

Synthesis of bionic glycoproteins for  
the treatment of uropathogenic *E. coli*

Natasha Emily Hatton

PhD

University of York

Chemistry

October 2021

## Abstract

This thesis first describes methods for the synthesis of bionic glycoproteins with potential activity against Uropathogenic *Escherichia coli*. Work to achieve this goal initially focused on the synthesis of constructs capable of binding to the FimH receptor; a trisaccharide ( $\alpha$ -D-mannopyranoside-(1  $\rightarrow$  3) -  $\alpha$ -D-mannopyranoside- (1  $\rightarrow$  4) 3-azidopropyl- $\beta$ -D-glucopyranoside) and two small mannose-based molecules. While the monosaccharide building blocks required for the trisaccharide synthesis were successfully synthesised, the small FimH-binding mannose-based species proved more suitable for the generation of bionic glycoproteins. One of the small mannose-based molecules was used in conjunction with on-resin copper-catalysed click ligation to synthesize three mannose-based probes capable of bio-conjugation to either colicin Ia or E9 proteins via organocatalyst-mediated protein aldol ligation (OPAL). Subsequently, in the first ever example of OPAL being used to conjugate glycans to proteins, these probes were used to synthesize a library of FimH-binding mannose-presenting colicin conjugates.

A selection of auto-aggregation and microscopy assays were conducted to determine whether the FimH-binding mannose-presenting colicin conjugates could induce aggregation of samples non-pathogenic *E. coli* strains. Unfortunately, the results of these experiments were inconclusive and further work is required to fully establish the biological activity of the mannose-based colicin conjugates.

This thesis also describes efforts towards the synthesis of trisaccharide ( $\alpha$ -D-mannopyranoside-(1  $\rightarrow$  3) -  $\alpha$ -D-mannopyranoside- (1  $\rightarrow$  4) 3-Azidopropyl- $\beta$ -D-glucopyranoside) Although completion of this synthesis was not achieved due to the timescale of this project, significant progress was made. Reported herein is the work performed thus far including a reliable method for the formation of  $\beta$ -mannosidic bonds (a notoriously difficult feat). In addition to investigating chemical methods for  $\beta$ -mannoside formation, enzymatic synthetic methods using the phosphorylase BT-1033 were also developed. To the best of our knowledge we present the first investigation into the substrate promiscuity of BT-1033 towards unnatural glucosamine analogues and mannose-1-phosphates.

## Contents

### Contents

Abstract.....	ii
Contents.....	iii
List of abbreviations.....	viii
List of figures.....	xi
List of schemes.....	xvii
List of tables.....	xxii
Acknowledgements.....	xxv
Declaration.....	xxvi
Chapter 1 Introduction .....	27
1.1    Section A .....	27
1.1.1    Structure of the urinary tract, urothelium and uroplakins .....	27
1.1.2    Urinary tract infections .....	28
1.1.3 <i>Uropathogenic Escherichia coli</i> pathogenesis pathway.....	30
1.1.4    FimH structure and catch bond mechanism.....	32
1.1.5    FimH binding pocket .....	34
1.1.6    Vaccines against targeting UTIs .....	37
1.1.7    Oligosaccharide based FimH inhibitors.....	40
1.1.8 $\alpha$ -configured D-Mannopyranoside based inhibitors .....	43
1.1.9    Use of polyvalent mannose scaffolds in FimH .....	58
1.2    Section B .....	65
1.2.1    Protein bio-conjugation methodologies .....	65
1.2.1.1    Canonical amino acid based protein bio-conjugation methodologies .....	65
1.2.1.2    Non-canonical protein bio-conjugation methodologies.....	68
1.2.2    Protein and peptide glycoconjugate constructs .....	75
1.2.3    Project aims .....	81
Chapter 2 Synthesis of monosaccharide building blocks.....	83
2.0 Aims.....	83
2.1 Design and synthesis of an oligosaccharide-based inhibitor .....	83
2.1.1 Reasoning behind monosaccharide synthesis .....	83
2.1.2 Design of monosaccharides.....	83
2.1.3 Design and synthesis of mannoside <b>2.2</b> .....	84
2.1.4 Design and synthesis of mannoside donors <b>2.1a</b> and <b>2.1b</b> .....	86
2.1.5 Synthesis of mannoside donors <b>2.1a</b> and <b>2.1b</b> .....	87
2.1.6    Synthesis of a GlcNAc acceptor .....	88
2.1.6.1 Initial use of trichloroacetyl protection .....	88

## Contents

2.1.6.2 Use of phthalimide protection .....	99
2.2 Design and synthesis of mannose squarate analogues .....	104
2.3 Summary and conclusions .....	109
Chapter 3 Synthesis of mannose-based inhibitor-linked OPAL probes for use in ligation .....	110
3.1 Introduction .....	110
3.2 Section aims .....	114
3.2 Results and discussion .....	114
3.2.1 Expression and purification of colicin E9 .....	114
3.2.2 Investigation into potential bio-conjugation techniques .....	116
3.2.3 Synthesis of a library of mannose-based inhibitor-linked OPAL probes.....	122
3.2.4 Conjugation of OPAL probe to colicin Ia and colicin E9 .....	133
3.3 Summary and conclusions .....	135
Chapter 4 Investigation into the biological applications of the colicin conjugates .....	136
4.1 Aims.....	136
4.2 Results and discussion .....	136
4.2.1 Use of aggregation assays .....	136
4.2.2 Use of microscopy .....	149
4.3 Summary and conclusions .....	152
Chapter 5 Use of chemical synthesis for the construction of $\beta$ -mannosides .....	153
5.1. Introduction .....	153
5.2 Section aims .....	160
5.3 Result and discussion .....	161
5.3.1 Exploration of chemical synthesis method for the synthesis of $\beta$ -mannosides .....	161
5.3.2 Further investigations into the synthesis of protected trisaccharide <b>5.19</b> .....	164
5.3.3 Optimisation of the final $\alpha$ -mannoside glycosylation in trisaccharide <b>1.4</b> .....	167
5.4 Summary and conclusions .....	174
Chapter 6 Use of enzymatic synthesis for the construction of $\beta$ -mannosides .....	175
6.1 Introduction into enzymatic methods for $\beta$ -mannoside synthesis.....	175
6.2 Section aims .....	181
6.3 Results and Discussion .....	181
6.3.1 Result of screening BT-1033 in reverse phosphorolysis with unnatural GlcNAc acceptors and mannose-1-phosphates .....	181
6.3.2. Establishing conversion rate of the BT-1033 catalysed reactions .....	187
6.3.4 Crystallography of BT-1033.....	212
6.3.5 Use of BT-1033 as a thioglycoligases .....	215
Chapter 7 Conclusion and future work.....	219

## Contents

Chapter 8 Experimental .....	224
8.1 General experimental .....	224
8.1.1 Non-chapter specific experimental procedures/information.....	224
8.1.2 Spectroscopic and spectrometric instruments and standard practices .....	224
8.1.3 Sodium dodecyl sulfate polyacrylamide gel electrophoresis (SDS-PAGE) analysis of proteins .....	226
8.1.4 General procedure for running a lectin blot.....	227
8.1.5 General procedure for running a Western blot.....	227
8.1.6 General method for Bradford assay.....	228
8.1.7 General biological kits used .....	228
8.1.8 Microscopy.....	228
8.2 Experimental for Chapter 2.....	229
8.2.1 Synthesis of 4-methylphenyl 2-benzyl-4,6- <i>O</i> -benzylidene-3- <i>O</i> - <i>p</i> -methoxybenzyl-1-thio- $\alpha$ -D- mannopyranoside <b>2.2</b> .....	229
8.2.2 Synthesis of 4-methylphenyl 2- <i>O</i> -acetyl-3,4,6-tri- <i>O</i> -benzyl-1-thio- $\alpha$ -D-mannopyranoside <b>2.1a</b> and 4-methylphenyl 2- <i>O</i> -benzoyl-3,4,6-tri- <i>O</i> -benzyl-1-thio- $\alpha$ -D-mannopyranoside <b>2.1b</b> ..	235
8.2.3 Synthesis of 4-methylphenyl 3,6-di- <i>O</i> -benzyl-2-deoxy-2- <i>N</i> -trichloroacetamido-1-thio- $\beta$ -D- glucopyranoside <b>2.26</b> .....	241
8.2.4 Synthesis of ethyl 3- <i>O</i> -benzoyl-4,6- <i>O</i> -benzylidene-2-deoxy-2- <i>N</i> -trichloroacetamido-1-thio- $\beta$ -D-glucopyranoside <b>2.3b</b> .....	248
8.2.5 Synthesis of 3-Azidopropyl 3,6-di- <i>O</i> -benzyl-2-deoxy-2-phthalimido-1- $\beta$ -D-glucopyranoside <b>2.3c</b> .....	253
8.2.6 Synthesis of squarate mannose analogues - <i>p</i> -[[(2-aminoethylamino)-2,3-dioxocyclobut-1- enyl]amino]phenyl $\alpha$ -D-mannopyranoside <b>2.53</b> and <i>p</i> -[[(1-amino-2-azidoethane)-2,3- dioxocyclobut-1-enyl]amino]phenyl $\alpha$ -D-mannopyranoside <b>2.54</b> .....	262
8.2.7 Synthesis of supporting compounds used in chapter 2 .....	268
8.3 Experimental for Chapter 3.....	270
8.3.1 Methodology for the expression and purification of Colicin E9 .....	270
8.3.2 Methodology for the bio-conjugation of mannose-based inhibitor <b>2.53</b> to colicin Ia using heterobifunctional linker <b>3.1</b> .....	271
8.3.3.1 Methodology for the bio-conjugation of active biotin linked (PEG) <sub>3</sub> OPAL probe <b>3.3</b> to colicin E9 .....	272
8.3.3.2 Methodology for the bio-conjugation of active biotin linked (PEG) <sub>3</sub> OPAL probe <b>3.3</b> to colicin Ia .....	273
8.3.4. Synthesis of Synthesis of (S)-2-(4-((3-(tert-butoxycarbonyl)-2,2-dimethyloxazolidin-4- yl)methyl)phenoxy)acetic acid <b>3.5</b> .....	274
8.3.5 Synthesis of required OPAL probes.....	278
8.3.6 Synthesis of mannose-based inhibitor linked colicin conjugates .....	299
8.4 Experimental for Chapter 4.....	307

## Contents

8.4.1 General methodology for the preparation of auto-aggregation samples using the initial auto-aggregation assay (Experiment one) .....	307
8.4.2 General methodology for the preparation of auto-aggregation samples using the redesigned auto-aggregation assay (Experiments two- five) .....	308
8.4.3 General methodology for the preparation of microscopy samples (Experiments six - eight) .....	310
8.5 Experimental for Chapter 5.....	311
8.5.1 Synthesis of $\beta$ -1,4-D-mannosyl-N-acetyl-D-glucosamine using chemical synthesis .....	311
8.5.2 Further investigations into the synthesis of protected trisaccharide <b>5.19</b> .....	319
8.5.3 Optimisation of the $\alpha$ -mannoside glycosylation.....	323
8.6 Experimental for Chapter 6.....	336
8.6.1 Expression and purification of BT-1033 .....	336
8.6.2 Reaction performed using BT-1033 .....	337
8.6.3 BT-1033 Crystallography .....	341
8.6.4 Investigation into BT-1033 thioglycoligases activity.....	341
Chapter 9 Appendix .....	i
9.1 Appendix for chapter 2 .....	i
9.1.1 Synthesis of 4-methylphenyl 2-benzyl-4,6-O-benzylidene-3-O-p-methoxybenzyl-1-thio- $\alpha$ -D-mannopyranoside <b>2.2</b> .....	i
9.1.2 Synthesis of 4-methylphenyl 2-O-acetyl-3,4,6-tri-O-benzyl-1-thio- $\alpha$ -D-mannopyranoside <b>2.1a</b> and 4-methylphenyl 2-O-benzoyl-3,4,6-tri-O-benzyl-1-thio- $\alpha$ -D-mannopyranoside <b>2.1b</b> ....	xiv
9.1.3 Synthesis of 4-methylphenyl 3,6-di-O-benzyl-2-deoxy-2-N-trichloroacetamido-1-thio- $\beta$ -D-glucopyranoside <b>2.26</b> .....	xxvi
9.1.4 Synthesis of ethyl 3-O-benzoyl-4,6-O-benzylidene-2-deoxy-2-N-trichloroacetamido-1-thio- $\beta$ -D-glucopyranoside <b>2.38</b> .....	xxxix
9.1.5 Synthesis of 3-Azidopropyl 3,6-di-O-benzyl-2-deoxy-2-phthalimido-1- $\beta$ -D-glucopyranoside <b>2.3c</b> .....	xlvii
9.1.6 Synthesis of squarate mannose analogues- <i>p</i> -[[(2-aminoethylamino)-2,3-dioxocyclobut-1-enyl]amino]phenyl $\alpha$ -D-mannopyranoside <b>2.53</b> and <i>p</i> -[[(1-amino-2-azidoethane)-2,3-dioxocyclobut-1-enyl]amino]phenyl $\alpha$ -D-mannopyranoside <b>2.54</b> .....	lxiv
9.1.7 Supporting compounds used in chapter 2 .....	lxxvii
9.2 Appendix for Chapter 3.....	lxxxv
9.2.1 Expression and purification of colicin E9 .....	lxxxv
9.2.2 Synthesis of Synthesis of (S)-2-(4-((3-(tert-butoxycarbonyl)-2,2-dimethyloxazolidin-4-yl)methyl)phenoxy)acetic acid <b>3.5</b> .....	lxxxvi
9.2.3 LCMS traces of OPAL probes <b>3.17</b> , <b>3.18</b> , <b>3.19</b> and <b>3.20</b> .....	xcv
9.2.4 SDS page gels, lectin blots and western blots for the colicin linked conjugates .....	ci
9.3 Appendix for Chapter 4.....	cvi

## Contents

9.3.1 General appendix .....	cvi
9.3.2 Results of experiment one, an auto-aggregation assay performed using the initial auto-aggregation assay method, investigating the effects of growth media and sample size .....	cvii
9.3.3 Results of experiment two, the screen performed using the redesigned auto-aggregation assay, investigating how factors such as starting OD <sub>600</sub> , incubation time and incubation temperature effects percentage auto-aggregation .....	cix
9.3.4 Results of experiment six, images of the microscopy samples imaged during the screening of microscopy conditions .....	cxvi
9.3.5 Results of experiment seven, images from the microscopy screen of samples incubated with mannose-based inhibitor linked (Gly-Ser) <sub>6</sub> colicin E9 conjugate .....	cxlii
9.3.6 Result of experiment eight, microscopy images of samples used in the positive control screen .....	cxlviii
9.4 Appendix for Chapter 5 .....	clv
9.4.1 Synthesis of $\beta$ -1,4-D-mannosyl-N-acetyl-D-glucosamine using chemical synthesis .....	clv
9.4.2 Further investigations into the synthesis of trisaccharide <b>5.19</b> .....	clxix
9.4.3 Work into the investigation into the optimisation of the $\alpha$ -mannoside glycosylation ..	clxxiv
9.5 Appendix for Chapter 6 .....	cxcviii
9.5.1 BT-1033 expression .....	cxcviii
9.5.2 BT-1033 catalysed reactions 1-42b .....	cci
9.5.3 Summary of ITag results .....	ccxxxv
9.5.4 NMR data .....	ccxxxviii
9.5.5 Crystal trays designs .....	ccxlv
9.5.6 BT-1033 catalysed reactions 43a-44b and enzyme free control reactions 45a and 45bcc	cxlvii
Chapter 10 References .....	ccl

## List of abbreviations

2,2 DMT	Benzylaldehyde dimethylacetal
Ac	Acetyl
Ac <sub>2</sub> O	Acetic anhydride
AgOTf	Silver trifluoromethanesulfonate
AlCl <sub>3</sub>	Aluminium chloride
ATR	attenuated total reflectance
BF <sub>3</sub> ·OEt <sub>2</sub>	Boron trifluoride etherate
BnBr	Benzyl bromide
Boc	tert-butyloxycarbonyl
Boc <sub>2</sub> O	Di-tert-butyl dicarbonate
BSA	bovine serum albumin
BSP	Benzenesulfinyl piperidine
Bu <sub>2</sub> SnO	Dibutyltin oxide
BzCl	Benzoyl chloride
cAMP	Cyclic AMP
CAP	Catabolite activator protein
CAZymes	carbohydrate-active enzymes
COVID-19	Corona virus disease 2019
CRP	cAMP receptor protein
CSA	Camphorsulfonic acid
CuAAC	Copper(I)-catalyzed alkyne-azide cycloaddition
DBMP	2,6-di-tert-butyl-4-methylpyridine
DCM	Dichloromethane
DDQ	2,3-Dichloro-5,6-dicyano-1,4-benzoquinone
DIBAL-H	Di-Isobutyl Aluminum Hydride
DIPEA	N,N-Diisopropylethylamine
DMAP	4-Dimethylaminopyridine
DMF	Dimethylformamide
DMSO	Dimethyl sulfoxide
DNA	Deoxyribonucleic acid
DNP	dinitrophenyl
DTBMP	2,6-Di-tert-butylpyridine
DTT	Dithiothreitol
<i>E. coli</i>	<i>Escherichia coli</i>
ECL	Enhanced chemiluminescence
EDC/NHS	ethyl(dimethylaminopropyl) carbodiimide / <i>N</i> -Hydroxysuccinimide
ESI	Electrospray ionization
Et <sub>2</sub> O	Diethyl ether
EtOAc	Ethyl acetate
FT-ICR	Fourier-transform ion cyclotron resonance
FTIR	Fourier transform infrared
GH	glycosyl hydrolases
GP	glycoside phosphorylases



## List of abbreviations

GT	glycosyl transferases
HEPES	4-(2-hydroxyethyl)-1-piperazineethanesulfonic acid
HR	High resolution
HSEt	Ethanethiol
HSiEt <sub>3</sub>	Triethylsilane
HSTol	4-methylbenzenethiol
	O-(1H-6-Chlorobenzotriazole-1-yl)-1,1,3,3-tetramethyluronium
HTCU	hexafluorophosphate
IAD	intermolecular aglycon delivery
IC <sub>50</sub>	half maximal inhibitory concentration
iPrOH	iso-propanol
IPTG	isopropyl β-d-thiogalactopyranoside
kDa	kilo Datons
<i>lac</i>	Lactose
LB	Luria Broth
LCMS	Liquid chromatography mass spectrometry
LPS	lipid polysaccharide
MALDI	Matrix-assisted laser desorption/ionization
m-CPBA	meta-Chloroperoxybenzoic acid
MeCN	Acetonitrile
MeOH	Methanol
MS	Mass spectrometry
4Å MS	4Å Molecular sieves
NEt <sub>3</sub>	Triethylamine
NGP	neighbouring group participation
NIS	N-Iodosuccinimide
NMR	Nuclear Magnetic Resonance
OD <sub>600</sub>	optical denisty at 600 nm
OPAL	Organocatalyst-mediated protein aldol ligation
PB	Phosphate buffer
PBS	Phosphate buffered saline
Pd/C	Palladium on carbon
PDVF	Polyvinylidene difluoride
PEG	Polyethylene glycol
Phth	Phthalimide
pKa	Acid dissociation constant
PMB	<i>para</i> -Methoxybenzyl
PMBCl	4-Methoxybenzyl chloride
PMSF	phenylmethanesulfonyl fluoride
r.t.	Room temperature
<i>R<sub>f</sub></i>	Retention factor
RNA	Ribonucleic acid
rpm	rotations per minute
SDS PAGE	Sodium dodecyl sulfate polyacrylamide gel electrophoresis

## List of abbreviations

SPAAC	Strain-promoted azide–alkyne cycloaddition
TBAI	Tetrabutylammonium iodide
TCA	Trichloroacetyl
TCEP	Tris(2-carboxyethyl)phosphine hydrochloride
Tf <sub>2</sub> O	Trifluoromethanesulfonic anhydride
TFA	Trifluoroacetic acid
TfOH	Trifluoromethanesulfonic acid
TG	transglycosidases
THF	Tetrahydrofuran
TIRF	Total Internal Reflection Fluorescence
TLC	Thin layer chromatography
TMSOTf	Trimethylsilyl trifluoromethanesulfonate
TRIS	tris(hydroxymethyl)aminomethane
TsOH	p-Toluenesulfonic acid
TTBP	2,4,6-Tri-tert-butylpyrimidine
UV	Ultraviolet
βMe	β mercaptoethanol

## List of figures

Figure 1-1. Structure of the urinary tract consisting of the upper urinary tract e.g. the kidneys and ureters and the lower urinary tract e.g. the bladder and the urethra .....	27
Figure 1-2. <b>a)</b> Structure of the urothelium with basal cells attached to a basement membrane, an intermediate layer and a layer of umbrella cells. <b>b)</b> Structure of the uroplakin plaque consisting of six heterodimeric units with each unit composed of two dimers UPIa/II and UPIb/IIIa. <b>c)</b> Structure of the heterodimer units where the green ellipse represents a high mannose containing N-glycan and the grey ellipses represent complex N-glycans. <b>d)</b> Structure of uroplakin Ia and <b>e)</b> structure of uroplakin Ib. Both structures consist of four transmembrane domains and have an approximate molecular weight of 30 kDa. <sup>8,9</sup> The green ellipses represent mannose residues, the blue squares represent glucosamine residues and the yellow ellipses represent galactose residues.....	28
Figure 1-3. Electron microscopy images of UPEC adhered to the urinary epithelial cell surface. <sup>22</sup> [Bars = 3 $\mu$ M (A) and 0.5 $\mu$ M (B)] .....	29
Figure 1-4. The pathogenesis cycle for UPEC consists of five stages: stage 1) colonization of the periurethral areas and the urethra, stage 2) movement of UPEC up the urethra, stage 3) UPEC adherence, stage 4) biofilm formation, stage 5) epithelial cell invasion and formation of intracellular bacterial population, and stage 6) colonization of the urinary tract and kidneys by UPEC followed by entry into the blood stream.....	30
Figure 1-5. Schematic diagram showing the three-stage membrane zipper mechanism thought to be used by UPEC during the invasion of the urothelium; <b>stage 1)</b> binding of UPEC to the urothelium, <b>stage 2)</b> localized rearrangement of the urothelium actin cytoskeleton, <b>stage 3)</b> envelopment and internalization of the bound UPEC .....	31
Figure 1-6. Structural organisation of the type 1 pilus which includes the following subunits: FimA (blue), FimC (gray), FimD (green rectangle), FimF (purple), FimG (green oval), and FimH (red). The position of the N-terminal domain (N, orange) and two C-terminal domains (C1, pink circle; C2, gray circle) relative to the transmembrane pore (green rectangle) in FimD are also indicated .....	31
Figure 1-7. Crystal structure of FimH (red) with a heptylmannoside (green) ligand bound in the N-terminal lectin domain (FimH <sub>LD</sub> ) (PDB ID 4LOV). <sup>44</sup> Residues with side chains shown as sticks (blue) are involved in non-covalent interactions with heptylmannoside, sodium ions (purple spheres) or water molecules (red spheres). The dashed lines (purple) denote short-range, non-covalent interactions. .	32
Figure 1-8. Catch bond mechanism for FimH binding to mannose in urethral lumen during a) no shear flow conditions where unbound and bound forms exist at equilibrium, and b) moderate shear flow conditions where the bound state is favoured. Under moderate shear flow conditions, the hydrodynamic drag on the micron-sized UPEC bacterium (not to scale) results in a physical force on the tether which activates the catch bond mechanism in FimH. The higher affinity binding to mannose under these conditions prevents the UPEC bacterium from being flushed out of the urinary tract during urination.....	34
Figure 1-9. A depiction of the majority of interactions that occur between mannose based pentasaccharide <b>1.1</b> and the extended FimH binding site. <sup>51</sup> Red indicates interactions mediated by Van der Waals, aromatic stacking and hydrophobic interactions, blue indicates interactions mediated by hydrogen bonding .....	35
Figure 1-10. <b>a)</b> Structure of FimH lectin domain when the tyrosine gate is open PDB 4AV0 <sup>57</sup> <b>b)</b> Structure of the FimH lectin domain when the tyrosine gate is closed PDB 4ATT <sup>58</sup> . Note the movement of the Tyr48 residue (blue) from facing the Asp47 residue (yellow) in the open conformer to facing the Thr51 residue (pink) in the closed conformer. The Arg98 residue (green) plays a role in stabilizing the surface loop conformation on which the Thr51 residue is located.....	36

## List of figures

Figure 1-11. Cartoon depiction of proposed mechanism of action for a typical anti-adhesion FimH-based vaccine. With antibodies binding to FimH thereby blocking UPEC adhering to mannose saturated N-glycans (green squares) located on the urothelium surface .....	39
Figure 1-12. Compares the structures of potent oligosaccharide based FimH inhibitors (oligosaccharides <b>1.2</b> , <b>1.3</b> , and trisaccharide <b>1.4</b> ) to weak oligosaccharide based FimH inhibitors (mannotriose <b>1.5</b> , mannopentaose <b>1.6</b> and Man $\alpha$ -1,3Man <b>1.7</b> ) .....	41
Figure 1-13. Structure of the potent FimH inhibitor oligomannoside <b>1.1</b> .....	42
Figure 1-14. Structure of the alkyl mannoside scaffold. Where n = 0-7 .....	43
Figure 1-15. Structure of p-nitrophenyl- $\alpha$ -mannoside <b>1.8</b> , p-Nitro-O-chlorophenyl- $\alpha$ -mannoside (pNoClP $\alpha$ Man) <b>1.9</b> and 4-methylumbelliferyl- $\alpha$ -mannoside (MeUmb $\alpha$ Man) <b>1.10</b> .....	44
Figure 1-16. Structure of biphenyl mannoside <b>1.11</b> .....	45
Figure 1-17. Structure of biphenyl mannoside <b>1.12</b> and biphenyl mannoside <b>1.13</b> .....	46
Figure 1-18. Structure of biphenyl mannoside <b>1.11</b> , biphenyl mannoside <b>1.14</b> , biphenyl mannoside <b>1.15</b> and biphenyl mannoside <b>1.16</b> .....	46
Figure 1-19. Structure of biphenyl mannoside <b>1.17</b> .....	47
Figure 1-20. Structure of some substituted biphenyl mannoside analogs with promising FimH activity and pharmacokinetic properties, <sup>94, 96</sup> such as dissociation constants ( $K_D$ ) and logP <sub>e</sub> values assessed using a parallel artificial membrane permeability (PAMP) assay .....	48
Figure 1-21. Structure of squarate mannoside <b>1.18</b> and squarate mannoside <b>1.19</b> .....	50
Figure 1-22. Structure of Diamide squarate mannoside <b>1.20</b> .....	51
Figure 1-23. Structure, IC <sub>50</sub> values and K <sub>D</sub> values of 2-O-n-heptyl-1,6-anhydro-D-glycero-D-galactitol <b>1.21</b> and n-heptyl $\alpha$ -D-mannopyranoside <b>1.22</b> <sup>98</sup> .....	52
Figure 1-24. Structure of thiazolylaminomannosides scaffold <b>1.1</b> and neothiazolylaminomannoside scaffold <b>1.2</b> and structure and IC <sub>50</sub> values of thiazolylaminomannosides <b>1.23</b> and neothiazolylaminomannoside <b>1.24</b> <sup>99</sup> .....	54
Figure 1-25. Structure and IC <sub>50</sub> value of indolinyphenyl <b>1.25</b> <sup>101</sup> .....	55
Figure 1-26. Structures of the $\alpha$ -D-Mannopyranoside based inhibitors, n-heptyl $\alpha$ -D-mannopyranoside <b>1.22</b> , biphenyl $\alpha$ -D-mannopyranoside derivatives <b>1.26</b> and <b>1.27</b> , indolylphenyl mannoside derivative <b>1.28</b> and squarate mannosides derivative <b>1.29</b> .....	56
Figure 1-27. Diagram showing two potential mechanisms whereby multivalent ligands can increase apparent binding affinity. <b>a</b> ) Clustering effect where a multivalent ligand binds to one receptor initially and then captures additional receptors as they diffuse into close proximity resulting in clustering of the ligand -bound receptors. <b>b</b> ) Induced aggregation whereby multivalent ligands bind to multiple lectins on different bacterial units cross linking them together .....	59
Figure 1-28. Structure of multivalent HM glycoconjugates series designed upon using a carbohydrate core where n= 0, 1,2 and 6 (when using $\beta$ -cyclodextrin core) .....	60
Figure 1-29. <b>a</b> ) The immune response induced by polysaccharide-based vaccines, <b>b</b> ) The immune response induced by protein glycoconjugate vaccines. ....	76
Figure 1-30. Structure of bi-galactose analogue <b>1.30</b> .....	78
Figure 1-31. Cartoon depiction of glycoconjugate induced UPEC aggregation .....	81
Figure 1-32. The four overall objectives of the project. Stage 1) Synthesis of a mannose based FimH inhibitor, stage 2) Protein bio-conjugation (colicin Ia PDB; 1CII <sup>222</sup> ), stage 3) BtuB binding (PDB; 3RGM <sup>223</sup> ) and TIRF microscopy and stage 4) UPEC aggregation and motility assay using digital holography .....	82
Figure 2-1. The structure of trisaccharide <b>1.4</b> .....	83
Figure 2-2. Retrosynthesis of trisaccharide <b>1.4</b> to give the three desired monosaccharide structures. Where R = Bz or Bn, R <sub>1</sub> = Bz, Ac or Bn, R <sub>2</sub> = HTCA or Phth .....	84
Figure 2-3. The structure of mannoside <b>2.2</b> .....	84

## List of figures

Figure 2-4. Structure of the dibenzylidene mannoside side product <b>2.9</b> obtained during 4,6-O-benzylidene acetal-protection of unprotected mannoside <b>2.6</b> .....	85
Figure 2-5. Structure of likely mannose dibutylstannylene acetal intermediate <b>2.10</b> formed during selective O-3 PMB protection .....	86
Figure 2-6. Structures of O-2 acetyl <b>2.1a</b> and O-2 benzoyl <b>2.1b</b> protected mannose thioglycoside donors .....	86
Figure 2-7. Structure of 3-azidopropyl-linked 1,4 GlcNPhth acceptor <b>2.16</b> .....	88
Figure 2-8. Simplified view of alternative selective benzylidene acetal ring opening pathways, where E represents an electrophile .....	94
Figure 2-9. Van der Marel’s benzylidene acetal NPhth protected S <sub>Et</sub> thioglycoside <b>2.28</b> and NHTCA protected S <sub>Tol</sub> thioglycoside <b>2.26</b> .....	95
Figure 2-10. Structure of the undesired product <b>2.34</b> from test glycosylation of donor <b>2.26</b> with 3-azidopropan-1-ol.....	96
Figure 2-11. Structure of Fairbanks and co-workers GlcNAc acceptor <sup>253</sup> .....	98
Figure 2-12. a) Depicts reductive amination reaction pathway, where R <sub>1</sub> = H for aldehydes and R <sub>1</sub> = either an alkyl or aryl group for ketones, b) depicts EDC/NSH coupling reaction pathway, where R <sub>2</sub> = protein when using direct coupling method and R <sub>2</sub> = a linker functionalised with either a maleimide, alkyne or azide motif when a functionalised linker approach is being used .....	108
Figure 3-1. Structure of colicin Ia, highlighted are the three different domains, the R-domain (green), the C-domain (yellow) and the T-domain (orange). PDB; 1CII <sup>222</sup> .....	110
Figure 3-2. Structure of colicin E9 highlighted are the three different domains, the R-domain (green), the C-domain (yellow) and the T-domain (orange). PDB; 5EW5 <sup>263</sup> .....	111
Figure 3-3. Crystal structure of spin-labelled BtuB T156R1, PDB; 3RGM <sup>223</sup> .....	112
Figure 3-4. Structure of the OmpF porin. PDB 2ZFG <sup>283</sup> .....	113
Figure 3-5. Structure of colicin IA (pink) bound to the Cir receptor (blue), PDB; 2HDI <sup>291</sup> .....	113
Figure 3-6. Structures of allolactose and IPTG.....	115
Figure 3-7. Structure of mannose-based inhibitors 2.53 and 2.54 .....	116
Figure 3-8. SDS-PAGE gel (stained with Coomassie) containing colicin Ia which has been subjected to ligation with mannose-based inhibitor-linked heterobifunctional linker <b>3.2</b> (lanes B-E) and unmodified colicin Ia (lanes F-I) .....	118
Figure 3-9. Lectin blot containing colicin Ia which has been subjected to ligation with mannose-based inhibitor-linked heterobifunctional linker <b>3.2</b> (lanes B-E) and unmodified colicin Ia (lanes F-I).....	118
Figure 3-10. The structure of biotin-linked OPAL probe <b>3.3</b> .....	120
Figure 3-11. Results of lectin blot containing colicin Ia which has been subjected to OPAL ligation with biotin-linked OPAL probe <b>3.3</b> (lanes B-E) and unmodified colicin Ia (lanes F-H).....	120
Figure 3-12. Results of lectin blot containing colicin E9 which has been subjected to OPAL ligation with biotin-linked OPAL probe <b>3.3</b> (lanes B-E) and unmodified colicin E9 (lanes F-H).....	120
Figure 3-13. Results of SDS-PAGE gel stained with Coomassie containing unmodified colicin Ia (lane B), colicin Ia which has been subjected to ligation with biotin-linked OPAL probe <b>3.3</b> (lane C), unmodified colicin E9 (lane D) and colicin E9 which has been subjected to ligation with biotin-linked OPAL probe <b>3.3</b> (lane E) .....	121
Figure 3-14. Depicts the mass spectroscopy results for probe <b>3.10</b> .....	126
Figure 3-15. Structure of probe <b>3.13</b> .....	127
Figure 3-16. Depicts mass spectrometry trace for probe <b>3.13</b> .....	127
Figure 3-17. Structure of probe <b>3.14</b> .....	128
Figure 3-18. Liquid chromatography trace of probe <b>3.14</b> .....	128
Figure 3-19. Mass spectrometry trace of probe <b>3.14</b> .....	129
Figure 3-20. Structure of probe <b>3.15</b> .....	129

## List of figures

Figure 3-21. Depicts the liquid chromatogram trace for probe <b>3.15</b> .....	130
Figure 3-22. Depicts mass spectrometry trace for probe <b>3.15</b> .....	130
Figure 3-23. Structure of biotin-linked probe <b>3.16</b> .....	131
Figure 3-24. Depicts the liquid chromatogram trace for probe <b>3.16</b> .....	131
Figure 3-25. Depicts mass spectrometry trace for probe <b>3.16</b> .....	132
Figure 3-26. Results of SDS-PAGE gel stained with Coomassie containing unmodified colicin E9 (lane B-D), and colicin E9 which has been subjected to OPAL ligation with mannose-based inhibitor-linked (Gly-Ser) OPAL probe <b>3.18</b> (lanes E-G) .....	133
Figure 3-27. Results of lectin blot containing unmodified colicin E9 (lanes B-E) and colicin E9 which has been subjected to OPAL ligation with mannose-based inhibitor-linked (Gly-Ser) OPAL probe <b>3.18</b> (lanes F-I) .....	133
Figure 3-28. Results of SDS-PAGE gel stained with Coomassie containing colicin Ia which has been subjected to OPAL ligation with mannose-based inhibitor-linked (Gly-Ser) <sub>3</sub> OPAL probe <b>3.17</b> (lanes B and C), unmodified colicin Ia (lane D and E), colicin E9 which has been subjected to OPAL ligation with mannose-based inhibitor-linked (Gly-Ser) <sub>3</sub> OPAL probe <b>3.17</b> (lanes F and G) and unmodified colicin E9. ....	134
Figure 3-29. Depicts the UV vis trace for a) biotin-linked OPAL probe <b>3.20</b> and b) Mannose-based inhibitor (Gly-Ser) OPAL probe <b>3.18</b> .....	135
Figure 4-1. Diagram depicting the expected LPS structures of both BW25113 and JW3596 adapted from <sup>318,319</sup> .....	138
Figure 4-2. Results of Experiment Two, which was designed to screen potential aggregation factors using the new auto-aggregation assay method. The results are plotted on the graph that corresponds to a sample starting OD <sub>600</sub> .....	142
Figure 4-3. Microscopy images of two of the samples where aggregation was observed in Experiment Six. a) active sample of BW25113 incubated 10 nM mannose-based inhibitor linked (Gly-Ser) colicin E9 conjugate, b) zoomed in section of image a, c) vortexed control sample of BW25113 incubated 10 nM mannose-based inhibitor linked (Gly-Ser) colicin E9 conjugate, d) active sample of BW25113 incubated with 1 μM mannose-based inhibitor linked (Gly-Ser) <sub>6</sub> colicin E9 conjugate, e) zoomed in section of image d, f) vortexed control sample of BW25113 incubated with 1 μM mannose-based inhibitor linked (Gly-Ser) <sub>6</sub> colicin E9 conjugate. Note images a, c, d and f were all taken a 20x magnification .....	150
Figure 5-1. Structure of a 1,2-O-cis-stannylene acetal of mannose .....	154
Figure 5-2. Structure of covalent α- triflate intermediate and contact ion pair intermediate .....	155
Figure 5-3. Structure of the <sup>3</sup> H <sub>4</sub> and <sup>4</sup> H <sub>3</sub> oxacarbenium ion conformations .....	156
Figure 5-4. Structure of disaccharide <b>5.18</b> .....	161
Figure 5-5. Structure of protected trisaccharide <b>5.19</b> .....	165
Figure 5-6. Structure of 1,2 benzyol mannose donor <b>2.1b</b> .....	168
Figure 6-1. Structures of unnatural GlcNAc acceptors <b>6.1-6.4</b> .....	182
Figure 6-2. Structure of the unnatural mannose phosphate analogues supplied by the Miller group .....	184
Figure 6-3. Conditions used for copper catalysed click reaction between an azide containing glycoside and imidazolium label <b>6.16</b> . Where R = OH for the unnatural GlcNAN <sub>3</sub> acceptor <b>6.1</b> and a mannosides for the disaccharides .....	188
Figure 6-4. Phyer2 predicted PDB structure of BT-1033 with suspected acid / base residue Aspartic acid residue 101 highlighted in pink .....	212
Figure 6-5. Images of promising BT-1033 crystals using conditions JCSG B8 (0.2 M MgCl <sub>2</sub> ·6H <sub>2</sub> O, 0.1 M TRIS, pH = 7.0, 10% w/v PEG 8000) and INDEX H8 (0.1 M magnesium formate dihydrate, 15% w/v PEG 3350) .....	213

## List of figures

Figure 6-6. Further promising images of BT-1033 crystals. Conditions H3 - 0.1 M magnesium formate dihydrate, 23% w/v PEG 3350, protein : reservoir 0.5 : 1.0; H4 - 0.1 M magnesium formate dihydrate, 23% w/v PEG 3350, protein : reservoir 1.0 : 1.0; H5 - 0.1 M magnesium formate dihydrate, 23% w/v PEG 3350, protein : reservoir 1.0 : 0.75; H6 - 0.1 M magnesium formate dihydrate, 23% w/v PEG 3350, protein : reservoir 1.0 : 0.5 .....	214
Figure 6-7. Structure of O-4-thiol-glucosamine acceptor <b>6.17</b> .....	215
Figure 8-1. Proton and carbon numbering for <sup>1</sup> H NMR and <sup>13</sup> C NMR data for mono and disaccharides .....	224
Figure 8-2. Reaction scheme for OPAL ligation of biotin-linked (PEG) <sub>3</sub> OPAL probe <b>3.3</b> to colicin E9272	
Figure 8-3. Reaction scheme for OPAL ligation of biotin-linked (PEG) <sub>3</sub> OPAL probe <b>3.3</b> to colicin Ia	273
Figure 8-4. Structure of mannose-based inhibitor linked OPAL probe <b>3.6</b> .....	278
Figure 8-5. Structure of mannose-based inhibitor linked OPAL probe <b>3.10</b> .....	281
Figure 8-6. Structure of mannose-based inhibitor linked (Gly-Ser) <sub>3</sub> OPAL probe <b>3.13</b> .....	283
Figure 8-7. Structure of active mannose-based inhibitor linked (Gly-Ser) <sub>3</sub> OPAL probe <b>3.17</b> .....	286
Figure 8-8. Structure of mannose-based inhibitor linked (Gly-Ser) OPAL probe <b>3.14</b> .....	287
Figure 8-9. active mannose-based inhibitor linked (Gly-Ser) OPAL probe <b>3.18</b> .....	289
Figure 8-10. Structure of mannose-based inhibitor linked (Gly-Ser) <sub>6</sub> OPAL probe <b>3.15</b> .....	290
Figure 8-11. Structure of active mannose-based inhibitor linked (Gly-Ser) <sub>6</sub> OPAL probe <b>3.19</b> .....	294
Figure 8-12. Structure of biotin linked (Ser-Gly) <sub>3</sub> OPAL probe <b>3.16</b> .....	295
Figure 8-13. Structure of active biotin linked (Ser-Gly) <sub>3</sub> OPAL probe <b>3.20</b> .....	298
Figure 9-1. Results of SDS-PAGE gel stained with Coomassie containing fraction 13-24 post HisTrap HP column purification of colicin E9 .....	lxxxv
Figure 9-2. Results of SDS-PAGE gel stained with Coomassie of fractions C7-D8 post gel filtration of colicin E9 .....	lxxxv
Figure 9-3. Structure of mannose-based inhibitor linked (Gly-Ser) OPAL probe <b>3.18</b> .....	xcv
Figure 9-4. Liquid chromatography trace for mannose-based inhibitor linked (Gly-Ser) OPAL probe <b>3.18</b> .....	xcv
Figure 9-5. Mass spectrometry trace for mannose-based inhibitor linked (Gly-Ser) OPAL probe <b>3.18</b> .....	xcvi
Figure 9-6. Structure of mannose-based inhibitor linked (Gly-Ser) <sub>3</sub> OPAL probe <b>3.17</b> .....	xcvi
Figure 9-7. Liquid chromatography trace for mannose-based inhibitor linked (Gly-Ser) <sub>3</sub> OPAL probe <b>3.17</b> .....	xcvii
Figure 9-8. Mass spectrometry trace for mannose-based inhibitor linked (Gly-Ser) <sub>3</sub> OPAL probe <b>3.17</b> .....	xcvii
Figure 9-9. Structure of mannose-based inhibitor linked (Gly-Ser) <sub>6</sub> OPAL probe <b>3.19</b> .....	xcviii
Figure 9-10. Liquid chromatography trace of mannose-based inhibitor linked (Gly-Ser) <sub>6</sub> OPAL probe <b>3.19</b> .....	xcviii
Figure 9-11. Mass spectrometry trace of mannose-based inhibitor linked (Gly-Ser) <sub>6</sub> OPAL probe <b>3.19</b> .....	xcix
Figure 9-12. Structure of biotin linked (Gly-Ser) <sub>3</sub> OPAL probe <b>3.20</b> .....	xcix
Figure 9-13. Liquid chromatography trace of biotin linked (Gly-Ser) <sub>3</sub> OPAL probe <b>3.20</b> .....	c
Figure 9-14. Mass spectrometry trace of biotin linked (Gly-Ser) <sub>3</sub> OPAL probe <b>3.20</b> .....	c
Figure 9-15. Results of SDS-PAGE gel stained with Coomassie, containing unmodified colicin Ia (lane B) and colicin Ia which has been subjected to ligation with mannose-based inhibitor linked (Gly-Ser) OPAL probe <b>3.18</b> (lane C).....	ci
Figure 9-16. Results of lectin blot containing unmodified colicin Ia (lanes B-E) and colicin Ia which has been subjected to OPAL ligation with mannose-based inhibitor linked (Gly-Ser) OPAL probe <b>3.18</b> (lanes F-I).....	ci

## List of figures

Figure 9-17. Results of SDS-PAGE gel stained with Coomassie, containing unmodified colicin E9 (lanes B and C) and colicin E9 which has been subjected to ligation with mannose-based inhibitor linked (Gly-Ser) <sub>3</sub> OPAL probe <b>3.17</b> (lanes D and E) .....	ci
Figure 9-18. Results of lectin blot containing unmodified colicin E9 (lanes B-D) and colicin E9 which has been subjected to ligation with mannose-based inhibitor linked (Gly-Ser) <sub>3</sub> OPAL probe <b>3.17</b> (lanes E-G) .....	cii
Figure 9-19. Results of SDS-PAGE gel stained with Coomassie, containing unmodified colicin Ia (lanes B and E) and colicin Ia which has been subjected to ligation with mannose-based inhibitor linked (Gly-Ser) <sub>3</sub> OPAL probe <b>3.17</b> (lanes F and I) .....	cii
Figure 9-20. Results of lectin blot containing unmodified colicin Ia (lanes B-E) and colicin Ia which has been subjected to ligation with mannose-based inhibitor linked (Gly-Ser) <sub>3</sub> OPAL probe <b>3.17</b> (lanes F-I) .....	cii
Figure 9-21. Results of SDS-PAGE gel stained with Coomassie, containing unmodified colicin E9 (lane B) and colicin E9 which has been subjected to ligation with mannose-based inhibitor linked (Gly-Ser) <sub>6</sub> OPAL probe <b>3.19</b> (lane C) .....	ciii
Figure 9-22. Results of lectin blot containing unmodified colicin E9 (lane B-E) and colicin E9 which has been subjected to ligation with mannose-based inhibitor linked (Gly-Ser) <sub>6</sub> OPAL probe <b>3.19</b> (lanes F-I) .....	ciii
Figure 9-23. Results of SDS-PAGE gel stained with Coomassie, containing unmodified colicin Ia (lane B) and colicin Ia which has been subjected to ligation with mannose-based inhibitor linked (Gly-Ser) <sub>6</sub> OPAL probe <b>3.19</b> .....	ciii
Figure 9-24. Results of lectin blot containing unmodified colicin Ia (lanes B - E) and colicin Ia which has been subjected to ligation with mannose-based inhibitor linked (Gly-Ser) <sub>6</sub> OPAL probe <b>3.19</b> (lanes F-I) .....	civ
Figure 9-25. Results of SDS-PAGE gel stained with Coomassie, containing unmodified colicin E9 (lanes B and C) and colicin E9 which has been subjected to ligation with biotin linked (Ser-Gly) <sub>3</sub> OPAL probe <b>3.20</b> (lanes D and E) .....	civ
Figure 9-26. Results of western blot containing unmodified colicin E9 (lanes B-D), colicin E9 which has been subjected to ligation with biotin linked (Ser-Gly) <sub>3</sub> OPAL probe <b>3.20</b> (lanes E-G) and biotinylated biovin serum albumin (lanes H-J) .....	civ
Figure 9-27. Results of SDS-PAGE gel stained with Coomassie, containing unmodified colicin Ia (lane B) and colicin Ia which has been subjected to ligation with biotin linked (Ser-Gly) <sub>3</sub> OPAL probe <b>3.20</b> (lane C) .....	cv
Figure 9-28. Results of western blot containing unmodified colicin E9 (lanes B-D) and colicin E9 which has been subjected to ligation with biotin linked (Ser-Gly) <sub>3</sub> OPAL probe <b>3.20</b> (lanes E-G) .....	cv
Figure 9-29. Plasmid map of BT-1033 pET-24 a(+), imaged using snap gene .....	cxcviii
Figure 9-30. HisTrap HP column trace .....	cxcviii
Figure 9-31. Results of SDS-PAGE gel stained with Coomassie of fractions 1-12 extracted from the HisTrap column .....	cxcix
Figure 9-32. Results of SDS-PAGE gel stained with Coomassie of fractions 13-21 extracted from the HisTrap column .....	cxcix
Figure 9-33. Gel filtration column trace .....	cc
Figure 9-34. Results of SDS-PAGE gel stained with Coomassie of fractions a6 to b11 extracted post gel filtration .....	cc



## List of schemes

Scheme 1-1. Reaction scheme for the synthesis of alkyl mannosides, by glycosylation with aliphatic alcohols proceeding using a AgOTf activation system.....	43
Scheme 1-2. Synthesis of ortho-substituted biphenyl mannosides. Reagents and conditions: Pathway <b>A + B</b> ; a) $\text{BF}_3 \cdot \text{Et}_2\text{O}$ , $\text{CH}_2\text{Cl}_2$ , reflux, 45 h, (25-75%); b) 3-substituted phenylboronic acid derivatives, cat. $\text{Pd}(\text{PPh}_3)_4$ , $\text{Cs}_2\text{CO}_3$ , dioxane/water (5/1), 80 °C, 1 h; c) cat. $\text{MeONa}$ , $\text{MeOH}$ , rt, 12 h, (b+c 3-64%); Pathway <b>C</b> ; d) $\text{MeNH}_2/\text{EtOH}$ , rt, e) bis(pinacolato)diboron, cat. $\text{Pd}(\text{dppf})\text{Cl}_2$ , $\text{KOAc}$ , $\text{DMSO}$ , 80 °C.....	49
Scheme 1-3. Reaction scheme for covalent bond formation between squarate mannoside <b>1.18</b> and the N-terminus of the FimH lectin (residue Phe1).....	50
Scheme 1-4. Synthetic pathway for the preparation of squarate mannosides. Reagents and reaction conditions; a) $\text{Pd}/\text{C}$ , $\text{H}_2$ , $\text{DMF}$ rt, 1 h; b) diethylsquarate, $\text{DMF}$ , rt, 12-14 h (a+b 55% b alone 63%); <sup>90</sup> c) ethylamine, $\text{NEt}_3$ , $\text{MeOH}$ , rt, 12h (63%) <sup>97</sup> .....	52
Scheme 1-5. Potential bio-conjugation reactions which can be performed on cysteine residues. $\text{S}_{\text{protein}}-\text{C}$ bond formation reactions include aminoethylation (buffer pH 8.9, 25 °C, 24 h), <sup>142</sup> treatment with iodoacetamide (buffer pH 8.2. r.t., 30 minutes), <sup>143</sup> maleimide ligation (buffer pH = 6.5 – 7.4, r.t.) and vinyl sulfone ligation (buffer pH = 8.5, r.t., 24 h). <sup>144</sup> $\text{S}_{\text{protein}}-\text{S}$ bond formation reactions include Dha formation (for formation methods see <sup>145</sup> ), disulfide formation and desulfurization of disulfides ( $\text{P}(\text{NMe})_3$ 2 eq, buffer, pH = 9.5, r.t., 12 h) <sup>146</sup> .....	65
Scheme 1-6. Reaction scheme for maleimide ligation including reaction conditions <sup>154</sup> and kinetic information <sup>148</sup> .....	66
Scheme 1-7. Reaction scheme for dual modification of a bromomaleimide .....	67
Scheme 1-8. Reaction scheme for vinyl sulfone mediated ligation. Displaying the reaction conditions used to conjugate rhodamine dye (R) to concanavalin A (protein) <sup>148</sup> .....	67
Scheme 1-9. Potential bio-conjugation reactions which can be performed on lysine residues, including the use of activated esters (buffer, pH 7.2 – 9, r.t., 30 minutes), isothiocyanates, isocyanates, sulfonyl chlorides (pH 8.0, r.t. – 37 °C, 1-2 h), <sup>165</sup> and reductive amination (buffer, pH 6.5 – 8.5 <sup>166</sup> r.t.) reactions .....	68
Scheme 1-10. Reaction scheme for CuAAC including reaction conditions and kinetics <sup>148</sup> .....	69
Scheme 1-11. Reaction scheme for SPAAC including kinetic parameters <sup>148</sup> .....	69
Scheme 1-12. Reaction scheme for the tetrazine ligation including kinetic parameters <sup>182</sup> .....	70
Scheme 1-13. Reaction scheme for hydrazone / oxime ligation including kinetic parameters for both hydrazone (with and without the nucleophilic catalyst aniline) <sup>138</sup> and oxime ligation <sup>148</sup> .....	71
Scheme 1-14. Reaction scheme and kinetic parameters for the a) Pictet-Spengler <sup>148</sup> and b) iso-Pictet-Spengler <sup>138</sup> .....	72
Scheme 1-15. Reaction scheme for OPAL ligation. Biotag = biotin, folate, azide or dansyl .....	73
Scheme 1-16. Reaction scheme for palladium decaging. Biotag = biotin, folate, azide and dansyl.....	73
Scheme 1-17. Reaction scheme for threonine-lysine dipeptide installation, oxidation and conjugation. Here biotag = biotin or dansyl .....	74
Scheme 1-18. Synthesis of pentavalent CTB-linked glycoconjugate <b>1.35</b> . Following an initial copper catalysed click reaction to attach pentasaccharide <b>1.31</b> to alkyne armed hydroxylamine linker <b>1.32</b> affording Boc protected hydroxylamine charged pentasacchride <b>1.33</b> . Following TFA mediated Boc deprotection pentasaccharide <b>1.34</b> was extracted and subjected to oxime ligation with the oxidised CTB mutant affording pentavalent CTB-linked glycoconjugate <b>1.35</b> .....	80
Scheme 2-1. Synthesis of wanted 1,3 mannoside <b>2.2</b> from D-mannose. Reagents and conditions a) $\text{Ac}_2\text{O}$ , pyridine, $\text{DMAP}$ , 0 °C- r.t., 12 h (80%); b) $\text{HSTol}$ , $\text{BF}_3 \cdot \text{Et}_2\text{O}$ , dry $\text{DCM}$ , 0 °C- r.t. 12 h, (62%); c) $\text{MeONa}$ , $\text{MeOH}$ , r.t., 62 h (80%); d) 2,2 DMT, $\text{CSA}$ , dry $\text{MeCN}$ , $\text{Et}_3\text{N}$ , r.t., 5 h (61%); e) $\text{Bu}_2\text{SnO}$ , dry	

List of schemes

toluene, 110 °C, 3h, PMBCl, CsF, dry DMF, 70 °C, 12 h (83%); f) BnBr, NaH, dry DMF, 0 °C- r.t, 2 h (36%) .....	85
Scheme 2-2. Synthesis of wanted 1,2 mannosides <b>2.1a</b> and <b>2.1b</b> from D-mannose. Reagents and conditions; a) Ac <sub>2</sub> O, pyridine, DMAP, 0 °C- r.t., 12 h, (94 %); b) i) 33 % HBr, AcOH, DCM, r.t., 1.5 h ii) 2,6-Lutidine, dry DCM, dry MeOH, r.t., 12 h, (i+ii = 51 %); c) NaOMe, MeOH, r.t., 1 h; d) NaH, BnBr, dry DMF, 0 °C- r.t., 12 h, (c + b = 50 %); e) AcOH, r.t., 1 h, (84 %); f) HSTol, BF <sub>3</sub> ·Et <sub>2</sub> O, dry DCM, 0 °C- r.t., 6 h (45 %); g) NaOMe, MeOH, r.t., 12h (89%); h) BzCl, DMAP, Pyridine, 0 °C- r.t., 2h, (78%) .....	87
Scheme 2-3. Depiction of ortho-ester formation with initial oxocarbenium ion formation followed by neighbouring group participation to form a β-linked acetoxonium ion <b>2.15</b> which is trapped by methanol under basic conditions to afford orthoester <b>2.11</b> .....	88
Scheme 2-4. Hydrogenation reaction of benzyl protected trisaccharide <b>2.17</b> to afford trisaccharide <b>1.4</b> .....	89
Scheme 2-5. Mechanism for TCA induce oxazoline ring formation. With initial oxocarbenium ion <b>2.18</b> formation, followed by neighbouring group participation of TCA to afford trichloroacetoxonium ion <b>2.19</b> .....	90
Scheme 2-6. Synthesis of 1,4 GlcNHTCA acceptor <b>2.3a</b> from D-glucosamine hydrochloride. Reagents and conditions; a) D-glucosamine hydrochloride, trichloroacetylchloride, NaHCO <sub>3</sub> , H <sub>2</sub> O, r.t., 1h; b) Ac <sub>2</sub> O, pyridine, DMAP, 0 °C - r.t., 12 h, (a+b 58%); c) HSTol, BF <sub>3</sub> ·Et <sub>2</sub> O, dry DCM, 0 °C- r.t., 12h, (16%); d) NaOMe, MeOH, r.t., 10 minutes, (80%); e) 2,2 DMT, CSA, dry MeCN, r.t., 5h, (87%); f) NaH, BnBr, dry DMF, 0 °C- r.t., 12 h (7%); g) triethylsilane, BF <sub>3</sub> ·Et <sub>2</sub> O, dry DCM, 0 °C, 2 minutes (6%); h) 1-benzenesulfinyl piperidine, trifluoromethanesulfonic anhydride, dry DCM, 4Å MS, 3-azidopropan-1-ol .....	91
Scheme 2-7. Two potential reaction pathways A and B for the formation of N-2 unprotected glucosamine <b>2.27</b> . NaH is represented as H <sup>-</sup> .....	93
Scheme 2-8. Mechanism proposed for selective benzylidene acetal ring opening to reveal a free O-4 .....	95
Scheme 2-9. Mechanism of trifluoromethanesulfonic anhydride activation of BSP <b>2.29</b> to afford activated BSP <b>2.30</b> .....	95
Scheme 2-10. Proposed mechanism for glycosylation of NHTCA protected thioglycoside <b>2.26</b> with 3-azidopropan-1-ol.....	96
Scheme 2-11. Synthesis of GlcNHTCA acceptor <b>2.3b</b> from D-glucosamine hydrochloride. Reagent and conditions; a) D-glucosamine hydrochloride, trichloroacetylchloride, NEt <sub>3</sub> , MeOH, 0 °C - r.t., 5 days; b) Ac <sub>2</sub> O, pyridine, DMAP, 0 °C- r.t., 12 h; c) EtSH, BF <sub>3</sub> ·OEt <sub>2</sub> , dry DCM, 0 °C - r.t., 12 h, (40%); d) NaOMe, MeOH, r.t., 2h (86%); e) 2,2 DMT, CSA, dry MeCN, NEt <sub>3</sub> , 65°C, r.t., 3h, (52%); f) BzCl, pyridine, DMAP, 0 °C - r.t., 1.5 h (66%); g) 1-benzenesulfinyl piperidine, trifluoromethanesulfonic anhydride, dry DCM, 4Å MS, 3-azidopropan-1-ol; h) Et <sub>3</sub> SiH, BF <sub>3</sub> ·Et <sub>2</sub> O/ TFA, dry DCM.....	97
Scheme 2-12. Synthesis of 1,4 GlcNPhth acceptor <b>2.3c</b> from D-glucosamine hydrochloride. Reagents and conditions: a) Phthalic anhydride, NaOH, NaHCO <sub>3</sub> , 1 : 2 MeOH : H <sub>2</sub> O, Acetone, r.t., 2 h, 50 °C, 1 h, r.t., 12h (50%); b) Ac <sub>2</sub> O, pyridine, DMAP, 0 °C - r.t., 6h, (87%); c) HSTol, BF <sub>3</sub> ·Et <sub>2</sub> O, dry DCM, 0 °C - r.t., 96 h, (85%); d) NaOMe, MeOH : DCM, r.t., 20 min, (99 %); e) 2,2-DMT, dry MeCN, CSA, NEt <sub>3</sub> , r.t., 12 h, (66%); f) NaH, BnBr, dry DMF, 0 °C- r.t., 6 h, (41%); g) BSP, TTBP, Tf <sub>2</sub> O, 3-azidopropan-1-ol, 4Å MS, dry DCE, -10 °C, 3 h, (79%); h) HSiEt <sub>3</sub> , TfOH, dry DCM, r.t., 20 minutes, (43%).....	99
Scheme 2-13. Mechanism of phthalimide addition.....	100
Scheme 2-14. Ring opening reaction using a hydride and acid combination to give either the open O-4 position (desired glycoside <b>2.3c</b> ) or 4,6-O-benzylidene acetal-cleaved glycoside <b>2.48</b> . Reagents- i) Acid + hydride .....	101
Scheme 2-15. Selective O-4 benzylidene acetal ring opening of 4,6-O-benzylidene acetal-protected glycoside <b>2.47</b> .....	102

## List of schemes

Scheme 2-16. Proposed 4-step chemical approach to the mannose squarate <b>2.49</b> from D-mannose .....	105
Scheme 2-17. Synthesis of mannose-based inhibitor <b>2.50</b> from D-mannose. Reagents and conditions, a) Ac <sub>2</sub> O, pyridine, DMAP, 0 °C - r.t., 12 h (80%); b) BF <sub>3</sub> ·OEt <sub>2</sub> , 4-nitrophenol, dry DCM, 0 °C - r.t., 60 h, (43%); c) i) NaOMe, MeOH, r.t. 20 minutes, ii) Pd/C, H <sub>2</sub> , dry MeOH, r.t., 12 h, (i + ii = 53%); d) Dimethyl squarate, dry MeOH, r.t., 4 h, (84%); e) N-Boc-1,2-Diaminoethane, NEt <sub>3</sub> , dry MeOH, r.t., 16 h, (43%); f) H <sub>2</sub> O : TfOH 1 : 1, r.t., 3 h (80%).....	106
Scheme 2-18. Synthesis of azide capped squarate ester <b>2.54</b> , using 1-amino-2-azidoethane. NEt <sub>3</sub> , MeOH, r.t., 16h, ≤ 67%.....	109
Scheme 3-1. Schematic depicting the pH-dependent reactions of heterobifunctional linker 3.1, which initially undergoes an EDC NHS reaction with mannoside based inhibitor 2.53 to afford mannose-based inhibitor-linked heterobifunctional linker 3.2, and then subsequently undergoes maleimide ligation to the free thiol unit located on colicin Ia.....	117
Scheme 3-2. Schematic for colicin Ia undergoing initial NaIO <sub>4</sub> -mediated oxidative cleavage of the N-terminal 1,2-amino alcohol to give an alpha oxo-aldehyde, which can subsequently be subjected to OPAL ligation with an aldehyde-charged probe, mediated by a proline tetrazole catalyst. (R = a biotag such as folate, dansyl and biotin) .....	119
Scheme 3-3. Reaction schematic for proposed conversion of peptide <b>3.4</b> to mannose-based inhibitor-linked OPAL probe <b>3.6</b> . Following initial attachment of mannose-based inhibitor <b>2.53</b> (step A) to afford Dde protected mannose-based inhibitor-linked peptide <b>3.7</b> , which is treated with 2% hydrazine in DMF (step B) to afford mannose-based inhibitor-linked peptide <b>3.8</b> . The revealed free amine residue allows for attachment of OPAL small molecule <b>3.5</b> (step C) affording protected mannose-based inhibitor-linked OPAL probe <b>3.9</b> , the final step is treatment with 95 : 2.5 : 2.5 TFA : H <sub>2</sub> O : triisopropylsilane to afford mannose-based inhibitor-linked OPAL probe <b>3.6</b> .....	123
Scheme 3-4. Schematic for the synthesis of mannose-based inhibitor-linked OPAL probe <b>3.10</b> from alkyne charged peptide <b>3.11</b> following initial on-resin copper-catalysed click with mannose-based inhibitor <b>2.54</b> to afford mannose-based inhibitor-linked peptide <b>3.12</b> , which undergoes acid-catalysed cleavage using the cleavage cocktail 95 : 2.5 : 2.5 TFA : H <sub>2</sub> O : triisopropylsilane .....	125
Scheme 3-5. General procedure for NaIO <sub>4</sub> oxidation of biotin and mannose-based inhibitor-linked OPAL probes <b>3.13</b> , <b>3.14</b> , <b>3.15</b> and <b>3.16</b> to form activated probes <b>3.17</b> , <b>3.18</b> , <b>3.19</b> and <b>3.20</b> .....	132
Scheme 4-1. Schematic of the initial auto-aggregation assay designed, based on that previously reported by Uhlin and co-workers <sup>315</sup> .....	137
Scheme 4-2. Schematic of the redesigned auto-aggregation assay .....	141
Scheme 5-1. a) The thermodynamic preferences which lead to α-mannoside formation, e.g. favourable orbital alignment and favourable dipole interactions. b) The kinetic preference for α-mannoside formation, e.g. neighbouring group participation .....	153
Scheme 5-2. Kahne's sulfoxide glycosylation protocol, where R = a protecting group such as OBn and OR' = the acceptor .....	154
Scheme 5-3. Mechanism of pre-activation and direct activation of mannose donors, where R = the acceptor .....	155
Scheme 5-4. Proposed mechanistic pathways accounting for the selectivity observed in glycosylations of benzylidene mannose donors <sup>334</sup> .....	157
Scheme 5-5. The general method used for mannose based intramolecular aglycon delivery. This process begins by tethering the acceptor to the O-2 position. Once tethered the glycosyl donor is activated, stimulating an intramolecular glycosylation which is followed by hydrolysis.....	158
Scheme 5-6. Reaction pathway for vinyl ether mediated intramolecular aglycon delivery. This pathway proceeds via an acid catalysed tethering mechanism followed by NIS-mediated activation of the glycosyl donor.....	158

## List of schemes

Scheme 5-7. Reaction pathway for temporary silicon tethered mediated intramolecular aglycon delivery. The reaction pathway proceeds with initial formation of the silicon tether at the O-2 position, followed by Tf <sub>2</sub> O mediated activation .....	159
Scheme 5-8. Reaction pathway for intramolecular aglycon delivery mediated by an oxidative tether using O-2-PMB. The pathway follows initial DDQ mediated oxidation, with subsequent glycosyl donor activation resulting in intramolecular glycosylation succeeded by a final work-up to afford the desired β-mannoside .....	159
Scheme 5-9. Depicts the gatekeeper approach to intramolecular aglycan delivery. This method follows the same mechanism as oxidative tethering, however the PMB group is attached to a solid support allowing for easy product purification .....	160
Scheme 5-10. Formation of disaccharide <b>5.21</b> from protected 1,3-mannose donor <b>5.20</b> and protected 1,4-glucosamine acceptor <b>2.3c</b> using Bols and co-workers pre-activation conditions.....	161
Scheme 5-11. Unsuccessful formation of disaccharide <b>5.18</b> from protected mannose donor <b>5.22</b> and protected glucosamine acceptor <b>2.3c</b> using Bols and co-workers conditions.....	162
Scheme 5-12. Formation of glycoside <b>5.23</b> from protected 1,3-mannose donor <b>2.2</b> and propan-2-ol using Crich and co-workers pre-activation conditions .....	162
Scheme 5-13. Formation of glycoside <b>5.23</b> from benzylidene acetal sulfoxide donor <b>5.22</b> and propan-1-ol using Bols and co-workers pre-activation conditions.....	163
Scheme 5-14. Formation of disaccharide <b>5.25</b> from protected 1,3-mannose donor <b>5.22</b> or <b>2.2</b> and 1,2,3,4-di-O-isopropylidene-α-D-galactopyranose <b>5.24</b> using a) Bols and co-workers unsuccessful direct activation conditions and b) Crich and co-workers successful pre-activation conditions .....	164
Scheme 5-15. Formation of disaccharide <b>5.18</b> from protected 1,3-mannose donor <b>2.2</b> and protected 1,4-glucosamine acceptor <b>2.3c</b> using Crich and co-workers pre-activation conditions .....	164
Scheme 5-16. Potential pathways by which NIS and TMSOTf mediated glycosylation occur to give glycoside <b>5.27</b> with complete α-selective.....	165
Scheme 5-17. Formation of glycoside <b>5.29</b> via an NIS and TMSOTf mediated glycosylation of protected 1,2-mannose donor <b>2.1b</b> and propan-2-ol .....	166
Scheme 5-18. Formation of disaccharide <b>5.30</b> via an NIS and TMSOTf mediated glycosylation of protected 1,2-mannose donor <b>2.1b</b> and 1,2,3,4 diisopropylidene galactose <b>5.24</b> .....	166
Scheme 5-19. Oxidation of disaccharide <b>5.18</b> using DDQ to give disaccharide <b>5.13</b> .....	166
Scheme 5-20. Formation of protected trisaccharide <b>5.19</b> via an NIS and TMSOTf mediated glycosylation of protected 1,2-mannose donor <b>2.1b</b> with disaccharide <b>5.31</b> .....	167
Scheme 6-1. Glycosylation mechanism of inverting GHs, proceeding by an S <sub>N</sub> 2-like reaction in which the base carboxyl group deprotonates a nucleophile (HOR'), facilitating nucleophilic attack on the anomeric position. This attack results in the formation of a oxocarbenium ion-like transition state, which collapses to afford a glycoside with inverted stereochemistry to the substrate <sup>353</sup> .....	175
Scheme 6-2. Glycosylation mechanism of retaining GHs, proceeding via a double displacement mechanism with initial displacement of a leaving group at the anomeric position (OR) by the carboxylate group acting as a nucleophile. This attack induces an oxocarbenium ion-like transition state which results in the formation of glycosyl-enzyme intermediate. The second carboxylate group (acid/base catalyst) catalyses the second displacement reaction by deprotonating an incoming nucleophile (HOR'), stimulating the nucleophile to attack the anomeric position. This induces the formation of a second oxocarbenium ion-like transition state which results in formation of a glycoside which has retained stereochemistry <sup>353</sup> .....	176
Scheme 6-3. Example schematic of a potential transglycosidases catalysed reaction .....	176
Scheme 6-4. Schematic of the S <sub>N</sub> i-like mechanism occurring via attack of the nucleophilic acceptor component at the same face as the leaving group, stimulating the formation of transition state, subsequently affording a glycoside <sup>356</sup> R= nucleophile mono or diphosphate.....	177

## List of schemes

Scheme 6-5. Example schematic for a phosphorylase mediated reaction, catalysing either the polymerisation of a sugar-1-phosphate to an acceptor (e.g. oligosacchride unit, monosaccharide sugar unit or aglycon unit) or phosphorolysis of a glycoside bond to afford a sugar-1-phosphate and an acceptor unit.....	178
Scheme 6-6. Proposed mechanistic pathway of MGP .....	179
Scheme 6-7. Schematic of the proposed mechanism of thioglycoligases with initial glycosylation of the donor to the nucleophilic residue (step a) followed by attack of the thiol containing acceptor. Here OR can represent a multitude of motifs, such as a protecting group (i.e. OPNP or OMe) or the continuation of the oligosaccharide chain.....	180
Scheme 7-1. The inhibition assay deigned to investigate the potential ability of the mannose-based inhibitor linked colicin conjugates to prevent adhesion of NU14 to RT4 cells.....	220
Scheme 7-2. An assay designed to monitor the effects of the mannose-based inhibitor linked colicin conjugates on UTI 89 motility .....	221
Scheme 7-3. Reaction scheme for the enzymatic conversion of a) mannose-1-phosphate and unnatural glucosamine acceptor <b>6.2</b> and b) mannose-1-phosphate and O-4-thiol-glucosamine acceptor <b>6.17</b> .....	223
Scheme 8-1. Reaction scheme for ligation of mannose-based inhibitor-linked heterobifunctional linker <b>3.2</b> to colicin Ia .....	271
Scheme 8-2. Reaction scheme for OPAL ligation of active mannose-based inhibitor linked (Gly-Ser) OPAL probe <b>3.18</b> to colicin Ia.....	299
Scheme 8-3. Reaction scheme for OPAL ligation of active mannose-based inhibitor linked (Gly-Ser) OPAL probe <b>3.18</b> to colicin E9.....	300
Scheme 8-4. Reaction scheme for OPAL ligation of active mannose-based inhibitor linked (Gly-Ser) <sub>3</sub> OPAL probe <b>3.17</b> to colicin Ia.....	301
Scheme 8-5. Reaction scheme for OPAL ligation of active mannose based inhibitor (Gly-Ser) <sub>3</sub> OPAL probe <b>3.17</b> to colicin E9 .....	302
Scheme 8-6. Reaction scheme for OPAL ligation of mannose-based inhibitor linked (Gly-Ser) <sub>6</sub> OPAL probe <b>3.19</b> to colicin Ia .....	303
Scheme 8-7. Reaction scheme for OPAL ligation of active mannose-based inhibitor linked (Gly-Ser) <sub>6</sub> OPAL probe <b>3.19</b> to colicin E9.....	304
Scheme 8-8. Reaction scheme for OPAL ligation of biotin linked OPAL probe <b>3.20</b> to colicin Ia .....	305
Scheme 8-9. Reaction scheme for OPAL ligation of biotin-linked (Ser-Gly) <sub>3</sub> OPAL probe <b>3.20</b> to colicin E9 .....	306

## List of tables

Table 1. Depicts the different $\alpha$ -D-mannopyranoside based inhibitors discussed above .....	57
Table 2. Summary of the multivalent heptamannoside structure discussed .....	61
Table 3. Summary of the organic scaffold used in the synthesis of mannose-based glycoclusters .....	63
Table 4. Reagents and reactions conditions trialled for the selective O-4 benzylidene acetal ring opening of 4,6-O-benzylidene acetal-protected glycoside <b>2.47</b> depicted in Scheme 2-15 .....	102
Table 5. Different reagent equivalents and reaction temperatures trialled for the selective O-4 benzylidene acetal ring opening of 4,6-O-benzylidene acetal-protected glycoside <b>2.47</b> depicted in Scheme 2-15 .....	103
Table 6. Different E. coli strains required for the auto-aggregation experiments, each strain's acceptor composition, and whether aggregation would be expected .....	139
Table 7. Results of Experiment One. Which used samples of E. coli grown in either LB or M9 media and incubated in either 2 mL or 1.5 mL samples. OD <sub>600</sub> measurements were recorded post-incubation .....	140
Table 8. Results of Experiment Three, an auto-aggregation assay using positive control samples made from E. coli strains BW25113 and JW3596, incubated at 37 °C with 10 nM biotin linked colicin E9 conjugate and 2 nM NeutrAvidin. This assay was only repeated once, with one active sample and one vortexed control sample made for each condition and one single OD <sub>600</sub> measurement taken of each sample. These measurements were used to calculate percentage auto-aggregation. Note the OD <sub>600</sub> measurements reported here are the values reported post dilution factor adjustment.....	143
Table 9. Results of Experiment Four, a second auto-aggregation assay performed on positive control samples of BW25113 with a higher starting OD <sub>600</sub> value of 6. ....	145
<b>Table 10.</b> Results of Experiment Five, an auto-aggregation assay performed on samples of BW25113 incubated with varying concentrations of each Mannose-based inhibitor linked (Gly-Ser) <sub>n</sub> colicin E9 conjugate. OD <sub>600</sub> measurements were made post sample incubation and were used to calculate percentage auto-aggregation. ....	147
Table 11. The various glycosylation conditions trialled in the synthesis of the $\alpha$ -linked disaccharide <b>5.30</b> and the results of these trial reactions.....	169
Table 12. The results of the various trial glycosylation performed to investigate the effects of donor protection on glycosylation yield.....	171
Table 13. The results of the various trial glycosylation performed using 1,2:5,6-di-O-isopropylidene- $\alpha$ -D-glucofuranose <b>5.39</b> as the acceptor.....	173
Table 14. BT-1033 reaction Entries 1-5; including starting reaction volume, starting donor and acceptor concentration, concentration of BT-1033, incubation time and whether LCMS suggested conversion had occurred .....	183
Table 15. BT-1033 reaction Entries 6-16; including starting reaction volume, starting donor and acceptor concentration, concentration of BT-1033, incubation time and whether LCMS analysis suggested conversion had occurred .....	185
Table 16. BT-1033 reaction Entries 2-16 conversion rate percentages calculated using an ITag reaction .....	189
Table 17. BT-1033 catalysed reaction Entries 17-28a; including starting reaction volume, starting donor and acceptor concentration, concentration of BT-1033, incubation time and whether conversion was suggested in the initial LCMS trace, and the conversion rate (%) measured using an ITag reaction. Reaction repeats are labelled "a" and "b." .....	192
Table 18. BT-1033 catalysed reaction Entries 28b, 29a and 29b; including starting reaction volume, starting donor and acceptor concentration, concentration of BT-1033, incubation time and whether	

## List of tables

conversion was suggested in the initial LCMS trace, and the conversion rate (%) measured using an ITag reaction. Reaction repeats are labelled “a” and “b.” .....	196
Table 19. BT-1033 catalysed reaction Entries 21b, 30a, 30b, 22b, 31a and 31b; including starting reaction volume, starting donor and acceptor concentration, concentration of BT-1033, incubation time and whether conversion was suggested in the initial LCMS trace, and the conversion rate (%) measured using an ITag reaction. Reaction repeats are labelled “a” and “b.” .....	198
Table 20. BT-1033 catalysed reaction Entries 23b, 32a, 32b, 24a, 33a and 33b; including starting reaction volume, starting donor and acceptor concentration, concentration of BT-1033, incubation time and whether conversion was suggested in the initial LCMS trace, and the conversion rate (%) measured using an ITag reaction. Reaction repeats are labelled “a” and “b.” .....	201
Table 21. BT-1033 catalysed reaction Entries 25b, 34a, 34b, 26b, 35a, 35b, 27b, 36a and 36b; including starting reaction volume, starting donor and acceptor concentration, concentration of BT-1033, incubation time and whether conversion was suggested in the initial LCMS trace, and the conversion rate (%) measured using an ITag reaction. Reaction repeats are labelled “a” and “b.” ..	204
Table 22. BT-1033 catalysed reaction Entries 37a, 37b, 38a, 38b, 39a, 39b, 40a, 40b, 41a, 41b, 42a and 42b; including starting reaction volume, starting donor and acceptor concentration, concentration of BT-1033, incubation time and whether conversion was suggested in the initial LCMS trace, and the conversion rate (%) measured using an ITag reaction. Reaction repeats are labelled “a” and “b.” .....	207
Table 23. BT-1033 catalysed reaction Entries 29 scale up and 34 scale up; including starting reaction volume, starting donor and acceptor concentration, concentration of BT-1033, incubation time and whether conversion was suggested in the initial LCMS trace, and the conversion rate (%) measured using an ITag reaction. Reaction repeats are labelled “a” and “b.” .....	211
Table 24. BT-1033 catalysed reaction Entries 43a, 43b, 44a, 44b, 45a, 45b; including starting reaction volume, starting donor and acceptor concentration, concentration of BT-1033, incubation time and whether conversion was suggested in the initial LCMS trace, and the conversion rate (%) measured using an ITag reaction. Reaction repeats are labelled “a” and “b.” .....	217
Table 25. The composition of the SDS-PAGE gels of varying acrylamide percentages. The resolving buffer is (1.5 M Tris-HCL, 0.4% SDS, pH 8.8). TEMED stands for Tetramethylethylenediamine. ....	226
Table 26. The compositions of the stacking gel used during SDS-PAGE. Stacking buffer is (0.5 M Tris-HCl, 0.4% SDS, pH 6.8) .....	226
Table 27. Information about the specific conditions used in Experiments 2-5, all of which were performed using the redesigned auto-aggregation assay methodology .....	cccix
Table 28. Provides information about the specific conditions used in Experiments 6-8 .....	310
Table 29. The reaction equivalents of each reagent used during each of the ITag reactions .....	338
Table 30. The concentrations of BT-1033 used to set up each crystal tray.....	341
Table 31. The primers designed for use in Quikchange™ Site-Directed Mutagenesis.....	342
Table 32. PCR reaction composition for Quikchange™ Site-Directed Mutagenesis .....	343
Table 33. The PCR reaction stages and conditions used during Quikchange™ Site-Directed Mutagenesis.....	343
Table 34. Shows the volumes in µL of the supplements required to prepare a 15 mL culture of supplemented M9 media.....	cvi
Table 35. Shows the antibiotic concentrations required for growth of each different E. coli strain ...	cvi
Table 36. Shows the results of the auto-aggregation assay designed to investigate the effects of growth media and samples size on auto-aggregation. The assay was performed using the initial auto-aggregation methodology as explained on page 307. Three repeat assays were performed on three different days, each sample was made in triplicate and each final OD <sub>600</sub> measurement was repeated three times, with the average measurement given in the table below. Note the OD <sub>600</sub> values reported	

## List of tables

in Table 36 are the values recorded post dilution factor adjustment and have been rounded to 2 decimal places.....	cvii
Table 37. Results of the auto-aggregation assay used to screen potential aggregation factors such as starting OD <sub>600</sub> , incubation time and incubation temperature. Three repeat assays were performed on three different days. One active sample and one vortexed control sample was made for each condition and a single final OD <sub>600</sub> measurement was made for both the active sample and the vortexed control sample, these values were adjusted for by the dilution factor and used to calculate percentage auto-aggregation using equation one. The three percentage auto-aggregation measurements collected for each sample was then averaged. Note the OD <sub>600</sub> values reported in Table 37 are the values recorded post dilution factor adjustment and the values have been rounded to 2 decimal places .....	cix
Table 38. The relative intensities of the ITag reagent <b>6.16</b> clicked acceptor and disaccharide peaks in each sample. These results have been used to calculate the total peak contribution of the ITag reagent <b>6.16</b> clicked acceptor and disaccharide peaks in each sample. Furthermore, this value can be used to find the percentage contribution of the disaccharide peak and thus the conversion rate of each reaction .....	ccxxxv
Table 39. Results of the two IPAP HSQC (13C HSQC with multiplicity editing) spectra for the two anomeric carbons and analysis of the results to give the <sup>1</sup> J <sub>CH</sub> coupling constants.....	ccxli



### Acknowledgements

I would like to thank all three of my supervisors, Dr Martin Fascione, Dr Christoph Baumann and Dr Laurence Wilson, for their support and guidance throughout this process. I would especially like to thank Dr Martin Fascione for providing me with the opportunity to acquire the biological skills I enjoyed learning so much throughout my time in the laboratory. I would also like to thank past and present members of the chemical biology group, especially Julia Walton, Tessa, Emily, Alexandra and Nick for answering my very basic biology questions. I would also like to thank Darshita and Katie, who share the challenges of carbohydrate synthesis with me and provide a sympathetic ear when yet again something has gone wrong!

A special thanks also goes to the collaborators I have had the privilege of working with; the Miller group (University of Keele), the Linclau group (University of Southampton) and the Galan group (University of Bristol). A further thanks goes to the technical staff in the Department of Chemistry; Dr Ed Bergström and Karl Heaton (mass spectrometry), Dr Alex Heyman and Heather Fish (NMR spectrometry) and Sam Hart (protein crystallography). I would also like to thank the Engineering and Physical Sciences Research Council (1944882) for research funding.

I would like to thank my family for their support throughout this process. Finally, I would like to thank Nick again for his continued encouragement and support.

## Declaration

### Declaration

I, Natasha Emily Hatton, declare that this thesis is a presentation of original work and I am the sole author. This work has not previously been presented for an award at this, or any other, University.

All sources are acknowledged as References. Contributions to this work by other researchers are indicated either when relevant figures are discussed or in the relevant experimental section.

Chapter 1- contains contence from the publication

Hatton, Natasha E., Baumann, Christoph G., Fascione, Martin Anthony, Developments in mannose-based treatments for Uropathogenic Escherichia coli induced urinary tract infections, ChemBioChem, 22, 613-629, doi: 10.1002/cbic.202000406 (2021).

I, Natasha Emily Hatton, am the first author of this above publication, and prepared the majority of the manuscript. A list of acknowlagments is available for this article.

## Chapter 1 Introduction

### 1.1 Section A

#### 1.1.1 Structure of the urinary tract, urothelium and uroplakins

The primary function of the urinary tract is to collect, transport, store and remove urine from the body, eliminating toxic waste products and metabolites generated by the kidneys.<sup>1</sup> The urinary tract can be anatomically categorized into two sub-sections: the upper urinary tract (e.g. the kidneys and the ureters)<sup>2</sup> and the lower urinary tract (e.g. the bladder and the urethra) (Figure 1-1).<sup>2</sup> The surface of the urinary tract is lined with a specialized epithelium known as urothelium.<sup>1</sup> The biochemical and morphological features of the urothelium vary depending on its location within the urinary tract.<sup>1</sup>

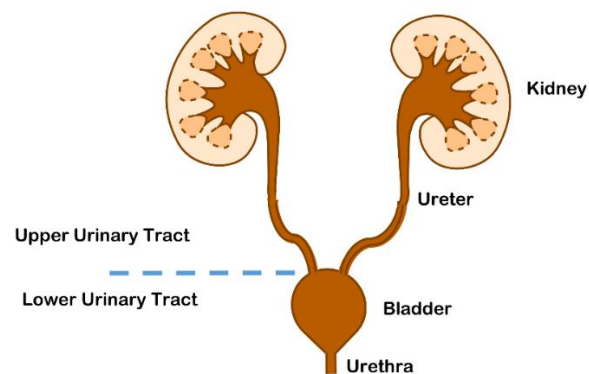


Figure 1-1. Structure of the urinary tract consisting of the upper urinary tract e.g. the kidneys and ureters and the lower urinary tract e.g. the bladder and the urethra

Generally, the urothelium is composed of three different layers; a basal cell layer attached to the basement membrane, an intermediate layer and an apical layer consisting of large hexagonal cells known as umbrella cells (Figure 1-2a).<sup>3</sup> Umbrella cells are multinucleated, highly differentiated and accumulate a large amount of uroplakin proteins on their surface. This accumulation leads to the forming of a two-dimensional plaque,<sup>1,4,5</sup> which acts as a barrier to water and other toxic materials in the urine.<sup>6</sup> In humans there are four different uroplakins (UP) proteins: UPIa, UPIb, UPII and UPIII.<sup>7</sup> These units come together to form a heterodimer (Figure 1-2b) with six of these heterodimers combining to form the uroplakin plaque (Figure 1-2c).<sup>3</sup> UPIa and UPIb belong to the tetraspanin family,<sup>3</sup> consisting structurally of four rod-like transmembrane domains. The first and second transmembrane domains are connected through a small extracellular loop, with a second large extracellular loop connecting the third and fourth transmembrane domains. The main difference between the two uroplakins is UPIa contains a high mannose glycan attached to the second extracellular domain at residue Asn169 (Figure 1-2d). In comparison, UPIb contains a tetraantennary fucosylated complex glycan attached to the second extracellular domain at the Asn131 residue (Figure 1-2e).<sup>3</sup> UPII and UPIIIa are each structurally composed of a single transmembrane domain.

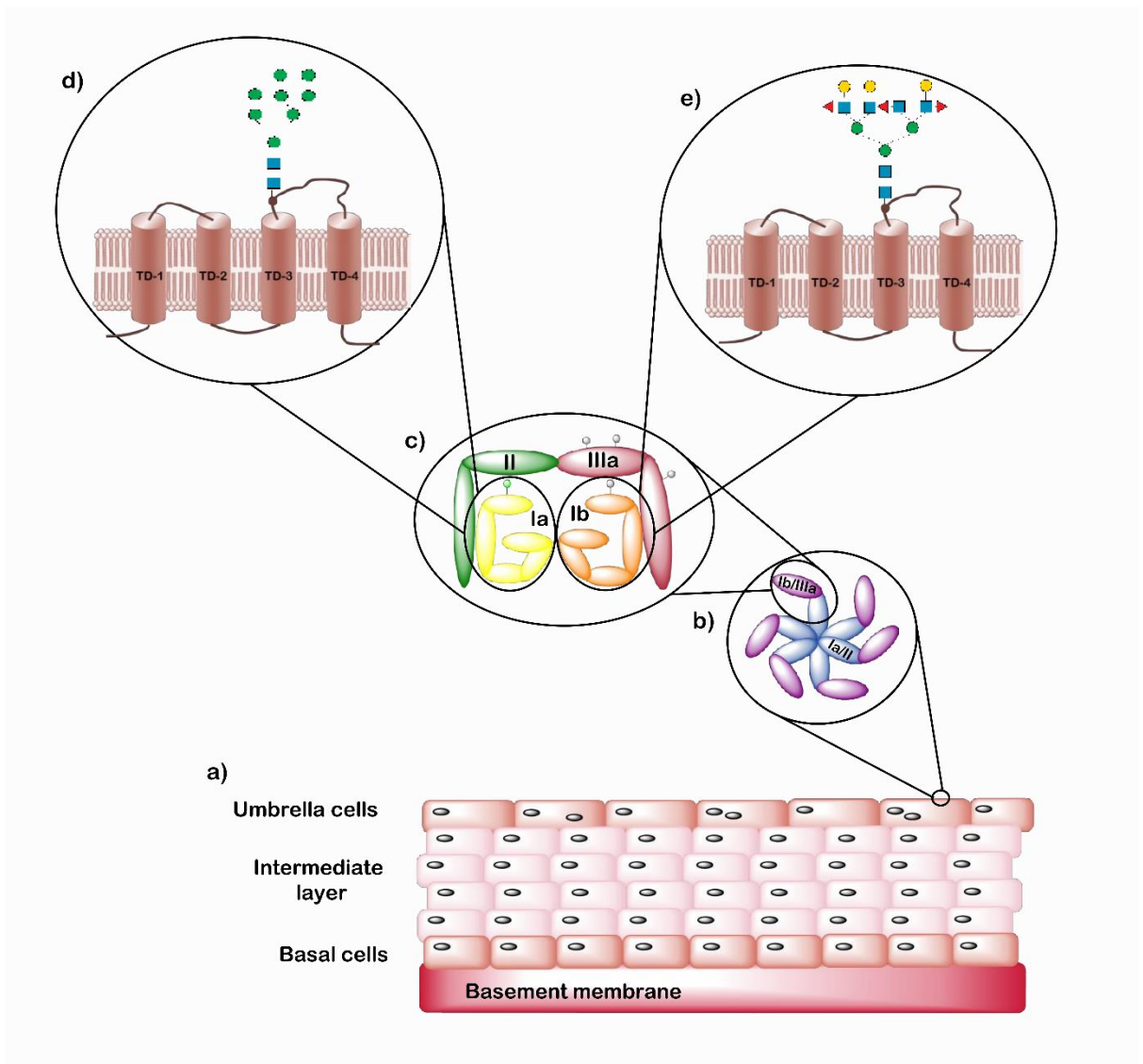


Figure 1-2. **a)** Structure of the urothelium with basal cells attached to a basement membrane, an intermediate layer and a layer of umbrella cells. **b)** Structure of the uroplakin plaque consisting of six heterodimeric units with each unit composed of two dimers UPIa/II and UPIb/IIIa. **c)** Structure of the heterodimer units where the green ellipse represents a high mannose containing N-glycan and the grey ellipses represent complex N-glycans. **d)** Structure of uroplakin Ia and **e)** structure of uroplakin Ib. Both structures consist of four transmembrane domains and have an approximate molecular weight of 30 kDa.<sup>8,9</sup> The green ellipses represent mannose residues, the blue squares represent glucosamine residues and the yellow ellipses represent galactose residues

### 1.1.2 Urinary tract infections

Urinary tract infections (UTIs) is the third most common type of infection experienced by humans after respiratory and gastro-intestinal infections.<sup>10</sup> Most UTI cases affect the lower urinary tract<sup>11</sup> and can be either symptomatic or asymptomatic,<sup>12</sup> with symptoms including increased urination frequency, pain during urination and blood in the urine.<sup>13</sup> If left untreated UTIs can result in kidney damage, allowing bacteria to enter the blood stream resulting in urosepsis. Urosepsis accounts for 5-7% of severe sepsis cases reported, with a mortality rate of between 25% and 60%.<sup>14</sup>

## Introduction

Women are significantly more likely to experience a UTI than men<sup>15</sup> due to the female urethrae being significantly shorter than a males (4 cm vs 20 cm).<sup>16</sup> Approximately 40-50% of women will experience a symptomatic UTI within their lifetime, with over half of these women suffering a relapse within six months.<sup>17</sup> Age is another well-recognized risk factor, with UTIs being the second most common form of infection in the non-institutionalized elderly population, accounting for 25% of infection cases.<sup>15</sup> Due to their weakened immune systems approximately 10% of males and 20% of females over the age of 80 suffer from an asymptomatic UTI.<sup>18</sup> Other risk factors for UTIs include urinary catheterization and diabetes.<sup>19</sup>

UTIs are caused by the invasion of foreign pathogens, with *Uropathogenic Escherichia coli* (UPEC) (Figure 1-3) being responsible for 80% of cases. *Staphylococcus saprophytics* accounts for a further 10-15%, and the remaining cases are caused by *Klebsiella*, *Enterobacter*, and *Proteus* species.<sup>20</sup> UTIs can be classed as uncomplicated or complicated. For a UTI to be classed as complicated the patient must also suffer from either an underlying illness such as diabetes, a structural malformation of the urinary tract, or an obstruction of urine flow.<sup>21</sup> Complicated UTIs are generally more difficult to treat,<sup>20</sup> meaning the infections are often chronic with several different Gram-positive and Gram-negative bacteria present.

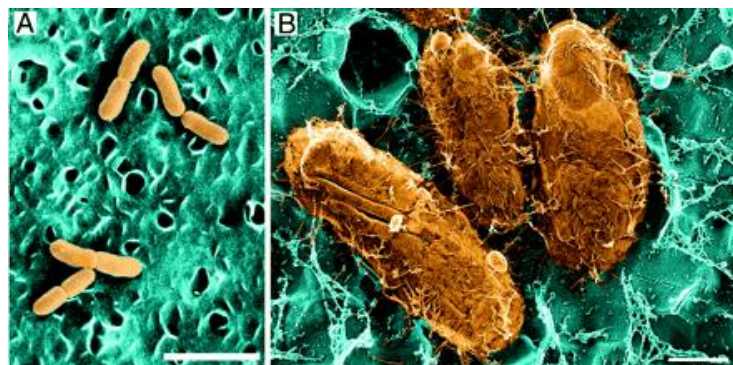


Figure 1-3. Electron microscopy images of UPEC adhered to the urinary epithelial cell surface.<sup>22</sup> [Bars = 3  $\mu$ M (A) and 0.5  $\mu$ M (B)]

Currently UTIs are treated with a course of antibiotic such as Nitrofurantoin or Trimethoprim.<sup>18</sup> However, an increasing problem observed in the treatment of UTIs is antibiotic resistance - studies demonstrate UPEC strains contain over 30 different resistance genes to trimethoprim, with clinical resistance occurring in 16.7% of cases.<sup>23</sup> Nitrofurantoin is still active against *E. coli*, with fewer cases of resistance being reported than with Trimethoprim. However, Nitrofurantoin has a higher incidence of significant side effects like pulmonary fibrosis,<sup>24</sup> and it is predicted that resistance to both antibiotics will increase. The enduring challenge of antibiotic resistance means that researching new effective treatments for UPEC-induced UTIs is a clinical priority.<sup>23</sup>

### 1.1.3 Uropathogenic *Escherichia coli* pathogenesis pathway

UPEC is responsible for the majority of reported uncomplicated UTI cases,<sup>17</sup> thus identifying new targets within UPEC could serve as the basis for developing new treatments for both acute and recurrent UTIs.

The six stages of UPEC pathogenesis are summarized in Figure 1-4.<sup>25</sup> The bacteria initially colonize the periurethral areas and the urethra, travelling up the urethra while growing as planktonic cells in the urine. While in the urinary tract, UPEC interacts with and adheres to the urothelium. Once adhered, UPEC grows on the surface of the umbrella cells of the urothelium forming a biofilm, facilitating invasion of the epithelial cells. Once within the umbrella cells UPEC can begin replicating, forming an intracellular bacterial population (IBC); this allows for further formation of a quiescent intracellular reservoir (QIR).<sup>26</sup> UPEC can then invade the intermediate layers of the urothelium and lay dormant. These bacteria are protected from antibiotic treatment, making them extremely difficult to eliminate and thus the source of many recurrent infections.<sup>27</sup> If untreated, UPEC will continue to colonize up the urinary tract, progressing to the kidneys.<sup>26</sup> This colonization can result in kidney tissue damage and provides UPEC access to the blood stream, resulting in urosepsis.

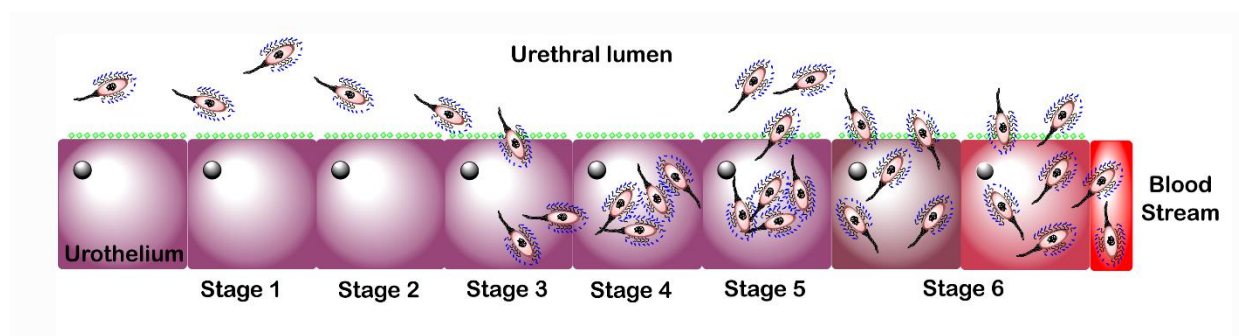


Figure 1-4. The pathogenesis cycle for UPEC consists of five stages: stage 1) colonization of the periurethral areas and the urethra, stage 2) movement of UPEC up the urethra, stage 3) UPEC adherence, stage 4) biofilm formation, stage 5) epithelial cell invasion and formation of intracellular bacterial population, and stage 6) colonization of the urinary tract and kidneys by UPEC followed by entry into the blood stream

Invasion of the urothelium by UPEC occurs via a membrane zippering mechanism.<sup>28, 29</sup> This mechanism is stimulated by UPEC binding to the urothelium, which activates a complex signalling cascade, resulting in localized rearrangement of the urothelium actin cytoskeleton.<sup>29</sup> The cytoskeleton rearrangement leads to the envelopment and internalization of the bound UPEC (Figure 1-5). This complex signalling cascade has been shown to be reliant on many factors, such as focal adhesions; e.g. Src,<sup>30</sup> phosphoinositide 3-kinase,<sup>29</sup> Rho-family GTPases; actin bundling and adaptor proteins, e.g.  $\alpha$ -actinin and vinculin,<sup>29, 31</sup> lipid raft components, e.g. caveolin-1,<sup>32</sup> and microtubules. Treatment of a host cell with a microtubule-disrupting agent, such as nocodazole or vinblastine, has been shown to inhibit host cell invasion by UPEC.<sup>33</sup>

## Introduction

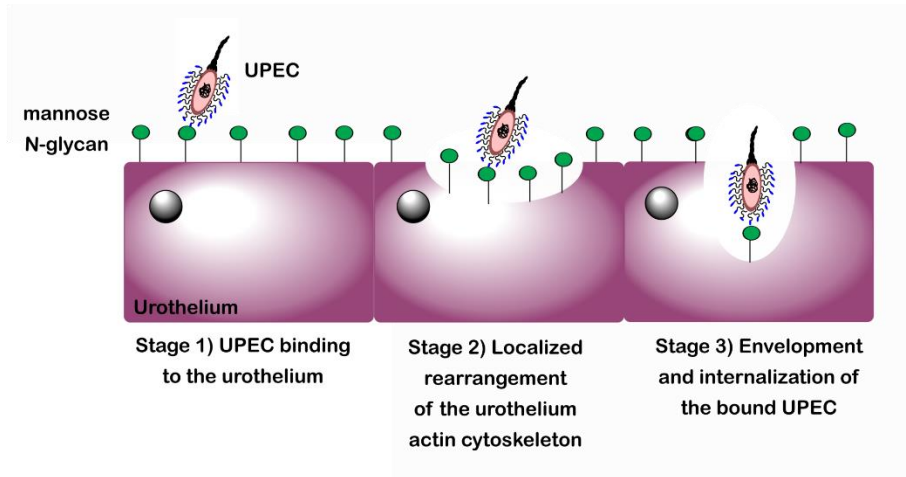


Figure 1-5. Schematic diagram showing the three-stage membrane zippering mechanism thought to be used by UPEC during the invasion of the urothelium; **stage 1**) binding of UPEC to the urothelium, **stage 2**) localized rearrangement of the urothelium actin cytoskeleton, **stage 3**) envelopment and internalization of the bound UPEC

Adhesion of UPEC to the urothelium is mediated by UPEC binding to terminal D-mannose units on UPIa. Without adhesion to the sugar UPEC would remain free in the urine and be removed from the bladder during urination, preventing the initial UPEC infection from progressing into a symptomatic UTI. To bind to terminal mannose units UPEC expresses multiple 3-micron long rod-like structures on their surface known as type 1 pili (Figure 1-6).<sup>34</sup> The type 1 pilus consists of multiple different subunits, including repeating units of the FimA protein, which form a 7 nm-thick right-handed helical rod. This rod is joined to a 3 nm-thick distal tip fibrillum, which itself is composed of three further subunits: two adapter proteins; FimF and FimG; and an adhesion protein, FimH.<sup>34</sup>

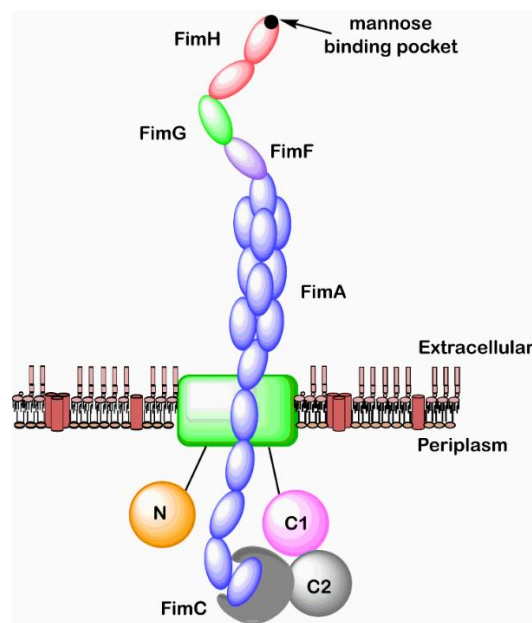


Figure 1-6. Structural organisation of the type 1 pilus which includes the following subunits: FimA (blue), FimC (gray), FimD (green rectangle), FimF (purple), FimG (green oval), and FimH (red). The position of the N-terminal domain (N, orange) and two C-terminal domains (C1, pink circle; C2, gray circle) relative to the transmembrane pore (green rectangle) in FimD are also indicated

## Introduction

The exact process by which the type 1 pilus adheres to the urinary tract was unknown for a long time. One of the original theories proposed was that adhesion was mediated by the repeating FimA units which comprised most of the type one pilus.<sup>35</sup> However, it is now recognized that the role of the repeating FimA units is to provide a structural scaffold.<sup>36</sup> A wealth of research conducted in the late 1980s discovered that the minor subunits, FimF, FimG and FimH, were involved in adhesion.<sup>37,38</sup> Christiansen and co-workers found that recombinant bacteria lacking either all three subunits or just FimH displayed no ability to bind to erythrocytes, indicating that FimH plays a critical role in adhesion.<sup>39</sup> Klemm and co-workers<sup>40</sup> confirmed this observation, providing direct evidence that FimH is responsible for mannose-mediated adhesion.<sup>40</sup>

### 1.1.4 FimH structure and catch bond mechanism

FimH is comprised of two domains (Figure 1-7). The first is a C-terminal pilin domain (FimH<sub>PD</sub>), which attaches FimH to the pilus rod<sup>41</sup> through the neighbouring subunit FimG. This attachment occurs by donor strand complementation,<sup>42</sup> and is an effective way of providing strong inter-molecular linkages through the donation of one  $\beta$ -strand from one subunit (e.g. FimG) into the  $\beta$ -sandwich of the neighbouring subunit (e.g. FimH<sub>P</sub>).<sup>43</sup> The second FimH domain is the N-terminal lectin domain (FimH<sub>LD</sub>), which contains a mannose-binding pocket<sup>41</sup> which can bind to mannose sugars on the urothelium, mediating adhesion of UPEC to the urinary tract.<sup>34</sup>

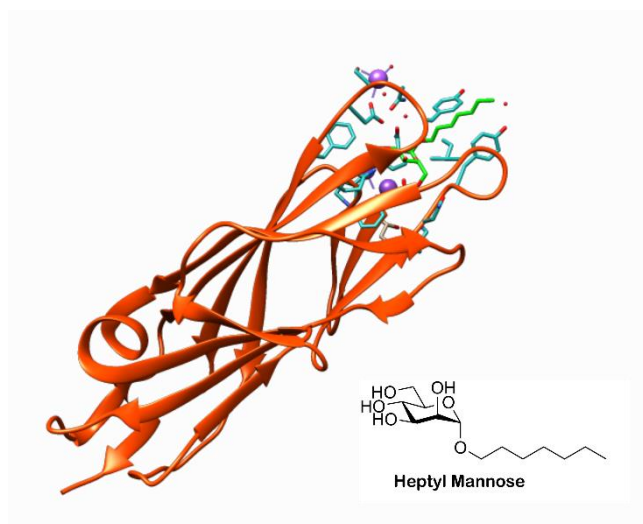


Figure 1-7. Crystal structure of FimH (red) with a heptylmannoside (green) ligand bound in the N-terminal lectin domain (FimH<sub>LD</sub>) (PDB ID 4LOV).<sup>44</sup> Residues with side chains shown as sticks (blue) are involved in non-covalent interactions with heptylmannoside, sodium ions (purple spheres) or water molecules (red spheres). The dashed lines (purple) denote short-range, non-covalent interactions



## Introduction

The two-domain structure of FimH allows the type-1 pilus to form a catch-bond when bound.<sup>42</sup> A catch-bond is a type of non-covalent interaction in which the dissociation lifetime of the bond increases when force is applied<sup>45</sup> (Figure 1-8). Wirtz and co-workers provided the first unequivocal evidence for the existence of catch-bonds.<sup>46</sup> Prior to this, catch-bonds were treated as one potential explanation for why the adhesion affinity of some bacteria (e.g. UPEC) increases in moderate shear flow. An alternative theory was the transport limiting binding model. This model, which has fallen out of favour, suggests that increased shear flow causes an increase in both dissociation and association rates, thus an enhancement in bacterial adhesion would have to be caused by an increase in bacterial association not a decrease in bacterial dissociation.<sup>47, 48</sup>

The catch-bond in FimH is biphasic, meaning under moderate force (such as that experienced by the sides of the urinary tract during urination) FimH binds to ligands with higher affinity, whereas exposure to higher shear flow leads to a decrease in binding affinity due to an increase in the dissociation rate for the FimH-ligand interaction.<sup>45</sup> Moderate mechanical force induces the separation of the FimH<sub>LD</sub> and FimH<sub>P</sub> subunits (Figure 1-8). This separation switches the lectin domain from a low affinity state to a high affinity state<sup>49, 50</sup> reducing the rate of spontaneous ligand release, resulting in a 1000-fold higher affinity of FimH for mannose sugars under moderate flow conditions compared with static conditions.<sup>42</sup> The relatively weaker affinity of FimH under static conditions favours invasion of UPEC along the urinary tract during static conditions, while the high affinity of FimH under moderate flow conditions enables UPEC to be retained in the urinary tract during urination. Glockshuber and co-workers<sup>42</sup> investigated how the different flow conformation states affect the binding of FimH to *N*-glycans. A mixture of synthetic  $\alpha$ -linked mono- and dimannosides were used to represent the natural terminal  $\alpha$ -D-mannoside moieties present on FimH targeted glycoproteins in the bladder.<sup>42</sup> Using these ligands, kinetic and structural characterization of the binding properties of FimH under both static and flow conditions could be investigated. It was demonstrated that the increased affinity of FimH under flow conditions compared to static conditions was ligand independent.<sup>42</sup> Glockshuber and co-workers further found that dimannosides bound with higher affinity compared to monosaccharides, with the difference in affinity determined by the rate of spontaneous ligand dissociation.<sup>42</sup> Under static conditions FimH binds to all natural terminal  $\alpha$ -D-mannoside structures with medium affinity, while under flow conditions FimH binds to all D-mannosides at a 2000-fold higher affinity with a 70,000-fold decrease in ligand dissociation rate and a 30-fold increase in ligand association rate.<sup>42</sup> Glockshuber and co-workers additionally found that even though FimH favours monovalent *N*-glycan binding when *N*-glycans are in short supply, each *N*-glycan can bind up to three FimH units at once.<sup>42</sup>

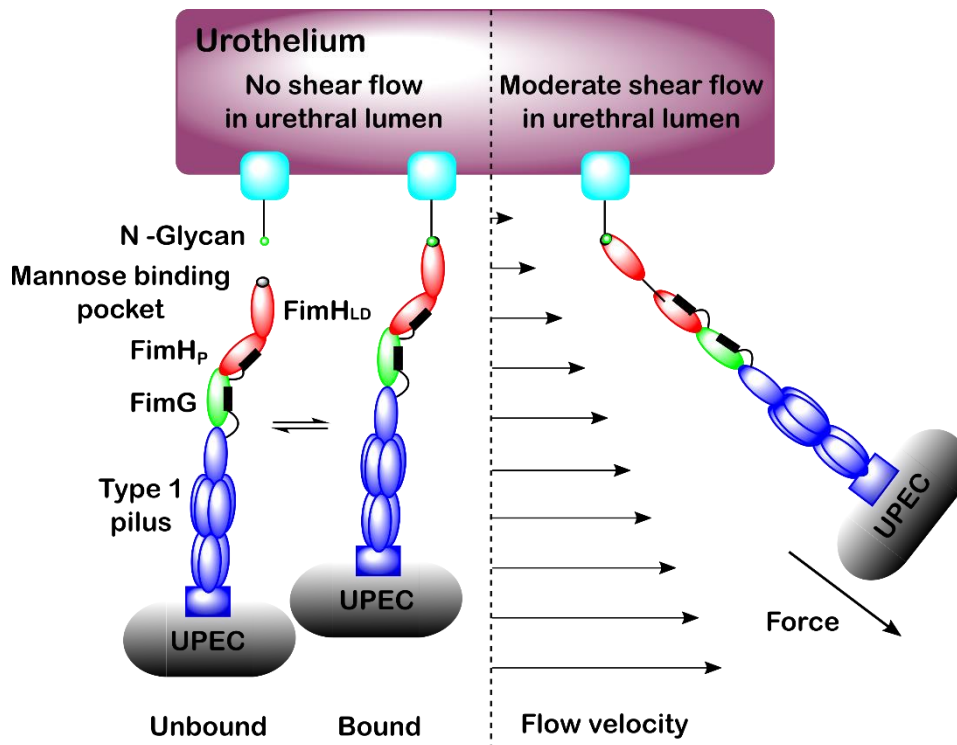


Figure 1-8. Catch bond mechanism for FimH binding to mannose in urethral lumen during a) no shear flow conditions where unbound and bound forms exist at equilibrium, and b) moderate shear flow conditions where the bound state is favoured. Under moderate shear flow conditions, the hydrodynamic drag on the micron-sized UPEC bacterium (not to scale) results in a physical force on the tether which activates the catch bond mechanism in FimH. The higher affinity binding to mannose under these conditions prevents the UPEC bacterium from being flushed out of the urinary tract during urination

### 1.1.5 FimH binding pocket

The FimH lectin domain contains 157 amino acids, which assemble to form an 11-stranded  $\beta$ -barrel structure.<sup>41</sup> Encompassed within the  $\beta$ -barrel structure is a polar binding pocket<sup>42</sup> (residues Asn46, Asp47, Asp54, Gln133, Asn135 and Asp140) to which terminal mannose units can engage in a complex network of hydrogen bonding and electrostatic interactions.<sup>41</sup> The polar binding pocket is surrounded by a hydrophobic region, (residues Phe1, Ile13 and Phe142)<sup>41</sup> which contains a tyrosine gate (residues Tyr48, Ile52, Thr51 and Tyr137).<sup>41</sup> This region provides support for the binding site through electrostatic interactions with the tyrosine gate, which is shown to be influential in the ability of ligands to enter the binding site.<sup>51</sup> Further interactive features of the FimH lectin domain are a small hydrophobic pocket<sup>52</sup> adjacent to the sugar binding pocket (residues Ile52, Tyr137 and Asn138),<sup>41</sup> a salt bridge (residues Arg98-Glu50) which facilitates further hydrogen bonding,<sup>52</sup> and the Tyr48 and Tyr137 residues, which partake in hydrophobic and ring stacking interactions<sup>52, 53</sup> as well as forming direct and water-mediated hydrogen bonds to ligands.<sup>53</sup> A summary of the main interactions that occur between the FimH lectin domain and mannose-based pentasaccharide **1.1** is presented in Figure 1-9.

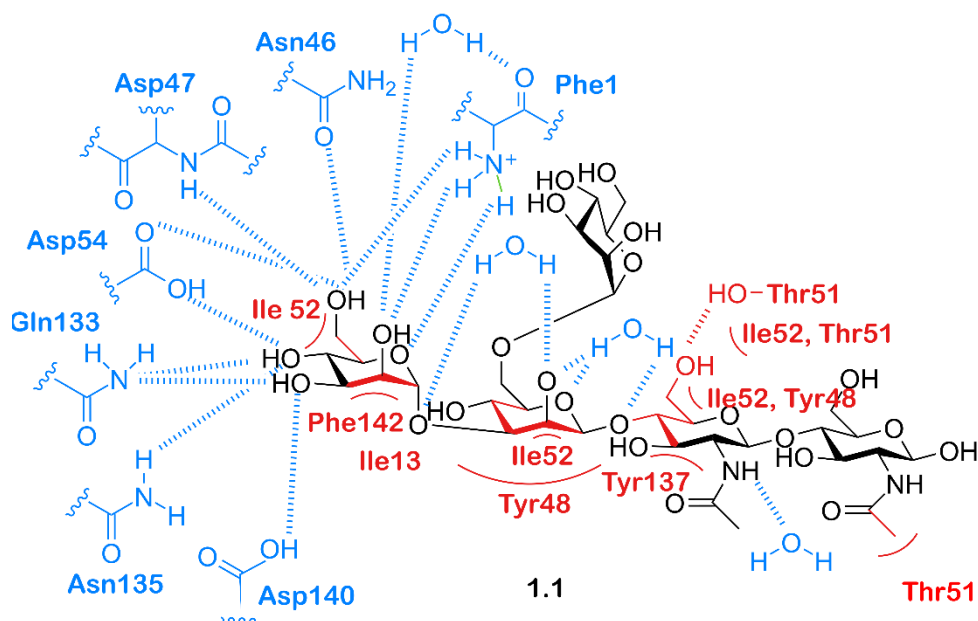


Figure 1-9. A depiction of the majority of interactions that occur between mannose based pentasaccharide **1.1** and the extended FimH binding site.<sup>51</sup> Red indicates interactions mediated by Van der Waals, aromatic stacking and hydrophobic interactions, blue indicates interactions mediated by hydrogen bonding

As depicted in Figure 1-9, the binding of a mannose-based ligand to the extended FimH binding site is the result of a complex network of interactions and hydrogen bonding. As such, small changes to the structure of the ligand can disrupt this binding network, resulting in either a decrease or complete loss of ligand affinity. Epimers of mannose (e.g. glucose and galactose) exhibit no inhibitory effects on FimH,<sup>41, 54, 55</sup> due to the lack of an axial C-2 hydroxyl group preventing them from partaking in critical interactions with the polar binding pocket. The five-membered sugar fructose, which like mannose contains an axial C-2 hydroxyl group, has been shown to have weak activity for FimH.<sup>54 41, 55</sup> A further stereochemical requirement exhibited by the FimH lectin domain is that the terminal mannose unit must be in the alpha orientation.<sup>56</sup> Terminal  $\alpha$ -mannosides can engage in water-mediated hydrogen bonding within the FimH lectin domain;<sup>41</sup> these interactions would not be possible if the mannoside was in the  $\beta$ -configuration.

A further characteristic of the extended FimH binding site that facilitates critical interactions with ligands are its hydrophobic residues. These residues surround the mannose binding pocket and consists of the hydrophobic support and tyrosine gate residues as well as residue Thr51, which extends out of the hydrophobic ridge along a hydrophobic groove.<sup>41</sup> Unlike the polar binding pocket, the tyrosine gate structure is flexible, interacting with ligands by a mixture of  $\pi$ -stacking and van der Waals interactions.<sup>41</sup> The flexibility of the tyrosine gate is the result of the Tyr48 residue being able to rotate, allowing for three different tyrosine gate conformations; open, closed and half open.<sup>57</sup> In its unbound resting state FimH adopts an open conformation; here the side chain of the Tyr48 residue is positioned

## Introduction

inwards facing residues Asp47 and Arg98 (Figure 1-10a).<sup>57</sup> In the closed gate conformation the Tyr48 residue shifts alignment towards the Thr51 residue (Figure 1-10b).<sup>58</sup> If the side chain of the Tyr48 residue is aligned somewhere between the open and closed position, then the gate is classified as half open.<sup>57</sup> When bound to a ligand the tyrosine gate can either remain in its open conformation or shift to the half open or closed conformation.<sup>57</sup> A conformational change often accompanies ligand binding in order to minimize Gibbs free energy, thus different ligands will bind to different conformational states.<sup>57, 58</sup> When a ligand is flexible and can extend out of the binding site like some oligomannosides,<sup>51</sup> the open conformation is adopted as this allows the second mannose residue in the oligosaccharide to interact with the Tyr48 residue of the binding site.<sup>52</sup> When a ligand contains a sterically rigid aglycone group (e.g. 1,4-biaryl group) the tyrosine gate will shift to the closed conformation, positioning the aglycone residue outside of the tyrosine gate. This conformational shift is favoured by the formation of strong  $\pi$ -stacking interactions between the aglycon and the outer side of the aromatic ring on the Tyr48 residue.<sup>52, 59</sup>

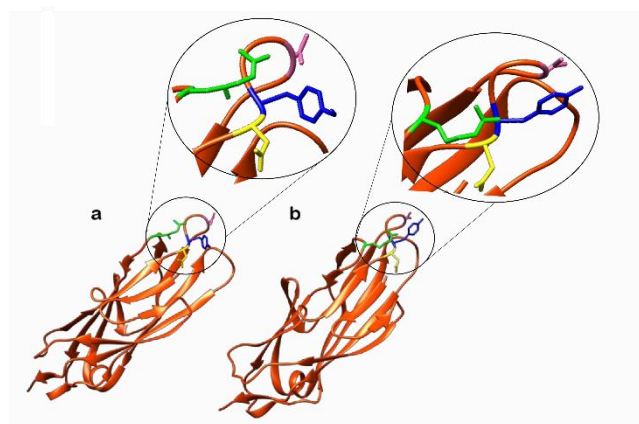


*Figure 1-10. a) Structure of FimH lectin domain when the tyrosine gate is open PDB 4AV0<sup>57</sup> b) Structure of the FimH lectin domain when the tyrosine gate is closed PDB 4ATT<sup>58</sup>. Note the movement of the Tyr48 residue (blue) from facing the Asp47 residue (yellow) in the open conformer to facing the Thr51 residue (pink) in the closed conformer. The Arg98 residue (green) plays a role in stabilizing the surface loop conformation on which the Thr51 residue is located*

### 1.1.6 Vaccines against targeting UTIs

Due to the prevalence of UTI cases and increasing resistance rates to current treatments, a wealth of research has been performed into both preventative and curative strategies to treat UTIs.

Preventative treatments have focused on the development of a vaccine. However, the development of a UTI targeting vaccine poses many challenges and many factors have to be taken into consideration. One major consideration is the high natural UTI recurrence rate, which suggests the immune systems of many patients are unable to mount an effective enough immune response to prevent secondary infections. The lack of a strong immune response could be the result of uropathogens being able to mask themselves and suppress the immune system.<sup>60</sup> This raises the argument to whether a vaccine would be able to activate the immune system to the extent needed to elicit immunity. A further consideration is that the process by which protective immunity occurs in the urinary tract is not well understood; as such designing a vaccine that targets this process is difficult. In addition, UPEC populations display high levels of diversity, making deciding on a target antigen challenging.<sup>60</sup>

Vaccines can generally be grouped into two broad categories: whole agent / whole cell vaccines and specific-antigen vaccines. Whole cell vaccines use either the whole microorganism in a weakened or inactive form or use a lysate of the microorganism, whereas specific-antigen vaccines include one or more antigen subunit. The majority of current vaccines licenced in the US target viruses (16 virus targeting vaccines vs 8 bacteria targeting vaccines)<sup>60</sup> with most using whole cell targeting. Many vaccines which bacteria opt for a specific-antigen approach due to safety considerations. There are currently three bacterial vaccines on the market that use whole agent targeting; e.g. tuberculosis, anthrax and typhoid fever.<sup>60</sup> A limitation of specific-antigen vaccines is that single antigens do not induce the same immune response as whole cells. Therefore, single antigen based vaccines are often less immunogenic and do not provide the same robust and long-lasting immune response as whole cell vaccines.<sup>60</sup> To increase the immunogenicity of a single antigen, vaccine formulations often include an adjuvant (e.g. aluminium salts, the squalene-based MF59, the LPS-derived monophosphoryl lipid A (MPL) and liposomes),<sup>60</sup> which serve to amplify the adaptive immune response in order to generate an effective immunological memory.<sup>61</sup>

Despite whole cell targeting being of limited use in the development of bacterial based vaccines, StroVac (Strathmann AG, Hamburg, Germany), a human targeting UTI vaccine, was developed using this process.<sup>60</sup> StroVac and SolcoUrovac (Solco Basel AG, Birsfelden, Switzerland and Protein Express, Cincinnati, OH, USA) are intramuscular polyvalent whole cell vaccines, both containing different compositions of ten strains of heat-killed uropathogens; six *E. coli* strains and

## Introduction

single strains of *Klebsiella pneumoniae*, *Proteus mirabilis*, *Morganella morganii*, and *Enterococcus faecalis*.<sup>60</sup> Though the first clinical trials using SolcoUrovac showed the vaccine to be protective against recurrent UTIs,<sup>62</sup> undesirable reactions were seen at the injection site.<sup>63</sup> The vaccine formulation was altered for pessary application and The Protein Expression company in Ohio, USA obtained a licence from Solco to produce Urovac.<sup>63</sup> Phase II and extended phase II clinical trials of the pessary formulation of UroVac found women treated with six doses at week 0, 1, 2, 6, 10 and 14 gained short-term protection from infections. However, by the end of the six-month study it was established that UroVac did not provide significant long-term protection from UTIs and did not induce an increase in UPEC specific serum, urinary or vaginal antibodies.<sup>64</sup>

OM-89 / Uro-Vaxom (OM Pharma, Myerlin, Switzerland) is another UTI vaccine sold in almost 40 countries.<sup>64</sup> Uro-Vaxom is administered as a daily oral capsule, and is composed of a mix of lyophilized membrane proteins from 18 UPEC strains.<sup>64</sup> Several double blind studies have been performed to assess Uro-Vaxom safety and efficacy.<sup>65,66</sup> Uro-Vaxom was found to significantly reduce UTI recurrence rates with only limited toxicity issues seen. The requirement for daily administration may limit Uro-Vaxom applications, due to issues with patient compliance.<sup>64-66</sup>

Two further whole-cell targeting UTI vaccines are Urvakol (Institute of Microbiology, Prague, Czech Republic) and Urostim (National Center of Infectious and Parasitic Diseases, Sofia, Bulgaria). These vaccines are administered by an oral daily dose and are composed of a mixture of inactivated uropathogens containing strains of *E. coli*, *P. mirabilis* and *E. faecalis*, with Urvakol also containing a strain of *Pseudomonas aeruginosa*, and Urostim containing a strain of *K. pneumonia*. Initial patient and animal studies of Urvakol and Urostim appear promising, but the ability of either vaccine to prevent recurrent UTIs has not been confirmed as well-structured clinical trials have not yet been completed.<sup>64</sup>

The development of a specific antigen vaccine which targets UTIs has been investigated. Adhesins such as FimH make attractive antigen candidates, as antibodies raised against them should block adhesion-host cell receptor binding and thus bacterial colonisation (Figure 1-11).<sup>67</sup> FimH is critical to UPECs pathogenesis but is not highly abundant on UPECs surface; FimH is therefore a good adhesion for vaccine development.<sup>60</sup>

## Introduction

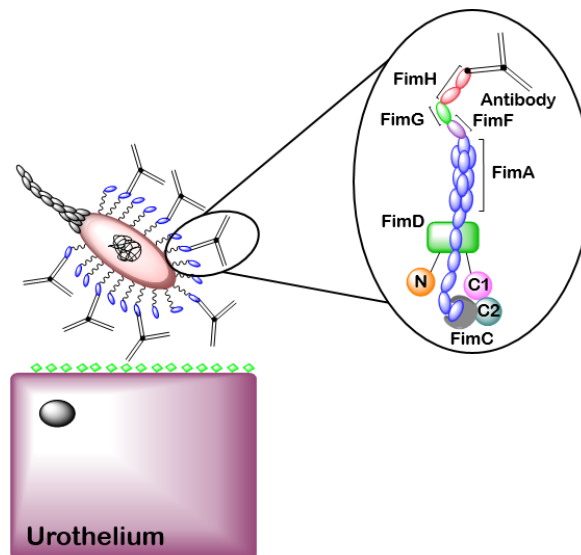


Figure 1-11. Cartoon depiction of proposed mechanism of action for a typical anti-adhesion FimH-based vaccine. With antibodies binding to FimH thereby blocking UPEC adhering to mannose saturated N-glycans (green squares) located on the urothelium surface

Langermann and co-workers have performed research into FimH targeting vaccines.<sup>68-70</sup> Antibodies were raised in mice to two different purified FimH protein complexes; the first complex contained the periplasmic chaperone FimC bound to the full length FimH protein (FimC-H) and the second complex contained a naturally occurring mannose-binding FimH truncate (FimHt) corresponding to the N-terminal two thirds of the FimH protein. Antibodies were further raised against the whole type 1 pili purified from ORN103/pSH2.<sup>68</sup> Initial results showed that both FimHt and FimC-H induced a strong, long-lasting immune response, which could be further increased by booster immunizations.<sup>68</sup> Using the flow cytometric method originally developed to evaluate rickettsia-cell attachment,<sup>71</sup> the *in vitro* ability of FimHt and FimC-H antibodies to prevent bacterial adhesion to urothelium cells was investigated. The results showed both FimHt and FimC-H antibodies had the ability to prevent *E. coli* NU14 from binding to the urothelium cells.<sup>68</sup>

Further work by Langermann and co-workers used mice models to investigate whether FimH vaccines could protect mice from developing UTIs. Mice were immunized with various FimH vaccines then infected with *E. coli* NU14, nine weeks after primary immunisation. Vaccinated mice showed a 100 to 1000-fold reduction in the number of organisms recovered from the bladder compared to control mice (mice treated with only adjuvant or FimC-immunized control mice).<sup>68</sup> Similar results were observed for mice vaccinated with the FimC-H vaccine, and mice vaccinated with the FimHt vaccine showed UTI protection lasting up to 29 weeks post immunisation.<sup>68</sup> Furthermore, Langermann and co-workers<sup>70</sup> used a murine cystitis model to demonstrate that immunisation with FimC-H and MF59.C1 reduced *in vivo* colonization of the bladder mucosa by UPEC by >99%.<sup>70</sup>

## Introduction

Murine models are useful tools in establishing the initial activity of a FimH vaccine. However, before starting human trials this activity should be verified using a nonhuman primate UTI model. Langermann and co-workers used *Cynomolgus monkeys* to further evaluate the activity of the FimC-H vaccine.<sup>69</sup> Four monkeys were vaccinated with FimC-H in MF59 adjuvant and their systemic IgG antibody levels were monitored over time.<sup>69</sup> Three of the four monkeys immunized showed an increase in production of FimH-specific IgG antibodies and displayed protection from type 1-piliated NU14 bacterial infections.<sup>69</sup>

The UPEC type 1 fimbria subunit vaccine, FimCH was bought to phase II clinical trials by MedImmune, Inc (MA, USA) in 1999. However, the vaccine was discontinued in 2003 as clinical trials failed to demonstrate sufficient clinical efficacy to warrant phase III clinical trials.<sup>64</sup> Since then Sequoia science have licenced the FimCH vaccine, changed the adjuvant<sup>72</sup> and entered it into clinical trials with the FDA granting the FimCH UTI vaccine fast track designation.<sup>73</sup>

ExPEC4V is a further UTI-targeting vaccine consisting of a tetravalent *E. coli* bio-conjugate. This vaccine was worked on by GlycoVaxyn and Janssen Pharmaceutical. ExPEC4V has undergone phase Ib clinical trials and was shown to be well tolerated and reduce the number of *E. coli* induced UTI cases in the vaccinated group, warranting further phase II clinical trials.<sup>74</sup>

### 1.1.7 Oligosaccharide based FimH inhibitors

FimH primarily targets large branched mannose-capped oligosaccharides found on *N*-glycosylated proteins which line the urinary tract<sup>41</sup> such as UPIa.<sup>75</sup> The preference of FimH for mannose-capped oligosaccharides can be seen in ligand affinity assays, with  $\alpha$ -D-mannose-capped oligosaccharides displaying 100-200 times greater affinity for FimH than  $\alpha$ -D-mannose monomers.<sup>41</sup> This increase in affinity is due to mannose-based oligosaccharides being able to interact with the extended FimH binding site.

Due to their role as natural FimH ligands and their ability to act as FimH inhibitors, much research has been performed into using mannose-capped oligosaccharides as a curative treatment for UPEC-induced UTIs. Sharon and co-workers<sup>76, 77</sup> investigated the ability of a large range of mannose glycosides and mannose-capped oligosaccharides to inhibit *E. coli*-induced yeast aggregation.<sup>76, 77</sup> The three most potent inhibitors were oligosaccharides **1.2**, **1.3** and trisaccharide **1.4** (Figure 1-12),<sup>76, 77</sup> with research suggesting that trisaccharide **1.4** is the optimal size for binding to the extended FimH binding site.<sup>76, 77</sup> Further investigation found that the high binding affinity displayed by trisaccharide **1.4** was due to a few key structural components. Firstly, trisaccharide **1.4** contains a Man- $\alpha$ 1,-3-Man linkage at the non-reducing terminus; this linkage has been shown to be highly preferential in FimH binding.<sup>78</sup> A second beneficial structural feature is the presence of a *N*-acetyl glucosamine sugar, as



neither mannotriose **1.5** nor mannopentaose **1.6** (Figure 1-12) exhibited significantly higher FimH binding affinity than Man- $\alpha$ 1,-3-Man **1.7** (Figure 1-12).<sup>78</sup> Furthermore, docking studies suggest that the structure of trisaccharide **1.4** allows both the central mannose unit and the GlcNAc unit to interact with the tyrosine gate, accounting for the high affinity displayed by trisaccharide **1.4**.<sup>78</sup>

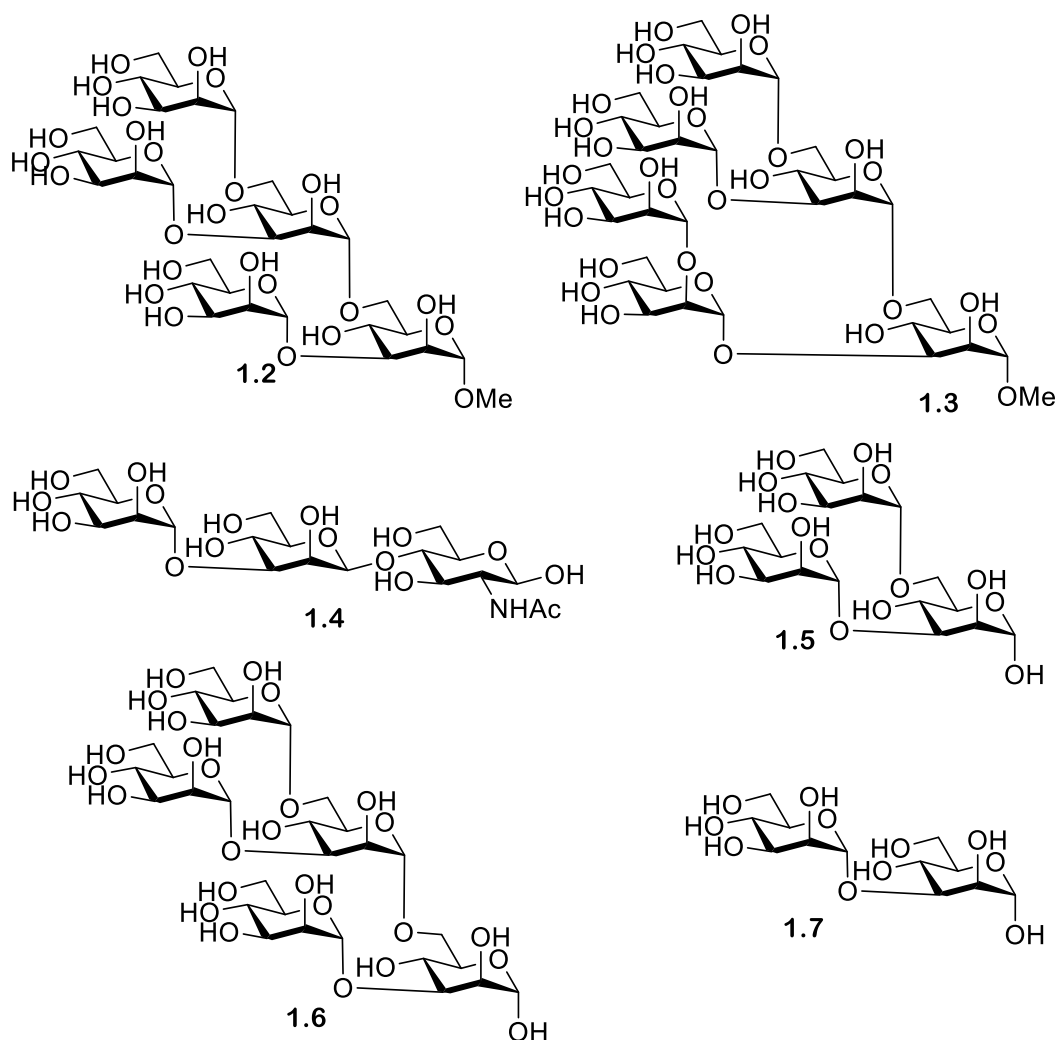


Figure 1-12. Compares the structures of potent oligosaccharide based FimH inhibitors (oligosaccharides **1.2**, **1.3**, and trisaccharide **1.4**) to weak oligosaccharide based FimH inhibitors (mannotriose **1.5**, mannopentaose **1.6** and Man- $\alpha$ 1,3Man **1.7**)

A further oligosaccharide with high affinity to FimH is oligosaccharide **1.1** (Figure 1-13,  $K_d = 20$  nM)<sup>78</sup>), displaying a 10-fold increase in affinity compared to Man- $\alpha$ 1,-3-Man.<sup>51, 78</sup> Oligosaccharide **1.1** contains a terminal chitobiose unit; these units are ubiquitous in nature, providing a bridge between mannosides and asparagine residues in the Asn-X-Ser/Thr motif found in *N*-linked glycoproteins.<sup>51</sup> Chitobiose units have been shown to interact with the extended FimH binding site. A crystal structure of oligomannoside **1.1** bound to the extended FimH receptor binding domain identified some of the key binding interactions.<sup>51</sup> Firstly, Man4 at the non-reducing end was shown to be anchored into the polar binding pocket. Further interactions were mediated through the tyrosine gate interacting with

the Man- $\alpha$ 1,3-Man- $\beta$ 1,4-GlcNAc backbone via the  $\alpha$ 1,3 and the first  $\beta$ 1,4 glycosidic linkages. The second mannose unit at the non-reducing end, Man5, was not directly recognized by FimH due to the unit partially extending out of the binding site. GlcNAc1 was also shown to partially exit the binding site, folding over residue Thr51. Man5 and GlcNAc1 displayed the most flexibility of all the saccharide units,<sup>51</sup> likely due to being the least closely bound to the extended FimH binding site. This crystal structure provides further evidence that trisaccharide **1.4** may construct the optimal motif for FimH binding, containing the critical Man- $\alpha$ 1,3-Man- $\beta$ 1,4-GlcNAc backbone needed for interactions with the extended FimH binding site.

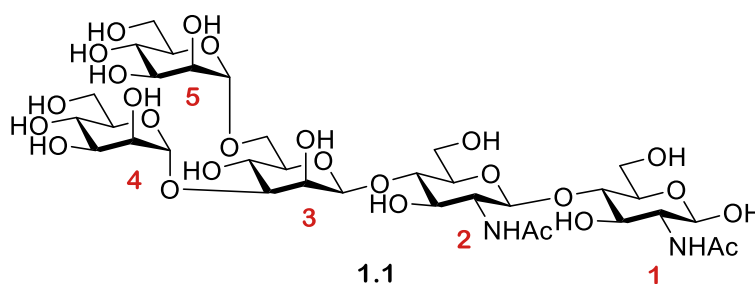


Figure 1-13. Structure of the potent FimH inhibitor oligomannoside 1.1

The oligomannoside structures discussed here were obtained by a number of different methods including chemical synthesis, isolation from yeast extract and isolation from the urine of patients suffering from mannosidosis and GM1 gangliosidosis.<sup>66 51, 78</sup>

Chemical synthesis is one of the most common methods used to obtain mannose-capped oligosaccharides. As is common in carbohydrate synthesis, the synthesis of these oligosaccharides relies on a complex scheme of protection, glycosylation and deprotection steps. To further add to this complexity, potent FimH inhibitors such as trisaccharide **1.4** and oligosaccharide **1.1** contain a critical  $\beta$ -mannosidic bond between the central mannose unit and the GlcNAc unit.  $\beta$ -Mannosidic bonds have long been recognized as the most difficult linkages to construct for carbohydrate chemists.<sup>79</sup> Over the last 25 years multiple groups have conducted a wealth of research into the development of  $\beta$ -mannosidic bonds, developing synthetic methods to afford  $\beta$ -mannosides in a high yielding and selective manner.<sup>79-84</sup> Despite this research, the requirement for pre-activation and need for specific mannoside donor protection groups (e.g. *O*-4,6 benzylidene protection)<sup>85, 86</sup> still makes  $\beta$ -mannoside synthesis challenging, and consequently many opt to prepare simpler  $\alpha$ -mannoside counterparts. A further factor resisting the use of mannose capped oligosaccharides as therapeutics is their size which makes them unlikely to be orally absorbed. Lack of oral absorption coupled with synthetic complexity, has therefore restricted the application of mannose-capped oligosaccharides, and as such many research groups have chosen to focus on the more easily synthesized  $\alpha$ -D-mannopyranoside based inhibitors as FimH antagonists.

### 1.1.8 $\alpha$ -configured D-Mannopyranoside based inhibitors

One of the first classes of D-mannopyranoside based FimH inhibitors were alkyl mannosides (Figure 1-14, Table 1, Entry 1, page 56). These were discovered serendipitously when De Greve and co-workers found butyl- $\alpha$ -D-mannoside occupied the mannose binding site.<sup>87</sup> Investigations found butyl- $\alpha$ -D-mannoside ( $K_d = 151$  nM) to bind to FimH with 15-30 times greater affinity than  $\alpha$ -D-mannose ( $K_d = 2.3$   $\mu$ M).<sup>87</sup> Further investigation into the binding affinity of alkyl mannosides found that in general binding affinity increases as alkyl chain length increases, with the binding affinity peaking for hept-D-mannoside ( $K_d = 5$  nM).<sup>87</sup> One theory explaining this trend is that increasing the chain length increases the van der Waals interactions with the hydrophobic groove and tyrosine gate, but once the alkyl chain is longer than a heptyl chain it extends beyond the hydrophobic region into solvent-exposed areas,<sup>41</sup> increasing the free binding energy and thus lowering binding affinity.

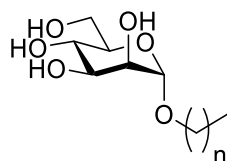
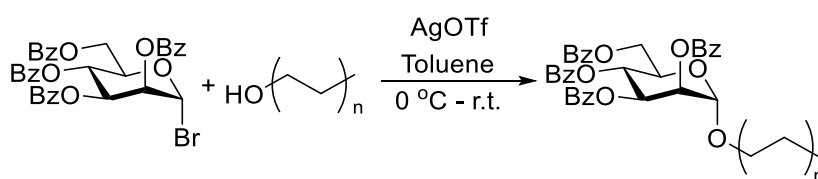


Figure 1-14. Structure of the alkyl mannoside scaffold. Where  $n = 0-7$

The alkyl mannosides used by De Greve and co-workers<sup>87</sup> were synthesized using a procedure reported by Tidén and co-workers<sup>88</sup> for the synthesis of octyl and tetradecyl mannosides. Here alkyl alcohols underwent silver triflate-promoted glycosylations to 2,3,4,6,-tetra-*O*-benzoyl- $\alpha$ -D-mannopyranosyl bromide (Scheme 1-1), followed by Zemplén deacylation to afford the deprotected alkyl mannoside ligand.



Scheme 1-1. Reaction scheme for the synthesis of alkyl mannosides, by glycosylation with aliphatic alcohols proceeding using a AgOTf activation system

Sharon and co-workers<sup>89</sup> reported aromatic  $\alpha$ -mannosides (Table 1, Entry 2, page 56) to be powerful inhibitors of the adherence of type 1 fimbriated *E. coli* to both yeast and intestinal epithelial cells. With *p*-nitrophenyl- $\alpha$ -mannoside **1.8** (Figure 1-15) shown to be approximately 70 times more effective than methyl  $\alpha$ -mannoside for both inhibiting yeast agglutination by *E. coli* 025 and inhibiting the adherence of *E. coli* 0128 to guinea pig ileal epithelial cells.<sup>76, 89</sup> The two most potent aromatic  $\alpha$ -mannoside inhibitors reported by Sharon and co-workers<sup>76, 89</sup> were *p*-nitro-*O*-chlorophenyl- $\alpha$ -mannoside (*p*NoClP $\alpha$ Man) **1.9** and 4-methylumbelliferyl- $\alpha$ -mannoside (MeUmb $\alpha$ Man) **1.10** (Figure

## Introduction

1-15). These analogs were shown to increase the inhibition of yeast agglutination by *E. coli* 025 by a factor of 717 (*p*NoClPaMan **1.9**) and 600 (MeUmbaMan **1.10**) compared to methyl  $\alpha$ -mannoside. A significant increase in inhibition of *E. coli* 0128 adherence to guinea pig ileal epithelial cells was also observed [470 times for (*p*NoClPaMan **1.9**) and 1015 times for (MeUmbaMan **1.10**) with respect to methyl  $\alpha$ -mannoside]. This increase in affinity displayed by FimH for aromatic  $\alpha$ -mannosides compared with methyl  $\alpha$ -mannoside is likely due to the aromatic side chain being able to establish favourable  $\pi$ - $\pi$  stacking interactions with the tyrosine gate.<sup>90</sup>

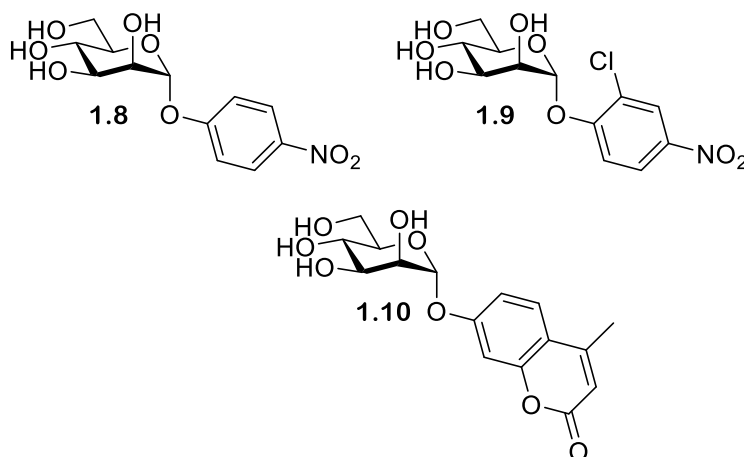


Figure 1-15. Structure of *p*-nitrophenyl- $\alpha$ -mannoside **1.8**, *p*-Nitro-*O*-chlorophenyl- $\alpha$ -mannoside (*p*NoClPaMan) **1.9** and 4-methylumbelliferyl- $\alpha$ -mannoside (MeUmbaMan) **1.10**

Building upon the high potency displayed by *p*-nitrophenyl- $\alpha$ -mannoside, Lindhorst and co-workers synthesized a series of *para*-substituted aryl  $\alpha$ -D-mannosides, with one analog achieving significantly higher potency than *p*-nitrophenyl- $\alpha$ -mannoside [relative inhibitory potential (RIP) of 1.6 vs 1].<sup>91</sup> Further work into the development of an aromatic  $\alpha$ -mannoside based inhibitor was performed by Han and co-workers.<sup>52</sup> Here they synthesized a series of aryl-substituted  $\alpha$ -D-phenylmannosides, evaluating their biological activity using a guinea pig red blood cell based hemagglutination (HA) assay. This assay measures the concentration of inhibitor needed for >90% HA inhibition, and this concentration is known as the hemagglutination inhibition (HAI) titre. The HAI titre of new compounds can be compared to that of other compounds in order to assess the potency of new compounds.

Han and co-workers synthesized an extensive series of aryl substituted  $\alpha$ -D-phenylmannosides functionalized with a variety of groups (Cl, NO<sub>2</sub>, CN, OMe, CO<sub>2</sub>Me, NHAc, CO<sub>2</sub>H, CONH<sub>2</sub>, CH<sub>2</sub>CO<sub>3</sub>Me) at either the *ortho*, *meta* or *para* position.<sup>52</sup> Generally, it was noted that phenylmannosides functionalized at the *ortho* and *meta* positions gave better potency than phenylmannosides functionalized at the *para* position. The most potent phenylmannoside contained a methyl ester group

at both *meta* positions, being three times more potent than the phenylmannoside containing a single *meta* methyl ester.<sup>52</sup>

Another well-investigated group of FimH-targeting analogs are biphenyl mannosides (Table 1, Entry 3, page 56).<sup>52, 59, 92, 93</sup> Han and co-workers hypothesized that the potency of aryl mannosides could be increased by the addition of a second aryl ring. This hypothesis was explored using analogs containing an additional aryl ring system in conjugation with the parent ring of the aryl mannoside. The most potent analog was biphenyl mannoside **1.11** (HAI = 1  $\mu$ M, IC<sub>50</sub> = 0.94  $\mu$ M)<sup>52</sup> which contained a methyl ester at the *meta* position of the second ring system (Figure 1-16). A high resolution X-ray crystal structure of biphenyl mannoside **1.11**, showed that both aromatic rings were able to partake in hydrophobic and  $\pi$ - $\pi$  stacking interactions with the closed Tyr-48 residue, with the methyl ester further able to hydrogen bond with the salt bridge (residues Arg-98 and Glu-50).<sup>52</sup>

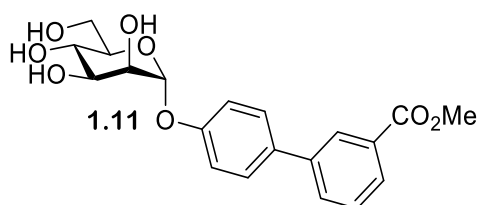


Figure 1-16. Structure of biphenyl mannoside **1.11**

Further SAR evaluation of the terminal biphenyl mannoside aryl ring identified two potent biphenyl mannosides: biphenyl mannoside **1.12** (HAI = 0.15  $\mu$ M) and biphenyl mannoside **1.13** (HAI = 0.37  $\mu$ M, IC<sub>50</sub> = 0.74  $\mu$ M)<sup>92</sup> (Figure 1-17).<sup>52</sup> Biphenyl mannoside **1.12** displayed good potency in the HAI assay, yet due to its insolubility could not be used in a biofilm assay.<sup>93</sup> However, biphenyl mannoside **1.13** was used in a biofilm assay and showed impressive activity, with an IC<sub>50</sub> of 0.74  $\mu$ M.<sup>93</sup> Initial dosing in mice established biphenyl mannoside **1.13** to be orally bioavailable and stable to metabolism, and the only metabolic degradation pathway detected was hydrolysis of the glycosidic bond. Metabolic degradation of biphenyl mannoside **1.13** should be minimal as >95% was excreted in the urine unchanged. Moreover, no apparent toxicity was observed up to a dose of 200 mg/kg, using physiological changes and survival as assessment parameters. Further investigation using an adapted preclinical murine model suggested that biphenyl mannoside **1.13** was effective at preventing infections, treating established UTIs and increasing the activity of antibiotic treatments.<sup>93</sup>

## Introduction

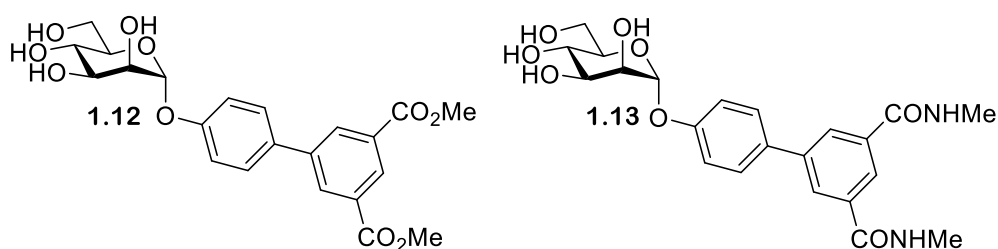


Figure 1-17. Structure of biphenyl mannoside **1.12** and biphenyl mannoside **1.13**

Han and co-workers previous work on  $\alpha$ -D-phenylmannosides showed that substitution at the *ortho* position with chloro and cyano groups could significantly increase potency.<sup>52</sup> Using widely available biphenyl mannoside **1.11** as a scaffold (Figure 1-18), Han and co-workers also synthesized a number of biphenyl mannosides substituted at the *ortho* position of the top ring, and observed the general potency trend  $\text{CF}_3 > \text{Cl} = \text{Me} > \text{OMe} > \text{F}$ .<sup>92</sup> One explanation for the increase in potency upon *ortho* substitution is that the presence of *ortho* substituents increases the hydrophobic contact with the tyrosine gate at residues Ile52 or Ile13. This explanation is supported by the potency trend seen above, as addition of a  $\text{CF}_3$  group would result in the largest increase in hydrophobic contact and thus the largest increase in potency. Further investigation was performed using biphenyl mannoside **1.14** ( $\text{IC}_{50} = 1.35 \mu\text{M}$ )<sup>92</sup> as a scaffold, with a similar potency trend observed:  $\text{CF}_3 > \text{Me} > \text{Cl}$ .<sup>92</sup> Two final analogs were synthesized; biphenyl mannoside **1.15** ( $\text{HAI} = 0.01 \mu\text{M}$ ,  $\text{IC}_{50} = 0.043 \mu\text{M}$ )<sup>92</sup> and biphenyl mannoside **1.16** ( $\text{HAI} = 0.02 \mu\text{M}$ ,  $\text{IC}_{50} = 0.073 \mu\text{M}$ )<sup>92</sup>, with both displaying increased potency to biphenyl mannoside **1.13** ( $\text{HAI} = 0.37 \mu\text{M}$ ).<sup>92</sup>

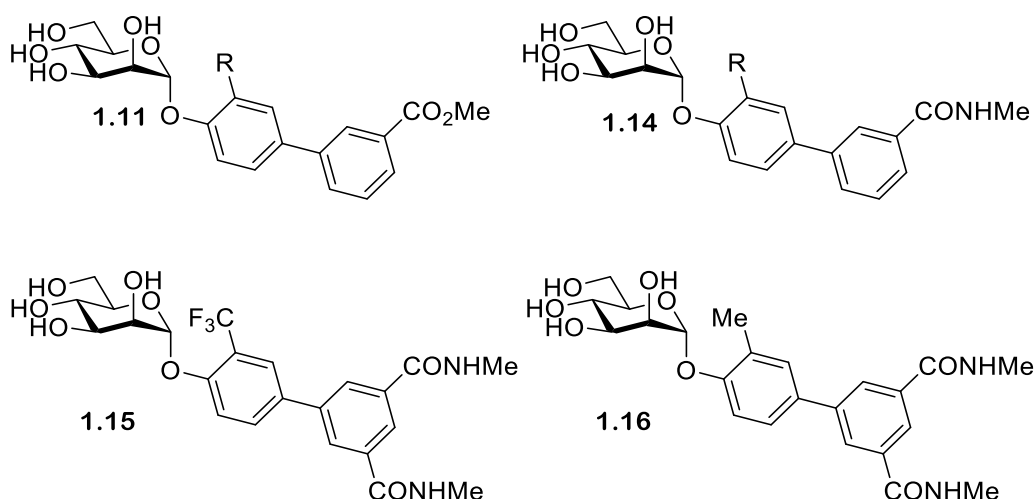


Figure 1-18. Structure of biphenyl mannoside **1.11**, biphenyl mannoside **1.14**, biphenyl mannoside **1.15** and biphenyl mannoside **1.16**

Biphenyl mannosides **1.15** and **1.16** displayed good potency, but their low  $\log(p)$  values of -6.27 and -8.46 respectively, suggest they would have poor oral absorption.<sup>92</sup> Biphenyl mannoside **1.17** (Figure 1-19) had a significantly higher  $\log(p)$  of -3.89, and therefore should have better oral absorption.<sup>92</sup> Pharmacokinetic studies in mice showed biphenyl mannoside **1.17** ( $IC_{50} = 0.16 \mu\text{M}$ )<sup>92</sup> to be a promising lead candidate, maintaining a concentration in the urine and plasma well above the predicted minimum effective concentration for over 6 h. Further *in vivo* tests used a chronic infection mouse model; this model uses C3H/HeN mice with chronic cystitis at two-weeks post-infection. The efficacy of compounds can be monitored by the number of colony forming units (CFU) present at selective time periods after compound administration.<sup>93</sup> Mice treated with biphenyl mannoside **1.17** showed a significant reduction of chronic cystitis six hours post-treatment; however, by 24 hours post-treatment the number of CFU had started to increase, but remained lower than in control mice.<sup>93</sup> This CFU increase was shown to be prevented by administering three doses of biphenyl mannoside **1.17** every eight hours. These *in vivo* experiments suggest that biphenyl mannoside **1.17** provided a promising lead compound which could be used in preclinical trials.<sup>93</sup>

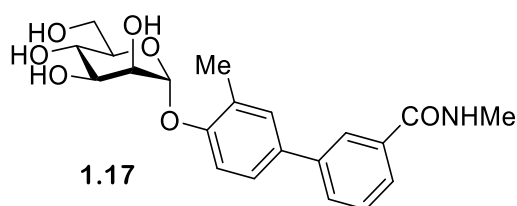


Figure 1-19. Structure of biphenyl mannoside **1.17**

A limitation of the antagonistic studies performed on previously designed biphenylmannosides and other  $\alpha$ -D-mannopyranoside based inhibitors are the methods used; e.g. a fluorescence polarization assay, an isothermal titration calorimetry (ITC) based assay, and a surface plasmon resonance (SPR)-based assay. These methods rely on the use of FimH<sub>LD</sub>,<sup>94</sup> which is locked in the high-affinity FimH conformation.<sup>44</sup> As discussed previously, the FimH lectin can adopt three conformational states; an unbound low-affinity conformation, a bound medium-affinity conformation which occurs under static conditions, and a bound high-affinity conformation which occurs under shear force.<sup>94</sup> Therefore, only measuring an antagonist affinity against one FimH conformation could limit the accuracy of the results. Antagonistic studies performed using most target-based assays and cell based assays (e.g. hemagglutinin assays or a flow cytometry based assay) are not affected by these inaccuracies, as they use *E. coli* cells producing FimH<sub>FL</sub>, which can adopt all three conformers.<sup>94</sup> Monomeric FimH<sub>FL</sub> is inherently unstable<sup>94, 95</sup> and thus a native model must be used instead. This model is composed of FimH expressed as a biomolecular complex, where the incomplete fold of FimH<sub>PD</sub> is complemented by a synthetic donor-strand peptide. Subsequently, comparison of the

## Introduction

binding affinities of a series of biphenyl analogs showed an approximate 100-fold decrease in affinity from FimH<sub>LD</sub> to FimH<sub>FL</sub>. Recent investigations into biphenyl mannoside affinity for FimH<sub>LD</sub> and FimH<sub>FL</sub> has led to the design of some promising substituted biphenyl mannoside analogs (Figure 1-20).<sup>94, 96</sup> These analogs display nanomolar potency against FimH<sub>FL</sub> and subnanomolar potencies against FimH<sub>LD</sub>, alongside promising pharmacokinetic properties.<sup>94, 96</sup>

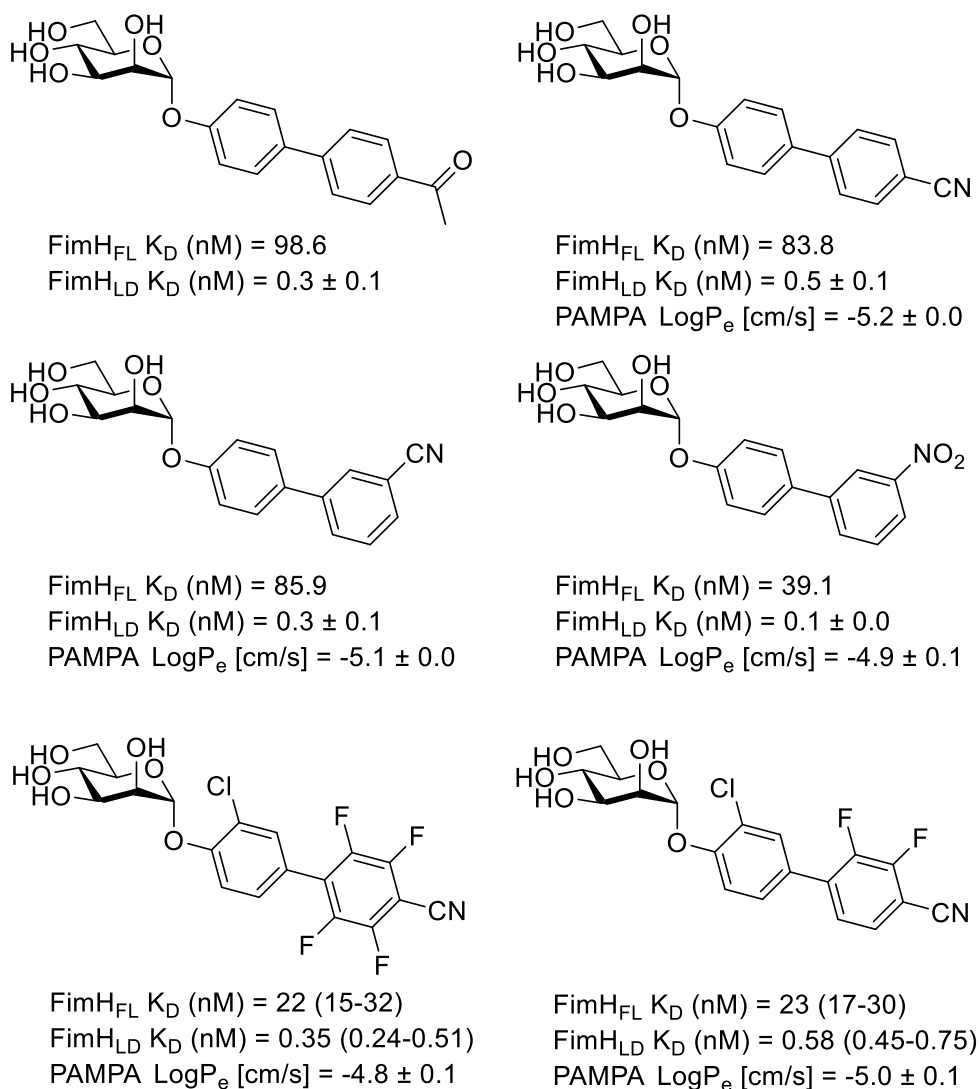


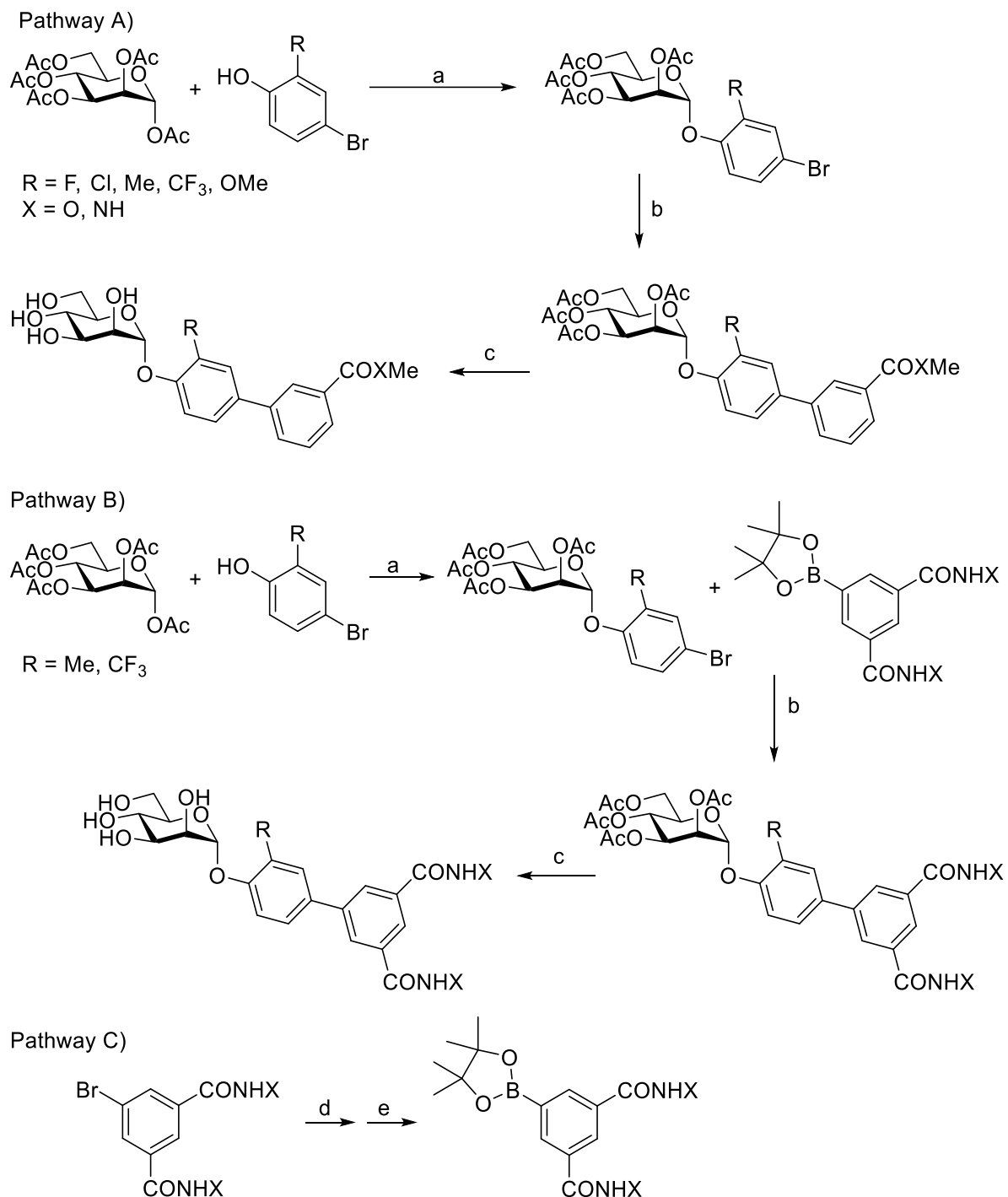
Figure 1-20. Structure of some substituted biphenyl mannoside analogs with promising FimH activity and pharmacokinetic properties,<sup>94, 96</sup> such as dissociation constants ( $K_D$ ) and logP<sub>e</sub> values assessed using a parallel artificial membrane permeability (PAMP) assay

The *ortho*-substituted biphenyl mannosides were synthesized via two routes (Scheme 1-2). Most analogs were synthesized using Pathway A. The first step of this pathway is Lewis acid mediated glycosylation of mannoside pentaacetate with a 2-substituted 4-bromophenol analog (step a). This is followed by a Suzuki cross-coupling with a commercially available 3-substituted phenylboronic acid derivative to give a protected *ortho*-substituted 4'-biphenyl mannoside (step b). The final step is a Zemplén deacetylation, affording the deprotected *ortho*-substituted 4'-biphenyl mannoside (step c).



## Introduction

Synthesis of the diamide analogs was performed using Pathway B, following the same initial and final steps as Pathway A (step a and d), but using a 3,5-di-(N-methylaminocarbonyl)-phenylboronic acid pinacol ester synthesized in-house (Pathway C) in the Suzuki cross-coupling reaction (step d).<sup>92</sup>



*Scheme 1-2. Synthesis of ortho-substituted biphenyl mannosides. Reagents and conditions: Pathway A + B; a) BF<sub>3</sub>·Et<sub>2</sub>O, CH<sub>2</sub>Cl<sub>2</sub>, reflux, 45 h, (25-75%); b) 3-substituted phenylboronic acid derivatives, cat. Pd(PPh<sub>3</sub>)<sub>4</sub>, Cs<sub>2</sub>CO<sub>3</sub>, dioxane/water (5/1), 80 °C, 1 h; c) cat. MeONa, MeOH, rt, 12 h, (b+c 3-64%); Pathway C; d) MeNH<sub>2</sub>/EtOH, rt, e) bis(pinacolato)diboron, cat. Pd(dppf)Cl<sub>2</sub>, KOAc, DMSO, 80 °C*

## Introduction

Lindhorst and co-workers used computer-based docking methods to predict the binding affinities of a number of FimH inhibitors; e.g. methyl mannose, *p*-Nitro-phenyl- $\alpha$ -mannoside and two squarate mannosides (squarate mannoside **1.18** and squarate mannoside **1.19**, Figure 1-21). An enzyme-linked immunosorbent assay (ELISA) was performed to test the inhibitors ability to inhibit type 1 fimbriae-mediated bacterial adhesion, with methyl mannose used as a standard (RIP = 1). Squarate mannosides **1.18** and **1.19** were shown to be the most potent inhibitors in the ELISA, with RIPs of 1600 and 6900, respectively.<sup>90</sup> For the inhibitors analysed the expected inverse trend between docking score and RIP was observed. One notable exception was squarate mannoside **1.18**, which had a predicted FimH affinity higher than that of squarate mannoside **1.19**. However, the ELISA showed squarate mannoside **1.19** to be 4 times more potent than squarate mannoside **1.18**.<sup>90</sup>

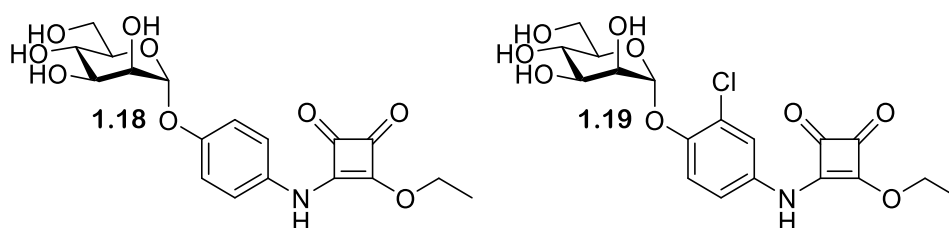
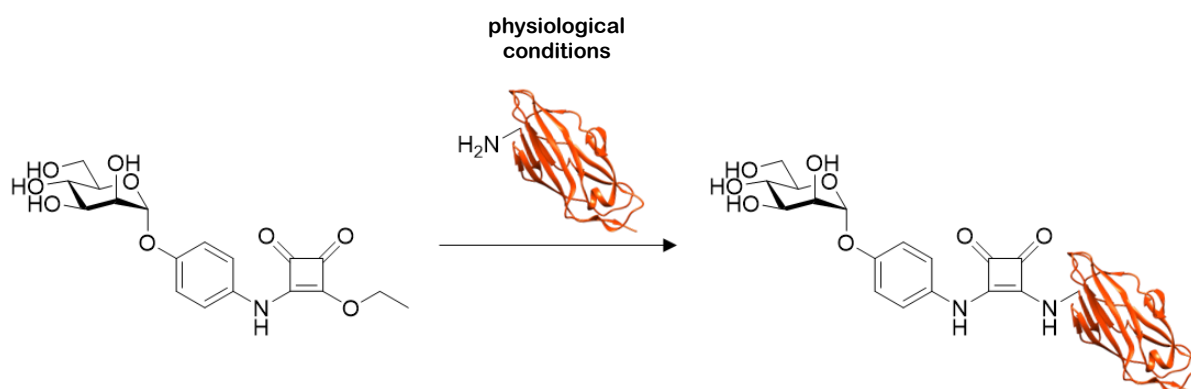


Figure 1-21. Structure of squarate mannoside **1.18** and squarate mannoside **1.19**

Following the discovery of squarate mannosides as potent FimH inhibitors<sup>90</sup> it was hypothesized that the high potency observed with these ligands could be the result of covalent bond formation between squarate mannoside **1.18** and the FimH binding site (Scheme 1-3 depicts the proposed conjugation of squarate mannoside **1.18** to a free amine on FimH, such as that on the N-terminus). To see if this type of reaction was possible, squarate mannoside **1.18** was reacted with a L-phenylalanine ester under physiological conditions (PBS buffer, pH 7.2).<sup>97</sup> Conversion of squarate mannoside **1.18** to the diamide was observed by mass spectrometry.<sup>97</sup>



Scheme 1-3. Reaction scheme for covalent bond formation between squarate mannoside **1.18** and the N-terminus of the FimH lectin (residue Phe1)

## Introduction

Further investigations were performed to see if cross-linking could occur within the carbohydrate recognition domain of FimH. For these investigations diamide squarate mannoside **1.20** (Figure 1-22) was synthesized as its structure prevents covalent cross-linking to FimH.<sup>97</sup> Diamide squarate mannoside **1.20** was shown to be a more potent inhibitor than squarate mannoside **1.18** (diamide squarate mannoside **1.20**  $IC_{50} = 6.38 \mu\text{M} \pm 3.7$  vs squarate mannoside **1.18**  $IC_{50} = 17.3 \mu\text{M} \pm 6.5$ ).<sup>97</sup> This provides strong evidence against the hypothesis that covalent cross-linking was responsible for the high potency previously observed with squarate mannoside analogues.<sup>97</sup> Docking studies provided further opposing evidence, as for covalent cross-linking to the carbohydrate recognition domain to occur a mannoside must be bound in an “upside-down” mode, a mode not supported by the performed docking studies.<sup>97</sup> Finally, samples of type 1-fimbriated *E. coli* were preincubated with different ligands prior to adhesion; if covalent cross-linking to the carbohydrate recognition domain of FimH was to occur then no bacterial adhesion would be possible after preincubation.<sup>97</sup> The observation of concentration dependent inhibition provided further opposition to the covalent cross-linking hypothesis.<sup>97</sup>

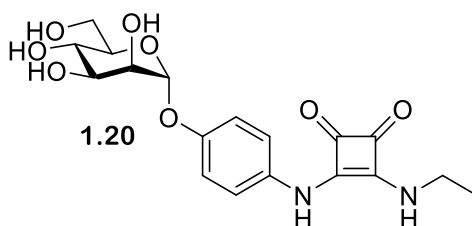
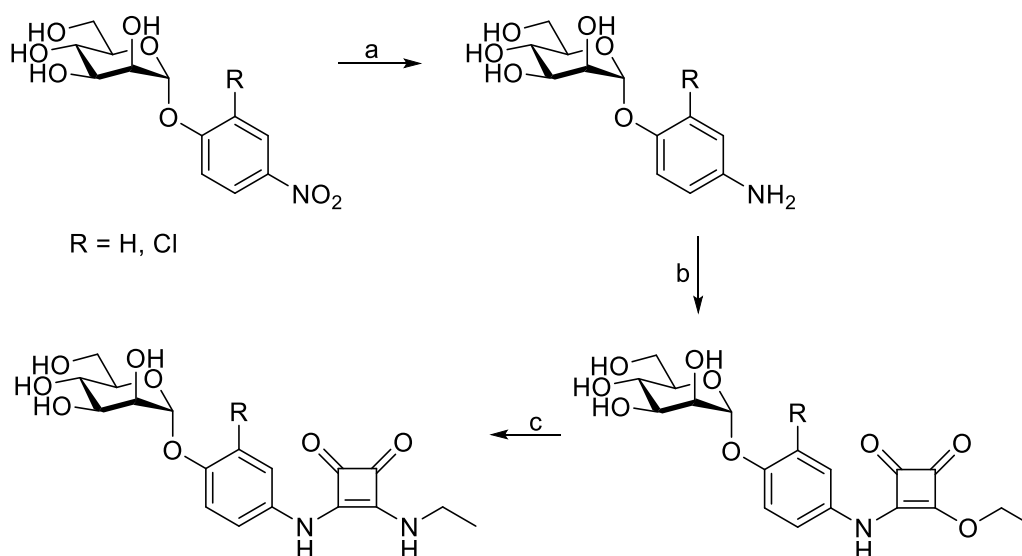


Figure 1-22. Structure of Diamide squarate mannoside **1.20**

The general pathway for squarate mannoside synthesis is summarised in Scheme 1-4. It proceeds by initial hydrogenation of a *p*-nitrophenyl  $\alpha$ -D-mannopyranoside derivative to afford a *p*-aminophenyl- $\alpha$ -D-mannopyranoside derivative (step a). This amino-derivative is further reacted with diethylsquarate (step b).<sup>90</sup> Extraction of a diamide squarate mannoside requires a further reaction; ethylamine addition mediated by  $\text{Et}_3\text{N}$  (step c).<sup>97</sup> Synthesis of squarate mannosides can be simplified by using *p*-aminophenyl- $\alpha$ -D-mannopyranoside derivatives as starting materials, excluding the need for a hydrogenation.<sup>90</sup>

### Introduction



Scheme 1-4. Synthetic pathway for the preparation of squarate mannosides. Reagents and reaction conditions; a) Pd/C, H<sub>2</sub>, DMF rt, 1 h; b) diethylsquarate, DMF, rt, 12-14 h (a+b 55% b alone 63%);<sup>90</sup> c) ethylamine, NEt<sub>3</sub>, MeOH, rt, 12h (63%)<sup>97</sup>

Septanoses (Table 1, Entry 5, page 56) were introduced by Ernst and co-workers<sup>98</sup> following the observation that methyl  $\beta$ -septanosides bound to the jackbean lectin concanavalin A (ConA) (another mannose-selective lectin).<sup>98</sup> Ernst and co-workers<sup>98</sup> used a competitive binding assay and ITC experiments to assess the potency of multiple septanose analogs on FimH<sub>LD</sub>. The results of these experiments showed 2-*O*-*n*-heptyl-1,6-anhydro-D-glycero-D-galactitol **1.21** (Figure 1-23) displayed a ten-fold lower potency for FimH than *n*-heptyl  $\alpha$ -D-mannopyranoside **1.22** (Figure 1-23) (IC<sub>50</sub> = 1.37  $\pm$  0.3  $\mu$ M vs 0.064  $\pm$  0.02  $\mu$ M, K<sub>D</sub> = 0.26  $\mu$ M vs 0.029  $\mu$ M).<sup>98</sup> Further investigations showed that while 2-*O*-*n*-heptyl-1,6-anhydro-D-glycero-D-galactitol **1.21** (Figure 1-23) establishes the same hydrogen bonding network at the FimH binding site as *n*-heptyl  $\alpha$ -D-mannopyranoside **1.22** (Figure 1-23),<sup>98</sup> the formation of this network results in a loss of conformational flexibility, causing a loss of entropy.<sup>98</sup>

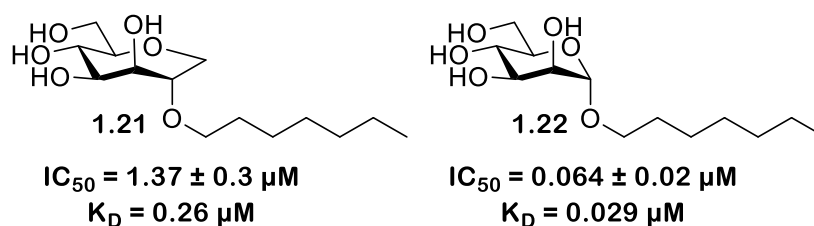


Figure 1-23. Structure, IC<sub>50</sub> values and K<sub>D</sub> values of 2-*O*-*n*-heptyl-1,6-anhydro-D-glycero-D-galactitol **1.21** and *n*-heptyl  $\alpha$ -D-mannopyranoside **1.22**<sup>98</sup>

## Introduction

Gouin and co-workers developed a further class of D-mannopyranoside based inhibitors: thiazolylaminomannosides (TazMan) and neothiazolylaminomannosides (NeoTazMan) (Table 1, Entry 6, page 56).<sup>99, 100</sup> A series of TazMan analogs were originally developed based on scaffold **1.1** (Figure 1-24); with the most potent analogue, thiazolylaminomannoside **1.23**, being 100-times more potent at preventing adherent-invasive *Escherichia coli* (AIEC) attaching to the intestinal cells compared to *n*-heptyl  $\alpha$ -D-mannopyranoside **1.22** (Figure 1-24).<sup>100</sup> Despite thiazolylaminomannoside **1.23** displaying high *in vitro* potency, it showed limited *in vivo* efficiency, likely due to having low pH stability and low water solubility; this restricts the applications of thiazolylaminomannoside **1.23**.<sup>100</sup> To combat these poor *in vivo* results, Gouin and co-workers synthesized a second neothiazolylaminomannoside (NeoTazMan) series based on scaffold **1.2** (Figure 1-24).<sup>99</sup> Thiazolylaminomannoside **1.23** NeoTazMans counterpart neothiazolylaminomannoside **1.24** (Figure 1-24) was shown to have improved *in vivo* properties, being stable to both enzymatic and acid hydrolysis. However, neothiazolylaminomannoside **1.24** was shown to be 2.8 times less potent than thiazolylaminomannoside **1.23** with an  $IC_{50}$  of 194 nM vs 70 nM.<sup>99</sup> These initial investigations show that both TazMan and NeoTazMan are effective FimH inhibitors. However, it is unknown how applicable these analogs are as therapeutics in the treatment of UPEC induced UTIs, as existing studies have only explored their applications in the treatment of Crohn's Disease.<sup>99, 100</sup>

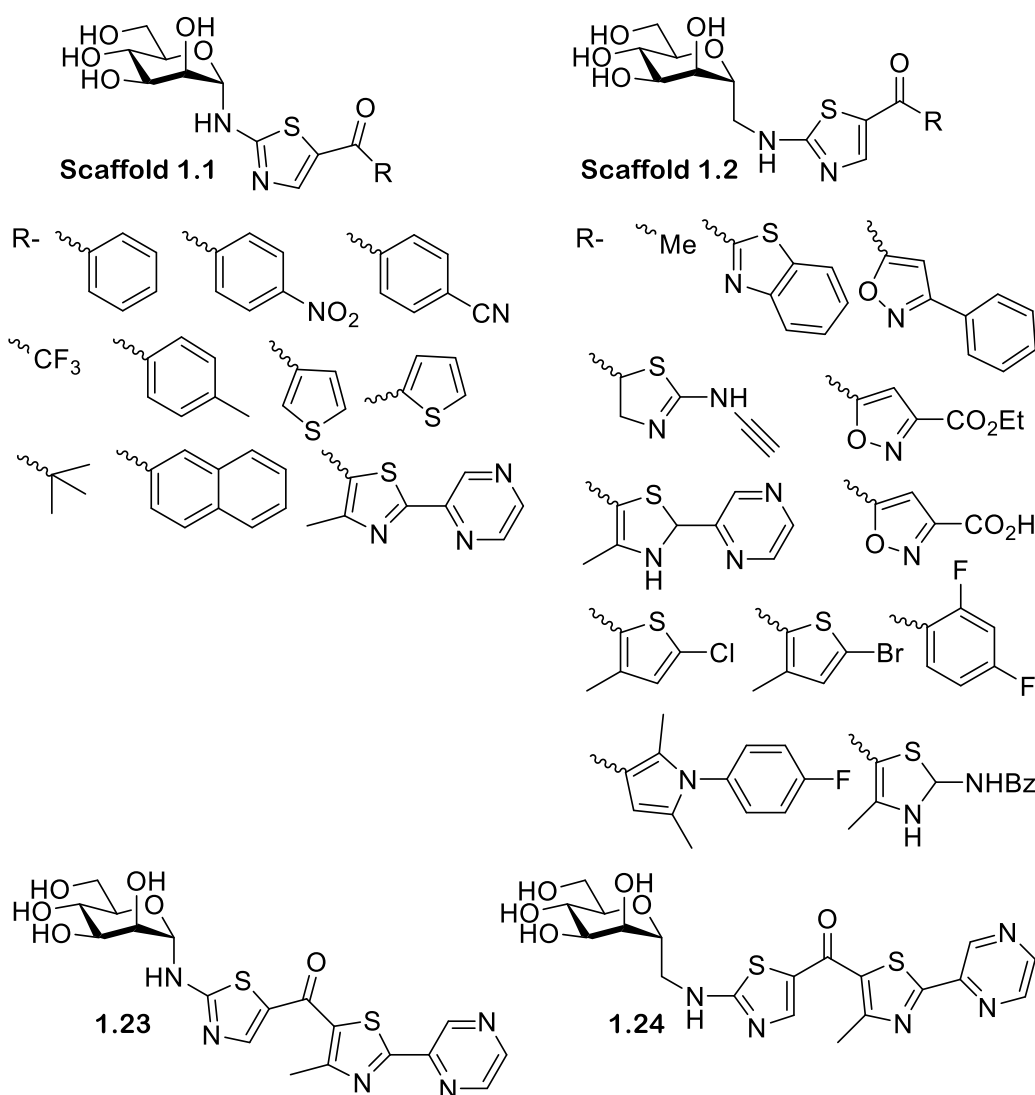


Figure 1-24. Structure of thiazolylaminomannosides scaffold **1.1** and neothiazolylaminomannoside scaffold **1.2** and structure and  $IC_{50}$  values of thiazolylaminomannosides **1.23** and neothiazolylaminomannoside **1.24**<sup>99</sup>

The final class of  $\alpha$ -D-mannopyranoside based inhibitors discussed in this review are indolynylmannosides (Table 1, Entry 7, page 56), which were first investigated by Ernst and co-workers.<sup>101</sup> Ernst and co-workers synthesized a series of indolylphenyl and indolynylphenyl  $\alpha$ -D-mannosides and then investigated their inhibitory and pharmacokinetic properties. The most promising analogue was indolynylphenyl **1.25** (Figure 1-25) achieving an  $IC_{50}$  of 20 nM.<sup>101</sup> Administering a low dose of indolynylphenyl **1.25** (1 mg / kg) to a mouse model achieved a minimum inhibitory concentration in the bladder for > 8 h.<sup>101</sup> Furthermore, a 1 mg / kg dose of indolynylphenyl **1.25** was shown to reduce colony-forming units in the bladder by a factor of 3.7 compared to untreated mice; this result is in line with the reduction seen in mice treated with ciprofloxacin (8 mg / kg).<sup>101</sup>

## Introduction

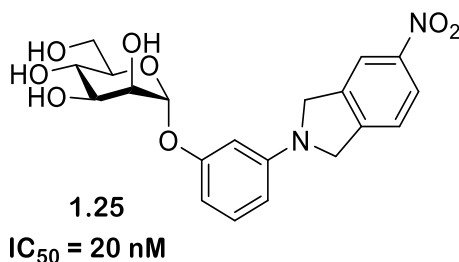


Figure 1-25. Structure and  $IC_{50}$  value of indolinyphenyl **1.25**<sup>101</sup>

A factor that must be considered when designing mannose-based inhibitors is selectivity, as humans possess other mannose binding lectins (e.g. human mannose binding proteins) meaning a lack of selectivity can result in off-target reactions. Ernst and co-workers<sup>102</sup> have previously investigated the selectivity of five potent FimH antagonists all with nM  $IC_{50}$  values (Figure 1-26) against eight human mannose receptors. If an analogue displayed  $10^5$  times greater potency for FimH over the mannose binding proteins it was classified as selective, and assumed to not cause adverse effects due to non-selective binding.<sup>102</sup> All inhibitors tested were shown to have a  $10^5$  fold lower affinity for the human mannose binding proteins than FimH, confirming their selectivity.<sup>102</sup> The FimH inhibitors have been optimized to contain hydrophobic substituents at their reducing end; these substituents can interact with the tyrosine gate located at the entrance of the FimH binding site. The tyrosine gate is a feature unique to FimH, which likely explains the selectivity displayed by these inhibitors.<sup>102</sup> Furthermore, multivalent ligand presentation is known to be hugely important in nature, and as the inhibitors investigated here are only capable of monovalent binding they likely only display low affinity for human mannose receptors.<sup>102</sup>

## Introduction

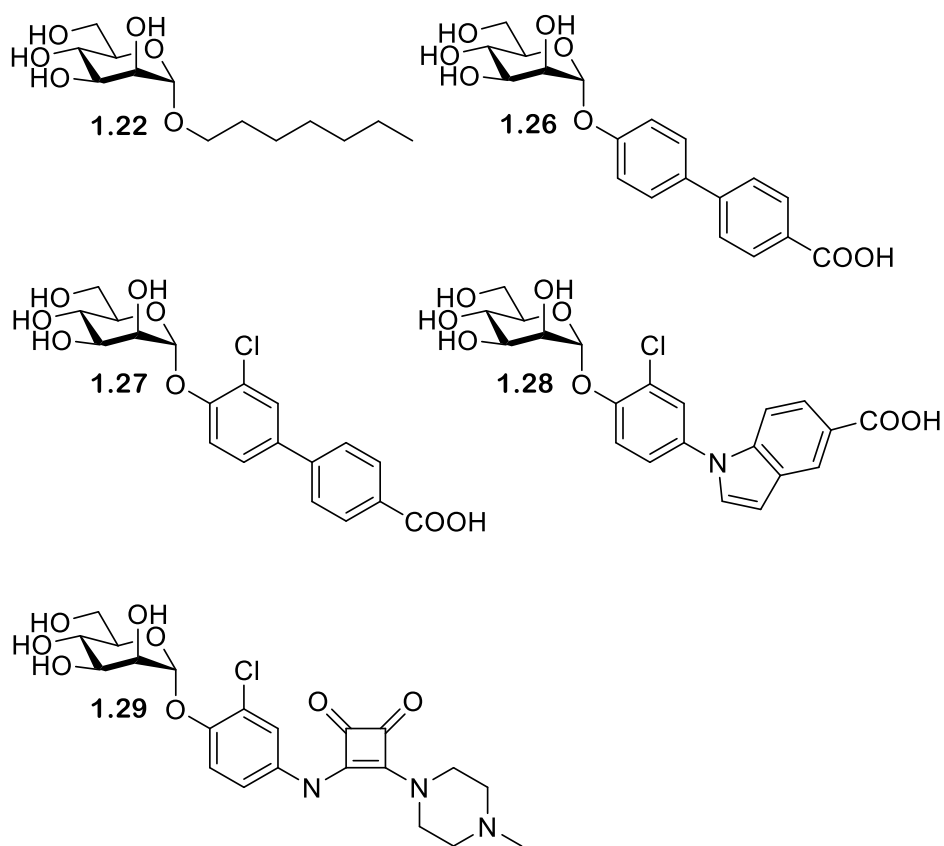
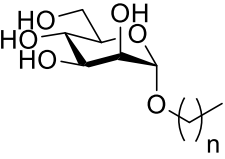
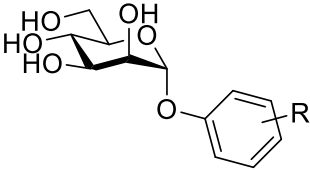
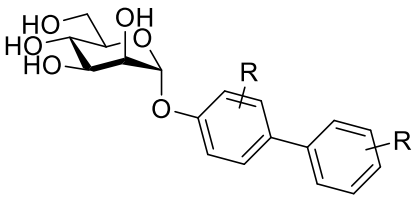
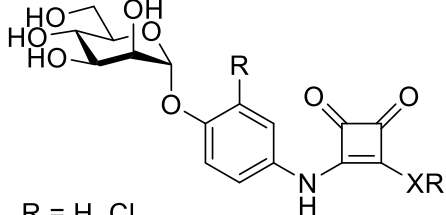
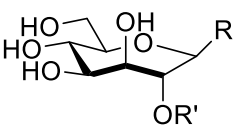


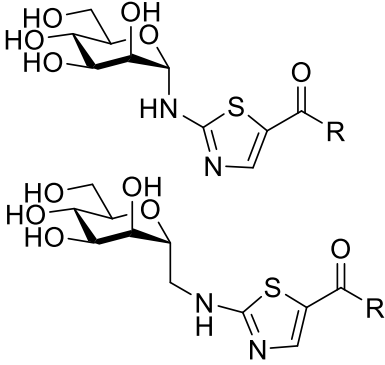
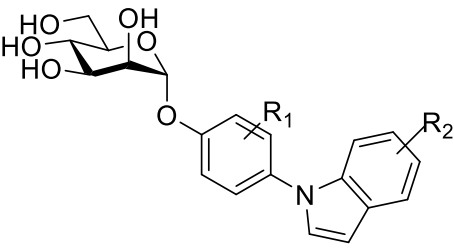
Figure 1-26. Structures of the  $\alpha$ -D-Mannopyranoside based inhibitors, *n*-heptyl  $\alpha$ -D-mannopyranoside **1.22**, biphenyl  $\alpha$ -D-mannopyranoside derivatives **1.26** and **1.27**, indolylphenyl mannose derivative **1.28** and squarate mannoses derivative **1.29**



## Introduction

Table 1. Depicts the different  $\alpha$ -D-mannopyranoside based inhibitors discussed above

Entry	Structure	Reference(s)
1) Alkyl mannosides	 <p style="text-align: center;"><math>n = 0-7</math></p>	87
2) Aryl mannosides	 <p style="text-align: center;"> <math>R = \text{NO}_2, \text{Cl}, \text{CN}, \text{OMe},</math>  <math>\text{CO}_2\text{Me}, \text{NHAc}, \text{CO}_2\text{H},</math>  <math>\text{CO}_2\text{NH}_2, \text{CH}_2\text{CO}_2\text{Me}, \text{ect}</math> </p>	52, 89-91
3) Biphenyl mannosides	 <p style="text-align: center;"> <math>R = \text{CO}_2\text{Me}, \text{CO}_2\text{NHMe},</math>  <math>\text{CF}_3, \text{Cl}, \text{Me}, \text{OMe}, \text{F},</math>  <math>\text{NO}_2, \text{CN}, \text{COMe}</math> </p>	52, 59, 92, 93, 96
4) Squarate mannosides	 <p style="text-align: center;"> <math>R = \text{H}, \text{Cl}</math>  <math>R' = \text{OMe}, \text{OEt}</math>  <math>X = \text{O}, \text{NH}</math> </p>	90, 97
5) Septanoses	 <p style="text-align: center;"> <math>R = \text{H}, \text{OMe}</math>  <math>R' = \text{H}, \text{C}_7\text{H}_{15}</math> </p>	98

6) Thiazolylamino mannosides (TazMan) and Neothiazolylam inomanosides (NeoTazMan)		99, 100
7) Indolynyl- mannosides		101

### 1.1.9 Use of polyvalent mannose scaffolds in FimH

In nature carbohydrate ligand presentation is mainly multivalent,<sup>102</sup> suggesting that the potency of  $\alpha$ -D-mannopyranoside based inhibitors may be limited due to only achieving monovalent targeting. The phenomenon describing how many multivalent ligands display greater affinity than their monovalent counterparts has been termed the “cluster glycoside effect”.<sup>103, 104</sup> Multivalent ligand presentation can increase lectin binding via multiple factors, including receptor clustering and cross-linking.<sup>105</sup> Receptor clustering occurs when monovalent lectins / ligands are anchored to the cell membrane. The presence of a multivalent binding species can capture receptors freely diffusing in the membrane, thus inducing receptor clustering (Figure 1-27). However, this mechanism is unlikely to occur in the bacterial outer membrane (OM) due to the restricted lateral diffusion of OM proteins.<sup>106</sup> Receptor clustering may occur by default in the bacterial OM near sites of beta-barrel transmembrane protein insertion (i.e. BAM complex will mediate insertion of FimD) due to the restricted lateral diffusion. As a consequence, the transmembrane FimD usher protein may already be present at the extracellular surface in clusters.<sup>105</sup> Multivalent ligand presentation can further increase lectin binding through cross-linking. Here, individual ligands on a multivalent species bind to lectins on separate target units, cross-linking them and aggregating bacteria together (Figure 1-27).<sup>105</sup> Due to the complexity of multivalent carbohydrate interactions, it is often an accumulation of multiple factors that cause the “cluster

glycoside effect". In the case of FimH it is likely that multivalent mannose-based ligands bind to multiple different FimH units, resulting in the formation of *E. coli* clusters. Multivalent glycomaterials attached to filters have been used to aggregate *E. coli* and remove it from solution.<sup>107, 108</sup>

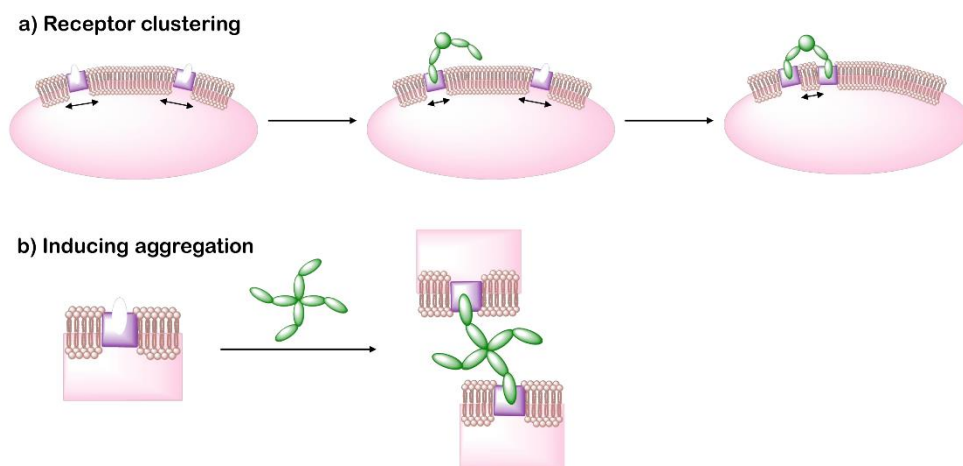


Figure 1-27. Diagram showing two potential mechanisms whereby multivalent ligands can increase apparent binding affinity. **a)** Clustering effect where a multivalent ligand binds to one receptor initially and then captures additional receptors as they diffuse into close proximity resulting in clustering of the ligand-bound receptors. **b)** Induced aggregation whereby multivalent ligands bind to multiple lectins on different bacterial units cross linking them together

There has been substantial research into the development of FimH-targeting polyvalent mannose scaffolds, with applications in the treatment of UPEC-induced UTIs. Multiple different polyvalent mannose scaffolds have been investigated with three of the major ones being multimeric heptylmannosides,<sup>109-113</sup> glycoclusters<sup>114-117</sup> and dendrimers.<sup>118-121</sup>

One of the most researched polyvalent scaffolds are multimeric heptylmannosides (Table 2, page 61); these aim to build upon the high-inhibitory potency displayed by heptyl  $\alpha$ -D-mannoside (HM) (Figure 1-7). Gouin and co-workers synthesized an initial series of multivalent glycoconjugates (Table 2, Entry 1, page 61) based on a 1,1,1-tris(hydroxymethyl)ethane or pentaerythritol core and measured their inhibitory potencies using a HAI-assay and a bladder binding assay (BBA) with human bladder cell line 5637.<sup>109</sup> Both the HAI titre and the BBA data showed a positive correlation between potency and valency.<sup>109</sup> A second multivalent HM glycoconjugates series (Figure 1-28, Table 2, Entry 2, page 61) was designed based on a carbohydrate core, with one heptamannoside analog tethered to a ring-opened  $\beta$ -cyclodextrin.<sup>110</sup> Binding affinity of this series was examined using HAI titre and ITC measurements. As with the previous series, HAI titre measurements showed a positive correlation between valency and potency, with the heptavalent opened  $\beta$ -cyclodextrin glycoconjugate achieving a titre in the nanomolar region (60 nM).<sup>110</sup> Though initial ITC measurements supported this trend, latter measurements varied, likely due to increased calorimetry noise reducing the accuracy of the  $K_d$  measurements.<sup>110</sup> Two further heptavalent  $\beta$ -cyclodextrin-linked HM glycoconjugates (Table 2, Entry

## Introduction

3, page 61) were synthesized using two different spacer lengths. Their biophysical properties were assessed using ITC, extracting  $K_d$  values and molar ratios. Both heptavalent  $\beta$ -cyclodextrin-linked glycoconjugates were significantly more potent than their monovalent counterparts, with  $K_d$  values in the nanomolar range.<sup>111</sup> Reverse titration measurements showed that the use of a shorter spacer unit led to superior potency ( $K_d = 2.9 \text{ nM} \pm 0.03$ ) compared to the use of a longer linker ( $K_d = 33.0 \text{ nM} \pm 6.6$ ), despite only achieving partial binding occupancy (molar ratios =  $3.01 \pm 0.03$  for the short spacer and =  $7.7 \pm 0.06$  for the longer spacer).<sup>111</sup> This suggests potency is not solely dependent on valency. The in vivo properties of both heptavalent  $\beta$ -cyclodextrin-linked glycoconjugates were assessed using a murine cystitis model with C3H/HeN mice. Both heptavalent glycoconjugates were shown to be 100 times more potent than their monovalent counterparts.<sup>111</sup>

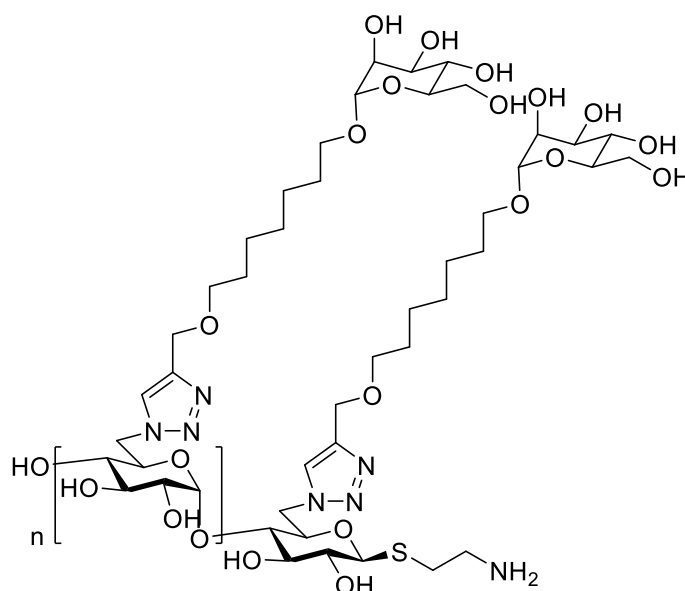
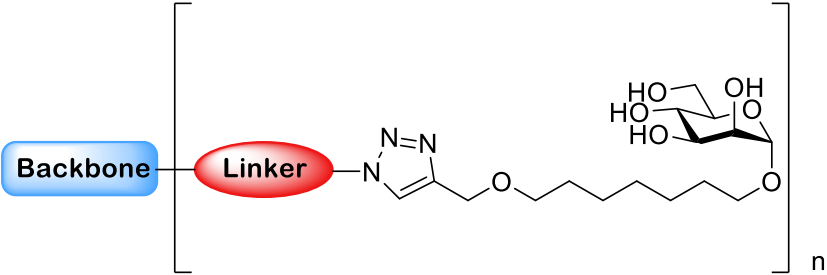
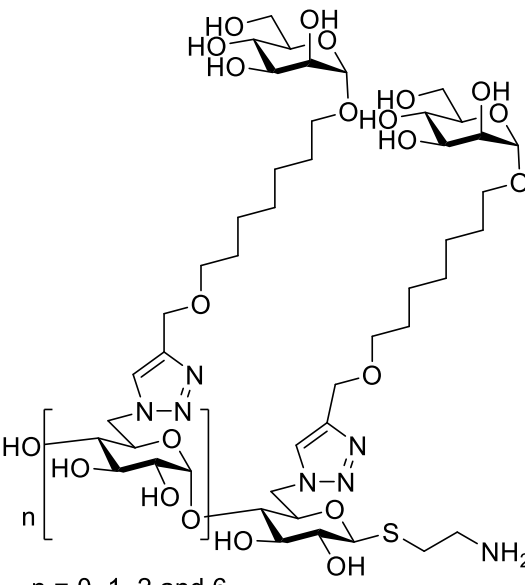
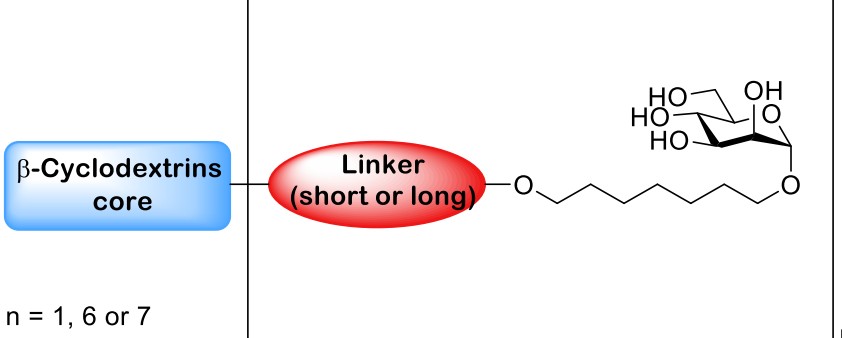


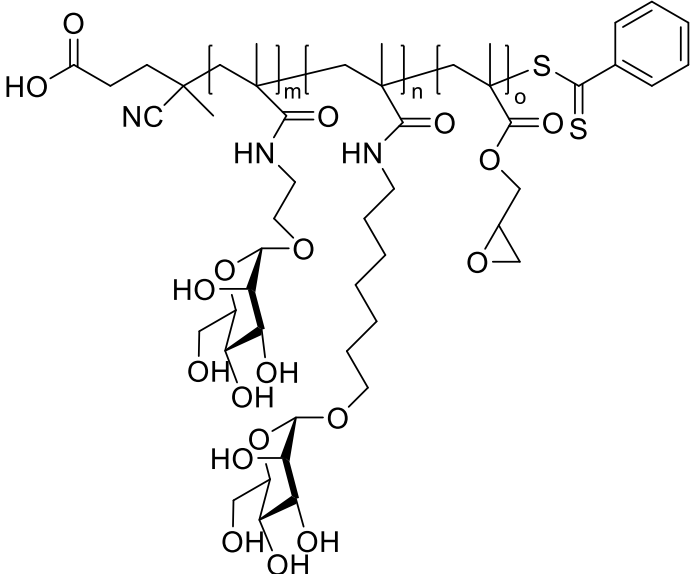
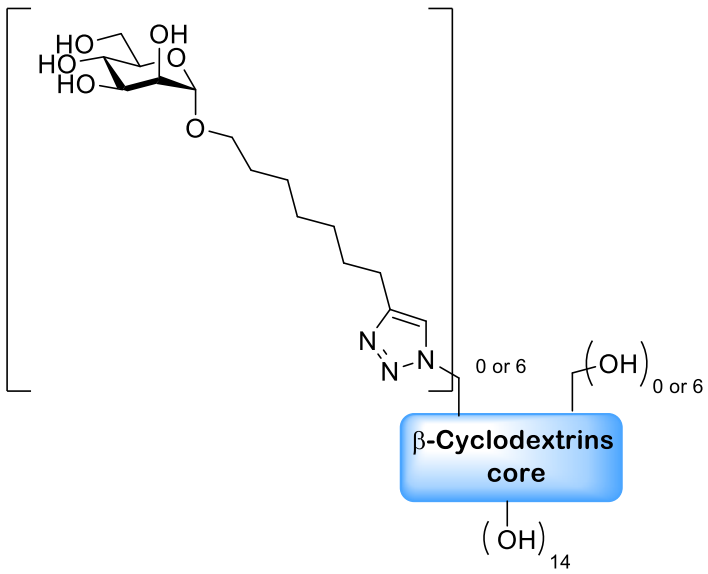
Figure 1-28. Structure of multivalent HM glycoconjugates series designed upon using a carbohydrate core where  $n=0, 1, 2$  and 6 (when using  $\beta$ -cyclodextrin core)

Further work into development of a multivalent heptylmannoside has investigated the design and use of glyconanoparticles<sup>113</sup> (Table 2, Entry 4, page 61) and multimeric heptyl-mannosides<sup>112</sup> (Table 2, Entry 5, page 61) in targeting adherent invasive *Escherichia coli* (AIEC), a bacterial strain present in the ileal lesion of Crohn's disease patients.<sup>112</sup>

## Introduction

Table 2. Summary of the multivalent heptamannoside structure discussed

Entry	Core unit	Reference
1)	 <p style="text-align: center;"><math>n = 1 - 4</math></p>	109
2)	 <p style="text-align: center;"><math>n = 0, 1, 2 \text{ and } 6</math></p>	110
3)	 <p style="text-align: center;"><math>n = 1, 6 \text{ or } 7</math></p>	111

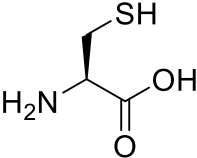
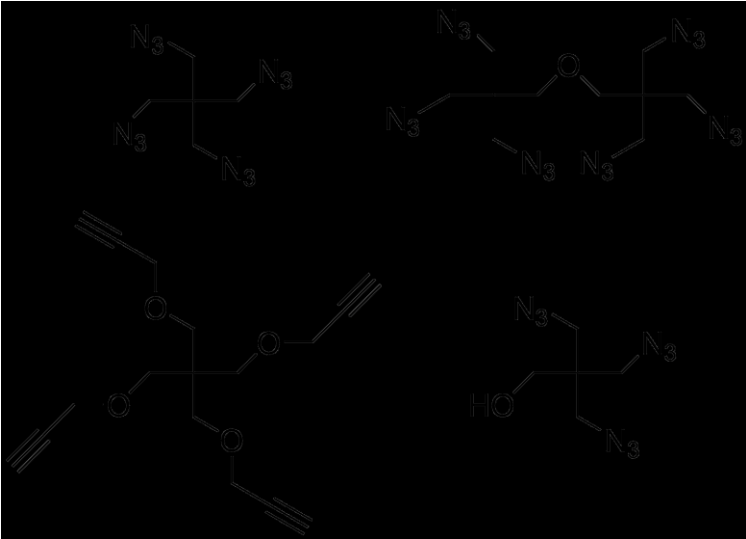
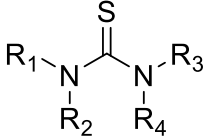
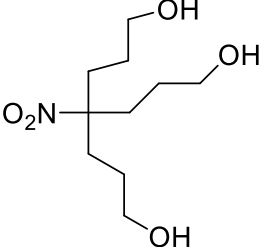
4)	 <p style="text-align: center;"><b>Core structure prior to polymerization-induced self assembly</b></p>	113
5)	 <p style="text-align: center;"><b>β-Cyclodextrins core</b></p>	112

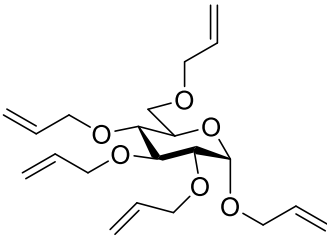
Mannose-based glycoclusters are a further polyvalent mannose scaffold that has been investigated. Multiple different glycocluster series have been synthesized using a variety of different backbone scaffolds (Table 3); e.g. cysteine residues (Table 3, Entry 1),<sup>114</sup> functionalized pentaerythritol (Table 3, Entry 2),<sup>115</sup> thiourea-bridged clusters (Table 3, Entry 3),<sup>116,122</sup> peptide-bridged clusters (Table 3, Entry 4)<sup>122</sup> and carbohydrate centred clusters (Table 3, Entry 5).<sup>117</sup> The *in vitro* efficacy of different glycocluster series have been assessed using a variety of methods; e.g. IC<sub>50</sub> measurements, inhibition

## Introduction

of baker's yeast agglutination assay, HAI titre, and ELISA. Generally, a positive correlation between potency and valency was observed. However, other factors such as scaffolds structure (e.g. inclusion of a phenyl unit in the scaffold) were shown to significantly contribute to potency.

*Table 3. Summary of the organic scaffold used in the synthesis of mannose-based glycoclusters*

Entry	Organic scaffold	Structure	Reference
1	Cysteine		114
2	Azide or alkyne bearing pentaerythritols		115
3	Thiourea-bridged clusters		116, 122
4	Peptide-bridged clusters		122

5	Carbohydrate centred cluster		117
---	------------------------------	--	-----

Investigations have also focused on the synthesis of a mannose-bearing dendrimer.<sup>118-121</sup> Roy and co-workers synthesized multiple series of mannose-bearing dendrimers using different scaffolds. One scaffold of particular note was the  $\alpha$ -amino-L-lysine scaffold, from which they synthesized a dendrimer containing 16 mannose units with a potency 500 times greater than methyl mannose (HAI titre = 1.0  $\mu$ M vs 500  $\mu$ M).<sup>119</sup>

Diamond nanoparticles can also serve as a polyvalent mannose scaffold. Mannose-functionalized diamond nanoparticles were originally applied to the detection and removal of *E. coli* from bacteria-polluted water.<sup>108</sup> More recently mannose-functionalized diamond nanoparticles have been demonstrated to be potent *E. coli* anti-adhesives, displaying impressive potency in a bladder cell adhesion assay (RIP = 9259 vs 1 for methyl mannose)<sup>123</sup> as well as reducing *E. coli* biofilm formation.<sup>123</sup>

A final scaffold discussed here is fullerenes. Copper-catalysed click chemistry was used to functionalize fullerenes with mannose moieties,<sup>124</sup> yielding three fullerene analogs bearing 12 mannoside units.<sup>125</sup> ITC and SPR showed these polyvalent analogs to be capable of multivalent binding and found that both polyvalent and monovalent analogs displayed a  $K_d$  in the nanomolar range.<sup>125</sup> A further HAI-assay was performed which found the polymeric fullerenes to be between 2.8-30 times more potent than their monomeric counterparts.

Other polyvalent mannose scaffolds reported include glycopeptides,<sup>121, 126</sup> polyvalent nanoparticles<sup>127</sup> and pillar[5]arene derivative.<sup>128</sup> Research into these scaffolds is in its infancy but initial *in vitro* investigations appear promising.

Oral administration is the preferred route for drug administration, and as such the applications of any analogue which cannot be orally administered are limited. Due to their large structure and high hydrogen bond donor and acceptor content, polyvalent mannosides are unlikely to be orally absorbed. This could severely limit their applications in the treatment of UTIs but also makes them potentially powerful candidates in the treatment of AIEC-induced Crohn's disease.<sup>113 112</sup> Indeed clinical trials are currently being performed on the use of multivalent inhibitor Sibofimloc (TAK-018/EB8018) in the treatment of Crohn's disease.<sup>129 130</sup>



## 1.2 Section B

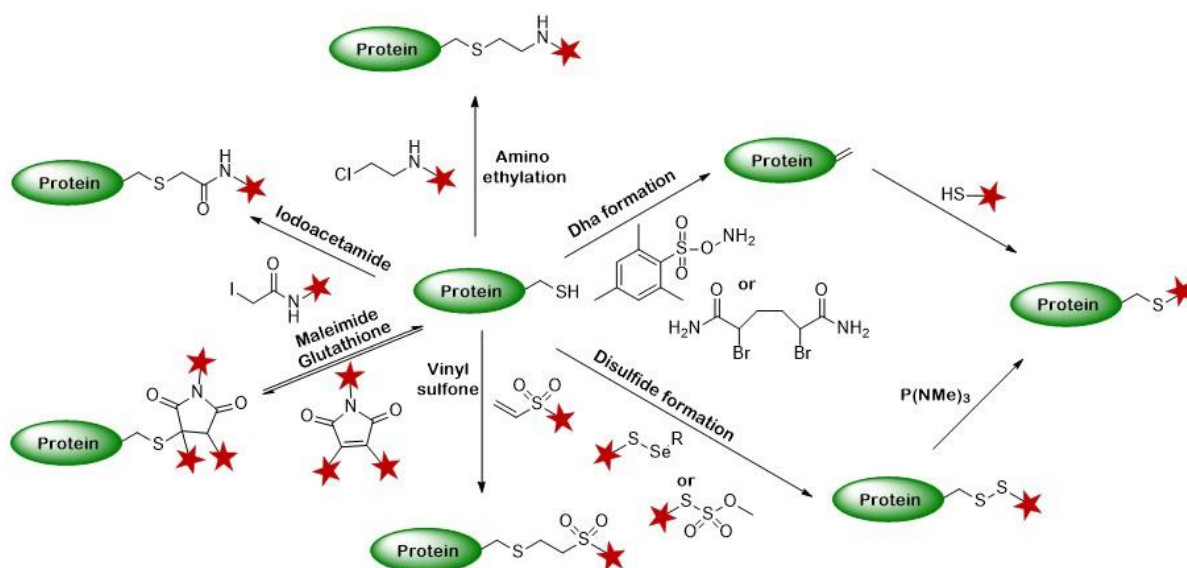
### 1.2.1 Protein bio-conjugation methodologies

Bio-conjugation of proteins to other macromolecules or small molecules is a vital tool that enables biological processes and interactions to be studied,<sup>131</sup> and allows pharmaceutical agents such as antibody drug conjugates (ADCs) to be developed.<sup>132</sup> A number of different site-selective protein bio-conjugation methods have been developed,<sup>133-139</sup> and some of the most widely utilised are discussed below.

#### 1.2.1.1 Canonical amino acid based protein bio-conjugation methodologies

Canonical amino acid-based protein ligation methodologies refer to protein bio-conjugation methods which target naturally encoded amino acids, such as cysteine and lysine residues. As many proteins may contain several of these amino acids in a surface-exposed position, these methods are often non site-specific.

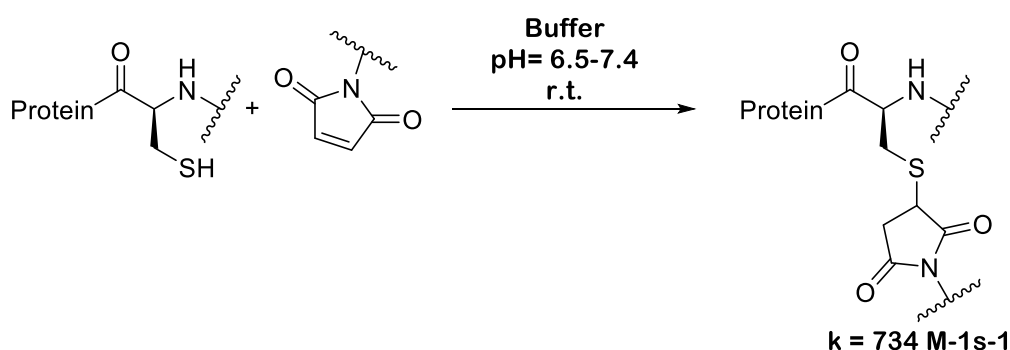
Cysteine residues are highly popular in canonical amino acid targeting, and there are multiple advantages for targeting cysteine residues. Of all the 20 canonical amino acids cysteine is the most robustly nucleophilic with its thiol moiety offering a unique reactive handle.<sup>140</sup> The high reactivity of the thiol group allows cysteine to participate in numerous different bio-conjugation methods, forming conjugates connected by either a  $S_{\text{protein}}-C$  or  $S_{\text{protein}}-S$  bond (Scheme 1-5).<sup>140</sup> A further advantage of targeting cysteine residues is their low abundance (< 2%)<sup>140, 141</sup> in proteins allows for potential single site targeting.



Scheme 1-5. Potential bio-conjugation reactions which can be performed on cysteine residues.  $S_{\text{protein}}-C$  bond formation reactions include aminoethylation (buffer pH 8.9, 25 °C, 24 h),<sup>142</sup> treatment with iodoacetamide (buffer pH 8.2, r.t., 30 minutes),<sup>143</sup> maleimide ligation (buffer pH = 6.5 – 7.4, r.t.) and vinyl sulfone ligation (buffer pH = 8.5, r.t., 24 h).<sup>144</sup>  $S_{\text{protein}}-S$  bond formation reactions include Dha formation (for formation methods see<sup>145</sup>), disulfide formation and desulfurization of disulfides ( $P(NMe)_3$  2 eq, buffer, pH = 9.5, r.t., 12 h)<sup>146</sup>

## Introduction

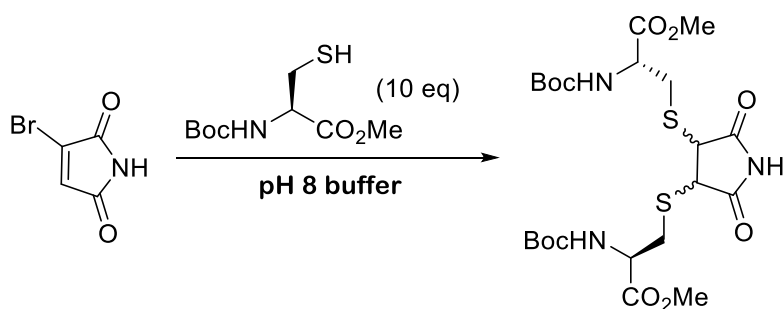
Maleimide ligation (Scheme 1-6) is one of the most popular site-selective bio-conjugation methods.<sup>147</sup> The success of maleimide ligations is largely due to their fast reaction times ( $k = 734 \text{ M}^{-1} \text{ s}^{-1}$ )<sup>148</sup> and wide availability of maleimide-functionalised linkers and probes. All these factors have allowed maleimide ligation to be employed for protein bio-conjugations in the pharmaceutical industry; specifically for the assembly of antibody drug conjugates, such as Trastuzumab emtansine, Brentuximab vedotin and Vadastuximab talirine.<sup>149</sup> Further applications of maleimide ligation are the development of a vaccine candidate for B cell lymphoma,<sup>150</sup> labelling proteins or peptides with fluorophores<sup>151</sup> for further use in assays or microscopy, synthesis of a peptide glycoconjugate with applications as a targeted potent HIV inhibitor<sup>152</sup> and the formation of protein-protein conjugates.<sup>153</sup>



*Scheme 1-6. Reaction scheme for maleimide ligation including reaction conditions<sup>154</sup> and kinetic information<sup>148</sup>*

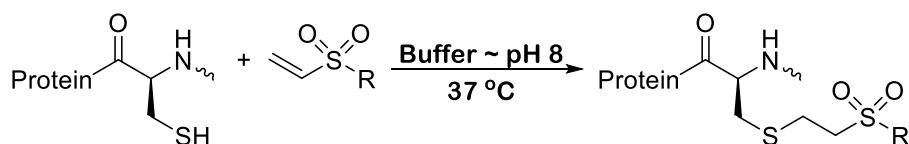
Though the products of maleimide ligations are often considered stable, it has been suggested that competing thiols could cause reversal via initial retro-Michael reactions.<sup>155</sup> Additionally, maleimide adducts can undergo hydrolysis leading to further decomposition of protein conjugates.<sup>155, 156</sup> More recently some bio-conjugation experiments have focused on the use of bromomaleimides. Bromomaleimides offer a method for making reversible conjugates, as they react rapidly and selectively with cysteine residues, yet upon treatment with TCEP the free cysteine can be regenerated. Furthermore, treatment of the thiomaleimides product with a base in methanol affords dehydroalanine; this reversibility is potentially important as in some conjugation reactions only temporary tethering is required.<sup>157</sup> A further advantage of using bromomaleimides is they allow dual modification (Scheme 1-7); an initial reaction with a cysteine residue displaces the bromine via nucleophilic substitution and a reaction with a second cysteine can then occur via Michael addition.<sup>158</sup>

## Introduction



Scheme 1-7. Reaction scheme for dual modification of a bromomaleimide

Vinyl sulfones<sup>137</sup> are an alternative Michael acceptor that can be selectively reacted with cysteine residues<sup>159</sup> (Scheme 1-8). At present vinyl sulfones are less widely used than maleimides due to their higher reactivity towards hydroxyl groups,<sup>160</sup> making off-target reactions more likely.

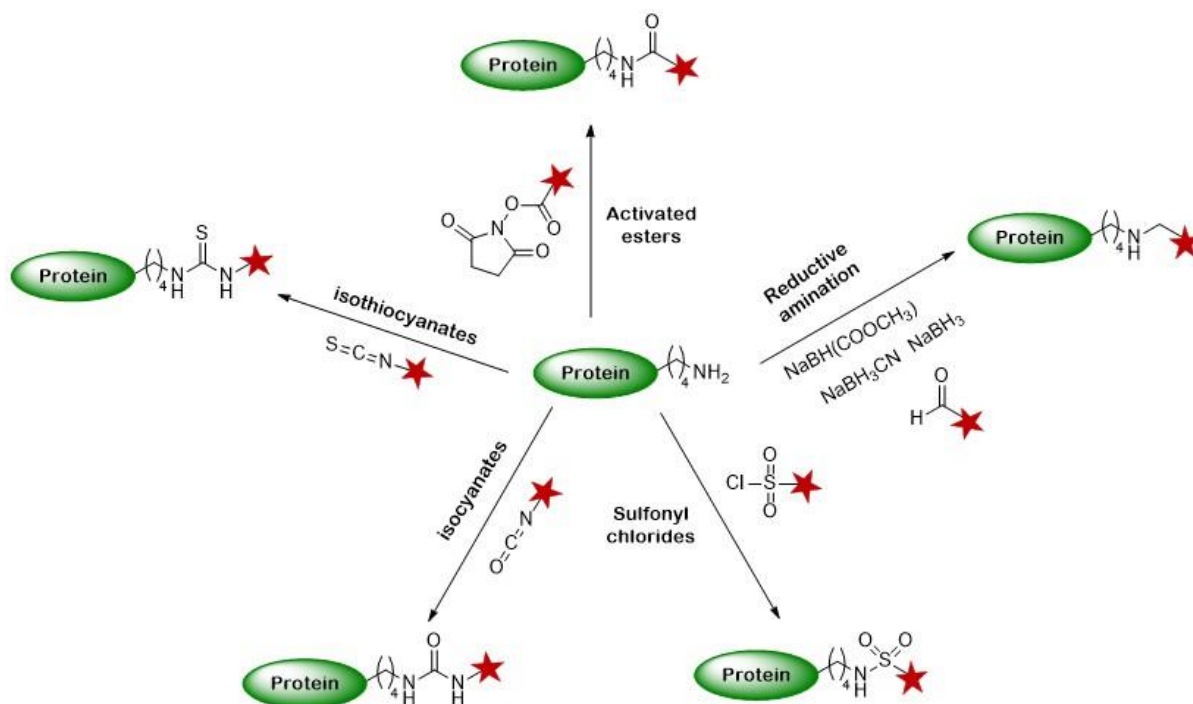


Scheme 1-8. Reaction scheme for vinyl sulfone mediated ligation. Displaying the reaction conditions used to conjugate rhodamine dye (R) to concanavalin A (protein)<sup>148</sup>

There are limitations associated with targeting cysteine residues. Firstly, the introduction of additional cysteine residues into proteins can result in intramolecular disulfide bond formation and protein misfolding. Furthermore, free cysteine residues can undergo promiscuous side reactions with co-factors such as metal ions. A final complication associated with protein cysteine mutants is that the introduction of a free cysteine residue can often lead to intermolecular disulfide bond formation, resulting in protein dimers which cannot undergo conjugation reactions; cysteine mutants thus require treatment with a reducing agent prior to conjugation.

Another canonical amino acid which is heavily targeted in bio-conjugation reactions is lysine, as a wide variety of different reactions can utilise the nucleophilic primary amine lysines present (Scheme 1-9).<sup>161</sup> Lysine residues are more prevalent than cysteine residues<sup>161</sup> and as such bio-conjugation methods targeting lysine residues are rarely site-selective. However, bio-conjugation methods targeting lysine residues have found a niche in the synthesis of conjugates where multiple conjugations are beneficial (*e.g.* glycoconjugate vaccines formulation).<sup>162-164</sup>

## Introduction



Scheme 1-9. Potential bio-conjugation reactions which can be performed on lysine residues, including the use of activated esters (buffer, pH 7.2 – 9, r.t., 30 minutes), isothiocyanates, isocyanates, sulfonyl chlorides (pH 8.0, r.t. – 37 °C, 1-2 h),<sup>165</sup> and reductive amination (buffer, pH 6.5 – 8.5<sup>166</sup> r.t.) reactions

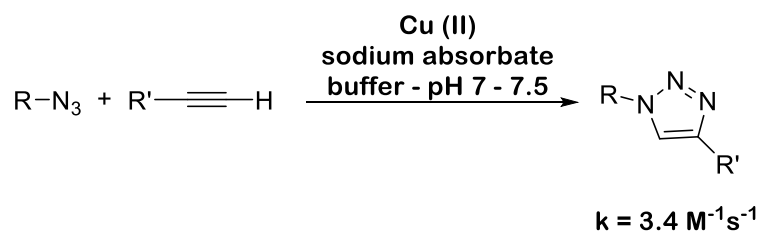
### 1.2.1.2 Non-canonical protein bio-conjugation methodologies

The major limitation of using canonical amino acids during bio-conjugations is the lack of site-selective. To overcome this limitation a number of site-specific bio-conjugation methodologies have been designed, relying on the installation of a unique functionality into the protein. The three most commonly installed functionalities are azides, alkynes and aldehydes. These functionalities can either be installed using unnatural amino acid (UAA) mutagenesis or via chemical or enzymatic treatment of the existing amino acid residues. It is not the purpose of this work to review UAA mutagenesis but previously published reviews are available.<sup>140, 167</sup>

Bio-conjugation methodologies which rely on an azide or alkyne moiety proceed via a cycloaddition reaction pathway. Here two or more unsaturated moieties combine to form a cyclic adduct in which there is a net reduction of the bond multiplicity. Most organic chemists are familiar with the Diels-Alder reaction between a conjugated diene and a substituted dienophile.<sup>168</sup> The two most well-studied cycloaddition-based bio-conjugation methods are azide-alkyne ligation<sup>133, 134</sup> and tetrazine ligation.<sup>136</sup> Both these ligations are classified as “click” chemistries due to their simplicity, speed, high reactant and product versatility, regioselectivity and high yield.<sup>169, 170</sup> Azide-alkyne ligation has been widely used within the literature since 2002, when both Sharpless and co-workers<sup>133</sup> and Meldal and co-workers<sup>134</sup> independently introduced the copper-catalysed azide-alkyne cycloadditions (CuAAC) (Scheme 1-10). CuAAC have been successfully used to label both proteins<sup>171</sup> and live cells,<sup>172</sup> and have been used in the formation of pharmaceutical analogues.<sup>173</sup> However, the use of Cu-

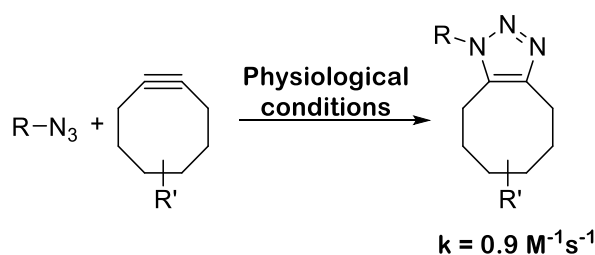
## Introduction

catalysed azide-alkyne ligations is limited, as Cu (I) is readily oxidised to Cu (II) in solution. For this reason, Cu (I) is often generated *in situ*, using a Cu (II) source and an excess of reducing agent, such as sodium ascorbate<sup>174</sup> or hydrazine.<sup>175</sup> The combination of Cu (I) and sodium ascorbate can lead to the generation of reactive oxygen species, which can further react with other chemical species to have a detrimental effect on experimental results.<sup>174</sup> This potential for side reactions, coupled with the high toxicity of Cu towards cells,<sup>176</sup> limits the experimental use of the Cu-catalysed azide-alkyne ligation, especially in cell-based assay experiments and protein ligations performed within living cells.



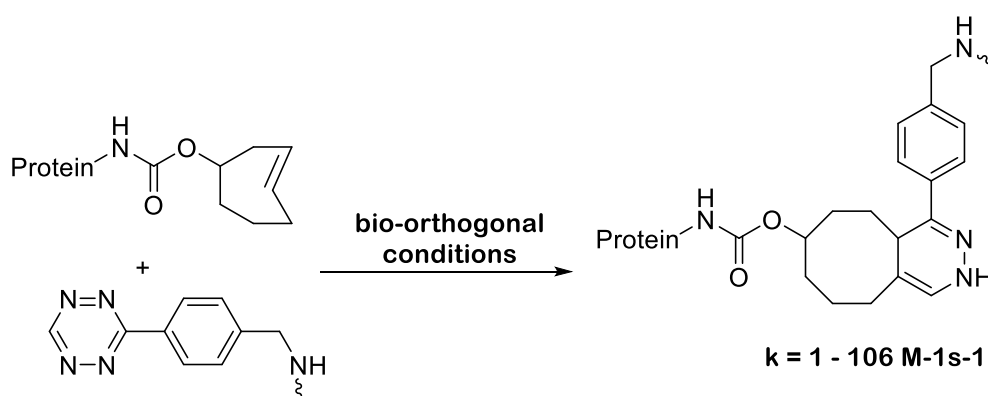
*Scheme 1-10. Reaction scheme for CuAAC including reaction conditions and kinetics<sup>148</sup>*

In 2004 Bertozzi and co-workers introduced the strain-promoted azide/alkyne cycloaddition (SPAAC)<sup>135</sup> (Scheme 1-11). The replacement of an unstrained alkyne with a strained cyclooctyne removed the need for a Cu catalyst, as the cyclic strain of the cyclooctyne accelerates the uncatalysed reaction with the azide. Since their introduction SPAAC ligations have proved to have many applications within chemical biology. One example is the development of an antibody-free western blot analysis method,<sup>177</sup> using an azide functionalised protein which is further coupled to an azadibenzocyclooctyne containing fluorescent probe.<sup>177</sup> Furthermore, SPAAC has been used to develop a new methodology for the synthesis of covalent protein-oligonucleotide conjugates.<sup>178</sup>



*Scheme 1-11. Reaction scheme for SPAAC including kinetic parameters<sup>148</sup>*

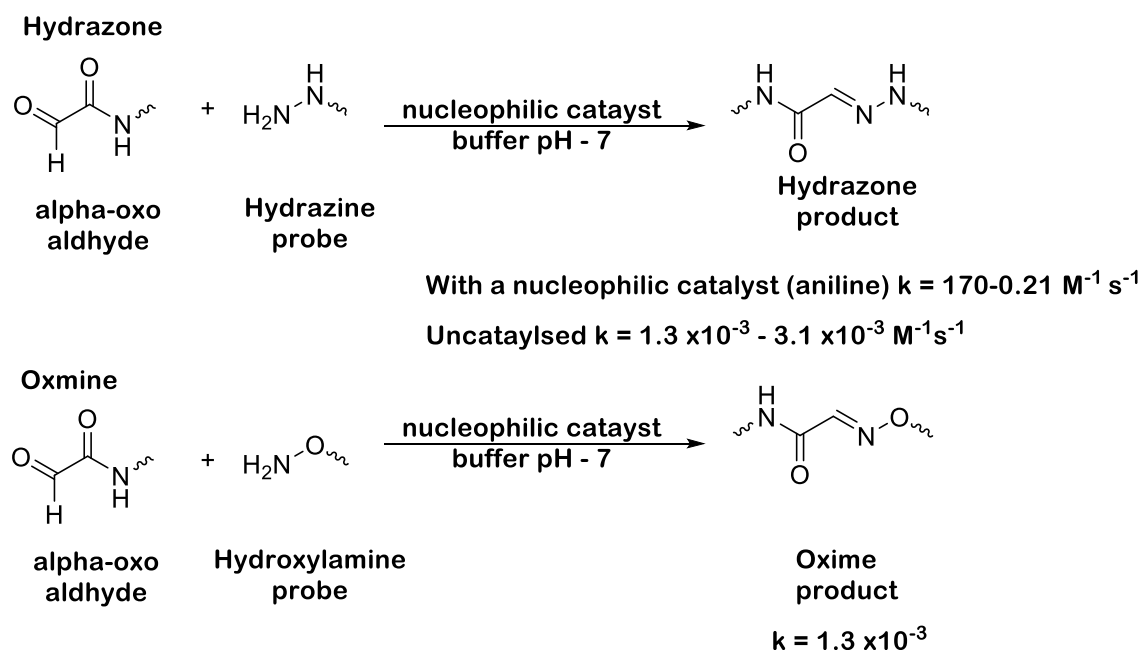
The increasingly popular tetrazine ligation to a strained alkene, such as a trans-cyclooctene derivative with a reactive tetrazine moiety, is an example of an inverse electron-demand Diels-Alder reaction (Scheme 1-12), which is followed by a retro [4+2] cycloaddition.<sup>136</sup> The tolerance of this reaction to a broad range of substrate functionalities and bio-orthogonal conditions, (such as water and cell media)<sup>136</sup> has meant tetrazine ligations have found numerous applications, in both chemical and cell biology. Tetrazine ligation has been successfully used to synthesise radiolabelled-F<sup>18</sup> conjugates which can be used in PET scan imaging of intraportally transplanted islet cells.<sup>179</sup> Tetrazine ligation has further been used in *in vitro* labelling experiments, Hilderbrand and co-workers<sup>180</sup> showed that the addition of a tetrazine conjugated fluorochrome could label pre-targeted antibodies both selectively and rapidly.<sup>180</sup> These examples showcase just a few of the applications of tetrazine ligation; further applications can be seen in a review paper on the subject.<sup>181</sup>



Scheme 1-12. Reaction scheme for the tetrazine ligation including kinetic parameters<sup>182</sup>

Hydrazone/oxime ligations (Scheme 1-13) involve the reaction of either a hydrazine or hydroxylamine/aminooxy reagent with an aldehyde to form either a hydrazone or oxime linkage.<sup>138</sup> Due to the ease of aldehyde-installation into proteins,<sup>138</sup> hydrazone/oxime ligations have also been applied to the conjugation of proteins to fluorescent probes.<sup>183-186</sup> Oxime ligations have been further showcased in the conjugation of carbohydrates to proteins, using proteins bearing a site-specifically installed formylglycine residue and complex aminoxy glycans.<sup>187, 188</sup> Oxime ligation has been further used to synthesise a nanobody conjugate which can selectively destroy HER2-positive breast cancer cells.<sup>189</sup> Although hydrazine or hydroxylamine functionalised probes are easy to synthesise, the C=N bond formed between protein and substrate via hydrazone/oxime ligation is susceptible to hydrolytic cleavage over time,<sup>190</sup> limiting the long term stability of the protein-conjugate. A further drawback of hydrazone/oxime ligation is that optimal reaction pH for both is pH 4.5,<sup>191</sup> which many proteins cannot tolerate without some denaturation occurring. The use of nucleophilic catalysts such as aniline can

overcome this problem however, allowing many proteins to undergo hydrazone/oxime ligation at neutral pH,<sup>191</sup> but even in these cases the concentrations of nucleophilic catalyst needed - often as much as 100 mM for oxime ligation<sup>192</sup> - can be toxic to live cells.<sup>192</sup>

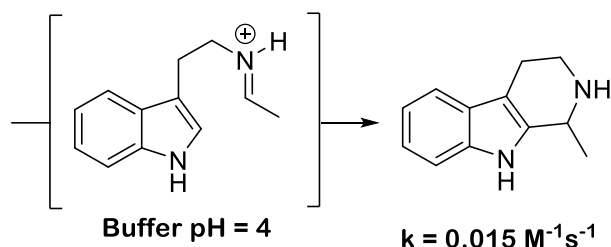
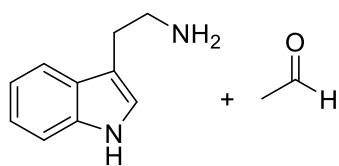


Scheme 1-13. Reaction scheme for hydrazone / oxime ligation including kinetic parameters for both hydrazone (with and without the nucleophilic catalyst aniline)<sup>138</sup> and oxime ligation<sup>148</sup>

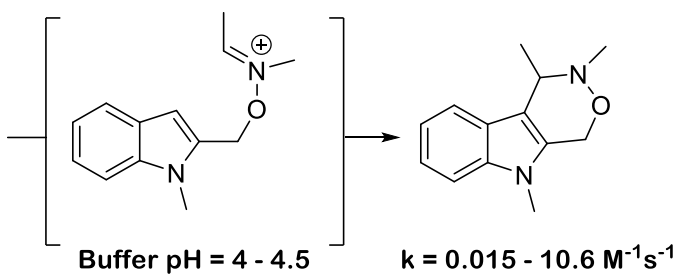
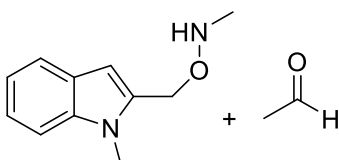
A further ligation methodology that targets protein aldehydes is the Pictet-Spengler reaction (Scheme 1-14a). This is the cyclisation reaction between tryptamines and aldehydes, following initial iminium formation with subsequent intramolecular cyclisation.<sup>138</sup> A variation of this reaction with improved kinetic performance is the iso-Pictet-Spengler reaction (Scheme 1-14b). Both the Pictet-Spengler and iso-Pictet-Spengler reaction result in the formation of a C-C bond between protein and substrate,<sup>193</sup> an attractive prospect in bio-orthogonal chemistry due to their anticipated greater stability under bio-orthogonal conditions. The iso-Pictet-spengler reaction has been successfully used to ligate PEGylated, biotinylated and fluorescent probes to glyoxyl-myoglobin, fGly-tagged maltose binding protein (MBP) and fGly-tagged Herceptin antibodies.<sup>193</sup> However, the applications of both the Pictet-Spengler and iso-Pictet-Spengler reaction are limited by the low reaction pH needed (e.g. pH 4)<sup>193</sup> and slow rate of reaction.

## Introduction

### a) Pictet-Spengler



### b) iso-Pictet-Spengler

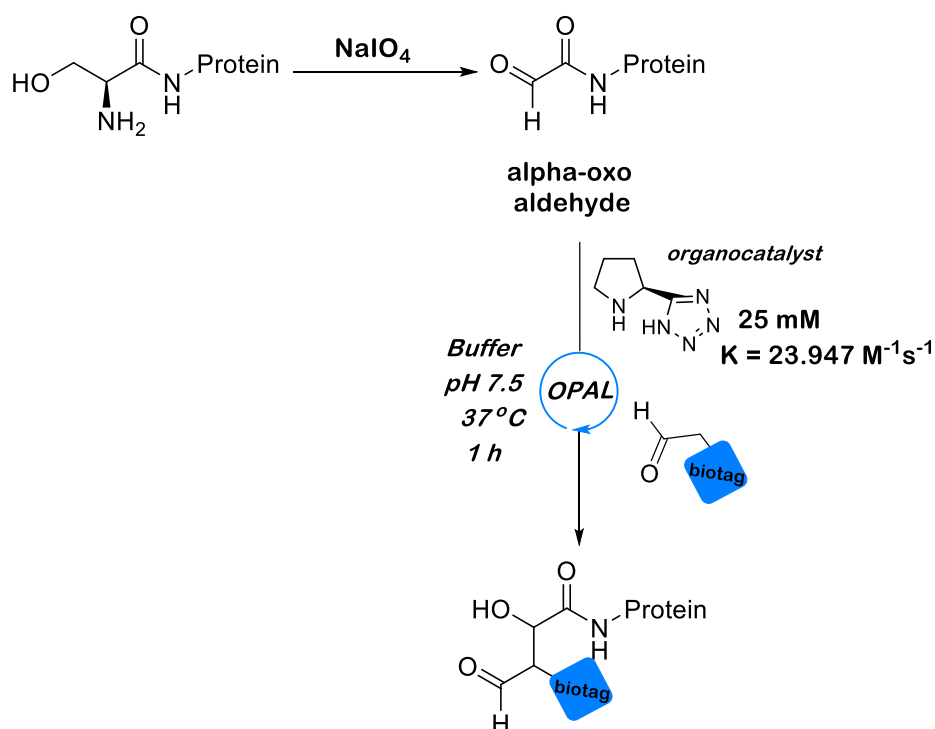


Scheme 1-14. Reaction scheme and kinetic parameters for the a) Pictet-Spengler<sup>148</sup> and b) iso-Pictet-Spengler<sup>138</sup>

A recently developed protein bio-conjugation method which also targets protein aldehydes is the organocatalyst-mediated protein cross-aldol ligation (OPAL), developed by Fascione and co-workers.<sup>139</sup> The OPAL ligation requires the presence of an  $\alpha$ -oxo aldehyde within the protein, which can readily be installed at the *N*-terminus by sodium periodate oxidation of the *N*-terminal serine or threonine residues, or via transamination of *N*-terminal glycine residues via pyridoxal 5-phosphate-mediated transamination (Scheme 1-15).<sup>139</sup> The installed  $\alpha$ -oxo aldehyde is then functionalised with an enolisable aldehyde containing OPAL probe and a proline-type catalyst, resulting in site-specific bio-conjugation via aldol condensation.<sup>139</sup>

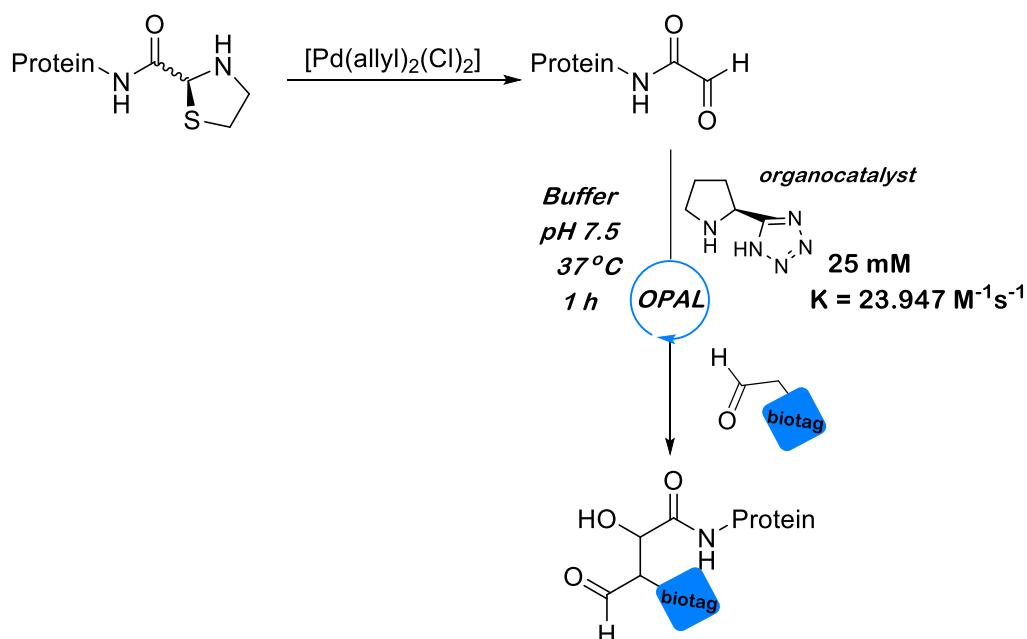


## Introduction



Scheme 1-15. Reaction scheme for OPAL ligation. Biotag = biotin, folate, azide or dansyl

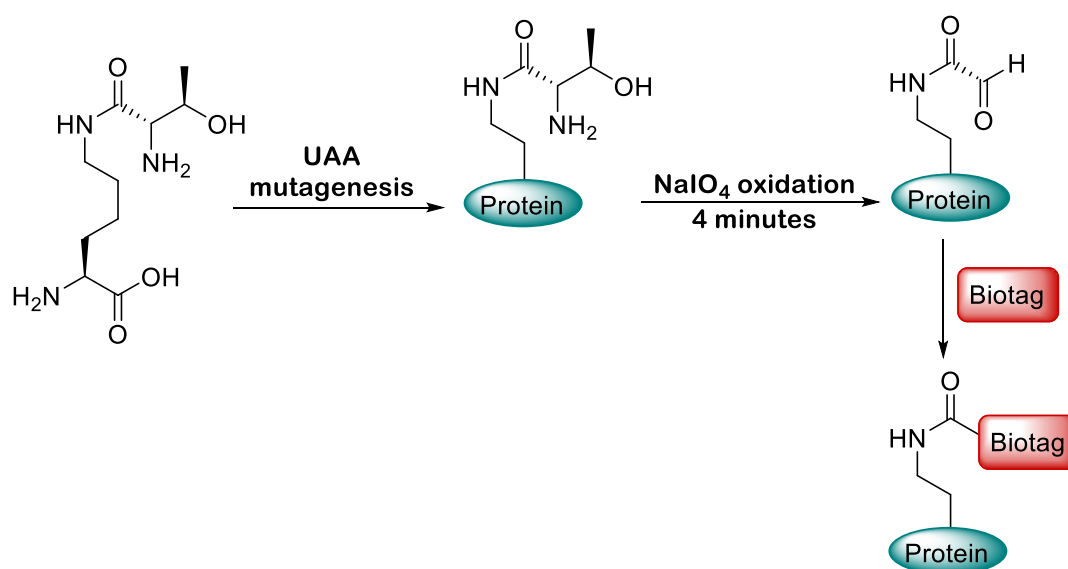
A potential limitation of OPAL ligation was that installation of an  $\alpha$ -oxo aldehyde was previously limited to the *N*-terminus.<sup>139</sup> However, the development of a palladium decaging<sup>194</sup> stratagem which involves the installation of a thiazolidine ring functionalised unnatural amino acid into the target protein, which can later be treated with palladium to reveal an  $\alpha$ -oxo aldehyde, has enabled OPAL ligation to also be performed at internal sites within proteins (Scheme 1-16).



Scheme 1-16. Reaction scheme for palladium decaging. Biotag = biotin, folate, azide and dansyl

## Introduction

More recently Fascione and co-workers introduced a new way of installing non-terminal  $\alpha$ -oxo aldehydes, using a threonine-lysine dipeptide which can again be introduced to a protein by UAA mutagenesis.<sup>195</sup> The threonine residue acts as a masked  $\alpha$ -oxo aldehyde which can be revealed upon  $\text{NaIO}_4$  oxidation. The  $\alpha$ -oxo aldehydes introduced by this method were further targeted by Strain-Promoted Alkyne-Nitrone Cycloaddition (SPANC) ligation with biotin and dansyl charged bicyclononyne (BCN) probes (Scheme 1-17).<sup>195</sup>



*Scheme 1-17. Reaction scheme for threonine-lysine dipeptide installation, oxidation and conjugation. Here biotag = biotin or dansyl*

Akin to the Pictet and iso-Pictet-Spengler ligations, the OPAL results in the formation of a stable C-C bond between protein and substrate. However, OPAL has superior kinetics and is far milder, occurring within 1 h at neutral pH.<sup>139</sup> As such the OPAL is more versatile than iso-Pictet-Spengler ligation. A further advantage of the OPAL over the aforementioned stratagems lies in the ability to perform a secondary ligation to the aldehyde species that is regenerated following the first aldol reaction.<sup>139</sup> Whereas performing dual modification on a protein has historically required the use of different bio-conjugation methods (e.g. oxime ligation and azide-cyclooctyne click ligation),<sup>196</sup> only a single  $\alpha$ -oxo aldehyde need be introduced if OPAL is to be used. This versatility has already been demonstrated via the successful ligation of azide, biotinylated, fluorescent and folate probes to multiple protein species, such as thioredoxin, myoglobin and green fluorescent protein (GFP).<sup>139</sup>

### 1.2.2 Protein and peptide glycoconjugate constructs

A major application of protein bio-conjugation is the construction of protein glycoconjugates. Protein glycoconjugates have been widely used in vaccine formulation, due to their cost-efficiency and ability to be produced in large quantities.<sup>197</sup>

Protein glycoconjugate vaccines were designed to overcome the issues displayed by purified polysaccharide vaccines. Purified polysaccharide vaccines against meningococcus and pneumococcus were developed in the 1970s.<sup>197</sup> Though these vaccines were shown to be partially immunogenic in adults they did not elicit an antibody response in children,<sup>197</sup> the vaccines target population, while it had previously been reported in 1929 that conjugation of a bacterial capsular polysaccharide to a carrier protein significantly increased the immunogenic response of the polysaccharide.<sup>198, 199</sup>

The difference in immune response between protein glycoconjugate vaccines and purified polysaccharide vaccines can be explained by the way the different structures interact with the immune system. Following immunization both vaccine types are taken up by the dendritic cells and transported to the lymph nodes.<sup>200</sup> Once at the lymph nodes the vaccine must interact with both B and T cells to stimulate the formation of germinal centres (GCs). These are sites within the lymph node and spleen where B cells proliferate, differentiate and mutate their antibody genes using somatic hypermutation.<sup>200</sup> Three main cells are required for GC formation; polysaccharide specific B-cells (which express the antibody on their surface as a receptor), follicular helper T-cells ( $T_{FH}$ , which recognise the protein carrier antigen presented on the surface of B-cells) and follicular dendritic cells (FDCs which contain and present the antigen to the B cells). The survival of B-cells located in GCs are reliant on their engagement with T-cells.<sup>200</sup>

Purified polysaccharides can bind to specific antibodies located on the surface of B-cells, however the polysaccharides do not fit into the major histocompatibility complex (MHC) cavity, preventing interactions between the B-cell and the  $T_{FH}$ -cells, inducing B-cell apoptosis (Figure 1-29a).<sup>197</sup> While protein glycoconjugates within vaccines also bind to specific B-cell antibodies via their polysaccharide units, their protein units can also be processed by B-cells to reveal a peptide which is recognised by the MHC cavity and displayed on the B-cell surface, promoting T-cell engagement and stimulating a GC reaction; this leads to the production of polysaccharide-specific antibodies and memory B-cells (Figure 1-29b).<sup>197</sup>

## Introduction

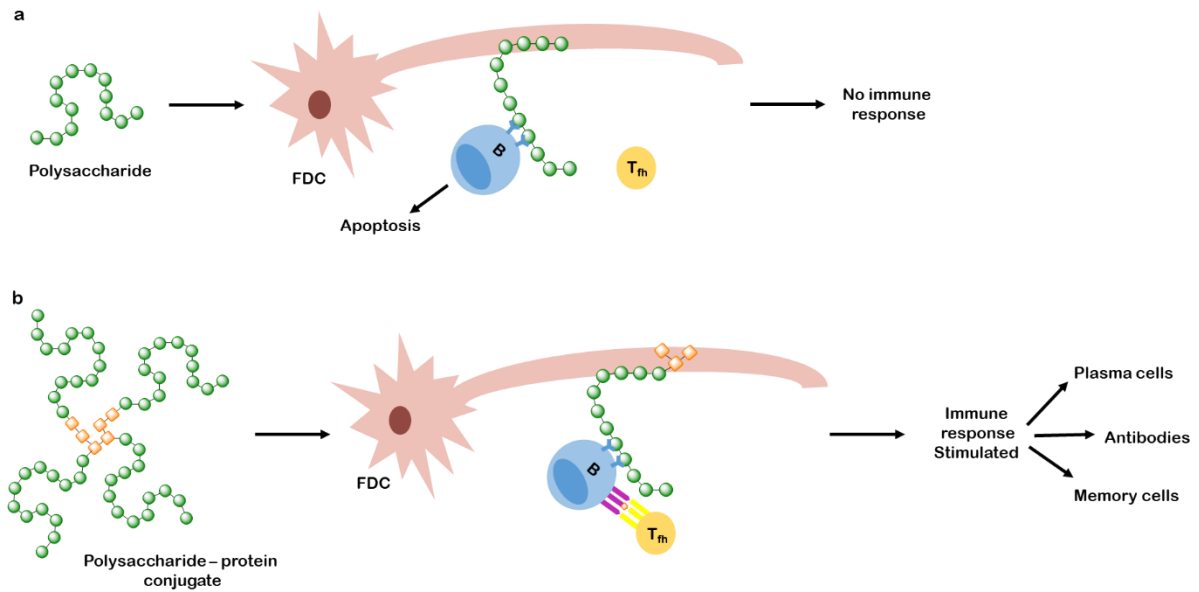


Figure 1-29. **a)** The immune response induced by polysaccharide-based vaccines, **b)** The immune response induced by protein glycoconjugate vaccines.

Protein glycoconjugate vaccines have been developed against a number of different diseases/pathogens such as *Mycobacterium tuberculosis*,<sup>201</sup> *Klebsiella pneumoniae*,<sup>202</sup> Meningitis,<sup>162, 203-205</sup> invasive nontyphoidal *Salmonella* (iNTS),<sup>163, 164, 206-208</sup> Typhoid fever,<sup>209-212</sup> *Pseudomonas aeruginosa*,<sup>204</sup> *Escherichia coli*<sup>204</sup> and *S. flexneri*.<sup>213</sup>

Immunisation with the capsular polysaccharide of *S. typhi* (Vi) has been demonstrated to provide immunity against typhoid fever,<sup>214, 215</sup> however, it was hypothesized that the immunogenic properties of Vi could be enhanced by protein coupling. Therefore, multiple studies have focused on the synthesis and applications of a Vi-protein glycoconjugate vaccine, with multiple different carrier proteins being investigated; these include Bovine serum albumin,<sup>210</sup> cholera toxin,<sup>210</sup> Tetanus toxoid,<sup>210, 212</sup> diphtheria toxin,<sup>210, 211</sup> and human serum albumin.<sup>209</sup> Diphtheria toxin is a popular protein carrier, and is often chosen due to its low cost and structural stability in the pH ranges encountered during bio-conjugation.<sup>211</sup> The majority of conjugate vaccines were shown to result in an increased immunogenic response, compared to treatment with Vi alone.<sup>209-212</sup>

A further disease to which a notable amount of research into conjugate vaccines has been dedicated is iNTS.<sup>163, 164, 206, 208</sup> Recent studies have focused on the use of the diphtheria toxin mutant CRM197 as a carrier protein.<sup>163, 164, 208</sup> Many of the conjugates to this protein were shown to elicit an immune response with a few proving to be promising candidate vaccines.<sup>163, 206</sup>

## Introduction

Conjugation of polysaccharides to carrier proteins can be achieved using a variety of non-site-selective methods. With many of the examples discussed above relying on the use of reductive amination<sup>163, 164, 206, 208, 209</sup> and / or linker molecules (e.g. adipic acid dihydrazide (ADH),<sup>163, 164, 208, 209</sup> 1-ethyl-3-(3-dimethylaminopropyl)carbodiimide (EDC),<sup>203, 211</sup> adipic acid bis(*N*-hydroxysuccinimide) (SIDEA),<sup>163, 164</sup> 4-(*N*-maleimido)-*n*-butanoyl).<sup>213</sup> These conjugation methods rely on amine functionalities<sup>162-164</sup> (e.g. like those presented by lysine side chains) and as such are not site-selective. Most proteins contain multiple lysine residues, and may also have an exposed *N*-terminus, and therefore multiple amine groups are often available for ligation, allowing for numerous polysaccharide additions. However, recently some protein glycoconjugate vaccines have also been synthesised using site-selective conjugation methods.<sup>216-218</sup>

Though the majority of previous research performed into protein glycoconjugates has focused on vaccine development, some studies have investigated alternative applications for protein glycoconjugates. One such example was the development of glycodendrinanoparticles designed to block viral infections.<sup>219</sup> The carrier protein used in this study was engineered monomeric Q $\beta$  (a bacterial capsid protein engineered to contain a L-homopropargylglycine (Hpg) residue); these monomers self-assembled to form a 180-copy multimer.<sup>219</sup> Cu-catalysed click-chemistry was then used to attach a mannose containing glycodendrimeric construct to the protein backbone, producing glycodendrinanoparticles containing up to 1,620 mannose units.<sup>219</sup> An ELISA demonstrated that the glycodendrinanoparticles could prevent DC-SIGN (dendritic cell-specific intercellular adhesion molecule-3-grabbing nonintegrin) from binding to mannosylated albumin, with an estimated IC<sub>50</sub> of 35-40 nM.<sup>219</sup> Further investigation found that the glycodendrinanoparticles were capable of blocking Ebola infection on T-lymphocytes and a human dendritic cell infection model, displaying an IC<sub>50</sub> in the picomolar range.<sup>219</sup>

Further work by Davis and co-workers produced dual-action glycodendriproteins capable of inhibiting bacterial aggregation, with *Actinomyces naeslundii* chosen as the target bacteria.<sup>220</sup> Here four different glycodendrimer scaffolds were synthesised, each containing between two and four galactose units.<sup>220</sup> The glycodendrimers were linked to a NHS-butyl methanethiosulfonate linker and reacted site-selectively with an engineered protein-degrading proteinase, subtilisin, from *Bacillus lentus*, via a free cystine residue.<sup>220</sup> The dual activity of the glycodendriproteins arise from the galactose residues binding to lectins on *Actinomyces naeslundii*, preventing bacterial host cell adhesion,<sup>220</sup> and furthermore, once a glycodendriprotein is bound to a bacterial lectin the protein-degrading proteinase induces degradation of the lectin, further preventing infection.<sup>220</sup> The activity of the glycodendriproteins was investigated using an enzyme-linked lectin assay (ELLA) with surface immobilised peanut agglutinin (PNA) used as a model galactose binding lectin. A positive trend was

## Introduction

observed between the number of galactose units present and an analogues potency. Further investigation was performed into the glycodendriproteins ability to inhibit co-aggregation of *A. naeslundii* and *Streptococcus orali*. The inhibitory potency of the glycodendriproteins was shown to be dependent on each analogues structure, with the bi-galactose analogue **1.30** (Figure 1-30) displaying the highest potency and achieving an  $IC_{50}$  in the nanomolar range.<sup>220</sup>

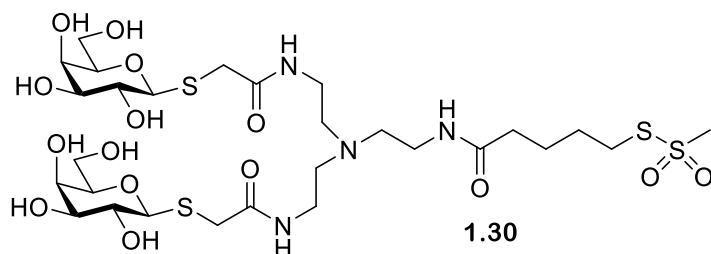


Figure 1-30. Structure of bi-galactose analogue **1.30**

Wang and co-workers<sup>152</sup> investigated the use of peptide glycoconjugates as HIV inhibitors, using a maleimide-activated high mannose oligosaccharide derived from oligosaccharide  $Man_9GlcNAc_2Asn$ . The maleimide activated oligosaccharide was then reacted with a cystine residue on a 36-mer HIV-1 gp41 peptide, T20, which had previously shown to be a potent inhibitor against HIV infection. HIV-1 primarily targets the macrophages and dendritic cells, these cells express mannose and oligomannose-specific receptors on their surface, therefore conjugating a mannose saturated oligosaccharide to HIV-1 gp41 peptide will allow more specific targeting of the macrophages and dendritic cells.<sup>152</sup>

Turnbull and co-workers also investigated the use of protein-glycoconjugates as therapeutic inhibitors, with their work focusing on the cholera toxin (CT).<sup>221</sup> The CT contains five identical CT B subunits (CTB) all of which contain a *N*-terminal threonine residue. Turnbull and co-workers used an inactive CTB mutant as a protein scaffold, and subjected the scaffold to a  $NaIO_4$ -mediated oxidative cleavage to afford five terminal aldehyde motifs.<sup>221</sup> The target pentasaccharide **1.31** was then subjected to a Cu-catalysed click reaction with alkyne-armed hydroxylamine linker **1.32** to afford pentasaccharide **1.33**, which displays a Boc-protected hydroxylamine-terminated appendage extending from the reducing terminus. Pentasaccharide **1.33** was subjected to Boc-deprotection affording pentasaccharide **1.34** and conjugated to the oxidised CTB mutant via oxime ligation, yielding pentavalent CTB-linked glycoconjugate **1.35** (Scheme 1-18).<sup>221</sup>

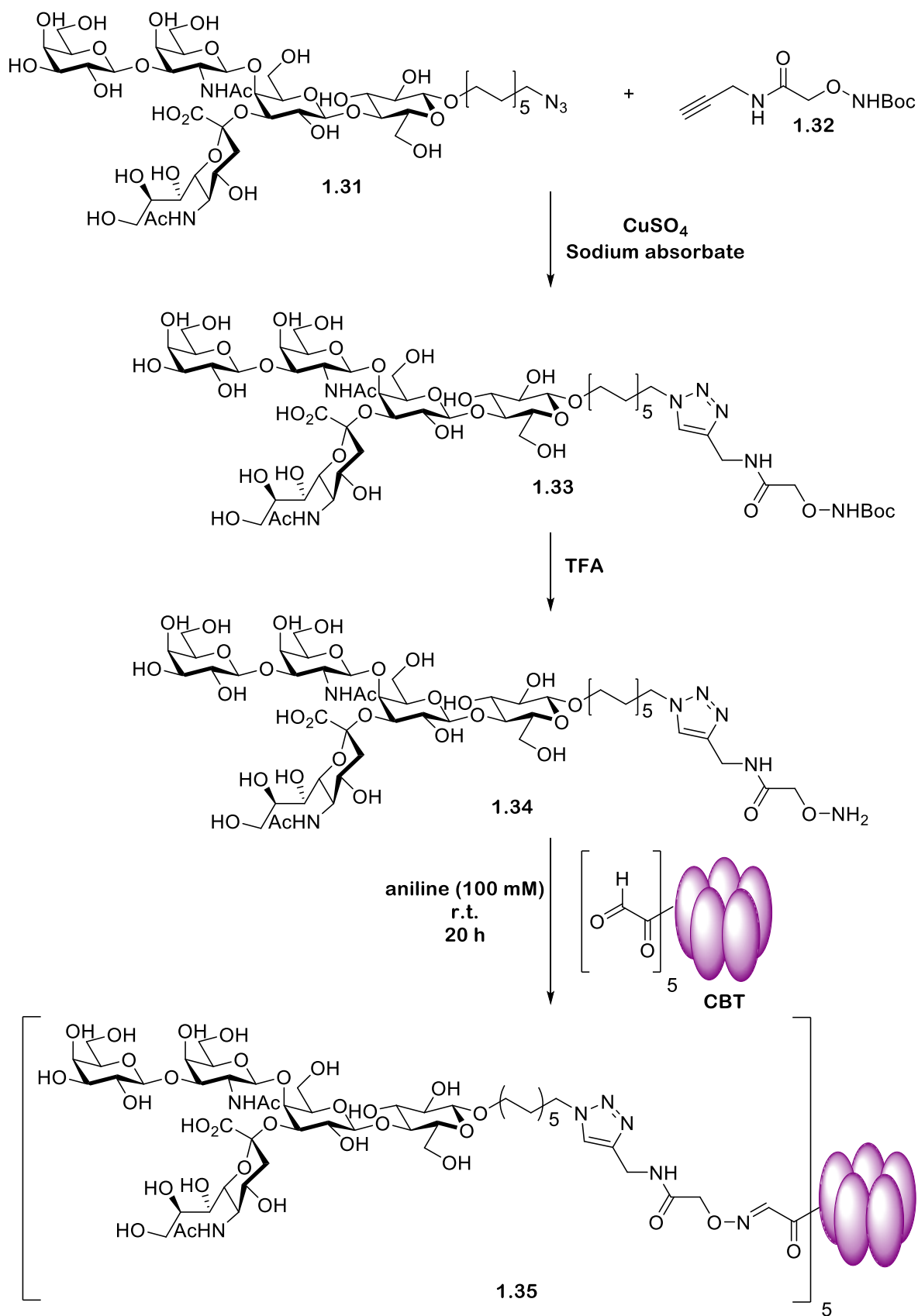
The biological properties of pentavalent CTB-linked glycoconjugate **1.35** were assessed using an ELLA and ITC.<sup>221</sup> The ELLA confirmed pentavalent CTB-linked glycoconjugate **1.35** to have impressive potency with a low  $IC_{50}$  value of 104 pM; 5100 times more potent than the pentasaccharide alone.<sup>221</sup> However, the ITC results disagree with those of the ELLA, finding pentavalent CTB-linked

## Introduction

glycoconjugate **1.35** to exhibit similar potency to the pentasaccharide (30 nM vs 43 nM), but it was suggested that the formation of random aggregates with modest binding affinities may have interfered with the ITC measurements.<sup>221</sup>

The examples discussed showcase the vast potential applications protein-glycoconjugates have as pathogenic inhibitors. Further investigation into this fertile area of research is thus both tantalising and could lead to the development of new targeted glycotherapeutic agents that could revolutionise the treatment of urinary tract infections.

## Introduction



*Scheme 1-18. Synthesis of pentavalent CTB-linked glycoconjugate 1.35. Following an initial copper catalysed click reaction to attach pentasaccharide 1.31 to alkyne armed hydroxylamine linker 1.32 affording Boc protected hydroxylamine charged pentasacchride 1.33. Following TFA mediated Boc deprotection pentasaccharide 1.34 was extracted and subjected to oxime ligation with the oxidised CTB mutant affording pentavalent CTB-linked glycoconjugate 1.35*



### 1.2.3 Project aims

The aim of this project is to employ a high affinity monovalent FimH inhibitor to achieve polyvalent *E. coli* targeting via colicin-linked glycoconjugates. Exposure of the colicin-linked glycoconjugate to *E. coli* should lead to initial high affinity binding of the colicin protein to its outer membrane target receptor. Once bound the colicin protein anchors the glycoconjugate to *E. coli*, potentially allowing the glycoconjugate linker to transverse the glycocalyx and display the high affinity FimH inhibitor on the *E. coli* surface. As each bacterium is capable of binding to multiple colicin-linked glycoconjugates, we aim to use this targeting approach to turn *E. coli* itself into a polyvalent mannose presenting scaffold, capable of binding to multiple FimH groups presented by other *E. coli* bacterium. We propose that this targeting approach will result in *E. coli* aggregation (Figure 1-31), preventing *E. coli* from binding to the urothelium umbrella cells and thus allowing removal of *E. coli* from the bladder during urination. This type of therapy is classified as an anti-adhesion therapy as it does not induce apoptosis, but instead prevents *E. coli* from reaching its target. As this selection pressure is mild it is unlikely to trigger a rapid evolutionary response from *E. coli*, and thus it is hoped that *E. coli* will be slow to develop resistance.

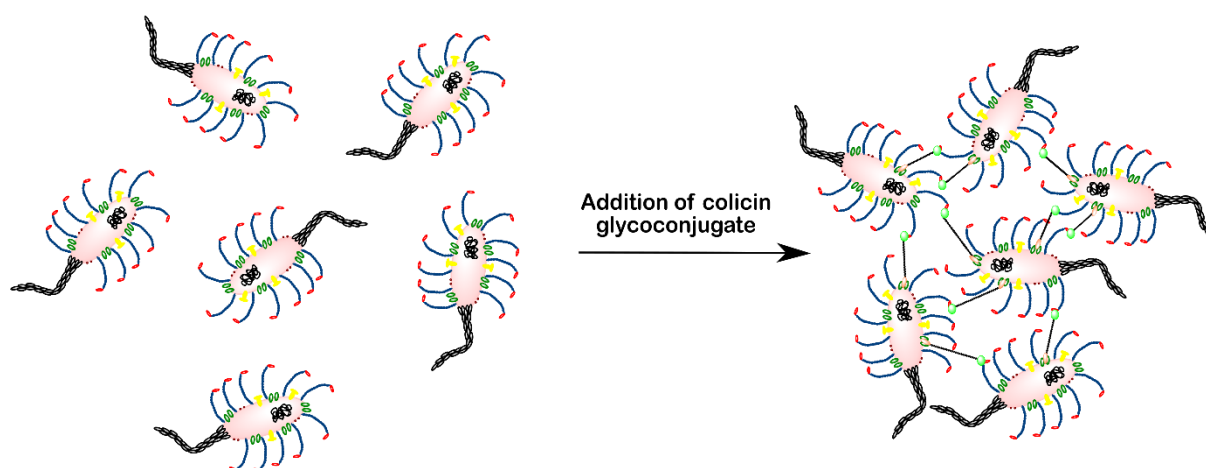


Figure 1-31. Cartoon depiction of glycoconjugate induced UPEC aggregation

The overall project aims can be divided into four objectives (Figure 1-32); 1) the synthesis of a high affinity FimH inhibitor, 2) bio-conjugation of the FimH inhibitor to a colicin protein affording a colicin linked glycoconjugate using OPAL methodology previously developed in the Fascione group, 3) analysis of the glycoconjugates ability to bind to its target receptor and 4) analysis of the glycoconjugates ability to adhere *E. coli*.

## Introduction

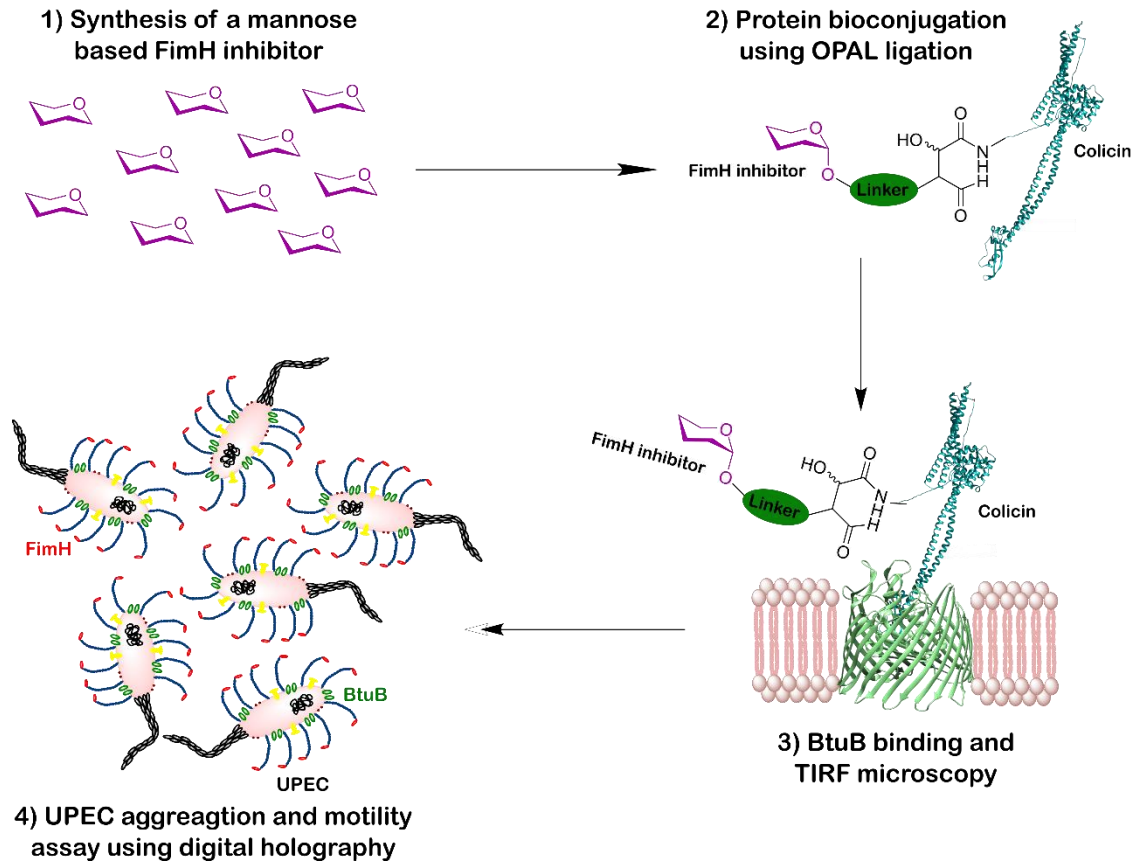


Figure 1-32. The four overall objectives of the project. Stage 1) Synthesis of a mannose based FimH inhibitor, stage 2) Protein bio-conjugation (colicin Ia PDB; 1CII<sup>222</sup>), stage 3) BtuB binding (PDB; 3RGM<sup>223</sup>) and TIRF microscopy and stage 4) UPEC aggregation and motility assay using digital holography

## Chapter 2 Synthesis of monosaccharide building blocks

### 2.0 Aims

The focus of the work in this chapter is the design and synthesis of mannose-based ligands for the UPEC adhesion protein FimH. These mannose-based ligands can then be used in the construction of the mannose-colicin bio-conjugates, which will subsequently be screened for their ability to induce UPEC aggregation in later chapters.

### 2.1 Design and synthesis of an oligosaccharide-based inhibitor

#### 2.1.1 Reasoning behind monosaccharide synthesis

Trisaccharide **1.4** (Figure 2-1) was initially chosen as a potential FimH-inhibiting oligosaccharide due to its relatively simple structure compared to other oligosaccharide based inhibitors. Trisaccharide **1.4** consists of three linear monosaccharide units, consequently, the protected monosaccharide precursors do not have to facilitate selective branching reactions, and are thus relatively simple to synthesise. Furthermore, previous studies have shown trisaccharide **1.4** to be a potent inhibitor of FimH, and even have suggested that trisaccharide **1.4** is the optimal size for binding to the FimH binding site.<sup>76,77</sup> The major interactions that trisaccharide **1.4** can achieve with the FimH lectin domain are depicted in Figure 1-9.

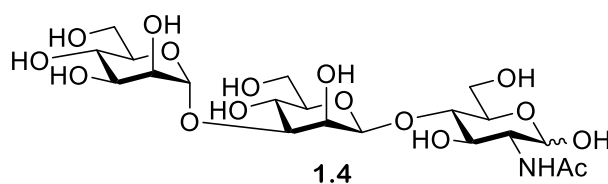


Figure 2-1. The structure of trisaccharide 1.4

#### 2.1.2 Design of monosaccharides

Retrosynthetic analysis of trisaccharide **1.4** was used to design the required monosaccharide building blocks (Figure 2-2). Three monosaccharides were designed – **2.1x**, **2.2** and **2.3x** (where **x** varies from **a**→**c**, Figure 2-6, Scheme 2-6, Scheme 2-11, Scheme 2-12). The glucosamine building block **2.3x** is unprotected at *O*-4, and can be used as a glycosyl acceptor with the benzylidene acetal protected mannose thioglycoside **2.2**, which itself is capable as acting as a  $\beta$ -selective glycosyl donor.<sup>224</sup> The resultant **2.3x-2.2** disaccharide can then serve as an glycosyl acceptor for  $\alpha$ -selective mannose thioglycoside **2.1x**. Note that an orthogonal protecting group is to be installed onto each mannoside unit, as this will allow for selective removal and further glycosylations.

## Synthesis of monosaccharide building blocks

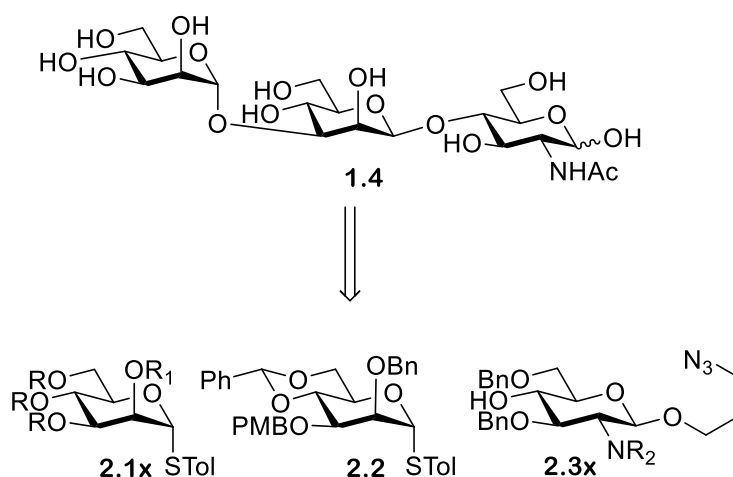


Figure 2-2. Retrosynthesis of trisaccharide **1.4** to give the three desired monosaccharide structures. Where  $R = Bz$  or  $Bn$ ,  $R_1 = Bz, Ac$  or  $Bn$ ,  $R_2 = HTCA$  or  $Phth$

### 2.1.3 Design and synthesis of mannoside **2.2**

The first donor synthesized was benzylidene protected mannoside **2.2** (Figure 2-3). Due to its placement within the trisaccharide a protection strategy which included temporary protection of *O*-3 and installation of a latent glycosyl donor at the anomeric position was required. The STol group located at the anomeric position of mannoside **2.2** can act as a selectively activated leaving group in glycosylation with a 1,4-protected glucosamine acceptor **2.3x** to afford a  $\beta$ -mannoside.<sup>80, 83, 86, 225-227</sup> The PMB ether located at *O*-3 can provide temporary protection as it can be orthogonally removed post-glycosylation with DDQ to reveal an unprotected *O*-3. This allows for a further  $\alpha$ -selective glycosylation at *O*-3 with protected mannose STol glycosyl donor **2.1x**.

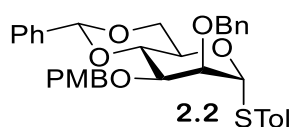
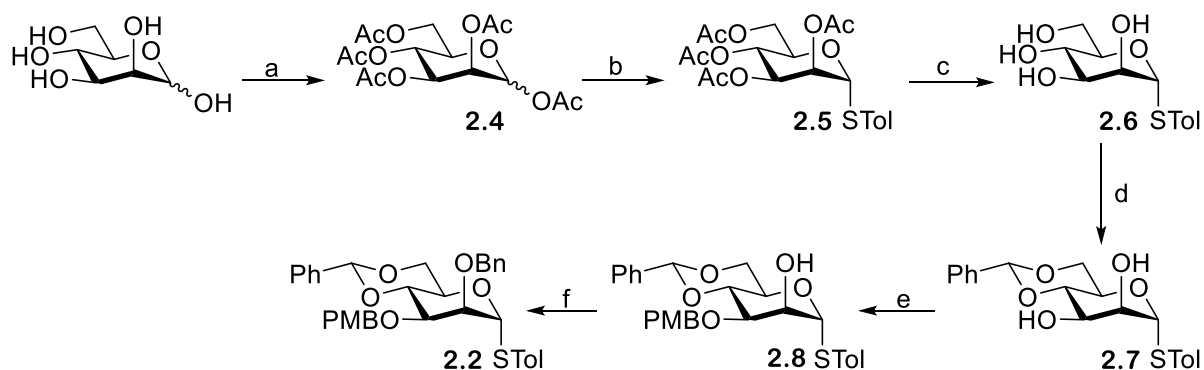


Figure 2-3. The structure of mannoside **2.2**

Benzylidene acetal protected thioglycoside **2.2** was synthesized via the synthetic pathway shown in Scheme 2-1. This pathway consists of 6-steps, with initial global acetylation of D-mannose to afford D-mannose pentaacetate **2.4** (Scheme 2-1, step a), followed by Lewis acid mediated attack on the anomeric centre with 4-methylbenzenethiol to afford thioglycoside **2.5** (Scheme 2-1, step b). This product was subsequently subjected to deacetylation using Zemplén conditions to reveal unprotected mannoside **2.6** (Scheme 2-1, step c), which was then protected with a benzylidene acetal, affording 4,6-O-benzylidene-acetal protected mannoside **2.7** (Scheme 2-1, step d). The *O*-3 position of protected mannoside **2.7** was then orthogonally protected with a PMB ether, affording PMB protected

## Synthesis of monosaccharide building blocks

mannoside **2.8** (Scheme 2-1, step e), which was then subjected to O-2 benzyl protection to afford the desired mannoside **2.2** (Scheme 2-1, step f).



*Scheme 2-1. Synthesis of wanted 1,3 mannoside **2.2** from D-mannose. Reagents and conditions a) Ac<sub>2</sub>O, pyridine, DMAP, 0 °C- r.t., 12 h (80%); b) HSTol, BF<sub>3</sub>·Et<sub>2</sub>O, dry DCM, 0 °C- r.t. 12 h, (62%); c) MeONa, MeOH, r.t., 62 h (80%); d) 2,2 DMT, CSA, dry MeCN, Et<sub>3</sub>N, r.t., 5 h (61%); e) Bu<sub>2</sub>SnO, dry toluene, 110 °C, 3h, PMBCl, CsF, dry DMF, 70 °C, 12 h (83%); f) BnBr, NaH, dry DMF, 0 °C- r.t., 2 h (36%)*

The choice of protecting groups strongly influences a donor's reactivity - the use of electron-donating protecting groups (e.g. benzyl groups) results in an armed donor, whereas the use of electron-withdrawing protecting groups (e.g. benzoyl groups) results in a disarmed donor.<sup>228</sup> Armed donors are more reactive than their disarmed counterparts, often leading to higher glycosylation yields.<sup>229</sup>

As a  $\beta$ -mannosidic bond is required between the central mannose unit and the glucosamine unit in trisaccharide **1.4**, a benzylidene acetal was installed at the O-4 and O-6 positions of unprotected mannoside **2.6**. Formation of the 4,6-acetal is thermodynamically favoured due to the high preference of the phenyl group to be in the equatorial position.<sup>230</sup> However, a lower yield than expected (61%) of 4,6-O-benzylidene acetal-protected mannoside **2.7** was afforded. This was due to the formation of dibenzylidene mannoside product **2.9** (Figure 2-4), where a 2,3-O-benzylidene ring is formed in addition to the 4,6-O-benzylidene ring due to the cis orientation of O-2 relative to O-3 on mannose.<sup>230</sup>

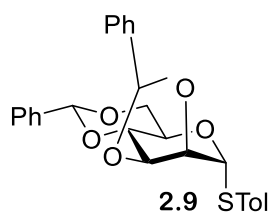


*Figure 2-4. Structure of the dibenzylidene mannoside side product **2.9** obtained during 4,6-O-benzylidene acetal-protection of unprotected mannoside **2.6***

## Synthesis of monosaccharide building blocks

The 4,6-*O*-benzylidene acetal-protected mannoside **2.7** was subsequently selectively protected at *O*-3 using a dibutyltin oxide-mediated benzylation with *p*-methoxybenzyl chloride (see Scheme 2-1). This reaction was performed in two stages. In the first stage 4,6-*O*-benzylidene acetal-protected mannoside **2.7** was reacted with dibutyltin oxide, likely resulting in the formation of dibutylstannylene acetal intermediate **2.10** (Figure 2-5). This intermediate was then reacted with *p*-methoxybenzyl chloride, affording PMB protected mannoside **2.8**. Previous work has shown that mannose dibutylstannylene acetals react preferentially at the equatorial OH, vicinal to the axial OH.<sup>231, 232</sup> I propose that this could be the result of dipole minimisation between the trans-axial *O*-2 and *O*-1 resulting in *O*-2 being less nucleophilic than *O*-3. This hypothesis would be consistent with PMB protected mannoside **2.8** being the only reaction product isolated.

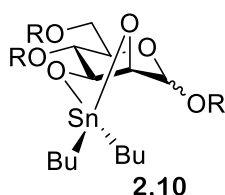


Figure 2-5. Structure of likely mannose dibutylstannylene acetal intermediate **2.10** formed during selective *O*-3 PMB protection

### 2.1.4 Design and synthesis of mannoside donors **2.1a** and **2.1b**

The decision to install an orthogonal protecting group at *O*-2 of the terminal trisaccharide mannose unit was made after examination of the crystal structure of the FimH binding site, which revealed free space directly above the final trisaccharide unit.<sup>51</sup> Using a terminal mannose unit bearing a temporary protecting group (which could be selectively removed after construction of the protected trisaccharide) would potentially allow for extension to form either a tetrasaccharide or a pentasaccharide. This would potentially allow the free space above the terminal trisaccharide unit to be explored. To achieve this goal, both *O*-2 acetyl **2.1a** and *O*-2 benzoyl **2.1b** protected thioglycoside donors were considered (Figure 2-6).

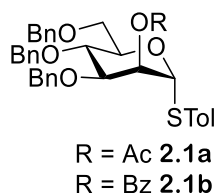


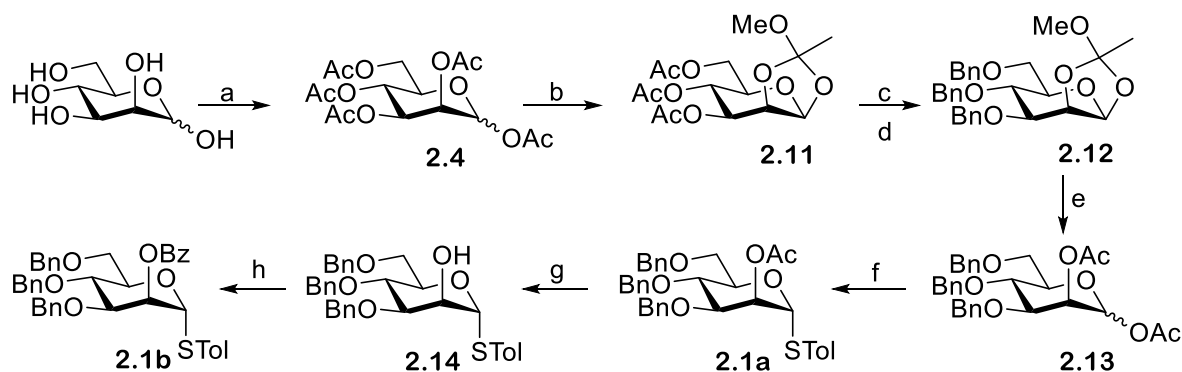
Figure 2-6. Structures of *O*-2 acetyl **2.1a** and *O*-2 benzoyl **2.1b** protected mannose thioglycoside donors

Careful consideration was taken when selecting the protecting groups for mannoside donors **2.1a** and **2.1b**. The choice of benzyl protection at the *O*-3, *O*-4, and *O*-6 positions should lead to an

armed donor with high reactivity,<sup>233</sup> while the presence of an electron-withdrawing ester protecting group (e.g. Bz or Ac) at *O*-2 should allow for neighbouring group participation during glycosylation.<sup>234</sup> Unlike benzyl groups, both benzoyl and acetyl groups are base-sensitive, providing a simple method for selective *O*-2 unmasking. Both mannoside donors **2.1a** and **2.1b** were therefore synthesized to enable investigation of the effect of steric hindrance on glycosylation yields.

### 2.1.5 Synthesis of mannoside donors **2.1a** and **2.1b**

The desired *O*-2 acetyl protected mannoside **2.1a** and *O*-2 benzoyl protected mannoside **2.1b** were synthesised using the seven-step pathway depicted in Scheme 2-2. After global acetylation *D*-mannose pentaacetate **2.4** was subjected to a selective 1,2-ortho esterification (Scheme 2-2, step b), affording 1,2-orthoester protected mannoside **2.11**. Deacetylation was then performed (Scheme 2-2, step c), revealing alcohols at *O*-3, *O*-4, and *O*-6 positions, and benzyl protection was subsequently performed (Scheme 2-2, step d) to afford fully protected orthoester **2.12**. The orthoester then underwent acid cleavage with acetic acid (Scheme 2-2, step e) affording mannoside **2.13**, followed by thioglycoside formation with 4-methylbenzenethiol (Scheme 2-2, step f) to afford *O*-2 acetyl protected mannoside **2.1a**. Two further synthetic steps were required to obtain the desired *O*-2 benzoyl protected mannoside **2.1b**; a base mediated deacetylation (affording mannoside **2.14**) followed by selective installation of a benzoyl protecting group at *O*-2 (Scheme 2-2, steps g and h).

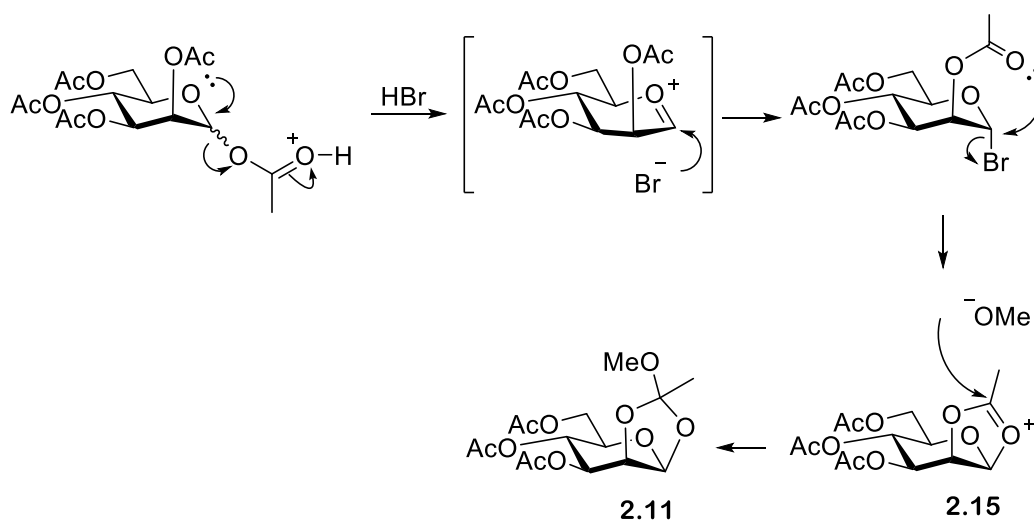


Scheme 2-2. Synthesis of wanted 1,2 mannosides **2.1a** and **2.1b** from *D*-mannose. Reagents and conditions; a)  $\text{Ac}_2\text{O}$ , pyridine, DAMP,  $0^\circ\text{C}$ - r.t., 12 h, (94 %); b) i) 33 % HBr, AcOH, DCM, r.t., 1.5 h ii) 2,6-Lutidine, dry DCM, dry MeOH, r.t., 12 h, (i+ii = 51 %); c) NaOMe, MeOH, r.t., 1 h; d) NaH, BnBr, dry DMF,  $0^\circ\text{C}$ - r.t., 12 h, (c + b = 50 %); e) AcOH, r.t., 1 h, (84 %); f) HSTol,  $\text{BF}_3\cdot\text{Et}_2\text{O}$ , dry DCM,  $0^\circ\text{C}$ - r.t., 6 h (45 %); g) NaOMe, MeOH, r.t., 12h (89%); h) BzCl, DMAP, Pyridine,  $0^\circ\text{C}$ - r.t., 2h, (78%)

Ortho esterification was used to achieve orthogonal protection of *O*-2. Orthoester formation allows for selective protection of the *O*-1 and *O*-2 positions, exploiting the cis orientation of *O*-1 and *O*-2 in mannose. In this reaction the *O*-2 acetate undergoes neighbouring group participation to form the transient  $\beta$ -linked acetoxonium ion **2.15** - this ion can be trapped under basic conditions by methanol to produce orthoester protected mannoside **2.11** (Scheme 2-3). The ortho esterification reaction afforded a significantly lower yield than that stated in literature: 51% vs 94%.<sup>236</sup> However, the

## Synthesis of monosaccharide building blocks

large scale of the reaction (17.17 g) resulted in enough 1,2-orthoester protected mannoside **2.11** (8.17 g) being obtained to enable the synthesis to be completed. If this ortho esterification reaction were to be repeated in the future, measures such as reaction scale-out and a fresh bottle of dry MeOH could be used to improve the reaction yield.



*Scheme 2-3. Depiction of ortho-ester formation with initial oxocarbenium ion formation followed by neighbouring group participation to form a 5-linked acetoxonium ion **2.15** which is trapped by methanol under basic conditions to afford orthoester **2.11***

### 2.1.6 Synthesis of a GlcNAc acceptor

#### 2.1.6.1 Initial use of trichloroacetyl protection

The synthesis of a glucosamine acceptor bearing a free hydroxyl at *O*-4 proved to be the most challenging monosaccharide synthesis of the project. A particularly challenging aspect in the design and synthesis of potential *O*-4 unprotected glucosamine acceptors was the installation of a bio-conjugation handle at the anomeric position (this bio-conjugation handle would ideally enable either direct protein attachment or serve as a point of attachment for a linker molecule), as selecting a handle that could both be easily installed and withstand the synthetic conditions needed to obtain trisaccharide **1.4** was challenging. Van der Marel and co-workers have previously reported the synthesis of 3-azidopropyl-linked GlcNPhth acceptor **2.16** (Figure 2-7),<sup>237</sup> demonstrating that 3-azidopropan-1-ol can be installed into a glucosamine unit. As such, 3-azidopropan-1-ol was initially selected as a potential bio-conjugation handle.

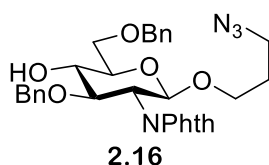
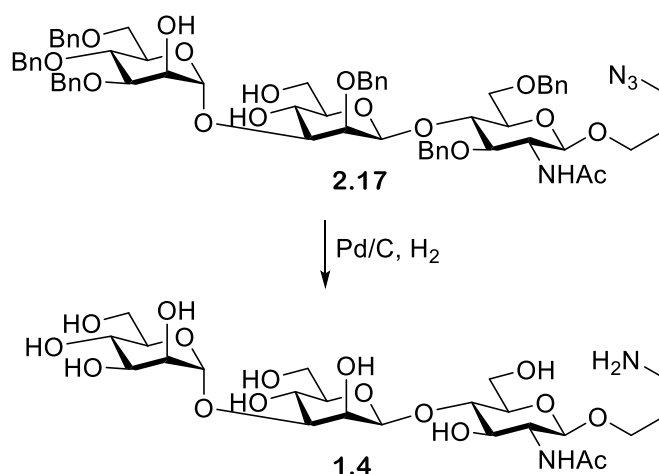


*Figure 2-7. Structure of 3-azidopropyl-linked 1,4 GlcNPhth acceptor **2.16***



## Synthesis of monosaccharide building blocks

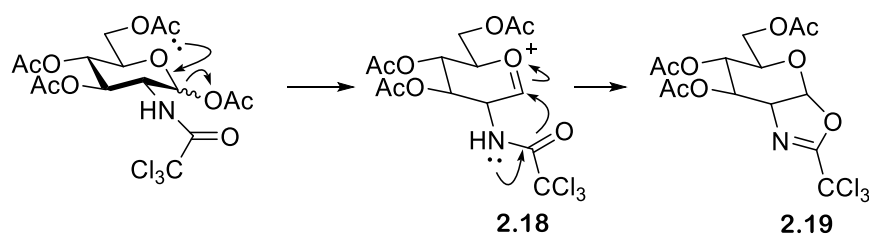
Unfortunately, the attractive azide motif present after 3-azidopropan-1-ol installation cannot be utilised during protein bio-conjugation, as the final deprotection step needed to afford trisaccharide **1.4** from benzyl protected trisaccharide **2.17** is hydrogenation, which reduces the azide motif to an amine (Scheme 2-4). However, this amine unit can itself facilitate downstream bio-conjugation reactions, as it can either be directly couple to proteins (via reaction with carboxylic acid or aldehyde motifs) or used as a point of attachment for a linker unit.



Scheme 2-4. Hydrogenation reaction of benzyl protected trisaccharide **2.17** to afford trisaccharide **1.4**

Seeberger and co-workers<sup>238</sup> have long been at the forefront of using trichloroacetyl (TCA) as an alternative *N*-2 protecting group to acetyl (Ac) and phthalimide (Phth). Like acetyl protection, TCA protection allows oxazoline ring formation, and thus affords increased stability (Scheme 2-5). However, unlike acetyl protection, TCA protection is reversible and can be removed using various conditions.<sup>239</sup> Reductive cleavage can be achieved via treatment with either Bu<sub>3</sub>SnH and AIBN,<sup>240, 241</sup> or with NaBH<sub>4</sub>.<sup>242</sup> TCA cleavage can also be achieved via treatment with Zn-Cu in acetic acid,<sup>243</sup> or via exposure to basic conditions.<sup>244, 245</sup> However, it should be noted that Nifantiev and co-workers found that basic cleavage of *N*-2 TCA groups proceeded slower than their *O*-3 acetyl counterparts and required heating to 50 °C.<sup>244</sup> Further note that additional TCA cleavage methods have also been reported.<sup>239</sup> An advantage of TCA protection over Phth protection is that the TCA group should withstand all the reaction conditions used during trisaccharide synthesis, Phth groups are more susceptible to base-catalysed hydrolysis than TCA,<sup>246</sup> and therefore the ability of Phth groups to withstand the conditions used during deacetylation is somewhat questionable.

## Synthesis of monosaccharide building blocks

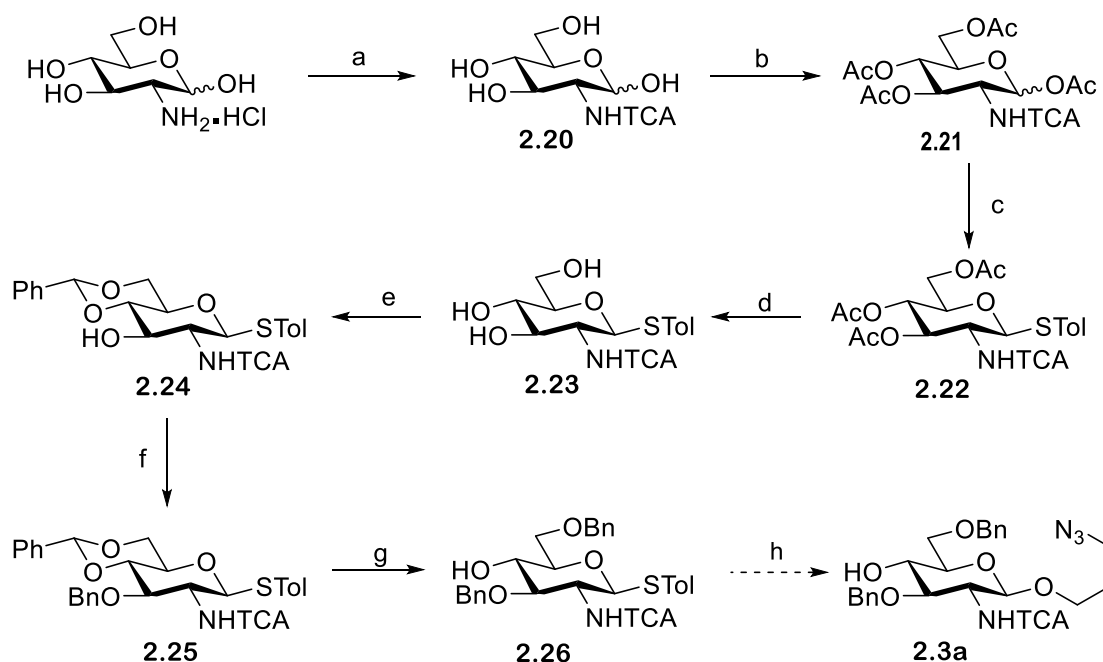


Scheme 2-5. Mechanism for TCA induce oxazoline ring formation. With initial oxocarbenium ion **2.18** formation, followed by neighbouring group participation of TCA to afford trichloroacetoxonium ion **2.19**

A potential issue with TCA protection is that, due to the presence of the three chlorine atoms, a TCA protecting group is more electron withdrawing than an Ac protecting group. This increased electron withdrawal could reduce the reactivity of both the anomeric and *O*-3 positions. However, we hypothesised that the electron withdrawing ability of TCA would only marginally limit reactivity, as Phth groups are also more electron withdrawing than Ac groups (pKa values for imides such as Phth vary between 8 - 10 whereas pKa values for amides (e.g. NHAc) can vary from 15 - 17).<sup>247</sup> Furthermore, previous research has shown that the *O*-4 of *N*-Phth glucose derivatives are more easily glycosylated than their *N*-acetyl protected counterparts.<sup>248</sup>

Synthesis of GlcNHTCA acceptor **2.3a** was attempted using the eight-step synthetic pathway shown in Scheme 2-6. This pathway follows initial TCA protection of D-glucosamine hydrochloride to afford TCA bearing glycoside **2.20**, which is then subjected to global acetylation to afford acetyl-protected glycoside **2.21**. Acetyl-protected glycoside **2.21** was then subjected to Lewis acid mediated thioglycoside formation with 4-methylbenzenethiol, affording STol glycosyl donor **2.22**. Thioglycoside **2.22** is subsequently subjected to deacetylation (affording triol **2.23**) followed by benzylidene acetal-protection to afford 4,6-*O*-benzylidene acetal-protected thioglycoside **2.24**. A benzyl protecting group was then installed at the *O*-3 position (affording thioglycoside **2.25**) before the 4,6-*O*-benzylidene acetal ring was selectively opened to reveal a free *O*-4, affording di-benzyl protected thioglycoside **2.26**. The final proposed synthetic step was glycosylation with 3-azidopropan-1-ol to afford the desired 4-OH GlcNHTCA acceptor **2.3a**.

## Synthesis of monosaccharide building blocks



Scheme 2-6. Synthesis of 1,4 GlcNHTCA acceptor **2.3a** from *D*-glucosamine hydrochloride. Reagents and conditions; a) *D*-glucosamine hydrochloride, trichloroacetylchloride, NaHCO<sub>3</sub>, H<sub>2</sub>O, r.t., 1h; b) Ac<sub>2</sub>O, pyridine, DMAP, 0 °C - r.t., 12 h, (a+b 58%); c) HSTol, BF<sub>3</sub>·Et<sub>2</sub>O, dry DCM, 0 °C - r.t., 12h, (16%); d) NaOMe, MeOH, r.t., 10 minutes, (80%); e) 2,2 DMT, CSA, dry MeCN, r.t., 5h, (87%); f) NaH, BnBr, dry DMF, 0 °C - r.t., 12 h (7%); g) triethylsilane, BF<sub>3</sub>·Et<sub>2</sub>O, dry DCM, 0 °C, 2 minutes (6%); h) 1-benzenesulfinyl piperidine, trifluoromethanesulfonic anhydride, dry DCM, 4 Å MS, 3-azidopropan-1-ol

Initial TCA protection of *N*-2 was successful, yet obtaining an accurate reaction yield was challenging due to NaCl being produced as a byproduct. TCA-bearing glycoside **2.20** and NaCl displayed similar solubilities in both water and methanol, complicating isolation of TCA-bearing glycoside **2.20**. TCA-bearing glycoside **2.20** was therefore used crude during global acetylation and the percentage yield was calculated over two steps.

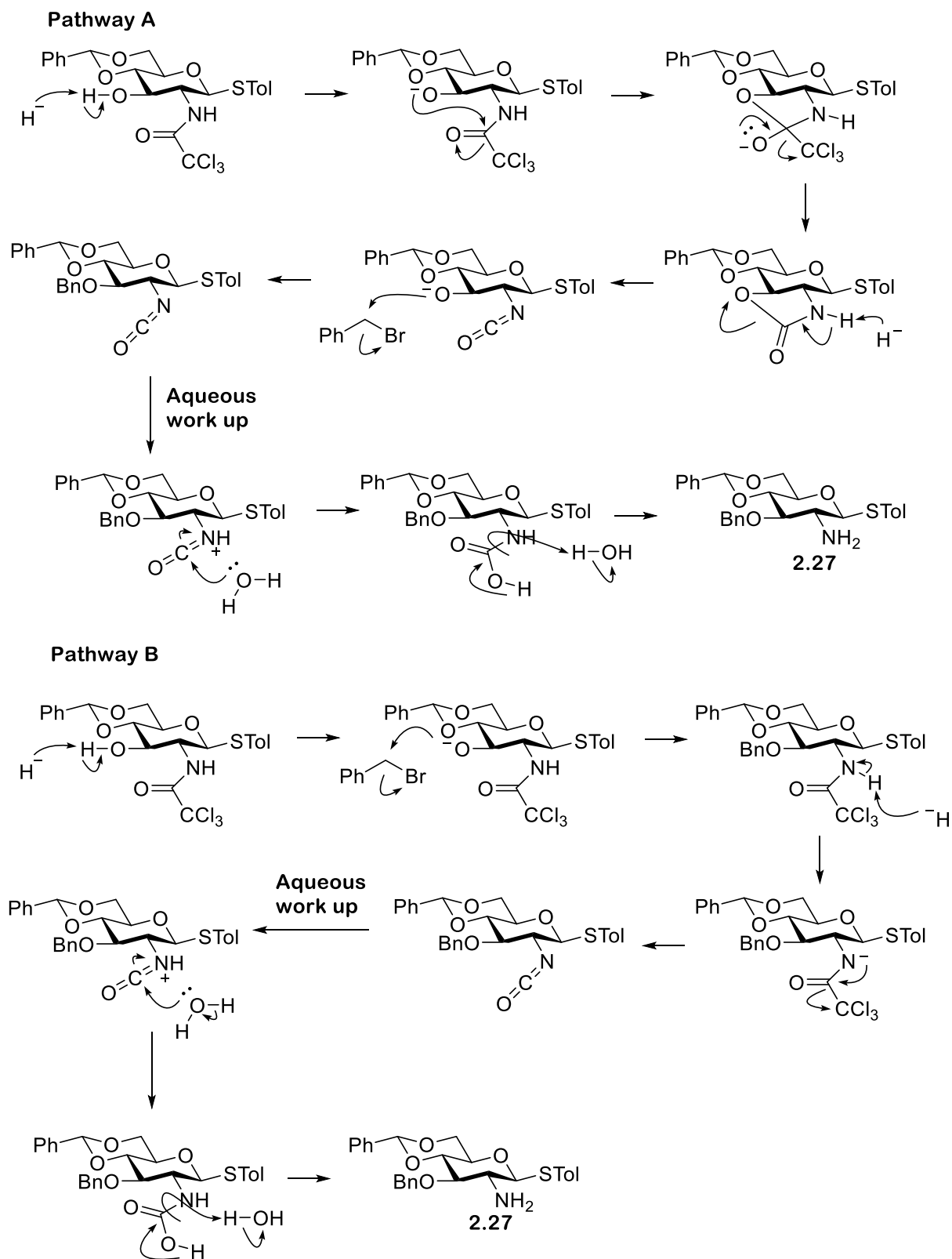
Unfortunately, the increased electron withdrawing ability of TCA was shown to impact reactivity, as diminished conversion of acetyl-protected glycoside **2.21** to thioglycoside **2.22** was observed. The increased electron withdrawing nature of TCA limits neighbouring group participation by disfavours the formation of the oxocarbenium ion *en route* to thioglycoside formation, resulting in a lower yield. As such, the reaction had to be repeated multiple times to afford enough product to be able to viably perform the next synthetic step. Other measures attempted in order to improve the reaction yield included the use of newly purchased 4-methylbenzenethiol and freshly distilled BF<sub>3</sub>·OEt, but neither of these changes resulted in a significantly improved reaction yield.

Benzoylation of the *O*-3 position of 4,6-*O*-benzylidene acetal protected thioglycoside **2.24** also proved challenging, with the first reaction attempt only affording a 7% yield of product **2.25**. The major product recovered from the reaction was observed to be *N*-2 unprotected glucosamine **2.27** (Scheme 2-7) which could be formed via two potential mechanisms. Both mechanisms A and B proceed via the

## Synthesis of monosaccharide building blocks

initial deprotonation of *O*-3 by NaH to afford an alkoxy anion. Pathway A suggests this anion could serve as a nucleophile which attacks at the amide carbon, resulting in oxazoline ring formation and loss of CCl<sub>3</sub>. Pathway A also suggests that if additional NaH is present it could deprotonate the amide nitrogen, which could result in isocyanate formation and the regeneration of the *O*-3 anion, which could subsequently react with benzyl bromide. The breakdown of the isocyanate by water during reaction workup would then release CO<sub>2</sub> and afford the observed *N*-2 unprotected glucosamine **2.27**. By comparison, pathway B suggests that oxazoline ring formation need not occur. In pathway B the *O*-3 anion initially generated simply reacts with benzyl bromide, and, in a comparable manner to that described in pathway A, the presence of excess NaH results in the deprotonation of the amide nitrogen and isocyanate formation. As the reaction was performed in dry DMF, it is likely that isocyanate breakdown occurred after the reaction, during the aqueous washes. Unfortunately, the current data offers no insights into the relative likelihoods of the two proposed pathways.

Synthesis of monosaccharide building blocks



Scheme 2-7. Two potential reaction pathways A and B for the formation of N-2 unprotected glucosamine **2.27**. NaH is represented as H<sup>-</sup>

Due to the issues encountered during *O*-3 benzyl protection, it was decided to use the 0.5 g of purified desired product **2.25** to trial the final two reaction steps. This would allow us to determine whether the synthetic scheme could be used to obtain the desired GlcNHTCA acceptor **2.3a**. If the final steps of the pathway proved fruitful then further investigations into improving benzylation yields could be performed.

It was decided that benzylidene acetal ring opening should be performed prior to glycosylation with 3-azidopropan-1-ol, as this would limit the quantity of expensive 3-azidopropan-1-ol required. Benzylidene acetal can be selectively opened to reveal either a free OH at *O*-4 or *O*-6. Wallin and co-workers<sup>249</sup> suggested two mechanistic pathways to explain how different reagent combinations result in different regioselectivity (Figure 2-8).<sup>249</sup> When a bulky Lewis acid (e.g.  $\text{AlCl}_3$ ) is present, Wallin and co-workers suggest that pathway A will be favoured due to reduced steric demands. However, when a smaller electrophile is present the mechanism is governed by the relative acidities of *O*-4 and *O*-6, resulting in pathway B being favoured.<sup>249</sup>

Pathway A

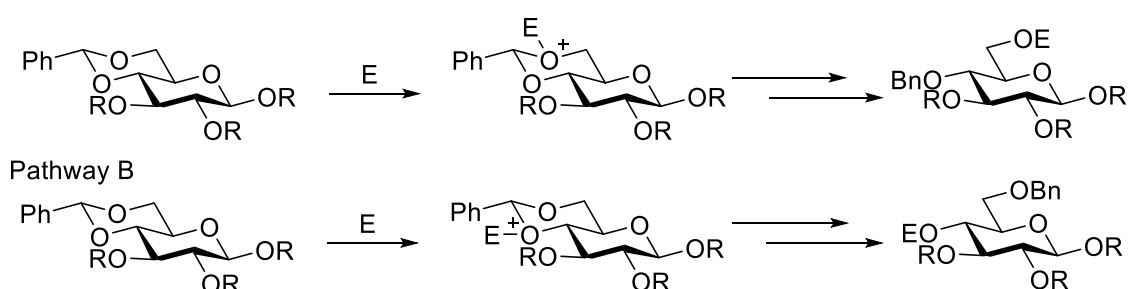
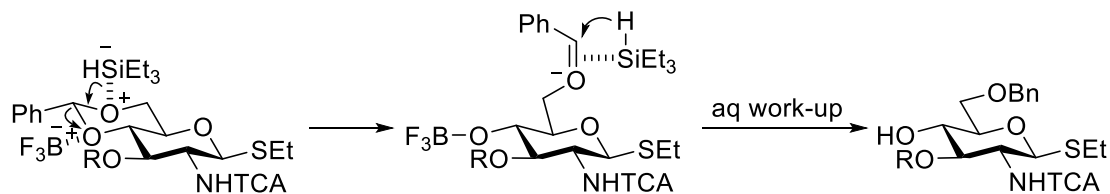


Figure 2-8. Simplified view of alternative selective benzylidene acetal ring opening pathways, where E represents an electrophile

A major problem with this initial mechanistic view is that it does not explain the regioselectivity observed when using the reducing agents  $\text{BH}_3\cdot\text{THF}$  or  $\text{BH}_3\cdot\text{NMe}_3$  in combination with  $\text{AlCl}_3$  in THF.<sup>250</sup> It was initially theorised that, due to its bulkiness,  $\text{AlCl}_3$  would preferentially coordinate to the less sterically hindered *O*-6 position, revealing a free *O*-6. However, these two reductive agents were shown to give the opposite regioselectivity, revealing a free *O*-4 position.<sup>250</sup> Ellervik and co-workers performed kinetic experiments to try and understand this effect, and concluded that the regioselectivity of reductive benzylidene acetals are not controlled by sterics but by electronics, with the most electrophilic species coordinating to the most nucleophilic oxygen (*O*-6).<sup>250</sup> Thus for our proposed reaction, which uses  $\text{Et}_3\text{SiH}$  and  $\text{BF}_3\cdot\text{OEt}_2$ , the regioselectivity can be explained by the coordination of the more electropositive  $\text{Et}_3\text{SiH}$  to *O*-6, where *O*-6 donates a lone pair of electrons into the silicon d-orbital. This coordination is stabilised by  $\text{BF}_3\cdot\text{OEt}_2$  coordinating to the *O*-4, and this

combined coordination results in the collapse of the benzylidene ring revealing a free *O*-4 (Scheme 2-8).



Scheme 2-8. Mechanism proposed for selective benzylidene acetal ring opening to reveal a free *O*-4

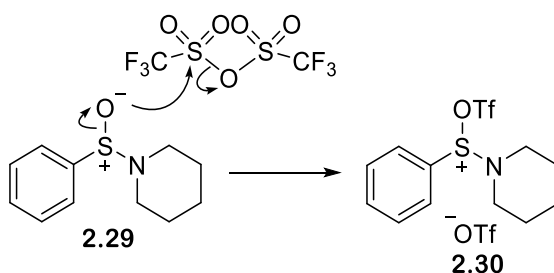
A selective *O*-4 benzylidene acetal opening was performed on 580 mg of thioglycoside **2.25** using  $\text{HSiEt}_3$  and  $\text{BF}_3 \cdot \text{OEt}_2$  for 2 min. The reaction was successful but low yielding due to a side-reaction of complete benzylidene acetal cleavage, meaning only 30 mg of purified product was isolated.

The final synthetic step required to afford the desired GlcNHTCA acceptor **2.3a** was glycosylation of di-benzyl protected thioglycoside **2.26** with 3-azidopropan-1-ol. A trial glycosylation was performed using the conditions of van der Marel and co-workers,<sup>237</sup> who had previously successfully glycosylated the benzylidene acetal protected SET thioglycoside donor **2.28** (Figure 2-9) bearing a Phth protecting group at *N*-2 to 3-azidopropan-1-ol with complete  $\beta$ -selectivity.



Figure 2-9. Van der Marel's benzylidene acetal NPhth protected SET thioglycoside **2.28** and NHTCA protected STol thioglycoside **2.26**

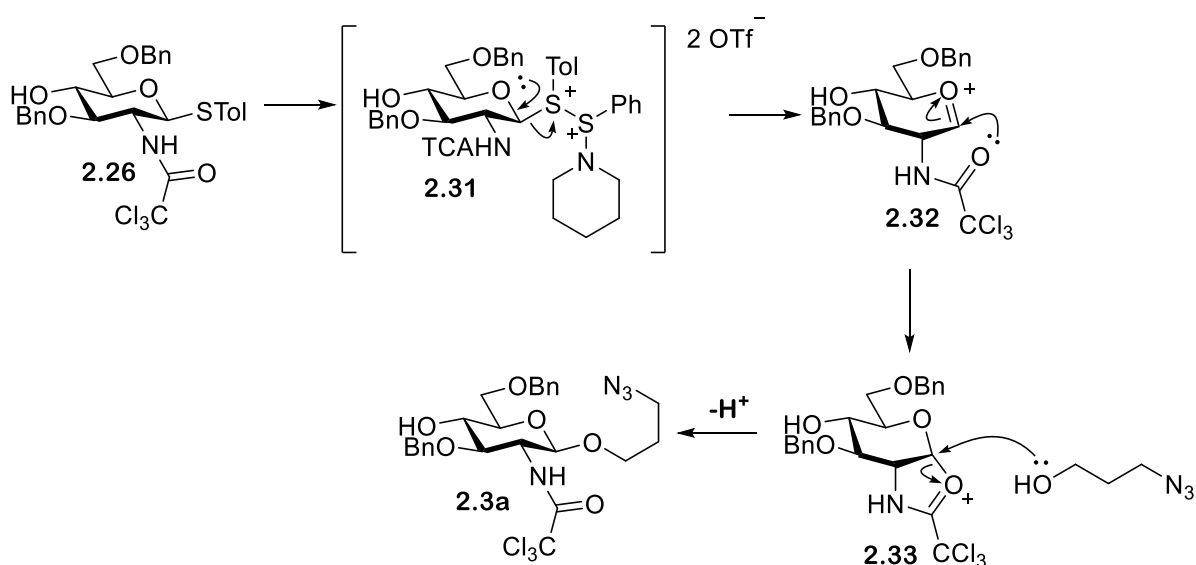
The thioglycoside activation conditions used by van der Marel and co-workers were based on the conditions developed by Crich and co-workers.<sup>251</sup> This approach proceeds via the generation of a potent thiophilic activator (activated BSP **2.30**) *in situ* through the use of  $\text{Tf}_2\text{O}$  and 1-benzenesulfonyl piperidine **2.29** (BSP) (Scheme 2-9).<sup>251</sup> The hindered base 2,4,6-tri-*tert*-butylpyrimidine (TTBP)<sup>225</sup> is also used to increase reaction rates, making its potency particularly suitable for disarmed donors.



Scheme 2-9. Mechanism of trifluoromethanesulfonic anhydride activation of BSP **2.29** to afford activated BSP **2.30**

## Synthesis of monosaccharide building blocks

The 3-azidopropan-1-ol glycosylation proceeds via the mechanism proposed in Scheme 2-10. Initially, STol reacts with activated BSP **2.30** to afford putative intermediate **2.31**. This increases the leaving group ability of the thioglycoside via oxocarbenium **2.32** formation. Neighbouring group participation by TCA forms a trichloroacetoxonium ion **2.33**, which is then attacked by 3-azidopropan-1-ol to form the desired GlcNHTCA product **2.3a**. Due to the low reactivity of the *O*-4 position excess 3-azidopropan-1-ol could be used during glycosylation without the formation of any side products. The low reactivity of the *O*-4 hydroxyl group has been credited to the steric hindrance around the *O*-4 position.<sup>229, 252</sup>



Scheme 2-10. Proposed mechanism for glycosylation of NHTCA protected thioglycoside **2.26** with 3-azidopropan-1-ol

A trial glycosylation using 3-azidopropan-1-ol and donor **2.26** was performed using BSP/Tf<sub>2</sub>O activation conditions. The reaction proved to be unsuccessful, with glycoside **2.34** (Figure 2-10) being isolated as the major product. Trace amounts of benzyl alcohol likely remained in the reaction mixture from the previous synthetic step (benzylidene acetal opening), and the use of pre-activation glycosylation conditions may have given benzyl alcohol the opportunity to act as a competing nucleophile, reacting with trichloroacetoxonium ion **2.33** prior to the addition of 3-azidopropan-1-ol. To avoid this side reaction occurring a change in the order of step h and i, was therefore proposed, with glycosylation with 3-azidopropan-1-ol being performed prior to benzylidene opening.

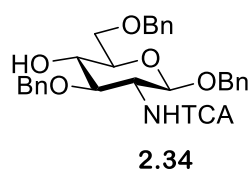
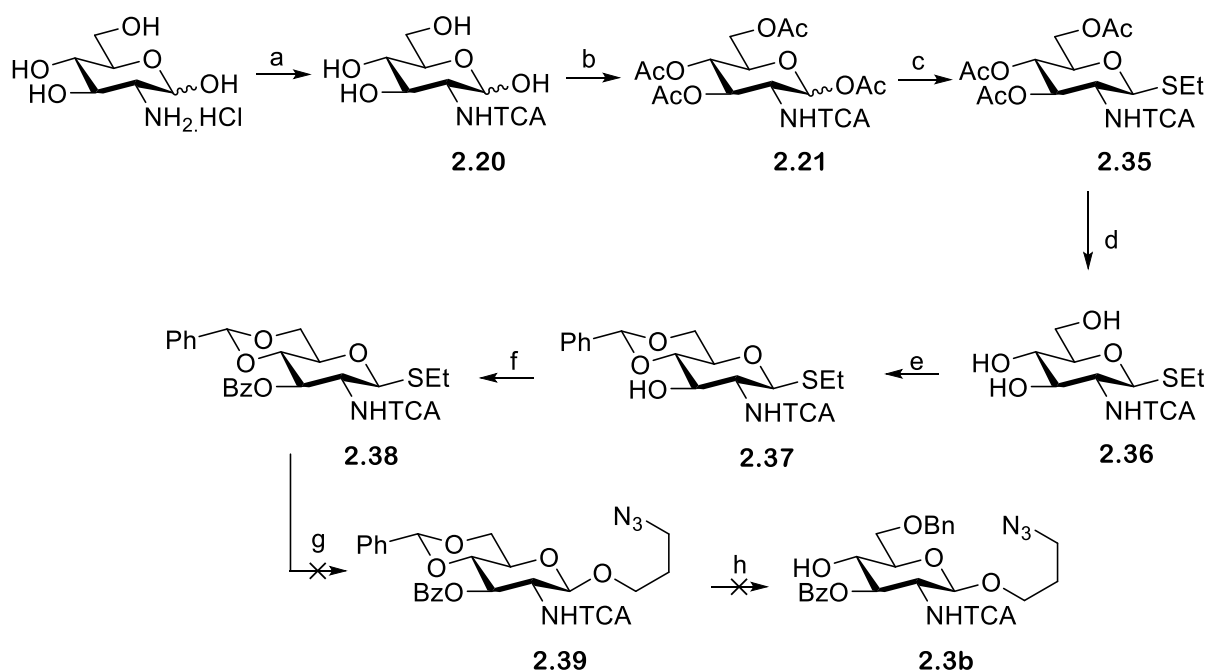


Figure 2-10. Structure of the undesired product **2.34** from test glycosylation of donor **2.26** with 3-azidopropan-1-ol



## Synthesis of monosaccharide building blocks

Due to multiple steps either failing or resulting in poor yields, a new synthetic route to the GlcNHTCA acceptor **2.3a** was designed (Scheme 2-11). This scheme contains three major changes compared to the original.



*Scheme 2-11. Synthesis of GlcNHTCA acceptor 2.3b from D-glucosamine hydrochloride. Reagent and conditions; a) D-glucosamine hydrochloride, trichloroacetylchloride,  $\text{NEt}_3$ , MeOH, 0 °C - r.t., 5 days; b)  $\text{Ac}_2\text{O}$ , pyridine, DMAP, 0 °C - r.t., 12 h; c) EtSH,  $\text{BF}_3 \cdot \text{OEt}_2$ , dry DCM, 0 °C - r.t., 12 h, (40%); d) NaOMe, MeOH, r.t., 2h (86%); e) 2,2 DMT, CSA, dry MeCN,  $\text{NEt}_3$ , 65°C, r.t., 3h, (52%); f) BzCl, pyridine, DMAP, 0 °C - r.t., 1.5 h (66%); g) 1-benzenesulfinyl piperidine, trifluoromethanesulfonic anhydride, dry DCM, 4 Å MS, 3-azidopropan-1-ol; h)  $\text{Et}_3\text{SiH}$ ,  $\text{BF}_3 \cdot \text{Et}_2\text{O}$ /TFA, dry DCM*

Due to the low and inconsistent yields observed during glycosylation with 4-methylbenzenethiol (8-48%), it was decided to substitute 4-methylbenzenethiol for the more nucleophilic ethanethiol. However, once again thioglycoside **2.35** was isolated in a lower yield than expected (40%). It was therefore theorised that the low glycosylation yields observed both here and previously for STol formation were not the result of the nucleophile chosen but instead were the result of TCA protection disarming the anomeric position.

The initial synthetic scheme used NaH as a base during *O*-3 benzyl ether protection (step f), yet NaH proved to result in irreversible cleavage of the TCA group. This presented a need for a new reagent combination. Fairbanks and co-workers<sup>253</sup> recently reported barium oxide and barium hydroxide as alternative reagents for NaH in benzylation reactions, and in their hands, usage of this combination improved their yield of GlcNAc acceptor **2.40** (Figure 2-11). However, in our hands benzylation of 4,6-*O*-benzylidene acetal-protected thioglycoside **2.37** using barium oxide and barium hydroxide was unsuccessful, with only starting material being isolated.

## Synthesis of monosaccharide building blocks

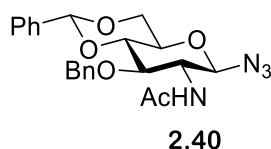


Figure 2-11. Structure of Fairbanks and co-workers GlcNAc acceptor<sup>253</sup>

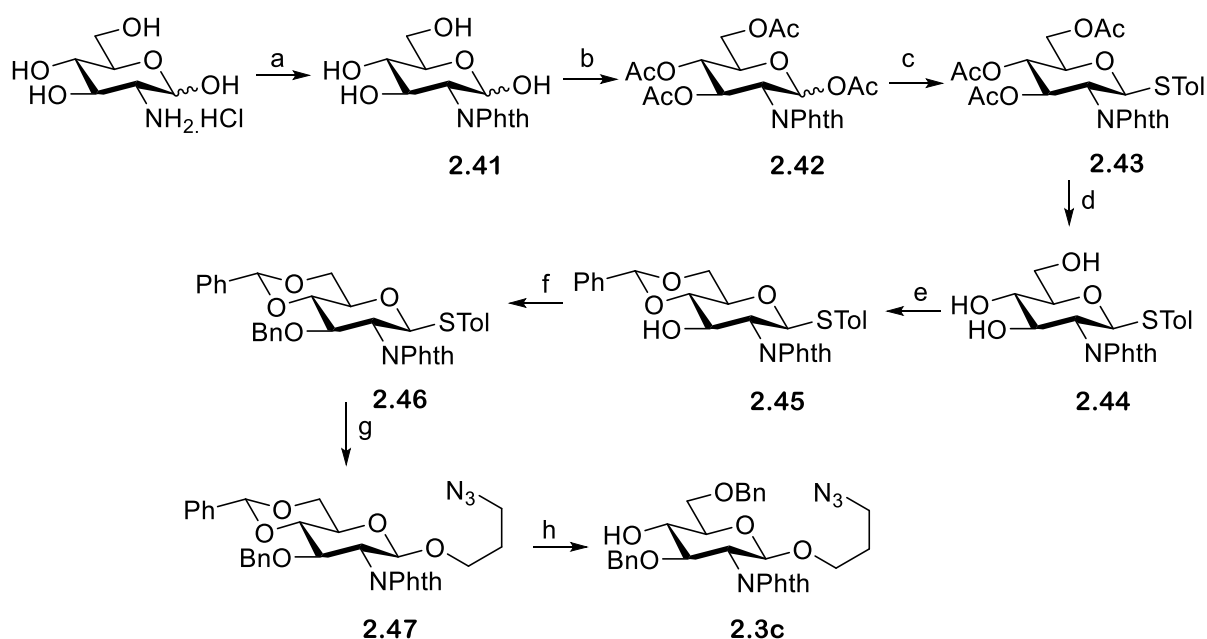
A further attempt at benzylation of the *O*-3 position of 4,6-*O*-benzylidene acetal-protected thioglycoside **2.37** was made using 1.1 eq of NaH and 1.5 eq of benzyl bromide. After 10 minutes a drop in  $R_f$  value was observed by TLC, yet post-work-up no reaction was shown to have occurred. A further reaction was set up using 1.5 eq of NaH, yet TLC analysis again suggested that no reaction had occurred. Additional NaH was added and the reaction mixture was stirred for 2 h, at which point TLC analysis indicated product formation. Unfortunately, only an 8% yield of the desired thioglycoside was isolated. This low reaction yield provides further support for the theory that TCA protection was actually deactivating both the anomeric and *O*-3 positions. Due to the difficulty observed during *O*-3 benzylation it was decided to replace the benzyl protecting group with a benzoyl protecting group. *O*-3 protection with a benzoyl group was therefore attempted, and benzoyl protected thioglycoside **2.38** was isolated in a 67% yield when using benzoyl chloride (with DMAP serving as a nucleophilic catalyst).

In a final alteration to the initially proposed reaction scheme, 3-azidopropan-1-ol glycosylation was performed prior to benzylidene acetal ring opening (Scheme 2-11). A trial glycosylation with 3-azidopropan-1-ol was performed on benzoyl protected thioglycoside **2.38**, again using van der Marel and co-workers method.<sup>237</sup> Unfortunately this reaction was again unsuccessful. The trial reaction was repeated at a higher temperature (0 °C vs -60 °C), yet the reaction was still unsuccessful. The installation of 3-azidopropan-1-ol was also attempted using the alternative glycosylation conditions of NIS and TMSOTf,<sup>254</sup> but again proved unfruitful. Due to the difficulties and low yields previously observed for reactions occurring at either the anomeric or *O*-3 positions, it was hypothesized that the electron withdrawing nature of the TCA protecting group may be hindering glycosylation with 3-azidopropan-1-ol. Notably van der Marel and co-workers used a less electron withdrawing Phth as a *N*-2 protecting group on their glucosamine donor.<sup>237</sup>

## Synthesis of monosaccharide building blocks

### 2.1.6.2 Use of phthalimide protection

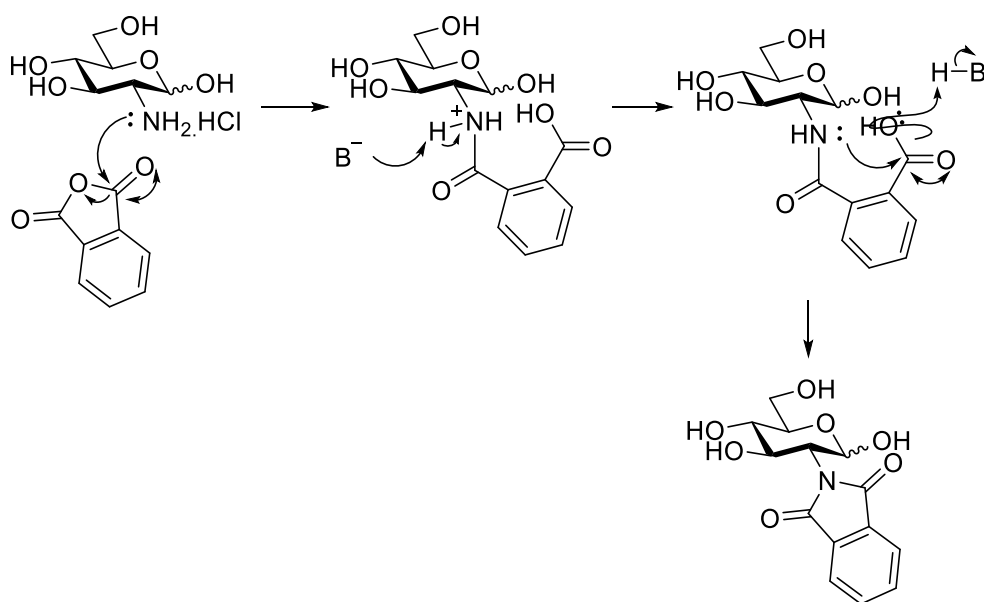
With it suspected that TCA protection at the *N*-2 position of glucosamine severely reduces the nucleophilicity of *O*-1 and *O*-3, a new GlcNPhth acceptor **2.3c** was designed. As Phth protection is less electron withdrawing than TCA this protecting group substitution should result in increased donor reactivity, helping to improve the low reaction yields previously noted during glycosylation or *O*-3 protection. GlcNPhth acceptor **2.3c** was synthesized via the route shown in Scheme 2-12. The transformations in this pathway are similar to those discussed in Scheme 2-6 (after the installation of the Phth group in the first step of the synthesis affording glycoside **2.41**).



Scheme 2-12. Synthesis of 1,4 GlcNPhth acceptor **2.3c** from *D*-glucosamine hydrochloride. Reagents and conditions: a) Phthalic anhydride, NaOH, NaHCO<sub>3</sub>, 1 : 2 MeOH : H<sub>2</sub>O, Acetone, r.t., 2 h, 50 °C, 1 h, r.t., 12h (50%); b) Ac<sub>2</sub>O, pyridine, DMAP, 0 °C - r.t., 6h, (87%); c) HSTol, BF<sub>3</sub>·Et<sub>2</sub>O, dry DCM, 0 °C - r.t., 96 h, (85%); d) NaOMe, MeOH : DCM, r.t., 20 min, (99 %); e) 2,2-DMT, dry MeCN, CSA, NEt<sub>3</sub>, r.t., 12 h, (66%); f) NaH, BnBr, dry DMF, 0 °C - r.t., 6 h, (41%); g) BSP, TTBP, Tf<sub>2</sub>O, 3-azidopropan-1-ol, 4 Å MS, dry DCE, -10 °C, 3 h, (79%); h) HSiEt<sub>3</sub>, TfOH, dry DCM, r.t., 20 minutes, (43%)

The mechanism of Phth protection is shown in Scheme 2-13, with the free amine attacking phthalic anhydride, initially opening the five-membered ring. Further reaction of the intermediary amide product is promoted by the favourable orbital overlap ahead of formation of the five-membered imide ring, which is locked in place by the aryl  $\pi$ -system.

## Synthesis of monosaccharide building blocks



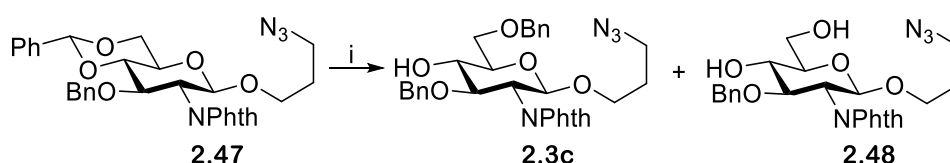
Scheme 2-13. Mechanism of phthalimide addition

In comparison to the synthesis of the GlcNHTCA acceptors **2.3a** and **2.3b**, the synthesis of GlcNPhth acceptor **2.3c** was significantly less challenging. One point to consider was the increased base sensitivity of Phth, as strongly basic conditions (e.g. pH 10) are required during deacetylation (step d) which could lead to cleavage of the Phth group in addition to the acetyl groups. To minimise this occurrence, the reaction time was reduced to 20 minutes. This change proved fruitful, yielding 99% mannoside **2.44** with no observable Phth protecting group cleavage.

One of the major advantages of Phth protection compared with TCA protection becomes apparent during formation of the thioglycoside in step c, benzyl protection in step f, and glycosylation with 3-azidopropan-1-ol in step g. The yield of thioglycoside formation was previously poor and inconsistent when using TCA protection, yet a yield of 85% of thioglycoside **2.43** was achieved using glycoside **2.42**. Previously, 3-*O* benzylation on 4,6-*O*-benzylidene acetal-protected thioglycoside **2.24** was either very low yielding or not observed at all, with TCA cleavage being the major side product. However, no such issues were observed in the benzylation of 4,6-*O*-benzylidene acetal-protected thioglycoside **2.45**, which proceeded in a 41% yield with no side-product formation being observed. Finally, while previous attempts at 3-azidopropan-1-ol glycosylation of di-benzyl protected thioglycoside **2.26** and benzoyl protected thioglycoside **2.38** were unsuccessful, 3-azidopropan-1-ol glycosylation with Phth protected thioglycoside **2.46** proceeded in a 79% yield, affording glycoside **2.47**. These improvements are likely a result of the less electron withdrawing nature of Phth compared to TCA, making both the anomeric and *O*-3 positions more reactive. This increase in reactivity enabled all steps in the Phth protected pathway to be completed, affording the benzylidene acetal protected GlcNPhth acceptor **2.3c**.

## Synthesis of monosaccharide building blocks

Substitution of TCA protection for Phth protection resulted in improved yields in many reaction steps (e.g. 4-methylbenzenethiol and 3-azidopropan-1-ol glycosylations and *O*-3 benzylidene protection). However, although an improvement in yield was observed during selective *O*-4 benzylidene acetal ring opening (37% vs 6%) the reaction still had to be repeated multiple times in order to obtain enough product to attempt a trial glycosylation. The major reason for the low yields observed during the reaction was the lack of control over the formation of the desired glycoside **2.3c**. If the reaction is left too long, or too many reactant eq are used, complete cleavage of the benzylidene ring occurs, affording diol **2.48** as the major reaction product (Scheme 2-14). Therefore, it was decided to optimise the reaction conditions by investigating different reagent combinations, reagent eq, reaction temperatures and solvent effects.



*Scheme 2-14. Ring opening reaction using a hydride and acid combination to give either the open *O*-4 position (desired glycoside **2.3c**) or 4,6-*O*-benzylidene acetal-cleaved glycoside **2.48**. Reagents- i) Acid + hydride*

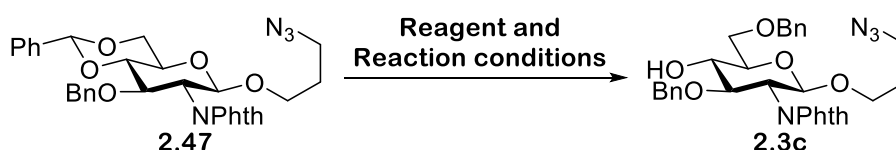
Initially,  $\text{Et}_3\text{SiH}$  and  $\text{BF}_3 \cdot \text{OEt}_2$  were the reagents chosen, as this reagent combination had previously been reported to liberate *O*-4.<sup>255</sup> However, upon testing only a 25% yield of desired glycoside **2.3c** was isolated (Table 4, Entry 1), with diol **2.48** being the major product. To try and improve the reaction yield, the quantity of both  $\text{Et}_3\text{SiH}$  and  $\text{BF}_3 \cdot \text{OEt}_2$  were increased (Table 4, Entry 2) and the reaction time was reduced. This actually had a detrimental effect, with diol **2.48** remaining the major product and no product **2.3c** being isolated.

Due to the poor yields observed with  $\text{BF}_3 \cdot \text{OEt}_2$ , it was decided to investigate the use of different Lewis acids. Van der Marel and co-workers<sup>237</sup> reported the use of  $\text{Et}_3\text{SiH}$  and TfOH to selectively open a benzylidene acetal at *O*-4, with an impressive 71% yield when using the conditions stated in Table 4, Entry 3. These conditions were replicated, and were successful, resulting in a 43% yield of the desired product **2.3c**, with minor amounts of starting material **2.47** and diol **2.48** also being isolated. Use of methyl triflate ( $\text{MeOTf}$ ) as an alternative Lewis acid was also investigated, but proved unsuccessful (Table 4, Entry 4), with no reaction being observed after 5 h at r.t. and with complete benzylidene acetal cleavage being observed after 16 h at r.t..

DIBAL-H has also been reported in the literature as a reagent which can perform selective *O*-4 benzylidene acetal ring openings on protected glycosides.<sup>256</sup> DIBAL-H was not originally selected for two reasons: i) firstly, due to the structure of desired product **2.3c**, it may remain complexed to aluminium even after workup, making extraction and purification difficult, and ii) secondly, a 10% KOH

## Synthesis of monosaccharide building blocks

solution is required during the workup procedure, which may be incompatible with the base-sensitive Phth protecting group. Nevertheless, a trial reaction was performed using a 1 M solution of DIBAL-H in toluene (0.15 mL) and a 0.2 M solution of 4,6-O-benzylidene acetal-protected glycoside **2.47** in toluene (0.263 mL) (Table 4, Entry 5). The reaction was monitored by TLC analysis, which showed the reaction to be complete after 20 minutes. However, the desired glycoside **2.3c** was not isolated post-workup. It is theorised that desired glycoside **2.3c** remained complexed to the aluminium, and thus entered the aqueous layer during extraction. Due to the presence of the base-sensitive Phth protecting group, excessive washing with 10% KOH aqueous solution in order to extract desired glycoside **2.3c** was unlikely to represent a viable solution to this problem.



Scheme 2-15. Selective O-4 benzylidene acetal ring opening of 4,6-O-benzylidene acetal-protected glycoside **2.47**

Table 4. Reagents and reactions conditions trialled for the selective O-4 benzylidene acetal ring opening of 4,6-O-benzylidene acetal-protected glycoside **2.47** depicted in Scheme 2-15

Entry	Reagents	Reaction conditions	Major product	Yield of <b>2.3c</b> (%)
1	Et <sub>3</sub> SiH (12 eq) BF <sub>3</sub> ·OEt <sub>2</sub> (2 eq)	DCM, 0 °C, 2 minutes	<b>2.48</b>	25%
2	Et <sub>3</sub> SiH (14 eq) BF <sub>3</sub> ·OEt <sub>2</sub> (3 eq)	DCM, 0 °C, 30 seconds	<b>2.48</b>	N/A
3	Et <sub>3</sub> SiH (3.3 eq) TfOH (3 eq)	DCM, -78 °C, 20 minutes	<b>2.3c</b>	43%
4	Et <sub>3</sub> SiH (3.3 eq) MeOTf (3 eq)	DCM, -78 °C – r.t., 16 h	<b>2.48</b>	N/A
5	DIBAL	1 M DIBAL in toluene 0.2 M <b>2.47</b> in toluene	N/A	N/A

## Synthesis of monosaccharide building blocks

The effect of reagent equivalents and reaction temperature was further investigated for both the Et<sub>3</sub>SiH and BF<sub>3</sub>·OEt<sub>2</sub> and the Et<sub>3</sub>SiH and TfOH systems. The acid eq of each system was reduced to 1 eq and two reaction samples were incubated at -78 °C. No reaction was observed in either sample, so both were warmed to 0 °C. This temperature increase did not result in a reaction, so both samples were further warmed to r.t. At this point the TfOH (Table 5 Entry 11) sample reacted to form a mixture of products; 10% starting material **2.47**, 10% desired glycoside **2.3c** and 50% diol **2.48**. Mass spectrometry showed the BF<sub>3</sub>·OEt<sub>2</sub> sample (Table 5 Entry 10) had also reacted, yielding a mixture of starting material **2.47** and diol **2.48**. Though these results demonstrate that both reaction temperature and acid eq play a role in controlling the formation of the desired glycoside **2.3c**, neither trial reaction afforded superior yields to that seen in Table 4 Entry 3. Therefore, all further trial reactions used 3.3 eq of TfOH and were performed at -78°C.

*Table 5. Different reagent equivalents and reaction temperatures trialled for the selective O-4 benzylidene acetal ring opening of 4,6-O-benzylidene acetal-protected glycoside **2.47** depicted in Scheme 2-15*

Entry	Reagent combinations	Reaction conditions	Major product	Yield of <b>2.3c</b> (%)
6	Et <sub>3</sub> SiH (3.3 eq) BF <sub>3</sub> ·OEt <sub>2</sub> (1 eq)	DCM, -78°C, 60 minutes	<b>2.47</b>	N/A
7	Et <sub>3</sub> SiH (3.3 eq) TfOH (1 eq)	DCM, -78°C, 60 minutes	<b>2.47</b>	N/A
8	Et <sub>3</sub> SiH (3.3 eq) BF <sub>3</sub> ·OEt <sub>2</sub> (1 eq)	DCM, 0 °C, 60 minutes	<b>2.47</b>	N/A
9	Et <sub>3</sub> SiH (3.3 eq) TfOH (1 eq)	DCM, 0 °C, 60 minutes	<b>2.47</b>	N/A
10	Et <sub>3</sub> SiH (3.3 eq) BF <sub>3</sub> ·OEt <sub>2</sub> (1 eq)	DCM, r.t., 60 minutes	<b>2.47</b> and <b>2.48</b>	N/A
11	Et <sub>3</sub> SiH (3.3 eq) TfOH (1 eq)	DCM, r.t., 60 minutes	<b>2.48</b>	10%

The final reaction factor investigated was reaction solvent, as all the previous reactions trialled using a hydride-Lewis acid combination has been performed in DCM. Due to the nature of the reaction it was decided not to trial any polar protic solvents (e.g. methanol), as it was hypothesised that hydrogen-bonding between the solvent and the reactants would increase the rate of ring cleavage, increasing the formation of diol biproduct **2.48**. As such, diethyl ether, toluene and acetonitrile were selected as potential alternative solvents. Unfortunately, 4,6-*O*-benzylidene acetal-protected glycoside **2.47** was shown to be insoluble in all three solvents at low temperatures, preventing any trial reactions from being conducted.

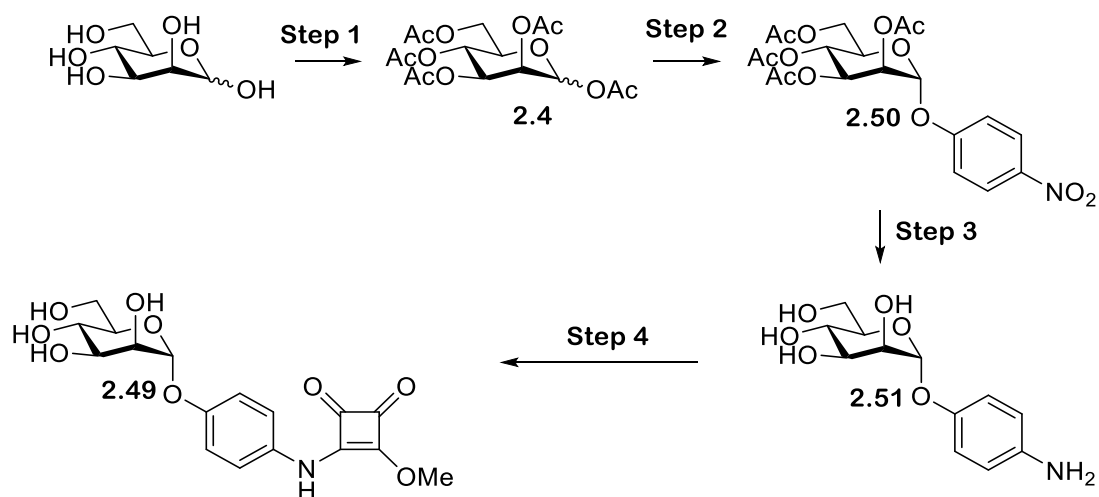
Somewhat disappointingly, in spite of extensive investigation into different reaction parameters, conditions that allow for both a high degree of control over the reaction and a high yield of desired glycoside **2.3c** could not be found. Van der Marel and co-workers<sup>237</sup> reaction conditions proved the most successful, affording a 43% yield of desired glycoside **2.3c** (Table 4, Entry 3). However, the inability to isolate the desired glycoside **2.3c** selectively and in high yields had a significant impact on this project, making it challenging to extract enough GlcPhth acceptor **2.3c** to complete proposed trisaccharide synthesis.

### 2.2 Design and synthesis of mannose squarate analogues

Due to the challenges associated with trisaccharide synthesis a simplified mannose-based inhibitor was targeted instead. A squarate mannoside scaffold was chosen for multiple reasons; firstly, squarate mannosides can be made via a simple synthetic pathway, with only four synthetic steps being required to obtain squarate mannoside **2.49** (Scheme 2-16). Furthermore, squarate mannosides have been shown in literature to have high affinity for FimH, with analogues achieving IC<sub>50</sub> values in the micromolar range.<sup>97</sup> A wide variety of squarate ester analogues can also be synthesised, with the terminal squarate methoxy group being easily substituted for an amine functionalised linker. This was an attractive prospect, as easy installation of multiple functional groups (e.g. amines or azide functionalities) enables the use of multiple bio-conjugation methods downstream during conjugate formation.



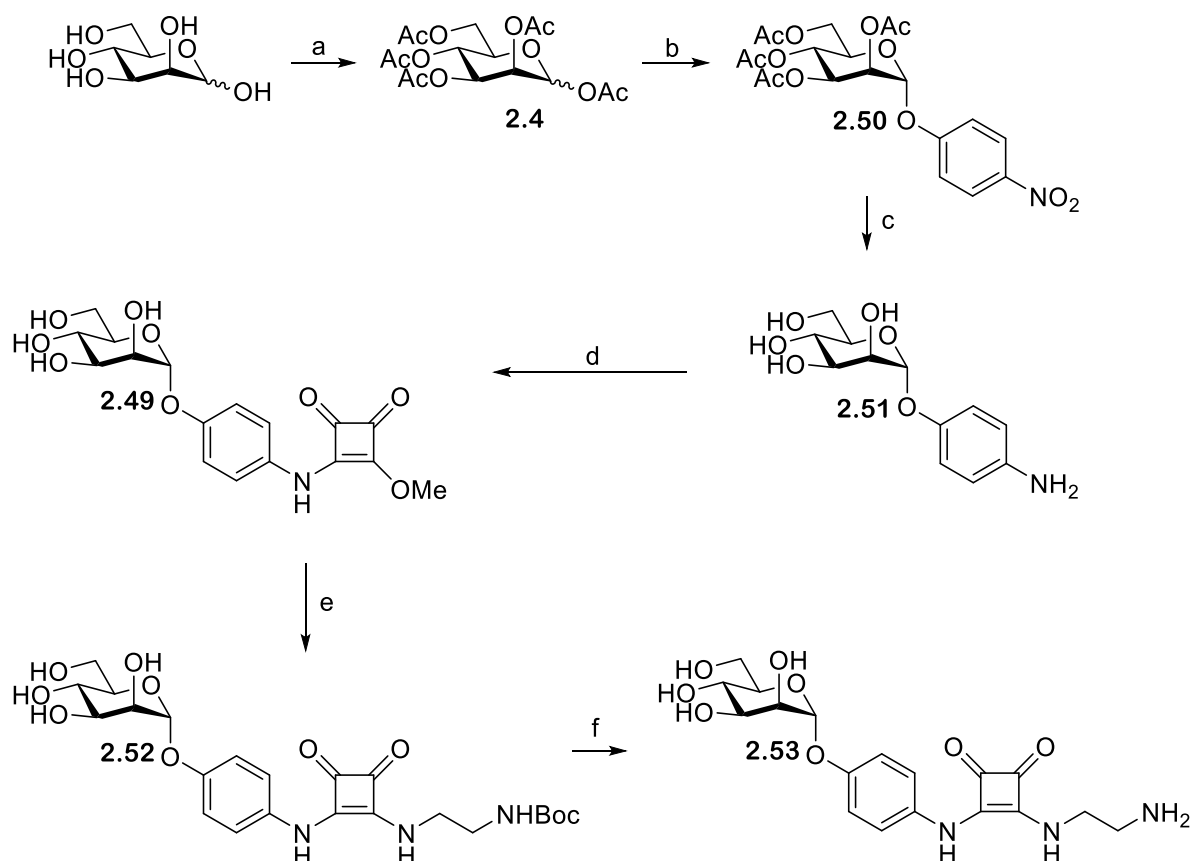
## Synthesis of monosaccharide building blocks



Scheme 2-16. Proposed 4-step chemical approach to the mannose squarate **2.49** from *D*-mannose

Amine terminated mannose-based inhibitor **2.49** was the first squarate mannoside analogue synthesized. Synthesis of this squarate ester was achieved (Scheme 2-17). The first synthetic step was peracetylation of mannose (step a, affording *D*-mannose pentaacetate **2.4**), followed by  $\text{BF}_3 \cdot \text{OEt}_2$  catalysed glycosylation with 4-nitrophenol (step b, affording mannoside **2.50**). Mannoside **2.50** was further subjected to deacetylation and subsequent hydrogenation, reducing the nitro group to an amine (step c, affording mannoside **2.51**). Once the amine group was revealed, squarate ester attachment was performed (step d, affording squarate-linked mannoside **2.49**), followed by *N*-Boc-1,2-diaminoethane addition (step e, affording mannoside **2.52**). Finally, Boc deprotection (step f) was performed, affording amine terminated mannose-based inhibitor **2.53**.

## Synthesis of monosaccharide building blocks



Scheme 2-17. Synthesis of mannose-based inhibitor **2.50** from *D*-mannose. Reagents and conditions, a)  $\text{Ac}_2\text{O}$ , pyridine, DMAP,  $0^\circ\text{C}$  - r.t., 12 h (80%); b)  $\text{BF}_3\cdot\text{OEt}_2$ , 4-nitrophenol, dry DCM,  $0^\circ\text{C}$  - r.t., 60 h, (43%); c) i) NaOMe, MeOH, r.t. 20 minutes, ii) Pd/C,  $\text{H}_2$ , dry MeOH, r.t., 12 h, (i + ii = 53%); d) Dimethyl squarate, dry MeOH, r.t., 4 h, (84%); e) *N*-Boc-1,2-Diaminoethane,  $\text{NEt}_3$ , dry MeOH, r.t., 16 h, (43%); f)  $\text{H}_2\text{O}$  : TfOH 1 : 1, r.t., 3 h (80%)

All synthetic stages were successful; though minor issues were encountered during the synthesis. One such issue was the low yield obtained in step b glycosylation of mannoside **2.4** with 4-nitrophenol which proceeded in a 43% yield. However, due to the large scale used, a sufficient quantity of mannoside **2.50** was obtained, enabling the continuation of the synthesis. Another issue encountered was the purification of squarate-linked mannoside **2.49**, as due to the polarity of the compound an appropriate chromatographic column system could not be found, making purification difficult when the reaction is performed on a small scale. This problem was overcome when the reaction was scaled-up, as on a larger scale the mannose squarate ester product precipitated out of solution, allowing isolation to be achieved via vacuum filtration. The final issue encountered was purification of amine terminated mannose-based inhibitor **2.53**. A 1:1 water : TfOH solution was used to remove the Boc protecting group, and the resultant acidic solution subsequently required neutralisation. Initially triethylamine was used, which led to a further issue regarding how to remove the resultant triethylamine salt. Due to the products polarity and solubility in water, purification was difficult as neither washing the compound with aqueous media or column chromatography could be used as purification methods. Purification was attempted using a size-exclusion column but was

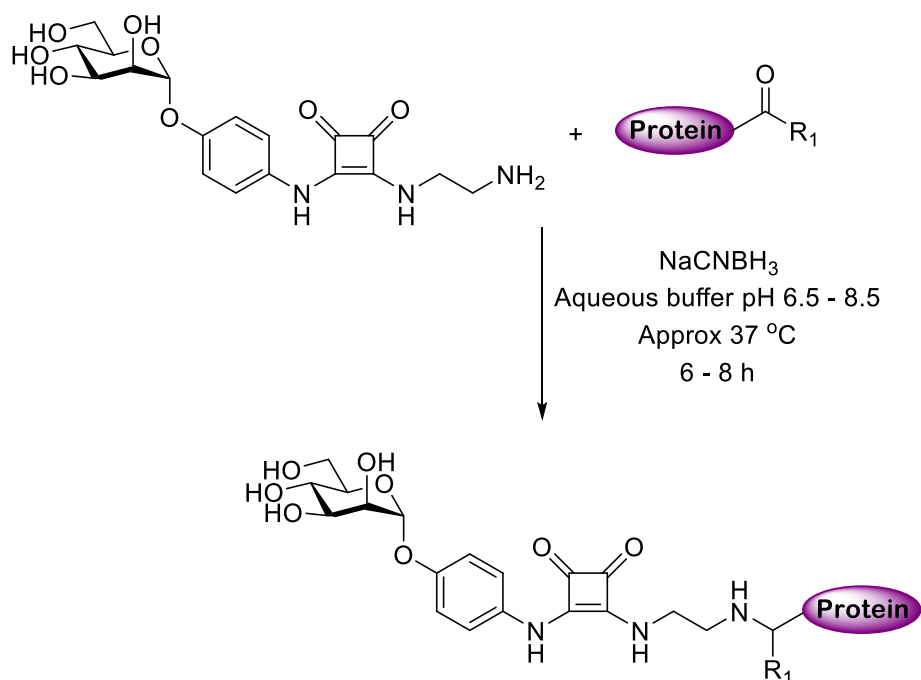
## Synthesis of monosaccharide building blocks

unsuccessful, with only triethylamine salts being isolated. An alternative neutralisation approach was thus chosen, in which basic resin (amberlite IRA-67 free base) was used to neutralise the solution and was subsequently removed via filtration, leaving no salts.

Installation of a terminal amine motif enables subsequent usage of multiple bio-conjugation techniques. Utilizing this amine functionality, amine terminated mannose-based inhibitor **2.53** can either be directly installed onto the protein of choice (e.g. via reductive amination or EDC/NHS coupling, see Figure 2-12), or attached to a heterobifunctional linker (by EDC/NHS coupling, see Figure 2-12 b) prior to protein bio-conjugation.

## Synthesis of monosaccharide building blocks

### a) Reductive amination



### b) EDC/NHS coupling

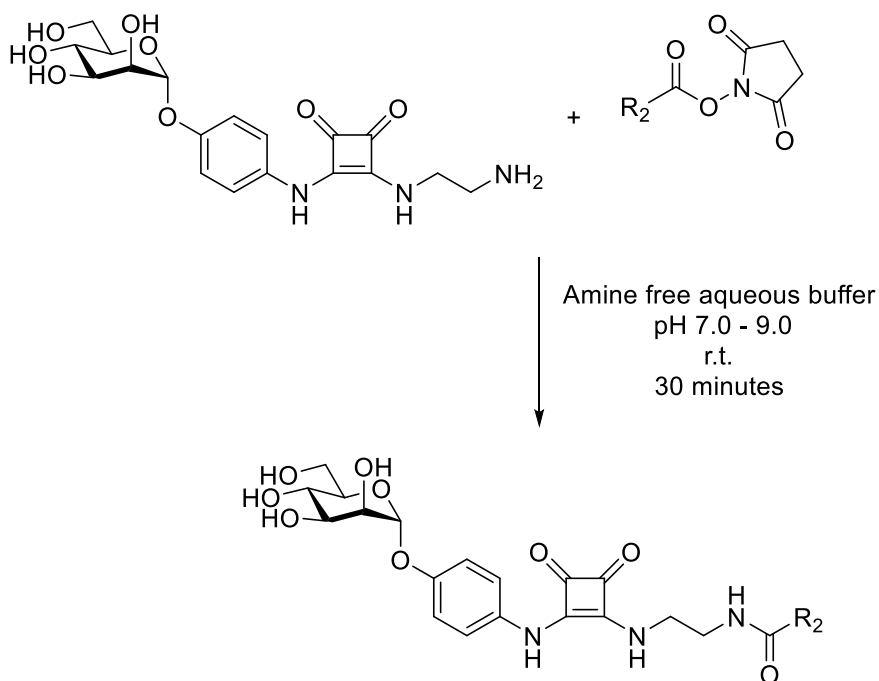
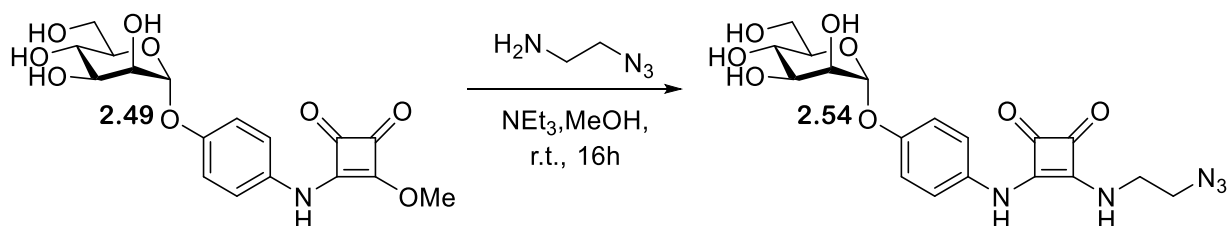


Figure 2-12. a) Depicts reductive amination reaction pathway, where  $R_1 = H$  for aldehydes and  $R_1 =$  either an alkyl or aryl group for ketones, b) depicts EDC/NHS coupling reaction pathway, where  $R_2 =$  protein when using direct coupling method and  $R_2 =$  a linker functionalised with either a maleimide, alkyne or azide motif when a functionalised linker approach is being used

## Synthesis of monosaccharide building blocks

A second squarate mannose analogue **2.54** was also synthesized (Scheme 2-18). This analogue was equipped with a terminal azide motif, enabling bio-conjugation via azide+alkyne click ligation. The synthesis of mannose-based inhibitor **2.54** follows the same initial four synthetic steps as the synthesis of amine capped mannose-based inhibitor **2.53**, but the two synthetic pathways deviate at squarate ester addition, with the Boc-protected ethylenediamine nucleophile being replaced with 1-amino-2-azidoethane, affording azide-capped squarate ester **2.54** (Scheme 2-18).



Scheme 2-18. Synthesis of azide capped squarate ester **2.54**, using 1-amino-2-azidoethane.  $\text{NEt}_3$ ,  $\text{MeOH}$ ,  $\text{r.t.}$ ,  $16\text{h}$ ,  $\leq 67\%$

### 2.3 Summary and conclusions

This chapter details the synthesis of two mannose squarate analogues which could be later used in bio-conjugation reactions to prepare a mannose-linked colicin conjugate. Two mannose squarate analogues were successfully synthesized (mannose squarate esters **2.53** and **2.54**), each equipped with a different bio-conjugation handle (e.g. amine motif or azide motif). This chapter also describes the design and synthesis of protected monosaccharide building blocks that could later be used in the synthesis of trisaccharide **1.4**.

## Chapter 3 Synthesis of mannose-based inhibitor-linked OPAL probes for use in ligation

### 3.1 Introduction

Colicins are small proteins produced by *E. coli* strains which carry the colicinogenic plasmid.<sup>257</sup> Colicins are used as an offensive weapon against competing *E. coli* strains, inducing apoptosis by a number of different mechanisms.<sup>258</sup> In this project the group A colicin E9<sup>257</sup> and group B colicin Ia<sup>257</sup> will be focused upon. Generally, group A colicins are encoded by small plasmids and are released into the surrounding medium where they are translocated into target *E. coli* cells using a Tol system.<sup>257</sup> In comparison, group B colicins are generally encoded by large plasmids and are not secreted. Group B colicins are usually translocated into the target *E. coli* using a TonB system.<sup>257</sup>

Colicin Ia (Figure 3-1) binds to the Cir outer membrane protein receptor with high affinity, with a reported  $K_{\text{assoc}}$  of  $1 \times 10^{10} \text{ M}^{-1}$  at  $37 \text{ }^\circ\text{C}$ ,<sup>259</sup> while colicin E9 (Figure 3-2) binds to the BtuB outer membrane receptor at nanomolar affinity.<sup>260</sup> Colicin Ia and colicin E9 are both composed of three distinct domains, the receptor domain (R) mediates binding to either the Cir or BtuB receptor, while the translocation domain (T) traverses the outer membrane and periplasmic space, delivering the channel forming domain (C) to the bacterial inner membrane.<sup>261, 262</sup> When in contact with the bacterial inner membrane, colicin Ia's C-domain undergoes a conformational change to form a voltage-gated ion channel in the plasma membrane,<sup>261</sup> resulting in an efflux of ions and thus apoptosis of *E. coli*.<sup>261</sup> In comparison, colicin E9 is an endonuclease toxin and induces apoptosis by degradation of bacterial genomic DNA.<sup>258</sup> For either colicin to exhibit an apoptotic effect they must be transported across the outer membrane.<sup>258</sup>

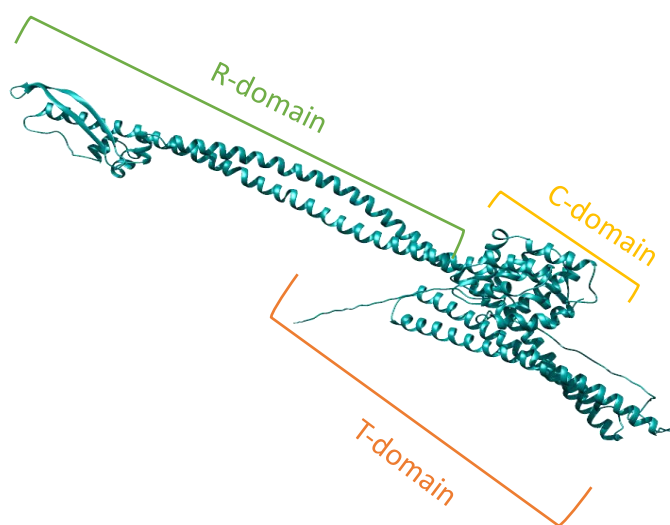


Figure 3-1. Structure of colicin Ia, highlighted are the three different domains, the R-domain (green), the C-domain (yellow) and the T-domain (orange). PDB; 1CII<sup>222</sup>

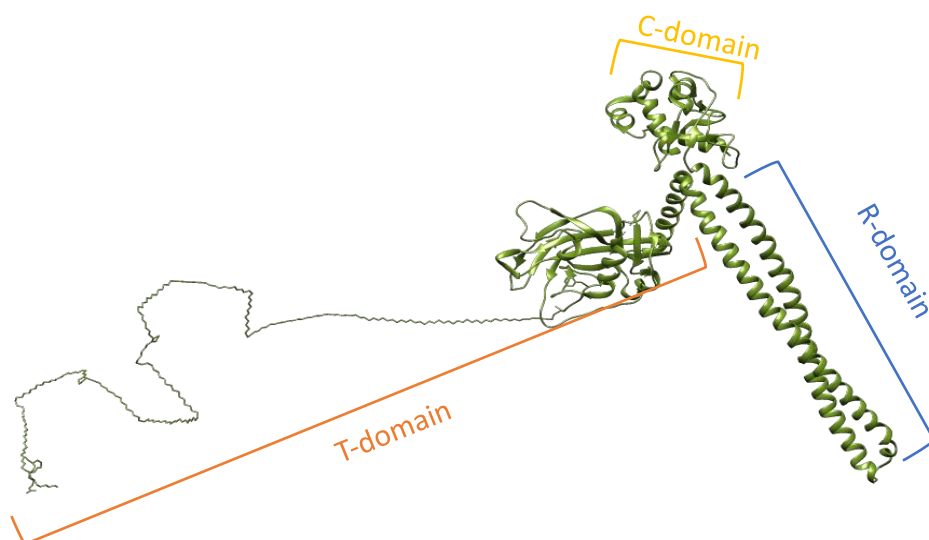


Figure 3-2. Structure of colicin E9 highlighted are the three different domains, the R-domain (green), the C-domain (yellow) and the T-domain (orange). PDB; 5EW5<sup>263</sup>

This project aims to exploit the high binding affinity of colicin Ia and E9 to their complementary receptors, while preventing either colicins from exhibiting an apoptotic effect on *E. coli*. This will be achieved by using colicin Ia and E9 mutants, both of which contain a ‘top lock’ disulfide bond within the R-domain. Installation of a disulfide bond within the R-domain of colicin E9 has previously been shown to inhibit toxicity, with toxic activity restored upon reduction of the disulfide with DTT.<sup>260</sup> It is thought that the increase in rigidity of the R-domain, caused by the installation of the disulfide bond, interferes with the translocation of colicin E9.<sup>258</sup> This principle should also apply to the addition of a disulfide bond to the R-domain of colicin Ia.

Colicins, like other bacteriocins, have therapeutic potential and are only effective against a narrow target range of bacteria, potentially allowing single bacteria strain targeting.<sup>264</sup> Furthermore, mammalian cells lack colicin target receptors, making off-target toxicity less likely.<sup>265</sup> Although this area of research is currently in its infancy, multiple studies have shown colicins exhibit antimicrobial properties,<sup>264-266</sup> with some investigations focusing on the use of colicin Ia<sup>264, 265</sup>. Though these results are promising, at present there is a lack of data regarding the potential toxicity and immunological effects of using colicins *in vivo*. In addition to potential antimicrobial activity, colicins have also been shown to exhibit anticancer activity on a number of different human tumour lines.<sup>267, 268</sup> Unfortunately, at present colicins only show mild selectivity for cancer cells over healthy cells, limiting their applications in cancer treatment.<sup>268</sup>

## Synthesis of mannose-based inhibitor-linked OPAL probes for use in ligation

Many group A colicins target the BtuB receptor, a highly abundant receptor (200 copies per cell)<sup>269</sup> located on the *E. coli* outer membrane and responsible for cyanocobalamin transport.<sup>257, 270</sup> The binding of cyanocobalamin to BtuB is calcium dependent, as depletion in calcium levels results in a 50-100 fold decrease in binding affinity.<sup>271</sup> The structure of the BtuB receptor (Figure 3-3) consists of a 22-stranded  $\beta$ -barrel with an *N*-terminal hatch domain embedded within the  $\beta$ -barrel lumen.<sup>272</sup> The BtuB receptor is TonB dependent, with a TonB protein forming part of the inner membrane complex responsible for producing the energy needed for transport of cyanocobalamin across the membrane.<sup>273-275</sup>

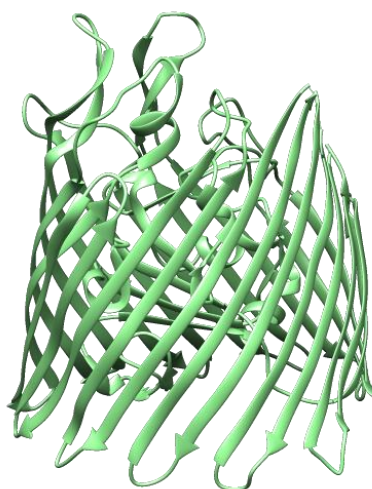


Figure 3-3. Crystal structure of spin-labelled BtuB T156R1, PDB; 3RGM<sup>223</sup>

In addition to the BtuB receptor, group A colicins require other embedded outer membrane proteins to cross the *E. coli* membrane.<sup>276</sup> Group A colicin toxicity has been shown to be dependent on either the OmpF or OmpC porin.<sup>277</sup> OmpF (Figure 3-4) is a non-specific pore protein which is highly abundant on the outer membrane of *E. coli*,<sup>278</sup> with each *E. coli* displaying over 100,000 copies.<sup>258, 279</sup> OmpF forms a trimeric structure, with each monomer consisting of a 16-stranded  $\beta$ -barrel.<sup>280</sup> Kleanthous and co-workers provided direct evidence that OmpF binds to the BtuB-ColE9 / Im9 complex on *E. coli*'s outer membrane, confirming the role of OmpF in the uptake of colicin E9.<sup>258</sup> Although both OmpF and BtuB are highly abundant on *E. coli*'s surface, they are rarely situated closely enough together to form a complex. Complex formation therefore relies on the diffusion of BtuB receptor across the outer membrane and collisional interactions with the relatively immobile OmpF.<sup>281</sup> The exact process by which OmpF facilitates colicin E9 translocation across the outer membrane is unknown, but there are currently multiple hypotheses all in their preliminary stages.<sup>282</sup>



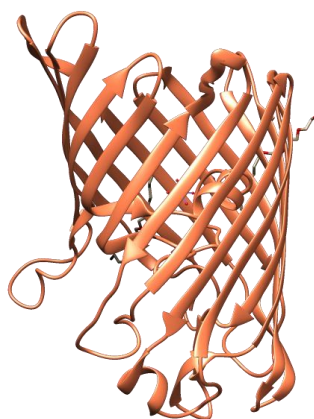


Figure 3-4. Structure of the OmpF porin. PDB 2ZFG <sup>283</sup>

The Cir receptor (Figure 3-5) is another highly abundant outer membrane protein receptor located on *E. coli*, with around 5000 receptors present on each *E. coli*.<sup>259</sup> Like the BtuB receptor, the Cir receptor consists of a 22-stranded transmembrane  $\beta$ -barrelled structure, with a *N*-terminal plug domain inserted within the  $\beta$ -barrel.<sup>284, 285</sup> The *N*-terminal domain contains a seven residue stretch called the TonB box; this stretch interacts with TonB proteins facilitating substrate uptake.<sup>284</sup> The main function of the Cir receptor is to bind and transport  $\text{Fe}^{3+}$  complexed to linear catecholates (e.g dihydroxybenzoyl serine) across the outer membrane.<sup>286</sup> The Cir receptor is additionally targeted by colicin Ia,<sup>285</sup> and has further been implicated in the uptake of catechol-substituted cephalosporins.<sup>287-290</sup> Finkelstein and co-workers found that, in addition to binding to the receptor binding domain of colicin Ia, the Cir receptor could also bind to the translocation domain weakly.<sup>284</sup> This result supports the hypothesis that translocation of colicin Ia involves two Cir receptors working independently, with one Cir receptor bound to the R domain of the colicin Ia and a second receptor bound to the T domain.<sup>284</sup>

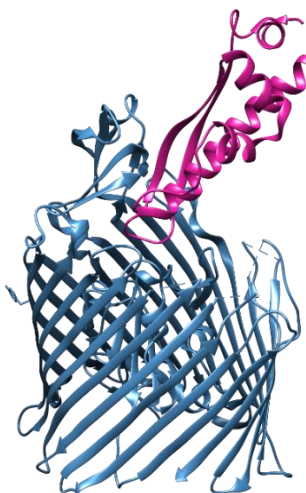


Figure 3-5. Structure of colicin IA (pink) bound to the Cir receptor (blue), PDB; 2HDI<sup>291</sup>

### 3.2 Section aims

The overall aim of this section is to synthesize a library of mannose-based inhibitor-linked colicin conjugates. To achieve this objective several bodies of work will have to be completed. Firstly, samples of colicin E9 need to be expressed and purified. Samples of colicin Ia containing a free cystine residue will be provided by the Baumann laboratory. Secondly, Potential bio-conjugation pathways will be explored, focusing on the use of either maleimide ligation or OPAL ligation. Maleimide ligation is well established in the literature with commercial probes available. However, for maleimide ligation to be utilised a colicin E9 mutant containing a free cystine residue would need to be designed, representing a significant time investment. Due to both colicin proteins possessing an *N*-terminal serine residue no mutants would be required for OPAL ligation. Nevertheless, OPAL ligation has previously not been used to ligate a glycan to a protein. Thus, if OPAL ligation is chosen, variously sized mannose-based inhibitor-linked OPAL probes would need to be synthesized. Finally, once a bio-conjugation pathway has been decided upon a library of mannose-based inhibitor-linked colicin conjugates will be synthesized.

### 3.2 Results and discussion

#### 3.2.1 Expression and purification of colicin E9

Expression and purification of colicin E9 was successfully performed in-house following the protocol attached in Experimental section 8.3.1.1 page 270. Colicin-expressing organisms protect themselves from the apoptotic effects of colicins by co-expressing a small cytoplasmic inhibitor known as an immunity protein (Im),<sup>292</sup> with the Im9 being expressed such that it is associated with colicin E9.<sup>293</sup> Preparatively, breakdown of the colicin E9 immunity complex can be achieved during Ni<sup>2+</sup> affinity purification, by engineering Im9 to contain a His<sub>6</sub> tag. The His<sub>6</sub>-tagged Im9 thus binds to the Ni<sup>2+</sup> affinity column, where after treatment with a denaturing buffer (pH 7.0, 20 mM K phosphate + 0.5 M NaCl + 6 M guanidine) stimulates the unfolding of colicin E9, releasing it from the bound Im9. Once separated, the denatured colicin E9 can be dialysed into a guanidine-free buffer (pH 7.0, 20 mM K phosphate + 0.5 M NaCl), where after it refolds.

The first attempt at expression and purification of colicin E9 was unsuccessful, as only a faint protein band was observed at 70 kDa post-Ni<sup>2+</sup> affinity purification. Furthermore, dialysis of these pooled fractions induced protein precipitation. The sample was centrifuged to afford a protein pellet and the resulting supernatant was concentrated, whereafter an absorbance measurement at 280 nm and an SDS-PAGE gel confirmed the supernatant sample did not contain a significant amount of protein.

The *lactose (lac)* operon in *E. coli* is a sequence of three structural genes necessary for the transport and metabolism of lactose.<sup>294</sup> One of these genes (*lacZ*) codes for  $\beta$ -galactosidase, an intracellular enzyme that cleaves lactose (a disaccharide) into glucose and galactose, another (*lacY*) codes for  $\beta$ -galactoside permease, a transmembrane protein that pumps  $\beta$ -galactosides (including lactose) into the cell, and the third (*lacA*) codes for  $\beta$ -galactoside transacetylase, an enzyme that transfers an acetyl group from acetyl-CoA to  $\beta$ -galactosides during metabolism.<sup>294</sup> *Lac* operon expression is regulated by the *lac* repressor and increases above basal levels when glucose levels are low<sup>295</sup>. The *lac* repressor binds specifically to DNA at the operator region of the *lac* operon<sup>296</sup> inhibiting *lac* operon transcription.<sup>297-299</sup> *E. coli* basally expresses the *lac* operon to a small degree, as small amounts of  $\beta$ -galactosidase and  $\beta$ -galactoside permease<sup>297</sup> are required to allow *E. coli* to respond to changes in lactose or glucose levels via the formation of the lactose metabolite allolactose,<sup>300</sup> an inducer of the *lac* operon.<sup>301</sup> When glucose levels are low or lactose levels are high, allolactose binds to the *lac* repressor, inducing an allosteric shape change,<sup>297, 299, 302</sup> destabilising the *lac* repressor-*lac* operon complex, resulting in increased transcription of the *lac* operon.<sup>297</sup> The 'hunger signal,' cyclic AMP (cAMP),<sup>303</sup> is produced by *E. coli* when glucose levels are low. cAMP can bind to Catabolite activator protein (CAP or cAMP receptor protein (CRP)),<sup>304, 305</sup> and the resulting complex binds to a specific site in the DNA of the *lac* promoter region,<sup>305, 306</sup> enhancing the binding of RNA polymerase to the promoter DNA of the *lac* operon.<sup>304, 305</sup>

In the plasmid construct used for colicin E9 expression, the genes needed for colicin E9 expression are located after a *lac* operon, and thus activation of the *lac* operon results in colicin E9 expression. Isopropyl  $\beta$ -D-1-thiogalactopyranoside (IPTG) is an allolactose mimic<sup>307</sup> (Figure 3-6), which when added to an *E. coli* culture results in activation of the *lac* operon and stimulation of gene expression. Low glucose levels prior to IPTG induction can result in leaking of the *lac* operon, and therefore keeping glucose levels high prior to IPTG-induced colicin E9 expression will minimise leaking of the *lac* operon. A second attempt at colicin E9 expression and purification was attempted, using LB media supplemented with glucose (final concentration = 0.4% w/v D-glucose). This supplementation was shown to increase expression of colicin E9 and 4.78 mg of purified colicin E9 was extracted for use during protein bio-conjugation experiments.

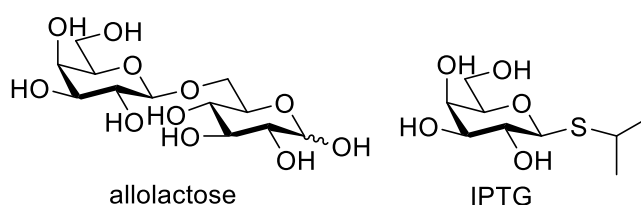


Figure 3-6. Structures of allolactose and IPTG

### 3.2.2 Investigation into potential bio-conjugation techniques

Following the successful synthesis of mannose-based inhibitors **2.53** and **2.54**, (Figure 3-7) the next task was to start investigating different potential bio-conjugation methods which could be used to append either inhibitor to a colicin protein. Mannose-based inhibitor **2.53** contains a terminal amine motif which allows utilization of bio-conjugation techniques like reductive amination (Figure 2-12a) and EDC NHS coupling (Figure 2-12b). Conversely, mannose-based inhibitor **2.54** has a terminal azide group, allowing exploration of click ligation methods such as CuAAC and SPAAC ligation.

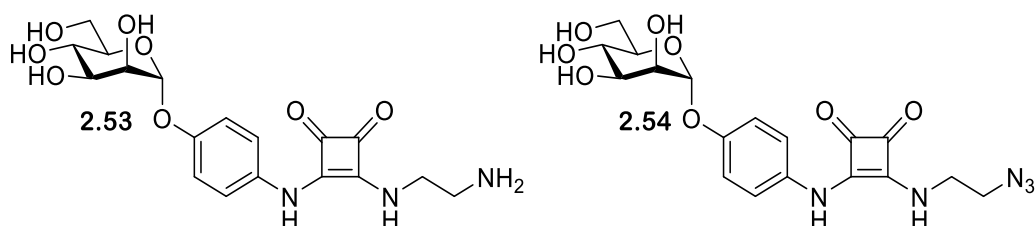
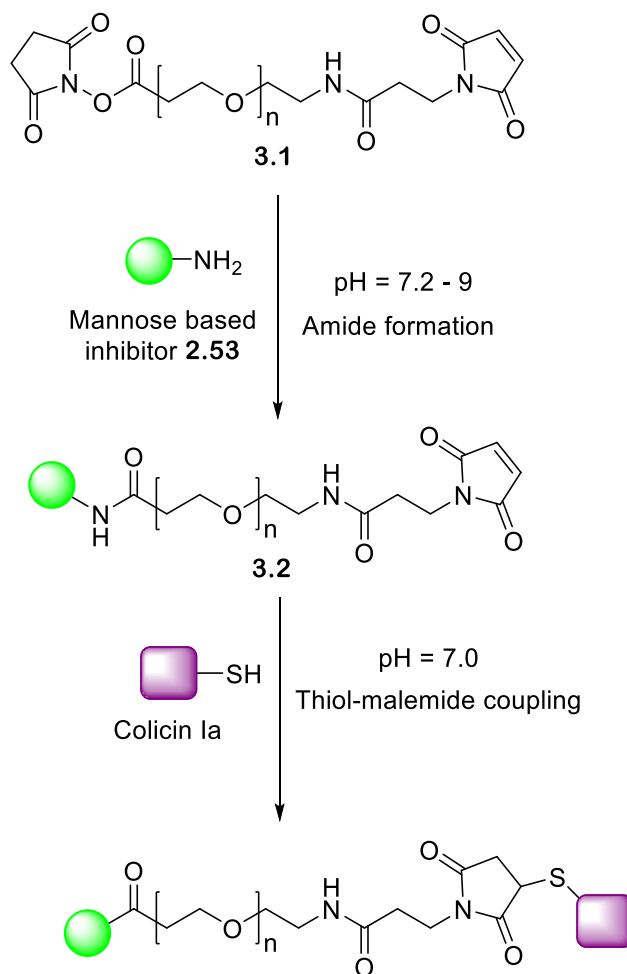


Figure 3-7. Structure of mannose-based inhibitors 2.53 and 2.54

Neither colicin Ia or E9 contain the appropriate motifs (an aldehyde / ketone motif for reductive amination or an alkyne motif for either CuAAC or SPAAC) to allow for direct installation of either mannose-based inhibitor. Consequently, a linker molecule will be required for conjugation. A commercially available compatible linker (heterobifunctional linker **3.1**, Scheme 3-1) was found for the conjugation of colicin Ia to mannose-based inhibitor **2.53**. Heterobifunctional linker **3.1** contains an NHS ester which can react with the terminal amine on mannose-based inhibitor **2.53**, as well as a maleimide motif which can react with the thiol group present at the free cysteine residue on colicin Ia. The reactivity of heterobifunctional linker **3.1** is pH dependant - at pH 7.2-9 amide formation is favoured, whereas at pH 7.0 maleimide ligation is favoured. This allows for selective addition of mannose-based inhibitor **2.53** to heterobifunctional linker **3.1**, to afford mannose-based inhibitor-linked heterobifunctional linker **3.2** prior to maleimide ligation with colicin Ia (Scheme 3-1).

## Synthesis of mannose-based inhibitor-linked OPAL probes for use in ligation



*Scheme 3-1. Schematic depicting the pH-dependent reactions of heterobifunctional linker 3.1, which initially undergoes an EDC NHS reaction with mannose based inhibitor 2.53 to afford mannose-based inhibitor-linked heterobifunctional linker 3.2, and then subsequently undergoes maleimide ligation to the free thiol unit located on colicin Ia*

Colicin Ia (70 kDa) is too large to be observed by mass spectroscopy on the FT-ICR. As such, maleimide conjugation of colicin Ia to mannose-based inhibitor-linked heterobifunctional linker **3.2** was monitored using a lectin blot mediated by a concanavalin A peroxidase conjugate. Concanavalin A is a mannose binding lectin<sup>308</sup> and horseradish peroxidase catalyses the oxidation of luminal to a range of substrates, including components of bioluminescent systems<sup>309-311</sup> causing the emission of UV light. The addition of an enhanced chemiluminescence (ECL) reagent amplifies luminescence allowing for detection via UV imaging. Concanavalin A will only bind to colicin Ia which has undergone conjugation to mannose-based inhibitor-linked heterobifunctional linker **3.2**, meaning only the conjugated colicin Ia is detectable under UV.

## Synthesis of mannose-based inhibitor-linked OPAL probes for use in ligation

Conjugation of mannose-based inhibitor **2.53** to colicin Ia using heterobifunctional linker **3.1** was performed. A lectin blot and a SDS-PAGE gel (Figure 3-8 and Figure 3-9) confirmed that the conjugation was successful. Like many proteins containing a free cysteine residue, colicin Ia shows a tendency to form disulfide-linked dimers.<sup>312</sup> In these disulfide-linked dimers, both the previously-free cysteine residues of the individual colicins are inaccessible for modification via maleimide ligation. As such, prior to maleimide ligation colicin Ia was treated with the thiol reducing agent  $\beta$ -mercaptoethanol ( $\beta$ Me). UV activity was observed in lanes B-E of the lectin blot (Figure 3-9) - these lanes all contained modified colicin Ia. Comparatively no UV activity was observed in lanes F-I, which contained unmodified colicin Ia. All lanes in the SDS-PAGE gel (Figure 3-8), contain a major band around 70 kDa for colicin Ia monomer. Lanes B-E also contain a minor band around 140 kDa for the colicin Ia dimer. A further interesting observation is that the major band in lanes B-E is higher than that in lanes F-I, providing further evidence that the conjugation of colicin Ia to mannose-based inhibitor-linked heterobifunctional linker **3.2** was successful.

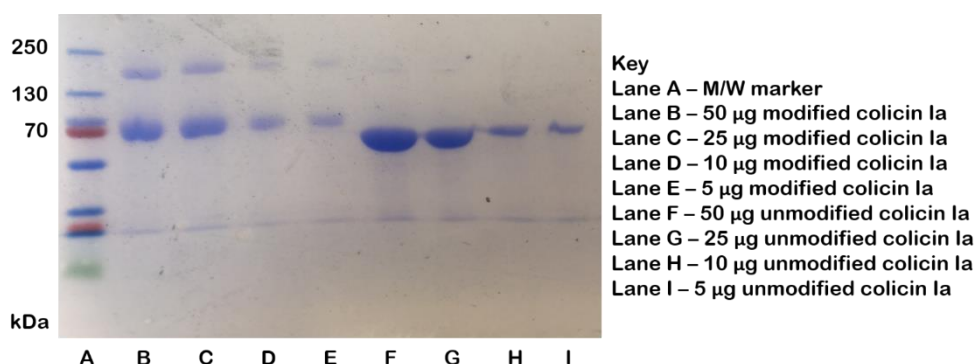


Figure 3-8. SDS-PAGE gel (stained with Coomassie) containing colicin Ia which has been subjected to ligation with mannose-based inhibitor-linked heterobifunctional linker **3.2** (lanes B-E) and unmodified colicin Ia (lanes F-I)

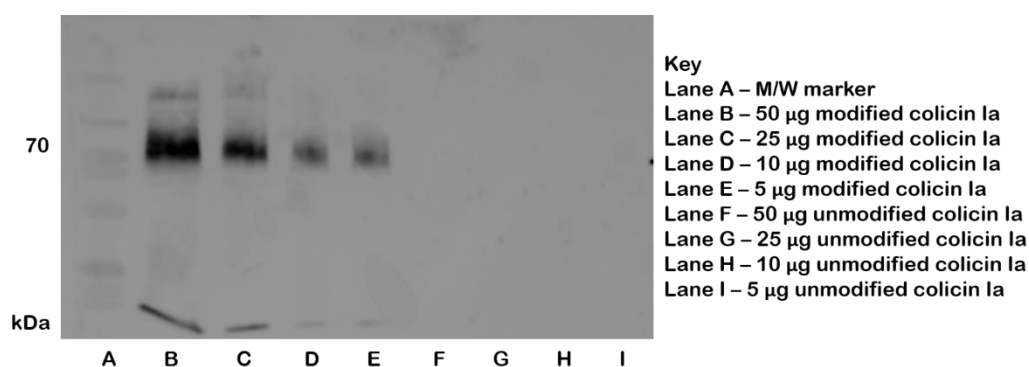
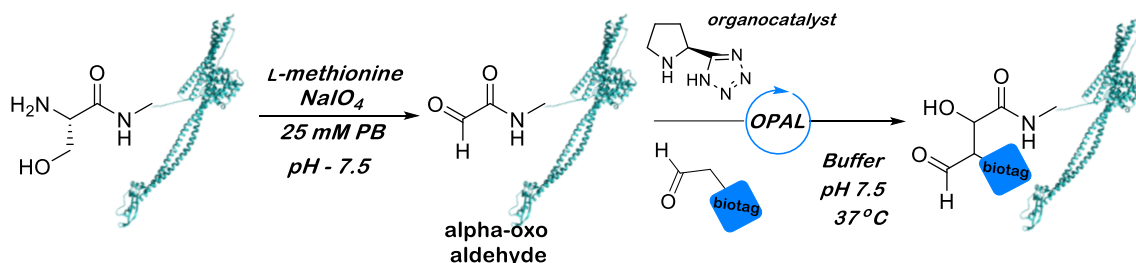


Figure 3-9. Lectin blot containing colicin Ia which has been subjected to ligation with mannose-based inhibitor-linked heterobifunctional linker **3.2** (lanes B-E) and unmodified colicin Ia (lanes F-I)

## Synthesis of mannose-based inhibitor-linked OPAL probes for use in ligation

Colicin E9 does not contain a free cystine residue, and therefore cannot undergo maleimide ligation. As such, a new bio-conjugation method was needed to afford a mannose-linked colicin E9 conjugate. Both colicin E9 and colicin Ia contain an *N*-terminal serine residue, meaning they can be readily subjected to OPAL ligation - a bio-conjugation method developed in the Fascione laboratory (Scheme 3-2).



*Scheme 3-2. Schematic for colicin Ia undergoing initial NaIO<sub>4</sub>-mediated oxidative cleavage of the N-terminal 1,2-amino alcohol to give an alpha oxo-aldehyde, which can subsequently be subjected to OPAL ligation with an aldehyde-charged probe, mediated by a proline tetrazole catalyst. (R = a biotag such as folate, dansyl and biotin)*

The preparation of an OPAL-ligated construct involves two steps, with the first being the oxidation of the *N*-terminal serine residue on either colicin Ia or colicin E9 using NaIO<sub>4</sub>, which functionalises the *N*-terminus with an alpha-oxo aldehyde via the oxidative cleavage of the 1,2-amino alcohol. This step is conducted in the presence of L-methionine to protect the protein from over-oxidation. Once the alpha-oxo aldehyde has been introduced, the colicin is then treated with a secondary amine organocatalyst (the tetrazole variant shown in scheme is the most effective known) and an active biomolecule-tagged OPAL probe (e.g. functionalised with biotin, folate, azide, or sugar units).

To test whether OPAL ligation would be an appropriate bio-conjugation technique, both colicin E9 and Ia were subjected to OPAL conjugation with biotin-linked OPAL probe **3.3**, synthesized by a previous group member (Figure 3-10). Western blots and an SDS-PAGE gel were used to determine that OPAL conjugation of both colicin Ia and E9 to biotin-linked OPAL probe **3.3** had been successful. The Western blots for both colicins (Figure 3-11 and Figure 3-12) showed background UV activity in all lanes, but both membranes showed significant UV activity in lanes B, C and D, all of which contained biotin-modified colicin. No significant UV activity was seen in lane E of either membrane, even though these lanes did contain biotin-modified colicin. This is likely due to the concentration of protein present being too low to exhibit UV activity. The SDS-PAGE gel (Figure 3-13) supports the Western blot findings as all lanes contain a major protein band around 70 kDa, indicative of the presence of monomeric colicin Ia or colicin E9.

Synthesis of mannose-based inhibitor-linked OPAL probes for use in ligation

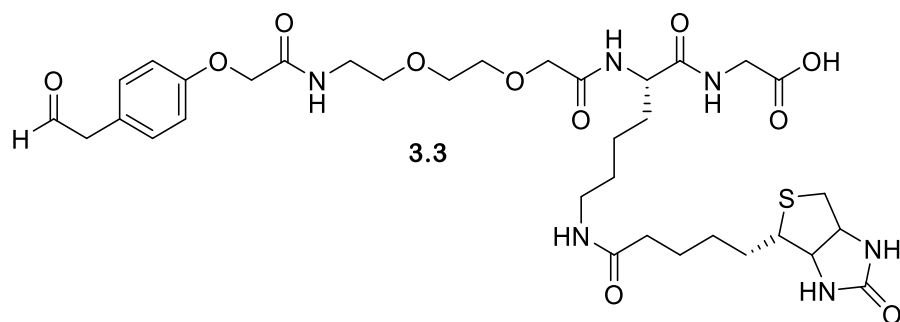


Figure 3-10. The structure of biotin-linked OPAL probe **3.3**

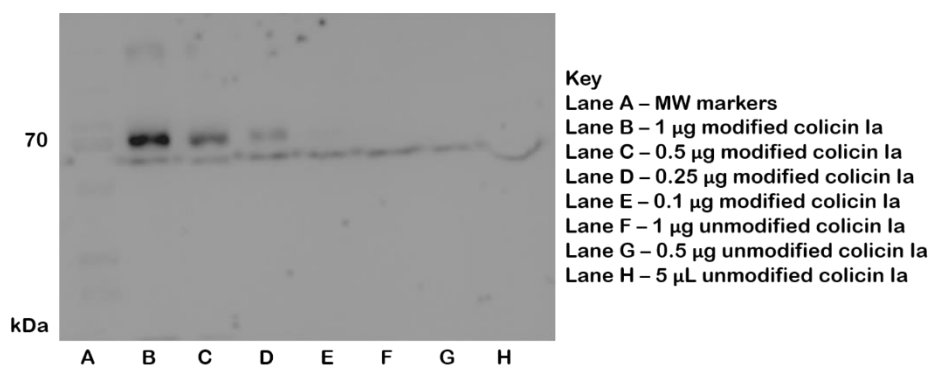


Figure 3-11. Results of lectin blot containing colicin Ia which has been subjected to OPAL ligation with biotin-linked OPAL probe **3.3** (lanes B-E) and unmodified colicin Ia (lanes F-H)

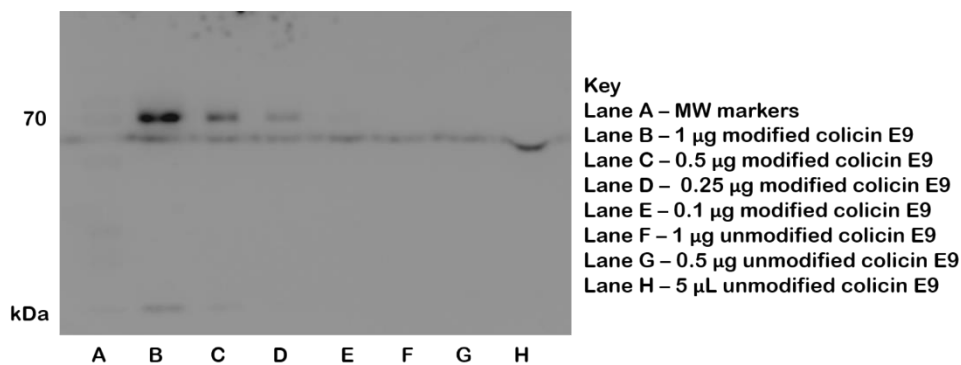
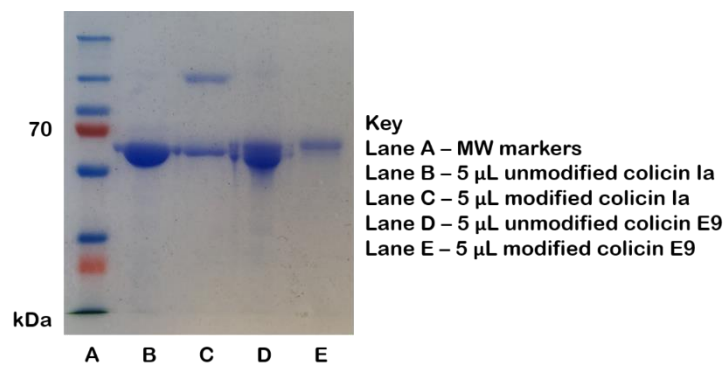


Figure 3-12. Results of lectin blot containing colicin E9 which has been subjected to OPAL ligation with biotin-linked OPAL probe **3.3** (lanes B-E) and unmodified colicin E9 (lanes F-H).



## Synthesis of mannose-based inhibitor-linked OPAL probes for use in ligation



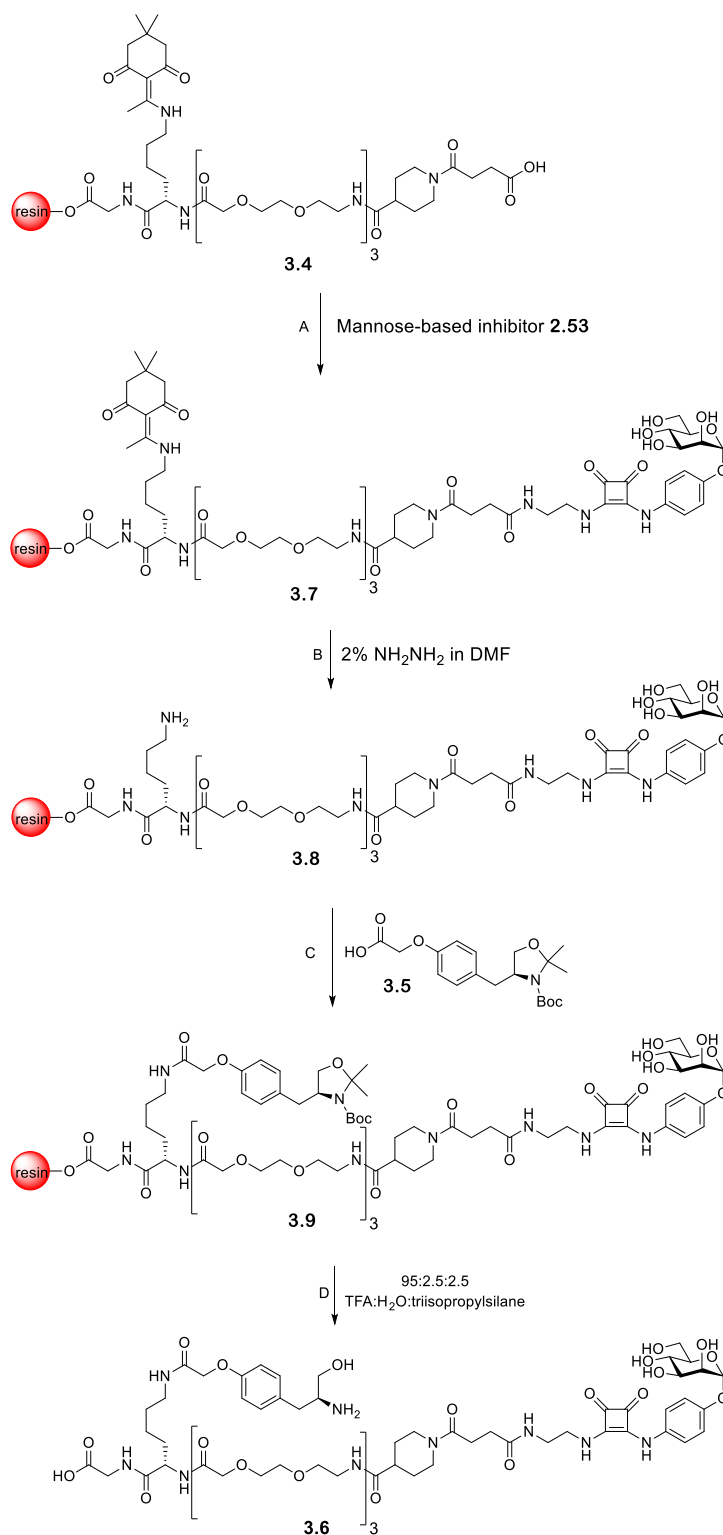
*Figure 3-13. Results of SDS-PAGE gel stained with Coomassie containing unmodified colicin Ia (lane B), colicin Ia which has been subjected to ligation with biotin-linked OPAL probe **3.3** (lane C), unmodified colicin E9 (lane D) and colicin E9 which has been subjected to ligation with biotin-linked OPAL probe **3.3** (lane E)*

### 3.2.3 Synthesis of a library of mannose-based inhibitor-linked OPAL probes

Once it had been proven that both colicin Ia and E9 underwent OPAL ligation, the development of a mannose-based inhibitor-linked OPAL probe became a priority. OPAL probe synthesis is typically conducted on a peptide synthesiser, and the commercial availability of amino acids containing dansyl and biotin units makes the incorporation of these groups into OPAL probes straightforward. As an amino acid functionalized with mannose-based inhibitor **2.53** or **2.54** is not commercially available, installation of either mannose-based inhibitor would be more challenging.

Peptide **3.4** (Scheme 3-3) was designed as an initial scaffold for a mannose-based inhibitor-linked OPAL probe. The key components in the design of peptide **3.4** are the PEG spacer units, which are installed to separate the points at which mannose-based inhibitor **2.53** and OPAL small molecule **3.5** will be attached. Furthermore, installation of piperidine-4-carboxylic acid prior to succinic anhydride installation prevents cyclisation of succinic anhydride, which if allowed to occur would prevent further peptide coupling. Succinic anhydride was included in the peptide design as a point of attachment for mannose-based inhibitor **2.53**. Due to the terminal amine present on mannose-based inhibitor **2.53**, traditional peptide coupling could not be used, but by reacting succinic anhydride with the terminal amine group on the peptide a carboxylic acid becomes installed, allowing mannose-based inhibitor **2.53** to itself be coupled to by amide bond formation (Scheme 3-3, step A). The second amino acid present in peptide **3.4** is Lys(Dde) - this serves as a point of attachment for OPAL small molecule **3.5**, as once the peptide backbone has been synthesised the Dde group can be deprotected using a solution of 2% hydrazine in DMF (Scheme 3-3, step B), revealing a free amine motif to which OPAL small molecule **3.5** can be coupled (Scheme 3-3, step C). The final stage of OPAL probe synthesis is resin cleavage (Scheme 3-3, step D) which yields mannose-based inhibitor-linked OPAL probe **3.6**.

## Synthesis of mannose-based inhibitor-linked OPAL probes for use in ligation



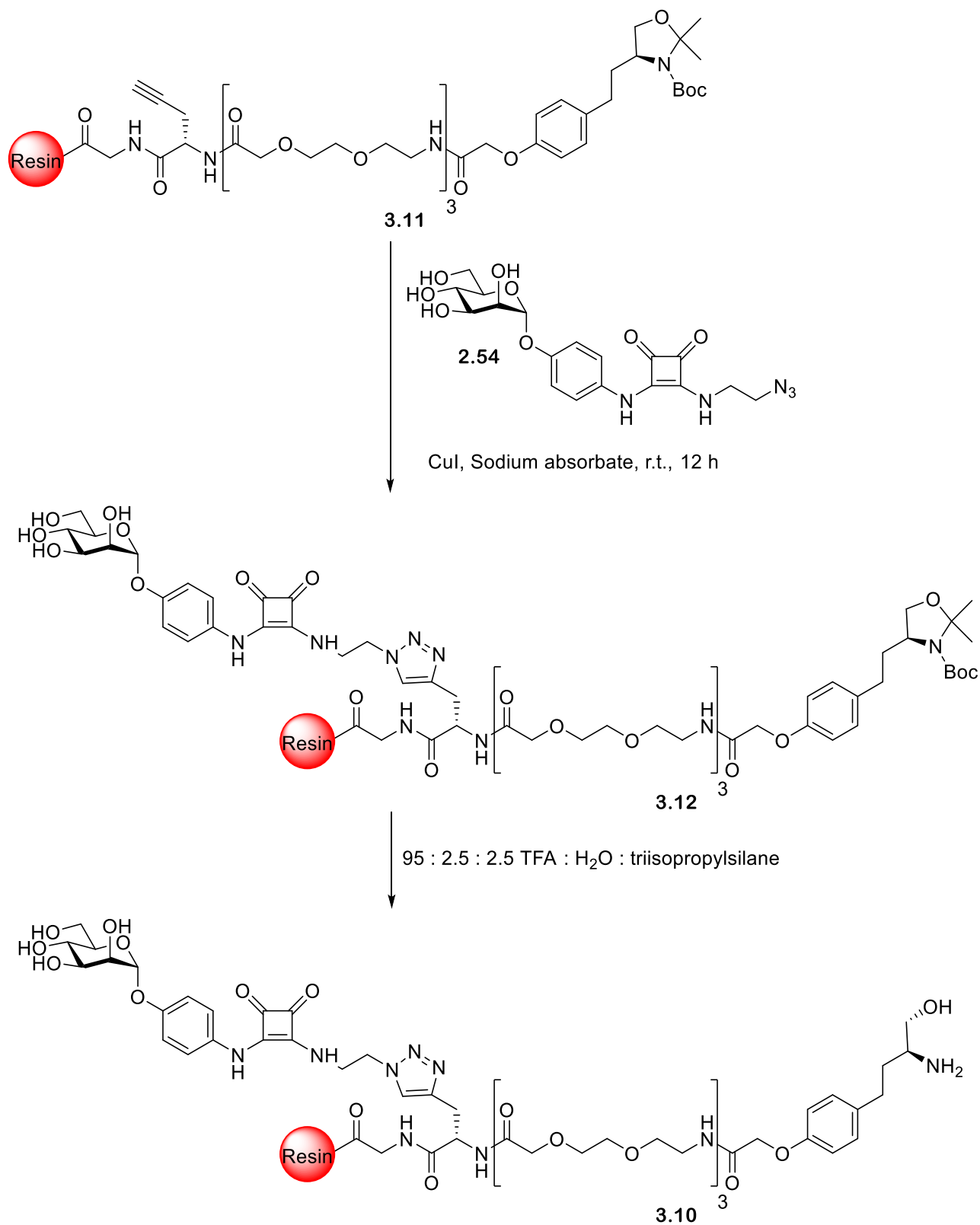
*Scheme 3-3. Reaction schematic for proposed conversion of peptide 3.4 to mannose-based inhibitor-linked OPAL probe 3.6. Following initial attachment of mannose-based inhibitor 2.53 (step A) to afford Dde protected mannose-based inhibitor-linked peptide 3.7, which is treated with 2% hydrazine in DMF (step B) to afford mannose-based inhibitor-linked peptide 3.8. The revealed free amine residue allows for attachment of OPAL small molecule 3.5 (step C) affording protected mannose-based inhibitor-linked OPAL probe 3.9, the final step is treatment with 95 : 2.5 : 2.5 TFA :  $\text{H}_2\text{O}$  : triisopropylsilane to afford mannose-based inhibitor-linked OPAL probe 3.6*

## Synthesis of mannose-based inhibitor-linked OPAL probes for use in ligation

Characterisation of mannose-based inhibitor-linked OPAL probe **3.6** was challenging, as liquid chromatography mass spectrometry (LCMS) traces only gave weak product mass signals at 1448.48 m/z, even at high concentrations of deprotected probe **3.6**. Fourier transform ion cyclotron resonance (FT-ICR) mass spectrometry, using both ESI and MALDI, further showed the presence of weak product mass signals. More interestingly, no common impurity peaks could be identified across all three mass spectra, suggesting the weak product peak intensity observed could be due to deprotected probe **3.6** being difficult to ionise during mass spectrometry. It was hypothesized that purification of deprotected probe **3.6** using an LH-20 column might increase its visibility in mass spectrometry analysis. Unfortunately, post-purification LCMS traces again displayed only a weak product peak, and it was thus decided to redesign the mannose-based inhibitor linked OPAL probe.

A paper by Sewald and co-workers<sup>313</sup> reported the use of Cu-catalysed click chemistry on-resin to produce a sugar-peptide glycoconjugate. Using this method would simplify the design of a mannose-based inhibitor-linked OPAL probe. As substituting the Fmoc-Lys(Dde)-OH residue for an Fmoc-L-propargylglycine residue provides an easy installation point for mannose-based inhibitor **2.54** (Scheme 3-4) - this further removes the need for piperidine-4-carboxylic acid and succinic anhydride, as OPAL small molecule **3.5** can be installed directly onto the peptide terminus.

Synthesis of mannose-based inhibitor-linked OPAL probes for use in ligation



Scheme 3-4. Schematic for the synthesis of mannose-based inhibitor-linked OPAL probe **3.10** from alkyne charged peptide **3.11** following initial on-resin copper-catalysed click with mannose-based inhibitor **2.54** to afford mannose-based inhibitor-linked peptide **3.12**, which undergoes acid-catalysed cleavage using the cleavage cocktail 95 : 2.5 : 2.5 TFA : H<sub>2</sub>O : triisopropylsilane

## Synthesis of mannose-based inhibitor-linked OPAL probes for use in ligation

Synthesis of mannose-based inhibitor-linked OPAL probe **3.10** (Scheme 3-4) was attempted. Unfortunately, mass spectrometry analysis showed only minor peaks present at  $m/z$  1248.51  $[M+H]^+$  (2.03%) (Figure 3-14) and  $m/z$  624.97  $[M+2H]^{2+}$  (25.18%), corresponding to probe **3.10** (Figure 3-14). The major products identified by mass spectrometry were an unknown major species ( $m/z$  1139.55  $[M+H]^+$  (4.38%) and 570.42  $[M+2H]^{2+}$  (100%)) and a second species whose mass corresponds to that of peptide **3.10** minus OPAL small molecule **3.5** (1041.44  $[M+H]^+$  (18.05%) and 521.32  $[M+2H]^{2+}$  (79.75%)). These results suggest that some peptide coupling reactions failed to reach completion, explaining the low yield of probe **3.10** obtained.

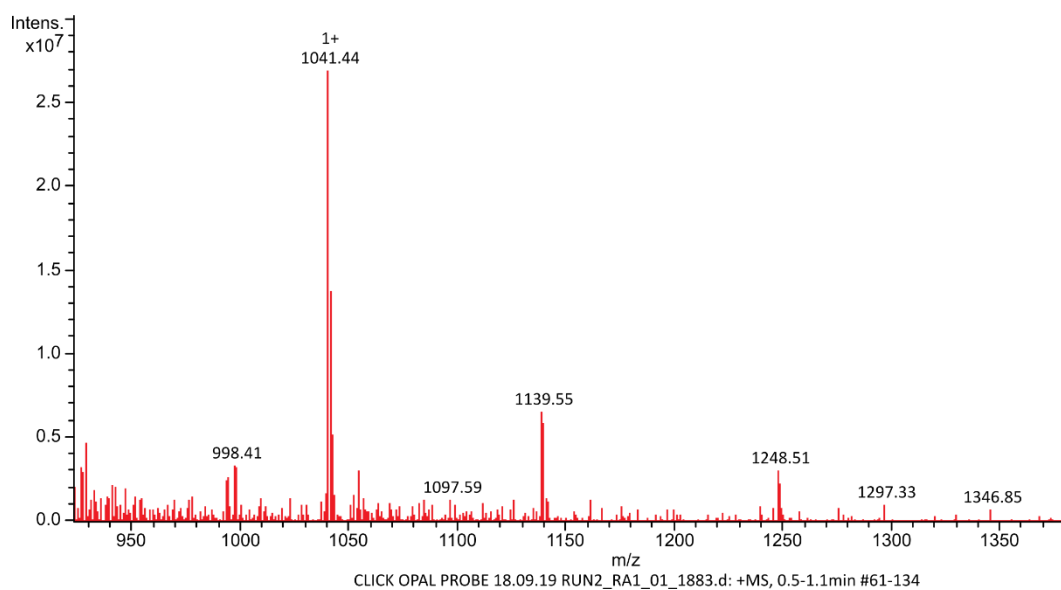


Figure 3-14. Depicts the mass spectroscopy results for probe **3.10**

Other members of the group have also experienced problems with peptide synthesis; all syntheses using the spacer unit 8-amino-3,6-dioxaoctanoic acid were proving problematic. Thus, it was decided to tweak the design of the mannose-based OPAL probe by replacing the PEG spacer units with six repeating alternating glycine and serine units to afford probe **3.13** (Figure 3-15). We hypothesize the use of glycine and serine units would increase probe **3.13** water-solubility and the ease with which probe **3.13** could be purified.

## Synthesis of mannose-based inhibitor-linked OPAL probes for use in ligation

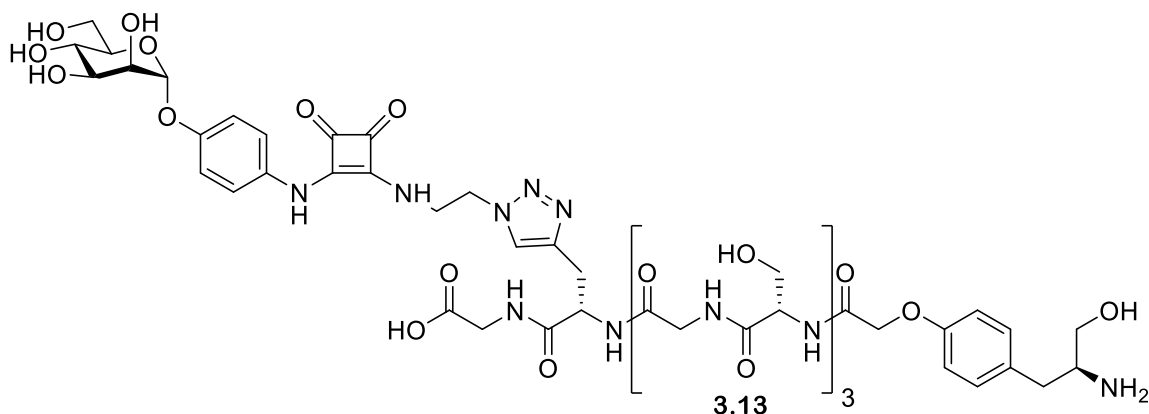


Figure 3-15. Structure of probe **3.13**

Mass spectrometry results showed the successful synthesis of probe **3.13**, with a peak at  $m/z$  1245.46  $[M+H]^+$  and a major peak at  $m/z$  623.35  $[M+2H]^{2+}$  (Figure 3-16).

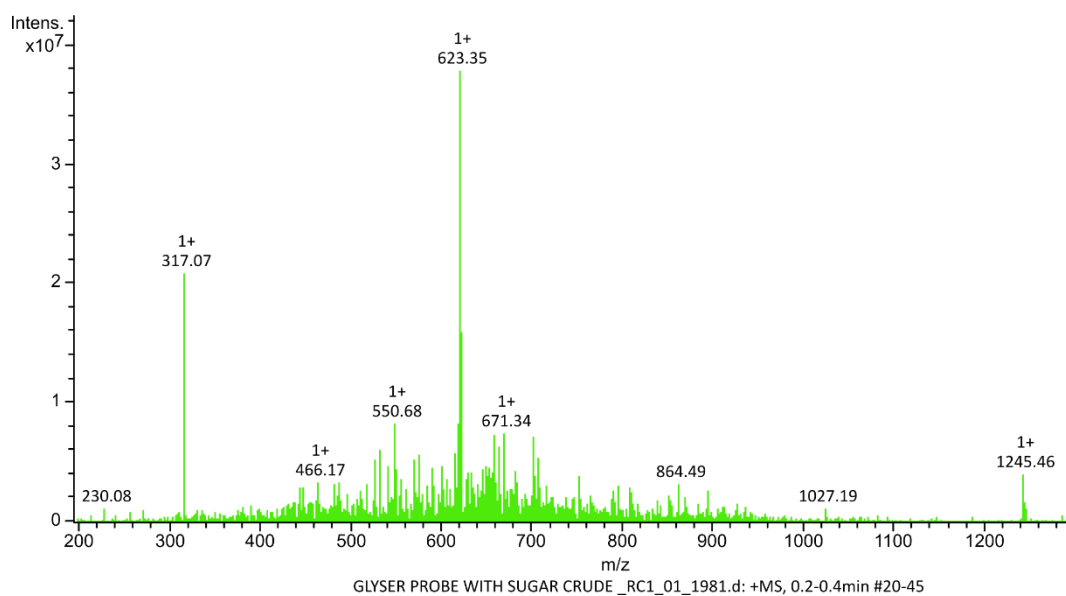


Figure 3-16. Depicts mass spectrometry trace for probe **3.13**

## Synthesis of mannose-based inhibitor-linked OPAL probes for use in ligation

It is currently hypothesized that the length of the OPAL probe linker will be a crucial variable in whether *E. coli* will aggregate upon exposure to the mannose-based inhibitor-linked colicin conjugates. If the linker is too short, initial binding of the conjugates colicin unit to its target receptor should still occur, yet the conjugates mannose unit will not extend beyond the glycocalyx of the bound *E. coli*. This would mean that binding to the FimH units on other *E. coli* would not be possible, and thus aggregation would not be facilitated. Probe **3.14** (Figure 3-17) was synthesised to test this theory - it contains only a single glycine serine repeat in its linker, and is thus significantly shorter than probe **3.13**. The successful synthesis of probe **3.14** was confirmed by LC-MS analysis (Figure 3-18 and Figure 3-19), which showed a major peak at  $m/z$  957.18  $[M+H]^+$  and a second peak at  $m/z$  480.20  $[M+2H]^{2+}$  (Figure 3-19).

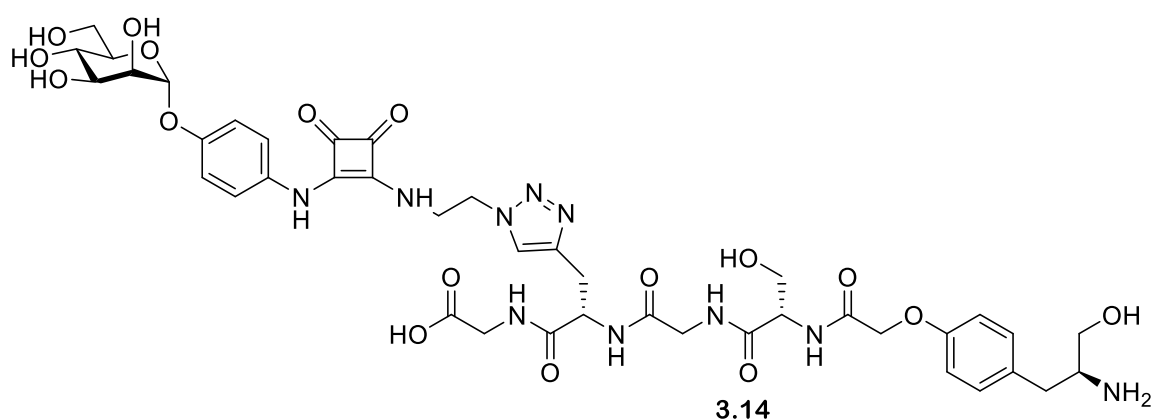


Figure 3-17. Structure of probe **3.14**

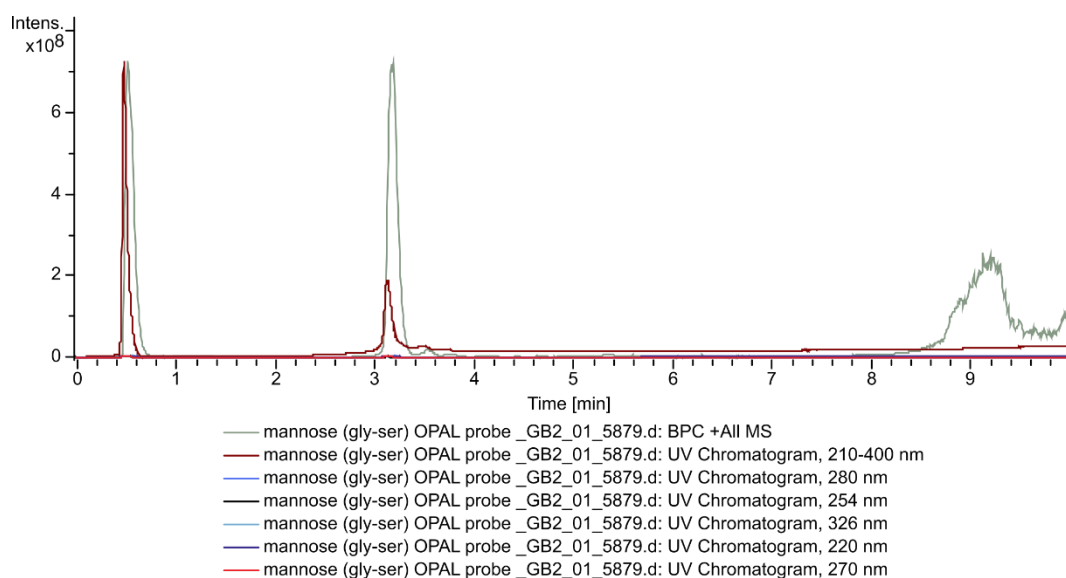


Figure 3-18. Liquid chromatography trace of probe **3.14**



## Synthesis of mannose-based inhibitor-linked OPAL probes for use in ligation

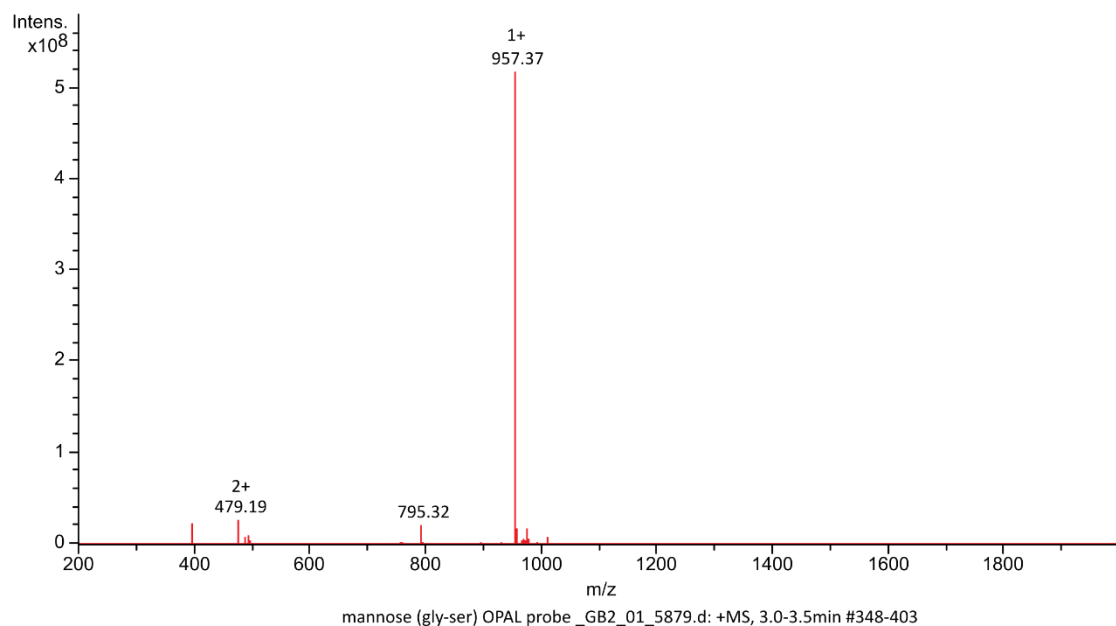


Figure 3-19. Mass spectrometry trace of probe **3.14**

Conversely, increasing the linker length will likely increase the linker's flexibility, and thus, if a linker is too long the mannose unit could bind to FimH units on the same *E. coli* to which the colicin is bound and would be unable to aggregate different *E. coli* cells together. To test this hypothesis a final mannose-based inhibitor-linked OPAL probe was synthesised containing six repeating glycine-serine units (probe **3.15**, Figure 3-20). LC-MS analysis confirmed the successful synthesis of probe **3.15** with a major peak at  $m/z$  839.57  $[M+2H]^{2+}$  and a second peak at  $m/z$  1678.45  $[M+H]^+$  (Figure 3-21 and Figure 3-22).

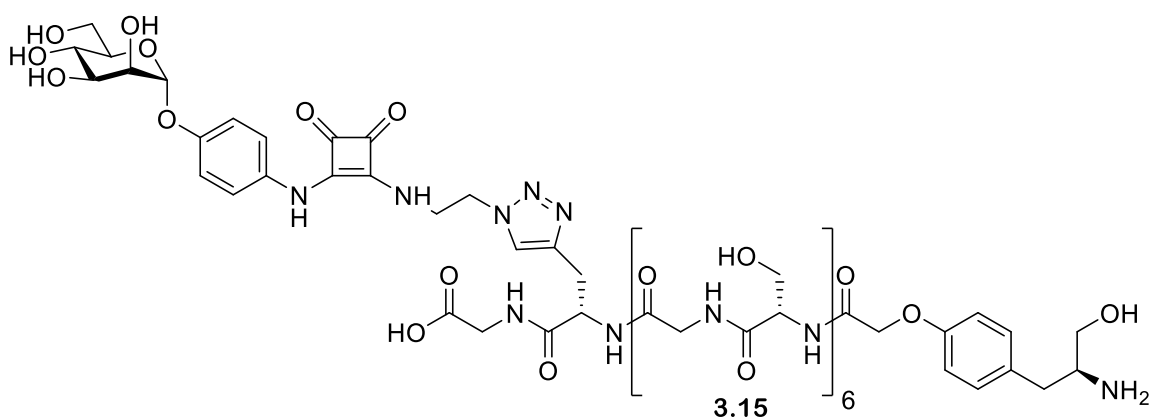


Figure 3-20. Structure of probe **3.15**

## Synthesis of mannose-based inhibitor-linked OPAL probes for use in ligation

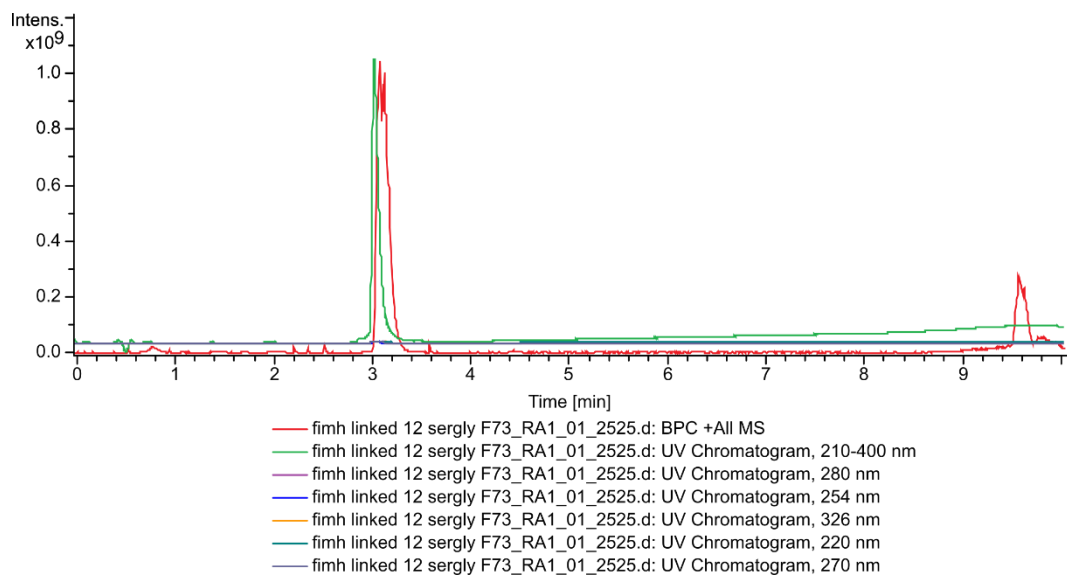


Figure 3-21. Depicts the liquid chromatogram trace for probe 3.15

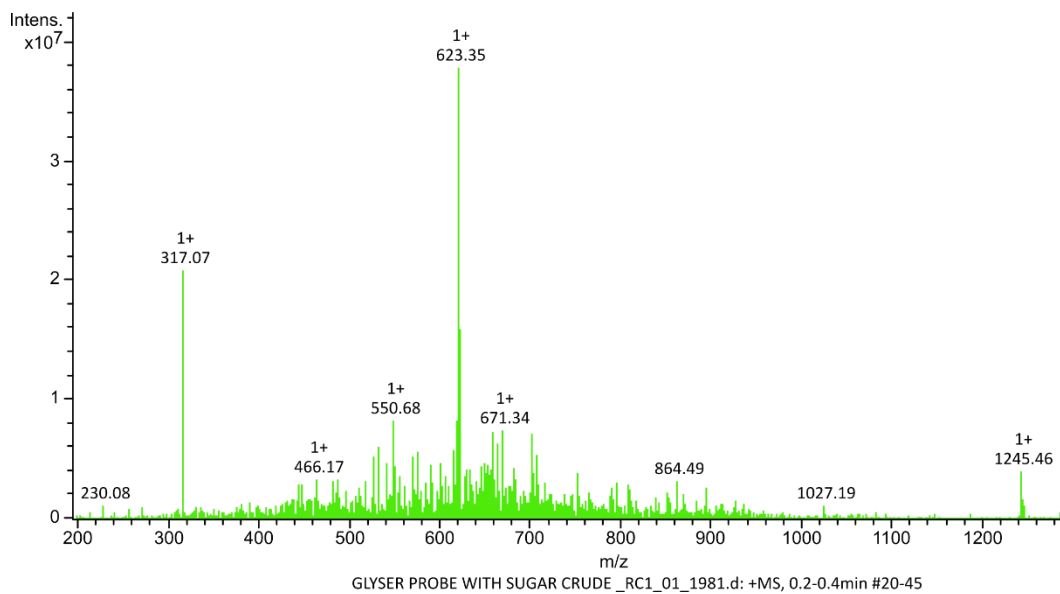


Figure 3-22. Depicts mass spectrometry trace for probe 3.15

## Synthesis of mannose-based inhibitor-linked OPAL probes for use in ligation

Prior to establishing whether the mannose-based inhibitor-linked colicin conjugates can induce *E. coli* aggregation, the effect of OPAL ligation on binding of colicins to their target receptors was investigated. To achieve this binding microscopy was to be performed using a biotin-linked colicin E9 conjugate and fluorescently labelled streptavidin. A new biotin-linked OPAL probe, (probe **3.16**, Figure 3-23) containing three serine-glycine spacer units was designed and synthesised, with its successful synthesis confirmed by LC-MS analysis (Figure 3-24 and Figure 3-25). By using a probe with the same spacer unit as the mannose-based inhibitor-linked OPAL probes, a more accurate reflection of how the mannose-based inhibitor-linked OPAL probes might affect binding would hopefully be obtained.

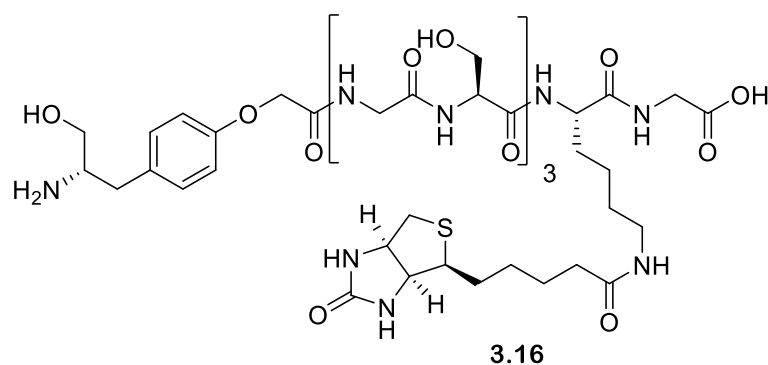


Figure 3-23. Structure of biotin-linked probe **3.16**

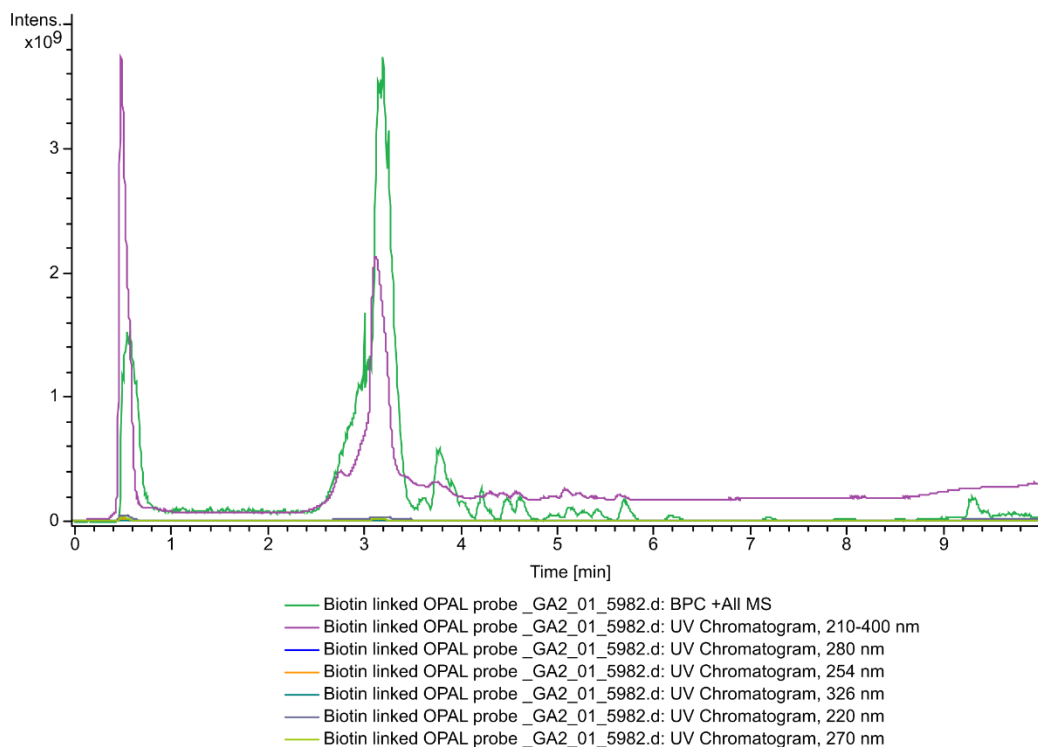


Figure 3-24. Depicts the liquid chromatogram trace for probe **3.16**

## Synthesis of mannose-based inhibitor-linked OPAL probes for use in ligation

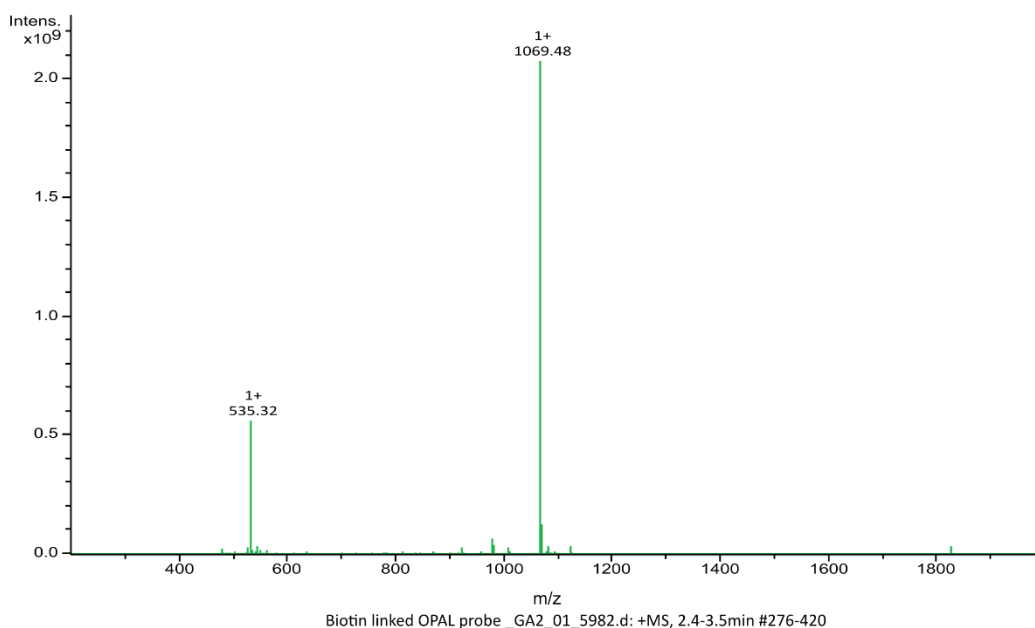
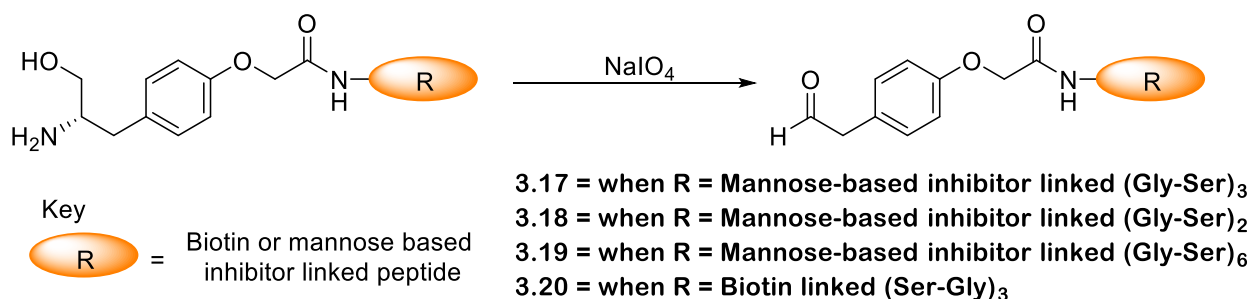


Figure 3-25. Depicts mass spectrometry trace for probe 3.16

Prior to OPAL conjugation, probes **3.13**, **3.14**, **3.15** and **3.16** needed to undergo  $\text{NaIO}_4$ -mediated oxidation (Scheme 3-5). Oxidation of the 1,2 amino alcohols to aldehydes afforded probes; **3.17**, **3.18**, **3.9** and **3.20**, all of which could be subjected to OPAL conjugation. The traditional oxidation procedure used on previously synthesised OPAL probes calls for approximately 5 eq of  $\text{NaIO}_4$  in addition to 10 eq of L-methionine (L-methionine serves to prevent over-oxidation of the protein). The mannose unit of mannose-based inhibitor contains a 1,2-cis diol which could undergo oxidation with  $\text{NaIO}_4$ . It was thus decided to adapt the oxidation procedure, lowering the eq of  $\text{NaIO}_4$  to one in the hopes that the increased reactivity of the 1,2-amino alcohol over the 1,2-cis diol would allow for selective oxidation. This assumption proved correct, as oxidation of all three mannose-based inhibitor-linked OPAL probes using the adapted method were successful and no oxidation of the 1,2-cis diols were observed.



Scheme 3-5. General procedure for  $\text{NaIO}_4$  oxidation of biotin and mannose-based inhibitor-linked OPAL probes **3.13**, **3.14**, **3.15** and **3.16** to form activated probes **3.17**, **3.18**, **3.19** and **3.20**

### 3.2.4 Conjugation of OPAL probe to colicin Ia and colicin E9

Each probe was subjected to OPAL ligation with both colicin E9 and Ia affording a total of eight colicin-linked glycoconjugates, six mannose-based inhibitor-linked (Gly-Ser)<sub>n</sub> colicin conjugates and two biotin-linked (Ser-Gly)<sub>3</sub> colicin conjugates.

The successful synthesis of all eight colicin conjugates was confirmed using an SDS-PAGE gel and either a lectin blot (for mannose-based inhibitor linked colicin conjugates) or a Western blot (for biotin-linked colicin conjugates). The SDS-PAGE gel and lectin blot of mannose-based inhibitor-linked (Gly-Ser) colicin E9 conjugate are presented in Figure 3-26 and Figure 3-27 respectively. It can be observed in the lectin blot that lanes B-E containing unmodified colicin E9 show no UV activity. However, lanes F and G both contain colicin E9 which has been subjected to OPAL ligation with mannose-based inhibitor-linked (Gly-Ser) OPAL probe and both show UV activity. Though lanes H and I contained colicin E9 which has been subjected to OPAL ligation no UV activity is observed in these lanes, most likely because too little protein is present in these lanes. The SDS-PAGE gel further supports the lectin blot showing the presence of a protein band at 70 kDa in all lanes. The lectin blots and SDS-PAGE gels for the other conjugates are attached in appendix section 9.2.4, page ci-cv.

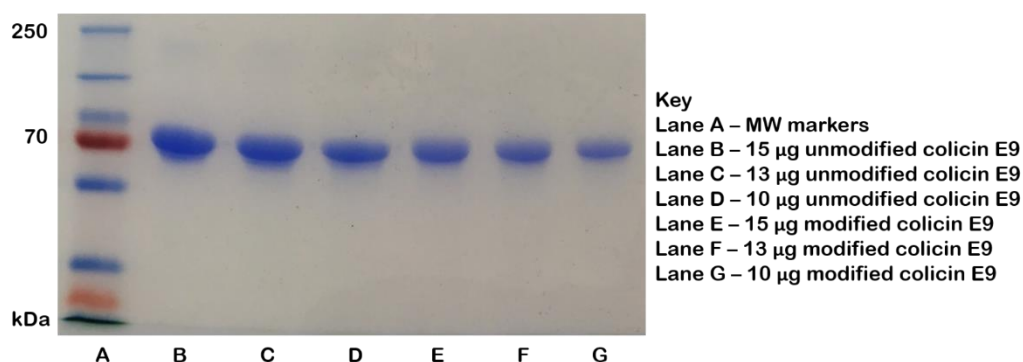


Figure 3-26. Results of SDS-PAGE gel stained with Coomassie containing unmodified colicin E9 (lane B-D), and colicin E9 which has been subjected to OPAL ligation with mannose-based inhibitor-linked (Gly-Ser) OPAL probe 3.18 (lanes E-G)

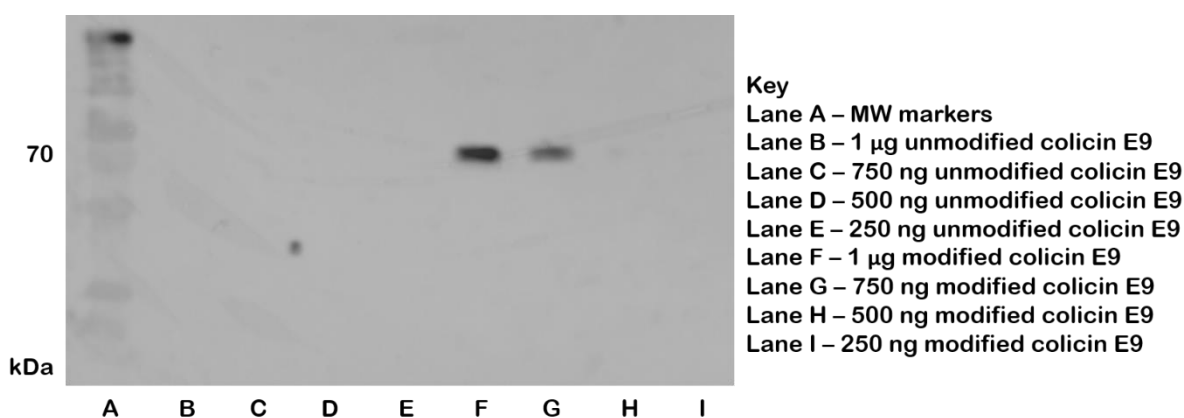


Figure 3-27. Results of lectin blot containing unmodified colicin E9 (lanes B-E) and colicin E9 which has been subjected to OPAL ligation with mannose-based inhibitor-linked (Gly-Ser) OPAL probe 3.18 (lanes F-I)

## Synthesis of mannose-based inhibitor-linked OPAL probes for use in ligation

A challenge encountered once the mannose-based inhibitor-linked colicin E9 conjugates had been synthesised was measuring their concentration accurately. Prior to conjugation UV/vis measurements at 280 nm had been used to calculate protein concentration, however, it was suspected that this measurement method was giving incorrect concentrations for the mannose-based inhibitor-linked colicin conjugates. The SDS-PAGE gel shown in Figure 3-28 confirms the concentration measurement inaccuracy - the concentrations of all the samples used in Figure 3-28 were calculated using absorbance at 280 nm, yet the intensity of the protein bands across the lanes are notably different. The protein bands at 70 kDa observed for unmodified colicin Ia (lanes D and E) and colicin E9 (lanes H and I) are significantly more intense than the bands observed for colicin E9 which has been subjected to ligation with mannose-based inhibitor-linked (Gly-Ser)<sub>3</sub> OPAL probe (lanes B and C for colicin Ia and lanes F and G for colicin E9).

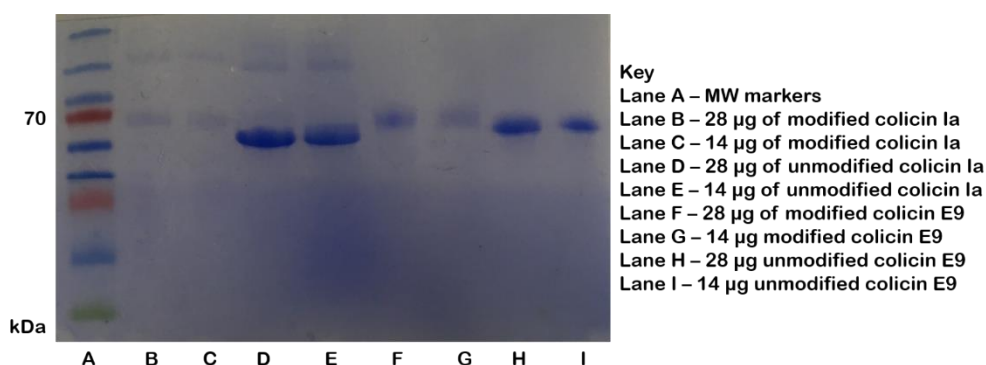


Figure 3-28. Results of SDS-PAGE gel stained with Coomassie containing colicin Ia which has been subjected to OPAL ligation with mannose-based inhibitor-linked (Gly-Ser)<sub>3</sub> OPAL probe **3.17** (lanes B and C), unmodified colicin Ia (lane D and E), colicin E9 which has been subjected to OPAL ligation with mannose-based inhibitor-linked (Gly-Ser)<sub>3</sub> OPAL probe **3.17** (lanes F and G) and unmodified colicin E9.

Both mannose-based inhibitor **2.53** and **2.54** contain a phenol group which could contribute to the 280 nm absorbance measurement. To confirm that it was this contribution preventing accurate values of protein concentration from being obtained, 1 mM samples of both mannose-based inhibitor-linked (Gly-Ser) OPAL probe **3.18** and biotin-linked (Ser-Gly)<sub>3</sub> OPAL probe **3.20** were prepared, and UV/vis traces were recorded (Figure 3-29). Mannose-based inhibitor-linked (Gly-Ser) OPAL probe **3.18** showed significant absorbance at 280 nm (15.313) compared to the biotin-linked (Ser-Gly)<sub>3</sub> OPAL probe **3.20** (absorbance = 0.2398 at 280 nm). These results support the hypothesis that the presence of the phenol unit in the mannose-based inhibitor linked OPAL probes prevents accurate measurement of the colicin conjugates protein concentration. A more accurate measure of the colicin-linked conjugates concentration was instead obtained using a Bradford assay.<sup>314</sup>

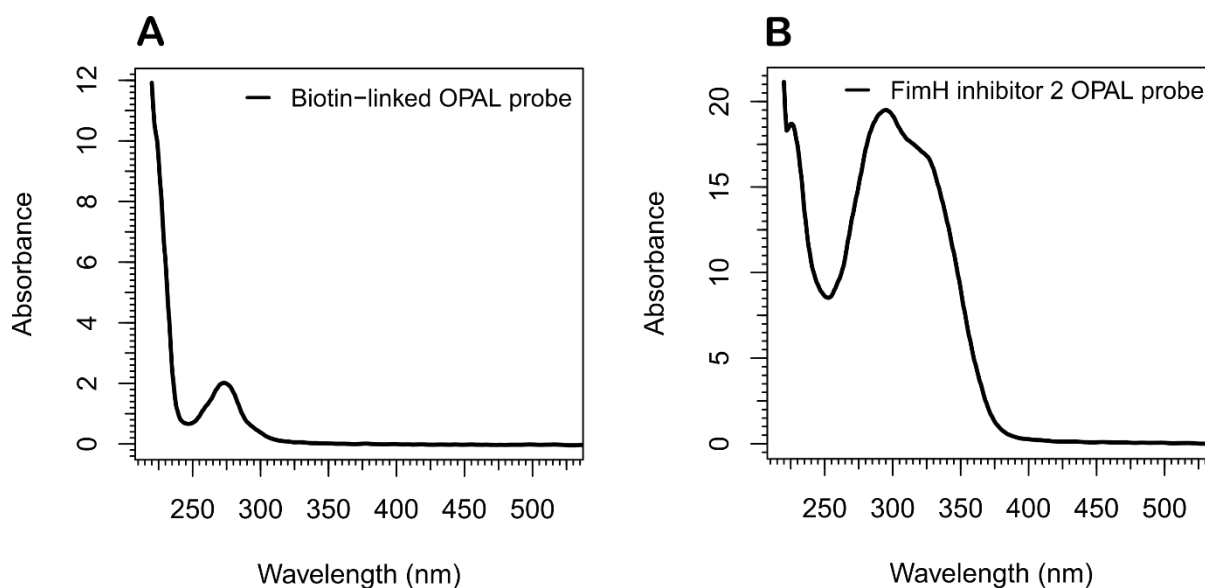


Figure 3-29. Depicts the UV vis trace for a) biotin-linked OPAL probe **3.20** and b) Mannose-based inhibitor (Gly-Ser) OPAL probe **3.18**

### 3.3 Summary and conclusions

In summary, this chapter covers a broad range of work. Firstly, the successful expression and purification of colicin E9 was performed, followed by the establishment of an OPAL ligation procedure for both colicin Ia and E9. This work has increased the breadth of OPAL ligation, being the first instance in which OPAL ligation has been used to append a sugar to a protein. Achieving this milestone required a significant amount of work, such as the design and synthesis of a mannose-based inhibitor-linked OPAL probe, which was achieved using on-resin copper catalysed click ligation. Furthermore, the traditional  $\text{NaIO}_4$ -mediated oxidative cleavage used to activate OPAL probes had to be adapted to prevent any oxidation of the 1,2-cis diol present on the mannose unit. All this work allowed for the successful synthesis of a library of mannose-based inhibitor-linked colicin Ia and E9 conjugates with variable linker lengths which can now have their biological properties investigated.

## Chapter 4 Investigation into the biological applications of the colicin conjugates

### 4.1 Aims

The aim of this chapter is to investigate the biological applications of the six mannose-based inhibitor-linked (Gly-Ser)<sub>n</sub> colicin conjugates synthesized in chapter 3, focusing mainly on whether any of these conjugates have the ability to induce *E. coli* aggregation as hypothesized at the beginning of this project. Unfortunately, due to COVID-19 preventing access to the University of York Biology Department, the originally planned experiments could not be performed, and thus alternative experiments using the equipment available in the Chemistry and occasionally Physics Departments were instead designed and performed. However, these experiments were shown to be no substitute for the originally planned experiments with the data being either inconclusive or inconsistent. This means that, despite our best efforts, the abilities of any of the mannose-based inhibitor-linked (Gly-Ser)<sub>n</sub> colicin conjugates to aggregate *E. coli* are still unknown.

### 4.2 Results and discussion

#### 4.2.1 Use of aggregation assays

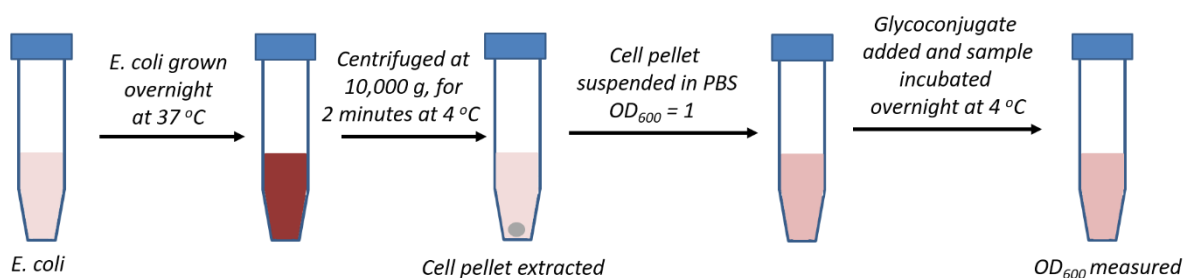
Initially we had planned to investigate the abilities of the six mannose-based inhibitor-linked (Gly-Ser)<sub>n</sub> colicin conjugates to induce *E. coli* aggregation using multiple microscopy techniques, the first of which was binding microscopy. Here we would use TIRF (Total Internal Reflection Fluorescence) microscopy with fluorescently labelled streptavidin to investigate whether the two biotin-linked (Gly-Ser)<sub>n</sub> colicin conjugates could bind to *E. coli* JW3596. This experiment would establish whether OPAL ligation at the N-terminus of both colicin units (E9 and Ia) impacted the binding of either to their target receptors. If either or both the biotin-linked (Gly-Ser)<sub>n</sub> colicin conjugates were shown to successfully bind to *E. coli* then experimental work would proceed to investigate whether any of the mannose-based inhibitor-linked (Gly-Ser)<sub>n</sub> colicin conjugates could induce *E. coli* aggregation. We originally planned to perform this work by treating samples of *E. coli* M1658 with each mannose-based inhibitor-linked (Gly-Ser)<sub>n</sub> colicin conjugate; these samples could then be imaged using TIRF microscopy allowing any aggregate formation to be observed. If aggregate formation was observed, then digital holographic microscopy would be used to confirm and further monitor the rate of aggregate formation.

The lack of regular access to a microscope meant that a substantial experimental redesign was required. Furthermore, any alternative experiments had to be performed using the equipment available within the Chemistry department. An auto-aggregation methodology previously used by Uhlin and co-workers<sup>315</sup> was found, and the general procedure by which the assay was conducted is summarised in Scheme 4-1. Following this methodology, an overnight culture of *E. coli* was harvested by centrifugation (10,000 xg, 2 minutes) and the resultant cell pellet is re-suspended in 1 x PBS to an



## Investigation into the biological applications of the colicin conjugates

OD<sub>600</sub> of 1. This solution was subsequently aliquoted into samples and if required the desired concentration of one of the mannose-based inhibitor-linked (Gly-Ser)<sub>n</sub> colicin conjugates could be added, the samples were then incubated overnight at 4 °C. Finally, an extract from the top of each sample was removed and diluted and an OD<sub>600</sub> measurement was taken. It is expected that any aggregates formed will sink to the bottom of the tube reducing the number of *E. coli* present at the top of a sample. Theoretically, this should mean that the lower the final OD<sub>600</sub> value the more aggregation that has occurred.



Scheme 4-1. Schematic of the initial auto-aggregation assay designed, based on that previously reported by Uhlin and co-workers<sup>315</sup>

Many bacterial strains, including *E. coli*, have a propensity to auto-aggregate. Auto-aggregation is a process via which bacteria of the same species form multicellular clumps which eventually settle at the bottom of a culture.<sup>316</sup> Auto-aggregation is often the first step of biofilm formation,<sup>316</sup> a critical stage in the pathogenic cycle of many bacteria. Generally, auto-aggregation is mediated by autoagglutinins - self-recognising surface structures such as proteins and exopolysaccharides.<sup>316</sup> Bacteria lipid polysaccharide (LPS) consists of three domains: the lipid A domain, the core oligosaccharide domain (containing both the inner and outer core) and the O-polysaccharide.<sup>317</sup> Uhlin and co-workers<sup>315</sup> demonstrated that changes in LPS composition affected biofilm formation. They investigated the effects of different *E. coli* mutants (with each mutant having a different LPS composition) on biofilm formation. The two deep rough mutants formed the strongest biofilm, significantly stronger than that formed by their parent strain, BW25113.<sup>315</sup>

Figure 4-1 depicts the expected LPS structure of both BW25113 and JW3596. JW3596 has a shorter LPS than BW25113, and thus should be expected to have a greater propensity towards aggregation than BW25113. As such, we will hereafter assume that if an aggregation assay is operational it will indicate that there is a greater degree of aggregation for JW3569 than for BW25113.

## Investigation into the biological applications of the colicin conjugates

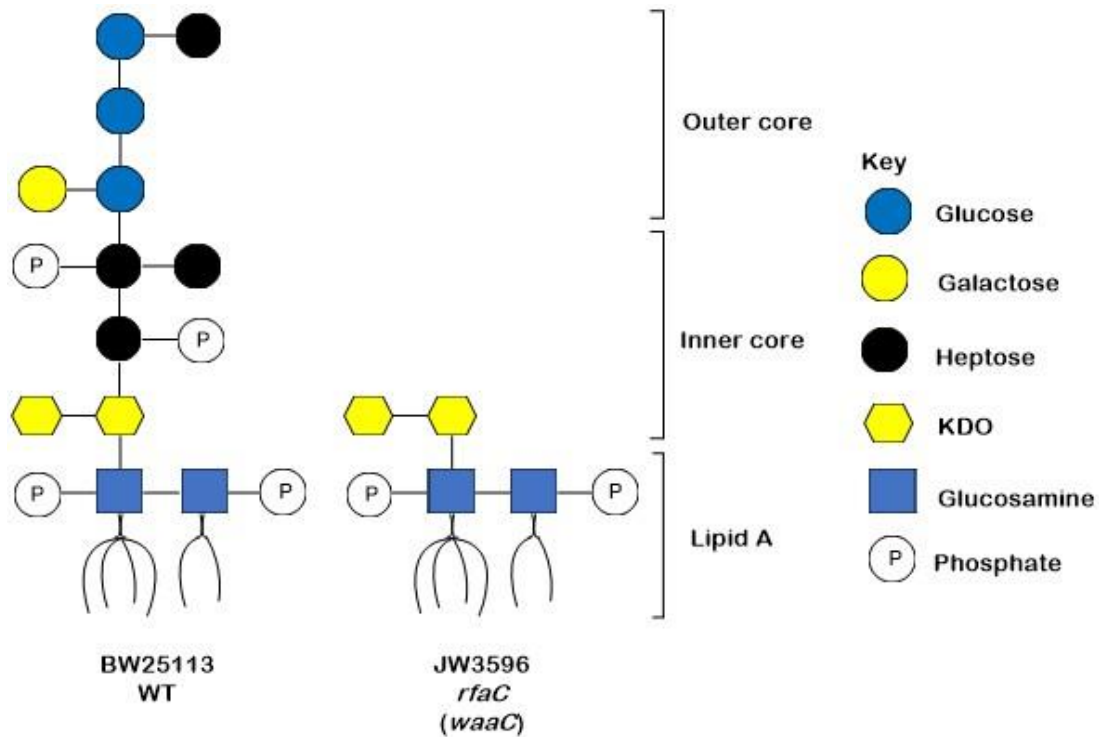


Figure 4-1. Diagram depicting the expected LPS structures of both BW25113 and JW3596 adapted from<sup>318,319</sup>

In addition to BW25113 and JW3596, three further knockout strains were selected from the Keio collection: JW4283 (*FimH*), RK5016 (*Btub*) and JW2142 (*Cir*) (see Table 6). All mannose-based inhibitor-linked (Gly-Ser)<sub>n</sub> colicin conjugates would be screened against *E. coli* strains BW25113, JW3596 and JW4283, with each conjugate additionally being tested against the knockout strain of the relevant colicin receptor (Table 6). As none of the mannose-based inhibitor-linked (Gly-Ser)<sub>n</sub> colicin conjugates should induce aggregation in the relevant knockout samples, identification of positive results should be simple; samples of BW25113 and JW3596 should have a lower final OD<sub>600</sub> value compared to those of samples of the relevant knockout strains.

## Investigation into the biological applications of the colicin conjugates

Table 6. Different *E. coli* strains required for the auto-aggregation experiments, each strain's receptor composition, and whether aggregation would be expected

<i>E. coli</i> strain	Contains FimH	Contains CirA receptor	Contains Btub receptor	Aggregation expected with	
				la conjugates	E9 conjugates
BW25113	Yes	Yes	Yes	Yes	Yes
JW3596	Yes	Yes	Yes	Yes	Yes
JW4283	No	Yes	Yes	No	No
RK5016	Yes	Yes	No	N/A	No
JW2142	Yes	No	Yes	No	N/A

Prior to using *E. coli* samples which contained one of the valuable mannose-based inhibitor-linked (Gly-Ser)<sub>n</sub> colicin conjugates, an auto-aggregation assay was performed using samples of *E. coli* only, to see whether the expected trend between samples of BW25113 and JW3596 would be observed (Experiment One, appendix section 9.3.2 page cvii). The auto-aggregation assay was run as described in experimental section 8.4.1, page 307 using samples of *E. coli* strains- BW25113, JW3596, JW4283 and JW2142. This aggregation assay was further used to investigate whether sample size (e.g. 1.5 mL vs 2 mL) or growth medium (M9 media vs LB media) affected auto-aggregation. The results of the auto-aggregation assay are shown in Table 7, where it can be seen that there is no significant difference in the final OD<sub>600</sub> values between samples of BW25113 and samples of JW3596. This potentially suggests that the auto-aggregation assay was not sensitive enough to detect the different auto-aggregation abilities of the two *E. coli* strains. The results in Table 7 also suggest that sample size and growth media have little impact on auto-aggregation.

## Investigation into the biological applications of the colicin conjugates

Table 7. Results of Experiment One. Which used samples of *E. coli* grown in either LB or M9 media and incubated in either 2 mL or 1.5 mL samples. OD<sub>600</sub> measurements were recorded post-incubation

<i>E. coli</i> strain	BW25113	JW3596	JW4283 (FimH minus)	JW2142 (CirA minus)
Conditions	OD <sub>600</sub> measurement following incubation			
2 mL using LB as growth media	0.84	0.81	0.80	0.59
1.5 mL using LB as growth media	0.75	0.76	0.74	0.60
2 mL using M9 as growth media	0.88	0.78	0.90	0.69
1.5 mL using M9 as growth media	0.85	0.84	0.86	0.68

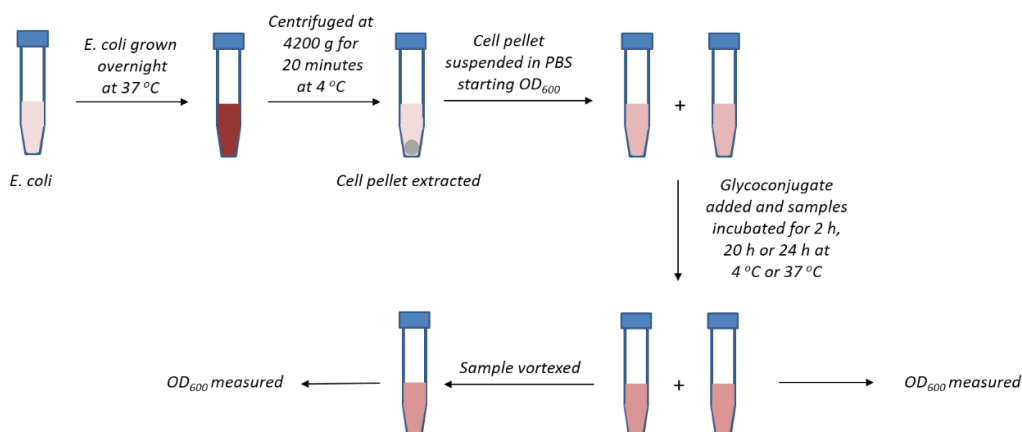
With the initial auto-aggregation assay not showing the expected trend between samples of BW25113 and JW3596, the literature was re-evaluated. Other previous studies using an auto-aggregation assays had used vortexed controls,<sup>320, 321</sup> wherein vortexed control samples are set up and incubated identically to their corresponding active sample, yet prior to OD<sub>600</sub> measurement the vortexed control samples are vortexed for a specified period of time (e.g. 30 seconds). Giordano and co-workers used the OD<sub>600</sub> measurements of the active sample and the vortexed control sample to calculate percentage auto-aggregation using Equation 1.<sup>320</sup>

**Equation 1.** Equation used to determine percentage auto-aggregation, here OD<sub>600</sub> Final is the OD<sub>600</sub> measurement of the active sample and OD<sub>600</sub> initial is the OD<sub>600</sub> measurement of the corresponding vortex control sample

$$\text{Percentage Auto-aggregation} = 100 \times \left( 1 - \left( \frac{OD_{600} \text{ Final}}{OD_{600} \text{ Initial}} \right) \right)$$

The auto-aggregation assay was redesigned in response to the literature findings, and the new assay is depicted in Scheme 4-2. The major change between this assay and the initial auto-aggregation assay is the inclusion of vortexed controls. The decision to include vortexed controls was made as it allowed extraction of percentage auto-aggregation measurements using Equation 1. Comparison of the percentage auto-aggregation values of samples should be more informative than comparing their final OD<sub>600</sub> measurements. A further advantage of the new auto-aggregation assay was that it allows easy screening of multiple conditions which could affect aggregation, such as starting OD<sub>600</sub>, incubation temperature, and incubation time.

## Investigation into the biological applications of the colicin conjugates

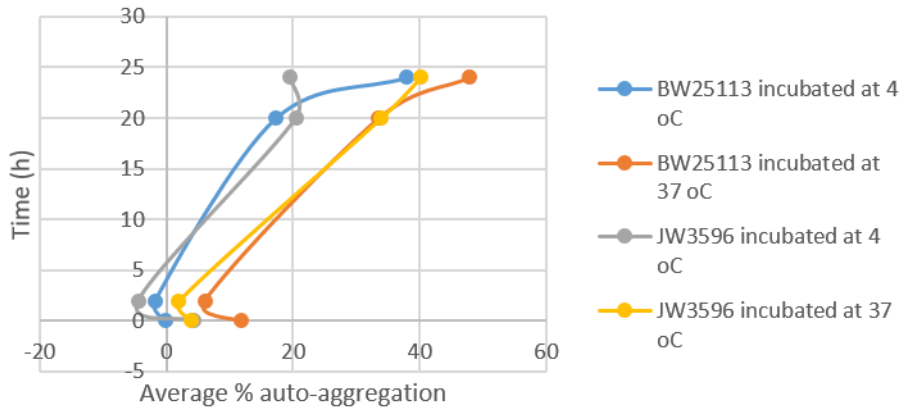


Scheme 4-2. Schematic of the redesigned auto-aggregation assay

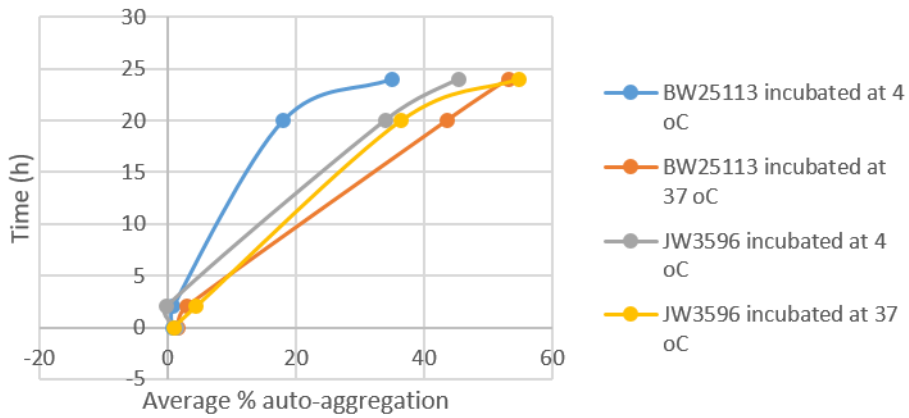
An auto-aggregation assay screen (Experiment Two) was set up to investigate a range of conditions such as starting OD<sub>600</sub> (1, 1.5 and 2), incubation time (0 h, 2 h, 20 h and 24 h) and incubation temperature (4 °C or 37 °C). All samples were made in accordance with experimental section 8.4.2, page 308, with the results attached in appendix section 9.3.3, page six. The assay was run in triplicate and the average percentage auto-aggregation for each sample was found and plotted on the corresponding graph (Figure 4-2). Due to the large number of samples run, the samples were split into three groups for analysis dependant on their starting OD<sub>600</sub>. The results of the auto-aggregation assay screen are shown in the graphs in Figure 4-2. The data was very challenging to analyse, suggesting only a few potential general trends. Firstly, there appears to be an increase in percentage auto-aggregation of samples incubated at 37 °C vs those incubated at 4 °C. One possible explanation for this difference in percentage auto-aggregation is increased growth could have occurred in samples incubated at 37 °C relative with those incubated at 4 °C. However, we propose that growth should be limited in 1 x PBS. Instead, we hypothesize that samples of the weakly-motile *E. coli* strain BW25113<sup>322</sup> incubated at 37 °C will have increased motility relative to those incubated at 4 °C, and consequently the *E. coli* in the 37 °C samples would be more likely to collide and induce aggregation. There further appears to be a positive trend between the starting OD<sub>600</sub> and the percentage auto-aggregation value seen after 24 h. The results shown in Figure 4-2 graph 1 suggest that after two hours there is a decrease in percentage auto-aggregation. As this trend is not seen consistently in Figure 4-2 graphs 2 and 3, it cannot be concluded whether it is significant. It is likely that insufficient aggregation had occurred in the active samples within 2 hours to give percentage auto-aggregation values significantly higher than those measured at the start. Unexpectedly, samples of JW3596 generally did not show increased percentage auto-aggregation compared to samples of BW25113. This was the second auto-aggregation assay which did not show the expected trend from the work of Uhlin and co-workers<sup>315</sup>, and thus it was decided that samples of *E. coli* alone could not be relied upon and an alternative positive control should be developed.

Investigation into the biological applications of the colicin conjugates

1 The results of the auto-aggregation assay of samples with a starting OD<sub>600</sub> of 1



2 The results of the auto-aggregation assay of samples with a starting OD<sub>600</sub> of 1.5



3 The results of the auto-aggregation assay of samples with a starting OD<sub>600</sub> of 2

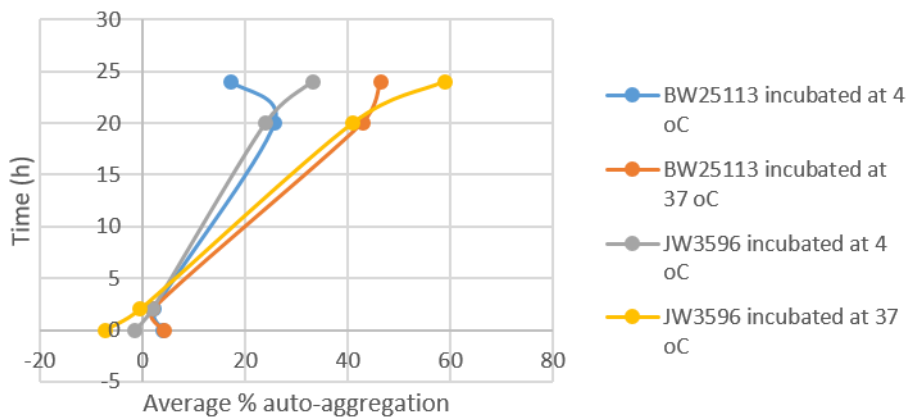


Figure 4-2. Results of Experiment Two, which was designed to screen potential aggregation factors using the new auto-aggregation assay method. The results are plotted on the graph that corresponds to a sample starting OD<sub>600</sub>

## Investigation into the biological applications of the colicin conjugates

The positive control designed used samples of *E. coli* incubated with 10 mM biotin linked colicin E9 conjugate and 2 mM NeutrAvidin. Binding of the colicin E9 unit to its target BtuB receptor on *E. coli* should leave the biotin unit freely presented on the surface of *E. coli*, and thus available for binding to NeutrAvidin. As NeutrAvidin can bind up to four biotin units,<sup>323</sup> it was theorised that the use of NeutrAvidin as the limiting reagent would induce the binding of multiple biotin units to a single NeutrAvidin, inducing aggregation. Positive control samples of BW25113 and JW3596 were set up in accordance with the methodology given in experimental section 8.4.2, page 308 (Experiment Three). The results of the Experiment Three auto-aggregation assay are shown in Table 8. As can be seen, the positive control samples of BW25113 show an increase in percentage auto-aggregation compared to the *E. coli* only samples, suggesting that aggregation has been induced above the baseline level of auto-aggregation. Conversely, positive control samples of JW3596 showed a percentage auto-aggregation similar to (if not below that) of the *E. coli* only controls. Interestingly, unlike previous auto-aggregation assays the *E. coli* only samples of JW3596 did show an increased percentage auto-aggregation compared to the *E. coli* only samples of BW25113.

*Table 8. Results of Experiment Three, an auto-aggregation assay using positive control samples made from E. coli strains BW25113 and JW3596, incubated at 37 °C with 10 nM biotin linked colicin E9 conjugate and 2 nM NeutrAvidin. This assay was only repeated once, with one active sample and one vortexed control sample made for each condition and one single OD<sub>600</sub> measurement taken of each sample. These measurements were used to calculate percentage auto-aggregation. Note the OD<sub>600</sub> measurements reported here are the values reported post dilution factor adjustment.*

Sample	OD <sub>600</sub> of active sample (±0.005)	OD <sub>600</sub> vortexed control (±0.005)	Percentage auto-aggregation (±0.05)
BW25113 OD <sub>600</sub> = 1.5 positive control	0.54	1.17	53.8
BW25113 OD <sub>600</sub> = 1.5 <i>E. coli</i> only	0.75	1.21	38.4
BW25113 OD <sub>600</sub> = 2 positive control	0.71	1.60	55.4
BW25113 OD <sub>600</sub> = 2 <i>E. coli</i> only	0.91	1.52	40.2
JW3596 OD <sub>600</sub> = 1.5 positive control	0.55	1.26	56.3
JW3596 OD <sub>600</sub> = 1.5 <i>E. coli</i> only	0.54	1.31	58.7

## Investigation into the biological applications of the colicin conjugates

JW3596 OD <sub>600</sub> = 2 positive control	0.72	1.50	52.3
JW3596 OD <sub>600</sub> = 2 <i>E. coli</i> only	0.55	1.58	65.5

It was theorised that further increasing the starting OD<sub>600</sub> from 1.5 or 2 to 6 or 7 would further exaggerate the difference in percentage auto-aggregation between the positive control samples and the *E. coli* only samples. However, the initial round of higher OD<sub>600</sub> positive control samples made with BW25113 afforded unanalysable results. Therefore, three alternative positive control samples of BW25113 were thus set up (Experiment Four, experimental section 8.4.2, page 308). These samples were assembled with increasing concentrations of the biotin-linked colicin E9 conjugate and NeutrAvidin (Table 9). In order to ascertain the minimum required concentration of colicin conjugate for aggregation, giving a bench mark for future assays using the mannose-based inhibitor-linked (Gly-Ser)<sub>n</sub> colicin conjugates. The concentrations of conjugate used in previous assays had been limited by the large sample sizes needed for final OD<sub>600</sub> measurements using the nanodrop spectrophotometer. Acquisition of a new filter for the plate reader (Victor Nivo™, multimode plate reader, PerkinElmer) allowed the use of smaller sample sizes (600 µL vs 1.5 mL), thus allowing higher colicin conjugate concentrations to be trialled. The results of the auto-aggregation assay are shown in Table 9, and show that the positive control samples have a higher percentage auto-aggregation than the *E. coli* only control. Furthermore, percentage auto-aggregation does not seem to significantly increase as the concentration of biotin-linked colicin E9 conjugate and NeutrAvidin increases, suggesting 10 nM of biotin linked colicin E9 conjugate and 2 mM NeutrAvidin is sufficient to induce maximum aggregation. However, a concerning observation was that OD<sub>600</sub> measurements made on the plate reader were not consistent with those made using the nanodrop spectrophotometer. When preparing the BW25113 sample for this auto-aggregation assay, a starting OD<sub>600</sub> of 6 was desired, and while a starting OD<sub>600</sub> of 6.185 was measured using the nanodrop spectrophotometer, the same sample gave a starting OD<sub>600</sub> of 2.49 when measured using the plate reader. Measurements of OD<sub>600</sub> values using the nanodrop spectrophotometer (DeNovix) cease to become accurate for readings above OD<sub>600</sub> = 1.7. As such, prior to being measured on either instrument the initial sample of BW25113 was diluted 1:6 with 1 x PBS. The resulting initial OD<sub>600</sub> measurements were then multiplied by the dilution factor to give the stated OD<sub>600</sub> values. Measuring diluted samples of BW25113 will reduce the accuracy of the initial OD<sub>600</sub> measurements, but this does not account for the large differences in starting OD<sub>600</sub> values seen between the two measurement methods. However, all final measurements were performed on the plate reader and as the percentage auto-aggregation values were calculated using these final



## Investigation into the biological applications of the colicin conjugates

measurements, therefore, the positive correlation observed between conjugate concentration and percentage auto-aggregation is valid.

*Table 9. Results of Experiment Four, a second auto-aggregation assay performed on positive control samples of BW25113 with a higher starting OD<sub>600</sub> value of 6.*

Sample	OD <sub>600</sub> of active sample (±0.005)	OD <sub>600</sub> vortexed control initial (±0.005)	Percentage auto-aggregation (±0.05)
10 nM Biotin linked colicin E9 conjugate and 2 nM NeutrAvidin	0.28	1.26	78.1
100 nM Biotin linked colicin E9 conjugate and 20 nM NeutrAvidin	0.25	1.30	81.7
1 µM Biotin linked colicin E9 conjugate and 200 nM NeutrAvidin	0.26	1.27	80.9
<i>E. coli</i> only	0.51	1.29	60.3

We therefore proceeded to a final auto-aggregation assay, using samples of BW25113 containing the mannose-based inhibitor-linked (Gly-Ser)<sub>n</sub> colicin E9 conjugates (Experiment Five). The samples were prepared as stated in experimental section 8.4.2, page 308 and the results of the auto-aggregation assay are shown in Table 10. Here a trend is seen between increasing the concentration of mannose-based inhibitor-linked (Gly-Ser)<sub>n</sub> colicin E9 conjugate from 10 nM to 100 nM and an increased percentage auto-aggregation value being observed. However, the percentage auto-aggregation values obtained for all colicin linked conjugates was similar to that obtained for the *E. coli* only control, in this experiment, however they were far greater than measured for the *E. coli* only control in experiment four.

## Investigation into the biological applications of the colicin conjugates

Therefore, until the experiment is completed in duplicate we cannot unequivocally conclude whether any of the mannose-based inhibitor-linked (Gly-Ser)<sub>n</sub> colicin E9 conjugates had the ability to induce aggregation of BW25113. Preparation of the auto-aggregation assay samples was extremely time and reagent intensive, and this, coupled with the issues encountered during the assay, led us to the decision to investigate an auxiliary method for measuring aggregation.

## Investigation into the biological applications of the colicin conjugates

**Table 10.** Results of Experiment Five, an auto-aggregation assay performed on samples of BW25113 incubated with varying concentrations of each Mannose-based inhibitor linked (Gly-Ser)<sub>n</sub> colicin E9 conjugate. OD<sub>600</sub> measurements were made post sample incubation and were used to calculate percentage auto-aggregation.

Colicin E9 linked conjugate	Concentration (nM)	OD <sub>600</sub> of active sample (±0.005)	OD <sub>600</sub> of vortexed control (±0.005)	Percentage auto-aggregation (±0.05)
Mannose-based inhibitor linked (Gly-Ser) colicin E9 conjugate	10	0.39	1.20	67.8
Mannose-based inhibitor linked (Gly-Ser) colicin E9 conjugate	100	0.28	1.20	76.5
Mannose-based inhibitor linked (Gly-Ser) <sub>3</sub> colicin E9 conjugate	10	0.26	1.15	77.3
Mannose-based inhibitor linked (Gly-Ser) <sub>3</sub> colicin E9 conjugate	100	0.25	1.19	79.4

Investigation into the biological applications of the colicin conjugates

Mannose-based inhibitor linked (Gly-Ser) <sub>6</sub> colicin E9 conjugate	10	0.32	1.2	72.1
Mannose-based inhibitor linked (Gly-Ser) <sub>6</sub> colicin E9 conjugate	100	0.26	1.19	78.1
<i>E. coli</i> only control		0.29	1.21	75.8

#### 4.2.2 Use of microscopy

We thus opted to explore microscopy techniques as an auxiliary method for measuring aggregation, fully aware that imaging of microscopy samples can be highly prone to sample bias and thus obtaining quantitative results regarding the extent of aggregation would be challenging. However, the issues observed during the aggregation assays meant that an auxiliary method would help to reinforce our observations regarding the abilities of the mannose-based inhibitor-linked (Gly-Ser)<sub>n</sub> colicin E9 conjugates to induce aggregation. Furthermore, the sample size required for microscopy imaging was significantly smaller than that required for an aggregation assay (60  $\mu$ L vs 600  $\mu$ L), meaning microscopy offered a way to quickly screen a large number of sample conditions for aggregate formation.

The initial microscopy samples screened a variety of different conditions, such as starting OD<sub>600</sub> (0.5, 1 or 2), mannose-based inhibitor-linked (Gly-Ser)<sub>n</sub> colicin E9 conjugate concentration (1  $\mu$ M, 100 nM and 10 nM), and different *E. coli* strains (BW25113 and JW3596). Each sample was set up in duplicate, meaning that each sample had a vortexed control (Experiment Six). Samples were prepared in accordance with experimental section 8.4.3, page 310 and microscopy images of each sample and its vortexed control are attached in appendix section 9.3.4, page cxvi.

Only two of the samples screened in Experiment Six were shown to induce aggregation. Both of these samples used BW25113 at a starting OD<sub>600</sub> of 0.5 (10 nM mannose-based inhibitor linked (Gly-Ser) colicin E9 conjugate and 1  $\mu$ M mannose-based inhibitor linked (Gly-Ser)<sub>6</sub> colicin E9 conjugate). Images of both samples and their vortexed controls are shown in Figure 4-3. Figure 4-3 (a-c) shows the results for 10 nM mannose-based inhibitor linked (Gly-Ser) colicin E9 conjugate and Figure 4-3 (d-f) shows the results for 1  $\mu$ M mannose-based inhibitor linked (Gly-Ser)<sub>6</sub> colicin E9 conjugate. As shown in Figure 4-3, aggregate formation is observed in the active samples and not the vortexed controls.

### Investigation into the biological applications of the colicin conjugates

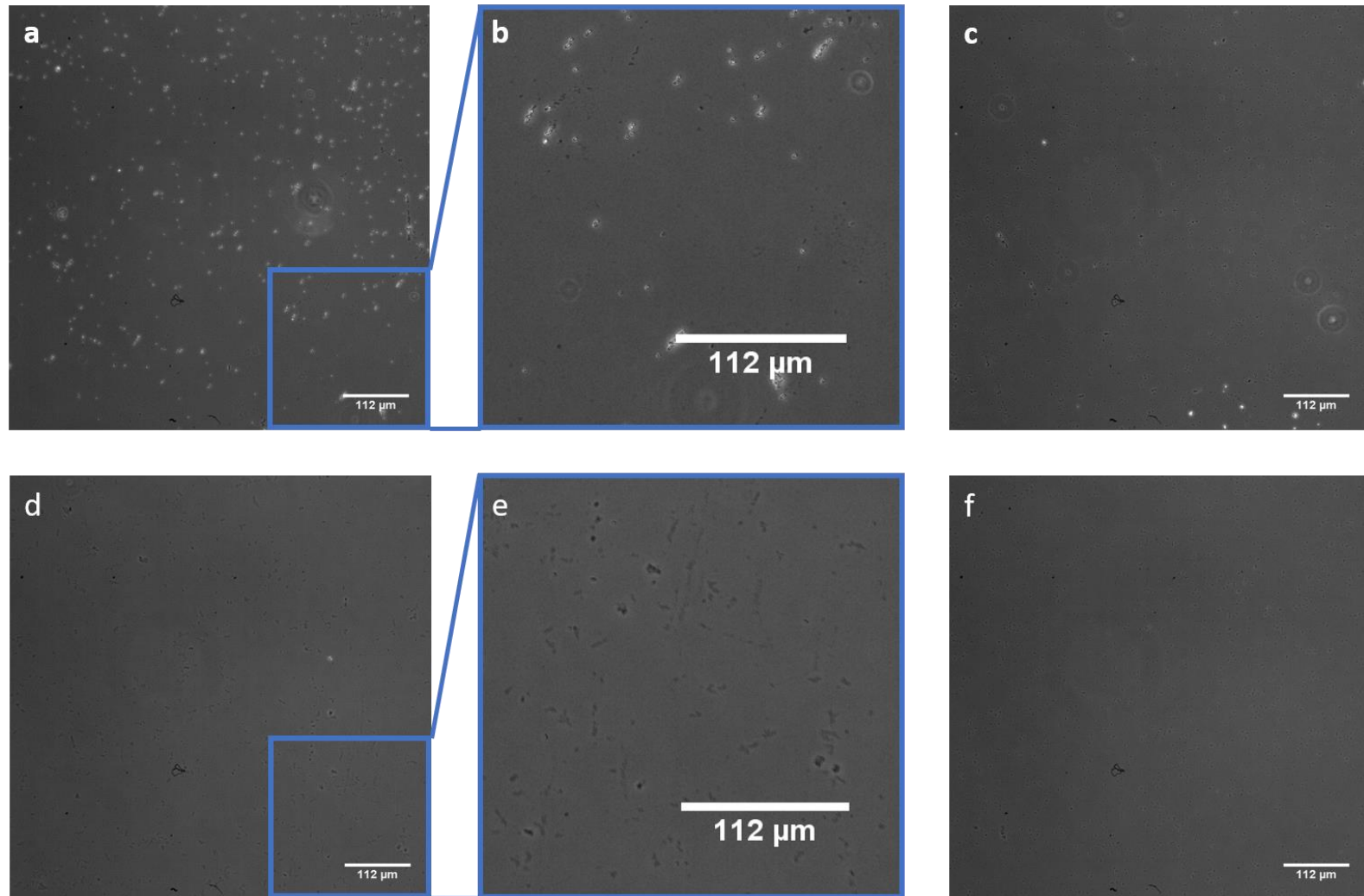


Figure 4-3. Microscopy images of two of the samples where aggregation was observed in Experiment Six. a) active sample of BW25113 incubated 10 nM mannose-based inhibitor linked (Gly-Ser) colicin E9 conjugate, b) zoomed in section of image a, c) vortexed control sample of BW25113 incubated 10 nM mannose-based inhibitor linked (Gly-Ser) colicin E9 conjugate, d) active sample of BW25113 incubated with 1  $\mu$ M mannose-based inhibitor linked (Gly-Ser)<sub>6</sub> colicin E9 conjugate, e) zoomed in section of image d, f) vortexed control sample of BW25113 incubated with 1  $\mu$ M mannose-based inhibitor linked (Gly-Ser)<sub>6</sub> colicin E9 conjugate. Note images a, c, d and f were all taken a 20x magnification

## Investigation into the biological applications of the colicin conjugates

Both samples in which aggregate formation was observed had a starting OD<sub>600</sub> of 0.5, and there are two potential hypotheses which could explain this correlation. Firstly, aggregation is more noticeable at lower bacterial levels, and alternatively, it was only at these lower bacterial concentrations where there was a high enough concentration of mannose-based inhibitor-linked (Gly-Ser)<sub>n</sub> colicin E9 conjugate to induce observable aggregate formation. An observation of note was aggregate formation was observed at 10 nM of mannose-based inhibitor linked (Gly-Ser) colicin E9 conjugate but not at 100 nM or 1 μM. This observation may be accounted for by occupation of all FimH binding sites by excess mannose conjugate which is free in solution rather than bound to surface colicin receptors.

Two further microscopy experiments were performed in an attempt to confirm whether conjugate addition induced aggregate formation in the 10 nM mannose-based inhibitor linked (Gly-Ser) colicin E9 conjugate sample. Firstly, samples of BW25113, JW4283 and RK5016 (starting OD<sub>600</sub> for all = 0.5) were incubated with either 1 μM and 100 nm of mannose-based inhibitor linked (Gly-Ser) colicin E9 conjugate (Experiment Seven). The microscopy samples were prepared in accordance with the method given in experimental section 8.4.3, page 310, and microscopy images of each sample and its vortexed control is also attached in Appendix section 9.3.5, page cxlii. Aggregate formation was not observed in any of these samples, highlighting the challenges presented by microscopy experiments for aggregation assays.

A third microscopy experiment was also performed. Here samples of BW25113 and RK5016 (starting OD<sub>600</sub> = 0.5) were incubated with 10 nM of biotin-linked colicin E9 conjugate and 2 nM of NeutrAvidin (Experiment Eight). Table 8 previously showed that incubation of samples of BW25113 under these conditions led to an increase in percentage auto-aggregation compared to samples of BW25113 only. The conditions used in the auto-aggregation assay reported in Table 8 are slightly different to those used to set up the microscopy samples - starting OD<sub>600</sub> values of 1.5 and 2 were used in the aggregation assay, whereas a starting OD<sub>600</sub> value of 0.5 was used to set up the microscopy samples. The microscopy samples and the relevant control samples were set up in accordance with experimental section 8.4.3, page 310) and microscopy images of each sample and its vortexed control are attached in appendix section 9.3.6, page cxlviii. None of the microscopy samples showed aggregate formation, yet the experiments we previously performed under similar conditions (experiments three and four) gave results suggestive of aggregate formation, again highlighting potential sampling bias. Currently, we propose more experiments are required in order to unequivocally conclude that any of the mannose-based inhibitor-linked (Gly-Ser)<sub>n</sub> colicin conjugates can induce *E. coli* aggregation.

### 4.3 Summary and conclusions

The aim of this chapter was to investigate the biological properties of the mannose-based inhibitor-linked (Gly-Ser)<sub>n</sub> colicin conjugates, mainly their ability to induce *E. coli* aggregation. Unfortunately, the results presented in this chapter are not yet unequivocal despite our best efforts to develop a robust assay / method for accurately measuring aggregate formation. Therefore, further work is required to explore the aggregative properties of the mannose-based inhibitor-linked (Gly-Ser)<sub>n</sub> colicin conjugates reported here.

An auto-aggregation assay was the first assay chosen to validate the biological applications of the mannose-based inhibitor-linked (Gly-Ser)<sub>n</sub> colicin conjugates. However, problems were encountered with this assay when samples of two different strains of *E. coli* did not show the expected trend in percentage auto-aggregation. These problems were further exacerbated by the inconsistent results on different spectrophotometers measured for samples of BW25113 incubated with the biotin-linked colicin E9 conjugate and NeutrAvidin. Finally, although samples of BW25113 incubated with varying concentrations of the mannose-based inhibitor-linked (Gly-Ser)<sub>n</sub> colicin E9 conjugates did show increased percentage auto-aggregation with increasing conjugate concentration, experimental repeats are required using control samples. Due to the large sample volumes required a further assay using higher concentrations of the conjugates was not possible. Another concern regarding the results of the auto-aggregation assays were the large differences in the OD<sub>600</sub> measurements recorded for identical samples using the nanodrop spectrophotometer and the plate reader. These issues necessitated the usage of an auxiliary validation method, and microscopy was chosen.

The use of microscopy to monitor aggregate formation had previously been avoided due to the high risk of sample bias. However, with auto-aggregation assays requiring reinforcement we decided to use microscopy to screen a number of different conditions (e.g. conjugate concentration, starting OD<sub>600</sub> and *E. coli* strain). Two conditions were identified as inducing aggregate formation (BW25113 OD<sub>600</sub> = 0.5, 10 nM mannose-based inhibitor linked (Gly-Ser) colicin E9 conjugate and BW25113 OD<sub>600</sub> = 0.5, 1 μM mannose-based inhibitor linked (Gly-Ser)<sub>6</sub> colicin E9 conjugate). However, further samples of BW25113 (starting OD<sub>600</sub> = 0.5) treated with 10 nM biotin-linked colicin E9 conjugate and 2 nM NeutrAvidin showed no aggregate formation despite previous auto-aggregation assays (experiments three and four) suggesting aggregation occurred. Therefore, further work will be required to unequivocally confirm our hypothesis, and potential investigation methods/approaches are discussed in chapter 7.

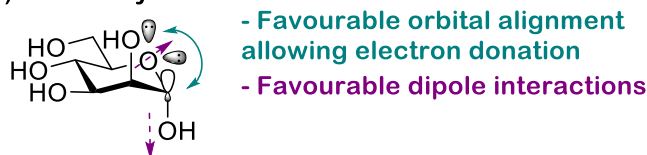


## Chapter 5 Use of chemical synthesis for the construction of $\beta$ -mannosides

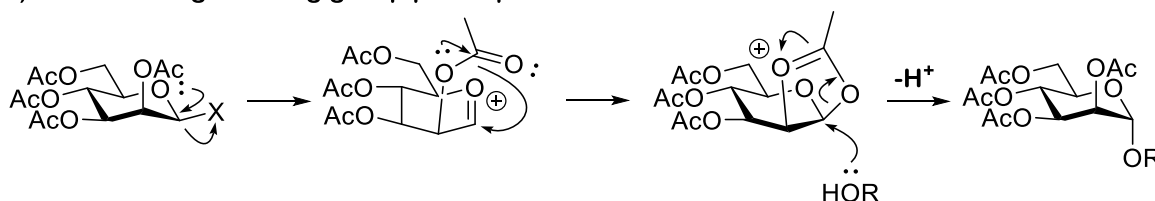
### 5.1. Introduction

$\beta$ -Mannosides are frequently seen within nature in various mannans, glycosphingolipids and lipopolysaccharides,<sup>80</sup> yet their synthesis remains a challenge for carbohydrate chemists. The main challenge in  $\beta$ -mannoside synthesis is that  $\alpha$ -mannoside formation is both thermodynamically and kinetically favoured (Scheme 5-1a); this makes finding synthetic conditions which favour  $\beta$ -mannoside formation difficult.<sup>324</sup> The thermodynamic preference for  $\alpha$ -mannosides is a direct consequence of the anomeric effect, which favours electronegative substituents adopting an axial orientation. This orientation is stabilised by both dipole minimisation and electron delocalisation from the axial lone pair on the ring oxygen to the antibonding orbital of the anomeric carbon (Scheme 5-1a).<sup>324</sup> Kinetic factors can further favour  $\alpha$ -mannoside formation; neighbouring group participation leads to the complete blockage of the  $\beta$ -face in the acetoxonium ion intermediate, promoting  $\alpha$ -mannoside formation (Scheme 5-1b).<sup>324, 325</sup>

#### a) Thermodynamic



#### b) Kinetic - Neighbouring group participation



Scheme 5-1. a) The thermodynamic preferences which lead to  $\alpha$ -mannoside formation, e.g. favourable orbital alignment and favourable dipole interactions. b) The kinetic preference for  $\alpha$ -mannoside formation, e.g. neighbouring group participation

Over the past 20 years a wealth of research has been dedicated to the development of reliable methods for  $\beta$ -mannosidic bond formation.<sup>80, 83, 84, 326, 327</sup> One of the first methods developed for  $\beta$ -mannosidic bond formation used mannose 1,2-*O*-cis-stannylene acetals donors (Figure 5-1).<sup>328</sup> The  $\beta$ -selectivity of this methodology can be accounted for by mannose 1,2-*O*-stannylene acetals favouring the cis-arrangement around the anomeric centre, leading to a glycosylation procedure which has been referred to as “glycosylation *via* a locked anomeric configuration”.<sup>328</sup> However, more recently other  $\beta$ -mannoside formation methodologies have been discovered which surpass the 50-57% conversion rate seen with mannose 1,2-*O*-stannylene acetals.<sup>328</sup>

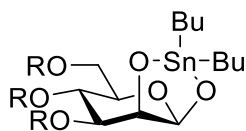
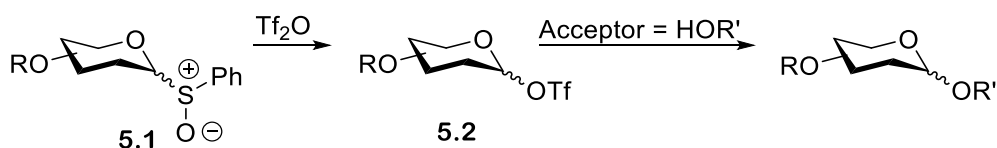


Figure 5-1. Structure of a 1,2-*O*-cis-stannylene acetal of mannose

Crich and co-workers have long led the development of  $\beta$ -mannoside chemistry,<sup>80, 329-331</sup> beginning with synthesis of  $\beta$ -mannopyranosides using primary alcohols via the sulfoxide method - a variation of the Kahne sulfoxide glycosylation protocol.<sup>80</sup> Kahne's glycosylation protocol uses a two-step methodology (Scheme 5-2),<sup>332</sup> firstly, a sulfoxide donor **5.1** is activated by  $\text{Tf}_2\text{O}$  at  $-78^\circ\text{C}$ , forming activated species **5.2**, before, species **5.2** undergoes glycosylation upon the addition of a glycosyl acceptor.<sup>332</sup>



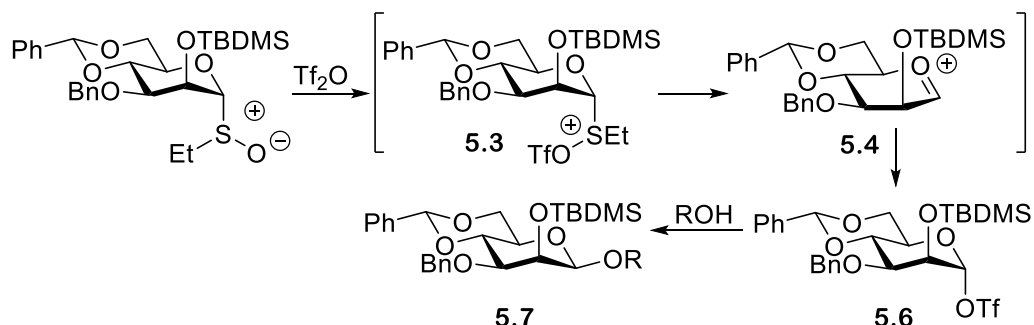
Scheme 5-2. Kahne's sulfoxide glycosylation protocol, where  $R$  = a protecting group such as  $\text{OBn}$  and  $\text{OR}'$  = the acceptor

Crich and co-workers adapted Kahne's sulfoxide glycosylation protocol for  $\beta$ -mannoside synthesis, developing three different protocols using benzylidene acetal protected sulfoxide donors (Scheme 5-3). Protocol A used a pre-activation methodology where  $\text{Tf}_2\text{O}$  was added to a 2:1 solution of the glycosyl donor and 2,6-di-*tert*-butyl-4-methylpyridine (DTBMP) in  $\text{Et}_2\text{O}$  / benzene at  $-78^\circ\text{C}$ . The glycosyl acceptor was added after the donor had undergone activation and the solution was warmed to  $0^\circ\text{C}$ .<sup>80</sup> This protocol was shown to consistently produce  $\beta$ -mannosides in high selectivity, with a maximum yield of 86% when a 4,6-*O*-benzylidene acetal protected donor was present.<sup>80</sup> Protocol A was adapted to give protocol C, in which the replacement of benzene with 1,4 dimethoxybenzene was shown to have no significant effect on glycosylation results.<sup>80</sup> Protocol B used a direct activation methodology, with  $\text{Tf}_2\text{O}$  added to a mixture of glycosyl donor, glycosyl acceptor and DTBMP; this protocol displayed no selectivity for  $\beta$ -mannoside formation, instead favouring  $\alpha$ -mannoside formation.<sup>80</sup>

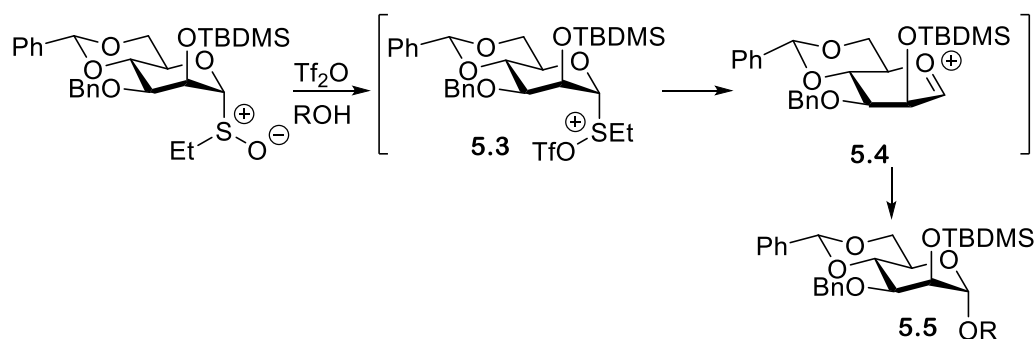
The selectivity of pre-activation protocols for  $\beta$ -mannoside formation can be explained mechanistically (Scheme 5-3).<sup>83</sup> In both direct activation and pre-activation protocols the glycosyl donor undergoes initial sulfoxide activation with  $\text{Tf}_2\text{O}$  to afford sulfoxonium ion **5.3**. In direct activation the formation of the sulfoxonium ion (**5.3**) precedes oxacarbenium ion formation (**5.4**) and subsequent attack at the  $\alpha$ -face by a glycosyl acceptor affording  $\alpha$ -mannoside **5.5** as a product.<sup>83</sup> In pre-activation protocols the lack of a glycosyl acceptor during activation leads to attack of oxacarbenium **5.4** ion by a triflate ion, forming a quasi-stable  $\alpha$ -triflate **5.6**. The blockage of the  $\alpha$ -face

facilitates stereoselective attack at the  $\beta$ -face upon glycosyl acceptor addition, affording  $\beta$ -mannoside **5.7** as a product.<sup>83</sup>

**Protocol A and C (pre-activation)**



**Protocol B (direct activation)**



*Scheme 5-3. Mechanism of pre-activation and direct activation of mannose donors, where R = the acceptor*

Crich and co-workers further proposed that for  $\beta$ -selectivity to be achieved the triflate ion must coordinate to the  $\alpha$ -face either covalently, forming an  $\alpha$ -triflate, or as an  $\alpha$ -oriented contact ion pair with the oxocarbenium ion (Figure 5-2).<sup>85</sup> The contact ion pair can become transiently separated by solvent, which leaves the  $\alpha$ -face exposed for attack, explaining the small amount of  $\alpha$ -mannoside formed during pre-activation protocols.

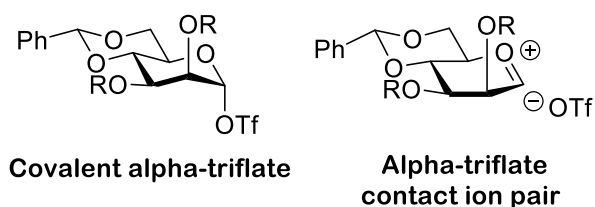


*Figure 5-2. Structure of covalent  $\alpha$ -triflate intermediate and contact ion pair intermediate*

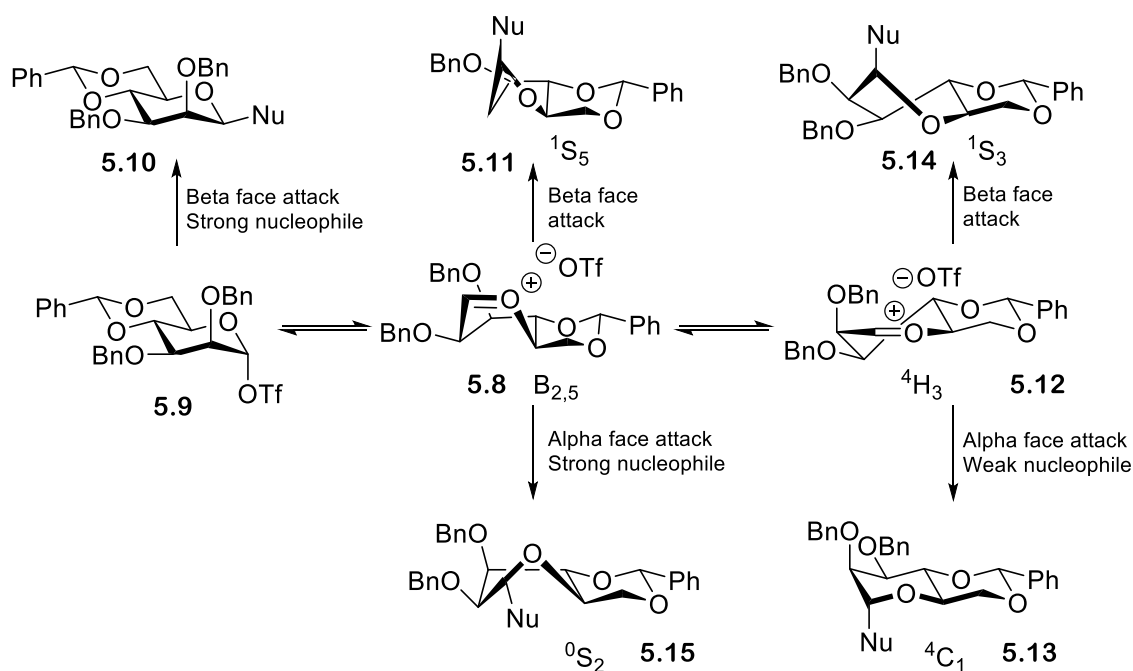
Protecting the *O*-4 and *O*-6 positions with a benzylidene acetal group was observed to reduce  $\alpha$ -mannoside formation. Crich and co-workers rationalised this reduction to be the result of the equilibrium shifting to favour covalent  $\alpha$ -triflate formation.<sup>85</sup> Further investigations into  $\beta$ -mannosides probed the influence of the nucleophilicity of glycosyl acceptors on the reaction mechanism and stereoselectivity. Mannose oxocarbenium ions likely exist in one of two half-chair conformations:<sup>333</sup> the  ${}^3H_4$  conformer and the  ${}^4H_3$  conformer (Figure 5-3). Though computational studies have previously obtained conflicting results regarding which conformer is preferential, biological data suggests that the  ${}^3H_4$  conformer is favoured.<sup>333</sup> This suggestion is further validated by computational studies of monosubstituted oxocarbenium ions which indicate a preference for the C-2 alkoxy group to favour the equatorial position and the alkoxy groups at C-3 and C-4 to strongly favour axial orientations.<sup>333</sup> Further backing for the adoption of the axial position by both C-3 and C-4 can be seen in glycoside hydrolysis rate studies.<sup>333</sup> It has been proposed that in the absence of a conformationally-restrictive protecting group, oxocarbenium ions mainly exist in the  ${}^3H_4$  conformer, but react via the less populated  ${}^4H_3$  conformer in a typical Curtin-Hammett kinetic scheme to afford high yields of the  $\alpha$ -mannoside.<sup>85</sup> Benzylidene acetal protection removes the  ${}^3H_4$  conformer from consideration, leaving only the  ${}^4H_3$  conformer, the more stable  $B_{2,5}$ -oxocarbenium ion **5.8** and the  ${}^4E$  conformer.<sup>85</sup>



Figure 5-3. Structure of the  ${}^3H_4$  and  ${}^4H_3$  oxocarbenium ion conformations

$\beta$ -mannoside formation is thought to rely upon the formation of the  $B_{2,5}$ -oxocarbenium ion **5.8**. This oxocarbenium ion can equilibrate to form  $\alpha$ -triflate **5.9**, which can then undergo an  $S_N2$ -like attack from a strong nucleophile to form  $\beta$ -mannoside **5.10** (Scheme 5-4).<sup>334</sup> Alternatively, the  $B_{2,5}$ -oxocarbenium ion **5.8** can undergo direct attack at the  $\beta$ -face with a weak nucleophile affording a  $\beta$ -mannoside with a  ${}^1S_5$  structure **5.11** (Scheme 5-4).  $\beta$ -mannoside formation is rarely stereoselective and minor amounts of the  $\alpha$ -mannoside is often observed. This observation is the result of the equilibration of  $B_{2,5}$ -oxocarbenium ion **5.8** to  ${}^4H_3$ -oxocarbenium ion **5.12** (Scheme 5-4). The  ${}^4H_3$ -oxocarbenium ion **5.12** can undergo attack at the  $\alpha$ -face by weak nucleophiles to afford the stable  ${}^4C_1$   $\alpha$ -mannoside **5.13** (Scheme 5-4).<sup>334</sup> Nucleophilic attack to form the  ${}^1S_3$  structure **5.14** and the  ${}^0S_2$  structure **5.15** rarely occurs due to the unfavourable nature of these structures (Scheme 5-4).

## Use of chemical synthesis for the construction of $\beta$ -mannosides



Scheme 5-4. Proposed mechanistic pathways accounting for the selectivity observed in glycosylations of benzylidene mannose donors<sup>334</sup>

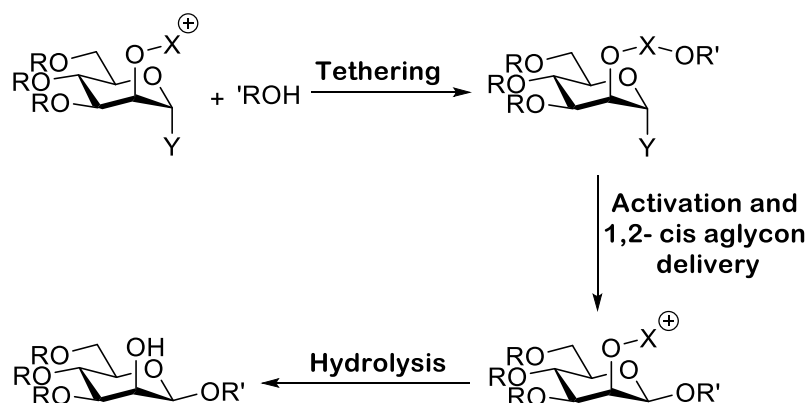
For many years Crich's method of pre-activation with  $\text{Tf}_2\text{O}$  was the gold standard for  $\beta$ -mannoside formation,<sup>80, 82, 83, 86, 335</sup> but recent studies have reported that pre-activation is not necessary to maintain  $\beta$ -stereoselectivity.<sup>336-338</sup> Bols and co-workers found 4,6-silylene protected thiomannosides<sup>79</sup> and 4,6-benzylidene acetal-protected mannosyl donors<sup>84</sup> could undergo  $\beta$ -selective glycosylations using direct activation with NIS/ $\text{TfOH}$ . Direct activation of benzylidene-acetal protected mannosyl donors using this method was shown to achieve similar yields and selectivity to that achieved using pre-activation methodologies<sup>84</sup> Though some entries using direct activation did display low  $\beta$ -selectivity, Bols and co-workers proved this to be the result of anomerisation of  $\beta$ -mannosides to  $\alpha$ -mannosides when insufficient base / acid scavenger species were present.<sup>84</sup>

Overall direct activation of benzylidene acetal-protected mannosyl donors is limited compared to pre-activation due to triflation of the acceptor alcohol occurring as a side reaction;<sup>84</sup> the extent of this side reaction is proportional to the acceptors nucleophilicity.<sup>326</sup> A practical advantage associated with the usage of this direct activation methodology over pre-activation methodologies is that the reaction can be performed at 25 °C instead of -78 °C.<sup>84</sup>

A further notable method for the formation of  $\beta$ -mannosides is intermolecular aglycon delivery (IAD). This approach works by temporarily tethering an aglycon moiety to the O-2 position of a glycosyl donor, then subsequently activating the glycosyl donor to promote a stereoselective intramolecular glycosylation affording (Scheme 5-5).<sup>339</sup> IAD has been applied to the synthesis of both

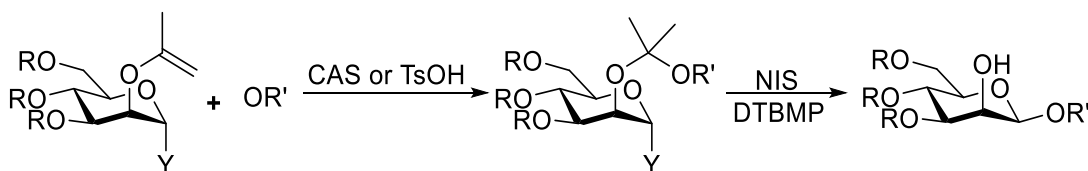
## Use of chemical synthesis for the construction of $\beta$ -mannosides

1,2 cis mannosidic and glycosidic bonds, using a variety of different tethering mechanisms. The tethering mechanisms relevant to  $\beta$ -mannoside formation are discussed below.



*Scheme 5-5. The general method used for mannose based intramolecular aglycon delivery. This process begins by tethering the acceptor to the O-2 position. Once tethered the glycosyl donor is activated, stimulating an intramolecular glycosylation which is followed by hydrolysis*

Much of the initial research into IAD was driven by a need to develop an effective method for  $\beta$ -mannoside formation. In 1991 Barresi and Hindsgaul introduced an IAD method using vinyl ethers (Scheme 5-6) which underwent an acid-catalysed (by either CSA or TsOH) tethering mechanism. This tethered intermediate was then activated with NIS inducing an intramolecular glycosylation reaction affording a  $\beta$ -mannoside.<sup>340</sup> To investigate whether the reaction proceeded by an intramolecular mechanism, methanol was added during NIS activation. If the reaction proceeded via an intramolecular pathway the addition of methanol should have no effect on product composition or yield, whereas if the glycosylation proceeded by an intermolecular pathway the methanol would act as a competing nucleophile, resulting in a yield reduction. No change to the product yield was observed, supporting the theory that the mechanism was intramolecular.<sup>341</sup> Due to both the low yields obtained during tethering reactions and the inability to form a  $\beta$  mannosidic bond to GlcNAc, vinyl ethers are now rarely used as tethers.<sup>339</sup>

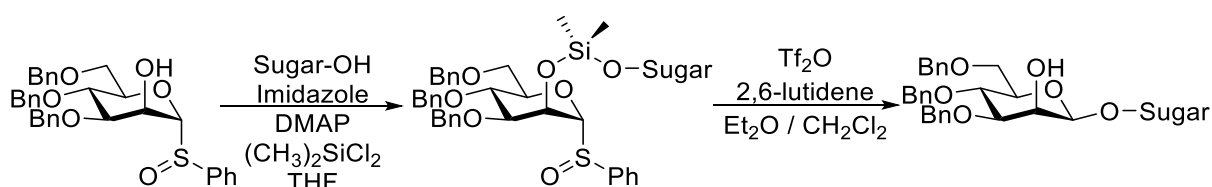


*Scheme 5-6. Reaction pathway for vinyl ether mediated intramolecular aglycon delivery. This pathway proceeds via an acid catalysed tethering mechanism followed by NIS-mediated activation of the glycosyl donor*

Stork and co-workers introduced the use of temporary silicon tethers (Scheme 5-7).<sup>342</sup> Once the silicon tether has formed the glycosyl sulfoxide donor can undergo activation at low temperatures, inducing an intramolecular glycosylation that generates  $\beta$ -mannosides in high yields (60-70%).<sup>342</sup> Initially, Stork and co-workers only used primary alcohol acceptors, meaning only O-6 linkages were

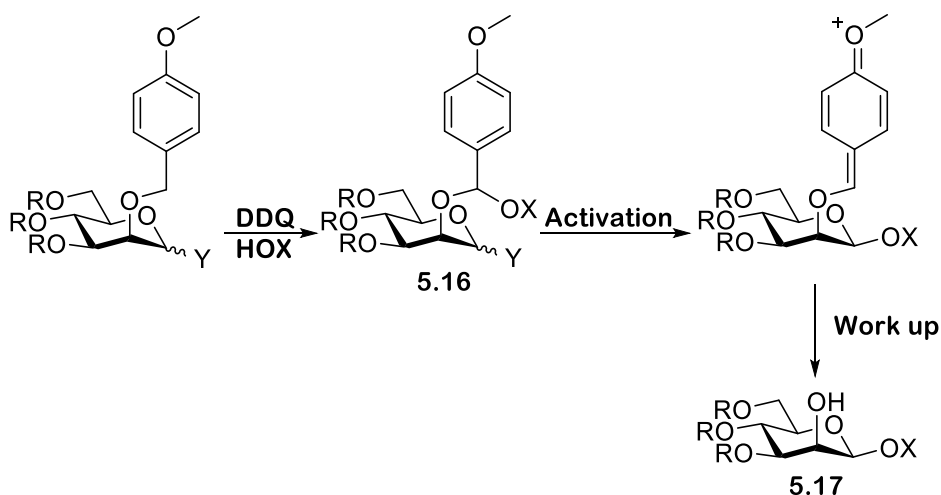
## Use of chemical synthesis for the construction of $\beta$ -mannosides

formed.<sup>342</sup> When the acceptor library was expanded to include secondary alcohols (e.g. *O*-3 and *O*-2) a decrease in average yield was observed (55-72%) with a further yield decrease observed when sterically hindered *O*-4 glycosyl acceptors were used (10-40%).<sup>343</sup> Bols and co-workers have since demonstrated temporary silicon tethering can be used reliably on glucose and galactose derivatives to synthesize 1,2-*cis* glycosidic bonds, achieving similar yields with primary, secondary and tertiary alcohols,<sup>344</sup> with the use of armed donors further increasing reaction yields.<sup>345</sup>



*Scheme 5-7. Reaction pathway for temporary silicon tethered mediated intramolecular aglycon delivery. The reaction pathway proceeds with initial formation of the silicon tether at the *O*-2 position, followed by  $Tf_2O$  mediated activation*

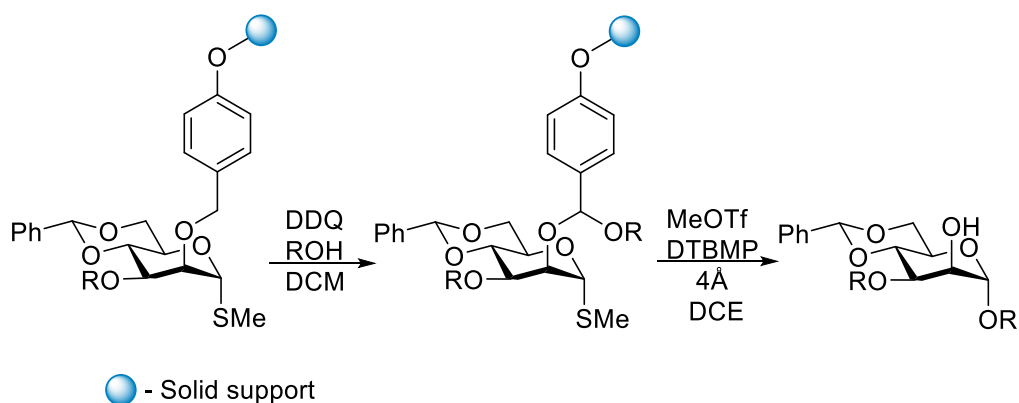
The most successful tethering approach to date for the formation of  $\beta$ -mannosides is oxidative tethering introduced by Ogawa and Ito.<sup>346</sup> The major advantage of oxidative tethering over the use of a vinyl and silyl tether is that oxidative tethering is high yielding for both 1°, and 2° alcohols including glucosamine (*O*-4).<sup>346</sup> A further advantage is that the tethering reaction is so efficient the tethered intermediate can be used crude.<sup>339</sup> Oxidative tethering predominantly uses a PMB protecting group at *O*-2, which undergoes DDQ mediated oxidation affording oxidised species **5.16**. Oxidised species **5.16** then undergoes activation and subsequent intramolecular glycosylation, affording the desired product **5.17** post work-up (Scheme 5-8).<sup>346</sup>



*Scheme 5-8. Reaction pathway for intramolecular aglycon delivery mediated by an oxidative tether using *O*-2-PMB. The pathway follows initial DDQ mediated oxidation, with subsequent glycosyl donor activation resulting in intramolecular glycosylation succeeded by a final work-up to afford the desired  $\beta$ -mannoside*

Multiple activation systems have shown success in oxidative tethering - the activation system AgOTf, SnCl<sub>2</sub> and DBMP has been shown to afford  $\beta$ -mannosides in good yields when using both *O*-4 glucose and glucosamine derivatives (40-70%),<sup>346</sup> and the activation of methyl thioglycoside donors using MeOTf and DTBMP has been shown to afford  $\beta$ -mannosides exclusively.<sup>339</sup>

The effect of protecting groups on glycosylation efficiency and stereoselectivity of oxidative tethering reactions has been investigated. The addition of a cyclic protecting group at the *O*-4 and *O*-6 positions has been shown to increase glycosylation efficiency.<sup>347</sup> Cyclohexylidene protection has been shown to be the most beneficial; this is likely due to the cyclic protecting group increasing ring-rigidity forcing an S<sub>N</sub>2-like reaction to occur, thus producing a  $\beta$ -linkage.<sup>347</sup> Ito and Ogawa further developed a solid phase approach (known as the gatekeeper approach) to IAD by attaching a solid support to the PMB group (Scheme 5-9).<sup>348</sup> The major advantage of this approach is that any unreacted material remains tethered to the solid support, making product isolation and purification easy. This approach has been successfully applied to the synthesis of a number of different  $\beta$ -mannosides, and has been shown to be near exclusively selective for  $\beta$ -mannoside formation.<sup>348</sup>



*Scheme 5-9. Depicts the gatekeeper approach to intramolecular aglycan delivery. This method follows the same mechanism as oxidative tethering, however the PMB group is attached to a solid support allowing for easy product purification*

## 5.2 Section aims

The aim of the work in this chapter is to initially investigate different chemical synthesis methods for  $\beta$ -mannoside formation, with the aim of establishing a reliable method for the synthesis of protected disaccharide **5.18**. The synthesis of protected disaccharide **5.18** is the biggest synthetic challenge presented in the project. Once protected disaccharide **5.18** was obtained it could be used in a final glycosylation with either mannoside **2.1a** or **2.1b** to afford protected trisaccharide **5.19**. It was anticipated that finding high yielding conditions for this final glycosylation would be significantly less challenging, as the formation of  $\alpha$ -mannosides is both thermodynamically and kinetically favoured.



### 5.3 Result and discussion

#### 5.3.1 Exploration of chemical synthesis method for the synthesis of $\beta$ -mannosides

One of the most challenging project aims was the synthesis of trisaccharide **1.4** and the formation of a  $\beta$ -mannosidic bond between the 1,3-mannose donor **2.2** and the 1,4-GlcNPhth acceptor **2.3c** (Figure 5-4).  $\beta$ -Mannosidic bonds are one of the most challenging bonds to synthesise in carbohydrate chemistry,<sup>79</sup> and making such a bond to the sterically hindered O-4 position<sup>343</sup> is especially challenging.

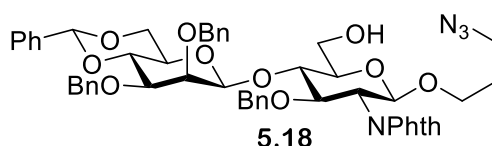
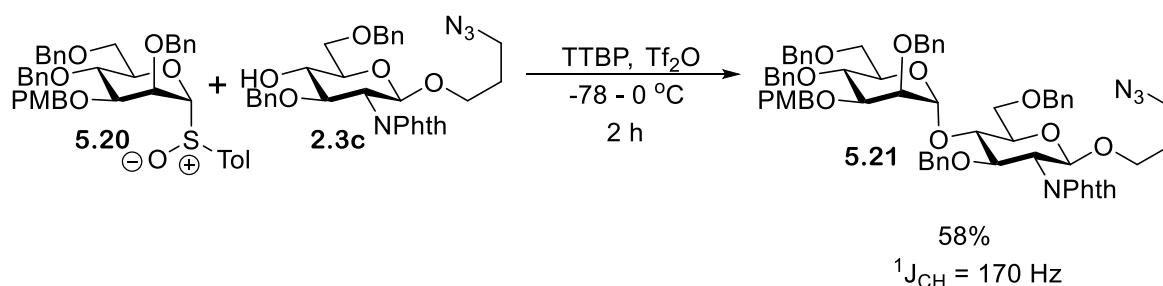


Figure 5-4. Structure of disaccharide **5.18**

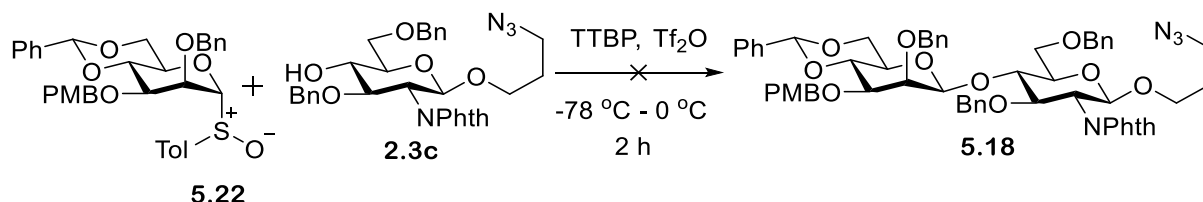
The first attempt made to synthesise a  $\beta$ -mannoside was unsuccessful but provided an opportunity to trial the Bols' glycosylation protocol and complete NMR characterisation of an  $\alpha$ -mannoside linkage for future comparison. The attempted glycosylation was performed using glycosyl sulfoxide donor **5.20** and GlcNPhth acceptor **2.3c**, trialling Bols and co-workers pre-activation conditions.<sup>84</sup> Disaccharide **5.21** was isolated as the major reaction product in a 59% yield, unfortunately, as expected NMR analysis using a proton coupled carbon spectrum showed disaccharide **5.21** to have a  $^1J_{CH}$  coupling constant of 170.9 Hz, which matches  $^1J_{CH}$  values reported for  $\alpha$ -mannosides<sup>349</sup> (Scheme 5-10).



Scheme 5-10. Formation of disaccharide **5.21** from protected 1,3-mannose donor **5.20** and protected 1,4-glucosamine acceptor **2.3c** using Bols and co-workers pre-activation conditions

The lack of stereoselectivity of this reaction is a result of the protecting groups present on glycosyl sulfoxide donor **5.20**, with both Bols and co-workers and Crich and co-workers previously reporting the necessity of using benzylidene acetal protected donors when synthesising  $\beta$ -mannosides.<sup>83, 84</sup>

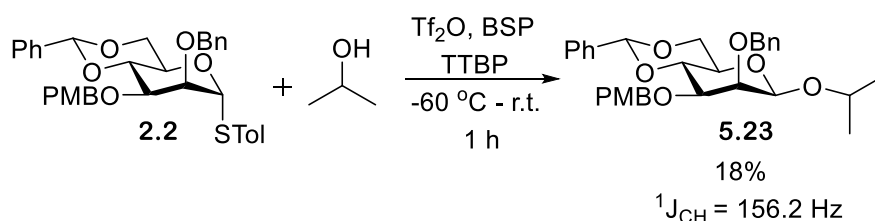
Consequently, sulfoxide donor **5.20** was redesigned to include a 4,6 benzylidene acetal ring. A second glycosylation was attempted using the same conditions as used previously, substituting sulfoxide donor **5.20** for benzylidene acetal sulfoxide donor **5.22**, however, TLC analysis showed no reaction occurred, with only hydrolysis of benzylidene acetal sulfoxide donor **5.22** observed (Scheme 5-11).



Scheme 5-11. Unsuccessful formation of disaccharide **5.18** from protected mannose donor **5.22** and protected glucosamine acceptor **2.3c** using Bols and co-workers conditions

The failure of this reaction was unexpected and prompted the evaluation of two different parameters. Firstly, the methodology being followed, as so far only Bols and co-worker's pre-activation technique had been attempted. Secondly, it was questioned whether benzylidene acetal sulfoxide donor **5.22** was reactive enough, as previously GlcNPhth acceptor **2.3c** had undergone a glycosylation with sulfoxide donor **5.20** to form disaccharide **5.21**.

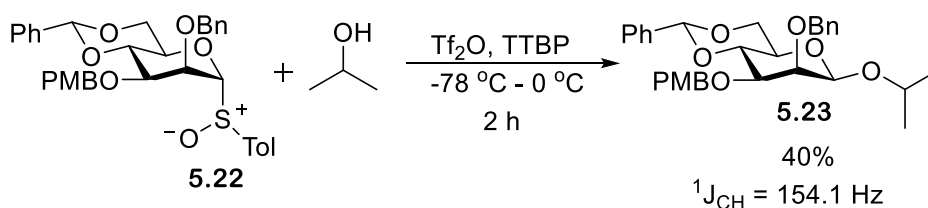
To test both these hypotheses we trialled many different glycosylation conditions using a simple propan-2-ol acceptor. The first reaction conditions tested were the Crich and co-worker's pre-activation conditions (Scheme 5-12).<sup>85</sup> These conditions vary from those used by Bols and co-worker's as they do not require sulfoxide formation and instead use BSP, TTBP and Tf<sub>2</sub>O as an activator combination.<sup>84</sup> The application of Crich and co-worker's conditions was successful in the glycosylation of benzylidene acetal donor **2.2** to propan-2-ol with an unoptimized 18% yield of glycoside **5.23** being extracted. NMR analysis confirmed the formation of a  $\beta$ -mannosidic bond with a <sup>1</sup>J<sub>CH</sub> coupling constant of 156.2 Hz.



Scheme 5-12. Formation of glycoside **5.23** from protected 1,3-mannose donor **2.2** and propan-2-ol using Crich and co-workers pre-activation conditions

## Use of chemical synthesis for the construction of $\beta$ -mannosides

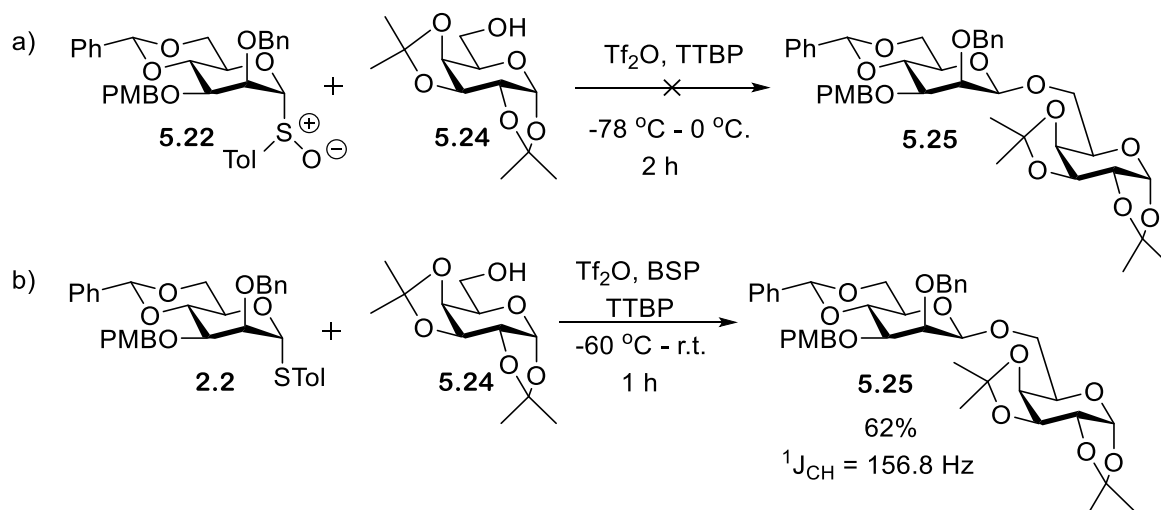
The other methods trialled included Bols and co-worker's direct activation and pre-activation methods.<sup>84</sup> No reaction occurred when Bols' direct activation methodology was trialled, with only starting material extracted. Bols' pre-activation methodology was successful affording a 40% yield of mannose glycoside **5.23** (Scheme 5-13).  $\beta$ -Stereoselectivity was confirmed via NMR spectroscopy using a proton coupled carbon spectra with a  $^1J_{\text{CH}}$  coupling constant of 154.1 Hz being measured. Although this coupling constant is slightly lower than that previously measured, I believe that this degree of error can be expected when using the manual measurement tool for coupling constants in the NMR analysis software Topspin 4.0.6.



Scheme 5-13. Formation of glycoside **5.23** from benzylidene acetal sulfoxide donor **5.22** and propan-1-ol using Bols and co-workers pre-activation conditions

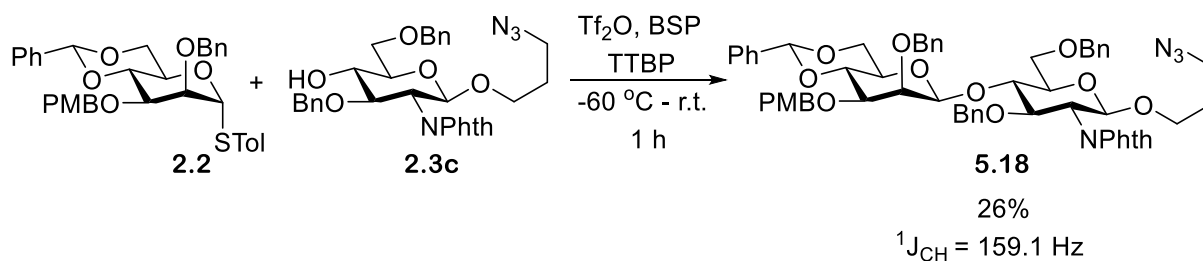
Due to the successful deployment of Crich and co-worker's and Bols and co-worker's pre-activation methodologies with propan-2-ol, it was decided to further test both these methods<sup>84, 85</sup> on another acceptor which better reflected the steric demands of GlcNPhth acceptor **2.3c**. 1,2,3,4-Di-*O*-isopropylidene- $\alpha$ -D-galactopyranose **5.24** was chosen due to its availability and low cost. Glycosylation of benzylidene acetal sulfoxide donor **5.22** to 1,2,3,4-di-*O*-isopropylidene- $\alpha$ -D-galactopyranose **5.24** using Bols and co-workers conditions was unsuccessful (Scheme 5-14a), with only hydrolysis of benzylidene acetal sulfoxide donor **5.22** being observed. However, pre-activation using Crich and co-workers conditions with benzylidene acetal donor **2.2** was successful, affording disaccharide **5.25** in a 62% yield, and NMR analysis suggested  $\beta$ -mannoside formation had occurred as a  $^1J_{\text{CH}}$  coupling constant of 156.8 Hz was recorded (Scheme 5-14b).

## Use of chemical synthesis for the construction of $\beta$ -mannosides



Scheme 5-14. Formation of disaccharide **5.25** from protected 1,3-mannose donor **5.22** or **2.2** and 1,2,3,4-di-O-isopropylidene- $\alpha$ -D-galactopyranose **5.24** using a) Bols and co-workers unsuccessful direct activation conditions and b) Crich and co-workers successful pre-activation conditions

Following the success of Crich and co-workers pre-activation conditions in both trial reactions, it was decided to further investigate the reaction scope by attempting a glycosylation of benzylidene acetal donor **2.2** to GlcNPhth acceptor **2.3c**.<sup>85</sup> Mass spectrometry and NMR analysis confirmed the formation of desired disaccharide **5.18** in an unoptimized 26% yield, with a  $^1J_{CH}$  coupling constant of 159.1 Hz confirming the formation of a  $\beta$ -mannosidic bond (Scheme 5-15).



Scheme 5-15. Formation of disaccharide **5.18** from protected 1,3-mannose donor **2.2** and protected 1,4-glucosamine acceptor **2.3c** using Crich and co-workers pre-activation conditions

### 5.3.2 Further investigations into the synthesis of protected trisaccharide **5.19**

Due to the requirement for an  $\alpha$ -mannosidic bond between 1,2-mannose donor **2.1b** and 1,3-mannose donor **2.2** in protected trisaccharide **5.19** (Figure 5-5). It was initially decided not to use a pre-activation glycosylation procedure for the final  $\alpha$ -selective glycosylation and to instead trial direct activation with NIS and TMSOTf.

Use of chemical synthesis for the construction of  $\beta$ -mannosides

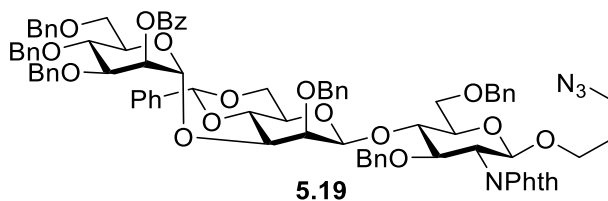
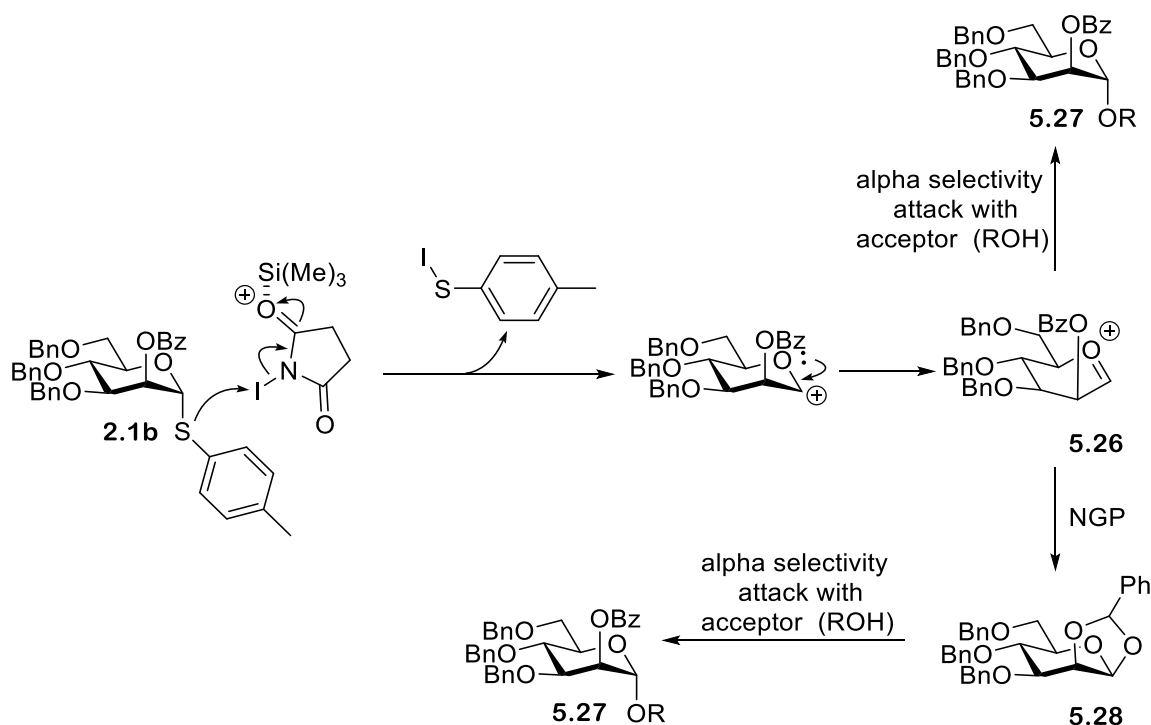


Figure 5-5. Structure of protected trisaccharide **5.19**

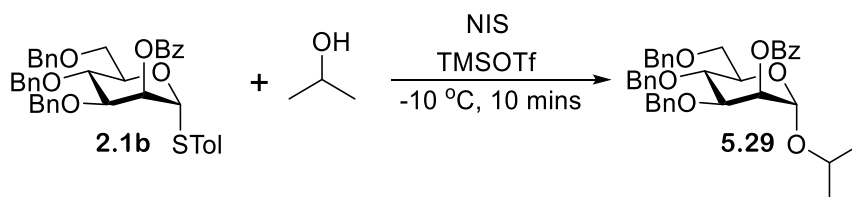
The major advantage of this methodology change is that glycosylation with NIS and TMSOTf does not require the formation of an unstable  $\alpha$ -triflate, with the mechanism instead thought to proceed by one of two pathways (Scheme 5-16). Both pathways follow the initial generation of an oxacarbenium ion **5.26**, which can either undergo direct attack at the anomeric position by a glycosyl acceptor to form mannoside **5.27**, or can be stabilised by neighbouring group participation (NGP) to form an intermediate ortho-ester containing mannoside **5.28**, which can subsequently undergo attack at the anomeric position by a glycosyl acceptor to form mannoside **5.27**. Both of these pathways induce retention at the anomeric stereocentre, generating an  $\alpha$ -mannosidic bond.



Scheme 5-16. Potential pathways by which NIS and TMSOTf mediated glycosylation occur to give glycoside **5.27** with complete  $\alpha$ -selective

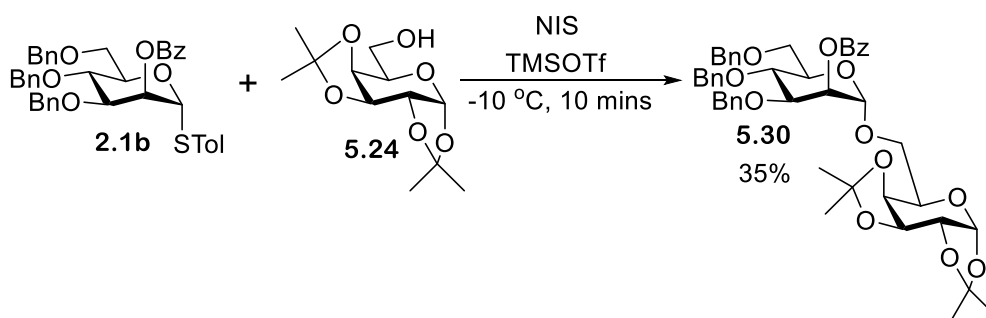
A NIS and TMSOTf mediated glycosylation was performed on 1,2-mannose donor **2.1b** using propan-2-ol as the glycosyl acceptor. The glycosylation was successful, however, purification was very challenging meaning  $\alpha$ -mannoside **5.29** was isolated in a crude mixture (Scheme 5-17). Specific

identification of undesired side-products within the crude mixture was not attempted, but conceptually formation of an orthoester would also have been possible under these reactions conditions.



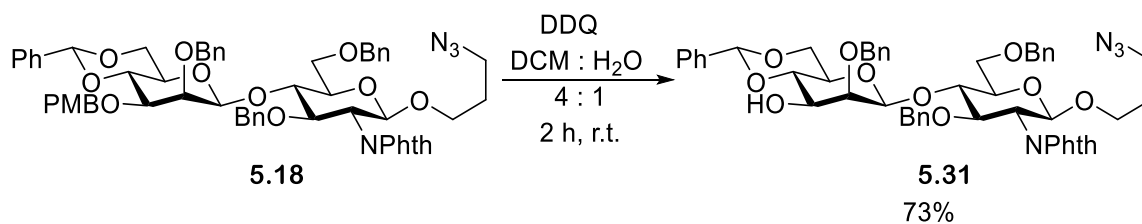
Scheme 5-17. Formation of glycoside **5.29** via an NIS and TMSOTf mediated glycosylation of protected 1,2-mannose donor **2.1b** and propan-2-ol

Following the successful synthesis of  $\alpha$ -mannoside **5.29**, a second trial reaction was performed using 1,2,3,4-di-*O*-isopropylidene- $\alpha$ -D-galactopyranose **5.24** as an acceptor. This glycosylation was also successful, with the presence of  $\alpha$ -mannoside **5.30** being confirmed by both mass spectrometry and NMR analysis (Scheme 5-18). It should be noted that glycosylation with 1,2,3,4-di-*O*-isopropylidene- $\alpha$ -D-galactopyranose **5.24** proceeded in a 35% yield.



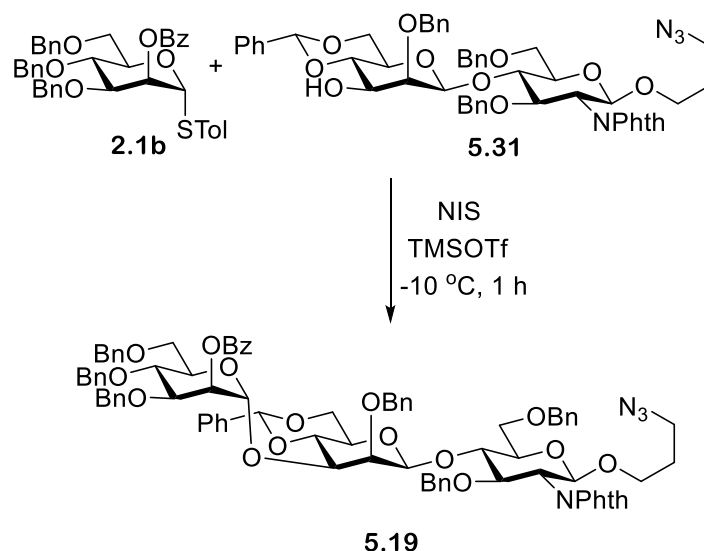
Scheme 5-18. Formation of disaccharide **5.30** via an NIS and TMSOTf mediated glycosylation of protected 1,2-mannose donor **2.1b** and 1,2,3,4 diisopropylidene galactose **5.24**

After the success of the two trial reactions, it was decided to trial the use of NIS and TMSOTf glycosylation conditions to the glycosylation of 1,2-mannose donor **2.1b** to protected disaccharide **5.18**. Before performing this trial reaction, disaccharide **5.18** underwent DDQ mediated oxidation affording disaccharide **5.31** in a 73% yield, this removed the PMB protecting group to reveal a free *O*-3 position (Scheme 5-19).



Scheme 5-19. Oxidation of disaccharide **5.18** using DDQ to give disaccharide **5.31**

Upon PMB removal, NIS and TMSOTf mediated glycosylation of 1,2-mannose donor **2.1b** to disaccharide **5.31** was performed. Mass spectrometry analysis confirmed the formation of trisaccharide **5.19** (Scheme 5-20), yet due to the reaction scale and low reaction yield of  $\leq 21\%$  purification was extremely challenging and unfortunately a clean NMR of trisaccharide **5.19** could not be obtained.



Scheme 5-20. Formation of protected trisaccharide **5.19** via an NIS and TMSOTf mediated glycosylation of protected 1,2-mannose donor **2.1b** with disaccharide **5.31**

### 5.3.3 Optimisation of the final $\alpha$ -mannoside glycosylation in trisaccharide **1.4**

The low yield observed in the  $\alpha$ -mannoside glycosylation was unexpected, as it had been presumed that due to  $\alpha$ -mannoside formation being both kinetically and thermodynamically favoured the reaction would proceed in a relatively high yield. For trisaccharide **5.19** to remain a valid target this final glycosylation needed to achieve a significantly higher yield, as other synthetic stages (i.e.  $\beta$ -mannoside formation and benzylidene acetal ring opening of 1,4-GlcNPhth acceptor **2.47**) were already severely limiting the amount of protected disaccharide **5.18** that could be obtained. It was thus decided to investigate different factors which might help to improve the glycosylation yield (e.g. the choice of protecting groups present on the donor and the glycosylation methodology). Due to the high value of protected disaccharide **5.18** a substitute acceptor was used during these trial reactions, with readily available 1,2,3,4-diisopropylidene galactose **5.24** initially being chosen.

The results of the different trial reactions are displayed in Tables 1, 2 and 3. The results achieved with *O*-2 benzoyl mannose donor **2.1b** (Figure 5-6) and 1,2,3,4-diisopropylidene galactose

**5.24** using direct activation with NIS and TMSOTf (Table 11, Entry 1) were treated as a standard to which other trial glycosylation yields could be compared. As none of the mannose donors investigated contained *O*-4, *O*-6-benzylidene acetal protection, all glycosylations proceeded with complete  $\alpha$ -stereoselectivity.

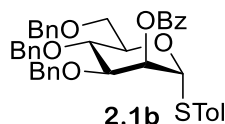


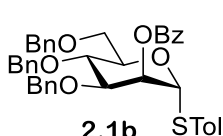
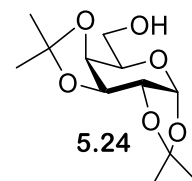
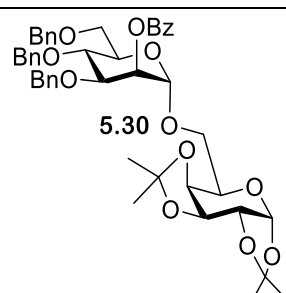
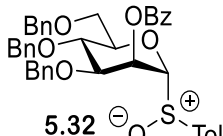
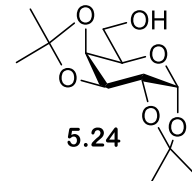
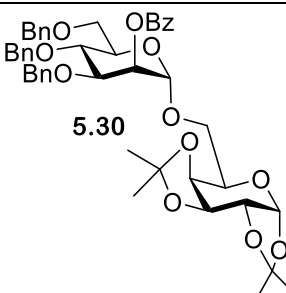
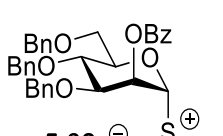
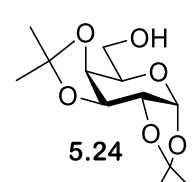
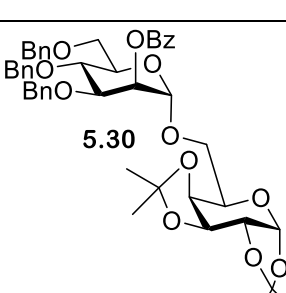
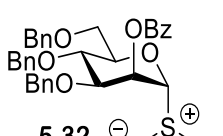
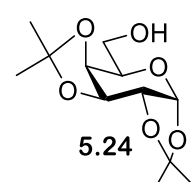
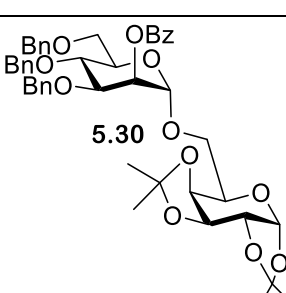
Figure 5-6. Structure of 1,2 benzoyl mannose donor **2.1b**

The first factor investigated was the glycosylation protocol: *e.g.* the order in which 1,2,3,4-diisopropylidene galactose **5.24** and Tf<sub>2</sub>O were added. Direct activation (Table 11 Entry 1, 35% yield) was initially substituted for pre-activation using Bols and co-worker's pre-activation with *O*-2 benzoyl mannose donor **5.32** (Table 11 Entry 2, 17% yield).<sup>84</sup> Though disaccharide **5.30** was successfully isolated Bols and co-worker's protocol achieved a significantly lower yield of only 17% compared to the standard reaction (Table 11 Entry 1, 35%). The final glycosylation protocol trialed involved direct activation with Tf<sub>2</sub>O and TTBP (Table 11 Entry 3, 35% yield). This protocol achieved a 35% yield, matching the yield achieved with the 1,2,3,4-diisopropylidene galactose standard. None of the protocols attempted achieved a greater glycosylation yield than the standard, and it was speculated that the desired disaccharide could have been lost or degraded during work-up. A second direct activation glycosylation with Tf<sub>2</sub>O and TTBP was performed, with the crude reaction mixture being directly loaded onto a silica column after reaction quenching (Table 11 Entry 4, 27% yield). This alteration seemingly had an adverse effect on the glycosylation yield, as the yield tabulated in Table 11 Entry 4 is lower than that of Table 11 Entry 3.



Use of chemical synthesis for the construction of  $\beta$ -mannosides

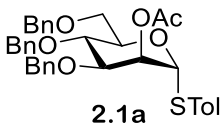
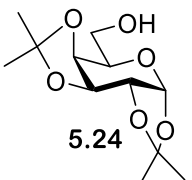
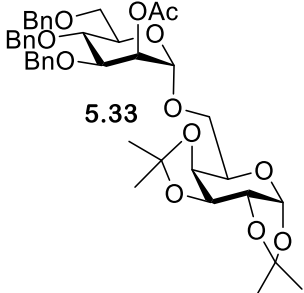
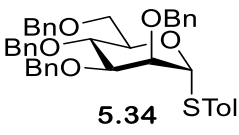
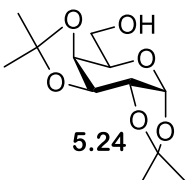
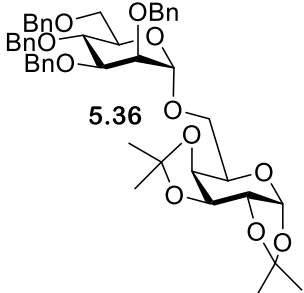
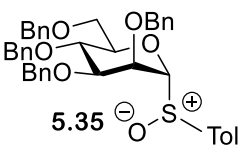
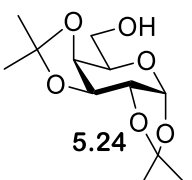
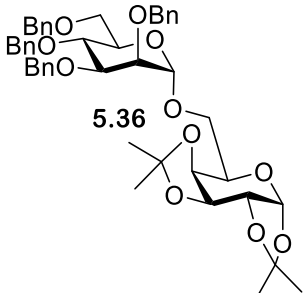
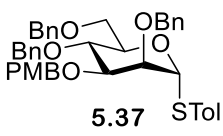
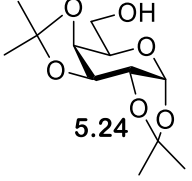
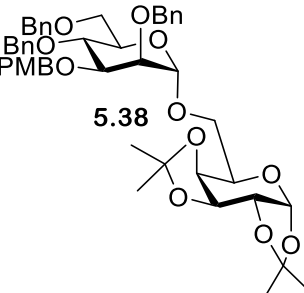
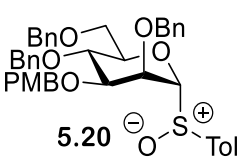
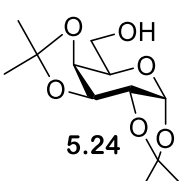
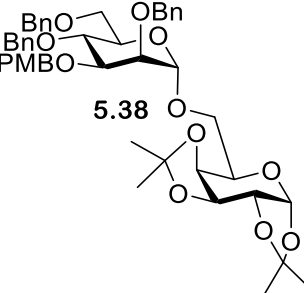
Table 11. The various glycosylation conditions trialed in the synthesis of the  $\alpha$ -linked disaccharide **5.30** and the results of these trial reactions.

Entry	Donor	Acceptor	Product	Method	Yield
1	 <p><b>2.1b</b> STol</p>	 <p><b>5.24</b></p>	 <p><b>5.30</b></p>	<p>NIS and TMSOTf</p> <p>Direct activation</p>	35%
2	 <p><b>5.32</b> <math>\ominus</math> O-S<math>^+</math> Tol</p>	 <p><b>5.24</b></p>	 <p><b>5.30</b></p>	<p>Tf<sub>2</sub>O, TTBP</p> <p>Pre- activation</p>	17%
3	 <p><b>5.32</b> <math>\ominus</math> O-S<math>^+</math> Tol</p>	 <p><b>5.24</b></p>	 <p><b>5.30</b></p>	<p>Tf<sub>2</sub>O, TTBP</p> <p>Direct activation</p>	35%
4	 <p><b>5.32</b> <math>\ominus</math> O-S<math>^+</math> Tol</p>	 <p><b>5.24</b></p>	 <p><b>5.30</b></p>	<p>Tf<sub>2</sub>O, TTBP</p> <p>Direct activation no work- up</p>	27%

The next glycosylation factor investigated was the protection strategy used on the 1,2-mannose donor, with the major focus being placed on what protecting group was present at *O*-2. Initially a benzoyl group was installed at the *O*-2 position of *O*-2 benzoyl mannose donor **2.1b** due to its electron-withdrawing nature and ability to undergo neighbouring group participation, thus increasing 1,2-trans-selectivity.<sup>350</sup> The replacement of the *O*-2 benzoyl group with an acetyl group allowed investigation into whether the steric demands of the benzoyl group effected glycosylation yield. Glycosylation with *O*-2 acetyl mannose donor **2.1a** was performed using NIS and TMSOTf (Table 12 Entry 1, 39% yield of  $\alpha$ -disaccharide **5.33**). The glycosylation was successful, yet did not achieve a significantly higher glycosylation yield than previously observed. It was therefore decided to investigate the effect of an electron donating group at *O*-2 on glycosylation yields. Glycosylation with *O*-2 benzyl protected mannose donor **5.34** and *O*-2 benzyl protected sulfoxide mannose donor **5.35** was performed using direct activation with NIS and TMSOTf (Table 12 Entry 2, 13% yield of  $\alpha$ -disaccharide **5.36**) and direct activation with Tf<sub>2</sub>O and TTBP (Table 12 Entry 3, 27% yield of  $\alpha$ -disaccharide **5.36**). Neither trial glycosylation afforded a yield of disaccharide greater than in Table 11 Entry 1 (35% yield). Finally, the effects of *O*-3 protection were investigated; *O*-3 PMB protected mannose donor **5.37** and *O*-3 PMB protected sulfoxide mannose donor **5.20**, previously used in  $\beta$ -mannoside trials, were subjected to glycosylation using direct activation with NIS and TMSOTf (Table 12 Entry 4, 37% yield of  $\alpha$ -disaccharide **5.38**) and direct activation with Tf<sub>2</sub>O and TTBP (Table 12 Entry 5). Direct activation with NIS and TMSOTf (Table 12 Entry 4) achieved a comparable yield to Table 11 Entry 1, (37% vs 35%), whilst direct activation with Tf<sub>2</sub>O and TTBP failed, with only hydrolysed and methylated donor being isolated.

Use of chemical synthesis for the construction of  $\beta$ -mannosides

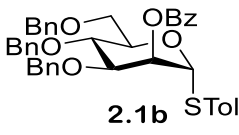
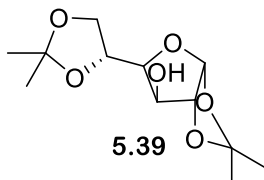
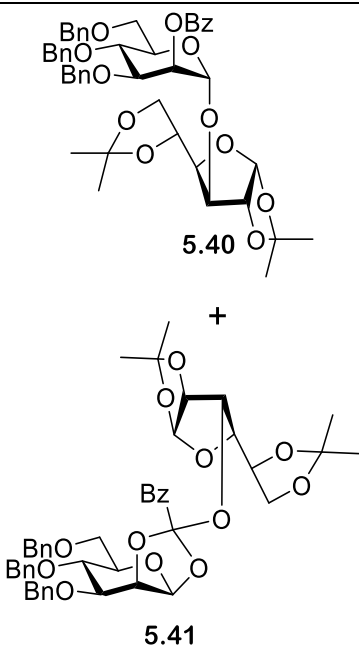
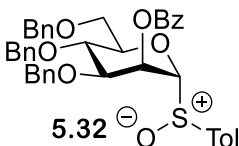
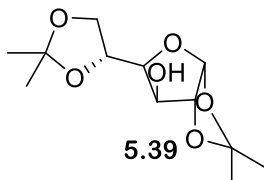
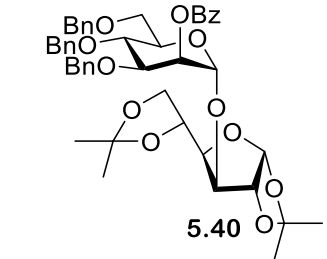
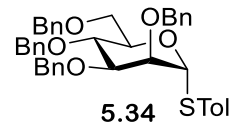
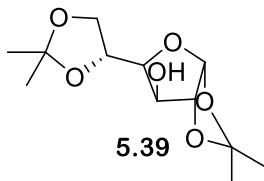
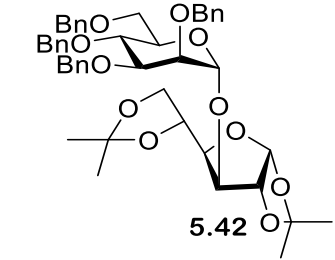
Table 12. The results of the various trial glycosylation performed to investigate the effects of donor protection on glycosylation yield.

Entry	Donor	Acceptor	Product	Method	Yield
1	 <p>2.1a STol</p>	 <p>5.24</p>	 <p>5.33</p>	NIS, TMSOTf  Direct activation	39%
2	 <p>5.34 STol</p>	 <p>5.24</p>	 <p>5.36</p>	NIS, TMSOTf  Direct activation	13%
3	 <p>5.35 <math>\ominus</math>-S<math>\oplus</math>-Tol</p>	 <p>5.24</p>	 <p>5.36</p>	Tf <sub>2</sub> O, TTBP  Direct activation	27%
4	 <p>5.37 STol</p>	 <p>5.24</p>	 <p>5.38</p>	NIS, TMSOTf  Direct activation	37%
5	 <p>5.20 <math>\ominus</math>-S<math>\oplus</math>-Tol</p>	 <p>5.24</p>	 <p>5.38</p>	Tf <sub>2</sub> O, TTBP  Direct activation	N/A

Due to none of the previous trials achieving a significantly greater glycosylation yield than that of the 1,2,3,4-diisopropylidene galactose standard established in Entry 1 of Table 11, it was decided to substitute the one factor all the trials had in common: the use of 1,2,3,4-diisopropylidene galactose **5.24** as an acceptor. 1,2,3,4-Diisopropylidene galactose **5.24** was substituted for 1,2:5,6-di-*O*-isopropylidene- $\alpha$ -D-glucofuranose **5.39**, and three trial reactions were performed. The first two trials used *O*-2 benzoyl protected mannose donor **2.1b** and *O*-2 benzoyl protected sulfoxide mannose donor **5.32**, undergoing direct activation with NIS and TMSOTf (Table 13, Entry 1, 25% yield of  $\alpha$ -disaccharide **5.40**) and direct activation with Tf<sub>2</sub>O and TTBP (Table 13, Entry 2, 33% yield of  $\alpha$ -disaccharide **5.40**). Initial results suggested that acceptor replacement led to an increase in yield, with both Table 13 Entry 1 and 2 reporting increased yields of disaccharide **5.40** (achieving yields of 40% and 33% respectively). However, upon NMR examination of Table 13 Entry 2, two products were identified: the desired disaccharide **5.40** and a suspected putative orthoester **5.41** in a 1 : 0.6 ratio. Both the desired disaccharide **5.40** and the suspected putative orthoester **5.41** have the same R<sub>f</sub> value and relative molecular mass, meaning that the two products can only be distinguished upon NMR analysis. Kong and co-workers reported that orthoesters could be converted to the desired disaccharide by addition of TMSOTf.<sup>351</sup> A trial reaction using these conditions was performed, yet no orthoester rearrangement was observed, with the integral ratio between disaccharide **5.40** and suspected putative orthoester **5.41** remaining 1 : 0.6. NMR examination of Entry 2 showed only one major product - disaccharide **5.40**. Some extra peaks were present on the NMR which were suggestive of the presence of a small amount of orthoester **5.41**, but none of these peaks were intense enough for unequivocal confirmation. A final trial was performed with *O*-2 benzyl protected donor **5.34**, which underwent direct activation with NIS and TMSOTf (Table 13, Entry 3, 18% yield). *O*-2 benzyl protection prevents neighbouring group participation meaning no orthoester formation could occur, and the desired disaccharide **5.42** was isolated in a 17% yield. These results highlight that the use of 1,2,3,4-diisopropylidene galactose as an acceptor was not the root cause of the low reaction yields observed.

Use of chemical synthesis for the construction of  $\beta$ -mannosides

Table 13. The results of the various trial glycosylation performed using 1,2:5,6-di-O-isopropylidene- $\alpha$ -D-glucofuranose **5.39** as the acceptor.

Entry	Donor	Acceptor	Product	Method	Yield
1	 <p><b>2.1b</b> STol</p>	 <p><b>5.39</b></p>	 <p><b>5.40</b></p> <p>+</p> <p><b>5.41</b></p>	<p>NIS, TMSOTf</p> <p>Direct activation</p>	<p>Product formation: 25%</p> <p>Orthoester formation: 15%</p>
2	 <p><b>5.32</b> <math>\ominus</math>-S<math>\oplus</math>-Tol</p>	 <p><b>5.39</b></p>	 <p><b>5.40</b></p>	<p>Tf<sub>2</sub>O, TTBP</p> <p>Direct activation</p>	33%
3	 <p><b>5.34</b> STol</p>	 <p><b>5.39</b></p>	 <p><b>5.42</b></p>	<p>NIS, TMSOTf</p> <p>Direct activation</p>	18%

With all different glycosylation variables (donor, acceptor and protocol) investigated and none of the changes resulting in a significant glycosylation yield increase, it was decided to move on from optimising the model system. One interesting observation is that a consistent side-product was not extracted from any of the trial reactions, though sometimes small amounts of hydrolysed or methylated donor were observed by mass spectrometry. This poses a question: What happens to the unreacted donor and acceptor? One potential suggestion is that the reactions were higher yielding than the glycosylation yields would suggest, but that the loss of compound during purification (e.g. work-up and column chromatography) had a large effect on the reported percentage yield – this is a particularly significant consideration when performing the reactions on such a small scale. This hypothesis cannot be definitively confirmed as increasing the reaction scale would likely result in increased donor hydrolysis.

The failure to improve the final  $\alpha$ -glycosylation yield was hugely disappointing, as such a low synthetic yield so late in the synthesis pathway would make obtaining a significant amount of protected trisaccharide **5.19** extremely challenging. This, coupled with the large mass loss which would accompany deprotection, led to trisaccharide **1.4** being dropped as a synthetic target, as the time required to obtain enough trisaccharide **1.4** to synthesise any colicin-linked conjugates was outside our timescale.

#### 5.4 Summary and conclusions

The work performed in this chapter allowed for the successful synthesis of protected disaccharide **5.18**, although the reaction yield was lower than hoped at 26%. Yield optimisation was not performed as it was decided to firstly establish whether the rest of the synthetic pathway to afford protected trisaccharide **5.19** could be performed before investing a significant amount of time into yield optimisation.

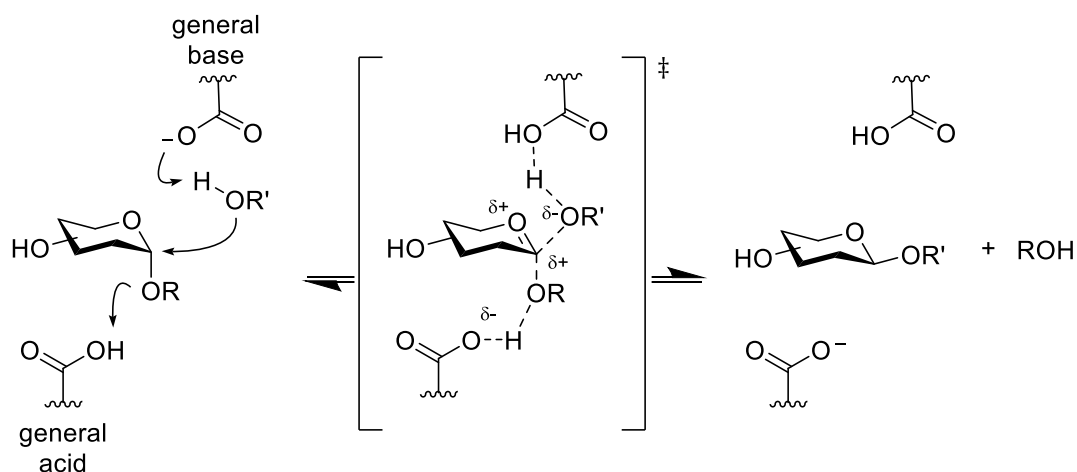
The synthesis of protected trisaccharide **5.19** was confirmed by mass spectrometry analysis. Unfortunately, not enough protected trisaccharide **5.19** could be extracted to obtain characterisation via NMR spectroscopy. This was because the final  $\alpha$ -glycosylation performed achieved an unexpectedly low yield, which called the future of trisaccharide **1.4** as a target into question. A large body of work was conducted investigating different glycosylation conditions in order to optimise the final glycosylation yield, yet unfortunately conditions which achieved a significantly higher yield than that obtained using the standard conditions (Table 11, Entry 1) were not found. With the low yields obtained in both the  $\beta$ - and  $\alpha$ - glycosylation reactions, and the low yields obtained in other synthetic steps, it was decided that trisaccharide **1.4** was not a viable synthetic target with respect to our time constraints.

## Chapter 6 Use of enzymatic synthesis for the construction of $\beta$ -mannosides

### 6.1 Introduction into enzymatic methods for $\beta$ -mannoside synthesis

There are several types of carbohydrate-active enzymes (CAZymes) which can be used for glycosylations,<sup>352-354</sup> some common ones are glycosyl hydrolases (GH), glycosyl transferases (GT), glycoside phosphorylases (GP) and transglycosidases (TG).

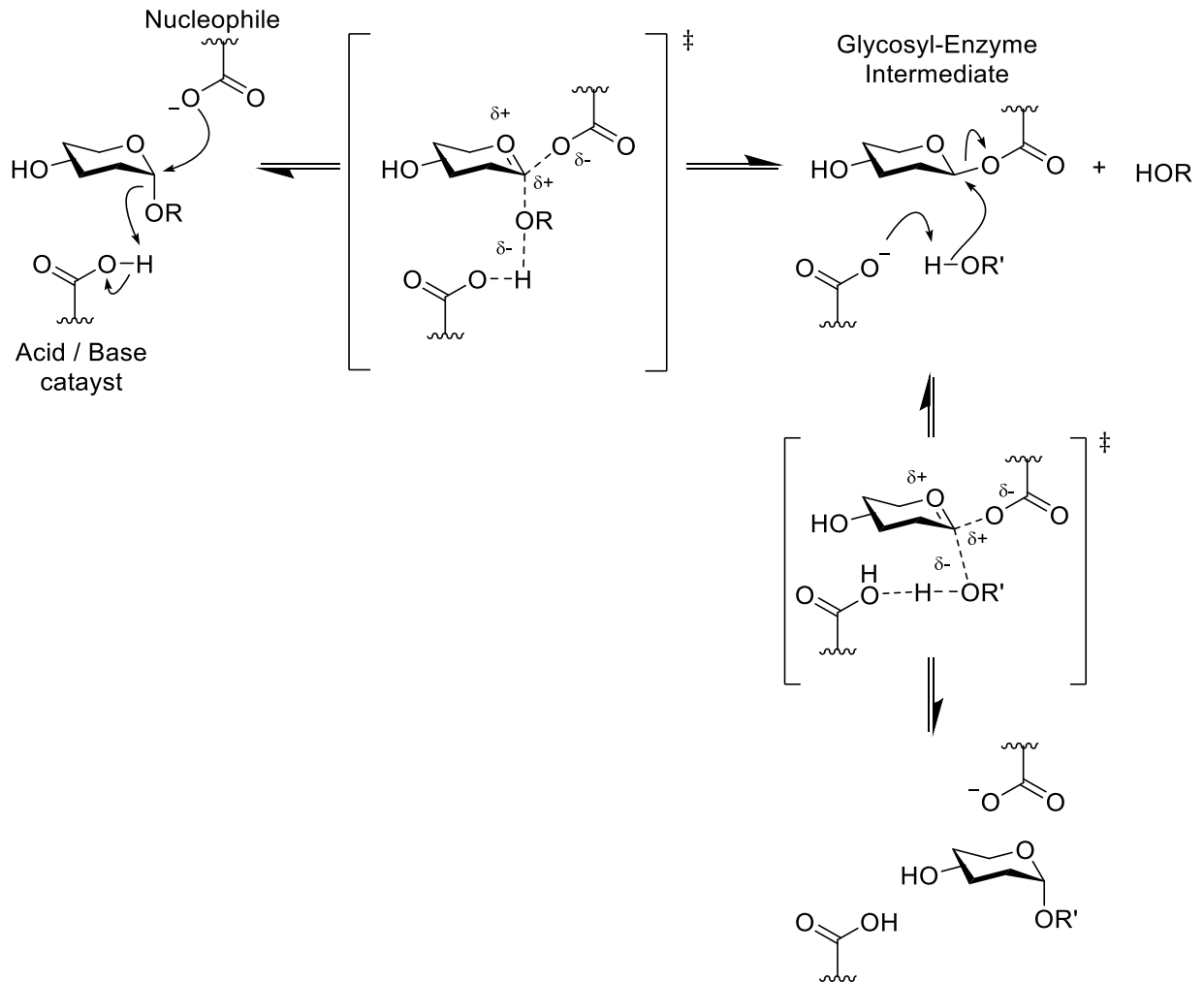
Hydrolysis of a glycosidic bond by GHs can result in either inversion or retention of stereochemistry at the anomeric position, dependant on the reaction mechanism followed. GHs which induce inversion of stereochemistry use a direct displacement mechanism in an  $S_N2$ -like reaction (Scheme 6-1).<sup>353</sup> The mechanism is reliant on the enzyme active site containing a pair of carboxyl groups located approximately 7-11 Å apart. One of these carboxyl groups functions as a general acid, protonating the glycosidic oxygen, while the second carboxyl group acts as a general base, activating incoming nucleophiles.<sup>353</sup> The mechanism proceeds via an oxocarbenium ion-like transition state.



*Scheme 6-1. Glycosylation mechanism of inverting GHs, proceeding by an  $S_N2$ -like reaction in which the base carboxyl group deprotonates a nucleophile ( $HOR'$ ), facilitating nucleophilic attack on the anomeric position. This attack results in the formation of an oxocarbenium ion-like transition state, which collapses to afford a glycoside with inverted stereochemistry to the substrate.<sup>353</sup>*

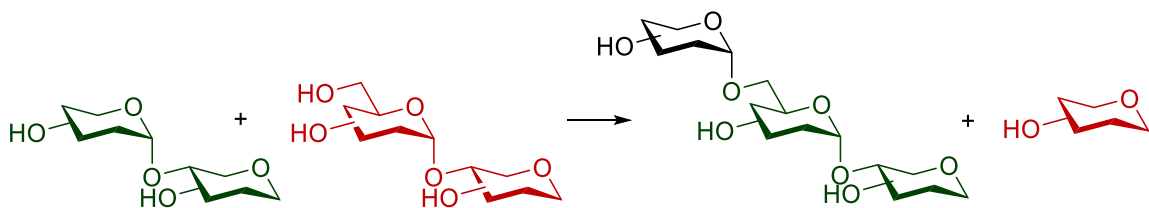
GHs which lead to a retention in stereochemistry proceed by a double-displacement reaction, via a covalently bound glycosyl-enzyme intermediate (Scheme 6-2).<sup>353, 355</sup> The presence of two active site carboxylate groups is likewise key to this mechanism. Interestingly, the distances between the carboxyl groups is smaller for retaining GHs compared to inverting GHs (5 Å vs 7-11 Å).<sup>353</sup> One carboxylate group functions as a general acid/base catalyst, while the other functions as a nucleophile, attacking the anomeric position of the glycoside forming a covalently bound glycosyl-enzyme intermediate.<sup>353</sup>

## Use of enzymatic synthesis for the construction of $\beta$ -mannosides



Scheme 6-2. Glycosylation mechanism of retaining GHs, proceeding via a double displacement mechanism with initial displacement of a leaving group at the anomeric position (OR) by the carboxylate group acting as a nucleophile. This attack induces an oxocarbenium ion-like transition state which results in the formation of glycosyl-enzyme intermediate. The second carboxylate group (acid/base catalyst) catalyses the second displacement reaction by deprotonating an incoming nucleophile (HOR'), stimulating the nucleophile to attack the anomeric position. This induces the formation of a second oxocarbenium ion-like transition state which results in formation of a glycoside which has retained stereochemistry<sup>353</sup>

Transglycosidases (TG) are classified amongst GH families; they have similar structures to many GHs and function via similar mechanistic strategies (Scheme 6-3).<sup>353</sup> The major difference between GHs and TGs is that TGs catalyse the hydrolysis of glycosidic linkages between sugars and transfer the aglycone moiety to a nucleophile hydroxyl on another sugar.<sup>353</sup>

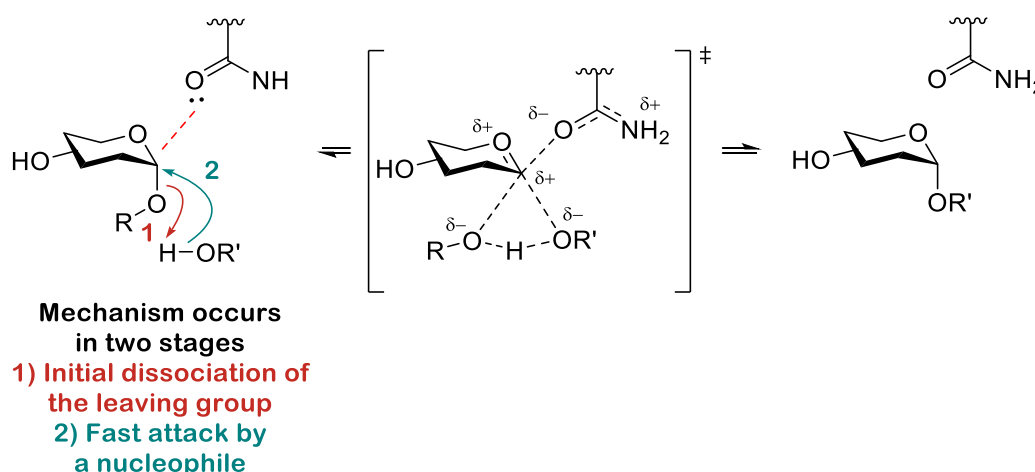


Scheme 6-3. Example schematic of a potential transglycosidase catalysed reaction



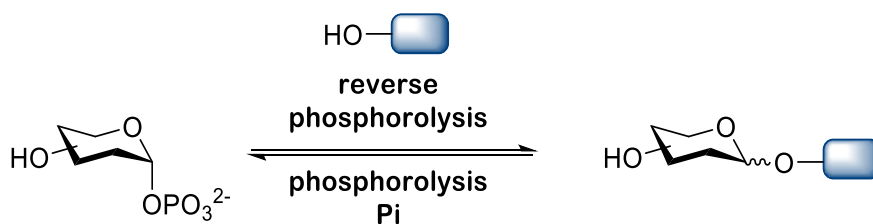
## Use of enzymatic synthesis for the construction of $\beta$ -mannosides

A further class of CAZymes are glycosyltransferases (GTs). These are enzymes which catalyse the transfer of sugar moieties from activated donor substrates to an acceptor, generating glycosidic linkages.<sup>353</sup> Reactions catalysed by GTs can result in either retention or inversion of stereochemistry,<sup>353</sup> with the mechanisms inducing inversion being believed to be very similar to those used by GHs.<sup>353</sup> Characterising the mechanism via which GTs induce stereochemical retention has proved challenging<sup>353</sup> and remains a highly debated topic.<sup>356</sup> Initially a double displacement mechanism was proposed, and while there is some evidence to suggest that some GTs families proceed via this mechanism<sup>356, 357</sup> accumulating enough evidence to solidify this theory for all GTs has proved challenging.<sup>353, 356</sup> This has led to the proposal of an  $S_Ni$ -like mechanism (Scheme 6-4) which occurs via initial dissociation of the leaving group quickly followed by attack of a nucleophile. This means the reaction has a single transition state in which the incoming nucleophile of the acceptor attacks the same face from which the leaving group departs.<sup>353</sup>



Scheme 6-4. Schematic of the  $S_Ni$ -like mechanism occurring via attack of the nucleophilic acceptor component at the same face as the leaving group, stimulating the formation of transition state, subsequently affording a glycoside<sup>356</sup> R= nucleophile mono or diphosphate

Glycoside phosphorylases (GPs) exploit the easy accessibility and relative stability of sugar-1-phosphates,<sup>358</sup> either through reversible phosphorolysis wherein sugar-1-phosphate donors can react with glycosyl acceptors in glycosidic bond forming reactions, or alternatively through phosphorolysis of oligosaccharides where in phosphate acts as a nucleophile to cleave the glycosidic linkage (Scheme 6-5).<sup>353</sup> Phosphorylases either show structural and mechanistic similarities with GHs or GTs,<sup>353</sup> inducing either stereochemical inversion or retention depending on which family they belong to.<sup>358</sup>



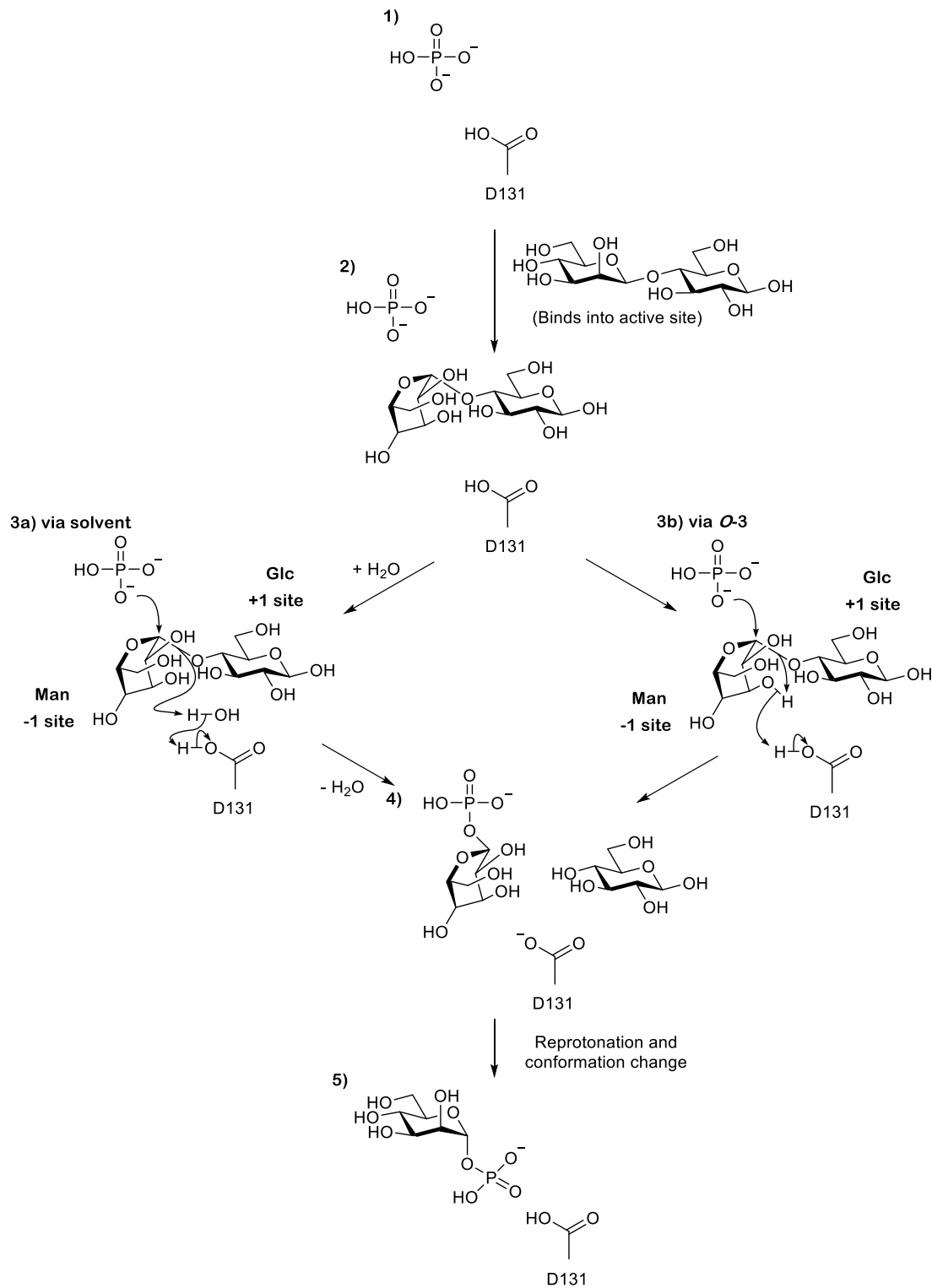
Scheme 6-5. Example schematic for a phosphorylase mediated reaction, catalysing either the polymerisation of a sugar-1-phosphate to an acceptor (e.g. oligosacchride unit, monosaccharide sugar unit or aglycon unit) or phosphorolysis of a glycoside bond to afford a sugar-1-phosphate and an acceptor unit

Specific GPs have been found for many different glycosides,<sup>358</sup> here we will focus in on  $\beta$ -1,4-D-mannosyl-*N*-acetyl-D-glucosamine phosphorylase (BT-1033), as its ability to turn over D-Man- $\beta$ -1,4-D-GlcNAc is of particular interest to this project.

BT-1033 is a GH130 phosphorylase found in the human gut microbe *Bacteroides thetaiotaomicron*, and was first reported by Nakai and co-workers<sup>359</sup> in 2013 and was proposed to catalyse the reversible phosphorolysis of D-Man- $\beta$ -1,4-D-GlcNAc.<sup>359</sup>

The sequence of BT-1033 has been analysed and compared to other GH-130 phosphorylases, with the results suggesting that residue Asp101 likely functions as the general acid/base.<sup>360</sup> Though little direct investigation into the mechanism of BT-1033 has been performed to date, there is a suggestion that the reaction mechanism of BT-1033 may be more complicated. The mechanism of 4-*O*- $\beta$ -D-mannosyl-D-glucose Phosphorylase (MGP), another GH130 phosphorylase, has been investigated and shown to be more complex than first thought.<sup>361</sup> Residue Asp131 in MGP had been hypothesized to function as a general acid/base, yet upon investigation it was revealed that the Asp131 residue was not close enough to the Glc-O4 atom to act as a direct proton source.<sup>361</sup> Though the exact mechanism by which MGP catalyses phosphorylation is still unclear, two alternative mechanisms have been proposed (Scheme 6-6).<sup>361</sup> The first proposes that a solvent molecule mediates protonation of the glycosidic bond (Scheme 6-6, pathway a) whereas, the second proposes a two-step protonation via the 3-OH of the mannose residue (Scheme 6-6, pathway b).<sup>361</sup>

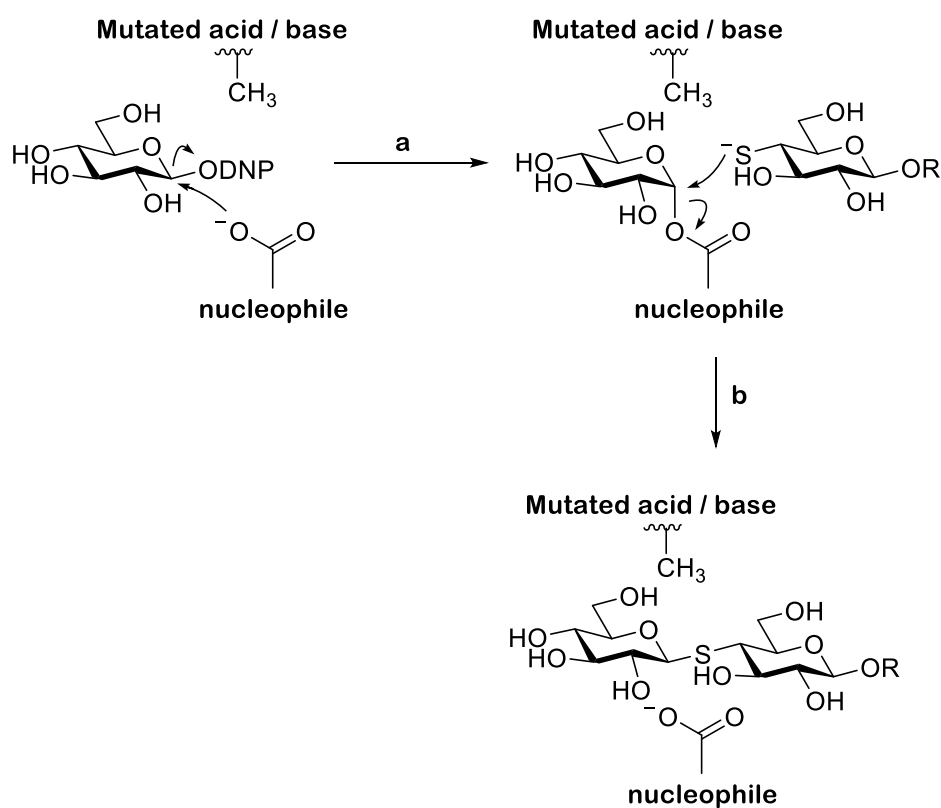
Use of enzymatic synthesis for the construction of  $\beta$ -mannosides



Scheme 6-6. Proposed mechanistic pathway of MGP

Glycosynthases are nucleophile mutants of retaining glycosidases that efficiently catalyse the synthesis of glycosidic bonds between activated fluoride donors and suitable acceptor sugars.<sup>362</sup> Mutation of the catalytic nucleophile renders glycosynthases void of hydrolytic activity.<sup>362, 363</sup>

In 2003 Withers and co-workers introduced thioglycoligases; these novel enzymes catalyse the synthesis of *S*-glycosidic linkages in oligosaccharides.<sup>364</sup> Thioglycosides are interesting non-hydrolysable sugar substitutes.<sup>365</sup> As explained above, the mechanism of retaining GHs is comprised of two steps (Scheme 6-7) and relies on two carboxylate residues within the active site; a catalytic nucleophile and a catalytic acid/base.<sup>366</sup> Withers and co-workers mutated retaining glycosidases so that they lacked the catalytic acid/base residue.<sup>366</sup> As both reaction steps are either acid or base catalysed, removal of the catalytic acid/base residue results in a significant rate reduction on both reaction stages.<sup>364</sup> However, these low reaction rates can be improved by using a donor with a good leaving group and an acceptor containing a strong nucleophile.<sup>364, 366</sup> If a donor possesses a good leaving group (e.g. dinitrophenyl, DNP) this will bypass the need for acid catalysis during the initial glycosylation step.<sup>364</sup> Furthermore, unlike many oxygen acceptors, strong nucleophiles such as thiol groups do not require base catalysis, and thus can attack the glycosyl-enzyme intermediate affording a thioglycoside.<sup>364</sup>



*Scheme 6-7. Schematic of the proposed mechanism of thioglycoligases with initial glycosylation of the donor to the nucleophilic residue (step a) followed by attack of the thiol containing acceptor. Here OR can represent a multitude of motifs, such as a protecting group (i.e. OPNP or OMe) or the continuation of the oligosaccharide chain*

## 6.2 Section aims

The work discussed in this chapter aims to explore the use of enzymatic methods for the synthesis of  $\beta$ -1,4-D-mannosyl-N-acetyl-D-glucosamine. The purpose of this investigation is to determine whether enzymatic methodologies offer a more consistent and high yielding alternative to the chemical synthesis pathways previously explored in Chapters 1 and 5. Furthermore, the substrate promiscuity of BT-1033 as a reverse phosphorylase will be investigated using a variety of unnatural glucosamine analogues and mannose-1-phosphate analogues. To do this an accurate protocol for measuring enzymatic conversion will need to be established. Finally, the potential of BT-1033 to function as a reverse phosphoro-thioligase will be investigated.

## 6.3 Results and Discussion

### 6.3.1 Result of screening BT-1033 in reverse phosphorolysis with unnatural GlcNAc acceptors and mannose-1-phosphates

BT-1033 was expressed and purified, following the methodology of Nakai and co-workers,<sup>359</sup> please see experimental section 8.6.1, page 336 and appendix section 9.5.1, page cxcviii for supporting data.

All the trial enzymatic reactions in this section were performed in 40 mM NaOAc, pH 5.5 buffer, supplemented with 15 mM MgCl<sub>2</sub> and all samples were incubated at 37 °C. Details regarding reaction scale, starting donor and acceptor concentration, starting and final BT-1033 concentrations and incubation time for each reaction can be found in tables 1-10. Post reaction termination LCMS traces are attached in appendix section 9.5.2, page cci and appendix section 9.5.6, page ccxlvii.

The first reaction attempted using BT-1033 was performed using the enzymes natural substrates: mannose-1-phosphate and GlcNAc (Table 14, Entry 1). BT-1033 was added to the reaction mixture to a concentration of 0.1  $\mu$ g/ $\mu$ L. The reaction was left at 37 °C for 24 h, where after LCMS analysis was used to examine the reaction mixture. A peak was detected at m/z 384, which is indicative of the presence of the desired disaccharide (Table 14, Entry 1). However, the major peak observed was at m/z 222, suggesting GlcNAc remained the dominant sugar species present in the reaction solution.

After demonstrating that the expressed BT-1033 could turn over its natural substrate, the substrate promiscuity of BT-1033 was investigated. Firstly, we decided to investigate the promiscuity of BT-1033 against unnatural GlcNAc acceptors (Figure 6-1). These unnatural glucosamine acceptors were synthesised by members of the Linclau group (University of Southampton).

## Use of enzymatic synthesis for the construction of $\beta$ -mannosides

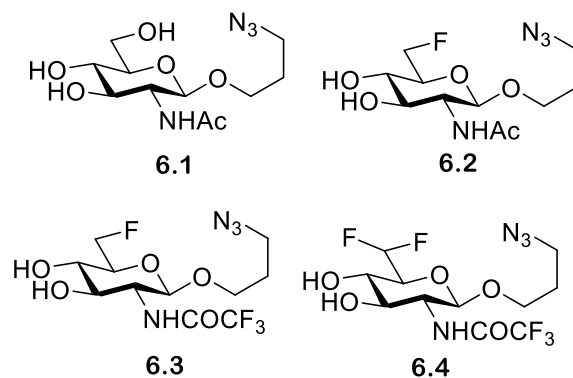


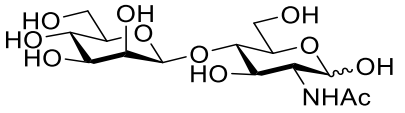
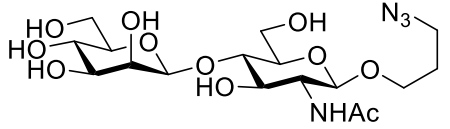
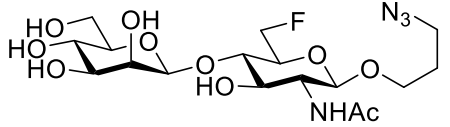
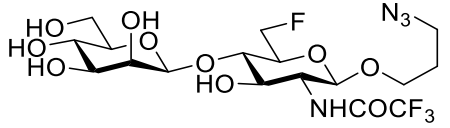
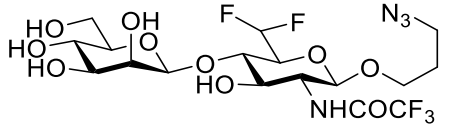
Figure 6-1. Structures of unnatural GlcNAc acceptors 6.1-6.4

The prospect of having a readily available azide handle on the disaccharide is attractive as it provides an easily accessible point for bio-conjugation. The first unnatural GlcNHAc acceptor investigated was unnatural GlcNAcN<sub>3</sub> acceptor **6.1**, the result of this trial reaction is shown in Table 14, Entry 2. LCMS analysis showed two distinct peaks on the liquid chromatogram, corresponding to the presence of GlcNAcN<sub>3</sub> **6.1** and the desired disaccharide (Table 14, Entry 2). Three further trial reactions were performed using fluorine containing unnatural GlcNAc acceptors **6.2**, **6.3** and **6.4** and mannose-1-phosphate as a donor (Table 14, Entries 3-5).

As summarized in Table 14 the results of the trial reactions suggest that BT-1033 successfully converted all four unnatural acceptors to some degree. However, the results of reaction Entries 4 and 5 using unnatural acceptors **6.3** and **6.4** produced some confusion. LCMS traces of both reactions displayed mass peaks corresponding to  $[M+NH_4]^+$  (at  $m/z$  540 for reaction Entry 4 and at  $m/z$  558 for reaction Entry 5, Table 14). However, neither LCMS trace displayed a peak corresponding to their respective acceptor's mass. Interestingly LCMS analysis of unnatural acceptors **6.3** and **6.4** also showed no mass peaks corresponding to the acceptor's mass. The LCMS traces of the unnatural acceptors did show peaks at  $m/z$  502 and 510 respectively, and these peaks were also seen in the LCMS traces of the respective BT-1033 catalysed reactions (Table 14, Entries 4 and 5). Unfortunately, no potential adduct pattern could be found to explain these peaks.

Use of enzymatic synthesis for the construction of  $\beta$ -mannosides

Table 14. BT-1033 reaction Entries 1-5; including starting reaction volume, starting donor and acceptor concentration, concentration of BT-1033, incubation time and whether LCMS suggested conversion had occurred

Reaction entry	Disaccharide product	Starting reaction scale ( $\mu$ L)	Starting donor concentration (mM)	Starting Acceptor concentration (mM)	BT-1033 concentration ( $\mu$ g/ $\mu$ L)	Incubation time (h)	Product observed in initial LCMS screening
1		30.6	250	250	0.094-0.073	24	Yes
2		30.6	250	250	0.094-0.073 to 0.18-0.14	24	Yes
3		30	85	85	0.096-0.074 to 0.188-0.145	26	Yes
4		30	250	250	0.096-0.074 to 0.188-0.145	26	?
5		30	250	250	0.096-0.074 to 0.188-0.145	26	?

## Use of enzymatic synthesis for the construction of $\beta$ -mannosides

After establishing that BT-1033 displayed catalytic activity against some unnatural GlcNAc analogues, particularly GlcNAcN<sub>3</sub> **6.1** the respective donor promiscuity was investigated further using this azide containing acceptor. The unnatural mannose-1-phosphate analogues trialled (Figure 6-2) were provided by the Miller group (University of Keele). The conditions used in the trial reactions are shown in Table 15.

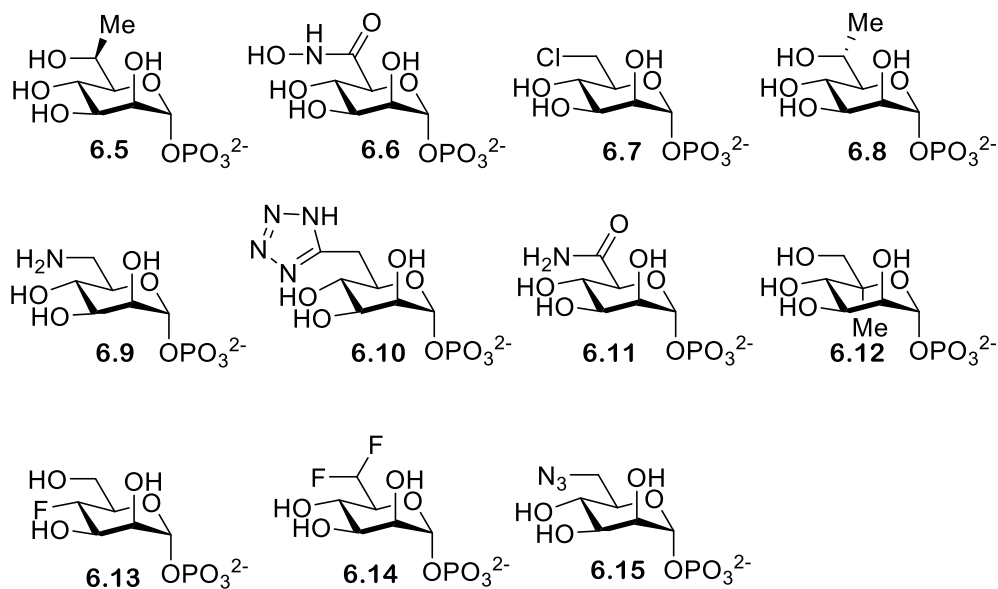
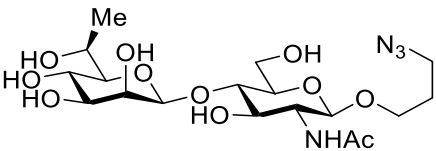
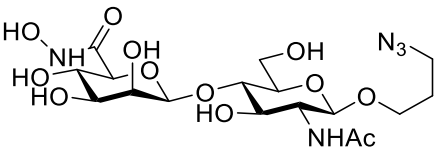
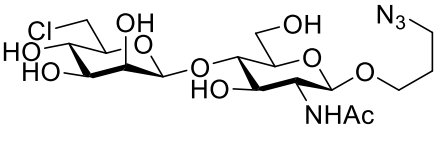
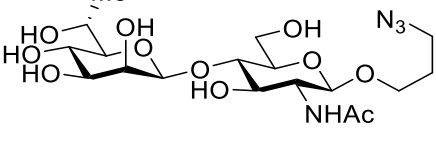
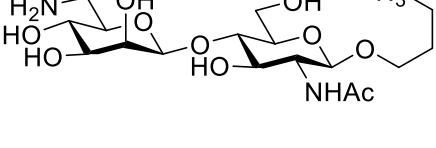


Figure 6-2. Structure of the unnatural mannose phosphate analogues supplied by the Miller group

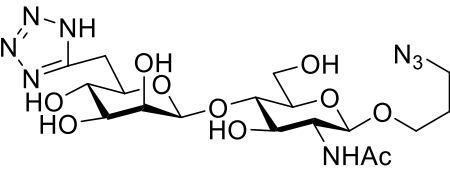
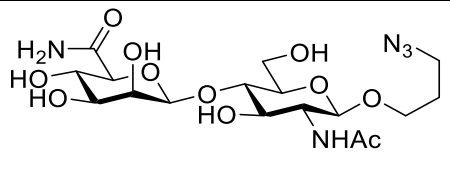
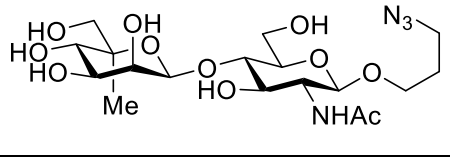
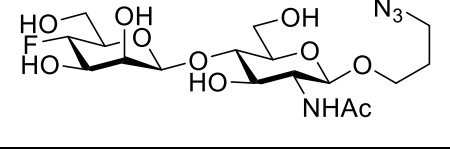
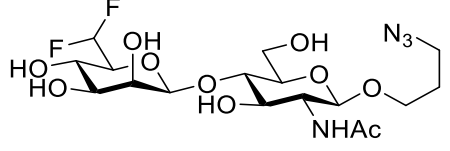


Use of enzymatic synthesis for the construction of  $\beta$ -mannosides

Table 15. BT-1033 reaction Entries 6-16; including starting reaction volume, starting donor and acceptor concentration, concentration of BT-1033, incubation time and whether LCMS analysis suggested conversion had occurred

Reaction entry	Disaccharide product	Reaction scale ( $\mu$ L)	Donor concentration at start (mM)	Acceptor concentration at start (mM)	BT-1033 concentration ( $\mu$ g/ $\mu$ L)	Incubation time (h)	Product observed in initial LCMS screening
6		19	210	263	0.10-0.078 to 0.29-0.22	72	Yes
7		20	250	250	0.096-0.074 to 0.28-0.21	72	No
8		20	250	250	0.096-0.074 to 0.28-0.21	72	Yes
9		15	250	250	0.096-0.074 to 0.28-0.21	72	Yes
10		20	250	250	0.096-0.074 to 0.28-0.21	72	No

Use of enzymatic synthesis for the construction of  $\beta$ -mannosides

Reaction entry	Disaccharide product	Reaction scale ( $\mu$ L)	Donor concentration at start (mM)	Acceptor concentration at start (mM)	BT-1033 concentration ( $\mu$ g/ $\mu$ L)	Incubation time (h)	Product observed in initial LCMS screening
11		12	188	188	0.12-0.093 to 0.34-0.26	72	No
12		20	250	250	0.096-0.074 to 0.28-0.21	72	No
13		20	250	250	0.096-0.074 to 0.28-0.21	72	Yes
14		20	250	250	0.096-0.074 to 0.28-0.21	72	Yes
15		15	250	250	0.096-0.074 to 0.28-0.21	72	Yes

Conversion was observed for seven of the eleven unnatural mannose-1-phosphate analogues trialled. There were no readily identifiable trends which rationalised why some analogues exhibited turnover while others did not. An initial hypothesis was that more sterically demanding donors were less likely to show conversion, yet the results did not fully support this hypothesis. Excluding analogue **6.9** (Table 15, Entry 10) all other unnatural mannose-1-phosphate analogues for which conversion was not observed contain an additional 6 position hydrogen bond acceptor (e.g. N for Entries 11, 12 and 7, O for Entries 12 and 7 and F for Entry 15, Table 15). Thus, it could be hypothesized that the lack of turnover seen for these analogues maybe accounted for by changes in the hydrogen bonding network within the enzyme active site. However, mannose-1-phosphate **6.15** (Table 15, Entry 16) was successfully turned over and contains an azido group, providing two further hydrogen bond acceptors at the 6-position. This observation strongly challenges the hypothesis that the presence of additional hydrogen bond acceptors was the reason conversion was not observed in Entries 10, 11, 12, 15 and 7, and at present the reason why conversion was not observed with these donors is unknown.

### 6.3.2. Establishing conversion rate of the BT-1033 catalysed reactions

Post reaction LCMS traces allowed for the determination of whether an unnatural analogue had undergone conversion. However, due to the acceptor and disaccharide having different ionisation abilities these traces do not provide accurate conversion rates. As such, numerous methods were trialled in the search of a method which could accurately measure enzymatic conversion rates. A few unsuccessful methods trialled were the use of an internal standard in NMR samples and the use of a standard GlcNAcN<sub>3</sub> curve obtained by LCMS. Galan and co-workers<sup>367</sup> recently developed the ITag methodology; here a copper-catalysed click reaction is used to covalently link alkyne-labelled Imidazolium-label **6.16** (ITag **6.16**) (Figure 6-3)<sup>367</sup> to an azide-labelled reporter. This method can be applied to any reaction which used one of the unnatural glucosamine acceptors **6.1**, **6.2**, **6.3** and **6.4** as an acceptor, as any remaining acceptor or disaccharide present will be tagged, resulting in the acceptor and disaccharide having essentially identical ionisation propensities and thereby allowing LCMS analysis to be used to calculate conversion rates. A sample of reaction Entries 2-16 was subjected to a reaction with ITag **6.16** (the Galan group, University of Bristol, provided a sample of ITag reagent **6.16** which was used in all the reactions presented in this chapter) and the resulting LCMS traces were analysed to extract the conversion rates shown in Table 16. The methodologies used for imidazolium labelling are reported in experimental section 8.6.2.3, page 337, with the results given in appendix section 9.5.3, page ccxxxv.

Use of enzymatic synthesis for the construction of  $\beta$ -mannosides

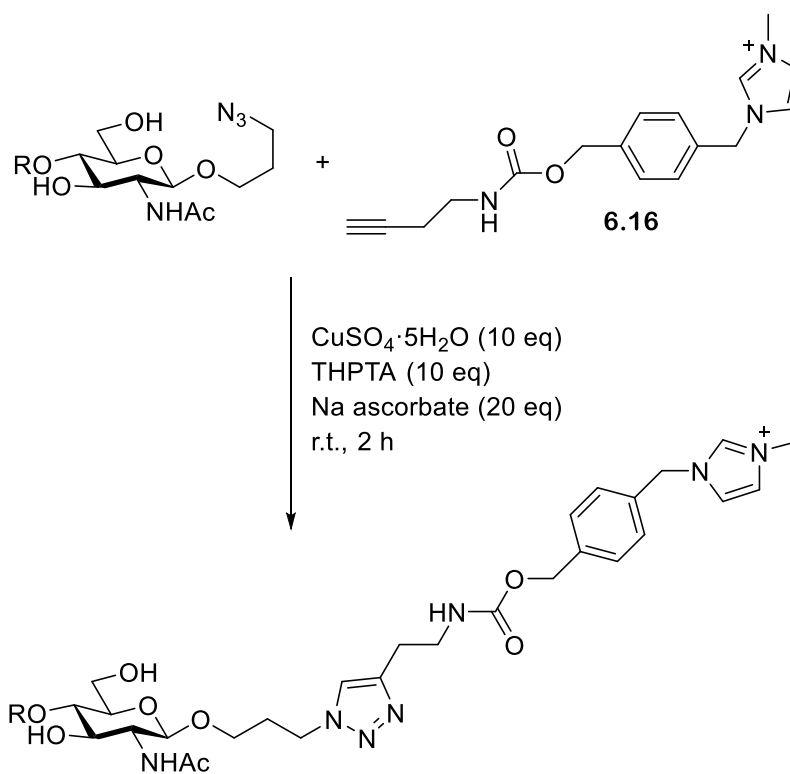


Figure 6-3. Conditions used for copper catalysed click reaction between an azide containing glycoside and imidazolium label 6.16. Where R = OH for the unnatural GlcNAN<sub>3</sub> acceptor 6.1 and a mannosides for the disaccharides

Use of enzymatic synthesis for the construction of  $\beta$ -mannosides

Table 16. BT-1033 reaction Entries 2-16 conversion rate percentages calculated using an ITag reaction

Reaction entry	Disaccharide product	Product observed in initial LCMS screening	Conversion rate measured (using ITag labelling) (%)
2		Yes	20
3		Yes	1
4		?	0.7
5		?	0.06
6		Yes	N/A
7		No	0.33
8		Yes	0.57
9		Yes	4
10		No	2
11		No	0.75
12		No	1.5

Use of enzymatic synthesis for the construction of  $\beta$ -mannosides

Reaction entry	Disaccharide product	Product observed in initial LCMS screening	Conversion rate measured (using ITag labelling) (%)
13		Yes	2
14		Yes	2
15		Yes	1.6
16		Yes	3.0 1.5

Due to the close resemblance to the natural substrates used by BT-1033, reaction 2 was treated as the pseudo native reaction to which other entries could be compared. Reaction Entries 3-16 (Table 16) achieved conversion yields significantly lower than that of reaction 2 (Table 16). A concern was that all the conversion values extracted for Entries 3-16 (Table 16) are below 5%.

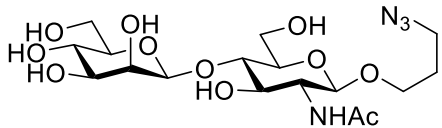
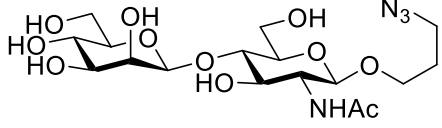
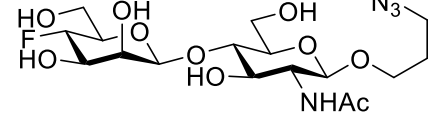
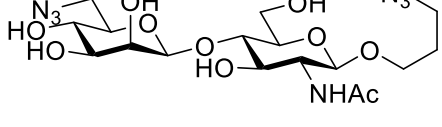
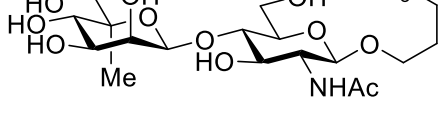
It was suspected that the conversion rate observed in Entries 3-16 may be limited via hydrolysis of the mannose-1-phosphate analogues. To test this hypothesis two further reactions were run (Table 17, Entries 17 and 18). Entry 17 contained 5 eq acceptor to 1 eq donor, whereas, Entry 18 contained 5 eq donor to 1 eq acceptor. The conversion rate for Entry 17 (2%) was shown to be significantly lower than that of Entry 2 (which used 1 eq of both donor and acceptor and achieved 20% conversion, Table 16). Conversely, Entry 18 was shown to have a significantly higher conversion rate (61%) compared to both Entry 2 and Entry 17, supporting the hypothesis that the limited conversion rates previously seen were due to donor hydrolysis limiting the amount of available donor.

With it established that increasing the donor concentration improved conversion rates a further ten trial reactions were set up (Table 17, Entries 19 to 28a) these reactions contained the unnatural monosaccharide units which had previously demonstrated turn over using initial LCMS analysis. All reactions were conducted in the presence of 5 eq of donor and were subsequently ITagged, and the results are shown in Table 17. All reaction entries achieved an increased conversion rate compared to their 1 eq donor counterparts. The highest yielding reaction was the pseudo native reaction (Table 17, Entry 28a), with the most promising unnatural monosaccharides being shown to be **6.7**, **6.12** and **6.2**, with all achieving conversion rates of 10% or more (Table 17, Entries 21, 22 and

25). Unnatural mannose-1-phosphates **6.13** and **6.15** achieved the lowest conversion yields of below 5% (Table 17, Entries 19 and 20), and were therefore excluded from any further investigations. Both unnatural glucosamine acceptors **6.3** and **6.4** were shown to achieve conversion rates of approximately 10-15% (Table 17, Entries 26 and 27), which are comparable to those attained by unnatural monosaccharide **6.7**, **6.12** and **6.2**. However, issues continued to be encountered during the initial LCMS analysis of the reactions performed on both unnatural glucosamine acceptors **6.3** and **6.4** (Table 17, Entries 25 and 26).

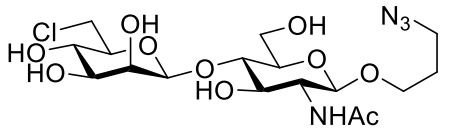
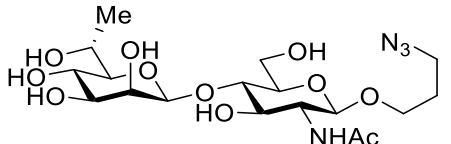
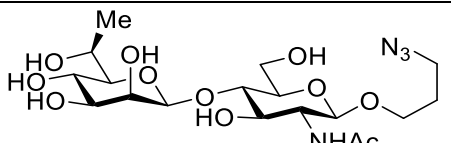
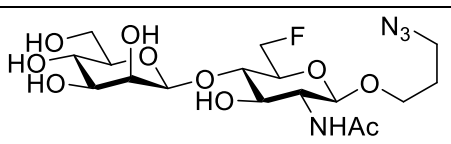
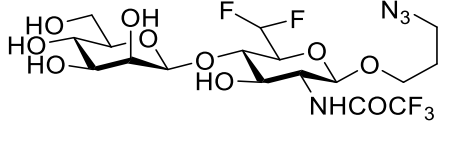
Use of enzymatic synthesis for the construction of  $\beta$ -mannosides

Table 17. BT-1033 catalysed reaction Entries 17-28a; including starting reaction volume, starting donor and acceptor concentration, concentration of BT-1033, incubation time and whether conversion was suggested in the initial LCMS trace, and the conversion rate (%) measured using an ITag reaction. Reaction repeats are labelled "a" and "b."

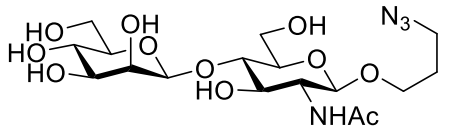
Reaction entry	Disaccharide product	Reaction scale ( $\mu$ L)	Donor concentration at start (mM)	Acceptor concentration at start (mM)	BT-1033 concentration ( $\mu$ g/ $\mu$ L)	Incubation time (h)	Product observed in initial LCMS screening	Conversion rate measured (using ITag labelling) (%)
17		30.2	60	300	0.096-0.074 to 0.28-0.21	48	Yes	2
18		30	625	125	0.096-0.074 to 0.28-0.21	48	Yes	61
19		10	250	50	0.096-0.074 to 0.24-0.185	72	Yes	5
20		10	250	50	0.096-0.074 to 0.24-0.185	72	Yes	3.5 di - 5
21a		10	250	50	0.096-0.074 to 0.24-0.185	72	Yes	19



Use of enzymatic synthesis for the construction of  $\beta$ -mannosides

Reaction entry	Disaccharide product	Reaction scale ( $\mu\text{L}$ )	Donor concentration at start (mM)	Acceptor concentration at start (mM)	BT-1033 concentration ( $\mu\text{g}/\mu\text{L}$ )	Incubation time (h)	Product observed in initial LCMS screening	Conversion rate measured (using ITag labelling) (%)
22a		10	250	50	0.096-0.074 to 0.24-0.185	72	Yes	10
23a		10	250	50	0.096-0.074 to 0.24-0.185	72	Yes	6
24a		10	250	50	0.096-0.074 to 0.24-0.185	72	Yes	7
25a		10	250	50	0.096-0.074 to 0.21-0.16	72	Yes	32
26a		10	250	50	0.096-0.074 to 0.21-0.16	72	Yes	13

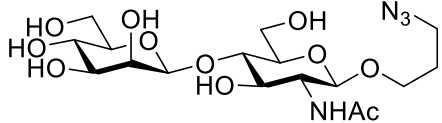
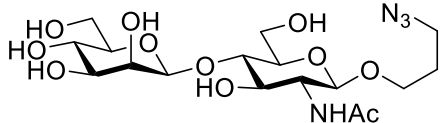
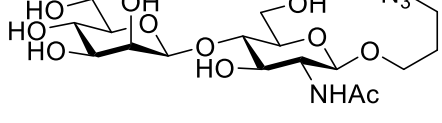
Use of enzymatic synthesis for the construction of  $\beta$ -mannosides

Reaction entry	Disaccharide product	Reaction scale ( $\mu$ L)	Donor concentration at start (mM)	Acceptor concentration at start (mM)	BT-1033 concentration ( $\mu$ g/ $\mu$ L)	Incubation time (h)	Product observed in initial LCMS screening	Conversion rate measured (using ITag labelling) (%)
28a		10	250	50	0.096-0.074 to 0.21-0.16	72	Yes	76

Further increasing the donor equivalence from 5 eq to 10 eq was shown to lead to a marginal increase in conversion rate in the pseudo native reaction, (conversion rates = 76% and 71% for Entries 28a and 28b vs 85% and 81% for Entries 29a and 29b, Table 17 and Table 18). However, due to this increase being only marginal its significance cannot be confirmed. To investigate the viability of this conversion rate increase, a second sample of Entry 28b and 29b was subjected to reaction with ITag reagent **6.16**, and conversion rates of 71% and 77% were achieved. These conversion rates are slightly lower than those previously achieved (77% vs 71% and 81% vs 77%) suggesting that there is between a 5-10% limit to the precision of conversion rate measurements made using the ITag reaction. This allowed us to set a precision limit of 5% on any conversion rate measured using the ITag methodology.

Use of enzymatic synthesis for the construction of  $\beta$ -mannosides

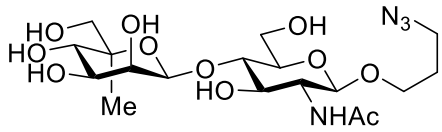
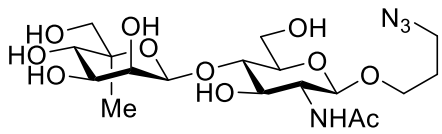
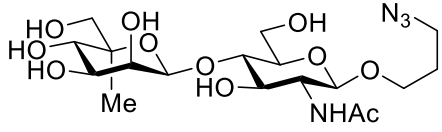
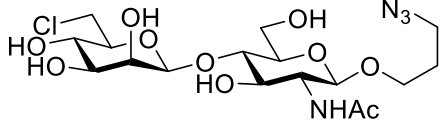
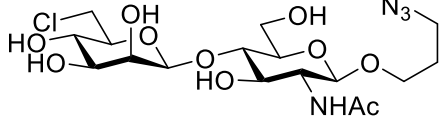
Table 18. BT-1033 catalysed reaction Entries 28b, 29a and 29b; including starting reaction volume, starting donor and acceptor concentration, concentration of BT-1033, incubation time and whether conversion was suggested in the initial LCMS trace, and the conversion rate (%) measured using an ITag reaction. Reaction repeats are labelled "a" and "b."

Reaction entry	Disaccharide product	Reaction scale ( $\mu$ L)	Donor concentration at start (mM)	Acceptor concentration at start (mM)	BT-1033 concentration ( $\mu$ g/ $\mu$ L)	Incubation time (h)	Product observed in initial LCMS screening	Conversion rate measured (using ITag labelling) (%)
28b		10	250	50	0.096-0.074 to 0.21-0.16	72	Yes	77/ 71
29a		10	500	50	0.096-0.074 to 0.21-0.16	72	Yes	85
29b		10	500	50	0.096-0.074 to 0.21-0.16	72	Yes	81/ 77

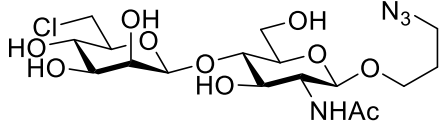
Repeat reactions were performed for Entries 21a to 22a (Table 17) and two further identical reactions were set up for each unnatural monosaccharide using 10 eq of donor to investigate whether this increase in donor equivalence would further increase the conversion rate. The results shown in Table 19 are for unnatural mannoside **6.7** and **6.12**, both of which had previously been shown to be promising analogues. Reaction Entry 21b (Table 19) achieved a comparable conversion rate to that of Entry 21a (21% vs 19%), with Entry 30a (Table 19) achieving a significantly higher conversion rate (37% vs 19%), suggesting that further increasing the donor equivalences led to an increase in conversion rate. The conversion rate measured in Entry 30b (Table 19) appears to be anomalous with only a 4% conversion rate being observed. An attempt was made to repeat reaction Entry 30b, yet this reaction attempt used a new stock of unnatural mannose-1-phosphate **6.12** which was supplied as a 2 : 1 mixture of  $\alpha$  :  $\beta$  anomers and initial LCMS analysis of the reaction suggested no conversion had occurred. As such, it was not possible to confirm whether Entry 30b was an anomalous result. Unnatural mannoside **6.7** had also previously been shown to be a promising analogue with reaction 22a (Table 17) achieving a conversion yield of 10%. However, reaction Entries 22b, 31a and 31b (Table 19) all achieved very poor conversion rates (0.7 – 3%) and it is suspected that the low conversion yield was due to the use of a new stock of unnatural mannoside **6.7**. A  $^1\text{H-NMR}$  spectrum of the new stock of unnatural mannoside **6.7** was taken and did not match the  $^1\text{H-NMR}$  spectrum provided by the Miller group, leading us to believe there had been significant decomposition of the stock, accounting for the low conversion rates observed.

Use of enzymatic synthesis for the construction of  $\beta$ -mannosides

Table 19. BT-1033 catalysed reaction Entries 21b, 30a, 30b, 22b, 31a and 31b; including starting reaction volume, starting donor and acceptor concentration, concentration of BT-1033, incubation time and whether conversion was suggested in the initial LCMS trace, and the conversion rate (%) measured using an ITag reaction. Reaction repeats are labelled "a" and "b."

Reaction entry	Disaccharide product	Reaction scale ( $\mu$ L)	Donor concentration at start (mM)	Acceptor concentration at start (mM)	BT-1033 concentration ( $\mu$ g/ $\mu$ L)	Incubation time (h)	Product observed in initial LCMS screening	Conversion rate measured (using ITag labelling) (%)
21b		10	150	30	0.096-0.074 to 0.21-0.16	72	Yes	21
30a		10	250	25	0.096-0.074 to 0.21-0.16	72	Yes	37
30b		10	250	25	0.096-0.074 to 0.21-0.16	72	Yes	4
22b		10	250	50	0.096-0.074 to 0.21-0.16	72	Yes	3
31a		10	500	50	0.096-0.074 to 0.21-0.16	72	Yes	2

Use of enzymatic synthesis for the construction of  $\beta$ -mannosides

Reaction entry	Disaccharide product	Reaction scale ( $\mu$ L)	Donor concentration at start (mM)	Acceptor concentration at start (mM)	BT-1033 concentration ( $\mu$ g/ $\mu$ L)	Incubation time (h)	Product observed in initial LCMS screening	Conversion rate measured (using ITag labelling) (%)
31b		10	500	50	0.096-0.074 to 0.21-0.16	72	Yes	0.7

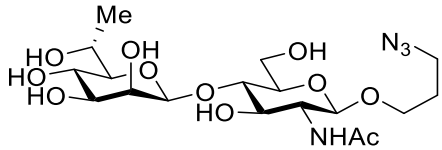
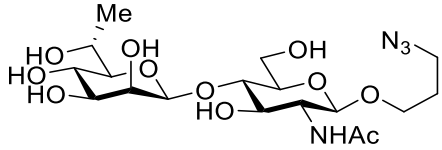
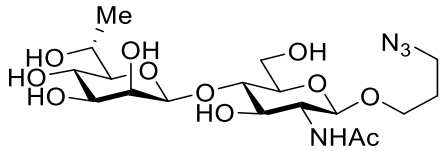
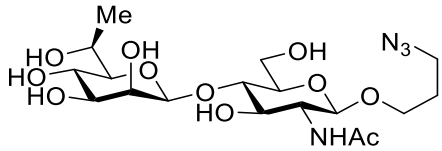
## Use of enzymatic synthesis for the construction of $\beta$ -mannosides

Previously reactions 23a and 24a (Table 17) had shown conversion rates of over 5% (6% and 7%). Further reactions using unnatural mannoside **6.8** (reactions 23b, 32a and 32b, Table 20) gave poor conversion rates of approximately 1%. These reactions were run using a new sample of unnatural mannoside **6.8**, so it could be speculated that issues with this sample could have caused the poor conversion rates observed. Unfortunately, this theory could not be confirmed as the sample of unnatural mannoside **6.8** consisted of only a few mg which were used in reactions 23b, 32a and 32b, and consequently there was not enough sample left for NMR analysis to investigate potential degradation. All further reactions performed on unnatural mannoside **6.5** (reactions 24b, 33a and 33b, Table 20) achieved similar conversion rates of 14%, 13% and 11% respectively. These conversion rates are higher than the 7% conversion rate previously observed in reaction 24, and these results appear to suggest that increasing the equivalences of unnatural mannoside **6.5** from 5 eq to 10 eq does not significantly increase the conversion rate observed.

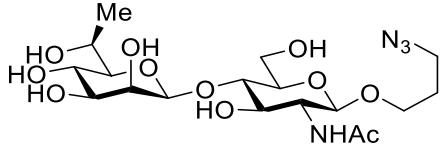
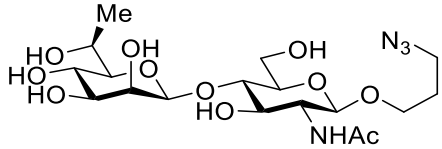


Use of enzymatic synthesis for the construction of  $\beta$ -mannosides

Table 20. BT-1033 catalysed reaction Entries 23b, 32a, 32b, 24a, 33a and 33b; including starting reaction volume, starting donor and acceptor concentration, concentration of BT-1033, incubation time and whether conversion was suggested in the initial LCMS trace, and the conversion rate (%) measured using an ITag reaction. Reaction repeats are labelled "a" and "b."

Reaction entry	Disaccharide product	Reaction scale ( $\mu$ L)	Donor concentration at start (mM)	Acceptor concentration at start (mM)	BT-1033 concentration ( $\mu$ g/ $\mu$ L)	Incubation time (h)	Product observed in initial LCMS screening	Conversion rate measured (using ITag labelling) (%)
23b		10	250	50	0.096-0.074 to 0.21-0.16	72	Yes	1
32a		10	500	50	0.096-0.074 to 0.21-0.16	72	Yes	1
32b		10	500	50	0.096-0.074 to 0.21-0.16	72	Yes	1
24b		10	250	50	0.096-0.074 to 0.21-0.16	72	Yes	14

Use of enzymatic synthesis for the construction of  $\beta$ -mannosides

Reaction entry	Disaccharide product	Reaction scale ( $\mu$ L)	Donor concentration at start (mM)	Acceptor concentration at start (mM)	BT-1033 concentration ( $\mu$ g/ $\mu$ L)	Incubation time (h)	Product observed in initial LCMS screening	Conversion rate measured by ITag (%)
33a		10	500	50	0.096-0.074 to 0.21-0.16	72	Yes	13
33b		10	500	50	0.096-0.074 to 0.21-0.16	72	Yes	11

## Use of enzymatic synthesis for the construction of $\beta$ -mannosides

The results for the three different unnatural acceptors varied highly. Reactions using unnatural glucosamine acceptor **6.2** showed impressive conversion rates of between 58-71% (Entries 25b, 34a, 34b, Table 21). Reaction Entries 25b, 34a and 34b demonstrated the trend that when donor equivalences were increased from 5 eq to 10 eq conversion rates increased, with conversion rates increasing from 59% to 69% / 71% between Entry 25b (Table 21) and Entries 34a and 34b (Table 21).

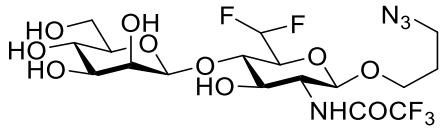
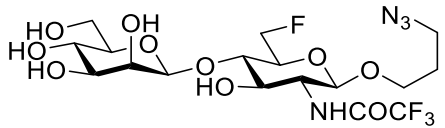
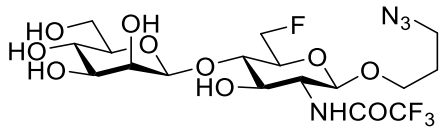
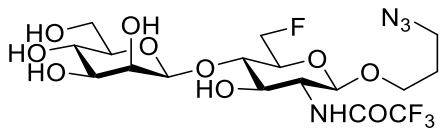
The data for unnatural glucosamine acceptors **6.3** and **6.4** was challenging to analyse. Initial analysis of the LCMS trace run after reaction termination of Entry 26a (Table 17) showed a notable mass peak corresponding to the mass of disaccharide. No notable significant mass peaks corresponding to either the disaccharide or glucosamine acceptor **6.4** could be identified on any of the initial LCMS spectrums for Entry 26b, Entry 35a and Entry 35b (Table 21). This corresponds with the reduced conversion rates observed in these reactions 2%, 2% and 1% respectively, all of which are significantly lower than the 13% conversion rate obtained for Entry 26a (Table 17). Reactions performed using unnatural glucosamine acceptor **6.3** (reaction Entries 27a (Table 17), 27b, 36a and 36b (Table 21)) showed no significant mass peaks for either acceptor **6.3** or the disaccharide on any of the initial LCMS traces taken post reaction termination. This result initially suggested glucosamine acceptor **6.3** was not being converted by BT-1033, yet the results of the ITag reactions suggested otherwise with conversion rates of between 10-30% being observed. The inconsistencies seen in the reactions discussed above, coupled with the issues encountered when analysing reaction Entries 4 and 5 (Table 14), suggest that the conversion rate results extracted for unnatural glucosamine acceptors **6.3** and **6.4** requires further investigation.

Use of enzymatic synthesis for the construction of  $\beta$ -mannosides

Table 21. BT-1033 catalysed reaction Entries 25b, 34a, 34b, 26b, 35a, 35b, 27b, 36a and 36b; including starting reaction volume, starting donor and acceptor concentration, concentration of BT-1033, incubation time and whether conversion was suggested in the initial LCMS trace, and the conversion rate (%) measured using an ITag reaction. Reaction repeats are labelled "a" and "b."

Reaction entry	Disaccharide product	Reaction scale ( $\mu$ L)	Donor concentration at start (mM)	Acceptor concentration at start (mM)	BT-1033 concentration ( $\mu$ g/ $\mu$ L)	Incubation time (h)	Product observed in initial LCMS screening	Conversion rate measured (using ITag labelling) (%)
25b		10	250	50	0.096-0.074 to 0.21-0.16	72	Yes	59
34a		10	500	50	0.096-0.074 to 0.21-0.16	72	Yes	71
34b		10	500	50	0.096-0.074 to 0.21-0.16	72	Yes	69
26b		10	250	50	0.096-0.074 to 0.21-0.16	72	No	2
35a		10	500	50	0.096-0.074 to 0.21-0.16	72	?	2

Use of enzymatic synthesis for the construction of  $\beta$ -mannosides

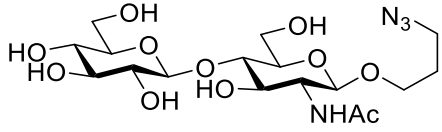
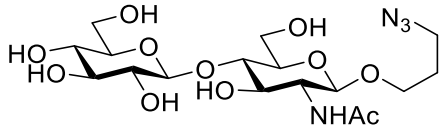
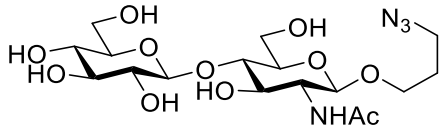
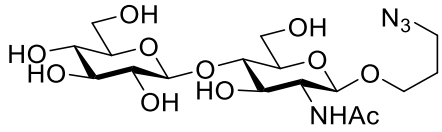
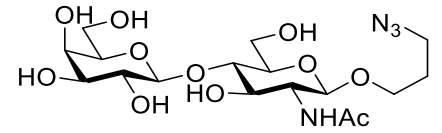
Reaction entry	Disaccharide product	Reaction scale ( $\mu$ L)	Donor concentration at start (mM)	Acceptor concentration at start (mM)	BT-1033 concentration ( $\mu$ g/ $\mu$ L)	Incubation time (h)	Product observed in initial LCMS screening	Conversion rate measured (using ITag labelling) (%)
35b		10	500	50	0.096-0.074 to 0.21-0.16	72	No	1
27b		10	250	50	0.096-0.074 to 0.21-0.16	72	No	37/ 30
36a		10	500	50	0.096-0.074 to 0.21-0.16	72	No	22
36b		10	500	50	0.096-0.074 to 0.21-0.16	72	No	10

## Use of enzymatic synthesis for the construction of $\beta$ -mannosides

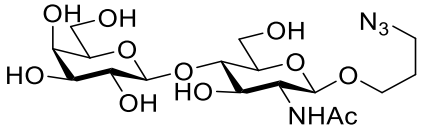
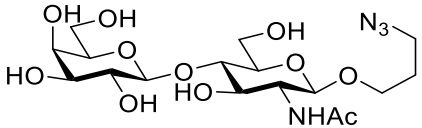
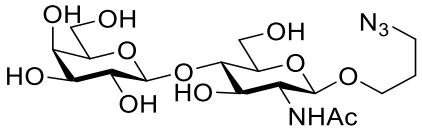
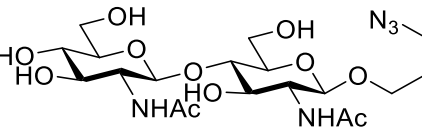
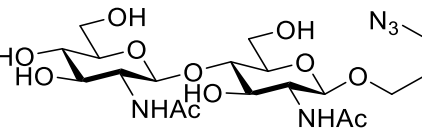
All previous trial reactions have used a mannose-1-phosphate analogue as a donor and a glucosamine analogue as an acceptor. We hypothesized that the use of a mannose-1-phosphate would be critical for BT-1033 turnover due to the axial orientation of *O*-2. Thus it was decided to explore this hypothesis by running further trial reactions using glucose-1-phosphate, galactose-1-phosphate and *N*-Acetyl glucosamine-1-phosphate as substitute donors. Duplicate reactions were run using both 5 eq and 10 eq of each donor, a sample of each reaction was reacted with ITag reagent **6.16**, with the conversion rate results shown in Table 22. None of the trial reactions displayed in Table 22 obtained a conversion rate above the previously set threshold level of 5%, supporting the theory that the axial *O*-2 on mannose-1-phosphate is critical to conversion.

Use of enzymatic synthesis for the construction of  $\beta$ -mannosides

Table 22. BT-1033 catalysed reaction Entries 37a, 37b, 38a, 38b, 39a, 39b, 40a, 40b, 41a, 41b, 42a and 42b; including starting reaction volume, starting donor and acceptor concentration, concentration of BT-1033, incubation time and whether conversion was suggested in the initial LCMS trace, and the conversion rate (%) measured using an ITag reaction. Reaction repeats are labelled "a" and "b."

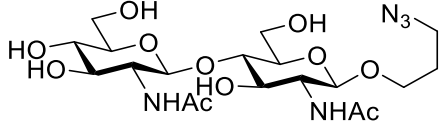
Reaction entry	Disaccharide product	Reaction scale ( $\mu$ L)	Donor concentration at start (mM)	Acceptor concentration at start (mM)	BT-1033 concentration ( $\mu$ g/ $\mu$ L)	Incubation time (h)	Product observed in initial LCMS screening	Conversion rate measured (using ITag labelling) (%)
37a		10	225	50	0.096-0.074 to 0.21-0.16	72	Yes	0.6
37b		10	225	50	0.096-0.074 to 0.21-0.16	72	Yes	0.6
38a		10	450	50	0.096-0.074 to 0.21-0.16	72	Yes	0.6
38b		10	450	50	0.096-0.074 to 0.21-0.16	72	Yes	0.46
39a		10	250	50	0.096-0.074 to 0.21-0.16	72	No	2

Use of enzymatic synthesis for the construction of  $\beta$ -mannosides

Reaction entry	Disaccharide product	Reaction scale ( $\mu$ L)	Donor concentration at start (mM)	Acceptor concentration at start (mM)	BT-1033 concentration ( $\mu$ g/ $\mu$ L)	Incubation time (h)	Product observed in initial LCMS screening	Conversion rate measured (using ITag labelling) (%)
39b		10	250	50	0.096-0.074 to 0.21-0.16	72	No	0.7
40a		10	500	50	0.096-0.074 to 0.21-0.16	72	No	0.7
40b		10	500	50	0.096-0.074 to 0.21-0.16	72	No	0.2
41a		10	225	50	0.096-0.074 to 0.21-0.16	72	Yes	0.3
41b		10	225	50	0.096-0.074 to 0.21-0.16	72	Yes	0.3



Use of enzymatic synthesis for the construction of  $\beta$ -mannosides

Reaction entry	Disaccharide product	Reaction scale ( $\mu$ L)	Donor concentration at start (mM)	Acceptor concentration at start (mM)	BT-1033 concentration ( $\mu$ g/ $\mu$ L)	Incubation time (h)	Product observed in initial LCMS screening	Conversion rate measured (using ITag labelling) (%)
42b		10	450	50	0.096-0.074 to 0.21-0.16	72	Yes	0.2

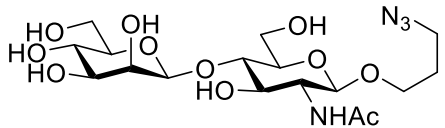
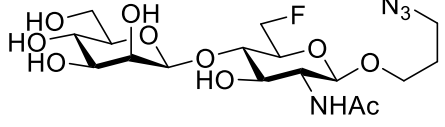
## Use of enzymatic synthesis for the construction of $\beta$ -mannosides

All previous reactions reported above have been performed on a test reaction scale in order to conserve both donor and acceptor; this has prevented purification of any reaction samples and thus prohibited the reaction stereoselectivity from being confirmed. Two scale-up reactions were performed (reaction Entries 29 and 34) and purified by size exclusion using a gel filtration, allowing for the extraction of a pure sample of each disaccharide (2.7 mg of disaccharide for entry 29 scale up and 1.3 mg of disaccharide for entry 34 scale up). These samples were submitted for NMR spectroscopy, with an IPAP-HSQC experiment<sup>368</sup> performed on the disaccharide from entry 29 scale up and a CLIP-HSQC experiment<sup>369</sup> was performed on the disaccharide from entry 34 scale up to measure each anomeric carbons  $^1J_{CH}$  coupling constant. The  $^1J_{CH}$  coupling constants extracted for the disaccharides were 162 Hz and 160 Hz and 159 Hz and 164 Hz respectively, confirming the  $\beta$ -selectivity of each disaccharide.<sup>361</sup>

The two scaled-up reactions gave lower conversion rates than their 10  $\mu$ L scale counterparts (e.g. conversion rate for Entry 29 scale up = 61% (Table 23) vs Entries 29a and 29b conversion rate = 85% and 77% / 81% (Table 18), conversion rate for Entry 34 scale up = 58% (Table 23) vs Entries 34a and 34b 71% and 69% (Table 21)). Currently, not enough scaled-up reactions have been performed to conclude whether increasing the reaction scale reduces the conversion rate, yet the data from Entries 29 and 34 scale up reactions (Table 23) does suggest that reaction scale could influence conversion rates.

Use of enzymatic synthesis for the construction of  $\beta$ -mannosides

Table 23. BT-1033 catalysed reaction Entries 29 scale up and 34 scale up; including starting reaction volume, starting donor and acceptor concentration, concentration of BT-1033, incubation time and whether conversion was suggested in the initial LCMS trace, and the conversion rate (%) measured using an ITag reaction. Reaction repeats are labelled "a" and "b."

Reaction entry	Disaccharide product	Reaction scale ( $\mu$ L)	Donor concentration at start (mM)	Acceptor concentration at start (mM)	BT-1033 concentration ( $\mu$ g/ $\mu$ L)	Incubation time (h)	Product observed in initial LCMS screening	Conversion rate measured (using ITag labelling) (%)
29 scale up		200	500	50	0.101 to 0.297	72	Yes	61
34 Scale up		154	500	50	0.1-0.77 to 0.29-0.22	72	Yes	58

#### 6.3.4 Crystallography of BT-1033

In an endeavour to further understand the catalytic mechanism of BT-1033 the crystallisation of the enzyme was attempted. However, prior to trialling crystallography conditions we obtained a predicted PDB model using Phyer2. (Figure 6-4).<sup>370</sup> The Phyer2 model of BT-1033 showed a 100% confidence agreement with the PDB template crystal structure used of  $\beta$ -1,4-mannopyranosyl-chitobiose phosphorylase at 1.60 Angstrom in complex with *N*-acetylglucosamine and inorganic phosphate (PDB - c4udgb).<sup>371</sup>



Figure 6-4. Phyer2 predicted PDB structure of BT-1033 with suspected acid / base residue Aspartic acid residue 101 highlighted in pink

Five initial 96-well crystal tray screens were set up with BT-1033 (PACT (molecular dimensions), AMSo<sub>4</sub> (molecular dimensions), Morpheus (molecular dimensions) (molecular dimensions), INDEX (Hampton research) and JCSG (molecular dimensions)). All plates were set up using the same protein sample with a concentration between 11.39 to 14.9  $\mu\text{g}/\mu\text{L}$  and using a 1 : 1 protein to buffer reservoir ratio. Protein crystallisation was observed in at least one well of each plate, with the most promising conditions being JCSG B8 and INDEX H8, both of which produced plate like crystals (Figure 6-5).

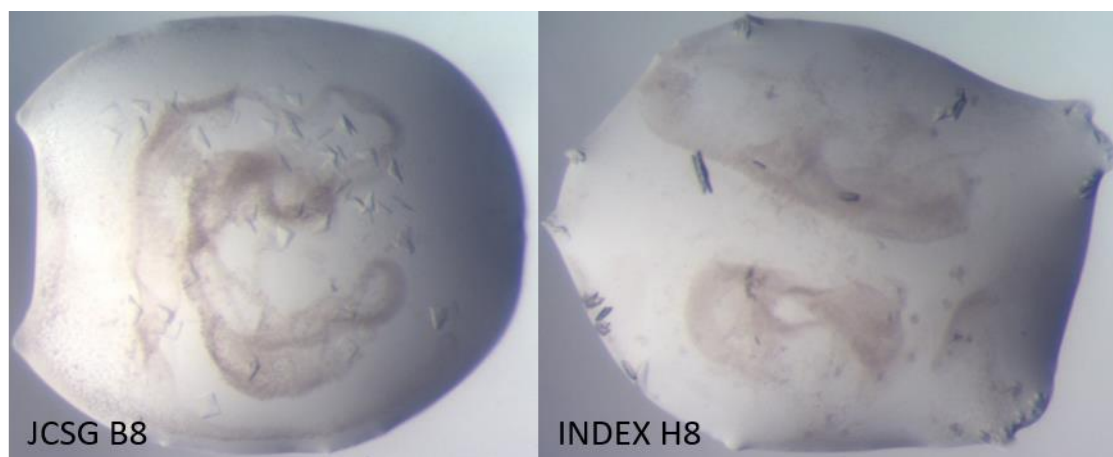


Figure 6-5. Images of promising BT-1033 crystals using conditions JCSG B8 (0.2 M  $MgCl_2 \cdot 6H_2O$ , 0.1 M TRIS, pH = 7.0, 10% w/v PEG 8000) and INDEX H8 (0.1 M magnesium formate dihydrate, 15% w/v PEG 3350)

While the formation of plate like crystals under these conditions was positive, the crystals had formed in a 96-well plate meaning they were relatively small and would likely be difficult to fish. Therefore, a further two 48-well plates were designed, one optimising the conditions present in JCSG B8 and the other optimising the conditions present in INDEX H8. The designs of these two plates are attached in appendix section 9.5.5, page ccxlv. It was hoped that using these two plates would permit the formation of larger protein crystals, allowing for easier crystal fishing and therefore, increasing the chance of a protein crystal structure being obtained. None of the conditions trialled on the optimised JCSG B8 based 48-well plate induced protein crystallisation, but protein crystallisation was observed in multiple conditions in the INDEX H8 based 48-well plate, with some examples being shown in Figure 6-6. The crystals formed in H6 of the H8 INDEX based plate were selected for crystal fishing along with the crystals in B8 of the JCSG plate. Four crystals from each condition were fished and these crystals were sent to Diamond for X-ray diffraction. Unfortunately, none of the BT-1033 protein crystals selected diffracted well enough to obtain an accurate protein crystal structure.

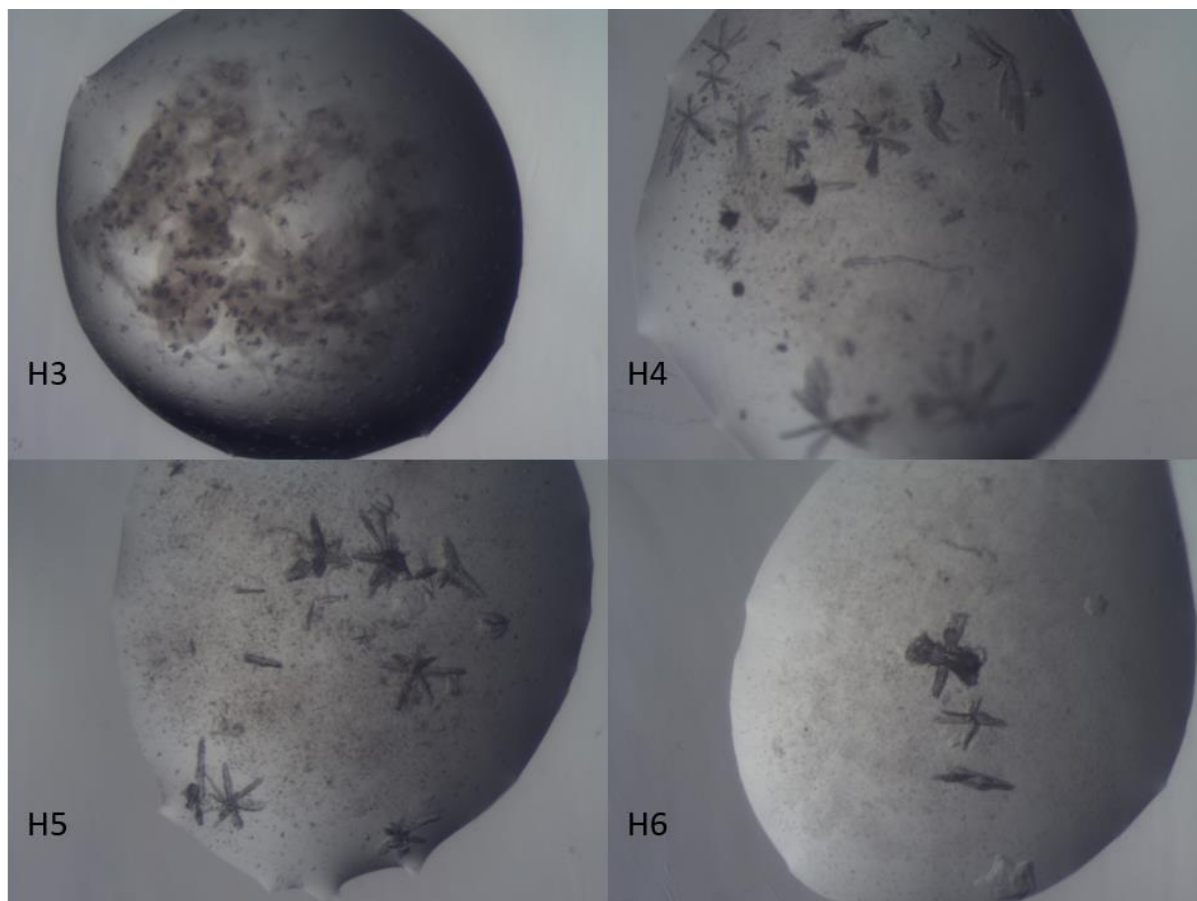


Figure 6-6. Further promising images of BT-1033 crystals. Conditions H3 - 0.1 M magnesium formate dihydrate, 23% w/v PEG 3350, protein : reservoir 0.5 : 1.0; H4 - 0.1 M magnesium formate dihydrate, 23% w/v PEG 3350, protein : reservoir 1.0 : 1.0; H5 - 0.1 M magnesium formate dihydrate, 23% w/v PEG 3350, protein : reservoir 1.0 : 0.75; H6 - 0.1 M magnesium formate dihydrate, 23% w/v PEG 3350, protein : reservoir 1.0 : 0.5

Due to time constraints no further BT-1033 protein crystal trays could be set up, and thus we were unable to obtain an accurate protein crystal structure for BT-1033. Future work should involve a further 48-well crystal tray based around the conditions used in row H of the INDEX H8 based plate (0.1 M magnesium formate dihydrate, 23% w/v PEG 3350), as larger BT-1033 crystals could allow for easier crystal fishing.

## 6.3.5 Use of BT-1033 as a thioglycoligases

Thioglycoligase rely on the use of donors which possess good leaving groups.<sup>364, 366</sup> Phosphate groups are suitable leaving groups in this regard. This led us to hypothesize that in addition to its phosphorylase activity BT-1033 could also exude activity as a thioglycoligase. As BT-1033 catalyses the reversible phosphorolysis of  $\beta$ -1,4-D-mannosyl-*N*-acetyl-D-glucosamine<sup>359</sup> achieving a high conversion yield can be challenging and requires an excess of mannose-1-phosphate to drive the reaction equilibrium in favour of product. Investigating potential thioglycoligase activity could help overcome this problem, providing a method for the formation of non-hydrolysable thioglycosides. To investigate this theory, it was decided to design two BT-1033 mutants, both of which would have their general acid base residue (Asp101)<sup>360</sup> mutated to either an alanine residue or a glycine residue. Furthermore, a member of the Miller group at Keele University synthesised *O*-4-thiol-glucosamine acceptor **6.17** (Figure 6-7) to allow testing of the BT-1033 mutants thioglycoligase activity once they were obtained.

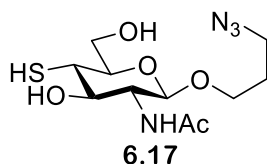


Figure 6-7. Structure of *O*-4-thiol-glucosamine acceptor **6.17**

However, we initially investigated the ability of wild type BT-1033 to convert *O*-4-thiol-glucosamine acceptor **6.17**. In the absence of a reducing agent *O*-4-thiol-glucosamine acceptor **6.17** exists as a dimer, and thus needs reducing prior to being used in an enzymatic reaction. To ensure *O*-4-thiol-glucosamine acceptor **6.17** remains in its monomeric form throughout the reaction, the reaction was performed in 40 mM NaOAc, 5 mM TCEP, pH 5.5 buffer. As no previous reactions had been performed in the presence of 5 mM TCEP, an additional pseudo native reaction was set up to see if the buffer change had a significant effect on conversion (Table 24, Entries 43a and 43b). The addition of 5 mM TCEP was shown to slightly reduce the observed conversion rate (73% and 59 % for Entries 43a and 43b (Table 24) vs 85% and 81/77% for Entries 29a and 29b (Table 18)). Two further reactions were set up, using *O*-4-thiol-glucosamine acceptor **6.17** (Table 24, Entries 44a and 44b), and these reactions showed the formation of the desired disaccharide on the initial post reaction termination LCMS traces, with the results of the ITag reaction estimating an approximate conversion rate of 34% (Table 24, Entries 44a and 44b). This conversion rate is significantly lower than that observed in trials of the pseudo native reactions which displayed conversion rates of between 59-85% seen (Entries 29a and 29b (Table 18), 43a and 43b (Table 24)). As *O*-4-thiol-glucosamine acceptor **6.17** is more nucleophilic than glucosamine acceptor **6.1**, two enzyme free control reactions were set up (Table 24, Entries 45a and 45b). This would confirm that any turnover observed in Table 24 Entries

## Use of enzymatic synthesis for the construction of $\beta$ -mannosides

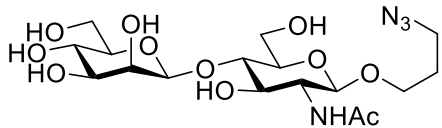
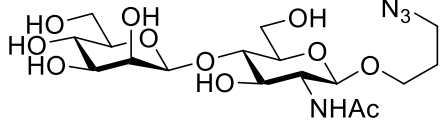
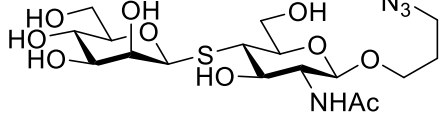
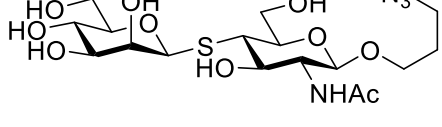
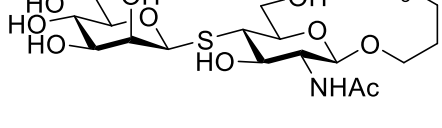
44a and 44b was catalysed by BT-1033 and was not the result of direct attack of *O*-4-thiol-glucosamine acceptor **6.17** on mannose-1-phosphate. The initial LCMS traces taken post reaction termination suggested no formation of the disaccharide in Table 24 Entries 45a and 45b, and further supported by the ITag reaction which suggested conversion rates of 1.4% and 1.3%. These conversion rates fall below the 5% degree of uncertainty, thus it was concluded that BT-1033 was responsible for the conversion observed in Table 24 reaction Entries 44a and 44b.

We had hoped to further expand this work by synthesising the two BT-1033 mutants discussed above. However, initial attempts at QuikChange<sup>®</sup> site-directed mutagenesis kit (Agilent Technologies) (see 342) were unsuccessful in obtaining the mutants, and the time constraints of the project has meant that the reason for the failure of QuikChange<sup>®</sup> site-directed mutagenesis has not been determined, and other mutagenesis methods have not yet been explored.

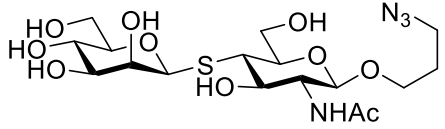


Use of enzymatic synthesis for the construction of  $\beta$ -mannosides

Table 24. BT-1033 catalysed reaction Entries 43a, 43b, 44a, 44b, 45a, 45b; including starting reaction volume, starting donor and acceptor concentration, concentration of BT-1033, incubation time and whether conversion was suggested in the initial LCMS trace, and the conversion rate (%) measured using an ITag reaction. Reaction repeats are labelled "a" and "b."

Reaction entry	Disaccharide product	Reaction scale ( $\mu$ L)	Donor concentration at start (mM)	Acceptor concentration at start (mM)	BT-1033 concentration ( $\mu$ g/ $\mu$ L)	Incubation time (h)	Product observed in initial LCMS screening	Conversion rate measured (using ITag labelling) (%)
43a		10	500	50	0.1 to 0.18	48	Yes	73
43b		10	500	50	0.1 to 0.18	48	Yes	59
44a		10	500	50	0.1 to 0.18	48	Yes	34
44b		10	500	50	0.1 to 0.18	48	Yes	34
45a		10	500	50	0	48	No	1.4

Use of enzymatic synthesis for the construction of  $\beta$ -mannosides

Reaction entry	Disaccharide product	Reaction scale ( $\mu$ L)	Donor concentration at start (mM)	Acceptor concentration at start (mM)	BT-1033 concentration ( $\mu$ g/ $\mu$ L)	Incubation time (h)	Product observed in initial LCMS screening	Conversion rate measured by ITag (%)
45b		10	500	50	0	48	No	1.3

### Chapter 7 Conclusion and future work

This thesis describes the successful synthesis of multiple monosaccharide building blocks (chapter 2) for use in the synthesis of colicin conjugates (chapter 3), protected disaccharide and a protected trisaccharide (chapter 5). In addition, this thesis describes the bespoke usage of OPAL bio-conjugation for conjugating specially synthesized sugar-linked OPAL probes to colicin units to afford colicin-linked conjugates (chapter 3). Attempts to analyse the biological properties of these conjugates are also discussed (chapter four). In addition, enzymatic synthetic methods using BT-1033 for the synthesis of  $\beta$ -1,4-D-mannosyl-N-acetyl-D-glucosamine and many unnatural  $\beta$ -1,4-D-mannosyl-N-acetyl-D-glucosamine analogues have been established, and initial efforts have been made to learn more about the structure and mechanism of action of BT-1033 (chapter 6).

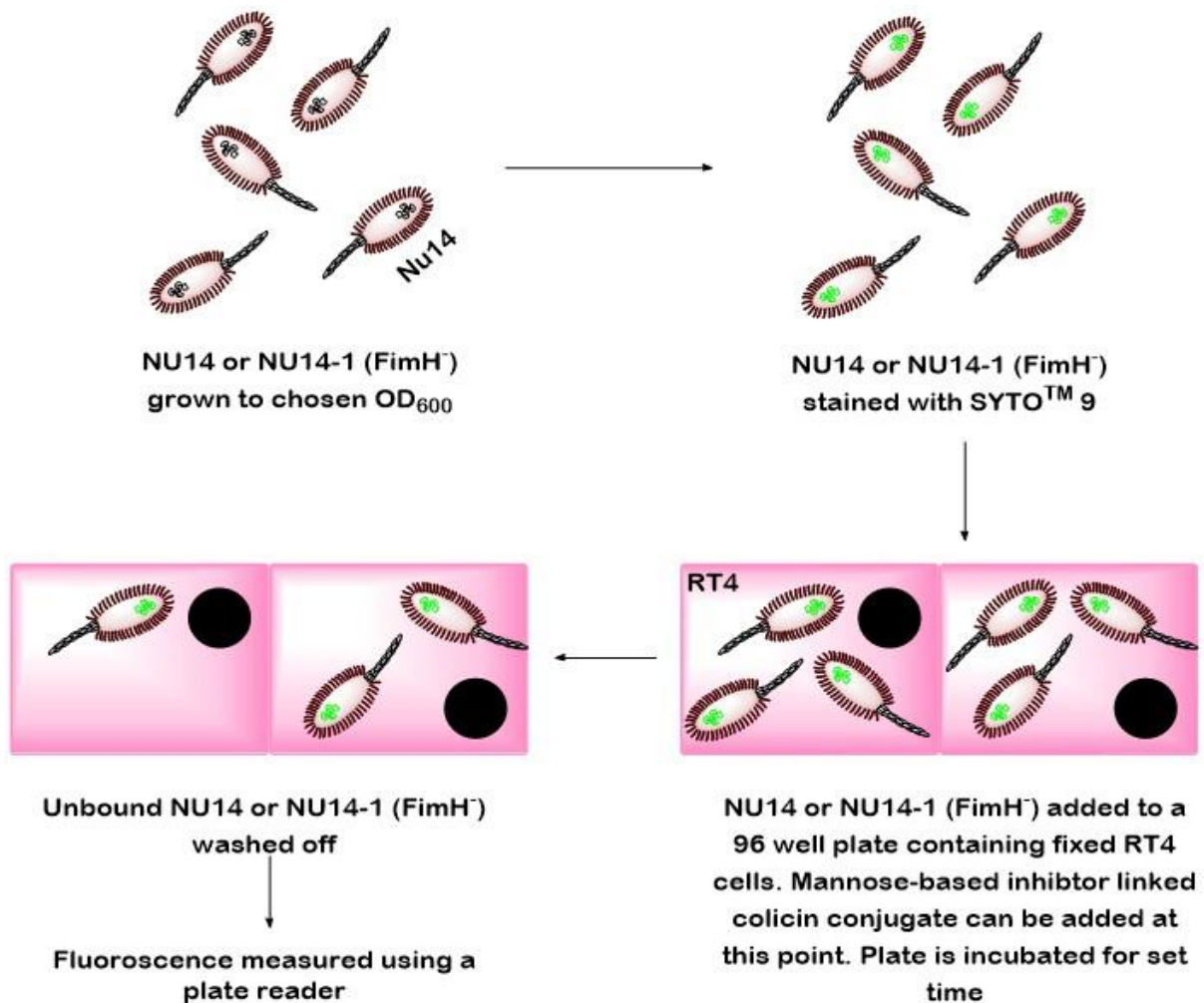
Chapter 2 focused on the synthesis of monosaccharide sugar units. Both mannose-based inhibitors **2.53** and **2.54**, were successfully synthesised, as were the requisite monosaccharide building blocks for the synthesis of protected trisaccharide **5.19**. Chapter 3 focused on the development of a successful method for the installation of mannose-based inhibitor **2.53** and **2.54** into three different OPAL probes. These probes were subsequently appended to both colicin E9 and Ia, affording six different mannose-based inhibitor linked colicin conjugates. Two further biotin-linked colicin conjugates were also prepared via similar methods. The results presented in these chapters fulfil the objectives outlined and thus no further work is required.

Chapter 4 aimed to investigate the biological properties of the mannose-based inhibitor linked colicin conjugates, principally their ability to induce *E. coli* aggregation. Due to limited access to the University of York Biology department, a mixture of auto-aggregation assays and microscopy imaging was used. Unfortunately, these experiments proved inconclusive, and consequently a significant amount of future work will be required to properly elucidate the biological properties of the mannose-based inhibitor linked colicin conjugates. To this end a collaboration has been established with the Southgate group in the University of York Biology Department, as the Southgate group has expertise in developing a range of cell and tissue culture systems for urothelium cells.

Preliminary discussions during this collaboration have led to the design of a new assay protocol, which is depicted in Scheme 7-1. This assay uses *E. coli* strain NU14, a clinical pyelonephritis isolate<sup>372</sup> and NU14-1 a FimH-minus mutant of NU14.<sup>68, 373</sup> The NU14 or NU14-1 will be grown to the chosen OD<sub>600</sub>, following this the cells will be stained with SYTO™ 9, a green fluorescent nucleic acid stain. The NU14 or NU14-1 can then be added to a 96 well plate containing fixed RT4 cells (a human bladder cancer cell line).<sup>374</sup> At this point the mannose based inhibitor linked colicin conjugates can be added. The 96 well plates will then be incubated for a set amount of time, and the wells subsequently

## Conclusion and future work

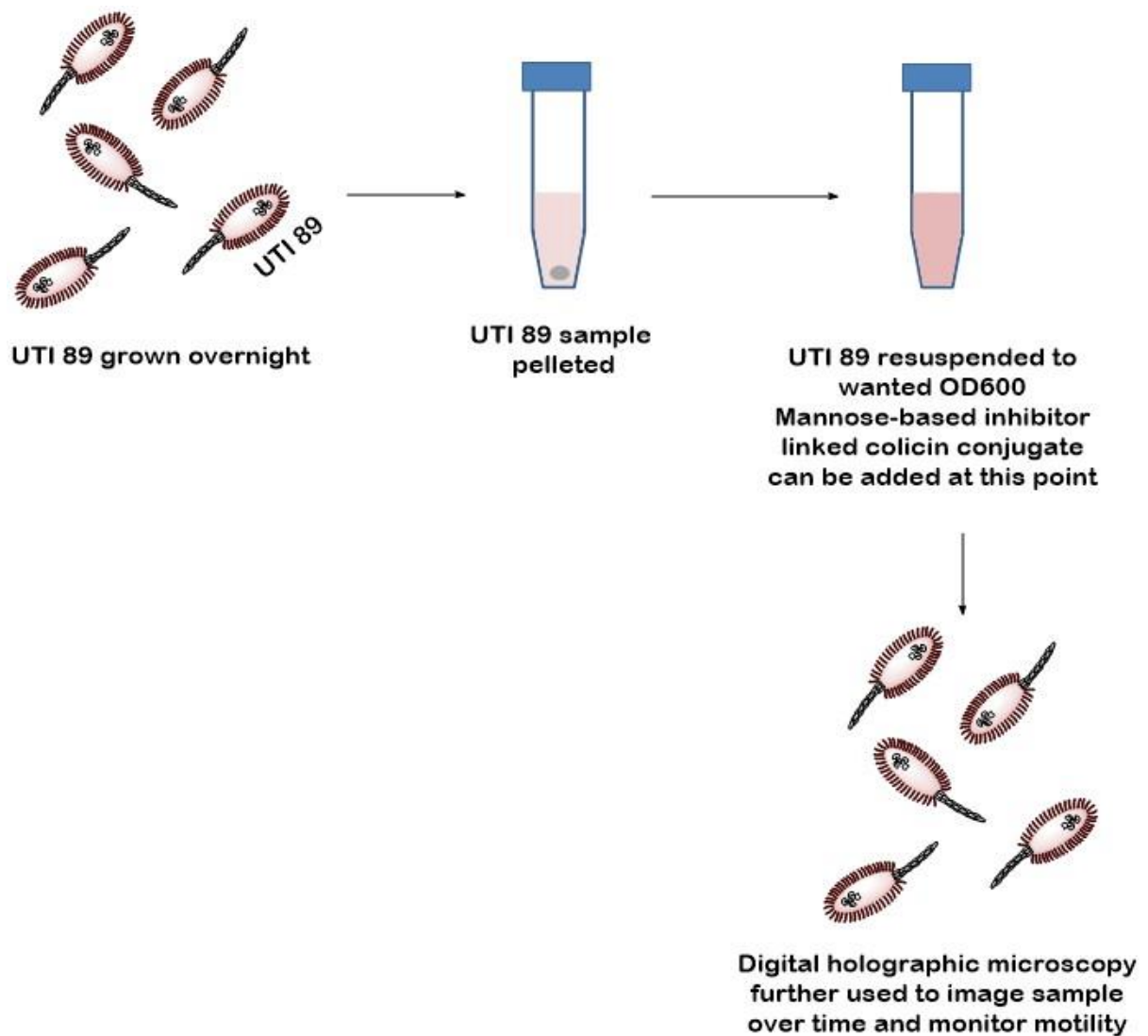
washed to remove any unbound NU14 or NU14-1. The fluorescence of each well can then be measured using a plate reader; theoretically the less *E. coli* bound to the RT4 cells the lower the fluorescence measurement of a well. Therefore, if the mannose-based inhibitor linked colicin conjugates are able to induce *E. coli* aggregation they should prevent binding of NU14 to RT4 cells lowering the fluorescence compared to that of a sample of NU14 only. Additionally, due to their lack of FimH, NU14-1 samples should struggle to adhere to the RT4 cells, and thus wells containing NU14-1 should have significantly lower fluorescence compared to wells containing NU14 only. With regards to further experiments, *E. coli* strain UTI 89 could be substituted for *E. coli* strain NU14 with minimal assay redesign. Currently, we do not possess a FimH-minus mutant for UTI 89 and thus control samples would have to be made using the competitive inhibitor methyl-mannose. As at sufficient methyl mannose concentrations binding of the FimH units on UTI 89 to the RT4 cells should be inhibited, allowing baseline fluorescence to be established.



Scheme 7-1. The inhibition assay designed to investigate the potential ability of the mannose-based inhibitor linked colicin conjugates to prevent adhesion of NU14 to RT4 cells

## Conclusion and future work

If the newly designed assay depicted in Scheme 7-1 proves that mannose-based inhibitor linked colicin conjugates prevent adhesion of NU14 to RT4 cells a further motility assay will be performed. This assay is depicted in Scheme 7-2. Here, *E. coli* UTI 89 would be grown overnight then pelleted and resuspended to the desired OD<sub>600</sub>. Mannose-based inhibitor linked colicin conjugates would then be added to the samples and digital holographic microscopy would be used to monitor sample motility. We hypothesize that if a mannose-based inhibitor linked colicin conjugate successfully induces aggregation this should result in an observable reduction in motility over time.



Scheme 7-2. An assay designed to monitor the effects of the mannose-based inhibitor linked colicin conjugates on UTI 89 motility

## Conclusion and future work

If the results of both the inhibition and motility assays are positive this would confirm our initial hypothesis that the mannose-based inhibitor linked colicin conjugates can inhibit *E. coli* binding by inducing aggregation. Further work could then be performed using a UTI mouse model to see if these effects are maintained *in vivo*. The potential applications of this work are huge as the mannose-based inhibitor linked colicin conjugates could potentially offer an alternative method for treating UPEC-induced UTIs, and unlike traditional antibiotic treatments (which kill the bacteria) UPEC removal via aggregation induction would not represent a strong selection pressure, and thus hopefully bacterial resistance to this treatment would evolve more slowly.

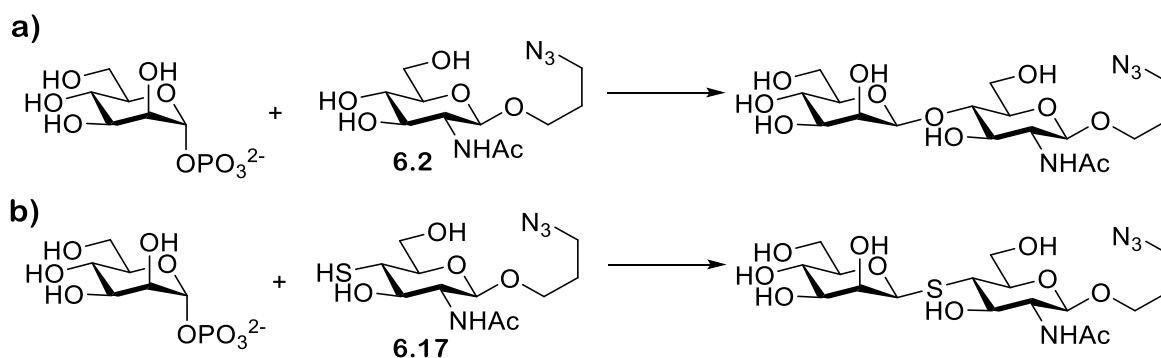
The work presented in chapter 5 focused on investigating chemical synthesis methods for  $\beta$ -mannosidic bond formation and the synthesis of protected trisaccharide **5.19**. Though a small amount of trisaccharide **5.19** was successfully synthesised and characterised by mass spectrometry, the glycosylation steps required were so low yielding that a clean sample of trisaccharide **5.19** could not be isolated. Furthermore, these low yields meant that extracting a significant amount of trisaccharide **5.19** would be extremely time and labour intensive. As such, we resolved to investigate other synthetic approaches and focus our efforts on easier synthetic targets.

Chapter 6 explored enzymatic methods of synthesising  $\beta$ -1,4-D-mannosyl-N-acetyl-D-glucosamine using BT-1033, and it was demonstrated that BT-1033 offers an alternative method for the synthesis of  $\beta$ -1,4-D-mannosyl-N-acetyl-D-glucosamine. The substrate promiscuity of BT-1033 was then investigated with a number of different unnatural monosaccharides, with the most promising analogues shown to be analogues **6.1**, **6.2**, **6.7** and **6.12**, which all showed promising conversion rates. Further work could initially focus on how reaction scale affects conversion rate. Additional work would also involve repeating a few of the reactions for which anomalous results were previously obtained, this would allow accurate conversion rates to be extracted. However, these reactions will have to wait until more of the respective unnatural mannose-1-phosphate analogues can be sourced.

Efforts were made to obtain a crystal structure of BT-1033 in chapter 6. Unfortunately, while crystallisation of BT-1033 was achieved, initial attempts to elucidate its structure by x-ray crystallography was unsuccessful and there was not enough time to set up further crystal trays. Setting up a further 48-well crystal tray, optimising the conditions used on the H row of the INDEX H8 based plate would likely facilitate the formation of larger BT-1033 crystals, and as larger crystals are more easily fished this would hopefully allow an accurate crystal structure to be obtained. Co-crystallisation of BT-1033 with mannose-1-phosphate could also be attempted, as the presence of a ligand bound to the active site could also help facilitate crystal formation. Obtaining the crystal structure of BT-1033 either with or without bound mannose-1-phosphate would provide valuable information about the

structure of BT-1033 and would better our understanding of how the enzymatic mechanism of BT-1033 may proceed.

The latter part of chapter 6 describes the investigation of the potential thioglycoligase activity of BT-1033. Unfortunately, due to an initial failure in preparing two bespoke BT-1033 mutants (active-site mutants in which the suspected acid/base residue has been replaced with an alanine or glycine residue) and time constraints, only a limited amount of work has been conducted and much future work is required. Further efforts should be made to obtain the two desired BT-1033 mutants; this could initially be done by screening further QuikChange™ PCR conditions such as dsDNA content, annealing temperature or incubation time. If QuikChange™ continues to prove challenging other site-directed mutagenesis methods could be trialled, and failing this plasmids containing the genes encoding for the mutants could be procured from Genscript Biotech. After the two BT-1033 enzyme mutants have been obtained, their abilities to convert unnatural glucosamine acceptor **6.2** and *O*-4-thiol-glucosamine acceptor **6.17** should be investigated (Scheme 7-3). If the BT-1033 alanine mutant possesses the predicted thioglycoligase activity then conversion of mannose-1-phosphate and *O*-4-thiol-glucosamine acceptor **6.17** to the wanted disaccharide (Scheme 7-3, reaction b) would be observed while no conversion of mannose-1-phosphate and unnatural glucosamine acceptor **6.2** (Scheme 7-3, reaction a) should be observed. The BT-1033 glycine mutant theoretically should show no conversion of either unnatural glucosamine acceptor **6.2** and *O*-4-thiol-glucosamine acceptor **6.17** (Scheme 7-3). There are wide-reaching implications associated with proving the thioglycoligase activity of BT-1033. In principle, if an acid/base alanine mutant of BT-1033 can function as a thioglycoligase, it is likely that acid/base alanine mutants of other GH-130s will also possess thioglycoligase activity, and this would lead to the development of reliable methods to synthesise a number of different thioglycosides. Thioglycosides have numerous applications as they offer a non-hydrolysable alternative to *O*-glycosides.



Scheme 7-3. Reaction scheme for the enzymatic conversion of a) mannose-1-phosphate and unnatural glucosamine acceptor **6.2** and b) mannose-1-phosphate and *O*-4-thiol-glucosamine acceptor **6.17**

## Chapter 8 Experimental

### 8.1 General experimental

#### 8.1.1 Non-chapter specific experimental procedures/information

The use of dry solvents is stated in individual methodologies. All dry solvents used were dried according to standard methods and solvents used for flash chromatography purposes were not dried prior to use. All chemical synthesis reactions were carried out in oven-dried glassware. Thin layer chromatography was carried out on Merck silica gel 60 F<sub>254</sub> pre-coated aluminium foil sheets and were visualised using UV light (254 nm) and stained with either a 5% sulphuric acid in EtOH stain (for sugars), Ninhydrin stain (for amines and BOC protected amines) and a PPh<sub>3</sub> stain followed by a Ninhydrin stain (for azides).

#### 8.1.2 Spectroscopic and spectrometric instruments and standard practices

<sup>1</sup>H-NMR (500 MHz) and <sup>13</sup>C-NMR (126 MHz) experiments were conducted using a Bruker AVIIIHD 500 instrument at The University of York Centre for Magnetic Resonance. <sup>1</sup>H-NMR (400 MHz) and <sup>13</sup>C-NMR (101 MHz) experiments were conducted using a JEOL 400 instrument at The University of York Centre for Magnetic Resonance. Me<sub>4</sub>Si was often used as an internal standard at either 0.1% or 1% when using chloroform-d as a NMR solvent. Multiplicities are given as singlet (s), doublet (d), triplet (t), doublet of doublets (dd), doublet of doublet of doublets (ddd), triplet of doublets (td), quartet of doublets (qd) or multiplet (m). Resonances were assigned using HH-COSY and CH-HSQC. All NMR chemical shifts (δ) were recorded in ppm and coupling constants (J) are reported in Hz. Topspin 4.0.6 and MestReNovax64 were primarily used for processing the spectral data. The notation of the chemical environments to which the <sup>1</sup>H and <sup>13</sup>C NMR data of mono- and disaccharides are assigned are described in Figure 8-1.

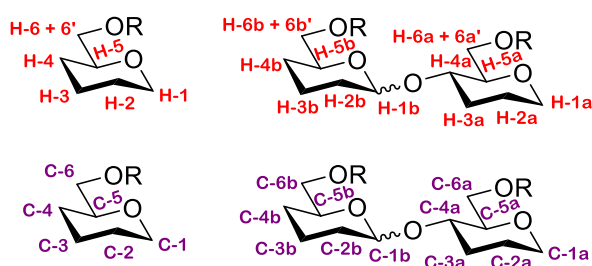


Figure 8-1. Proton and carbon numbering for <sup>1</sup>H NMR and <sup>13</sup>C NMR data for mono and disaccharides

UV-vis spectra were recorded using a nanodrop spectrophotometer (DeNovix). Fourier transform infrared (FTIR) spectra were recorded on a PerkinElmer UATR 2 spectrometer using the attenuated total reflectance (ATR) technique. Optical rotations were measured using a Bellingham and Stanley ADP 450 Automatic Digital Peltier Controlled Polarimeter equipped with a 589 nm LED.



## Experimental

Concentration is denoted as “c” and was calculated as grams per 100 millilitres (g / 100 mL) whereas the solvent is indicated in parenthesis (c, solvent).

ESI-MS experiments used for the characterisation of chemically synthesised molecules were conducted using a Bruker micrOTOF mass spectrometer coupled to an Agilent 1200 series LC system. More details regarding the ESI-LC/MS analysis of OPAL probes and enzymatically synthesised sugars can be found below.

### *ESI-LC/MS of OPAL probes and enzymatically synthesised sugars*

LC-MS analysis was performed on a Dionex UltiMate® 3000 Ci Rapid Separation LC system equipped with an UltiMate® 3000 photodiode array detector probing at 250-400 nm coupled to a HCT ultra ETD 11 (Bruker Daltonics) ion trap spectrometer, using Chromeleon® 6.80 SR12 software (ThermoScientific), Compass 1.3 for esquire HCT build 581.3, esquireControl version 6.2, Build 62.24 software (Bruker Daltonics) and Bruker compass HyStar 3.2-SR2, HyStar version 3.2, Build 44 software (Bruker Daltonics) at The University of York Centre of Excellence in Mass Spectrometry (CoEMS). Data analysis was performed using ESI compass 1.3 DataAnalysis, Version 4.4 software (Bruker Daltonics). All peptide/protein mass spectrometry was conducted in positive ion mode unless otherwise stated.

### *General analysis of OPAL probes (minus probe 3.13) and post ITag enzymatic reactions*

Samples were analysed using a Symmetry C18 5 µm 3.0 x 150 mm reverse-phase column. Water + 0.1% formic acid by volume (solvent A) and acetonitrile + 0.1% formic acid (solvent B) were used as a mobile phase at a flow rate of 300 µL min<sup>-1</sup> at room temperature. A multi-step gradient of 7.5 min was programmed as follows: 95% A for 1.0 min, followed by a linear gradient to 95% B over 6.5 min, followed by 95% B for an additional 1.0 min. A linear gradient to 95% A was used to equilibrate the column.

### *General analysis of enzymatically synthesised sugars*

Samples were analysed using a hydrophilic interaction chromatography (HILIC) column. Water + 0.1% formic acid by volume (solvent A) and acetonitrile + 0.1% formic acid (solvent B) were used as a mobile phase at a flow rate of 500 µL min<sup>-1</sup> at r.t. A multi-step gradient of 10.5 min was programmed as follows: 5% A for 2.5 min, followed by a linear gradient to 5% B over 6 min, followed by 5% B for an additional 1 min. A linear gradient to 5% A was used to equilibrate the column.

### *Other samples (notably probe 3.13)*

These samples were analysed without the use of a column. Analysis was performed at r.t. HPLC-grade water with 0.1% (v/v) formic acid (solvent A) and acetonitrile with 0.1% (v/v) formic acid (solvent B) were used as the mobile phase at a 1:1 ratio over the course of 3 min as follows: 50 µL min<sup>-1</sup> to 250 µL min<sup>-1</sup> for 1 min, 250 µL min<sup>-1</sup> for 1 min, followed by 1000 µL min<sup>-1</sup> for 1 min.

## Experimental

Samples made for LCMS were made using a 50% (v/v) HPLC grade water/acetonitrile, 1% formic acid solution.

### 8.1.3 Sodium dodecyl sulfate polyacrylamide gel electrophoresis (SDS-PAGE) analysis of proteins

SDS-PAGE was often used for the analysis of protein expression, purification and bio-conjugation experiments. A 10% acrylamide gel was used during colicin E9 expression purification and subsequent bio-conjugation experiments with colicin Ia and colicin E9, whereas a 12% acrylamide gel was used during the expression and purification of BT-1033. SDS-PAGE gels were poured in-house using a specialised kit. The recipes used to prepare the gels is shown in Table 25.

Table 25. The composition of the SDS-PAGE gels of varying acrylamide percentages. The resolving buffer is (1.5 M Tris-HCl, 0.4% SDS, pH 8.8). TEMED stands for Tetramethylethylenediamine.

Component	10% Acrylamide gel	12% Acrylamide gel
H <sub>2</sub> O / mL	4	3.2
Resolving buffer / mL	2.5	2.5
30% acrylamide stock / mL	3.3	4.2
20% ammonium persulfate solution / $\mu$ L	50	50
TEMED / $\mu$ L	10	10

Once set, a stacking gel was placed on top of the main gel, with a comb inserted to create sample lanes. The recipe for preparing the stacking gel is given in Table 26.

Table 26. The compositions of the stacking gel used during SDS-PAGE. Stacking buffer is (0.5 M Tris-HCl, 0.4% SDS, pH 6.8)

Component	Quantity
H <sub>2</sub> O / mL	3.2
Stacking buffer / mL	1.3
30% acrylamide stock / mL	0.5
20% ammonium persulfate solution / $\mu$ L	12.5
TEMED / $\mu$ L	8

Once the SDS PAGE gels were fully prepared, including stacker gel and sample lanes, the SDS PAGE gels were ready to be loaded with samples. Colicin Ia and E9 samples were mixed with a non-reducing buffer (2% SDS, 50 mM Tris-HCl, 0.1 % bromophenol, 10% glycerol) and boiled for 2 min prior to running on the SDS PAGE gel. BT-1033 samples were mixed with 5 x concentrated reducing buffer (10% SDS, 10 mM 2-mercaptoethanol, 20% glycerol, 200 mM Tris-HCl pH 6.8, 0.05% bromophenol

## Experimental

blue) and boiled for 5 min prior to running on the SDS-PAGE gel. The molecular weight markers used were "PageRuler Plus Prestained Protein Ladder" (ThermoScientific). Each gel was run at 200 V for 30-80 min in SDS running buffer (25 mM Tris, 192 mM Gly, pH not adjusted). Protein loading is noted in the captions of the relevant figures.

If the SDS PAGE gels were not being used in either lectin or Western blots they were fixed via gel emersion in a fixing solution (40% water, 50% EtOH, 10% AcOH) which was gently rocked for between 20-60 minutes. The fixed gels were then immersed in a solution of 0.1% Coomassie Brilliant Blue R-50 (in 40% water, 50% EtOH, 10% AcOH), and were gently rocked for between 20-60 minutes. The Coomassie stained gels were then destained via emersion in a destaining solution (50% water, 40% EtOH, 10% AcOH) and were gently rocked overnight with the solution replaced when saturated.

### 8.1.4 General procedure for running a lectin blot

The blots were assembled using 12 layers of blotting paper and one layer of nitrocellulose membrane which has previously been soaked in transfer buffer (25 mM Tris-HCl pH = 8.3, 192 mM glycine, 20% MeOH) for 10 minutes and a SDS-PAGE gel which had been run but not stained. The blots were assembled in the following order - 6 layers blotting paper, nitrocellulose membrane, 10% SDS-PAGE gel and 6 layers of blotting paper. The gels were transferred to the nitrocellulose membranes using a Trans-Blot®Turbo™ transfer system running at 1.3 A constant; up to 25 V for 30 minutes. The membranes were then incubated in 1 x PBS and 2% tween® 20 for 5 minutes with gentle rocking followed by two further washes with 1 x PBS (5 minutes with gentle rocking). The membranes were then incubated with 10 mL 1 x PBS containing 0.05% tween® 20 (Sigma Aldrich), 1 mM CaCl<sub>2</sub>, 1 mM MnCl<sub>2</sub> and 1 mM MgCl<sub>2</sub> and 5 pM lectin peroxidase (Sigma Aldrich). The blots were incubated at r.t. for 16 h and then incubated with 4 mL Amersham (Cytiva) for five minutes. Finally the blots were imaged using a Syngene G:BOX Chemi XRQ equipped with a Synoptic 4.0 MP camera, with GeneSyn software (Version 1.5.70).

### 8.1.5 General procedure for running a Western blot

The blots were assembled using 12 layers of blotting paper and one 10% SDS PAGE gel all previously soaked in transfer buffer (25 mM Tris-HCl pH = 8.3, 192 mM glycine, 20% MeOH) for 10 min. A further layer of Polyvinylidene difluoride (PVDF) membrane was used which had been soaked in methanol (30 seconds), water (30 seconds) and transfer buffer (25 mM Tris-HCl pH = 8.3, 192 mM glycine, 20% MeOH) (10 min). The blots were assembled in the following order - 6 layers blotting paper, PVDF membrane, 10% SDS PAGE gel and 6 layers of blotting paper. The gels were transferred to the PVDF membrane using a Trans-Blot®Turbo™ transfer system running at 1.3 A constant; up to 25 V for 30 minutes. The membranes were transferred to a 1 x PBS solution 5% milk solution and incubated overnight at 4 °C with gentle agitation. The membranes were incubated with either 2.5 µL (1 : 4000)

## Experimental

of HRP-Conjugated Streptavidin, (1.25 mg/mL, Thermo Scientific Pierce) or 500 ng of Biotin antibody (HRP) (GeneTex) for 1 h. The membranes were washed twice with 1 x PBS 0.1% tween® 20 (Sigma Aldrich) and once with 1 x PBS, all washes were performed for five minutes with gentle agitation. The blots were incubated with 4 mL of Amersham (Cytiva) for five minutes and the blots were imaged using a Syngene G:BOX Chemi XRQ equipped with a Synoptic 4.0 MP camera, with GeneSyn software (Version 1.5.70).

### 8.1.6 General method for Bradford assay

Thermo Scientific™ Pierce™ Coomassie Plus (Bradford) Assay Kit was used.

Standards of bovine serum albumin (BSA) were prepared between 1-25 µg/mL by diluting stock BSA into the relevant protein storage buffer for colicin Ia, colicin E9 and BT-1033. 150 µL of each standard/sample was mixed with 150 µL of Coomassie reagent and the samples were vortexed and incubated for 10 minutes at r.t.. The absorbance at 595 nm was measured for each standard and protein sample using a nanodrop spectrophotometer (DeNovix). The protein concentration was determined from a linear standard curve produced from the BSA standards.

### 8.1.7 General biological kits used

The kits listed below were used using the methods described in the manuals provided with the kits:

- Stellar™ competent cells (TakaRa)

- BL-21 (DE3) competent *E. coli* (New England Biolabs)

- QIA prep® spin miniprep kits (QIAGEN)

- BugBuster® Protein extraction reagent (Novagen)

### 8.1.8 Microscopy

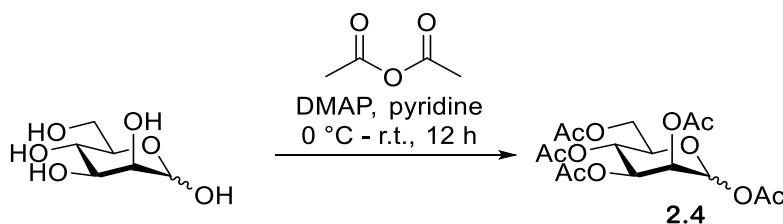
Samples were prepared in accordance with Experimental section 8.4.3, page 310. A 10 µL of each sample was taken from the bottom of each eppendorf and applied to a microscopy slide. A cover slip was applied and the samples were imaged (using phase contrast imaging) on a Nikon Eclipse Ti-E microscope equipped with a Mikrotron MC-1362 camera and an EPIX E4 frame grabber running EPIX PIXCI software.

## Experimental

### 8.2 Experimental for Chapter 2

#### 8.2.1 Synthesis of 4-methylphenyl 2-benzyl-4,6-*O*-benzylidene-3-*O*-*p*-methoxybenzyl-1-thio- $\alpha$ -D-mannopyranoside **2.2**

##### 8.2.1.1 Synthesis of *D*-mannose pentaacetate **2.4**<sup>375</sup>



Acetic anhydride (42 mL, 410 mmols) was added to a solution of D-mannose (20 g, 100 mmols) and DMAP (cat) in pyridine (42 mL) at 0 °C affording a cloudy white solution. The reaction mixture was warmed to r.t. and stirred for a further 12 h, affording a clear yellow solution. The solution was concentrated *in vacuo*, affording a caramel coloured oil, which was diluted with DCM (40 mL), washed with water (40 mL), 1 M HCl acid solution (40 mL) and saturated NaHCO<sub>3</sub> solution (40 mL). The solution was dried (MgSO<sub>4</sub>) and concentrated *in vacuo* to afford a caramel oil of **2.4** which was used crude in following reactions (35 g, 89 mmols, 80%); R<sub>f</sub> = 0.5 (2:1 Hexane : EtOAc).

<sup>1</sup>H NMR (400 MHz, CDCl<sub>3</sub>)  $\delta$  6.09 (d,  $J_{1,2}$  = 2.0 Hz, 1H, H-1), 5.35 (m, 2H, H-3, H-4), 5.27 (dd,  $J_{2,3}$  = 2.5 Hz,  $J_{1,2}$  = 2.0 Hz, 1H, H-2), 4.29 (dd,  $J_{6a,6b}$  = 12.4 Hz,  $J_{5,6a}$  = 4.8 Hz, 1H, H-6a), 4.11 (dd,  $J_{6a,6b}$  = 12.4 Hz,  $J_{5,6b}$  = 2.5 Hz, 1H, H-6b), 4.06 (m, 1H, H-5), 2.19 (s, 3H, CH<sub>3</sub> (OAc)), 2.18 (s, 3H, CH<sub>3</sub> (OAc)), 2.10 (s, 3H, CH<sub>3</sub> (OAc)), 2.06 (s, 3H, CH<sub>3</sub> (OAc)), 2.01 (s, 3H, CH<sub>3</sub> (OAc)).

<sup>13</sup>C NMR (101 MHz, CDCl<sub>3</sub>)  $\delta$  170.8 (1C), 170.2 (1C), 169.9 (1C), 169.7 (1C), 168.2 (1C), (C=O), 90.7 (1C, C-1), 70.7 (1C, C-5), 68.8 (1C, C-3/C-4), 68.4 (1, C-2), 65.6 (1C, C-3/ C-4), 62.2 (1C, C-6), 21.0 (1C, CH<sub>3</sub>), 20.9 (1C, CH<sub>3</sub>), 20.8 (1C, CH<sub>3</sub>), 20.8 (2C, CH<sub>3</sub>).

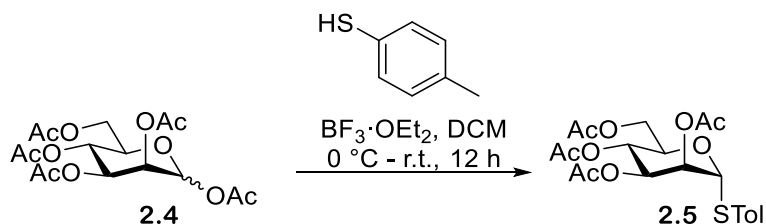
(ESI)HRMS – C<sub>16</sub>H<sub>22</sub>NaO<sub>11</sub><sup>+</sup> ([M+Na]<sup>+</sup>) requires m/z 413.1060: found m/z 413.1056

$[\alpha]_D^{25}$  = + 29.26 (c 1, DCM)

IR – 2973 (C-H), 1748 (C=O), 1370 (C-O), 1217 (C-O)

## Experimental

### 8.2.1.2 Synthesis of 4-methylphenyl 2,3,4,6-tetra-O-acetyl-1-thio- $\alpha$ -D-mannopyranoside **2.5** <sup>376</sup>



Due to the large quantity of starting material the reaction was performed in two batches, the procedure was the same for both.

$\text{BF}_3 \cdot \text{Et}_2\text{O}$  (1<sup>st</sup> batch = 11 mL, 48 mmols, 1.5 eq. 2<sup>nd</sup> batch = 19 mL, 86 mmols, 1.5 eq) was added dropwise to a solution of **2.4** (1<sup>st</sup> batch = 12 g, 32 mmols, 1 eq. 2<sup>nd</sup> batch = 22 g, 57 mmols) and 4-methylbenzenethiol (1<sup>st</sup> batch 5.2 g, 42 mmols, 1.3 eq. 2<sup>nd</sup> batch 9.2 g, 74 mmols, 1.3 eq) in dry DCM (50 mL) at 0 °C under  $\text{N}_2$ . The reaction mixture was warmed to r.t. and stirred for 12 h to afford a clear purple solution. The solution was washed with water (2 x 30 mL) and saturated  $\text{NaHCO}_3$  solution (30 mL), dried ( $\text{MgSO}_4$ ) and concentrated *in vacuo* to afford a caramel oil. The oil was purified using column chromatography eluting with a graduated solvent system of 2.5 : 1 hexane : EtOAc to 2 : 1 hexane : EtOAc. This afforded a caramel oil of **2.5** (25 g, 53 mmols, 62%);  $R_f = 0.54$  (1.5 : 1 Hexane : EtOAc).

$^1\text{H}$  NMR (400 MHz,  $\text{CDCl}_3$ )  $\delta$  7.38 (d,  $J_{\text{HAr}} = 7.9$  Hz, 2H, HAr), 7.12 (d,  $J_{\text{HAr}} = 7.9$  Hz, 2H, HAr), 5.49 (m, 1H, H-2), 5.41 (s, 1H, H-1), 5.32 (m, 2H, H-3, H-4), 4.55 (m, 1H, H-5), 4.30 (dd,  $J_{6a,6b} = 12.3$  Hz,  $J_{5,6a} = 5.7$  Hz, 1H, H-6a), 4.10 (dd,  $J_{6a,6b} = 12.3$  Hz,  $J_{5,6b} = 3.0$  Hz, 1H, H-6b), 2.32 (s, 3H,  $\text{CH}_3$  (STol)), 2.14 (s, 3H,  $\text{CH}_3$  (OAc)), 2.07 (s, 3H,  $\text{CH}_3$  (OAc)), 2.06 (s, 3H,  $\text{CH}_3$  (OAc)), 2.01 (s, 3H,  $\text{CH}_3$  (OAc)).

$^{13}\text{C}$  NMR (101 MHz,  $\text{CDCl}_3$ )  $\delta$  170.7 (s, 1C, C=O), 170.1 (s, 1C, C=O), 169.9 (s, 1C, C=O), 169.9 (s, 1C, C=O), 138.6, 132.8, 130.1, 128.9, (CAr), 86.1 (s, 1C, C-1), 70.9 (s, 1C, C-2), 69.5 (s, 1C, C-5), 69.5 (s, 1C, C-3/C-4), 66.5 (s, 1C, C-3/C-4), 62.6 (s, 1C, C-6), 21.3 (s, 1C,  $\text{CH}_3$  (STol)), 21.1 (s, 1C,  $\text{CH}_3$  (OAc)), 20.8 (s, 1C,  $\text{CH}_3$ , (OAc)), 20.8 (s, 1C,  $\text{CH}_3$  (OAc)), 20.7 (s, 1C,  $\text{CH}_3$  (OAc)).

Note that NMR does contain an impurity due to orthoester formation. The impurity is present in a ratio of 1: 0.1 desired product to impurity and cannot be removed by flash column chromatography as it has the same  $R_f$  as the product.

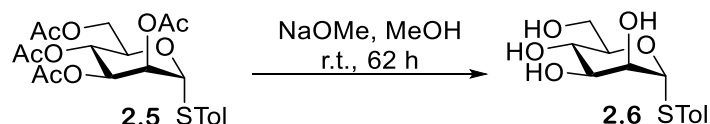
(ESI)HRMS –  $\text{C}_{21}\text{H}_{26}\text{NaO}_9\text{S}^+$  ( $[\text{M}+\text{Na}]^+$ ) requires  $m/z$  477.1195: found  $m/z$  477.1201

$[\alpha]_D^{25} = +84.1$  (c 1, DCM)

IR – 2943 (C-H), 1741 (C=O), 1214 (C-O)

## Experimental

### 8.2.1.3 Synthesis of 4-methylphenyl 1-thio- $\alpha$ -D-mannopyranoside **2.6**<sup>377</sup>



Due to the large quantity of starting material the reaction was performed in two batches, the procedure was the same for both.

NaOMe solution was added dropwise to a solution of **2.5** (1<sup>st</sup> batch = 13 g, 30 mmols, 1 eq, 2<sup>nd</sup> batch = 12 g, 26 mmols) in MeOH (40 mL) until pH 10 was reached, affording a colourless solution. The reaction mixture was stirred for 62 h at r.t. affording a colourless solution with a white precipitate. TLC examination showed that the precipitate in both batches and the solution of batch 1 was pure but the solution of batch 2 contained impurities. Both precipitates were collected *via* vacuum filtration and both solutions were neutralised using dowex, which was then removed *via* filtration. The filtrates were then combined with the solution of batch 1 and concentrated *in vacuo*, affording a white powder of **2.6**. The impure solution was purified by column chromatography, eluting with a graduated solvent system of 1 : 1 hexane : EtOAc to 7 : 1 DCM : MeOH affording a white powder of **2.6** (13 g, 44 mmols, 80%);  $R_f = 0.3$  (EtOAc) was extracted.

<sup>1</sup>H NMR (400 MHz, CDCl<sub>3</sub>)  $\delta$  7.41 (dd,  $J_{\text{HAr}} = 8.0$  Hz,  $J_{\text{HAr}} = 2.1$  Hz, 2H, HAr), 7.14 (dd,  $J_{\text{HAr}} = 8.0$  Hz,  $J_{\text{HAr}} = 2.1$  Hz, 2H, HAr), 5.35 (s, 1H, H-1), 4.63 (s, 3H, OH), 4.09 – 4.02 (m, 2H, H-2, H-5), 3.84-3.66 (m, 4H, H-3, H-4, H-6a, H-6b), 2.31 (s, 3H, CH<sub>3</sub>).

<sup>13</sup>C NMR (101 MHz, CDCl<sub>3</sub>)  $\delta$  137.6, 132.2, 130.7, 129.5, (CAr), 89.5 (1C, C-1), 74.2 (1C, C-5), 72.4 (1C, C-2), 71.8 (1C, C-4), 67.3 (1C, C-3), 61.3 (1C, C-6), 19.8 (1C, CH<sub>3</sub>).

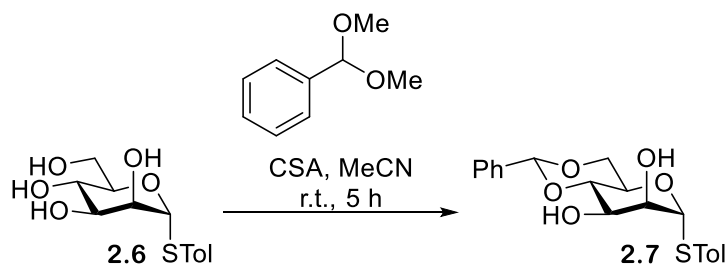
(ESI)HRMS – C<sub>13</sub>H<sub>18</sub>NaO<sub>5</sub>S<sup>+</sup> ([M+Na]<sup>+</sup>) requires m/z 309.0773: found m/z 309.0766

$[\alpha]_D^{25} = +215.3$  (c 1, MeOH)

IR- 3247 (O-H), 2904 (C-H), 1983 (C-H), 1491 (C=C), 1068 (C-O)

## Experimental

### 8.2.1.4 Synthesis of 4-methylphenyl 4,6-O-benzylidene-1-thio- $\alpha$ -D-mannopyranoside **2.7**<sup>378</sup>



Due to the large quantity of starting material the reaction was performed in two batches, the procedure was the same for both.

2,2 DMT (1<sup>st</sup> batch = 8.2 mL, 54 mmols, 2 eq, 2<sup>nd</sup> batch = 4.8 mL, 31 mmols, 2 eq) was added to a solution of **2.6** (8.1 g, 28 mmols, 1 eq / 4.7 g, 16 mmols) and CSA (approx. 0.61 g / 0.36 g) in dry MeCN at r.t. The reaction mixture was stirred for 5 h, affording a clear solution.  $\text{NEt}_3$  was added to quench the reaction and the solution was concentrated *in vacuo* to afford a white solid. This solid was purified using column chromatography eluting with a graduated solvent system of 22 : 1 DCM : MeOH to 16 : 1 DCM : MeOH, affording a white crystalline solid of **2.7** (10 g, 27 mmols, 61%);  $R_f = 0.52$  (1 : 1 Hexane : EtOAc).

*NMR*- Note that due to the presence of multiplets in the spectrum there was not enough information to determine which individual signal can be assigned to chemical environment H-3

$^1\text{H}$  NMR (400 MHz,  $\text{CDCl}_3$ )  $\delta$  7.47 (m, 2H, HAr), 7.37 (m, 5H, HAr), 7.18 (m, 2H, HAr), 5.63 (s, 1H, CHPh), 5.54 (d,  $J_{2,\text{OH}} = 4.2$  Hz, 1H, OH), 5.37 (d,  $J_{1,2} = 1.0$  Hz, 1H, H-1), 4.07 (m, 2H, H-3, H-5), 3.96 (m, 2H, H-2, H-4), 3.74 (m, 2H, H-6a/b), 2.29 (s, 3H,  $\text{CH}_3$ ).

$^{13}\text{C}$  NMR (101 MHz,  $\text{CDCl}_3$ ) 137.9, 137.3, 132.01, 129.93, 128.1, 126.4, (CAr), 101.2 (1C, CHPh), 89.7 (1C, C-1), 78.5 (1C, C4), 72.4 (1C, C-2), 68.1 (1C, C-6), 67.6 (1C, C-3/5), 65.2 (1C, C3/5), 20.7 (1C,  $\text{CH}_3$ ).  
(ESI)HRMS –  $\text{C}_{20}\text{H}_{22}\text{NaO}_5\text{S}^+$  ( $[\text{M}+\text{Na}]^+$ ) requires  $m/z$  397.1086: found  $m/z$  397.1077

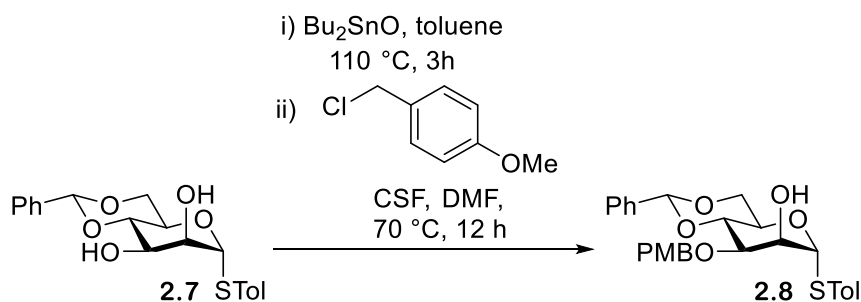
$[\alpha]_D^{25} = +167.2$  (c 1, DCM)

*IR* – 3217 (O-H), 2917 (C-H), 1986 (C-H), 1492 (C=C), 1087 (C-O)



## Experimental

### 8.2.1.5 Synthesis of 4-methylphenyl 4,6-O-benzylidene-3-O-p-methoxybenzyl-1-thio- $\alpha$ -D-mannopyranoside **2.8**



$\text{Bu}_2\text{SnO}$  (6.5 g, 26 mmols, 1.3 eq) was added to a solution of **2.7** (7.4 g, 20 mmols) in dry toluene at r.t affording a cloudy white solution. The solution was heated to  $110\text{ }^\circ\text{C}$  and refluxed for 3 hours, affording a colourless solution. The solution was concentrated *in vacuo*, affording a cloudy oil, which was dissolved in dry DMF. CSF (3.3 g, 22 mmols, 1.1 eq) was added and the solution was stirred for 5 minutes at which point PMBCl (3.5 mL, 26 mmols, 1.3 eq) was added affording a clear yellow solution. The solution was stirred at  $70\text{ }^\circ\text{C}$  for 12 h under  $\text{N}_2$ , affording a cloudy yellow solution. The solution was concentrated *in vacuo* to afford a yellow oil. The oil was diluted with DCM (50 mL), washed (2 x 50 mL water), dried ( $\text{MgSO}_4$ ) and concentrated *in vacuo* to afford a thick orange oil. This oil was purified using column chromatography, eluting with a graduated solvent system of 8 : 1 Hexane : EtOAc to 7 : 1 DCM : MeOH, affording a light yellow oil of **2.8** (8.1 g, 16 mmols, 83%);  $R_f = 0.54$  (2 : 1 Hexane : EtOAc)

$^1\text{H}$  NMR (500 MHz,  $\text{CDCl}_3$ )  $\delta$  7.51 (dd,  $J_{\text{HAr}} = 7.7\text{ Hz}$ ,  $J_{\text{HAr}} = 1.7\text{ Hz}$ , 2H, HAr Ph), 7.38 (m, 3H, HAr Ph), 7.33 (d,  $J_{\text{HAr}} = 8.1\text{ Hz}$ , 2H, HAr STol), 7.29 (d,  $J_{\text{HAr}} = 8.7\text{ Hz}$ , 2H, HAr PMB), 7.12 (d,  $J_{\text{HAr}} = 8.1\text{ Hz}$ , 2H, HAr STol), 6.88 (d,  $J_{\text{HAr}} = 8.7\text{ Hz}$ , 2H, HAr PMB), 5.61 (s, 1H, CHPh), 5.50 (d,  $J_{1,2} = 1.0\text{ Hz}$ , 1H, H-1), 4.81 (d,  $J_{\text{CH}_2} = 11.5\text{ Hz}$ , 1H,  $\text{CH}_2$ ), 4.66 (d,  $J_{\text{CH}_2} = 11.5\text{ Hz}$ , 1H,  $\text{CH}_2$ ), 4.34 (td,  $J_{5,6a} = 9.8\text{ Hz}$ ,  $J_{5,6b} = 9.8\text{ Hz}$ ,  $J_{4,5} = 4.8\text{ Hz}$ , 1H, H-5), 4.23 (dd,  $J_{2,3} = 3.8\text{ Hz}$ ,  $J_{1,2} = 1.0\text{ Hz}$ , 1H, H-2), 4.20 (dd,  $J_{3,4} = 10.0\text{ Hz}$ ,  $J_{4,5} = 4.8\text{ Hz}$ , 1H, H-4), 4.12 (dd,  $J_{5,6a} = 9.8\text{ Hz}$ ,  $J_{6a,6b} = 9.8\text{ Hz}$ , 1H, H-6a), 3.95 (dd,  $J_{3,4} = 10.0\text{ Hz}$ ,  $J_{2,3} = 3.8\text{ Hz}$ , 1H, H-3), 3.84 (dd,  $J_{5,6b} = 9.8\text{ Hz}$ ,  $J_{6a,6b} = 9.8\text{ Hz}$ , 1H, H-6b), 3.81 (s, 3H,  $\text{OCH}_3$ ), 2.84 (s, 1H, OH), 2.33 (s, 3H,  $\text{CH}_3$ ).

$^{13}\text{C}$  NMR (126 MHz,  $\text{CDCl}_3$ )  $\delta$  159.5, 138.0, 137.5, 132.4, 130.0, 129.8, 129.6, 129.4, 129.0, 128.2, 126.1, 114.0, (C-Ar), 101.6 (1C, CHPh), 88.1 (1C, C-1), 79.0 (1C, C-4), 75.4 (1C, C-3), 72.9 (1C,  $\text{CH}_2$ ), 71.3 (1C, C-2), 68.6 (1C, C-6), 64.5 (1C, C-5), 55.3 (1C,  $\text{OCH}_3$ ), 21.1 (1C,  $\text{CH}_3$ ).

(ESI)HRMS –  $\text{C}_{28}\text{H}_{30}\text{NaO}_6\text{S}^+$  ( $[\text{M}+\text{Na}]^+$ ) requires  $m/z$  517.1661: found  $m/z$  517.1665

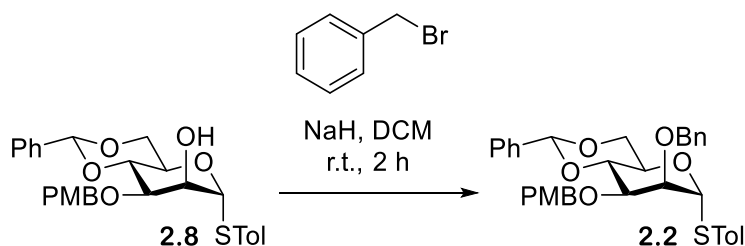
$[\alpha]_D^{25} = +158.4$  (c 1, DCM)

IR- 3425 (O-H), 2899 (C-H), 1979 (C-H), 1512 (C=C), 1085 (C-O)

No literature reference for characterisation could be found

## Experimental

### 8.2.1.6 Synthesis of 4-methylphenyl 2-benzyl-4,6-O-benzylidene-3-O-p-methoxybenzyl-1-thio- $\alpha$ -D-mannopyranoside **2.2**



NaH (0.32 g, 13 mmols, 1.5 eq) was added to a solution of **2.8** (3.7 g, 9.0 mmols) in dry DMF (20 mL) at 0 °C and the resultant mixture stirred for 5 minutes. BnBr (1.6 mL, 13 mmols, 1.5 eq) was then added dropwise and the resultant solution was stirred at r.t. for 2 h, affording a clear solution. The solution was concentrated *in vacuo*, diluted with DCM, washed with water (20 mL), dried (MgSO<sub>4</sub>) and concentrated *in vacuo* to afford a colourless oil. The oil was purified by column chromatography, eluting with a graduated solvent system of 15 : 1 Hexane : EtOAc to 3 : 1 Hexane : EtOAc, affording a colourless oil of **2.2** (1.9 g, 3.3 mmols, 36%); *R<sub>f</sub>* = 0.84 (2 : 1 Hexane : EtOAc).

<sup>1</sup>H NMR (500 MHz, CDCl<sub>3</sub>)  $\delta$  7.52 (dd, *J*<sub>HAr</sub> = 7.8 Hz, *J*<sub>HAr</sub> = 1.6 Hz, 2H, HAr), 7.30 (m, 12H, HAr), 7.10 (d, *J*<sub>HAr</sub> = 8.0 Hz, 2H, HAr), 6.86 (dd, *J*<sub>HAr</sub> = 6.6 Hz, *J*<sub>HAr</sub> = 2.0 Hz, 2H, HAr), 5.64 (s, 1H, CHPh), 5.41 (d, *J*<sub>1,2</sub> = 1.3 Hz, 1H, H-1), 4.73 (d, *J*<sub>CH2</sub> = 11.8 Hz, 1H, CH<sub>2</sub>), 4.70 (s, 2H, CH<sub>2</sub>), 4.58 (d, *J*<sub>CH2</sub> = 11.8 Hz, 1H, CH<sub>2</sub>), 4.28 (m, 1H, H-3), 4.27 (m, 1H, H-5), 4.21 (dd, *J*<sub>6a,6b</sub> = 10.0 Hz, *J*<sub>5,6a</sub> = 4.3 Hz, 1H, H-6a), 3.98 (dd, *J*<sub>2,3</sub> = 3.2 Hz, *J*<sub>1,2</sub> = 1.3 Hz, 1H, H-2), 3.95 (dd, *J*<sub>3,4</sub> = 3.2 Hz, *J*<sub>4,5</sub> = 9.6 Hz, 1H, H-4), 3.87 (m, 1H, H-6b), 3.81 (s, 3H, OCH<sub>3</sub>), 2.31 (s, 3H, CH<sub>3</sub>).

<sup>13</sup>C NMR (126 MHz, CDCl<sub>3</sub>)  $\delta$  159.3, 138.0, 137.8, 137.7, 132.3, 130.5, 129.9, 129.4, 128.9, 128.4, 128.2, 128.1, 127.8, 126.1, 113.8, (CAr), 101.5 (1C, CHPh), 87.5 (1C, C-1), 79.1 (1C, C-3), 78.0 (1C, C-2), 75.8 (C-4), 73.0 (1C, CH<sub>2</sub>), 72.7 (1C, CH<sub>2</sub>), 68.6 (1C, C-6), 65.4 (1C, C-5), 55.3 (1C, OCH<sub>3</sub>), 21.1 (1C, CH<sub>3</sub>).

(ESI)HRMS – C<sub>35</sub>H<sub>37</sub>O<sub>6</sub>S<sup>+</sup> ([M+H]<sup>+</sup>) requires *m/z* 585.2311: found *m/z* 585.2310.

$[\alpha]_D^{20} = +100.14$  (*c* 1, CHCl<sub>3</sub>)

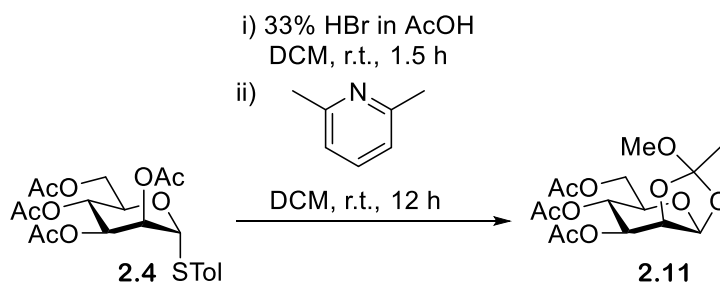
IR – 3032 (C-H), 2918 (C-H), 1959 (C-H), 1611 (C=C), 1087 (C-O), 1042 (C-O).

No literature reference for characterisation could be found

## Experimental

### 8.2.2 Synthesis of 4-methylphenyl 2-*O*-acetyl-3,4,6-tri-*O*-benzyl-1-thio- $\alpha$ -D-mannopyranoside **2.1a** and 4-methylphenyl 2-*O*-benzoyl-3,4,6-tri-*O*-benzyl-1-thio- $\alpha$ -D-mannopyranoside **2.1b**

#### 8.2.2.1 Synthesis of 3,4,6-tri-*O*-acetyl-1,2-*O*-(1-methoxyethylidene)- $\beta$ -D-mannopyranose **2.11** <sup>379</sup>



A solution of 33% hydrobromic acid in acetic acid (51 mL) was added dropwise to a solution of **2.4** (17 g, 44 mmols) in dry DCM (50 mL) at r.t., affording a yellow solution. The solution was stirred for 1.5 hours, then a mixture of ice and water (40 mL) was added to the solution. The aqueous layer of the solution was washed with DCM (2 x 40 mL) and the combined organic extractions were washed with saturated NaHCO<sub>3</sub> solution (2 x 40 mL), dried (MgSO<sub>4</sub>) and concentrated *in vacuo*, affording a yellow oil of the crude bromine. 2,6 lutidene (10 mL) was added dropwise over a 5-minute period to the solution of the crude bromine in dry DCM (50 mL) and dry MeOH (50 mL). The reaction mixture was stirred at r.t for 12 h, affording a yellow solution. The solution was diluted with DCM (50 mL), washed with saturated NaHCO<sub>3</sub> solution (2 x 100 mL), CuSO<sub>4</sub> solution (2 x 100 mL) and water (50 mL), dried (MgSO<sub>4</sub>) and concentrated *in vacuo*, affording an off-white solid. The solid was wash with diethyl ether affording a white solid of **2.11** (8.2 g, 23 mmols, 51%); R<sub>f</sub> = 0.60 (2: 1 Hexane : EtOAc).

<sup>1</sup>H NMR (500 MHz, CDCl<sub>3</sub>)  $\delta$  5.50 (d,  $J_{1,2}$  = 2.5 Hz, 1H, H-1), 5.30 (dd,  $J_{3,4}$  = 9.7 Hz,  $J_{4,5}$  = 9.7 Hz, 1H, H-4), 5.15 (dd,  $J_{3,4}$  = 9.7 Hz,  $J_{2,3}$  = 4.0 Hz, 1H, H-3), 4.62 (dd,  $J_{2,3}$  = 4.0 Hz,  $J_{1,2}$  = 2.5 Hz, 1H, H-2), 4.24 (dd,  $J_{6a,6b}$  = 12.1 Hz,  $J_{5,6a}$  = 4.8 Hz, 1H, H-6a), 4.15 (dd,  $J_{6a,6b}$  = 12.1 Hz,  $J_{5,6b}$  = 2.6 Hz, 1H, H-6b), 3.68 (ddd,  $J_{4,5}$  = 9.7 Hz,  $J_{5,6a}$  = 4.8 Hz,  $J_{5,6b}$  = 2.6 Hz, 1H, H-5), 3.28 (s, 3H, OCH<sub>3</sub>), 2.12 (s, 3H, CH<sub>3</sub>), 2.07 (s, 3H, CH<sub>3</sub>), 2.05 (s, 3H, CH<sub>3</sub>), 1.74 (s, 3H, CH<sub>3</sub>).

<sup>13</sup>C NMR (126 MHz, CDCl<sub>3</sub>)  $\delta$  170.6 (1C), 170.4 (1C), 169.4 (1C), (C=O), 124.5 (1C, C), 97.4 (1C, C-1), 76.6 (1C, C-2), 71.3 (1C, C-5), 70.6 (1C, C-3), 65.5 (1C, C-4), 62.3 (1C, C-6), 49.9 (1C, OCH<sub>3</sub>), 24.3 (1C, CH<sub>3</sub>), 20.7 (1C, CH<sub>3</sub>), 20.7 (1C, CH<sub>3</sub>), 20.6 (1C, CH<sub>3</sub>).

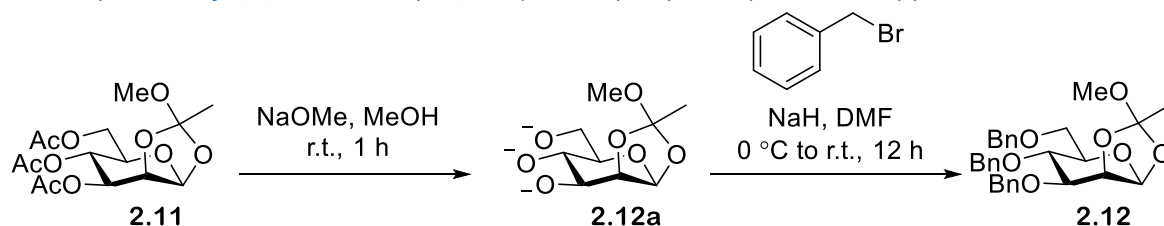
(ESI)HRMS - C<sub>15</sub>H<sub>22</sub>NaO<sub>10</sub><sup>+</sup> ([M+Na]<sup>+</sup>) requires m/z 385.1111: found m/z 385.1120

$[\alpha]_D^{25}$  = - 12.2 (c 1, DCM)

IR – 2958 (C-H), 1967 (C-H), 1736 (C=O), 1209 (C-O) 1051 (C-O)

## Experimental

### 8.2.2.2 Synthesis of 3,4,6-tri-O-benzyl-1,2-O-(methoxyethylidene)- $\beta$ -D-mannopyranose **2.12**<sup>379</sup>



NaOMe solution was added dropwise to a solution of **2.11** (8.2 g, 23 mmols) in MeOH (40 mL) until pH 10 was reached, affording a clear solution. The reaction mixture was stirred for 1 h at r.t. and subsequently concentrated *in vacuo*. This afforded a white foamy solid of **2.12a** which was dried *via* vacuum for 30 minutes before being dissolved in dry DMF and cooled to 0 °C. NaH (3.2 g, 140 mmols, 6 eq) was added to the solution of **2.12a** and stirred at 0 °C for 10 minutes. BnBr (16 mL, 140 mmols, 6 eq) was then added dropwise, affording a light yellow solution. This solution was warmed to r.t. and stirred for 12 h. The solution was then diluted with MeOH and contracted *in vacuo* to afford a caramel coloured oil. The oil was dissolved in DCM and washed with water (40 mL) and saturated NaCl solution (40 mL), dried (MgSO<sub>4</sub>) and concentrated *in vacuo* to afford a caramel coloured oil. This oil was purified by column chromatography, eluting with a graduated solvent system of 10 : 1 Hexane : EtOAc to 4 : 1 Hexane : EtOAc, affording white crystals of **2.12** (5.8 g, 12 mmols, 50%); R<sub>f</sub> = 0.42 (2 : 1 Hexane : EtOAc).

<sup>1</sup>H NMR (500 MHz, CDCl<sub>3</sub>)  $\delta$  7.39 (dd,  $J_{\text{HAr}} = 8.0$  Hz,  $J_{\text{HAr}} = 1.5$  Hz, 2H, HAr), 7.32 (m, 6H, HAr), 7.29 (m, 4H, HAr), 7.27 (m, 1H, HAr), 7.23 (dd,  $J_{\text{HAr}} = 7.5$  Hz,  $J_{\text{HAr}} = 1.5$  Hz, 2H, HAr), 5.34 (d,  $J_{1,2} = 2.5$  Hz, 1H, H-1), 4.90 (d,  $J_{\text{CH}_2} = 10.8$  Hz, 1H, CH<sub>2</sub>), 4.78 (d,  $J_{\text{CH}_2} = 1.52$  Hz, 2H, CH<sub>2</sub>), 4.60 (dd,  $J_{\text{CH}_2} = 11.0$  Hz,  $J_{\text{CH}_2} = 3.0$  Hz, 2H, CH<sub>2</sub>), 4.54 (d,  $J_{\text{CH}_2} = 12.6$  Hz, 1H, CH<sub>2</sub>), 4.40 (dd,  $J_{2,3} = 3.9$  Hz,  $J_{1,2} = 2.5$  Hz, 1H, H-2), 3.92 (dd,  $J_{3,4} = 9.4$  Hz,  $J_{3,4} = 9.4$  Hz, 1H, H-4), 3.72 (m, 3H, H-3, H-6a, H-6b), 3.42 (ddd,  $J_{4,5} = 9.4$  Hz,  $J_{5,6a} = 4.7$  Hz,  $J_{5,6b} = 2.6$  Hz, 1H, H-5), 3.28 (s, 3H, OCH<sub>3</sub>), 1.73 (s, 3H, CH<sub>3</sub>).

<sup>13</sup>C NMR (126 MHz, CDCl<sub>3</sub>)  $\delta$  138.2, 137.8, 128.5, 128.4, 128.3, 128.0, 128.0, 127.8, 127.5, 127.5, (CAr), 124.0 (1C, C), 97.6 (1C, C-1), 79.0 (1C, C-3), 77.1 (1C, C-2), 75.2 (1C, CH<sub>2</sub>), 74.2 (1C, C-4), 74.2 (1C, C-5), 73.4 (1C, CH<sub>2</sub>), 72.4 (1C, CH<sub>2</sub>), 69.0 (1C, C-6), 49.8 (1C, OCH<sub>3</sub>), 24.4 (1C, CH<sub>3</sub>).

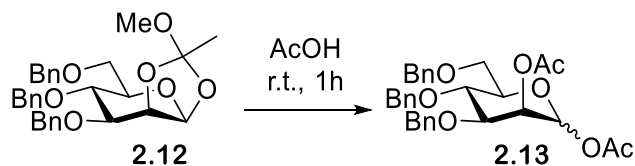
(ESI)HRMS - C<sub>30</sub>H<sub>34</sub>NaO<sub>7</sub><sup>+</sup> ([M+Na]<sup>+</sup>) requires m/z 529.2202: found m/z 529.2211

$[\alpha]_D^{25} = +12.1$  (c 1, DCM)

IR – 2900 (C-H), 1967 (C-H), 1453 (C=C), 1026 (C-O)

## Experimental

### 8.2.2.3 Synthesis 1,2-di-O-acetyl-3,4,6-tri-O-benzyl- $\alpha$ -D-mannopyranoside **2.13**<sup>380</sup>



**1.12** (5.8 g, 12 mmols) was dissolved in AcOH (40 mL) and the solution was stirred at r.t. for 1 h, affording a clear solution. The solution was concentrated *in vacuo* to afford a clear oil. This oil was diluted with EtOAc, washed with water (40 mL), dried (MgSO<sub>4</sub>) and concentrated *in vacuo*, affording a clear oil of **1.13** (5.2 g, 9.6 mmols, 84%); R<sub>f</sub> = 0.60 (2 : 1 Hexane : EtOAc).

<sup>1</sup>H NMR (400 MHz, CDCl<sub>3</sub>)  $\delta$  7.31 (m, 13H, HAr), 7.16 (dd,  $J_{\text{HAr}} = 7.0$ ,  $J_{\text{HAr}} = 2.2$  Hz, 2H, HAr), 6.12 (d,  $J_{1,2} = 2.0$  Hz, 1H, H-1), 5.36 (dd,  $J_{1,2} = 2.0$  Hz,  $J_{2,3} = 2.0$  Hz, 1H, H-2), 4.86 (d,  $J_{\text{CH}_2} = 10.6$  Hz, 1H, CH<sub>2</sub>), 4.73 (d,  $J_{\text{CH}_2} = 11.1$  Hz, 1H, CH<sub>2</sub>), 4.68 (d,  $J_{\text{CH}_2} = 12.0$  Hz, 1H, CH<sub>2</sub>), 4.52 (m, 3H, CH<sub>2</sub>), 3.97 (m, 2H, H-3,4), 3.82 (m, 2H, H-5,6a), 3.69 (dd,  $J_{6a,6b} = 10.7$  Hz,  $J_{5,6b} = 1.24$  Hz, 1H, H-6b), 2.17 (s, 3H, CH<sub>3</sub>), 2.07 (s, 3H, CH<sub>3</sub>).

<sup>13</sup>C NMR (101 MHz, CDCl<sub>3</sub>)  $\delta$  170.3 (1C, C=O), 168.6 (1C, C=O), 138.2 (2C), 137.8, 128.6, 128.5, 128.5, 128.3, 128.1, 128.1, 128.0, 128.0, 127.8, (C-Ar), 91.4 (1C, C-1), 77.8 (1C, C-3), 75.5 (1C, CH<sub>2</sub>), 73.9 (1C, CH<sub>2</sub>), 73.8 (1C, C-5), 73.7 (1C, C-4), 72.1 (1C, CH<sub>2</sub>), 68.6 (1C, C-6), 67.6 (1C, C-2), 21.2 (1C, CH<sub>3</sub>), 21.1 (1C, CH<sub>3</sub>).

(ESI)HRMS - C<sub>30</sub>H<sub>34</sub>NaO<sub>7</sub><sup>+</sup> ([M+Na]<sup>+</sup>) requires m/z 557.2151: found m/z 557.2163

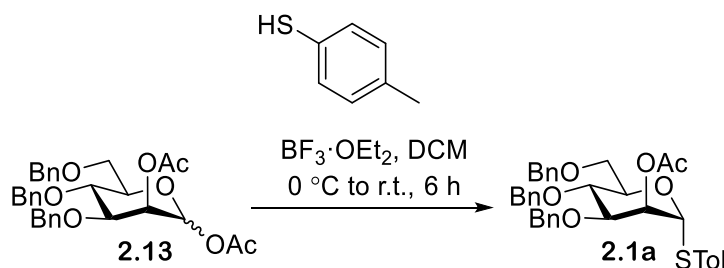
$[\alpha]_D^{25} = +8.6$  (c 0.25, DCM)

IR – 2920 (C-H), 1976 (C-H), 1747 (C=O), 1496 (C=C), 1214 (C-O), 1100 (C-O)

## Experimental

### 8.2.2.4 Synthesis of 4-methylphenyl 2-O-acetyl-3,4,6-tri-O-benzyl-1-thio- $\alpha$ -D-mannopyranoside **2.1a**

381



The reaction was performed in two batches the same procedure was used for both.

$\text{BF}_3 \cdot \text{Et}_2\text{O}$  (batch 1 = 3 mL, 15 mmols, 1.5 eq, batch 2 = 1.5 mL, 5 mmols, 1.5 eq) was added dropwise to a solution of **2.13** (batch 1 = 5.2 g, 9.7 mmols, 1 eq, batch 2 = 1.8 g, 3.3 mmols) and 4-methylbenzenethiol (batch 1 = 1.6 g, 13 mmols, 1.3 eq, batch 2 = 0.54 g, 4.3 mmols, 1.3 eq) in dry DCM at 0 °C under  $\text{N}_2$ , affording a clear light orange solution. The reaction mixture was warmed to r.t. and stirred for 6 h, affording a clear orange/ pink solution. The solution was washed with water (2 x 40 mL) and saturated  $\text{NaHCO}_3$  solution (40 mL), dried ( $\text{MgSO}_4$ ) and concentrated *in vacuo* to afford a light orange oil. The oil was purified by column chromatography, eluting with a solvent system of 3 : 1 hexane : EtOAc, affording a light yellow oil of **2.1a** (3.5 g, 5.8 mmols, 45%);  $R_f = 0.82$  (2 : 1 Hexane : EtOAc).

The product is mixed with ortho ester (from which it could not be separated) in a 1 : 0.2 ratio.

$^1\text{H}$  NMR (500 MHz,  $\text{CDCl}_3$ )  $\delta$  7.32 (m, 15H, HAr), 7.19 (dd,  $J_{\text{HAr}} = 7.9$  Hz,  $J_{\text{HAr}} = 1.8$  Hz, 15H, 2H, HAr), 7.04 (dd,  $J_{\text{HAr}} = 8.0$  Hz, 2H, HAr), 5.59 (dd,  $J_{1,2} = 1.7$  Hz,  $J_{2,3} = 1.7$  Hz, 1H, H-2), 5.45 (d,  $J_{1,2} = 1.7$  Hz, 1H, H-1), 4.88 (d,  $J_{\text{CH}_2} = 10.8$  Hz, 1H,  $\text{CH}_2$ ), 4.72 (d,  $J_{\text{CH}_2} = 11.2$  Hz, 1H,  $\text{CH}_2$ ), 4.65 (d,  $J_{\text{CH}_2} = 12.0$  Hz, 1H,  $\text{CH}_2$ ), 4.56 (d,  $J_{\text{CH}_2} = 11.2$  Hz, 1H,  $\text{CH}_2$ ), 4.51 (d,  $J_{\text{CH}_2} = 10.8$  Hz, 1H,  $\text{CH}_2$ ), 4.45 (d,  $J_{\text{CH}_2} = 12.0$  Hz, 1H,  $\text{CH}_2$ ), 4.34 (m, 1H, H-5), 3.94 (m, 2H, H-4, H-3), 3.85 (dd,  $J_{6a,6b} = 10.8$  Hz,  $J_{5,6a} = 5.0$  Hz, 1H, H-6a), 3.72 (dd,  $J_{6a,6b} = 10.8$  Hz,  $J_{5,6b} = 2.0$  Hz, 1H, H-6b), 2.30 (s, 3H,  $\text{CH}_3$ ), 2.13 (s, 3H,  $\text{CH}_3$ ).

$^{13}\text{C}$  NMR (126 MHz,  $\text{CDCl}_3$ )  $\delta$  171.7 (C=O), 139.7, 139.6, 139.2, 139.0, 133.7, 131.2, 129.8, 129.7, 129.6, 129.5, 129.2, 129.2, 129.1, 129.0, 128.9, (CAr), 87.9 (1C, C-1), 79.8 (1C, C-3), 76.6 (1C,  $\text{CH}_2$ ), 75.9 (1C, C-4), 74.7 (1C,  $\text{CH}_2$ ), 73.8 (1C, C-5), 73.2 (1C,  $\text{CH}_2$ ), 71.7 (1C, C-2), 70.3 (1C, C-6), 22.4 (2C, 2 x  $\text{CH}_3$ ).

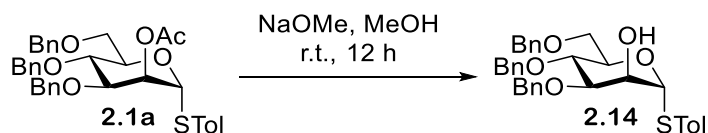
(ESI)HRMS -  $\text{C}_{36}\text{H}_{38}\text{NaO}_6\text{S}^+$  ( $[\text{M}+\text{Na}]^+$ ) requires  $m/z$  621.2287: found  $m/z$  621.2296

$[\alpha]_D^{25} = +34.7$  (c 1, DCM)

IR – 2864 (C-H), 1742 (C=O), 1494 (C=C), 1228 (C-O), 1087 (C-O)

## Experimental

### 8.2.2.5 Synthesis of 4-methylphenyl 3,4,6-tri-O-benzyl-1-thio- $\alpha$ -D-mannopyranoside **2.14**<sup>381</sup>



A NaOMe solution was added dropwise to a solution of **2.1a** (3.5 g, 5.8 mmols) in MeOH (20 mL) until pH 10 was reached, affording a clear solution. The solution was stirred at r.t. for 12 h, neutralised with dowex and concentrated *in vacuo*, affording a white solid of **2.14** (2.9 g, 5.3 mmols, 89%);  $R_f = 0.67$  (2 : 1 Hexane : EtOAc).

$^1\text{H}$  NMR (500 MHz,  $\text{CDCl}_3$ )  $\delta$  7.35 (m, 7H, HAr), 7.30 (m, 8H, HAr), 7.20 (m, 2H, HAr), 7.04 (d,  $J_{\text{HAr}} = 8.2$  Hz, 2H, HAr), 5.53 (d,  $J_{1,2} = 1.5$  Hz, 1H, H-1), 4.84 (d,  $J_{\text{CH}_2} = 10.8$  Hz, 1H,  $\text{CH}_2$ ), 4.70 (d,  $J_{\text{CH}_2} = 2.6$  Hz,  $\text{CH}_2$ ), 4.60 (d,  $J_{\text{CH}_2} = 12.0$  Hz,  $\text{CH}_2$ ), 4.53 (d,  $J_{\text{CH}_2} = 10.8$  Hz, 1H,  $\text{CH}_2$ ), 4.44 (d,  $J_{\text{CH}_2} = 12.0$  Hz,  $\text{CH}_2$ ), 4.31 (ddd,  $J_{4,5} = 9.5$  Hz,  $J_{5,6a} = 4.6$  Hz,  $J_{5,6b} = 1.8$  Hz, 1H, H-5), 4.24 (dd,  $J_{2,3} = 3.0$  Hz,  $J_{1,2} = 1.5$  Hz), 1H, H-2), 3.90 (m, 2H, H-3, H-4), 3.79 (dd,  $J_{6a,6b} = 10.8$  Hz,  $J_{5,6a} = 4.6$  Hz), 1H, H-6a), 3.68 (dd,  $J_{6a,6b} = 10.8$  Hz,  $J_{5,6b} = 1.8$  Hz, 1H, H-6b), 2.29 (s, 3H,  $\text{CH}_3$ ).

$^{13}\text{C}$  NMR (126 MHz,  $\text{CDCl}_3$ )  $\delta$  138.2, 138.2, 137.7, 137.6, 132.2, 129.9, 129.8, 128.6, 128.4, 128.3, 128.1, 128.0, 127.9, 127.8, 127.7, 127.6, (CAr), 87.7 (1C, C-1), 80.3 (1C, C-3), 75.2 (1C,  $\text{CH}_2$ ), 74.5 (1C,  $\text{CH}_2$ ), 73.4 (1C,  $\text{CH}_2$ ), 72.2 (1C, C-5), 72.1 ( $\text{CH}_2$ ), 69.8 (1C, C-2), 68.8 (1C, C-6), 21.1 (1C,  $\text{CH}_3$ ).

(ESI)HRMS -  $\text{C}_{34}\text{H}_{36}\text{NaO}_5\text{S}^+$  ( $[\text{M}+\text{Na}]^+$ ) requires  $m/z$  579.2181: found  $m/z$  579.2136

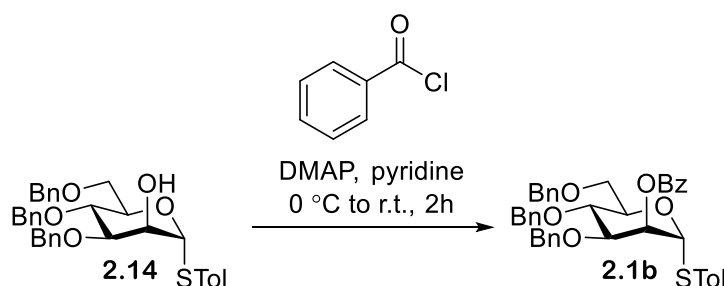
$[\alpha]_D^{25} = +200.5$  (c 1, DCM)

IR – 3406.85 (O-H), 2867 (C-H), 1972 (C-H), 1493 (C=C), 1084 (C-O)

## Experimental

### 8.2.2.6 Synthesis of 4-methylphenyl 2-O-benzoyl-3,4,6-tri-O-benzyl-1-thio- $\alpha$ -D-mannopyranoside **2.1b**

382



Benzoyl chloride was added to a solution of **2.14** (5.7 g, 0.01 mmols) and DMAP (cat) in pyridine (50 mL) at 0 °C. The reaction mixture was stirred at r.t. for 2 h, affording a clear solution. The solution was concentrated *in vacuo*, diluted with DCM, washed with water (2 x 50 mL), 1 M HCl (50 mL), saturated NaHCO<sub>3</sub> solution (50 mL) and saturated NaCl solution (50 mL). The solution was dried (MgSO<sub>4</sub>) and concentrated *in vacuo*, affording a light-yellow oil. The oil was purified by column chromatography, eluting with a solvent system of 7 : 1 hexane : EtOAc. This afforded a light yellow oil of **2.1b** (4.2 g, 6.4 mmols, 78%); R<sub>f</sub> = 0.8 (2 : 1 Hexane : EtOAc).

<sup>1</sup>H NMR (500 MHz, CDCl<sub>3</sub>)  $\delta$  8.13 (d,  $J_{\text{HAr}} = 7.7$  Hz, 2H, HAr), 7.55 (t,  $J_{\text{HAr}} = 7.5$  Hz, 1H, HAr), 7.41 (m, 6H, HAr), 7.28 (m, 11H, HAr), 7.19 (d,  $J_{\text{HAr}} = 7.6$  Hz, 2H, HAr), 7.02 (d,  $J_{\text{HAr}} = 7.8$  Hz, 2H, HAr), 6.02 (m, 1H, H-2), 4.86 (m, 3H, 2x CH<sub>2</sub>, H-1), 4.75 (d,  $J_{\text{CH}_2} = 11.8$  Hz, 1H, CH<sub>2</sub>), 4.60 (d,  $J_{\text{CH}_2} = 11.8$  Hz, 1H, CH<sub>2</sub>), 4.55 (dd,  $J_{\text{CH}_2} = 12.2$  Hz,  $J_{\text{CH}_2} = 12.2$  Hz, 2H, CH<sub>2</sub>), 3.95 (dd,  $J_{3,4} = 9.3$  Hz,  $J_{4,5} = 9.3$  Hz, 1H, H-4), 3.88 (d,  $J_{6a/6b, 5} = 2.5$  Hz, 2H, H6a, H6b), 3.76 (dd,  $J_{3,4} = 9.3$  Hz,  $J_{2,3} = 2.8$  Hz, 1H, H-3), 3.60 (m, 1H, H-5), 2.26 (s, 3H, CH<sub>3</sub>).

<sup>13</sup>C NMR (126 MHz, CDCl<sub>3</sub>)  $\delta$  165.8 (1C, C=O), 138.6, 138.2, 137.7, 137.6, 133.1, 132.0, 130.3, 130.2, 129.7, 128.3, 128.3, 128.3, 128.2, 128.0, 127.7, 127.7, 127.5, 127.4, (CAr), 85.7 (1C, C-1), 81.5 (1C, C-3), 79.9 (1C, C-5), 75.3 (1C, CH<sub>2</sub>), 74.1 (1C, C-4), 73.4 (1C, CH<sub>2</sub>), 71.6 (1C, CH<sub>2</sub>), 70.7 (1C, C-2), 69.4 (1C, C-6), 21.1 (1C, CH<sub>3</sub>).

(ESI)HRMS -C<sub>41</sub>H<sub>40</sub>NaO<sub>6</sub>S<sup>+</sup> ([M+Na]<sup>+</sup>) requires m/z 683.2443: found m/z 683.2466

$[\alpha]_D^{25} = -51.31$  (c 1, DCM)

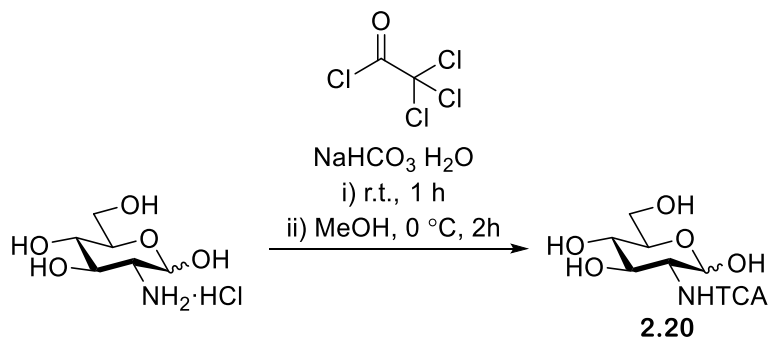
IR – 3030 (C-H), 2864 (C-H), 1984 (C-H), 1720 (C=O), 1493 (C=C), 1451 (C=C), 1266 (C-O), 1089 (C-O).



## Experimental

### 8.2.3 Synthesis of 4-methylphenyl 3,6-di-O-benzyl-2-deoxy-2-N-trichloroacetamido-1-thio-β-D-glucopyranoside **2.26**

#### 8.2.3.1 Synthesis of 2-deoxy-2-trichloroacetamido-α/β-D-glucopyranose **2.20**<sup>240</sup> method 1



Trichloroacetyl chloride (7.8 mL, 80 mmols, 1.5 eq) was added dropwise to a solution of D-glucosamine hydrochloride (10 g, 47 mmols) and NaHCO<sub>3</sub> (12 g, 140 mmols, 3 eq) in water (100 mL) over an hour period, affording a clear solution. The reaction mixture was stirred at r.t. or 1 h. The solution was concentrated *in vacuo*, affording a wet white powder. The powder was diluted with MeOH (100mL) and the resulting mixture stirred for 2 h at 0 °C, after which time a white precipitate could be observed suspended within the solution. The solution was filtered *via* vacuum, removing the white precipitate. The filtrate was concentrated *in vacuo*, affording a white foam of **2.20**. **2.20** was used crude in its subsequent reaction.

Note that due to some salt remaining in the product an accurate mass or percentage yield could not be determined, as such the crude product was instead taken forward into the next reaction.

<sup>1</sup>H NMR (400 MHz, DMSO) δ 8.68 (d, *J* = 8.3 Hz, 1H, NH<sub>α</sub>), 8.31 (d, *J* = 3.4 Hz 1H, NH<sub>β</sub>), 5.04 (d, *J* = 3.4 Hz, 1H, H-1<sub>α</sub>), 4.65 (d, *J* = 8.3 Hz, 1H, H-1<sub>β</sub>).

<sup>13</sup>C NMR (101 MHz, DMSO) δ 161.6 (1C, C=O), 92.8 (1C, CCl<sub>3</sub>), 89.7 (1C, C-1), 73.4 (1C, C-5), 72.3 (1C, C-4), 70.8 (1C, C-3), 61.0 (1C, C-2), 57.1 (1C, C-6).

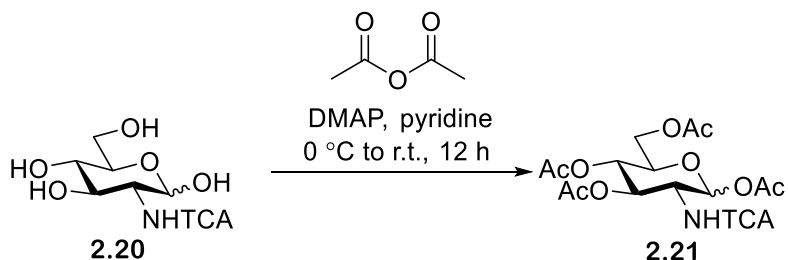
(ESI)HRMS - C<sub>8</sub>H<sub>12</sub>O<sub>6</sub>NNa<sup>35</sup>Cl<sub>3</sub><sup>+</sup> ([M+Na]<sup>+</sup>) requires *m/z* 345.9623: found *m/z* 345.9627

C<sub>8</sub>H<sub>12</sub>O<sub>6</sub>NNa<sup>35</sup>Cl<sub>3</sub> : C<sub>8</sub>H<sub>12</sub>O<sub>6</sub>NNa<sup>35</sup>Cl<sub>2</sub><sup>37</sup>Cl : C<sub>8</sub>H<sub>12</sub>O<sub>6</sub>NNa<sup>35</sup>Cl<sup>37</sup>Cl<sub>2</sub> ratio of peak intensities = 3.3 : 3.1 : 1

IR- 3327 (O-H), 2956 (C-H), 2933 (C-H), 2856 (C-H), 1655 (C=O), 1334 (C-O), 1025 (C-O).

## Experimental

### 8.2.3.2 Synthesis of 1,3,4,6-tetra-O-acetyl-2-deoxy-2-trichloroacetamido- $\alpha/\beta$ -D-glucopyranose **2.21**<sup>240</sup>



Acetic anhydride (30 mL) was added to a solution of **2.20** (15g, 46 mmols) and DMAP (cat) in pyridine (30 mL) at 0 °C. The reaction mixture was warmed to r.t. and stirred for 12 h, affording a dark orange solution. The solution was concentrated *in vacuo* to afford a dark brown oil. The oil was diluted in DCM (30 mL), washed with water (30 mL), 1 M HCl solution (30 mL) and saturated NaHCO<sub>3</sub> solution (30 mL). The solution was dried (MgSO<sub>4</sub>) and concentrated *in vacuo*, affording a light caramel coloured foam of **2.21** (13 g, 26 mmols, 58%); R<sub>f</sub> = 0.64 (1 : 1 Hexane : EtOAc).

<sup>1</sup>H NMR (500 MHz, MeOD)  $\delta$  6.20 (d,  $J_{1\alpha,2\alpha}$  = 3.8 Hz, 1H, H-1 $\alpha$ ), 5.90 (d,  $J_{1\beta,2\beta}$  = 8.2 Hz, 1H, H-1 $\beta$ ), 5.46 (dd,  $J_{2\alpha,3\alpha}$  = 11.1 Hz,  $J_{3\alpha,4\alpha}$  = 9.2 Hz, 1H, H-3 $\alpha$ ), 5.42 (dd,  $J_{2\beta,3\beta}$  = 10.0 Hz,  $J_{3\beta,4\beta}$  = 9.2 Hz, 1H, H-3 $\beta$ ), 5.13 (dd,  $J_{4\alpha,5\alpha}$  = 10.5 Hz,  $J_{3\alpha,4\alpha}$  = 9.5 Hz, 1H, H-4 $\alpha$ ), 5.06 (dd,  $J_{4\beta,5\beta}$  = 10.2 Hz,  $J_{3\beta,4\beta}$  = 9.5 Hz, 1H, H-4 $\beta$ ), 4.40 (dd,  $J_{2\alpha,3\alpha}$  = 11.1 Hz,  $J_{1\alpha,2\alpha}$  = 3.8 Hz, 1H, H-2 $\alpha$ ), 4.31 (dd,  $J_{6\alpha,6b\alpha}$  = 12.5 Hz,  $J_{5\alpha,6a\alpha}$  = 4.0 Hz, 1H, H-6 $\alpha\alpha$ ), 4.30 (dd,  $J_{6\beta,6b\beta}$  = 12.5 Hz,  $J_{5\beta,6a\beta}$  = 4.5 Hz, 1H, H-6 $\alpha\beta$ ), 4.19 (ddd,  $J_{4\alpha,5\alpha}$  = 10.5 Hz,  $J_{5\alpha,6a\alpha}$  = 4.0 Hz,  $J_{5\alpha,6b\alpha}$  = 2.2 Hz, 1H, H-5 $\alpha$ ), 4.12 (dd,  $J_{2\beta,3\beta}$  = 10.0 Hz,  $J_{1\beta,2\beta}$  = 8.2 Hz, 1H, H-2 $\beta$ ), 4.07 (dd,  $J_{6\alpha,6b\alpha}$  = 12.5 Hz,  $J_{5\alpha,6b\alpha}$  = 2.2 Hz, 1H, H-6 $b\alpha$ ), 4.06 (dd,  $J_{6\alpha,6b\alpha}$  = 12.5 Hz,  $J_{5,6b}$  = 2.3 Hz, 1H, H-5 $\beta$ ), 3.94 (ddd,  $J_{4,5}$  = 10.2 Hz,  $J_{5,6a}$  = 4.5 Hz,  $J_{5,6b}$  = 2.3 Hz, 1H, H-6 $b\beta$ ), 2.17 (s, 3H, CH<sub>3</sub> $\alpha$ ), 2.06 (s, 3H, CH<sub>3</sub> $\beta$ ), 2.05 (s, 3H, CH<sub>3</sub> $\beta$ ), 2.05 (s, 3H, CH<sub>3</sub> $\alpha$ ), 2.02 (s, 3H, CH<sub>3</sub> $\alpha$ ), 2.01 (s, 3H, CH<sub>3</sub> $\beta$ ), 1.98 (s, 3H, CH<sub>3</sub> $\alpha$ ), 1.97 (s, 3H, CH<sub>3</sub> $\beta$ ).

<sup>13</sup>C NMR (126 MHz, MeOD)  $\delta$  171.3 (1C, C=O $\alpha$ ), 171.3 (1C, C=O $\beta$ ), 171.0 (1C, C=O $\alpha$ ), 170.5 (1C, C=O $\beta$ ), 170.2 (1C, C=O $\alpha$ ), 170.2 (1C, C=O $\beta$ ), 169.6 (1C, C=O $\alpha$ ), 169.4 (1C, C=O $\beta$ ), 163.4 (1C, NHCO $\beta$ ), 163.4 (1C, NHCO $\alpha$ ), 92.4 (1C, CCl<sub>3</sub>), 91.8 (1C, C-1 $\beta$ ), 82.7 (1C, C-1 $\alpha$ ), 72.9 (1C, C-5 $\beta$ ), 72.1 (1C, C-3 $\beta$ ), 70.5 (1C, C-3 $\alpha$ ), 70.0 (1C, C-5 $\alpha$ ), 68.8 (1C, C-4 $\alpha$ ), 68.7 (1C, C-4 $\beta$ ), 61.9 (1C, C-6 $\beta$ ), 61.9 (1C, C-6 $\alpha$ ), 54.9 (1C, C-2 $\beta$ ), 53.2 (1C, C-2 $\alpha$ ), 19.7 (2C, CH<sub>3</sub>), 19.6 (2C, CH<sub>3</sub>), 19.6 (4C, CH<sub>3</sub>), 19.5 (1C, CH<sub>3</sub>), 19.5 (1C, CH<sub>3</sub>).

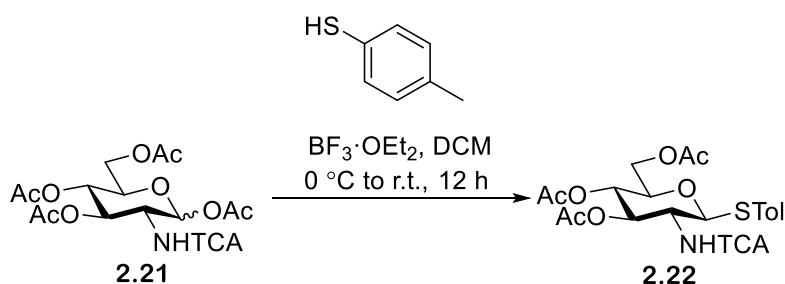
(ESI)HRMS - C<sub>16</sub>H<sub>20</sub>O<sub>10</sub>NNa<sup>35</sup>Cl<sub>3</sub><sup>+</sup> ([M+Na]<sup>+</sup>) requires m/z 514.0050: found m/z 514.0047  
 C<sub>16</sub>H<sub>20</sub>O<sub>10</sub>NNa<sup>35</sup>Cl<sub>3</sub> : C<sub>16</sub>H<sub>20</sub>O<sub>10</sub>NNa<sup>35</sup>Cl<sub>2</sub><sup>37</sup>Cl : C<sub>16</sub>H<sub>20</sub>O<sub>10</sub>NNa<sup>35</sup>Cl<sup>37</sup>Cl<sub>2</sub> ratio of peak intensities = 3.1 : 3 : 1

$[\alpha]_D^{25}$  = - 6.0 (c 1, DCM)

IR- 3314 (N-H), 2957 (C-H), 1743 (C=O), 1662 (N-H), 1210 (C-O), 1035 (C-O), 841 (C-Cl)

## Experimental

### 8.2.3.3 Synthesis of 4-methylphenyl 3,4,6-tri-O-acetyl-2-deoxy-2-trichloroacetamido-1-thio-β-D-glucopyranoside **2.22**<sup>383</sup>



$\text{BF}_3 \cdot \text{Et}_2\text{O}$  (4.7 mL, 39 mmols, 1.5 eq) was added dropwise to a solution of **2.21** (13 g, 26 mmols) and 4-methylbenzenethiol (4.2 g, 34 mmols, 1.3 eq) in dry DCM (40 mL) at 0 °C under  $\text{N}_2$ . The reaction mixture was warmed to r.t. and stirred for 12 h, affording a clear orange solution. The solution was washed with water (2 x 40 mL) and saturated  $\text{NaHCO}_3$  solution (40 mL), dried ( $\text{MgSO}_4$ ) and concentrated *in vacuo* to afford a dark orange oil. The oil was purified using column chromatography, eluting with a graduated solvent system of 4:1 Hexane : EtOAc to 1 : 1 Hexane : EtOAc. This afforded a white solid of **2.22** (2.7 g, 4.8 mmols, 18%);  $R_f = 0.65$  (1.5 : 1 Hexane : EtOAc).

$^1\text{H}$  NMR (500 MHz,  $\text{CDCl}_3$ )  $\delta$  7.41 (d,  $J_{\text{HAr}} = 8.0$  Hz, 2H, HAr), 7.12 (d,  $J_{\text{HAr}} = 8.0$  Hz, 2H, HAr), 7.04 (d,  $J_{\text{NH},2} = 9.1$  Hz, 1H, NH), 5.34 (dd,  $J_{2,3} = 9.8$  Hz,  $J_{3,4} = 9.8$  Hz, 1H, H-3), 5.07 (dd,  $J_{3,4} = 9.8$  Hz,  $J_{4,5} = 9.8$  Hz, 1H, H-4), 4.77 (d,  $J_{1,2} = 10.4$  Hz, 1H, H-1), 4.23 (dd,  $J_{6a,6b} = 12.3$  Hz,  $J_{5,6a} = 5.2$  Hz, 1H, H-6a), 4.18 (dd,  $J_{6a,6b} = 12.3$  Hz,  $J_{5,6b} = 2.4$  Hz, 1H, H-6b), 3.99 (ddd,  $J_{1,2} = 10.4$  Hz,  $J_{2,3} = 9.8$  Hz,  $J_{\text{NH},2} = 9.1$  Hz, 1H, H-2), 3.74 (ddd,  $J_{4,5} = 9.8$  Hz,  $J_{5,6a} = 5.2$  Hz,  $J_{5,6b} = 2.4$  Hz, 1H, H-5), 2.35 (s, 3H,  $\text{CH}_3$ ), 2.09 (s, 3H,  $\text{CH}_3$ ), 2.00 (s, 3H,  $\text{CH}_3$ ), 1.92 (s, 3H,  $\text{CH}_3$ ).

$^{13}\text{C}$  NMR (126 MHz,  $\text{CDCl}_3$ )  $\delta$  171.0 (1C, C=O (OAc)), 170.6 (1C, C=O (OAc)), 169.2 (1C, C=O (OAc)), 161.6 (1C, C=O (TCA)), 139.1, 134.1, 129.8, 127.5, (CAr), 92.3 (1C,  $\text{CCl}_3$ ), 86.6 (1C, C-1), 76.0 (1C, C-5), 73.2 (1C, C-3), 68.3 (1C, C-4), 62.3 (1C, C-6), 54.4 (1C, C-2), 21.2 (1C,  $\text{CH}_3$  (STol)), 20.7 (1C,  $\text{CH}_3$  (OAc)), 20.6 (1C,  $\text{CH}_3$  (OAc)), 20.4 (1C,  $\text{CH}_3$ , (OAc)).

(ESI)HRMS -  $\text{C}_{21}\text{H}_{24}\text{O}_8\text{NNa}^{35}\text{Cl}_3\text{S}^+$  ( $[\text{M}+\text{Na}]^+$ ) requires  $m/z$  578.0186: found  $m/z$  578.0170

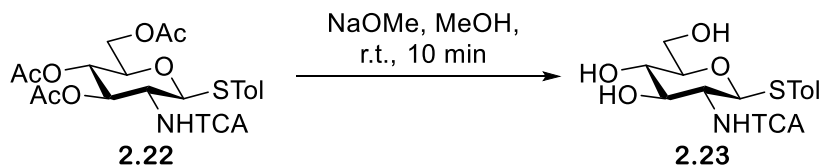
$\text{C}_{21}\text{H}_{24}\text{O}_8\text{NNa}^{35}\text{Cl}_3\text{S}$  :  $\text{C}_{21}\text{H}_{24}\text{O}_8\text{NNa}^{35}\text{Cl}_2^{37}\text{ClS}$  :  $\text{C}_{21}\text{H}_{24}\text{O}_8\text{NNa}^{35}\text{Cl}^{37}\text{Cl}_2\text{S}$  ratio of peak intensities = 3.3 : 3.2 : 1

$[\alpha]_D^{25} = -10.7$  (c 1, DCM)

*IR*- 3370 (N-H), 2923 (C-H). 1742 (C=O), 1693 (C=O), 1524 (C=C), 1213 (C-O), 1040 (C-O). 822 (C-Cl)

## Experimental

### 8.2.3.4 Synthesis of 4-methylphenyl 2-deoxy-2-trichloroacetamido-1-thio- $\beta$ -D-glucopyranoside **2.23**



A NaOMe solution was added dropwise to a solution of **2.22** (11 g, 4.6 mmols) in MeOH (30 mL) until the solution reached pH 10. The reaction mixture was stirred for 10 minutes at r.t. to afford a cloudy white solution. The solution was neutralised with dowex and concentrated *in vacuo*, yielding a white powder of **2.23** (7.0 g, 16 mmols, 80%);  $R_f = 0.78$  (1 : 1 Hexane : EtOAc).

$^1\text{H}$  NMR (500 MHz, MeOD)  $\delta$  7.41 (d,  $J_{\text{HAr}} = 8.0$  Hz, 2H, HAr), 7.11 (d,  $J_{\text{HAr}} = 8.0$  Hz, 2H, HAr), 4.86 (d, 1H, H-1), 3.88 (dd,  $J = 12.0$  Hz,  $J = 1.9$  Hz, 1H, H-6a), 3.71 (m, 2H, H-2, H-6b), 3.61 (dd,  $J = 9.8$  Hz,  $J = 8.3$  Hz, 1H, H-3), 3.34 (m, 2H, H-4, H-5), 2.31 (s, 3H, CH<sub>3</sub>).

$^{13}\text{C}$  NMR (126 MHz, MeOD)  $\delta$  164.0 (1C, C=O), 138.9, 133.4, 131.4, 130.6, (CAr), 94.2 (1C, CCl<sub>3</sub>), 88.3 (1C, C-1), 82.1 (1C, C-5), 76.6 (1C, C-3), 72.0 (1C, C-4), 62.8 (1C, C-6), 57.9 (1C, C-2), 21.1 (1C, CH<sub>3</sub>).

(ESI)HRMS - C<sub>15</sub>H<sub>18</sub><sup>35</sup>Cl<sub>3</sub>NNaO<sub>5</sub>S<sup>+</sup> ([M+Na]<sup>+</sup>) requires m/z 451.9869: found m/z 451.9872

C<sub>15</sub>H<sub>18</sub>O<sub>5</sub>NNa<sup>35</sup>Cl<sub>3</sub>S : C<sub>15</sub>H<sub>18</sub>O<sub>5</sub>NNa<sup>35</sup>Cl<sub>2</sub><sup>37</sup>ClS : C<sub>15</sub>H<sub>18</sub>O<sub>5</sub>NNa<sup>35</sup>Cl<sup>37</sup>Cl<sub>2</sub>S ratio of peak intensities = 2.9 : 3 : 1

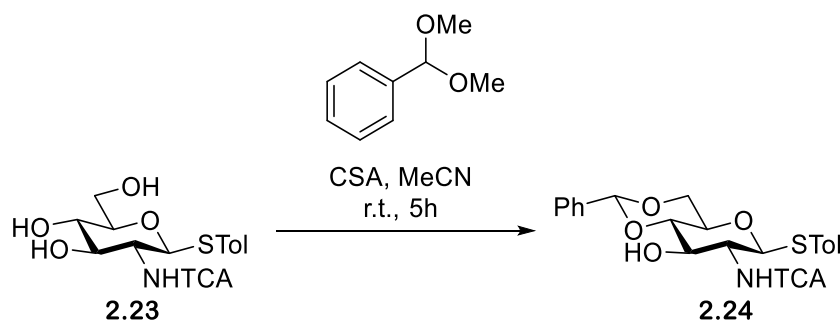
$[\alpha]_D^{25} = +3.8$  (c 1, MeOH)

IR- 3334 (O-H), 2921 (C-H), 1683 (C=O), 1424 (C=C), 1278 (C-N), 816 (C-Cl)

No literature reference quoting NMR data could not be found.

## Experimental

### 8.2.3.5 Synthesis of 4-methylphenyl 4,6-O-benzylidene-2-deoxy-2-trichloroacetyl- $\beta$ -D-glucopyranoside **2.24**<sup>384</sup>



2,2 DMT (4.9 mL, 32 mmols, 2 eq) was added to an acidified solution of **2.23** (7.0 g, 16 mmols) and CSA in dry MeCN, affording a light-yellow solution. The reaction mixture was stirred at r.t. for 5 h.  $\text{NEt}_3$  (2 mL) was added then to quench the reaction, and the solution was concentrated *in vacuo* to yield a white solid. The solid was purified by column chromatography, eluting with a graduated solvent system of 4 : 1 Hexane : EtOAc to 10 : 1 DCM : MeOH. This affording a white solid of **2.24** (7.2 g, 14 mmols, 87%);  $R_f = 0.78$  (2 : 1 Hexane : EtOAc).

$^1\text{H}$  NMR (500 MHz,  $\text{CDCl}_3$ )  $\delta$  7.45 (m, 2H, HAr), 7.40 (d,  $J_{\text{HAr}} = 8.0$  Hz, 2H, HAr), 7.36 (dd,  $J_{\text{HAr}} = 5.0$  Hz,  $J_{\text{HAr}} = 1.7$  Hz, 3H, HAr), 7.14 (d,  $J_{\text{HAr}} = 8.0$  Hz, 2H, HAr), 6.96 (d,  $J_{\text{NH},2} = 7.6$  Hz, 1H, NH), 5.52 (s, 1H, CHPh), 5.08 (d,  $J_{1,2} = 10.3$  Hz, 1H, H-1), 4.37 (dd,  $J_{6a,6b} = 10.3$  Hz,  $J_{5,6a} = 4.6$  Hz, 1H, H-6a), 4.25 (dd,  $J_{2,3} = 9.2$  Hz,  $J_{3,4} = 9.2$  Hz, 1H, H-3), 3.77 (dd,  $J_{5,6b} = 10.3$  Hz,  $J_{6a,6b} = 10.3$  Hz, 1H, H-6b), 3.50 (m, 3H, H-2, H-3, H-5), 2.35 (s, 3H,  $\text{CH}_3$ ).

$^{13}\text{C}$  NMR (126 MHz,  $\text{CDCl}_3$ )  $\delta$  162.0 (1C, C=O), 139.1, 136.8, 133.9, 130.0, 129.4, 128.4, 127.3, 126.3 (CAr), 101.9 (1C, CHPh), 92.4 (1C,  $\text{CCl}_3$ ), 85.5 (1C, C-1), 81.3 (1C, C-5), 71.3 (1C, C-3), 70.4 (1C, C-4), 68.5 (1C, C-6), 57.5 (C-5), 21.2 (1C,  $\text{CH}_3$ ).

(ESI)HRMS -  $\text{C}_{22}\text{H}_{22}^{35}\text{Cl}_3\text{NNaO}_5\text{S}^+$  ( $[\text{M}+\text{Na}]^+$ ) requires  $m/z$  540.0182: found  $m/z$  540.0170

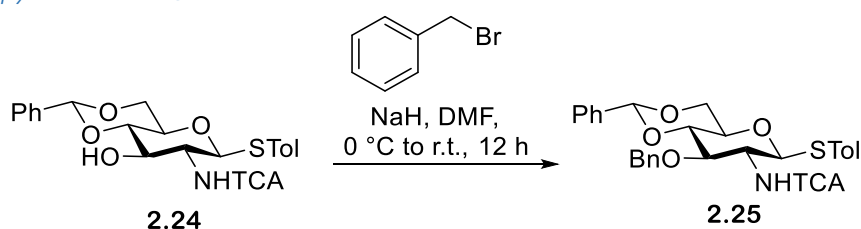
$\text{C}_{22}\text{H}_{22}^{35}\text{Cl}_3\text{NNa}^{35}\text{Cl}_3\text{S} : \text{C}_{22}\text{H}_{22}^{35}\text{Cl}_3\text{NNa}^{35}\text{Cl}_2^{37}\text{ClS} : \text{C}_{22}\text{H}_{22}^{35}\text{Cl}_3\text{NNa}^{35}\text{Cl}^{37}\text{Cl}_2\text{S}$  ratio of peak intensities = 2.8 : 2.6 : 1

$[\alpha]_D^{25} = -16.7$  ( $c$  1, DCM)

$\text{IR}$ - 3556 (O-H), 3318 (N-H), 2862 (C-H), 1690 (C=O), 1536 (C=C), 1076 (C-O), 819 (C-Cl)

## Experimental

### 8.2.3.6 Synthesis of 4-methylphenyl 3-O-benzyl-4,6-O-benzylidene-2-deoxy-2-N-trichloroacetamido-1-thio-β-D-glucopyranoside **2.25**



NaH (0.62 g, 26 mmols, 2 eq) was added to a solution of **2.24** (7.0 g, 13 mmols) in dry DMF (30 mL) at 0°C, and the reaction mixture stirred for 10 minutes. BnBr (3.1 mL, 26 mmols, 2 eq) was then added to the reaction mixture, and the mixture warmed to r.t. and stirred for 12 h, affording a light-yellow solution. The solution was concentrated *in vacuo*, diluted with DCM (30 mL), washed with water (30 mL), dried (MgSO<sub>4</sub>) and concentrated *in vacuo* to yield a clear oil. The oil was purified by column chromatography, eluting with a graduated solvent system of 4 : 1 Hexane : EtOAc to 3 : 1 Hexane : EtOAc. This afforded a clear oil of **2.25** (0.57 g, 0.93 mmols, 7%); R<sub>f</sub> = 0.71 (2 : 1 Hexane : EtOAc).

*NMR*- sample was used crude so data was not collected

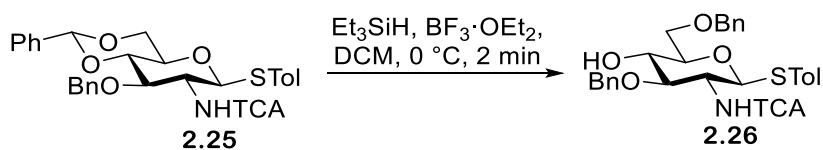
(ESI)HRMS - C<sub>29</sub>H<sub>28</sub><sup>35</sup>Cl<sub>3</sub>NNaO<sub>5</sub>S<sup>+</sup> ([M+Na]<sup>+</sup>) requires m/z 630.0651: found m/z 630.0669

Speculative isotope ratio not obtained

No literature reference for characterisation could be found

## Experimental

### 8.2.3.7 Synthesis of 4-methylphenyl 3,6-di-O-benzyl-2-deoxy-2-N-trichloroacetamido-1-thio-β-D-glucopyranoside **2.26**



$\text{Et}_3\text{SiH}$  (1.7 mL, 11 mmols, 12 eq) was added to a solution of **2.25** (0.58 g, 0.9 mmols) in dry DCM (10 mL) at  $0^\circ\text{C}$  and the resultant solution stirred at  $0^\circ\text{C}$  for 2 minutes.  $\text{BF}_3 \cdot \text{Et}_2\text{O}$  (0.23 mL, 1.8 mmols, 2 eq) was added to the reaction mixture and the mixture stirred for a further 2 minutes to afford a clear solution. The solution was washed with water (2 x 10 mL), saturated  $\text{NaHCO}_3$  solution (10 mL) and saturated  $\text{NaCl}$  solution (10 mL), dried ( $\text{MgSO}_4$ ) and concentrated *in vacuo*, affording a clear oil. The oil was purified by column chromatography, eluting with a graduated solvent system of 4 : 1 Hexane : EtOAc to 2 : 1 Hexane : EtOAc. This afforded a crude clear oil of **2.26** (0.031 g, 0.051 mmols, 6%)  $R_f = 0.88$  (1 : 1 Hexane : EtOAc). **2.26** was used crude in subsequent reactions.

A known impurity ( $\text{HOCH}_2\text{Bn}$ ) is present in the raw spectra. Peaks attributable to **2.26** are reported below:

$^1\text{H}$  NMR (400 MHz,  $\text{CDCl}_3$ )  $\delta$  7.41-7.06 (m, 18H HAr), 6.80 (d,  $J_{\text{HAr}} = 8.0$  Hz, 1H, HAr), 5.06 (d,  $J_{1,2} = 10.1$  Hz, H-1), 4.83 (d,  $J_{\text{CH}_2} = 11.0$  Hz, 1H,  $\text{CH}_2$ ), 4.67 (d,  $J_{\text{CH}_2} = 11.0$  Hz, 1H,  $\text{CH}_2$ ), 4.62 (d,  $J_{\text{CH}_2} = 12.1$  Hz, 1H,  $\text{CH}_2$ ), 4.55 (d,  $J_{\text{CH}_2} = 12.1$  Hz, 1H,  $\text{CH}_2$ ), 4.07 (d,  $J_{\text{CH}_2} = 2.1$  Hz, 2H,  $\text{CH}_2$  impurity), 3.87 (dd,  $J = 10.0$  Hz,  $J = 8.2$  Hz, 1H, H-3), 3.76 (m, 2H, H6, H6'), 3.58 (td,  $J = 10.0$  Hz,  $J = 2.3$  Hz, 1H, H-4), 3.51 (m, 1H, H-5), 3.41 (m, 1H, H-2), 2.32 (s, 3H,  $\text{CH}_3$ ).

$^{13}\text{C}$  NMR (101 MHz,  $\text{CDCl}_3$ )  $\delta$  161.6 (C=O), 140.8, 139.1, 138.7, 137.9, 136.2, 133.8, 130.9, 130.0, 129.8, 128.9, 128.6, 128.6, 128.0, 127.9, 127.9, 127.0, 126.2 (CAr), 92.6 (1C,  $\text{CCl}_3$ ), 84.9 (1C, C-1), 81.3 (1C, C-3), 78.2 (1C, C-5), 73.9 (1C,  $\text{CH}_2$ ), 73.1 (1C, C-4), 72.9 (1C,  $\text{CH}_2$ ), 70.5 (1C, C-6), 56.6 (1C, C-5), 38.5 (1C,  $\text{CH}_2$  impurity), 21.4 (1C,  $\text{CH}_3$ ).

(ESI)HRMS -  $\text{C}_{29}\text{H}_{30}\text{Cl}_3\text{NNaO}_5\text{S}^+$  ( $[\text{M}+\text{Na}]^+$ ) requires  $m/z$  632.0808: found  $m/z$  632.0798

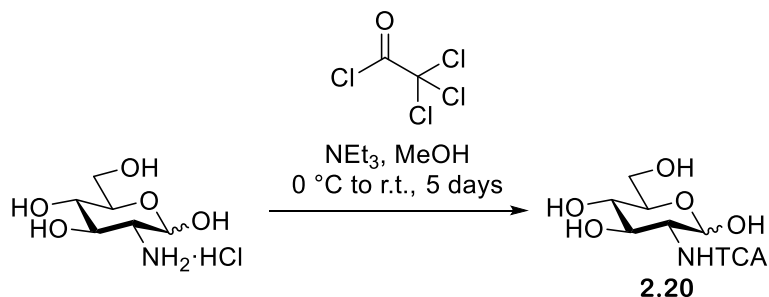
$\text{C}_{29}\text{H}_{30}\text{O}_5\text{NNa}^{35}\text{Cl}_3\text{S}$  :  $\text{C}_{29}\text{H}_{30}\text{O}_5\text{NNa}^{35}\text{Cl}_2^{37}\text{ClS}$  :  $\text{C}_{29}\text{H}_{30}\text{O}_5\text{NNa}^{35}\text{Cl}^{37}\text{Cl}_2\text{S}$  ratio of peak intensities = 2.8 : 2.7 : 1

No literature reference for characterisation could be found

## Experimental

### 8.2.4 Synthesis of ethyl 3-*O*-benzoyl-4,6-*O*-benzylidene-2-deoxy-2-*N*-trichloroacetamido-1-thio- $\beta$ -D-glucopyranoside **2.3b**

#### 8.2.4.1 Synthesis of 2-deoxy-2-trichloroacetamido- $\alpha/\beta$ -D-glucopyranose **2.20** method 2



Due to the large quantity of starting material the reaction was performed in two batches of equal size, the procedure was the same for both batches.

Trichloroacetyl chloride (13 mL, 93 mmols, 1.3 eq) was added dropwise to a solution of D-glucosamine hydrochloride (20 g, 93 mmols) and triethylamine (30 ml, 220 mmols, 2.3 eq) in MeOH at  $0\text{ }^\circ\text{C}$ . The reaction mixture was warmed to r.t. and stirred for 5 days, affording a white cloudy solution. The solution was filtered through celite and concentrated *in vacuo* to dryness, yielding a white solid of **2.20**. Compound **2.20** was used crude in subsequent reactions.

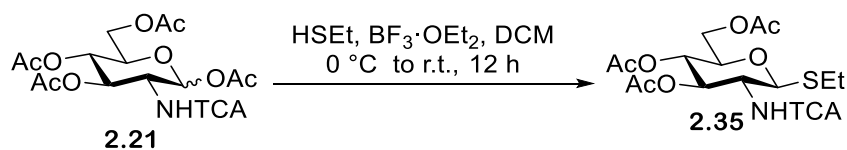
Analysed data was identical to that previously collected in the lab, and this feedstock was used crude.

For compound data please see page 241



## Experimental

### 8.2.4.2 Synthesis of ethyl-3,4,6-tri-O-acetyl-2-deoxy-2-(trichloroethoxycarbonylamido)-1-thio- $\beta$ -D-glucopyranoside **2.35**<sup>385</sup>



Due to the large quantities required, the reaction was performed in 3 batches.

$\text{BF}_3\cdot\text{Et}_2\text{O}$  (batch 1 + 2 = 6.5 mL, 53 mmols, 1 eq, batch 3 = 2.3 mL, 19 mmols) was added dropwise to a solution of **2.21** (batch 1 + 2 = 26 g, 53 mmols, 1 eq, batch 3 = 9.4 g, 19 mmols, 1 eq) and ethanethiol (batch 1 + 2 = 5.7 mL, 79 mmols, 1.5 eq, batch 3 = 2 mL, 28 mmols, 1.5 eq) in dry DCM (50 mL) at 0 °C under  $\text{N}_2$ . The reaction mixture was warmed to r.t. and stirred for 12 h, affording a clear orange solution. The solution was washed with water (2 x 50 mL) and saturated  $\text{NaHCO}_3$  solution (50 mL), dried ( $\text{MgSO}_4$ ) and concentrated *in vacuo* to afford a dark orange oil. The oil was purified using column chromatography, eluting with a graduated solvent system of 4:1 Hexane : EtOAc to 1 : 1 Hexane : EtOAc. This afforded a white solid of **2.35** (**2.35 $\alpha$** : 4 g, 8.1 mmols, **2.35 $\beta$** : 20 g, 40 mmols, total = 40%) ;  $R_f \alpha = 0.56$ ,  $R_f \beta = 0.49$  (1.5 : 1 Hexane : EtOAc).

$^1\text{H}$  NMR (500 MHz,  $\text{CCl}_2\text{D}_2$ )  $\delta$  6.91 (d,  $J_{\text{NH},2} = 9.4$  Hz, 1H, NH), 5.31 (dd,  $J_{3,4} = 9.6$  Hz,  $J_{4,5} = 9.6$  Hz, 1H, H-4), 5.10 (dd,  $J_{2,3} = 9.6$  Hz,  $J_{3,4} = 9.6$  Hz, 1H, H-3), 4.70 (d,  $J_{1,2} = 10.3$  Hz, 1H, H-1), 4.23 (dd,  $J_{6a,6b} = 12.3$  Hz,  $J_{5,6a} = 5.2$  Hz, 1H, H-6a), 4.12 (dd,  $J_{6a,6b} = 12.3$  Hz,  $J_{5,6b} = 2.4$  Hz, 1H, H-6b), 4.05 (dd,  $J_{1,2} = 10.3$  Hz,  $J_{2,3} = 9.6$  Hz, 1H, H-2), 3.76 (ddd,  $J_{4,5} = 9.6$  Hz,  $J_{5,6a} = 5.2$  Hz,  $J_{5,6b} = 2.4$  Hz, 1H, H-5), 2.71 (qd,  $J_{\text{CH}_2, \text{CH}_2} = 16.2$  Hz,  $J_{\text{CH}_2, \text{CH}_3} = 7.4$  Hz, 2H,  $\text{CH}_2$ ), 2.06 (s, 3H,  $\text{CH}_3$ ), 2.02 (s, 3H,  $\text{CH}_3$ ), 2.00 (s, 3H,  $\text{CH}_3$ ), 1.26 (t, 3H,  $\text{CH}_3$ ).

$^{13}\text{C}$  NMR (126 MHz,  $\text{CCl}_2\text{D}_2$ )  $\delta$  172.2 (1C, C=O), 171.8 (1C, C=O), 170.6 (1C, C=O), 163.0 (1C, NHC=O), 93.5 (1C,  $\text{CCl}_3$ ), 85.3 (1C, C-1), 77.4 (1C, C-5), 74.3 (1C, C-4), 69.6 (1C, C-3), 63.5 (1C, C-6), 56.2 (1C, C-2), 25.8 (1C,  $\text{SCH}_2$ ), 21.8 (1C,  $\text{COCH}_3$ ), 21.7 (2C,  $\text{COCH}_3$ ), 16.1 (1C,  $\text{CH}_2\text{CH}_3$ ).

(ESI)HRMS -  $\text{C}_{16}\text{H}_{22}^{35}\text{Cl}_3\text{NNaO}_8\text{S}^+$  ( $[\text{M}+\text{Na}]^+$ ) requires  $m/z$  516.0029: found  $m/z$  516.0023

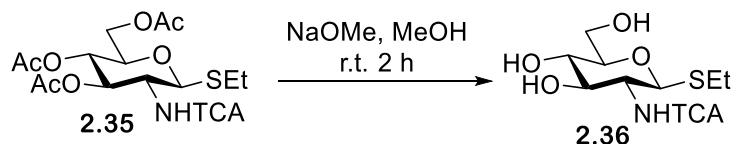
$\text{C}_{16}\text{H}_{22}\text{O}_8\text{NNa}^{35}\text{Cl}_3\text{S}$  :  $\text{C}_{16}\text{H}_{22}\text{O}_8\text{NNa}^{35}\text{Cl}_2^{37}\text{ClS}$  :  $\text{C}_{16}\text{H}_{22}\text{O}_8\text{NNa}^{35}\text{Cl}^{37}\text{Cl}_2\text{S}$  ratio of peak intensities = 3.3 : 3 : 1

$[\alpha]_D^{25} = -23.4$  (c 1, DCM)

*IR*- 3340 (N-H), 2964 (C-H), 1741 (C=O), 1524 (N-H), 1220 (C-O), 1033 (C-O), 820 (C-Cl)

## Experimental

### 8.2.4.3 Synthesis of ethyl 2-deoxy-2-N-trichloroacetamido-1-thio-β-D-glucopyranoside **2.36** <sup>386</sup>



A NaOMe solution was added dropwise to a solution of **2.35** (16 g, 33 mmols) in MeOH (50 mL) until the solution reached pH 10. The reaction mixture was stirred for 2 h at r.t. affording a cloudy white solution. The solution was neutralised with dowex and concentrated *in vacuo* to yield a white powder of **2.36** (10 g, 28 mmols, 86%);  $R_f = 0.51$  (7 : 1 DCM : MeOH). **2.36** was used crude in subsequent reactions.

$^1\text{H}$  NMR (500 MHz, MeOD)  $\delta$  4.67 (d,  $J_{1,2} = 10.0$  Hz, 1H, H-1), 3.88 (dd,  $J_{6a,6b} = 12.0$  Hz,  $J_{5,6a} = 1.6$  Hz, 1H, H-6a), 3.75 (dd,  $J_{1,2} = 10.0$  Hz,  $J_{2,3} = 10.0$  Hz, 1H, H-2), 3.68 (dd,  $J_{6a,6b} = 12.0$  Hz,  $J_{5,6b} = 5.4$  Hz, 1H, H-6b), 3.61 (dd,  $J_{2,3} = 10$  Hz,  $J_{3,4} = 8.2$  Hz, 1H, H-3), 3.32 (m, 2H, H-4, H-5), 2.73 (qd,  $J_{\text{CH}_2, \text{CH}_2} = 12.5$  Hz,  $J_{\text{CH}_2 \text{CH}_3} = 7.4$  Hz, 2H, CH<sub>2</sub>), 1.25 (t,  $J_{\text{CH}_2 \text{CH}_3} = 7.4$  Hz, 1H, CH<sub>3</sub>).

$^{13}\text{C}$  NMR (126 MHz, MeOD)  $\delta$  164.0 (1C, C=O), 94.1 (1C, CCl<sub>3</sub>), 84.8 (1C, C-1), 82.2 (1C, C-5), 76.5 (1C, C-3), 72.2 (1C, C-4), 62.9 (1C, C-6), 58.1 (1C, C-2), 24.9 (1C, CH<sub>2</sub>), 15.2 (1C, CH<sub>3</sub>).

(ESI)HRMS - C<sub>10</sub>H<sub>16</sub><sup>35</sup>Cl<sub>3</sub>NNaO<sub>5</sub>S<sup>+</sup> ([M+Na]<sup>+</sup>) requires m/z 389.9712: found m/z 389.9732

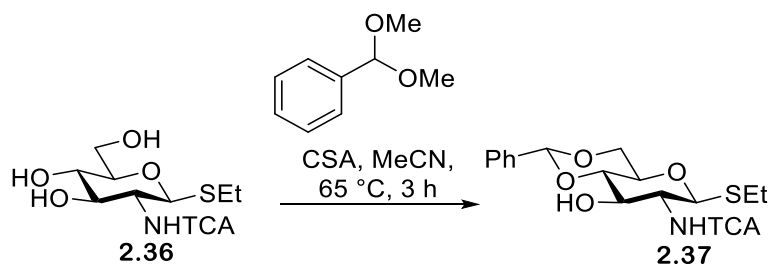
C<sub>10</sub>H<sub>16</sub>O<sub>5</sub>NNa<sup>35</sup>Cl<sub>3</sub>S : C<sub>10</sub>H<sub>16</sub>O<sub>5</sub>NNa<sup>35</sup>Cl<sub>2</sub><sup>37</sup>ClS : C<sub>10</sub>H<sub>16</sub>O<sub>5</sub>NNa<sup>35</sup>Cl<sup>37</sup>Cl<sub>2</sub>S ratio of peak intensities = 2.7 : 2.5 : 1

IR- 3307 (O-H), 2927 (C-H), 1686 (C=O), 1526 (N-H), 1262 (C-N), 1021 (C-O), 818 (C-Cl)

$[\alpha]_D^{25} = -12.28$  (c 0.29, MeOH)

## Experimental

### 8.2.4.4 Synthesis of ethyl 4,6-O-benzylidene-2-deoxy-2-N-trichloroacetamido-1-thio-β-D-glucopyranoside **2.37**<sup>244</sup>



2,2 DMT (8.4 mL, 56 mmols, 2 eq) was added to an acidified solution of **2.36** (10 g, 28 mmols) and CSA in dry MeCN, affording a light-yellow solution. The reaction mixture was heated to 65 °C and stirred for 3 h. The reaction was quenched with NEt<sub>3</sub> (3 mL) and the solution was concentrated *in vacuo* to yield an orange solid. The solid was purified by column chromatography, eluting with a graduated solvent system of 4:1 Hexane : EtOAc to 10 : 1 DCM : MeOH. This afforded a white solid of **2.37** (6.5 g, 14 mmols, 50%); R<sub>f</sub> = 0.78 (2 : 1 Hexane : EtOAc).

<sup>1</sup>H NMR (500 MHz, MeOD) δ 7.49 (dd, *J*<sub>HAr</sub> = 5.2 Hz, *J*<sub>HAr</sub> = 2.1 Hz, 2H, HAr), 7.34 (dd, *J*<sub>HAr</sub> = 5.2 Hz, *J*<sub>HAr</sub> = 2.1 Hz, 3H, HAr), 5.61 (s, 1H, CH<sub>2</sub>Ph), 4.78 (d, 10.2 Hz, 1H, H-1), 4.30 (dd, *J*<sub>6a,6b</sub> = 10.2 Hz, *J*<sub>5,6a</sub> = 4.7 Hz, 1H, H-6a), 3.89 (m, 2H, H-2, H-3), 3.78 (dd, *J*<sub>5,6b</sub> = 10.2 Hz, *J*<sub>6a,6b</sub> = 10.2 Hz, 1H, H-6b), 3.57 (dd, *J*<sub>4,5</sub> = 9.2 Hz, *J*<sub>3,4</sub> = 9.2 Hz, 1H, H-4), 3.50 (ddd, *J*<sub>5,6a</sub> = 10.2 Hz, *J*<sub>4,5</sub> = 9.2 Hz, *J*<sub>5,6a</sub> = 4.7 Hz, 1H, H-5), 2.71 (qd, *J*<sub>CH<sub>2</sub>CH<sub>2</sub></sub> = 12.6 Hz, *J*<sub>CH<sub>2</sub>CH<sub>3</sub></sub> = 7.3 Hz, 2H, CH<sub>2</sub>), 1.26 (t, *J*<sub>CH<sub>2</sub>CH<sub>3</sub></sub> = 7.3 Hz, 3H, CH<sub>3</sub>).

<sup>13</sup>C NMR (126 MHz, MeOD) δ 139.0 (1C, C=O), 129.9, 129.0, 127.4, (CAr), 102.9 (1C, CH<sub>2</sub>Ph), 94.0 (1C, CCl<sub>3</sub>), 85.6 (1C, C-1), 82.8 (1C, C-5), 73.1 (1C, C-3), 71.9 (1C, C-4), 69.5 (1C, C-6), 58.4 (1C, C-2), 25.1 (1C, CH<sub>2</sub>), 15.4 (1C, CH<sub>3</sub>).

(ESI)HRMS - C<sub>20</sub>H<sub>29</sub><sup>35</sup>Cl<sub>3</sub>NNaO<sub>5</sub>S<sup>+</sup> ([M+Na]<sup>+</sup>) requires m/z 478.0025: found m/z 478.0014

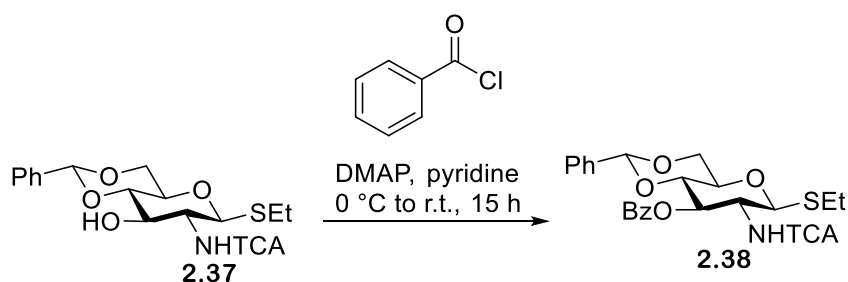
C<sub>20</sub>H<sub>29</sub>O<sub>5</sub>NNa<sup>35</sup>Cl<sub>3</sub>S : C<sub>20</sub>H<sub>29</sub>O<sub>5</sub>NNa<sup>35</sup>Cl<sub>2</sub><sup>37</sup>ClS : C<sub>20</sub>H<sub>29</sub>O<sub>5</sub>NNa<sup>35</sup>Cl<sup>37</sup>Cl<sub>2</sub>S ratio of peak intensities = 2.9 : 2.8 : 1

[α]<sub>D</sub><sup>25</sup> = - 50.6 (c 0.5, DCM)

IR- 3550 (O-H), 3314 (N-H), 2878 (C-H), 2471 (C-H), 1984 (C-H), 1681 (C=O), 1530 (N-H), 1425 (C=C), 1079 (C-O), 745 (C-Cl).

## Experimental

### 8.2.4.5 Synthesis of ethyl 3,6-di-O-benzyl-2-deoxy-2-N-trichloroacetamido-1-thio-β-D-glucopyranoside **2.38**



Benzoyl chloride (0.57 mL, 5.0 mmols, 1.5 eq) was added to a solution of **2.37** (1.5 g, 3.3 mmols) and DMAP (cat) in pyridine at 0 °C. The reaction mixture was warmed to r.t. and stirred for 1.5 hours, affording a brown solution. The solution was concentrated *in vacuo*, dissolved in DCM (15 mL), washed with water (15 mL), dried (MgSO<sub>4</sub>) and concentrated *in vacuo* to afford a brown oil. The oil was purified by column chromatography, eluting with a graduated solvent system of 5 : 1 Hexane : EtOAc to 2 : 1 Hexane : EtOAc. This yielded a white foam of **2.38** (2.9 g, 5.1 mmols, 66%); *R<sub>f</sub>* = 0.61 ( 2 : 1 Hexane : EtOAc).

<sup>1</sup>H NMR (500 MHz, CDCl<sub>3</sub>) δ 8.01 (dd, *J*<sub>HAr</sub> = 8.3 Hz, *J*<sub>HAr</sub> = 1.2 Hz, 2H, HAr), 7.84 (d, *J*<sub>HAr</sub> = 10 Hz, 1H, NH), 7.59 (m, 1H, HAr), 7.44 (m, 2H, HAr), 7.40 (m, 2H, HAr), 7.31 (m, 3H, HAr), 5.95 (dd, *J*<sub>2,3</sub> = 9.8 Hz, *J*<sub>3,4</sub> = 9.8 Hz, 1H, H-3), 5.54 (s, 1H, CH<sub>2</sub>Ph), 4.78 (d, *J*<sub>1,2</sub> = 10.5 Hz, 1H, H-1), 4.47 (ddd, *J*<sub>1,2</sub> = 10.53 Hz, *J*<sub>2,3</sub> = 10 Hz, *J*<sub>NH,2</sub> = 10 Hz, 1H, H-2), 4.05 (dd, *J*<sub>5,6a</sub> = 9.0 Hz, *J*<sub>6a,6b</sub> = 3.6 Hz, 1H, H-6a), 3.90 (dd, *J*<sub>3,4</sub> = 9.30 Hz, *J*<sub>4,5</sub> = 9.30 Hz, 1H, H-4), 3.71 (m, 2H, H-5, H-6b), 2.60 (qd, *J*<sub>CH<sub>2</sub>-CH<sub>2</sub></sub> = 12.50 Hz, *J*<sub>CH<sub>2</sub>-CH<sub>3</sub></sub> = 7.30 Hz, 2H, CH<sub>2</sub>), 1.25 (t, *J*<sub>CH<sub>3</sub>-CH<sub>3</sub></sub> = 7.30), 3H, CH<sub>3</sub>).

<sup>13</sup>C NMR (126 MHz, CDCl<sub>3</sub>) δ 167.7 (1C, C=O), 162.4 (1C, C=O), 137.0, 134.0, 130.0, 128.9, 128.6, 128.1, 125.7, (CAr), 100.9 (1C, CH<sub>2</sub>Ph), 92.2 (1C, CCl<sub>3</sub>), 84.5 (1C, C-1), 79.1 (1C, C-4), 73.8 (1C, C-3), 70.5 (1C, C-5), 68.3 (1C, C-6), 54.7 (1C, C-2), 24.4 (1C, CH<sub>2</sub>), 14.9 (1C, CH<sub>3</sub>).

(ESI)HRMS - C<sub>24</sub>H<sub>24</sub><sup>35</sup>Cl<sub>3</sub>NO<sub>6</sub>S<sup>+</sup> ([M+Na]<sup>+</sup>) requires *m/z* 582.0288: found *m/z* 582.0286

C<sub>24</sub>H<sub>24</sub>O<sub>6</sub>NNa<sup>35</sup>Cl<sub>3</sub>S : C<sub>24</sub>H<sub>24</sub>O<sub>6</sub>NNa<sup>35</sup>Cl<sub>2</sub><sup>37</sup>ClS : C<sub>24</sub>H<sub>24</sub>O<sub>6</sub>NNa<sup>35</sup>Cl<sup>37</sup>Cl<sub>2</sub>S ratio of peak intensities = 3.3 : 3 : 1

[α]<sub>D</sub><sup>25</sup> = - 61.8 (c 1, DCM)

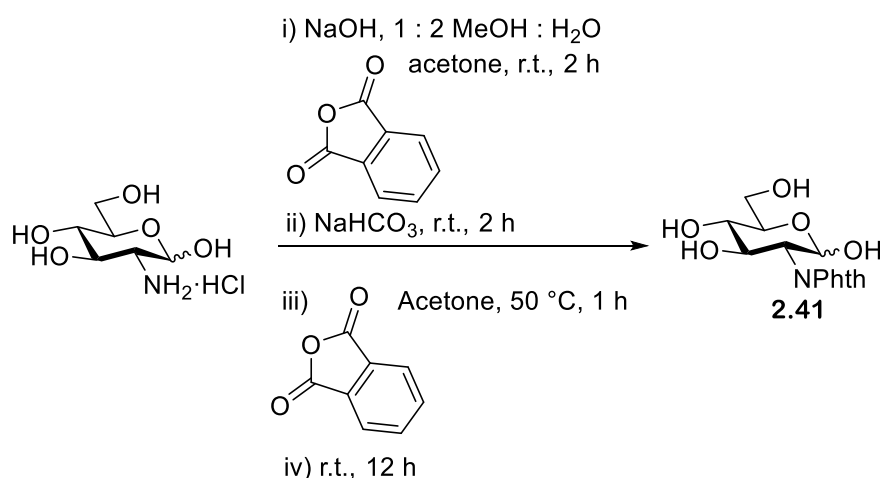
*IR*- 3342 (N-H), 2925 (C-H), 1990 (C-H), 1726 (C=O), 1690 (C=O), 1600 (N-H), 1523 (C=C), 1249 (C-O), 1069 (C-O), 819 (C-Cl).

No literature reference for characterisation could be found

## Experimental

### 8.2.5 Synthesis of 3-Azidopropyl 3,6-di-O-benzyl-2-deoxy-2-phthalimido-1-β-D-glucopyranoside **2.3c**

#### 8.2.5.1 Synthesis of 2-deoxy-2-phthalimido-D-glucopyranose **2.41**<sup>387</sup>



Sodium hydroxide (3.7 g, 90 mmols) was added slowly to a solution of D-glucosamine hydrochloride (20 g, 90 mmols, 1 eq) in 1 : 2 MeOH : H<sub>2</sub>O (120 mL). The reaction mixture was stirred at r.t. to afford a clear solution. A solution of Phthalic anhydride (16 g, 1108 mmols, 1.2 eq) in acetone (80 mL) was then added dropwise to the reaction mixture. The solution was stirred at r.t. for 2 h, affording an initial thick white precipitate. NaHCO<sub>3</sub> (16 g, 190 mmols, 2 eq) was then added and the reaction mixture stirred at r.t. for 2 h, affording a cloudy white solution. A solution of Phthalic anhydride (6 g, 40 mmols, 0.5 eq) in acetone (40 mL) was added dropwise to the reaction mixture. The reaction mixture was heated to 50 °C and stirred for 1 h, affording a light-yellow solution. The solution was then cooled to r.t. and stirred for 12 h, affording a yellow solution. The solution was then acidified to pH 1.5 using 1 M HCl solution, and the the solution placed in the freezer for 4 h. This resulted in the formation of a white precipitate, which was collected *via* Bunker filtration and washed with cold water. The filtrate was concentrated to a half its original volume *in vacuo* and placed back in the freezer for 4 h to yield more precipitate that could be isolated - this process was repeated 2 further times. The total mass of **2.41** that was collected was 16.37 g (53 mmols, 54%).

<sup>1</sup>H NMR (500 MHz, DMSO) δ 7.72 (dd, *J*<sub>Ar</sub> = 6.8 Hz, *J*<sub>Ar</sub> = 1 Hz, 1H, HAr), 7.55 (m, 1H, HAr), 7.50 (m, 2H, HAr), 5.06 (d, *J*<sub>1,2</sub> = 3.5 Hz, 1H, H-1), 3.75 (dd, *J*<sub>2,3</sub> = 8.3 Hz, *J*<sub>1,2</sub> = 3.5 Hz, 1H, H-2), 3.64 (m, 3H, H-3, H-5, H-6a), 3.50 (m, 1H, H-6b), 3.18 (m, 1H, H-4).

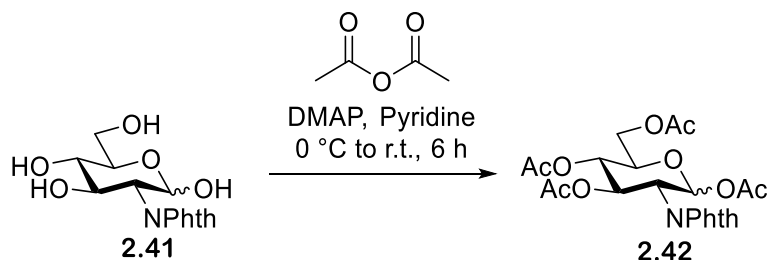
<sup>13</sup>C NMR (126 MHz, DMSO) δ 169.0 (1C, C=O), 168.9 (1C, C=O), 131.2, 129.7, 129.4, 128.5, (CAr), 91.0 (1C, C-1), 72.5 (1C, C-3/5), 71.3 (1C, C-4), 71.0 (1C, C-3/5), 61.6 (1C, C-6), 55.5 (1C, C-2).

(ESI)HRMS - C<sub>14</sub>H<sub>16</sub>NO<sub>7</sub><sup>+</sup> ([M+H]<sup>+</sup>) requires *m/z* 310.0927: found *m/z* 310.0923

IR- 3308 (O-H), 3254 (O-H), 2960 (C-H), 2875 (C-H), 2653 (C-H), 1708 (C=O), 1616 (C=C), 1559 (C=C), 1037 (C-O).

## Experimental

### 8.2.5.2 Synthesis of 1,3,4,6-tetra-O-acetyl-2-deoxy-2-phthalimido-D-glucopyranose **2.42** <sup>388</sup>



Acetic anhydride (30 mL) was added dropwise to a solution of **2.41** (15 g, 50 mmols) and DMAP in pyridine (30 mL) at 0 °C. The reaction mixture was warmed to r.t. and stirred for 6 h, affording a light-yellow solution. Ice cold water (5 mL) was added to the solution dropwise, affording a fine white precipitate. The precipitate containing solution was added to a beaker of cold water (40 mL) whereupon a thick white precipitate developed. DCM (40 mL) was added to dissolve the precipitate and the organic layer was extracted and washed with cold water (40 mL), 5% HCl solution (2 x 40 mL), cold water (40 mL) and saturated NaHCO<sub>3</sub> solution (40 mL), affording a light-yellow solution. This solution was dried (MgSO<sub>4</sub>) and concentrated *in vacuo* to yield a white foam of **2.42** (21 g, 44 mmols, 87%); *R<sub>f</sub>* = 0.38 (2 : 1 Hexane : EtOAc).

<sup>1</sup>H NMR (500 MHz, CDCl<sub>3</sub>) δ 7.85 (dd, *J*<sub>HAr</sub> = 5.5 Hz, *J*<sub>HAr</sub> = 3.0 Hz, 2H, HAr), 7.75 (dd, *J*<sub>HAr</sub> = 5.5 Hz, *J*<sub>HAr</sub> = 3.0 Hz, 2H, HAr), 6.56 (dd, *J*<sub>2,3</sub> = 11.5 Hz, *J*<sub>3,4</sub> = 9.2 Hz, 1H, H-3), 6.30 (d, *J*<sub>1,2</sub> = 3.4 Hz, 1H, H-1), 5.17 (dd, *J*<sub>4,5</sub> = 10.2 Hz, *J*<sub>3,4</sub> = 9.2 Hz, 1H, H-4), 4.73 (dd, *J*<sub>2,3</sub> = 11.5 Hz, *J*<sub>1,2</sub> = 3.4 Hz, 1H, H-2), 4.37 (dd, *J*<sub>6a,6b</sub> = 12.3 Hz, *J*<sub>5,6a</sub> = 3.8 Hz, 1H, H-6a), 4.22 (ddd, *J*<sub>4,5</sub> = 10.2 Hz, *J*<sub>5,6a</sub> = 3.8 Hz, *J*<sub>5,6b</sub> = 2.0 Hz, 1H, H-5), 4.14 (dd, *J*<sub>6a,6b</sub> = 12.3 Hz, *J*<sub>5,6b</sub> = 2.0 Hz, 1H, H-6b), 2.12 (s, CH<sub>3</sub>), 2.09 (s, CH<sub>3</sub>), 2.06 (s, CH<sub>3</sub>), 1.87 (s, CH<sub>3</sub>).

<sup>13</sup>C NMR (126 MHz, CDCl<sub>3</sub>) δ 170.7 (1C), 170.0 (1C), 169.8 (1C), 169.5 (1C), 169.3 (1C), 168.6 (1C), (C=O), 134.5, 129.0, 128.2, 123.7, (CAr), 90.5 (1C, C-1), 70.2 (1C, C-5), 69.4 (1C, C-4), 67.0 (1C, C-3), 61.5 (1C, C-6), 52.8 (1C, C-2), 21.0 (1C, CH<sub>3</sub>), 20.7 (1C, CH<sub>3</sub>), 20.6 (2C, CH<sub>3</sub>).

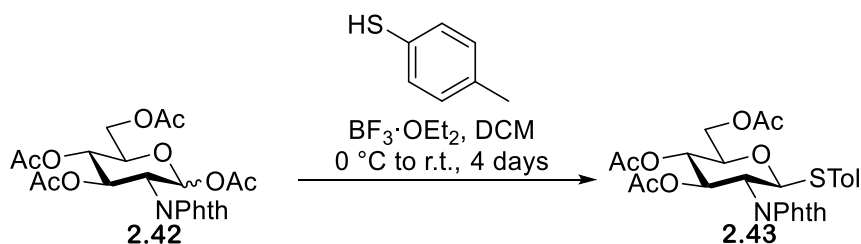
(ESI)HRMS - C<sub>22</sub>H<sub>23</sub>NNaO<sub>11</sub><sup>+</sup> ([M+Na]<sup>+</sup>) requires *m/z* 500.1169: found *m/z* 500.1173

[α]<sub>D</sub><sup>25</sup> = + 73.4 (c 1, DCM)

IR- 2939 (C-H), 1732 (C=O), 1715 (C=O), 1368 (C=C), 1214 (C-O), 1030 (C-O), 1012 (C-O).

## Experimental

### 8.2.5.3 Synthesis of 4-methylphenyl 3,4,6-tri-O-acetyl-2-deoxy-2-phthalimido-1-thio-β-D-glucopyranoside **2.43**<sup>389</sup>



$\text{BF}_3 \cdot \text{OEt}_2$  (8.1 mL, 66 mmols, 1.5 eq) was added dropwise to a solution of **2.42** (21 g, 44 mmols) and 4-methylbenzenethiol (7.1 g, 57 mmols, 1.3 eq) in dry DCM (200 mL) at 0 °C under  $\text{N}_2$ . The reaction mixture was stirred at r.t. for 4 days, affording a clear solution. The solution was washed with water (100 mL), saturated  $\text{NaHCO}_3$  solution (100 mL), dried ( $\text{MgSO}_4$ ) and concentrated *in vacuo* to yield an orange oil. The oil was purified by column chromatography, eluting with a graduated solvent system of 8 : 1 Hexane : EtOAc to 7 : 1 DCM : MeOH. This afforded a white solid of **2.43** (20 g, 37 mmols, 85%);  $R_f = 0.7$  (1 : 1 Hexane : EtOAc).

$^1\text{H}$  NMR (500 MHz,  $\text{CDCl}_3$ )  $\delta$  7.87 (dd,  $J_{\text{HAr}} = 5.5$  Hz,  $J_{\text{HAr}} = 3.2$  Hz, 2H, HAr (Phth)), 7.75 (dd,  $J_{\text{HAr}} = 5.5$  Hz,  $J_{\text{HAr}} = 3.2$  Hz, 2H, HAr (Phth)), 7.30 (d,  $J_{\text{HAr}} = 8.0$  Hz, 2H, HAr (STol)), 7.07 (d,  $J_{\text{HAr}} = 8.0$  Hz, 2H, HAr (STol)), 5.78 (dd,  $J_{4,5} = 10.2$  Hz,  $J_{3,4} = 9.2$  Hz, 1H, H-3), 5.65 (d,  $J_{1,2} = 10.4$  Hz, 1H, H-1), 5.12 (dd,  $J_{2,3} = 10.4$  Hz,  $J_{3,4} = 9.2$  Hz, 1H, H-4), 4.32 (dd,  $J_{1,2} = 10.4$  Hz,  $J_{2,3} = 10.4$  Hz, 1H, H-2), 4.28 (dd,  $J_{6a,6b} = 12.2$  Hz,  $J_{5,6a} = 5.0$  Hz, 1H, H-6a), 4.21 (dd,  $J_{6a,6b} = 12.2$  Hz,  $J_{5,6a} = 5.0$  Hz, 1H, H-6b), 3.88 (ddd,  $J_{4,5} = 10.2$  Hz,  $J_{5,6a} = 5.0$  Hz,  $J_{5,6b} = 2.3$  Hz, 1H, H-5), 2.33 (s, 3H,  $\text{CH}_3$  (STol)), 2.11 (s, 3H,  $\text{CH}_3$  (OAc)), 2.02 (s, 3H,  $\text{CH}_3$  (OAc)), 1.83 (s, 3H,  $\text{CH}_3$  (OAc)).

$^{13}\text{C}$  NMR (126 MHz,  $\text{CDCl}_3$ )  $\delta$  170.6 (1C), 170.1 (1C), 169.4 (1C), (C=O, OAc), 167.8 (1C), 167.0 (1C), (C=O, Phth), 138.4, 134.4, 134.3, 133.9, 131.6, 131.2, 129.6, 126.7, 123.7, (CAr), 83.1 (1C, C-1), 75.9 (1C, C-5), 71.7 (1C, C-3), 68.7 (1C, C-4), 62.2 (1C, C-6), 53.6 (1C, C-2), 21.2 (1C,  $\text{CH}_3$  (STol)), 20.8 (1C,  $\text{CH}_3$  (OAc)), 20.6 (1C,  $\text{CH}_3$  (OAc)), 20.4 (1C,  $\text{CH}_3$  (OAc)).

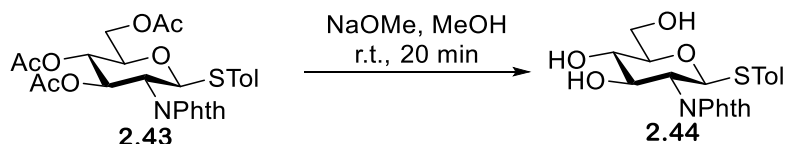
(ESI)HRMS -  $\text{C}_{27}\text{H}_{27}\text{NNaO}_9\text{S}^+$  ( $[\text{M}+\text{Na}]^+$ ) requires  $m/z$  564.1304: found  $m/z$  564.1304

$[\alpha]_D^{25} = +41.2$  (c 1, DCM)

IR- 2953 (C-H), 1737 (C=O), 1715 (C=O), 1381 (C=C), 1211 (C-O), 1037 (C-O).

## Experimental

### 8.2.5.4 Synthesis of 4-methylphenyl 2-deoxy-2-phthalimido-1-thio- $\beta$ -D-glucopyranoside **2.44** <sup>390</sup>



A NaOMe solution was added dropwise to a solution of **2.43** (20 g, 37 mmols) in a 1 : 1 mixture of MeOH : DCM (100mL : 100 mL) until pH 10 was reached. The reaction mixture was stirred at r.t. for 20 minutes, affording a clear solution with a white precipitate. The precipitate was removed *via* vacuum filtration and the filtrate was neutralised with dowex, which itself was subsequently removed *via* filtration, leaving a clear solution. This solution was concentrated *in vacuo*, affording a white solid of **2.44** (16 g, 36 mmols, 99%);  $R_f = 0.66$  (EtOAc).

$^1\text{H}$  NMR (500 MHz,  $\text{CD}_2\text{Cl}_2$  / MeOD)  $\delta$  7.85 (m, 1H, HAr (Phth)), 7.80 (m, 1H, HAr (Phth)), 7.74 (m, 2H, HAr (Phth)), 7.23 (d,  $J_{\text{HAr}} = 8.1$  Hz, 2H, HAr (STol)), 7.03 (d,  $J_{\text{HAr}} = 8.1$  Hz, 2H, HAr (STol)), 5.52 (d,  $J_{1,2} = 10.4$  Hz, 1H, H-1), 4.20 (m, 1H, H-3), 4.08 (m, 1H, H-2), 3.86 (dd,  $J_{6a,6b} = 12.0$  Hz,  $J_{6a,5} = 1.8$  Hz, 1H, H-6a), 3.74 (m, 1H, H-6b), 3.44 (m, 2H, H-4, H-5), 2.25 (s, 3H,  $\text{CH}_3$ ).

$^{13}\text{C}$  NMR (126 MHz,  $\text{CD}_2\text{Cl}_2$  / MeOD)  $\delta$  168.5 (1C), 168.1 (1C), (C=O), 138.1, 134.2, 132.2, 131.7, 131.5, 129.5, 128.8, 123.4, 123.0, (CAr), 84.2 (1C, C-1), 80.4 (1C, C-4), 72.3 (1C, C-3), 71.1 (1C, C-5), 61.8 (1C, C-6), 56.1 (1C, C-2), 20.5 (1C,  $\text{CH}_3$ ).

(ESI)HRMS -  $\text{C}_{21}\text{H}_{21}\text{NNaO}_6\text{S}^+$  ( $[\text{M}+\text{Na}]^+$ ) requires  $m/z$  438.0987: found  $m/z$  438.0978

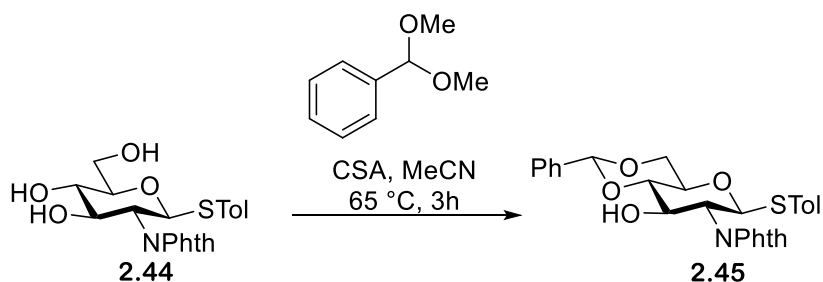
$[\alpha]_D^{25} = +91.38$  (c 0.4, MeOH)

IR- 3313 (O-H), 2918 (C-H), 1991 (C-H), 1769 (C=O), 1700 (C=O), 1392 (C=C), 1085 (C-O), 1013 (C-O).



## Experimental

### 8.2.5.5 Synthesis of 4-methylphenyl 4,6-O-benzylidene-2-deoxy-2-phthalimido-1-thio- $\beta$ -D-glucopyranoside **2.45**<sup>391</sup>



2,2 DMT (8.4 mL, 50 mmols, 1.5 eq) was added dropwise to an acidic solution of **2.44** (16 g, 37 mmols) and CSA (cat) in dry MeCN (200 mL), affording a clear light-yellow solution. The solution was stirred at r.t. for 12 h, affording a cloudy white solution which was neutralised with NEt<sub>3</sub> and concentrated *in vacuo* to yield a clear oil. This oil was purified by column chromatography, eluting with a graduated solvent system of 6 : 1 Hexane : EtOAc to 1 : 1 Hexane : EtOAc. This yielded a white solid of **2.45** (12 g, 24 mmols, 66%); R<sub>f</sub> = 0.49 (2:1 Hexane : EtOAc).

<sup>1</sup>H NMR (500 MHz, CDCl<sub>3</sub>)  $\delta$  7.89 (d, J<sub>HAr</sub> = 4.8 Hz, 1H, HAr (Phth)), 7.84 (d, J<sub>HAr</sub> = 4.8 Hz, 1H, HAr (Phth)), 7.74 (m, 2H, HAr (Phth)), 7.47 (m, 2H, HAr (Ph)), 7.36 (m, 3H, HAr (Ph)), 7.27 (m, 2H, HAr (STol)), 7.06 (d, J<sub>HAr</sub> = 8.0 Hz, 2H, HAr (STol)), 5.62 (d, J<sub>1,2</sub> = 10.5 Hz, 1H, H-1), 5.55 (s, 1H, CHPh), 4.61 (ddd, J<sub>2,3</sub> = 10.0 Hz, J<sub>3,4</sub> = 9.5 Hz, J<sub>3,OH</sub> = 3.4 Hz, 1H, H-3), 4.38 (dd, J<sub>6a,6b</sub> = 10.3 Hz, J<sub>5,6a</sub> = 4.8 Hz, 1H, H-6a), 4.30 (dd, J<sub>1,2</sub> = 10.5 Hz, J<sub>2,3</sub> = 10.0 Hz, 1H, H-2), 3.80 (dd, J<sub>6a,6b</sub> = 10.3 Hz, J<sub>5,6b</sub> = 10.3 Hz, 1H, H-6b), 3.67 (ddd, J<sub>5,6b</sub> = 10.3 Hz, J<sub>4,5</sub> = 9.5 Hz, J<sub>5,6a</sub> = 4.8 Hz, 1H, H-5), 3.57 (dd, J<sub>3,4</sub> = 9.5 Hz, J<sub>4,5</sub> = 9.5 Hz, 1H, H-4), 2.51 (d, J<sub>3,OH</sub> = 3.4 Hz, 1H, OH), 2.30 (s, 3H, CH<sub>3</sub>).

<sup>13</sup>C NMR (126 MHz, CDCl<sub>3</sub>)  $\delta$  168.3 (1C), 167.5 (1C), (C=O), 138.5, 136.9, 134.2, 133.4, 131.7, 131.6, 129.7, 129.4, 128.4, 127.8, 126.3, 123.9, 123.4, (CAr), 102.0 (1C, CHPh), 84.5 (1C, C-1), 81.9 (1C, C-4), 70.3 (1C, C-5), 69.8 (1C, C-3), 68.6 (1C, C-6), 55.6 (1C, C-2), 21.2 (1C, CH<sub>3</sub>).

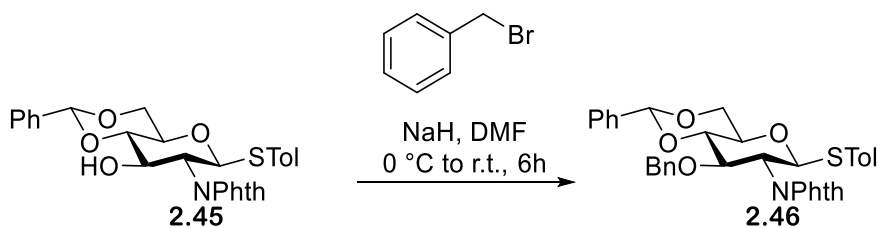
(ESI)HRMS - C<sub>28</sub>H<sub>25</sub>NNaO<sub>6</sub>S<sup>+</sup> ([M+Na]<sup>+</sup>) requires m/z 526.1300: found m/z 526.1305

$[\alpha]_D^{25} = +34.5$  (c 1, DCM)

IR- 3468 (O-H), 2866 (C-H), 1978 (C-H), 1774 (C=O), 1707 (C=O), 1383 (C=C), 1071 (C-O).

## Experimental

### 8.2.5.6 Synthesis of 4-methylphenyl 3-O-benzyl-4,6-O-benzylidene-2-deoxy-2-phthalimido-1-thio- $\beta$ -D-glucopyranoside **2.46**<sup>392</sup>



NaH (0.86 g, 36 mmols, 1.5 eq) was added to a solution of **2.45** (12 g, 24 mmols) in dry DMF (100 mL) at 0 °C, and the reaction mixture stirred at 0°C for 10 minutes. BnBr (4.3 mL, 36 mmols, 1.5 eq) was then added dropwise to the reaction mixture, and the mixture stirred at r.t. for 6 h, affording a clear solution. The solution was concentrated *in vacuo*, yielding a colourless oil. The oil was dissolved in DCM (100 mL) washed with water (3 x 100 mL), saturated NaCl solution (100 mL), dried (MgSO<sub>4</sub>) and concentrated *in vacuo*. The oil was purified by column chromatography, eluting with a graduated solvent system of 8 : 1 Hexane : EtOAc to 3 : 1 Hexane : EtOAc. This afforded a white solid of **2.46** (5.9 g, 9.9 mmols, 41%)

<sup>1</sup>H NMR (500 MHz, CDCl<sub>3</sub>)  $\delta$  7.86 (d,  $J_{\text{HAr}} = 6.9$  Hz, 1H, HAr Phth), 7.71 (m, 2H, HAr Phth), 7.63 (d,  $J_{\text{HAr}} = 6.9$  Hz, 1H, HAr Phth), 7.50 (dd,  $J_{\text{HAr}} = 8.0$  Hz,  $J_{\text{HAr}} = 1.6$  Hz, 2H, HAr Ph), 7.38 (m, 4H, HAr Ph), 7.24 (d,  $J_{\text{HAr}} = 8.0$  Hz, 2H, HAr Ph), 7.04 (d,  $J_{\text{HAr}} = 8.0$  Hz, 2H, HAr Ph), 6.98 (d,  $J_{\text{HAr}} = 7.5$  Hz, 2H, HAr STol), 6.90 (m, 2H, HAr STol), 5.60 (s, 1H, CHPh), 5.54 (d,  $J_{1,2} = 10.4$  Hz, 1H, H-1), 4.76 (d,  $J_{\text{CH}_2} = 12.3$  Hz, 1H, CH<sub>2</sub>), 4.48 (d,  $J_{\text{CH}_2} = 12.3$  Hz, 1H, CH<sub>2</sub>), 4.40 (m, 2H, H-3, H-6a), 4.26 (dd,  $J_{1,2} = 10.4$  Hz,  $J_{2,3} = 10.4$  Hz, 1H, H-2), 3.83 (dd,  $J_{5,6b} = 9.6$  Hz,  $J_{6a,6b} = 9.6$  Hz, 1H, H-6b), 3.77 (dd,  $J_{3,4} = 9.6$  Hz,  $J_{4,5} = 9.6$  Hz, 1H, H-4), 3.68 (td,  $J_{4,5} = 9.6$  Hz,  $J_{5,6b} = 9.6$  Hz,  $J_{5,6a} = 4.8$  Hz, 1H, H-5), 2.29 (s, 3H, CH<sub>3</sub>).

<sup>13</sup>C NMR (126 MHz, CDCl<sub>3</sub>)  $\delta$  167.8 (1C), 167.2 (1C), (C=O), 138.4, 137.7, 137.3, 134.0, 133.8, 133.5, 131.6, 129.7, 129.0, 128.6, 128.3, 128.2, 128.0, 127.7, 127.4, 127.0, 126.1, 123.5, 123.3, (CAr), 101.3 (1C, CHPh), 84.3 (1C, C-1), 82.8 (1C, C-4), 75.5 (1C, C-3), 74.2 (1C, CH<sub>2</sub>), 70.4 (1C, C-5), 68.7 (1C, C-6), 54.8 (1C, C-2), 21.1 (1C, CH<sub>3</sub>).

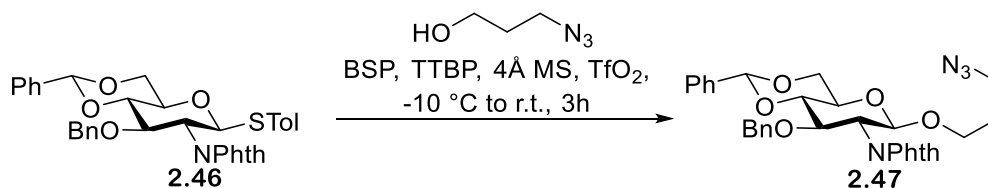
(ESI)HRMS - C<sub>35</sub>H<sub>31</sub>NNaO<sub>6</sub>S<sup>+</sup> ([M+Na]<sup>+</sup>) requires m/z 616.1770: found m/z 616.1773

$[\alpha]_D^{25} = +67.3$  (c 1, DCM)

IR- 2975 (C-H), 2098 (C-H), 1994 (C-H), 1775 (C=O), 1716 (C=O), 1382 (C=C), 1049 (C-O).

## Experimental

### 8.2.5.7 Synthesis of 3-Azidopropyl 3-O-benzyl-4,6-O-benzylidene-2-deoxy-2-phthalimido-1-β-D-glucopyranoside **2.47**<sup>237</sup>



**2.46** (0.8 g, 1.3 mmols) was dissolved in dry DCE, cooled to -10 °C and placed under N<sub>2</sub>, affording a clear solution. BSP (0.3 g, 1.5 mmols, 1.2 eq), TTBP (0.7 g, 2.8 mmols, 2.2 eq) and 4 Å molecular sieves were added, and the solution placed under N<sub>2</sub> and stirred at -10 °C for 5 minutes, affording a white cloudy solution. Tf<sub>2</sub>O (0.5 mL, 2.8 mmols, 2.2 eq) was added to the reaction mixture, resulting in a deep red solution which was stirred for 5 minutes. 3-azidopropan-1-ol was then added to the solution, and the reaction mixture warmed to r.t. and stirred for 3 h, affording a white solution. The solution was filtered through celite, washed with saturated NaHCO<sub>3</sub> solution (20 mL), dried (MgSO<sub>4</sub>) and concentrated *in vacuo*, affording a colourless oil. The oil was purified by column chromatography, eluting with a graduated solvent system of 8 : 1 Hexane : EtOAc to 3 : 1 Hexane : EtOAc. This yielded a white solid of **2.47** (0.6 g, 1 mmol, 79 %, β-only); R<sub>f</sub> = 0.55 (2 : 1 Hexane : EtOAc).

<sup>1</sup>H NMR (500 MHz, CDCl<sub>3</sub>) δ 7.83 (dd, *J*<sub>HAr</sub> = 5.4 Hz, *J*<sub>HAr</sub> = 3.0 Hz, 1H, HAr), 7.72 (m, 2H, HAr), 7.52 (dd, *J*<sub>HAr</sub> = 8.0 Hz, *J*<sub>HAr</sub> = 1.5 Hz, 2H, HAr), 7.39 (m, 4H, HAr), 6.99 (m, 3H, HAr), 6.89 (dd, *J*<sub>HAr</sub> = 5.9 Hz, *J*<sub>HAr</sub> = 1.4 Hz, 2H, HAr), 5.62 (s, 1H, CHPh), 5.20 (d, *J*<sub>1,2</sub> = 8.5 Hz, 1H, H-1), 4.80 (d, *J*<sub>CH2</sub> = 12.4 Hz, 1H, CH<sub>2</sub> Bn), 4.50 (d, *J*<sub>CH2</sub> = 12.4 Hz, 1H, CH<sub>2</sub> Bn), 4.41 (m, 2H, H-3, H-6a), 4.20 (dd, *J*<sub>1,2</sub> = 8.5 Hz, *J*<sub>2,3</sub> = 1.8 Hz, 1H, H-2), 3.83 (m, 3H, H-6b, H-4, CH<sub>2</sub>), 3.65 (td, *J*<sub>4,5</sub> = 9.8 Hz, *J*<sub>5,6b</sub> = 9.8 Hz, *J*<sub>5,6a</sub> = 4.9 Hz, 1H, H-5), 3.48 (m, 1H, CH<sub>2</sub>), 3.15 (m, 2H, CH<sub>2</sub>), 1.68 (m, 2H, CH<sub>2</sub>).

<sup>13</sup>C NMR (126 MHz, CDCl<sub>3</sub>) δ 167.7 (1C, C=O), 146.5 (1C, C=O), 137.9, 137.3, 134.1, 133.9, 131.5, 129.0, 128.3, 128.0, 128.0, 127.5, 127.4, 126.0, 123.5, 123.3 (CAr), 101.3 (1C, CPh), 98.9 (1C, C-1), 83.1 (1C, C-4), 74.5 (1C, C-3), 74.1 (1C, CH<sub>2</sub>), 68.7 (1C, C-6), 66.3 (1C, CH<sub>2</sub>), 66.1 (1C, C-5), 55.8 (1C, C-2), 47.8 (1C, CH<sub>2</sub>), 28.8 (1C, CH<sub>2</sub>).

(ESI)HRMS - C<sub>31</sub>H<sub>31</sub>N<sub>4</sub>NaO<sub>7</sub><sup>+</sup> ([M+Na]<sup>+</sup>) requires *m/z* 593.2021: found *m/z* 593.2009

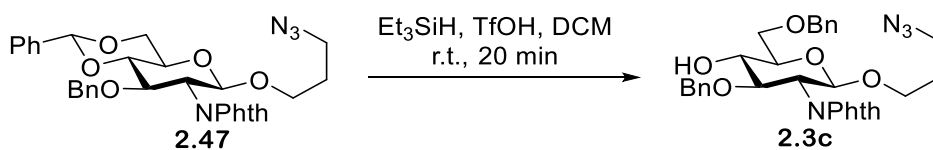
[α]<sub>D</sub><sup>25</sup> = + 31.3 (*c* 1, DCM)

IR- 3064 (C-H), 2944 (C-H), 2875 (C-H), 2096 (N=N=N), 1775 (C=O), 1711 (C=O), 1385 (C=C), 1103 (C-O), 1080 (C-O).

## Experimental

### 8.2.5.8 Synthesis of 3-Azidopropyl 3,6-di-O-benzyl-2-deoxy-2-phthalimido-1-β-D-glucopyranoside **2.3c**

237



Et<sub>3</sub>SiH (0.45 mL, 2.6 mmols, 3.3 eq) was added dropwise to a solution of **2.47** (0.49 g, 0.86 mmols) in dry DCM (20 mL) under N<sub>2</sub>. The reaction mixture was stirred for 2 minutes and TfOH (0.23 mL, 0.88 mmols, 3 eq) was added. The reaction mixture was stirred at r.t. for 20 minutes affording a colourless solution. The solution was washed with water (20 mL), saturated NaHCO<sub>3</sub> solution (20 mL) and saturated NaCl solution (20 mL). The solution was dried (MgSO<sub>4</sub>) and concentrated *in vacuo* to yield a colourless oil. The oil was purified by column chromatography, eluting with a graduated solvent system of 6 : 1 Hexane : EtOAc to 3 : 1 Hexane : EtOAc. This yielded a colourless oil of **2.3c** (0.21 g, 0.37 mmols, 43%); R<sub>f</sub> = 0.3 (2 : 1 Hexane : EtOAc).

<sup>1</sup>H NMR (500 MHz, CDCl<sub>3</sub>) δ 7.81 (m, 1H, HAr), 7.69 (m, 3H, HAr), 7.36 (m, 4H, HAr), 7.30 (m, 1H, HAr), 7.05 (dd, *J*<sub>HAr</sub> = 7.2 Hz, *J*<sub>HAr</sub> = 1.8 Hz, 2H, HAr), 6.94 (dd, *J*<sub>HAr</sub> = 5.3 Hz, *J*<sub>HAr</sub> = 1.8 Hz, 3H, HAr), 5.14 (d, *J*<sub>1,2</sub> = 8.5 Hz, 1H, H-1), 4.75 (d, *J*<sub>CH2</sub> = 12.5 Hz, 1H, CH<sub>2</sub> Bn), 4.64 (d, *J*<sub>CH2</sub> = 12.1 Hz, 1H, CH<sub>2</sub> Bn), 4.58 (d, *J*<sub>CH2</sub> = 12.1 Hz, 1H, CH<sub>2</sub> Bn), 4.53 (d, *J*<sub>CH2</sub> = 12.5 Hz, CH<sub>2</sub> Bn), 4.23 (dd, *J*<sub>2,3</sub> = 10.6 Hz, *J*<sub>3,4</sub> = 8.4 Hz, 1H, H-3), 4.15 (dd, *J*<sub>2,3</sub> = 10.6 Hz, *J*<sub>1,2</sub> = 8.5 Hz, 1H, H-2), 3.81 (m, 4H, H-4, H-6a, H-6b, CH<sub>2</sub>), 3.64 (ddd, *J* = 9.7 Hz, *J* = 9.7 Hz, *J* = 4.8 Hz, 1H, H-5), 3.46 (m, 1H, CH<sub>2</sub>), 3.11 (m, 2H, CH<sub>2</sub>), 2.99 (d, *J*<sub>4,OH</sub> = 2.5 Hz, 1H, OH), 1.65 (m, 2H, CH<sub>2</sub>).

<sup>13</sup>C NMR (126 MHz, CDCl<sub>3</sub>) δ 168.4 (1C), 167.7 (1C), (C=O), 138.2, 137.6, 133.9, 131.6, 128.5, 128.2, 127.9, 127.9, 127.8, 127.4, 123.3, (CAr), 98.4 (1C, C-1), 78.7 (1C, C-3), 74.3 (2C, C-4, CH<sub>2</sub>), 73.8 (1C, CH<sub>2</sub>), 73.7 (1C, C-5), 70.6 (1C, C-6), 66.1 (1C, CH<sub>2</sub>), 55.3 (1C, C-2), 48.0 (1C, CH<sub>2</sub>), 28.8 (1C, CH<sub>2</sub>).

(ESI)HRMS - C<sub>31</sub>H<sub>32</sub>N<sub>4</sub>NaO<sub>7</sub><sup>+</sup> ([M+Na]<sup>+</sup>) requires m/z 595.2169: found m/z 595.2163

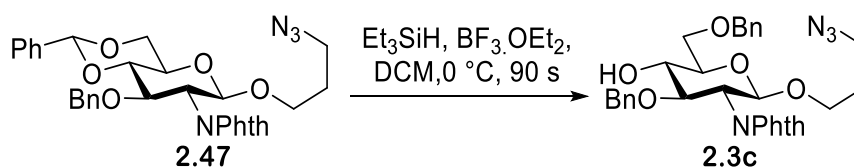
[α]<sub>D</sub><sup>25</sup> = + 20.3 (c 1, DCM)

IR- 3473 (O-H), 3030 (C-H), 2874 (C-H), 2095 (N=N=N), 1774 (C=O), 1709 (C=O), 1387 (C=C), 1066 (C-O), 1109 (C-O).

## Experimental

### 8.2.5.9 Synthesis of 3-Azidopropyl 3,6-di-O-benzyl-2-deoxy-2-phthalimido-1-β-D-glucopyranoside **2.3c**

237



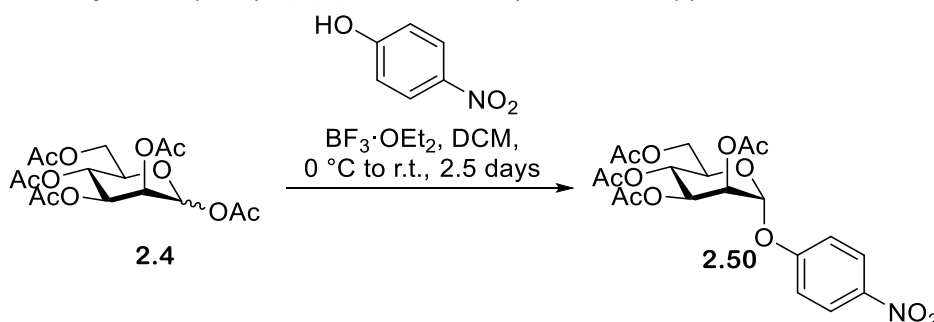
$\text{Et}_3\text{SiH}$  (0.16 mL, 1.0 mmols, 12 eq) was added dropwise to a solution of **2.47** (0.05 g, 0.09 mmols) in dry DCE (50 mL) under  $\text{N}_2$  at  $0^\circ\text{C}$ . The reaction mixture was stirred for 2 minutes and  $\text{BF}_3 \cdot \text{EtO}_2$  (0.2 mL, 0.17 mmols, 2 eq) was added. The reaction mixture was stirred at r.t. for 90 seconds, affording a colourless solution. The solution was washed with water (2 x 20 mL), saturated  $\text{NaHCO}_3$  solution (10 mL) and saturated  $\text{NaCl}$  solution (10 mL). The solution was dried ( $\text{MgSO}_4$ ) and concentrated *in vacuo*, affording a colourless oil. The oil was purified by column chromatography, eluting with a graduated solvent system of 6 : 1 Hexane : EtOAc to 3 : 1 Hexane : EtOAc. This yielded a colourless oil of **2.3c** (0.01 g, 0.017 mmols, 25%);  $R_f = 0.3$  (2 : 1 Hexane : EtOAc).

For compound data please see page 260

## Experimental

8.2.6 Synthesis of squarate mannose analogues - *p*-[[(2-aminoethylamino)-2,3-dioxocyclobut-1-enyl]amino]phenyl  $\alpha$ -D-mannopyranoside **2.53** and *p*-[[(1-amino-2-azidoethane)-2,3-dioxocyclobut-1-enyl]amino]phenyl  $\alpha$ -D-mannopyranoside **2.54**

8.2.6.1 Synthesis of 4-Nitrophenyl 2,3,4,6-tetra-*O*-acetyl- $\alpha$ -D-mannopyranoside **2.50** <sup>393, 394</sup>



$\text{BF}_3 \cdot \text{OEt}_2$  (1.5 mL, 12 mmols, 3 eq) was added dropwise to a solution of **2.4** at  $0^\circ\text{C}$  (1.6 g, 3.9 mmols) and 4-nitrophenol (1.1 g, 7.8 mmols, 2 eq) in dry DCM (10 mL) at r.t. under  $\text{N}_2$ . The reaction mixture was stirred for 2.5 days, affording an orange solution. The solution was quenched with saturated  $\text{NaHCO}_3$  solution (10 mL) and the organic layer extracted, washed with saturated  $\text{NaCl}$  solution (10 mL), dried ( $\text{MgSO}_4$ ) and concentrated *in vacuo* to yield an orange oil. This oil was purified using column chromatography, eluting with a graduated solvent system of 3 : 1 Hexane : EtOAc to 1 : 1 Hex : EtOAc. The semi-crude product was recrystallized from methanol, affording white crystals of **2.50** (0.8 g, 1.7 mmols, 43%);  $R_f = 0.58$  (3:1 Toluene : EtOAc).

$^1\text{H}$  NMR (500 MHz,  $\text{CDCl}_3$ )  $\delta$  8.23 (d,  $J_{\text{HAr}} = 9.30$  Hz, 2H, HAr), 7.22 (d,  $J_{\text{HAr}} = 9.30$  Hz, 2H, HAr), 5.63 (d,  $J_{1,2} = 1.8$  Hz, 1H, H-1), 5.54 (dd,  $J_{3,4} = 10.0$  Hz,  $J_{2,3} = 3.4$  Hz, 1H, H-3), 5.46 (dd,  $J_{2,3} = 3.4$  Hz,  $J_{1,2} = 1.8$  Hz, 1H, H-2), 5.38 (dd,  $J_{3,4} = 10.0$  Hz,  $J_{4,5} = 10.0$  Hz, 1H, H-4), 4.27 (dd,  $J_{6a,6b} = 12.3$  Hz,  $J_{5,6a} = 5.5$  Hz, 1H, H-6a), 4.08 (dd,  $J_{6a,6b} = 12.3$  Hz,  $J_{5,6b} = 2.3$  Hz, 1H, H-6b), 4.02 (ddd,  $J_{4,5} = 10.0$  Hz,  $J_{5,6a} = 5.5$  Hz,  $J_{5,6b} = 2.3$  Hz, 1H, H-5), 2.22 (s, 3H,  $\text{CH}_3$ ), 2.06 (s, 3H,  $\text{CH}_3$ ), 2.05 (s, 3H,  $\text{CH}_3$ ), 2.02 (s, 3H,  $\text{CH}_3$ ).

$^{13}\text{C}$  NMR (126 MHz,  $\text{CDCl}_3$ )  $\delta$  170.4 (1C), 169.9 (1C), 169.9 (1C), 169.6 (1C), (C=O), 160.1, 143.2, 125.8, 116.5, (CAr), 95.7 (1C, C-1), 69.8 (1C, C-5), 68.9 (1C, C-2), 68.5 (1C, C-3), 65.6 (1C, C-4), 61.9 (1C, C-6), 20.8 (1C,  $\text{CH}_3$ ), 20.6 (1C,  $\text{CH}_3$ ), 20.6 (1C,  $\text{CH}_3$ ), 20.6 (1C,  $\text{CH}_3$ ).

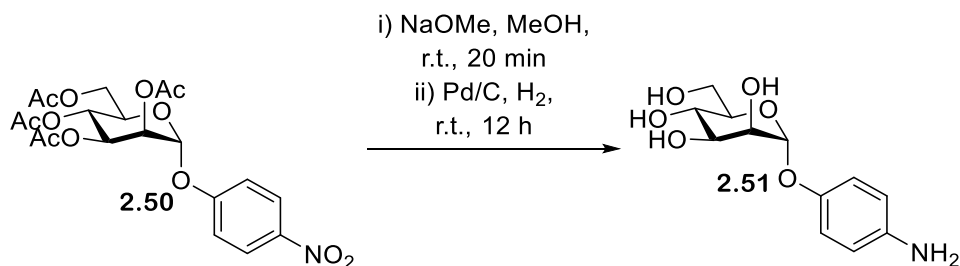
(ESI)HRMS –  $\text{C}_{20}\text{H}_{23}\text{O}_{12}\text{NNa}^+$  ( $[\text{M}+\text{Na}]^+$ ) requires  $m/z$  492.1118: found  $m/z$  492.1121

$[\alpha]_D^{25} = +94.40$  (c 1, DCM)

*IR* – 3127 (C-H), 2973 (C-H), 1954 (C-H), 1742 (C=O), 1592 (C=C), 1519 (N-O), 1343 (N-O), 1214 (C-O), 1025 (C-O).

## Experimental

### 8.2.6.2 Synthesis of 4-Aminophenyl $\alpha$ -D-mannopyranoside **2.51** <sup>395</sup>



A NaOMe solution was added dropwise to a solution of **2.50** (0.75 g 1.6 mmols) in MeOH (10 mL) until pH 10 was reached. The reaction mixture was stirred at r.t. for 20 minutes, affording a clear solution. The solution was neutralised with dowex which was subsequently removed *via* filtration to leave a clear solution. The solution was concentrated *in vacuo*, affording a white solid which was dried *in vacuo* for 2 h. The solid was then dissolved in dry MeOH (10 mL) and Pd/C (cat) was added to the solution. The vessel was placed under nitrogen, and then degassed before backfilling with H<sub>2</sub>. The reaction mixture was stirred at r.t for 12 h then filtered through celite and concentrated *in vacuo* to yield a white solid of **2.51** (0.24 g, 0.84 mmol, 53%).

<sup>1</sup>H NMR (500 MHz, MeOD)  $\delta$  6.89 (d,  $J_{\text{HAr}} = 9.0$  Hz, 2H, HAr), 6.68 (d,  $J_{\text{HAr}} = 9.0$  Hz, 2H, HAr), 5.28 (d,  $J_{1,2} = 1.80$  Hz, 1H, H-1), 3.98 (dd,  $J_{2,3} = 3.3$  Hz,  $J_{1,2} = 1.8$  Hz, 1H, H-2), 3.88 (dd,  $J_{3,4} = 9.2$  Hz,  $J_{2,3} = 3.3$  Hz, 1H, H-3), 3.75 (m, 3H, H-4, H-6a, H-6b), 3.67 (ddd,  $J = 9.6$ ,  $J = 4.7$  Hz,  $J = 2.4$  Hz, 1H, H-5).

<sup>13</sup>C NMR (126 MHz, MeOD)  $\delta$  150.9, 143.5, 119.2, 117.8 (CAr), 101.3 (1C, C-1), 75.1 (1C, C-5), 72.4 (1C, C-3), 72.2 (1C, C-2), 68.4 (1C, C-4), 62.7 (1C, C-6).

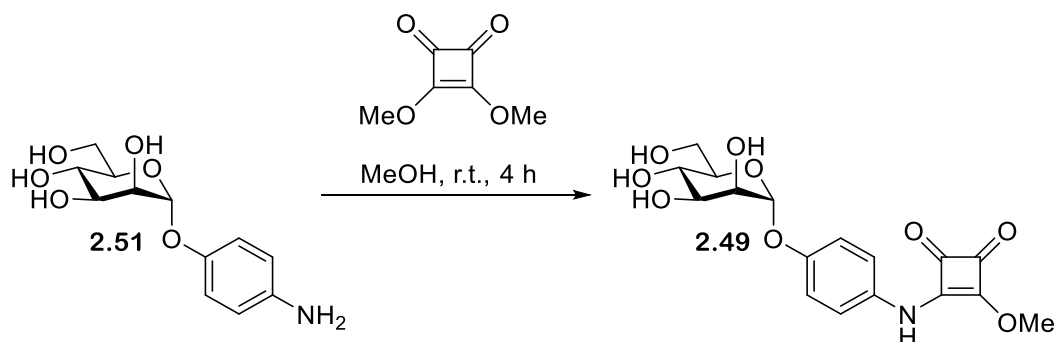
(ESI)HRMS – C<sub>12</sub>H<sub>18</sub>O<sub>6</sub>NNa<sup>+</sup> ([M+Na]<sup>+</sup>) requires m/z 294.0954: found m/z 294.0940

$[\alpha]_D^{25} = -244.75$  (c 1, MeOH)

IR – 3317 (O-H), 2939 (C-H), 2469 (C-H), 1510 (C=C), 1050 (C-O), 1019 (C-O).

## Experimental

### 8.2.6.3 Synthesis of *p*-[*N*-(2-Methoxy-3,4-dioxocyclobut-1-enyl)aminophenyl] $\alpha$ -D-mannopyranoside **2.49** <sup>396</sup>



3,4-dimethoxycyclobut-3-ene-1,2-dione (7.1 g, 0.05 mols) was added to **2.51** (13.6 g, 0.05 mols, 1 eq) in dry methanol and the reaction mixture was stirred at r.t. for 4 h to afford a white cloudy solution containing a precipitate. The precipitate was isolated by filtration, and was dried *in vacuo* to yield a white solid of **2.49** (16.6 g, 0.043 mols, 87%).

<sup>1</sup>H NMR (500 MHz, DMSO)  $\delta$  10.69 (s, 1H, NH), 7.25 (s, 2H, HAr), 7.07 (dd,  $J_{\text{HAr}} = 9.0$  Hz,  $J_{\text{HAr}} = 1.92$  Hz, 2H, HAr), 5.30 (d,  $J_{1,2} = 1.5$  Hz, 1H, H-1), 4.98 (d,  $J_{2,\text{OH}} = 4.5$  Hz, 1H, OH (H-2)), 4.81 (d,  $J_{4,\text{OH}} = 5.6$  Hz, OH (H-4)), 4.72 (d,  $J_{3,\text{OH}} = 5.9$  Hz, 1H, OH (H-3)), 4.44 (dd,  $J_{6a,\text{OH}} = 6.0$  Hz,  $J_{6b,\text{OH}} = 6.0$  Hz, OH (H-6)), 4.36 (s, 3H, CH<sub>3</sub>), 3.81 (m, 1H, H-2), 3.66 (m, 1H, H-3), 3.60 (ddd,  $J_{6a} = 11.6$  Hz,  $J_{6a} = 5.7$  Hz,  $J_{6a,5} = 1.7$  Hz, 1H, H-6a), 3.46 (m, 2H, H-4, H-6b), 3.40 (ddd,  $J_5 = 9.2$  Hz,  $J_5 = 5.9$  Hz,  $J_{5,6a} = 1.7$  Hz, 1H, H-5).

<sup>13</sup>C NMR (126 MHz, DMSO)  $\delta$  183.9 (1C, C=O), 169.4 (1C, C=O), 153.7 (1C, C), 132.6 (1C, C), 121.5, 119.0, 117.0, 115.0 (CAr), 99.7 (1C, C-1), 75.4 (1C, C-5), 71.1, (1C, C-3), 70.5 (1C, C-2), 67.2 (1C, C-4), 61.5 (1C, C-6), 60.8 (1C, CH<sub>3</sub>).

(ESI)HRMS – C<sub>17</sub>H<sub>19</sub>O<sub>9</sub>NNa<sup>+</sup> ([M+Na]<sup>+</sup>) requires *m/z* 404.0958: found *m/z* 404.0947

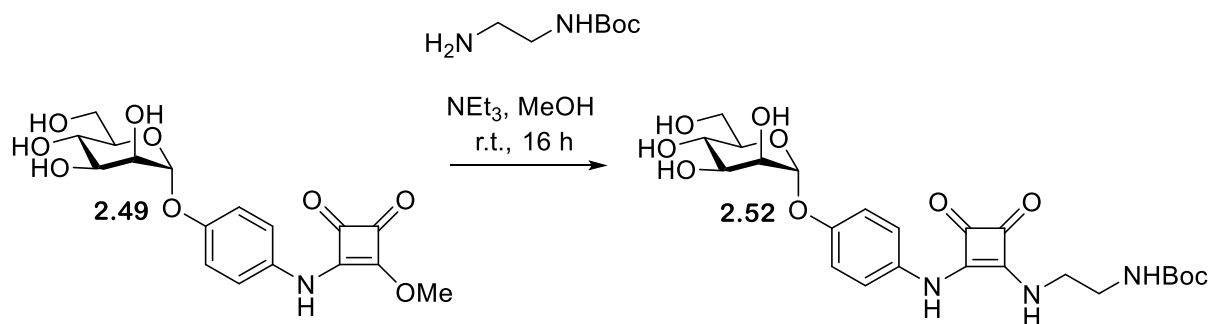
$[\alpha]_D^{25} = +111.22$  (c 1, DMSO)

IR – 3438, (O-H), 3264 (N-H), 3077 (C-H), 2940 (C-H), 1809 (C=O), 1711 (C=O), 1626 (C=C), 1594 (C=C), 1366 (C-O), 1088 (C-O).



## Experimental

### 8.2.6.4 Synthesis of [N-[4-( $\alpha$ -D-mannopyranosyloxy)phenyl]-N'-[(2'-tert-butylloxycarbonylamido)ethyl]]squaric acid diamide **2.52**<sup>396, 397</sup>



*N*-Boc-1,2-Diaminoethane (0.21 g, 1.3 mmols, 2 eq) was added to a solution of **2.49** (0.25 g, 0.65 mmols) and  $\text{NEt}_3$  (0.380 mL) in dry methanol (2 mL). The reaction mixture was stirred at r.t. for 16 h forming a cloudy white solution. The solution was neutralized with dowex, filtered and concentrated *in vacuo*, affording a white solid. The solid was purified using column chromatography, eluting with a solvent system of 3 : 1 EtOAc : MeOH. This afforded a colourless solid of **2.52** (0.13 g, 0.28 mmols, 43%);  $R_f = 0.31$  (2:1 Hexane : EtOAc).

$^1\text{H}$  NMR (500 MHz, DMSO)  $\delta$  10.00 (s, 1H, NH), 7.95 (s, 1H, NH), 7.38 (d,  $J_{\text{HAr}} = 9.0$  Hz, 2H, HAr), 7.06 (d,  $J_{\text{HAr}} = 9.0$  Hz, 2H, HAr), 6.94 (s, 1H, NH), 5.28 (d,  $J_{1,2} = 1.6$  Hz, H-1), 4.98 (d,  $J_{2,\text{OH}} = 4.0$  Hz, 1H, OH (H-2)), 4.80 (d,  $J_{4,\text{OH}} = 5.6$  Hz, 1H, OH (H-4)), 4.72 (d,  $J_{3,\text{OH}} = 5.3$  Hz, 1H, OH (H-3)), 4.45 (t,  $J_{6,\text{OH}} = 5.7$  Hz, 1H, OH (H-6)), 3.81 (s, 1H, H-2), 3.66 (m, 1H, H-3), 3.60 (m, 3H,  $\text{CH}_2$ , H-6a), 3.46 (m, 3H, H-4, H-5, H-6b), 3.13 (dd,  $J_{\text{CH}_2} = 11.9$  Hz, 6.2 Hz, 2H,  $\text{CH}_2$ ), 1.35 (s, 9H,  $\text{CH}_3$ ).

$^{13}\text{C}$  NMR (126 MHz, DMSO)  $\delta$  183.7 (1C, C=O), 180.9 (1C, C=O), 169.8 (1C, C=O), 164.2 (1C, C), 156.2 (CAr), 152.6 (1C, C), 134.2, 119.6, 118.4 (CAr), 99.9 (1C, C-1), 78.3 (1C C (Boc)), 75.3 (1C, C-5), 71.1 (1C, C-3), 70.6 (1C, C-2), 67.2 (1C, C-4), 61.5 (1C, C-6), 44.1 (1C,  $\text{CH}_2$ ), 41.5 (1C,  $\text{CH}_2$ ), 28.6 (3C,  $\text{CH}_3$ ).

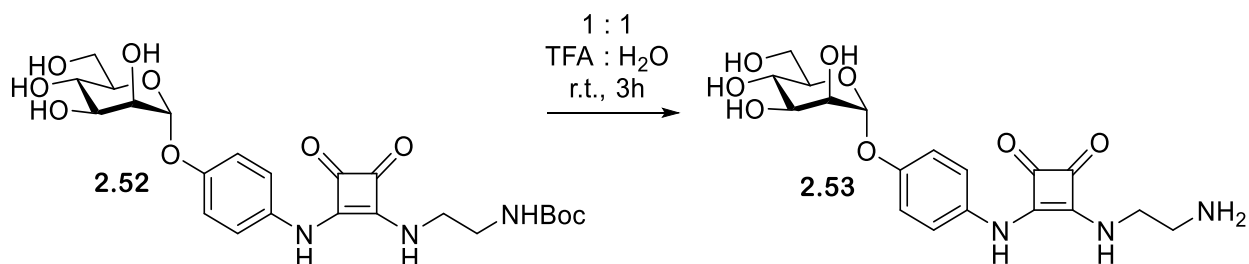
(ESI)HRMS –  $\text{C}_{23}\text{H}_{31}\text{N}_3\text{NaO}_{10}^+$  ( $[\text{M}+\text{Na}]^+$ ) requires  $m/z$  532.1907: found  $m/z$  532.1916

$[\alpha]_D^{25} = +73.22$  (c 1, DMSO)

IR – 3292 (O-H), 3210 (N-H), 2977 (C-H), 2933 (C-H), 1795 (C=O), 1671 (C=O), 1577 (C=C), 1231 (C-O), 1004 (C-O).

## Experimental

### 8.2.6.5 Synthesis of *p*-[[(2-aminoethylamino)-2,3-dioxocyclobut-1-enyl]amino]phenyl $\alpha$ -D-mannopyranoside **2.53**<sup>397</sup>



**2.52** (0.08 g, 0.16 mmols), was dissolved in a 1 : 1 solution of H<sub>2</sub>O : TFA (4 mL : 4 mL) affording a clear solution which was stirred at r.t. for 3 h. The solution was concentrated *in vacuo*, co-evaporating with toluene to yield a clear gel. The gel was dissolved in MeOH and neutralised with a free base resin. The resin was removed *via* filtration to leave a clear solution which was concentrated *in vacuo* to yield a crude colourless solid containing **2.53** (52 mg,  $\leq$  0.13 mmols,  $\leq$  81%).

<sup>1</sup>H NMR (500 MHz, DMSO)  $\delta$  7.37 (d,  $J_{\text{HAr}} = 8.8$  Hz, 2H, HAr), 7.06 (d,  $J_{\text{HAr}} = 8.8$  Hz, 2H, HAr), 5.29 (d,  $J_{1,2} = 1.5$  Hz, 1H, H-1), 3.82 (dd,  $J_{2,3} = 3.0$  Hz,  $J_{1,2} = 1.5$  Hz, 1H, H-2), 3.66 (m, 3H, CH<sub>2</sub>, H-3), 3.60 (dd,  $J = 11.5$  Hz,  $J = 1.5$  Hz, 1H, H-6a), 3.48 (m, 2H, H-6b, H-4), 3.42 (m, 1H, H-5), 2.88 (t,  $J_{\text{CH}_2} = 5.9$  Hz, 2H, CH<sub>2</sub>).

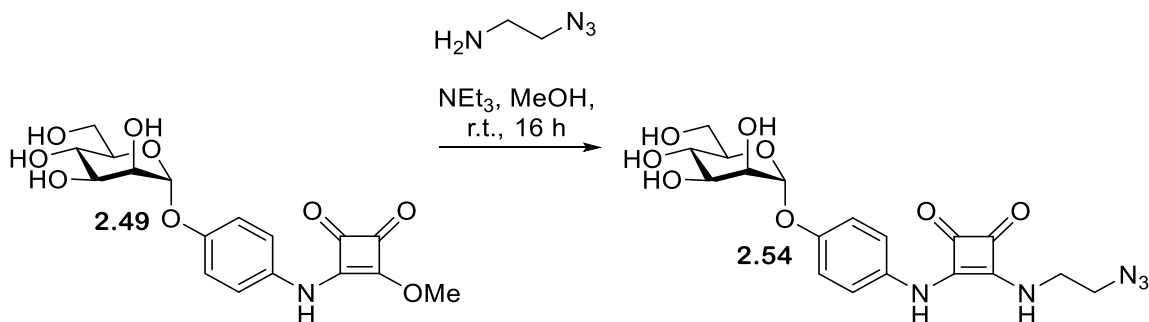
<sup>13</sup>C NMR (126 MHz, DMSO)  $\delta$  184.0 (1C, C=O), 180.9 (1C, C=O), 169.7 (1C, C), 164.4 (1C, C), 152.7, 134.1, 119.9, 118.3, (CAr), 99.8 (1C, C-1), 75.2 (1C, C-5), 71.0 (1C, C-3), 70.5 (1C, C-2), 67.3 (1C, C-4), 61.2 (1C, C-6), 44.5 (1C, CH<sub>2</sub>), 41.5 (1C, CH<sub>2</sub>).

(ESI)HRMS – C<sub>18</sub>H<sub>23</sub>N<sub>3</sub>NaO<sub>8</sub><sup>+</sup> ([M+Na]<sup>+</sup>) requires *m/z* 432.1383: found *m/z* 432.1377

IR – 3363 (O-H), 3249 (O-H), 2946 (C-H), 2907 (C-H), 1799 (C=O), 1652 (C=O), 1546 (C=C), 1511 (C=C), 1436 (C=C), 1183 (C-O), 1124 (C-O).

## Experimental

### 8.2.6.6 Synthesis of *p*-[[(1-amino-2-azidoethane)-2,3-dioxocyclobut-1-enyl]amino]phenyl $\alpha$ -D-mannopyranoside **2.54**



$\text{NEt}_3$  (0.12 mL, 1.3 mmols, 1.5 eq) was added dropwise to a solution of **2.49** (0.33 g, 0.87 mmols) and 1-amino-2-azidoethane (0.15 g, 1.7 mmols, 2 eq) in dry MeOH (20 mL). The reaction was stirred at r.t for 16 h, affording a light-yellow solution. The solution was neutralized with dowex and concentrated *in vacuo* to yield a crude yellow solid containing **2.54** (0.26 g,  $\leq 0.75$  mmols,  $\leq 67\%$ ). Compound was used crude in peptide synthesis.

**NMR**- Note NMR showed a mixture of product to starting at a ratio of 1: 0.27. Furthermore, though a new bottle of DMSO was used a large water peak can still be seen between 3.67-3.38, meaning integration values measured in this region were inaccurate and therefore the number of environments present was determined using the HSQC spectra. Furthermore, despite multiple attempts a  $^{13}\text{C}$  spectrum which showed intense enough peaks for full analysis could not be obtained (as here the C=O peaks and a few CAr peaks cannot be discerned). Below is the rough analysis of the  $^{13}\text{C}$  spectrum which could be completed. A paper by Taylor and co-workers<sup>398</sup> was used to help identify the squarate peaks.

$^1\text{H}$  NMR (500 MHz, DMSO)  $\delta$  7.35 (d,  $J_{\text{HAr}} = 8.8$  Hz, 2H, HAr), 7.05 (d,  $J_{\text{HAr}} = 8.8$  Hz, 2H, HAr), 5.27 (d,  $J_{1,2} = 1.6$  Hz, 1H, H-2), 3.81 (m, 1H, H-2), 3.76 (dd,  $J_{\text{CH}_2} = 6.01$  Hz, 2H,  $\text{CH}_2$ ), 3.65 (dd,  $J = 9.3$  Hz,  $J = 3.5$  Hz, 1H, H-3), 3.59-3.53 (m, 3H, H-6a,  $\text{CH}_2$ ), 3.50-3.39 (m, 3H, H-6b, H-4, H-5).

$^{13}\text{C}$  NMR (126 MHz, DMSO)  $\delta$  164.0 (C), 152.3 (C), 119.5, 117.9, (CAr), 99.4 (1C, C-1), 74.9 (1C, C-5), 70.7 (1C, C-2), 70.1 (1C, C-2), 66.7 (1C, C-4), 61.0 (1C, C-6), 51.3 (1C,  $\text{CH}_2$ ), 43.1 (1C,  $\text{CH}_2$ ).

(ESI)HRMS –  $\text{C}_{18}\text{H}_{21}\text{N}_5\text{NaO}_8^+$  ( $[\text{M}+\text{Na}]^+$ ) requires  $m/z$  458.1288: found  $m/z$  458.1286

*IR*- 3253 (O-H), 2931 (C-H), 2102 ( $\text{N}_3$ ), 1796 (C=O), 1660 (C=O), 1612 (C=O) 1570 (C=C), 1540 (C=C), 1520 (C=C) 1004 (C-O)

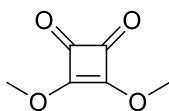
As sample was impure no  $[\alpha]_{\text{D}}^{25}$  was taken

No literature reference for characterisation could be found

## Experimental

### 8.2.7 Synthesis of supporting compounds used in chapter 2

#### 8.2.7.1 Synthesis of 3,4-dimethoxycyclobut-3-ene-1,2-dione<sup>399</sup>



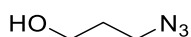
Trimethyl orthoformate was added to a solution of 3,4-dihydroxy-3-cyclobutene-1,2-diol in methanol. The reaction mixture was refluxed at 56 °C for 24 h, affording a colourless solution. The solution was concentrated *in vacuo* to yield a crude colourless oil. This oil was purified by column chromatography, eluting with a graduated solvent system of 3:1 Hex : EtOAc to 5 : 1 DCM : MeOH. This yielded white crystals of 3,4-dimethoxycyclobut-3-ene-1,2-dione (2.0 g, 0.014 mols, 78%).

<sup>1</sup>H NMR (500 MHz, CDCl<sub>3</sub>) δ 4.37 (s, 6H, OCH<sub>3</sub>).

<sup>13</sup>C NMR (126 MHz, CDCl<sub>3</sub>) δ 189.20 (2C, C=O), 184.50 (2C, C-3,4), 61.04 (2C, CH<sub>3</sub>).

(ESI)HRMS – C<sub>6</sub>H<sub>6</sub>NaO<sub>4</sub><sup>+</sup> ([M+Na]<sup>+</sup>) requires m/z 165.0998: found m/z 165.0158

#### 8.2.7.2 Synthesis of 3-Azidopropanol<sup>400</sup>



NaN<sub>3</sub> (19 g, 0.29 mols, 3.5 eq) was added slowly to a solution of 3-bromopropanol (7.4 mL, 0.081 mols) in DMF (70 mL). The reaction mixture was stirred vigorously at r.t. for 12 h, affording a white cloudy solution. The solution was concentrated *in vacuo*, diluted with Et<sub>2</sub>O (50 mL) and washed with water (1 x 50 mL) and saturated NaCl (1 x 50 mL). The aqueous layer was washed with Et<sub>2</sub>O (5 x 50 mL) and the organic fractions were combined, dried (MgSO<sub>4</sub>) and concentrated *in vacuo* to yield a light yellow oil. This oil was purified by column chromatography, eluting with a solvent system of 1 : 1 (Et<sub>2</sub>O : Hexane). This yielded a colourless oil of 3-Azidopropanol (10 g, 0.095 mols, 60%); R<sub>f</sub> = 0.66 (3 : 1 Et<sub>2</sub>O : Hexane).

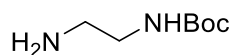
<sup>1</sup>H NMR (500 MHz, CDCl<sub>3</sub>) δ 3.74 (dd, *J* = 9.8 Hz, *J* = 6.0 Hz, 2H, CH<sub>2</sub>), 3.44 (t, *J* = 6.0 Hz, 2H, CH<sub>2</sub>), 2.25 (s, 1H, OH), 1.83 (pentet *J* = 6.0 Hz, 2H, CH<sub>2</sub>).

<sup>13</sup>C NMR (126 MHz, CDCl<sub>3</sub>) δ 59.79 (1C, CH<sub>2</sub>), 48.68 (1C, CH<sub>2</sub>), 31.45 (1C, CH<sub>2</sub>).

IR – 3336 (O-H), 2944 (C-H), 2882 (C-H), 2000 (N<sub>3</sub>), 1258 (C-O), 1049 (C-O)

## Experimental

### 8.2.7.3 Synthesis of N-BOC-1,2-Diaminoethane <sup>401</sup>



To a solution of 1,2-diaminoethane (3 mL, 0.045 mols, 10 eq) in  $\text{CHCl}_3$  (100 mL) was added dropwise at 0 °C a solution of di-tertbutyldicarbonate (1g, 4.5 mmols) in  $\text{CHCl}_3$ . The reaction mixture was stirred at r.t. for 16 h, affording a cloudy white solution. The solution was washed with brine (6 x 100 mL) and water (1 x 100 mL), dried ( $\text{MgSO}_4$ ) and concentrated *in vacuo* to yield a colourless oil of N-BOC-1,2-Diaminoethane (0.59, 3.7 mmols, 81%).

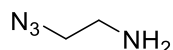
$^1\text{H}$  NMR (500 MHz,  $\text{CDCl}_3$ )  $\delta$  5.13 (s, 1H,  $\text{NH}$ ), 3.15 (m, 2H,  $\text{CH}_2$ ), 2.77 (t,  $J = 5.9$  Hz, 2H,  $\text{CH}_2$ ), 2.18 (s, 2H,  $\text{NH}_2$ ), 1.41 (s, 9H,  $\text{CH}_3$ ).

$^{13}\text{C}$  NMR (126 MHz,  $\text{CDCl}_3$ )  $\delta$  156.4 (1C,  $\text{C}=\text{O}$ ), 79.3 (1C,  $\text{C}$ ), 43.2 (1C,  $\text{CH}_2$ ), 41.8 (1C,  $\text{CH}_2$ ), 28.5 (s, 3C,  $\text{CH}_3$ ).

(ESI)HRMS –  $\text{C}_7\text{H}_{16}\text{O}_2\text{NaN}_2^+$  ( $[\text{M}+\text{Na}]^+$ ) requires  $m/z$  183.2068: found  $m/z$  183.1104.

IR – 3354 (N-H), 2975 (C-H), 2932 (C-H), 2864 (C-H), 1681 (C=O), 1161 (C-O).

### 8.2.7.4 Synthesis of 1-amino-2-azidoethane <sup>402</sup>



2-Chloroethanamine-hydrochloride (3.0 g, 26 mmols) was dissolved in water (20 mL) and  $\text{NaN}_3$  (5.0 g, 78 mmols, 3 eq) was added. The reaction mixture was stirred at 80 °C for 16 h, affording a clear solution. The solution was cooled to r.t. and  $\text{NaOH}$  was added. The solution was then concentrated *in vacuo* to afford a colourless oil. The oil was purified by column chromatography, eluting with a graduated solvent system of 100 % EtOAc to 5 : 1 DCM : MeOH. This afforded a clear oil of 1-amino-2-azidoethane (0.31 g, 3.6 mmols, 13%);  $R_f = 0.45$  (5 : 1 DCM : MeOH).

$^1\text{H}$  NMR (500 MHz, MeOD)  $\delta$  4.99 (m, 2H,  $\text{NH}_2$ ), 3.68 (dd,  $J = 5.4$  Hz,  $J = 5.4$  Hz, 2H,  $\text{CH}_2$ ), 3.06 (dd,  $J = J = 5.4$  Hz,  $J = 5.4$  Hz, 2H,  $\text{CH}_2$ ).

$^{13}\text{C}$  NMR (126 MHz, MeOD)  $\delta$  50.8 (1C,  $\text{CH}_2$ ), 40.3 (1C,  $\text{CH}_2$ ).

(ESI)HRMS –  $\text{C}_2\text{H}_7\text{N}_4^+$  ( $[\text{M}+\text{H}]^+$ ) requires  $m/z$  86.1060: found  $m/z$  87.0661

IR- 2925 (C-H), 2101 ( $\text{N}_3$ ).

### 8.3 Experimental for Chapter 3

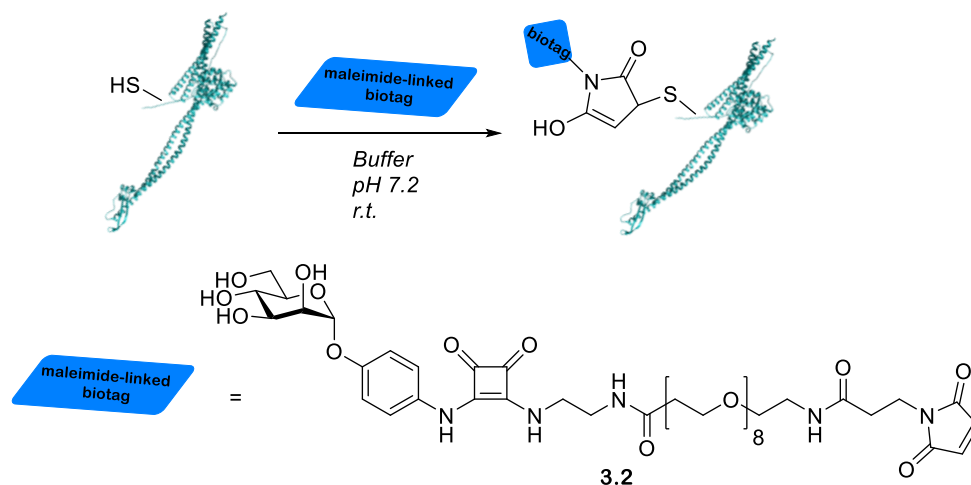
#### 8.3.1 Methodology for the expression and purification of Colicin E9

Two 500 mL cultures were grown and combined for purification.

An *E. coli* BL21 (DE3) (New England Biolabs) transformant harbouring the expression plasmid was grown at 37 °C in 5 mL of Luria broth (LB) media (1% NaCl, 1% tryptone and 0.5% yeast extract) containing 100 µg/mL ampicillin and 0.4% w/v D-glucose for 7 h with shaking at 150 rpm. 50 mL of LB media containing 100 µg/mL ampicillin and 0.4% w/v D-glucose was inoculated with the starter culture and grown overnight at 37 °C with shaking at 150 rpm. 500 mL of LB media containing 100 µg/mL ampicillin and 0.4% w/v D-glucose was inoculated with the overnight culture and was grown to an  $OD_{600} = 0.6$ . The expression was induced by 1 mM isopropyl β-D-thiogalactopyranoside and was incubated for 18 h at 37 °C with shaking at 150 rpm. The cells were harvested by centrifugation 6000 rpm for 12 minutes at 4 °C. The resulting cell pellet was resuspended in 35 mL of 20 mM K-phosphate pH 7.0, 0.5 M NaCl, 1 mM PMSF and lysozyme (add ~10 mg/35 ml) and disrupted by sonication (soniprep 150) (30 s pulse for 10 minutes). The supernatant was collected by centrifugation 20,000 × g for 30 minutes at 4 °C and filtered through a 0.45 µm pore syringe and applied to a HisTrap HP column (5 mL, Cytiva) equilibrated with 20 mM K-phosphate pH 7.0, 0.5 M NaCl, 5 mM imidazole using an AKTA start (Cytiva). The protein was eluted using a linear gradient of 20 mM K-phosphate pH 7.0, 0.5 M NaCl, 5 mM imidazole and 20 mM K-phosphate pH 7.0, 0.5 M NaCl, 6 M guanidine HCl. Fractions containing recombinant protein (colicin E9) were pooled, dialyzed against 20 mM K-phosphate pH 7.0, 0.5 M NaCl and concentrated (Sartorius vivaspin6 30,000 MWCO). The recombinant protein was further purified using gel filtration (Hiload 16/600, superdex 200pg, Cytiva) equilibrated with 20 mM K-phosphate pH 7.0, 0.5 M NaCl. The fractions containing recombinant protein (colicin E9) were pooled and concentrated (Sartorius vivaspin6 30,000 MWCO). The protein concentration was determined spectrophotometrically at 280 nm using an extinction coefficient of 46,075. The procedure yielded 4.78 mg of purified colicin E9.

## Experimental

### 8.3.2 Methodology for the bio-conjugation of mannose-based inhibitor **2.53** to colicin Ia using heterobifunctional linker **3.1**



*Scheme 8-1. Reaction scheme for ligation of mannose-based inhibitor-linked heterobifunctional linker **3.2** to colicin Ia*

Mannose-based inhibitor **2.53** (stock 1 M in DMSO, 3  $\mu$ L, final concentration 500 mM) was added to NHS-(PEG)<sub>8</sub>-Maleimide linker **3.1** (stock 500 mM in DMSO, 3  $\mu$ L, final concentration 250 mM) in a 0.5 mL Eppendorf tube. The solution was mixed by swirling the pipette tip and was incubated in the dark at r.t. for 30 minutes. The reaction mixture was added to a solution of colicin Ia (100  $\mu$ L, 100  $\mu$ M in 1 x PBS pH 7.2) which had been pre-treated with  $\beta$ Me via 3  $\times$  2  $\mu$ L additions of  $\beta$ Me stock over 30 minutes (stock 137 mM in water, final concentration 10% (v/v)), while being incubated in the dark at r.t. The reaction was purified using a PD SpinTrap G25 desalting column (GE Healthcare Life Sciences), eluting into 20 mM K phosphate, 500 mM NaCl pH 7.0 for analysis or further manipulation.

## Experimental

### 8.3.3.1 Methodology for the bio-conjugation of active biotin linked (PEG)<sub>3</sub> OPAL probe **3.3** to colicin E9

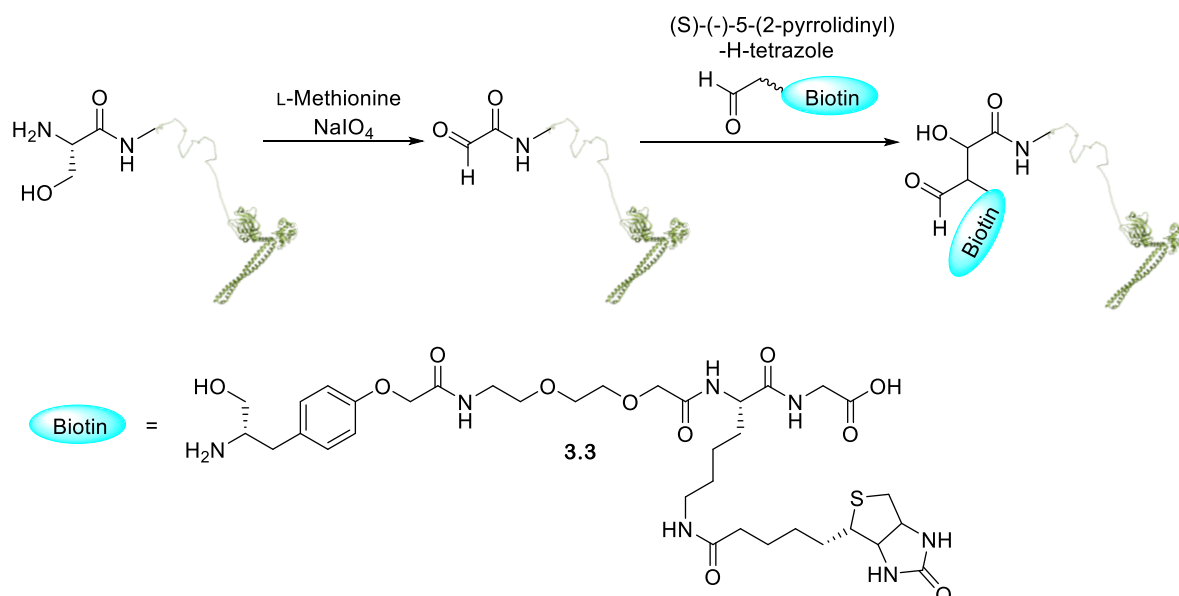


Figure 8-2. Reaction scheme for OPAL ligation of biotin-linked (PEG)<sub>3</sub> OPAL probe **3.3** to colicin E9

A solution of colicin E9 (100  $\mu$ L of 100  $\mu$ M stock in 25 mM PB pH 7.5) was charged with L-methionine (1  $\mu$ L of 66 mM stock in 0.1 M PB, 0.1 NaCl, pH 7.0) and NaIO<sub>4</sub> (1  $\mu$ L of 33 mM stock in 0.1 M PB, 0.1 NaCl, pH 7.0). The solution was mixed by gentle pipette tip swirling and allowed to sit on ice in the dark for 4 minutes. The reaction mixture was immediately purified using a PD SpinTrap G25 desalting column (GE Healthcare Life Sciences), eluting into 100  $\mu$ L of 25 mM PB pH 7.5. The reaction was charged with (S)-(-)-5-(2-pyrrolidinyl)-H-tetrazole (20  $\mu$ L of 200 mM stock in 25 mM PB pH 7.5) and biotin OPAL probe **3.3** (40  $\mu$ L of 4 mM stock in 25 mM PB pH 7.5). The solution was mixed via pipette tip swirling and incubated for 1 h at 37  $^{\circ}$ C. The reaction mixture was purified using a PD SpinTrap G25 desalting column (GE Healthcare Life Sciences), eluting into 20 mM K phosphate, 500 mM NaCl pH 7.0 for analysis and further manipulation.



## Experimental

### 8.3.3.2 Methodology for the bio-conjugation of active biotin linked (PEG)<sub>3</sub> OPAL probe **3.3** to colicin Ia

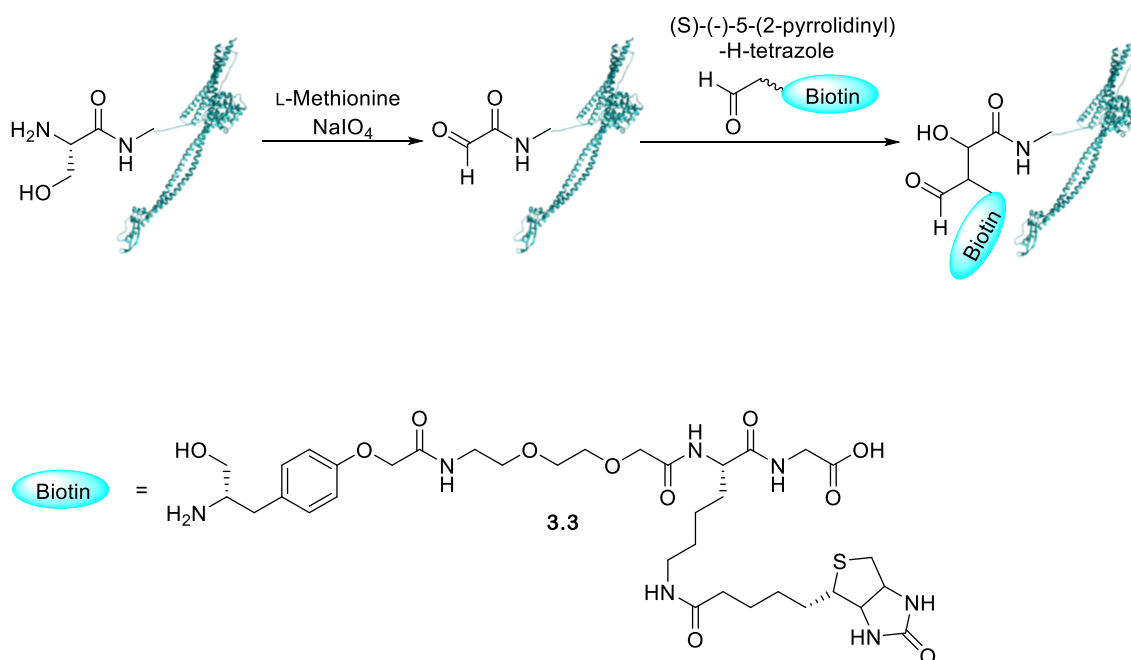


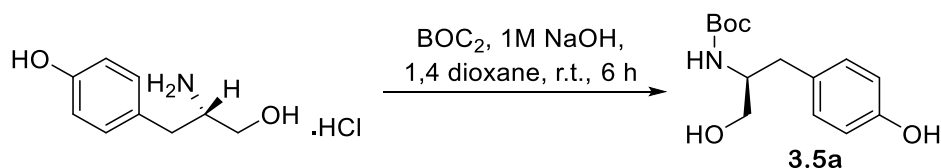
Figure 8-3. Reaction scheme for OPAL ligation of biotin-linked (PEG)<sub>3</sub> OPAL probe **3.3** to colicin Ia

$\beta$ Me (stock 137 mM in water, 10  $\mu$ L, final concentration 10% (v/v)) was added to a solution of colicin Ia (100  $\mu$ L of 100  $\mu$ M stock in 25 mM PB pH 7.5) in a 0.5 mL Eppendorf. The solution was mixed by pipette tip swirling and left at r.t. for 5 minutes. L-methionine (1  $\mu$ L of 66 mM stock in 0.1 M PB, 0.1 NaCl, pH 7.0) and NaIO<sub>4</sub> (1  $\mu$ L of 33 mM stock in 0.1 M PB, 0.1 NaCl, pH 7.0) were added to the reaction mixture. The solution was mixed by gentle pipette tip swirling and allowed to sit on ice in the dark for 4 minutes. The reaction mixture was immediately purified using a PD SpinTrap G25 desalting column (GE Healthcare Life Sciences), eluting into 100  $\mu$ L of 25 mM PB pH 7.5. The reaction was charged with (S)-(-)-5-(2-pyrrolidinyl)-H-tetrazole (20  $\mu$ L of 200 mM stock in 25 mM PB pH 7.5) and biotin-linked (PEG)<sub>3</sub> OPAL probe **3.3** (40  $\mu$ L of 4 mM stock in 25 mM PB pH 7.5). The solution was mixed via pipette tip swirling and incubated for 1 h at 37  $^{\circ}$ C. The reaction mixture was purified using a PD SpinTrap G25 desalting column (GE Healthcare Life Sciences), eluting into 20 mM K phosphate, 500 mM NaCl pH 7.0 for analysis and further manipulation.

## Experimental

### 8.3.4. Synthesis of Synthesis of (S)-2-(4-((3-(tert-butoxycarbonyl)-2,2-dimethyloxazolidin-4-yl)methyl)phenoxy)acetic acid **3.5**

#### 8.3.4.1 Synthesis of (S)-tert-butyl (1-hydroxy-3-(4-hydroxyphenyl)propan-2-yl)carbamate **3.5a** <sup>139</sup>



$\text{Boc}_2\text{O}$  (4.4 g, 20 mmol) was added to a solution of L-tyrosinol hydrochloride (4 g, 20 mmols) in 1 M NaOH (40 mL, 2eq) and dry 1,4 dioxane (40 mL), affording a colourless solution which was stirred for 6 h at r.t. The solution was concentrated *in vacuo*, affording a cloudy oil. This oil was dissolved in EtOAc (10 mL), washed with 5% citric acid (10 mL) and water (10 mL), dried ( $\text{MgSO}_4$ ) and concentrated *in vacuo* to yield a cloudy oil. This oil was purified by column chromatography, eluting with a graduated solvent system of 100% Hexane to 100% EtOAc, yielding a white foam of **3.5a** (2.8 g, 1.0 mmols, 52%);  $R_f = 0.5$  (1 : 1 Hex : EtOAc).

$^1\text{H}$  NMR (500 MHz, MeOD) rotA(\*): rotB(^) = ~50:50  $\delta$  7.03 (d,  $J_{\text{HAr}} = 8.3$  Hz, 2H, HAr), 6.70 (d,  $J_{\text{HAr}} = 8.3$  Hz, 2H HAr), 3.69 (m, 1H,  $\text{CHN}$ ), 3.47 (m, 2H,  $\text{CH}_2\text{O}$ ), 2.76 (dd,  $J_{\text{CH}_2} = 13.7$  Hz,  $J_{\text{CH}_2} = 6.2$  Hz, 1H, Ar $\text{CH}_2$ ), 2.58 (dd,  $J_{\text{HAr}} = 13.2$  Hz,  $J_{\text{HAr}} = 7.8$  Hz, 1H, Ar $\text{CH}_2$ ), 1.38 (s, 9H,  $\text{CH}_3$ ).

$^{13}\text{C}$  NMR (126 MHz, MeOD)  $\delta$  158.3(1C, C=O), 157.0, 131.5, 130.9, 116.3, (CAr), 80.0 (1C, C), 64.6 (1C,  $\text{CH}_2\text{O}$ ), 55.7 (1C,  $\text{CHN}$ ), 37.8 (1C, Ar $\text{CH}_2$ ), 29.0 (1C,  $\text{CH}_3$ ).

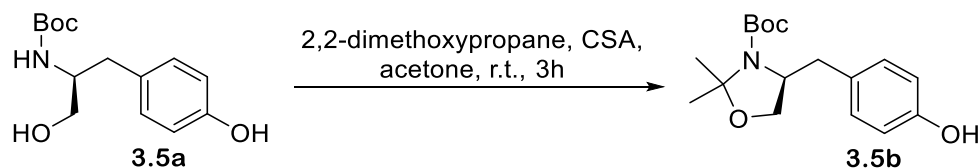
(ESI)HRMS – Calculated  $\text{C}_{14}\text{H}_{21}\text{NNaO}_4$ : 290.1368. Found  $[\text{M}+\text{Na}]^+$  290.1361

$[\alpha]_D^{25}$  - - 19.55(c 1, MeOH)

IR- 3356 (O-H), 2977 (C-H), 2931 (C-H), 1682 (C=O), 1515 (C=C), 1393 (C-O), 1245 (C-O), 1166 (C-O).

## Experimental

### 8.3.4.2 Synthesis of (*S*)-*tert*-butyl 4-(4-hydroxybenzyl)-2,2-dimethyloxazolidine-3-carboxylate **3.5b**<sup>139</sup>



2,2-dimethoxypropane (3.5 mL, 28 mmols, 3 eq) was added dropwise to an acidified solution of **3.5a** (2.5 g, 9.4 mmols) and CSA (cat) in anhydrous acetone (20 mL). The reaction mixture was stirred at r.t. for 3 h, affording a clear solution. The solution was neutralised with  $\text{NEt}_3$  and concentrated *in vacuo* to yield a clear oil. This oil was purified by column chromatography, eluting with a graduated solvent system of 100% hexane to 100% EtOAc, yielding a white solid of **3.5b** (2.4 g, 7.8 mmols, 83 %);  $R_f = 0.42$  (3 : 1 Hex : EtOAc).

both rotomers present 1:1 ratio

$^1\text{H}$  NMR (500 MHz,  $\text{CDCl}_3$ ) rotA(\*): rotB(^) = ~50:50  $\delta$  7.04 (m, 4H, HAr), 6.82 (d,  $J_{\text{HAr}} = 8.0$  Hz, 2H, HAr), 6.76 (d,  $J_{\text{HAr}} = 8.0$  Hz, 2H, HAr), 4.07 (m, 1H,  $\text{CHN}$  a), 3.94 (m, 1H,  $\text{CHN}$  b), 3.80-3.77 (m, 4H,  $\text{CH}_2\text{O}$  a + b), 3.11 (d,  $J_{\text{CH}_2} = 13.1$  Hz, 1H,  $\text{ArCH}_2$  b), 3.01 (d,  $J_{\text{CH}_2} = 11.5$  Hz, 1H,  $\text{ArCH}_2$  a), 2.60 (m, 2H,  $\text{ArCH}_2$  a + b), 1.63 (s, 3H,  $\text{CH}_3$ ), 1.56 (s, 3H,  $\text{CH}_3$ ), 1.53 (s, 18H,  $\text{CH}_3$ ), 1.50 (3H,  $\text{CH}_3$ ), 1.47 (3H,  $\text{CH}_3$ ).

$^{13}\text{C}$  NMR (126 MHz,  $\text{CDCl}_3$ )  $\delta$  155.0, 154.9, 152.4, 151.9, 130.6 (2C), 130.4 (2C), 129.8, 129.7, 115.6 (2C), 115.5 (2C), 94.2, 93.8, 80.7, 80.1, 66.0, 65.8, 59.4, 59.3, 38.6, 37.5, 28.6 (2C), 28.5 (2C), 27.5, 26.8, 24.5, 23.3.

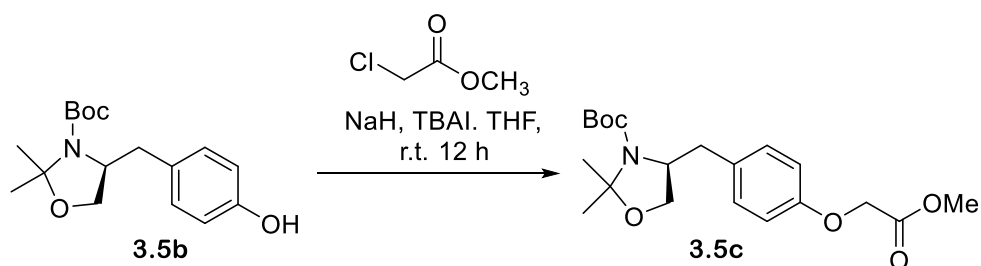
(ESI)HRMS - Calculated  $\text{C}_{17}\text{H}_{25}\text{NNaO}_4$ : 330.1681. Found  $[\text{M}+\text{Na}]^+$  330.1661

$[\alpha]_D^{25}$  - - 38.32(c 1,  $\text{CH}_2\text{Cl}_2$ )

IR- 3358 (O-H), 2980 (C-H), 2936 (C-H), 2877 (C-H), 1665 (C=O), 1515 (C=C), 1366 (C-O), 1325 (C-O), 1092 (C-O).

## Experimental

### 8.3.4.3 Synthesis of (S)-tert-butyl 4-(4-(2-methoxy-2-oxoethoxy)benzyl)-2,2-dimethyloxazolidene-3-carboxylate **3.5c**<sup>139</sup>



NaH (0.56 g, 24 mmols, 3eq) was added to a solution of **3.5b** (2.4 g, 7.8 mmols) in dry THF and the reaction mixture was stirred for 20 minutes, affording a cloudy solution. The solution was treated with TBAI (0.29 g, 0.78 mmols, 0.1 eq) and methylchloroacetate (6.4 mL, 20 mmols, 2.5 eq), and the reaction mixture was stirred at r.t. for 12 h. The reaction mixture was quenched with MeOH (2 mL) and concentrated *in vacuo*, affording a colourless oil. This oil was dissolved in DCM (20 mL) and washed with Na<sub>2</sub>S<sub>2</sub>O<sub>3</sub> (20 mL) and water (20 mL), dried (MgSO<sub>4</sub>) and concentrated *in vacuo* to afford a colourless oil. This oil was purified by column chromatography, eluting with a graduated solvent system of 100% Hexane to 100% EtOAc. This afforded a white solid of **3.5c** (2.0 g, 5.3 mmols, 67%); R<sub>f</sub> = 0.68 (5 : 2 Hex : EtOAc).

<sup>1</sup>H NMR (500 MHz, CDCl<sub>3</sub>), rotA(\*): rotB(^) = ~50:50 δ 7.16 (d, J<sub>HAr</sub> = 8.0 Hz, 2H, HAr), 7.11 (d, J<sub>HAr</sub> = 8.0 Hz, 2H, HAr), 6.84 (dd, J<sub>HAr</sub> = 9.0 Hz, J<sub>HAr</sub> = 9.0 Hz, 4H, HAr), 4.62 (s, 2H, CH<sub>2</sub>CO<sub>2</sub>Me both rotomers), 4.06 (m, 1H, CHN\*), 3.92 (m, 1H, CHN^), 3.80 (s, 5H, CH<sub>3</sub> both rotomers) 3.78 (s, 3H, CH<sub>3</sub>^), 3.75 (ddd, 4H, CH<sub>2</sub>O both rotomers), 3.14 (d, J = 13.0 Hz, 1H, ArCH<sub>2</sub>\*), 3.03 (d, J = 11.0 Hz, 1H, ArCH<sub>2</sub>^), 2.61 (dd, J = 13.2 Hz, J = 11.0 Hz, 2H, ArCH<sub>2</sub> both rotomers), 1.62 (s, 3H, CH<sub>3</sub>), 1.51 (s, 21H, CH<sub>3</sub>), 1.49 (3H, CH<sub>3</sub>), 1.45 (s, 3H, CH<sub>3</sub>).

<sup>13</sup>C NMR (126 MHz, CDCl<sub>3</sub>) δ 169.5, 156.5, 152.3, 151.7, 131.8, 130.6, 130.4, 114.8, 114.7, 94.1, 93.6, 80.2, 79.7, 66.1, 65.9, 65.4, 59.2, 52.3, 38.8, 37.7, 28.6, 28.5, 27.5, 26.9, 24.5, 23.3.

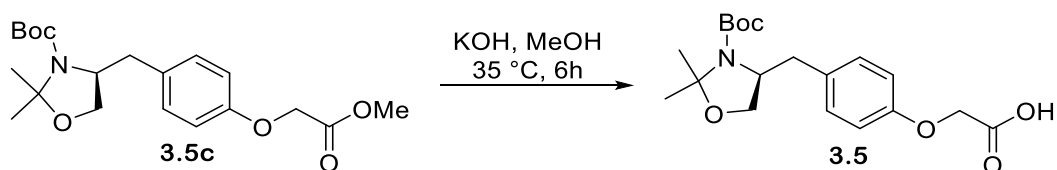
(ESI)HRMS - Calculated C<sub>20</sub>H<sub>29</sub>NNaO<sub>6</sub>: 402.1893. Found [M+Na]<sup>+</sup> 402.1886

[α]<sub>D</sub><sup>25</sup> - -34.38(c 1, CH<sub>2</sub>Cl<sub>2</sub>)

IR- 2979 (C-H), 2936 (C-H), 2874 (C-H), 1694 (C=O), 1512 (C=C), 1388 (C-O), 1366 (C-O).

## Experimental

### 8.3.4.4 Synthesis of (S)-2-(4-((3-(tert-butoxycarbonyl)-2,2-dimethyloxazolidin-4-yl)methyl)phenoxy)acetic acid **3.5** <sup>139</sup>



KOH (0.52 g, 9.2 mmols, 2 eq) was added to a solution of **3.5c** (1.8 g, 4.6 mmols) in MeOH (30 mL). The reaction mixture was stirred for 6 h at 35 °C, affording a clear solution. This solution was concentrated *in vacuo* to yield a white solid. This solid was subsequently dissolved in water (20 mL) and washed twice with diethyl ether (20 mL). The aqueous layer was then acidified using 6 M HCl and white crystals of **3.5** precipitated on standing. These crystals were collected *via* filtration and dried *in vacuo* to yield **3.5** (1 g, 2.7 mmols, 60%).

<sup>1</sup>H NMR (500 MHz, CDCl<sub>3</sub>), rotA(\*): rotB(^) = ~50:50 δ 7.15 (m, 4H, HAr), 6.85 (t, *J*<sub>HAr</sub> = 7.5 Hz, 4H, HAr), 4.66 (s, 4H, CH<sub>2</sub>CO<sub>2</sub>Me both rotomers), 4.04 (m, 1H, CHN\*), 3.93 (m, 1H, CHN^), 3.78-3.75 (m, 2H, CH<sub>2</sub>O\*), 3.72 (d, *J* = 9.0 Hz, 2H, CH<sub>2</sub>O^), 3.08 (d, *J* = 13.2 Hz, 1H, ArCH<sub>2</sub>\*), 3.02 (d, *J* = 13.2 Hz, 1H, ArCH<sub>2</sub>^), 2.63 (d, *J* = 13.2 Hz, 1H, ArCH<sub>2</sub>\*), 2.61 (d, *J* = 13.2 Hz, 1H, ArCH<sub>2</sub>^), 1.57 (s, 3H, CH<sub>3</sub>), 1.50 (s, 21H, CH<sub>3</sub>), 1.45 (s, 6H, CH<sub>3</sub>).

<sup>13</sup>C NMR (126 MHz, CDCl<sub>3</sub>) δ 172.5, 172.3, 156.7, 152.7, 152.1, 132.6, 132.5, 131.0, 130.9, 115.0, 114.9, 94.4, 94.1, 80.8, 80.0, 66.4, 66.2, 65.5, 59.6, 59.5, 39.0, 37.9, 28.7, 28.6, 27.6, 26.9, 24.7, 23.4.

(ESI)HRMS - Calculated C<sub>19</sub>H<sub>27</sub>NNaO<sub>6</sub>: 388.1736. Found [M+Na]<sup>+</sup> 388.1727

[α]<sub>D</sub><sup>25</sup> - -27.54 (c 1, CH<sub>2</sub>Cl<sub>2</sub>)

IR- 2981 (C-H), 2936 (C-H), 2877 (C-H), 1695 (C=O), 1512 (C=C), 1390 (C-O).

## Experimental

### 8.3.5 Synthesis of required OPAL probes

#### 8.3.5.1 Synthesis of mannose-based inhibitor linked OPAL probe 3.6

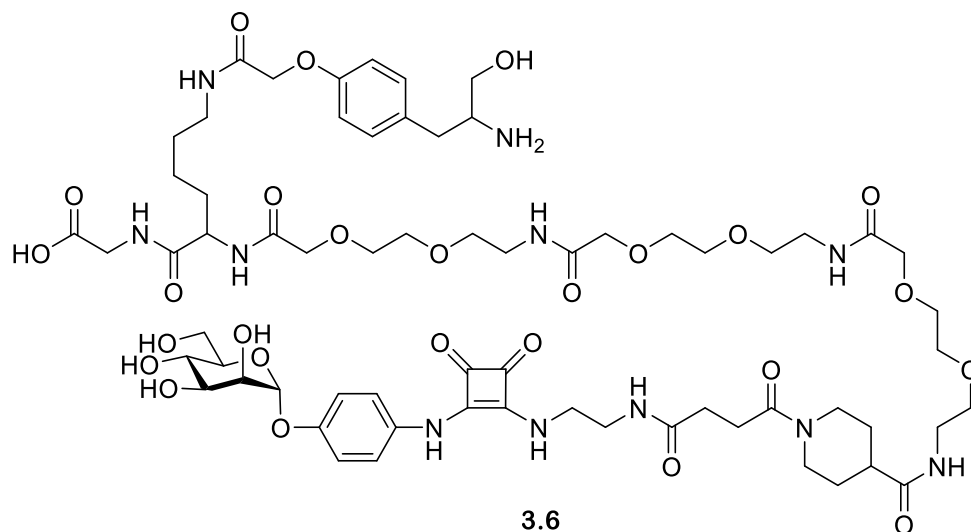


Figure 8-4. Structure of mannose-based inhibitor linked OPAL probe 3.6

H-Gly-2-CITrt resin was weighed out into an SPPS cartridge fitted with a PTFE stopcock, swollen in DMF for 30 minutes and then filtered.

DIPEA (98  $\mu$ L, 0.56 mmols, 11 eq) was added to a solution of Fmoc-Lys-(Dde)-COOH (141 mg, 0.26 mmols, 5 eq) and HTCU (107 mg, 0.26 mmols, 5 eq) dissolved in the minimum volume of DMF. The resultant solution was then immediately added to the swollen H-Gly-2-CITrt resin. The reaction mixture was gently agitated by rotation for 1 h and the resin was filtered off and washed with DMF (3 x 2 minutes with rotation). A solution of 20% piperidine in DMF was added to the resin and gently agitated by rotation for 2 minutes. The resin was filtered off and this process was repeated four more times, followed by washing with DMF (5 x 2 minutes with rotation).

DIPEA (98  $\mu$ L, 0.56 mmols, 11 eq) was then added to a solution of Fmoc-8-amino-3,6-dioxaoctanoic acid (102 mg, 0.26 mmols, 5 eq) and HTCU (107 mg, 0.26 mmols, 5 eq) dissolved in the minimum volume of DMF. The resultant solution was then immediately added to the resin. The reaction mixture was gently agitated by rotation for 1 h and the resin was filtered off and washed with DMF (3 x 2 minutes with rotation). A solution of 20% piperidine in DMF was added to the resin and gently agitated by rotation for 2 minutes. The resin was filtered off and this process was repeated four more times, followed by washing with DMF (5 x 2 minutes with rotation).

DIPEA (98  $\mu$ L, 0.56 mmols, 11 eq) was then added to a solution of Fmoc-8-amino-3,6-dioxaoctanoic acid (102 mg, 0.26 mmols, 5 eq) and HTCU (107 mg, 0.26 mmols, 5 eq) dissolved in the minimum volume of DMF. The resultant solution was then immediately added to the resin. The reaction mixture was gently agitated by rotation for 1 h and the resin was filtered off and washed with DMF (3 x 2 minutes with rotation). A solution of 20% piperidine in DMF was added to the resin and

## Experimental

gently agitated by rotation for 2 minutes. The resin was filtered off and this process was repeated four more times, followed by washing with DMF (5 x 2 minutes with rotation).

DIPEA (98  $\mu$ L, 0.56 mmols, 11 eq) was then added to a solution of Fmoc-8-amino-3,6-dioxaoctanoic acid (102 mg, 0.26 mmols, 5 eq) and HTCU (107 mg, 0.26 mmols, 5 eq) dissolved in the minimum volume of DMF. The resultant solution was then immediately added to the resin. The reaction mixture was gently agitated by rotation for 1 h and the resin was filtered off and washed with DMF (3 x 2 minutes with rotation). A solution of 20% piperdine in DMF was added to the resin and gently agitated by rotation for 2 minutes. The resin was filtered off and repeated four more times, followed by washing with DMF (5 x 2 minutes with rotation).

DIPEA (98  $\mu$ L, 0.56 mmols, 11 eq) was added to a solution of 1-Fmoc-piperidine-4-carboxylic acid (93 mg, 0.26 mmols, 5 eq) and HTCU (107 mg, 0.26 mmols, 5 eq) dissolved in the minimum volume of DMF. The resultant solution was then immediately added to the resin. The reaction mixture was gently agitated by rotation for 1 h and the resin was filtered off and washed with DMF (3 x 2 minutes with rotation). A solution of 20% piperdine in DMF was added to the resin and gently agitated by rotation for 2 minutes. The resin was filtered off and this process was repeated four more times, followed by washing with DMF (5 x 2 minutes with rotation).

DIPEA (98  $\mu$ L, 0.56 mmols, 11 eq) was added to a solution of succinic anhydride (27 mg, 0.26 mmols, 5 eq) dissolved in the minimum volume of DMF. The resultant solution was then immediately added to the resin. The reaction mixture was gently agitated by rotation for 1 h and the resin was filtered off and washed with DMF (3 x 2 minutes with rotation). A solution of 20% piperdine in DMF was added to the resin and gently agitated by rotation for 2 minutes. The resin was filtered off and this process was repeated four more times, followed by washing with DMF (5 x 2 minutes with rotation).

DIPEA (98  $\mu$ L, 0.56 mmols, 11 eq) was added to a solution of Mannose-based inhibitor **2.53** (108 mg, 0.26 mmols, 5 eq) and HTCU (107 mg, 0.26 mmols, 5 eq) dissolved in the minimum volume of DMF. The resultant solution was then immediately added to the resin. The reaction mixture was gently agitated by rotation for 1 h and the resin was filtered off and washed with DMF (3 x 2 minutes with rotation). A solution of 20% piperdine in DMF was added to the resin and gently agitated by rotation for 2 minutes. The resin was filtered off and this process was repeated four more times, followed by washing with DMF (5 x 2 minutes with rotation).

A freshly prepared solution of 2% (v/v) hydrazine monohydrate in DMF was then added to the resin and gently agitated by rotation for 5 minutes. The resin was filtered off and the process was repeated once more, followed by several washes with DMF (5 x 2 minutes with rotation).

## Experimental

DIPEA (98  $\mu$ L, 0.56 mmols, 11 eq) was added to a solution of OPAL small molecule **3.5** (102 mg, 0.26 mmols, 5 eq) and HTCU (107 mg, 0.26 mmols, 5 eq) dissolved in the minimum volume of DMF. The resultant solution was then immediately added to the resin. The reaction mixture was gently agitated by rotation for 1 h and the resin was filtered off and washed with DMF (5 x 2 minutes with rotation).

The resin was washed with DCM (3 x 2 minutes with rotation) and MeOH (3 x 2 minutes with rotation). The resin was dried on a vacuum manifold and further dried on a high vacuum line overnight. A solution of cleavage cocktail (95:2.5:2.5 TFA:H<sub>2</sub>O:triisopropylsilane) was added to the resin and gently agitated by rotation for 1 h. The reaction mixture was drained into ice-cold Et<sub>2</sub>O and centrifuged at 4000 rpm at 4 °C until pelleted (ca 5-10 minutes). The supernatant was carefully decanted and then subsequently resuspended, centrifuged and supernatant decanted three more times. The precipitated peptide pellet was dissolved in water and lyophilised to obtain a powder.

Purification of deprotected probe **3.6** was attempted using sephadex LH-20 resin (GE healthcare) in MeOH.



## Experimental

### 8.3.5.2 Synthesis of mannose-based inhibitor linked OPAL probe 3.10

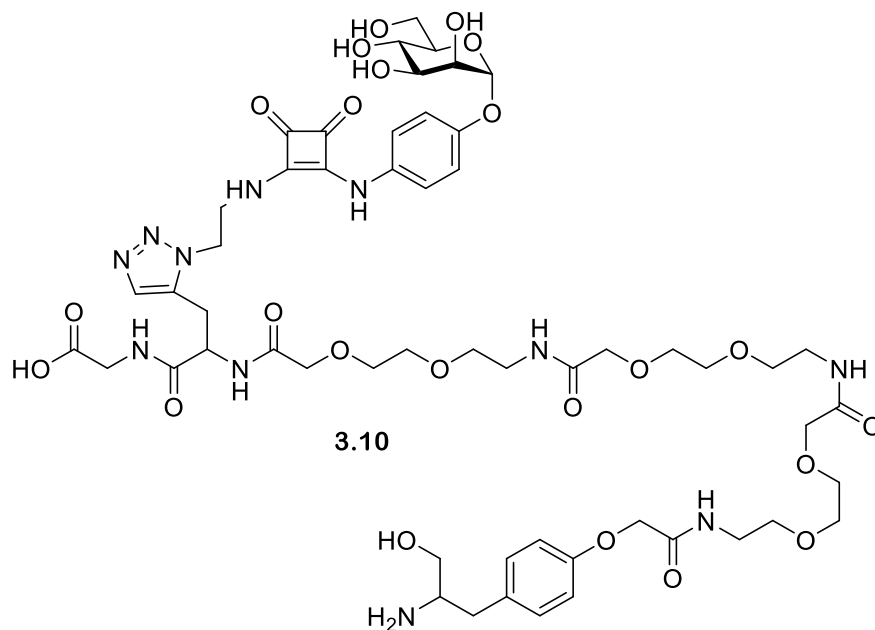


Figure 8-5. Structure of mannose-based inhibitor linked OPAL probe 3.10

H-Gly-2-CITrt resin was weighed out into an SPPS cartridge fitted with a PTFE stopcock, swollen in DMF for 30 minutes and then filtered.

DIPEA (98  $\mu$ L, 0.56 mmols, 11 eq) was added to a solution of Fmoc-propargyl-Gly-OH (89 mg, 0.26 mmols, 5 eq) and HTCU (107 mg, 0.26 mmols, 5 eq) dissolved in the minimum volume of DMF. The resultant solution was then immediately added to the resin. The reaction mixture was gently agitated by rotation for 1 h and the resin was filtered off and washed with DMF (3 x 2 minutes with rotation). A solution of 20% piperidine in DMF was added to the resin and gently agitated by rotation for 2 minutes. The resin was filtered off and this process was repeated four more times, followed by washing with DMF (5 x 2 minutes with rotation).

DIPEA (98  $\mu$ L, 0.56 mmols, 11 eq) was added to a solution of Fmoc-8-amino-3,6-dioxaoctanoic acid (102 mg, 0.26 mmols, 5 eq) and HTCU (107 mg, 0.26 mmols, 5 eq) dissolved in the minimum volume of DMF. The resultant solution was then immediately added to the resin. The reaction mixture was gently agitated by rotation for 1 h and the resin was filtered off and washed with DMF (3 x 2 minutes with rotation). A solution of 20% piperidine in DMF was added to the resin and gently agitated by rotation for 2 minutes. The resin was filtered off and this process was repeated four more times, followed by washing with DMF (5 x 2 minutes with rotation).

DIPEA (98  $\mu$ L, 0.56 mmols, 11 eq) was added to a solution of Fmoc-8-amino-3,6-dioxaoctanoic acid (102 mg, 0.26 mmols, 5 eq) and HTCU (107 mg, 0.26 mmols, 5 eq) dissolved in the minimum volume of DMF. The resultant solution was then immediately added to the resin. The reaction mixture was gently agitated by rotation for 1 h and the resin was filtered off and washed with DMF (3 x 2

## Experimental

minutes with rotation). A solution of 20% piperdine in DMF was added to the resin and gently agitated by rotation for 2 minutes. The resin was filtered off and this process was repeated four more times, followed by washing with DMF (5 x 2 minutes with rotation).

DIPEA (98  $\mu$ L, 0.56 mmols, 11 eq) was added to a solution of Fmoc-8-amino-3,6-dioxaoctanoic acid (102 mg, 0.26 mmols, 5 eq) and HTCUC (107 mg, 0.26 mmols, 5 eq) dissolved in the minimum volume of DMF. The resultant solution was then immediately added to the resin. The reaction mixture was gently agitated by rotation for 1 h and the resin was filtered off and washed with DMF (3 x 2 minutes with rotation). A solution of 20% piperdine in DMF was added to the resin and gently agitated by rotation for 2 minutes. The resin was filtered off and this process was repeated four more times, followed by washing with DMF (5 x 2 minutes with rotation).

DIPEA (98  $\mu$ L, 0.56 mmols, 11 eq) was added to a solution of OPAL small molecule **3.5** (102 mg, 0.26 mmols, 5 eq) and HTCUC (107 mg, 0.26 mmols, 5 eq) dissolved in the minimum volume of DMF. The resultant solution was then immediately added to the resin. The reaction mixture was gently agitated by rotation for 1 h and the resin was filtered off and washed with DMF (5 x 2 minutes with rotation).

DIPEA (1 mL, 5.75 mmols, 55 eq) was added to a solution of Mannose based inhibitor **2.53** (46 mg, 0.105 mmols, 1eq), sodium absorbate (31 mg, 0.156 mmols, 1.5 eq) and copper iodide (60 mg, 0.315 mmols, 3 eq) dissolved in DMF (2.5 mL) and the solution was added to resin. The reaction mixture was gently agitated by rotation for 12 h and the resin was filtered off and washed with H<sub>2</sub>O (3 x 2 minutes with rotation), iPrOH (3 x 2 minutes with rotation), DMF (3 x 2 minutes with rotation), iPrOH (3 x 2 minutes with rotation), DMF (3 x 2 minutes with rotation).

The resin was washed with DCM (3 x 2 minutes with rotation) and MeOH (3 x 2 minutes with rotation). The resin was dried on a vacuum manifold and further dried on a high vacuum line overnight. A solution of cleavage cocktail (95:2.5:2.5 TFA:H<sub>2</sub>O:triisopropylsilane) was added to the resin and gently agitated by rotation for 1 h. The reaction mixture was drained into ice-cold Et<sub>2</sub>O and centrifuged at 4000 rpm at 4 °C until pelleted (ca 5-10 minutes). The supernatant was carefully decanted and then subsequently resuspended, centrifuged and supernatant decanted three more times. The precipitated peptide pellet was dissolved in water and lyophilised to obtain a powder.

## Experimental

### 8.3.5.3 Synthesis of mannose-based inhibitor linked (Gly-Ser)<sub>3</sub> OPAL probe 3.13

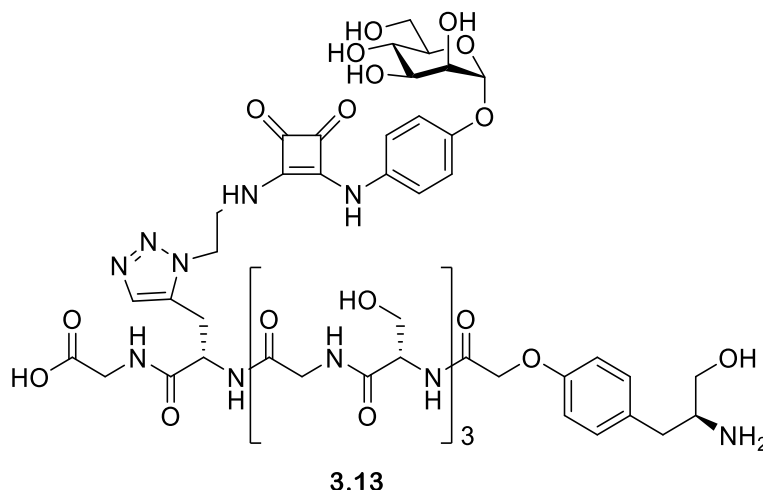


Figure 8-6. Structure of mannose-based inhibitor linked (Gly-Ser)<sub>3</sub> OPAL probe 3.13

H-Gly-2-CITrt resin was weighed out into an SPPS cartridge fitted with a PTFE stopcock, swollen in DMF for 30 minutes and then filtered.

DIPEA (98  $\mu$ L, 0.56 mmols, 11 eq) was added to a solution of Fmoc-propargyl-Gly-OH (89 mg, 0.26 mmols, 5 eq) and HCTU (107 mg, 0.26 mmols, 5 eq) dissolved in the minimum volume of DMF. The resultant solution was then immediately added to the resin. The reaction mixture was gently agitated by rotation for 1 h and the resin was filtered off and washed with DMF (3 x 2 minutes with rotation). A solution of 20% piperidine in DMF was added to the resin and gently agitated by rotation for 2 minutes. The resin was filtered off and this process was repeated four more times, followed by washing with DMF (5 x 2 minutes with rotation).

DIPEA (98  $\mu$ L, 0.56 mmols, 11 eq) was added to a solution of Fmoc-Gly-OH (79 mg, 0.26 mmols, 5 eq) and HCTU (107 mg, 0.26 mmols, 5 eq) dissolved in the minimum volume of DMF. The resultant solution was then immediately added to the resin. The reaction mixture was gently agitated by rotation for 1 h and the resin was filtered off and washed with DMF (3 x 2 minutes with rotation). A solution of 20% piperidine in DMF was added to the resin and gently agitated by rotation for 2 minutes. The resin was filtered off and this process was repeated four more times, followed by washing with DMF (5 x 2 minutes with rotation).

DIPEA (98  $\mu$ L, 0.56 mmols, 11 eq) was added to a solution of Fmoc-Ser(tBu)-OH (101 mg, 0.26 mmols, 5 eq) and HCTU (107 mg, 0.26 mmols, 5 eq) dissolved in the minimum volume of DMF. The resultant solution was then immediately added to the resin. The reaction mixture was gently agitated by rotation for 1 h and the resin was filtered off and washed with DMF (3 x 2 minutes with rotation). A solution of 20% piperidine in DMF was added to the resin and gently agitated by rotation for 2 minutes. The resin was filtered off and this process was repeated four more times, followed by washing with DMF (5 x 2 minutes with rotation).

## Experimental

DIPEA (98  $\mu$ L, 0.56 mmols, 11 eq) was added to a solution of Fmoc-Gly-OH (79 mg, 0.26 mmols, 5 eq) and HTCU (107 mg, 0.26 mmols, 5 eq) dissolved in the minimum volume of DMF. The resultant solution was then immediately added to the resin. The reaction mixture was gently agitated by rotation for 1 h and the resin was filtered off and washed with DMF (3 x 2 minutes with rotation). A solution of 20% piperdine in DMF was added to the resin and gently agitated by rotation for 2 minutes. The resin was filtered off and this process was repeated four more times, followed by washing with DMF (5 x 2 minutes with rotation).

DIPEA (98  $\mu$ L, 0.56 mmols, 11 eq) was added to a solution of Fmoc-Ser(tBu)-OH (101 mg, 0.26 mmols, 5 eq) and HTCU (107 mg, 0.26 mmols, 5 eq) dissolved in the minimum volume of DMF. The resultant solution was then immediately added to the resin. The reaction mixture was gently agitated by rotation for 1 h and the resin was filtered off and washed with DMF (3 x 2 minutes with rotation). A solution of 20% piperdine in DMF was added to the resin and gently agitated by rotation for 2 minutes. The resin was filtered off and this process was repeated four more times, followed by washing with DMF (5 x 2 minutes with rotation).

DIPEA (98  $\mu$ L, 0.56 mmols, 11 eq) was added to a solution of Fmoc-Gly-OH (79 mg, 0.26 mmols, 5 eq) and HTCU (107 mg, 0.26 mmols, 5 eq) dissolved in the minimum volume of DMF. The resultant solution was then immediately added to the resin. The reaction mixture was gently agitated by rotation for 1 h and the resin was filtered off and washed with DMF (3 x 2 minutes with rotation). A solution of 20% piperdine in DMF was added to the resin and gently agitated by rotation for 2 minutes. The resin was filtered off and this process was repeated four more times, followed by washing with DMF (5 x 2 minutes with rotation).

DIPEA (98  $\mu$ L, 0.56 mmols, 11 eq) was added to a solution of Fmoc-Ser(tBu)-OH (101 mg, 0.26 mmols, 5 eq) and HTCU (107 mg, 0.26 mmols, 5 eq) dissolved in the minimum volume of DMF. The resultant solution was then immediately added to the resin. The reaction mixture was gently agitated by rotation for 1 h and the resin was filtered off and washed with DMF (3 x 2 minutes with rotation). A solution of 20% piperdine in DMF was added to the resin and gently agitated by rotation for 2 minutes. The resin was filtered off and this process was repeated four more times, followed by washing with DMF (5 x 2 minutes with rotation).

DIPEA (98  $\mu$ L, 0.56 mmols, 11 eq) was added to a solution of OPAL small molecule **3.5** (102 mg, 0.26 mmols, 5 eq) and HTCU (107 mg, 0.26 mmols, 5 eq) dissolved in the minimum volume of DMF. The resultant solution was then immediately added to the resin. The reaction mixture was gently agitated by rotation for 1 h and the resin was filtered off and washed with DMF (5 x 2 minutes with rotation).

## Experimental

DIPEA (1 mL, 5.75 mmols, 55 eq) was added to a solution of Mannose-based inhibitor **2.54** (46 mg, 0.105 mmols, 1eq), sodium absorbate (31 mg, 0.156 mmols, 1.5 eq) and copper iodide (60 mg, 0.315 mmols, 3 eq) dissolved in DMF (2.5 mL) and the solution was added to resin. The reaction mixture was gently agitated by rotation for 12 h and the resin was filtered off and washed with H<sub>2</sub>O (3 x 2 minutes with rotation), iPrOH (3 x 2 minutes with rotation), DMF (3 x 2 minutes with rotation), iPrOH (3 x 2 minutes with rotation), DMF (3 x 2 minutes with rotation).

The resin was washed with DCM (3 x 2 minutes with rotation) and MeOH (3 x 2 minutes with rotation). The resin was dried on a vacuum manifold and further dried on a high vacuum line overnight. A solution of cleavage cocktail (95:2.5:2.5 TFA:H<sub>2</sub>O:triisopropylsilane) was added to the resin and gently agitated by rotation for 1 h. The reaction mixture was drained into ice-cold Et<sub>2</sub>O and centrifuged at 4000 rpm at 4 °C until pelleted (ca 5-10 minutes). The supernatant was carefully decanted and then subsequently resuspended, centrifuged and supernatant decanted three more times. The precipitated peptide pellet was dissolved in water and lyophilised to obtain a powder.

Probe **3.13** was purified using sephadex LH-20 resin (GE healthcare) in MeOH

## Experimental

### 8.3.5.4 Synthesis of mannose-based inhibitor linked (Gly-Ser)<sub>3</sub> OPAL probe **3.17**

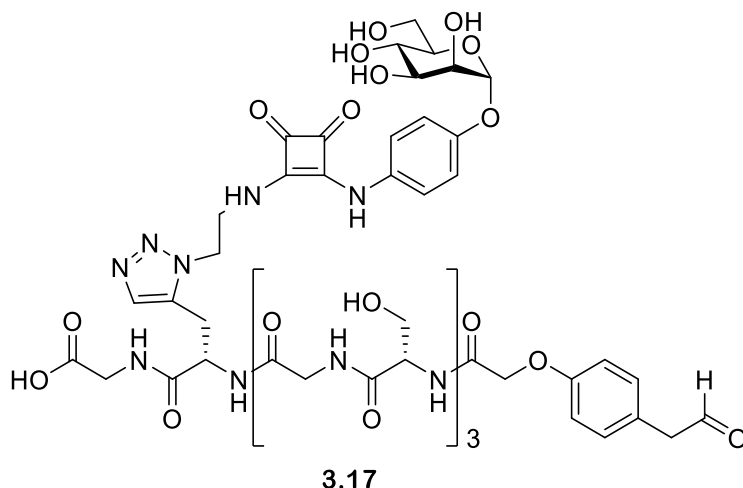


Figure 8-7. Structure of active mannose-based inhibitor linked (Gly-Ser)<sub>3</sub> OPAL probe **3.17**

To a solution of mannose-based inhibitor linked (Gly-Ser)<sub>3</sub> OPAL probe **3.13** (500  $\mu$ L, 16 mM, 10 mg, in 0.1 M PB, 0.1 M NaCl, pH = 7.0) was added NaIO<sub>4</sub> (72  $\mu$ L, 112 mM, in 0.1 M PB, 0.1 M NaCl, pH = 7.0) in 6  $\times$  12  $\mu$ L increments. The reaction was mixed thoroughly, and allowed to sit for 3 minutes on ice in the dark. The solution was then loaded onto a solid phase extraction cartridge (Grace Davison Extract Clean, 8 ml reservoir, Fisher Scientific) equilibrated with water/acetonitrile. After initial washing with water, the product was eluted over a gradient of acetonitrile. The product was then diluted with water, and subsequently lyophilised to give **3.17** as a pale yellow, fluffy powder (3.5 mg, 36%).

## Experimental

### 8.3.5.5 Synthesis of mannose-based inhibitor linked (Gly-Ser) OPAL probe 3.14

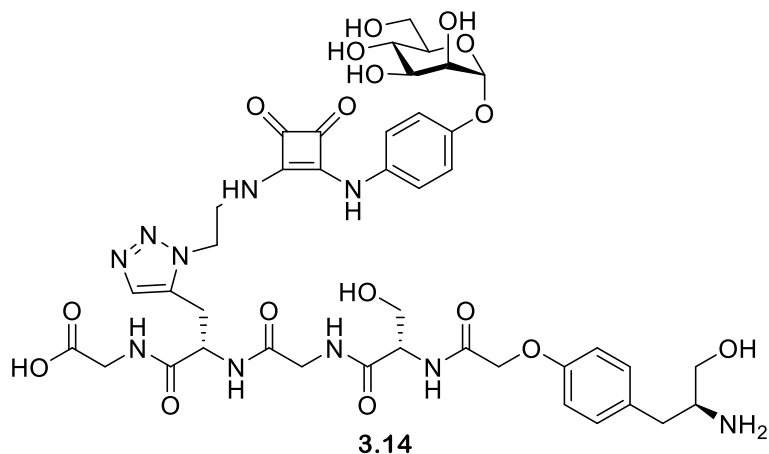


Figure 8-8. Structure of mannose-based inhibitor linked (Gly-Ser) OPAL probe 3.14

H-Gly-2-CITrt resin was weighed out into an SPPS cartridge fitted with a PTFE stopcock, swollen in DMF for 30 minutes and then filtered.

DIPEA (98  $\mu$ L, 0.56 mmols, 11 eq) was added to a solution of Fmoc-propargyl-Gly-OH (89 mg, 0.26 mmols, 5 eq) and HCTU (107 mg, 0.26 mmols, 5 eq) dissolved in the minimum volume of DMF. The resultant solution was then immediately added to the resin. The reaction mixture was gently agitated by rotation for 1 h and the resin was filtered off and washed with DMF (3 x 2 minutes with rotation). A solution of 20% piperidine in DMF was added to the resin and gently agitated by rotation for 2 minutes. The resin was filtered off and this process was repeated four more times, followed by washing with DMF (5 x 2 minutes with rotation).

DIPEA (98  $\mu$ L, 0.56 mmols, 11 eq) was added to a solution of Fmoc-Gly-OH (79 mg, 0.26 mmols, 5 eq) and HCTU (107 mg, 0.26 mmols, 5 eq) dissolved in the minimum volume of DMF. The resultant solution was then immediately added to the resin. The reaction mixture was gently agitated by rotation for 1 h and the resin was filtered off and washed with DMF (3 x 2 minutes with rotation). A solution of 20% piperidine in DMF was added to the resin and gently agitated by rotation for 2 minutes. The resin was filtered off and this process was repeated four more times, followed by washing with DMF (5 x 2 minutes with rotation).

DIPEA (98  $\mu$ L, 0.56 mmols, 11 eq) was added to a solution of Fmoc-Ser(tBu)-OH (101 mg, 0.26 mmols, 5 eq) and HCTU (107 mg, 0.26 mmols, 5 eq) dissolved in the minimum volume of DMF. The resultant solution was then immediately added to the resin. The reaction mixture was gently agitated by rotation for 1 h and the resin was filtered off and washed with DMF (3 x 2 minutes with rotation). A solution of 20% piperidine in DMF was added to the resin and gently agitated by rotation for 2 minutes. The resin was filtered off and this process was repeated four more times, followed by washing with DMF (5 x 2 minutes with rotation).

## Experimental

DIPEA (98  $\mu$ L, 0.56 mmols, 11 eq) was added to a solution of OPAL small molecule **3.5** (102 mg, 0.26 mmols, 5 eq) and HTCUC (107 mg, 0.26 mmols, 5 eq) dissolved in the minimum volume of DMF. The resultant solution was then immediately added to the resin. The reaction mixture was gently agitated by rotation for 1 h and the resin was filtered off and washed with DMF (5 x 2 minutes with rotation).

DIPEA (1 mL, 5.75 mmols, 55 eq) was added to a solution of mannose-based inhibitor **2.54** (46 mg, 0.105 mmols, 1eq), sodium absorbate (31 mg, 0.156 mmols, 1.5 eq) and copper iodide (60 mg, 0.315 mmols, 3 eq) dissolved in DMF (2.5 mL) and the solution was added to resin. The reaction mixture was gently agitated by rotation for 12 h and the resin was filtered off and washed with H<sub>2</sub>O (3 x 2 minutes with rotation), iPrOH (3 x 2 minutes with rotation), DMF (3 x 2 minutes with rotation), iPrOH (3 x 2 minutes with rotation), DMF (3 x 2 minutes with rotation).

The resin was washed with DCM (3 x 2 minutes with rotation) and MeOH (3 x 2 minutes with rotation). The resin was dried on a vacuum manifold and further dried on a high vacuum line overnight. A solution of cleavage cocktail (95:2.5:2.5 TFA:H<sub>2</sub>O:triisopropylsilane) was added to the resin and gently agitated by rotation for 1 h. The reaction mixture was drained into ice-cold Et<sub>2</sub>O and centrifuged at 4000 rpm at 4 °C until pelleted (ca 5-10 min). The supernatant was carefully decanted and then subsequently resuspended, centrifuged and supernatant decanted three more times. The precipitated peptide pellet was dissolved in water and lyophilised to obtain a powder.



## Experimental

### 8.3.5.6 Synthesis of mannose-based inhibitor linked (Gly-Ser) OPAL probe **3.18**

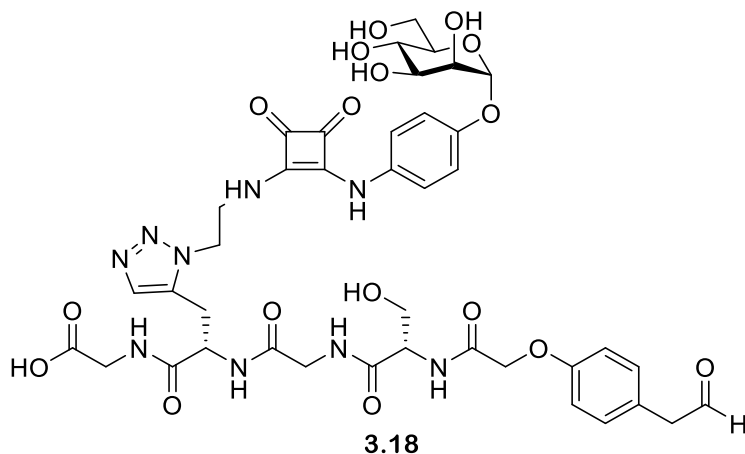


Figure 8-9. active mannose-based inhibitor linked (Gly-Ser) OPAL probe **3.18**

To a solution of Mannose-based inhibitor linked (Gly-Ser) click OPAL probe **3.14** (500  $\mu$ L, 14 mM, 6.7 mg, in 0.1 M PB, 0.1 M NaCl, pH = 7.0) was added NaIO<sub>4</sub> (63  $\mu$ L, 112 mM, in 0.1 M PB, 0.1 M NaCl, pH = 7.0). The reaction was mixed thoroughly and allowed to sit for 3 minutes on ice in the dark. The solution was then loaded onto a solid phase extraction cartridge (Grace Davison Extract Clean, 8 ml reservoir, Fisher Scientific) equilibrated with water/acetonitrile. After initial washing with water, the product was eluted over a gradient of acetonitrile. The product was then diluted with water, and subsequently lyophilised to give **3.18** as a pale yellow, fluffy powder (4 mg, 62%).

## Experimental

### 8.3.5.7 Synthesis of mannose-based inhibitor linked (Gly-Ser)<sub>6</sub> OPAL probe 3.15

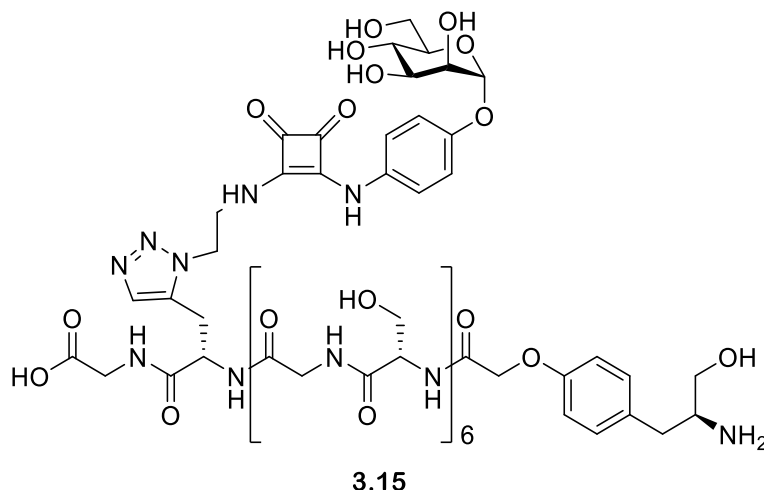


Figure 8-10. Structure of mannose-based inhibitor linked (Gly-Ser)<sub>6</sub> OPAL probe 3.15

H-Gly-2-CITrt resin was weighed out into an SPPS cartridge fitted with a PTFE stopcock, swollen in DMF for 30 minutes and then filtered.

DIPEA (98  $\mu$ L, 0.56 mmols, 11 eq) was added to a solution of Fmoc-propargyl-Gly-OH (89 mg, 0.26 mmols, 5 eq) and HCTU (107 mg, 0.26 mmols, 5 eq) dissolved in the minimum volume of DMF. The resultant solution was then immediately added to the resin. The reaction mixture was gently agitated by rotation for 1 h and the resin was filtered off and washed with DMF (3 x 2 minutes with rotation). A solution of 20% piperidine in DMF was added to the resin and gently agitated by rotation for 2 minutes. The resin was filtered off and this process was repeated four more times, followed by washing with DMF (5 x 2 minutes with rotation).

DIPEA (98  $\mu$ L, 0.56 mmols, 11 eq) was added to a solution of Fmoc-Gly-OH (79 mg, 0.26 mmols, 5 eq) and HCTU (107 mg, 0.26 mmols, 5 eq) dissolved in the minimum volume of DMF. The resultant solution was then immediately added to the resin. The reaction mixture was gently agitated by rotation for 1 h and the resin was filtered off and washed with DMF (3 x 2 minutes with rotation). A solution of 20% piperidine in DMF was added to the resin and gently agitated by rotation for 2 minutes. The resin was filtered off and this process was repeated four more times, followed by washing with DMF (5 x 2 minutes with rotation).

DIPEA (98  $\mu$ L, 0.56 mmols, 11 eq) was added to a solution of Fmoc-Ser(tBu)-OH (101 mg, 0.26 mmols, 5 eq) and HCTU (107 mg, 0.26 mmols, 5 eq) dissolved in the minimum volume of DMF. The resultant solution was then immediately added to the resin. The reaction mixture was gently agitated by rotation for 1 h and the resin was filtered off and washed with DMF (3 x 2 minutes with rotation). A solution of 20% piperidine in DMF was added to the resin and gently agitated by rotation for 2 minutes. The resin was filtered off and this process was repeated four more times, followed by washing with DMF (5 x 2 minutes with rotation).

## Experimental

DIPEA (98  $\mu$ L, 0.56 mmols, 11 eq) was added to a solution of Fmoc-Gly-OH (79 mg, 0.26 mmols, 5 eq) and HTCU (107 mg, 0.26 mmols, 5 eq) dissolved in the minimum volume of DMF. The resultant solution was then immediately added to the resin. The reaction mixture was gently agitated by rotation for 1 h and the resin was filtered off and washed with DMF (3 x 2 minutes with rotation). A solution of 20% piperdine in DMF was added to the resin and gently agitated by rotation for 2 minutes. The resin was filtered off and this process was repeated four more times, followed by washing with DMF (5 x 2 minutes with rotation).

DIPEA (98  $\mu$ L, 0.56 mmols, 11 eq) was added to a solution of Fmoc-Ser(tBu)-OH (101 mg, 0.26 mmols, 5 eq) and HTCU (107 mg, 0.26 mmols, 5 eq) dissolved in the minimum volume of DMF. The resultant solution was then immediately added to the resin. The reaction mixture was gently agitated by rotation for 1 h and the resin was filtered off and washed with DMF (3 x 2 minutes with rotation). A solution of 20% piperdine in DMF was added to the resin and gently agitated by rotation for 2 minutes. The resin was filtered off and this process was repeated four more times, followed by washing with DMF (5 x 2 minutes with rotation).

DIPEA (98  $\mu$ L, 0.56 mmols, 11 eq) was added to a solution of Fmoc-Gly-OH (79 mg, 0.26 mmols, 5 eq) and HTCU (107 mg, 0.26 mmols, 5 eq) dissolved in the minimum volume of DMF. The resultant solution was then immediately added to the resin. The reaction mixture was gently agitated by rotation for 1 h and the resin was filtered off and washed with DMF (3 x 2 minutes with rotation). A solution of 20% piperdine in DMF was added to the resin and gently agitated by rotation for 2 minutes. The resin was filtered off and this process was repeated four more times, followed by washing with DMF (5 x 2 minutes with rotation).

DIPEA (98  $\mu$ L, 0.56 mmols, 11 eq) was added to a solution of Fmoc-Ser(tBu)-OH (101 mg, 0.26 mmols, 5 eq) and HTCU (107 mg, 0.26 mmols, 5 eq) dissolved in the minimum volume of DMF. The resultant solution was then immediately added to the resin. The reaction mixture was gently agitated by rotation for 1 h and the resin was filtered off and washed with DMF (3 x 2 minutes with rotation). A solution of 20% piperdine in DMF was added to the resin and gently agitated by rotation for 2 minutes. The resin was filtered off and this process was repeated four more times, followed by washing with DMF (5 x 2 minutes with rotation).

DIPEA (98  $\mu$ L, 0.56 mmols, 11 eq) was added to a solution of Fmoc-Gly-OH (79 mg, 0.26 mmols, 5 eq) and HTCU (107 mg, 0.26 mmols, 5 eq) dissolved in the minimum volume of DMF. The resultant solution was then immediately added to the resin. The reaction mixture was gently agitated by rotation for 1 h and the resin was filtered off and washed with DMF (3 x 2 minutes with rotation). A solution of 20% piperdine in DMF was added to the resin and gently agitated by rotation for 2 minutes.

## Experimental

The resin was filtered off and this process was repeated four more times, followed by washing with DMF (5 x 2 minutes with rotation).

DIPEA (98  $\mu$ L, 0.56 mmols, 11 eq) was added to a solution of Fmoc-Ser(tBu)-OH (101 mg, 0.26 mmols, 5 eq) and HCTU (107 mg, 0.26 mmols, 5 eq) dissolved in the minimum volume of DMF. The resultant solution was then immediately added to the resin. The reaction mixture was gently agitated by rotation for 1 h and the resin was filtered off and washed with DMF (3 x 2 minutes with rotation). A solution of 20% piperdine in DMF was added to the resin and gently agitated by rotation for 2 minutes. The resin was filtered off and this process was repeated four more times, followed by washing with DMF (5 x 2 minutes with rotation).

DIPEA (98  $\mu$ L, 0.56 mmols, 11 eq) was added to a solution of Fmoc-Gly-OH (79 mg, 0.26 mmols, 5 eq) and HCTU (107 mg, 0.26 mmols, 5 eq) dissolved in the minimum volume of DMF. The resultant solution was then immediately added to the resin. The reaction mixture was gently agitated by rotation for 1 h and the resin was filtered off and washed with DMF (3 x 2 minutes with rotation). A solution of 20% piperdine in DMF was added to the resin and gently agitated by rotation for 2 minutes. The resin was filtered off and this process was repeated four more times, followed by washing with DMF (5 x 2 minutes with rotation).

DIPEA (98  $\mu$ L, 0.56 mmols, 11 eq) was added to a solution of Fmoc-Ser(tBu)-OH (101 mg, 0.26 mmols, 5 eq) and HCTU (107 mg, 0.26 mmols, 5 eq) dissolved in the minimum volume of DMF. The resultant solution was then immediately added to the resin. The reaction mixture was gently agitated by rotation for 1 h and the resin was filtered off and washed with DMF (3 x 2 minutes with rotation). A solution of 20% piperdine in DMF was added to the resin and gently agitated by rotation for 2 minutes. The resin was filtered off and this process was repeated four more times, followed by washing with DMF (5 x 2 minutes with rotation).

DIPEA (98  $\mu$ L, 0.56 mmols, 11 eq) was added to a solution of Fmoc-Gly-OH (79 mg, 0.26 mmols, 5 eq) and HCTU (107 mg, 0.26 mmols, 5 eq) dissolved in the minimum volume of DMF. The resultant solution was then immediately added to the resin. The reaction mixture was gently agitated by rotation for 1 h and the resin was filtered off and washed with DMF (3 x 2 minutes with rotation). A solution of 20% piperdine in DMF was added to the resin and gently agitated by rotation for 2 minutes. The resin was filtered off and this process was repeated four more times, followed by washing with DMF (5 x 2 minutes with rotation).

DIPEA (98  $\mu$ L, 0.56 mmols, 11 eq) was added to a solution of Fmoc-Ser(tBu)-OH (101 mg, 0.26 mmols, 5 eq) and HCTU (107 mg, 0.26 mmols, 5 eq) dissolved in the minimum volume of DMF. The resultant solution was then immediately added to the resin. The reaction mixture was gently agitated by rotation for 1 h and the resin was filtered off and washed with DMF (3 x 2 minutes with rotation).

## Experimental

A solution of 20% piperidine in DMF was added to the resin and gently agitated by rotation for 2 minutes. The resin was filtered off and this process was repeated four more times, followed by washing with DMF (5 x 2 minutes with rotation).

DIPEA (98  $\mu$ L, 0.56 mmols, 11 eq) was added to a solution of OPAL small molecule **3.5** (102 mg, 0.26 mmols, 5 eq) and HTCUC (107 mg, 0.26 mmols, 5 eq) dissolved in the minimum volume of DMF. The resultant solution was then immediately added to the resin. The reaction mixture was gently agitated by rotation for 1 h and the resin was filtered off and washed with DMF (5 x 2 minutes with rotation).

DIPEA (1 mL, 5.75 mmols, 55 eq) was added to a solution of mannose-based inhibitor **2.54** (46 mg, 0.105 mmols, 1 eq), sodium absorbate (31 mg, 0.156 mmols, 1.5 eq) and copper iodide (60 mg, 0.315 mmols, 3 eq) dissolved in DMF (2.5 mL) and the solution was added to resin. The reaction mixture was gently agitated by rotation for 12 h and the resin was filtered off and washed with H<sub>2</sub>O (3 x 2 minutes with rotation), iPrOH (3 x 2 minutes with rotation), DMF (3 x 2 minutes with rotation), iPrOH (3 x 2 minutes with rotation), DMF (3 x 2 minutes with rotation).

The resin was washed with DCM (3 x 2 minutes with rotation) and MeOH (3 x 2 minutes with rotation). The resin was dried on a vacuum manifold and further dried on a high vacuum line overnight. A solution of cleavage cocktail (95:2.5:2.5 TFA:H<sub>2</sub>O:triisopropylsilane) was added to the resin and gently agitated by rotation for 1 h. The reaction mixture was drained into ice-cold Et<sub>2</sub>O and centrifuged at 4000 rpm at 4 °C until pelleted (ca 5-10 minutes). The supernatant was carefully decanted and then subsequently resuspended, centrifuged and supernatant decanted three more times. The precipitated peptide pellet was dissolved in water and lyophilised to obtain a powder.

Probe **3.15** was purified using Bio-Gel P-2 resin (BIORAD) in water.

## Experimental

### 8.3.5.8 Synthesis of mannose-based inhibitor linked (Gly-Ser)<sub>6</sub> OPAL probe **3.19**

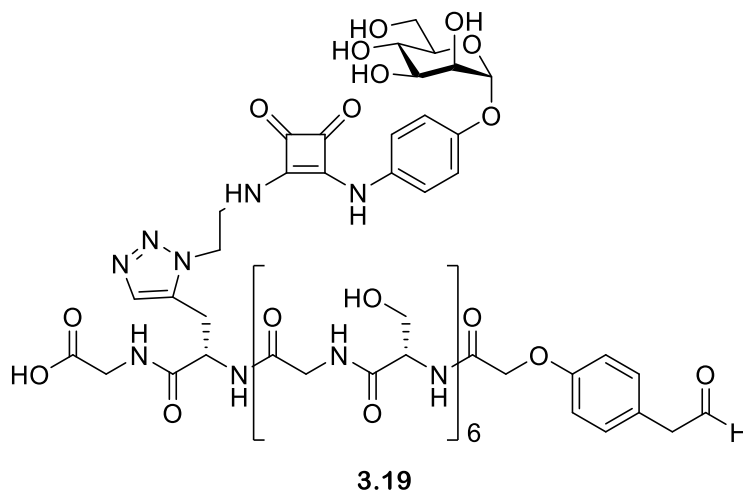


Figure 8-11. Structure of active mannose-based inhibitor linked (Gly-Ser)<sub>6</sub> OPAL probe **3.19**

To a solution of mannose-based inhibitor linked (Gly-Ser)<sub>6</sub> OPAL probe **3.15** (160  $\mu$ L, 15 mM, 4 mg, in 0.1 M PB, 0.1 M NaCl, pH = 7.0) was added NaIO<sub>4</sub> (22  $\mu$ L, 112 mM, in 0.1 M PB, 0.1 M NaCl, pH = 7.0) in 2 11  $\mu$ L increments. The reaction was mixed thoroughly, and allowed to sit for 3 minutes on ice in the dark. The solution was then loaded onto a solid phase extraction cartridge (Grace Davison Extract Clean, 8 ml reservoir, Fisher Scientific) equilibrated with water/acetonitrile. After initial washing with water, the product was eluted over a gradient of acetonitrile. The product was then diluted with water, and subsequently lyophilised to give **3.19** as a pale yellow, fluffy powder (3.8 mg, 96%).

## Experimental

### 8.3.5.9 Synthesis of biotin linked (Ser-Gly)<sub>3</sub>OPAL probe 3.16

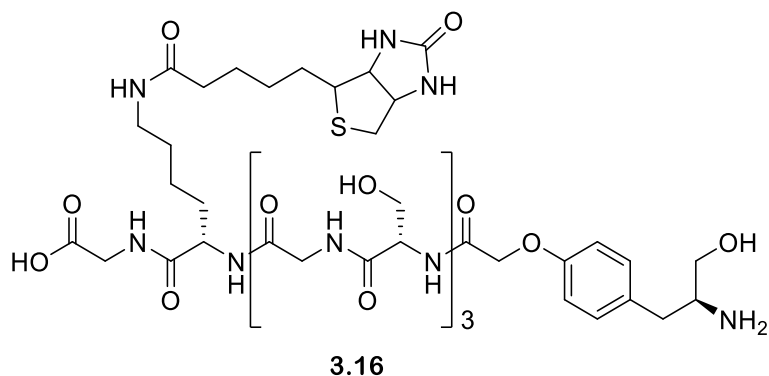


Figure 8-12. Structure of biotin linked (Ser-Gly)<sub>3</sub> OPAL probe 3.16

H-Gly-2-ClTrt resin was weighed out into an SPPS cartridge fitted with a PTFE stopcock, swollen in DMF for 30 minutes and then filtered.

DIPEA (98  $\mu$ L, 0.56 mmols, 11 eq) was added to a solution of Fmoc-propargyl-Gly-OH (158 mg, 0.26 mmols, 5 eq) and HTCU (107 mg, 0.26 mmols, 5 eq) dissolved in the minimum volume of DMF. The resultant solution was then immediately added to the resin. The reaction mixture was gently agitated by rotation for 1 h and the resin was filtered off and washed with DMF (3 x 2 minutes with rotation). A solution of 20% piperidine in DMF was added to the resin and gently agitated by rotation for 2 minutes. The resin was filtered off and this process was repeated four more times, followed by washing with DMF (5 x 2 minutes with rotation).

DIPEA (98  $\mu$ L, 0.56 mmols, 11 eq) was added to a solution of Fmoc-Ser(tBu)-OH (101 mg, 0.26 mmols, 5 eq) and HTCU (107 mg, 0.26 mmols, 5 eq) dissolved in the minimum volume of DMF. The resultant solution was then immediately added to the resin. The reaction mixture was gently agitated by rotation for 1 h and the resin was filtered off and washed with DMF (3 x 2 minutes with rotation). A solution of 20% piperidine in DMF was added to the resin and gently agitated by rotation for 2 minutes. The resin was filtered off and this process was repeated four more times, followed by washing with DMF (5 x 2 minutes with rotation).

DIPEA (98  $\mu$ L, 0.56 mmols, 11 eq) was added to a solution of Fmoc-Gly-OH (79 mg, 0.26 mmols, 5 eq) and HTCU (107 mg, 0.26 mmols, 5 eq) dissolved in the minimum volume of DMF. The resultant solution was then immediately added to the resin. The reaction mixture was gently agitated by rotation for 1 h and the resin was filtered off and washed with DMF (3 x 2 minutes with rotation). A solution of 20% piperidine in DMF was added to the resin and gently agitated by rotation for 2 minutes. The resin was filtered off and this process was repeated four more times, followed by washing with DMF (5 x 2 minutes with rotation).

DIPEA (98  $\mu$ L, 0.56 mmols, 11 eq) was added to a solution of Fmoc-Ser(tBu)-OH (101 mg, 0.26 mmols, 5 eq) and HTCU (107 mg, 0.26 mmols, 5 eq) dissolved in the minimum volume of DMF. The

## Experimental

resultant solution was then immediately added to the resin. The reaction mixture was gently agitated by rotation for 1 h and the resin was filtered off and washed with DMF (3 x 2 minutes with rotation). A solution of 20% piperidine in DMF was added to the resin and gently agitated by rotation for 2 minutes. The resin was filtered off and this process was repeated four more times, followed by washing with DMF (5 x 2 minutes with rotation).

DIPEA (98  $\mu$ L, 0.56 mmols, 11 eq) was added to a solution of Fmoc-Gly-OH (79 mg, 0.26 mmols, 5 eq) and HTCU (107 mg, 0.26 mmols, 5 eq) dissolved in the minimum volume of DMF. The resultant solution was then immediately added to the resin. The reaction mixture was gently agitated by rotation for 1 h and the resin was filtered off and washed with DMF (3 x 2 minutes with rotation). A solution of 20% piperidine in DMF was added to the resin and gently agitated by rotation for 2 minutes. The resin was filtered off and this process was repeated four more times, followed by washing with DMF (5 x 2 minutes with rotation).

DIPEA (98  $\mu$ L, 0.56 mmols, 11 eq) was added to a solution of Fmoc-Ser(tBu)-OH (101 mg, 0.26 mmols, 5 eq) and HTCU (107 mg, 0.26 mmols, 5 eq) dissolved in the minimum volume of DMF. The resultant solution was then immediately added to the resin. The reaction mixture was gently agitated by rotation for 1 h and the resin was filtered off and washed with DMF (3 x 2 minutes with rotation). A solution of 20% piperidine in DMF was added to the resin and gently agitated by rotation for 2 minutes. The resin was filtered off and this process was repeated four more times, followed by washing with DMF (5 x 2 minutes with rotation).

DIPEA (98  $\mu$ L, 0.56 mmols, 11 eq) was added to a solution of Fmoc-Gly-OH (79 mg, 0.26 mmols, 5 eq) and HTCU (107 mg, 0.26 mmols, 5 eq) dissolved in the minimum volume of DMF. The resultant solution was then immediately added to the resin. The reaction mixture was gently agitated by rotation for 1 h and the resin was filtered off and washed with DMF (3 x 2 minutes with rotation). A solution of 20% piperidine in DMF was added to the resin and gently agitated by rotation for 2 minutes. The resin was filtered off and this process was repeated four more times, followed by washing with DMF (5 x 2 minutes with rotation).

DIPEA (98  $\mu$ L, 0.56 mmols, 11 eq) was added to a solution of OPAL small molecule **3.5** (102 mg, 0.26 mmols, 5 eq) and HTCU (107 mg, 0.26 mmols, 5 eq) dissolved in the minimum volume of DMF. The resultant solution was then immediately added to the resin. The reaction mixture was gently agitated by rotation for 1 h and the resin was filtered off and washed with DMF (5 x 2 minutes with rotation).

The resin was washed with DCM (3 x 2 minutes with rotation) and MeOH (3 x 2 minutes with rotation). The resin was dried on a vacuum manifold and further dried on a high vacuum line overnight. A solution of cleavage cocktail (95:2.5:2.5 TFA:H<sub>2</sub>O:triisopropylsilane) was added to the resin and



## Experimental

gently agitated by rotation for 1 h. The reaction mixture was drained into ice-cold Et<sub>2</sub>O and centrifuged at 4000 rpm at 4 °C until pelleted (ca 5-10 minutes). The supernatant was carefully decanted and then subsequently resuspended, centrifuged and supernatant decanted three more times. The precipitated peptide pellet was dissolved in water and lyophilised to obtain a powder.

## Experimental

### 8.3.5.10 Synthesis of biotin linked (Ser-Gly)<sub>3</sub> OPAL probe **3.20**

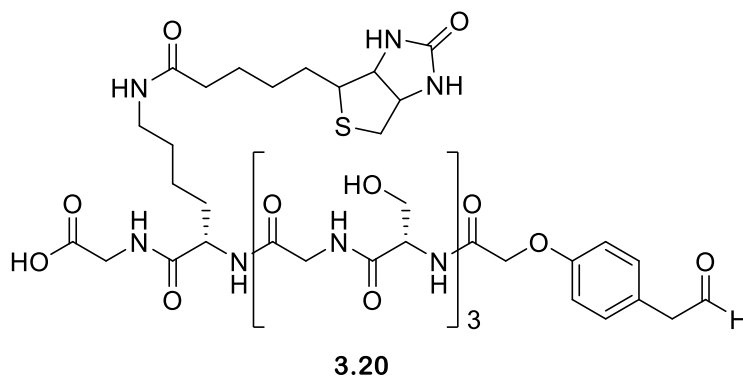


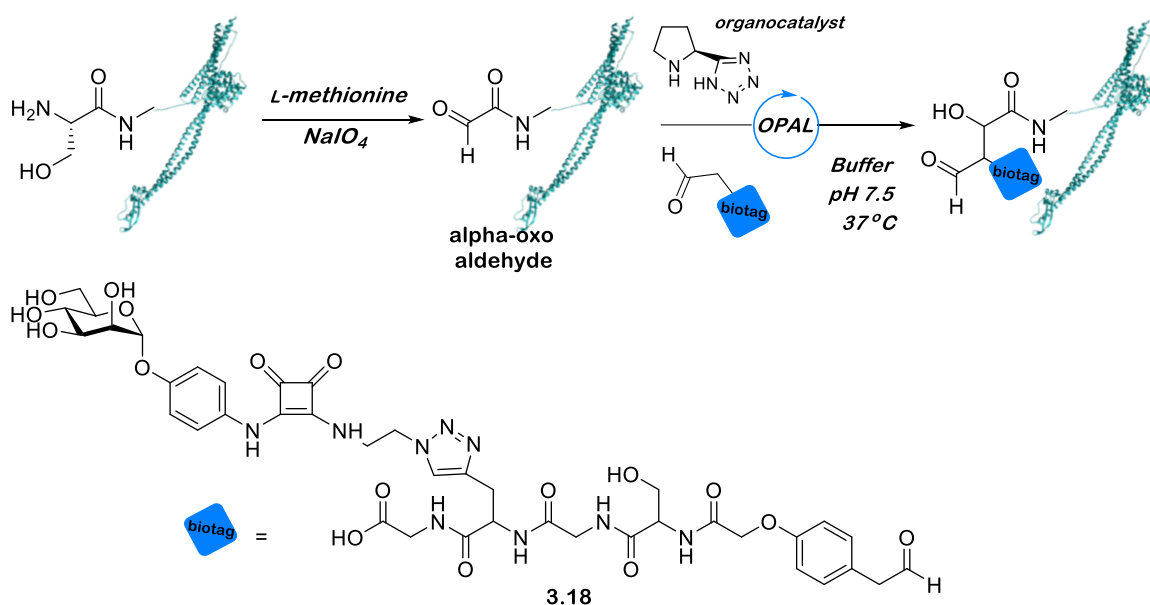
Figure 8-13. Structure of active biotin linked (Ser-Gly)<sub>3</sub> OPAL probe **3.20**

To a solution of biotin linked (Ser-Gly)<sub>3</sub> OPAL probe **3.16** (500  $\mu$ L, 9.4 mM, 5 mg, in 0.1 M PB, 0.1 M NaCl, pH = 7.0) was added NaIO<sub>4</sub> (42  $\mu$ L, 112 mM, in 0.1 M PB, 0.1 M NaCl, pH = 7.0) in 6 x 7  $\mu$ L additions. The reaction was mixed thoroughly and allowed to sit for 3 minutes on ice in the dark. The solution was then loaded onto a solid phase extraction cartridge (Grace Davison Extract Clean, 8 ml reservoir, Fisher Scientific) equilibrated with water/acetonitrile. After initial washing with water, the product was eluted over a gradient of acetonitrile. The product was then diluted with water, and subsequently lyophilised to give **3.20** as a pale yellow, fluffy powder (4 mg, 82%).

## Experimental

### 8.3.6 Synthesis of mannose-based inhibitor linked colicin conjugates

#### 8.3.6.1 Methodology for the bio-conjugation of active mannose-based inhibitor linked (Gly-Ser) OPAL probe **3.18** to colicin Ia glycoconjugate

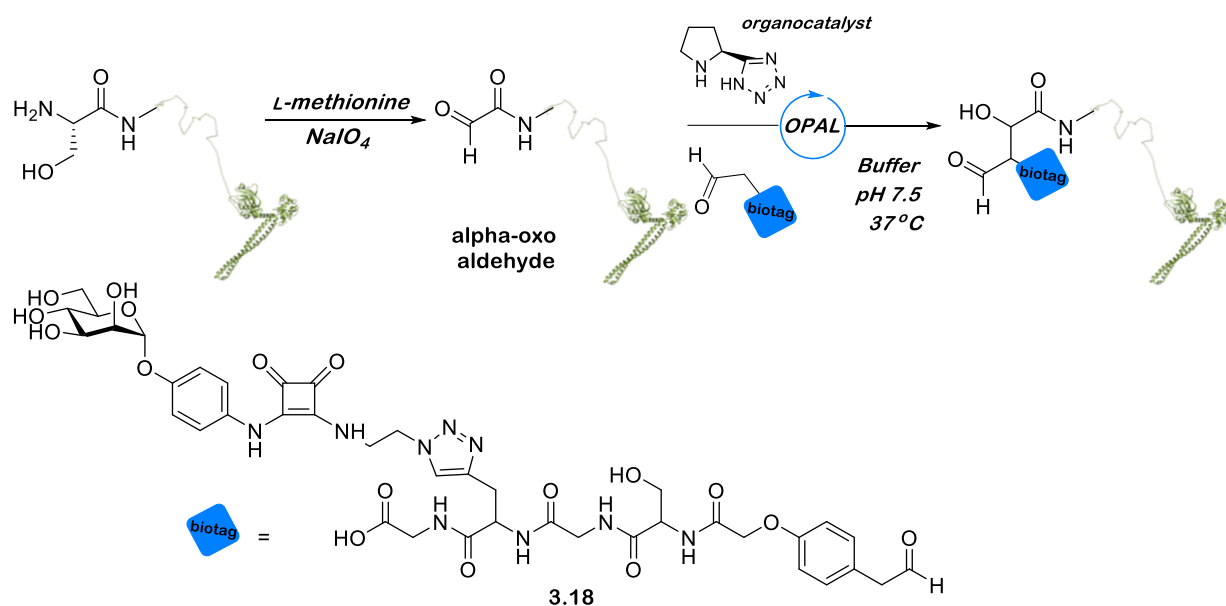


Scheme 8-2. Reaction scheme for OPAL ligation of active mannose-based inhibitor linked (Gly-Ser) OPAL probe **3.18** to colicin Ia

βMe (137 mM stock in water, 10 μL, final concentration 10% (v/v)) was added to a solution of colicin Ia (100 μL of 100 μM stock in 25 mM PB pH 7.5) in a 0.5 mL Eppendorf, mixed by pipette tip swirling and left at r.t. for 5 minutes. The solution was charged with L-methionine (1 μL of 66 mM stock in 0.1 M PB, 0.1 NaCl, pH 7.0) and NaIO<sub>4</sub> (1 μL of 33 mM stock in 0.1 M PB, 0.1 NaCl, pH 7.0) and mixed by gentle pipette tip swirling. The solution was incubated on ice in the dark for 4 minutes. The reaction mixture was immediately purified using a PD SpinTrap G25 desalting column (GE Healthcare Life Sciences), eluting into 100 μL of 25 mM PB pH 7.5. The reaction mixture was charged with (S)-(-)-5-(2-pyrrolidinyl)-H-tetrazole (20 μL of 200 mM stock in 25 mM PB pH 7.5) and probe **3.18** (40 μL of 4 mM stock in 25 mM PB pH 7.5). The solution was mixed via pipette tip swirling and incubated for 1 h at 37 °C. The reaction mixture was purified using a PD SpinTrap G25 desalting column (GE Healthcare Life Sciences), eluting into 20 mM K phosphate, 500 mM NaCl pH 7.0 for analysis and further manipulation.

## Experimental

### 8.3.6.2 Methodology for the bio-conjugation of active mannose-based inhibitor linked (Gly-Ser) OPAL probe **3.18** to colicin E9

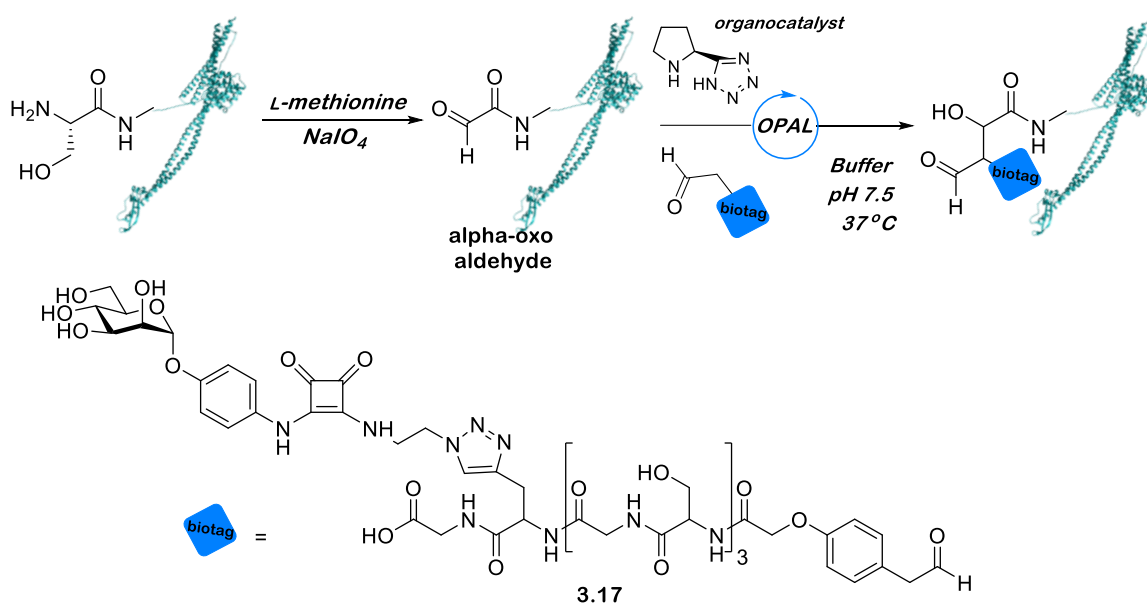


Scheme 8-3. Reaction scheme for OPAL ligation of active mannose-based inhibitor linked (Gly-Ser) OPAL probe **3.18** to colicin E9

A solution of colicin E9 (100  $\mu$ L of 78  $\mu$ M stock in 25 mM PB pH 7.5) was charged with *L*-methionine (0.78  $\mu$ L of 66 mM stock in 0.1 M PB, 0.1 NaCl, pH 7.0) and NaIO<sub>4</sub> (0.78  $\mu$ L of 33 mM stock in 0.1 M PB, 0.1 NaCl, pH 7.0). The solution was mixed by gentle pipette tip swirling and allowed to sit on ice in the dark for 4 minutes. The reaction mixture was immediately purified using a PD SpinTrap G25 desalting column (GE Healthcare Life Sciences), eluting into 100  $\mu$ L of 25 mM PB pH 7.5. The reaction mixture was charged with (S)-(-)-5-(2-pyrrolidinyl)-H-tetrazole (15.6  $\mu$ L of 200 mM stock in 25 mM PB pH 7.5) and probe **3.18** (31.2  $\mu$ L of 4 mM stock in 25 mM PB pH 7.5). The solution was mixed via pipette tip swirling and incubated for 1 h at 37 °C. The reaction mixture was purified using a PD SpinTrap G25 desalting column (GE Healthcare Life Sciences), eluting into 20 mM K phosphate, 500 mM NaCl pH 7.0 for analysis and further manipulation.

## Experimental

### 8.3.6.3 Methodology for the bio-conjugation of active mannose-based inhibitor linked (Gly-Ser)<sub>3</sub> OPAL probe **3.17** to colicin Ia

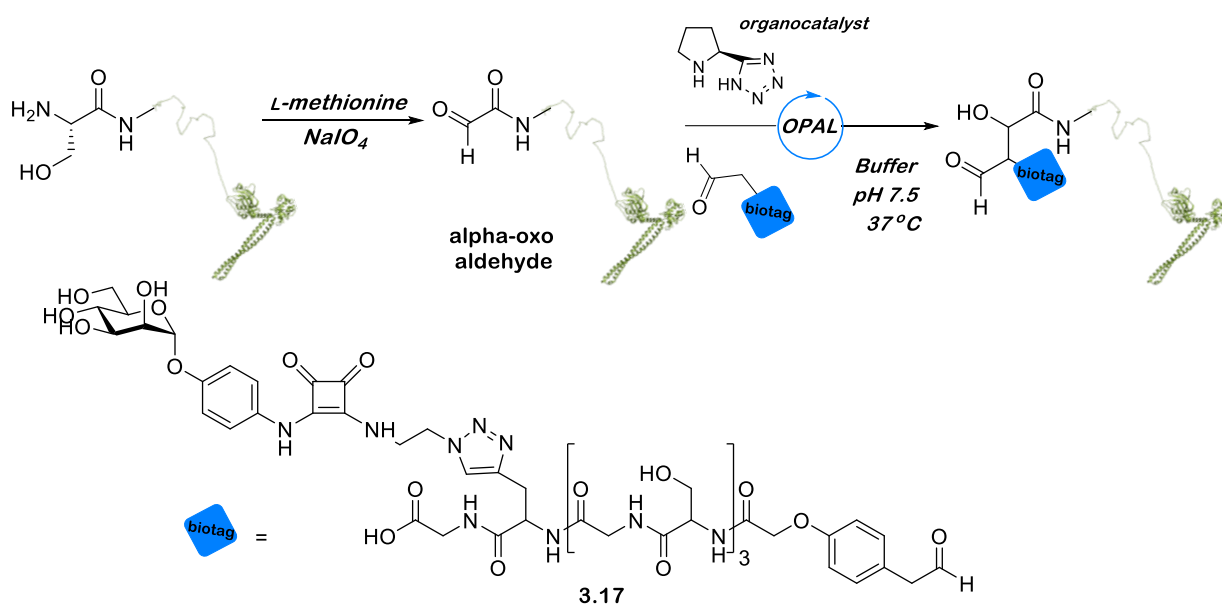


Scheme 8-4. Reaction scheme for OPAL ligation of active mannose-based inhibitor linked (Gly-Ser)<sub>3</sub> OPAL probe **3.17** to colicin Ia

$\beta$ Me (137 mM stock in water, 10  $\mu$ L, final concentration 10% (v/v)) was added to a solution of colicin Ia (100  $\mu$ L of 100  $\mu$ M stock in 25 mM PB pH 7.5) in a 0.5 mL Eppendorf, mixed by pipette tip swirling and left at r.t. for 5 minutes. The solution was charged with L-methionine (1  $\mu$ L of 66 mM stock in 0.1 M PB, 0.1 NaCl, pH 7.0) and NaIO<sub>4</sub> (1  $\mu$ L of 33 mM stock in 0.1 M PB, 0.1 NaCl, pH 7.0) and mixed by gentle pipette tip swirling. The solution was incubated on ice in the dark for 4 minutes. The reaction mixture was immediately purified using a PD SpinTrap G25 desalting column (GE Healthcare Life Sciences), eluting into 100  $\mu$ L of 25 mM PB pH 7.5. The reaction mixture was charged with (S)-(-)-5-(2-pyrrolidinyl)-H-tetrazole (20  $\mu$ L of 200 mM stock in 25 mM PB pH 7.5) and probe **3.17** (40  $\mu$ L of 4 mM stock in 25 mM PB pH 7.5). The solution was mixed via pipette tip swirling and incubated for 1 h at 37 °C. The reaction mixture was purified using a PD SpinTrap G25 desalting column (GE Healthcare Life Sciences), eluting into 20 mM K phosphate, 500 mM NaCl pH 7.0 for analysis and further manipulation.

## Experimental

### 8.3.6.4 Methodology for the bio-conjugation of active mannose-based inhibitor linked (Gly-Ser)<sub>3</sub> OPAL probe **3.17** to colicin E9

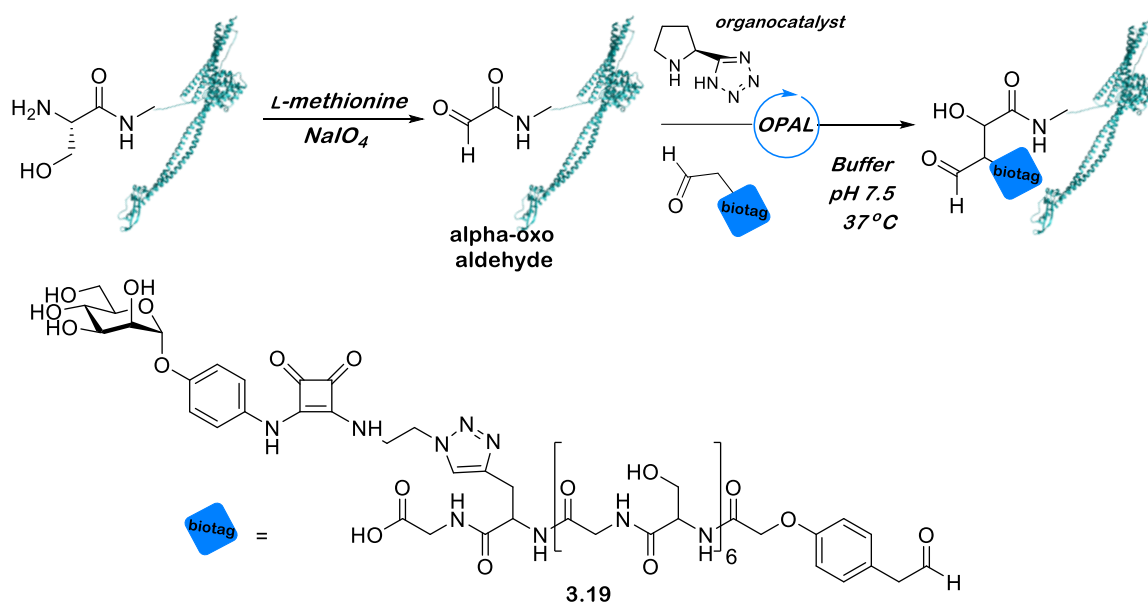


Scheme 8-5. Reaction scheme for OPAL ligation of active mannose based inhibitor (Gly-Ser)<sub>3</sub> OPAL probe **3.17** to colicin E9

A solution of colicin E9 (100  $\mu$ L of 78  $\mu$ M stock in 25 mM PB pH 7.5) was charged with *L*-methionine (1  $\mu$ L of 66 mM stock in 0.1 M PB, 0.1 NaCl, pH 7.0) and NaIO<sub>4</sub> (1  $\mu$ L of 33 mM stock in 0.1 M PB, 0.1 NaCl, pH 7.0). The solution was mixed by gentle pipette tip swirling and allowed to sit on ice in the dark for 4 minutes. The reaction mixture was immediately purified using a PD SpinTrap G25 desalting column (GE Healthcare Life Sciences), eluting into 100  $\mu$ L of 25 mM PB pH 7.5. The reaction mixture was charged with (S)-(-)-5-(2-pyrrolidinyl)-H-tetrazole (20  $\mu$ L of 200 mM stock in 25 mM PB pH 7.5) and probe **3.17** (40  $\mu$ L of 4 mM stock in 25 mM PB pH 7.5). The solution was mixed via pipette tip swirling and incubated for 1 h at 37 °C. The reaction mixture was purified using a PD SpinTrap G25 desalting column (GE Healthcare Life Sciences), eluting into 20 mM K phosphate, 500 mM NaCl pH 7.0 for analysis and further manipulation.

## Experimental

### 8.3.6.5 Methodology for the bio-conjugation of active mannose-based inhibitor linked (Gly-Ser)<sub>6</sub> OPAL probe **3.19** to colicin Ia

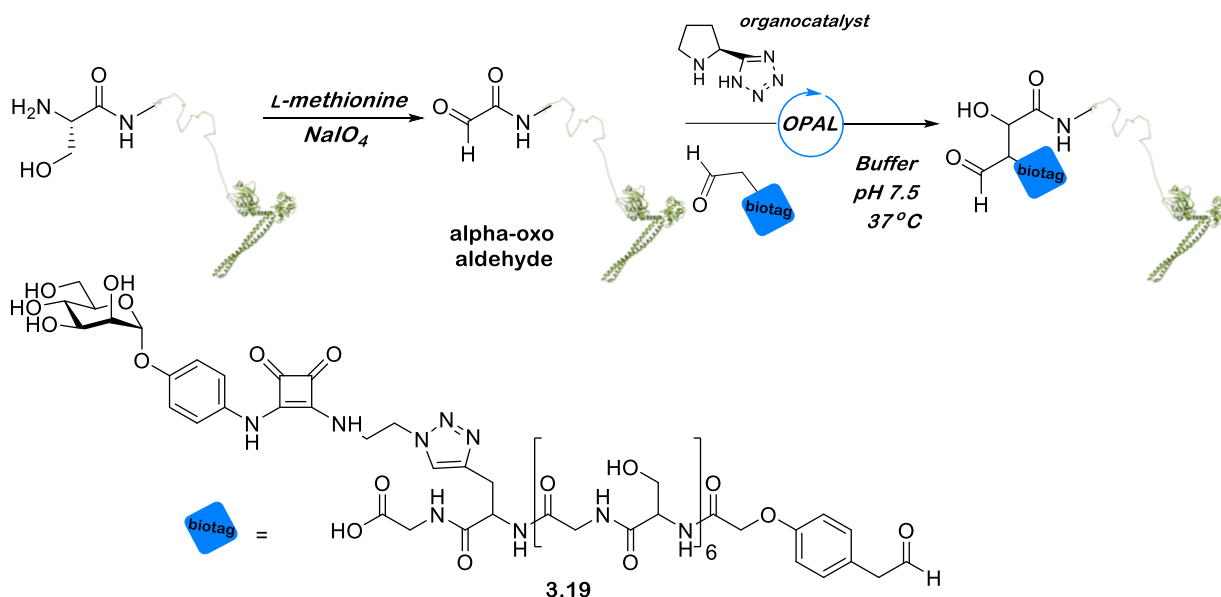


Scheme 8-6. Reaction scheme for OPAL ligation of mannose-based inhibitor linked (Gly-Ser)<sub>6</sub> OPAL probe **3.19** to colicin Ia

$\beta$ Me (137 stock mM in water, 10  $\mu$ L, final concentration 10% (v/v)) was added to a solution of colicin Ia (100  $\mu$ L of 26  $\mu$ M stock in 25 mM PB pH 7.5) in a 0.5 mL Eppendorf, mixed by pipette tip swirling and left at r.t. for 5 minutes. The solution was charged with L-methionine (0.5  $\mu$ L of 33 mM stock in 0.1 M PB, 0.1 NaCl, pH 7.0) and NaIO<sub>4</sub> (0.5  $\mu$ L of 16.5 mM stock in 0.1 M PB, 0.1 NaCl, pH 7.0) and mixed by gentle pipette tip swirling. The solution was incubated on ice in the dark for 4 minutes. The reaction mixture was immediately purified using a PD SpinTrap G25 desalting column (GE Healthcare Life Sciences), eluting into 100  $\mu$ L of 25 mM PB pH 7.5. The reaction mixture was charged with (S)-(-)-5-(2-pyrrolidinyl)-H-tetrazole (13.7  $\mu$ L of 200 mM stock in 25 mM PB pH 7.5) and probe **3.19** (27  $\mu$ L of 4 mM stock in 25 mM PB pH 7.5). The solution was mixed via pipette tip swirling and incubated for 1 h at 37 °C. The reaction mixture was purified using a PD SpinTrap G25 desalting column (GE Healthcare Life Sciences), eluting into 20 mM K phosphate, 500 mM NaCl pH 7.0 for analysis and further manipulation.

## Experimental

### 8.3.6.6 Methodology for the bio-conjugation of active mannose-based inhibitor linked (Gly-Ser)<sub>6</sub> OPAL probe **3.19** to colicin E9



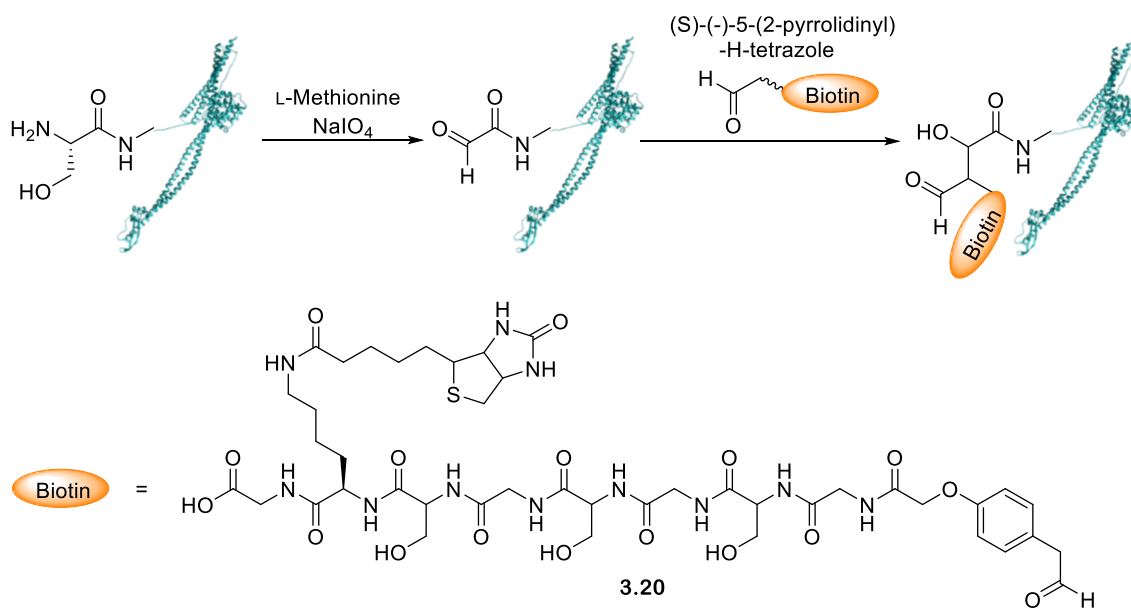
Scheme 8-7. Reaction scheme for OPAL ligation of active mannose-based inhibitor linked (Gly-Ser)<sub>6</sub> OPAL probe **3.19** to colicin E9

A solution of colicin E9 (100  $\mu\text{L}$  of 81  $\mu\text{M}$  stock in 25 mM PB pH 7.5) was charged with L-methionine (0.8  $\mu\text{L}$  of 66 mM stock in 0.1 M PB, 0.1 NaCl, pH 7.0) and NaIO<sub>4</sub> (0.8  $\mu\text{L}$  of 33 mM stock in 0.1 M PB, 0.1 NaCl, pH 7.0). The solution was mixed by gentle pipette tip swirling and allowed to sit on ice in the dark for 4 minutes. The reaction mixture was immediately purified using a PD SpinTrap G25 desalting column (GE Healthcare Life Sciences), eluting into 100  $\mu\text{L}$  of 25 mM PB pH 7.5. The reaction mixture was charged with (S)-(-)-5-(2-pyrrolidinyl)-H-tetrazole (10.5  $\mu\text{L}$  of 200 mM stock in 25 mM PB pH 7.5) and probe **3.19** (21.2  $\mu\text{L}$  of 4 mM stock in 25 mM PB pH 7.5). The solution was mixed via pipette tip swirling and incubated for 1 h at 37 °C. The reaction mixture was purified using a PD SpinTrap G25 desalting column (GE Healthcare Life Sciences), eluting into 20 mM K phosphate, 500 mM NaCl pH 7.0 for analysis and further manipulation.



## Experimental

### 8.3.6.7 Methodology for the bio-conjugation of active biotin-linked (Ser-Gly)<sub>3</sub> OPAL probe **3.20** to colicin Ia

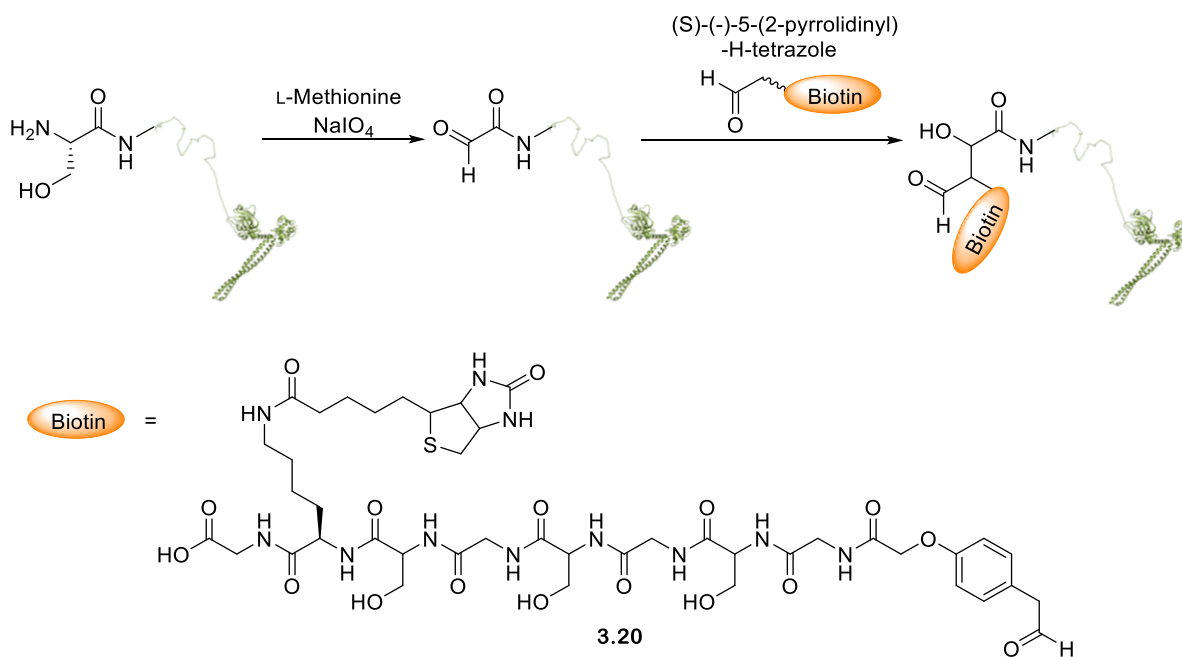


*Scheme 8-8. Reaction scheme for OPAL ligation of biotin linked OPAL probe **3.20** to colicin Ia*

$\beta$ Me (stock 137 mM in water, 10  $\mu$ L, final concentration 10% (v/v)) was added to a solution of colicin Ia (100  $\mu$ L of 32  $\mu$ M stock in 25 mM PB pH 7.5) in a 0.5 mL Eppendorf, the solution was mixed by pipette tip swirling and left at r.t. for 5 minutes. L-methionine (1  $\mu$ L of 22 mM stock in 0.1 M PB, 0.1 NaCl, pH 7.0) and NaIO<sub>4</sub> (1  $\mu$ L of 11 mM stock in 0.1 M PB, 0.1 NaCl, pH 7.0) were added to the reaction mixture. The solution was mixed by gentle pipette tip swirling and allowed to sit on ice in the dark for 4 minutes. The reaction mixture was immediately purified using a PD SpinTrap G25 desalting column (GE Healthcare Life Sciences), eluting into 100  $\mu$ L of 25 mM PB pH 7.5. The reaction was charged with (S)-(-)-5-(2-pyrrolidinyl)-H-tetrazole (2.4  $\mu$ L of 200 mM stock in 25 mM PB pH 7.5) and biotin OPAL probe **3.20** (4.8  $\mu$ L of 4 mM stock in 25 mM PB pH 7.5). The solution was mixed via pipette tip swirling and incubated for 1 h at 37 °C. The reaction mixture was purified using a PD SpinTrap G25 desalting column (GE Healthcare Life Sciences), eluting into 20 mM K phosphate, 500 mM NaCl pH 7.0 for analysis and further manipulation.

## Experimental

### 8.3.6.8 Methodology for the bio-conjugation of active biotin-linked (Ser-Gly)<sub>3</sub> OPAL probe **3.20** to colicin E9



Scheme 8-9. Reaction scheme for OPAL ligation of biotin-linked (Ser-Gly)<sub>3</sub> OPAL probe **3.20** to colicin E9

A solution of colicin E9 (100  $\mu$ L of 52.6  $\mu$ M stock in 25 mM PB pH 7.5) was charged with L-methionine (0.5  $\mu$ L of 66 mM stock in 0.1 M PB, 0.1 NaCl, pH 7.0) and NaIO<sub>4</sub> (0.5  $\mu$ L of 33 mM stock in 0.1 M PB, 0.1 NaCl, pH 7.0). The solution was mixed by gentle pipette tip swirling and allowed to sit on ice in the dark for 4 minutes. The reaction mixture was immediately purified using a PD SpinTrap G25 desalting column (GE Healthcare Life Sciences), eluting into 100  $\mu$ L of 25 mM PB pH 7.5. The reaction was charged with (S)-(-)-5-(2-pyrrolidinyl)-H-tetrazole (2.5  $\mu$ L of 200 mM stock in 25 mM PB pH 7.5) and biotin OPAL probe **3.20** (5  $\mu$ L of 4 mM stock in 25 mM PB pH 7.5). The solution was mixed via pipette tip swirling and incubated for 1 h at 37  $^{\circ}$ C. The reaction mixture was purified using a PD SpinTrap G25 desalting column (GE Healthcare Life Sciences), eluting into 20 mM K phosphate, 500 mM NaCl pH 7.0 for analysis and further manipulation

## Experimental

### 8.4 Experimental for Chapter 4

#### 8.4.1 General methodology for the preparation of auto-aggregation samples using the initial auto-aggregation assay (Experiment one)

Glycerol stocks of the required *E. coli* strains were used to inoculate a culture of either supplemented M9 media (recipe attached in Appendix section 9.3.1.1, page cvi) or LB-miller media (1% NaCl, 1% tryptone and 0.5% yeast extract), containing the respective concentrations of antibiotics (see Appendix section 9.3.1.2, page cvi). Each culture was grown overnight at 37 °C with shaking at 220 rpm. The bacteria were then harvested by centrifugation 4,200 × g, 2 minutes, 4 °C. The supernatant was removed and the cell pellet was resuspended in 1 x PBS to an OD<sub>600</sub> of 1, measured using a nanodrop spectrophotometer (DeNovix). The *E. coli* was then aliquoted to the appropriate sample volume and the samples were incubated at 4 °C overnight. A 500 µL extract was then taken from the top of each sample and diluted with 350 µL of 1 x PBS. An OD<sub>600</sub> measurement of this sample was then taken using a nanodrop spectrophotometer (DeNovix) and the recorded values were adjusted by the dilution factor.

## Experimental

### 8.4.2 General methodology for the preparation of auto-aggregation samples using the redesigned auto-aggregation assay (Experiments two- five)

Glycerol stocks of the respective *E. coli* strains were used to inoculate cultures of LB-miller media (1% NaCl, 1% tryptone and 0.5% yeast extract) containing the required concentrations of antibiotics (see page cvi for details). The cultures were grown at 37 °C overnight with shaking at 220 rpm. The bacteria were then harvested by centrifugation 4,200 × g, 20 minutes, 4 °C. The supernatant was removed and the bacteria cells were resuspended in 1 x PBS to the desired OD<sub>600</sub>, measured using a nanodrop spectrophotometer (DeNovix) (see Table 27 for details on starting OD<sub>600</sub> values). The *E. coli* were then aliquoted and the required amounts of colicin E9 conjugates and NeutrAvidin were added. Each sample was made in duplicate to give an active sample and a vortexed control. The samples were then incubated under the required conditions (see Table 27). Following incubation, one of the duplicate samples was vortexed for 30 seconds, and the final OD<sub>600</sub> values of each sample was measured using either the nanodrop spectrophotometer (DeNovix). Here the top 500 µL of each sample was removed and diluted with 350 µL of 1 x PBS and an OD<sub>600</sub> measurement was made, and the measured OD<sub>600</sub> value adjusted using the dilution factor. Alternatively, a victor Nivo™, multimode plate reader, PerkinElmer was used for final OD<sub>600</sub> measurements - here the top 200 µL of each sample was taken and added to a 96 well plate and an OD<sub>600</sub> measurement was made. Following final OD<sub>600</sub> measurements Equation 1 was then used to calculate percentage auto-aggregation.

$$\text{Percentage Auto-aggregation} = 100 \times \left(1 - \left(\frac{OD_{600}Final}{OD_{600}Initial}\right)\right)$$

## Experimental

*Table 27. Information about the specific conditions used in Experiments 2-5, all of which were performed using the redesigned auto-aggregation assay methodology*

Experiment	<i>E. coli</i> strain used	Starting OD <sub>600</sub>	Sample size	Incubation time (h)	Incubation temperature (°C)	Method for final OD <sub>600</sub> measurement
Two	BW25113, JW3596	1, 1.5, 2	1.5 mL	0, 2, 20 and 24	4 and 37	Nanodrop spectrophotometer (DeNovix)
Three	BW25113, JW3596	1.5, 2	1.5 mL	Overnight	37	Nanodrop spectrophotometer (DeNovix)
Four	BW25113	6	600 µL	24	37	Victor Nivo™, multimode plate reader, PerkinElmer
Five	BW25113	6	600 µL	24	37	Victor Nivo™, multimode plate reader, PerkinElmer

## Experimental

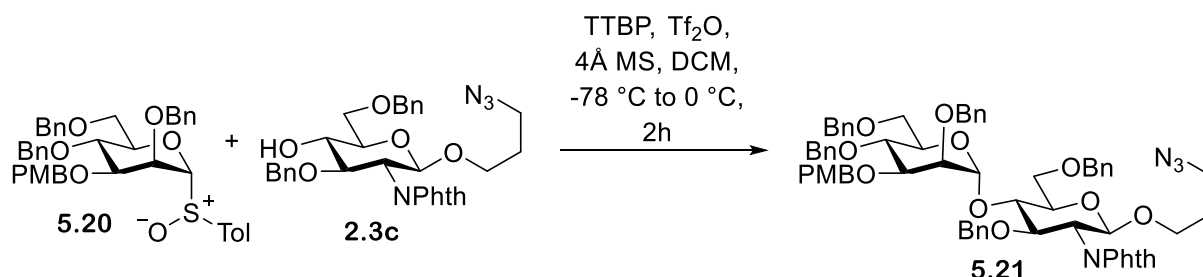
### 8.4.3 General methodology for the preparation of microscopy samples (Experiments six - eight)

Glycerol stocks of the respective *E. coli* strains were used to inoculate a culture of LB-miller media (1% NaCl, 1% tryptone and 0.5% yeast extract) containing the required concentrations of antibiotics (see page cvi for details). The cultures were grown overnight at 37 °C with shaking at 220 rpm, and the bacteria were then harvested using centrifugation 4,200 × g for 20 minutes at 4 °C. The bacteria were resuspended in 1 x PBS to the desired starting OD<sub>600</sub> (see Table 28), as measured using a nanodrop spectrophotometer (DeNovix). The *E. coli* were aliquoted and the appropriate amounts of the colicin E9 conjugates and NeutrAvidin were added to give 60 µL samples, with each sample being made in duplicate to give an active sample and a vortexed control. The samples were incubated under the conditions stated in Table 28. Following incubation, the vortexed control samples were vortexed for 30 seconds and the bottom 10 µL of each sample was taken and placed on a microscopy slide for imaging, using a Nikon Eclipse Ti-E microscope (image taken using Phase Contrast Imaging) equipped with a Mikrotron MC-1362 camera and visualised using EPIX E4 frame grabber running EPIX PIXCI software. The images were taken at either x 20 or x 40 magnification.

Table 28. Provides information about the specific conditions used in Experiments 6-8

Experiments	<i>E. coli</i> strains used	Starting OD <sub>600</sub>	Incubation time (h)	Incubation temperature (°C)
Six	BW25113, JW3596	2, 1, 0.5	9.5	37
Seven	BW25113, JW4283, RK5016	0.5	21.25	37
Eight	BW25113, RK5016	0.5	22	37

## 8.5 Experimental for Chapter 5

8.5.1 Synthesis of  $\beta$ -1,4-D-mannosyl-N-acetyl-D-glucosamine using chemical synthesis8.5.1.1 Synthesis of 2,4,6-O-benzyl-3-O-p-methoxybenzyl- $\alpha$ -D-mannopyranoside-(1  $\rightarrow$  4) 3-Azidopropyl (3,6-di-O-benzyl- $\beta$ -D-glucopyranoside) **5.21** using Bols and co-workers methodology<sup>84</sup>

A mixture of **5.20** (0.076 g, 0.11 mmols) and TTBP (0.055 g, 0.22 mmols, 1.5 eq) was co-evaporated 3 times with toluene and dried *in vacuo* overnight. 4Å MS (0.2 g) were added to the reaction mixture, which was then placed under N<sub>2</sub>, dissolved in DCM (2 mL) and cooled to -78 °C affording a cloudy solution. Tf<sub>2</sub>O (0.022 mL, 0.13 mmols, 2 eq) was added and the solution was stirred for 30 minutes affording a pink solution. **2.3c** (0.094 g, 0.16 mmols, 1.5 eq) was added to the solution and the reaction mixture was warmed to 0 °C over 2 h at which point the reaction was quenched with NEt<sub>3</sub> (0.2 mL) affording a white solution. The solution was diluted with DCM (5 mL) and EtOAc (5 mL), filtered through celite, washed with water (3 x 10 mL), saturated NaCl solution (1 x 10 mL), dried (MgSO<sub>4</sub>) and concentrated *in vacuo*, affording a colourless oil. The oil was purified by column chromatography, eluting with a graduated solvent system of 4 : 1 Hexane : EtOAc to 2 : 1 Hexane : EtOAc. This afforded a colourless oil of **5.21** (0.073 g, 0.068 mmols, 59%,  $\alpha$  only) R<sub>f</sub> = 0.78 (3:1 Hexane : EtOAc).

<sup>1</sup>H NMR (500 MHz, CDCl<sub>3</sub>)  $\delta$  7.66 (m, 3H, H<sub>Ar</sub>), 7.28 (m, 14H, H<sub>Ar</sub>), 7.19 (m, 10H, H<sub>Ar</sub>), 6.94 (d,  $J_{\text{HAr}}$  = 7.4 Hz, 2H, H<sub>Ar</sub>), 6.88 (t,  $J_{\text{HAr}}$  = 7.4 Hz, 2H, H<sub>Ar</sub>), 6.79 (d, 2H, H<sub>Ar</sub>), 5.28 (d,  $J_{1a,2a}$  = 1.4 Hz, 1H, H-1b), 5.06 (d,  $J_{1b,2b}$  = 8.20 Hz, 1H, H-1a), 4.85 (d, 1H, CH<sub>2</sub>), 4.62 (d, 1H, CH<sub>2</sub>), 4.56 (d, 2H, CH<sub>2</sub>), 4.51 (dd, 2H, CH<sub>2</sub>), 4.48 (d, 2H, CH<sub>2</sub>), 4.46 (d, 1H, CH<sub>2</sub>), 4.42 (d, 2H, CH<sub>2</sub>), 4.28 (dd,  $J$  = 10.5 Hz, 8.74 Hz, 1H, H-3a), 4.15 (m, 2H, H-2a, CH<sub>2</sub>), 3.98 (dd,  $J$  = 9.4 Hz, H-4b), 3.84 (m, 6H, H-4a, H-6(a), H-6'(a), H-5b, H-3b, CH<sub>2</sub>), 3.72 (s, 4H, H-2b, OCH<sub>3</sub>), 3.68 (d,  $J$  = 4.7 Hz, 1H, H-6(b)), 3.60 (m, 2H, H6'(b), H-5a), 3.44 (m, 1H, CH<sub>2</sub>), 3.09 (m, 2H, CH<sub>2</sub>), 1.70 (m, 2H, CH<sub>2</sub>).

<sup>13</sup>C NMR (101 MHz, CDCl<sub>3</sub>)  $\delta$  159.1 (2C, C=O), 138.5, 138.4, 138.4, 138.2, 137.7, 133.8, 133.8, 131.4, 130.5, 129.2, 128.3, 128.3, 128.3, 128.3, 128.2, 128.1, 128.0, 127.7, 127.6, 127.5, 127.4, 127.4, 127.2, 127.2, 123.3, 113.7 (C<sub>Ar</sub>), 100.3 (1C,  $J_{\text{CH}}$  = 170.9 Hz, C-1b), 98.1 (1C,  $J_{\text{CH}}$  = 159 Hz, C-1a), 80.5 (1C, C-3a), 79.4 (1C, C-3b), 79.8 (1C, C-5b), 75.7 (1C, C-2b), 75.0 (1C, CH<sub>2</sub>), 74.9 (1C, C-5a), 74.9 (1C, C-4b), 74.3 (1C, CH<sub>2</sub>), 73.4 (1C, CH<sub>2</sub>), 73.3 (1C, CH<sub>2</sub>), 73.1 (1C, C-4a), 72.3 (1C, CH<sub>2</sub>), 72.0 (1C, CH<sub>2</sub>), 69.5 (1C, C-6a), 69.4 (1C, C-6b), 66.0 (1C, CH<sub>2</sub>), 55.6 (1C, C-2a), 55.2 (1C, OCH<sub>3</sub>), 48.0 (1C, CH<sub>2</sub>).

(ESI)HRMS – C<sub>66</sub>H<sub>68</sub>N<sub>4</sub>NaO<sub>13</sub><sup>+</sup> ([M+Na]<sup>+</sup>) requires m/z 1147.4681: found m/z 1147.4675

$[\alpha]_D^{25}$  = + 34.3 (c 1, CH<sub>2</sub>Cl<sub>2</sub>)

## Experimental

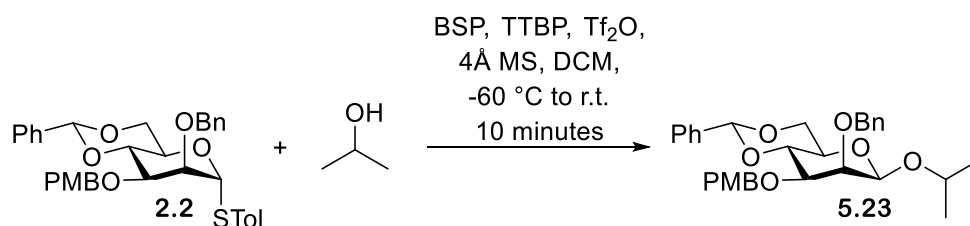
*IR* – 3030 (C-H), 2867 (C-H), 2097 (N=N=N), 1988 (C-H), 1775 (C=O), 1712 (C=O), 1387 (C=C), 1361 (C=C), 1248 (C-O), 1049 (C-O), 1027 (C-O).

No literature reference for characterisation could be found



## Experimental

### 8.5.1.2 Synthesis of 2-propanol 2-benzyl-4,6-O-benzylidene-3-O-p-methoxybenzyl- $\beta$ -D-mannopyranoside **5.23** using Crich and co-worker's methodology<sup>85</sup>



**2.2** was dried under vacuum overnight. Tf<sub>2</sub>O (0.019 mL, 0.11 mmols, 1.3 eq) was added to a solution of **2.2** (0.05 g, 0.085 mmols), BSP (0.02 g, 0.1 mmols, 1.2 eq) and TTBP (0.034 g, 0.14 mmols, 1.6 eq) in dry DCM (2mL) at -60 °C under N<sub>2</sub> affording a red solution. The solution was stirred for 5 minutes and 2-propanol (0.007 mL, 0.1 mmols, 1.2 eq) was added. The reaction mixture was stirred for a further 2 minutes at -60 °C and then warmed to r.t. and stirred for 10 minutes affording a white cloudy solution. The solution was filtered through celite, washed with saturated NaHCO<sub>3</sub> solution (1x 5 mL) and saturated NaCl solution (1 x 5 mL), dried (MgSO<sub>4</sub>) and concentrated *in vacuo*, affording a clear oil. The oil was purified by column chromatography, eluting with a graduated solvent system of 5 : 1 Toluene : EtOAc to 1 : 1 Toluene : EtOAc. This afforded a colourless oil of **5.23** (0.008 g, 0.015 mmols, 18%,  $\beta$  only).

<sup>1</sup>H NMR (500 MHz, CDCl<sub>3</sub>)  $\delta$  7.48 (m, 3H, HAr), 7.36 (m, 4H, HAr), 7.28 (m, 3H, HAr), 7.18 (d,  $J_{\text{HAr}} = 8.60$  Hz, 1H, HAr), 6.81 (d,  $J_{\text{HAr}} = 8.60$  Hz, 1H, HAr), 5.60 (s, 1H, CHPh), 4.97 (d,  $J_{\text{CH}_2} = 12.6$  Hz, 1H, CH<sub>2</sub>), 4.87 (1H,  $J_{\text{CH}_2} = 12.6$  Hz, 1H, CH<sub>2</sub>), 4.59 (d,  $J_{\text{CH}_2} = 10.0$  Hz, 1H, CH<sub>2</sub>), 4.52 (d,  $J_{\text{CH}_2} = 10$  Hz, 1H, CH<sub>2</sub>), 4.51 (s, 1H, H-1), 4.27 (dd,  $J_{6a,6b} = 10.4$  Hz,  $J_{5,6a} = 4.8$  Hz, H-6a), 4.18 (dd,  $J_{3,4} = 9.8$  Hz,  $J_{4,5} = 9.8$  Hz, 1H, H-4), 3.97 (m, 1H, CH), 3.92 (m, 1H, H-6b), 3.81 (d,  $J_{2,3} = 2.8$  Hz, 1H, H-2), 3.79 (s, 1H, OCH<sub>3</sub>), 3.55 (dd,  $J_{3,4} = 9.8$  Hz,  $J_{2,3} = 2.8$  Hz, 1H, H-3), 3.29 (ddd,  $J_{5,6b} = 14.3$  Hz,  $J_{4,5} = 9.8$  Hz,  $J_{5,6b} = 4.9$  Hz, 1H, H-5), 1.26 (d,  $J_{\text{CH}} = 6.1$  Hz, CH<sub>3</sub>), 1.14 (d,  $J_{\text{CH}} = 6.1$  Hz, 3H, CH<sub>3</sub>).

<sup>13</sup>C NMR (126 MHz, CDCl<sub>3</sub>)  $\delta$  159.1, 138.6, 137.7, 130.4, 130.1, 129.1, 128.9, 128.8, 128.7, 128.6, 128.1, 128.0, 127.4, 126.0, (CAr), 101.4 (1C, CHPh), 100.2 (1C, C-1,  $J_{\text{CH}} = 156.2$  Hz), 78.6 (1C, C-4), 77.7 (1C, C-3), 76.3 (1C, C-2), 74.6 (1C, CH<sub>2</sub>), 72.0 (1C, CH<sub>2</sub>), 71.4 (1C, CH), 68.7 (1C, C-6), 67.6 (1C, C-5), 55.3 (1C, OCH<sub>3</sub>), 23.5 (1C, CH<sub>3</sub>), 21.6 (1C, CH<sub>3</sub>).

(ESI)HRMS – C<sub>31</sub>H<sub>36</sub>NaO<sub>7</sub><sup>+</sup> ([M+Na]<sup>+</sup>) requires m/z 543.2359: found m/z 543.2351

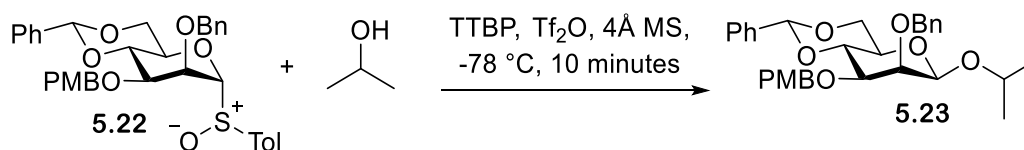
$[\alpha]_D^{25} = -35.35$  (c 0.4, CH<sub>2</sub>Cl<sub>2</sub>)

IR – 2968 (C-H), 2922 (C-H), 2864 (C-H), 1716 (C=O), 1593 (C=C), 1514 (C=C), 1335 (C-O), 1087 (C-O)

No literature reference for characterisation could be found

## Experimental

### 8.5.1.3 Synthesis of 2-propanol 2-benzyl-4,6-O-benzylidene-3-O-p-methoxybenzyl- $\beta$ -D-mannopyranoside **5.23** using Bols and co-worker's pre-activation methodology<sup>84</sup>



A mixture of **5.22** (0.076 g, 0.11 mmols, 1eq) and TTBP (0.055 g, 0.22 mmols, 1.5 eq) were co-evaporated 3 times with toluene and dried *in vacuo* overnight. Tf<sub>2</sub>O was added dropwise to a solution of **5.22** (0.044 g, 0.073 mmols), TTBP (0.035 g, 0.14 mmols, 2eq) and 4 Å MS (0.2 g) in dry DCM under N<sub>2</sub> at -78 °C affording a red solution which was stirred for 30 minutes. 2-propanol was added, and the solution was stirred for 10 minutes at -78 °C affording a white solution which was quenched with NEt<sub>3</sub>. The reaction mixture was filtered through celite affording a clear solution. The solution was washed with water (3 x 5 mL), saturated NaCl solution (1 x 5 mL), dried (MgSO<sub>4</sub>) and concentrated *in vacuo*, affording a pale-yellow oil. The oil was purified by column chromatography, eluting with a graduated solvent system of 1 : 1 Toluene : EtOAc to 1 : 1 Tol :EtOAc. This afforded a colourless oil of **5.23** (0.015 g, 0.088 mmols, 40%,  $\beta$  only).

<sup>1</sup>H NMR- Matches that as reported previously for **5.23**, Page 313

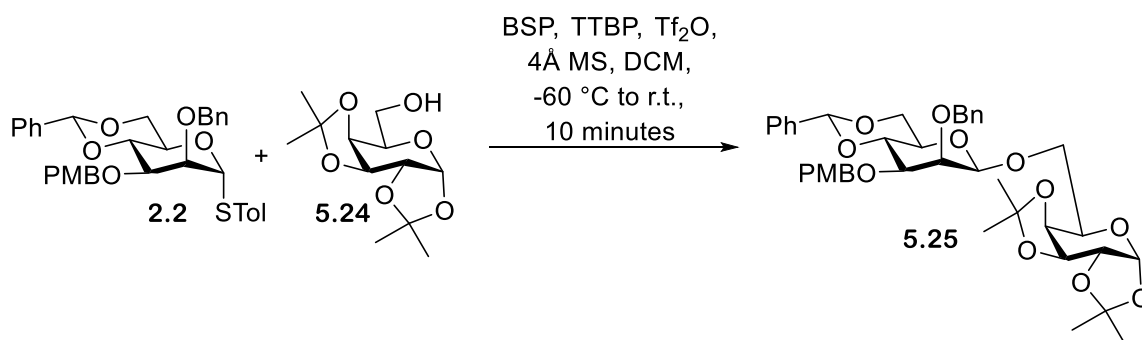
<sup>13</sup>C NMR- Matches that as reported previously for **5.23** with a  $J_{CH} = 154.1$  Hz, Page 313

Mass spectroscopy- Matches that as reported previously for **5.23**, Page 313

No literature reference for characterisation could be found

## Experimental

### 8.5.1.4 Synthesis 2-benzyl-4,6-O-benzylidene-3-O-p-methoxybenzyl- $\beta$ -D-mannopyranoside-(1 $\rightarrow$ 6)-1,2,3,4-di-O-isopropylidene- $\alpha$ -D-galactopyranose **5.25** using Crich and co-worker's methodology<sup>85</sup>



**2.2** and **5.24** were dried under vacuum overnight. Tf<sub>2</sub>O (0.019 mL, 0.11 mmols, 1.3 eq) was added to a solution of **2.2** (0.05, 0.085 mmols), BSP (0.02 g, 0.1 mmols, 1.2 eq) and TTBP (0.034 g, 0.14 mmols, 1.6 eq) in dry DCM (2mL) at -60 °C under N<sub>2</sub> affording a red solution. The solution was stirred for 5 minutes and **5.24** (0.026 g, 0.1 mmols, 1.2 eq) was added. The reaction mixture was stirred for a further 2 minutes at -60 °C and then warmed to r.t. and stirred for 10 minutes affording a white cloudy solution. The solution was filtered through celite, washed with saturated NaHCO<sub>3</sub> solution (1x 5 mL) and saturated NaCl solution (1 x 5 mL), dried (MgSO<sub>4</sub>) and concentrated *in vacuo* forming a clear oil. The oil was purified by column chromatography, eluting with a graduated solvent system of 5 : 1 Toluene : EtOAc to 1 : 1 Toluene : EtOAc. This afforded a colourless oil of **5.25** (0.038 g, 0.053 mmols, 62%,  $\beta$  only).

<sup>1</sup>H NMR (500 MHz, CDCl<sub>3</sub>)  $\delta$  7.49 (d,  $J_{\text{HAr}} = 7.6$  Hz, 4H, HAr), 7.35 (m, 5H, HAr), 7.28 (d,  $J_{\text{HAr}} = 7.8$  Hz, 1H, HAr), 7.14 (d,  $J_{\text{HAr}} = 8.7$  Hz, 2H, HAr (PMB)), 6.80 (d,  $J_{\text{HAr}} = 8.7$  Hz, 2H, HAr (PMB)), 5.60 (s, 1H, CHPh), 5.58 (d,  $J_{1,2} = 5.0$  Hz, 1H, H-1a), 5.00 (d,  $J_{\text{CH}_2} = 12.3$  Hz, 1H, CH<sub>2</sub>), 4.89 (d,  $J_{\text{CH}_2} = 12.3$  Hz, 1H, CH<sub>2</sub>), 4.62 (dd,  $J_{3,4} = 7.8$  Hz,  $J_{2,3} = 2.5$  Hz, 1H, H-3a), 4.54 (s, 1H, H-1b), 4.52 (d,  $J_{\text{CH}_2} = 12.1$  Hz, 1H, CH<sub>2</sub>), 4.48 (d,  $J_{\text{CH}_2} = 12.1$  Hz, 1H, CH<sub>2</sub>), 4.34 (dd,  $J_{1,2} = 5.0$  Hz,  $J_{2,3} = 2.5$  Hz, 1H, H-2a), 4.29 (dd,  $J_{6a,6b} = 10.3$  Hz,  $J_{5,6a} = 4.8$  Hz, 1H, H-6b), 4.22 (dd,  $J_{3,4} = 7.8$  Hz,  $J_{4,5} = 1.7$  Hz, 1H, H-4a), 4.16 (m, 2H, H-4b, H6a), 4.09 (ddd,  $J_{5,6b} = 8.3$  Hz,  $J_{4,5} = 1.7$  Hz,  $J_{5,6a} = 1.7$  Hz, 1H, H-5a), 3.98 (d,  $J_{2,3} = 3.1$  Hz, 1H, H-2b), 3.92 (dd,  $J_{5,6b} = 10.3$  Hz,  $J_{6a,6b} = 10.3$  Hz, 1H, H-6'b), 3.79 (s, 3H, OCH<sub>3</sub>), 3.63 (dd,  $J_{6a,6b} = 10.8$  Hz,  $J_{5,6b} = 8.3$  Hz, 1H, H-6'a), 3.52 (dd,  $J_{2,3} = 9.8$  Hz,  $J_{3,4} = 9.8$  Hz, 1H, H-3b), 3.31 (ddd,  $J_{4,5} = 14.2$  Hz,  $J_{5,6b} = 10.3$  Hz,  $J_{5,6a} = 4.8$  Hz, 1H, H-5b), 1.50 (s, 3H, CH<sub>3</sub>), 1.45 (s, 3H, CH<sub>3</sub>), 1.35 (s, 3H, CH<sub>3</sub>), 1.33 (s, 3H, CH<sub>3</sub>).

<sup>13</sup>C NMR (126 MHz, CDCl<sub>3</sub>)  $\delta$  159.1, 138.4, 137.6, 130.3, 129.2, 128.8, 128.2, 128.2, 127.5, 126.1, 113.7, 109.6, 108.8, (CAr), 103.00 (1C,  $J_{\text{CH}} = 156.8$  Hz, C-1b), 101.4 (1C, CHPh), 96.4 (1C,  $J_{\text{CH}} = 176.4$  Hz, C-1a), 78.5 (1C, C-4b), 77.0 (1C, C-3b), 75.0 (1C, C-2b), 74.6 (1C, CH<sub>2</sub>), 71.8 (1C, CH<sub>2</sub>), 71.6 (1C, C-4a), 70.8 (1C, C-3a), 70.5 (1C, C-2a), 70.1 (1C, C-6a), 68.6 (1C, C-6b), 68.0 (1C, C-5a), 67.6 (1C, C-5b), 55.2 (1C, OCH<sub>3</sub>), 26.1 (1C, CH<sub>3</sub>), 26.0 (1C, CH<sub>3</sub>), 25.1 (1C, CH<sub>3</sub>), 24.4 (1C, CH<sub>3</sub>).

(ESI)HRMS – C<sub>40</sub>H<sub>48</sub>NaO<sub>12</sub><sup>+</sup> ([M+Na]<sup>+</sup>) requires m/z 743.3034: found m/z 743.3051

$[\alpha]_D^{25} = -66.17$  (c 0.4, CH<sub>2</sub>Cl<sub>2</sub>)

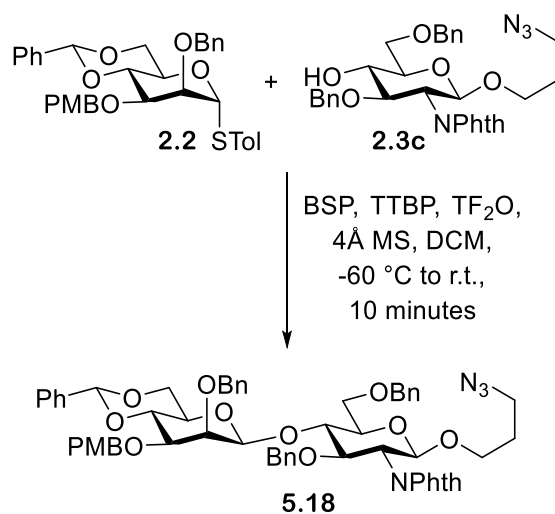
## Experimental

IR- 2922 (C-H), 2856 (C-H), 1732 (C=O), 1608 (C=C), 1360 (C-O), 1068 (C-O)

No literature reference for characterisation could be found

## Experimental

### 8.5.1.5 Synthesis of 2-benzyl-4,6-O-benzylidene-3-O-p-methoxybenzyl- $\beta$ -D-mannopyranoside-(1 $\rightarrow$ 4)-3-Azidopropyl (3,6-di-O-benzyl- $\beta$ -D-glucopyranoside) **5.18** using Crich and co-worker's methodology<sup>85</sup>



**2.2** and **2.3c** were dried under vacuum overnight.  $\text{TF}_2\text{O}$  (0.070 mL, 0.43 mmols, 1.3 eq) was added to a solution of **2.2** (0.19, 0.33 mmols), BSP (0.08 g, 0.4 mmols, 1.2 eq) and TTBP (0.13 g, 0.53 mmols, 1.6 eq) in dry DCM (2 mL) at  $-60 \text{ }^\circ\text{C}$  under  $\text{N}_2$  affording a red solution. The solution was stirred for 5 minutes and **2.3c** (0.23 g, 0.4 mmols, 1.2 eq) was added. The reaction mixture was stirred for a further 2 minutes at  $-60 \text{ }^\circ\text{C}$  and then warmed to r.t. and stirred for 10 minutes affording a white cloudy solution. The solution was filtered through celite, washed with saturated  $\text{NaHCO}_3$  solution (1x 5 mL) and saturated NaCl solution (1 x 5 mL), dried ( $\text{MgSO}_4$ ) and concentrated *in vacuo* forming a clear oil. The oil was purified by column chromatography, eluting with a solvent system of 8 : 1 Toluene : EtOAc. This afforded a colourless oil of **5.18** (0.089 g, 0.088 mmols, 26%,  $\beta$  only).

$^1\text{H NMR}$  (700 MHz,  $\text{CDCl}_3$ )  $\delta$  7.68 (s, 2H, HAr), 7.46 (dd,  $J_{\text{HAr}} = 15.2 \text{ Hz}$ ,  $J_{\text{HAr}} = 7.0 \text{ Hz}$ , 4H, HAr), 7.34 (m, 8H, HAr), 7.29 (m, 4H, HAr), 7.23 (d,  $J_{\text{HAr}} = 8.5 \text{ Hz}$ , 3H, HAr), 6.93 (m, 2H, HAr), 6.85 (s, 1H, HAr), 6.84 (m, 4H, HAr), 5.51 (s, 1H, CHPh), 5.11 (d,  $J_{1,2} = 8.50 \text{ Hz}$ , 1H, H-1a), 4.86 (m, 3H,  $\text{CH}_2$ ), 4.66 (d,  $J_{\text{CH}_2} = 11.8 \text{ Hz}$ , 1H,  $\text{CH}_2$ ), 4.64 (d,  $J_{\text{CH}_2} = 12.1 \text{ Hz}$ , 1H,  $\text{CH}_2$ ), 4.53 (s, 1H, H-1b), 4.52 (d,  $J_{\text{CH}_2} = 11.8 \text{ Hz}$ , 1H,  $\text{CH}_2$ ), 4.43 (d,  $J_{\text{CH}_2} = 12.5 \text{ Hz}$ , 1H,  $\text{CH}_2$ ), 4.40 (d,  $J_{\text{CH}_2} = 12.1 \text{ Hz}$ , 1H,  $\text{CH}_2$ ), 4.23 (dd,  $J_{2,3} = 10.7 \text{ Hz}$ ,  $J_{3,4} = 8.6 \text{ Hz}$ , 1H, H-3a), 4.17 (dd,  $J_{6a,6b} = 10.8 \text{ Hz}$ ,  $J_{5,6a} = 4.8 \text{ Hz}$ , 1H, H-6b), 4.14 (dd,  $J_{2,3} = 10.7 \text{ Hz}$ ,  $J_{1,2} = 8.5 \text{ Hz}$ , 1H, H-2a), 4.06 (dd,  $J_{3,4} = 9.7 \text{ Hz}$ ,  $J_{4,5} = 9.7 \text{ Hz}$ , H-4b), 4.01 (dd,  $J_{3,4} = 8.6 \text{ Hz}$ ,  $J_{4,5} = 1.2 \text{ Hz}$ , H-4a), 3.85 (dt,  $J_{\text{CH}_2} = 9.7 \text{ Hz}$ ,  $J_{\text{CH}_2} = 5.0 \text{ Hz}$ , 1H,  $\text{CH}_2$ ), 3.78 (s, 3H,  $\text{OCH}_3$ ), 3.72 (d,  $J_{2,3} = 3.0 \text{ Hz}$ , H-2b), 3.65 (dd,  $J_{6a,6b} = 10.9 \text{ Hz}$ ,  $J_{6a,5} = 2.0 \text{ Hz}$ , 1H, H-6a), 3.56 (dd,  $J_{6a,6b} = 10.9 \text{ Hz}$ ,  $J_{5,6a} = 10.9 \text{ Hz}$ , 1H, H-6'a), 3.54 (dd,  $J_{6a,6b} = 10.8 \text{ Hz}$ ,  $J_{5,6b} = 3.5 \text{ Hz}$ , 1H, H-6'b), 3.47 (m, 2H,  $\text{CH}_2$ , H-5a), 3.40 (d,  $J_{3,4} = 9.7 \text{ Hz}$ ,  $J_{2,3} = 3.0 \text{ Hz}$ , 1H, H-3b), 3.15 (m, 2H,  $\text{CH}_2$ , H-5b), 3.11 (m, 1H,  $\text{CH}_2$ ), 1.68 (m, 2H,  $\text{CH}_2$ ).

$^{13}\text{C NMR}$  (150 MHz,  $\text{CDCl}_3$ )  $\delta$  159.16 (2C, C=O), 138.8, 138.7, 137.8, 137.7, 133.8, 131.6, 130.6, 129.1, 128.8, 128.8, 128.6, 128.3, 128.2, 128.2, 128.0, 127.9, 127.8, 127.8, 127.6, 126.9, 126.1, 123.4, 113.7, (CAr), 102.0 (1C,  $J_{\text{CH}} = 159.1 \text{ Hz}$ , C-1b), 101.3 (1C, CHPh), 98.4 (1C,  $J_{\text{CH}} = 165.7 \text{ Hz}$ , C-1a), 79.5 (1C, C-4a), 78.7 (1C, C-4b), 78.0 (1C, C-3b), 77.1 (1C, C-3a), 76.9 (1C, C-2b), 75.0 (1C,  $\text{CH}_2$ ), 74.8 (1C, C-5a), 74.7 (1C,  $\text{CH}_2$ ), 73.6 (1C,  $\text{CH}_2$ ), 72.3 (1C,  $\text{CH}_2$ ), 68.6 (1C, C-6a), 68.5 (1C, C-6b), 67.4 (1C, C-5b), 66.0 (1C,  $\text{CH}_2$ ), 55.7 (1C, C-2a), 55.3 (1C,  $\text{OCH}_3$ ), 48.0 (1C,  $\text{CH}_2$ ), 28.9 (1C,  $\text{CH}_2$ ).

## Experimental

(ESI)HRMS –  $C_{60}H_{62}N_4NaO_{12}^+$  ( $[M+Na]^+$ ) requires  $m/z$  1055.4055: found  $m/z$  1055.4070.

$[\alpha]_D^{25} = 0$  ( $c$  1,  $CH_2Cl_2$ )

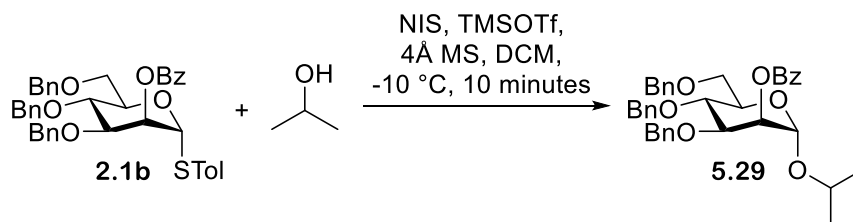
*IR*- 3032 (C-H), 2922 (C-H), 2854 (C-H), 2097 (N=N=N), 1775 (C=O), 1713 (C=O), 1611 (C=C), 1513 (C=C), 1454 (C=C), 1387 (C=C), 1083 (C-O).

No literature reference for characterisation could be found.

## Experimental

### 8.5.2 Further investigations into the synthesis of protected trisaccharide **5.19**

#### 8.5.2.1 Synthesis of 2-propyl 2-O-benzoyl-3,4,6-tri-O-benzyl- $\alpha$ -D-mannopyranoside **5.29**



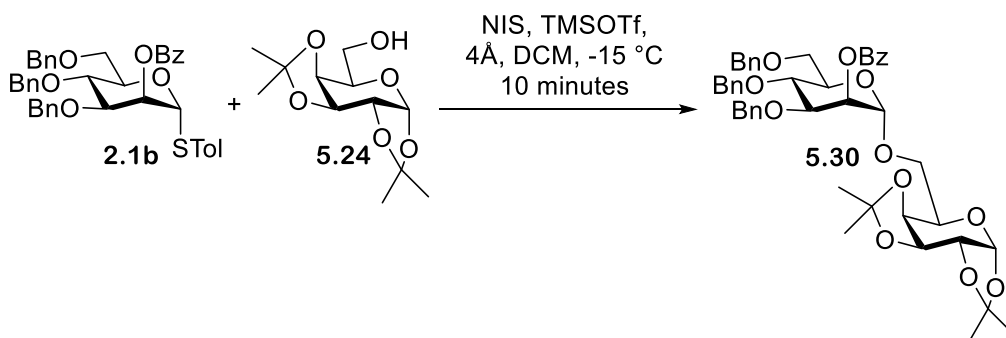
**2.1b** (0.05 g, 0.075 mmols, 1.3 eq) was dried *in vacuo* overnight. NIS (0.021 g, 0.097 mmols, 1.3 eq of **2.1b**) was added to a solution of **2.1b**, 2-propanol (0.004 mL, 0.057 mmols) and 4 Å molecular sieves (0.2 g) in DCM (2 mL) under N<sub>2</sub> at -10 °C. The reaction mixture was stirred for 5 minutes and TMSOTf (0.002 mL, 0.011 mmols, 0.2 eq of **2.1b**) was added dropwise affording a pink solution. The solution was stirred at -10 °C under nitrogen for 10 minutes. The reaction was quenched with NEt<sub>3</sub> (0.2 mL) affording a yellow solution. The solution was filtered through celite, washed with Na<sub>2</sub>S<sub>2</sub>O<sub>3</sub> (1 x 5 mL), saturated NaHCO<sub>3</sub> solution (1 x 5 mL), dried (MgSO<sub>4</sub>) and concentrated *in vacuo*, affording a colourless oil. The oil was purified by column chromatography, eluting with a graduated solvent system of 8 : 1 Hexane : EtOAc to 6 : 1 Hexane : EtOAc. This afforded a crude mixture containing **5.29** (0.027 g, 0.045 mmols); R<sub>f</sub> = 0.64 (4 : 1 Hexane : EtOAc).

(ESI)HRMS – C<sub>37</sub>H<sub>40</sub>NaO<sub>7</sub><sup>+</sup> ([M+Na]<sup>+</sup>) requires m/z 619.2672: found m/z 619.2666.

*Literature reference for characterisation*- P. Peng and R. R. Schmidt, *J. Am. Chem. Soc.*, 2015, **137**, 12653-12659.

## Experimental

### 8.5.2.2 Synthesis of 2-O-(benzoyl-3,4,6-tri-O-benzyl- $\alpha$ -D-mannopyranoside)-(1 $\rightarrow$ 6)-1,2,3,4-di-O-isopropylidene- $\alpha$ -D-galactopyranose **5.30**<sup>403</sup> using NIS and TMSOTf



**2.1b** (0.05 g, 0.075 mmols, 1.3 eq) and **5.24** (0.015 g, 0.057 mmols) were dried overnight under vacuum. NIS (0.022 g, 0.098 mmols, 1.3 eq of **2.1b**) was added to a solution of **2.1b**, **5.24** and 4Å MS in dry DCM (3 mL) at -15°C under N<sub>2</sub>. The reaction mixture was stirred for 10 minutes at -10°C at which point TMSOTf (0.002 mL, 0.01 mmols, 0.2 eq of **2.1b**) was added dropwise to the solution affording a pink solution. The solution was stirred for 10 minutes and quenched with NEt<sub>3</sub> affording a light-yellow solution. The solution was filtered through celite, washed with Na<sub>2</sub>S<sub>2</sub>O<sub>3</sub> (1 x 5 mL) and saturated NaHCO<sub>3</sub> solution (1 x 5 mL), dried (MgSO<sub>4</sub>) and concentrated *in vacuo*, affording a light-yellow oil. The oil was purified by column chromatography, eluting with a graduated solvent system of 4 : 1 Hexane : EtOAc to 1 : 1 Hexane : EtOAc. This afforded a colourless oil of **5.30** (0.016 g, 0.02 mmols, 35%,  $\alpha$ -only); R<sub>f</sub> = 0.7 (2.5 : 1 Hexane : EtOAc).

<sup>1</sup>H NMR (500 MHz, CDCl<sub>3</sub>)  $\delta$  8.00 (dd,  $J_{\text{HAr}} = 8.3$  Hz,  $J_{\text{HAr}} = 1.2$  Hz, 2H, HAr), 7.54 (m, 1H, HAr), 7.33 (m, 12H, HAr), 7.24 (m, 3H, HAr), 7.18 (dd,  $J_{\text{HAr}} = 7.5$  Hz,  $J_{\text{HAr}} = 1.8$  Hz, 2H, HAr), 5.65 (dd,  $J_{1,2} = 2.0$  Hz,  $J_{2,3} = 2.0$  Hz, 1H, H-2b), 5.51 (d,  $J_{1,2} = 5.0$  Hz, H-1a), 5.02 (d,  $J_{1,2} = 2.0$  Hz, 1H, H-1b), 4.85 (d,  $J_{\text{CH}_2} = 10.8$  Hz, 1H, CH<sub>2</sub>), 4.80 (d,  $J_{\text{CH}_2} = 11.3$  Hz, 1H, CH<sub>2</sub>), 4.75 (d,  $J_{\text{CH}_2} = 11.9$  Hz, 1H, CH<sub>2</sub>), 4.62 (dd,  $J_{3,4} = 7.9$  Hz,  $J_{2,3} = 2.4$  Hz, 1H, H-3a), 4.56 (d,  $J_{\text{CH}_2} = 11.3$  Hz, 1H, CH<sub>2</sub>), 4.53 (d,  $J_{\text{CH}_2} = 10.8$  Hz, 1H, CH<sub>2</sub>), 4.52 (d,  $J_{\text{CH}_2} = 11.9$  Hz, 1H, CH<sub>2</sub>), 4.31 (dd,  $J_{1,2} = 5.0$  Hz,  $J_{2,3} = 2.4$  Hz, 1H, H-2a), 4.24 (dd,  $J_{3,4} = 7.9$  Hz,  $J_{4,5} = 1.7$  Hz, 1H, H-4a), 4.11 (m, 2H, H-4b, H-3b), 3.96 (ddd,  $J_{5,6a} = 6.6$  Hz,  $J_{6a,6b} = 6.6$  Hz,  $J_{4,5} = 1.7$  Hz, 1H, H-5a), 3.90 (m, 2H, H-5b, H-6b), 3.82 (dd,  $J_{6a,6b} = 10.2$  Hz,  $J_{5,6a} = 6.6$  Hz, 1H, H-6a), 3.76 (m, 1H, H-6'b), 3.73 (dd,  $J_{6a,6b} = 10.2$  Hz,  $J_{5,6a} = 6.6$  Hz, 1H, H-6'a), 1.53 (s, 3H, CH<sub>3</sub>), 1.43 (3H, CH<sub>3</sub>), 1.35 (3H, CH<sub>3</sub>), 1.33 (s, 3H, CH<sub>3</sub>).

<sup>13</sup>C NMR (126 MHz, CDCl<sub>3</sub>)  $\delta$  165.6 (1C, C=O), 138.5, 138.4, 138.1, 133.1, 129.9, 129.8, 128.4, 128.3, 128.3, 128.2, 128.0, 127.6, 127.6, 127.5, 127.4, (CAr), 109.4 (1C, C), 108.6 (1C, C), 97.9 (1C, C-1b), 96.3 (1C, C-1a), 78.2 (1C, C-3b), 75.3 (1C, CH<sub>2</sub>), 74.3 (1C, C-4b), 73.4 (1C, CH<sub>2</sub>), 71.8 (1C, C-5b), 71.6 (1C, CH<sub>2</sub>), 70.8 (1C, C-4a), 70.6 (1C, C-2a), 70.6 (1C, C-3a), 69.0 (1C, C-6b), 68.9 (1C, C-2b), 66.2 (1C, C-6a), 65.9 (1C, C-5a), 26.1 (1C, CH<sub>3</sub>), 25.9 (1C, CH<sub>3</sub>), 24.9 (1C, CH<sub>3</sub>), 24.5 (1C, CH<sub>3</sub>).

(ESI)HRMS – C<sub>46</sub>H<sub>52</sub>NaO<sub>12</sub><sup>+</sup> ([M+Na]<sup>+</sup>) requires m/z 819.3356: found m/z 819.3342.

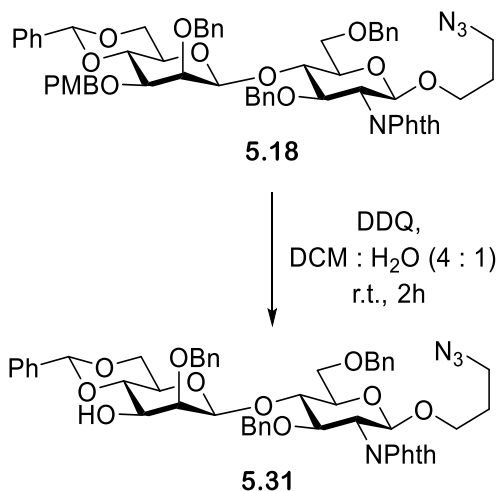
[ $\alpha$ ]<sub>D</sub><sup>25</sup> = - 16.10 (c 1, CH<sub>2</sub>Cl<sub>2</sub>)

IR –2986 (C-H), 2918 (C-H), 2849 (C-H), 1721 (C=O), 1453 (C=C), 1381 (C=C), 1371 (C=C), 1265 (C-O), 1210 (C-O), 1097 (C-O), 1067 (C-O).



## Experimental

### 8.5.2.3 Synthesis of 2-benzyl-4,6-O-benzylidene- $\alpha$ -D-mannopyranoside-(1 $\rightarrow$ 3)-3-Azidopropyl (3,6-Di-O-benzyl- $\beta$ -D-glucopyranoside) **5.31**



DDQ (0.012g, 0.094 mmols, 2 eq) was added to a solution of **5.18** (0.048 g, 0.047 mmols) in DCM : H<sub>2</sub>O (4 : 1 mL). The reaction mixture was stirred at r.t. for 2 h, affording a yellow solution. The solution was washed with water (3 x 5mL), dried (MgSO<sub>4</sub>) and concentrated *in vacuo*, affording a light-yellow oil. The oil was purified by column chromatography, eluting with a graduated solvent system of 5 : 1 Hexane : EtOAc to 1: 1 Hexane : EtOAc. This afforded a colourless oil of **5.31** which was used crude (0.032 g, 0.035 mmols); R<sub>f</sub> = 0.40 (2 : 1 Hex : EtOAc).

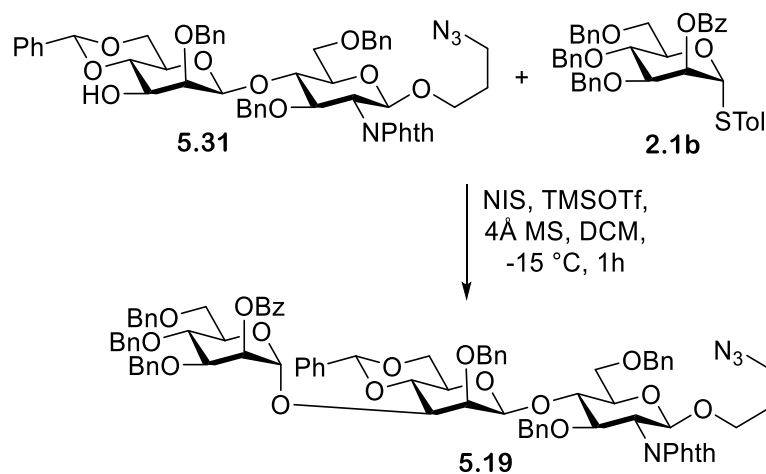
*NMR*- Awaiting clean NMR, rough one gathered showing removal of PMB however, also appeared to show rotomers.

(ESI)HRMS – C<sub>27</sub>H<sub>28</sub>NaO<sub>6</sub>S<sup>+</sup> ([M+Na]<sup>+</sup>) requires m/z 935.3479: found [M+Na]<sup>+</sup> 935.3505.

No literature reference for characterisation could be found

## Experimental

### 8.5.2.4 Synthesis of 2-O-benzoyl-3,4,6-tri-O-benzyl- $\alpha$ -D-mannopyranoside-(1 $\rightarrow$ 3) 2-O-benzyl-4,6-O-benzylidene-3-O-p-methoxybenzyl- $\alpha$ -D-mannopyranoside- (1 $\rightarrow$ 4) 3-Azidopropyl (3,6-Di-O-benzyl- $\beta$ -D-glucopyranoside) **5.19**



**2.1b** (0.03 g, 0.046 mmols, 1.3 eq) and **5.31** (0.032 g, 0.035 mmols) were dried *in vacuo* overnight. NIS (0.013 g, 0.059 mmols, 1.3 eq of donor) was added to a solution of **2.1b**, **5.31** and 4Å MS (0.3 g) in dry DCM (3 mL) at -15 °C under N<sub>2</sub>. The reaction mixture was stirred for 10 minutes at -10 °C at which point TMSOTf (0.002 mL, 0.009 mmols, 0.2 eq of donor) was added dropwise affording a pink solution. The reaction mixture was stirred for 1 h at -10 °C and quenched with NEt<sub>3</sub> (0.2 mL) affording a pink solution. The solution was filtered through celite, washed with Na<sub>2</sub>S<sub>2</sub>O<sub>3</sub> (1 x 5 mL) and saturated NaHCO<sub>3</sub> solution (1 x 5 mL), dried (MgSO<sub>4</sub>) and concentrated *in vacuo*, affording a light-yellow oil. The oil was purified by column chromatography, eluting with a solvent system of 8 : 1 Toluene : EtOAc. This afforded a crude colourless oil of **5.19** (0.011 g, 0.0075 mmols, ≤21%); R<sub>f</sub> = 0.48 (5 : 1 Toluene : EtOAc).

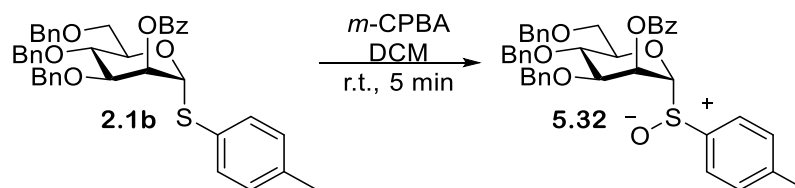
(ESI)HRMS – C<sub>85</sub>H<sub>84</sub>N<sub>4</sub>NaO<sub>18</sub><sup>+</sup> ([M+Na]<sup>+</sup>) requires m/z 1471.5678: found m/z 1471.5743.

No literature reference for characterisation could be found

## Experimental

### 8.5.3 Optimisation of the $\alpha$ -mannoside glycosylation

#### 8.5.3.1 Synthesis of 4-methylphenylsulfenyl 2-O-benzoyl-3,4,6-tri-O-benzyl-1-thio- $\alpha$ -D-mannopyranoside **5.32**



*m*-CPBA (0.052 g, 0.30 mmols, 2 eq) was added to a solution of **2.1b** (0.1 g, 0.15 mmols) in dry DCM (5 mL) and the reaction mixture was stirred at r.t. for 5 minutes. The reaction was quenched with  $\text{NaHCO}_3$  and the organic layer was extracted, washed with saturated NaCl solution (5 mL), dried ( $\text{MgSO}_4$ ) and concentrated *in vacuo*, affording a colourless oil. The oil was purified by column chromatography, eluting with a graduated solvent system of 5 : 1 Hexane : EtOAc to 1 : 1 Hexane : EtOAc. This afforded a colourless oil of **5.32** (0.032 g, 0.47 mmols, 31%);  $R_f = 0.5$  (3 : 1 Hexane : EtOAc).

$^1\text{H}$  NMR (500 MHz,  $\text{CDCl}_3$ )  $\delta$  7.98 (d,  $J_{\text{HAr}} = 8.2$  Hz, 2H, HAr), 7.54 (d,  $J_{\text{HAr}} = 8.2$  Hz, 3H, HAr), 7.28 (m, 19 H, HAr), 6.23 (dd,  $J_{2,3} = 3.2$  Hz,  $J_{1,2} = 2.0$  Hz, 1H, H-2), 4.89 (d,  $J_{\text{CH}_2} = 10.8$  Hz, 1H,  $\text{CH}_2$ ), 4.86 (d,  $J_{\text{CH}_2} = 11.3$  Hz, 1H,  $\text{CH}_2$ ), 4.69 (d,  $J_{1,2} = 2.0$  Hz, 1H, H-1), 4.65 (d,  $J_{\text{CH}_2} = 11.3$  Hz, 1H,  $\text{CH}_2$ ), 4.61 (d,  $J_{\text{CH}_2} = 11.9$  Hz, 1H,  $\text{CH}_2$ ), 4.53 (d,  $J_{\text{CH}_2} = 10.8$  Hz, 1H,  $\text{CH}_2$ ), 4.48 (d,  $J_{\text{CH}_2} = 11.9$  Hz, 1H,  $\text{CH}_2$ ), 4.41 (dd,  $J_{3,4} = 9.5$  Hz,  $J_{2,3} = 3.2$  Hz, 1H, H-3), 4.26 (dt,  $J_{4,5} = 9.6$  Hz,  $J_{5,6} = 3.3$  Hz, 1H, H-5), 4.05 (dd,  $J_{4,5} = 9.6$  Hz, 1H,  $J_{3,4} = 9.6$  Hz, 1H, H-4), 3.70 (d,  $J_{5,6} = 3.4$  Hz, 2H, H-6), 2.36 (s, 3H,  $\text{CH}_3$ ).

$^{13}\text{C}$  NMR (126 MHz,  $\text{CDCl}_3$ )  $\delta$  164.9 (1C, C=O), 142.1, 138.2, 138.1, 138.0, 137.6, 133.2, 130.0, 129.9, 129.6, 128.4, 128.3, 128.2, 127.9, 127.7, 127.6, 127.6, 124.4 (CAr), 96.0 (1C, C-1), 78.1 (1C, C-3), 77.4 (1C, C-5), 75.2 (1C,  $\text{CH}_2$ ), 73.6 (1C, C-4), 73.5 (1C, 1C,  $\text{CH}_2$ ), 71.9 (1C,  $\text{CH}_2$ ), 69.2 (1C, C-6), 66.3 (1C, C-2), 21.5 (1C,  $\text{CH}_3$ ).

(ESI)HRMS -  $\text{C}_{41}\text{H}_{40}\text{NaO}_7\text{S}^+$  ( $[\text{M}+\text{Na}]^+$ ) requires  $m/z$  699.2392: found  $m/z$  699.2386

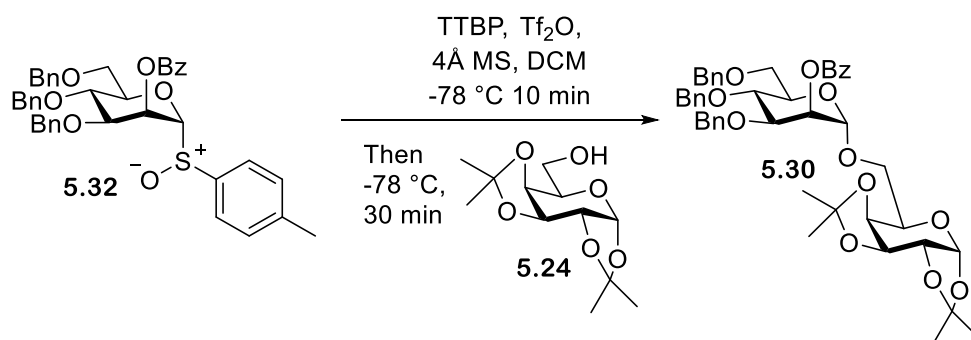
$[\alpha]_D^{25} = -23.54$  (c 1, DCM)

IR – 3094 (C-H), 3062 (C-H), 3031 (C-H), 2923 (C-H), 2866 (C-H), 1722 (C=O), 1495 (C=C), 1452 (C=C), 1203 (C-O), 1092 (C-O), 1040 (C-O), 1027 (C-O).

No literature reference for characterisation could be found.

## Experimental

### 8.5.3.2 Synthesis of 2-O-(benzoyl-3,4,6-tri-O-benzyl- $\alpha$ -D-mannopyranoside)-(1 $\rightarrow$ 6)-1,2,3,4-di-O-isopropylidene- $\alpha$ -D-galactopyranose **5.30**<sup>403</sup> using pre-activation with Bols and co-workers method<sup>84</sup>

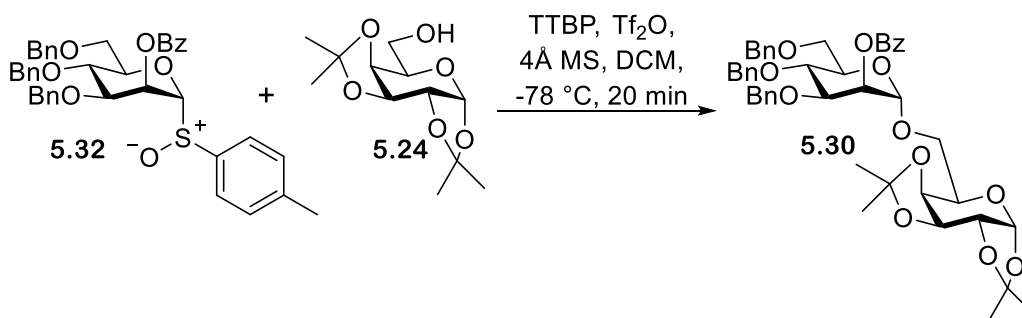


**5.32** (0.064 g, 0.094 mmols) **5.24** (0.036 g, 0.14 mmols, 1.5 eq) and TTBP (0.044 g, 0.18 mmols, 2 eq) were dried overnight under vacuum. Tf<sub>2</sub>O (0.031 mL, 0.11 mmols, 1.2 eq) was added dropwise to a solution of **5.32**, TTBP and 4 Å MS (0.5 g) in dry DCM (5 mL) at -78 °C under N<sub>2</sub> affording a dark red solution. The solution was stirred for 10 minutes and **5.24** was added dropwise (in 1 mL dry DCM), the reaction mixture was stirred at -78 °C for 30 minutes and quenched with NEt<sub>3</sub> (0.4 mL) affording a colourless solution. The solution was filtered through celite washed with saturated NaHCO<sub>3</sub> solution (5 mL) and saturated NaCl solution (5 mL), dried (MgSO<sub>4</sub>) and concentrated *in vacuo*, affording a yellow oil. The oil was purified by column chromatography, eluting with a graduated solvent system of 4 : 1 Hexane : EtOAc to 100% EtOAc. This afforded a colourless oil of **5.30** (0.013 g, 0.016 mmols, 17%,  $\alpha$ -only); R<sub>f</sub> = 0.7 (2.5 : 1 Hexane : EtOAc).

For compound data please see page 320

## Experimental

### 8.5.3.3 Synthesis of 2-O-(benzoyl-3,4,6-tri-O-benzyl- $\alpha$ -D-mannopyranoside)-(1 $\rightarrow$ 6)-1,2,3,4-di-O-isopropylidene- $\alpha$ -D-galactopyranose **5.30**<sup>403</sup> using direct activation with Bols and co-workers method<sup>84</sup>



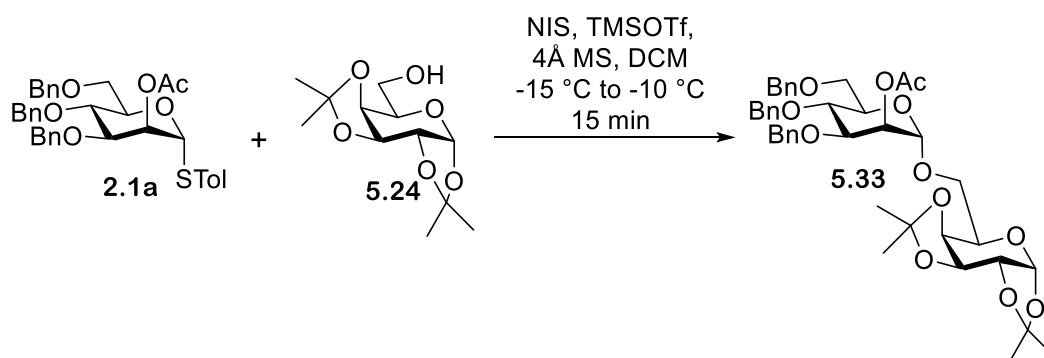
**5.32** (0.054 g, 0.080 mmols) **5.24** (0.031 g, 0.12 mmols, 1.5 eq) and TTBP (0.039 g, 0.16 mmols, 2 eq) were dried overnight under vacuum. Tf<sub>2</sub>O (0.016 mL, 0.096 mmols, 1.2 eq) was added dropwise to a solution of **5.32**, **5.24**, TTBP and 4 Å MS (0.5 g) in dry DCM (5 mL) at -78 °C under N<sub>2</sub> affording a cloudy colourless solution. The reaction mixture was stirred for 20 minutes and quenched with NEt<sub>3</sub> (0.2 mL) and MeOH (0.2 mL) affording a cloudy colourless solution. The solution was filtered through celite washed with water (5 mL) and saturated NaCl solution (5 mL), dried (MgSO<sub>4</sub>) and concentrated *in vacuo*, affording a colourless oil. The oil was purified by column chromatography, eluting with a graduated solvent system of 4 : 1 Hexane : EtOAc to 100% EtOAc. This afforded a crude colourless oil of **5.30** (0.032 g, 0.047 mmols, 54%); R<sub>f</sub> = 0.7 (2.5 : 1 Hexane : EtOAc). Note NMR showed impurity peak a 1 : 0.3 ratio so more likely amount (0.022 g, 0.033 mmols, 35%,  $\alpha$ -only).

For compound data please see page 320

Note a few impurity peaks are present on the NMR (product to impurity ratio 1 : 0.3). These impurity peaks are most likely attributable to either **5.32** or hydrolysed **5.32**.

## Experimental

### 8.5.3.4 Synthesis of 2-O-(acetyl-3,4,6-tri-O-benzyl- $\alpha$ -D-mannopyranoside)-(1 $\rightarrow$ 6)-1,2,3,4-di-O-isopropylidene- $\alpha$ -D-galactopyranose **5.33**<sup>404</sup> using NIS and TMSOTf



**2.1a** (0.05 g, 0.084 mmols, 1.3 eq) and **5.24** (0.016 g, 0.064 mmols) were dried overnight under vacuum. NIS (0.025 g, 0.11 mmols, 1.3 eq of **2.1a**) was added to a solution of **2.1a**, **5.24** and 4Å MS in dry DCM (3 mL) at -15 °C under N<sub>2</sub>. The reaction mixture was stirred for 10 minutes at -10 °C at which point TMSOTf (0.003 mL, 0.017 mmols, 0.2 eq of **2.1a**) was added dropwise to the solution affording a pink solution. The solution was stirred for 15 minutes and quenched with NEt<sub>3</sub> affording a light-yellow solution. The solution was filtered through celite, washed with Na<sub>2</sub>S<sub>2</sub>O<sub>3</sub> (5 mL), dried (MgSO<sub>4</sub>) and concentrated *in vacuo*, affording a light-yellow oil. The oil was purified by column chromatography, eluting with a graduated solvent system of 4 : 1 Hexane : EtOAc to 100% EtOAc. This afforded a colourless oil of **5.33**<sup>405</sup> (0.020 g, 0.027 mmols, 32%,  $\alpha$ -only); R<sub>f</sub> = 0.52 (2.5 : 1 Hexane : EtOAc).

<sup>1</sup>H NMR (500 MHz, CDCl<sub>3</sub>)  $\delta$  7.28 (m, 13H, HAR), 7.15 (dd,  $J_{\text{HAr}} = 7.7$  Hz,  $J_{\text{HAr}} = 2.2$  Hz, 2H, HAR), 5.50 (d,  $J_{1,2} = 5.0$  Hz, 1H, H-1a), 5.40 (dd,  $J_{2,3} = 3.3$  Hz,  $J_{1,2} = 1.7$  Hz, 1H, H-2b), 4.90 (d,  $J_{1,2} = 1.7$  Hz, 1H, H-1b), 4.84 (d,  $J_{\text{CH}_2} = 10.6$  Hz, 1H, CH<sub>2</sub>), 4.71 (d,  $J_{\text{CH}_2} = 10.6$  Hz, 1H, CH<sub>2</sub>), 4.68 (s, 1H, CH<sub>2</sub>), 4.60 (dd,  $J_{3,4} = 8.0$  Hz,  $J_{2,3} = 2.4$  Hz, 1H, H-3a), 4.53 (d,  $J_{\text{CH}_2} = 10.6$  Hz, 1H, CH<sub>2</sub>), 4.50 (d,  $J_{\text{CH}_2} = 10.6$  Hz, 1H, CH<sub>2</sub>), 4.47 (d,  $J_{\text{CH}_2} = 10.6$  Hz, 1H, CH<sub>2</sub>), 4.30 (dd,  $J_{1,2} = 5.0$  Hz,  $J_{2,3} = 2.4$  Hz, 1H, H-2a), 4.21 (dd,  $J_{3,4} = 8.0$  Hz,  $J_{4,5} = 2.0$  Hz, H-4a), 3.98 (dd,  $J_{3,4} = 9.3$  Hz,  $J_{2,3} = 3.3$  Hz, 1H, H-3b), 3.91 (m, 2H, H-5a, H-4b), 3.80 (m, 3

<sup>13</sup>C NMR (126 MHz, CDCl<sub>3</sub>)  $\delta$  170.4 (1C, C=O), 138.4, 138.3, 138.0, 128.4, 128.3, 128.1, 127.9, 127.8, 127.7, 127.6, 127.5, 109.4, 108.6, (CAr), 97.9 (1C, C-1b), 96.3 (1C, C-1a), 78.2 (1C, C-3b), 75.1 (1C, CH<sub>2</sub>), 74.3 (1C, C-4b), 73.4 (1C, CH<sub>2</sub>), 71.9 (1C, CH<sub>2</sub>), 71.5 (1C, C-5b), 70.8 (1C, C-4a), 70.6 (1C, C-2a), 70.6 (1C, C-3a), 68.7 (1C, C-6b), 68.7 (1C, C-2b), 66.2 (1C, C-6a), 66.0 (1C, C-5a), 26.2 (1C, CH<sub>3</sub>), 26.0 (1C, CH<sub>3</sub>), 24.9 (1C, CH<sub>3</sub>), 24.5 (1C, CH<sub>3</sub>), 21.14 (1C, CH<sub>3</sub>).

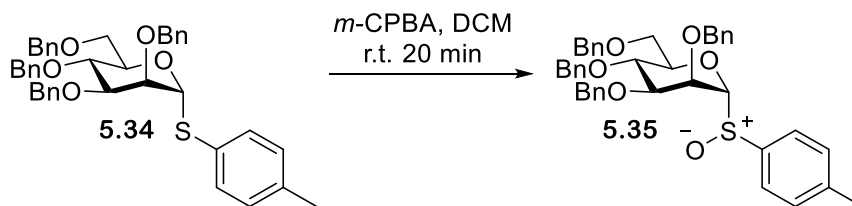
(ESI)HRMS - C<sub>41</sub>H<sub>50</sub>NaO<sub>12</sub><sup>+</sup> ([M+Na]<sup>+</sup>) requires m/z 757.3200: found m/z 757.3198

$[\alpha]_D^{25} = -11.46$  (c 1, DCM)

IR – 3031 (C-H), 2917 (C-H), 2853 (C-H), 1745 (C=O), 1725 (C=O), 1453 (C=C), 1370 (C=C), 1235 (C=O), 1211 (C=O), 1139 (C-O), 1095 (C-O), 1068 (C-O), 1027 (C-O), 1003 (C-O).

## Experimental

### 8.5.3.5 Synthesis of 4-methylphenylsulfenyl 2,3,4,6-tetra-O-benzyl-1-thio- $\alpha$ -D-mannopyranoside **5.35**



*m*-CPBA (0.03 g, 0.18 mmols, 1.5 eq) was added to a solution of **5.34** (0.08 g, 0.12 mmols) in dry DCM (3 mL), the reaction mixture was stirred at r.t. for 20 minutes affording a colourless solution. The solution was washed with saturated NaHCO<sub>3</sub> solution (5 mL), dried (MgSO<sub>4</sub>) and concentrated *in vacuo*, affording a colourless oil. The oil was purified by column chromatography, eluting with a graduated solvent system of 100% hexane to 100% EtOAc. This afforded a colourless oil of **5.35** (0.028 g, 0.042 mmols, 35%); R<sub>f</sub> = 0.6 (2 : 1 Hexane : EtOAc).

<sup>1</sup>H NMR (500 MHz, CDCl<sub>3</sub>) δ 7.46 (d, *J*<sub>HAr</sub> = 8.2 Hz, 2H, HAr), 7.30 (m, 18H, HAr), 7.18 (m, 4H, HAr), 4.92 (d, *J*<sub>CH2</sub> = 11.0 Hz, 1H, CH<sub>2</sub>), 4.64 (s, 2H, CH<sub>2</sub>), 4.58 (d, *J*<sub>CH2</sub> = 2.6 Hz, 2H, CH<sub>2</sub>), 4.53 (m, 3H, CH<sub>2</sub> H-1), 4.45 (m, 2H, CH<sub>2</sub> H-2), 4.20 (dd, *J*<sub>3,4</sub> = 9.5 Hz, *J*<sub>2,3</sub> = 3.3 Hz, 1H, H-3), 4.10 (ddd, *J*<sub>4,5</sub> = 9.5 Hz, *J*<sub>5,6'</sub> = 5.7 Hz, *J*<sub>5,6</sub> = 2.0 Hz, H-5), 4.00 (dd, *J*<sub>3,4</sub> = 9.5 Hz, *J*<sub>4,5</sub> = 9.5 Hz, 1H, H-4), 3.73 (dd, *J*<sub>6,6'</sub> = 10.5 Hz, *J*<sub>6,5</sub> = 2.0 Hz, 1H, H-6), 3.66 (dd, *J*<sub>6,6'</sub> = 10.5 Hz, *J*<sub>5,6'</sub> = 5.7 Hz, H-6'), 2.36 (s, 3H, CH<sub>3</sub>).

<sup>13</sup>C NMR (126 MHz, CDCl<sub>3</sub>) δ 141.8, 138.4, 138.2, 138.1, 138.0, 137.6, 129.9, 128.4, 128.4, 128.3, 128.3, 128.0, 127.9, 127.9, 127.7, 127.7, 127.7, 127.6, 127.6, 124.5 (CAr), 96.0 (1C, C-1), 79.6 (1C, C-3), 77.7 (1C, C-5), 75.2 (1C, CH<sub>2</sub>), 74.0 (1C, C-4), 73.4 (1C, CH<sub>2</sub>), 72.5 (1C, CH<sub>2</sub>), 72.1 (1C, CH<sub>2</sub>), 71.6 (1C, C-2), 69.5 (1C, C-6), 21.4 (1C, CH<sub>3</sub>).

(ESI)HRMS - C<sub>41</sub>H<sub>42</sub>NaO<sub>6</sub>S<sup>+</sup> ([M+Na]<sup>+</sup>) requires *m/z* 685.2600: found *m/z* 685.2604

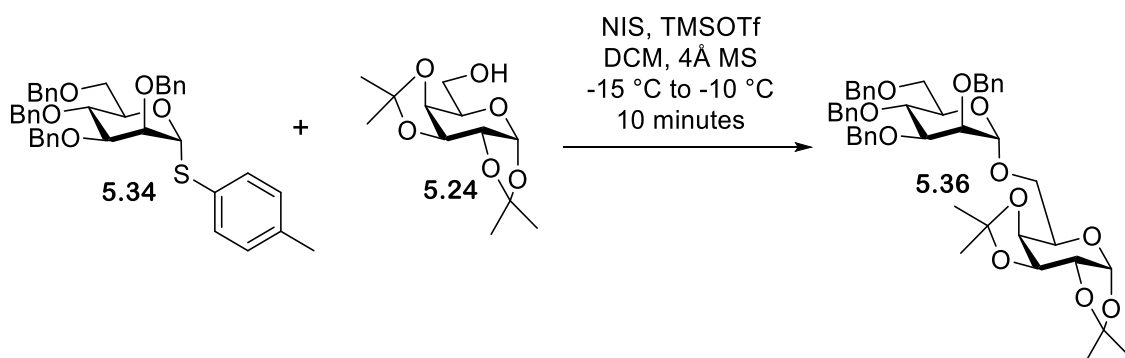
[ $\alpha$ ]<sub>D</sub><sup>25</sup> = -27.15 (*c* 1, CH<sub>2</sub>Cl<sub>2</sub>)

IR – 3030 (C-H), 2921 (C-H), 2866 (C-H), 1495 (C=C), 1454 (C=C), 1367 (C=C), 1208 (C-O), 1100 (C-O), 1040 (C-O), 1028 (C-O).

No literature reference for characterisation could be found.

## Experimental

### 8.5.3.6 Synthesis of 2,3,4,6-tetra-O-benzyl- $\alpha$ -D-mannopyranosyl-(1->6)-1,2:3,4-di-O-isopropylidene- $\alpha$ -D-galactopyranoside **5.36**<sup>406</sup> using direct activation with NIS and TMSOTf



**5.34** (0.05 g, 0.077 mmols, 1.3 eq) and **5.24** (0.015 g, 0.059 mmols) were dried overnight under vacuum. NIS (0.023 g, 0.1 mmols, 1.3 eq of **5.34**) was added to a solution of **5.34**, **5.24** and 4Å MS in dry DCM (3 mL) at -15 °C under N<sub>2</sub>. The reaction mixture was stirred for 10 minutes at -10 °C at which point TMSOTf (0.003 mL, 0.015 mmols, 0.2 eq of **5.34**) was added dropwise to the solution affording a pink solution. The solution was stirred for 15 minutes and quenched with NEt<sub>3</sub> affording a light-yellow solution. The solution was filtered through celite, washed with Na<sub>2</sub>S<sub>2</sub>O<sub>3</sub> (5 mL), saturated NaHCO<sub>3</sub> solution (5 mL), dried (MgSO<sub>4</sub>) and concentrated *in vacuo*, affording a light-yellow oil. The oil was purified by column chromatography, eluting with a graduated solvent system of 100% hexane to 100% EtOAc. This afforded a colourless oil of **5.36** (0.006 g, 0.0076 mmols, 13%,  $\alpha$ -only); R<sub>f</sub> = 0.65 (2.5 : 1 Hexane : EtOAc).

<sup>1</sup>H NMR (500 MHz, CDCl<sub>3</sub>)  $\delta$  7.31 (m, 14H, HAR), 7.24 (m, 4H, HAR), 7.15 (dd,  $J_{\text{HAr}} = 7.7$  Hz,  $J_{\text{HAr}} = 2.3$  Hz, 2H, HAR), 5.51 (d,  $J_{1,2} = 5.0$  Hz, 1H, H-1a), 5.00 (d,  $J_{1,2} = 1.8$  Hz, 1H, H-1b), 4.86 (d,  $J_{\text{CH}_2} = 10.6$  Hz, 1H, CH<sub>2</sub>), 4.73 (d,  $J_{\text{CH}_2} = 2.9$  Hz, 2H, CH<sub>2</sub>), 4.67 (d,  $J_{\text{CH}_2} = 12.2$  Hz, 1H, CH<sub>2</sub>), 4.60 (dd,  $J_{3,4} = 8.0$  Hz,  $J_{2,3} = 2.5$  Hz, 1H, H-3a), 4.58 (d,  $J_{\text{CH}_2} = 2.9$  Hz, 2H, CH<sub>2</sub>), 4.52 (m, 2H, CH<sub>2</sub>), 4.31 (dd,  $J_{1,2} = 5.0$  Hz,  $J = 2.5$  Hz, 1H, H-2a), 4.15 (dd,  $J_{3,4} = 8.0$  Hz,  $J_{4,5} = 1.8$  Hz, 1H, H-4a), 4.01 (dd,  $J_{3,4} = 9.2$  Hz,  $J_{4,5} = 9.2$  Hz, 1H, H-4b), 3.96 (m, 1H, H-5a), 3.90 (dd,  $J_{3,4} = 9.2$  Hz,  $J_{2,3} = 3.0$  Hz, 1H, H-3b), 3.82 (dd,  $J_{2,3} = 3.0$  Hz,  $J_{1,2} = 1.8$  Hz, 1H, H-2b), 3.78 (m, 3H, H-6a, H-6b, H-5b), 3.70 (m, 2H, H-6'a, H-6'b), 1.50 (s, 3H, CH<sub>3</sub>), 1.43 (s, 3H, CH<sub>3</sub>), 1.32 (s, 6H, CH<sub>3</sub>).

<sup>13</sup>C NMR (126 MHz, CDCl<sub>3</sub>)  $\delta$  138.6, 138.5, 138.4, 138.4, 128.3, 128.3, 128.3, 128.0, 127.8, 127.6, 127.5, 127.5, 127.4, 127.4, 109.4, 108.6 (CAr), 97.3 (1C, C-1b), 96.4 (1C, C-1a), 80.0 (1C, C-3b), 75.1 (1C, CH<sub>2</sub>), 74.8 (1C, C-4b), 74.6 (1C, C-2b), 73.3 (1C, CH<sub>2</sub>), 72.3 (1C, CH<sub>2</sub>), 72.1 (1C, C-5b), 72.1 (1C, CH<sub>2</sub>), 70.9 (C-4a), 70.7 (C-3a), 70.6 (1C, C-2a), 69.1 (1C, C-6b), 65.4 (1C, C-6a), 65.3 (1C, C-5a), 26.1 (1C, CH<sub>3</sub>), 26.0 (1C, CH<sub>3</sub>), 24.9 (1C, CH<sub>3</sub>), 24.6 (1C, CH<sub>3</sub>).

(ESI)HRMS - C<sub>46</sub>H<sub>54</sub>NaO<sub>11</sub><sup>+</sup> ([M+Na]<sup>+</sup>) requires m/z 805.3564: found m/z 805.3565

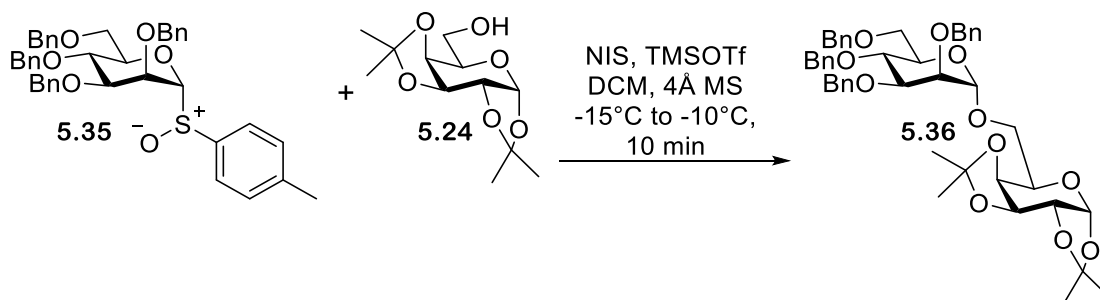
$[\alpha]_D^{25} = -30.30$  (c 1, DCM)

IR – 3071 (C-H), 3030 (C-H), 2992 (C-H), 2920 (C-H), 1497 (C=C), 1454 (C=C), 1382 (C=C), 1256 (C-O), 1210 (C-O), 1167 (C-O), 1102 (C-O), 1069 (C-O), 1027 (C-O), 1005 (C-O).



## Experimental

### 8.5.3.7 Synthesis of 2,3,4,6-tetra-O-benzyl- $\alpha$ -D-mannopyranosyl-(1 $\rightarrow$ 6)-1,2:3,4-di-O-isopropylidene- $\alpha$ -D-galactopyranoside **5.36**<sup>406</sup> using direct activation with with Bols and co-workers method<sup>84</sup>

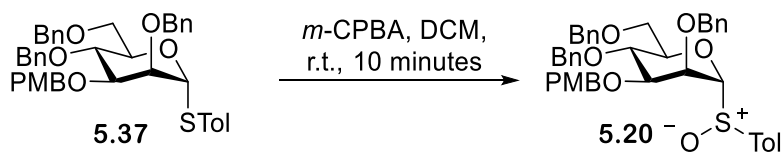


**5.35** (0.063 g, 0.095 mmols) **5.24** (0.036 g, 0.14 mmols, 1.5 eq) and TTBP (0.047 g, 0.19 mmols, 2 eq) were dried overnight under vacuum. Tf<sub>2</sub>O (0.018 mL, 0.11 mmols, 1.2 eq) was added dropwise to a solution of donor, acceptor, TTBP and 4Å MS (0.5 g) in dry DCM (5 mL) at -78 °C under N<sub>2</sub> affording a cloudy colourless solution. The reaction mixture was stirred for 20 minutes and quenched with NEt<sub>3</sub> (0.2 mL) and MeOH (0.2 mL) affording a cloudy colourless solution. The solution was filtered through celite washed with water (5 mL) and saturated NaCl solution (5 mL), dried (MgSO<sub>4</sub>) and concentrated *in vacuo*, affording a colourless oil. The oil was purified by column chromatography, eluting with a graduated solvent system of 100% hexane to 100% EtOAc. This afforded a colourless oil of **5.36** (0.020 g, 0.026 mmols, 27%,  $\alpha$ -only); R<sub>f</sub> = 0.65 (2.5 : 1 Hexane : EtOAc).

For compound data please see page 328

## Experimental

### 8.5.3.8 Synthesis of 4-methylphenylsulfenyl tri-2, 4, 6-O-benzyl-3-O-p-methoxybenzyl- $\alpha$ -D-mannopyranoside **5.20**



*m*-CPBA (0.052 g, 0.3 mmols, 2 eq) was added to a solution of **5.37** (0.1 g, 0.15 mmols) in dry DCM (1.2 mL) and stirred at r.t. for 10 minutes affording a clear solution. The solution was quenched with NaHCO<sub>3</sub> (10 mL), separated, washed with water (1 x 10 mL), brine (1 x 10 mL), dried (MgSO<sub>4</sub>) and concentrated *in vacuo*, affording a clear oil. The oil was purified by column chromatography, eluting with a graduated solvent system of 3 : 1 Hexane : EtOAc to 2 : 1 Hexane : EtOAc. This afforded a colourless oil of **5.20** (0.1 g, 0.14 mmols, 81%); R<sub>f</sub> = 0.42 (3 : 1 Hexane EtOAc).

<sup>1</sup>H NMR (500 MHz, CDCl<sub>3</sub>)  $\delta$  7.45 (d,  $J_{\text{HAr}} = 8.0$  Hz, 2H, HAr (PMB)), 7.28 (m, 15H, HAr), 7.20 (dd,  $J_{\text{HAr}} = 7.8$  Hz,  $J_{\text{HAr}} = 1.8$  Hz, 2H, HAr (Ph)), 7.17 (d,  $J_{\text{HAr}} = 8.0$  Hz, 2H, HAr (PMB)), 6.85 (d,  $J_{\text{HAr}} = 8.7$  Hz, 2H, HAr (STol)), 4.91 (d,  $J_{\text{CH}_2} = 10.9$  Hz, 1H, CH<sub>2</sub>), 4.58 (m, 3H, CH<sub>2</sub>), 4.56 (d,  $J_{\text{CH}_2} = 5.8$  Hz, 1H, CH<sub>2</sub>), 4.54 (d,  $J_{\text{CH}_2} = 4.1$  Hz, 1H, CH<sub>2</sub>), 4.53 (s, 1H, H-1), 4.50 (d,  $J_{\text{CH}_2} = 10.9$  Hz, 1H, CH<sub>2</sub>), 4.44 (d,  $J_{\text{CH}_2} = 11.8$  Hz, 1H, CH<sub>2</sub>), 4.42 (dd,  $J_{3,4} = 3.2$  Hz,  $J_{1,2} = 1.9$  Hz, 1H, H-2), 4.18 (dd,  $J_{3,4} = 9.5$  Hz,  $J_{2,3} = 3.2$  Hz, 1H, H-3), 4.10 (ddd,  $J_{4,5} = 9.5$  Hz,  $J_{5,6b} = 5.8$  Hz,  $J_{5,6a} = 1.6$  Hz, 1H, H-5), 3.96 (dd,  $J_{3,4} = 9.5$  Hz,  $J_{4,5} = 9.5$  Hz, 1H, H-4), 3.80 (s, 3H, OCH<sub>3</sub>), 3.72 (dd,  $J_{6a,6b} = 10.8$  Hz,  $J_{5,6a} = 1.6$  Hz, 1H, H-6a), 3.65 (dd,  $J_{6a,6b} = 10.8$  Hz,  $J_{5,6b} = 5.8$  Hz, 1H, H-6b), 2.39 (s, 3H, CH<sub>3</sub>).

<sup>13</sup>C NMR (126 MHz, CDCl<sub>3</sub>)  $\delta$  159.3, 141.8, 138.4, 138.3, 138.1, 137.7, 130.2, 129.9, 129.6, 128.4, 128.3, 128.3, 128.0, 127.9, 127.8, 127.7, 127.7, 127.6, 124.5, 113.8, (CAr), 96.0 (1C, C-1), 79.2 (1C, C-3), 77.7 (1C, C-5), 75.1 (1C, CH<sub>2</sub>), 74.0 (1C, C-4), 73.4 (1C, CH<sub>2</sub>), 72.5 (1C, CH<sub>2</sub>), 71.8 (1C, CH<sub>2</sub>), 71.6 (1C, C-2), 69.6 (1C, C-6), 55.3 (1C, OCH<sub>3</sub>), 21.5 (1C, CH<sub>3</sub>).

(ESI)HRMS – C<sub>42</sub>H<sub>44</sub>NaO<sub>7</sub>S<sup>+</sup> ([M+Na]<sup>+</sup>) requires *m/z* 715.2705: found *m/z* 715.2722.

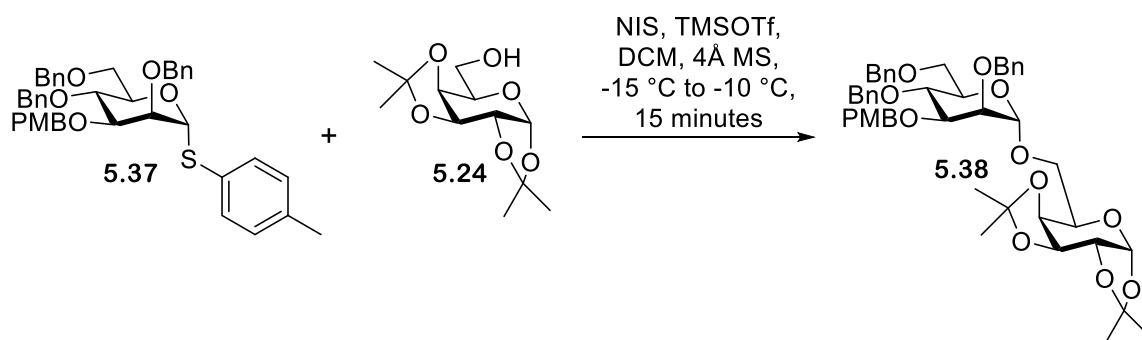
$[\alpha]_D^{25} = -40.1$  (c 1, CH<sub>2</sub>Cl<sub>2</sub>)

IR – 3030 (C-H), 2922 (C-H), 2864 (C-H), 1984 (C-H), 1513 (C=C), 1495 (C=C), 1247 (C-O), 1097 (C-O), 1035 (S=O).

No literature reference for characterisation could be found

## Experimental

### 8.5.3.9 Synthesis of tri-2, 4, 6-O-benzyl-3-O-p-methoxybenzyl-1-thio- $\alpha$ -D-mannopyranoside -(1->6)-1,2:3,4-di-O-isopropylidene- $\alpha$ -D-galactopyranoside using direct activation with NIS and TMSOTf 5.38



**5.37** (0.05 g, 0.074 mmols, 1.3 eq) and **5.24** (0.015 g, 0.057 mmols) were dried overnight under vacuum. NIS (0.021 g, 0.09 mmols, 1.3 eq of **5.37**) was added to a solution of **5.37**, **5.24** and 4Å MS in dry DCM (3 mL) at -15 °C under N<sub>2</sub>. The reaction mixture was stirred for 10 minutes at -10 °C at which point TMSOTf (0.003 mL, 0.015 mmols, 0.2 eq of **5.37**) was added dropwise to the solution affording a pink solution. The solution was stirred for 15 minutes and quenched with NEt<sub>3</sub> affording a light-yellow solution. The solution was filtered through celite, washed with Na<sub>2</sub>S<sub>2</sub>O<sub>3</sub> (5 mL), saturated NaHCO<sub>3</sub> (5 mL), dried (MgSO<sub>4</sub>) and concentrated *in vacuo*, affording a light-yellow oil. The oil was purified by column chromatography, eluting with a graduated solvent system of 100% hexane to 100% EtOAc. This afforded a colourless oil of **5.38** (0.017 g, 0.021 mmols, 37%,  $\alpha$ -only); R<sub>f</sub> = 0.63 (2 : 1 Hexane : EtOAc).

<sup>1</sup>H NMR (500 MHz, CDCl<sub>3</sub>)  $\delta$  7.31 (m, 11H, HAR), 7.24 (m, 4H, HAR), 7.16 (dd,  $J_{\text{HAR}} = 7.8$  Hz,  $J_{\text{HAR}} = 2.2$  Hz, 2H, HAR), 6.83 (dd,  $J_{\text{HAR}} = 6.7$  Hz,  $J_{\text{HAR}} = 2.0$  Hz, 2H, HAR), 5.52 (d,  $J_{1,2} = 5.0$  Hz, 1H, H-1a), 5.00 (d,  $J_{1,2} = 1.8$  Hz, 1H, H-1b), 4.85 (d,  $J_{\text{CH}_2} = 10.9$  Hz, 1H, CH<sub>2</sub>), 4.73 (s, 2H, CH<sub>2</sub>), 4.67 (d,  $J_{\text{HAR}} = 12.1$  Hz, 1H, CH<sub>2</sub>), 4.59 (dd,  $J_{3,4} = 8.0$  Hz,  $J_{2,3} = 2.5$  Hz, 1H, H-3a), 4.52 (d,  $J_{\text{CH}_2} = 12.1$  Hz, 1H, CH<sub>2</sub>), 4.51 (s, 2H, CH<sub>2</sub>), 4.49 (d,  $J_{\text{CH}_2} = 10.9$  Hz, 1H, CH<sub>2</sub>), 4.31 (dd,  $J_{1,2} = 5.0$  Hz,  $J_{2,3} = 2.5$  Hz, 1H, H-2a), 4.15 (dd,  $J_{3,4} = 8.0$  Hz,  $J_{4,5} = 1.8$  Hz, 1H, H-4a), 3.97 (m, 2H, H-5a, H-5b), 3.89 (dd,  $J_{3,4} = 9.4$  Hz,  $J_{2,3} = 3.1$  Hz, 1H, H-3b), 3.80 (s, 3H, OCH<sub>3</sub>), 3.78 (m, 4H, H-2b, H-4b, H-6b, H6a), 3.69 (m, 2H, H-6'b, H-6'a), 1.50 (s, 3H, CH<sub>3</sub>), 1.43 (s, 3H, CH<sub>3</sub>), 1.33 (s, 6H, CH<sub>3</sub>).

<sup>13</sup>C NMR (126 MHz, CDCl<sub>3</sub>)  $\delta$  159.1, 138.5, 138.4, 138.4, 130.7, 129.2, 128.3, 128.2, 127.9, 127.7, 127.7, 127.5, 127.5, 127.4, 113.7, 109.3, 108.6, (CAR), 97.3 (1C, C-1b), 96.3 (1C, C-1a), 79.8 (1C, C-3b), 75.1 (1C, CH<sub>2</sub>), 74.8 (1C, C-5b), 74.6 (1C, C-4b), 73.3 (1C, CH<sub>2</sub>), 72.4 (1C, CH<sub>2</sub>), 72.1 (1C, C-2b), 71.8 (1C, CH<sub>2</sub>), 70.9 (1C, C-4a), 70.7 (1C, C-3a), 70.6 (1C, C-2a), 69.2 (1C, C-6b), 65.4 (1C, C-6a), 65.3 (1C, C-5a), 55.3 (1C, OCH<sub>3</sub>), 26.1 (1C, CH<sub>3</sub>), 25.9 (1C, CH<sub>3</sub>), 24.9 (1C, CH<sub>3</sub>), 24.7 (1C, CH<sub>3</sub>).

(ESI)HRMS - C<sub>47</sub>H<sub>56</sub>NaO<sub>12</sub><sup>+</sup> ([M+Na]<sup>+</sup>) requires m/z 835.3669: found [M+Na]<sup>+</sup> 835.3667

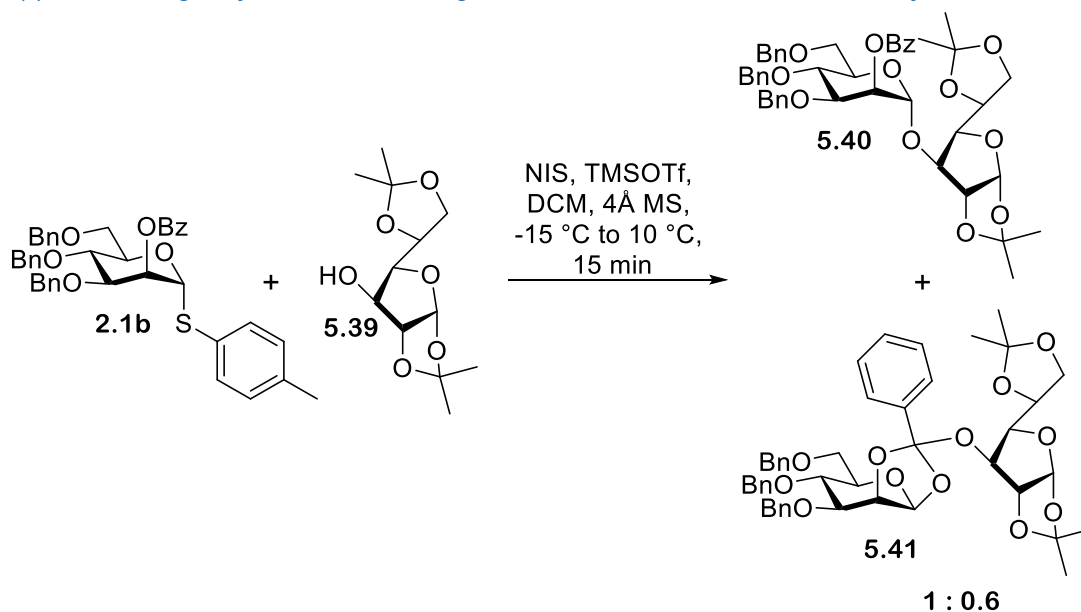
$[\alpha]_D^{25} = -3.9$  (c 1, DCM)

IR – 3063 (C-H), 3031 (C-H), 2996 (C-H), 2917 (C-H), 2869 (C-H), 1454 (C=C), 1382 (C=C), 1303 (C=C), 1250 (C-O), 1211 (C-O), 1172 (C-O), 1100 (C-O), 1070 (C-O), 1004 (C-O).

No literature reference for characterisation could be found.

## Experimental

### 8.5.3.10 Synthesis of 2-O-(benzoyl-3,4,6-tri-O-benzyl- $\alpha$ -D-mannopyranoside)-(1 $\rightarrow$ 3)-1,2:5,6-Di-O-isopropylidene- $\alpha$ -D-glucofuranose **5.39** using direct activation with NIS and TMSOTf



**2.1b** (0.05 g, 0.075 mmols, 1.3 eq) and **5.39** (0.015 g, 0.057 mmols) were dried overnight under vacuum. NIS (0.022 g, 0.09 mmols, 1.3 eq of **2.1b**) was added to a solution of **2.1b**, **5.39** and 4Å MS (0.3 g) in dry DCM (3 mL) at -15 °C under N<sub>2</sub>. The reaction mixture was stirred for 10 minutes at -10 °C at which point TMSOTf (0.003 mL, 0.015 mmols, 0.2 eq of **2.1b**) was added dropwise to the solution affording a pink solution. The solution was stirred for 15 minutes and quenched with NEt<sub>3</sub> affording a light-yellow solution. The solution was filtered through celite, washed with Na<sub>2</sub>S<sub>2</sub>O<sub>3</sub> (5 mL), saturated NaHCO<sub>3</sub> solution (5 mL), dried (MgSO<sub>4</sub>) and concentrated *in vacuo*, affording a light-yellow oil. The oil was purified by column chromatography, eluting with a graduated solvent system of 100% hexane to 100% EtOAc. This afforded a colourless oil of **5.40** and **5.41** (0.018 g, 0.023 mmols, 40% (25% **5.40** : 15 % **5.41**),  $\alpha$ -only); R<sub>f</sub> = 0.68 (2 : 1 Hexane : EtOAc).

Note NMR was impure with a 1 : 0.6 ratio of product : orthoester

<sup>1</sup>H NMR (500 MHz, CDCl<sub>3</sub>)  $\delta$  8.06 (m, 4H), 7.55 (m, 2H), 7.31 (m, 28H), 7.18 (m, 4H), 5.98 (d,  $J_{1,2}$  = 3.6 Hz, 0.6, H-1a orthoester), 5.80 (d,  $J_{1,2}$  = 3.6 Hz, 1H, H-1a), 5.65 (dd,  $J_{2,3}$  = 3.4 Hz,  $J_{1,2}$  = 2.0 Hz, 1H, H-2b), 5.62 (dd,  $J_{2,3}$  = 3.4 Hz,  $J_{1,2}$  = 2.0 Hz, 0.6H, H-2b orthoester), 5.27 (d,  $J_{1,2}$  = 2.0 Hz, 1H, H-1b), 5.03 (d,  $J_{1,2}$  = 2.0 Hz, 0.6H, H-1b orthoester), 4.86 (d,  $J_{\text{CH}_2}$  = 10.6 Hz, 1H, CH<sub>2</sub>), 4.78 (d,  $J_{\text{CH}_2}$  = 11.2 Hz, 1H, CH<sub>2</sub>), 4.77 (d,  $J_{\text{CH}_2}$  = 11.4 Hz, 0.6H, CH<sub>2</sub> orthoester), 4.74 (d,  $J_{\text{CH}_2}$  = 11.9 Hz, 0.6H, CH<sub>2</sub> orthoester), 4.73 (d,  $J_{\text{CH}_2}$  = 11.9 Hz, 1H, CH<sub>2</sub>), 4.67 (d,  $J_{1,2}$  = 3.6 Hz, 1H, H-2a), 4.54 (m, 6H, 3 x CH<sub>2</sub>, 4 x CH<sub>2</sub> orthoester, H-2a orthoester), 4.32 (d,  $J_{3,4}$  = 2.6 Hz, 1H, H-3a), 4.30 (m, 0.6H, H-3a orthoester), 4.21 (m, 1.6H, H-5a, H-5a orthoester), 4.14 (dd,  $J_{6,6'}$  = 8.3 Hz,  $J_{5,6}$  = 6.2 Hz 1H, H-6a), 4.06 (m, 4.2H, H-3b, H-3b orthoester, H-4a, H-5b, H-5b orthoester), 3.98 (dd,  $J_{6,6'}$  = 8.3 Hz,  $J_{5,6'}$  = 5.4 Hz, 1H, H-6'a), 3.89 (m, 2.6H, H-6b, H-4b, H-4b orthoester), 3.77 (m, 4H, H-4a orthoester, H6'b, H6b orthoester, H-6'b orthoester, H-6a orthoester, H-6'a orthoester) 1.48 (s, 3H, CH<sub>3</sub>), 1.46 (s, 1.5H, CH<sub>3</sub>), 1.37 (s, 3H, CH<sub>3</sub>), 1.35 (s, 1.5H, CH<sub>3</sub>), 1.33 (s, 1.5H, CH<sub>3</sub>), 1.32 (s, 1.5H, CH<sub>3</sub>), 1.32 (s, 3H, CH<sub>3</sub>), 1.24 (s, 3H, CH<sub>3</sub>).

## Experimental

$^{13}\text{C}$  NMR (126 MHz,  $\text{CDCl}_3$ )  $\delta$  165.6 (1C, C=O orthoester), 165.4 (1C, C=O), 138.6, 138.5, 138.3, 138.1, 138.0, 137.8, 133.2, 133.1, 129.9, 129.9, 129.8, 128.4, 128.4, 128.4, 128.4, 128.3, 128.3, 128.2, 128.2, 128.1, 128.1, 127.9, 127.8, 127.7, 127.6, 127.6, 127.5, 127.5, 127.4, (CAr), 112.2 (1C, C orthoester), 112.0 (1C, C), 109.4 (2C, C, actual and orthoester), 106.4 (1C, C-1a orthoester), 105.3 (1C, C-1a), 100.9 (1C, C), 98.8 (1C, C-1b), 97.5 (1C, C-1b orthoester), 84.1 (1C, C-2a orthoester), 83.6 (1C, C-2a), 81.4 (1C, C-4a), 80.8 (1C, C-3a), 79.2 (1C, C-3a orthoester), 77.9 (1C, C-5b orthoester), 77.9 (1C, C-5b), 75.5 (1C,  $\text{CH}_2$ ), 75.1 (1C,  $\text{CH}_2$  orthoester), 75.0 (1C, C-5a orthoester), 74.2 (2C, C-3b, C-3b orthoester), 73.6 (1C,  $\text{CH}_2$ ), 73.4 (1C,  $\text{CH}_2$  orthoester), 72.5 (1C, C-4b), 72.3 (1C, C-5a), 71.7 (1C, C-4b orthoester), 71.6 (1C,  $\text{CH}_2$ ), 71.5 (1C,  $\text{CH}_2$  orthoester), 70.9 (1C, C-4a orthoester), 69.1 (1C, C-6b), 69.0 (1C, C-6b orthoester), 68.9 (1C, C-2b orthoester), 68.4 (1C, C-2b), 67.8 (1C, C-6a), 67.4 (1C, C-6a orthoester), 27.2 (1C,  $\text{CH}_3$  orthoester), 26.8 (1C,  $\text{CH}_3$ ), 26.8 (1C,  $\text{CH}_3$ ), 26.5 (1C,  $\text{CH}_3$  orthoester), 26.1 (1C,  $\text{CH}_3$ ), 25.2 (1C,  $\text{CH}_3$ ), 23.9 (1C,  $\text{CH}_3$  orthoester), 23.9 (1C,  $\text{CH}_3$  orthoester).

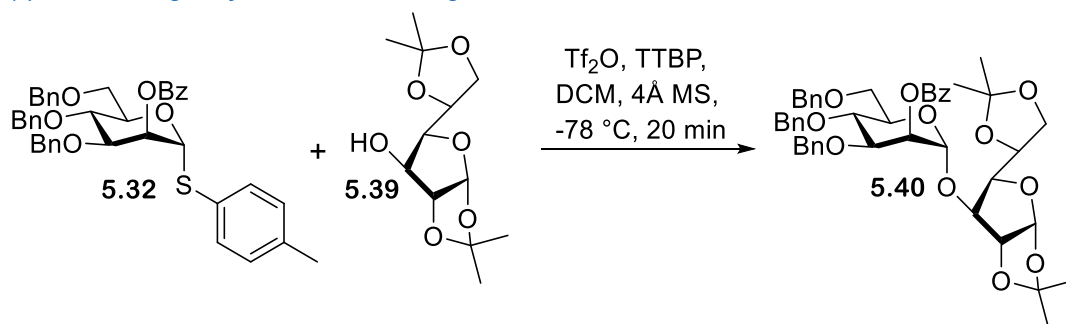
(ESI)HRMS -  $\text{C}_{46}\text{H}_{52}\text{NaO}_{12}^+$  ( $[\text{M}+\text{Na}]^+$ ) requires  $m/z$  819.3356: found  $m/z$  819.3372

IR – 2986 (C-H), 2932 (C-H), 1724 (C=O), 1264 (C-O), 1071 (C-O), 1022 (C-O)

No literature reference for characterisation could be found but previously synthesized by<sup>407</sup>

## Experimental

### 8.5.3.11 Synthesis of 2-O-(benzoyl-3,4,6-tri-O-benzyl- $\alpha$ -D-mannopyranoside)-(1 $\rightarrow$ 3)-1,2:5,6-Di-O-isopropylidene- $\alpha$ -D-glucofuranose **5.39** using direct activation with with Bols and co-workers method<sup>84</sup>



**5.32** (0.05 g, 0.075 mmols) **5.39** (0.028 g, 0.11 mmols, 1.5 eq) and TTBP (0.037 g, 0.15 mmols, 2 eq) were dried overnight under vacuum.  $\text{Tf}_2\text{O}$  (0.015 mL, 0.09 mmols, 1.2 eq) was added dropwise to a solution of donor, acceptor, TTBP and 4 Å MS (0.5 g) in dry DCM (5 mL) at  $-78\text{ }^\circ\text{C}$  under  $\text{N}_2$  affording a cloudy colourless solution. The reaction mixture was stirred for 20 minutes and quenched with  $\text{NEt}_3$  (0.2 mL) and MeOH (0.2 mL) affording a cloudy colourless solution. The solution was filtered through celite washed with water (5 mL) and saturated NaCl solution (5 mL), dried ( $\text{MgSO}_4$ ) and concentrated *in vacuo*, affording a colourless oil. The oil was purified by column chromatography, eluting with a graduated solvent system of 100% hexane to 100% EtOAc. This afforded a crude colourless oil of **5.40** (0.020 g, 0.025 mmols, 33%,  $\alpha$ -only);  $R_f = 0.68$  (2 : 1 Hexane : EtOAc).

$^1\text{H}$  NMR did show extra peaks in the aromatic and anomeric regions however when overlaid these did not match the orthoester peaks.

$^1\text{H}$  NMR (500 MHz,  $\text{CDCl}_3$ )  $\delta$  8.06 (dd,  $J_{\text{HAr}} = 8.2\text{ Hz}$ ,  $J_{\text{HAr}} = 1.4\text{ Hz}$ , 2H, HAr), 7.32 (m, 14H, HAr), 7.24 (m, 2H, HAr), 7.20 (dd,  $J_{\text{HAr}} = 7.7\text{ Hz}$ ,  $J_{\text{HAr}} = 2.4\text{ Hz}$ , 2H, HAr), 5.85 (d,  $J_{1,2} = 3.4\text{ Hz}$ , 1H, H-1a), 5.65 (dd,  $J_{1,2} = 2.0\text{ Hz}$ ,  $J_{2,3} = 2.0\text{ Hz}$ , 1H, H-2b), 5.27 (d,  $J_{1,2} = 2.0\text{ Hz}$ , 1H, H-1b), 4.86 (d,  $J_{\text{CH}_2} = 10.6\text{ Hz}$ , 1H,  $\text{CH}_2$ ), 4.79 (d,  $J_{\text{CH}_2} = 11.2\text{ Hz}$ , 1H,  $\text{CH}_2$ ), 4.73 (d,  $J_{\text{CH}_2} = 11.9\text{ Hz}$ , 1H,  $\text{CH}_2$ ), 4.68 (d,  $J_{1,2} = 3.4\text{ Hz}$ , 1H, H-2a), 4.57 (d,  $J_{\text{CH}_2} = 11.2\text{ Hz}$ , 1H,  $\text{CH}_2$ ), 4.55 (d,  $J_{\text{CH}_2} = 11.9\text{ Hz}$ , 1H,  $\text{CH}_2$ ), 4.52 (d,  $J_{\text{CH}_2} = 10.6\text{ Hz}$ , 1H,  $\text{CH}_2$ ), 4.32 (d,  $J_{3,4} = 2.7\text{ Hz}$ , 1H, H-3a), 4.22 (m, 1H, H-5a), 4.14 (dd,  $J_{6,6'} = 8.6\text{ Hz}$ ,  $J_{5,6} = 5.4\text{ Hz}$ , 1H, H-6a), 4.06 (m, 3H, H-3b, H-4a, H-5b), 3.97 (dd,  $J_{6,6'} = 8.6\text{ Hz}$ ,  $J_{5,6'} = 5.4\text{ Hz}$ , 1H, H-6'a), 3.89 (m, 2H, H-4b, H-6b), 3.83 (m, 1H, H-6'b), 1.48 (s, 3H,  $\text{CH}_3$ ), 1.38 (s, 3H,  $\text{CH}_3$ ), 1.31 (s, 3H,  $\text{CH}_3$ ), 1.25 (s, 3H,  $\text{CH}_3$ ).

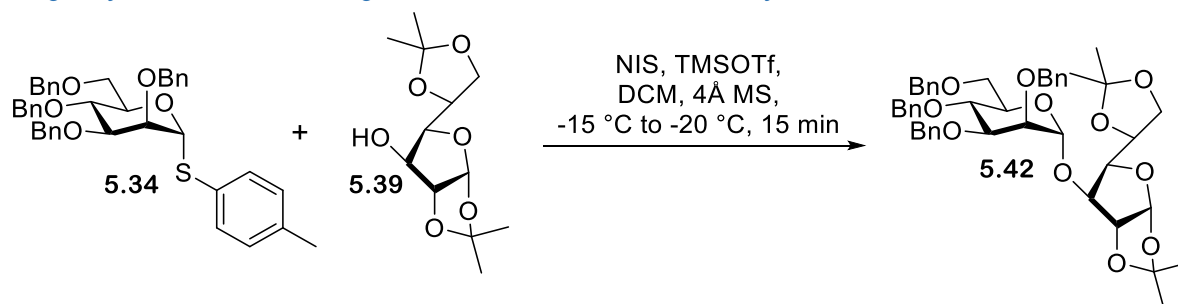
$^{13}\text{C}$  NMR (126 MHz,  $\text{CDCl}_3$ )  $\delta$  165.4 (1C, C=O), 138.3, 138.1, 137.8, 133.2, 129.9, 129.8, 129.7, 128.4, 128.4, 128.3, 128.2, 128.1, 127.8, 127.7, 127.6, 127.6, 125.8, (CAr), 112.0 (1C, C), 109.4 (1C, C), 105.3 (1C, C-1a), 98.8 (1C, C-1b), 83.6 (1C, C-2a), 81.4 (1C, C-4a), 80.8 (1C, C-3a), 77.9 (1C, C-5b), 75.5 (1C,  $\text{CH}_2$ ), 74.2 (1C, C-3b), 73.6 (1C,  $\text{CH}_2$ ), 72.5 (1C, C-4b), 72.3 (1C, C-5a), 71.6 (1C,  $\text{CH}_2$ ), 69.1 (C-6b), 68.4 (C-2b), 67.8 (C-6a), 26.8 (1C,  $\text{CH}_3$ ), 26.8 (1C,  $\text{CH}_3$ ), 26.1 (1C,  $\text{CH}_3$ ), 25.2 (1C,  $\text{CH}_3$ ).

Mass spectroscopy- please see page 332

No literature reference for characterisation could be found but previously synthesized by<sup>407</sup>

## Experimental

### 8.5.3.12 Synthesis of 2,3,4,6-tetra-O-benzyl- $\alpha$ -D-mannopyranosyl-(1 $\rightarrow$ 3)-1,2:5,6-Di-O-isopropylidene- $\alpha$ -D-glucufuranose **5.41**<sup>408</sup> using direct activation with NIS TMSOTf



**5.34** (0.05 g, 0.077 mmols, 1.3 eq) and **5.39** (0.015 g, 0.058 mmols) were dried overnight under vacuum. NIS (0.022 g, 0.1 mmols, 1.3 eq of **5.34**) was added to a solution of **5.34**, **5.39** and 4Å MS in dry DCM (3 mL) at -15 °C under N<sub>2</sub>. The reaction mixture was stirred for 10 minutes at -10 °C at which point TMSOTf (0.003 mL, 0.015 mmols, 0.2 eq of **5.34**) was added dropwise to the solution affording a pink solution. The solution was stirred for 15 minutes and quenched with NEt<sub>3</sub> affording a light-yellow solution. The solution was filtered through celite, washed with Na<sub>2</sub>S<sub>2</sub>O<sub>3</sub> (5 mL), saturated NaHCO<sub>3</sub> solution (5 mL), dried (MgSO<sub>4</sub>) and concentrated *in vacuo*, affording a light-yellow oil. The oil was purified by column chromatography, eluting with a graduated solvent system of 100% hexane to 100% EtOAc. This afforded a colourless oil of **5.42** (0.008 g, 0.01 mmols, 18%,  $\alpha$ -only); R<sub>f</sub> = 0.70 (2 : 1 Hexane : EtOAc).

<sup>1</sup>H NMR (500 MHz, CDCl<sub>3</sub>)  $\delta$  7.36 (m, 4H, HAr), 7.32 (m, 4H, HAr), 7.28 (m, 10H, HAr), 7.17 (dd,  $J_{\text{HAr}} = 7.7$  Hz,  $J_{\text{HAr}} = 2.4$  Hz, 2H, HAr), 5.80 (d,  $J_{1,2} = 3.5$  Hz, 1H, H-1a), 5.22 (d,  $J_{1,2} = 1.9$  Hz, 1H, H-1b), 4.88 (d,  $J_{\text{CH}_2} = 10.5$  Hz, 1H, CH<sub>2</sub>), 4.74 (d,  $J_{\text{CH}_2} = 12.2$  Hz, 1H, CH<sub>2</sub>), 4.67 (s, 1H, CH<sub>2</sub>), 4.65 (m, 1H, CH<sub>2</sub>, H-2a), 4.55 (m, 3H, CH<sub>2</sub>), 4.49 (d,  $J_{\text{CH}_2} = 10.5$  Hz, 1H, CH<sub>2</sub>), 4.25 (d,  $J_{3,4} = 1.6$  Hz, 1H, H-3a), 4.00 (m, 3H, H-4a, H-5a, H-6a), 3.99 (m, 2H, H6'a, H4b), 3.80 (m, 4H, H-3b, H-5b, H-6b, H-6'b), 3.76 (dd,  $J_{2,3} = 3.1$  Hz,  $J_{1,2} = 1.9$  Hz, 1H, H-2b), 1.47 (s, 3H, CH<sub>3</sub>), 1.40 (s, 3H, CH<sub>3</sub>), 1.32 (s, 3H, CH<sub>3</sub>), 1.21 (s, 3H, CH<sub>3</sub>).

<sup>13</sup>C NMR (126 MHz, CDCl<sub>3</sub>)  $\delta$  138.4, 138.3, 138.2, 138.1, 128.4, 128.4, 128.3, 128.3, 128.1, 127.8, 127.8, 127.7, 127.7, 127.6, 127.6, 127.5, (CAr), 111.92 (1C, C), 109.3 (1C, C), 105.3 (1C, C-1a), 98.9 (1C, C-1b), 83.7 (1C, C-2a), 81.4 (1C, C-4a), 80.6 (1C, C-3a), 79.6 (1C, C-5b), 75.3 (1C, CH<sub>2</sub>), 74.8 (1C, C-4b), 74.3 (1C, C-2b), 73.5 (1C, CH<sub>2</sub>), 72.7 (1C, C-3b), 72.6 (1C, C-5a), 72.3 (1C, CH<sub>2</sub>), 72.1 (1C, CH<sub>2</sub>), 69.3 (C-6b), 67.7 (C-6a), 26.9 (1C, CH<sub>3</sub>), 26.8 (1C, CH<sub>3</sub>), 26.1 (1C, CH<sub>3</sub>), 25.5 (1C, CH<sub>3</sub>).

(ESI)HRMS - C<sub>46</sub>H<sub>54</sub>NaO<sub>11</sub><sup>+</sup> ([M+Na]<sup>+</sup>) requires m/z 805.3564: found m/z 805.3578

$[\alpha]_D^{25} = + 3.60$  (c 1, DCM)

IR – 3035 (C-H), 2992 (C-H), 2928 (C-H), 2853 (C-H), 1497 (C=C), 1451 (C=C), 1372 (C=C), 1214 (C-O), 1075 (C-O), 1027 (C-O).

### 8.6 Experimental for Chapter 6

#### 8.6.1 Expression and purification of BT-1033

Method obtained from<sup>359</sup>

An *E. coli* BL21 (DE3) (New England Biolabs) transformant harbouring the expression plasmid was grown at 37 °C in 200 mL Luria broth (LB) media (1% NaCl, 1% tryptone and 0.5% yeast extract) containing 25 µg/µL kanamycin with shaking at 200 rpm until the culture reached an OD<sub>600</sub> of 0.6. Expression of BT-1033 was then induced by 0.1 mM isopropyl β-D-thiogalactopyranoside (IPTG) and was incubated for 24 h at 18 °C with shaking 200 rpm. The cells were harvested by centrifugation 20,000 × g for 20 minutes at 4 °C. The cell pellet was resuspended in 50 mL of 50 mM HEPES-NaOH, 500 mM NaCl, pH 7.0 buffer containing pepstatin (final concentration 1 µM), ABDSF (final concentration 0.2 mM) and benzonase (20 µL of 2.5 U per µL) and disrupted by sonication (Soniprep 150) (30 s pulses repeated 12 times with 30 s intermission between pulses). The supernatant was collected by centrifugation 20,000 × g, 20 minutes at 4 °C, filtered through a 0.22 µm syringe and applied to a HisTrap HP column (5 mL, Cytiva) equilibrated with 50 mM HEPES-NaOH, 500 mM NaCl, 10 mM imidazole pH 7.0 buffer using an AKTA start (Cytiva). The protein was eluted using a linear gradient of 50 mM HEPES-NaOH, 500 mM NaCl, 22 mM imidazole pH 7.0 buffer to 50 mM HEPES-NaOH, 500 mM NaCl, 400 mM imidazole pH 7.0 buffer. The fractions containing the recombinant protein (BT-1033) were pooled and dialysed into 10 mM HEPES-NaOH, pH 7.0 buffer and concentrated (Sartorius vivaspin6 10,000 MWCO). The recombinant protein (BT-1033) was further purified using a gel filtration column (Hiload 16/600, superdex 200 pg, Cytiva) equilibrated with 10 mM HEPES-NaOH, 150 mM NaCl, pH 7.0 buffer. The fractions containing the recombinant protein were pooled and concentrated (Sartorius vivaspin6 10,000 MWCO). The concentration of BT-1033 protein was determined spectrophotometrically at 280 nm using the calculated theoretical extinction coefficient of 28860 mol<sup>-1</sup> dm<sup>3</sup> cm<sup>-1</sup> and the reported extinction coefficient of 37,823 mol<sup>-1</sup> dm<sup>3</sup> cm<sup>-1</sup>.<sup>359</sup> The procedure yielded approximately 3.7 to 4.8 mg of purified BT-1033.



## Experimental

### 8.6.2 Reaction performed using BT-1033

#### *8.6.2.1 BT-1033 catalysed reactions general reaction set up procedure for Entries 1-42b*

A solution of 40 mM NaOAc, pH 5.5 was charged with MgCl<sub>2</sub> (from a stock in 40 mM NaOAc, pH 5.5 buffer) to a final concentration 15 mM MgCl<sub>2</sub>. **Acceptor** (in 40 mM NaOAc, pH 5.5 buffer), **Donor** (in 40 mM NaOAc, pH 5.5) and BT-1033 (in either 10 mM HEPES-NaOH, 150 mM NaCl, pH 7.0 buffer; or 9 : 1 40 mM NaOAc, pH 5.5 buffer : 10 mM HEPES-NaOH, 150 mM, NaCl, pH 7.0 buffer) were added to the 40 mM NaOAc + 15 mM MgCl<sub>2</sub>, pH 5.5 solution. After 24 h and/or 48 h a further addition of BT-1033 in either 10 mM HEPES-NaOH, 150 mM NaCl, pH 7.0 buffer; or 9 : 1 40 mM NaOAc, pH 5.5 buffer : 10 mM HEPES-NaOH, 150 mM, NaCl, pH 7.0 buffer) was added if required. The reactions were incubated at 37 °C for the time stated in Table 14-Table 23. Please refer to Table 14-Table 23 for details about the individual reactions.

#### *8.6.2.2 BT-1033 catalysed reactions general reaction termination procedure*

Reaction samples were diluted 1:1 with 40 mM NaOAc, pH 5.5 buffer and the resultant sample then further diluted 1:1 with EtOH. The samples were then centrifuged at 12,300 × g for 10 minutes and the supernatant was collected. The cell pellet was then resuspended in EtOH (the volume of EtOH added was equivalent to the previous volume of EtOH used to dilute the sample). The samples were then once-more centrifuged at 12,300 × g for 10 minutes and the supernatant collected and combined with the previous supernatant. The sample supernatants were then diluted with water (to reduce the EtOH content to below 10%) and lyophilised prior to further analysis.

#### *8.6.2.3 BT-1033 general ITAG procedure used*

A sample of reporter (in H<sub>2</sub>O) was charged with a solution of ITag reagent **6.16** (in DMSO). The solution was then mixed and further charged with a premixed solution of CuSO<sub>4</sub>·5H<sub>2</sub>O and THPTA (of appropriate concentrations in H<sub>2</sub>O). Finally, the reaction was charged with a solution of sodium ascorbate (of appropriate concentration in H<sub>2</sub>O). The reaction mixtures were stirred and incubated at r.t. for 2 h with 300 rpm. The reaction mixtures were lyophilised for further analysis. The reaction equivalents used for each reaction are tabulated in Table 29.

## Experimental

Table 29. The reaction equivalents of each reagent used during each of the ITag reactions

Reaction entry	Equivalences of reporter N <sub>3</sub>	Equivalences of reporter Itag reagent <b>6.16</b>	Equivalences of CuSO <sub>4</sub>	Equivalences of THPTA	Equivalences of sodium ascorbate
2	1	1	10	10	20
3	1	1	12	12	24
4	1	1	10	10	20
5	1	1	10	10	20
6	1	1	10	10	20
7	1	1	10	10	20
7 scale-up	1	1	10	10	20
8	1	1	10	10	20
9	1	1	10	10	20
10	1	1	10	10	20
11	1	1	10	10	20
12	1	1	10	10	20
13	1	1	10	10	20
14	1	1	10	10	20
15	1	1	10	10	20
16	1	1	10	10	20
17	1	1	10	10	20
18	1	1	10	10	20
19	1	5	50	50	100
20	1	5	50	50	100
21a	1	5	50	50	100
21b	1	1	10	10	20
22a	1	5	50	50	100
22b	1	5	50	50	100
23a	1	5	50	50	100
23b	1	1	10	10	20
24a	1	5	50	50	100
24b	1	1	10	10	20
25a	1	1	10	10	20
25b	1	5	50	50	100
26a	1	1	10	10	20
26b	1	5	50	50	100
27a	1	5	50	50	100
27b	1	5	50	50	100

Experimental

27b repeat ITag	1	1	10	10	20
28a	1	5	50	50	100
28b	1	5	50	50	100
28b repeat ITag	1	1	10	10	20
29a	1	5	50	50	100
29b	1	5	50	50	100
29b repeat ITag	1	1	10	50	100
29 scale-up	1	1	10	10	20
30a	1	1	10	10	20
30b	1	1	10	10	20
31a	1	5	50	50	100
31b	1	5	50	50	100
32a	1	1	10	10	20
32b	1	1	10	10	20
33a	1	1	10	10	20
33b	1	1	10	10	20
34a	1	5	50	50	100
34b	1	5	50	50	100
35a	1	5	50	50	100
35b	1	5	50	50	100
36a	1	5	50	50	100
36b	1	5	50	50	100
37a	1	1	10	10	20
37b	1	1	10	10	20
38a	1	1	10	10	20
38b	1	1	10	10	20
39a	1	1	10	10	20
39b	1	1	10	10	20
40a	1	1	10	10	20
40b	1	1	10	10	20
41a	1	1	10	10	20
41b	1	1	10	10	20
42a	1	1	10	10	20
42b	1	1	10	10	20
43a	1	1	10	10	20
43b	1	1	10	10	20
44a	1	1	10	10	20
44b	1	1	10	10	20
45a	1	1	10	10	20
45b	1	1	10	10	20

## Experimental

### 8.6.2.4 Purification procedure used for Entry 29 scale up, Entry 34 scale up, Table 23

Purification was performed using a column containing Bio-Gel P-2 resin (BIO RAD) which had been equilibrated into water. The crude sugar sample was loaded on to the column in 2 mL of water, and the column was run in water (approximate flow rate between 12 mL / h – 30 mL / h). The fractions containing the desired disaccharide were identified using LCMS and were combined and lyophilised prior to further analysis.

Mass of disaccharide extracted from BT-1033 Entry 29 scale up (Table 23) = 2.7 mg (58%)

Mass of disaccharide extracted from BT-1033 Entry 34 scale up (Table 23) = 1.3 mg (36%)

### 8.6.2.5 NMR analysis of Disaccharide extracted from BT-1033 Entry 29 scale up

$^1\text{H}$  (600 MHz,  $\text{D}_2\text{O}$ )  $\delta$  4.66 (s, 1H, H-1b), 4.41 (m, 1H, H-1a), 3.95 (d,  $J_{2,3} = 3.1$  Hz, 1H, H-2b), 3.86 (m, 1H,  $\text{CH}_2$ ), 3.80 (m, 2H, H-6a, H-6b), 3.62 (m, H-6'a, H-6'b, H-5a, H-5b, H-2a), 3.55 (m, 2H, H-3b,  $\text{CH}_2$ ), 3.46 (m, 2H, H-4b, H-3a/H-4a), 3.31 (m, 1H, H-3a/H-4a), 3.26 (m, 2H,  $\text{CH}_2$ ), 1.94 (s, 3H,  $\text{CH}_3$ ), 1.73 (p,  $J_{\text{CH}_2} = 6.4$  Hz,  $\text{CH}_2$ ).

$^{13}\text{C}$  (150 MHz,  $\text{D}_2\text{O}$ )  $\delta$  174.5 (1C, C=O), 101.1 (1C,  $J_{\text{CH}} = 162$  Hz, C-1a), 100.0 (1C,  $J_{\text{CH}} = 160$  Hz, C-1b), 78.9 (1C, X), 76.4 (1C, X), 74.5 (1C, X), 72.7 (1C, C-3b), 72.2 (1C, X), 70.5 (1C, C-2b), 67.1 (1C,  $\text{CH}_2$ ), 66.5 (1C, X), 60.8 (1C, C-6a/b), 60.1 (1C, C-6a/6b), 54.9 (1C, X), 47.7 (1C,  $\text{CH}_2$ ), 28.0 (1C,  $\text{CH}_2$ ), 22.1 (1C,  $\text{CH}_3$ ).

X= 2a, 3a, 4a, 5a, 4b, 5b

### 8.6.2.6 NMR analysis of Disaccharide extracted from BT-1033 Entry 34 scale up

Unfortunately, the NMR data gathered here was difficult to fully analyse, mainly due to there being one too-few peaks in the  $^1\text{H}$  spectrum with respect with how many  $^1\text{H}$  environments would be expected. However, we believe it likely (due to evidence from two-dimensional NMR techniques) that an additional  $^1\text{H}$  peak is located under the residual solvent  $\text{D}_2\text{O}$  peak. Furthermore, the  $^{13}\text{C}$  spectrum is also missing a C=O environment signal (although this signal would be from a quaternary carbon, and thus would be expected to be of low intensity). However, rough analysis of both the  $^1\text{H}$  and  $^{13}\text{C}$  spectra has been performed and a CLIP-HSQC experiment has been performed to extract the  $J_{\text{CH}}$  coupling constants for both the anomeric carbons.

$^1\text{H}$  (700 MHz,  $\text{D}_2\text{O}$ )  $\delta$  4.70 (s, 1H), 4.58 (d,  $J = 7.9$  Hz), 4.09 (d,  $J = 3.3$  Hz), 3.97 (td,  $J = 10.7$  Hz,  $J = 6.0$ , 1H), 3.94 (dd,  $J = 12.4$  Hz,  $J = 2.3$  Hz, 1H), 3.84 (m, 1H), 3.75 (m, 5H), 3.67 (m, 2H), 3.59 (dd, 1H), 3.44 (m, 1H), 3.38 (m, 2H), 2.06 (s, 3H), 1.85 (m, 2H)

$^{13}\text{C}$  (175 MHz,  $\text{D}_2\text{O}$ )  $\delta$  101.3 ( $J_{\text{CH}} = 159$  Hz, C-1a), 100.0 ( $J_{\text{CH}} = 164$  Hz, C-1b), 82.3, 81.5, 77.6, 76.4, 72.8, 72.0, 70.7, 67.6, 66.5, 60.9, 55.1, 47.8, 28.2, 22.1

## Experimental

### 8.6.3 BT-1033 Crystallography

#### 8.6.3.1 Procedure for setting up a crystal tray

All 96- and 48-well crystal trays were set up using the Mosquito<sup>®</sup> LCP ttp labtech. All plates were made using an approximate concentration of between 10-15  $\mu\text{g}/\mu\text{L}$  BT-1033 (9.40 – 14.9  $\mu\text{g}/\mu\text{L}$ , see Table 30 for details). All 96-well plates were set up using a protein : reservoir ratio of 100 nL : 100 nL. The conditions used in both the 48-well plates (Index H8 based plate and JCSG B8 based plate) are attached in Appendix section 9.5.5, page ccxlv. A protein : reservoir ratio of 1 : 1 was used to prepare the JCSG B8 based plate, whereas the protein : reservoir ratio was varied in the Index H8 based plate (see appendix section 9.5.5, page ccxlv). The plates were imaged using a LEICA M212s microscope and images were taken using a CMEX DC500C camera (Euromex) (software- ImageFocus 4, Euromex).

Table 30. The concentrations of BT-1033 used to set up each crystal tray

Plate	Concentration of BT-1033 used
96-wells plates - PACT, AM <sub>4</sub> SO <sub>4</sub> , Morpheus, INDEX and JCSG plates	9.4 – 12.3 $\mu\text{g}/\mu\text{L}$
48 well plates – Index H8 based plate, JCSG B8 based plate	Lanes A-G - 9.4 – 12.3 $\mu\text{g}/\mu\text{L}$ Lane H 11.4- 14.9 $\mu\text{g}/\mu\text{L}$

### 8.6.4 Investigation into BT-1033 thioglycoligases activity

#### 8.6.4.1 BT-1033 catalysed reactions general reaction set up procedure for Entries 43a-44b

A solution of 40 mM NaOAc, 26 mM TCEP, pH 5.5 buffer was charged with MgCl<sub>2</sub> (in 40 mM NaOAc, pH 5.5 buffer) to a final concentration of 15 mM MgCl<sub>2</sub>. **Donor** (in 40 mM NaOAc, pH 5.5 buffer), **Acceptor** (in 40 mM NaOAc, pH 5.5 buffer) and BT-1033 (in 9 : 1 40 mM NaOAc, pH 5.5 buffer : 10 mM HEPES-NaOH, 150 mM NaCl, pH 7.0 buffer) were then added. The final concentration of TCEP in the resultant solution was 4.94 mM). The reactions were then incubated at 37 °C for the times tabulated in Table 24. After 24 h and/or 48 h a further addition of BT-1033 in either 10 mM HEPES-NaOH, 150 mM NaCl, pH 7.0 buffer; or 9 : 1 40 mM NaOAc, pH 5.5 buffer : 10 mM HEPES-NaOH, 150 mM, NaCl, pH 7.0 buffer) was added if required. Please see Table 24 for details about individual reactions, see experimental section 8.6.2.2, page 337, see experimental section 8.6.2.3, page 337 for the general ITag procedure, see Table 29 for details on ITag reaction equivalents, and see Table 38 for ITag reaction results.

## Experimental

### 8.6.4.2 Enzyme free control general reaction set up procedure for Entries 45a and 45b

A solution of 40 mM NaOAc, 26 mM TCEP, pH 5.5 buffer was charged with MgCl<sub>2</sub> (in 40 mM NaOAc, pH 5.5 buffer) to a final concentration of 15 mM MgCl<sub>2</sub>. **Donor** (in 40 mM NaOAc, pH 5.5 buffer) and **Acceptor** (in 40 mM NaOAc, pH 5.5 buffer) were then added. The final concentration of TCEP in the resultant solution was 4.94 mM). The reactions were then incubated at 37 °C for the times tabulated in Table 24. (See Table 24 for reaction conditions, see experimental section 8.6.2.2, page 337 for the general reaction termination procedure, see experimental section 8.6.2.3, page 337 for the general ITag procedure, see Table 29 for detail on ITag reaction equivalents, and see Table 38 for ITag results).

### 8.6.4.3 Attempt at preparing the BT-1033 mutants

A Quikchange™ Site-Directed Mutagenesis Kit (Agilent Technologies) was used to attempt to modify BT-1033\_pET-24(+) (which codes for the WT BT-1033 protein) to prepare plasmids coding for two different BT-1033 mutants. The method followed is described in the Quikchange™ Site-Directed Mutagenesis Kit instruction manual. The primers designed are shown in Table 31 and the composition of the Quikchange™ PCR reaction mixture is shown in Table 32.

Table 31. The primers designed for use in Quikchange™ Site-Directed Mutagenesis

Oligo name	Sequence (5' → 3')	Length (bp)	GC%	Tm (Å °C)
a302c_for (D to A)	CCACGTAACACGCGGGGCATATTTATATTCGGATTC	36	47.2	63.9
a302c_rev (D to A)	GAATCCGAATATAAATATGCCCCGCGTGTTACGTGG	36	47.2	63.9
a302g_for (D to G)	CCACGTAACACGCGGGCCATATTTATATTCGGATTC	36	42.7	63.9
a302g_rev (D to G)	GAATCCGAATATAAATATGCCCCGCGTGTTACGTGG	36	47.2	63.9

## Experimental

Table 32. PCR reaction composition for Quikchange™ Site-Directed Mutagenesis

Reaction components	Quantity
Reaction buffer (x 10)	5 µL
BT-1033 plasmid (the dsDNA template)	15 – 35 ng*
Forward primer	125 ng
Reverse primer	125 ng
dNTP mix	1 µL
PfuTurbo DNA polymerase (2.5 U / µL)	1 µL
Double-distilled water	to 50 µL

\*Note amount of dsDNA template was varied during a screen of Quikchange™ Site-Directed Mutagenesis conditions.

Table 33. The PCR reaction stages and conditions used during Quikchange™ Site-Directed Mutagenesis

Step	Temperature (°C)	Time (s)	Cycles
Initial denature	95	30	1
Denaturation	95	30	12 or 16*
Annealing	55	60	
Extension	68	366	

\*Multiple attempts at making the alanine BT-1033 mutant were attempted, cycle number was varied between attempts to see if it could improve outcome.

Following temperature cycling, the reaction mixture was placed on ice for 2 minutes to cool the reaction to  $\leq 37$  °C. The reaction mixtures were then transformed into XL1-blue supercompetent cells and the cells plated (onto LB-kana agar) as detailed in the Quikchange™ Site-Directed Mutagenesis kit instruction manual. Alternatively, the reaction mixtures were transformed into Stellar™ Competent Cells (Takara Bio Inc). Colonies were selected and plasmids were harvested using a QIAprep Spin Miniprep Kit.

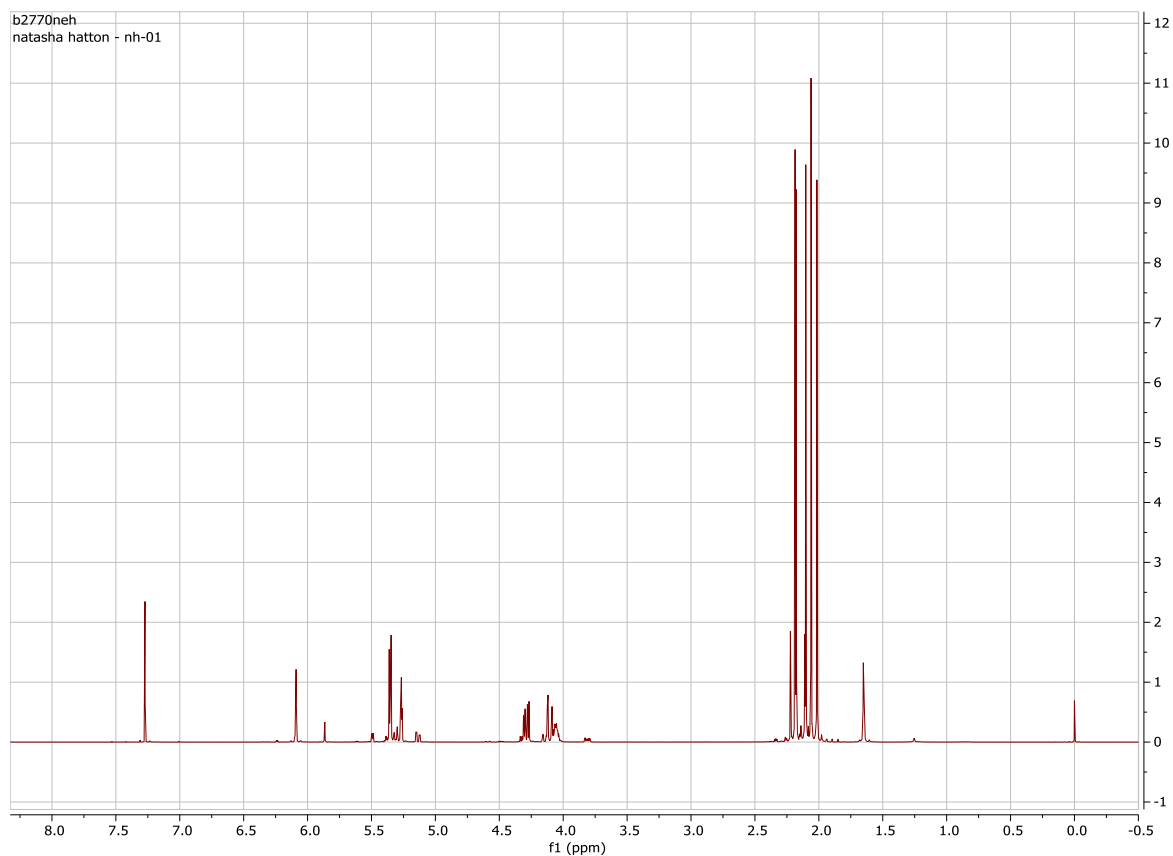
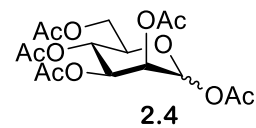
# Appendix

## Chapter 9 Appendix

### 9.1 Appendix for chapter 2

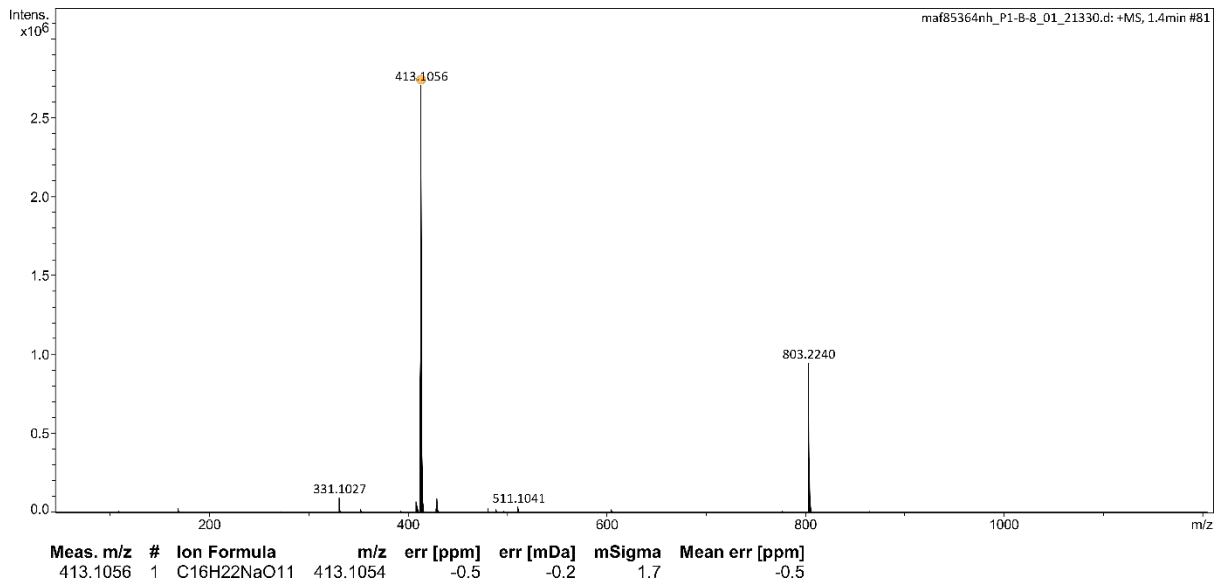
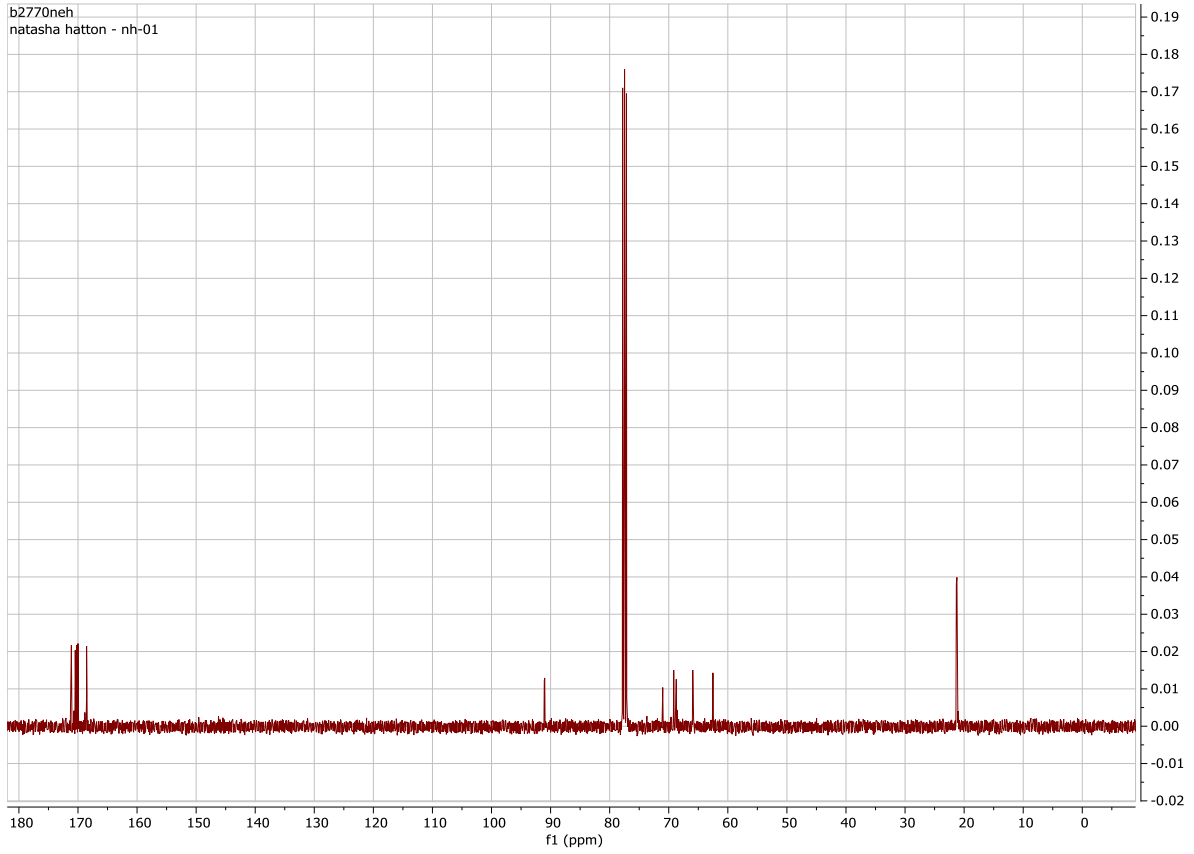
#### 9.1.1 Synthesis of 4-methylphenyl 2-benzyl-4,6-O-benzylidene-3-O-*p*-methoxybenzyl-1-thio- $\alpha$ -D-mannopyranoside **2.2**

##### 9.1.1.1 *D*-Mannose pentaacetate **2.4**

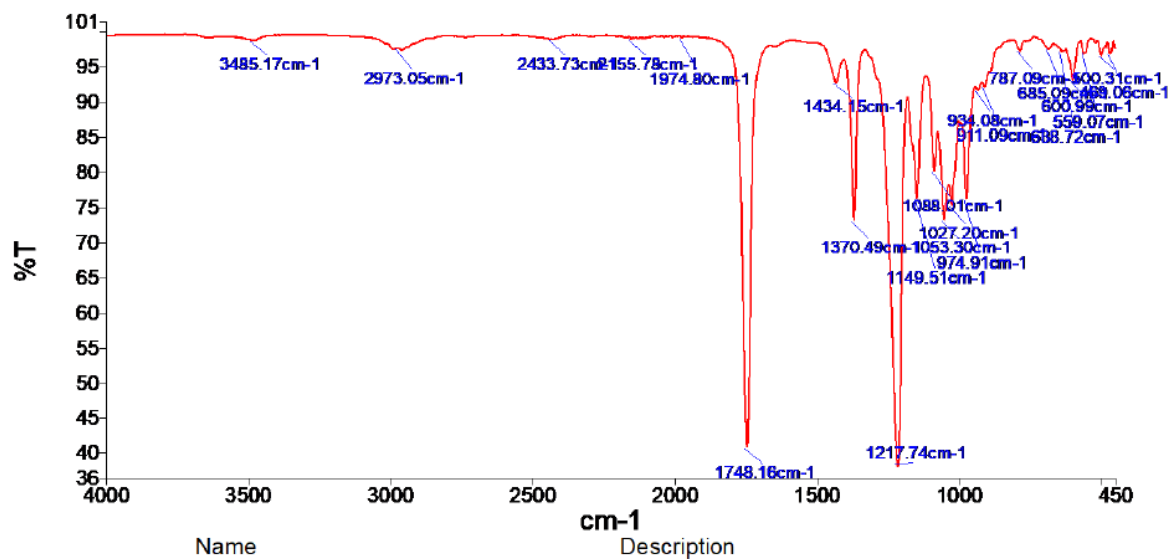




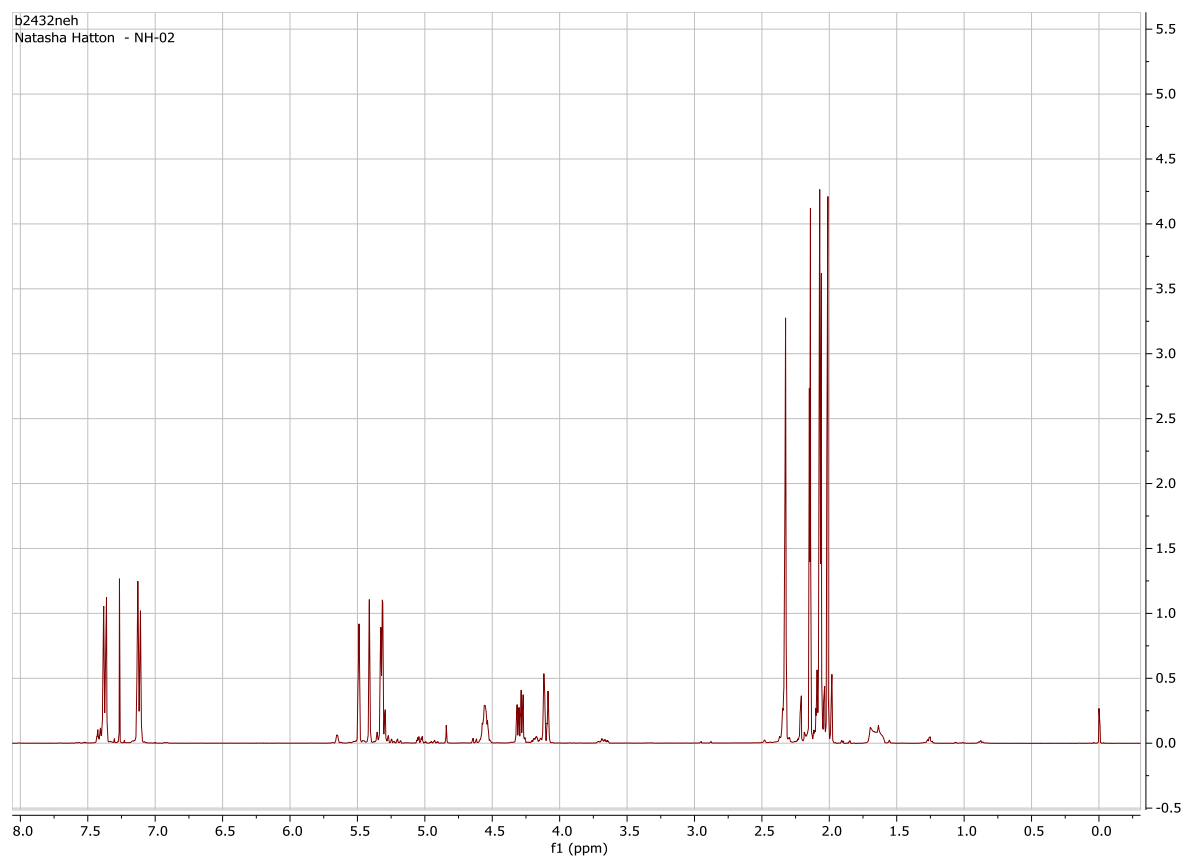
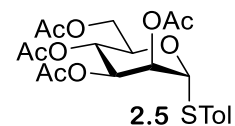
# Appendix



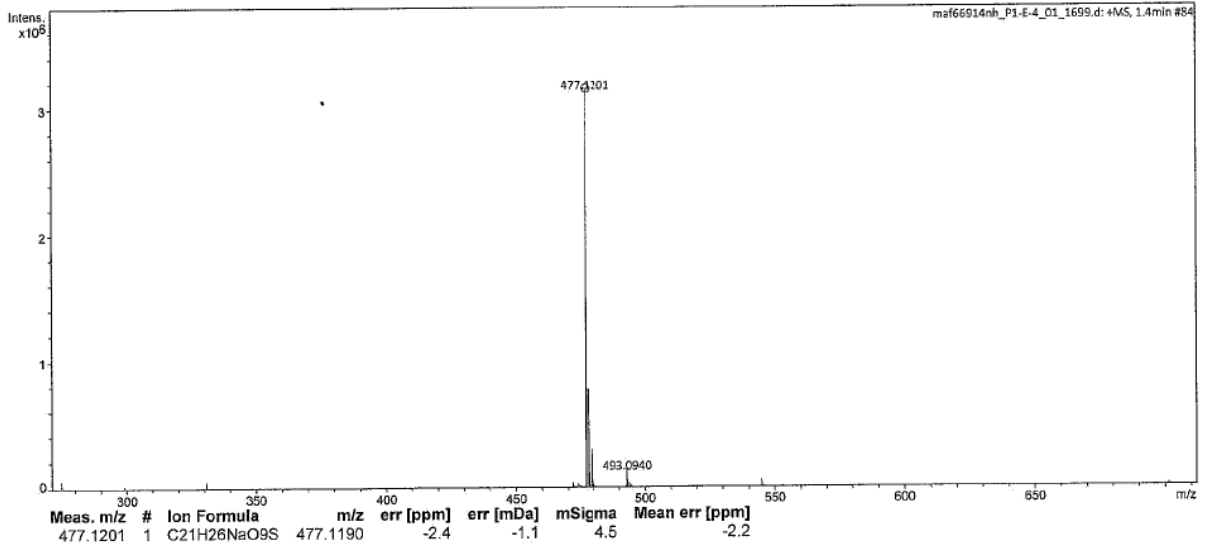
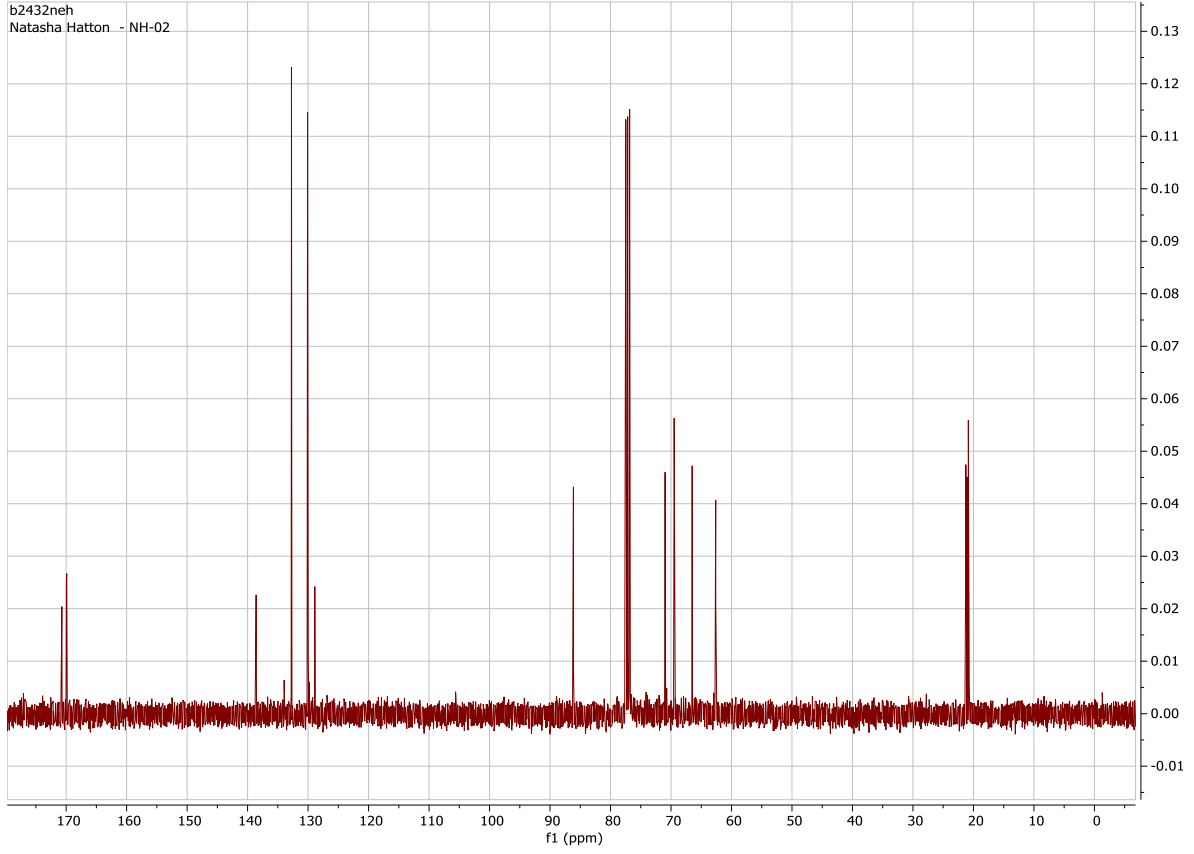
## Appendix



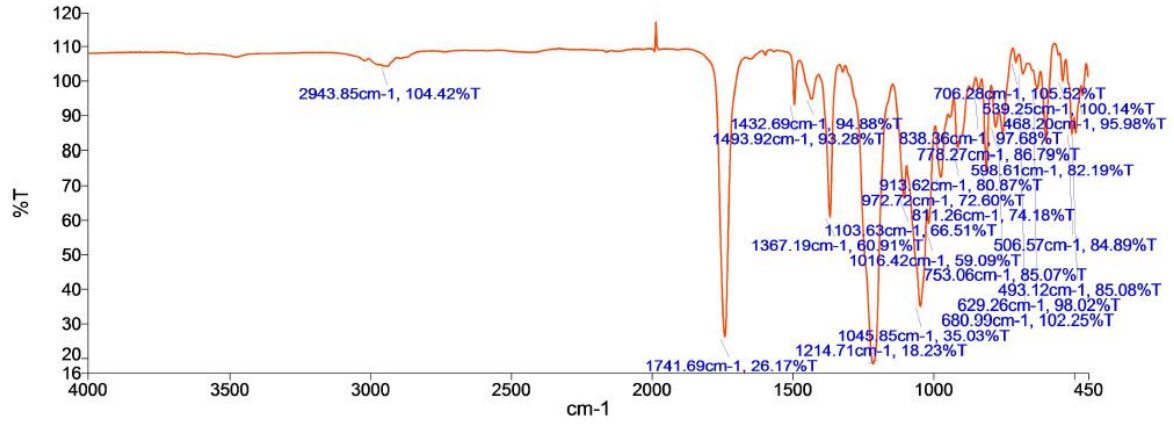
### 9.1.1.2 4-Methylphenyl 2,3,4,6-tetra-O-acetyl-1-thio- $\alpha$ -D-mannopyranoside 2.5



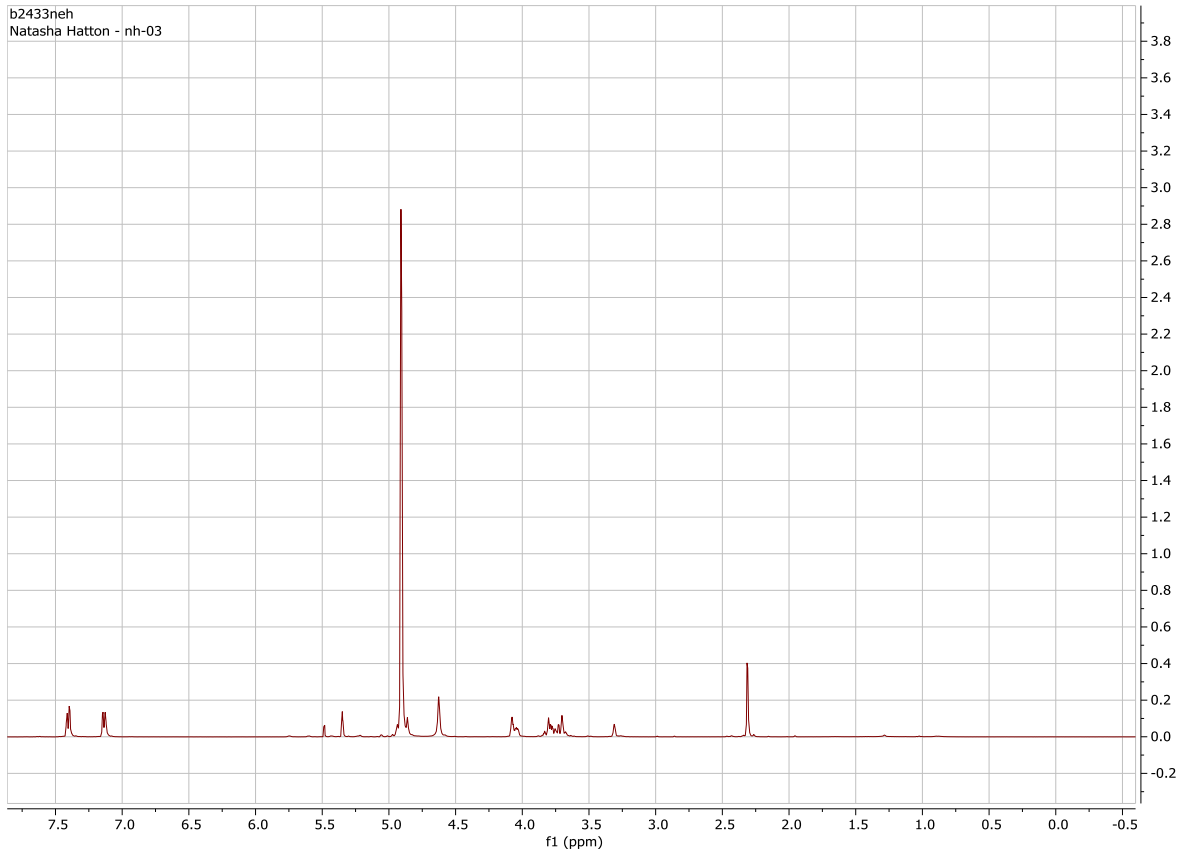
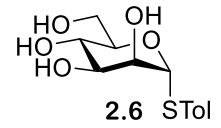
# Appendix



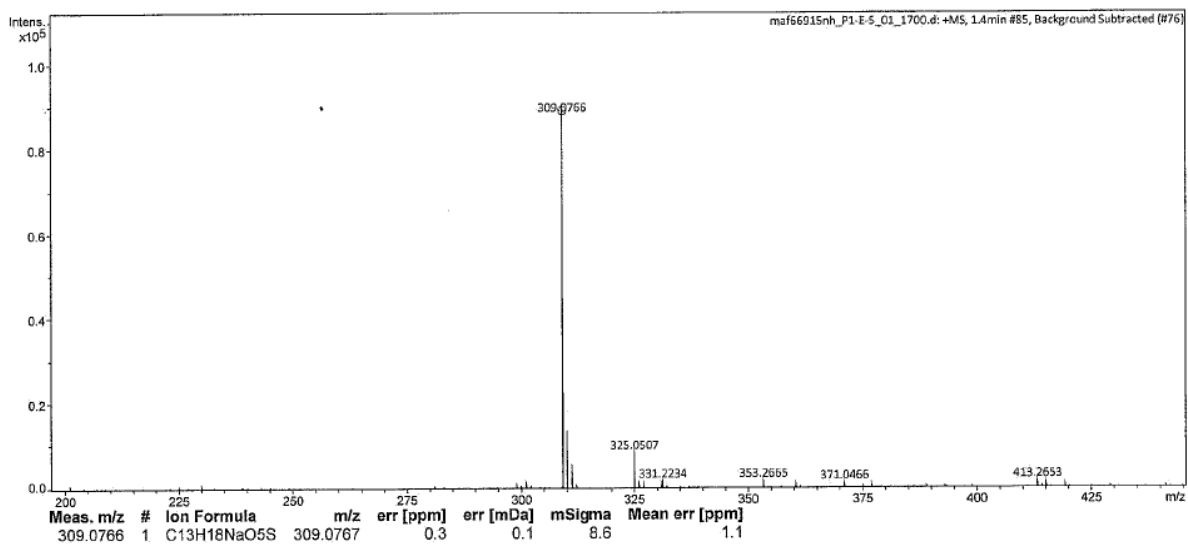
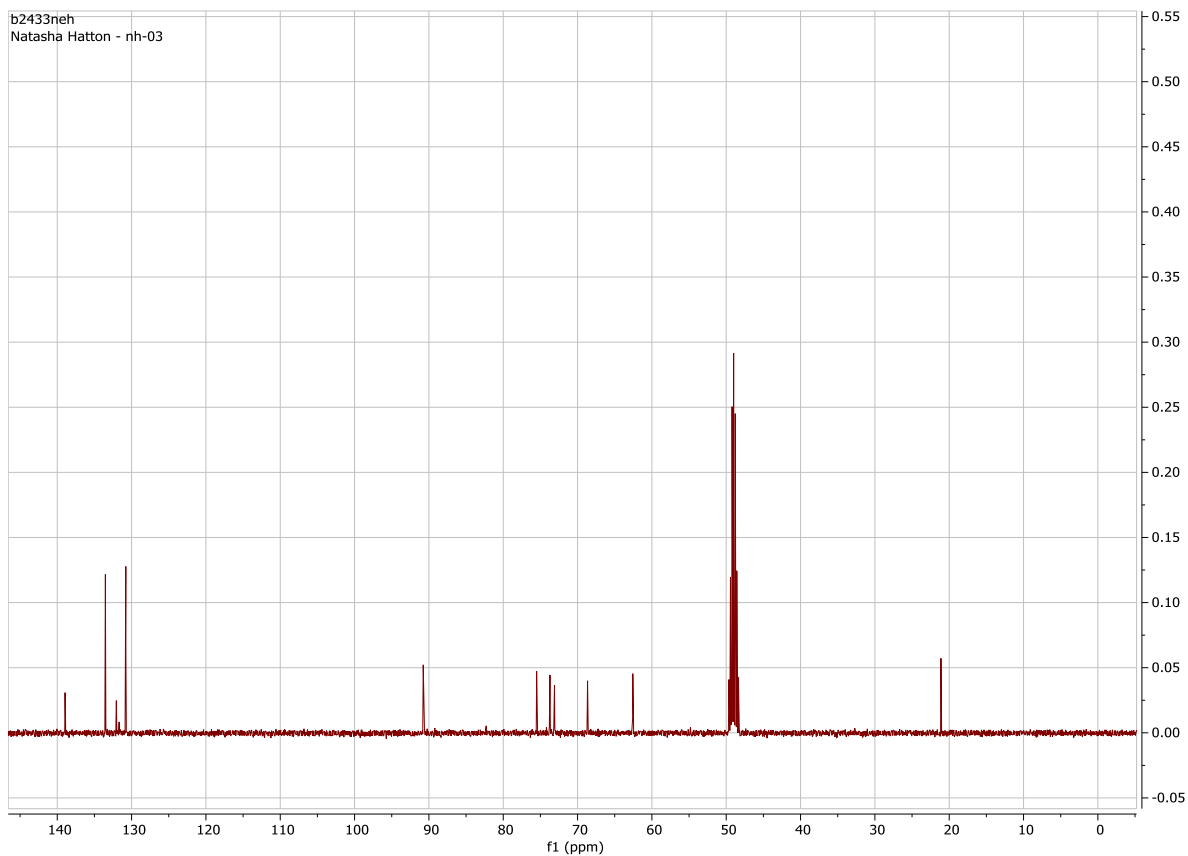
# Appendix



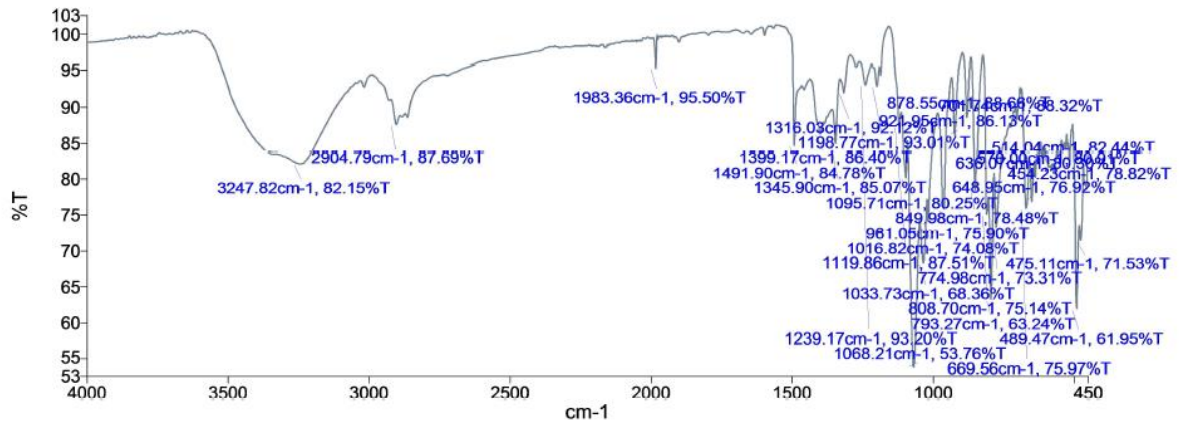
## 9.1.1.3 4-Methylphenyl 1-thio- $\alpha$ -D-mannopyranoside 2.6



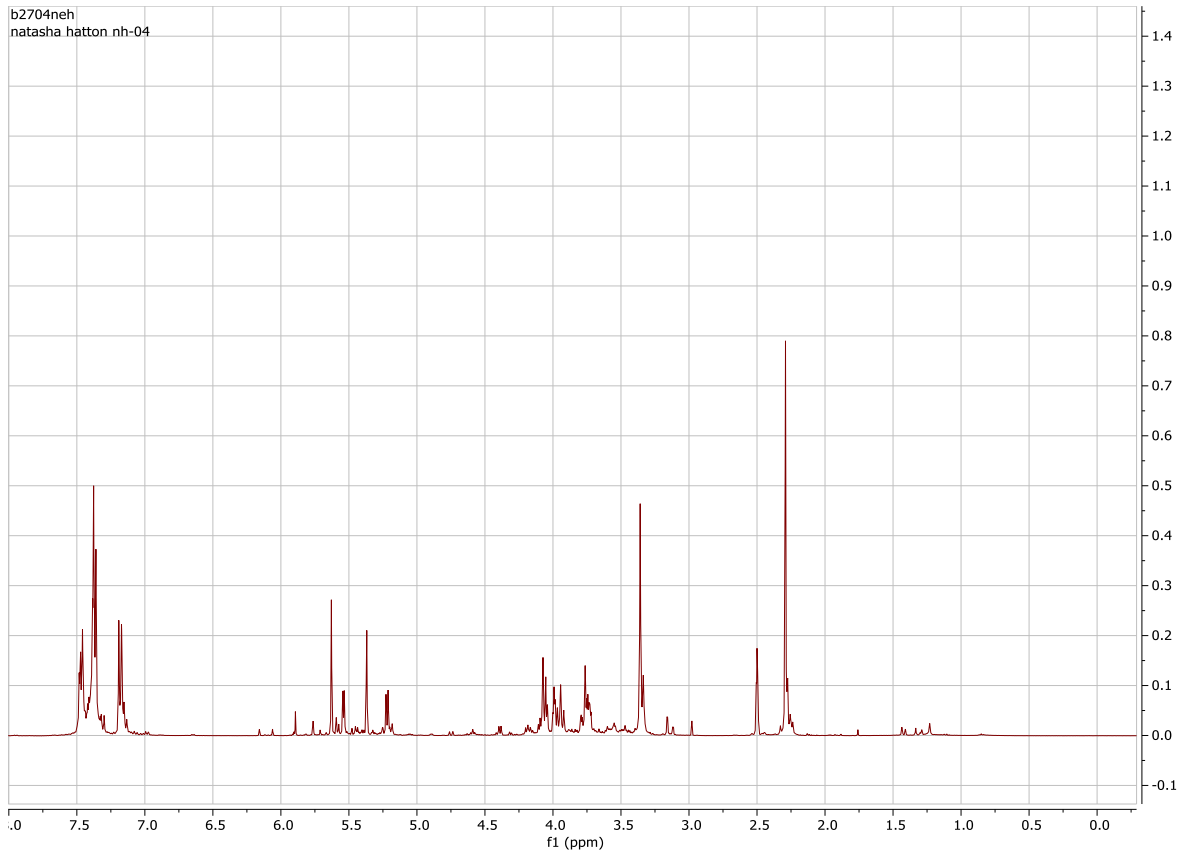
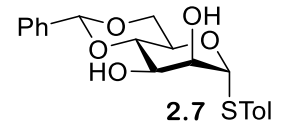
# Appendix



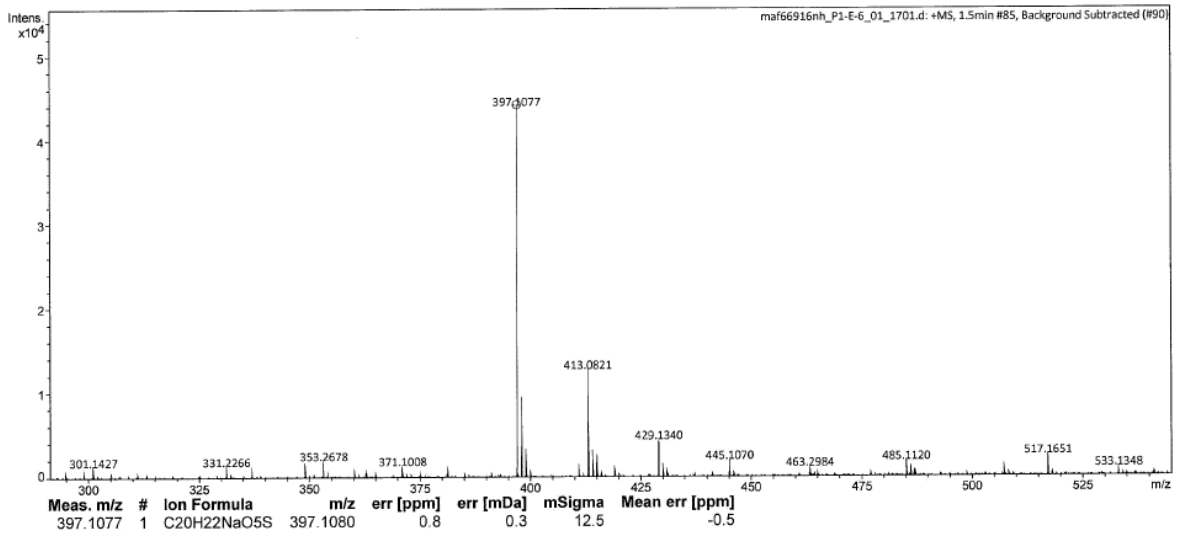
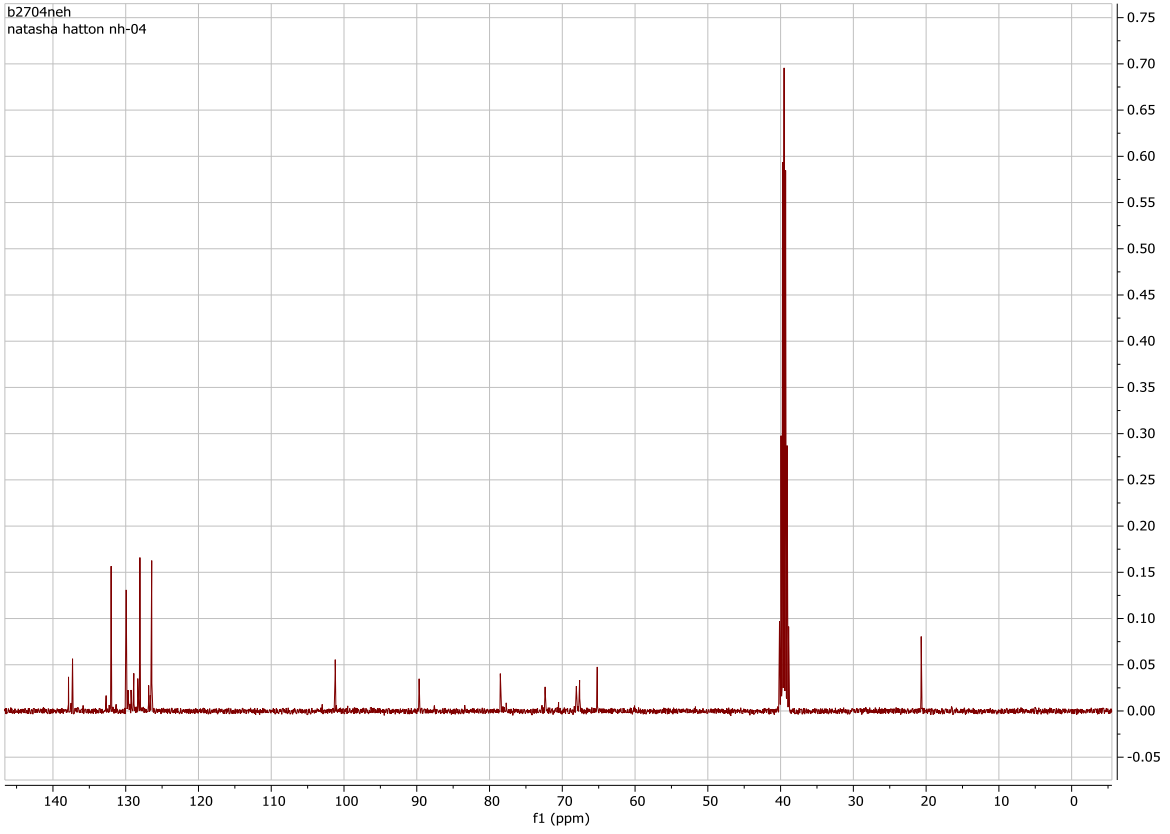
# Appendix



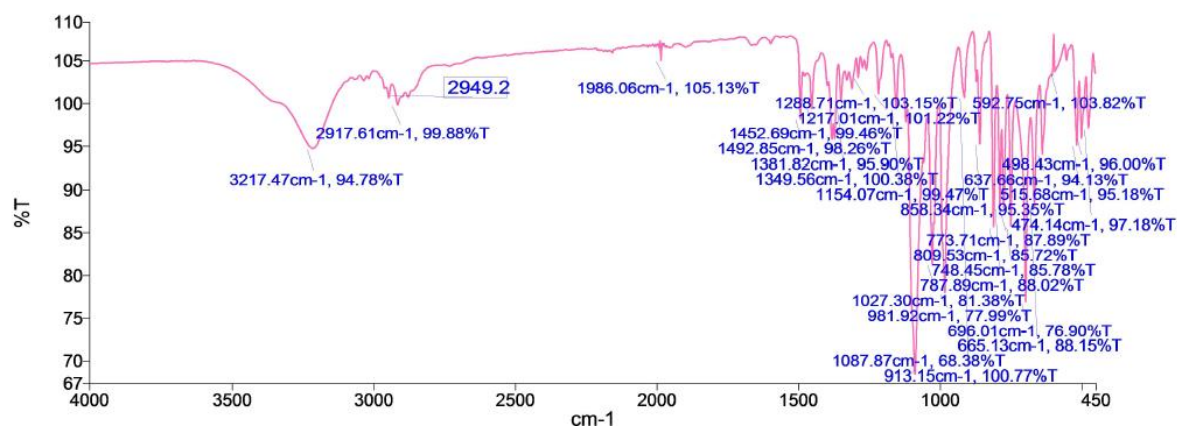
## 9.1.1.4 4-Methylphenyl 4,6-O-benzylidene-1-thio- $\alpha$ -D-mannopyranoside 2.7



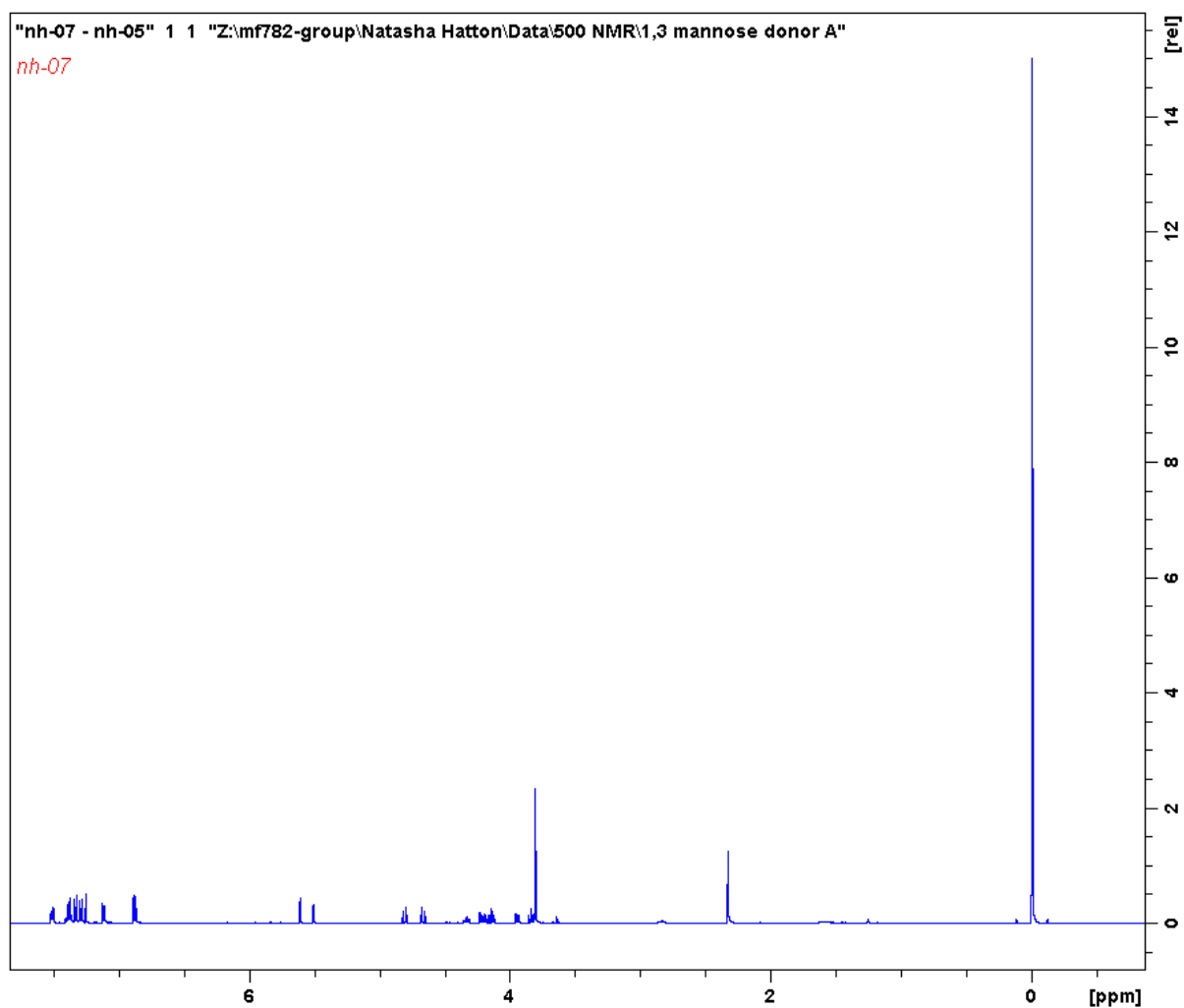
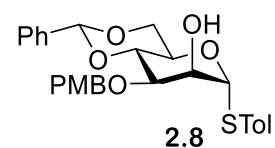
# Appendix



## Appendix

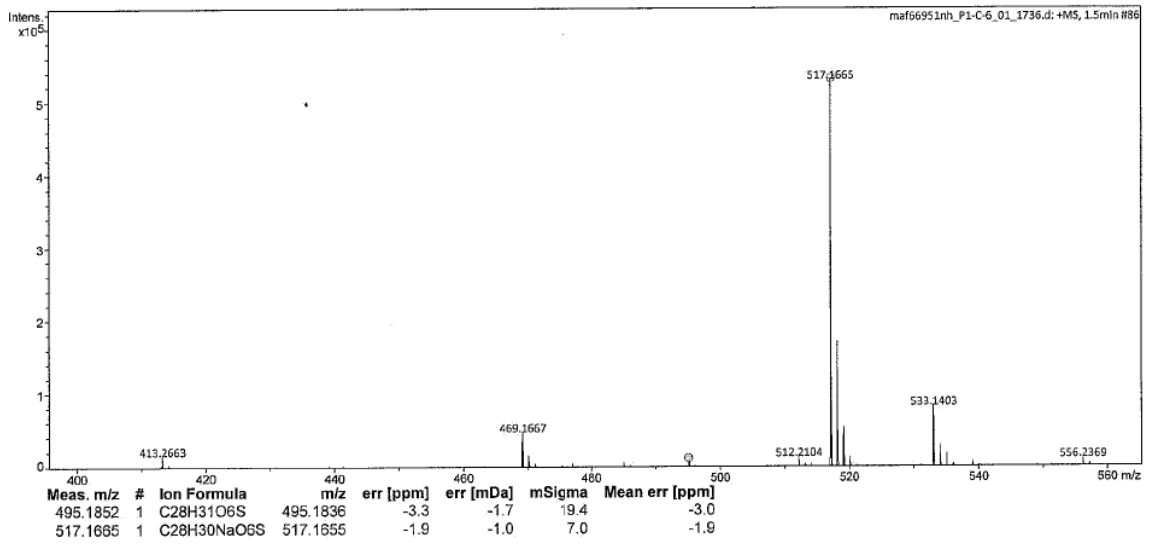
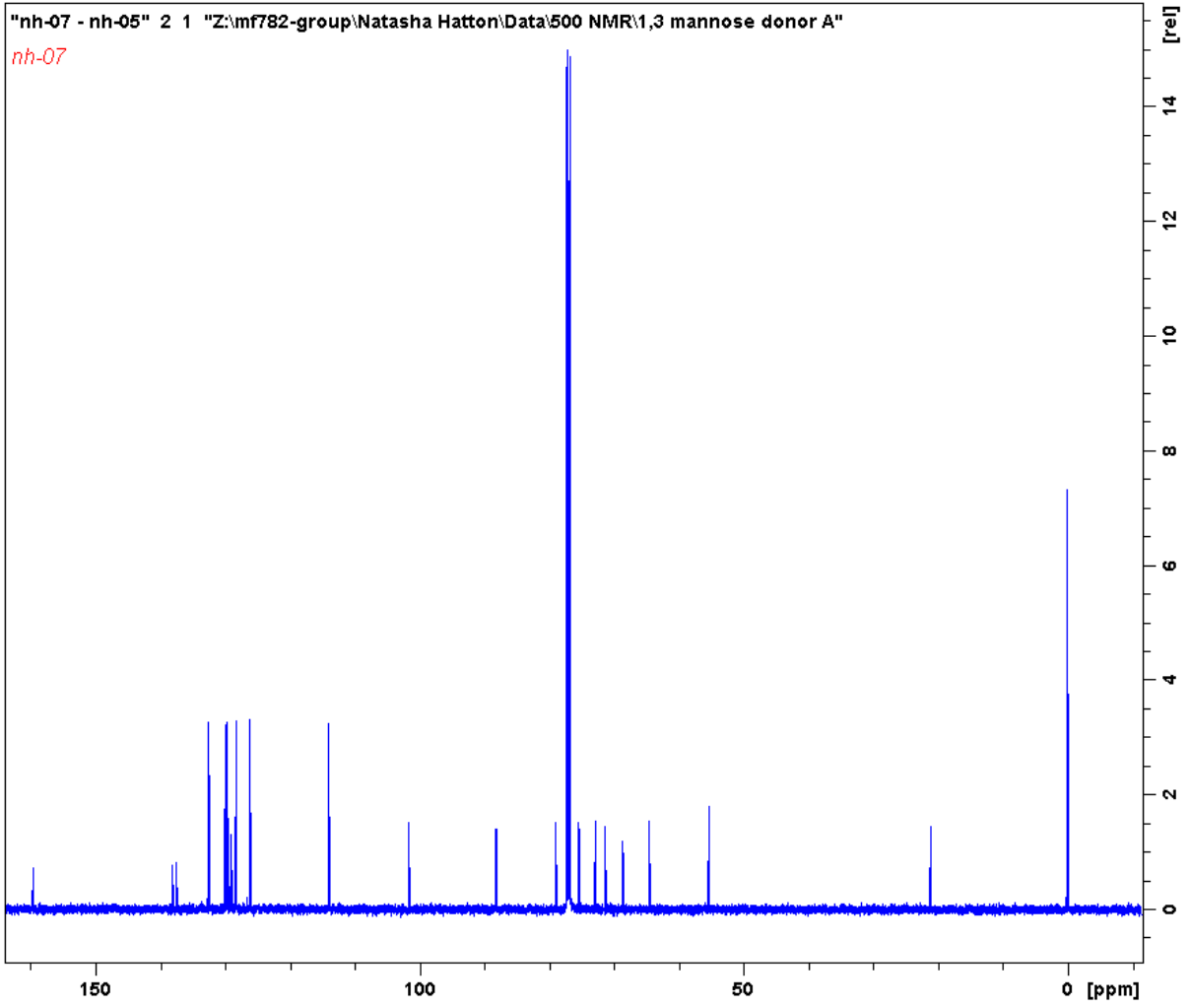


### 9.1.1.5 4-Methylphenyl 4,6-O-benzylidene-3-O-p-methoxybenzyl-1-thio- $\alpha$ -D-mannopyranoside 2.8

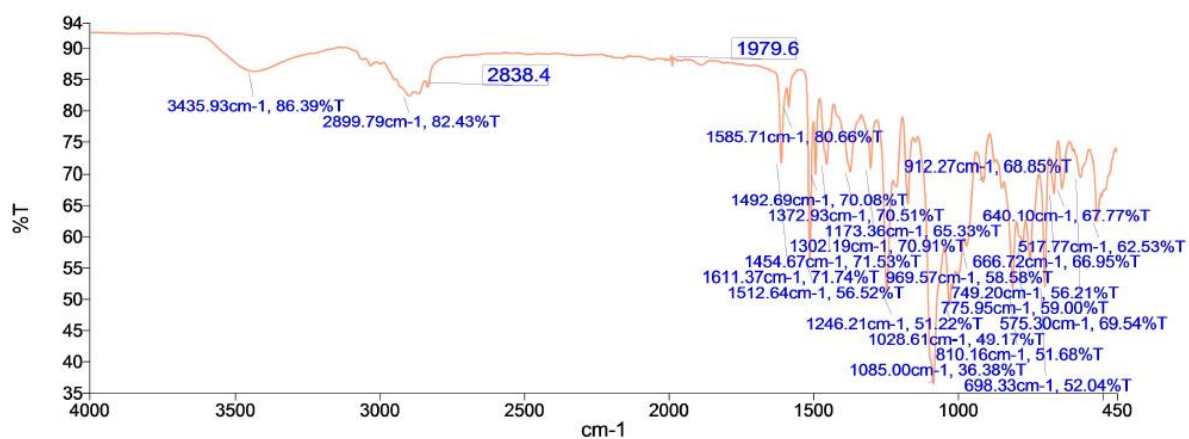




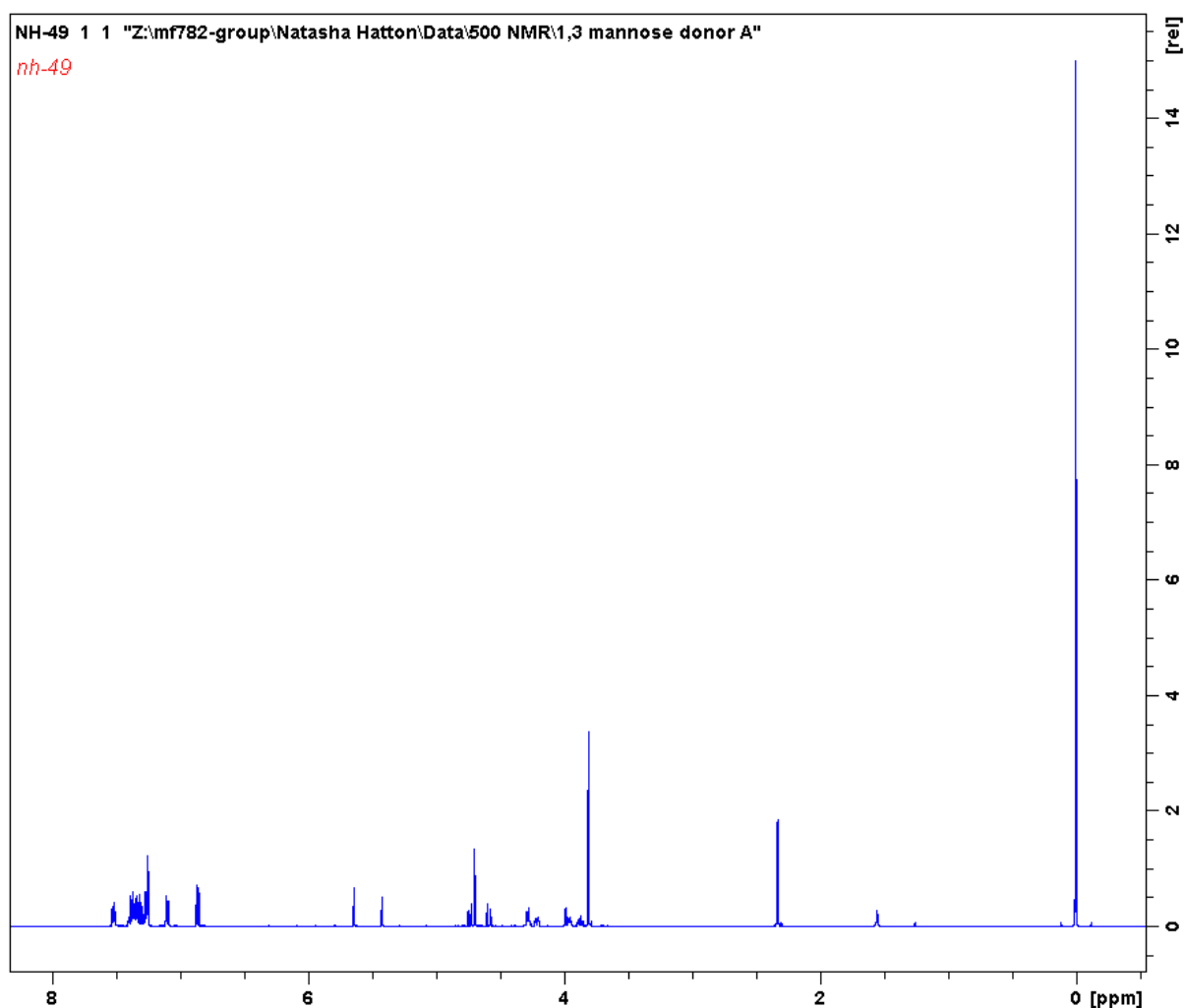
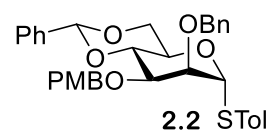
Appendix



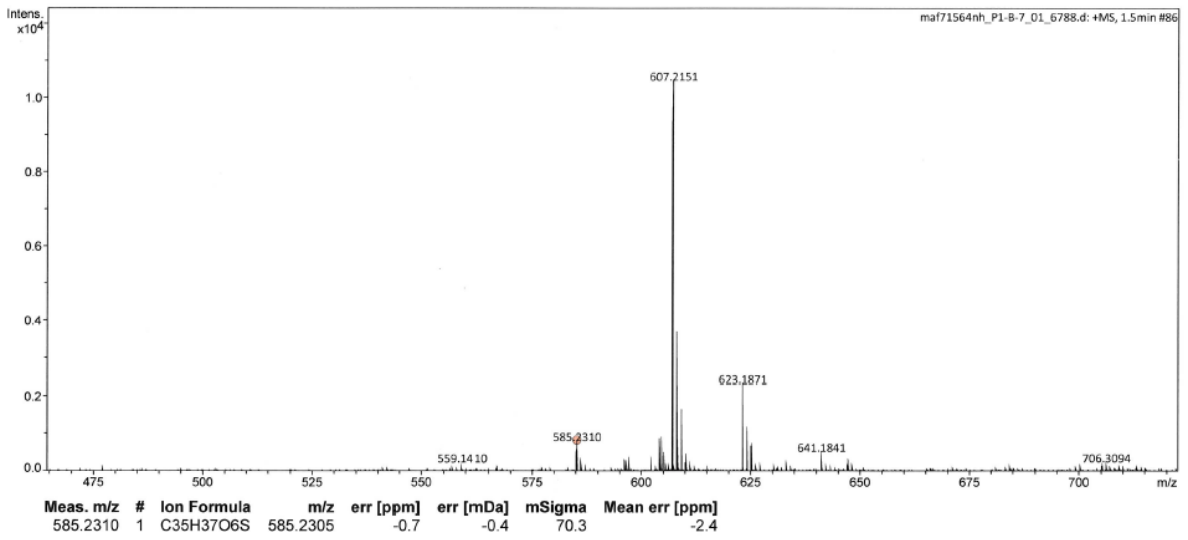
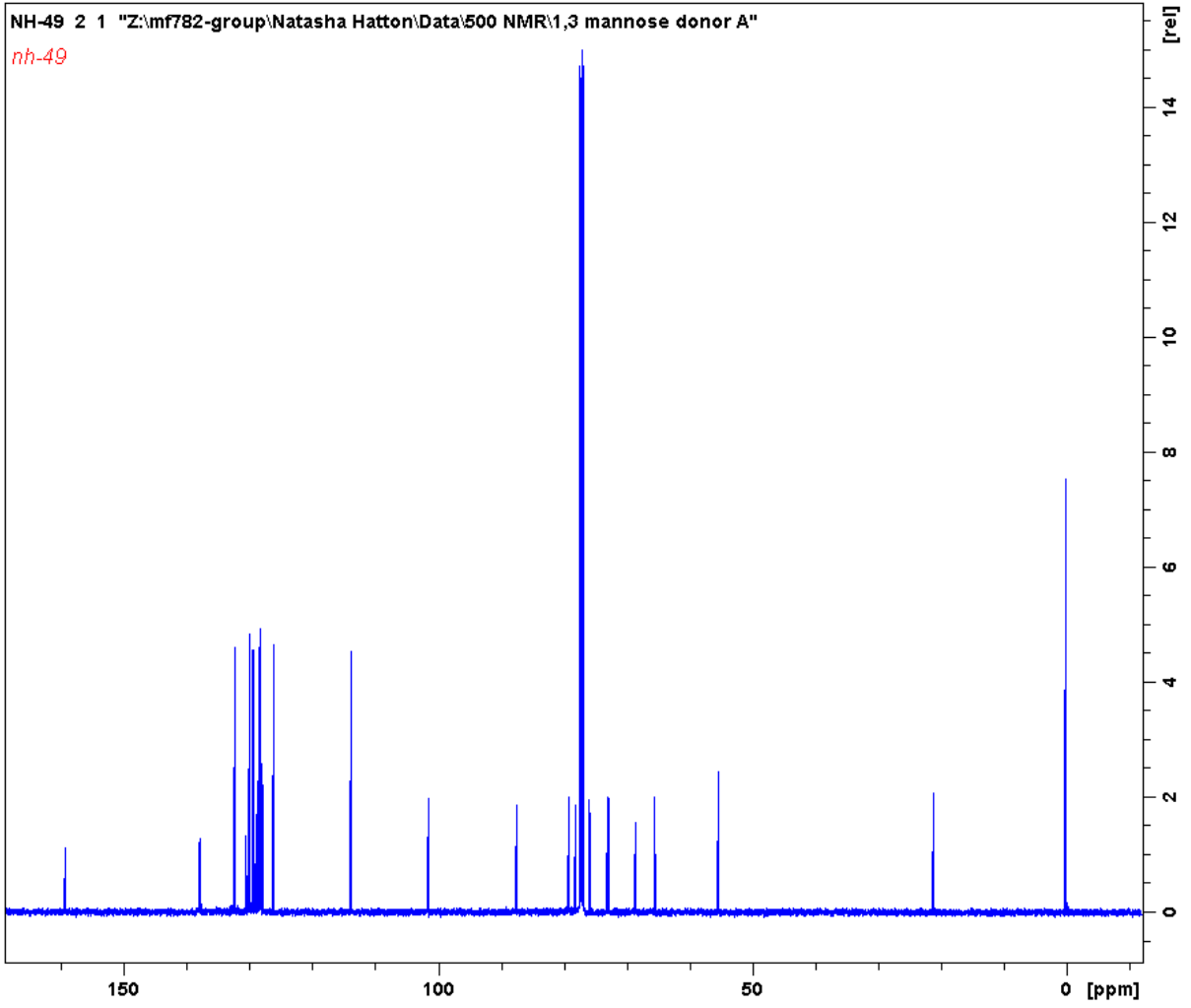
## Appendix



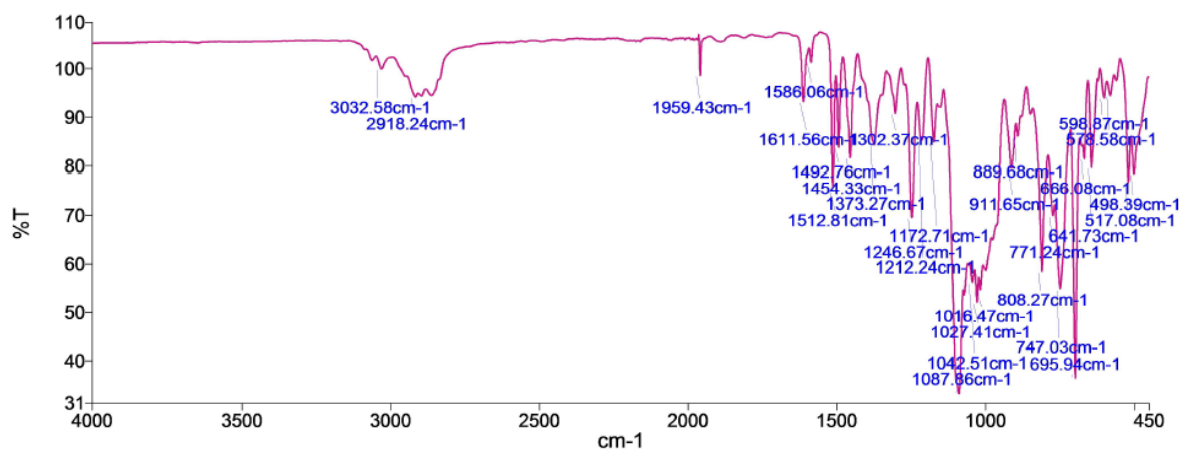
### 9.1.1.6 4-Methylphenyl 2-benzyl-4,6-O-benzylidene-3-O-p-methoxybenzyl-1-thio- $\alpha$ -D-mannopyranoside 2.2



# Appendix



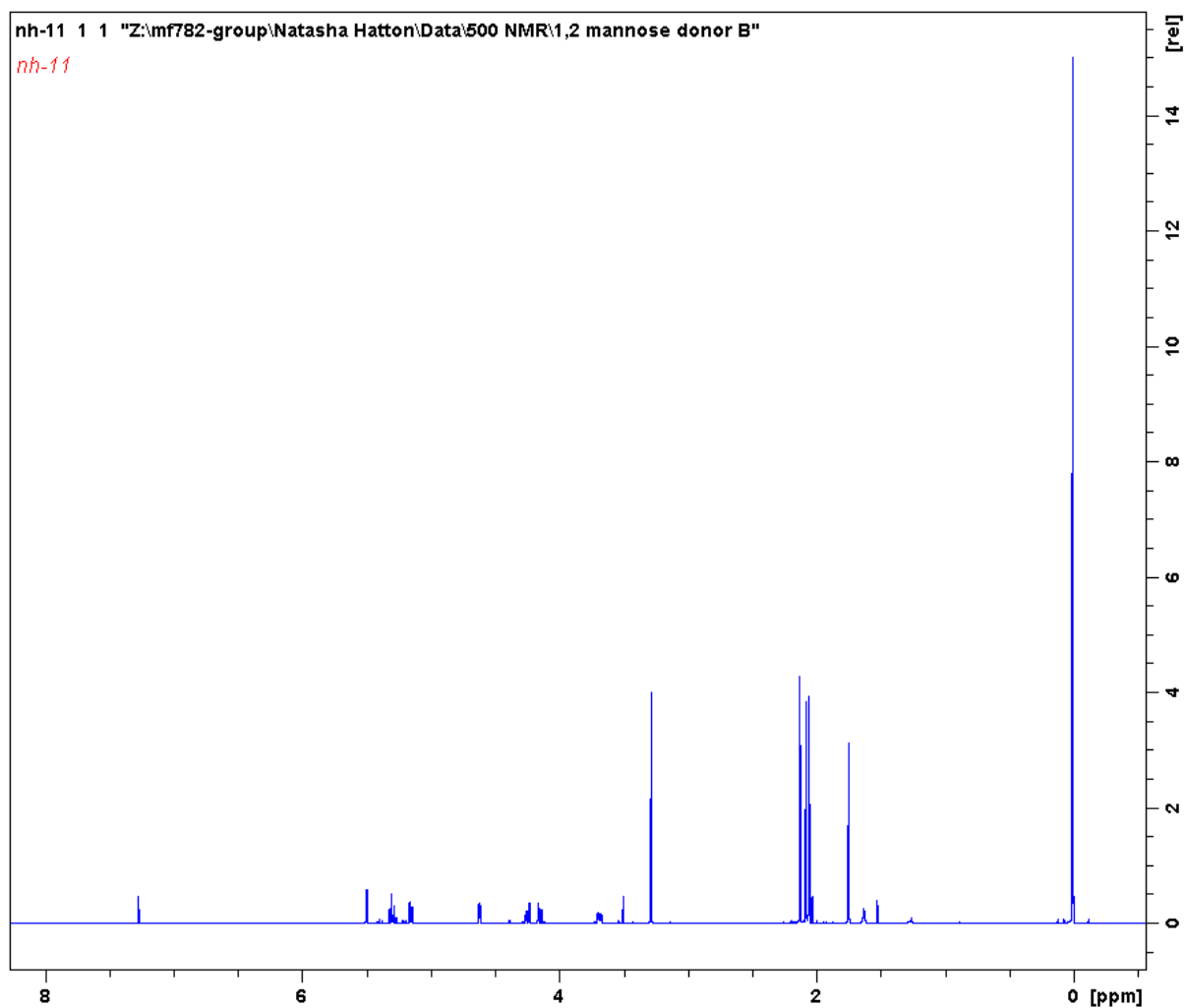
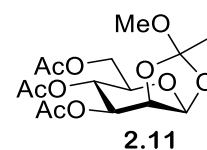
# Appendix



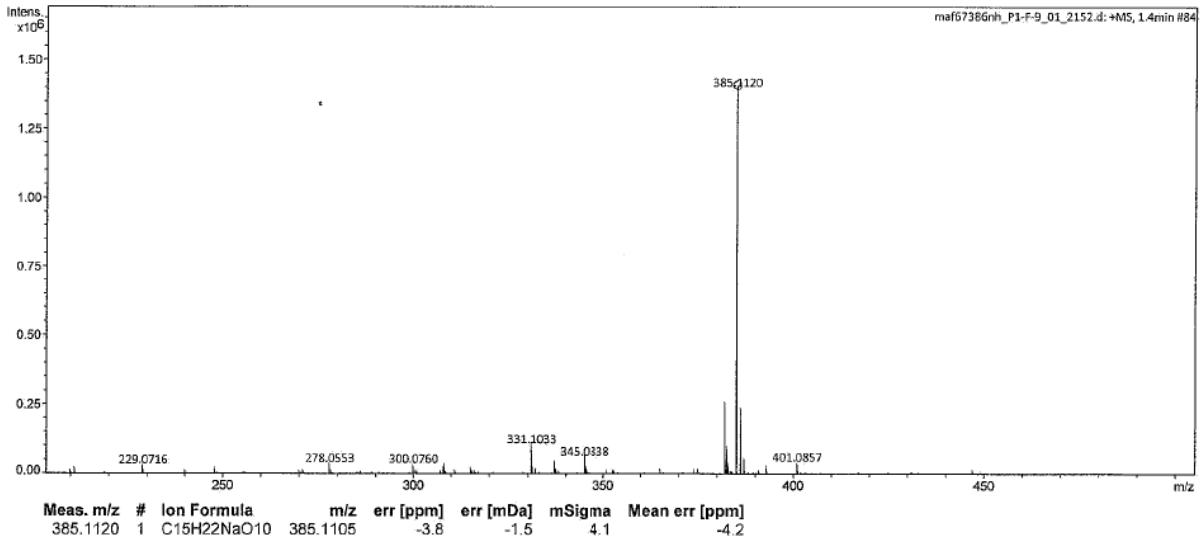
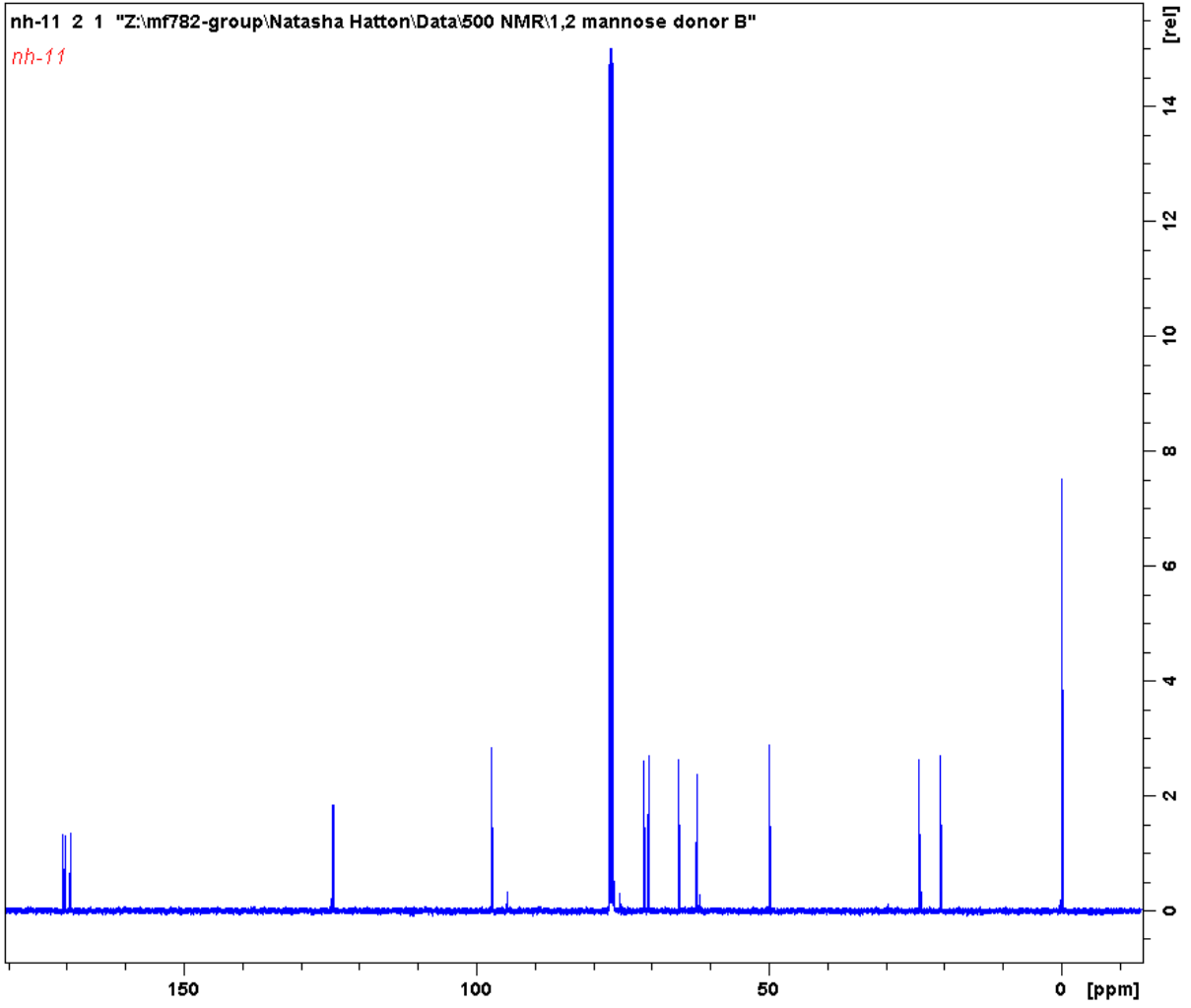
## Appendix

### 9.1.2 Synthesis of 4-methylphenyl 2-*O*-acetyl-3,4,6-tri-*O*-benzyl-1-thio- $\alpha$ -D-mannopyranoside **2.1a** and 4-methylphenyl 2-*O*-benzoyl-3,4,6-tri-*O*-benzyl-1-thio- $\alpha$ -D-mannopyranoside **2.1b**

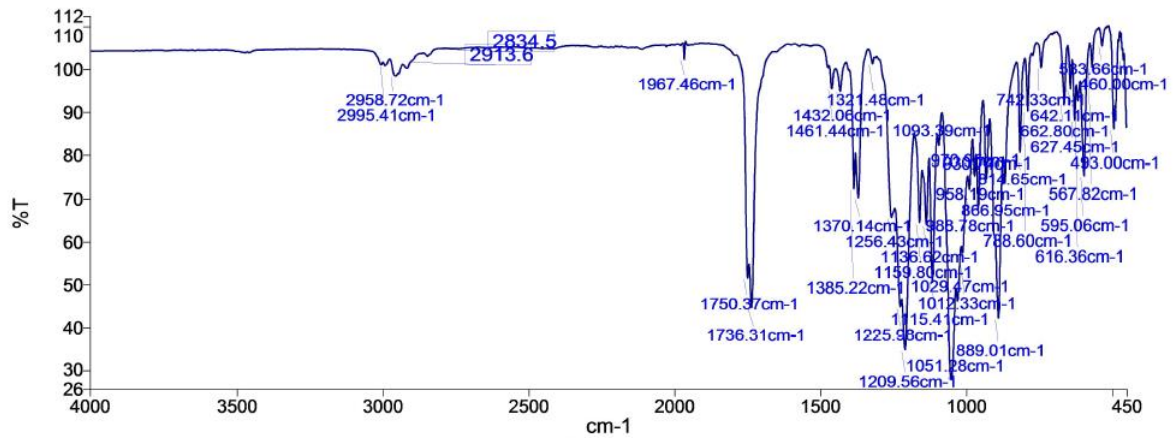
#### 9.1.2.1 3,4,6-Tri-*O*-acetyl-1,2-*O*-(1-methoxyethylidene)- $\beta$ -D-mannopyranose **2.11**



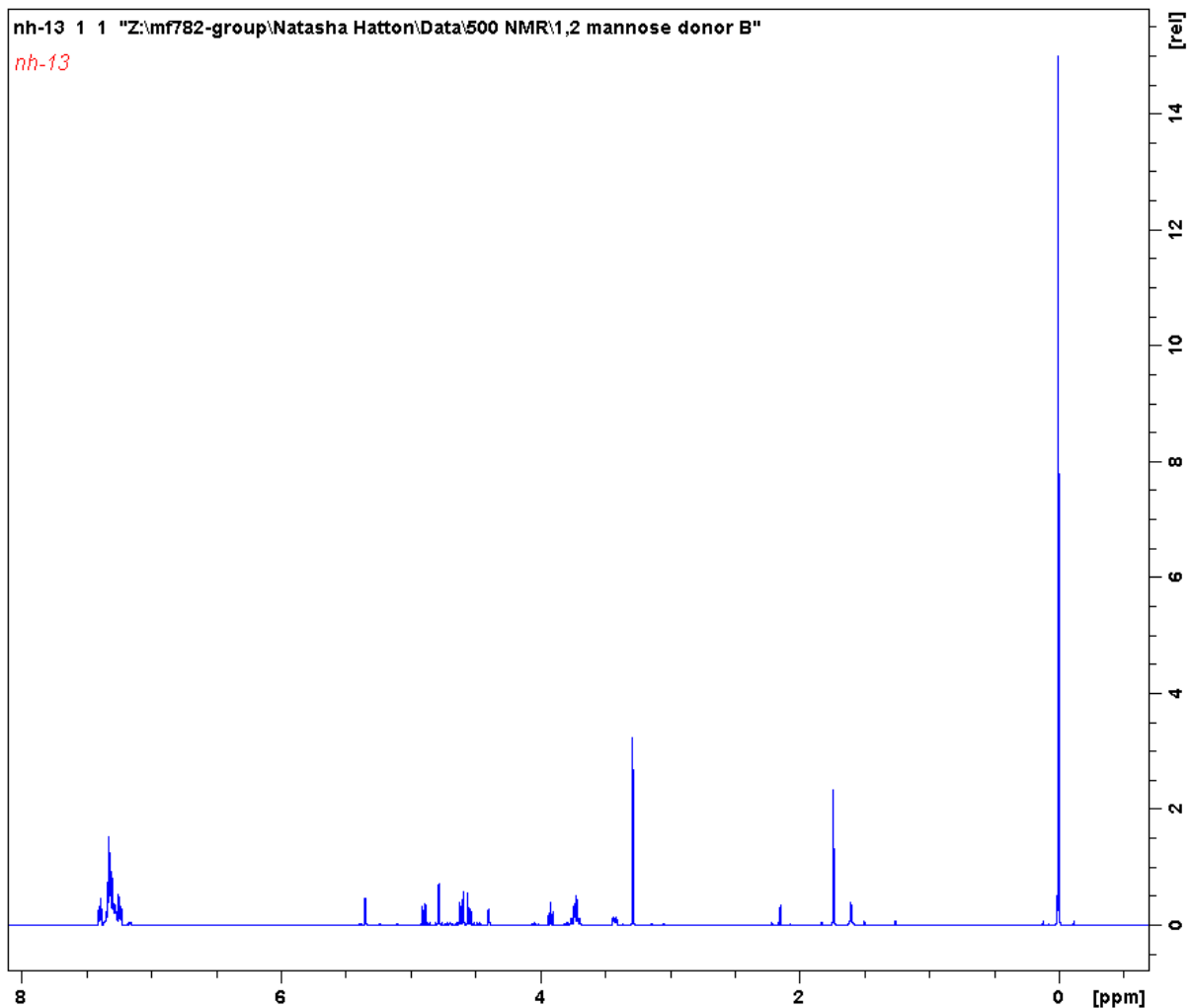
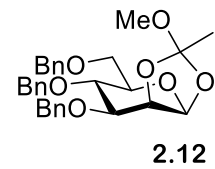
Appendix



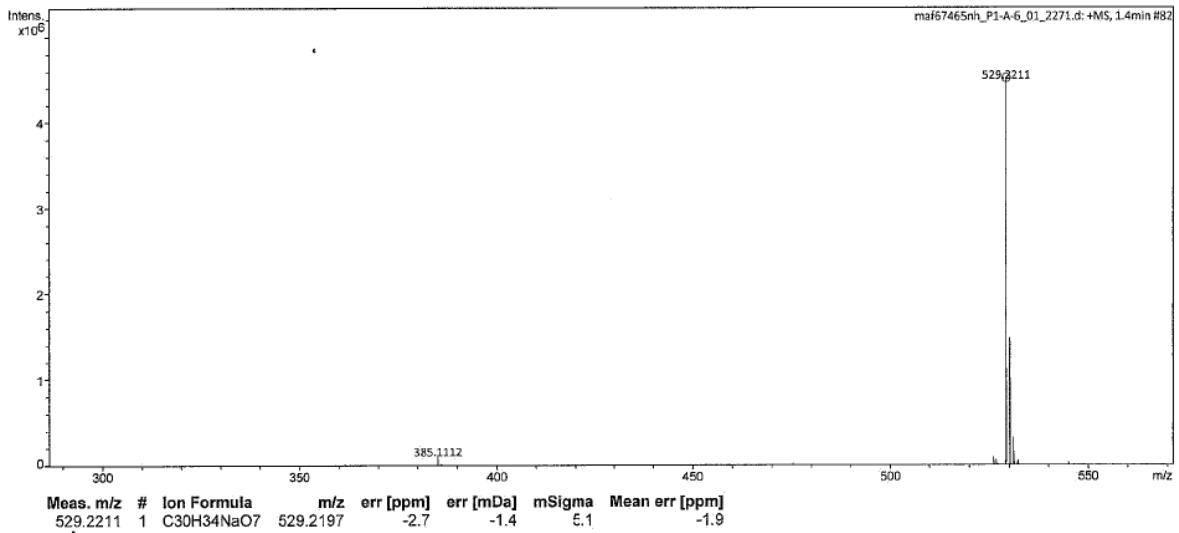
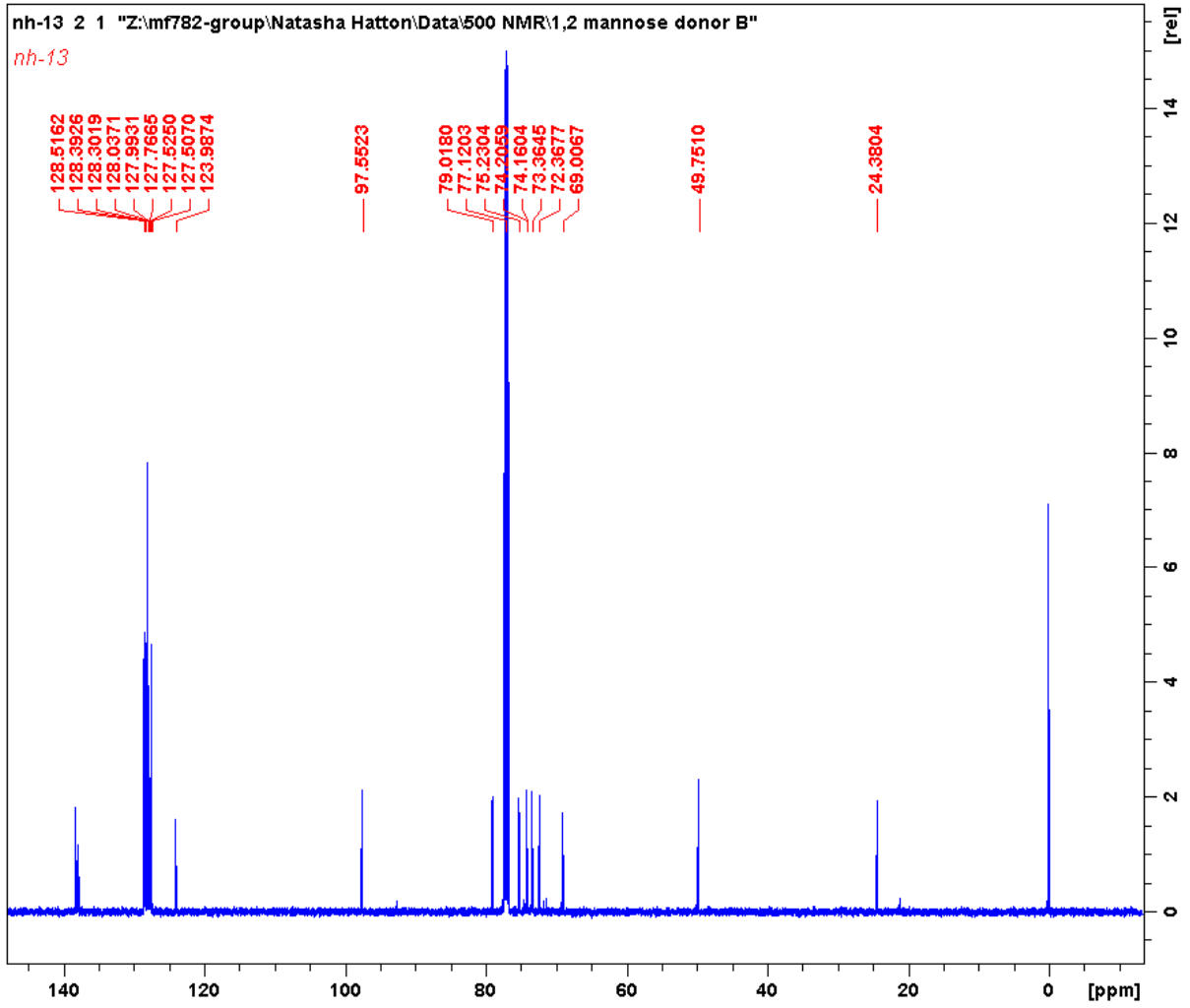
# Appendix



## 9.1.2.2 3,4,6-Tri-O-benzyl-1,2-O-(methoxyethylidene)-β-D-mannopyranose 2.12

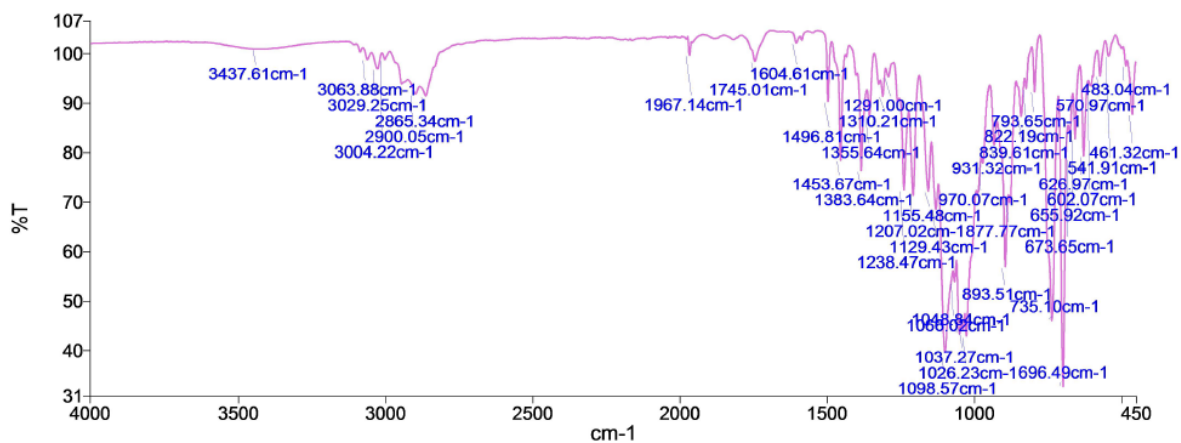


Appendix

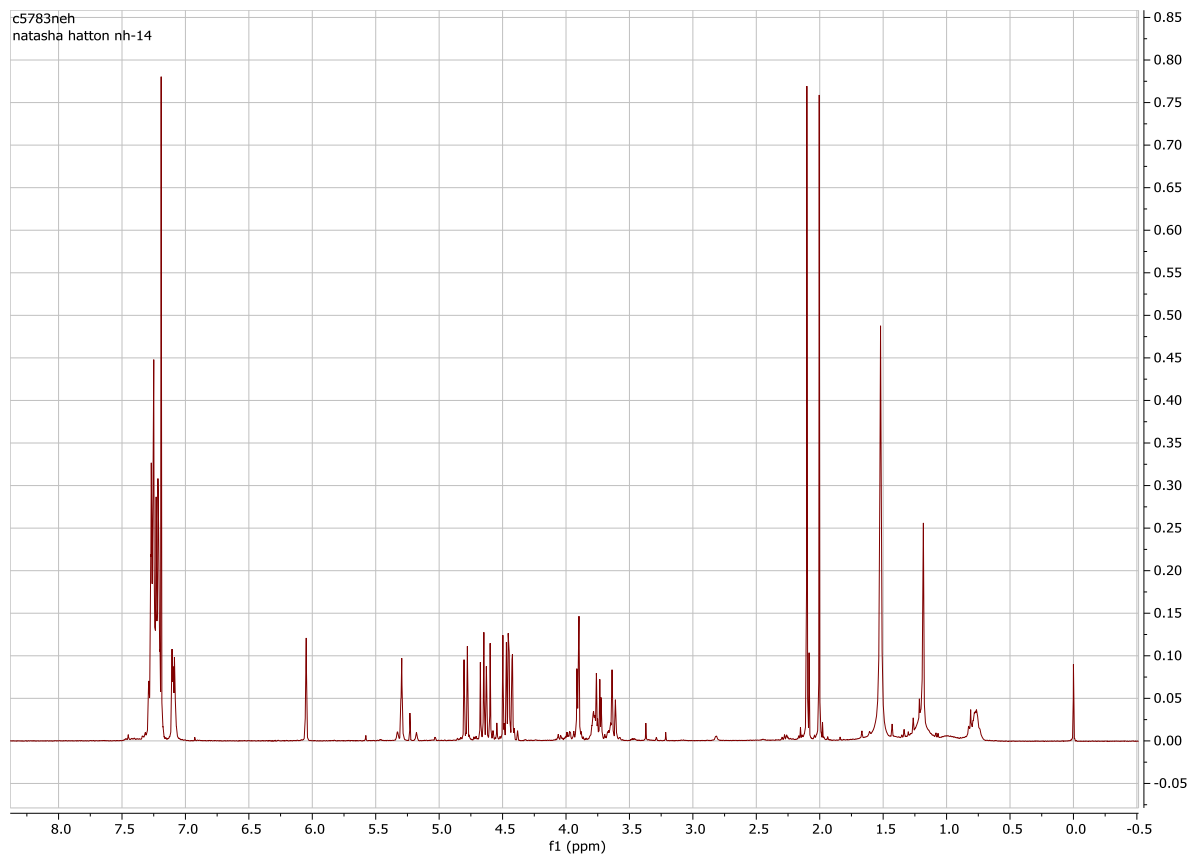
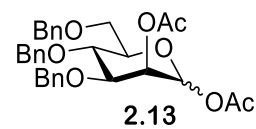




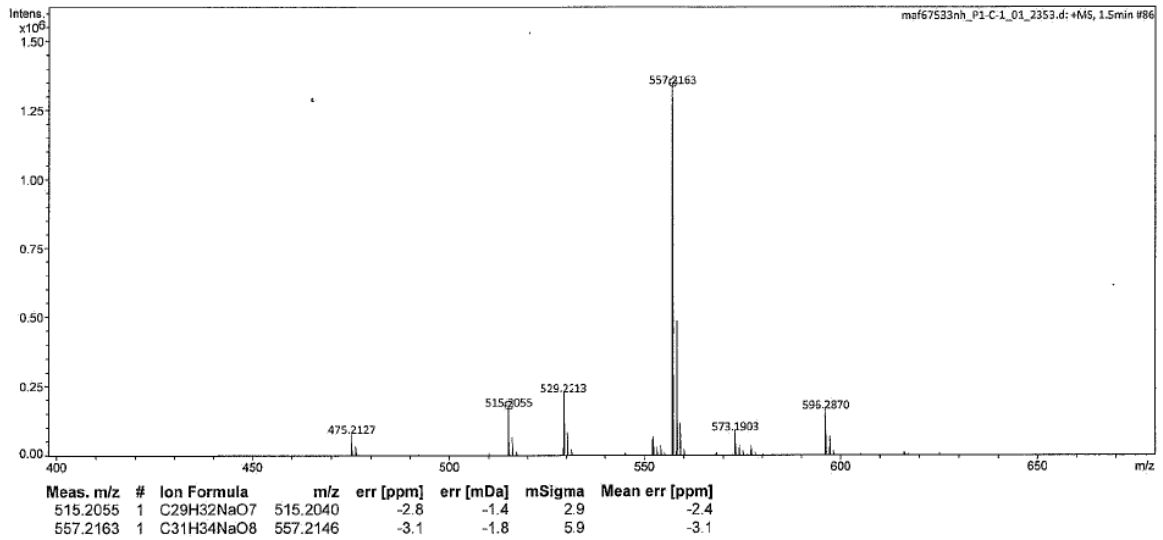
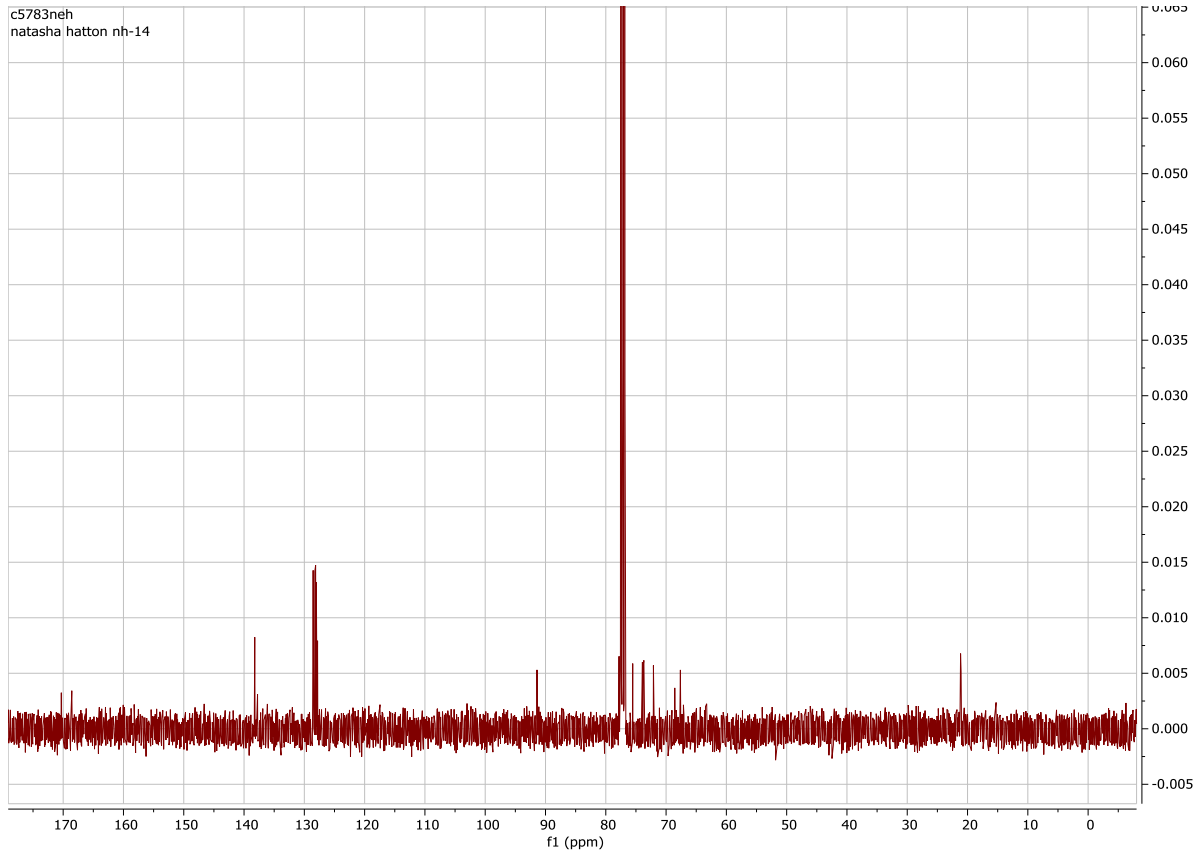
## Appendix



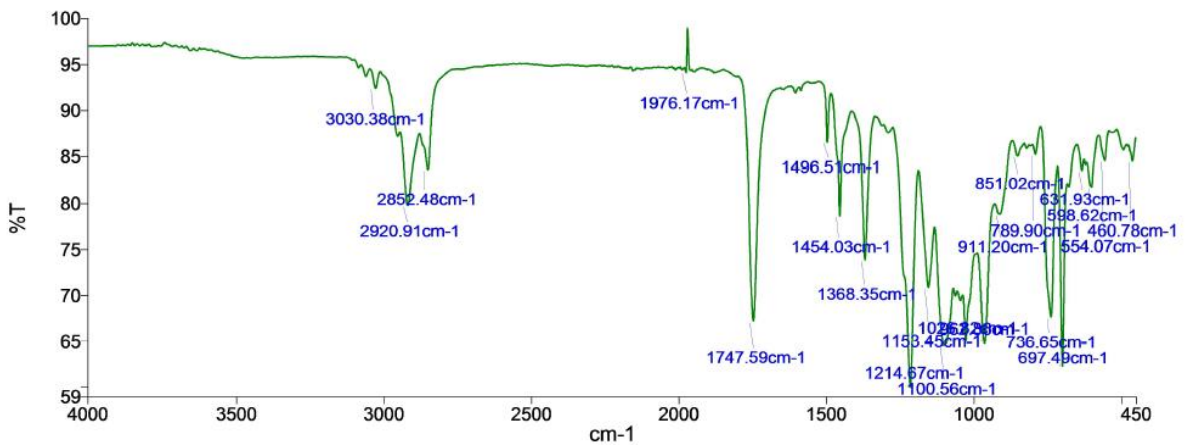
### 9.1.2.3 1,2-Di-O-acetyl-3,4,6-tri-O-benzyl- $\alpha$ -D-mannopyranoside 2.13



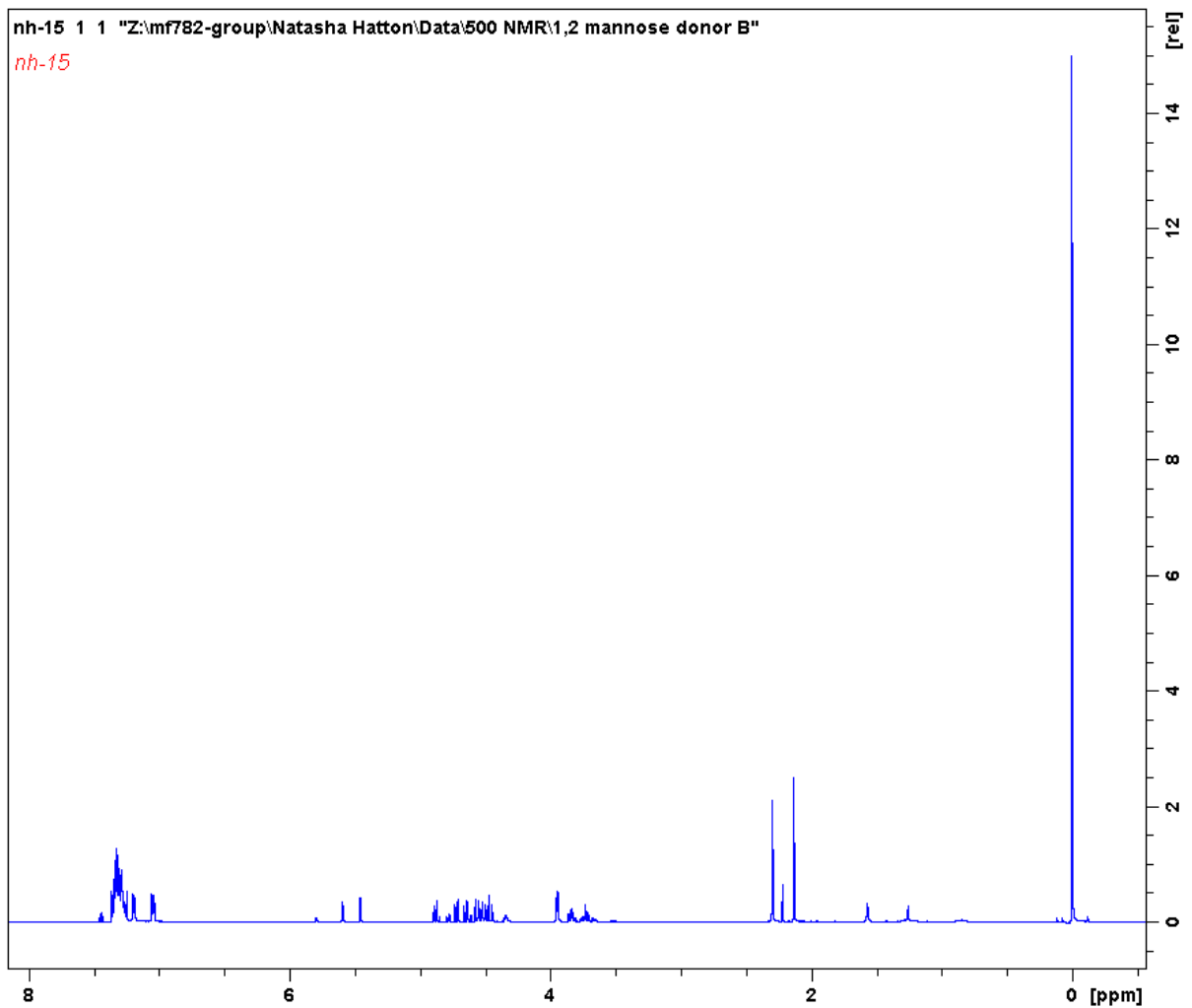
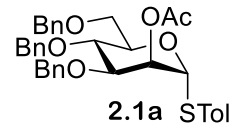
# Appendix



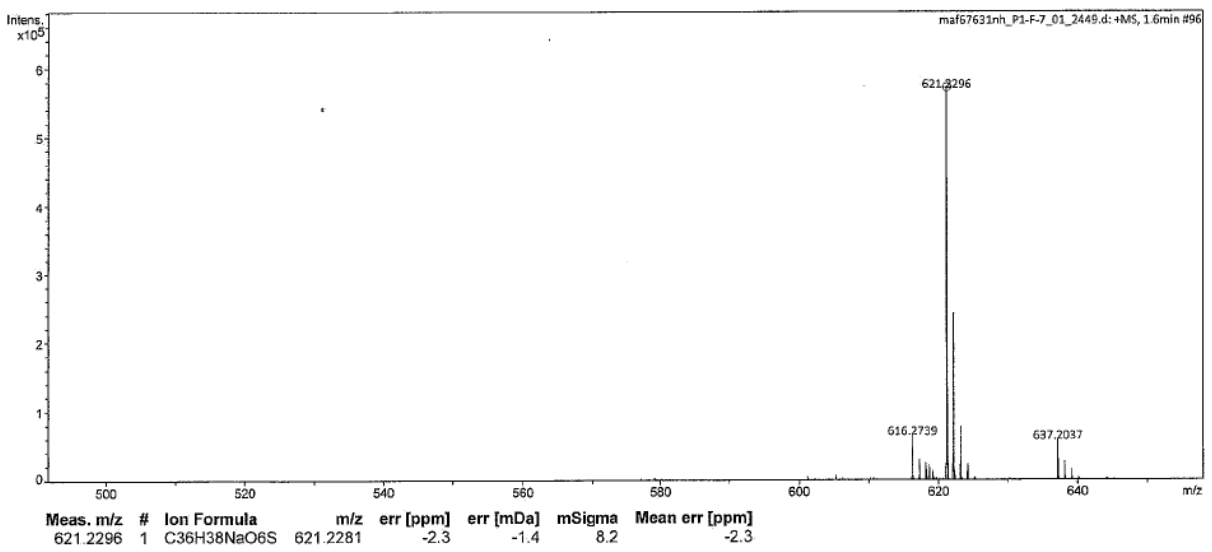
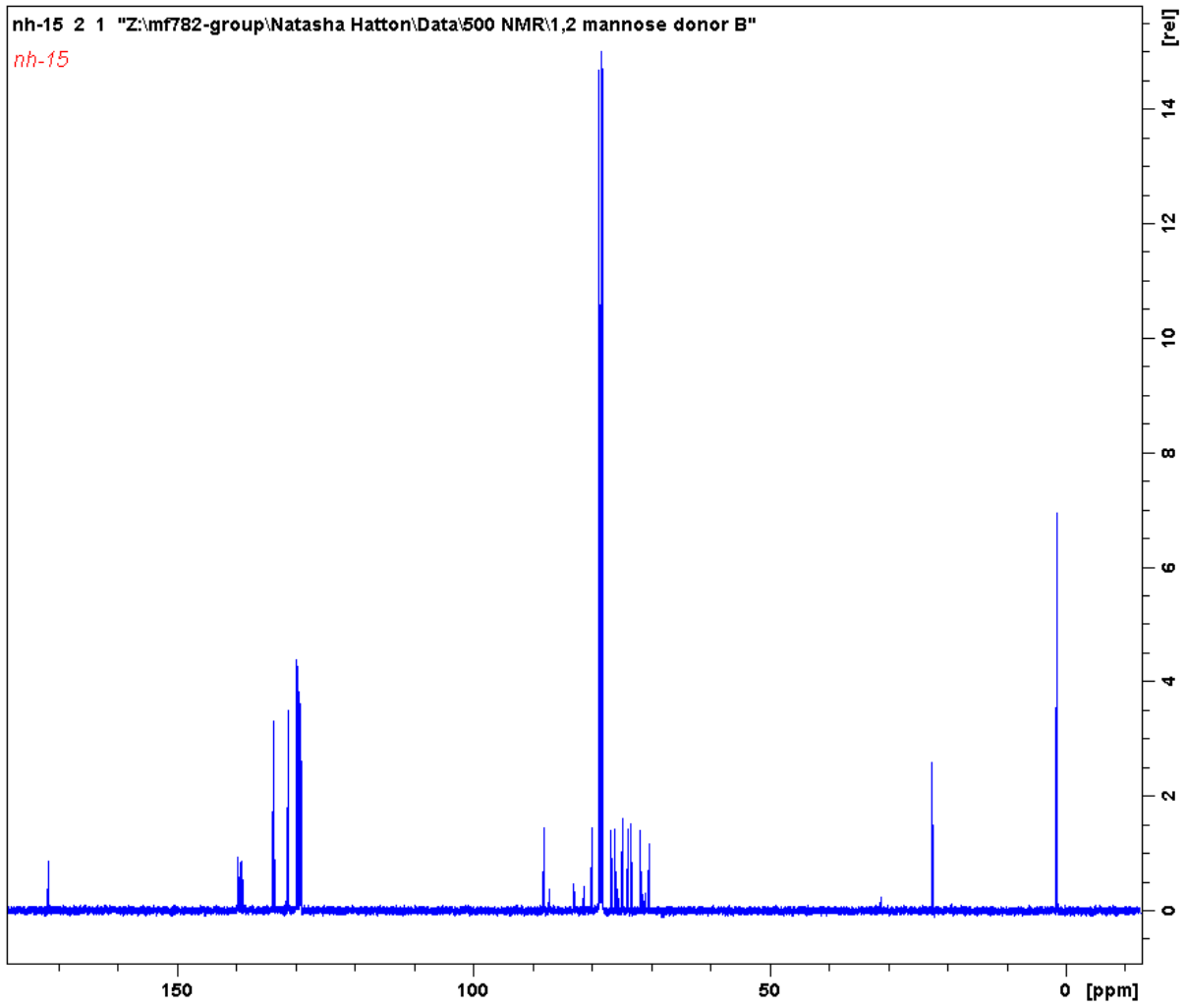
# Appendix



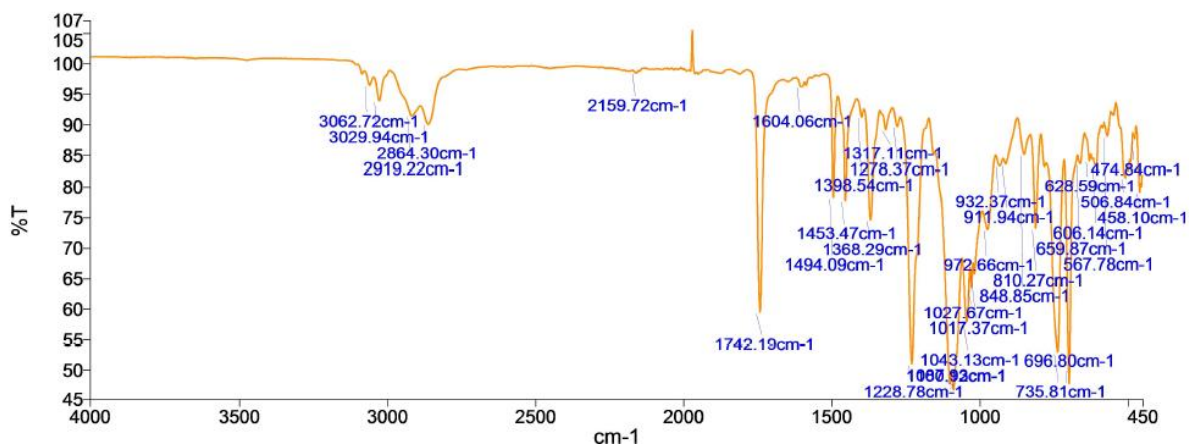
## 9.1.2.4 4-Methylphenyl 2-O-acetyl-3,4,6-tri-O-benzyl-1-thio- $\alpha$ -D-mannopyranoside 2.1a



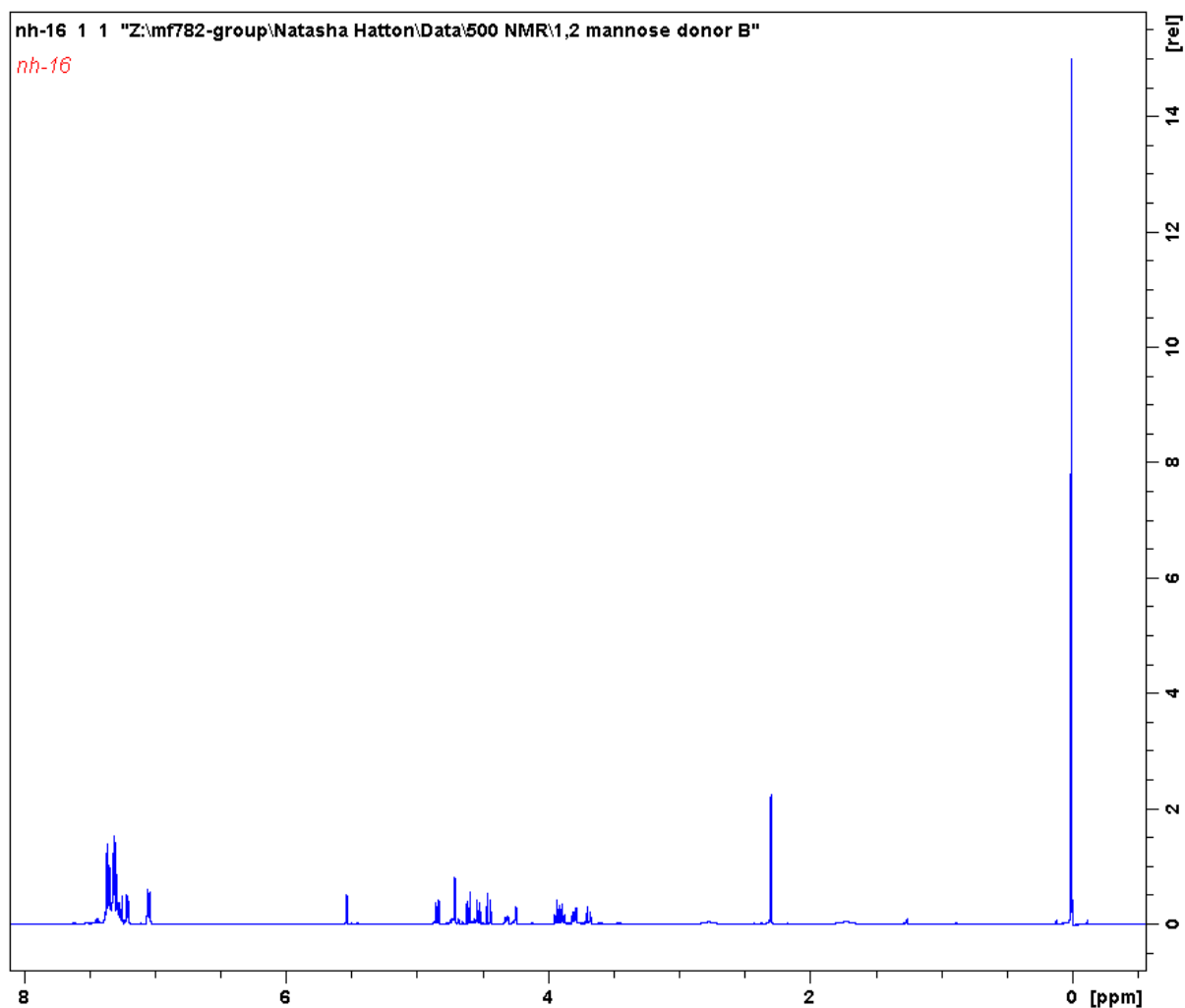
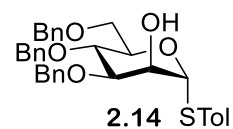
Appendix



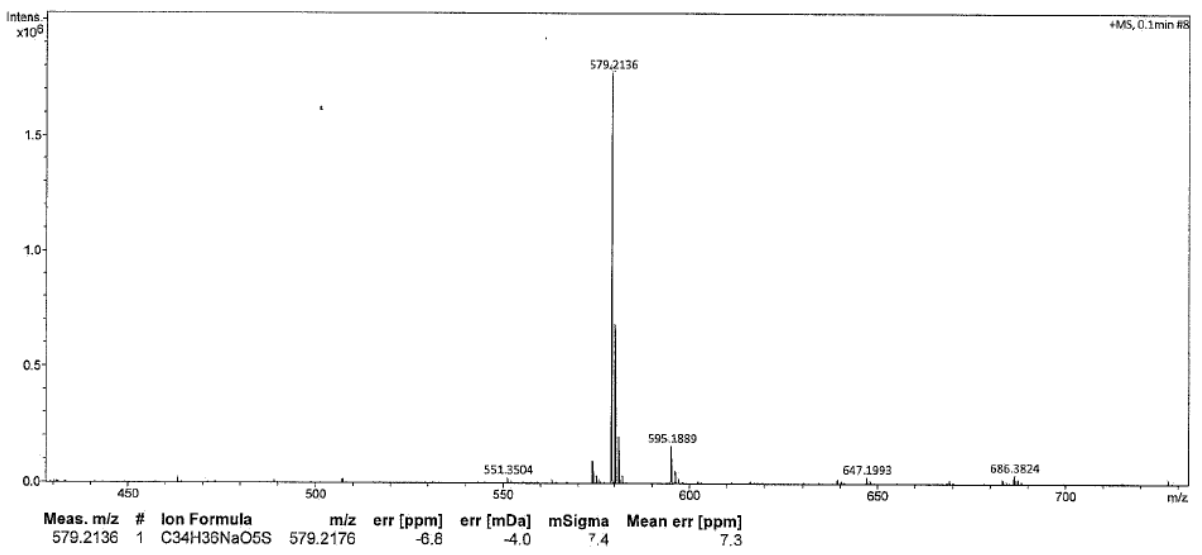
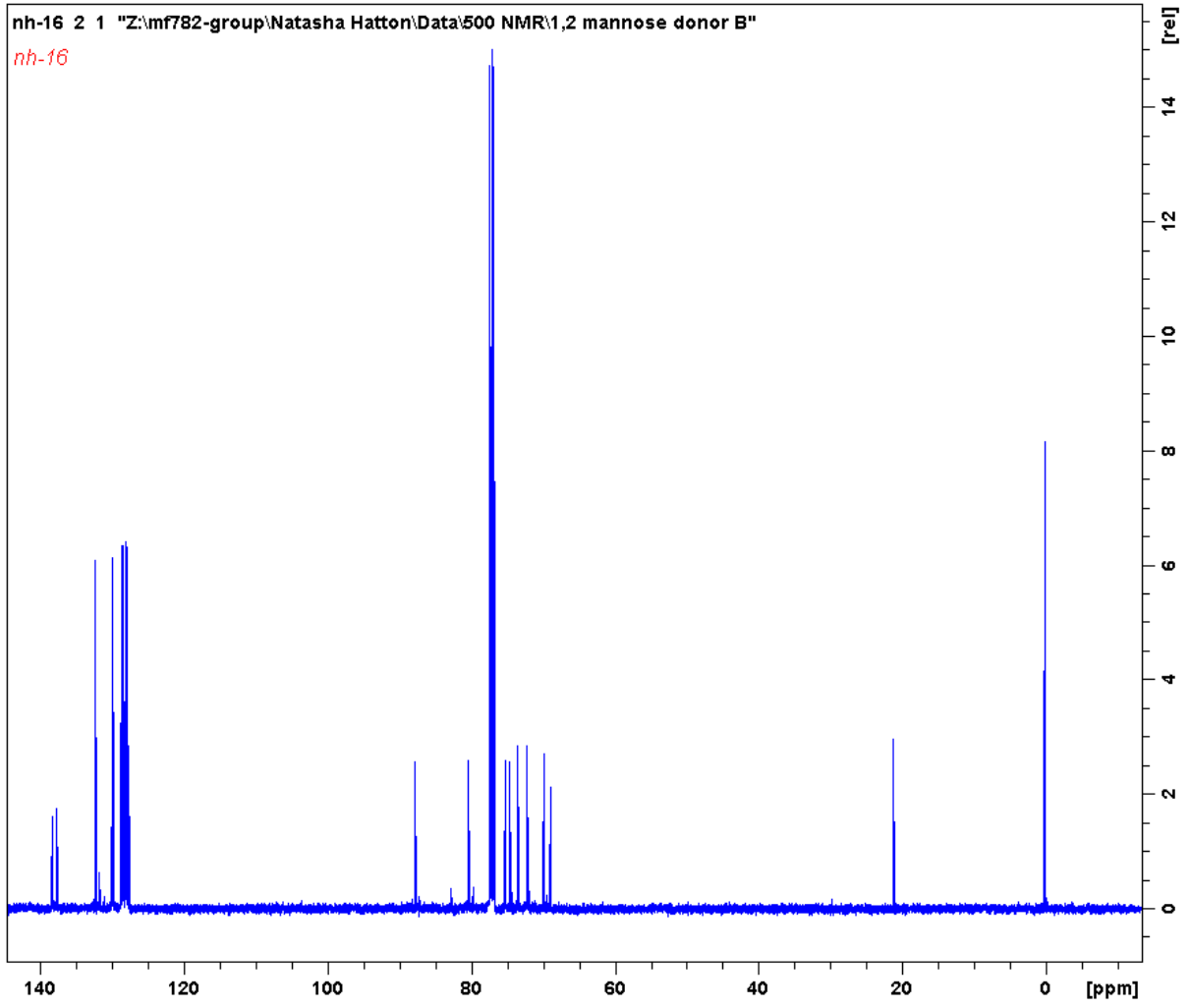
## Appendix



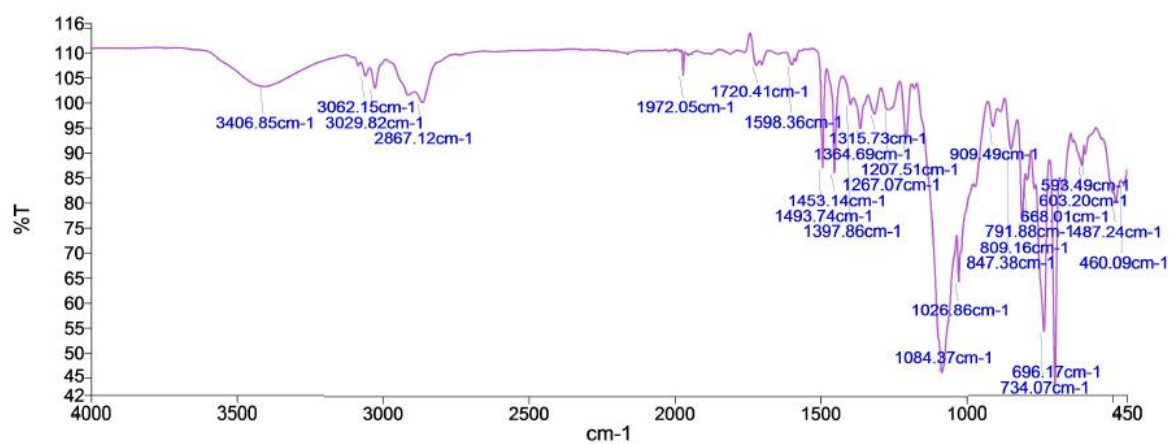
### 9.1.2.5 4-Methylphenyl 3,4,6-tri-O-benzyl-1-thio- $\alpha$ -D-mannopyranoside 2.14



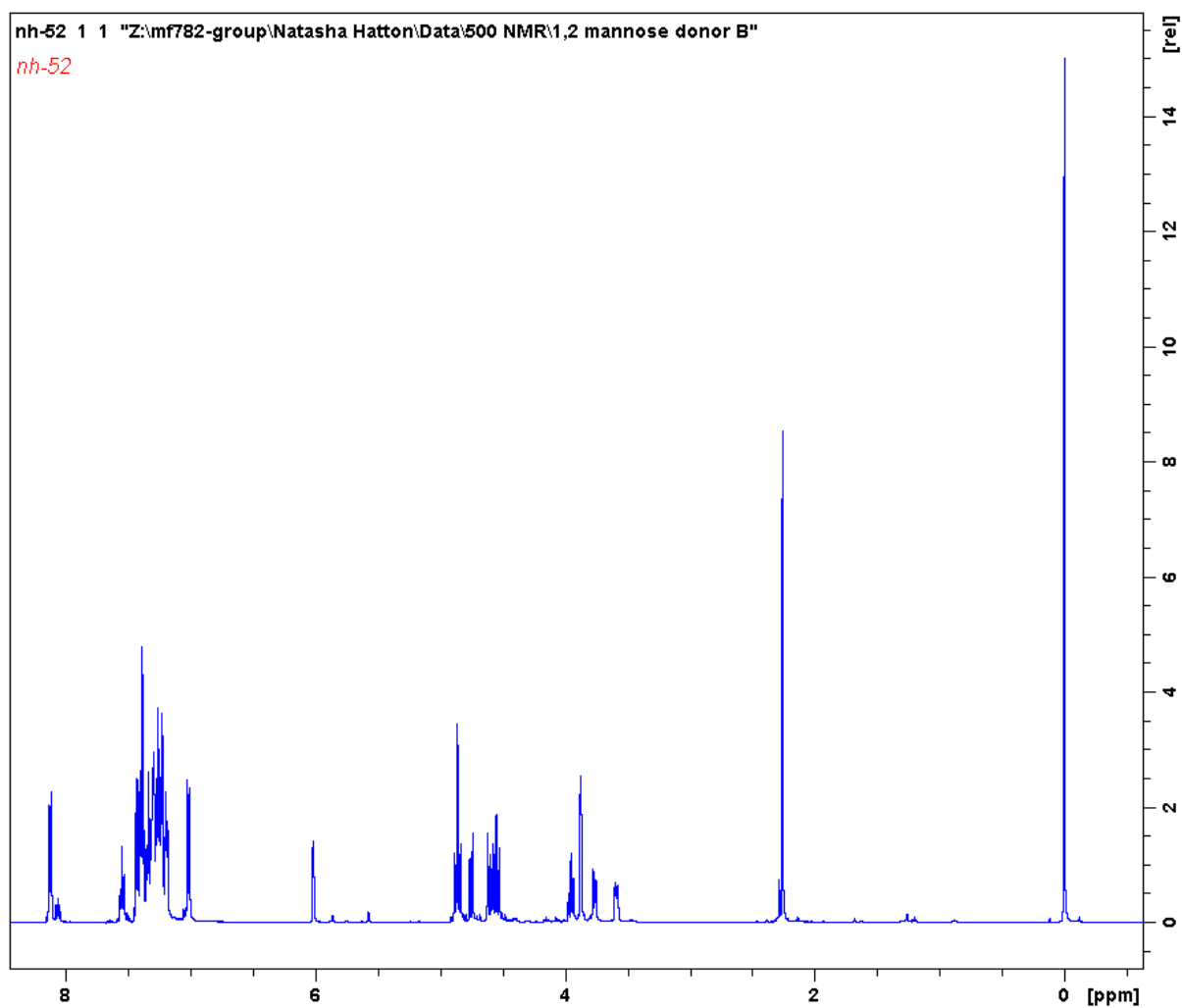
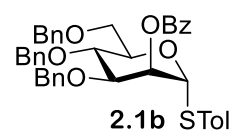
Appendix



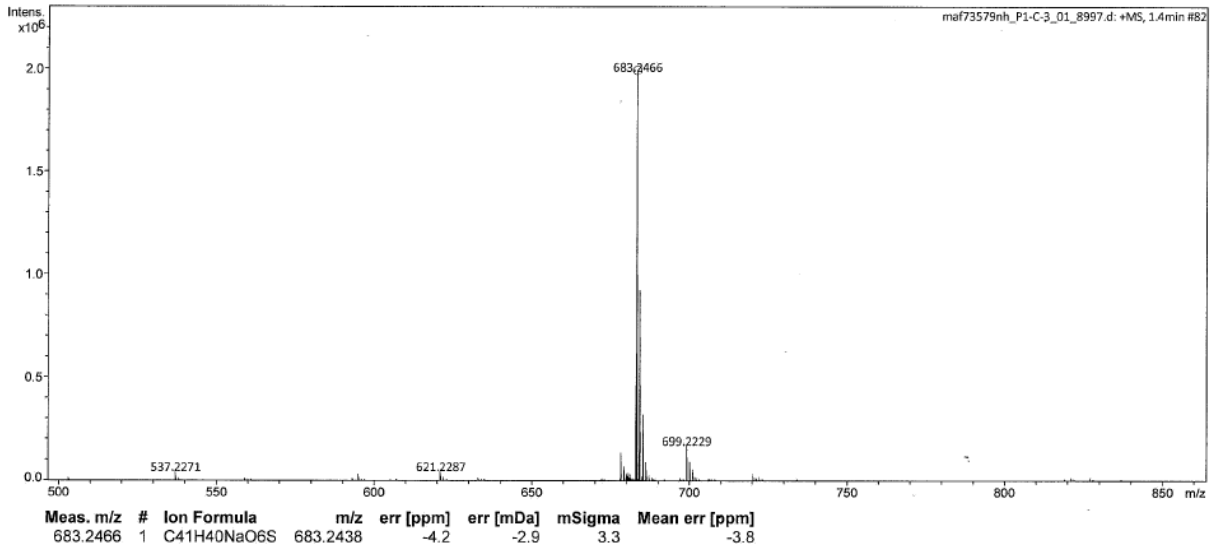
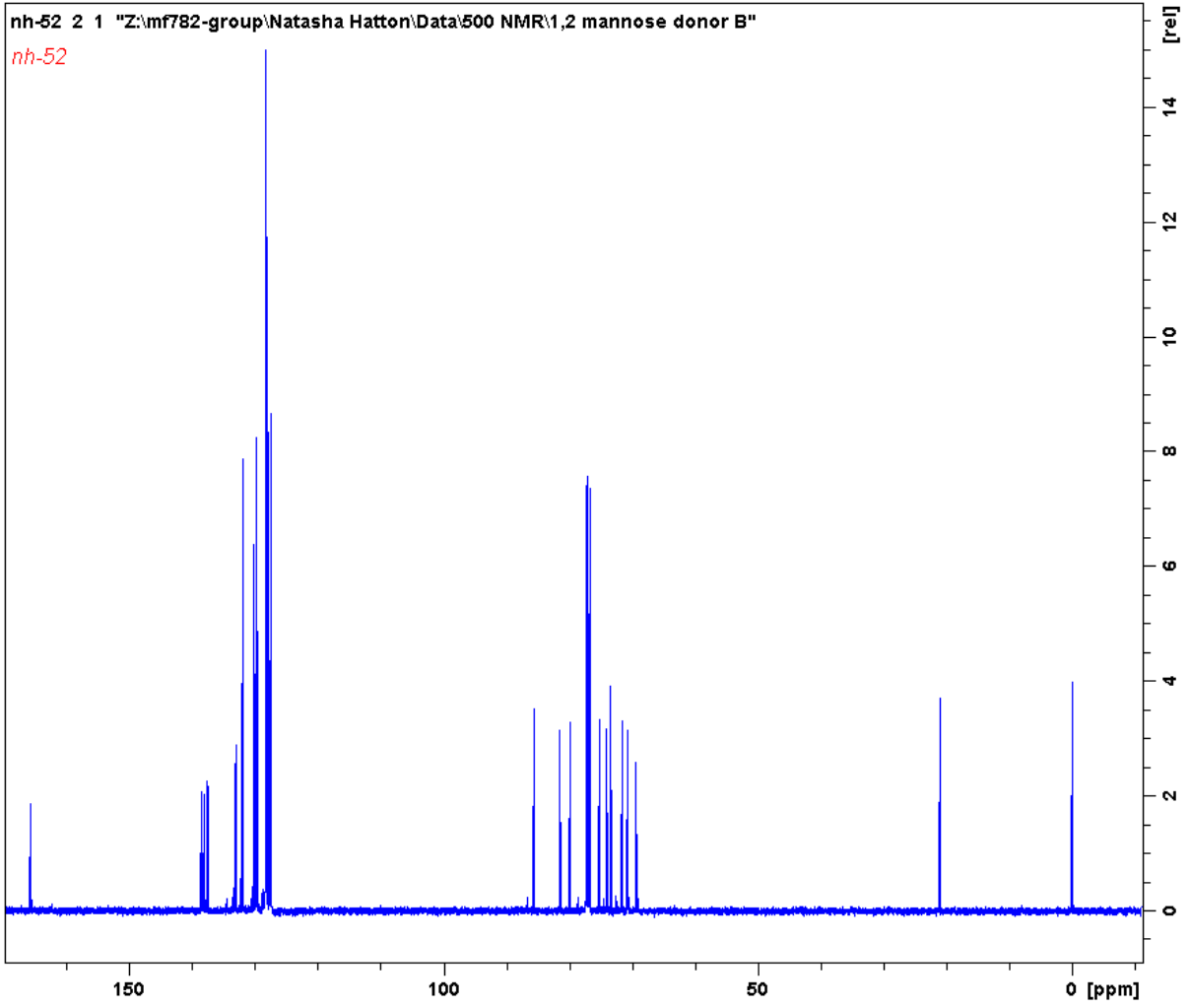
## Appendix



### 9.1.2.6 4-Methylphenyl 2-O-benzoyl-3,4,6-tri-O-benzyl-1-thio- $\alpha$ -D-mannopyranoside **2.1b**

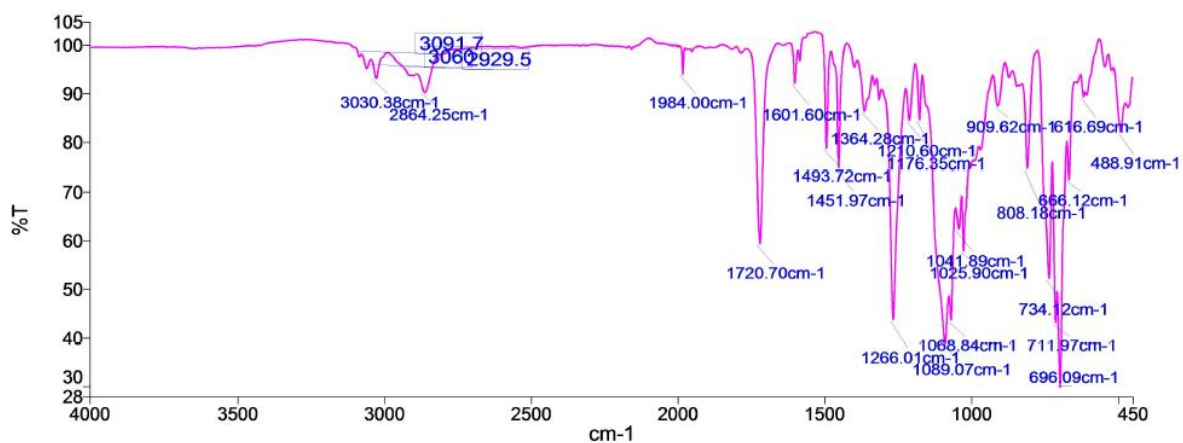


Appendix



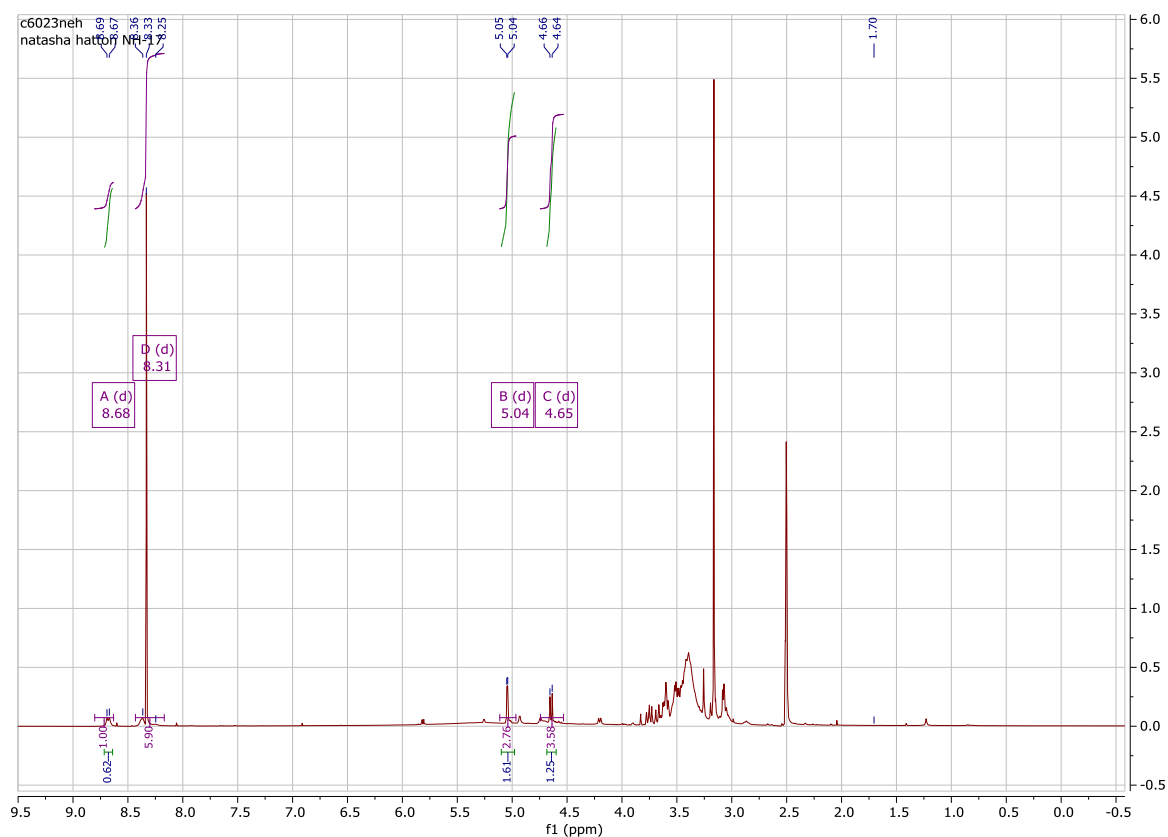
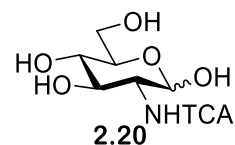


## Appendix

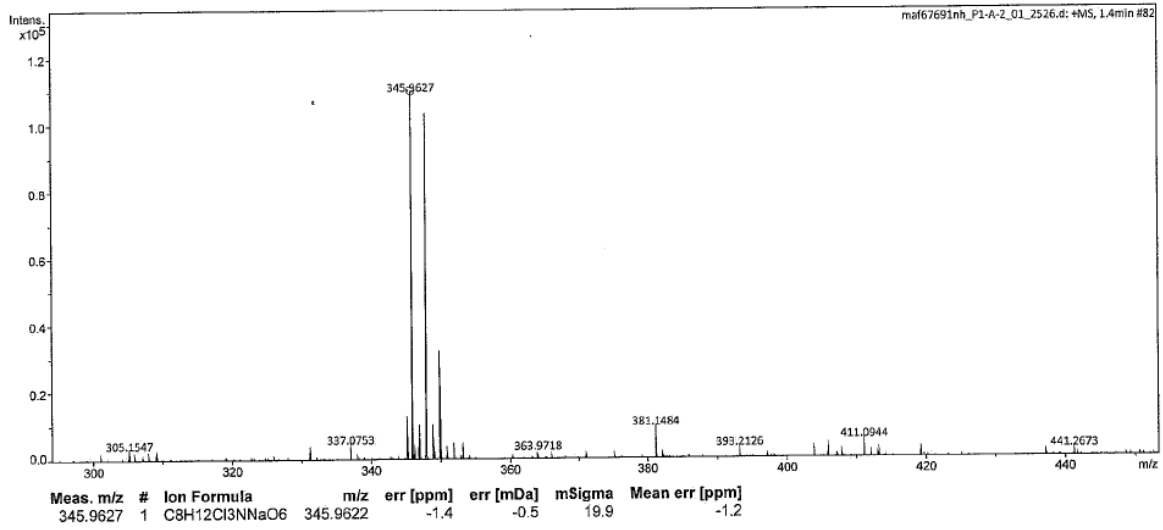
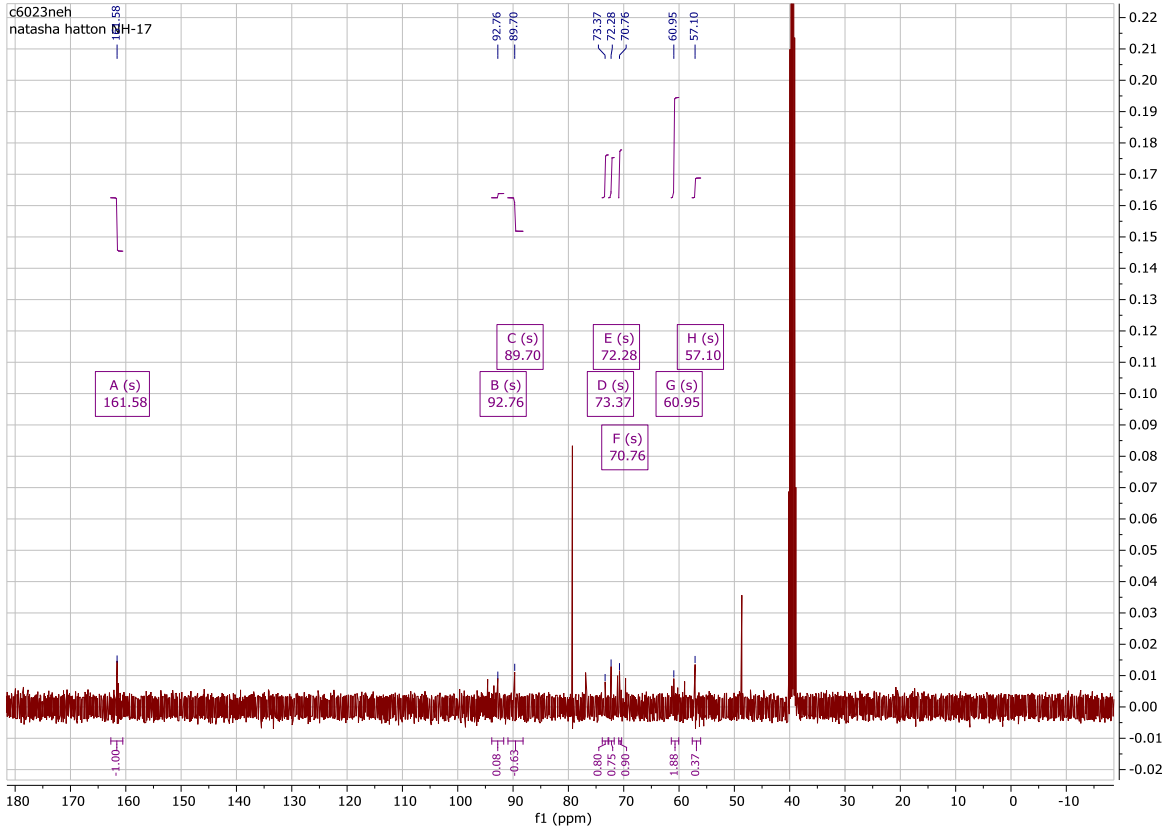


### 9.1.3 Synthesis of 4-methylphenyl 3,6-di-*O*-benzyl-2-deoxy-2-*N*-trichloroacetamido-1-thio- $\beta$ -D-glucopyranoside **2.26**

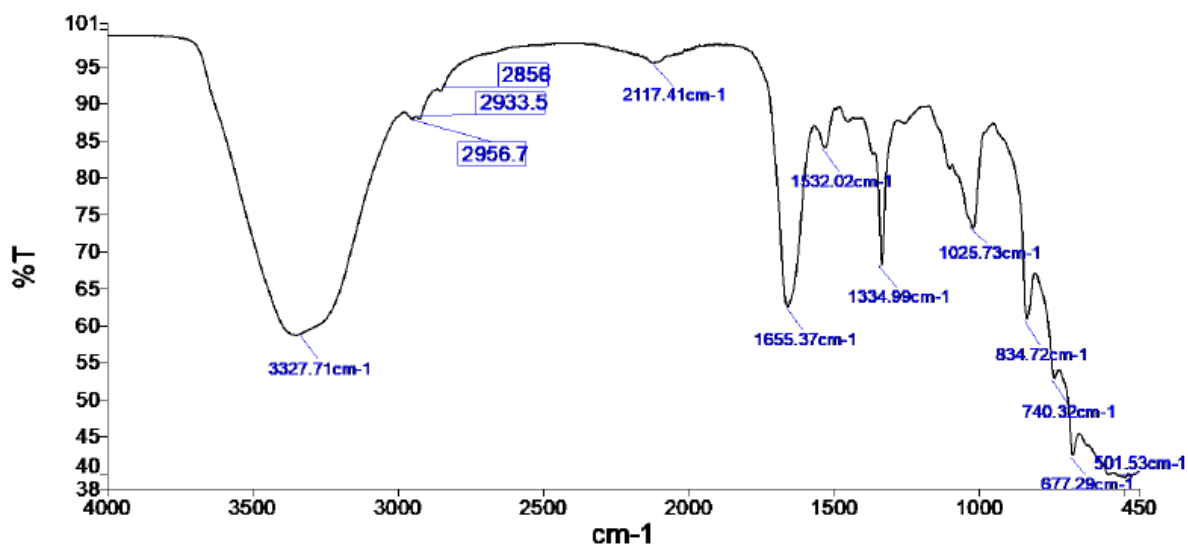
#### 9.1.3.1 2-Deoxy-2-trichloroacetamido- $\alpha/\beta$ -D-glucopyranose **2.20**



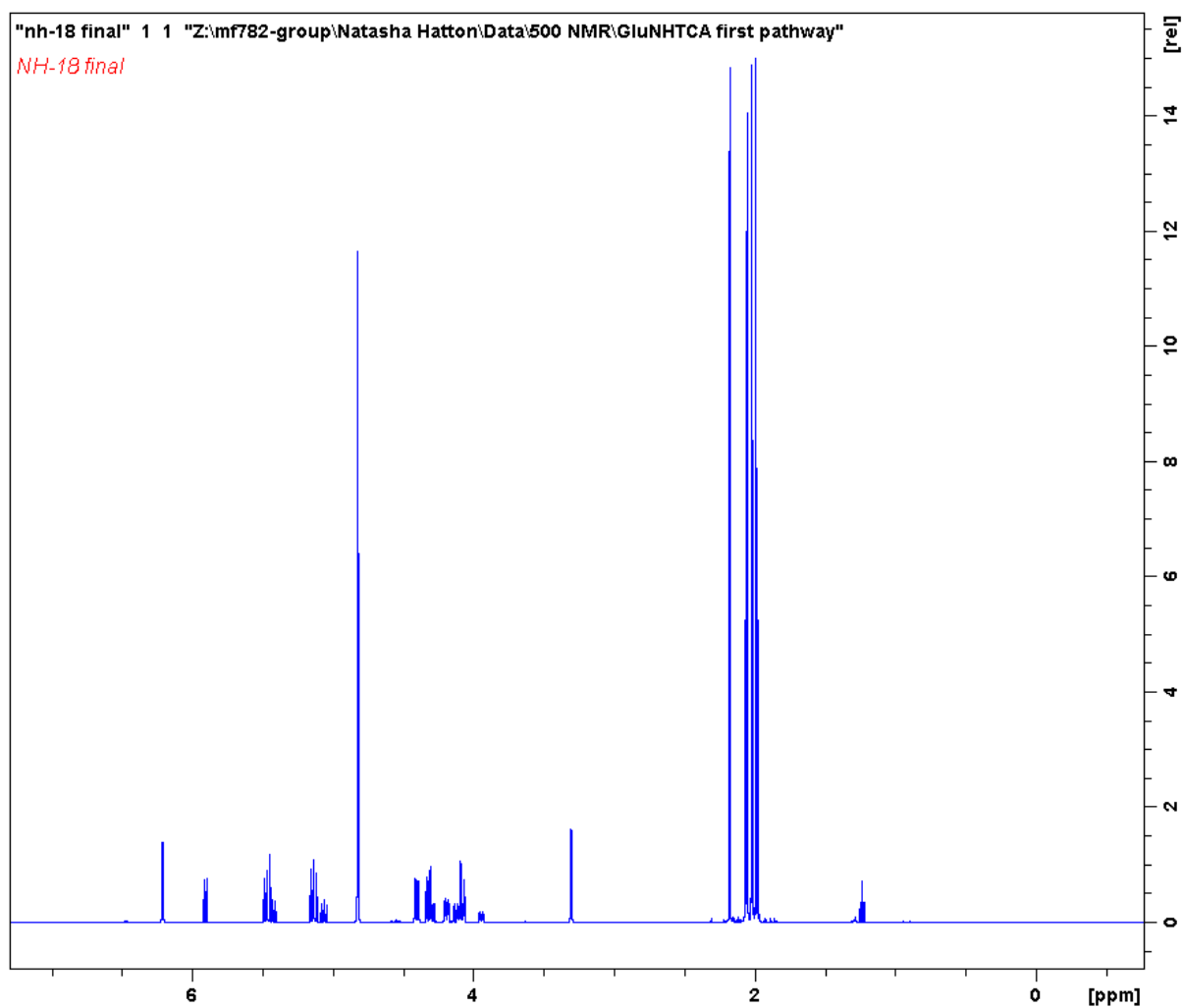
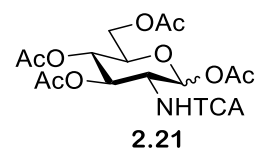
# Appendix



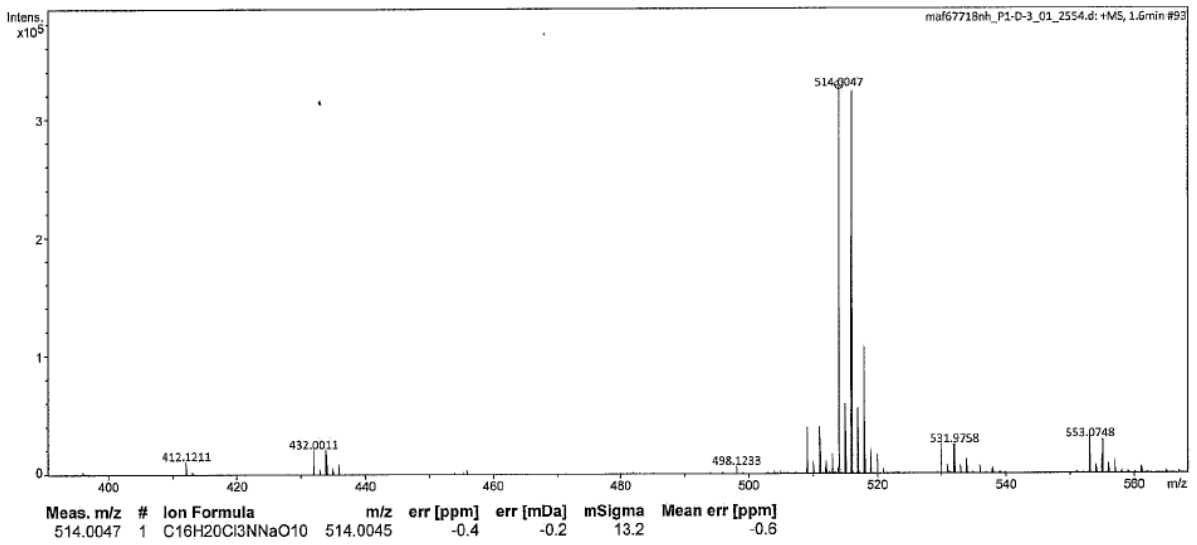
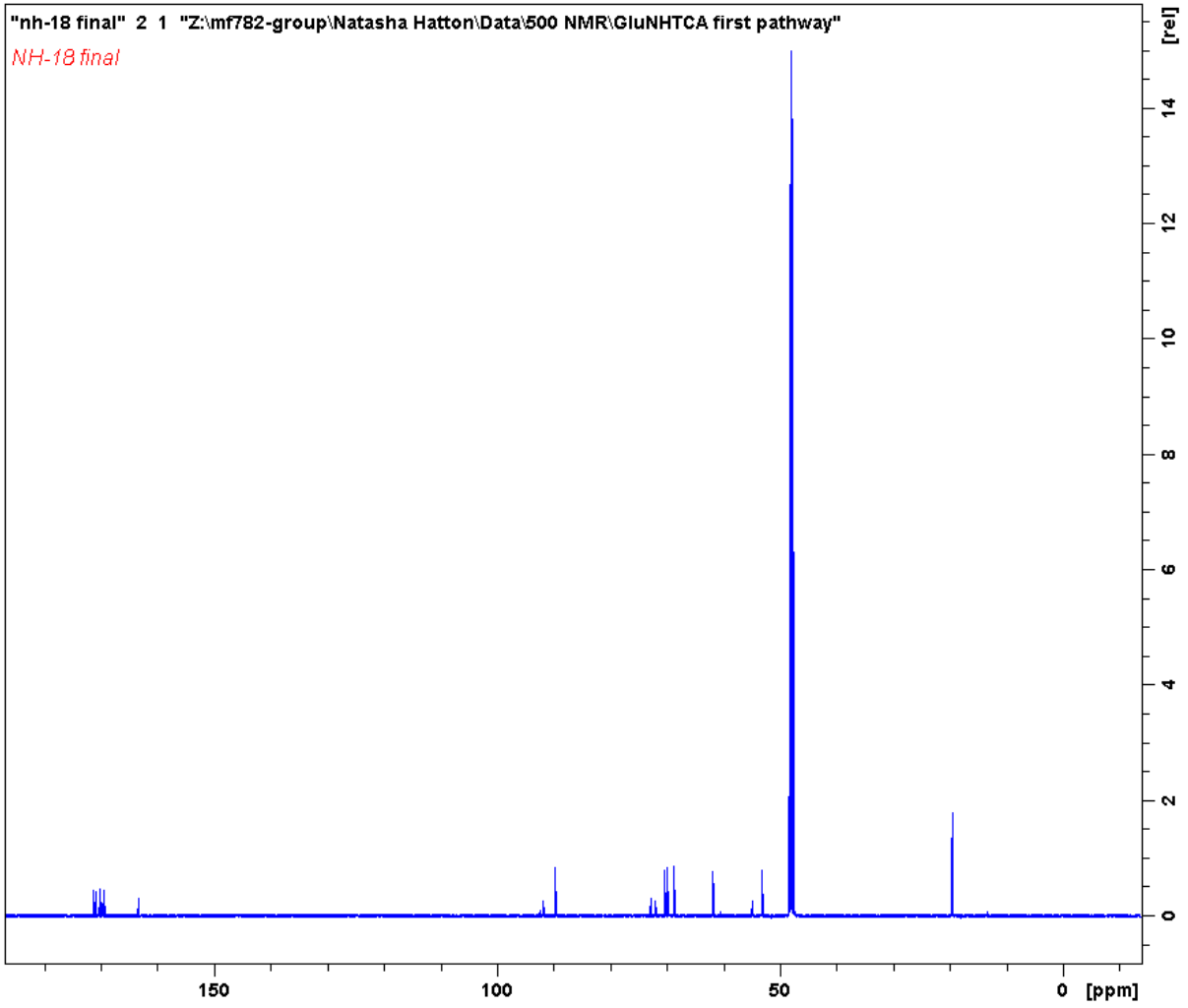
## Appendix



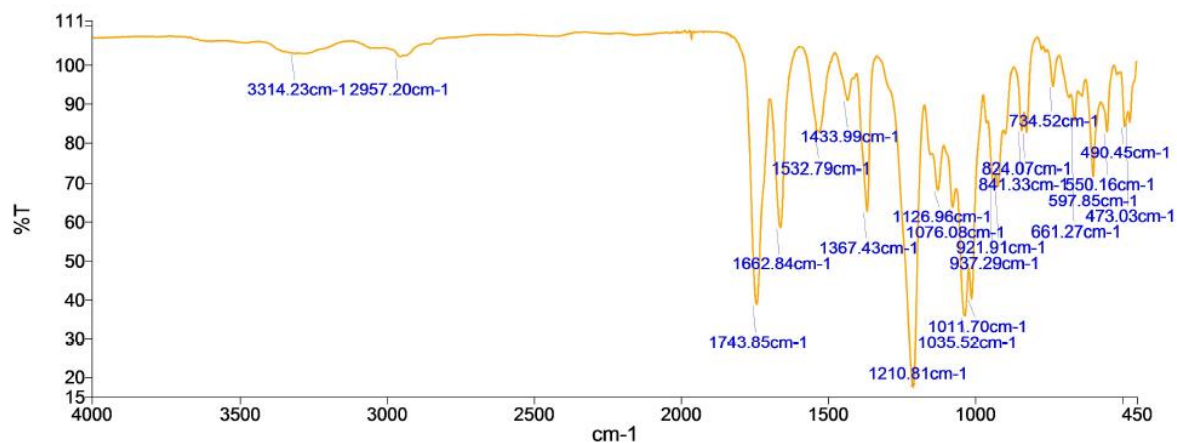
### 9.1.3.2 1,3,4,6-Tetra-O-acetyl-2-deoxy-2-trichloroacetamido- $\alpha/\beta$ -D-glucopyranose 2.21



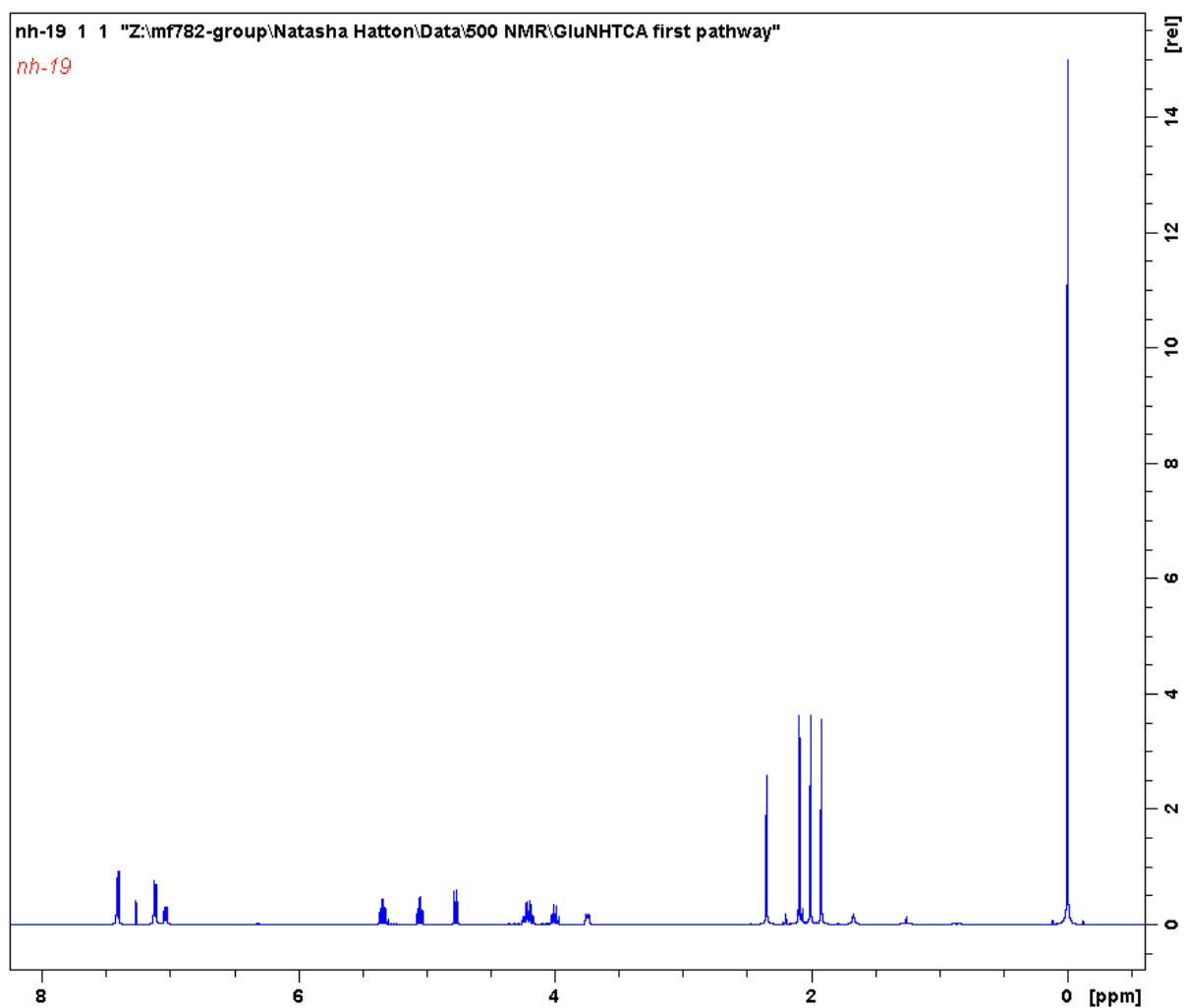
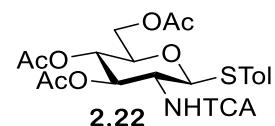
Appendix



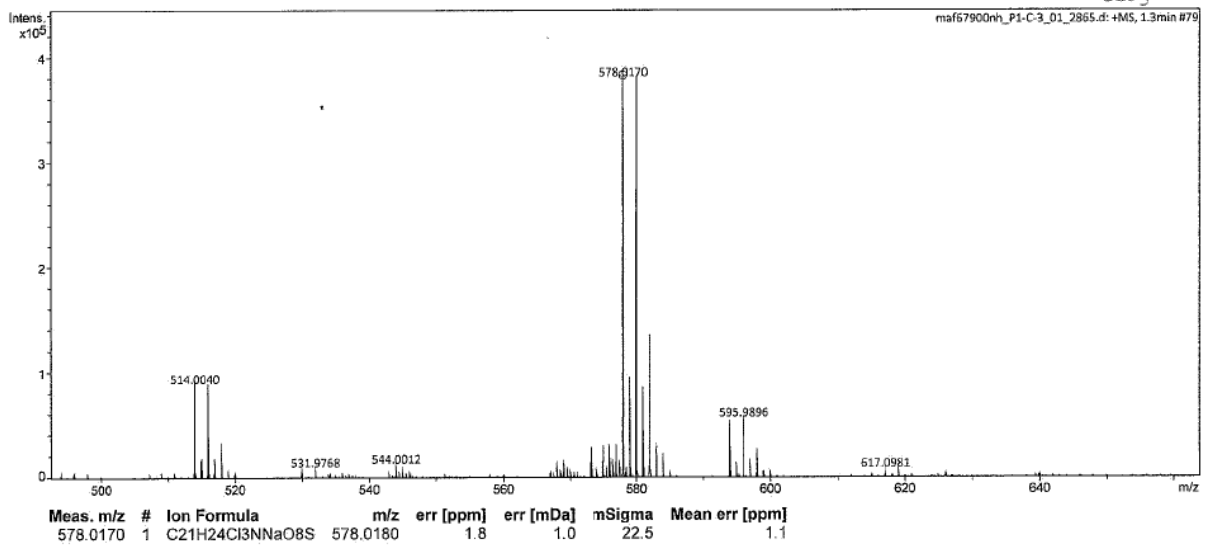
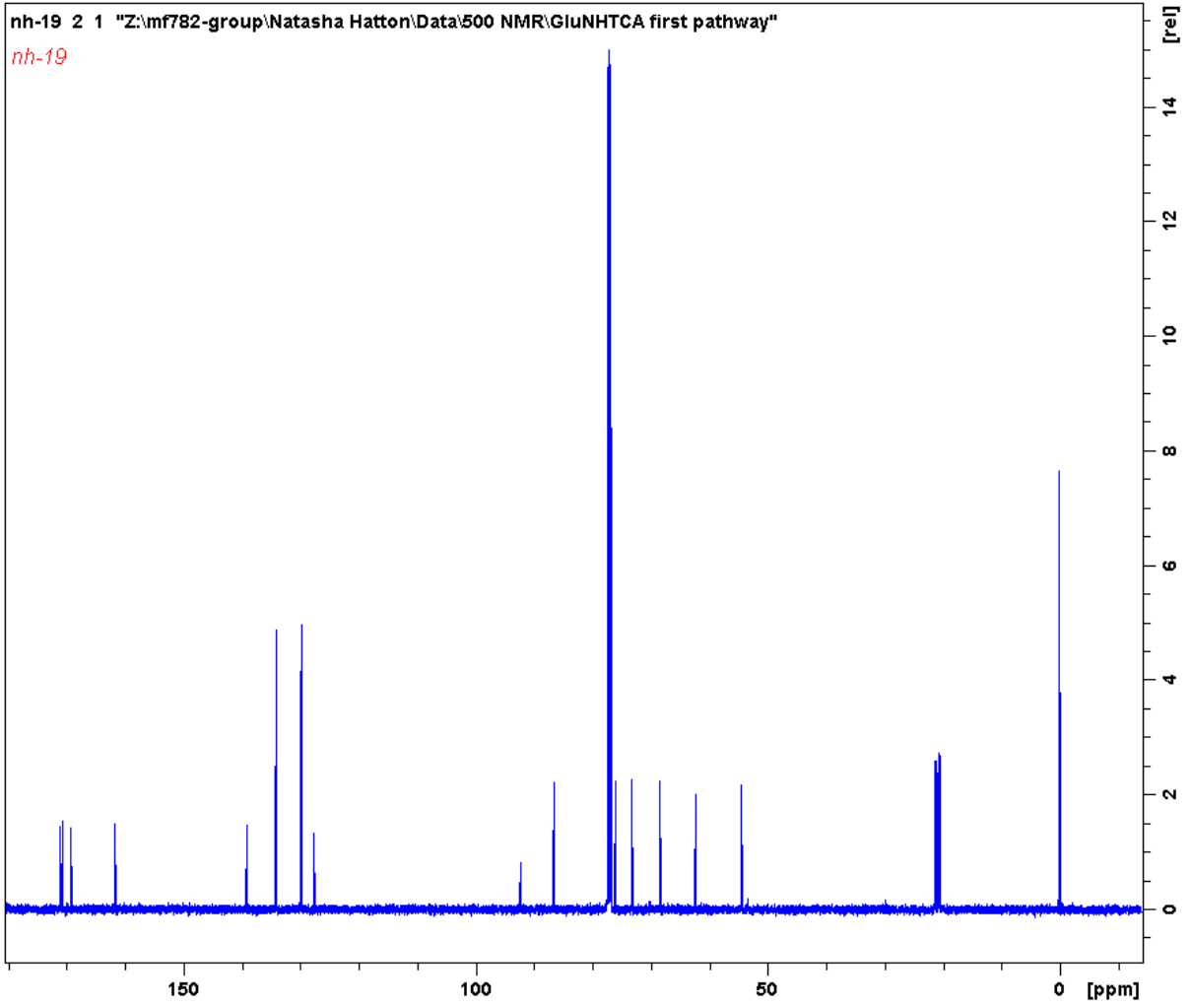
## Appendix



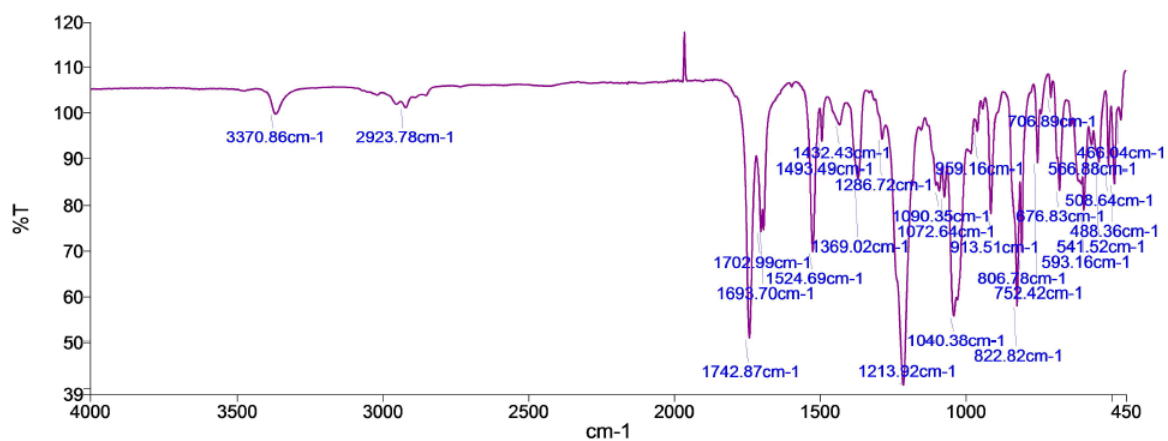
### 9.1.3.3 4-Methylphenyl 3,4,6-tri-O-acetyl-2-deoxy-2-trichloroacetamido-1-thio-β-D-glucopyranoside 2.22



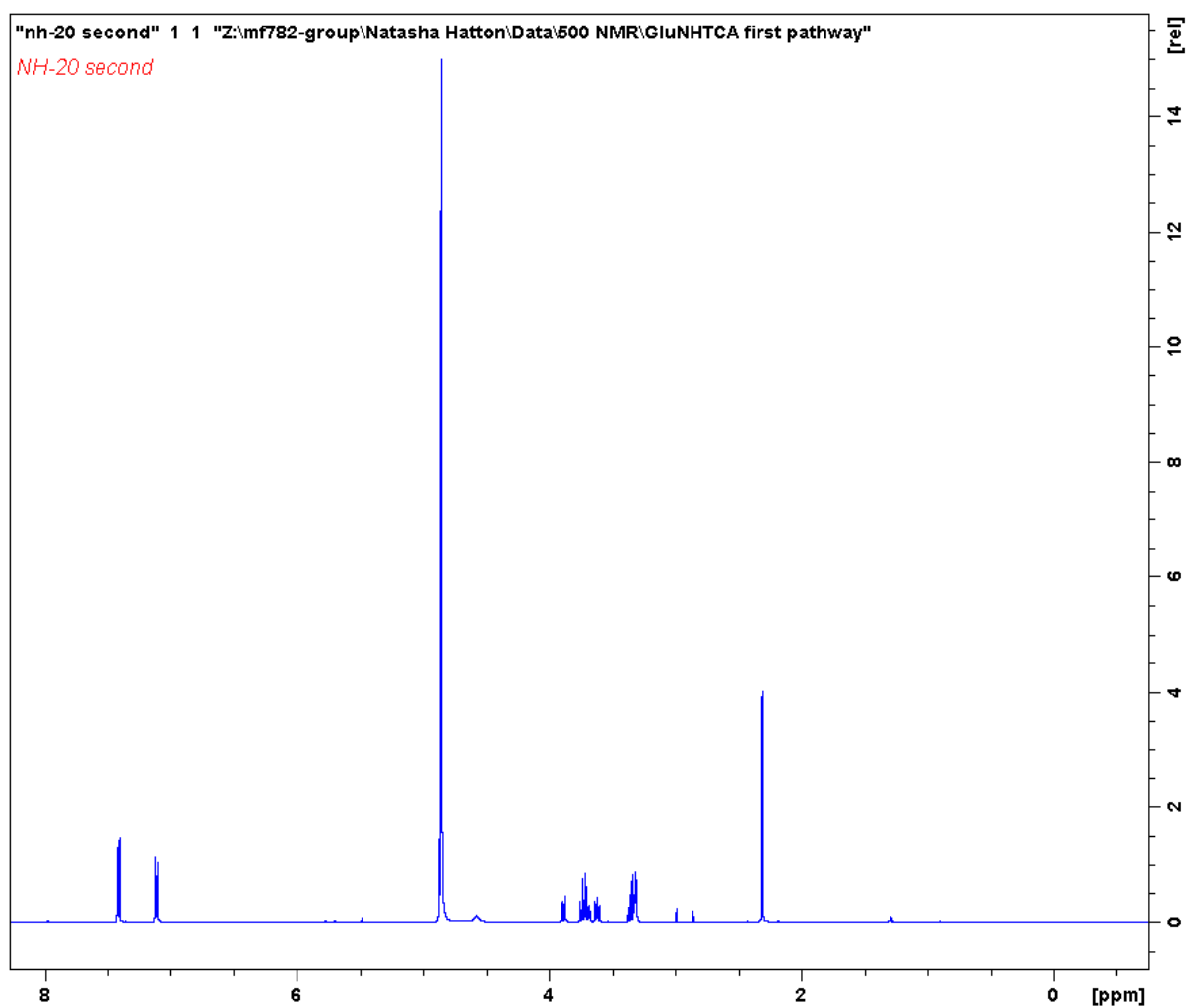
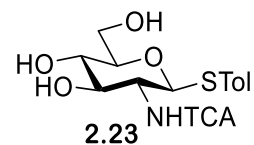
Appendix



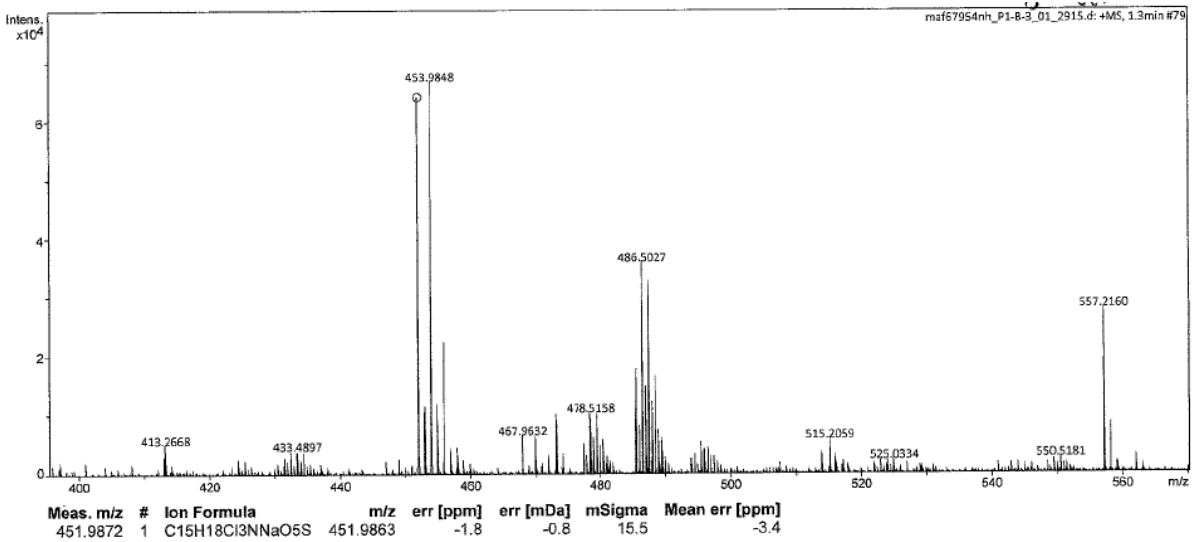
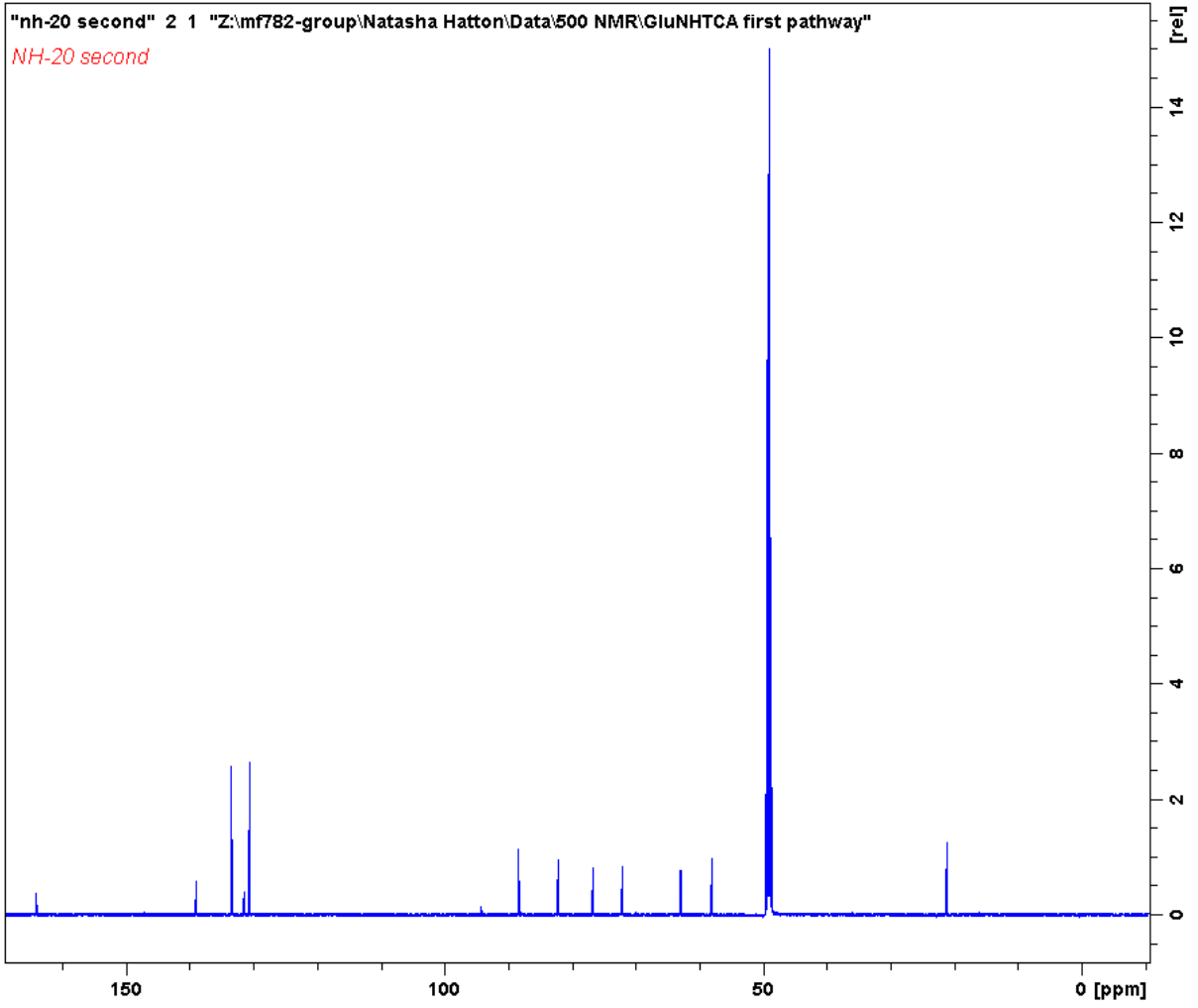
## Appendix



### 9.1.3.4 4-Methylphenyl 2-deoxy-2-trichloroacetamido-1-thio-β-D-glucopyranoside 2.23

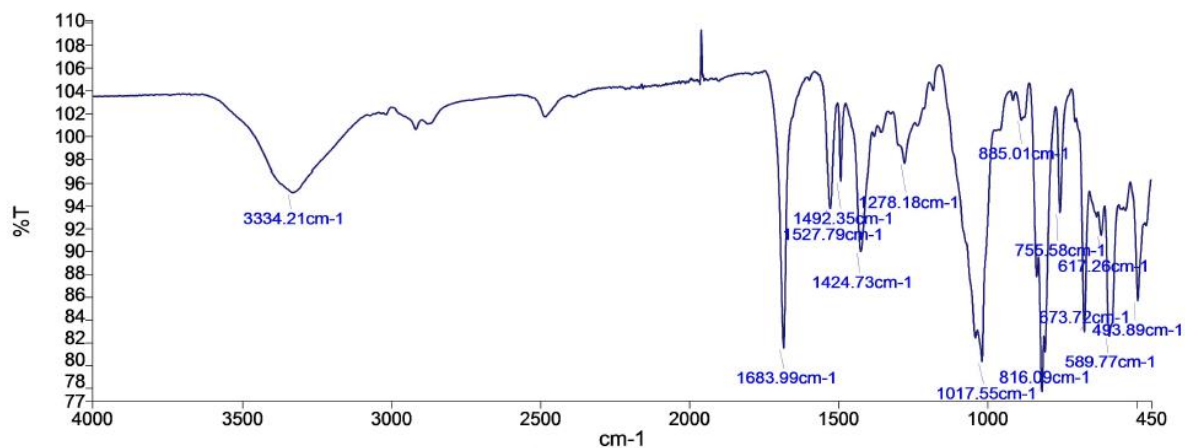


Appendix

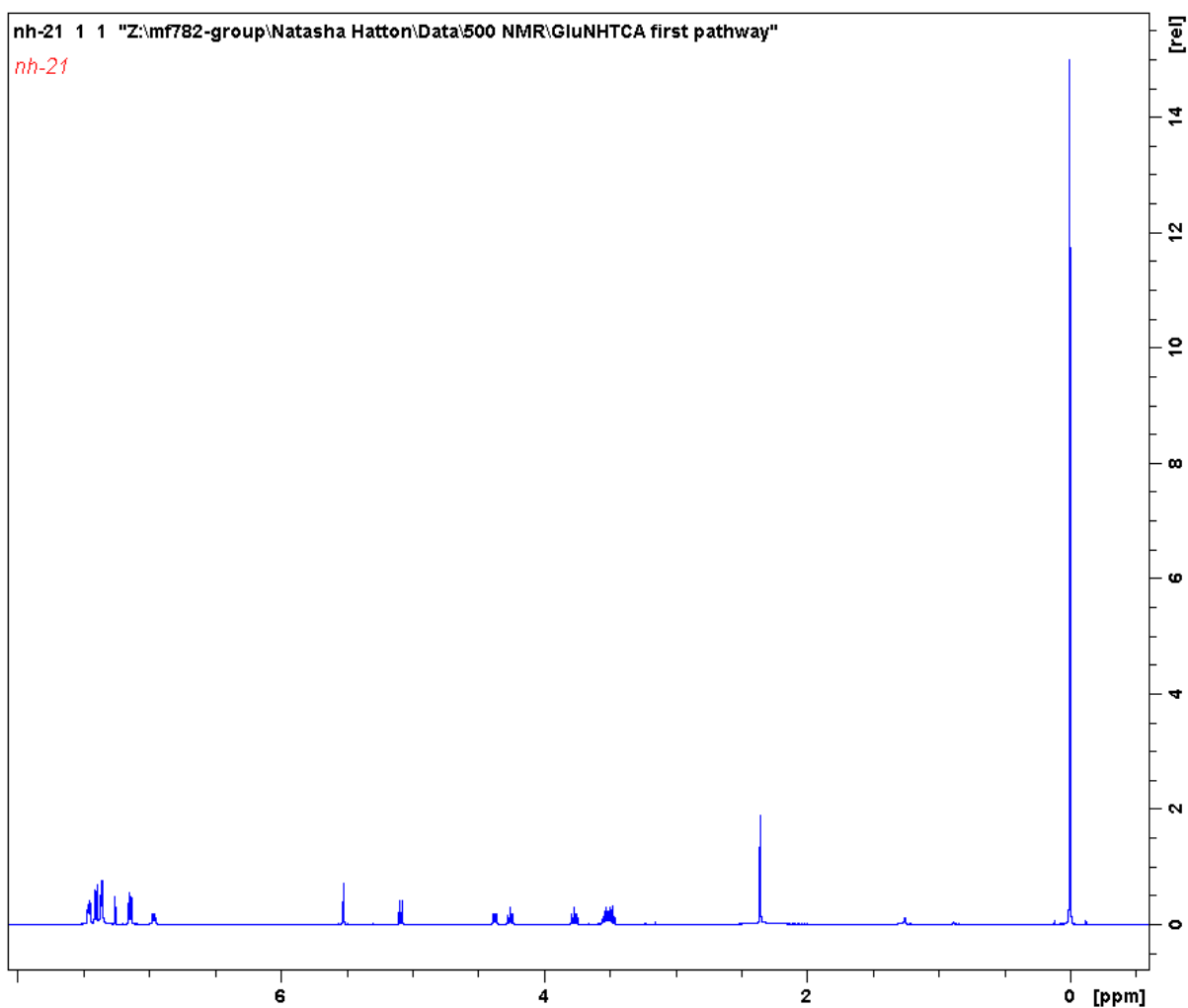
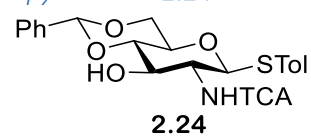




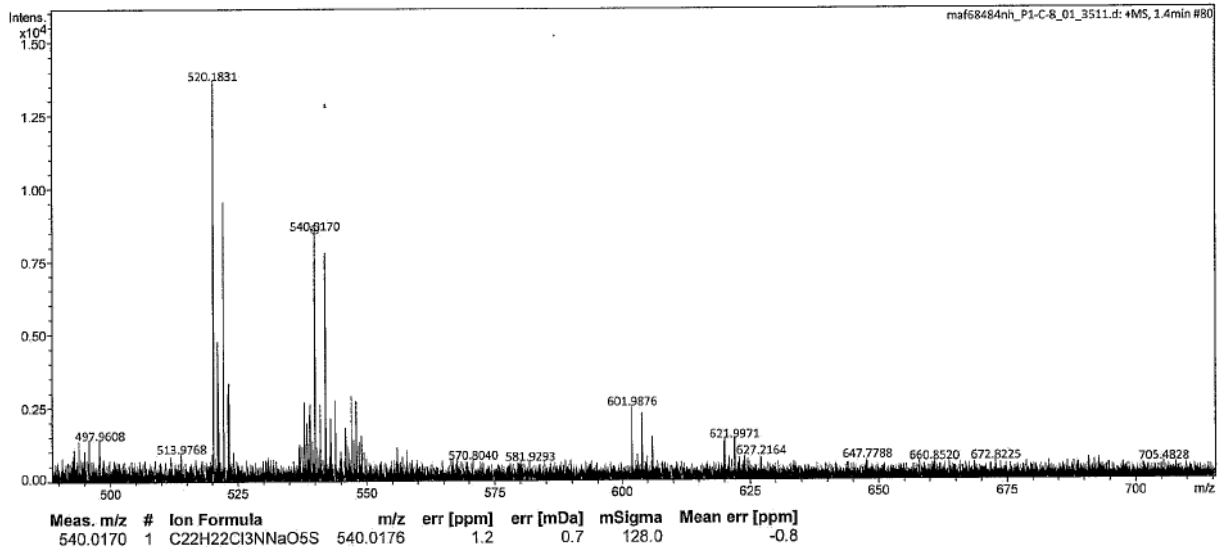
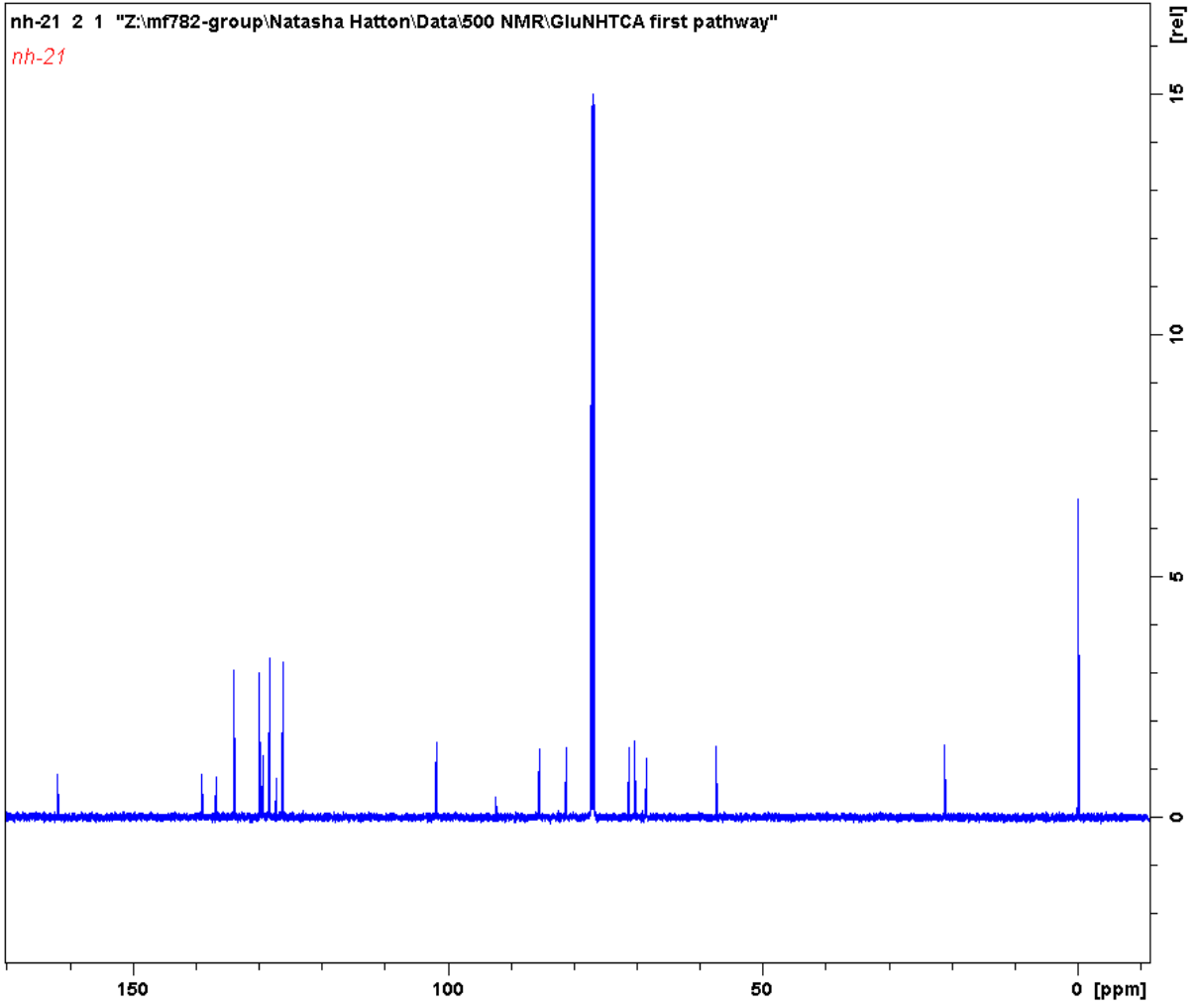
## Appendix



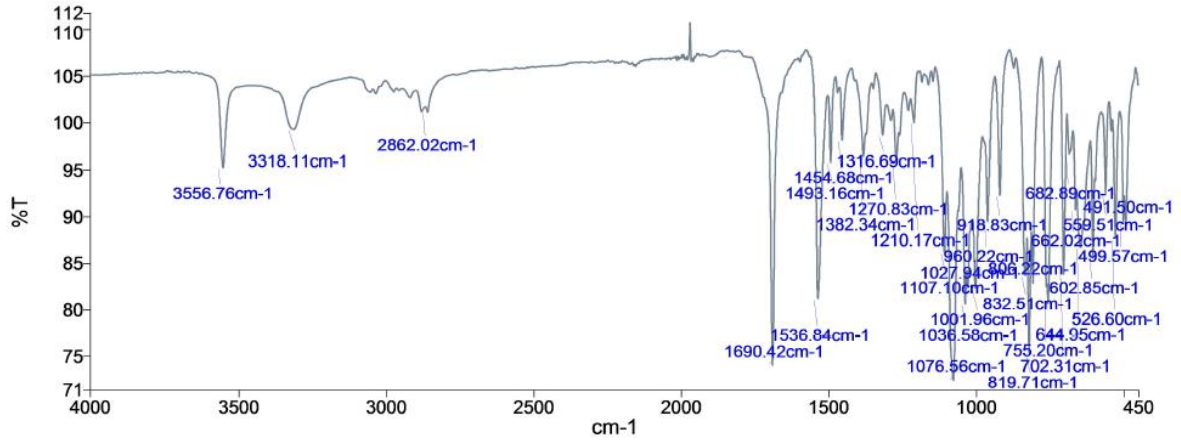
### 9.1.3.5 4-Methylphenyl 4,6-O-benzylidene-2-deoxy-2-trichloroacetyl- $\beta$ -D-glucopyranoside 2.24



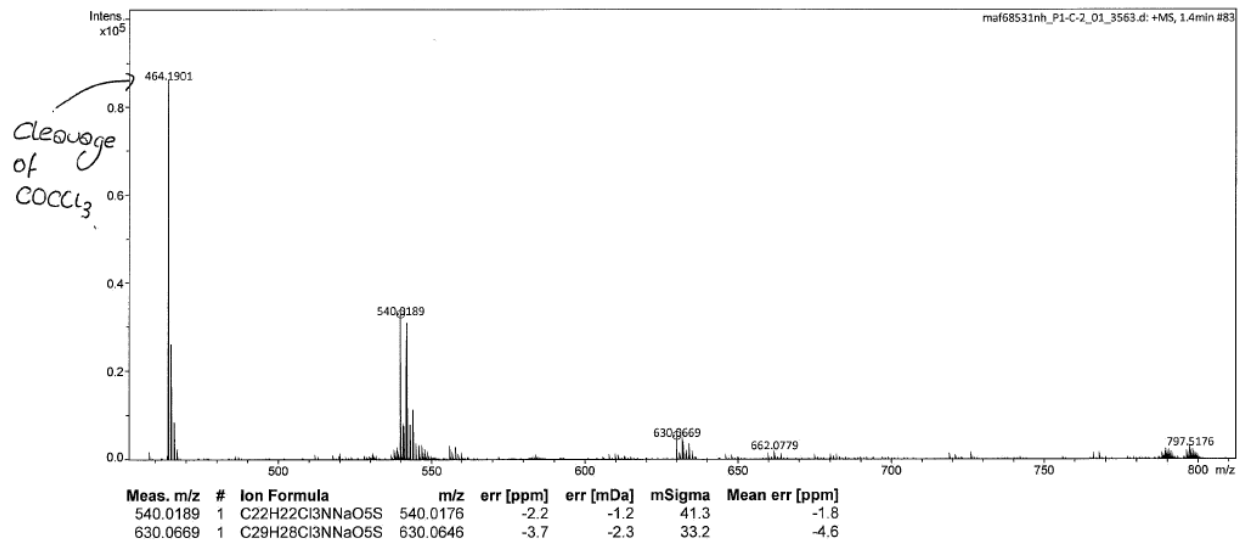
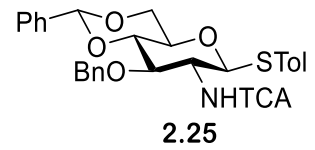
Appendix



## Appendix

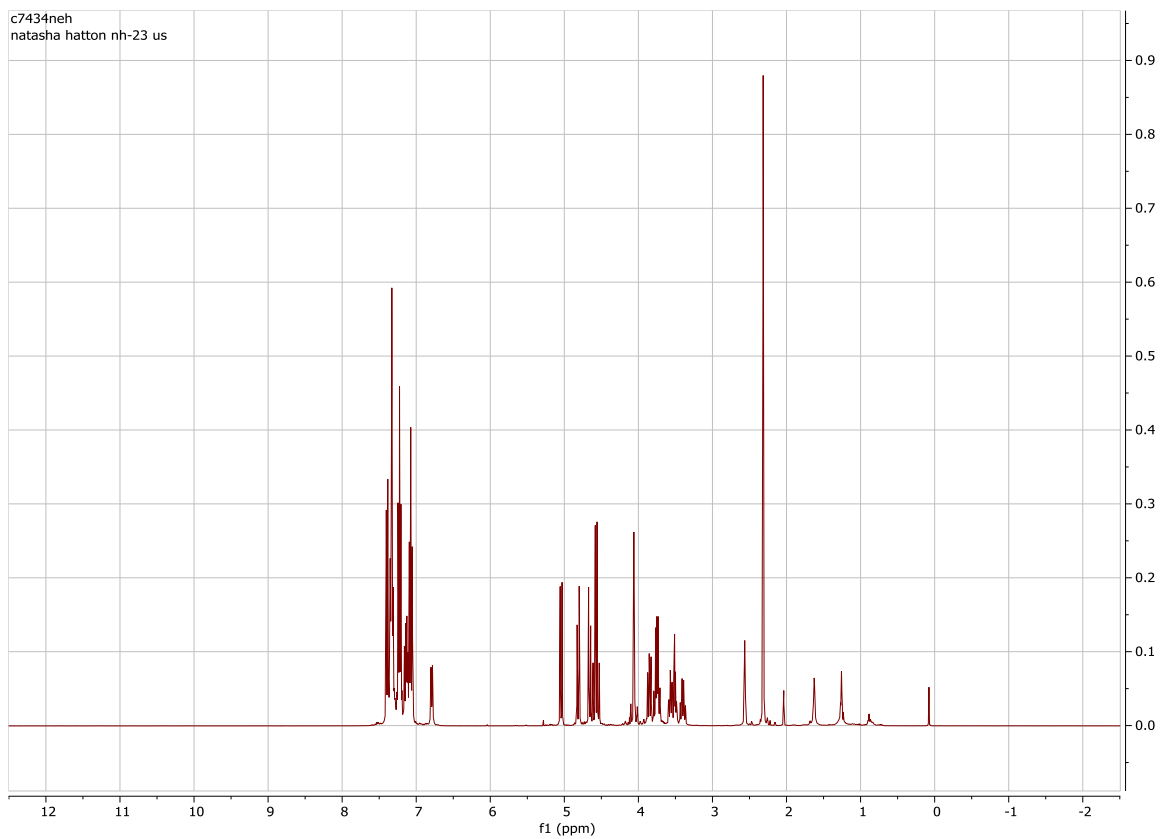
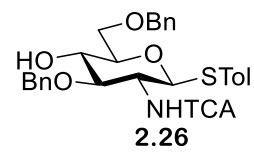


9.1.3.6 4-Methylphenyl 3-O-benzyl-4,6-O-benzylidene-2-deoxy-2-N-trichloroacetamido-1-thio-β-D-glucopyranoside **2.25**

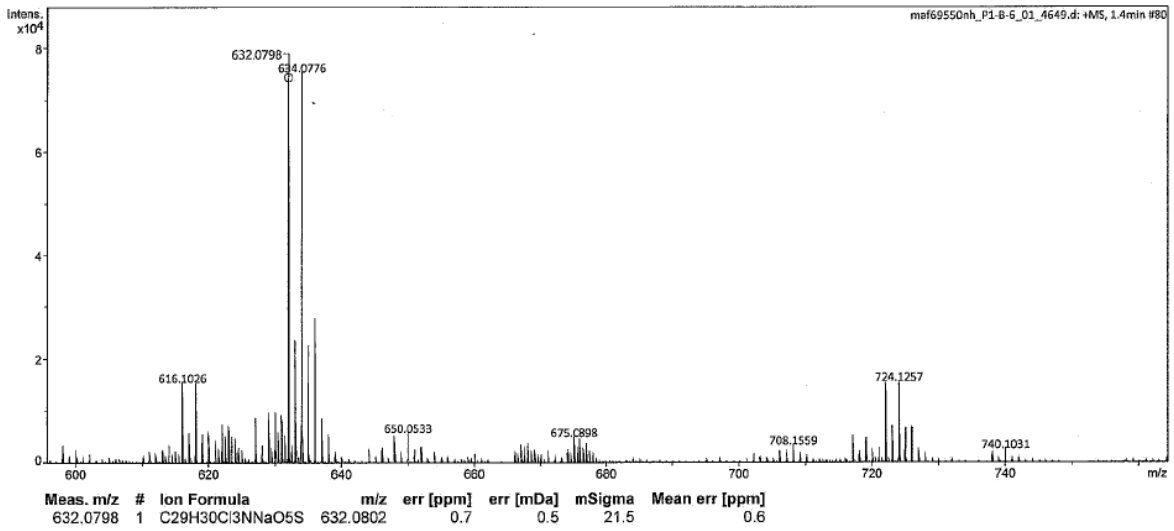
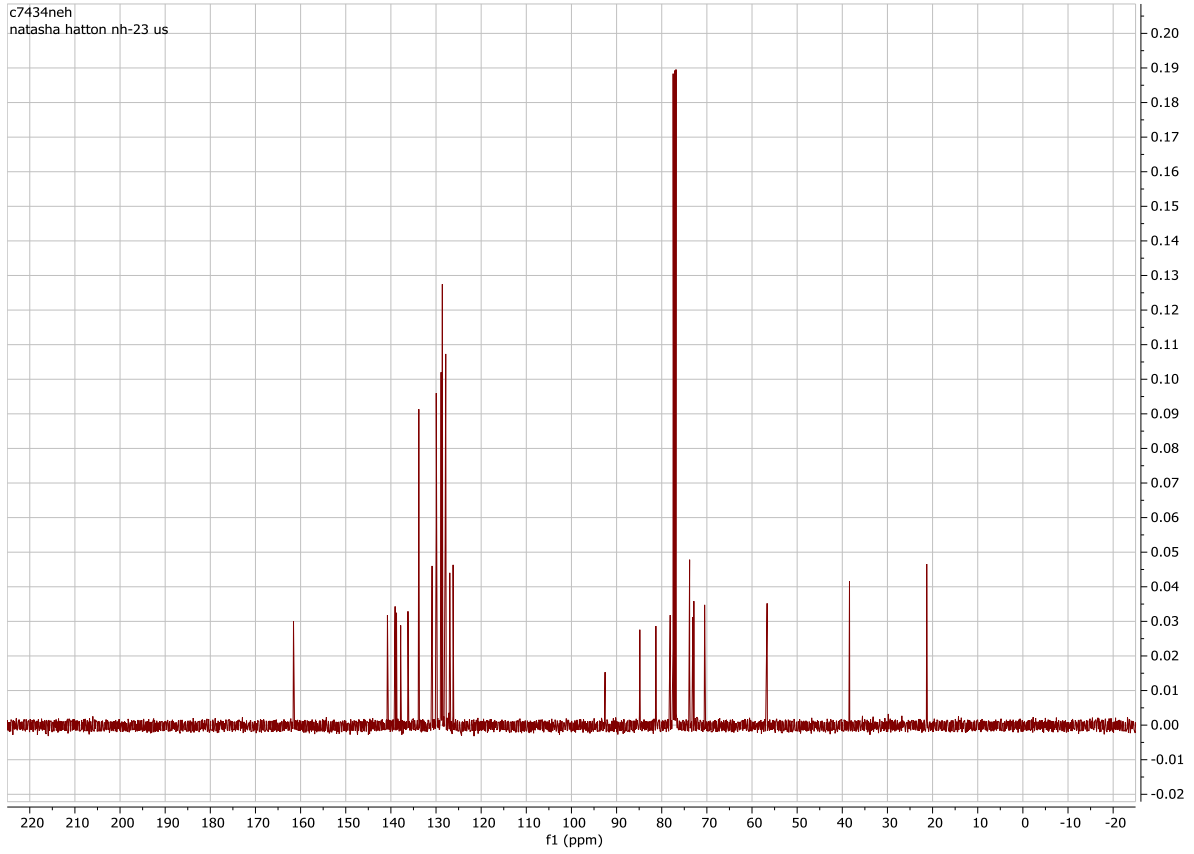


Appendix

9.1.3.7 4-Methylphenyl 3,6-di-O-benzyl-2-deoxy-2-N-trichloroacetamido-1-thio-β-D-glucopyranoside  
2.26



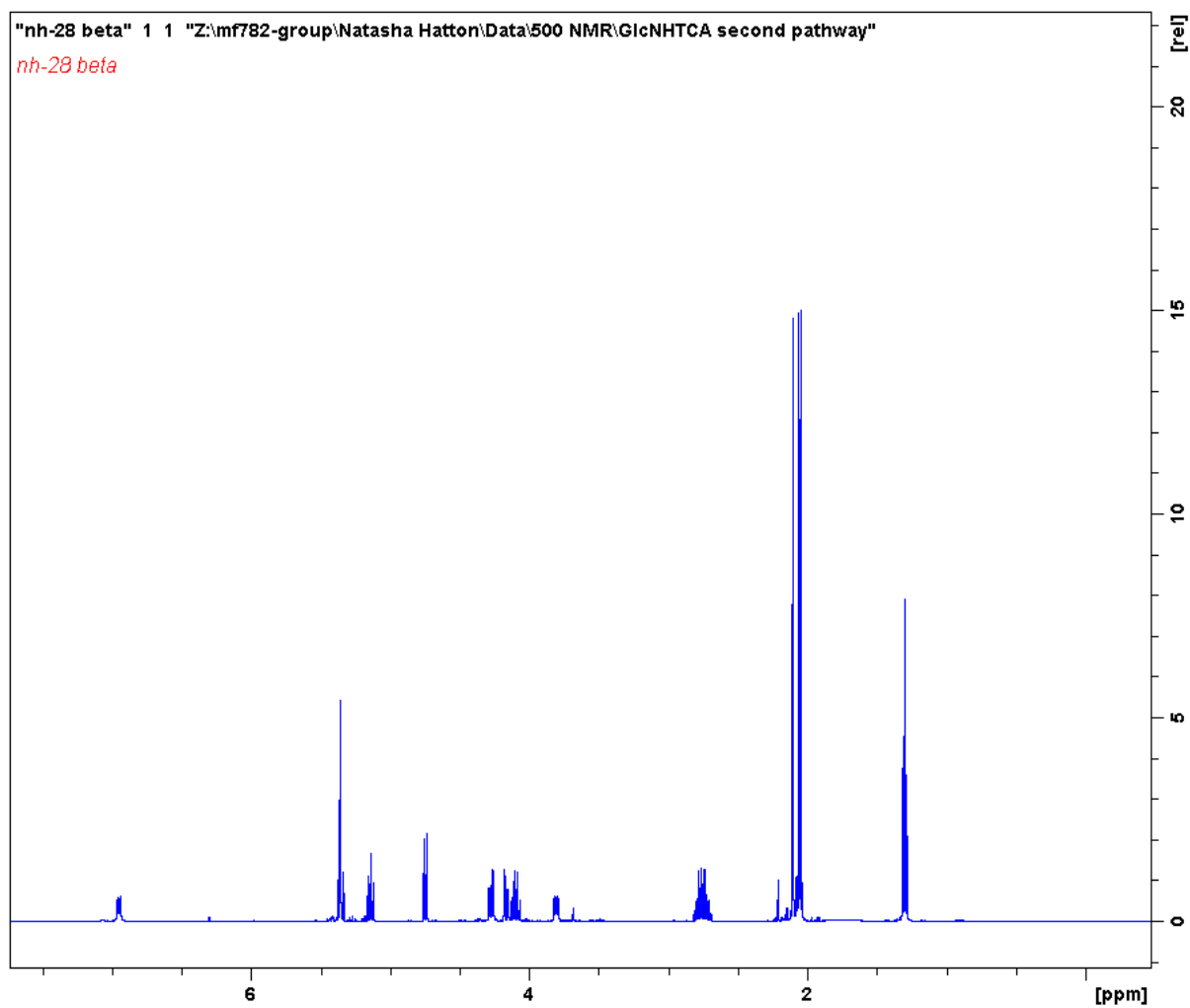
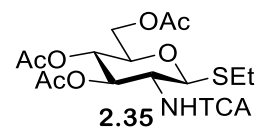
# Appendix



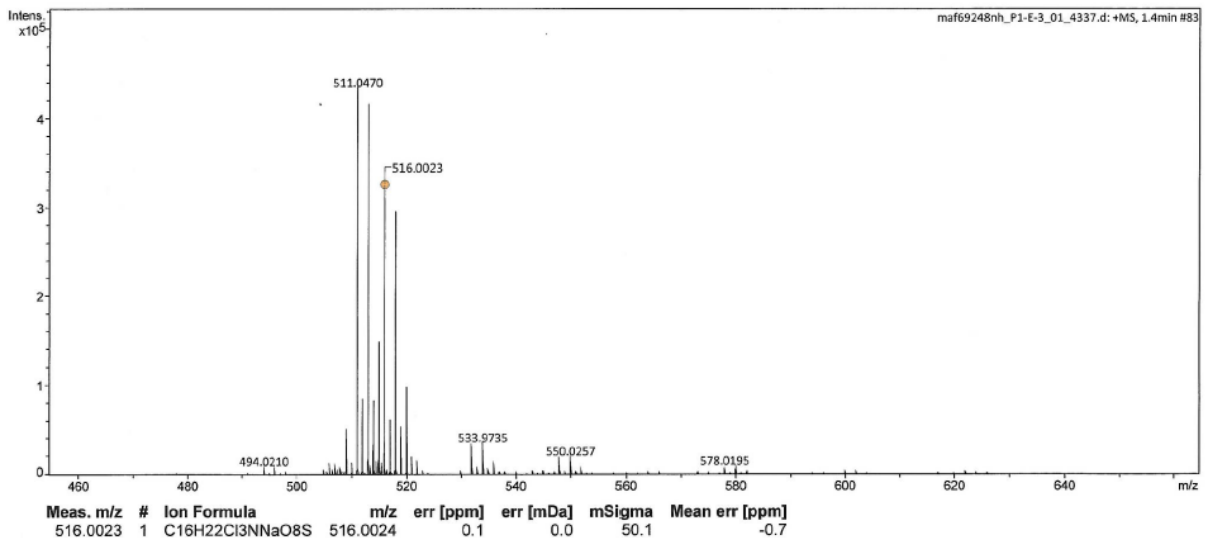
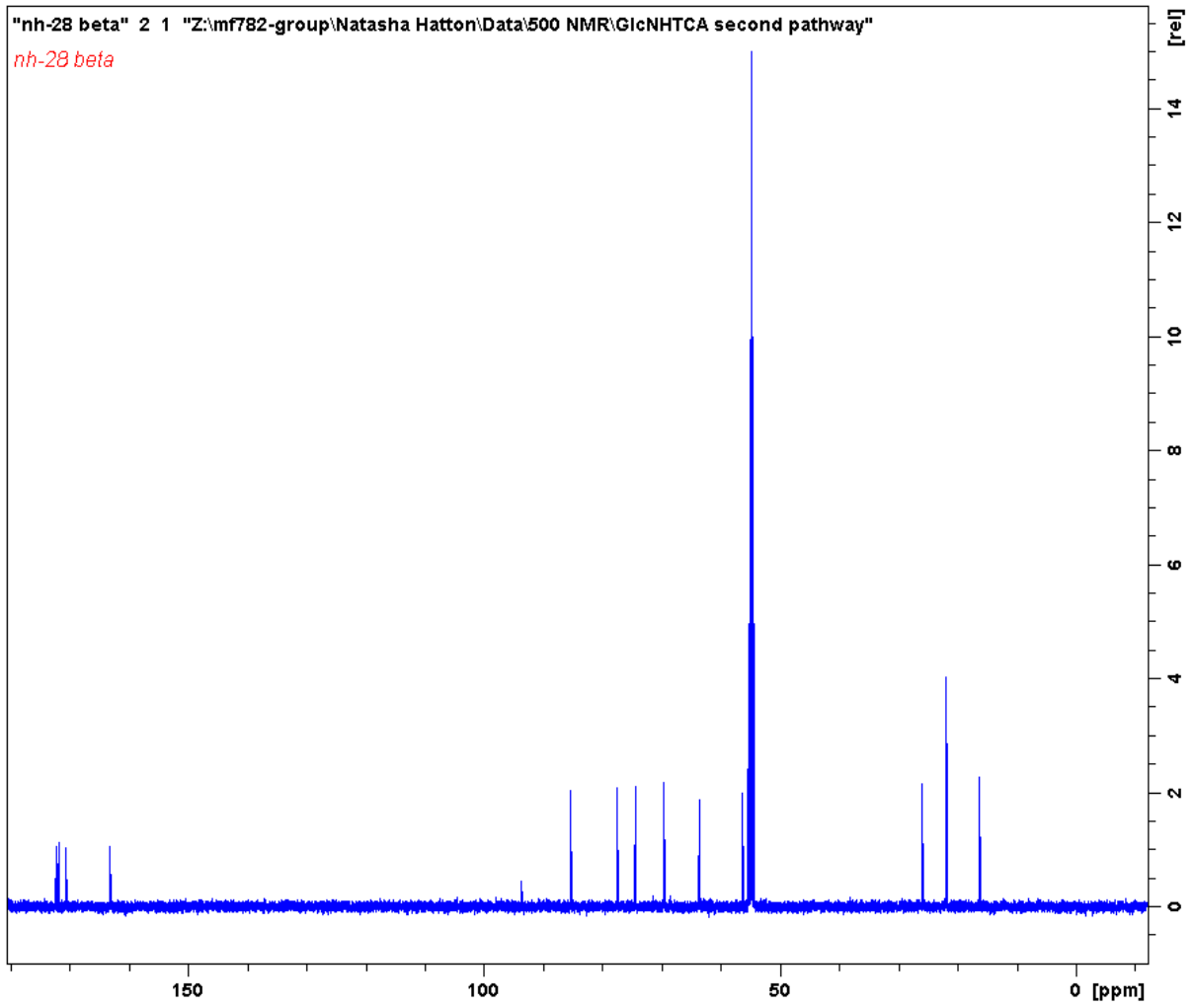
## Appendix

### 9.1.4 Synthesis of ethyl 3-*O*-benzoyl-4,6-*O*-benzylidene-2-deoxy-2-*N*-trichloroacetamido-1-thio- $\beta$ -D-glucopyranoside **2.38**

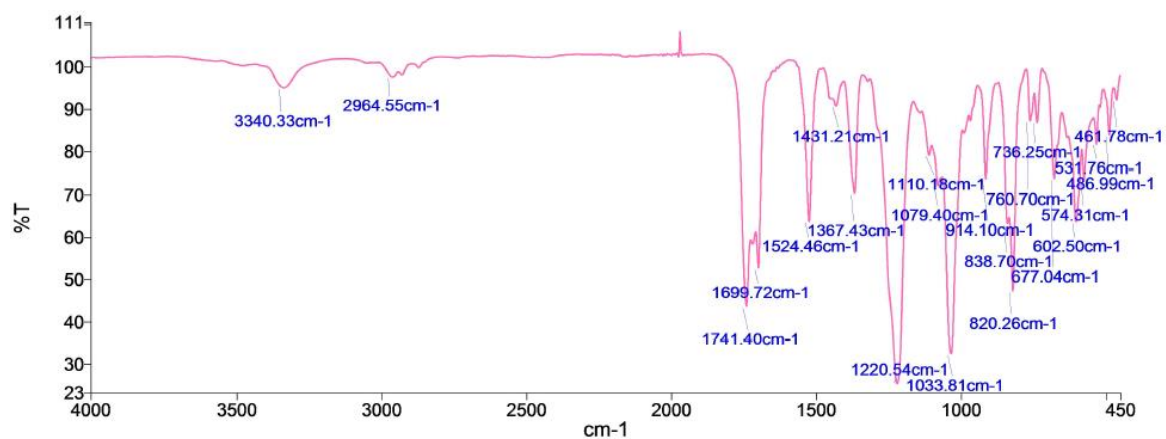
#### 9.1.4.1 Ethyl-3,4,6-tri-*O*-acetyl-2-deoxy-2-(trichloroethoxycarbonylamido)-1-thio- $\beta$ -D-glucopyranoside **2.35**



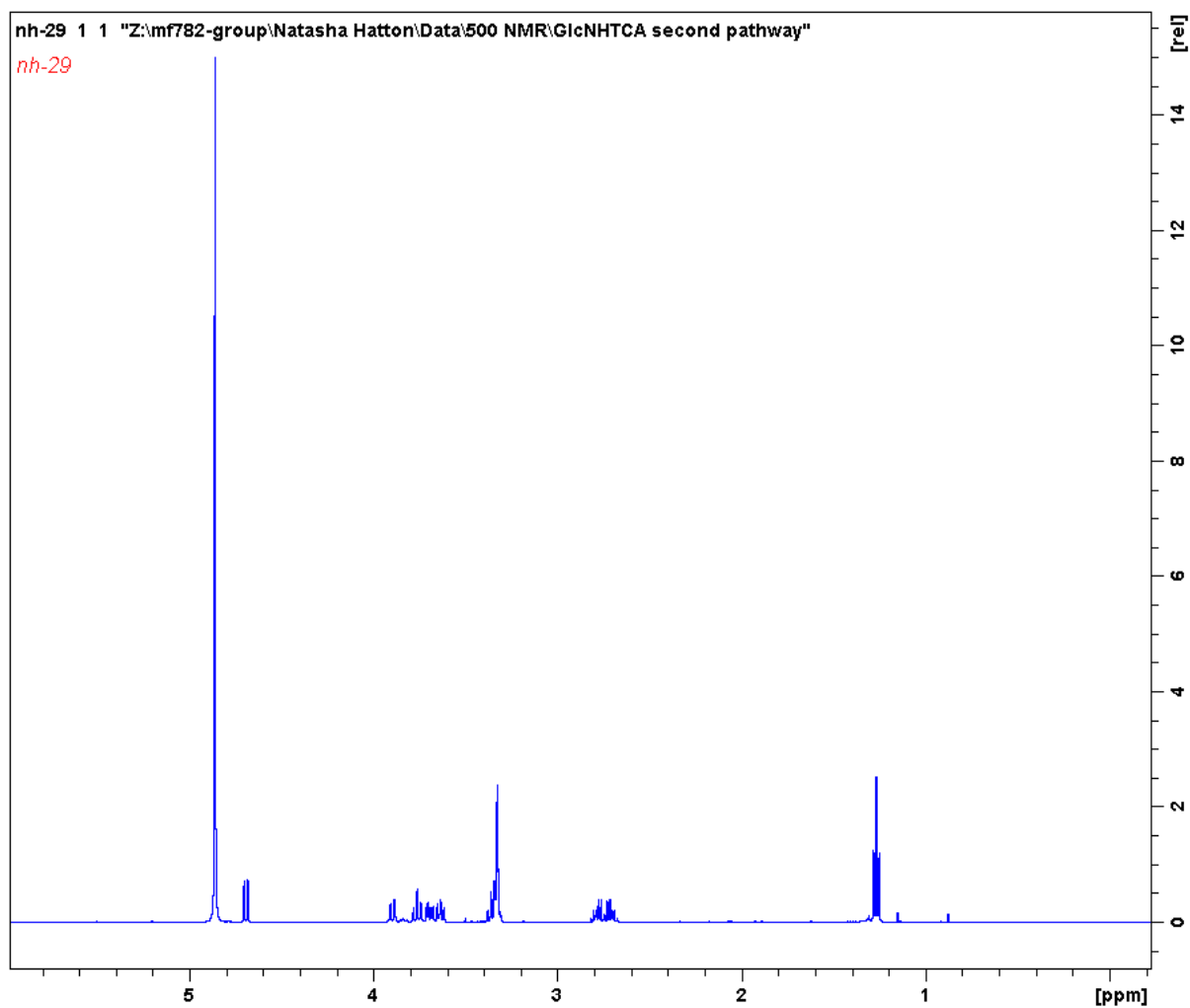
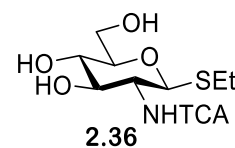
# Appendix



## Appendix

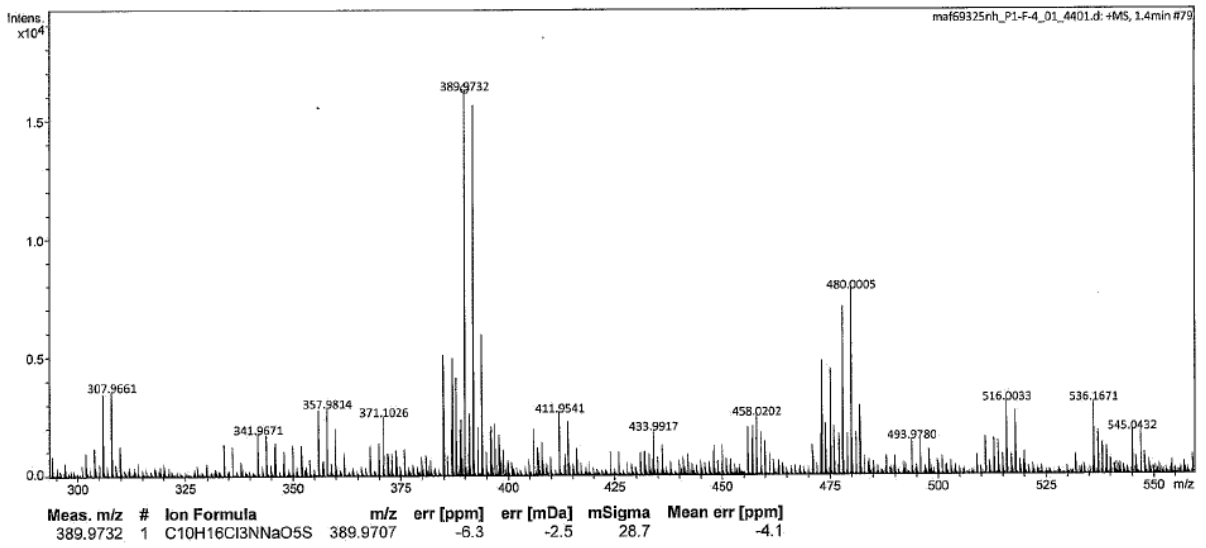
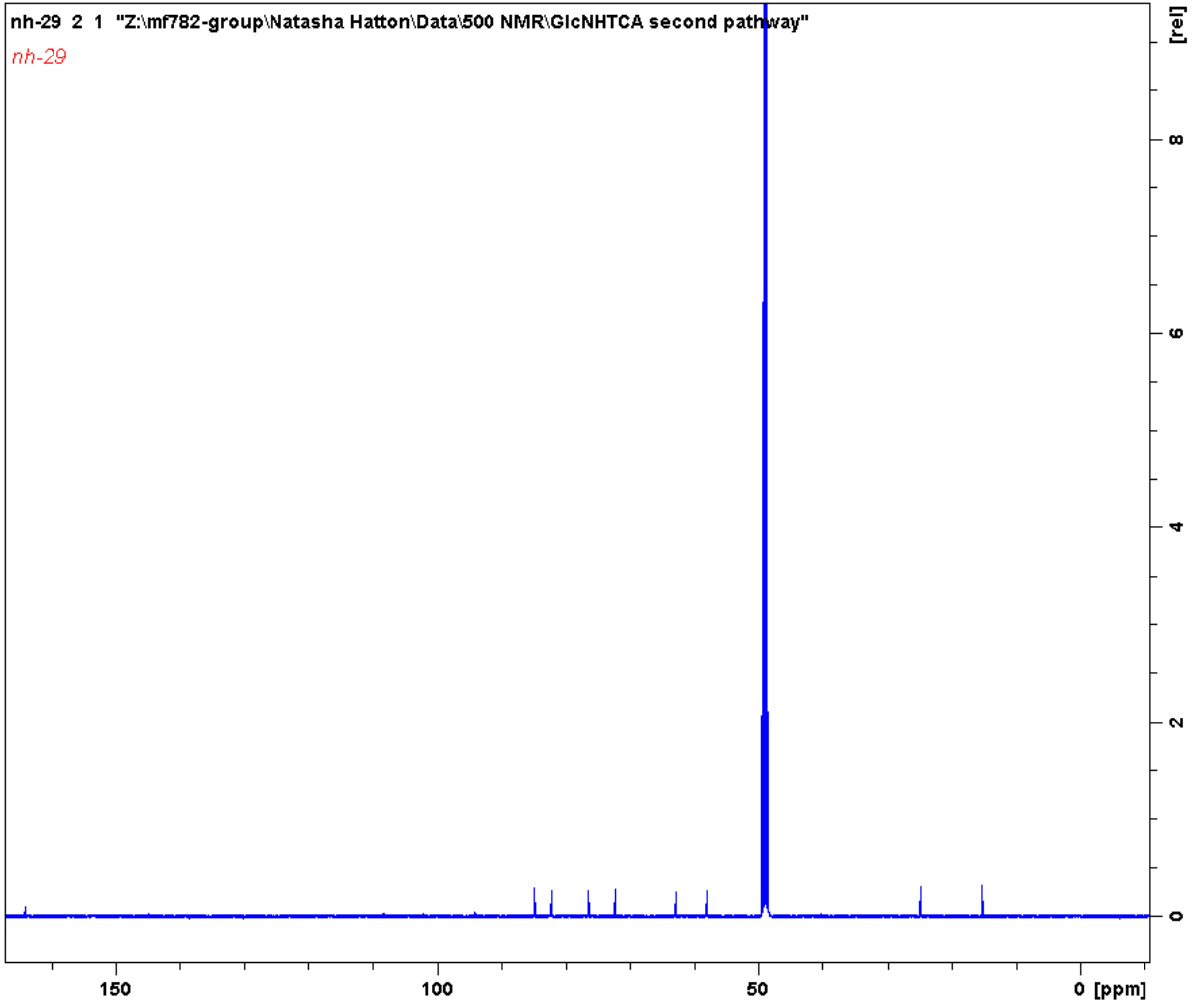


### 9.1.4.2 Ethyl 2-deoxy-2-N-trichloroacetamido-1-thio-β-D-glucopyranoside 2.36

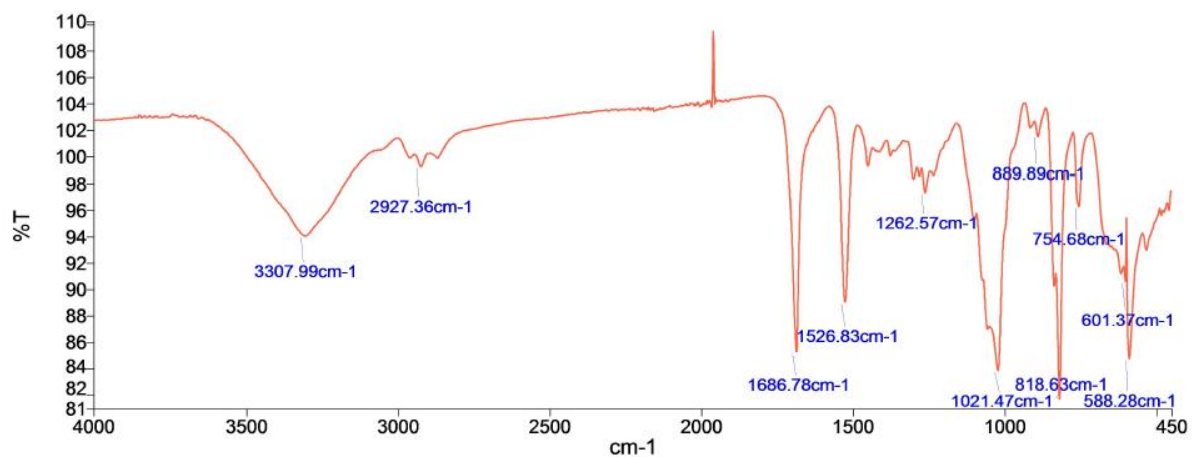




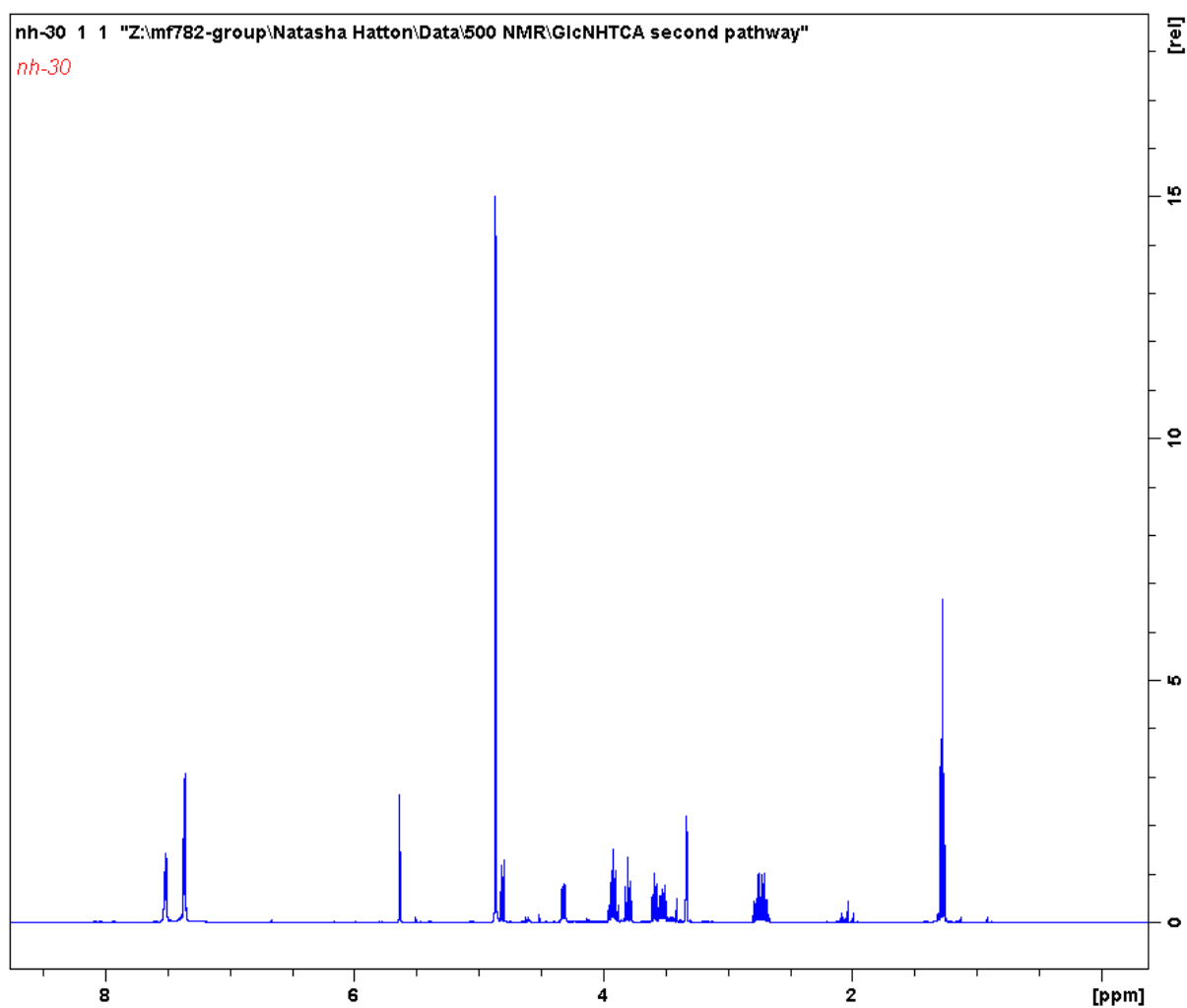
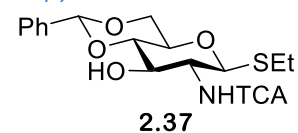
Appendix



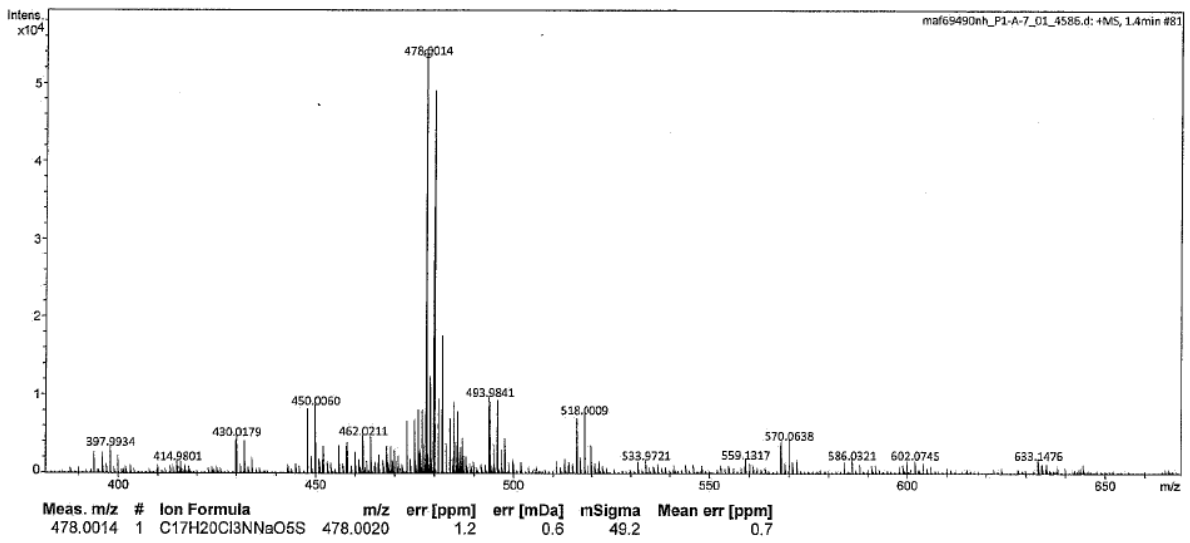
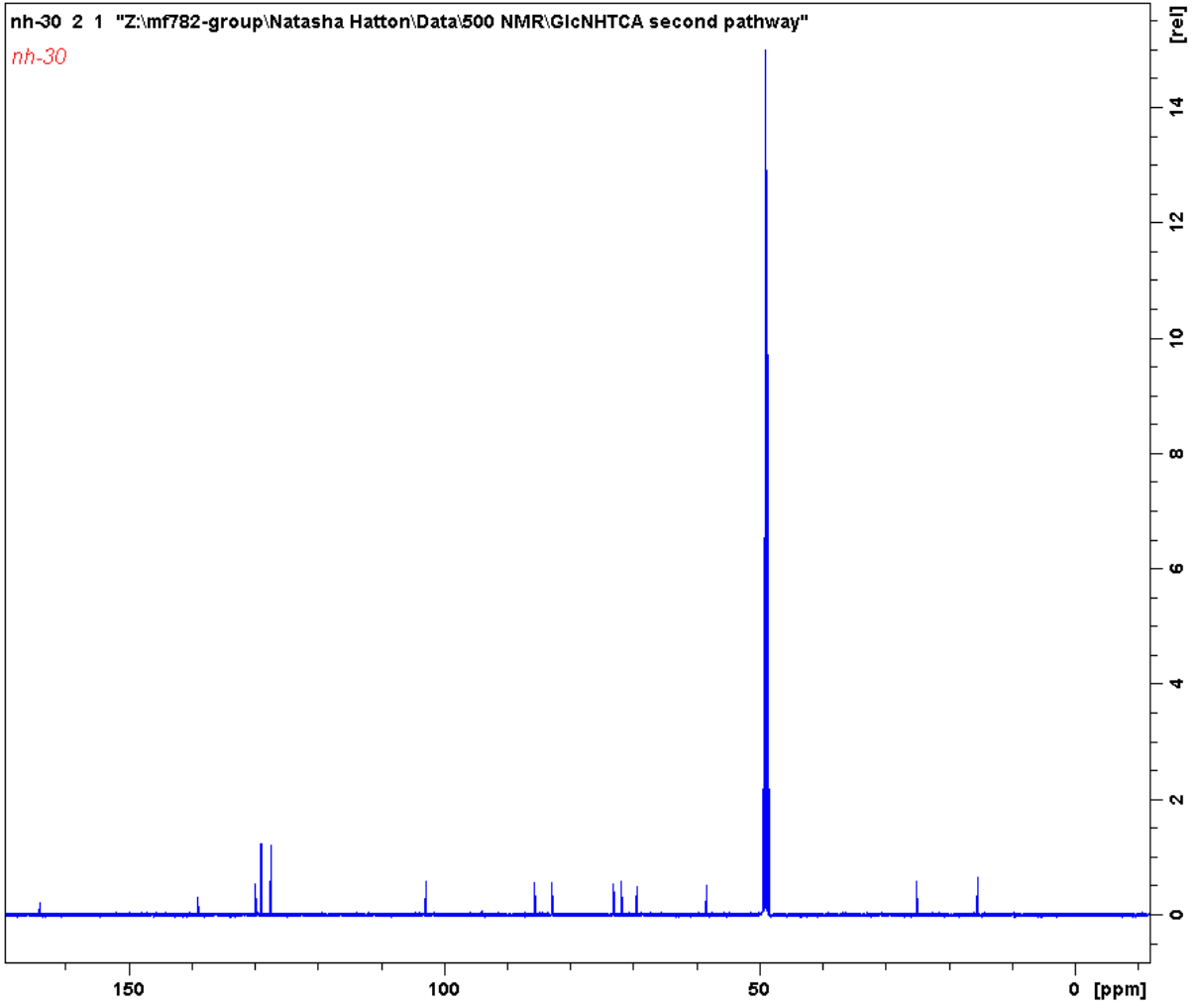
## Appendix



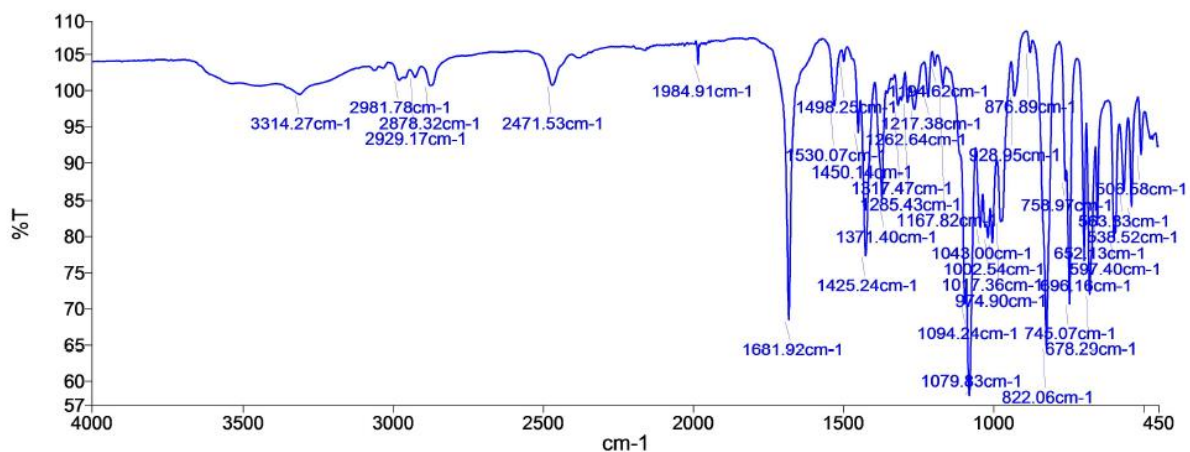
### 9.1.4.3 Ethyl 4,6-O-benzylidene-2-deoxy-2-N-trichloroacetamido-1-thio-β-D-glucopyranoside 2.37



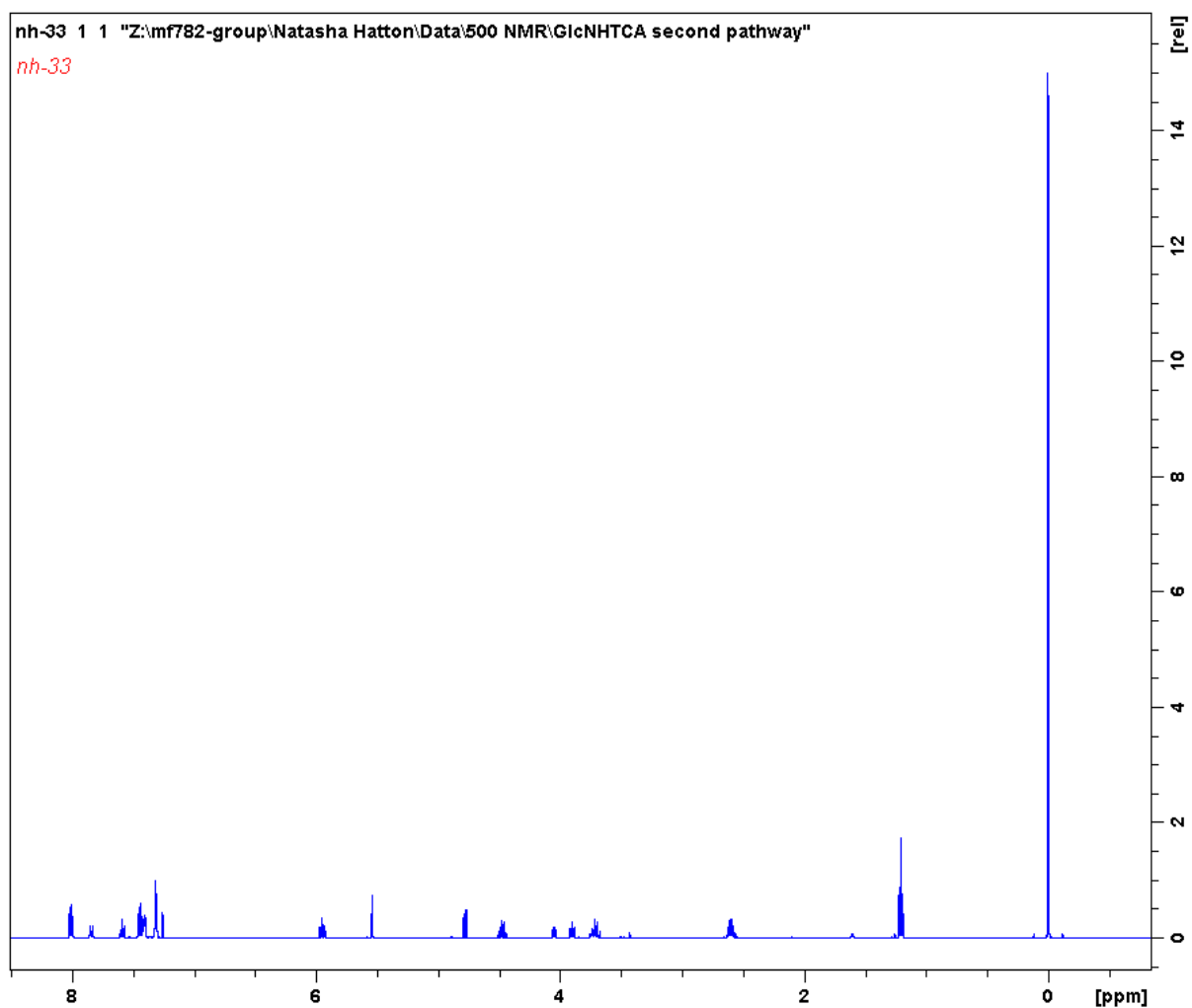
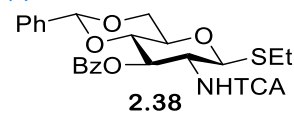
Appendix



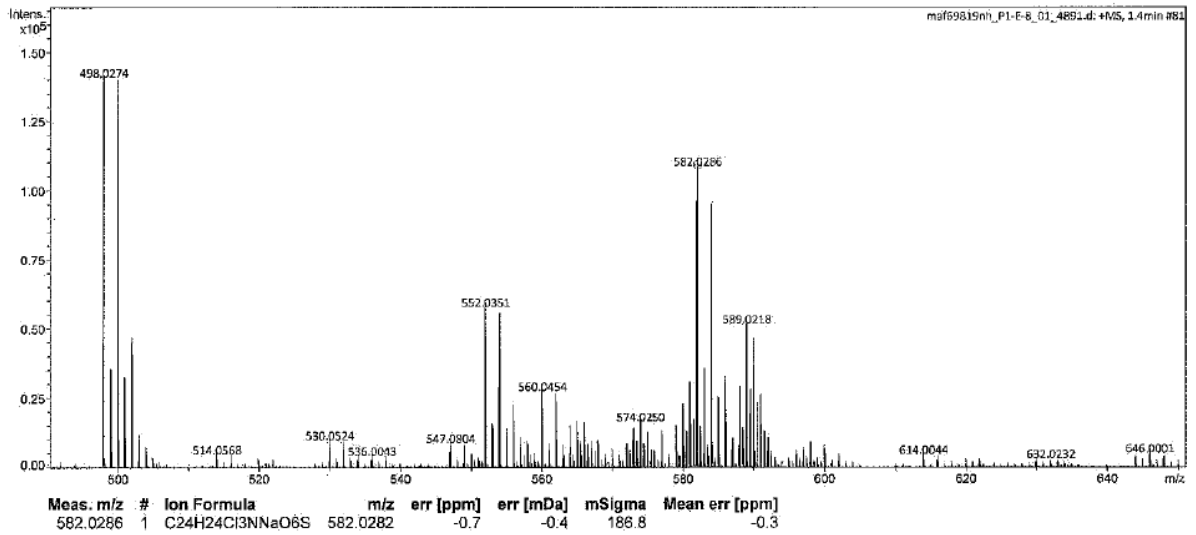
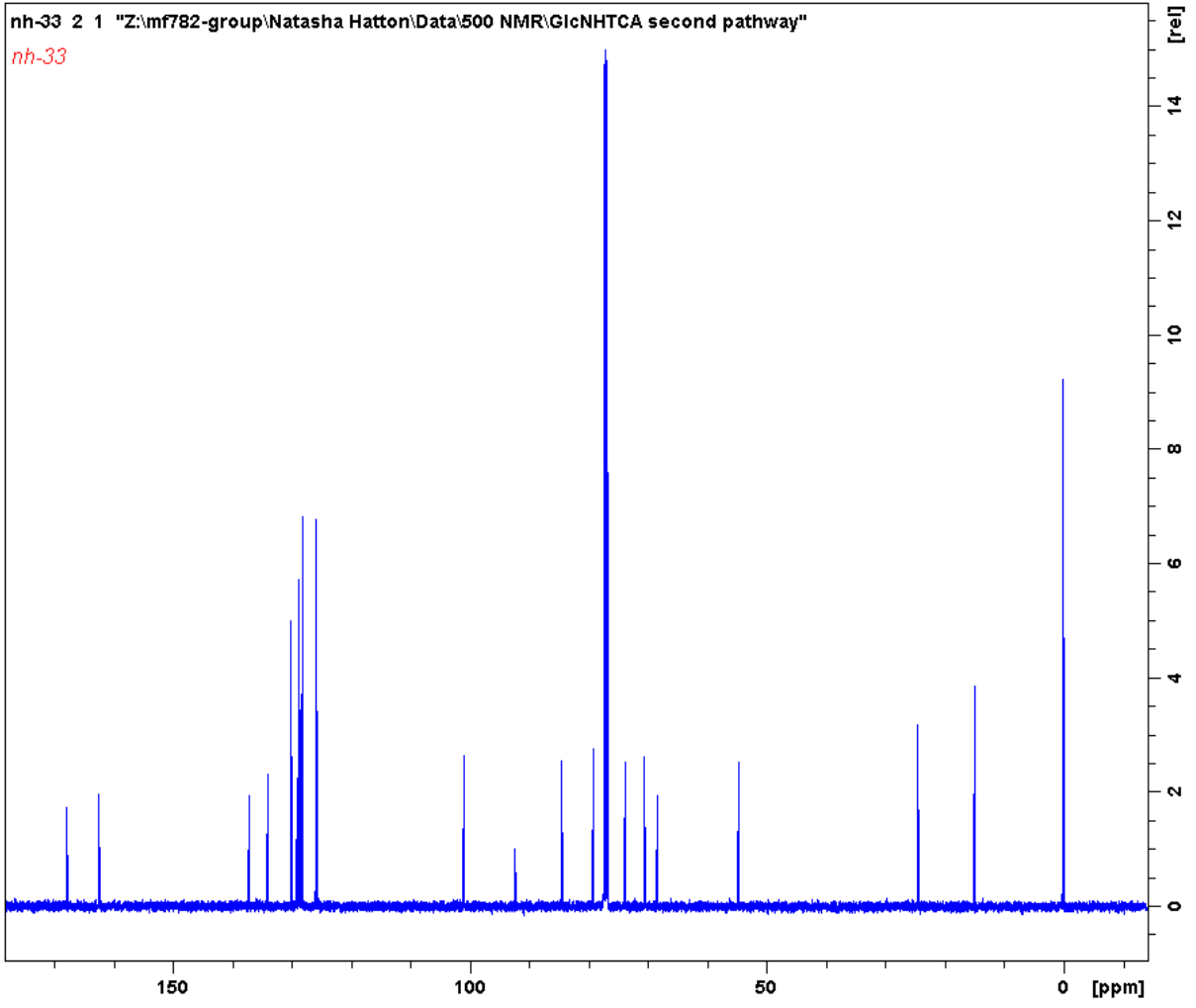
## Appendix



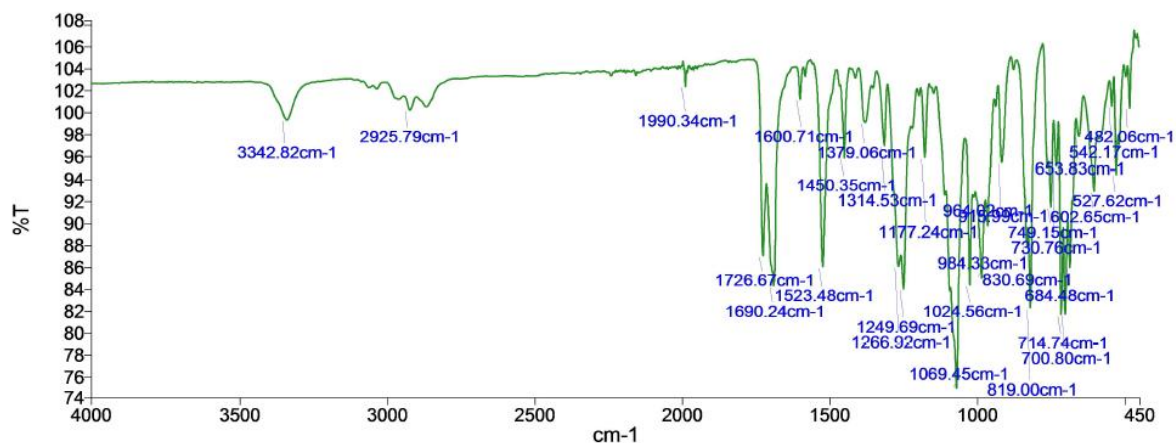
### 9.1.4.4 Ethyl 3,6-di-O-benzyl-2-deoxy-2-N-trichloroacetamido-1-thio-β-D-glucopyranoside **2.38**



Appendix

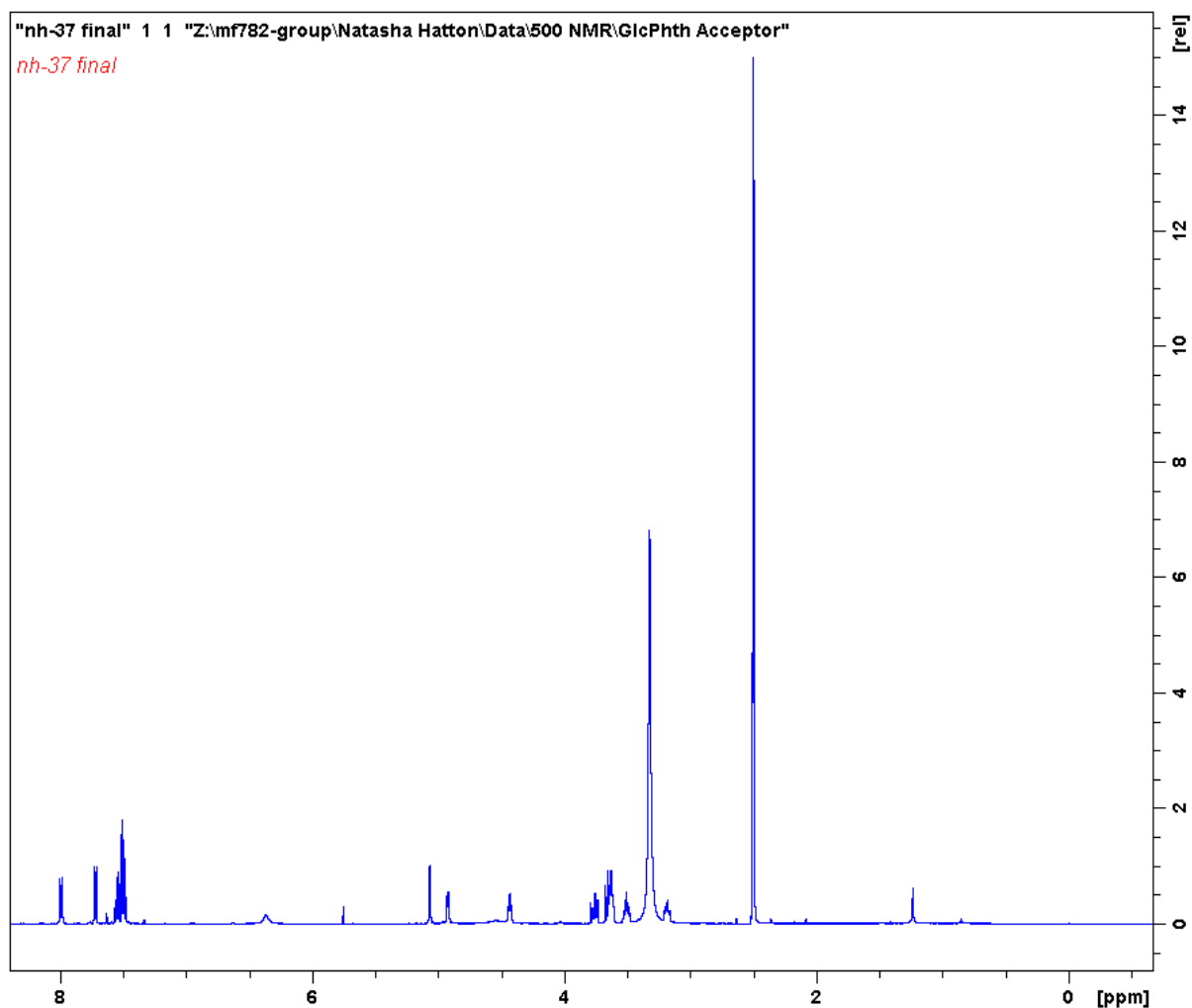
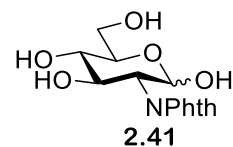


## Appendix

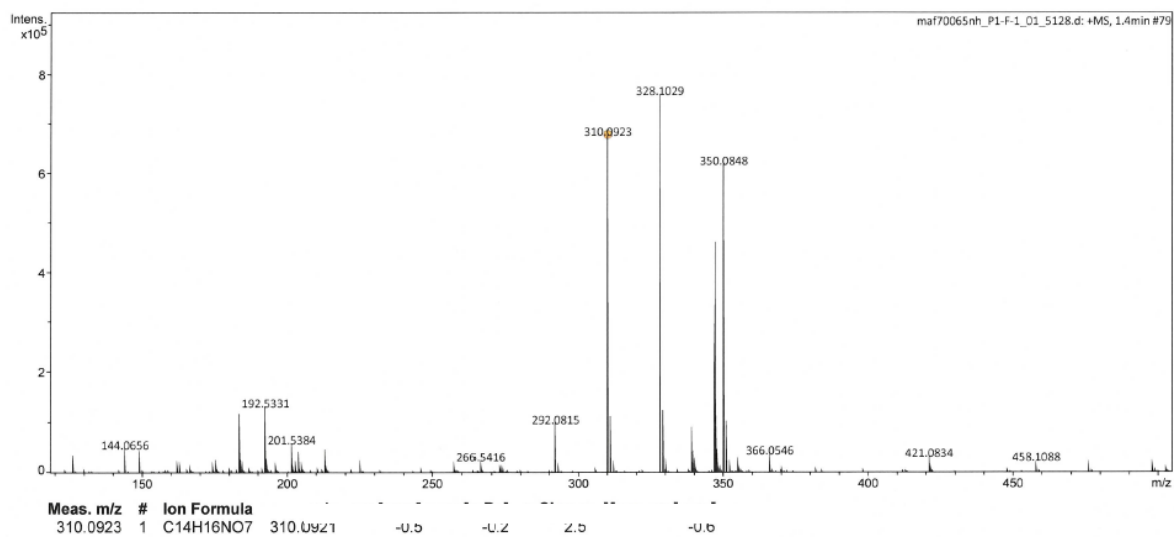
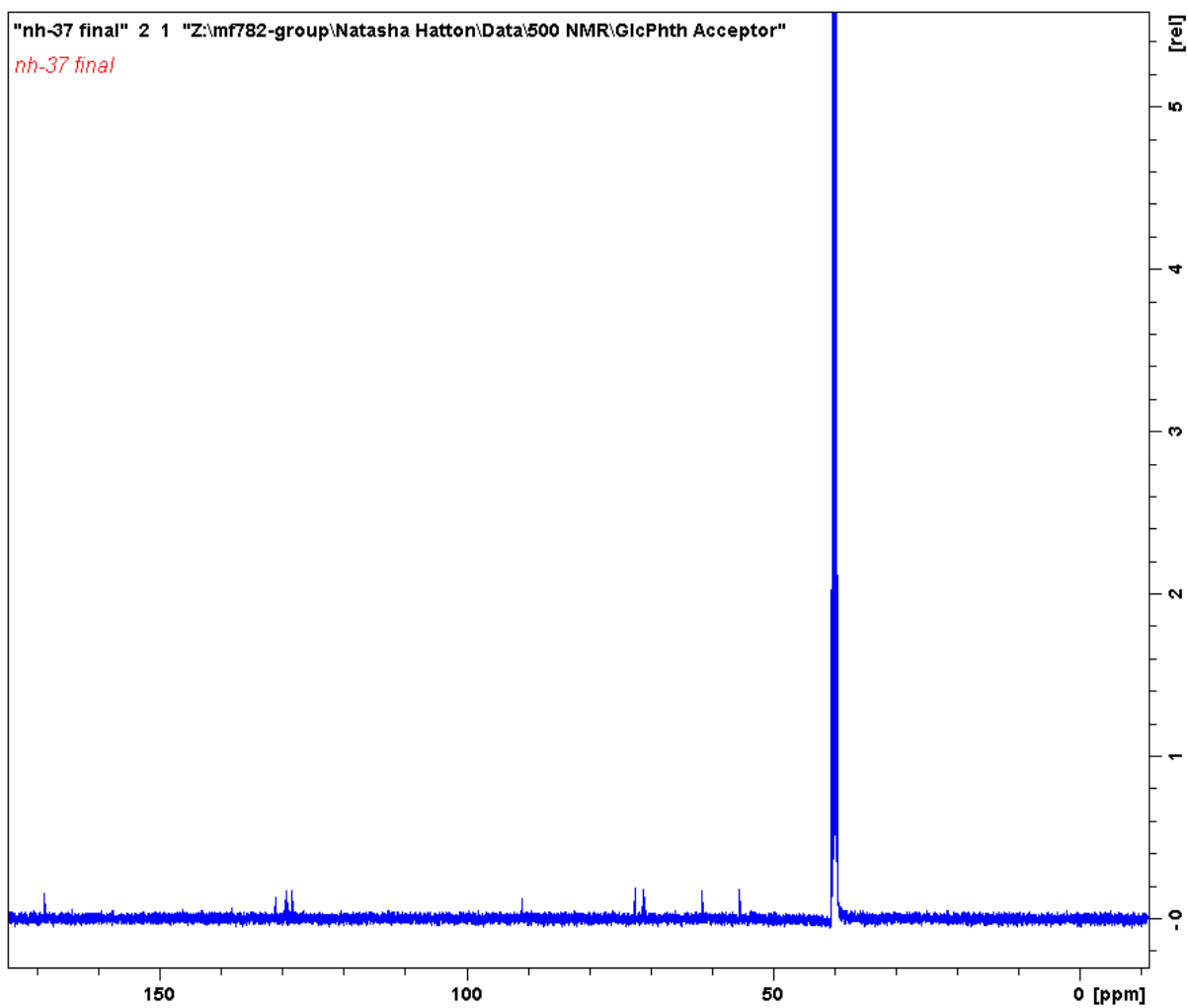


### 9.1.5 Synthesis of 3-Azidopropyl 3,6-di-O-benzyl-2-deoxy-2-phthalimido-1- $\beta$ -D-glucopyranoside **2.3c**

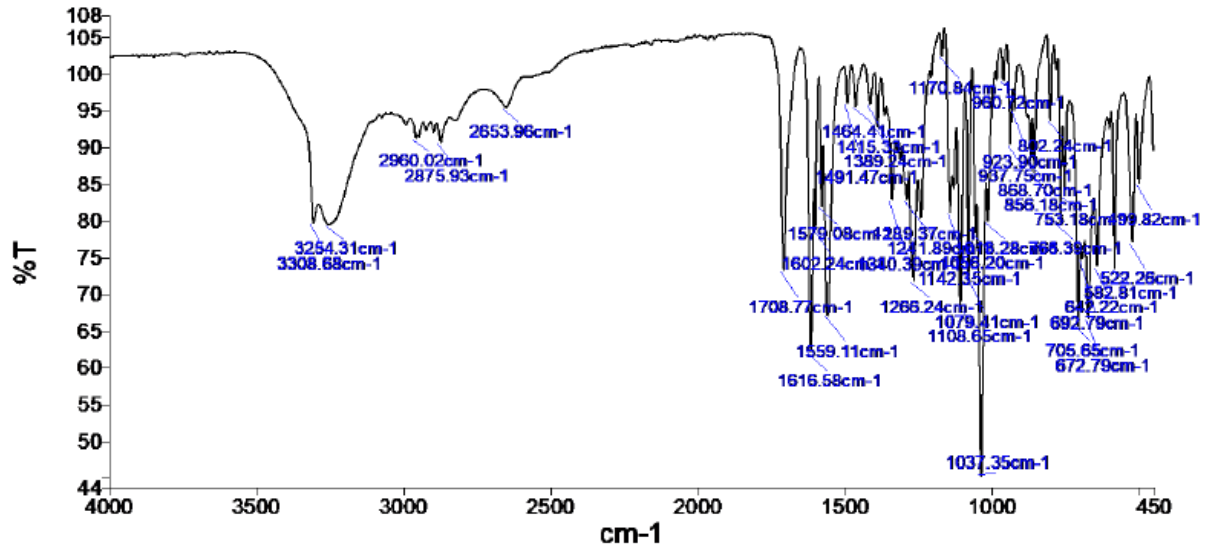
#### 9.1.5.1 2-Deoxy-2-phthalimido-D-glucopyranose **2.41**



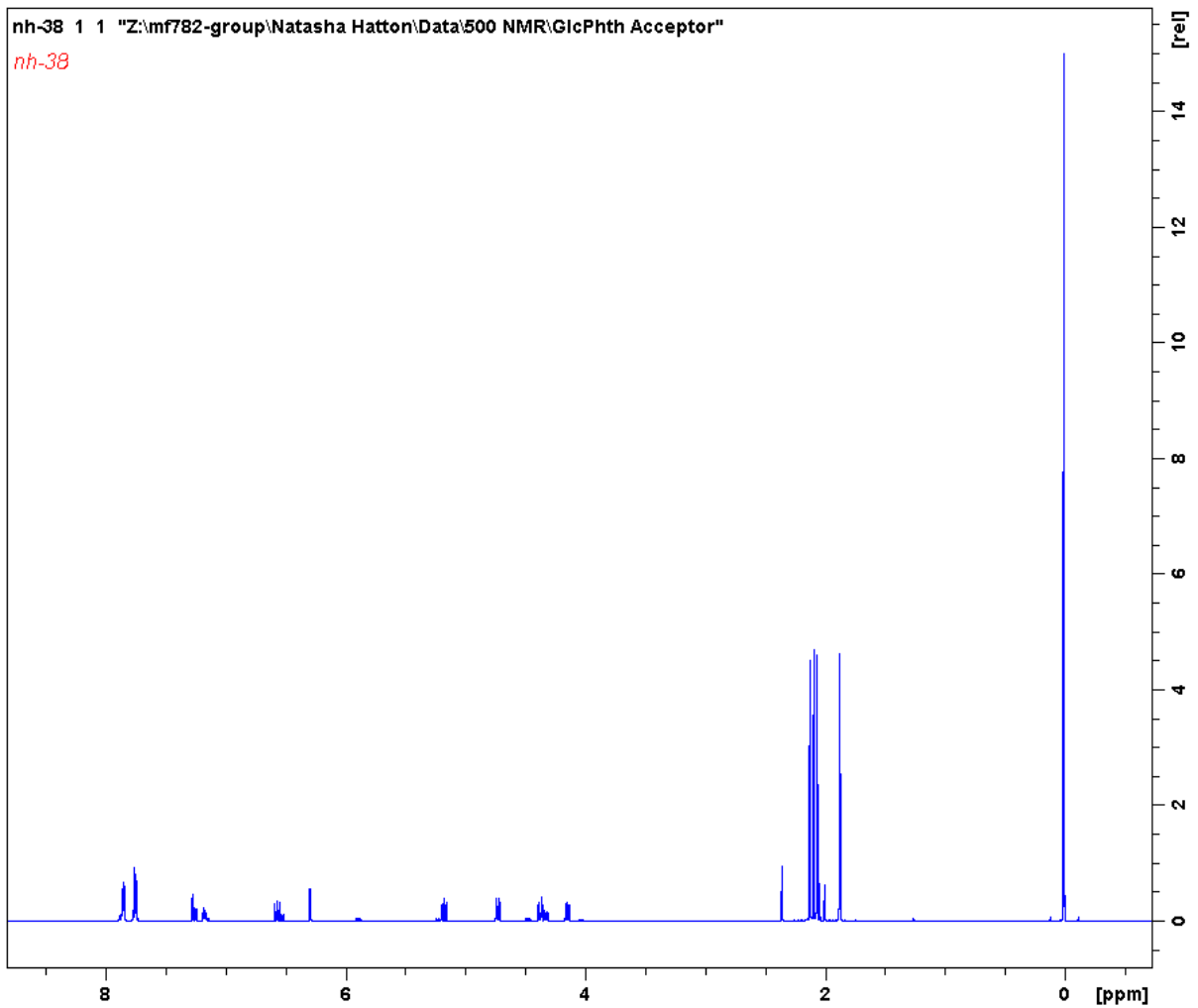
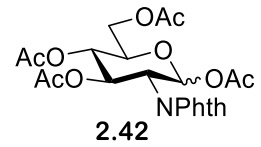
Appendix



Appendix

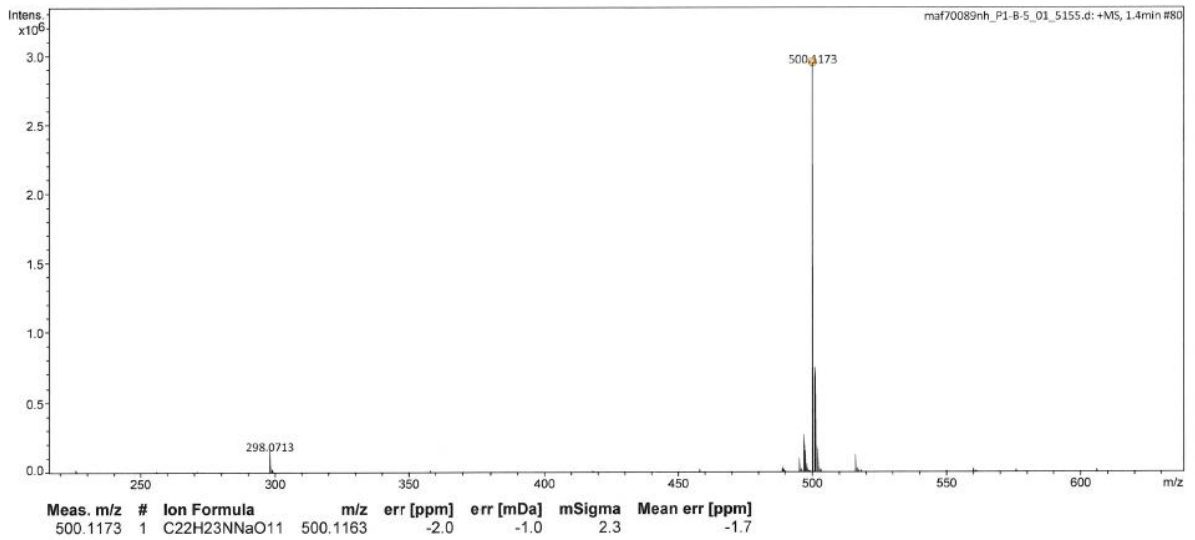
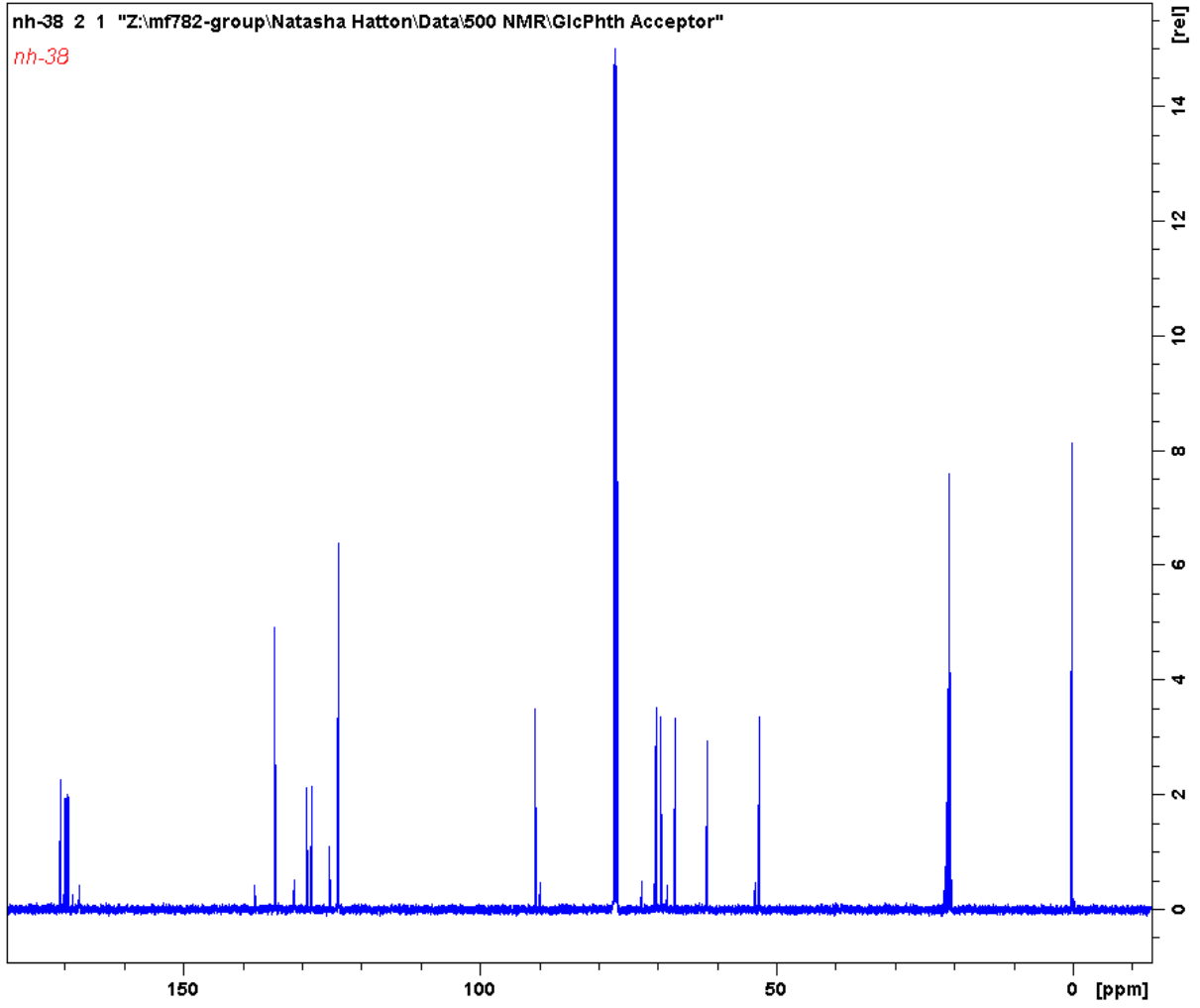


9.1.5.2 1,3,4,6-Tetra-O-acetyl-2-deoxy-2-phthalimido-D-glucopyranose 2.42

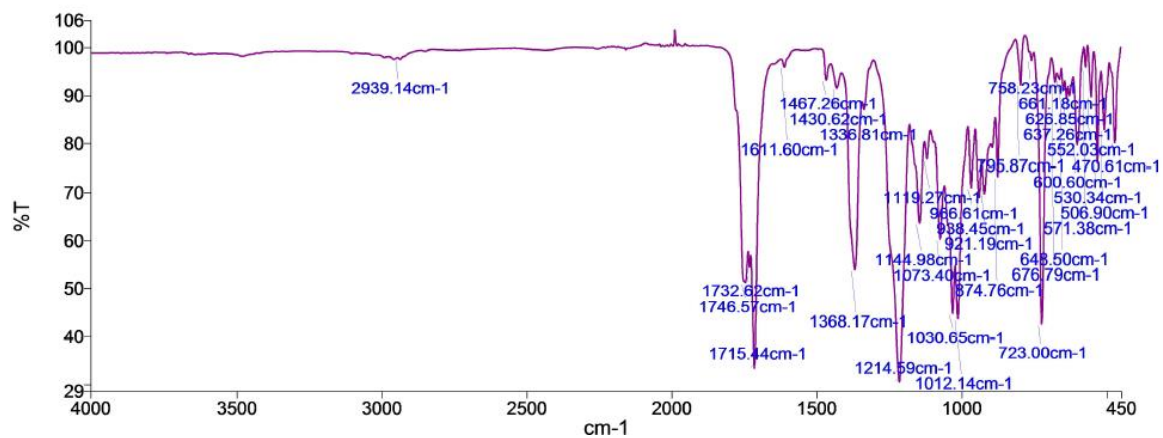




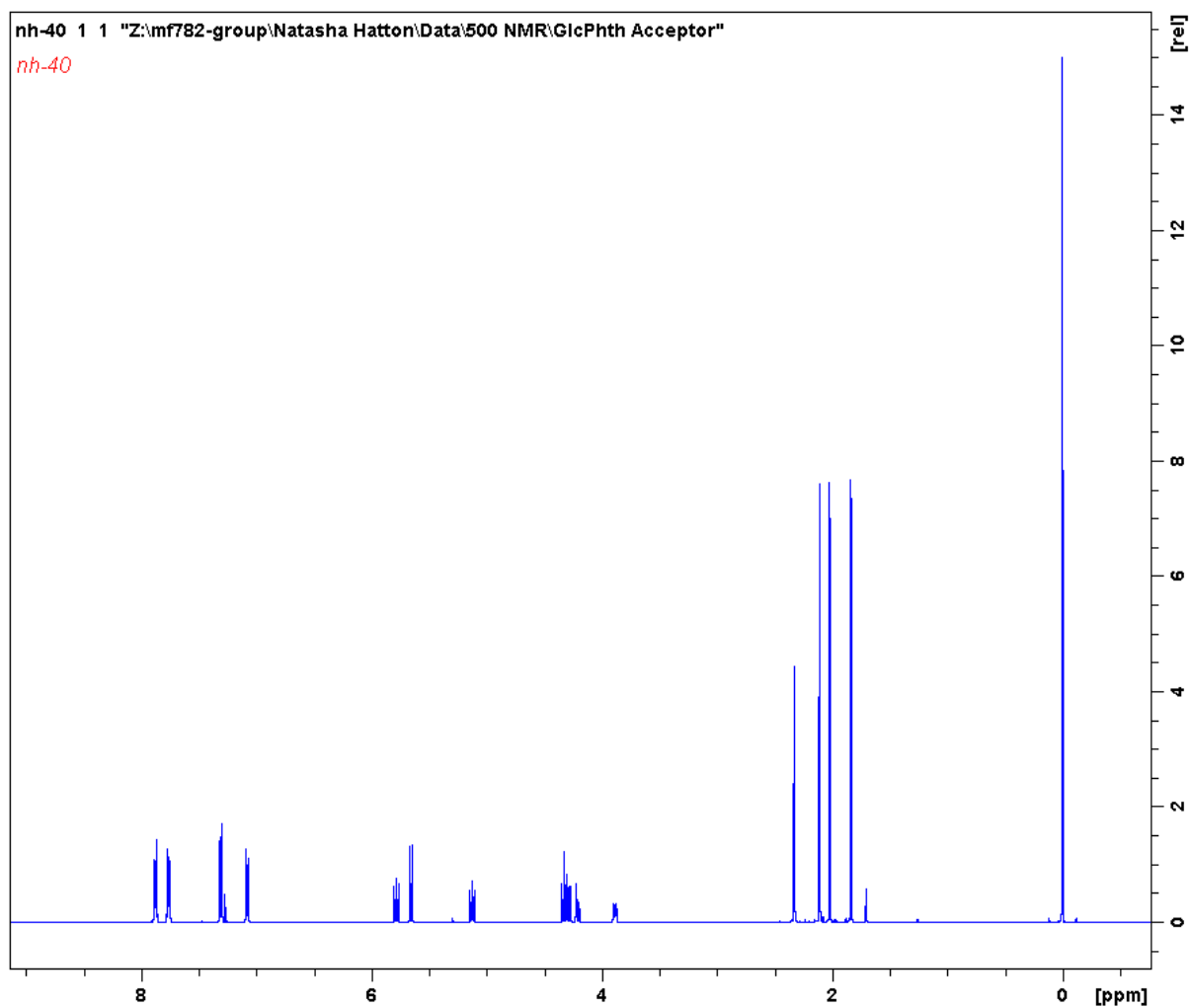
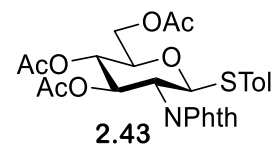
# Appendix



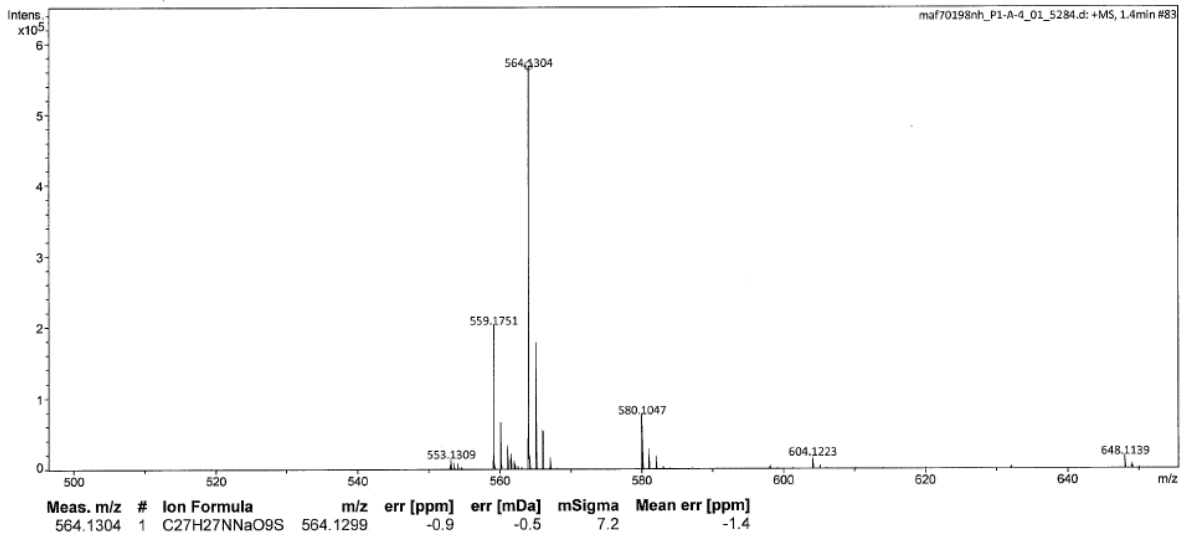
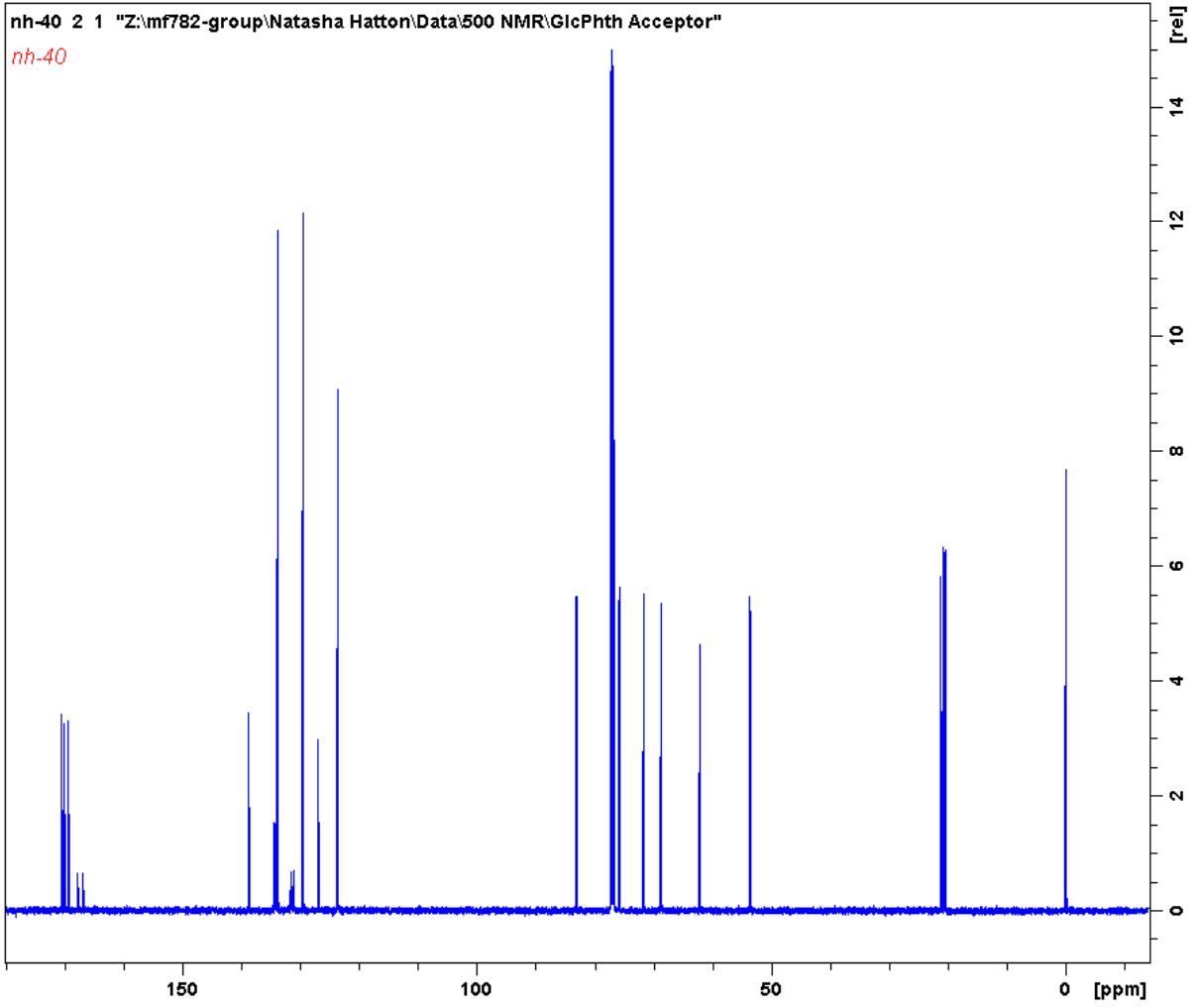
## Appendix



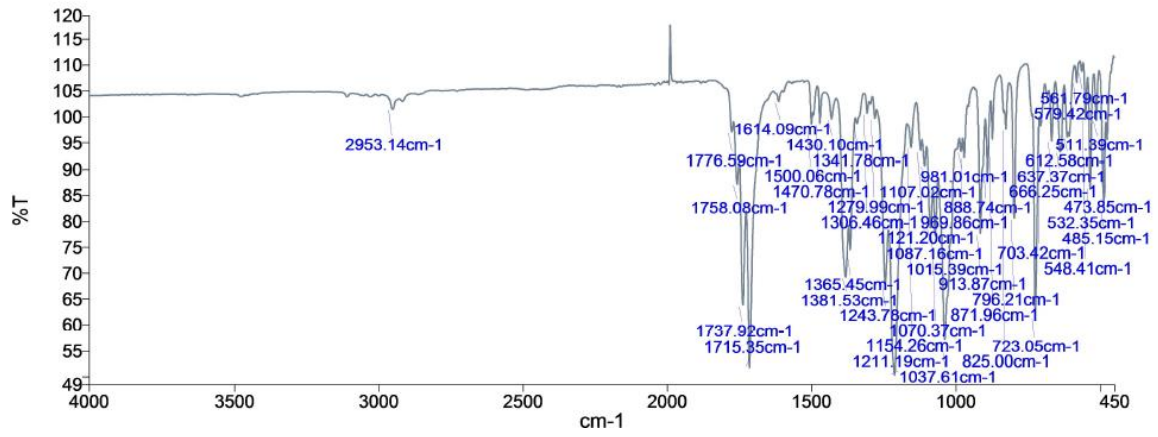
### 9.1.5.3 4-Methylphenyl 3,4,6-tri-O-acetyl-2-deoxy-2-phthalimido-1-thio- $\beta$ -D-glucopyranoside **2.43**



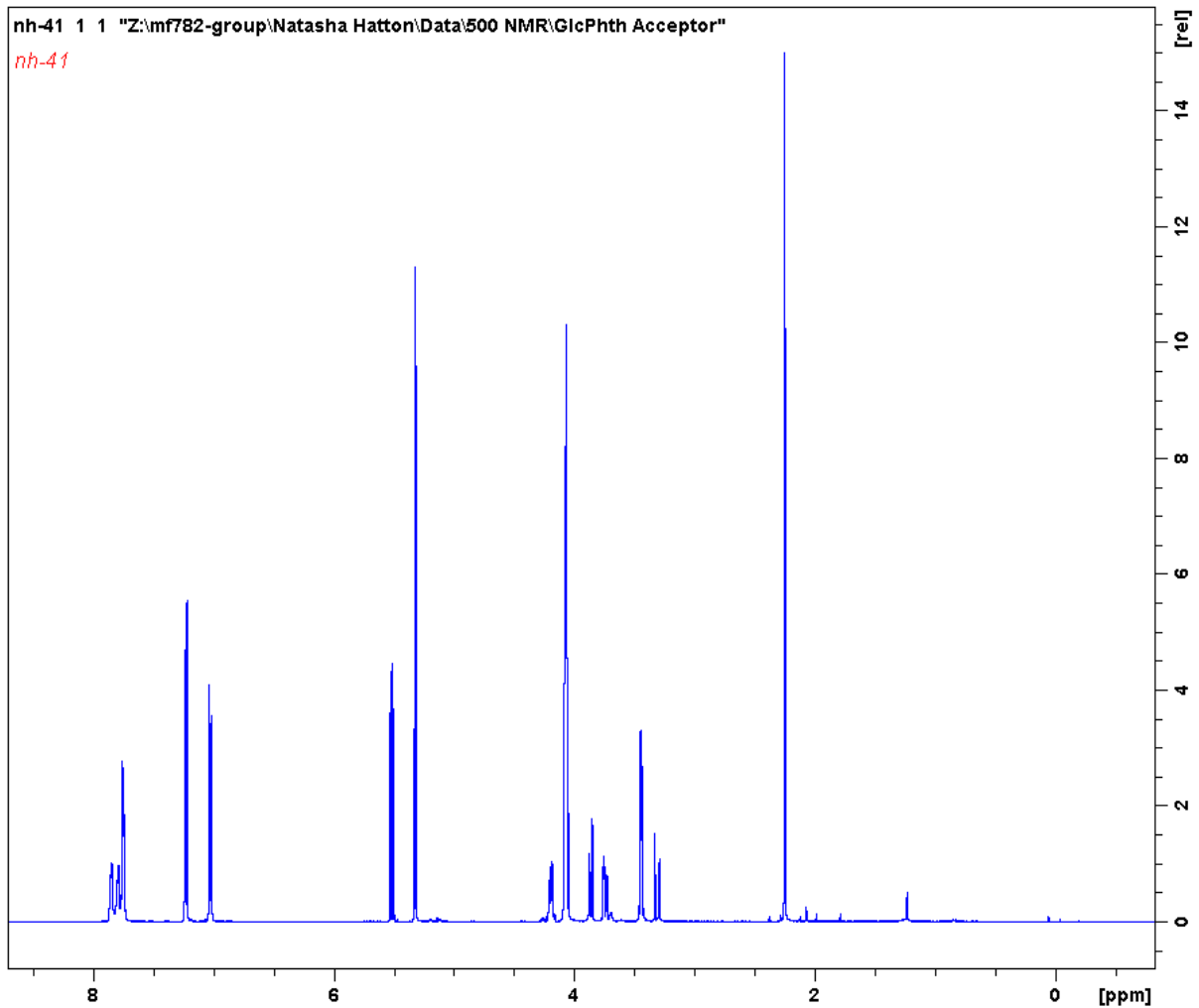
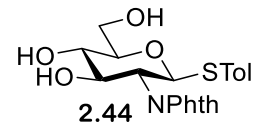
Appendix



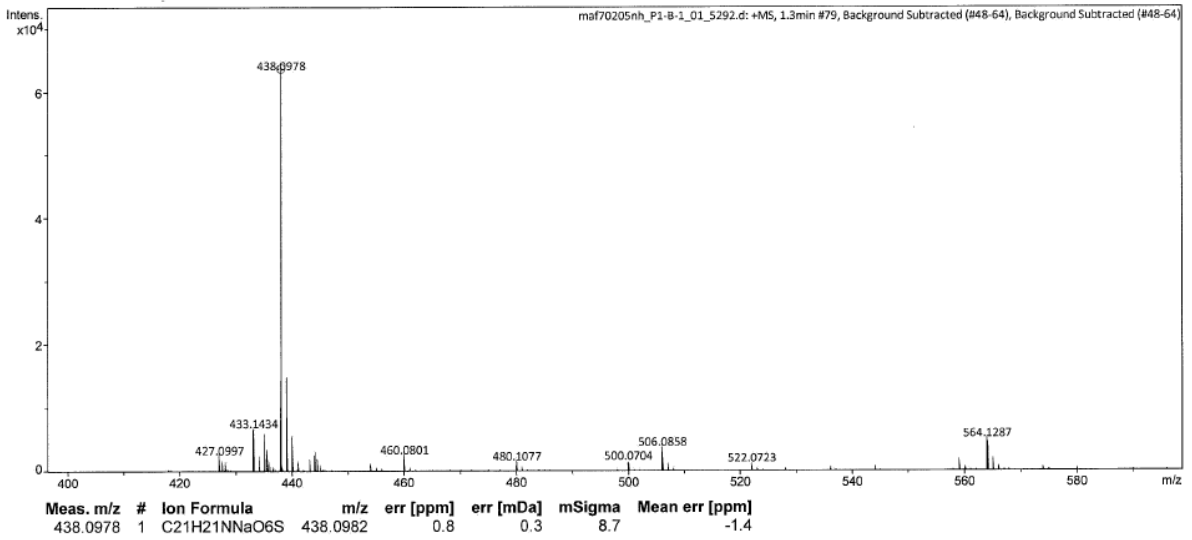
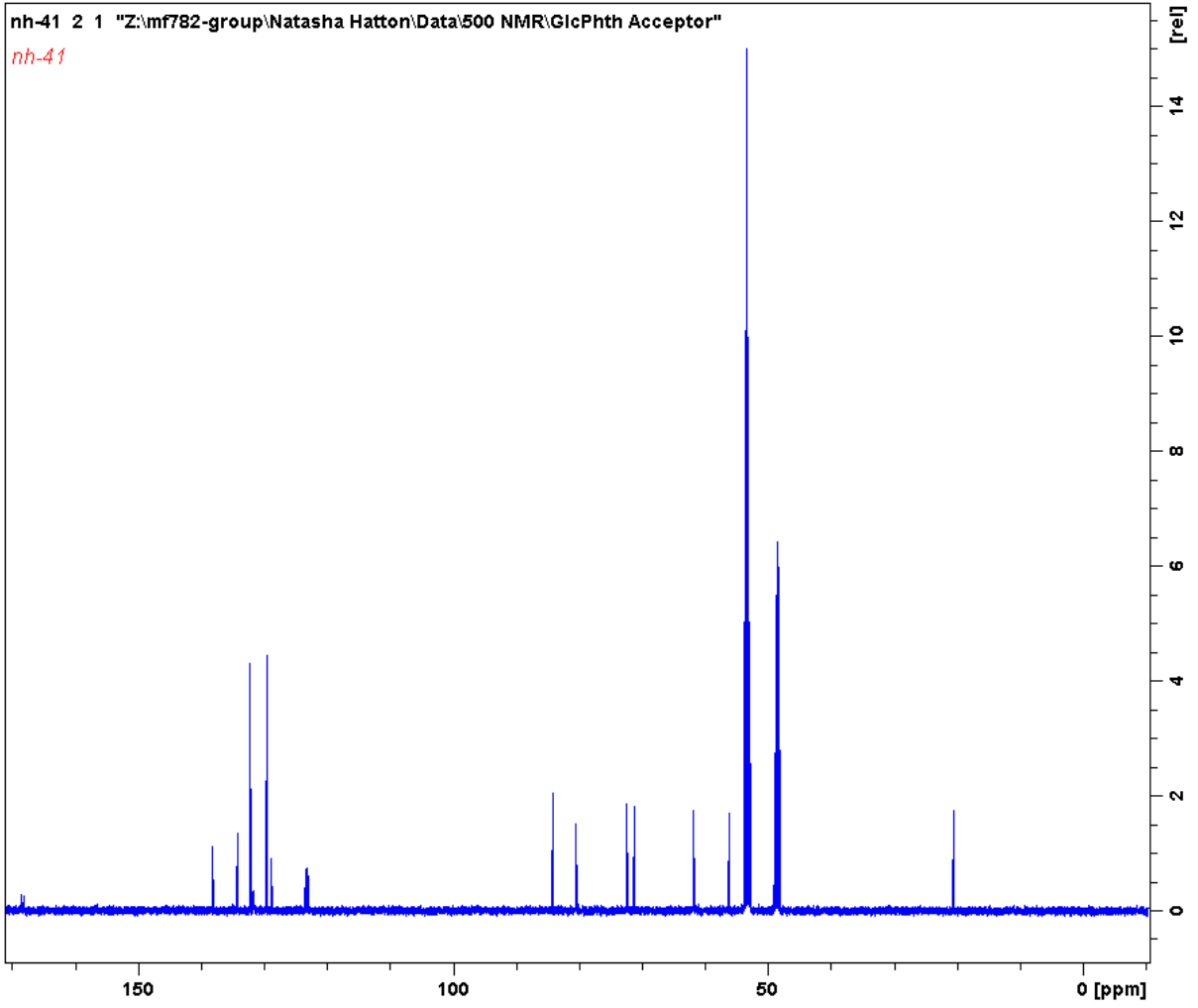
## Appendix



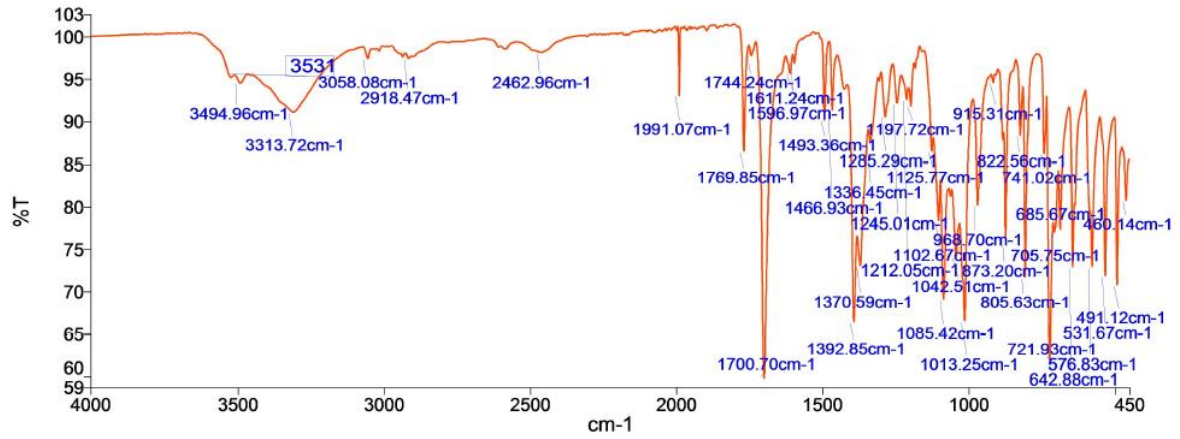
### 9.1.5.4 4-Methylphenyl 2-deoxy-2-phthalimido-1-thio-β-D-glucopyranoside 2.44



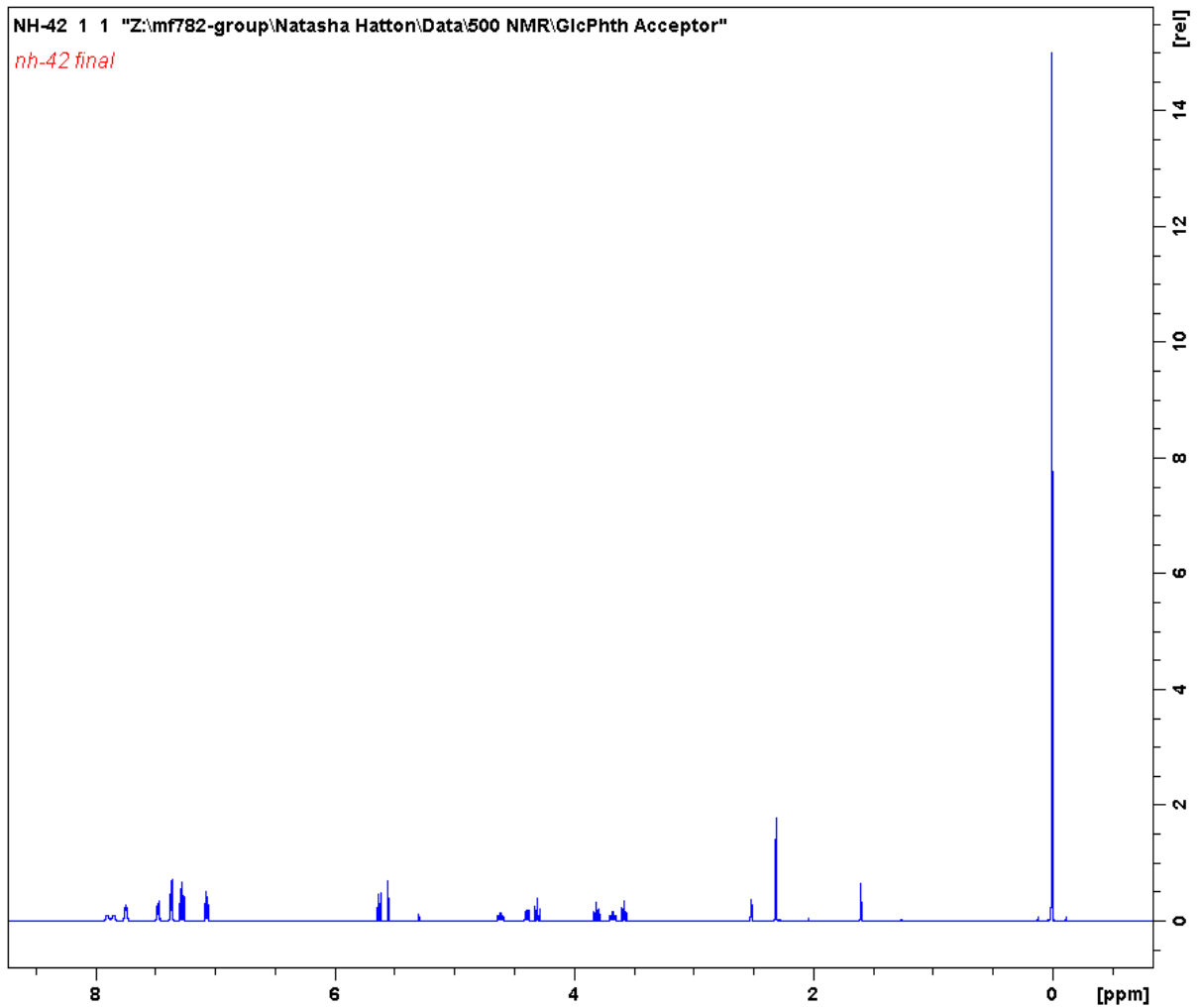
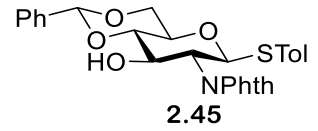
Appendix



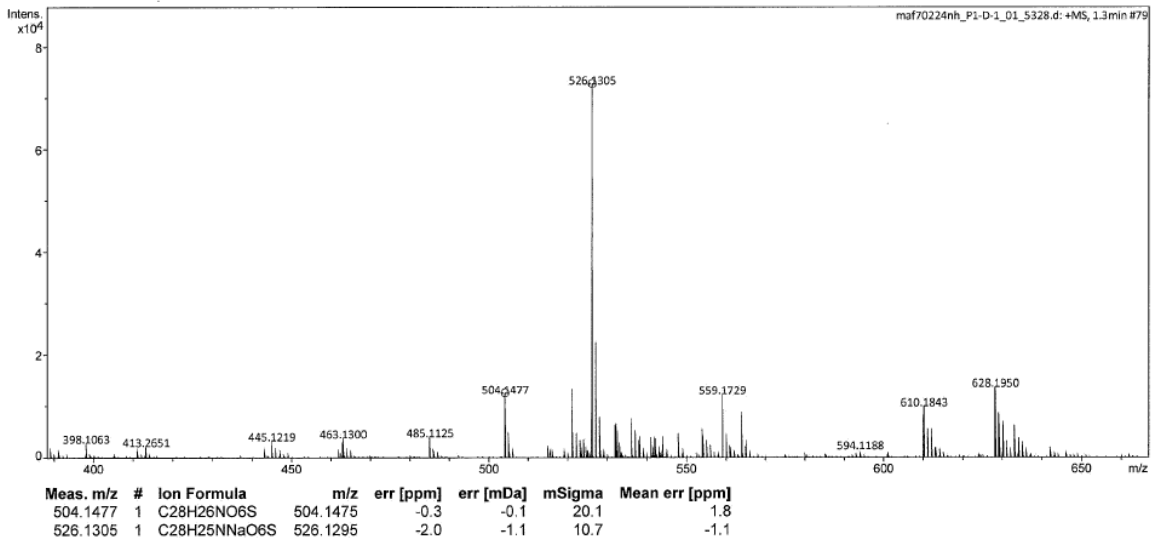
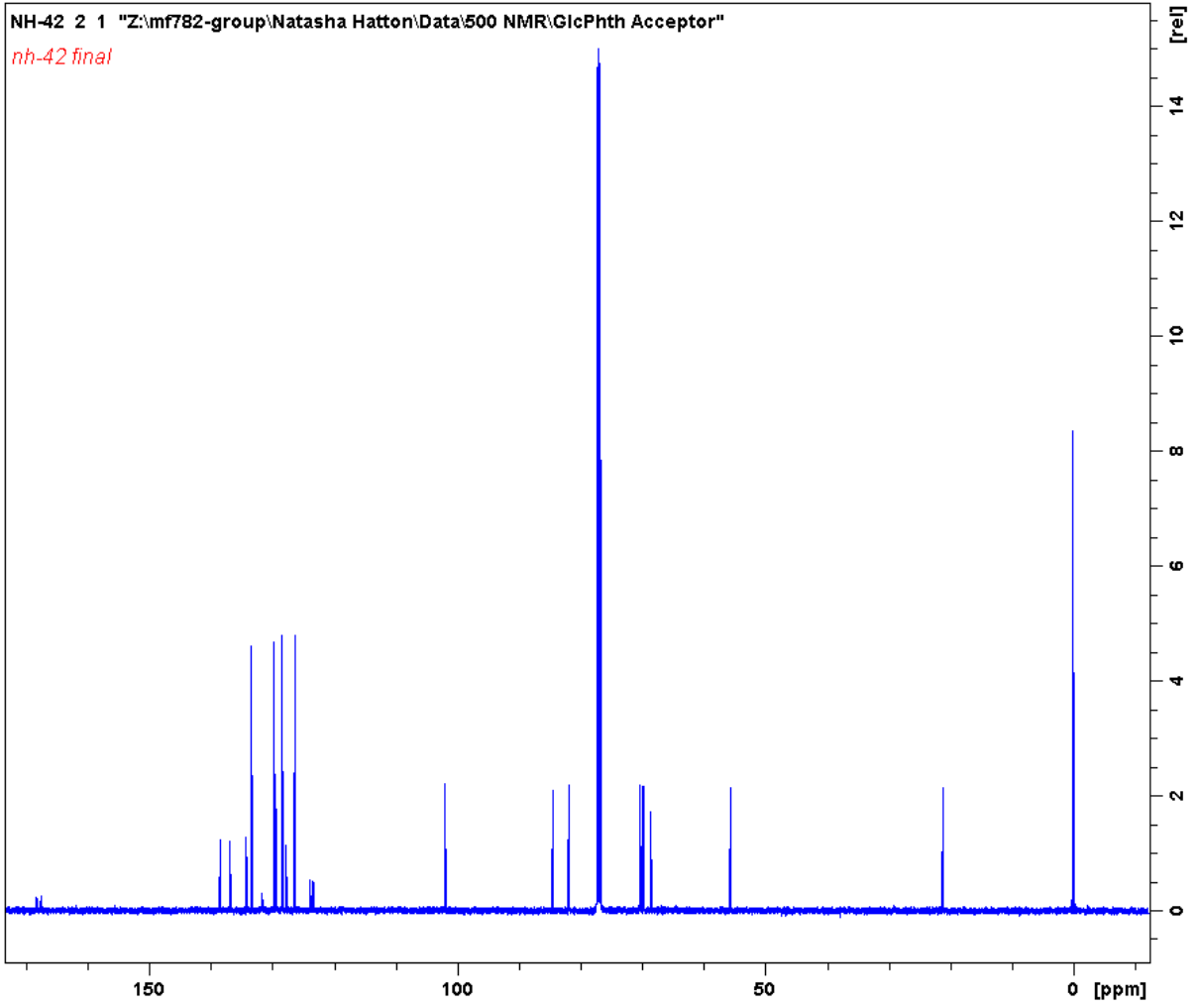
## Appendix



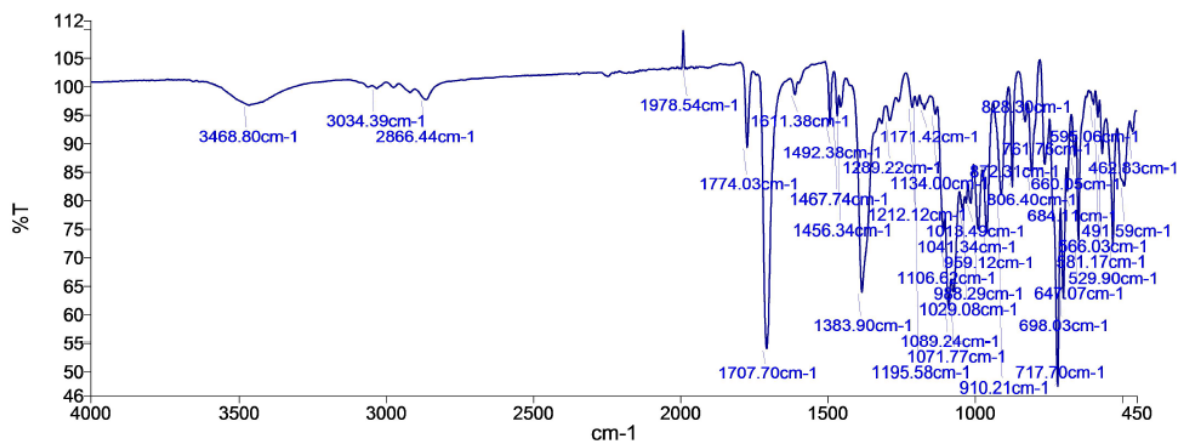
### 9.1.5.5 4-Methylphenyl 4,6-O-benzylidene-2-deoxy-2-phthalimido-1-thio-β-D-glucopyranoside 2.45



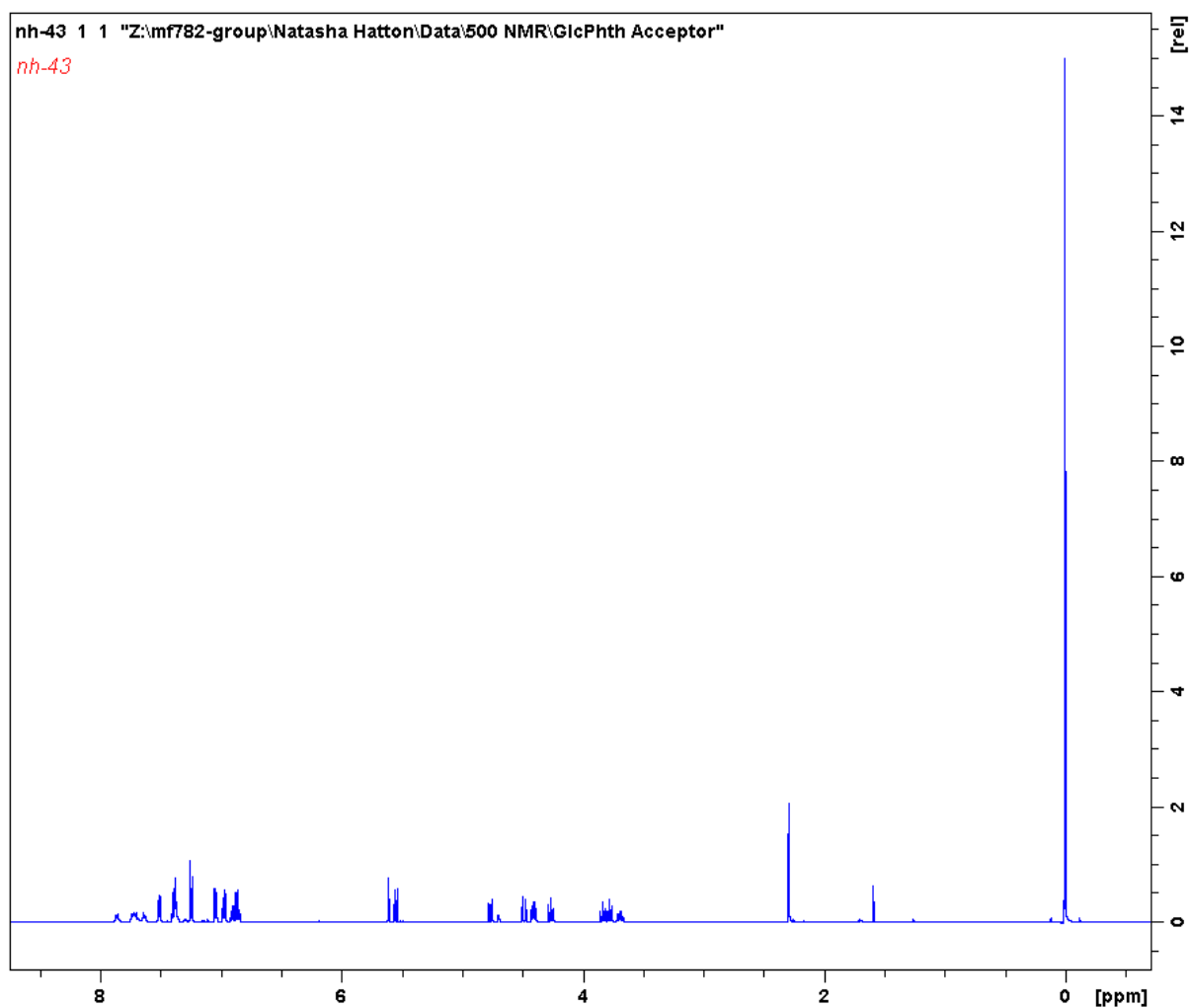
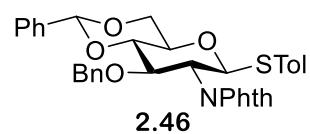
# Appendix



## Appendix

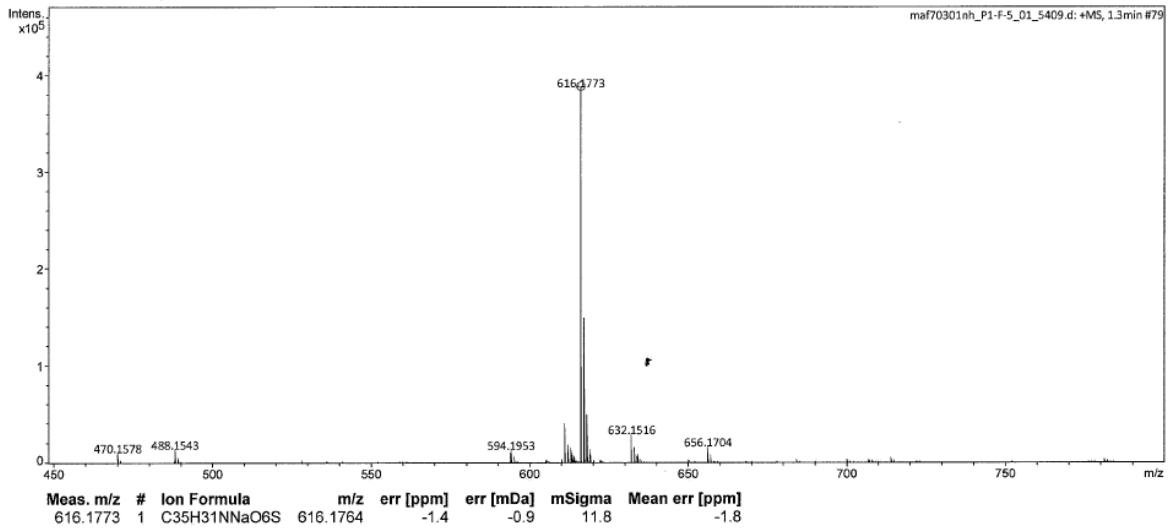
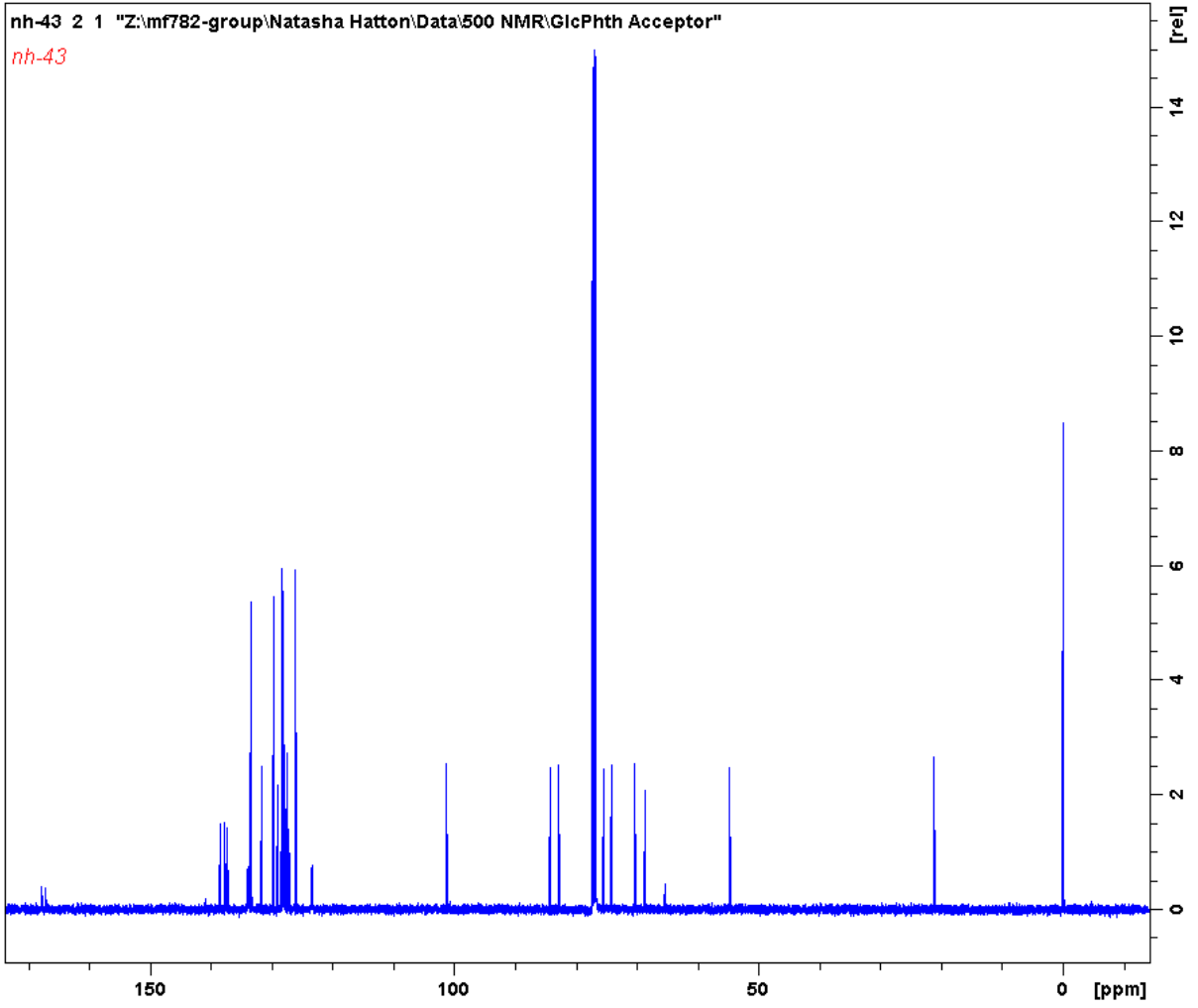


9.1.5.6 *p*-Methylphenyl 3-*O*-benzyl-4,6-*O*-benzylidene-2-deoxy-2-phthalimido-1-thio- $\beta$ -D-glucopyranoside **2.46**

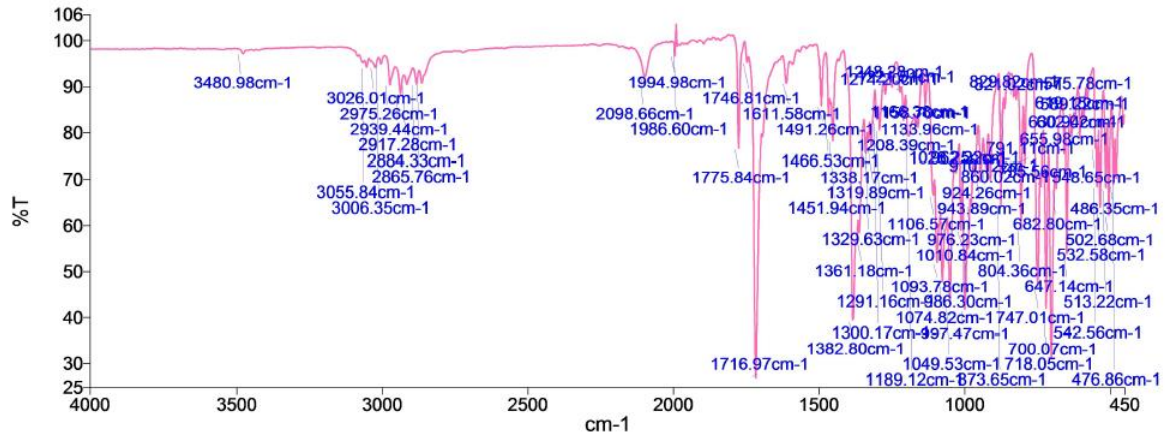




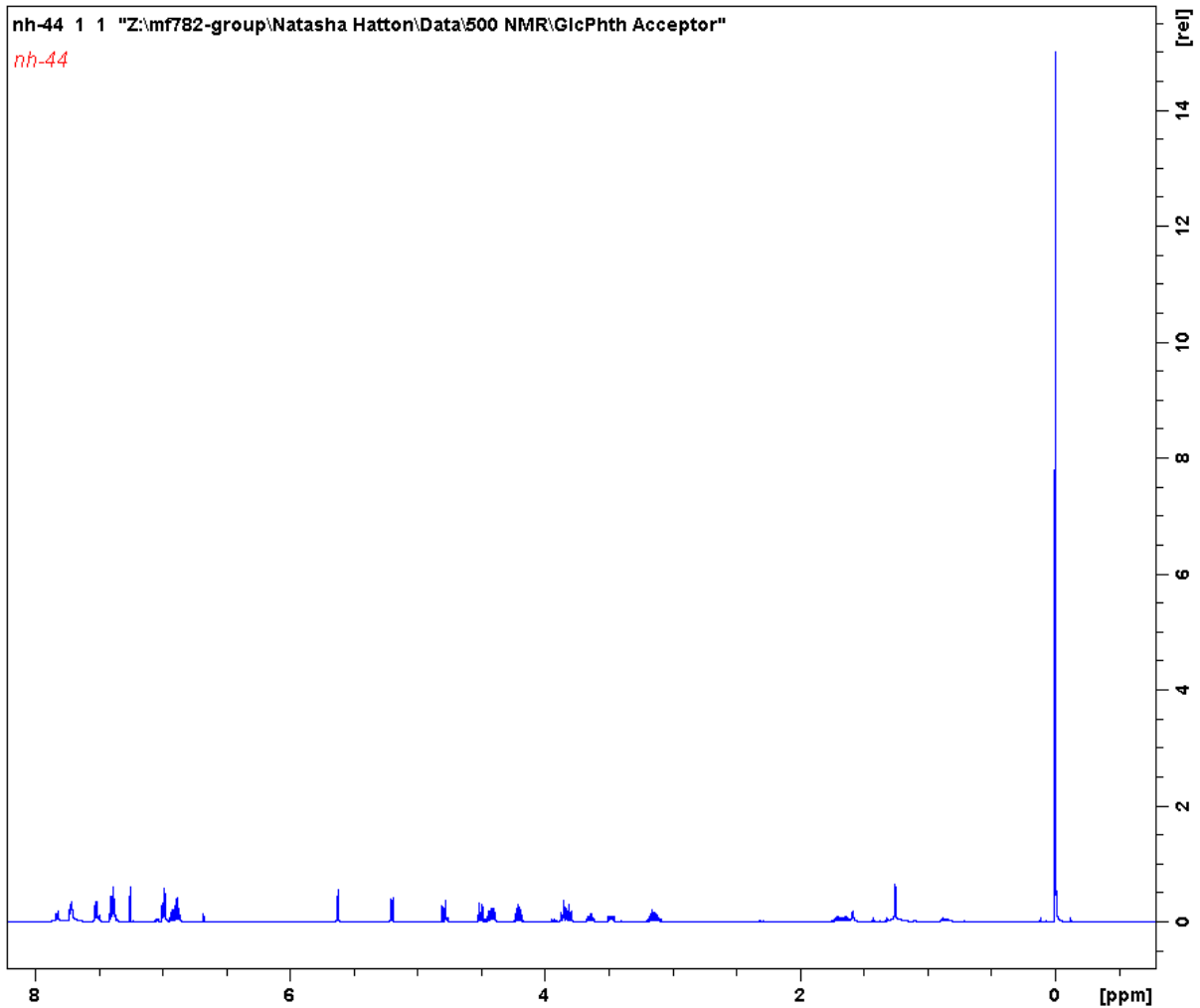
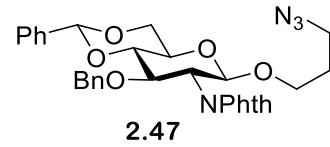
Appendix



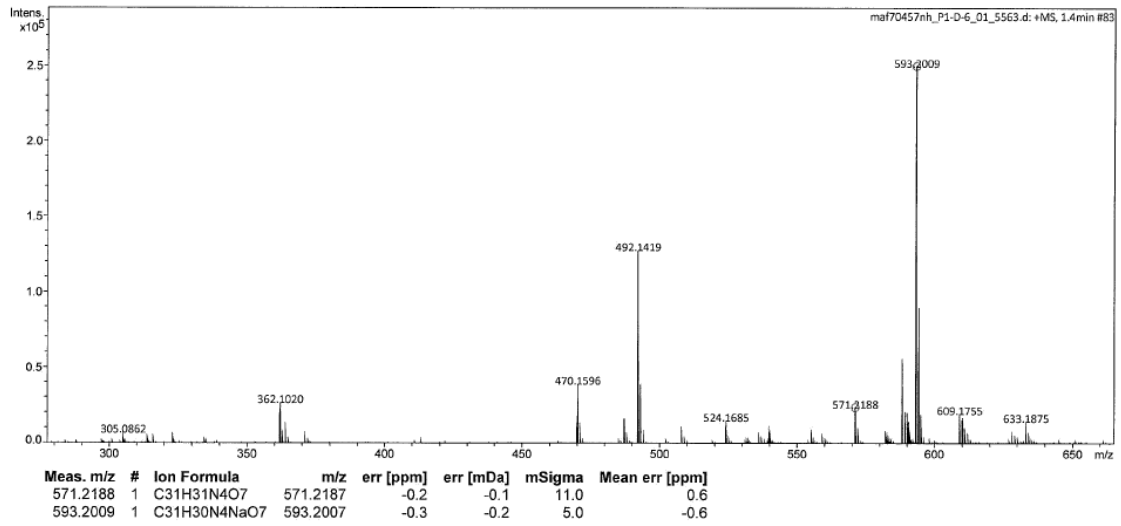
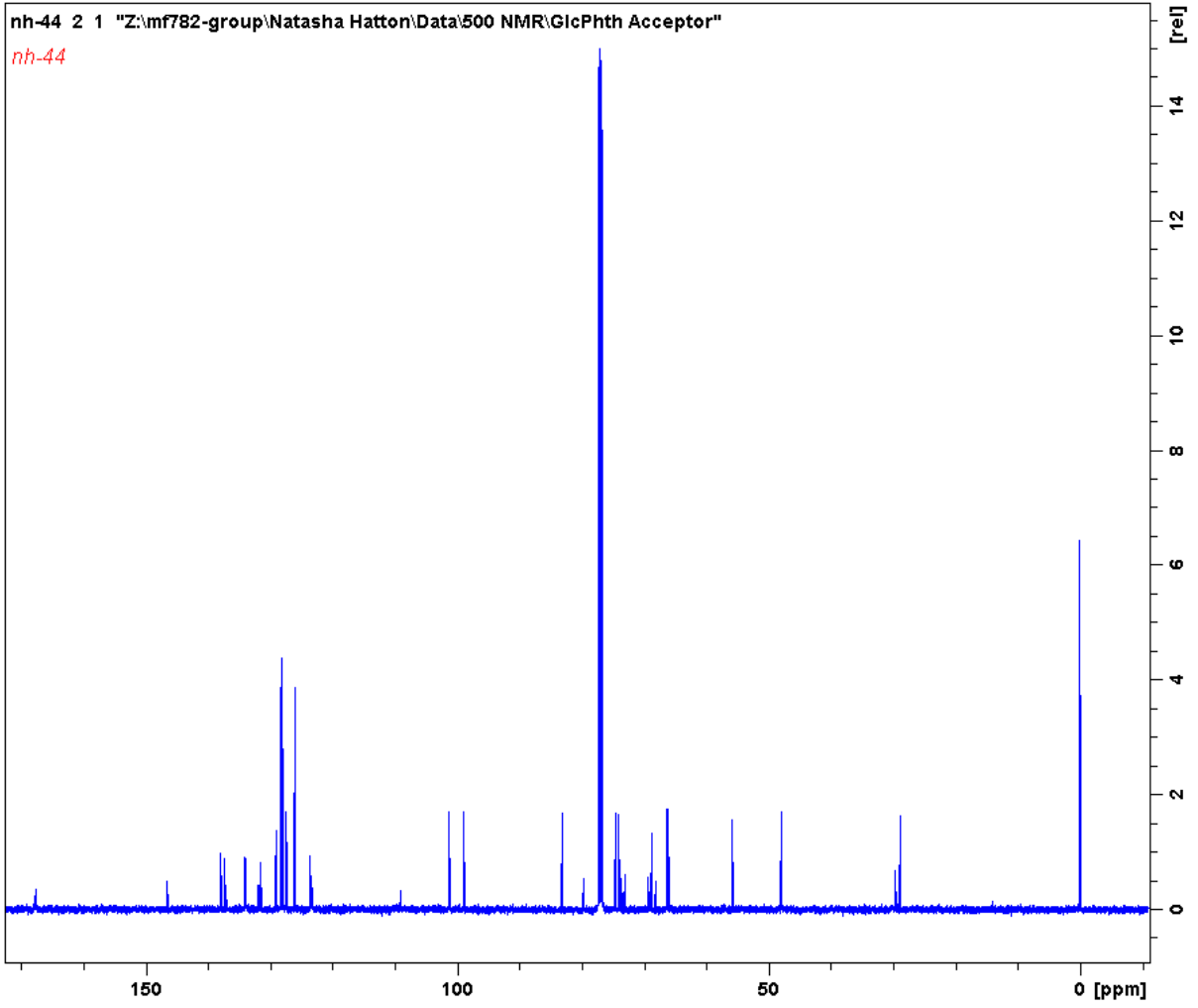
# Appendix



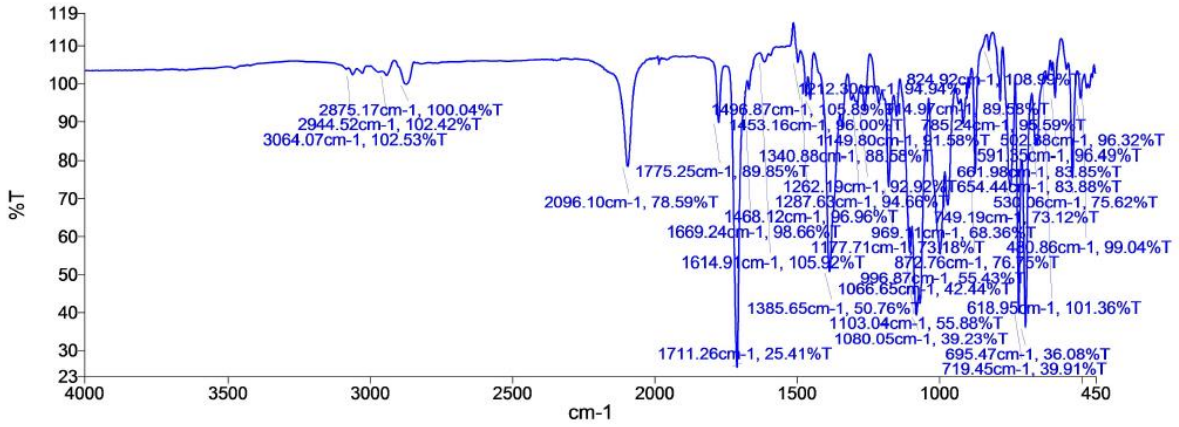
## 9.1.5.7 3-Azidopropyl 3-O-benzyl-4,6-O-benzylidene-2-deoxy-2-phthalimido-1-β-D-glucopyranoside 2.47



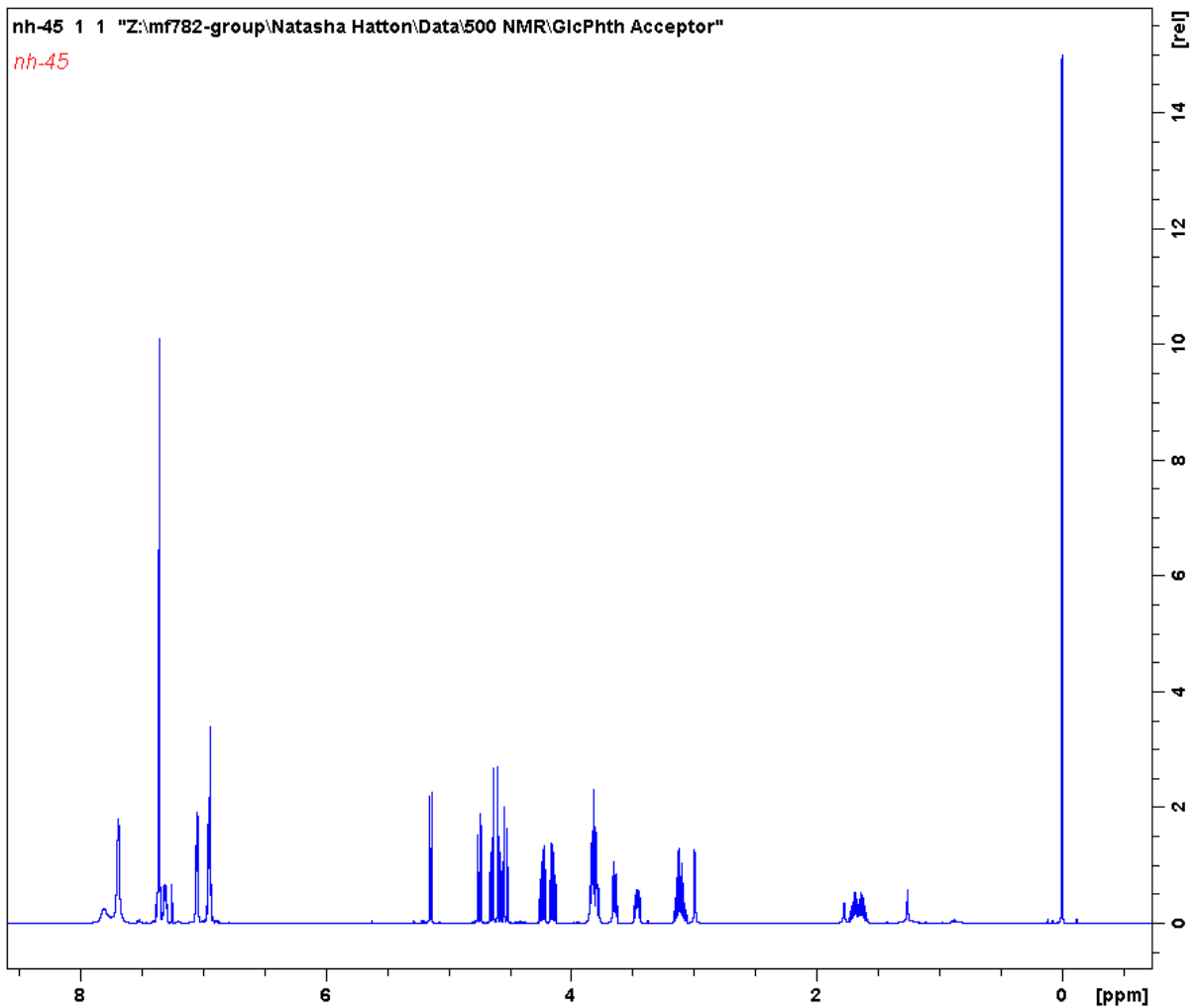
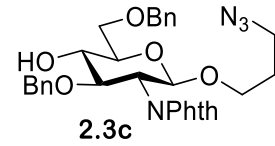
# Appendix



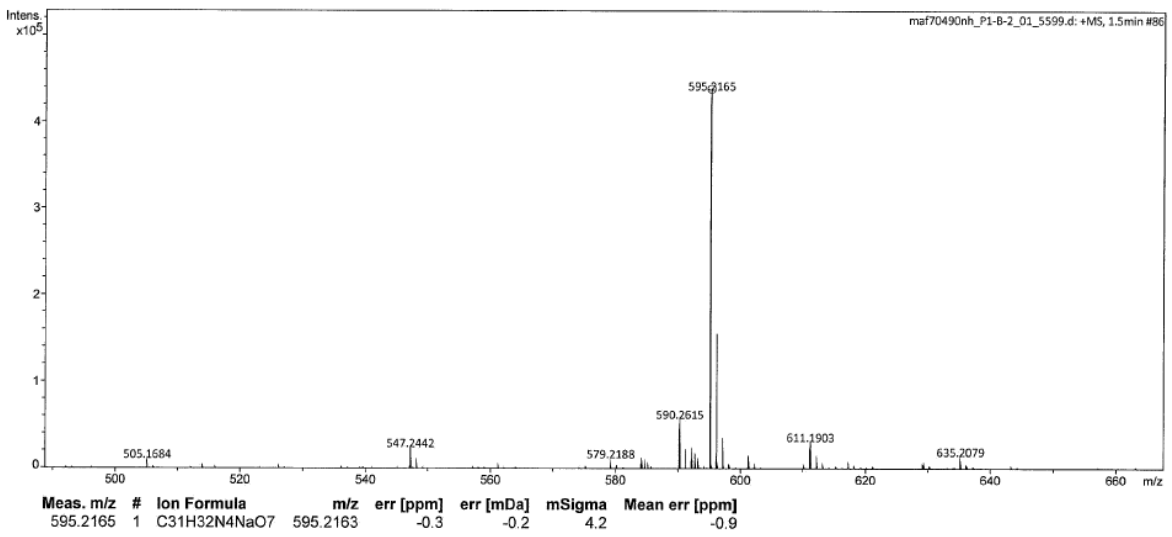
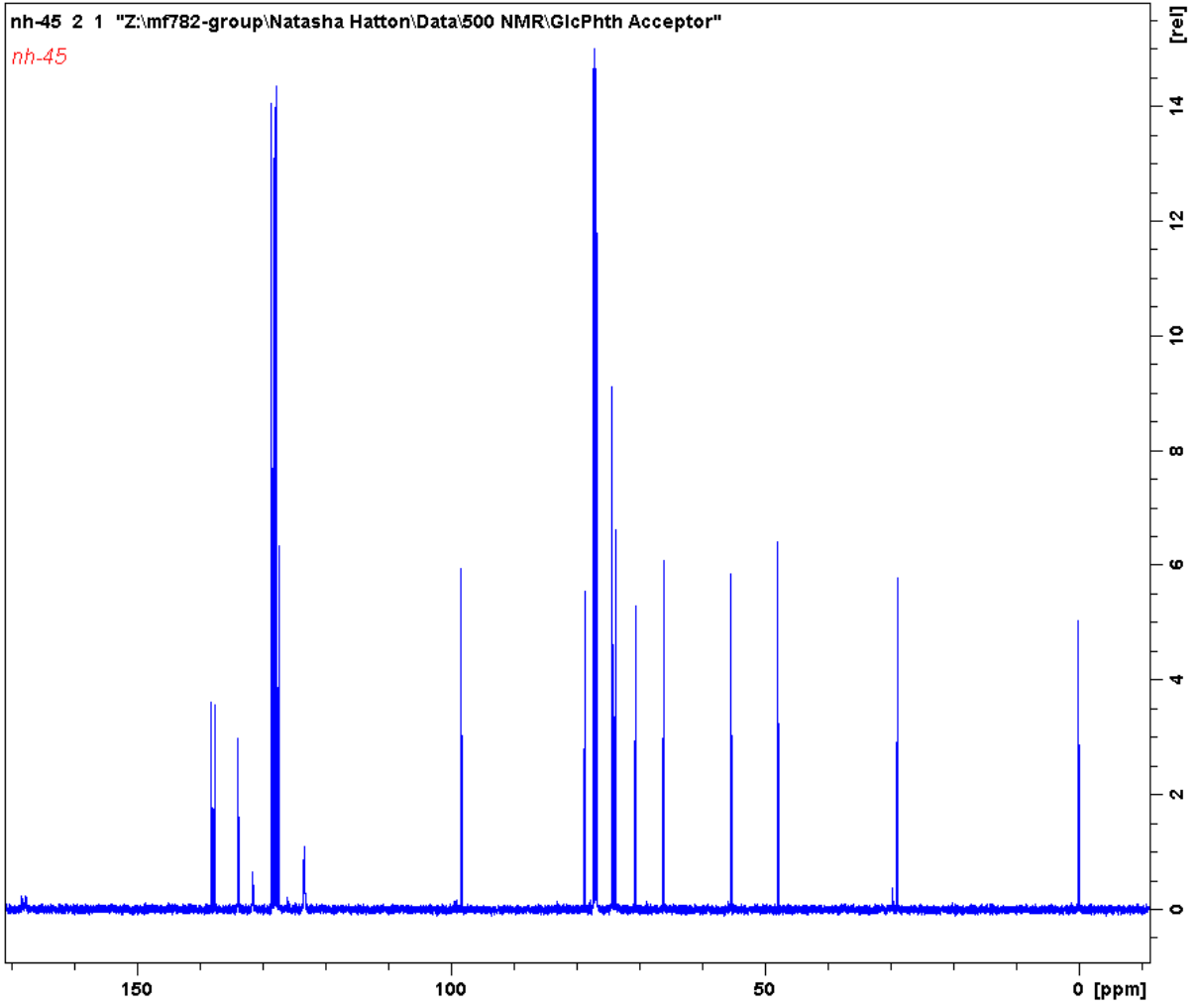
## Appendix



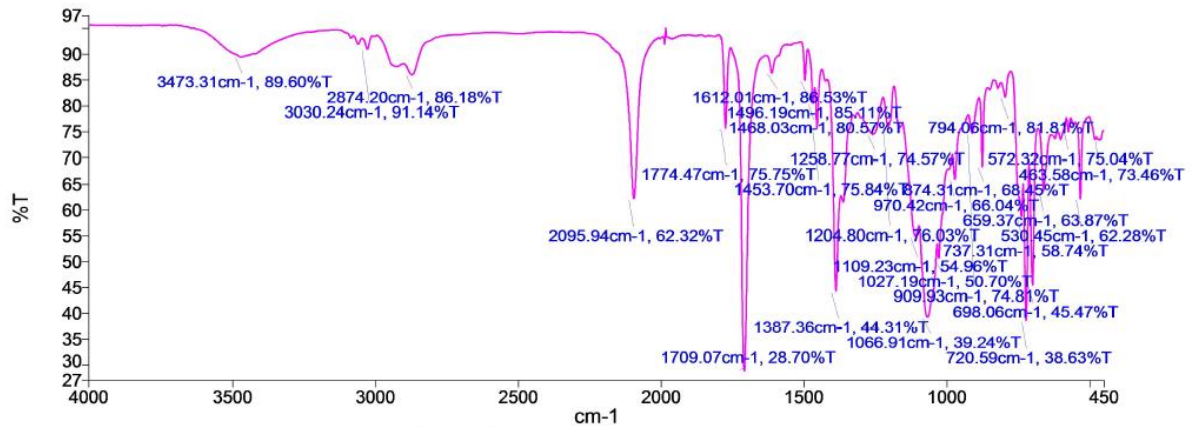
### 9.1.5.8 3-Azidopropyl 3,6-di-O-benzyl-2-deoxy-2-phthalimido-1-β-D-glucopyranoside 2.3c



Appendix



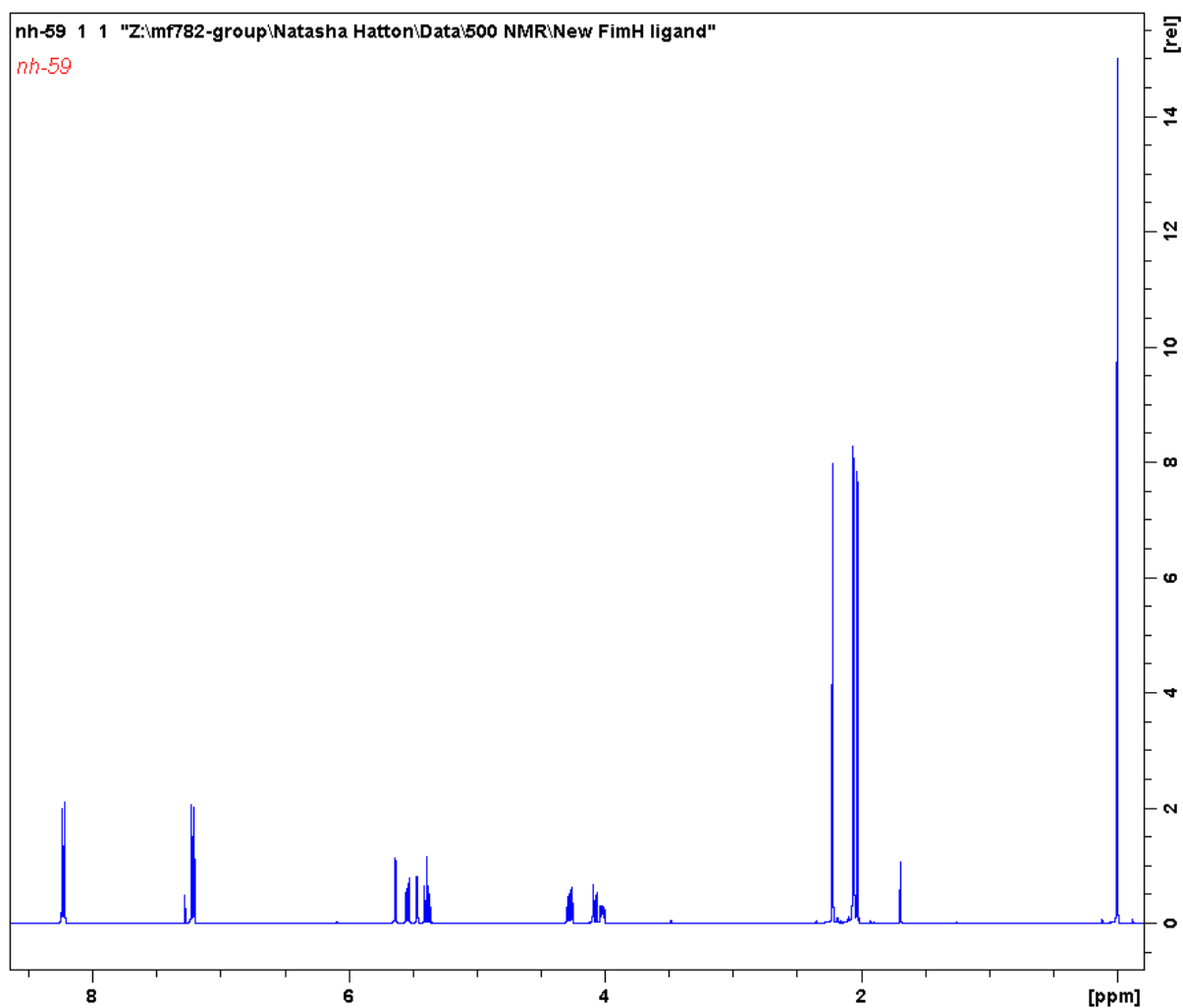
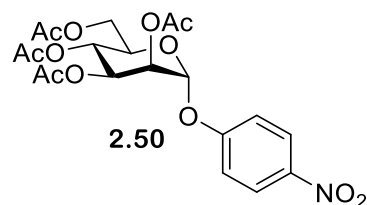
# Appendix



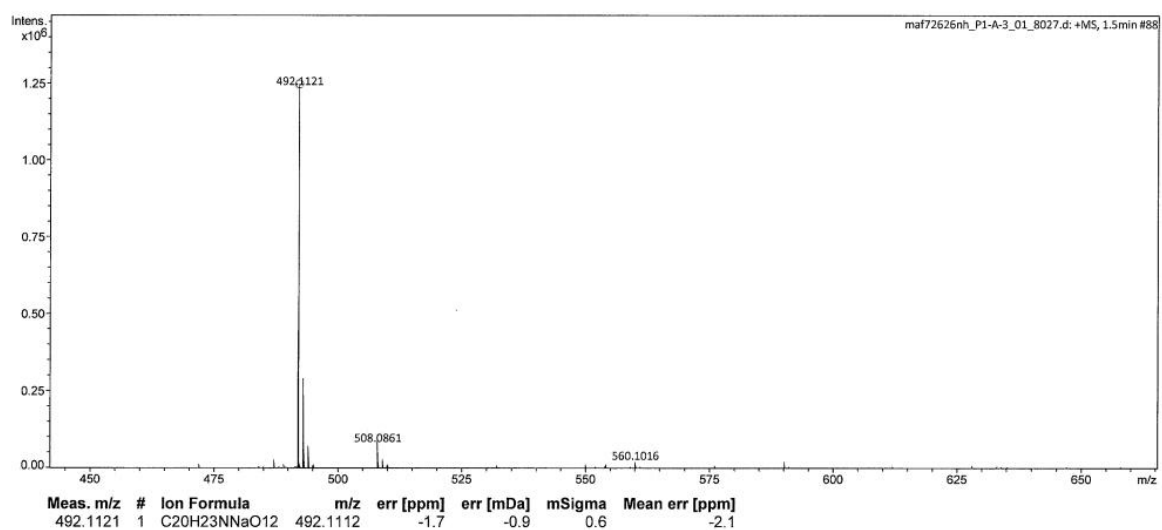
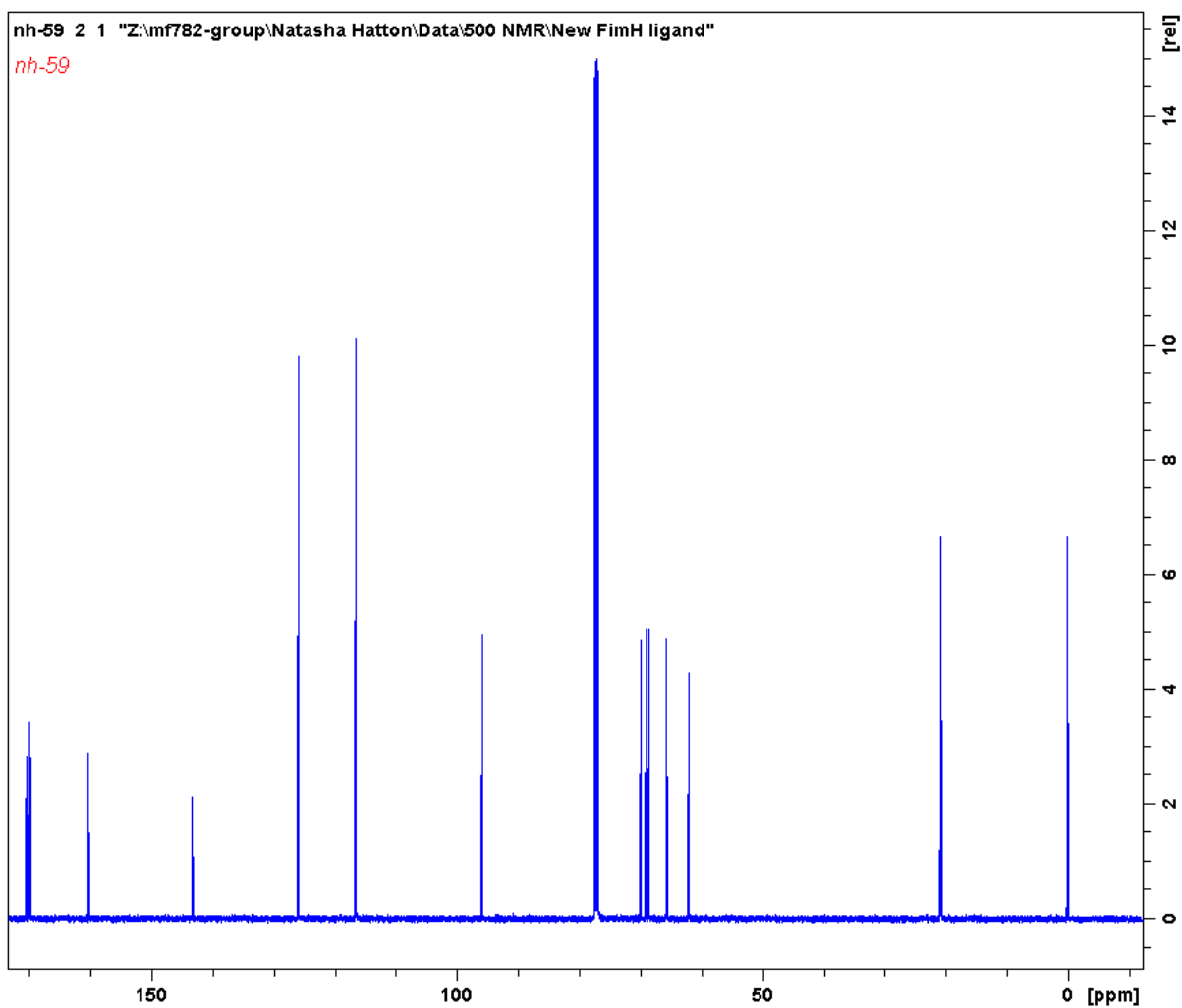
## Appendix

9.1.6 Synthesis of squarate mannose analogues- *p*-[[(2-aminoethylamino)-2,3-dioxocyclobut-1-enyl)amino]phenyl  $\alpha$ -D-mannopyranoside **2.53** and *p*-[[(1-amino-2-azidoethane)-2,3-dioxocyclobut-1-enyl)amino]phenyl  $\alpha$ -D-mannopyranoside **2.54**

9.1.6.1 4-Nitrophenyl 2,3,4,6-tetra-*O*-acetyl- $\alpha$ -D-mannopyranoside **2.50**

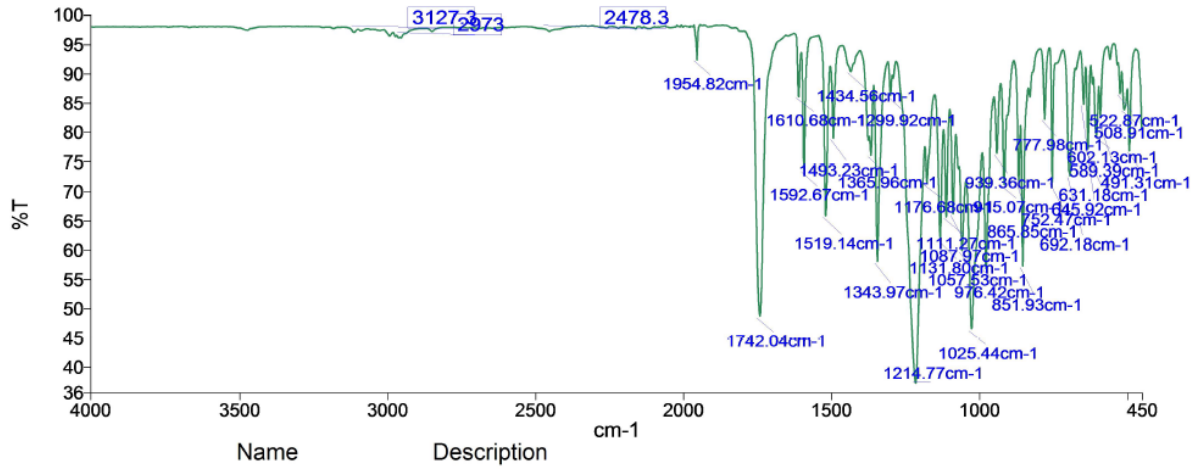


# Appendix

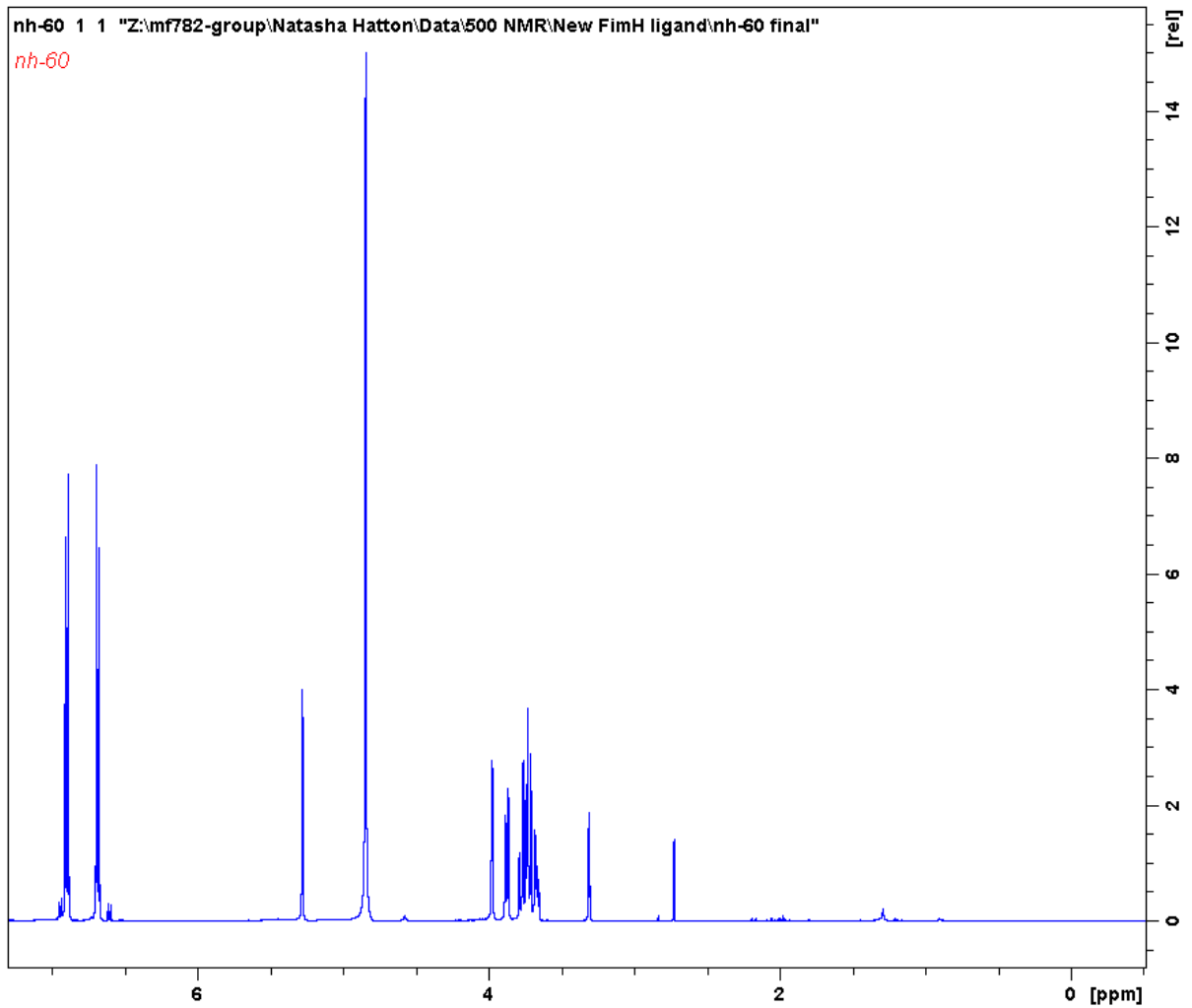
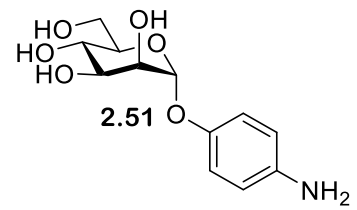




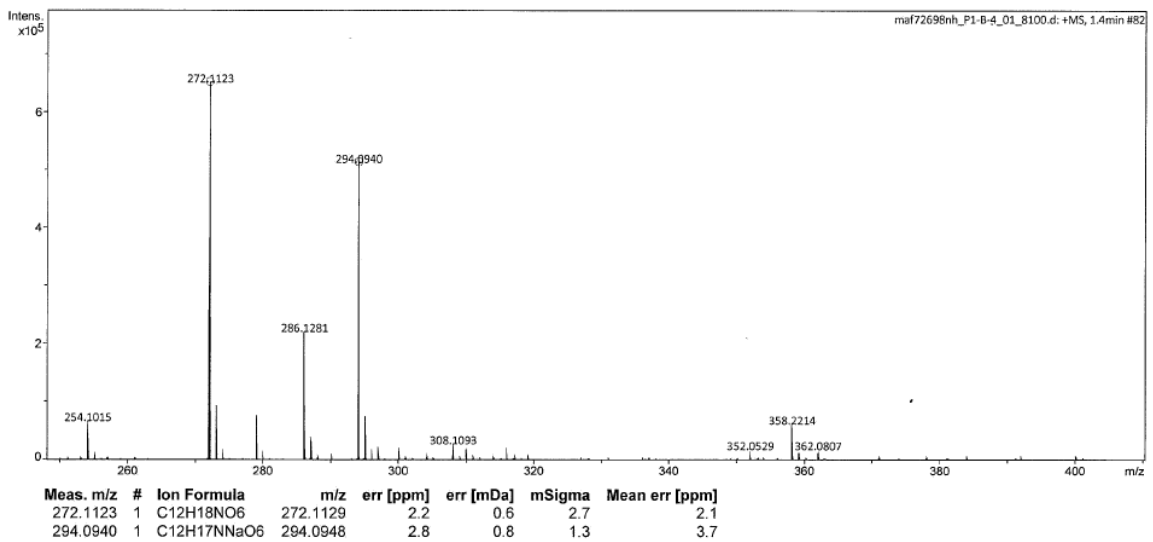
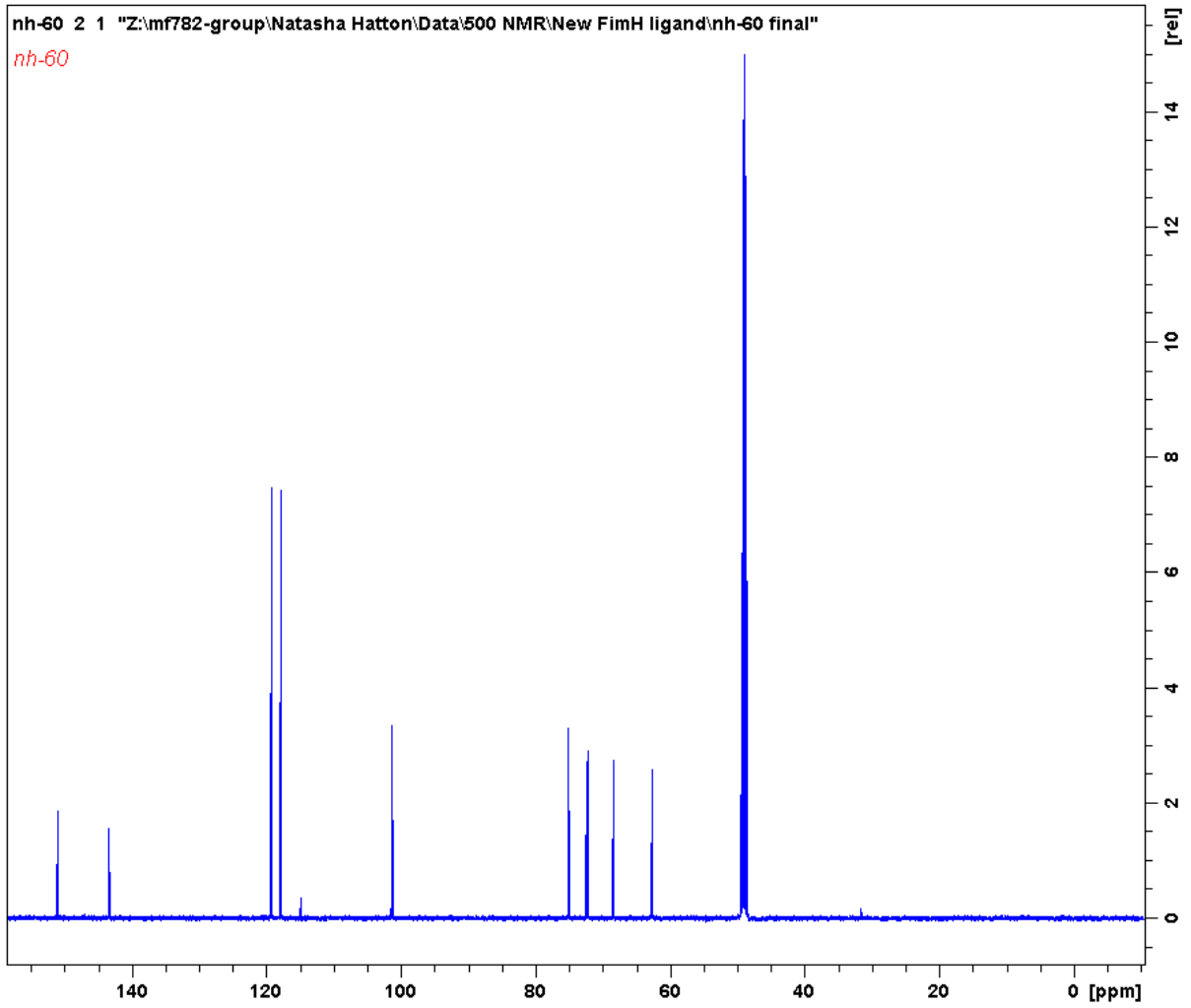
# Appendix



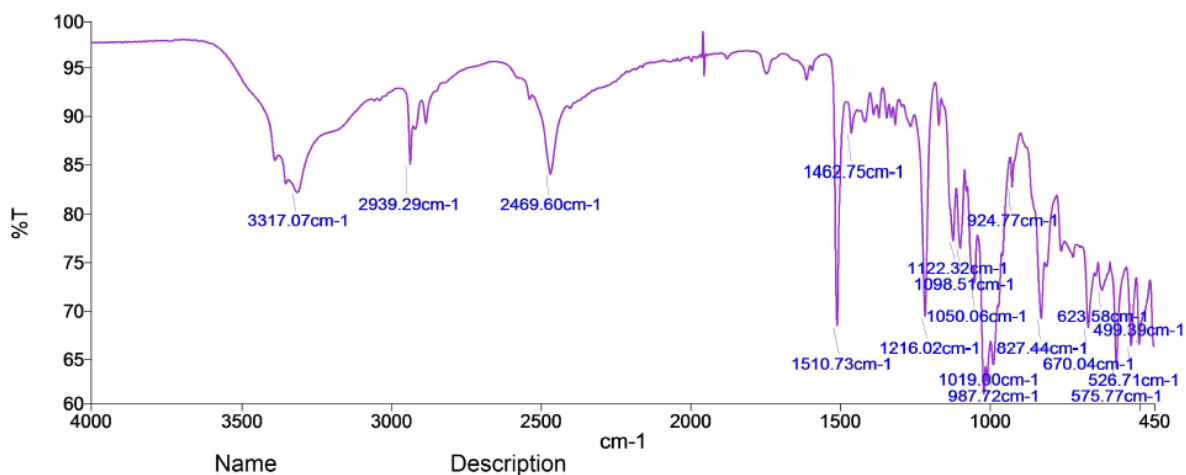
## 9.1.6.2 4-Aminophenyl $\alpha$ -D-mannopyranoside 2.51



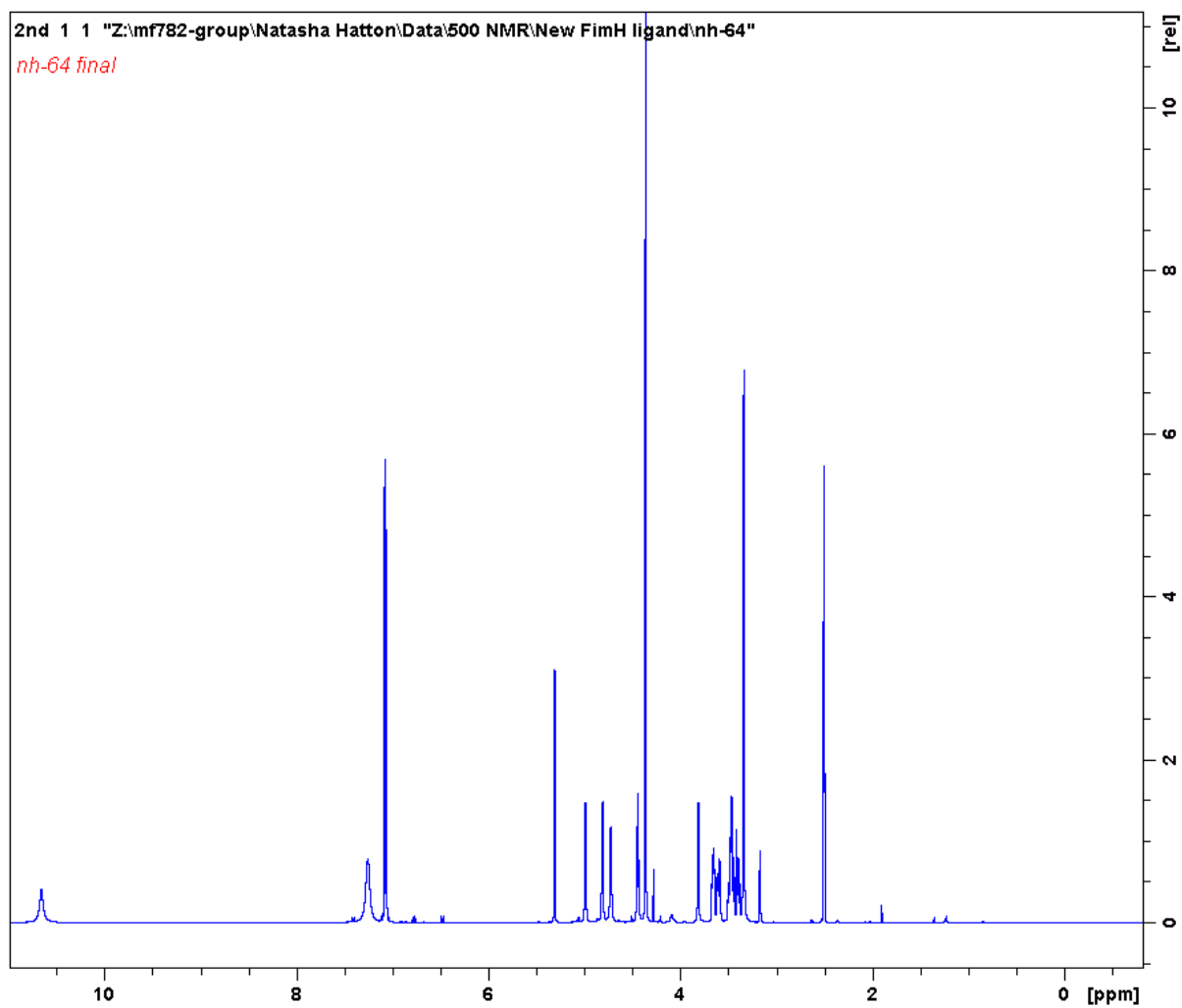
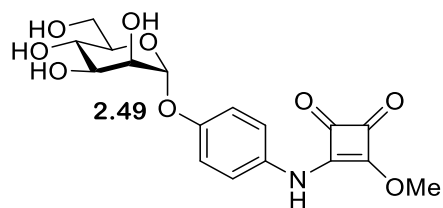
# Appendix



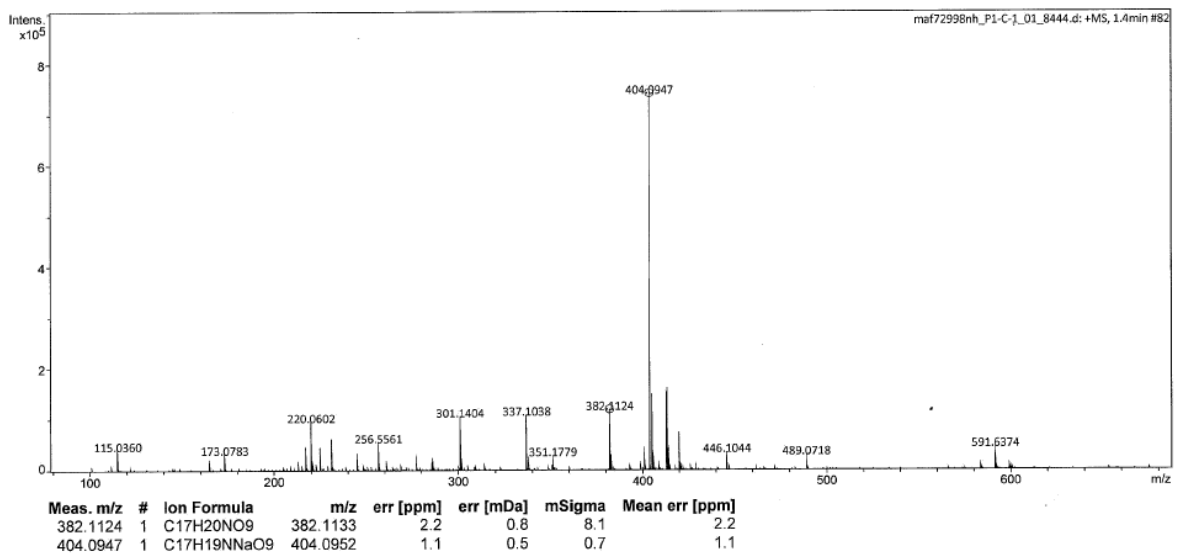
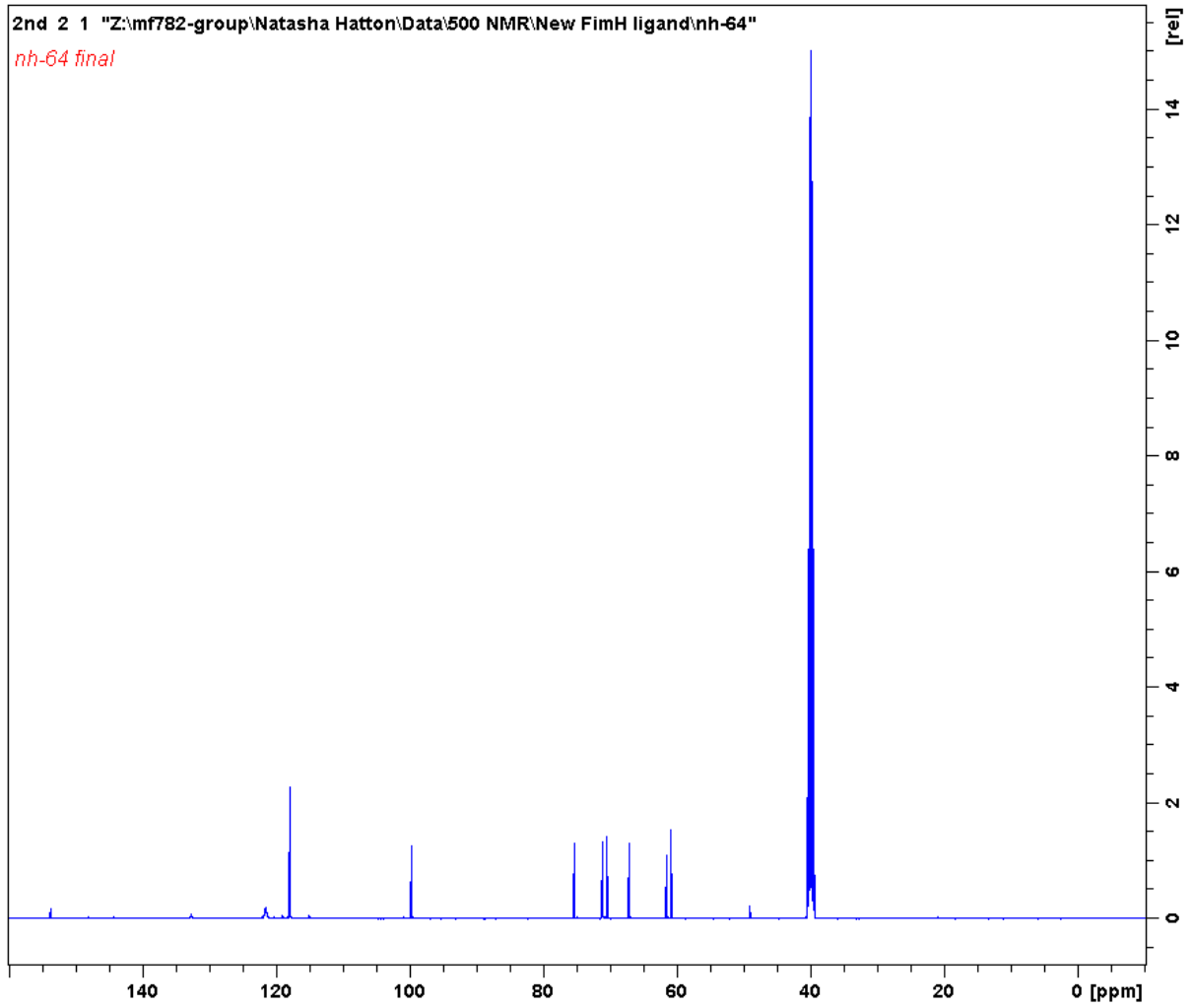
## Appendix



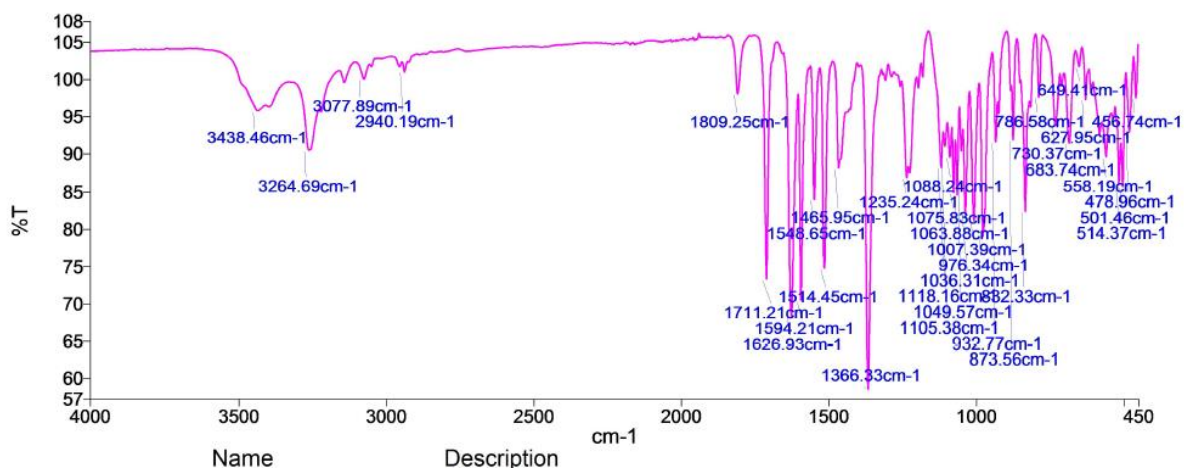
### 9.1.6.4 *p*-[*N*-(2-Methoxy-3,4-dioxocyclobut-1-enyl)aminophenyl] $\alpha$ -D-mannopyranoside **2.49**



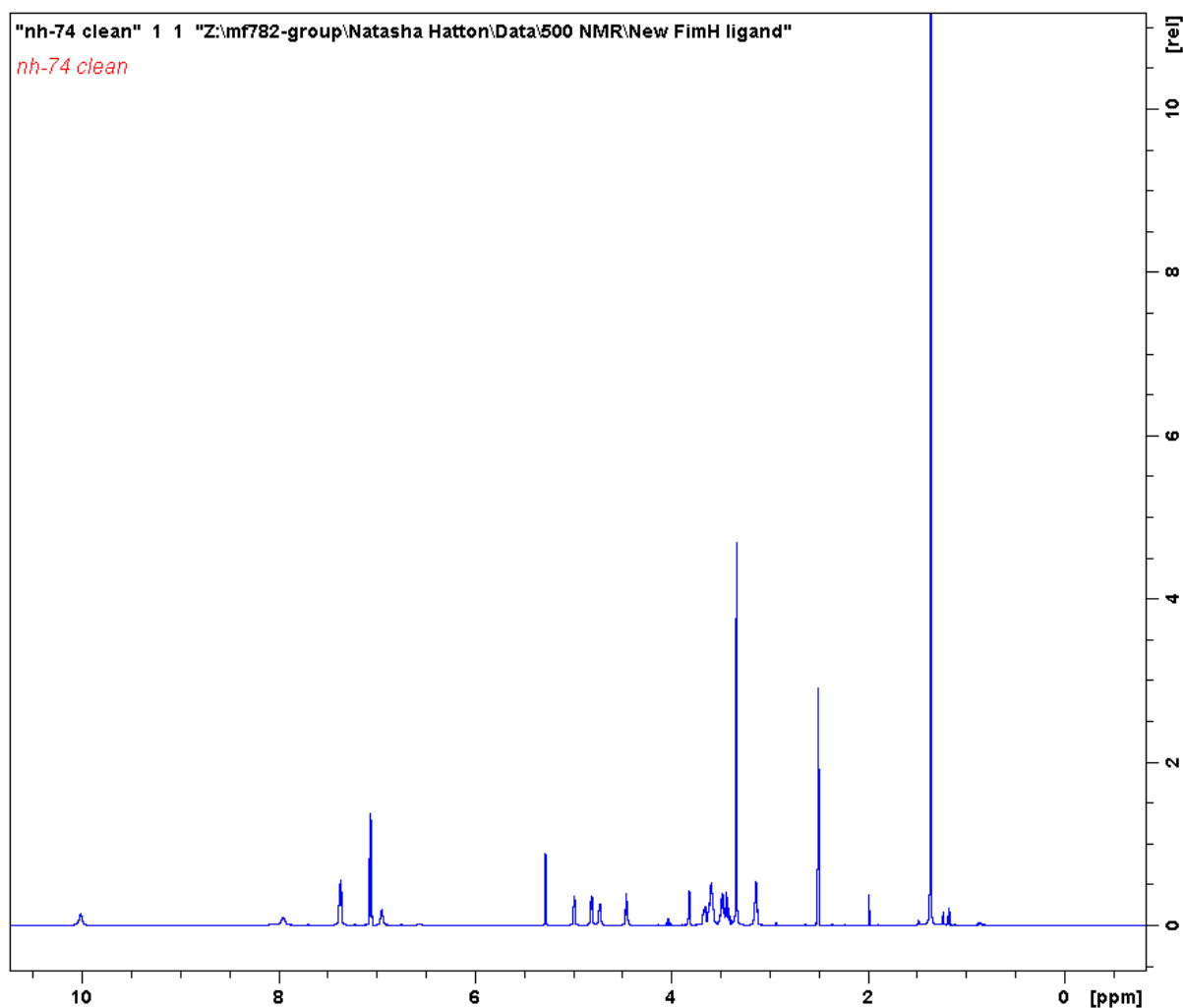
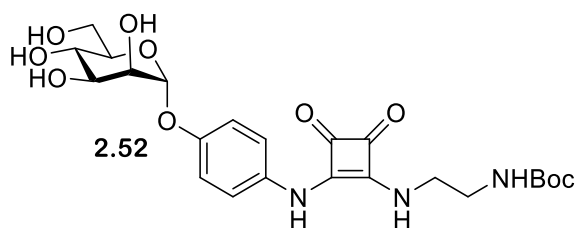
# Appendix



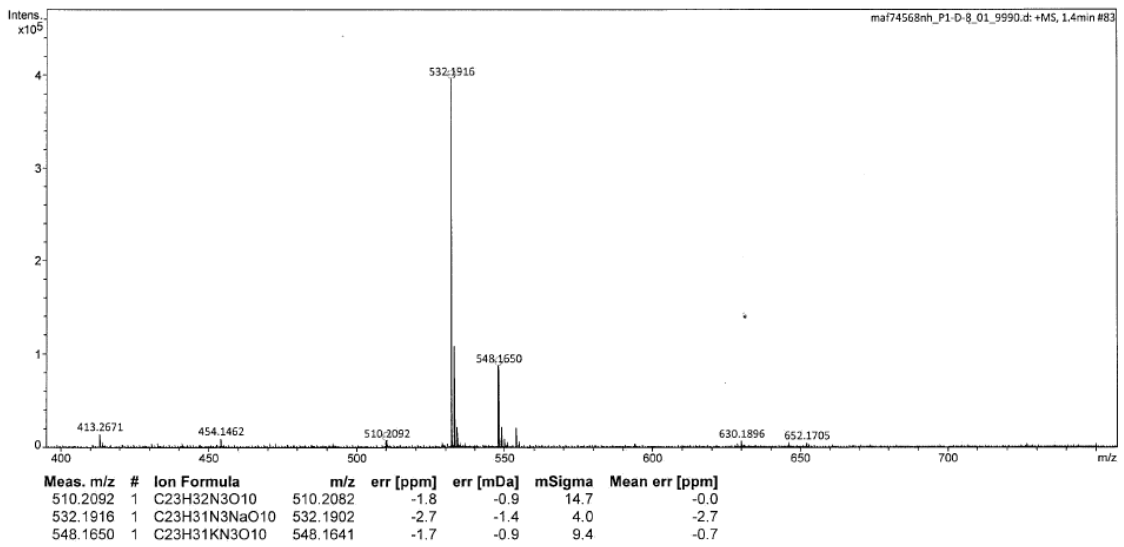
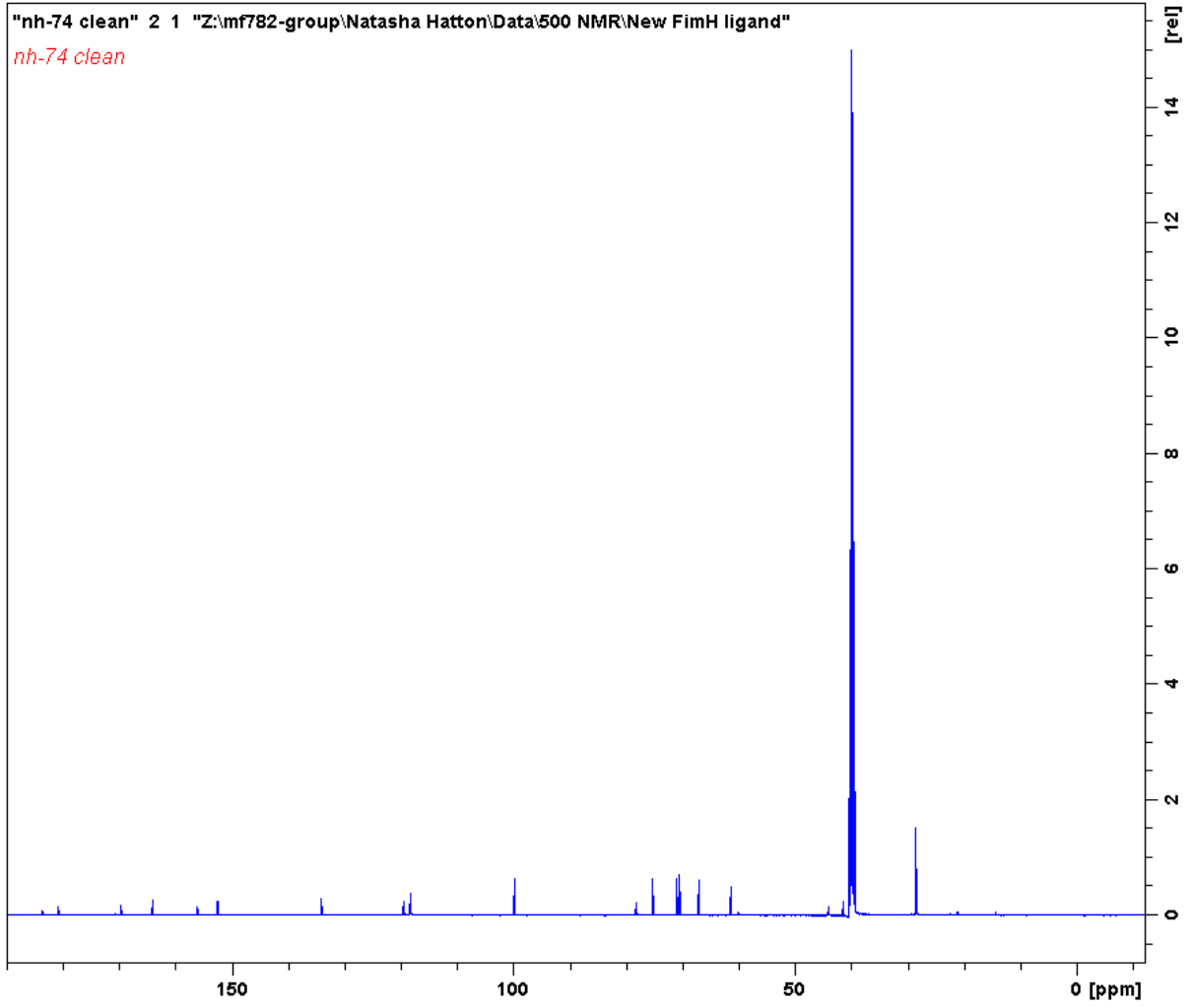
## Appendix



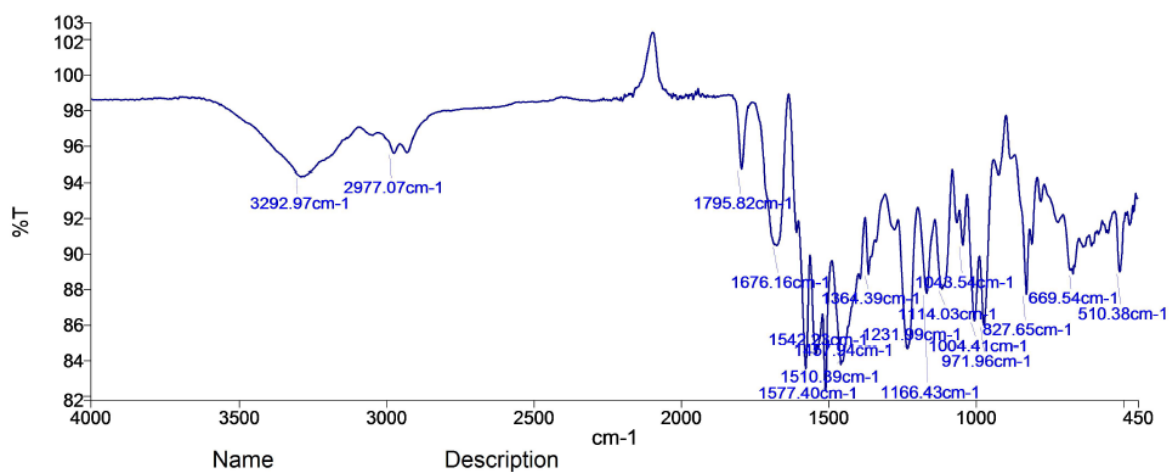
9.1.6.5 [N-[4-( $\alpha$ -D-Mannopyranosyloxy)phenyl]-N'-[(2'-tert-butyloxycarbonylamido)ethyl]]squaric acid diamide 2.52



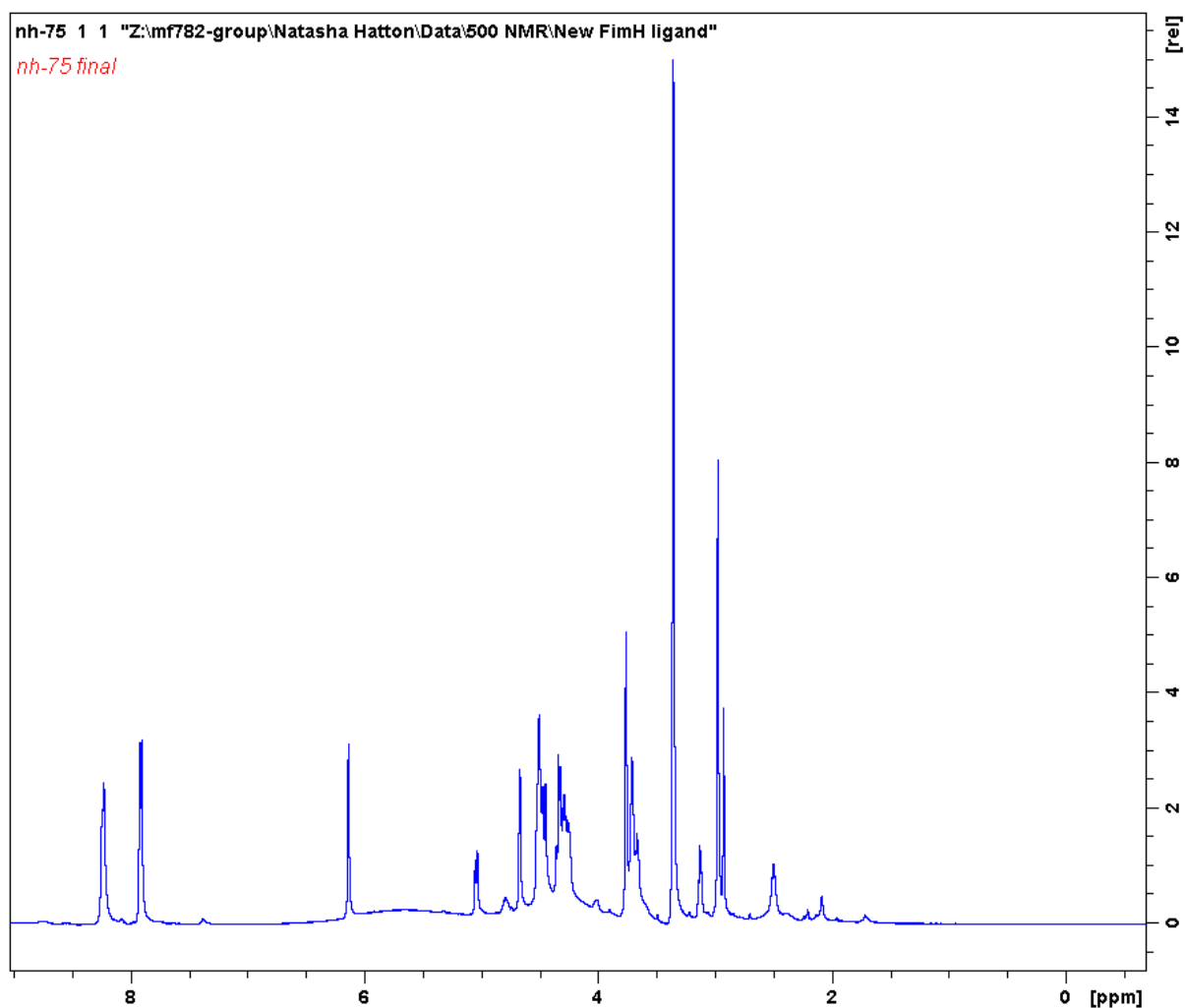
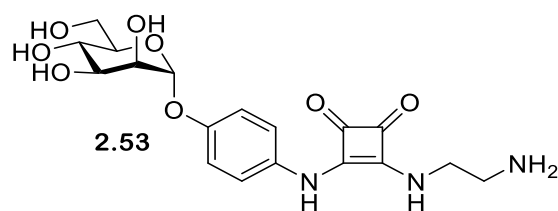
# Appendix



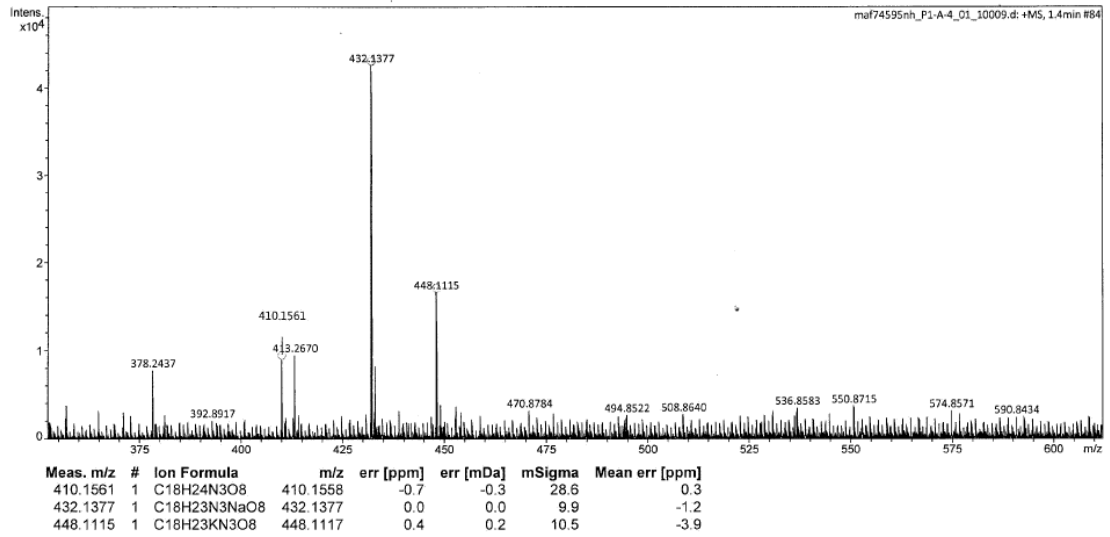
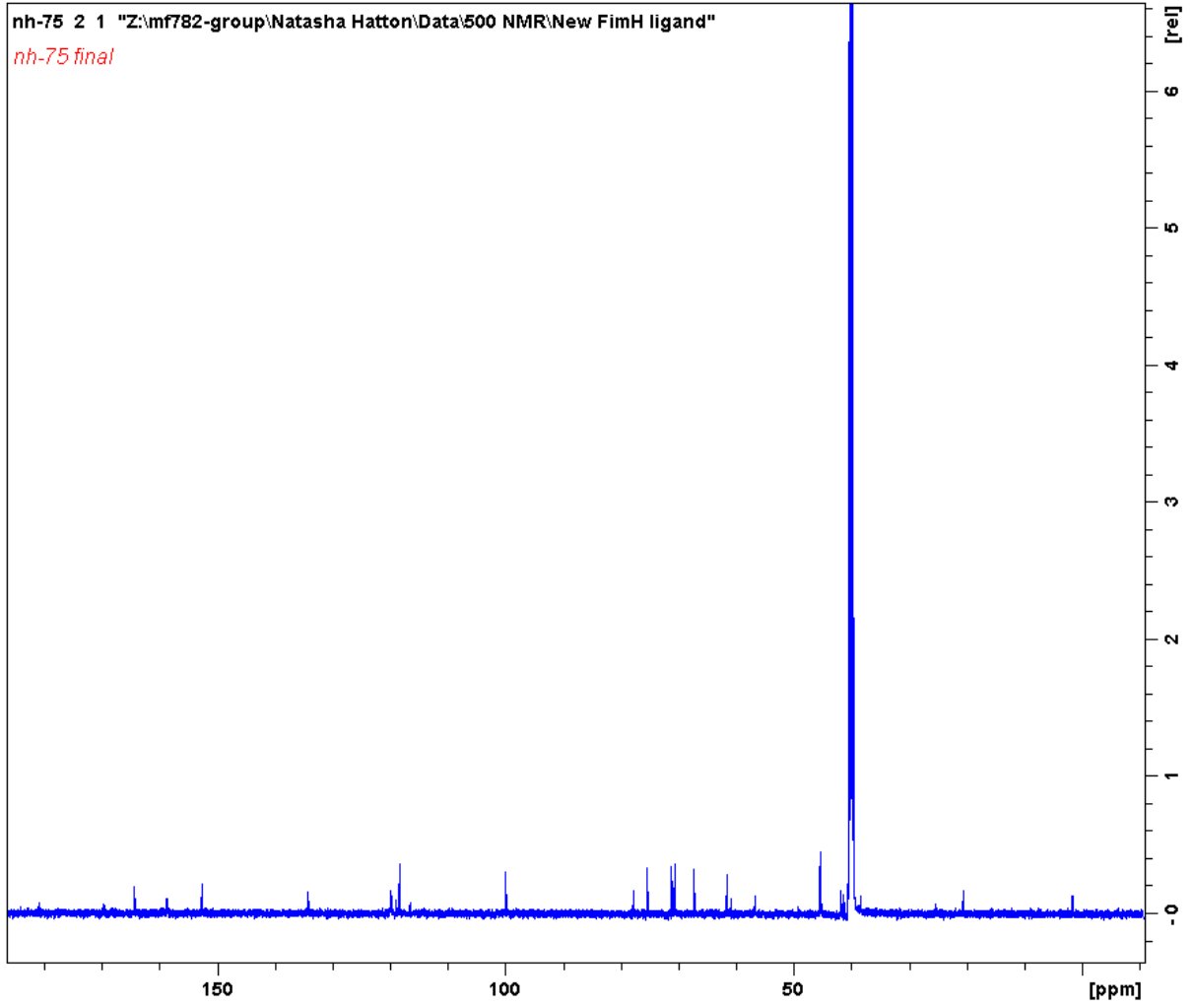
## Appendix



1.6.5 *p*-[[(2-Aminoethylamino)-2,3-dioxocyclobut-1-enyl]amino]phenyl  $\alpha$ -D-mannopyranoside  
2.53

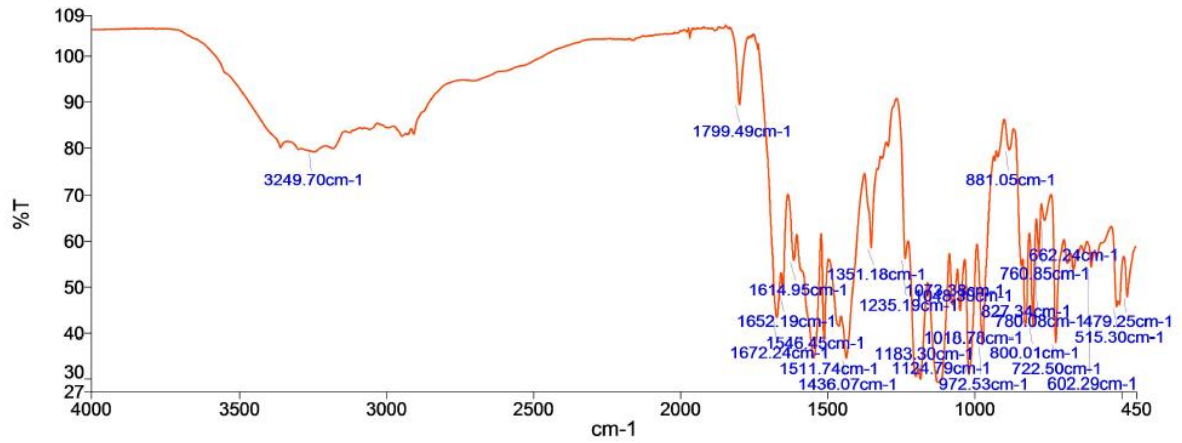


Appendix

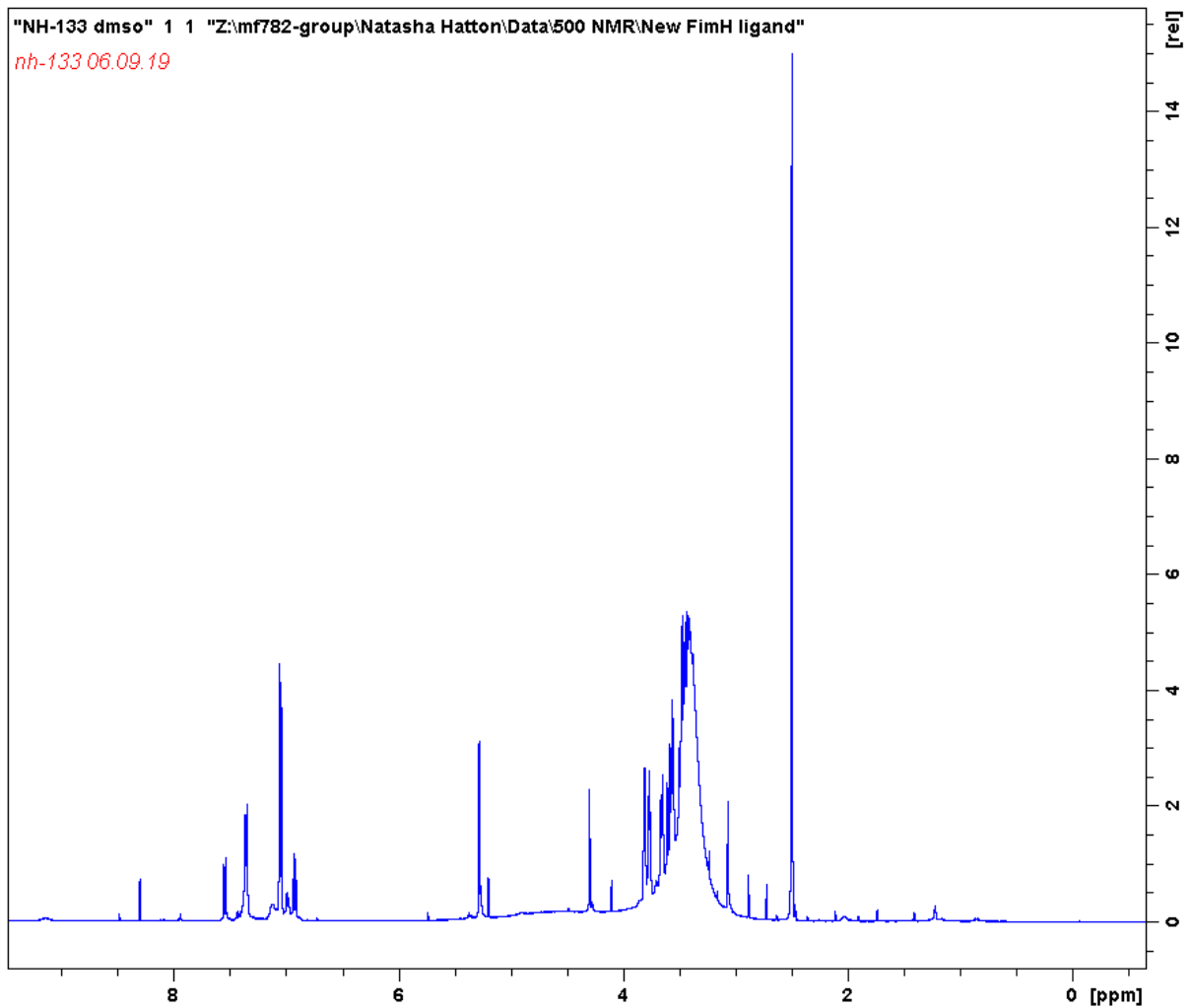
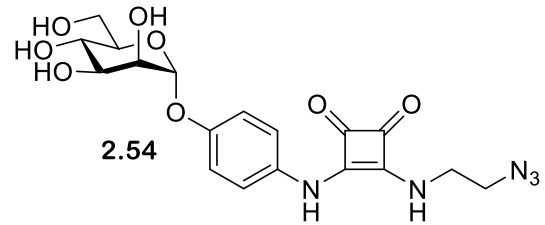




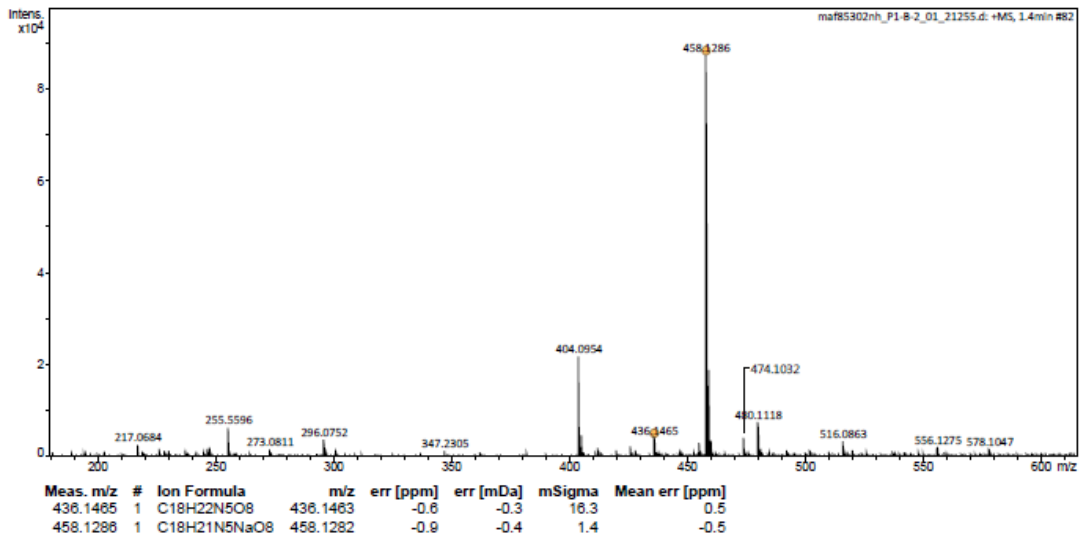
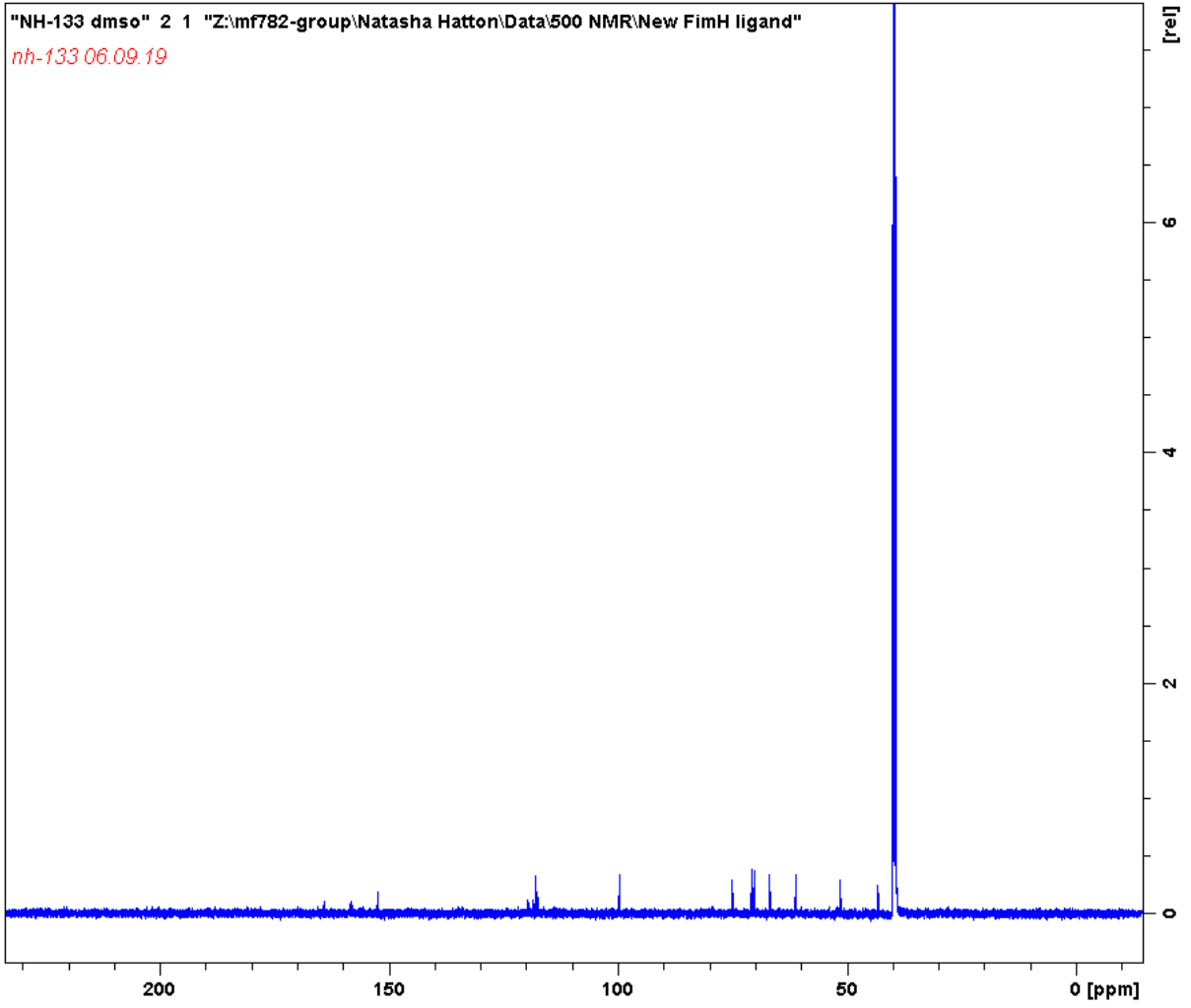
## Appendix



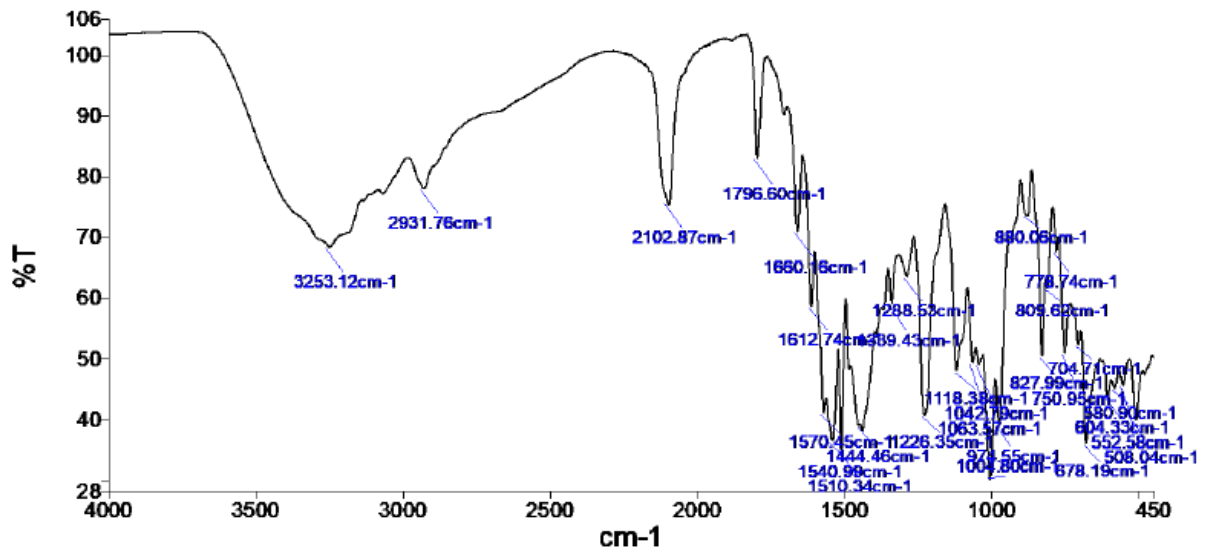
### 9.1.6.6 *p*-[[(1-Amino-2-azidoethane)-2,3-dioxocyclobut-1-enyl]amino]phenyl $\alpha$ -D-mannopyranoside 2.54



Appendix



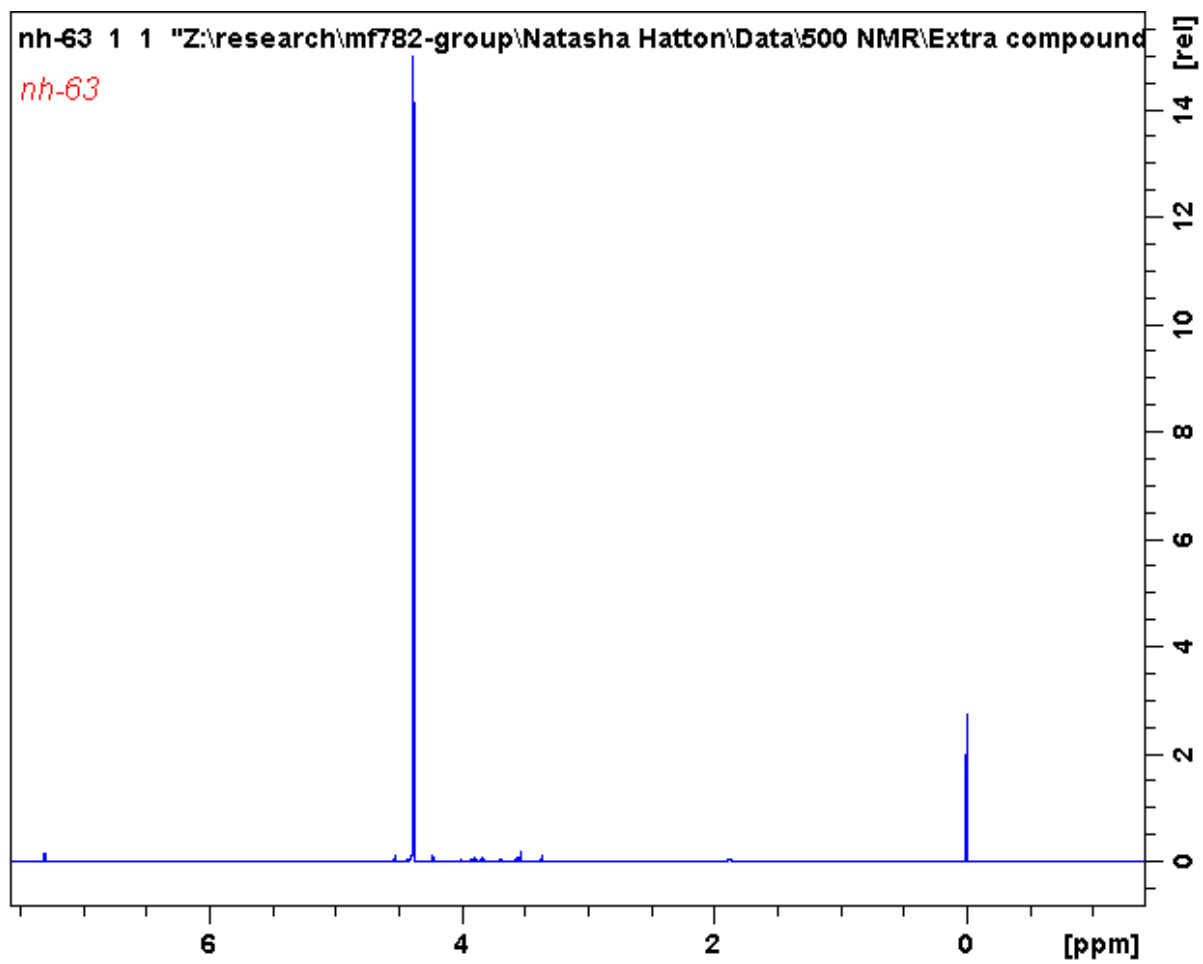
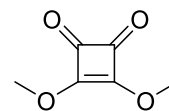
Appendix



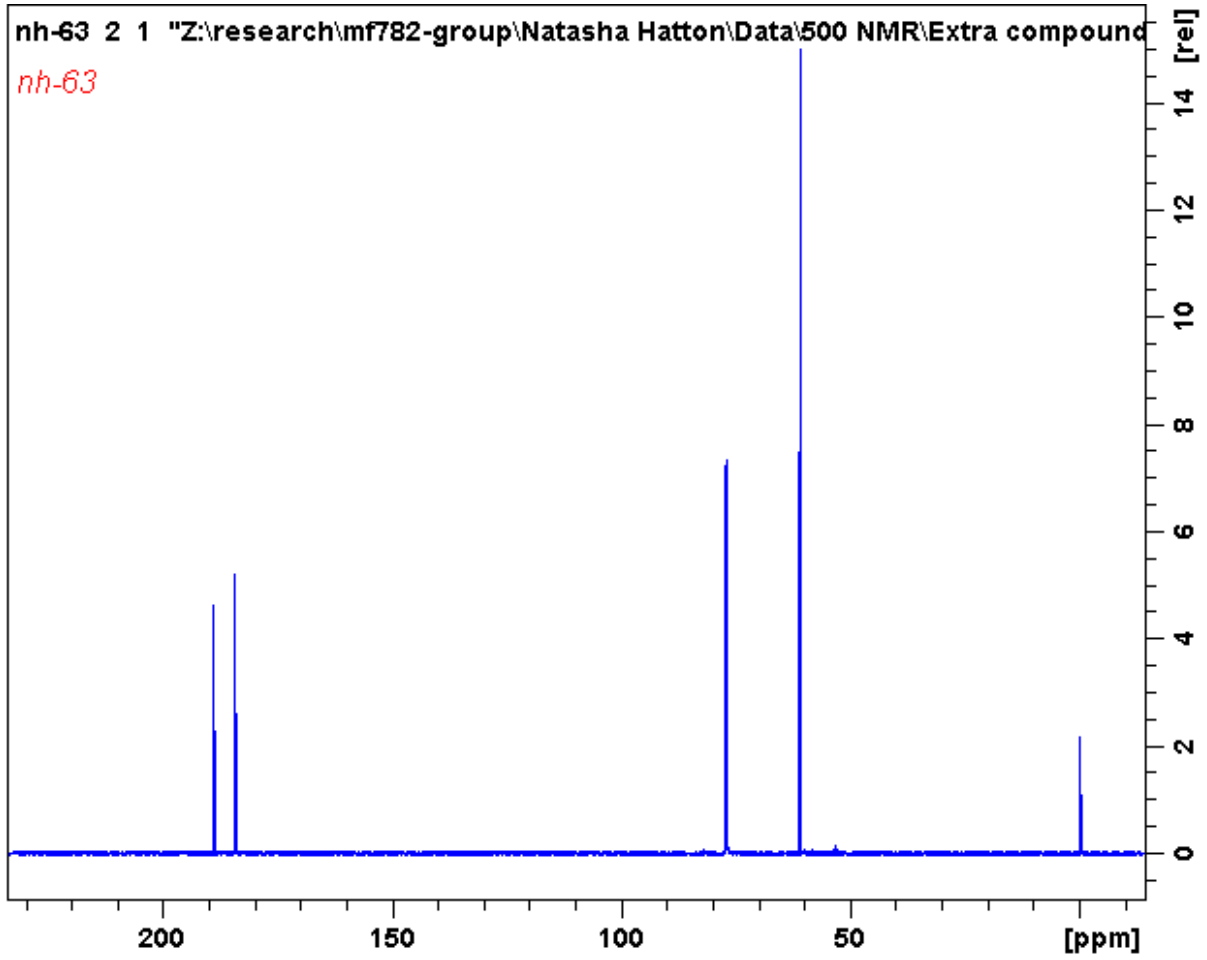
Appendix

9.1.7 Supporting compounds used in chapter 2

9.1.7.1 3,4-dimethoxycyclobut-3-ene-1,2-dione



Appendix

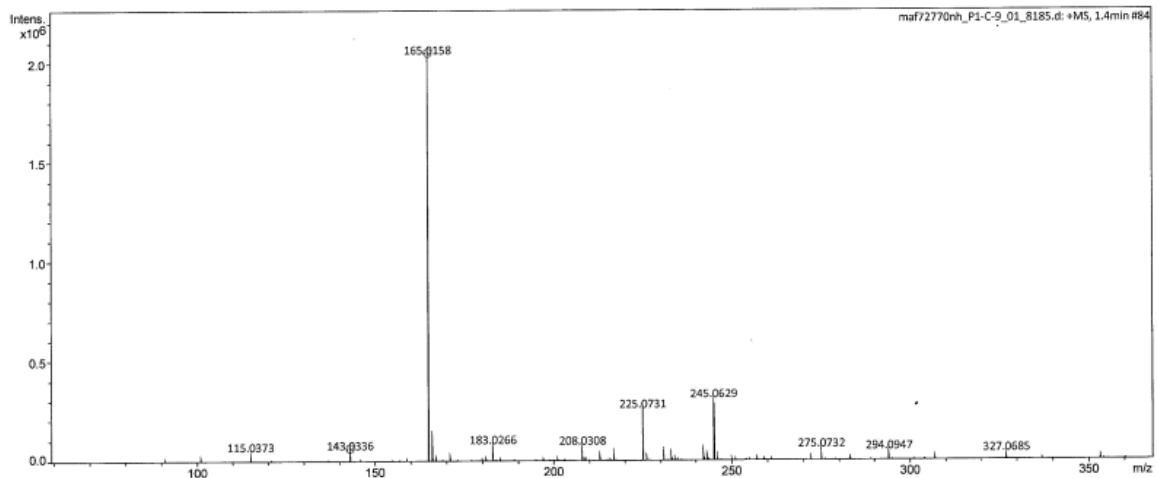


York - Chemistry - Mass Spectrometry Service Report

NH-63

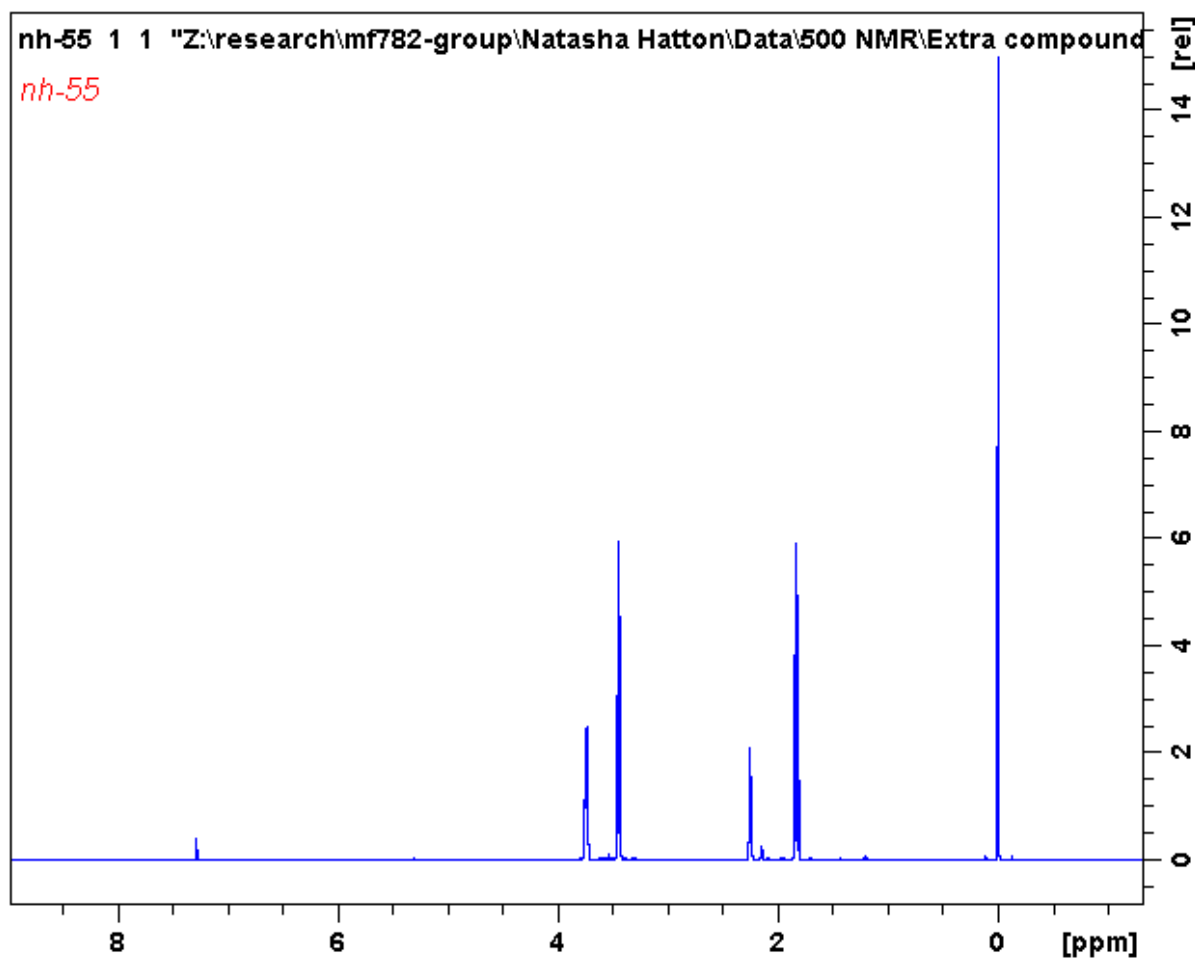
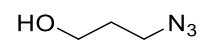
Analysis Information

Analysis Filename maf72770nh\_P1-C-9\_01\_8185.d Acquisition Date 10/10/2018 14:57:55  
Method ESI\_low mass\_2c1s.m Instrument compact  
Submission Name maf72770nh ESI Positive

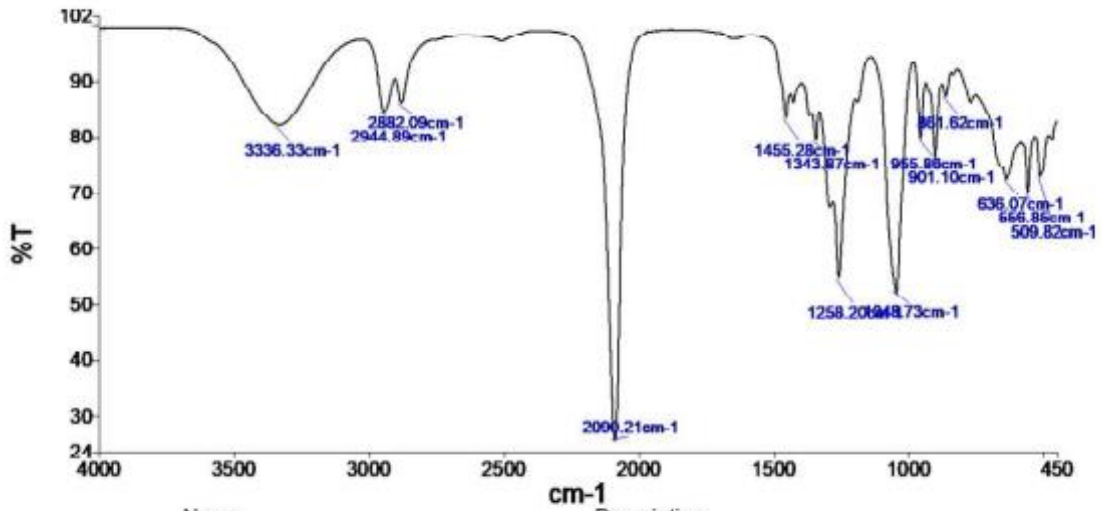
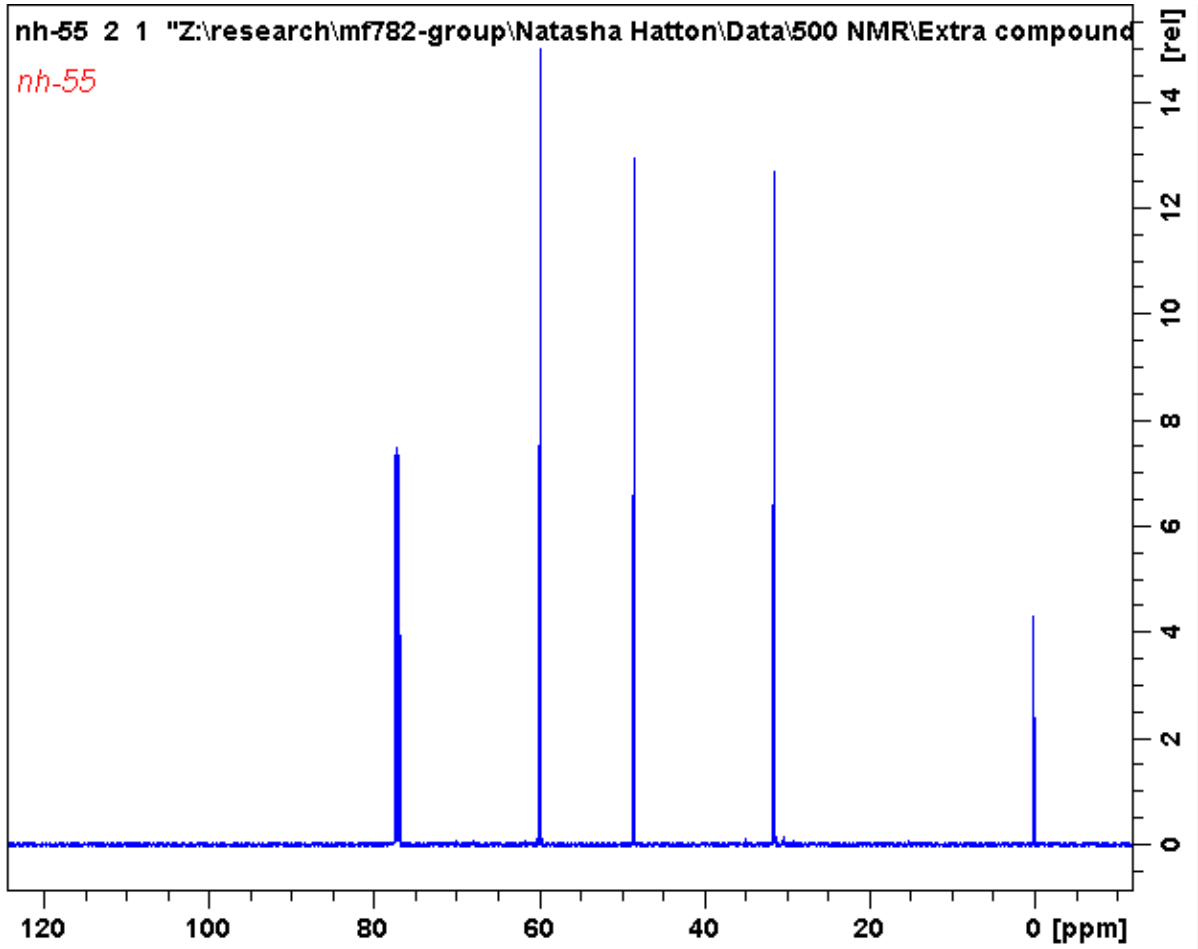


Meas. m/z	#	Ion Formula	m/z	err [ppm]	err [mDa]	mSigma	Mean err [ppm]
143.0336	1	C6H7O4	143.0339	2.2	0.3	11.3	2.5
165.0158	1	C6H6NaO4	165.0158	0.5	0.1	1.2	0.9

## 9.1.7.2 3-Azidopropanol

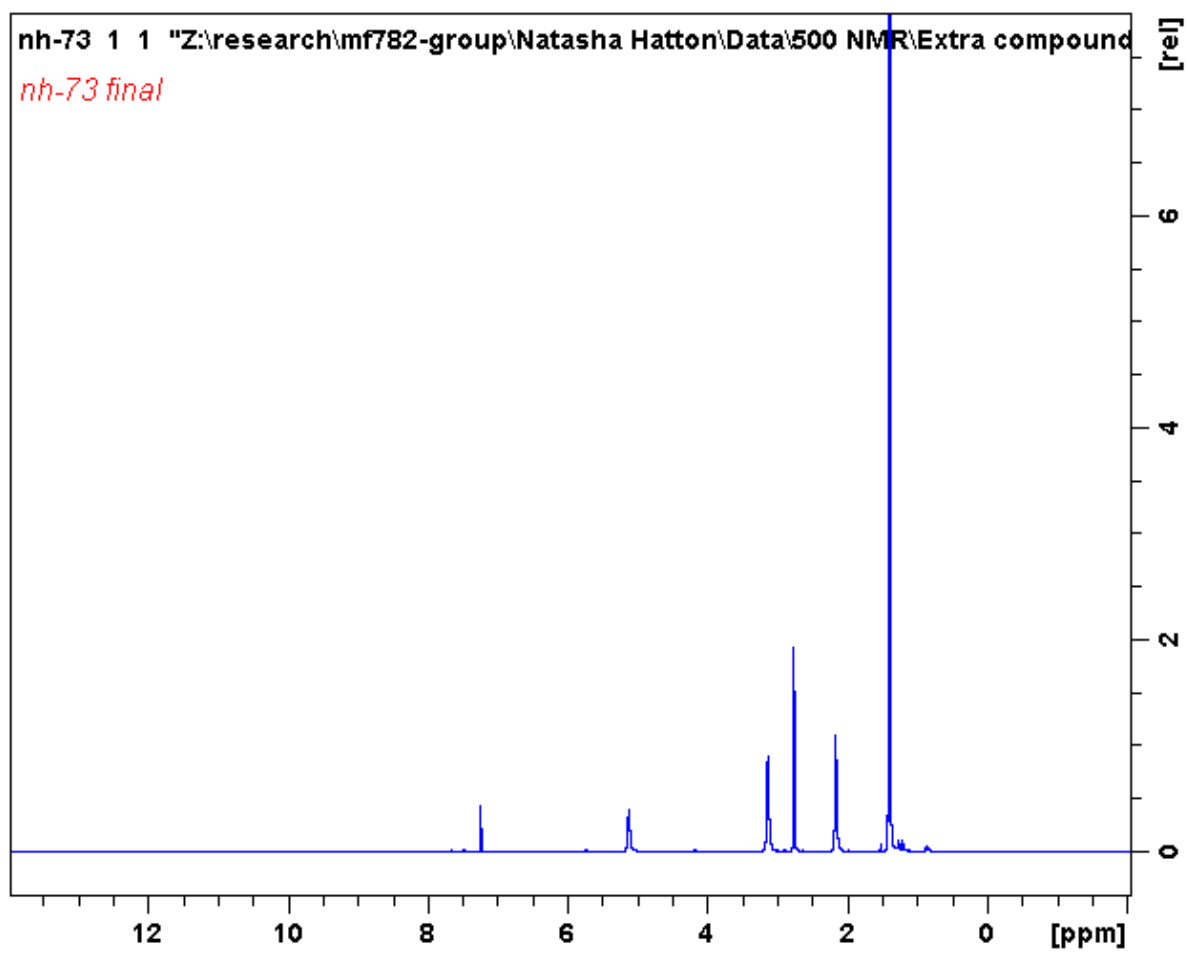
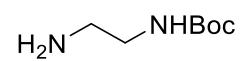


Appendix



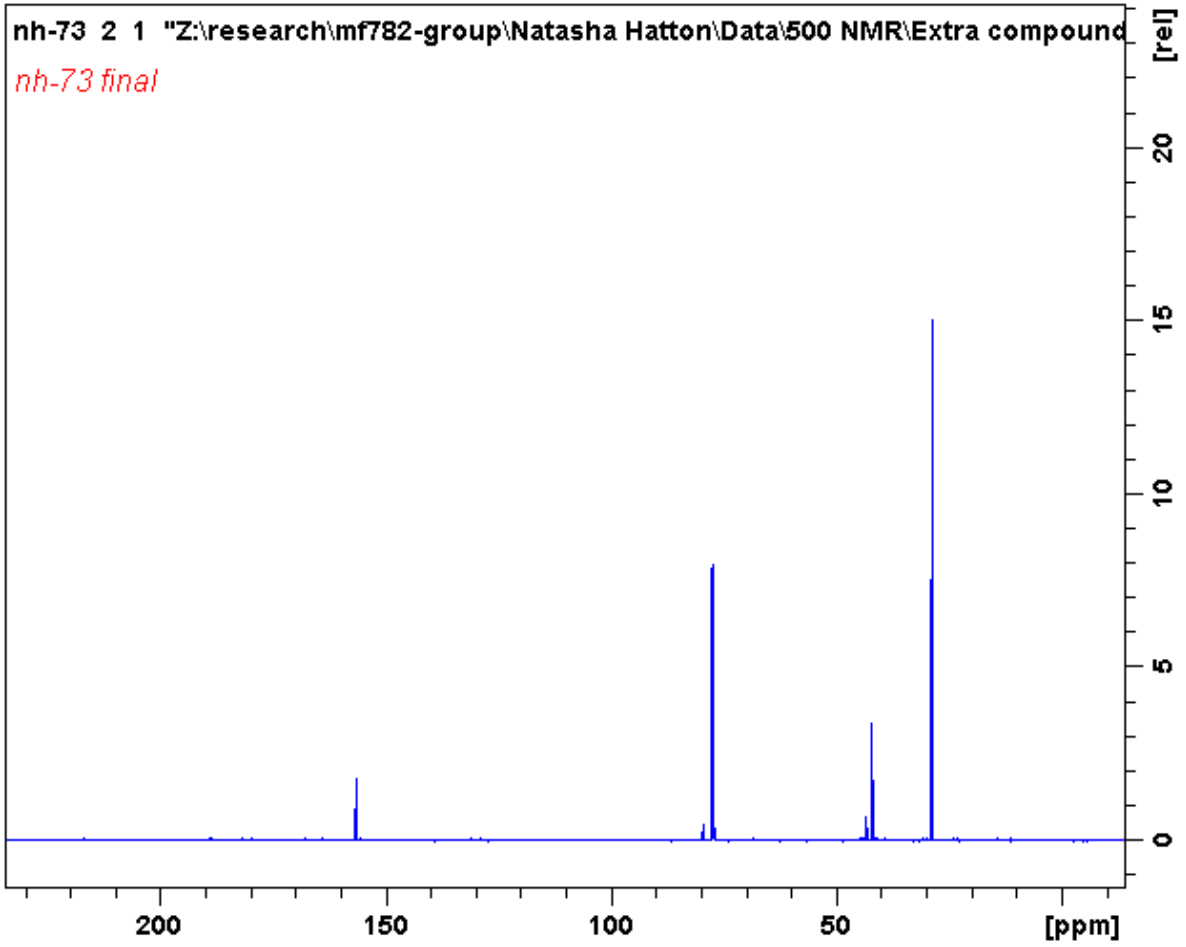
Name Description  
Administrator 1431 Sample 1431 By Administrator Date Tuesday, December 01 2020

## 9.1.7.3 N-BOC-1,2-Diaminoethane





Appendix

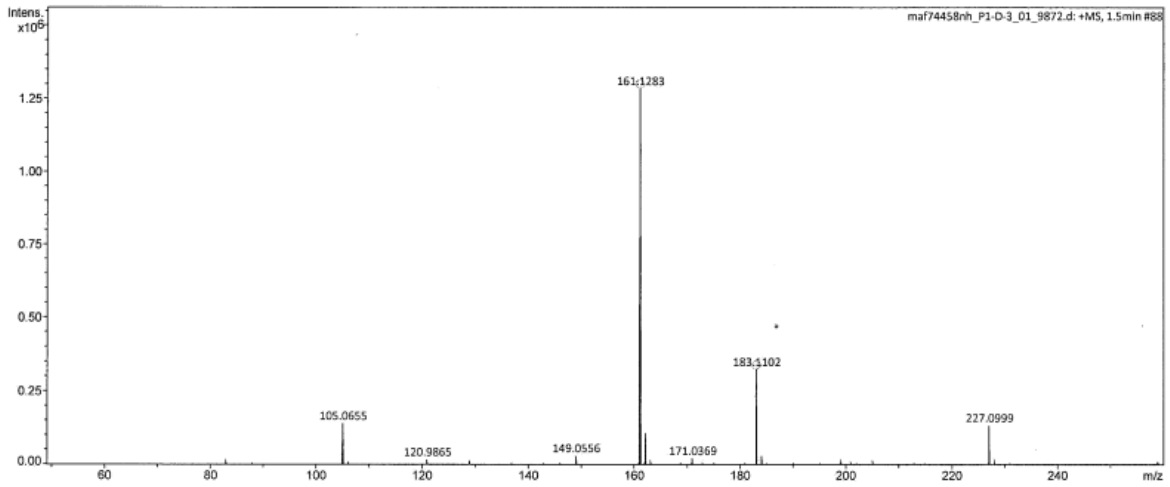


York - Chemistry - Mass Spectrometry Service Report

NH-61

Analysis Information

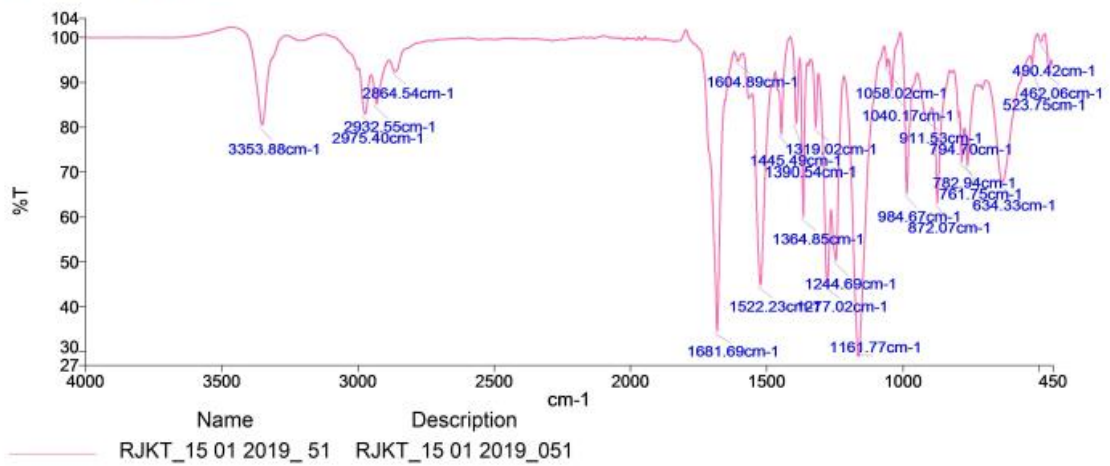
Analysis Filename maf74458nh\_P1-D-3\_01\_9872.d Acquisition Date 10/01/2019 15:13:58  
 Method ESI\_low mass\_2c1s.m Instrument compact  
 Submission Name maf74458nh ESI Positive



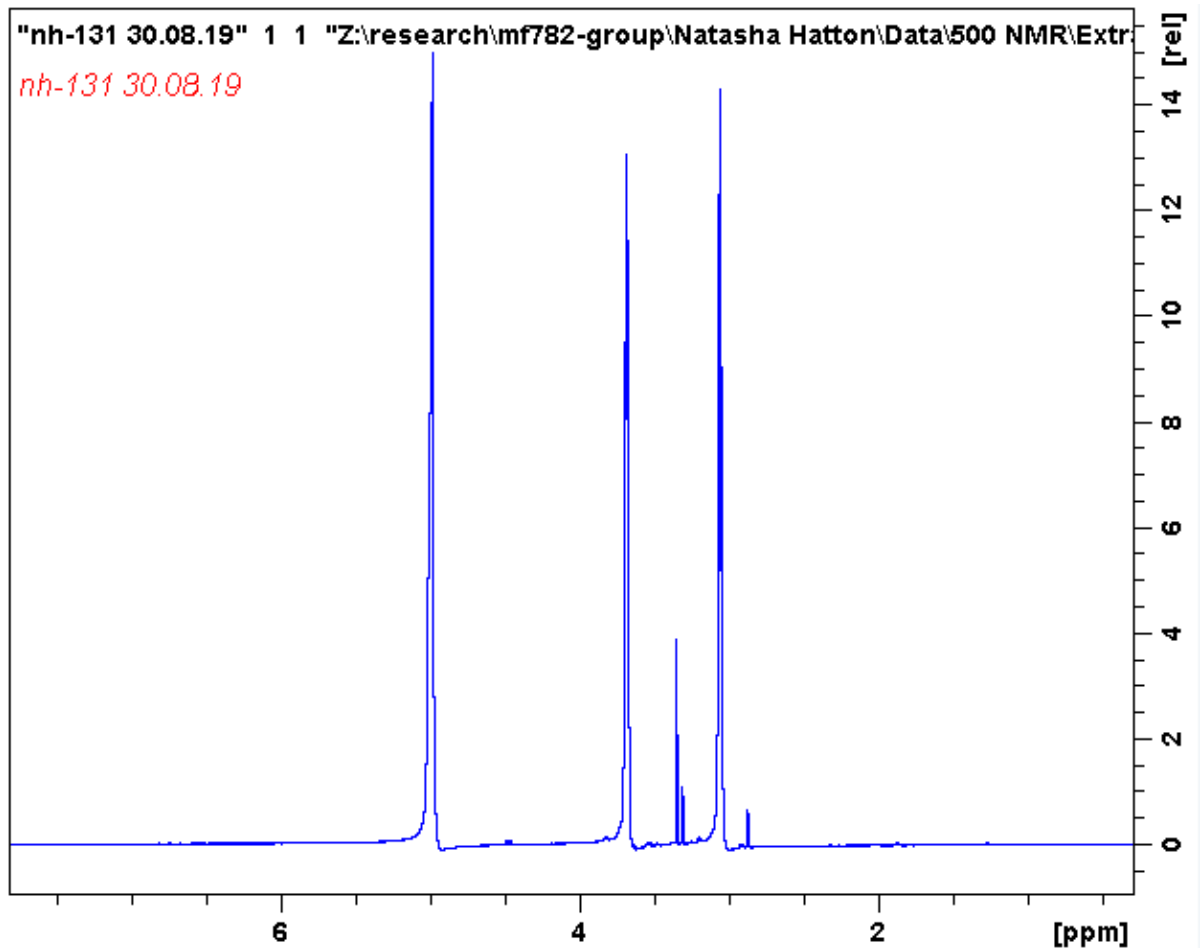
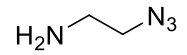
Meas. m/z	#	Ion Formula	m/z	err [ppm]	err [mDa]	mSigma	Mean err [ppm]
161.1283	1	C7H17N2O2	161.1285	0.9	0.1	1.8	0.4
183.1102	1	C7H16N2NaO2	183.1104	1.0	0.2	3.2	0.6

Appendix

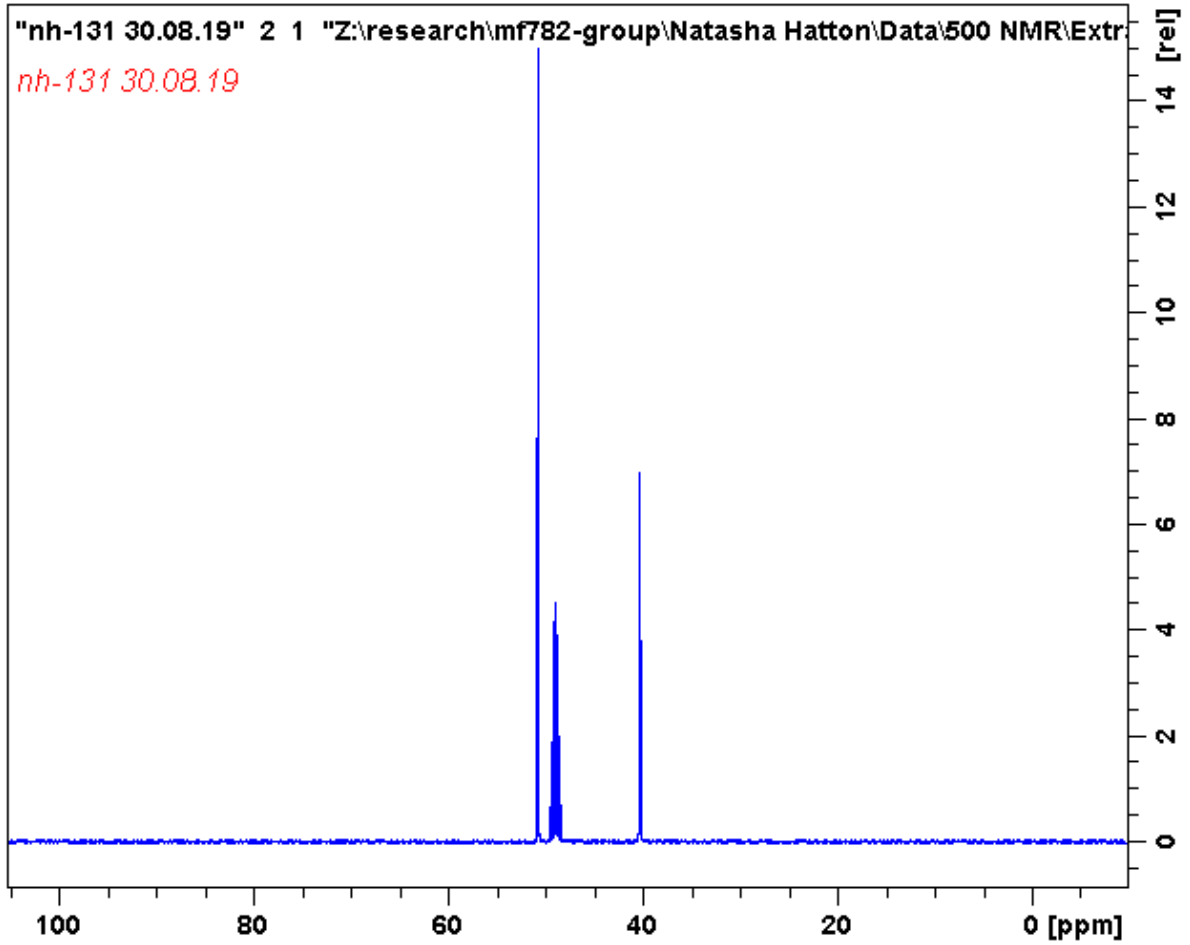
Peak Table Graph



9.1.7.4 1-amino-2-azidoethane



Appendix

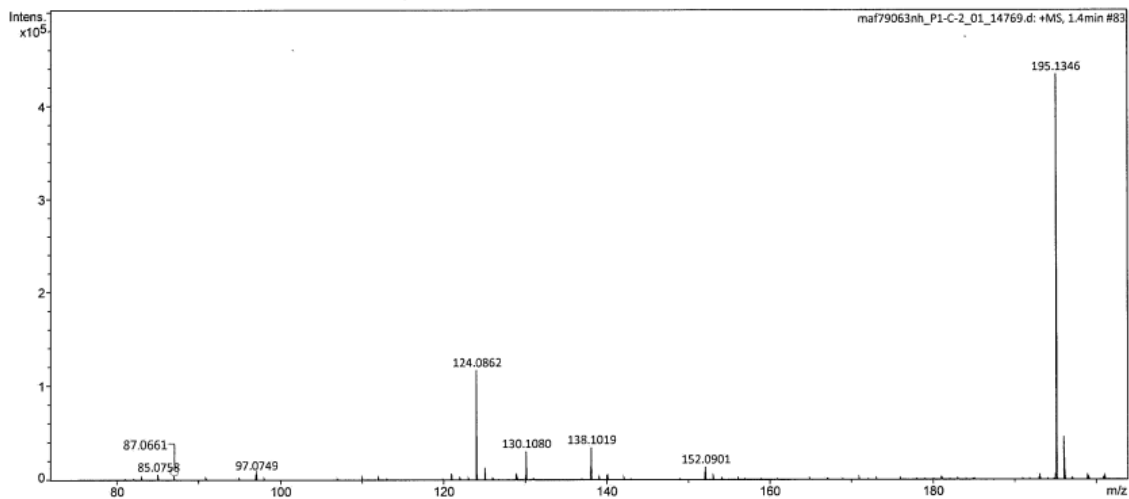
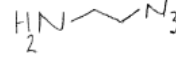


York - Chemistry - Mass Spectrometry Service Report

NH-131

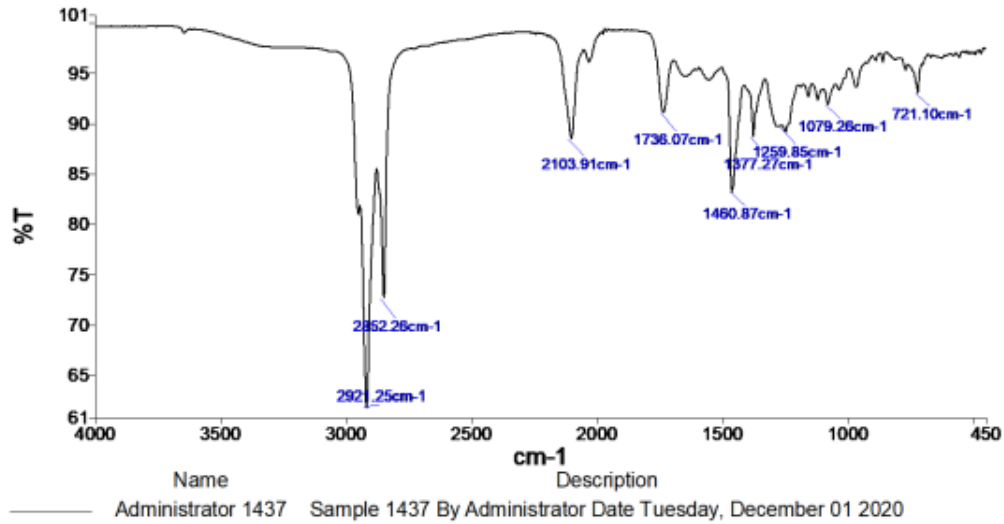
Analysis Information

Analysis Filename maf79063nh\_P1-C-2\_01\_14769.d Acquisition Date 20/08/2019 10:54:00  
 Method ESI\_low mass\_2c1s.m Instrument compact  
 Submission Name maf79063nh ESI Positive



Meas. m/z	#	Ion Formula	m/z	err [ppm]	err [mDa]	mSigma	Mean err [ppm]
87.0661	1	C <sub>2</sub> H <sub>7</sub> N <sub>4</sub>	87.0665	5.4	0.5	n.a.	3.1

## Appendix



### 9.2 Appendix for Chapter 3

#### 9.2.1 Expression and purification of colicin E9

##### 9.2.1.1 Gel post HisTrap HP column

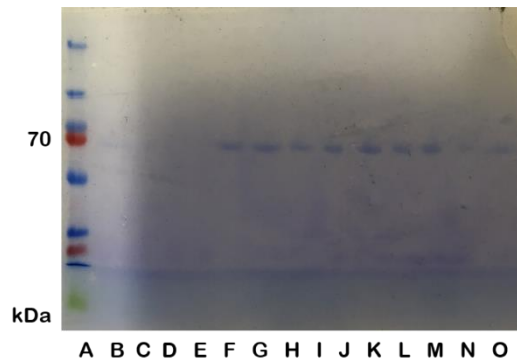


Figure 9-1. Results of SDS-PAGE gel stained with Coomassie containing fraction 13-24 post HisTrap HP column purification of colicin E9

##### 9.2.1.2 Gel post gel filtration

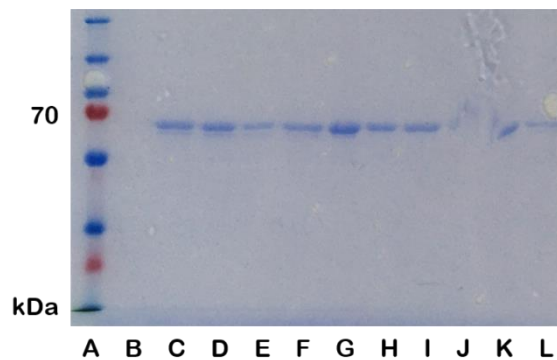
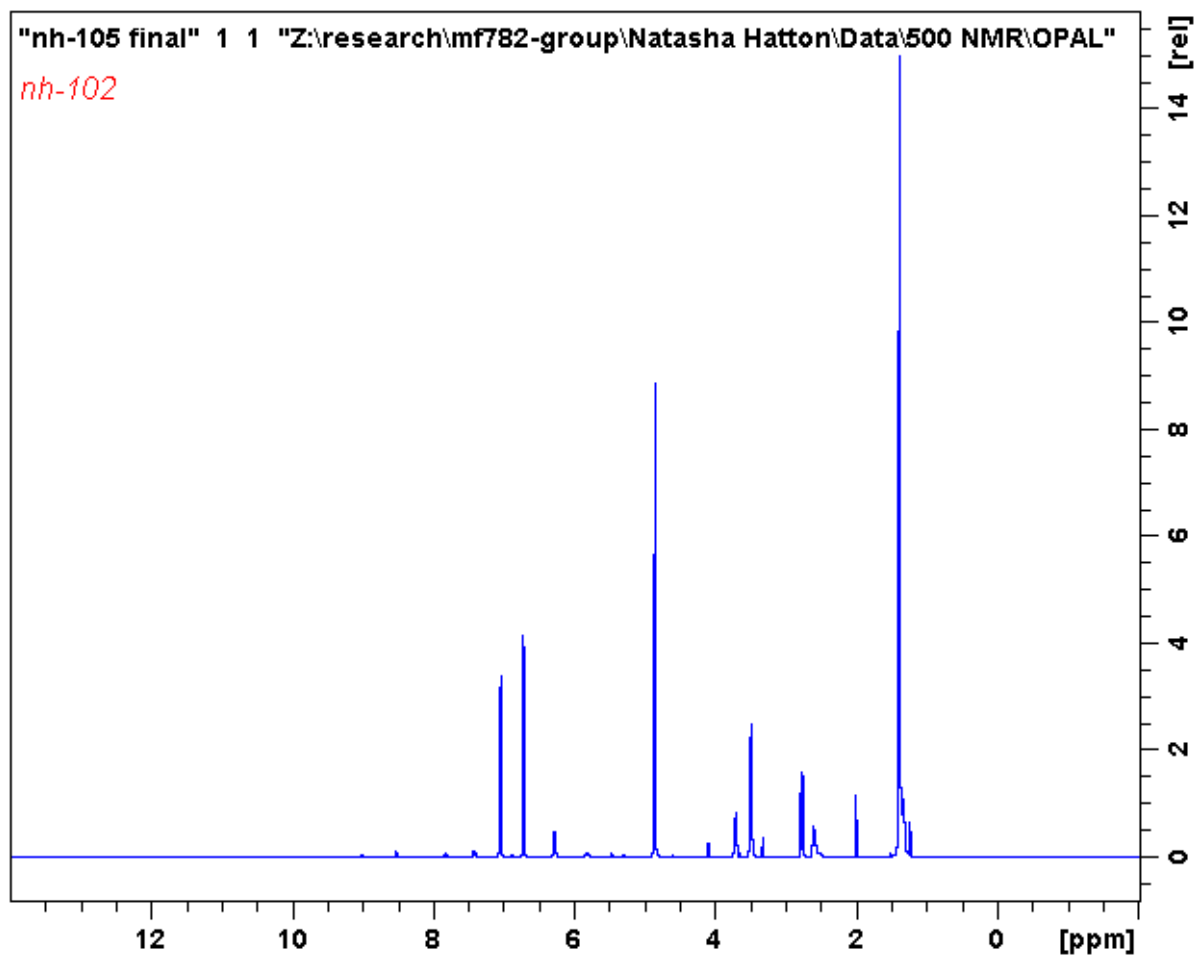
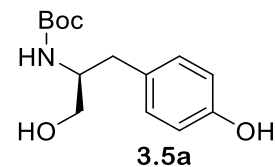


Figure 9-2. Results of SDS-PAGE gel stained with Coomassie of fractions C7-D8 post gel filtration of colicin E9

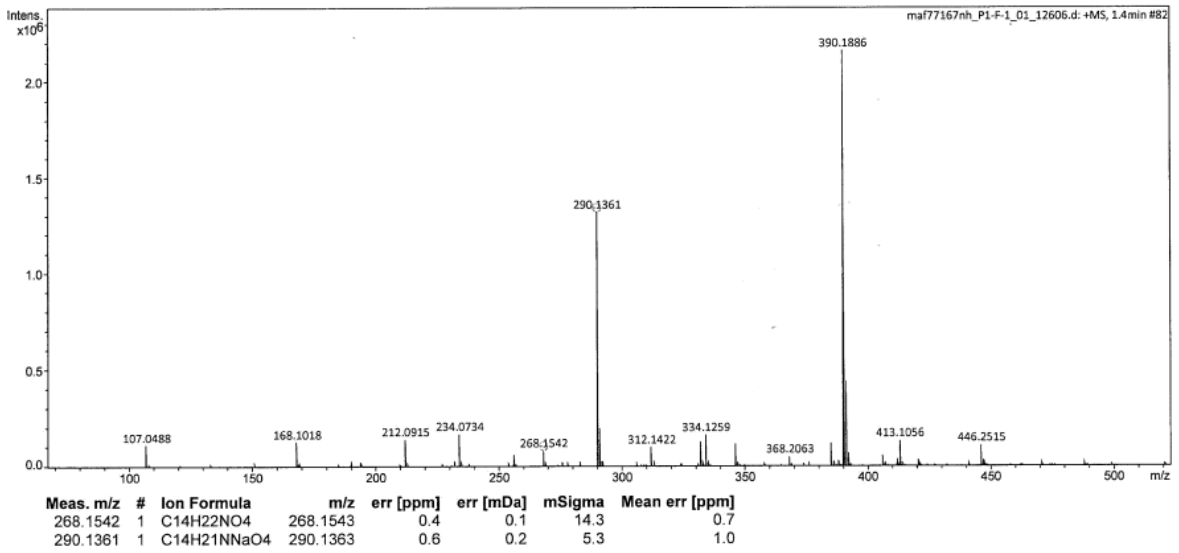
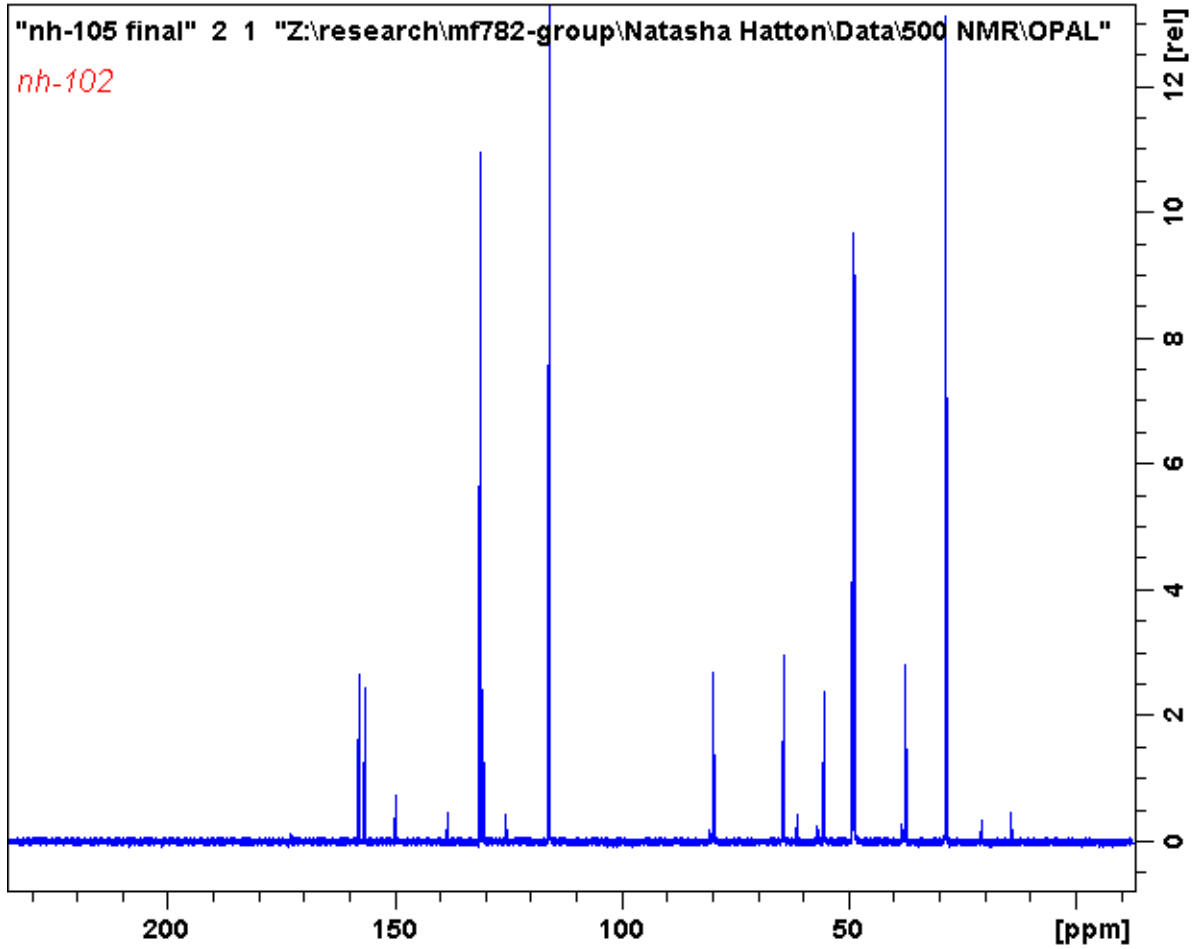
## Appendix

### 9.2.2 Synthesis of Synthesis of (S)-2-(4-((3-(tert-butoxycarbonyl)-2,2-dimethyloxazolidin-4-yl)methyl)phenoxy)acetic acid **3.5**

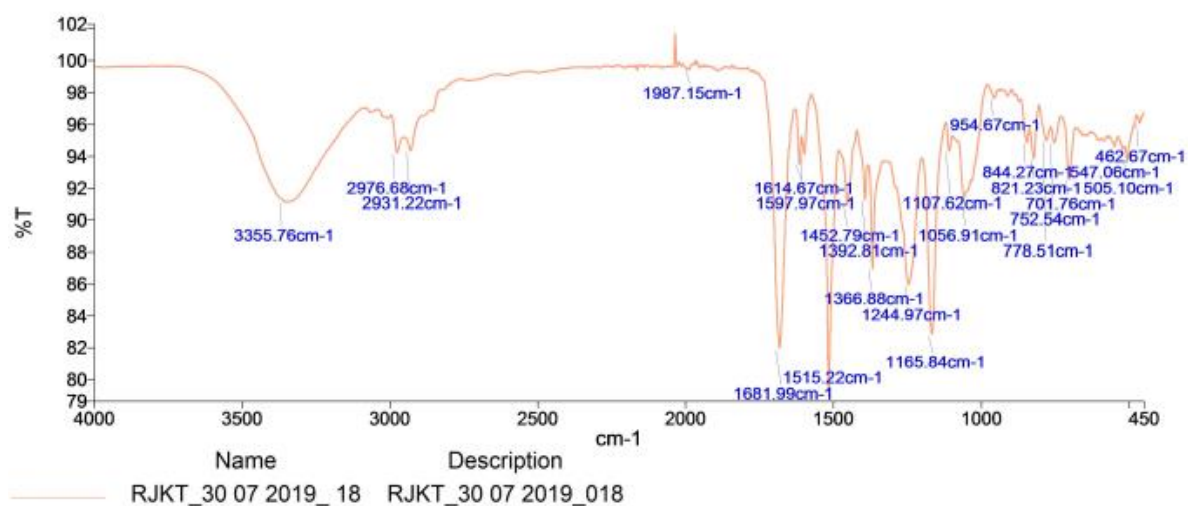
#### 9.2.2.1 Synthesis of (S)-tert-butyl (1-hydroxy-3-(4-hydroxyphenyl)propan-2-yl)carbamate **3.5a**



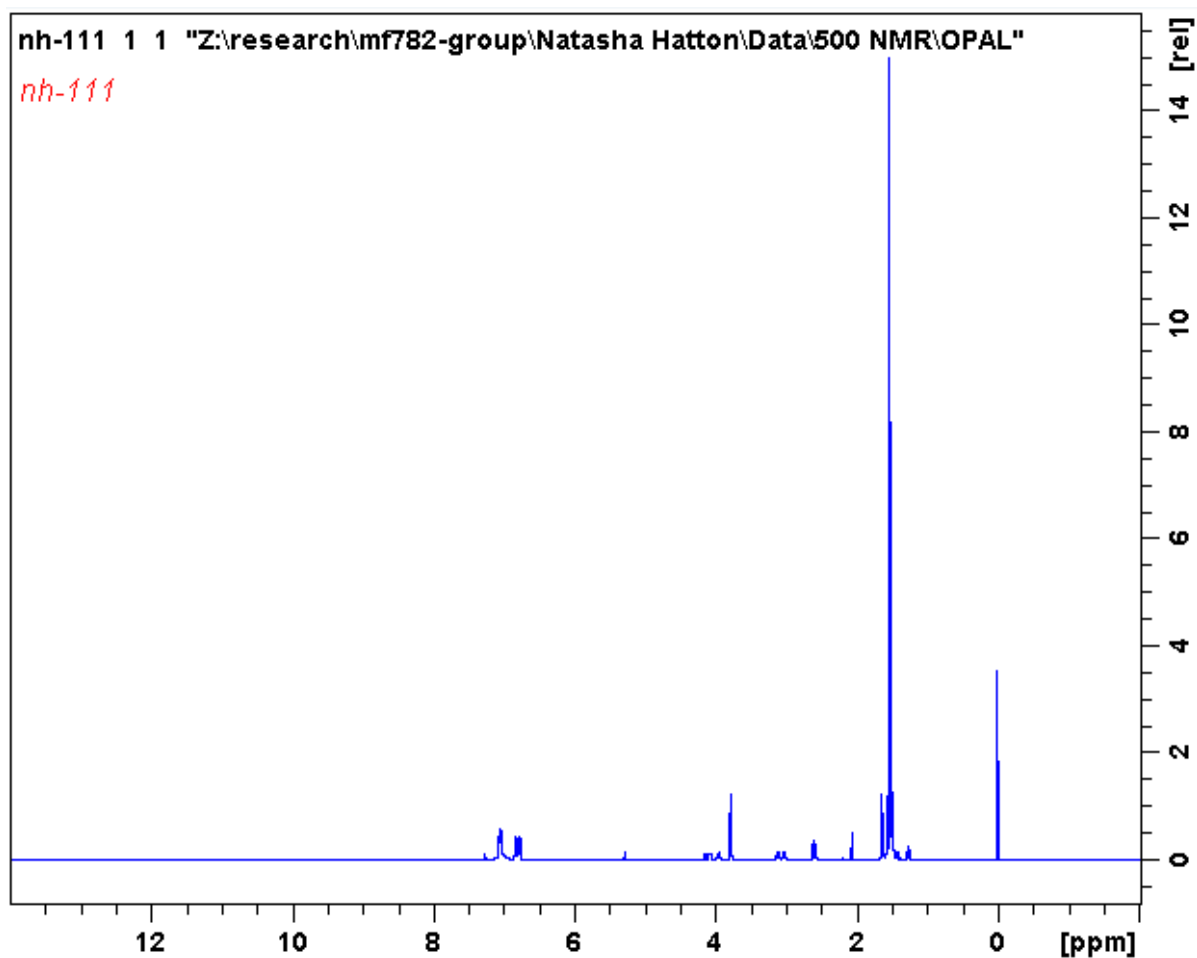
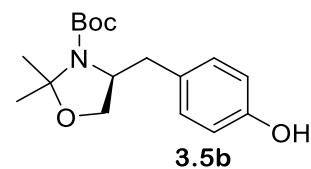
Appendix



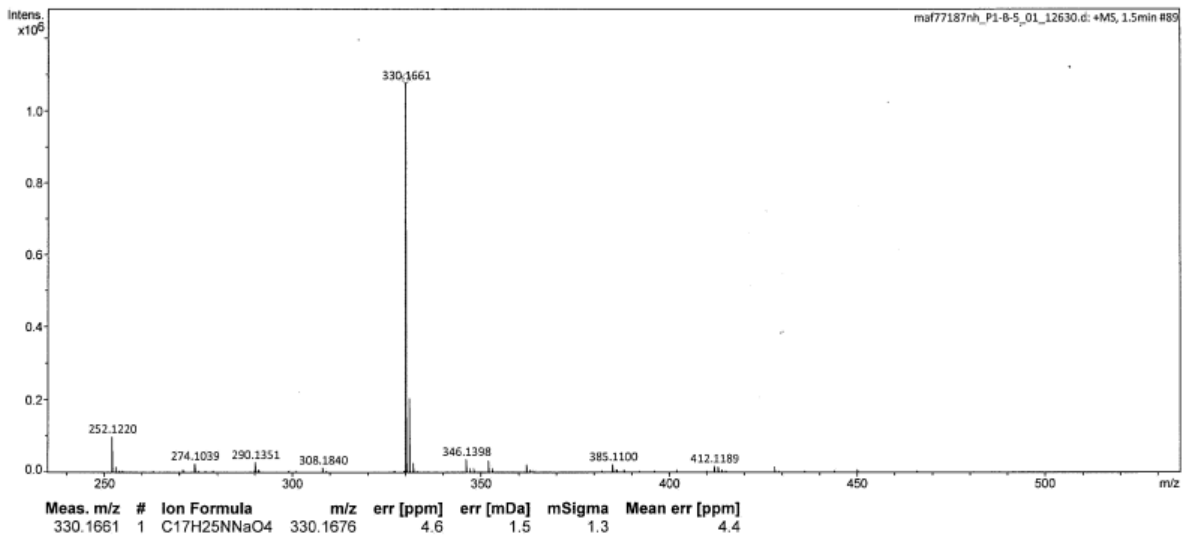
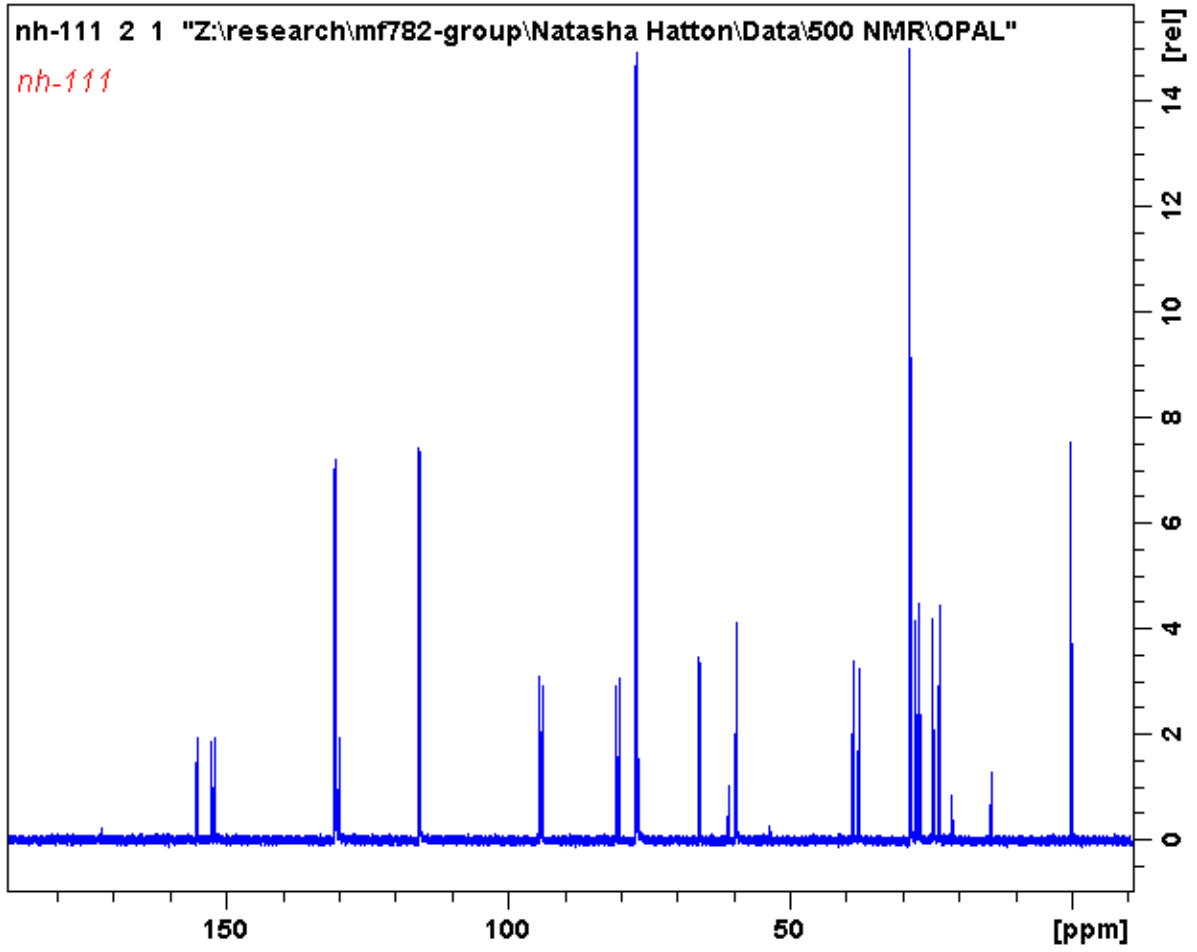
## Appendix



### 9.2.2.2 Synthesis of (*S*)-*tert*-butyl 4-(4-hydroxybenzyl)-2,2-dimethyloxazolidine-3-carboxylate **3.5b**



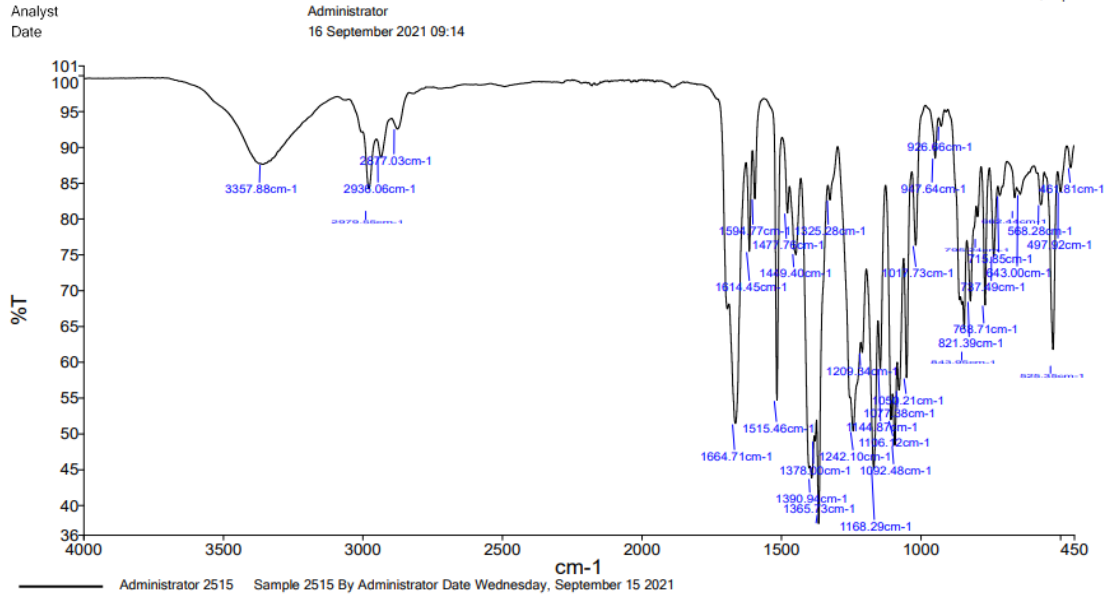
Appendix





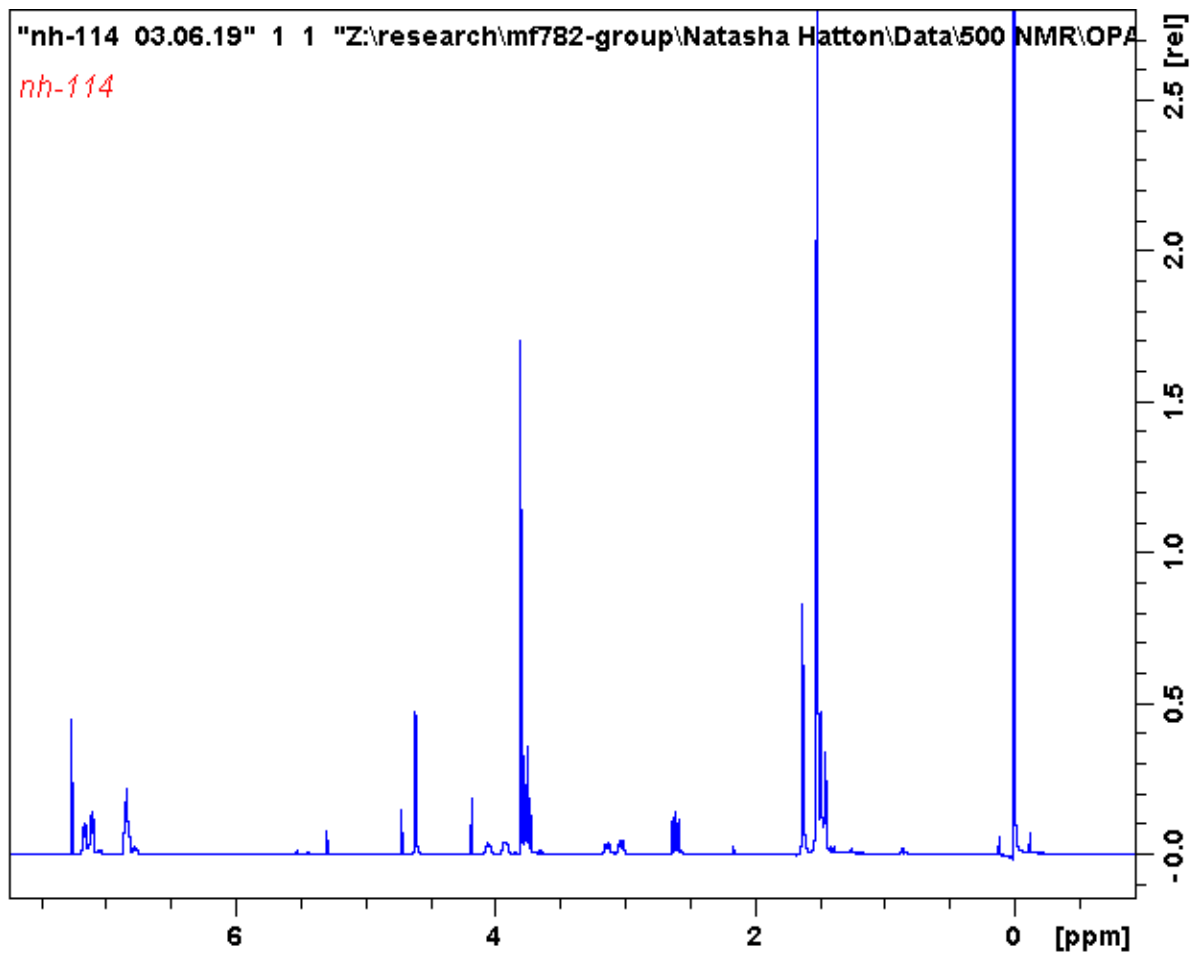
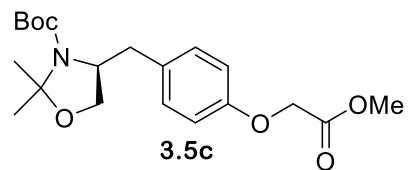
# Appendix

PerkinElmer Spectrum Version 10.5.4  
16 September 2021 09:14

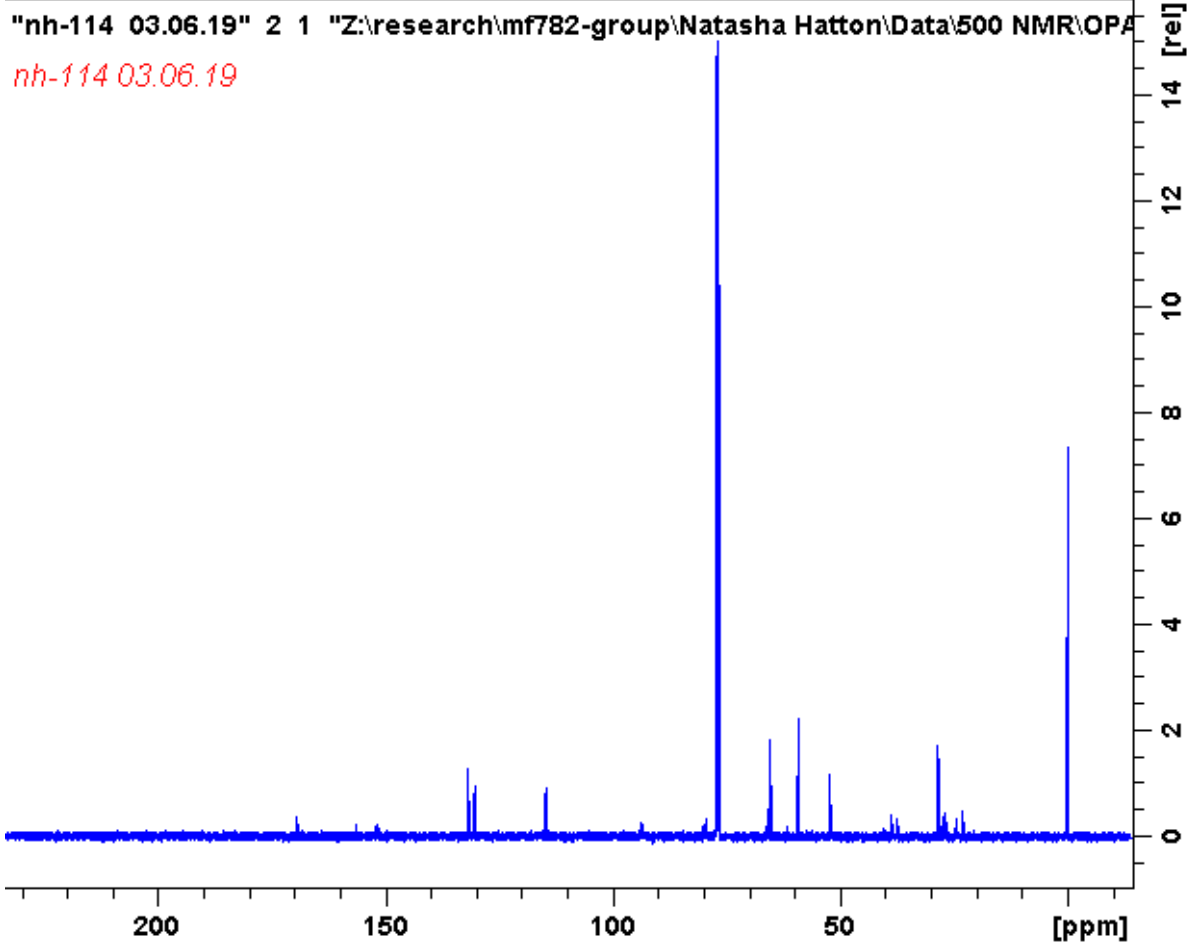


Appendix

9.2.2.3. *S*-tert-butyl 4-(4-(2-methoxy-2-oxoethoxy)benzyl)-2,2-dimethylloxazolidene-3-carboxylate **3.5c**



Appendix

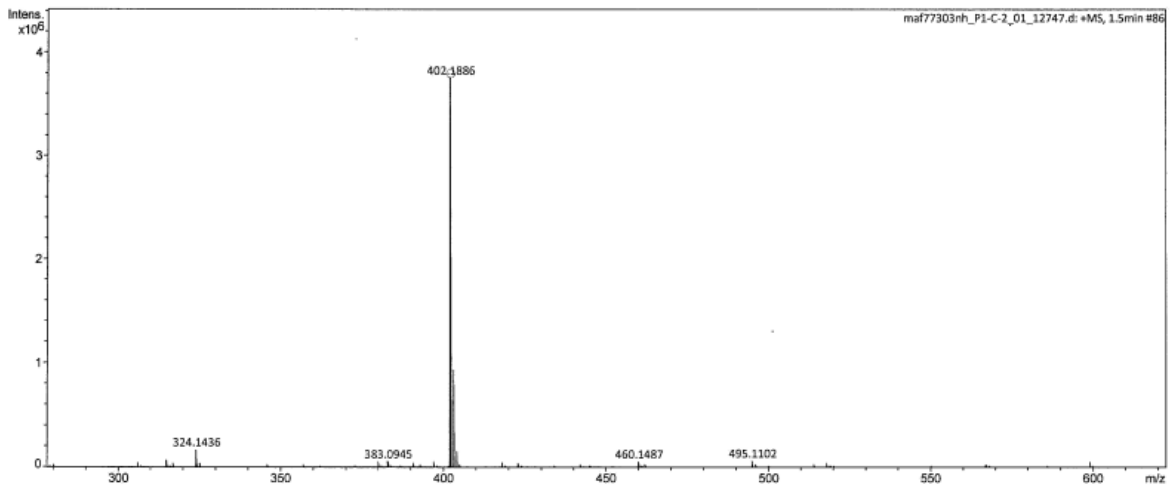


York - Chemistry - Mass Spectrometry Service Report

NH-114

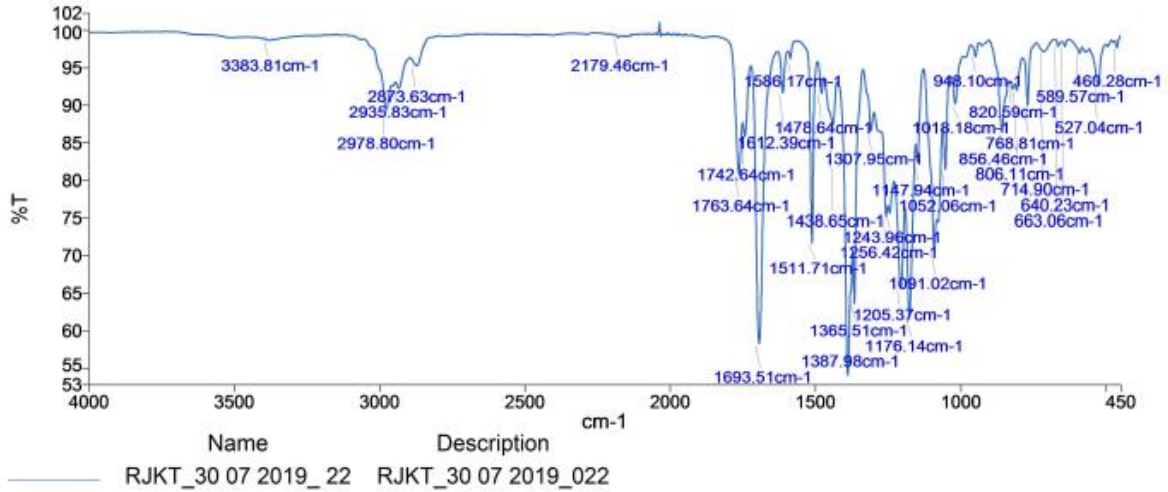
Analysis Information

Analysis Filename	maf77303nh_P1-C-2_01_12747.d	Acquisition Date	21/05/2019 08:56:09
Method	ESI_low mass_2c1s.m	Instrument	compact
Submission Name	maf77303nh	ESI	Positive

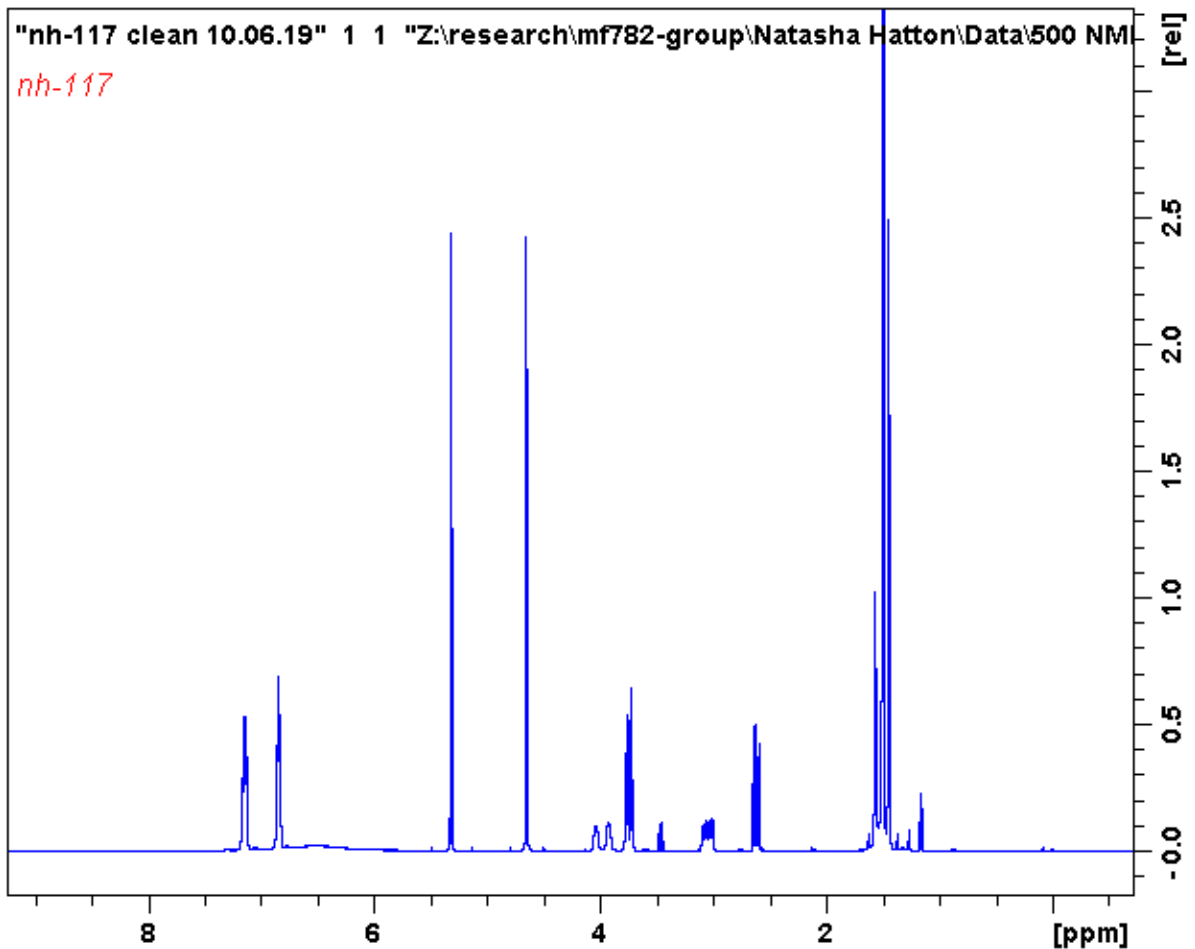
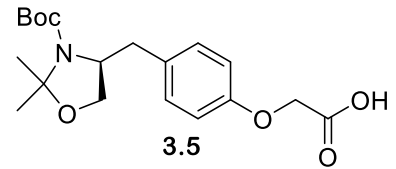


Meas. m/z	#	Ion Formula	m/z	err [ppm]	err [mDa]	mSigma	Mean err [ppm]
402.1886	1	C <sub>20</sub> H <sub>29</sub> NNaO <sub>6</sub>	402.1887	0.3	0.1	14.1	0.3

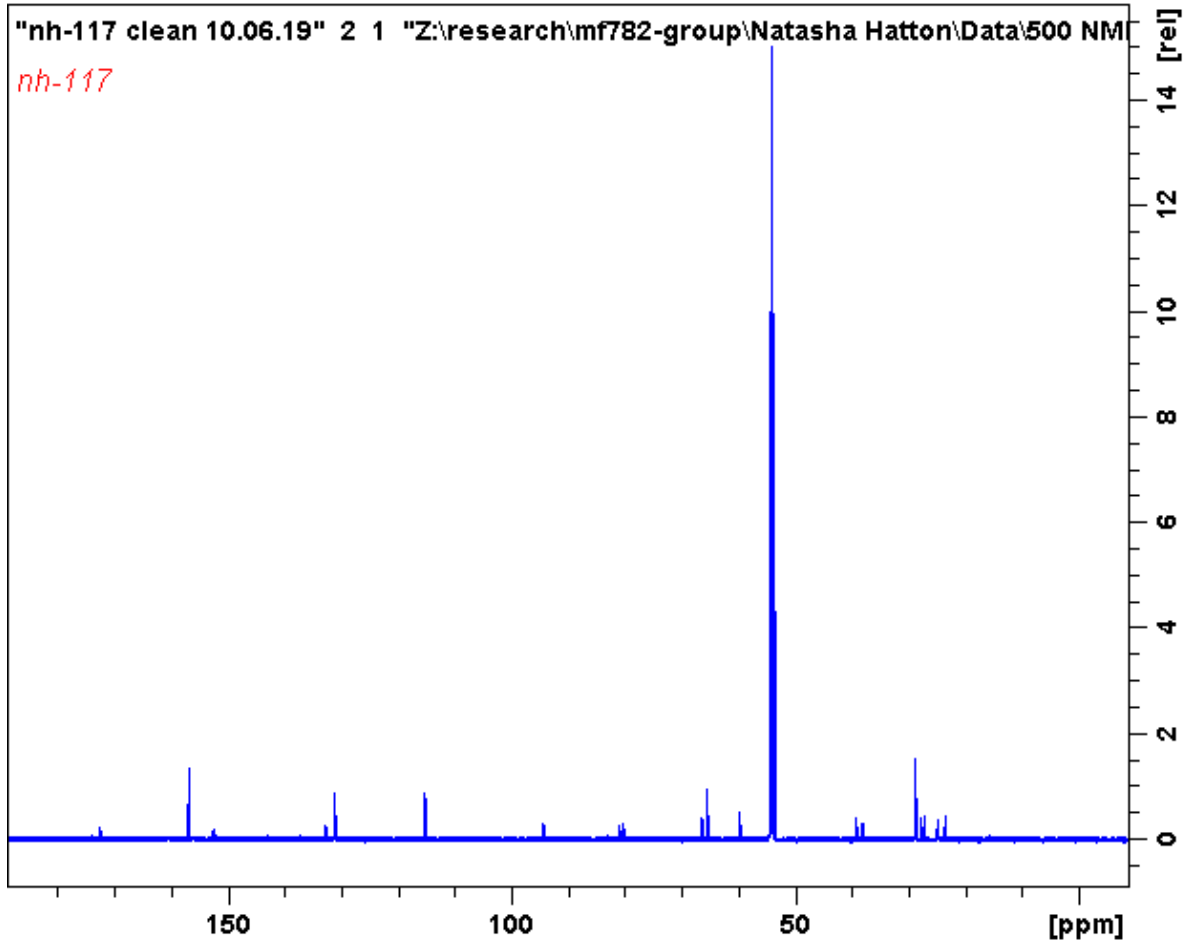
Appendix



9.2.2.2 (S)-2-(4-((3-(tert-butoxycarbonyl)-2,2-dimethyloxazolidin-4-yl)methyl)phenoxy)acetic acid 3.5



Appendix

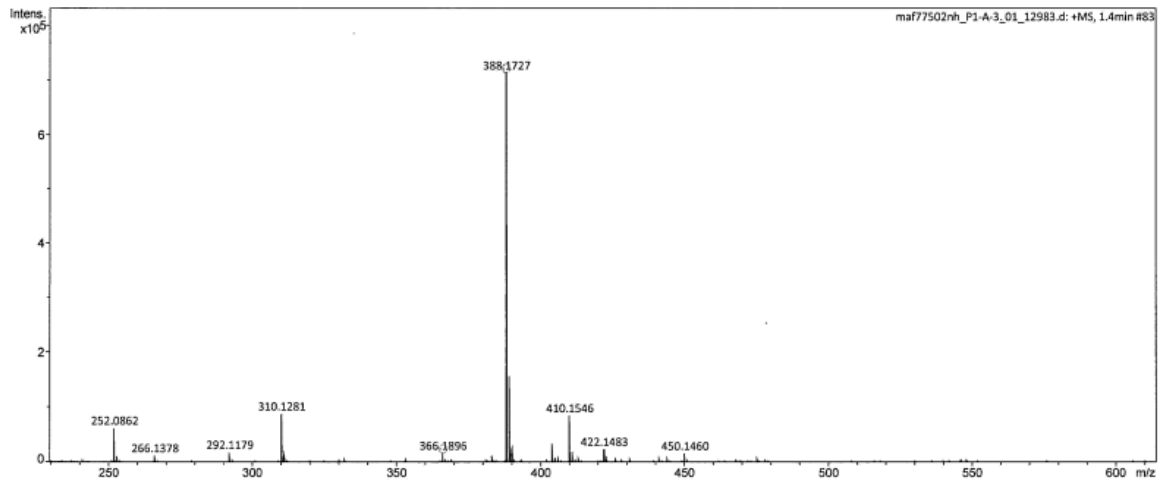


York - Chemistry - Mass Spectrometry Service Report

NH-117

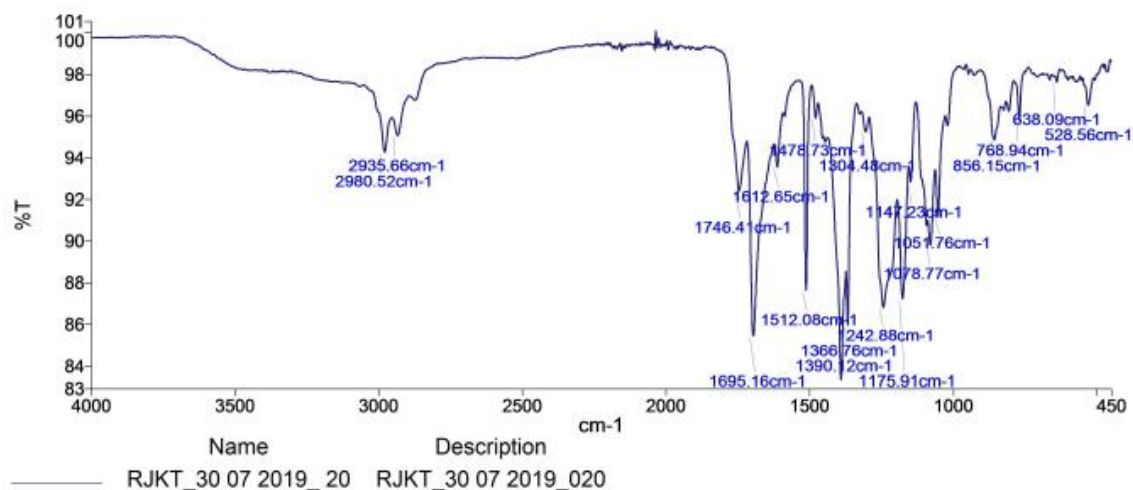
Analysis Information

Analysis Filename maf77502nh\_P1-A-3\_01\_12983.d Acquisition Date 30/05/2019 14:32:43  
Method ESI\_low mass\_2c1s.m Instrument compact  
Submission Name maf77502nh ESI Positive



Meas. m/z	#	Ion Formula	m/z	err [ppm]	err [mDa]	mSigma	Mean err [ppm]
366.1896	1	C <sub>19</sub> H <sub>28</sub> NO <sub>6</sub>	366.1911	4.1	1.5	16.5	1.3
388.1727	1	C <sub>19</sub> H <sub>27</sub> NNaO <sub>6</sub>	388.1731	1.0	0.4	3.3	1.0

## Appendix



### 9.2.3 LCMS traces of OPAL probes 3.17, 3.18, 3.19 and 3.20

#### 9.2.3.1 Mannose-based inhibitor linked (Gly-Ser) OPAL probe 3.18

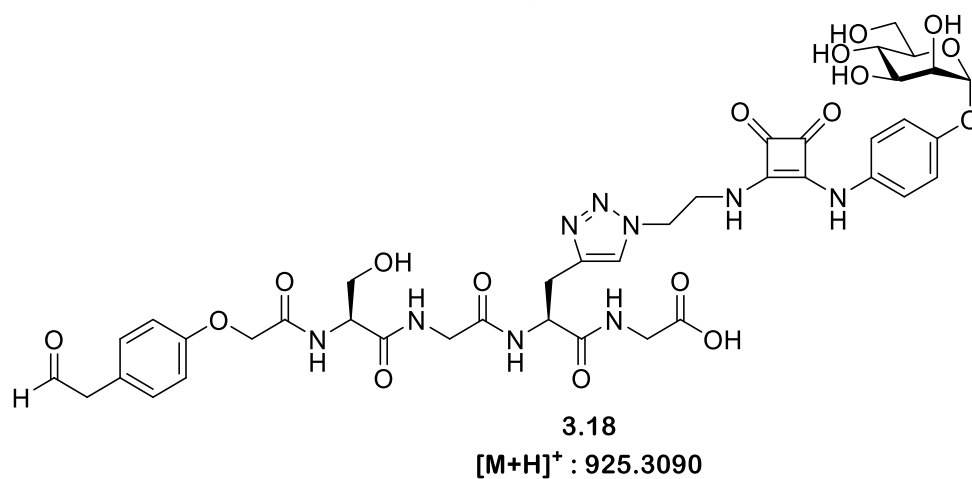


Figure 9-3. Structure of mannose-based inhibitor linked (Gly-Ser) OPAL probe 3.18

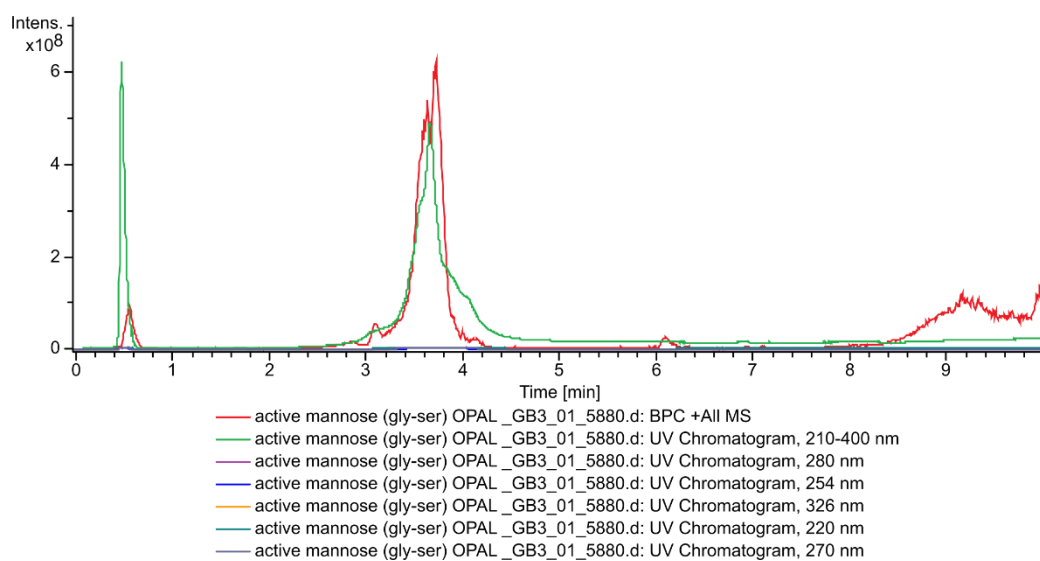


Figure 9-4. Liquid chromatography trace for mannose-based inhibitor linked (Gly-Ser) OPAL probe 3.18

## Appendix

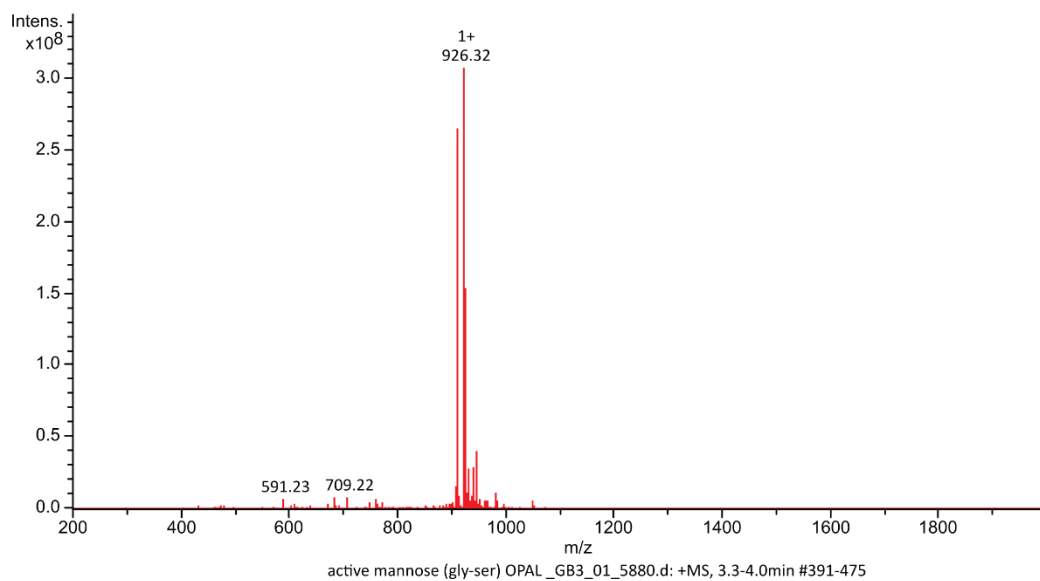


Figure 9-5. Mass spectrometry trace for mannose-based inhibitor linked (Gly-Ser) OPAL probe **3.18**

### 9.2.3.2 Mannose-based inhibitor linked (Gly-Ser)<sub>3</sub> OPAL probe **3.17**

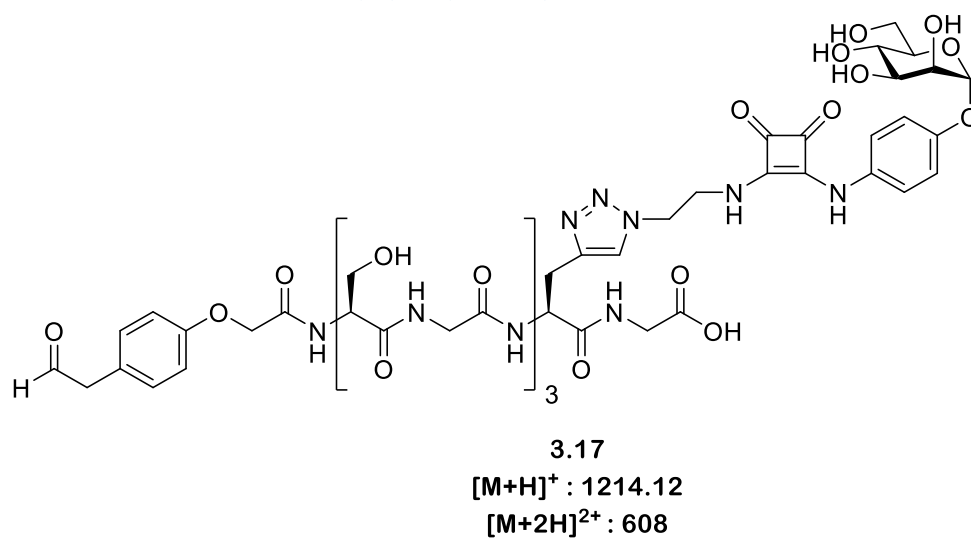


Figure 9-6. Structure of mannose-based inhibitor linked (Gly-Ser)<sub>3</sub> OPAL probe **3.17**

## Appendix

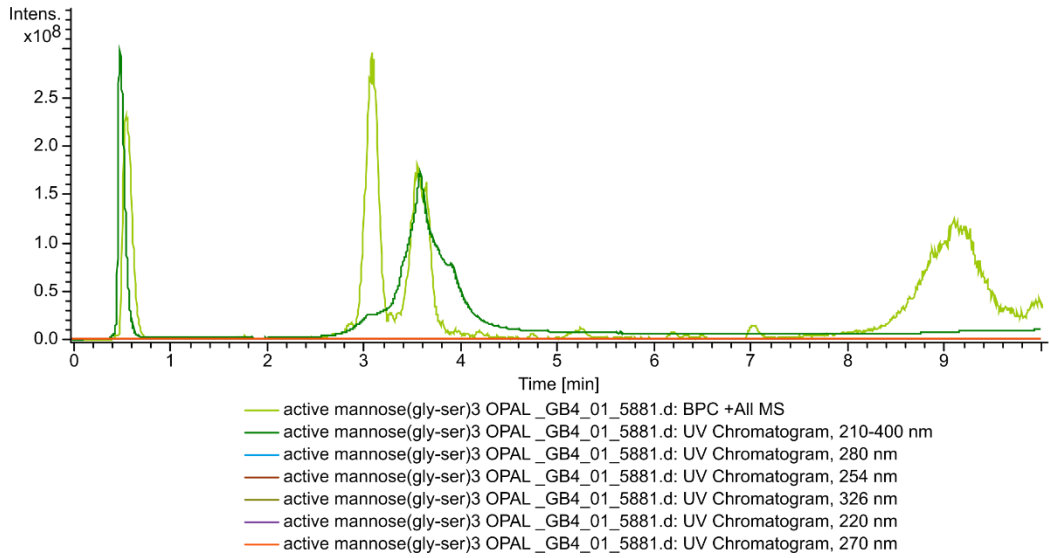


Figure 9-7. Liquid chromatography trace for mannose-based inhibitor linked (Gly-Ser)<sub>3</sub> OPAL probe 3.17

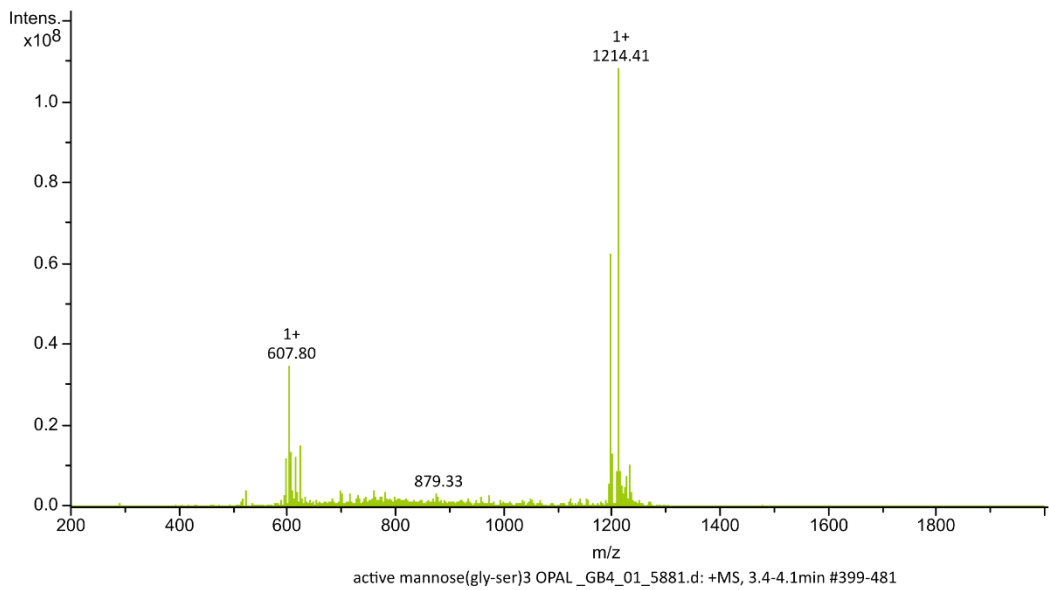


Figure 9-8. Mass spectrometry trace for mannose-based inhibitor linked (Gly-Ser)<sub>3</sub> OPAL probe 3.17



## Appendix

### 9.2.3.3 Mannose-based inhibitor linked (Gly-Ser)<sub>6</sub> OPAL probe 3.19

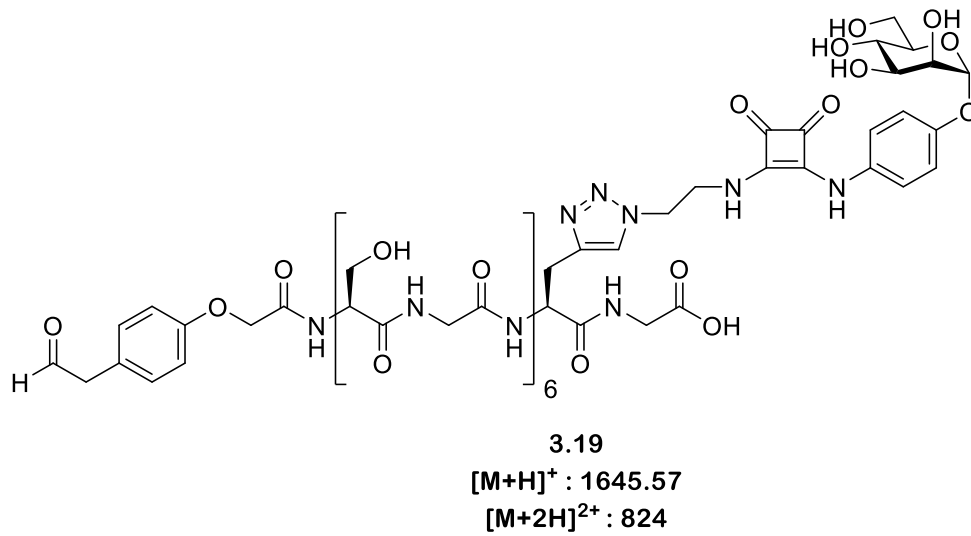


Figure 9-9. Structure of mannose-based inhibitor linked (Gly-Ser)<sub>6</sub> OPAL probe 3.19

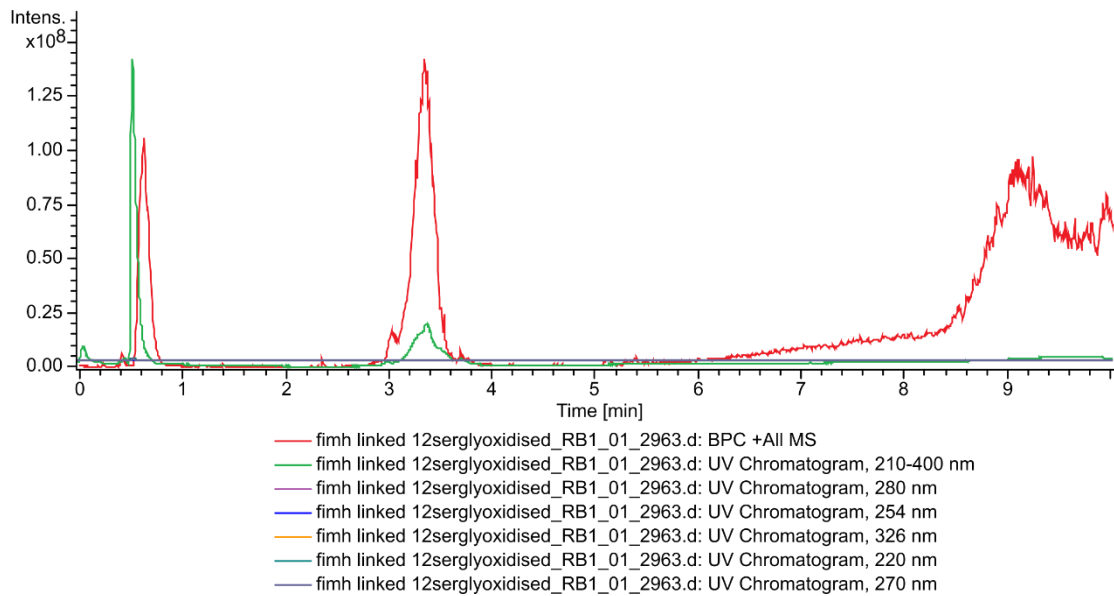


Figure 9-10. Liquid chromatography trace of mannose-based inhibitor linked (Gly-Ser)<sub>6</sub> OPAL probe 3.19

## Appendix

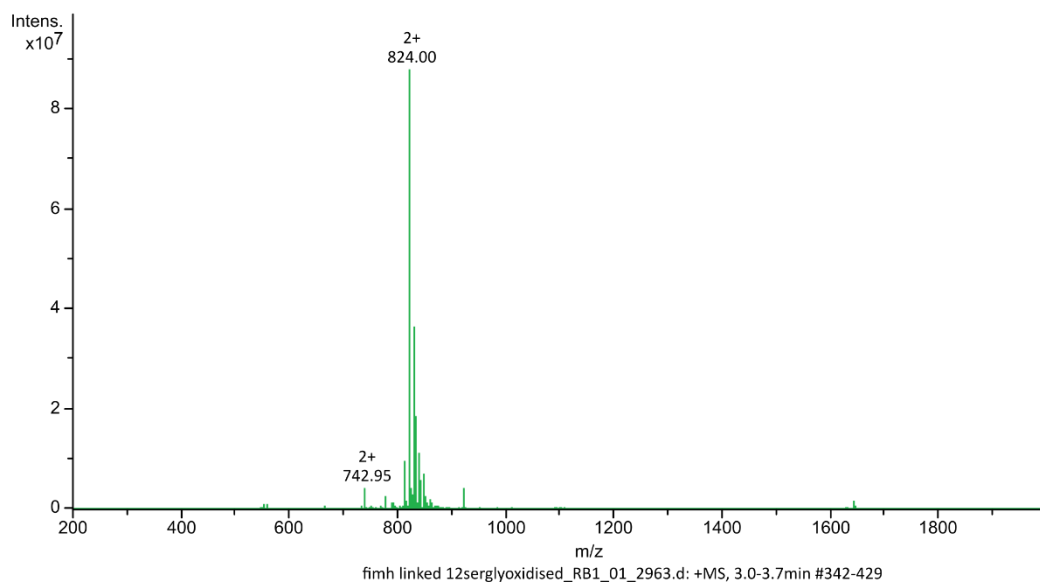


Figure 9-11. Mass spectrometry trace of mannose-based inhibitor linked (Gly-Ser)<sub>6</sub> OPAL probe **3.19**

### 9.2.3.4 Biotin linked (Gly-Ser)<sub>3</sub> OPAL probe **3.20**

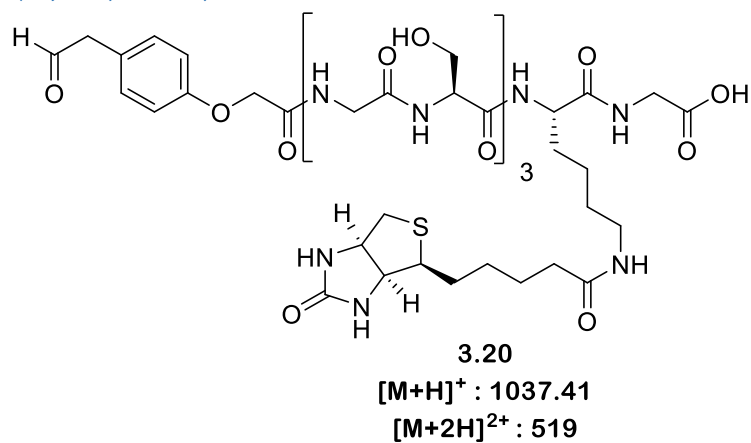


Figure 9-12. Structure of biotin linked (Gly-Ser)<sub>3</sub> OPAL probe **3.20**

## Appendix

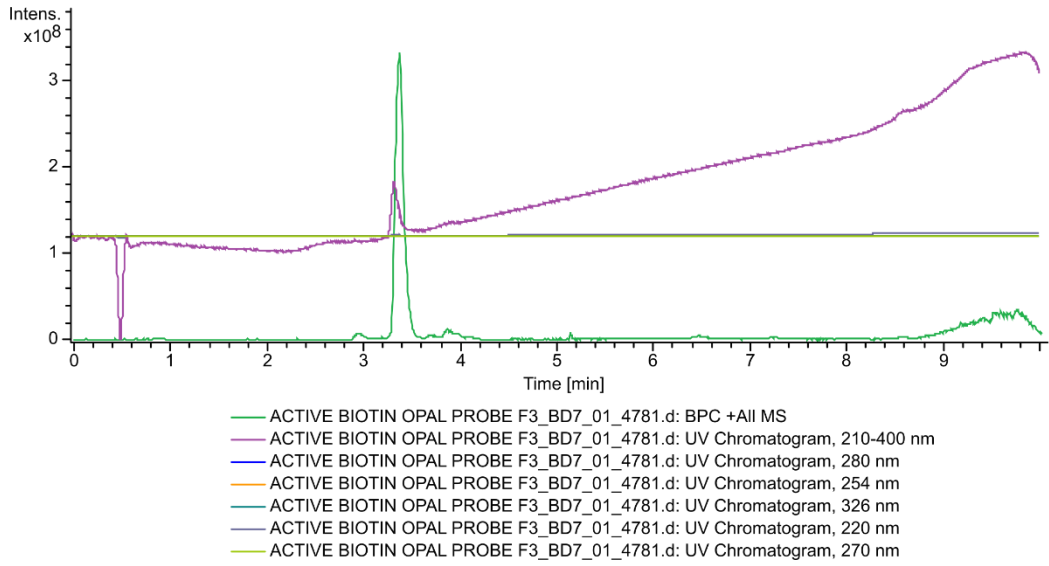


Figure 9-13. Liquid chromatography trace of biotin linked (Gly-Ser)<sub>3</sub> OPAL probe 3.20

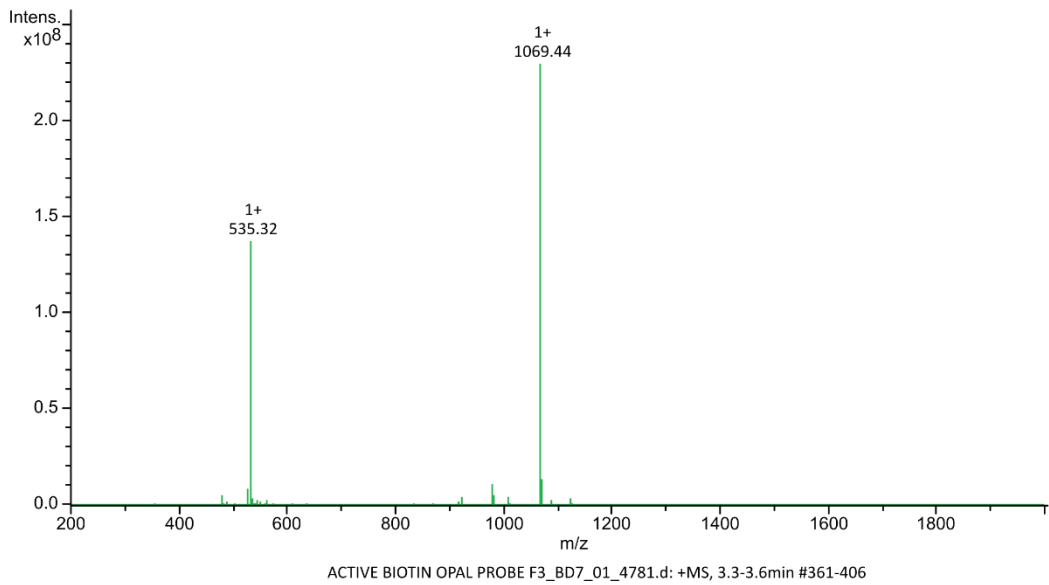


Figure 9-14. Mass spectrometry trace of biotin linked (Gly-Ser)<sub>3</sub> OPAL probe 3.20

## Appendix

### 9.2.4 SDS page gels, lectin blots and western blots for the colicin linked conjugates

#### 9.2.4.1 Mannose-based inhibitor linked (Gly-Ser) colicin Ia conjugate

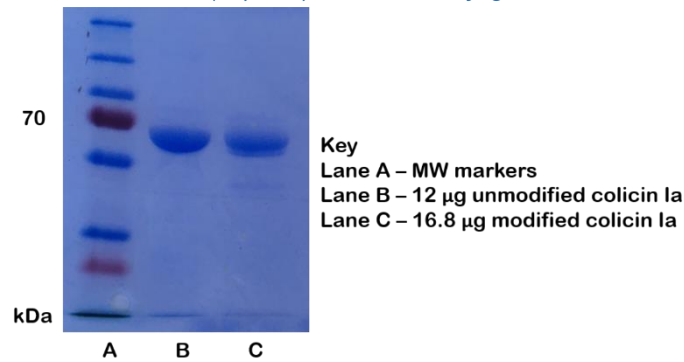


Figure 9-15. Results of SDS-PAGE gel stained with Coomassie, containing unmodified colicin Ia (lane B) and colicin Ia which has been subjected to ligation with mannose-based inhibitor linked (Gly-Ser) OPAL probe 3.18 (lane C)

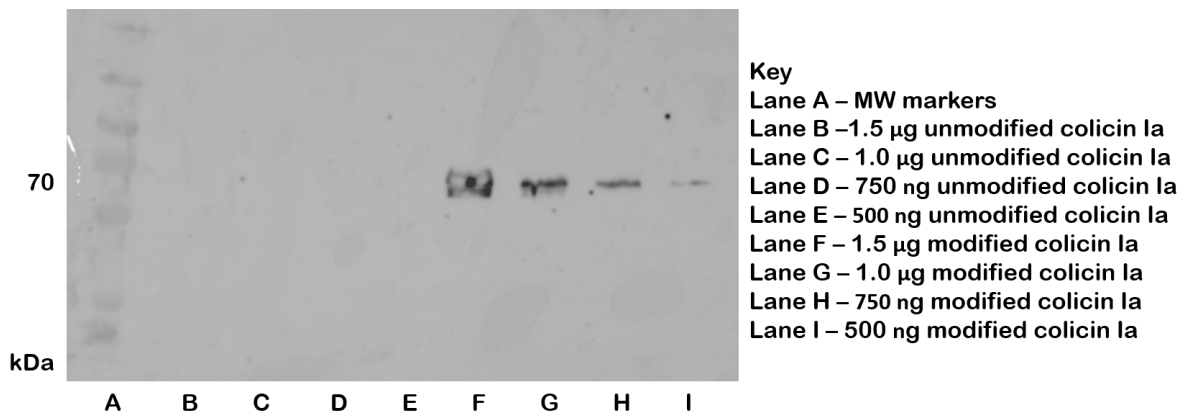


Figure 9-16. Results of lectin blot containing unmodified colicin Ia (lanes B-E) and colicin Ia which has been subjected to OPAL ligation with mannose-based inhibitor linked (Gly-Ser) OPAL probe 3.18 (lanes F-I)

#### 9.2.4.2 Mannose-based inhibitor linked (Gly-Ser)<sub>3</sub> colicin E9 conjugate

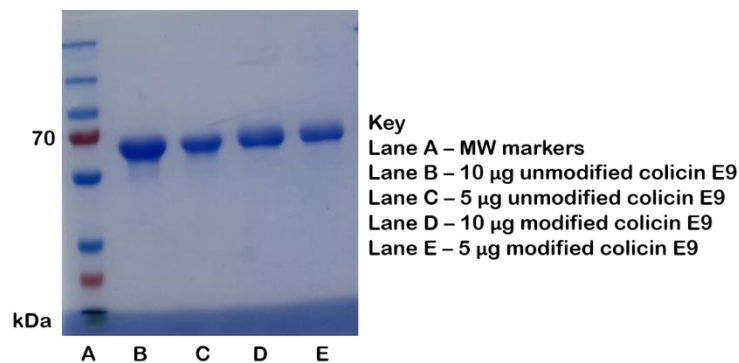


Figure 9-17. Results of SDS-PAGE gel stained with Coomassie, containing unmodified colicin E9 (lanes B and C) and colicin E9 which has been subjected to ligation with mannose-based inhibitor linked (Gly-Ser)<sub>3</sub> OPAL probe 3.17 (lanes D and E)

## Appendix

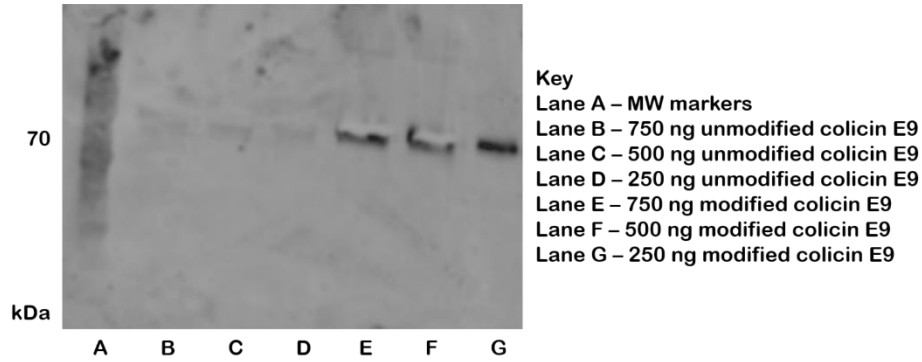


Figure 9-18. Results of lectin blot containing unmodified colicin E9 (lanes B-D) and colicin E9 which has been subjected to ligation with mannose-based inhibitor linked (Gly-Ser)<sub>3</sub> OPAL probe 3.17 (lanes E-G)

### 9.2.4.3 Mannose-based inhibitor linked (Gly-Ser)<sub>3</sub> colicin Ia conjugate

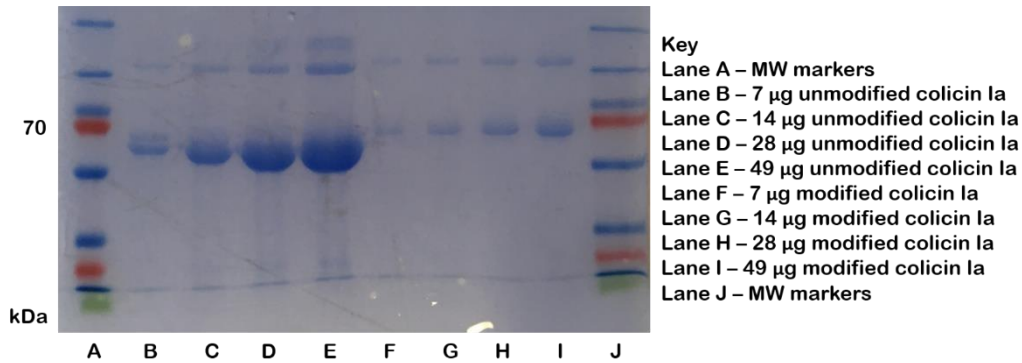


Figure 9-19. Results of SDS-PAGE gel stained with Coomassie, containing unmodified colicin Ia (lanes B and E) and colicin Ia which has been subjected to ligation with mannose-based inhibitor linked (Gly-Ser)<sub>3</sub> OPAL probe 3.17 (lanes F and I)

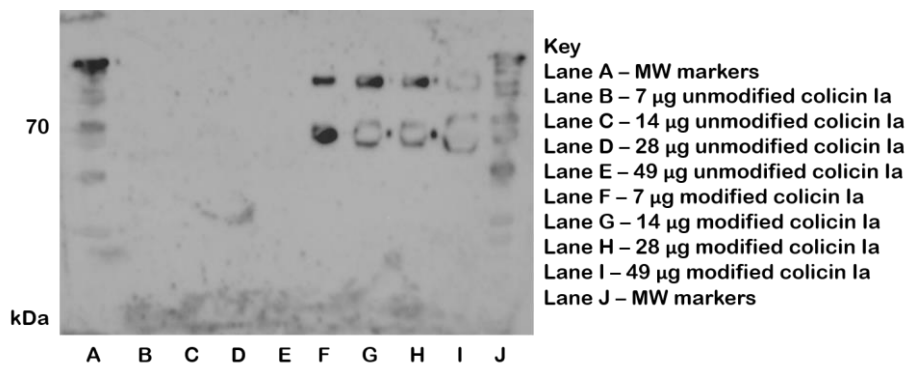


Figure 9-20. Results of lectin blot containing unmodified colicin Ia (lanes B-E) and colicin Ia which has been subjected to ligation with mannose-based inhibitor linked (Gly-Ser)<sub>3</sub> OPAL probe 3.17 (lanes F-I)

## Appendix

### 9.2.4.4 Mannose-based inhibitor linked (Gly-Ser)<sub>6</sub> colicin E9 conjugate

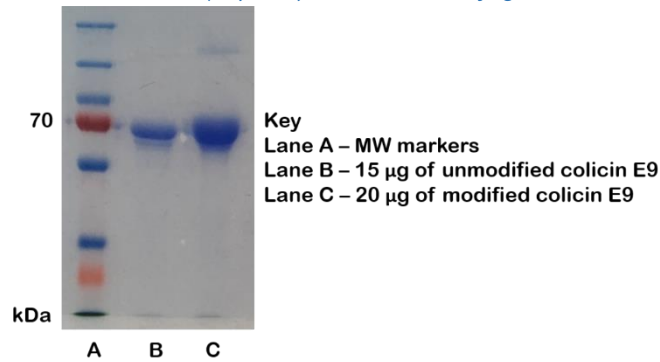


Figure 9-21. Results of SDS-PAGE gel stained with Coomassie, containing unmodified colicin E9 (lane B) and colicin E9 which has been subjected to ligation with mannose-based inhibitor linked (Gly-Ser)<sub>6</sub> OPAL probe 3.19 (lane C)

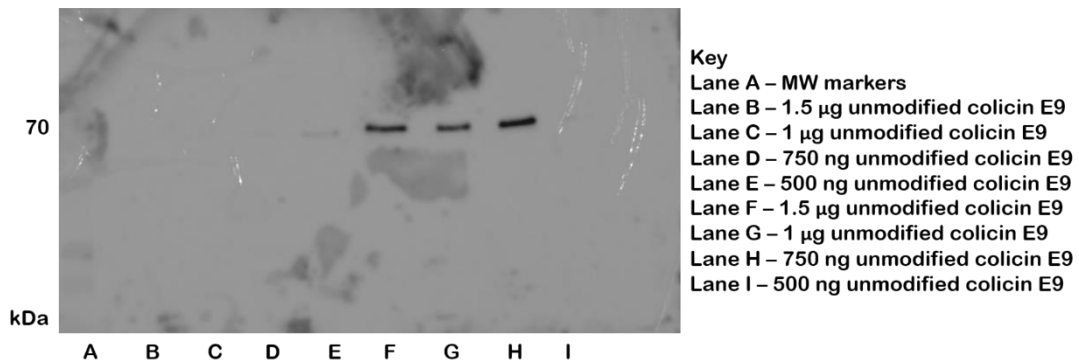


Figure 9-22. Results of lectin blot containing unmodified colicin E9 (lane B-E) and colicin E9 which has been subjected to ligation with mannose-based inhibitor linked (Gly-Ser)<sub>6</sub> OPAL probe 3.19 (lanes F-I)

### 9.2.4.5 Mannose-based inhibitor linked (Gly-Ser)<sub>6</sub> colicin Ia conjugate

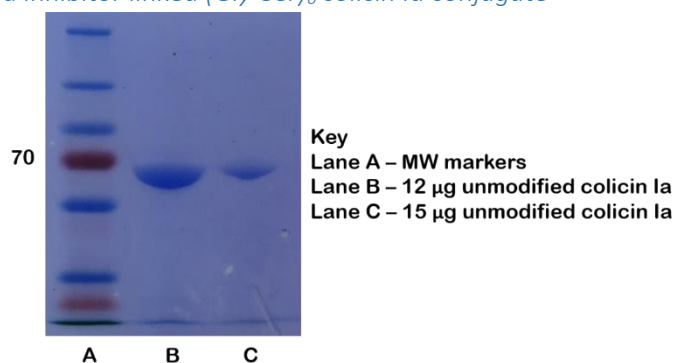


Figure 9-23. Results of SDS-PAGE gel stained with Coomassie, containing unmodified colicin Ia (lane B) and colicin Ia which has been subjected to ligation with mannose-based inhibitor linked (Gly-Ser)<sub>6</sub> OPAL probe 3.19

Appendix

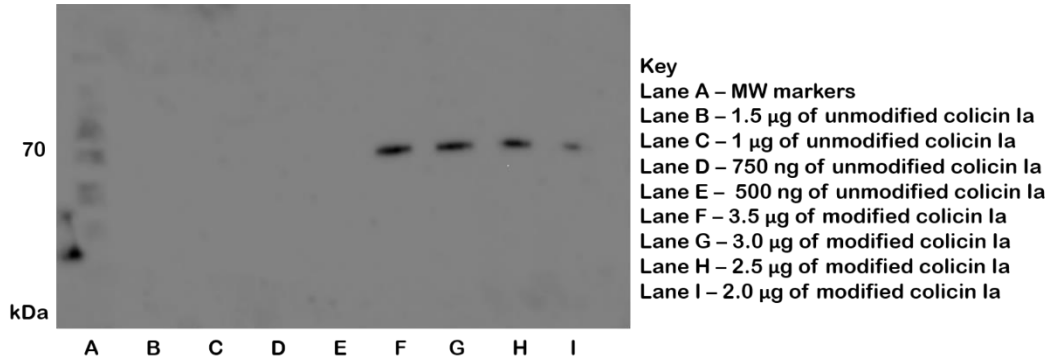


Figure 9-24. Results of lectin blot containing unmodified colicin Ia (lanes B - E) and colicin Ia which has been subjected to ligation with mannose-based inhibitor linked (Gly-Ser)<sub>6</sub> OPAL probe 3.19 (lanes F-I)

9.2.4.6 Biotin linked (Gly-Ser)<sub>3</sub> colicin E9 conjugate

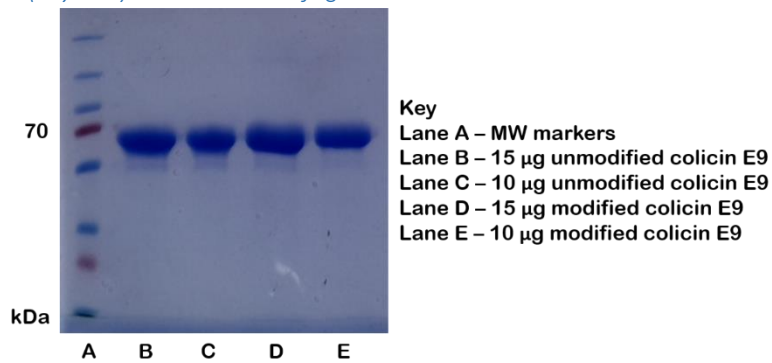


Figure 9-25. Results of SDS-PAGE gel stained with Coomassie, containing unmodified colicin E9 (lanes B and C) and colicin E9 which has been subjected to ligation with biotin linked (Ser-Gly)<sub>3</sub> OPAL probe 3.20 (lanes D and E)

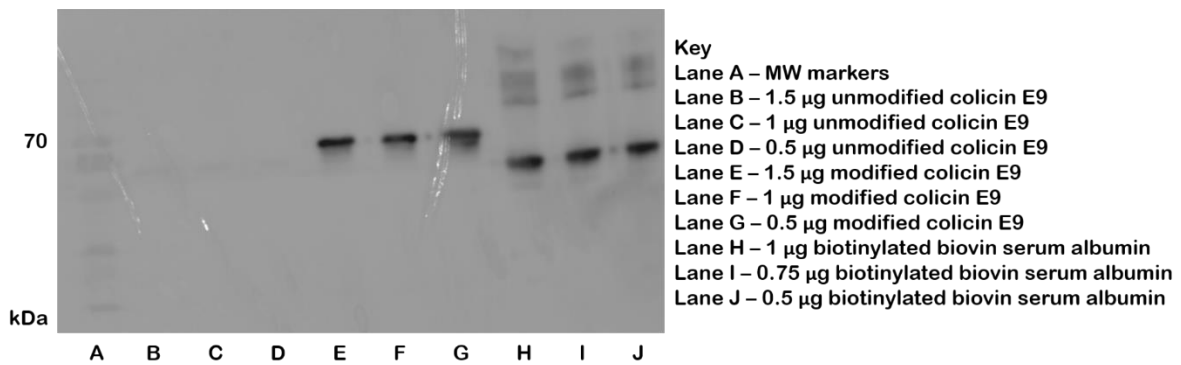


Figure 9-26. Results of western blot containing unmodified colicin E9 (lanes B-D), colicin E9 which has been subjected to ligation with biotin linked (Ser-Gly)<sub>3</sub> OPAL probe 3.20 (lanes E-G) and biotinylated bovin serum albumin (lanes H-J)

## Appendix

### 9.2.4.7 Biotin linked (Gly-Ser)<sub>3</sub> colicin Ia conjugate

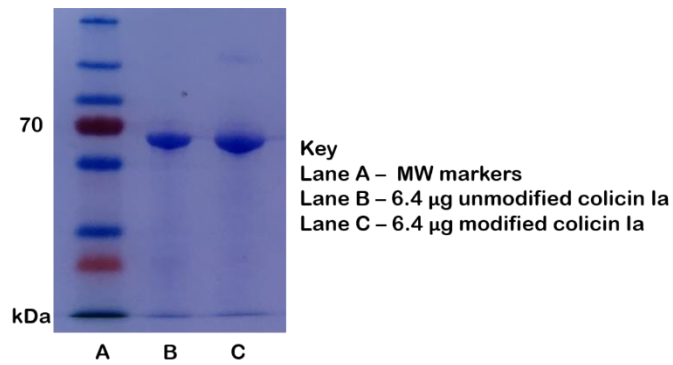


Figure 9-27. Results of SDS-PAGE gel stained with Coomassie, containing unmodified colicin Ia (lane B) and colicin Ia which has been subjected to ligation with biotin linked (Ser-Gly)<sub>3</sub> OPAL probe **3.20** (lane C)

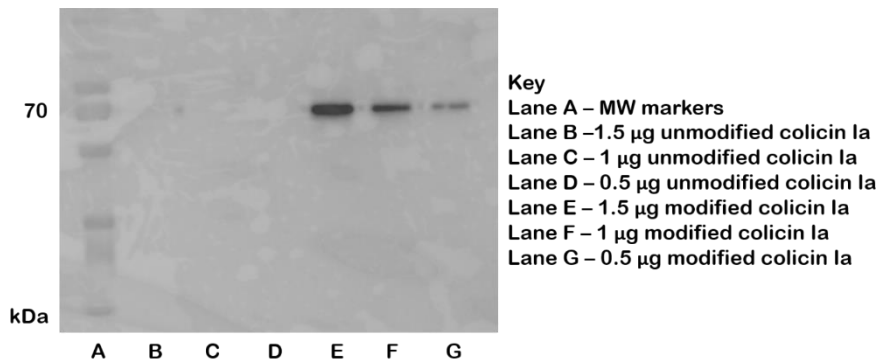


Figure 9-28. Results of western blot containing unmodified colicin E9 (lanes B-D) and colicin E9 which has been subjected to ligation with biotin linked (Ser-Gly)<sub>3</sub> OPAL probe **3.20** (lanes E-G)



## Appendix

### 9.3 Appendix for Chapter 4

#### 9.3.1 General appendix

##### 9.3.1.1 Recipe for supplemented M9 media

Using a 15 mL culture of M9 media (48 mM Na<sub>2</sub>HPO<sub>4</sub>, 22 mM KH<sub>2</sub>PO<sub>4</sub>, 8.6 mM NaCl)

#### M9 salts, vitamins and carbon/nitrogen sources

Table 34. Shows the volumes in  $\mu\text{L}$  of the supplements required to prepare a 15 mL culture of supplemented M9 media

Supplement	Volume ( $\mu\text{L}$ )
1 M MgSO <sub>4</sub>	30
1 M CaCl <sub>2</sub>	1.5
100 mM FeSO <sub>4</sub>	15
100 g/L NH <sub>4</sub> Cl	150
20% (w/v) D-glucose	300
20% (w/v) casamino acids	37.5
1% (w/v) thiamine	3
1% (w/v) L- Proline	3
1% (w/v) L- Arginine	3
1% (w/v) L- Methionine	3

##### 9.3.1.2 Antibiotic concentrations required for growth of each *E. coli* strain

Table 35. Shows the antibiotic concentrations required for growth of each different *E. coli* strain

<i>E. coli</i> strain	Antibiotic conditions
BW25113	None
JW3596 (Deep rough LSP)	Kanomycin 30 $\mu\text{g}/\text{mL}$
JW4283 (FimH minus)	Kanomycin 30 $\mu\text{g}/\text{mL}$
JW2142 (Cir minus)	Kanomycin 30 $\mu\text{g}/\text{mL}$
RK5016 (BtuB minus)	None

## Appendix

### 9.3.2 Results of experiment one, an auto-aggregation assay performed using the initial auto-aggregation assay method, investigating the effects of growth media and sample size

*Table 36. Shows the results of the auto-aggregation assay designed to investigate the effects of growth media and samples size on auto-aggregation. The assay was performed using the initial auto-aggregation methodology as explained on page 307. Three repeat assays were performed on three different days, each sample was made in triplicate and each final OD<sub>600</sub> measurement was repeated three times, with the average measurement given in the table below. Note the OD<sub>600</sub> values reported in Table 36 are the values recorded post dilution factor adjustment and have been rounded to 2 decimal places.*

Set	1				2				3				Overall Average
Sample	1	2	3	Average	1	2	3	Average	1	2	3	Average	
Conditions													
BW25133, LB media, 2 mL	0.93	0.82	0.89	0.88	0.74	0.74	0.78	0.75	0.85	0.89	0.89	0.87	0.84
JW3596, LB media, 2 mL	0.79	0.82	0.79	0.80	0.78	0.75	0.86	0.79	0.85	0.80	0.87	0.84	0.81
JW4283, LB media, 2 mL	0.89	0.86	0.77	0.84	0.76	0.72	0.75	0.74	0.84	0.88	0.77	0.83	0.80
JW2142, LB media, 2 mL	0.63	1.00*	0.57	0.60	0.25	0.23	0.44	0.33	0.86	0.78	0.86	0.83	0.59
BW2513, LB media, 1.5 mL	0.73	0.72	0.81	0.75	0.66	0.70	0.67	0.68	0.76	0.82	0.85	0.81	0.75
JW3596, LB media, 1.5 mL	0.78	0.67	0.76	0.74	0.78	0.77	0.79	0.78	N/A*	N/A*	N/A*	N/A*	0.76
JW4283, LB media, 1.5 mL	0.76	0.83	0.79	0.79	0.67	0.68	0.81	0.72	0.71	0.70	0.73	0.72	0.74

Appendix

JW2142, LB media, 1.5 mL	0.77	0.60	0.60	0.60	0.39	0.42	0.40	0.41	0.76	0.82	0.84	0.81	0.60
BW2513, M9 media, 2 mL	0.88	0.86	0.815	0.85	0.95	0.98	0.81	0.91	0.91	0.87	0.87	0.88	0.88
JW3596, M9 media, 2 mL	0.87	0.80	0.89	0.85	0.74	0.70	0.58	0.67	0.82	0.76	0.85	0.81	0.78
JW4283, M9 media, 2 mL	0.92	0.86	0.95	0.91	0.93	0.79	0.81	0.84	0.93	0.98	0.96	0.96	0.90
JW2142, M9 media, 2 mL	0.77	0.77	0.86	0.80	0.59	0.60	0.51	0.57	0.68	0.72	0.73	0.71	0.69
BW2513, M9 media, 1.5 mL	0.89	0.80	0.89	0.86	0.64	0.82	0.90	0.86	0.84	0.85	0.74	0.81	0.85
JW3596, M9 media, 1.5 mL	0.78	0.86	0.72	0.79	0.92	0.83	0.77	0.84	0.92	0.87	0.88	0.89	0.84
JW4283, M9 media, 1.5 mL	0.88	0.82	0.83	0.84	0.92	0.75	0.83	0.83	0.86	0.93	N/A*	0.90	0.86
JW2142, M9 media, 1.5 mL	0.72	0.53	0.52	0.59	0.64	0.65	0.77	0.69	0.79	0.77	0.76	0.78	0.68

\*discounted from average calculations, N/A\* measurement was not obtained

## Appendix

9.3.3 Results of experiment two, the screen performed using the redesigned auto-aggregation assay, investigating how factors such as starting OD<sub>600</sub>, incubation time and incubation temperature effects percentage auto-aggregation.

*Table 37. Results of the auto-aggregation assay used to screen potential aggregation factors such as starting OD<sub>600</sub>, incubation time and incubation temperature. Three repeat assays were performed on three different days. One active sample and one vortexed control sample was made for each condition and a single final OD<sub>600</sub> measurement was made for both the active sample and the vortexed control sample, these values were adjusted for by the dilution factor and used to calculate percentage auto-aggregation using equation one. The three percentage auto-aggregation measurements collected for each sample was then averaged. Note the OD<sub>600</sub> values reported in Table 37 are the values recorded post dilution factor adjustment and the values have been rounded to 2 decimal places*

Set	1			2			3			
Conditions	OD <sub>600</sub> final	OD <sub>600</sub> initial	Percentage auto-aggregation	OD <sub>600</sub> final	OD <sub>600</sub> initial	Percentage auto-aggregation	OD <sub>600</sub> final	OD <sub>600</sub> initial	Percentage auto-aggregation	Average percentage auto-aggregation
BW25113 OD <sub>600</sub> = 1, 4 °C, 0 h	N/A*	N/A*	N/A*	1.02	1.04	1.34	1.09	1.07	-1.64	-0.15
BW25113 OD <sub>600</sub> = 1, 4 °C, 2 h	1.10	1.03	-6.35	1.20	N/A*	N/A*	0.98	1.01	2.79	-1.78
BW25113 OD <sub>600</sub> = 1, 4 °C, 20 h	0.81	1.01	20.37	0.75	0.79	5.45	0.72	0.98	26.27	17.36
BW25113 OD <sub>600</sub> = 1, 4 °C, 24 h	0.61	0.92	33.73	N/A*	N/A*	N/A*	0.60	1.04	42.30	38.02
BW25113 OD <sub>600</sub> = 1, 37 °C, 0 h	N/A*	N/A*	N/A*	1.08	1.36	20.61	1.05	1.09	2.91	11.76
BW25113 OD <sub>600</sub> = 1, 37 °C, 2 h	0.94	0.94	0	0.89	0.89	0	0.90	1.09	17.32	6.10

Appendix

BW25113 OD <sub>600</sub> = 1, 37 °C, 20 h	0.44	0.70	37.68	0.71	0.74	4.05*	0.60	0.85	29.40	33.54
BW25113 OD <sub>600</sub> = 1, 37 °C, 24 h	0.31	0.77	59.48	0.38	0.81	53.89	0.56	0.80	30.29	47.89
BW25113 OD <sub>600</sub> = 1.5, 4 °C, 0 h	N/A*	N/A*	N/A*	1.65	1.63	-1.45	1.52	1.57	3.19	0.87
BW25113 OD <sub>600</sub> = 1.5, 4 °C, 2 h	1.65	1.65	0	1.51	1.51	0	1.50	1.54	2.44	0.93
BW25113 OD <sub>600</sub> = 1.5, 4 °C, 20 h	1.27	1.48	13.72	1.22	1.61	24.13	1.26	1.51	16.41	18.09
BW25113 OD <sub>600</sub> = 1.5, 4 °C, 24 h	0.83	1.41	40.66	N/A*	N/A*	N/A*	1.11	1.57	29.51	35.08
BW25113 OD <sub>600</sub> = 1.5, 37 °C, 0 h	N/A*	N/A*	N/A*	1.64	1.64	0	1.52	1.57	3.19	1.59
BW25113 OD <sub>600</sub> = 1.5, 37 °C, 2 h	1.43	1.49	4.15	1.37	1.43	4.09	1.38	1.39	0.77	3.00

Appendix

BW25113 OD <sub>600</sub> = 1.5, 37 °C, 20 h	0.60	1.32	54.98	0.87	1.34	35.37	0.73	1.23	40.74	43.70
BW25113 OD <sub>600</sub> = 1.5, 37 °C, 24 h	0.62	1.33	53.22	0.41	1.16	64.24	0.72	1.25	42.25	53.24
BW25113 OD <sub>600</sub> = 2, 4 °C, 0 h	N/A	N/A	N/A	1.95	2.01	2.97	1.98	2.08	4.92	3.94
BW25113 OD <sub>600</sub> = 2, 4 °C, 2 h	1.82	1.81	-0.69	1.78	1.87	4.96	1.97	2.03	2.68	2.31
BW25113 OD <sub>600</sub> = 2, 4 °C, 20 h	1.32	1.84	28.30	1.38	1.91	27.81	1.56	1.97	20.85	25.65
BW25113 OD <sub>600</sub> = 2, 4 °C, 24 h	1.21	N/A*	N/A*	N/A*	N/A*	N/A*	1.60	1.93	17.13	17.13
BW25113 OD <sub>600</sub> = 2, 37 °C, 0 h	N/A*	N/A*	N/A*	1.88	1.95	3.39	1.98	2.08	4.92	4.15
BW25113 OD <sub>600</sub> = 2, 37 °C, 2 h	1.81	1.82	0.24	1.72	1.76	1.77	1.87	1.94	4.06	2.02
BW25113 OD <sub>600</sub> = 2, 37 °C, 20 h	0.92	1.57	41.12	0.90	1.52	40.83	0.87	1.63	46.76	42.90

Appendix

BW25113 OD <sub>600</sub> = 2, 37 °C, 24 h	0.61	1.48	58.59	0.70	0.98	28.46	0.78	1.62	52.23	46.43
JW3596 (DR LPS) OD <sub>600</sub> = 1, 4 °C, 0 h	N/A*	N/A*	N/A*	1.10	1.09	-0.76	0.96	1.06	9.23	4.23
JW3596 (DR LPS) OD <sub>600</sub> = 1, 4 °C, 2 h	0.95	0.98	3.25	1.05	0.94	-12.07	N/A*	N/A*	N/A*	-4.41
JW3596 (DR LPS) OD <sub>600</sub> = 1, 4 °C, 20 h	0.65	0.96	32.25	0.87	1.02	14.92	0.85	0.99	14.31	20.49
JW3596 (DR LPS) OD <sub>600</sub> = 1, 4 °C, 24 h	0.55	0.67	17.21	N/A*	N/A*	N/A*	0.79	1.01	21.80	19.50
JW3596 (DR LPS) OD <sub>600</sub> = 1, 37 °C, 0 h	N/A*	N/A*	N/A*	1.04	1.12	6.52	1.07	1.09	1.33	3.92
JW3596 (DR LPS) OD <sub>600</sub> = 1, 37 °C, 2 h	1.79	1.78	-0.43	0.95	0.95	0	0.95	1.01	6.29	1.98
JW3596 (DR LPS)	0.56	0.81	31.67	N/A*	N/A*	N/A*	0.54	0.84	36.28	33.97

Appendix

OD <sub>600</sub> = 1, 37 °C, 20 h										
JW3596 (DR LPS) OD <sub>600</sub> = 1, 37 °C, 24 h	0.50	0.78	36.01	0.51	0.82	37.56	0.42	0.83	47.23	40.27
JW3596 (DR LPS) OD <sub>600</sub> = 1.5, 4 °C, 0 h	N/A*	N/A*	N/A*	1.67	1.64	-2.27	1.54	1.62	5.14	1.43
JW3596 (DR LPS) OD <sub>600</sub> = 1.5, 4 °C, 2 h	1.68	1.67	-0.24	1.58	1.54	-2.63	1.50	1.53	2.38	-0.16
JW3596 (DR LPS) OD <sub>600</sub> = 1.5, 4 °C, 20 h	1.02	1.58	35.52	0.98	1.51	33.96	1.09	1.62	32.37	33.95
JW3596 (DR LPS) OD <sub>600</sub> = 1.5, 4 °C, 24 h	0.89	1.87	52.48	N/A*	N/A*	N/A*	0.95	1.53	38.22	45.35
JW3596 (DR LPS) OD <sub>600</sub> =	N/A*	N/A*	N/A*	1.65	1.63	-1.40	1.53	1.58	3.27	0.93



Appendix

1.5, 37 °C, 0 h										
JW3596 (DR LPS) OD <sub>600</sub> = 1.5, 37 °C, 2 h	1.47	1.56	5.46	1.36	1.43	5.08	1.37	1.41	2.73	4.42
JW3596 (DR LPS) OD <sub>600</sub> = 1.5, 37 °C, 20 h	0.77	1.32	41.19	0.94	1.34	29.74	0.74	1.20	38.54	36.49
JW3596 (DR LPS) OD <sub>600</sub> = 1.5, 37 °C, 24 h	0.61	1.15	47.22	0.46	1.26	63.16	0.56	1.23	54.25	54.87
JW3596 (DR LPS) OD <sub>600</sub> = 2, 4 °C, 0 h	N/A*	N/A*	N/A*	2.02	2.00	-1.53	1.99	1.96	-1.28	-1.41
JW3596 (DR LPS) OD <sub>600</sub> = 2, 4 °C, 2 h	1.96	1.99	1.48	1.84	1.85	0.29	1.88	1.96	3.96	1.91
JW3596 (DR LPS) OD <sub>600</sub> = 2, 4 °C, 20 h	1.49	1.93	22.70	1.39	1.97	29.10	1.53	1.92	20.51	24.12

Appendix

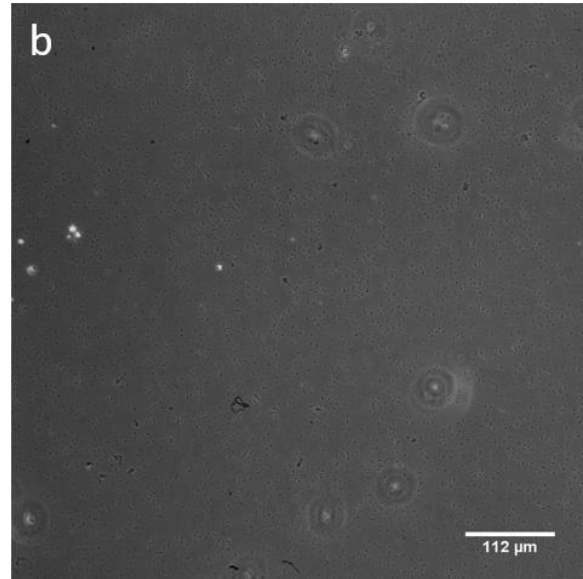
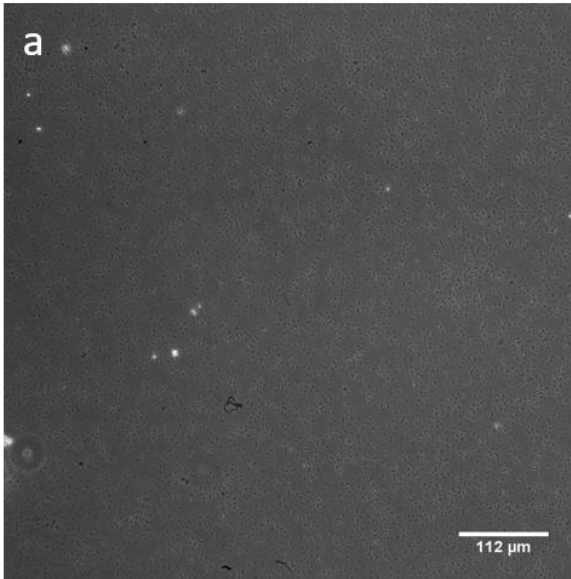
JW3596 (DR LPS) OD <sub>600</sub> = 2, 4 °C, 24 h	1.07	1.55	30.65	N/A*	N/A*	N/A*	1.34	2.09	35.86	33.25
JW3596 (DR LPS) OD <sub>600</sub> = 2, 37 °C, 0 h	N/A*	N/A*	N/A*	2.02	1.78	-13.46	1.99	1.96	-1.28	-7.37
JW3596 (DR LPS) OD <sub>600</sub> = 2, 37 °C, 2 h	0.96	0.92	-4.61	1.74	1.73	-1.03	1.83	1.91	4.31	-0.44
JW3596 (DR LPS) OD <sub>600</sub> = 2, 37 °C, 20 h	0.91	1.70	46.51	1.04	1.65	37.13	0.97	1.62	39.70	41.11
JW3596 (DR LPS) OD <sub>600</sub> = 2, 37 °C, 24 h	0.42	1.54	72.66	0.77	1.65	53.00	0.79	1.63	51.19	58.94

\*discounted from average calculations, N/A\* measurement was not obtained

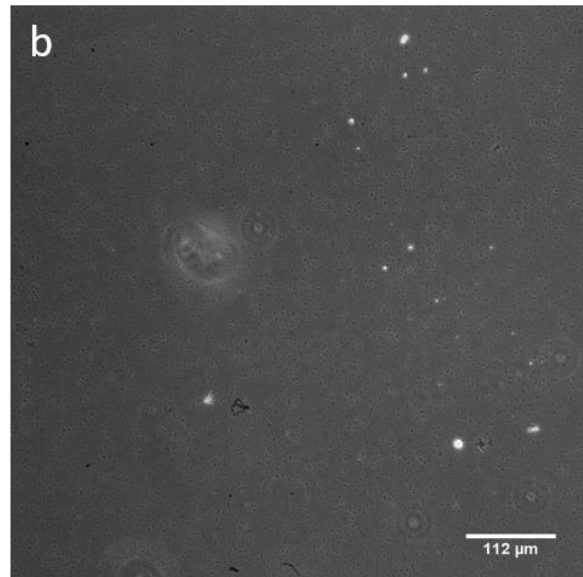
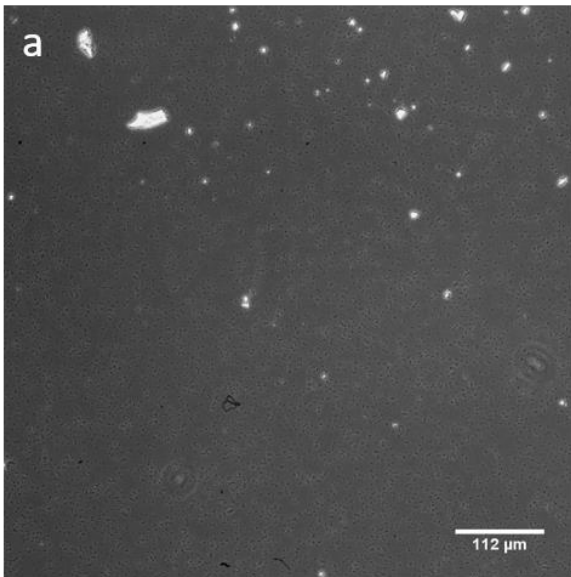
## Appendix

9.3.4 Results of experiment six, images of the microscopy samples imaged during the screening of microscopy conditions

*BW25113, incubated with 1  $\mu\text{M}$  of mannose-based inhibitor linked (Gly-Ser) colicin E9 conjugate, using a starting  $OD_{600}$  of 2. a) active sample, b) vortexed control, both taken at x 20 magnification*

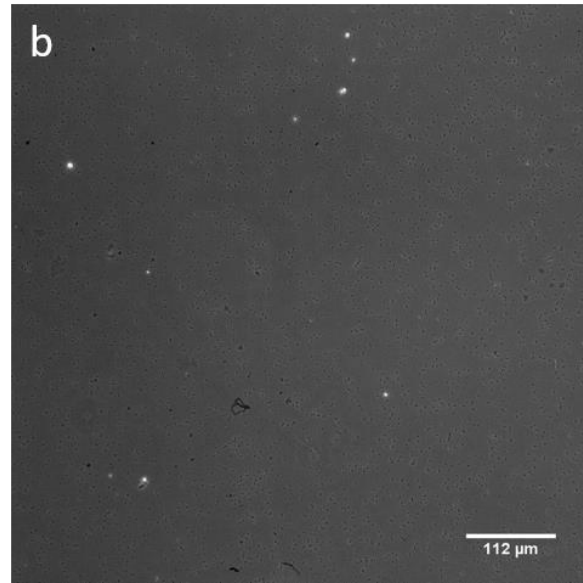
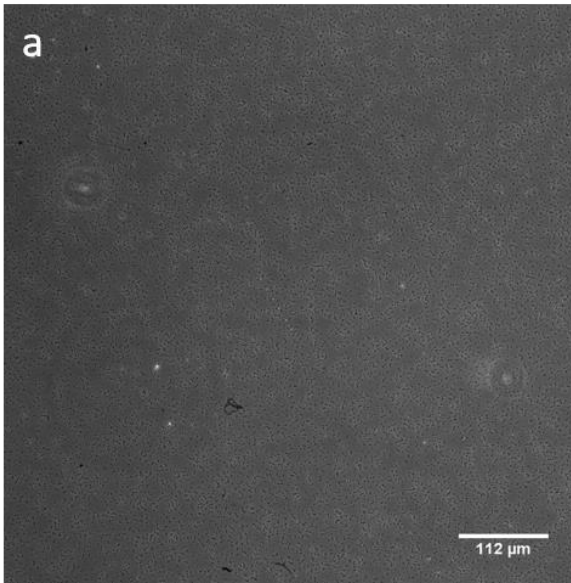


*BW25113, incubated with 100 nm of mannose-based inhibitor linked (Gly-Ser) colicin E9 conjugate, using a starting  $OD_{600}$  of 2. a) active sample, b) vortexed control, both taken at x 20 magnification*

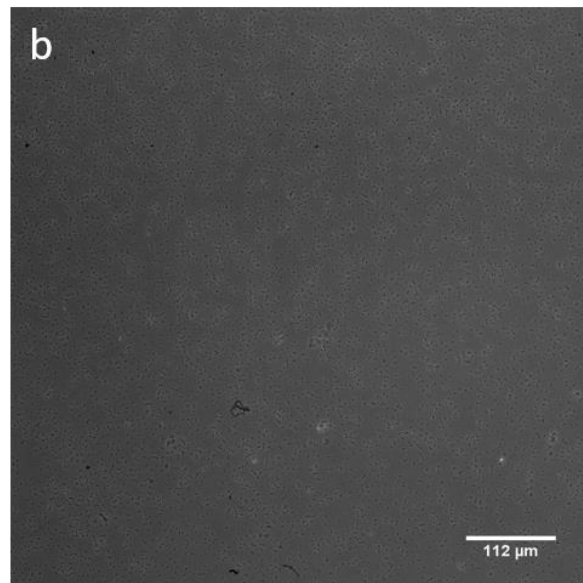
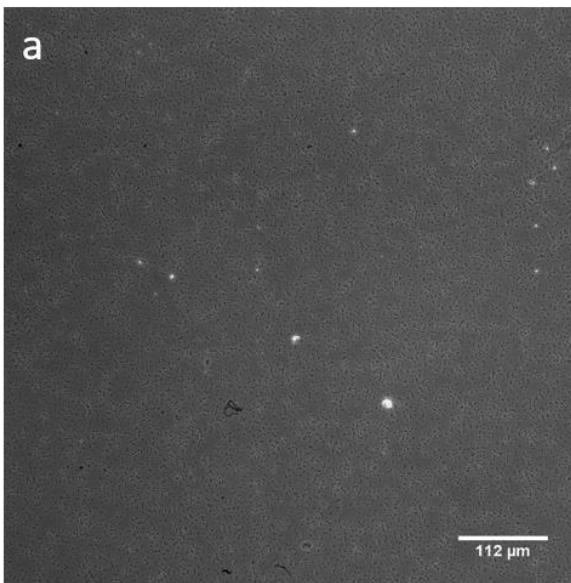


## Appendix

*BW25113, incubated with 10 nM of mannose-based inhibitor linked (Gly-Ser) colicin E9 conjugate, using a starting  $OD_{600}$  of 2. a) active sample, b) vortexed control, both taken at x 20 magnification*

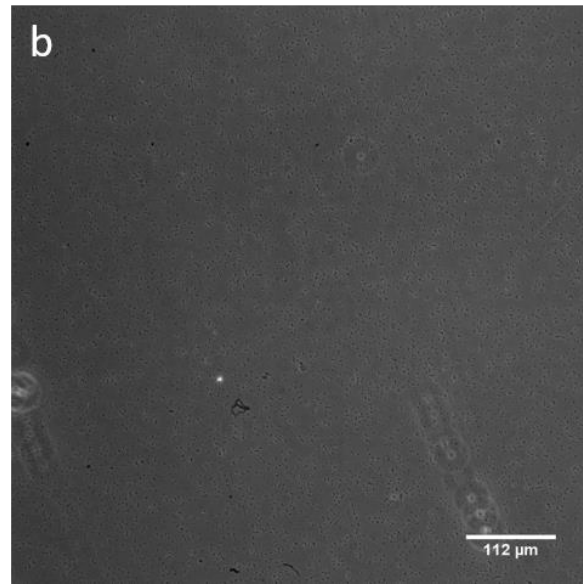
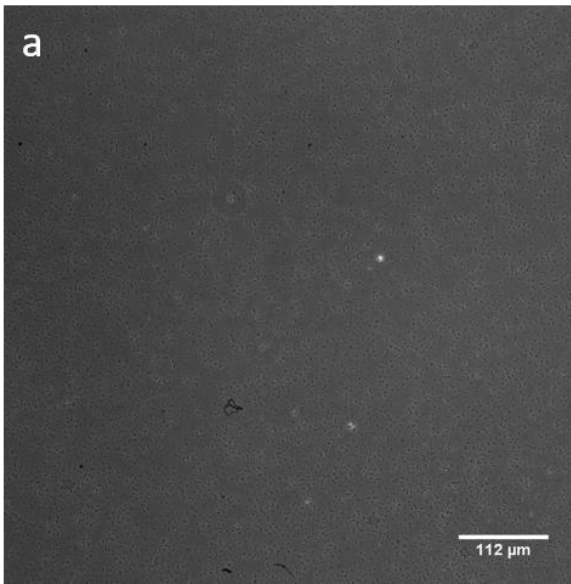


*BW25113, incubated with 1  $\mu\text{M}$  of mannose-based inhibitor linked (Gly-Ser)<sub>3</sub> colicin E9 conjugate, using a starting  $OD_{600}$  of 2. a) active sample, b) vortexed control, both taken at x 20 magnification*

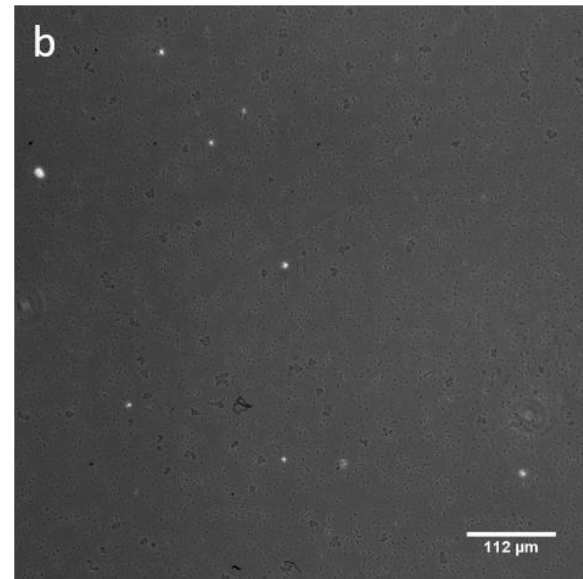
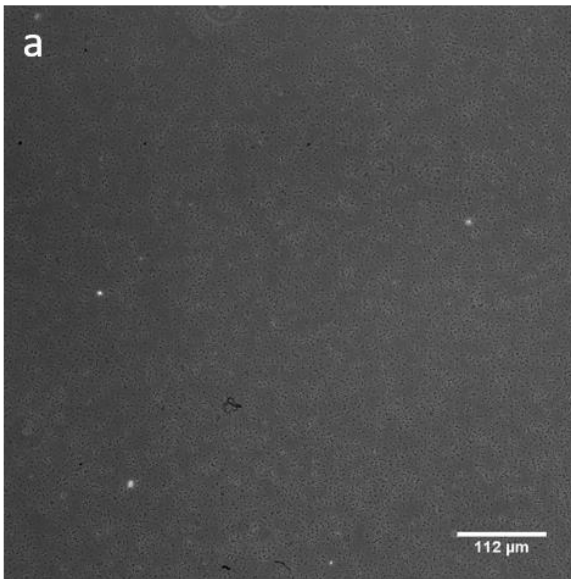


## Appendix

*BW25113, incubated with 100 nM of mannose-based inhibitor linked (Gly-Ser)<sub>3</sub> colicin E9 conjugate, using a starting OD<sub>600</sub> of 2. a) active sample, b) vortexed control, both taken at x 20 magnification*

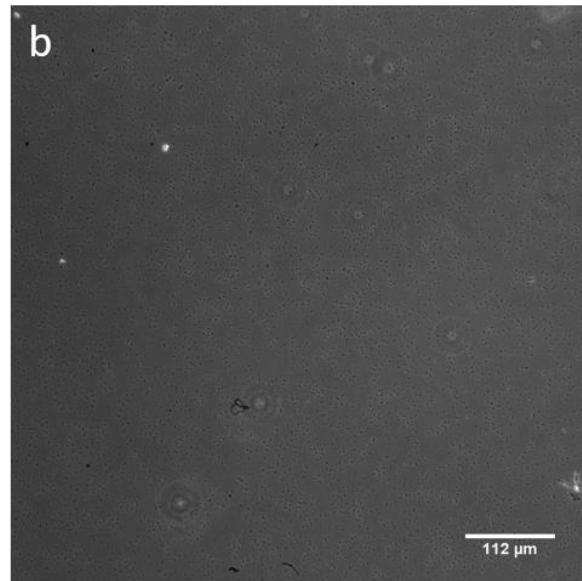
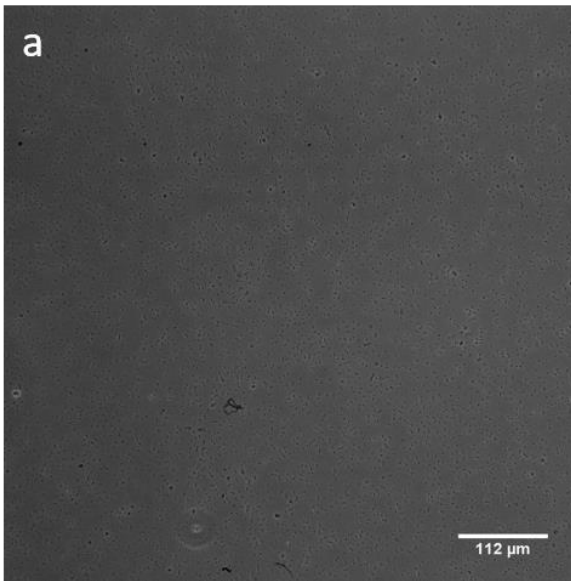


*BW25113, incubated with 10 nM of mannose-based inhibitor linked (Gly-Ser)<sub>3</sub> colicin E9 conjugate, using a starting OD<sub>600</sub> of 2. a) active sample, b) vortexed control, both taken at x 20 magnification*

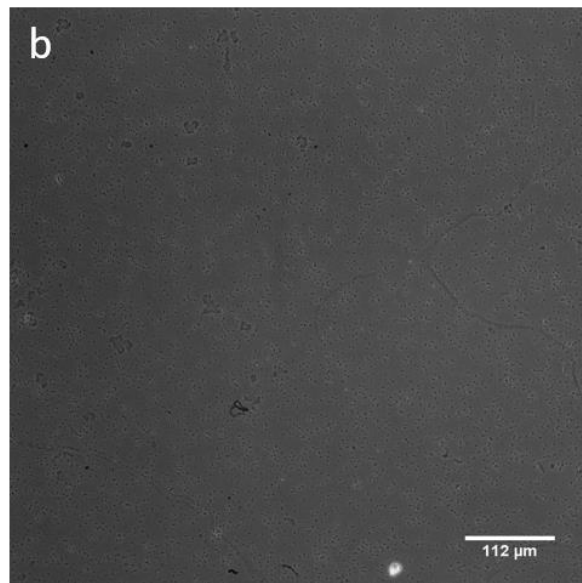
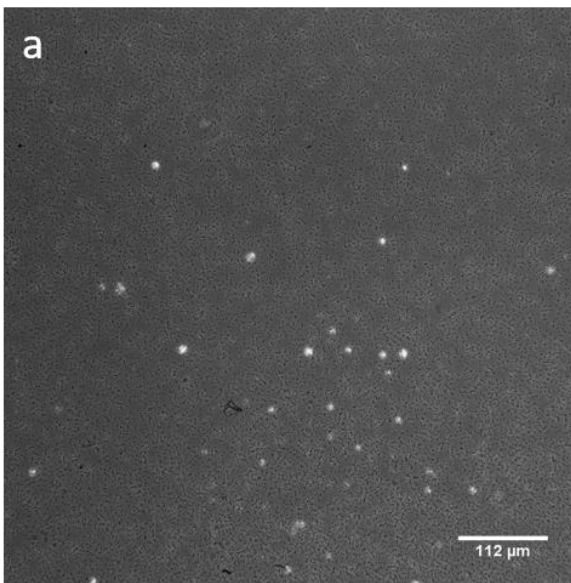


## Appendix

*BW25113, incubated with 1  $\mu\text{M}$  of mannose-based inhibitor linked (Gly-Ser)<sub>6</sub> colicin E9 conjugate, using a starting OD<sub>600</sub> of 2. a) active sample, b) vortexed control, both taken at x 20 magnification*

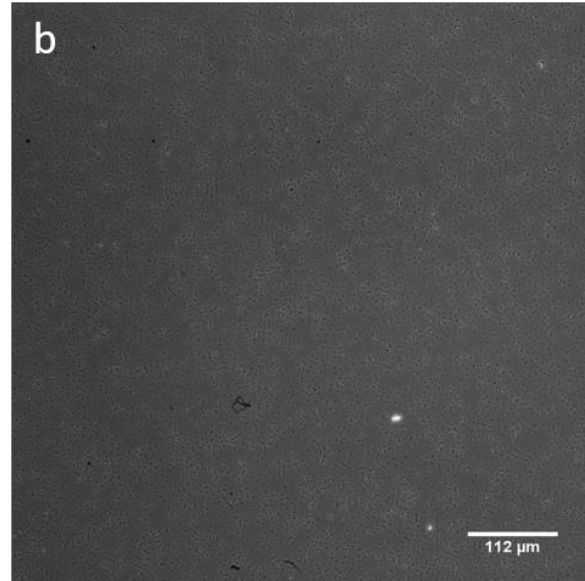
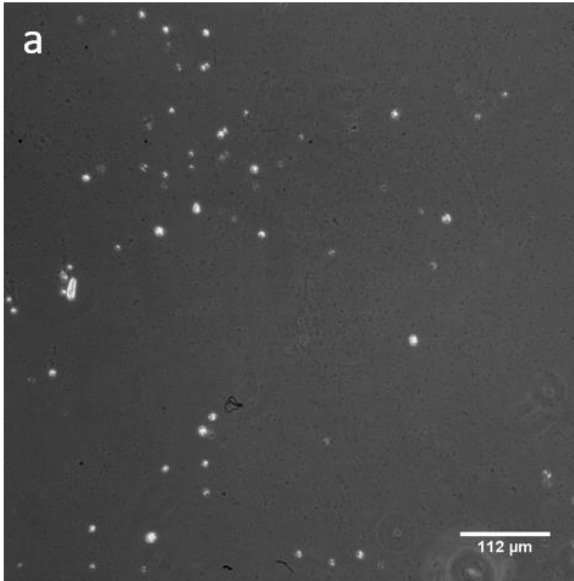


*BW25113, incubated with 100 nM of mannose-based inhibitor linked (Gly-Ser)<sub>6</sub> colicin E9 conjugate, using a starting OD<sub>600</sub> of 2. a) active sample, b) vortexed control, both taken at x 20 magnification*

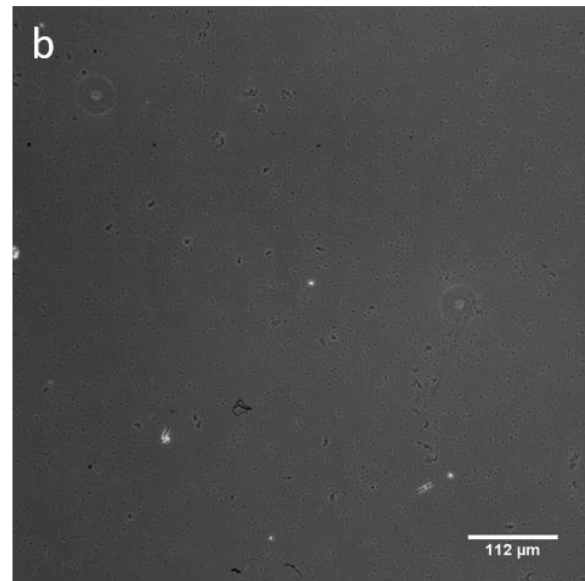
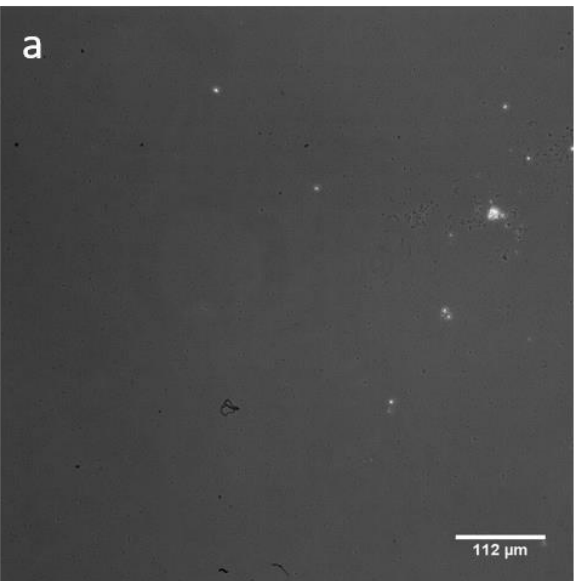


## Appendix

*BW25113, incubated with 10 nM of mannose-based inhibitor linked (Gly-Ser)<sub>6</sub> colicin E9 conjugate, using a starting OD<sub>600</sub> of 2. a) active sample, b) vortexed control, both taken at x 20 magnification*

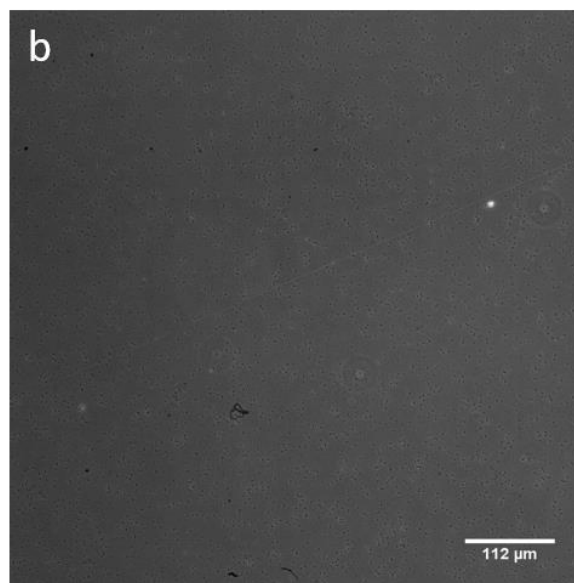
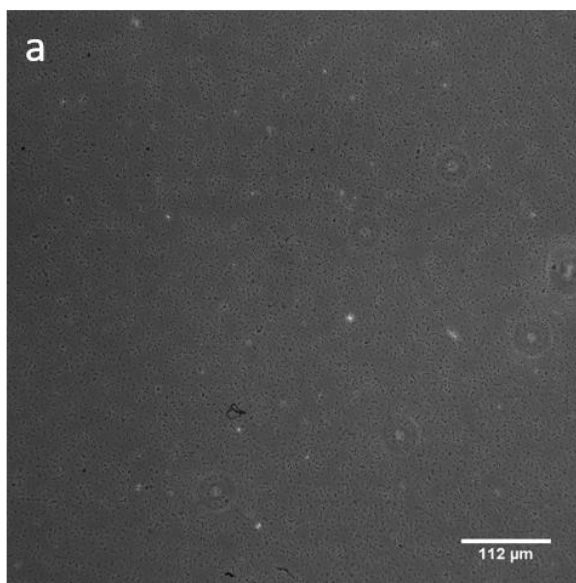


*BW25113, incubated with 1 μM of mannose-based inhibitor linked (Gly-Ser) colicin E9 conjugate, using a starting OD<sub>600</sub> of 1. a) active sample, b) vortexed control, both taken at x 20 magnification*

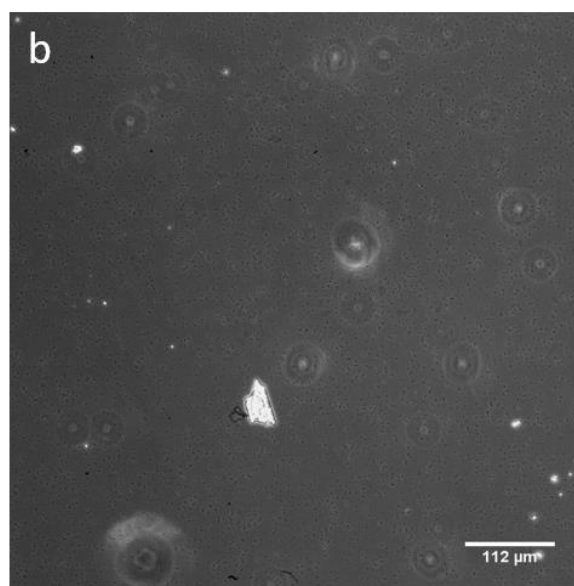
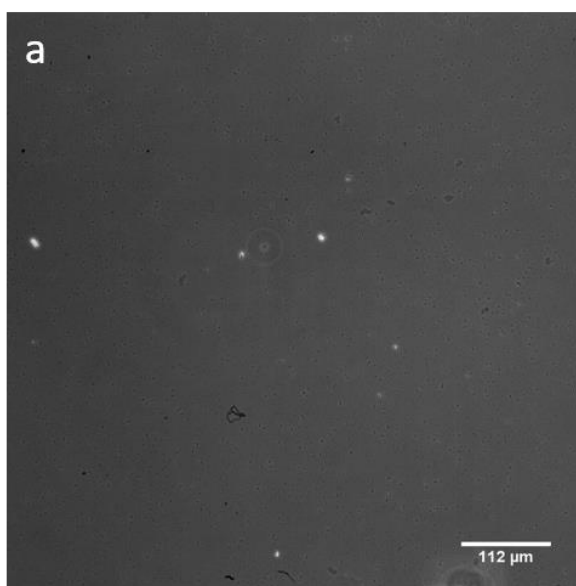


## Appendix

*BW25113, incubated with 100 nM of mannose-based inhibitor linked (Gly-Ser) colicin E9 conjugate, using a starting  $OD_{600}$  of 1. a) active sample, b) vortexed control, both taken at x 20 magnification*



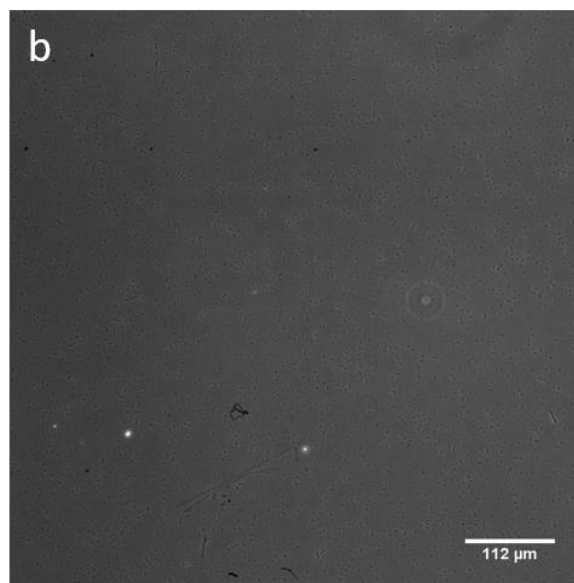
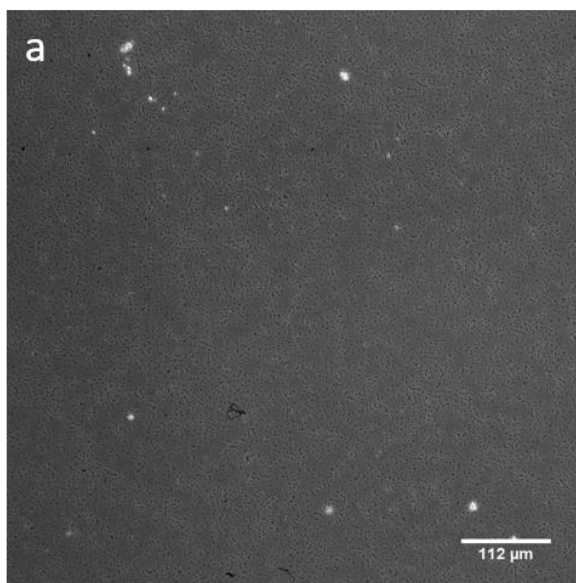
*BW25113, incubated with 10 nM of mannose-based inhibitor linked (Gly-Ser) colicin E9 conjugate, using a starting  $OD_{600}$  of 1. a) active sample, b) vortexed control, both taken at x 20 magnification*



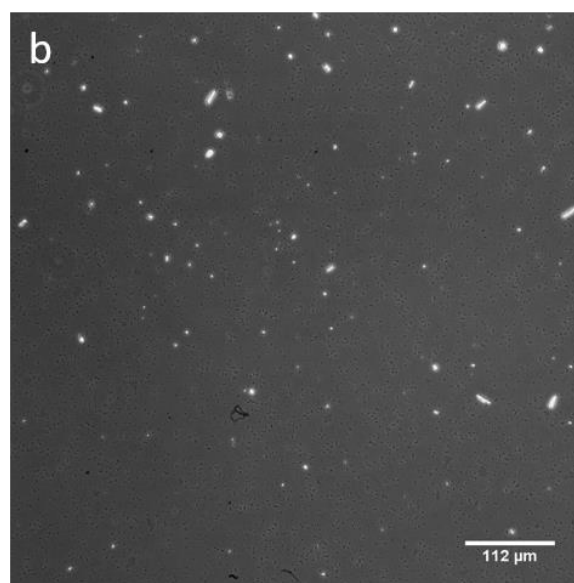
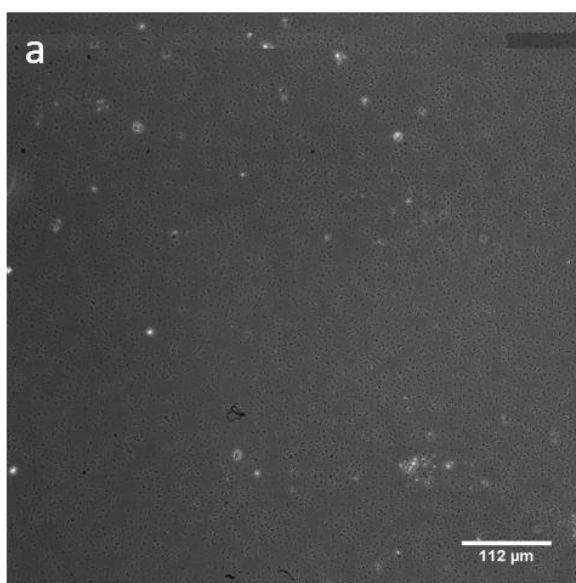


## Appendix

*BW25113, incubated with 1  $\mu$ M of mannose-based inhibitor linked (Gly-Ser)<sub>3</sub> colicin E9 conjugate, using a starting OD<sub>600</sub> of 1. a) active sample, b) vortexed control, both taken at x 20 magnification*

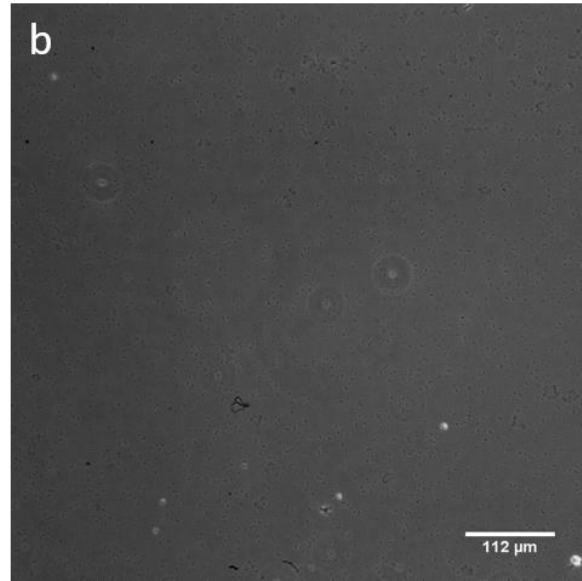
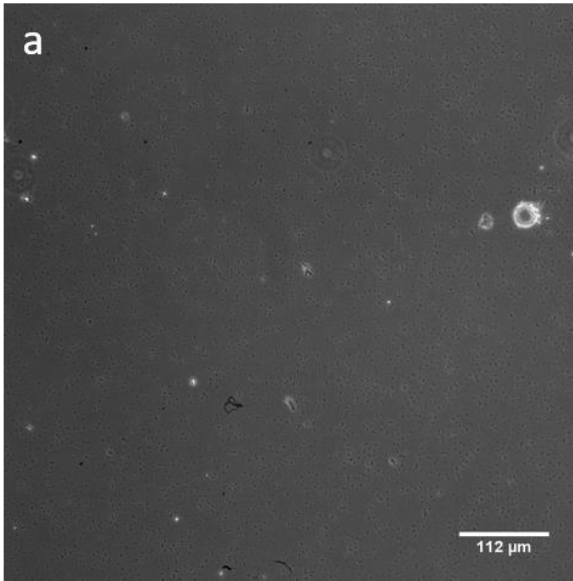


*BW25113, incubated with 100 nM of mannose-based inhibitor linked (Gly-Ser)<sub>3</sub> colicin E9 conjugate, using a starting OD<sub>600</sub> of 1. a) active sample, b) vortexed control, both taken at x 20 magnification*

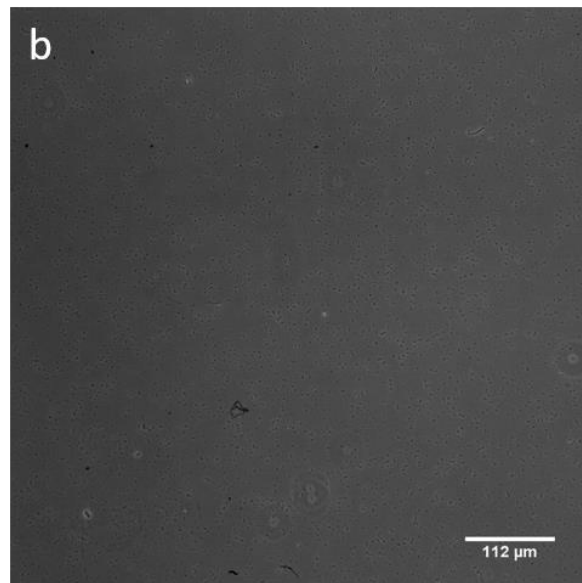
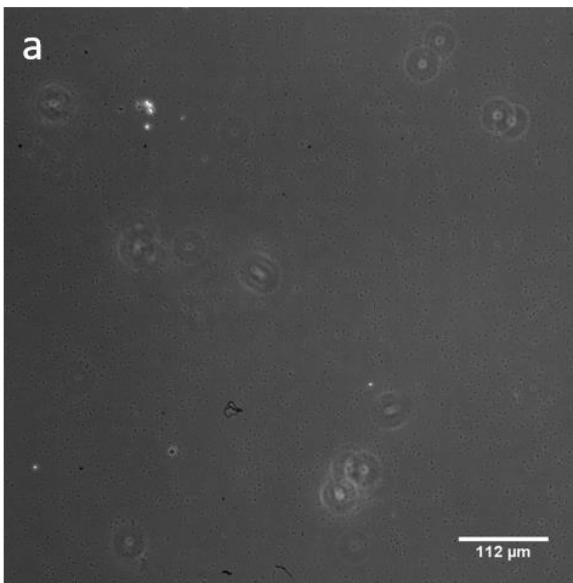


## Appendix

*BW25113, incubated with 1  $\mu\text{M}$  of mannose-based inhibitor linked (Gly-Ser)<sub>6</sub> colicin E9 conjugate, using a starting OD<sub>600</sub> of 1. a) active sample, b) vortexed control, both taken at x 20 magnification*

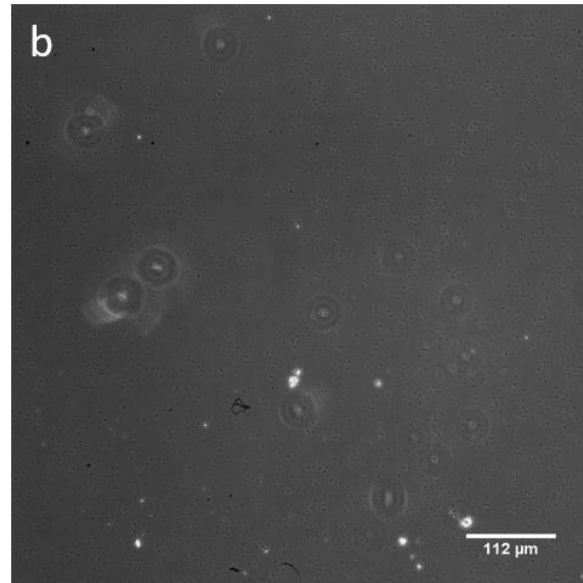
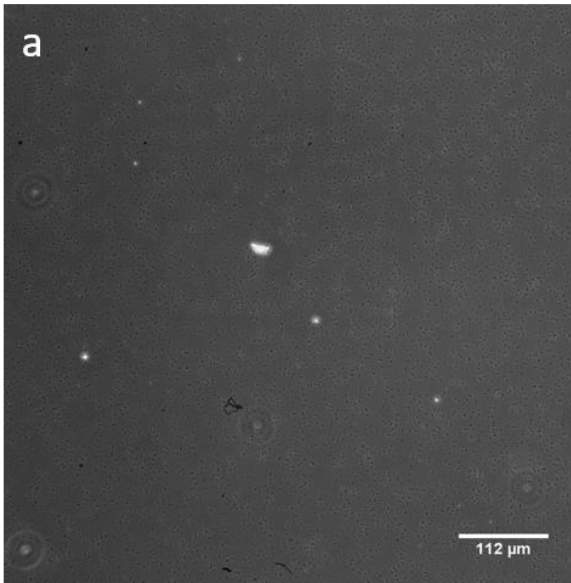


*BW25113, incubated with 100 nM of mannose-based inhibitor linked (Gly-Ser)<sub>6</sub> colicin E9 conjugate, using a starting OD<sub>600</sub> of 1. a) active sample, b) vortexed control, both taken at x 20 magnification*

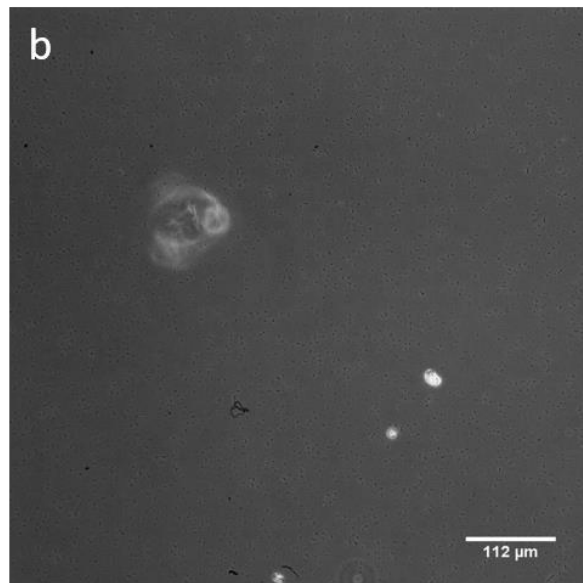
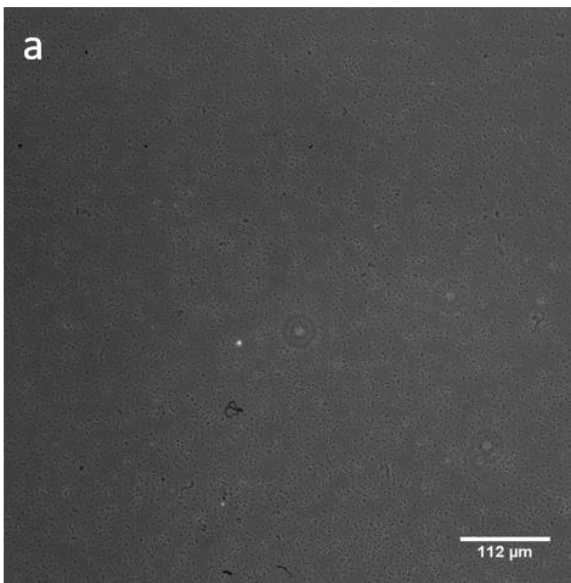


## Appendix

*BW25113, incubated with 10 nM of mannose-based inhibitor linked (Gly-Ser)<sub>6</sub> colicin E9 conjugate, using a starting OD<sub>600</sub> of 1. a) active sample, b) vortexed control, both taken at x 20 magnification*

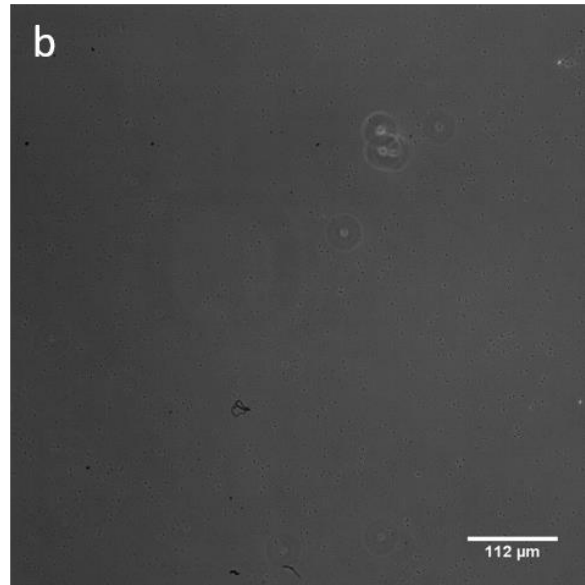
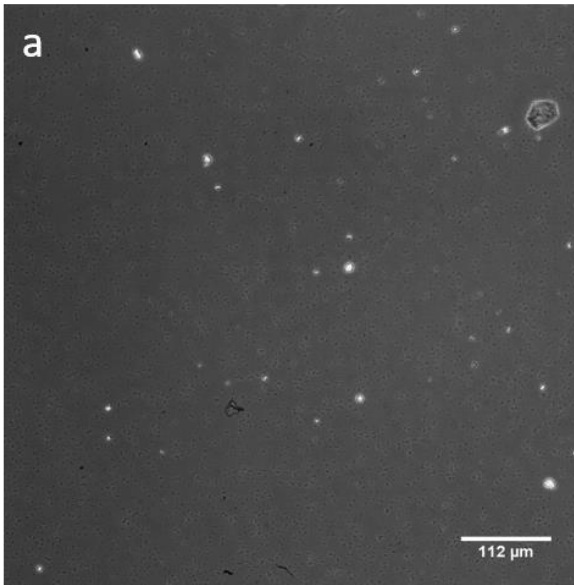


*BW25113, incubated with 1 μM of mannose-based inhibitor linked (Gly-Ser) colicin E9 conjugate, using a starting OD<sub>600</sub> of 0.5. a) active sample, b) vortexed control, both taken at x 20 magnification*

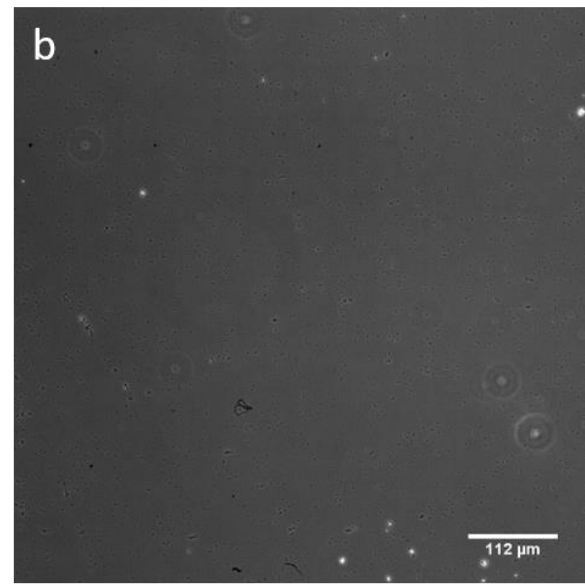
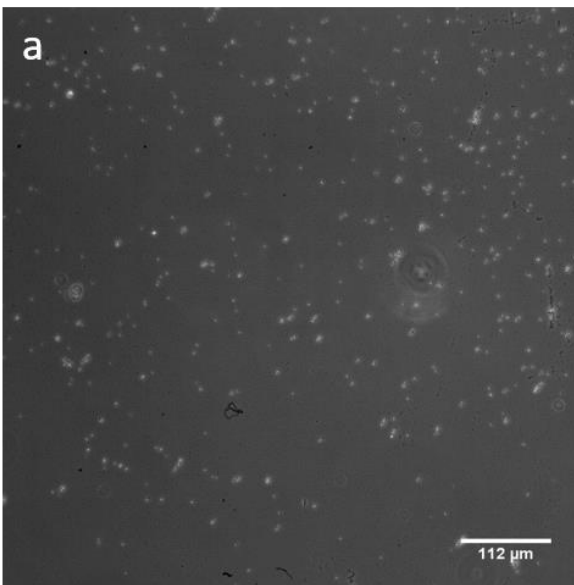


## Appendix

*BW25113, incubated with 100 nM of mannose-based inhibitor linked (Gly-Ser) colicin E9 conjugate, using a starting OD<sub>600</sub> of 0.5. a) active sample, b) vortexed control, both taken at x 20 magnification*

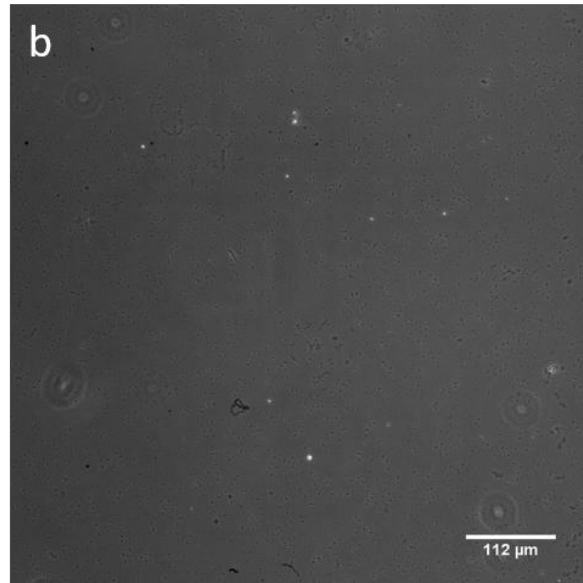
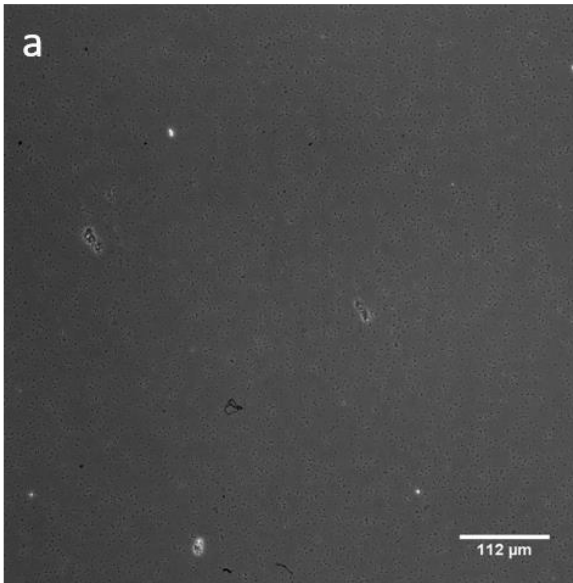


*BW25113, incubated with 10 nM of mannose-based inhibitor linked (Gly-Ser) colicin E9 conjugate, using a starting OD<sub>600</sub> of 0.5. a) active sample, b) vortexed control, both taken at x 20 magnification*

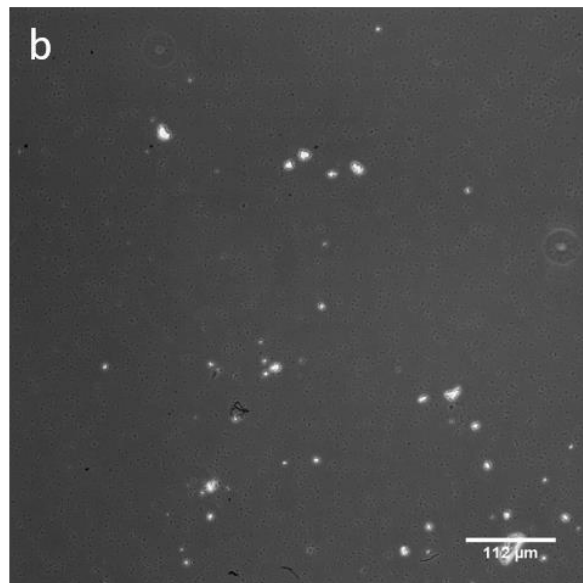
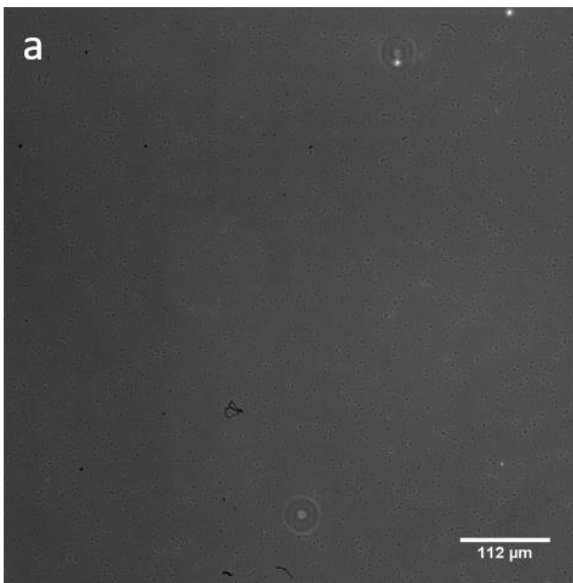


## Appendix

*BW25113, incubated with 1  $\mu\text{M}$  of mannose-based inhibitor linked (Gly-Ser)<sub>3</sub> colicin E9 conjugate, using a starting OD<sub>600</sub> of 0.5. a) active sample, b) vortexed control, both taken at x 20 magnification*

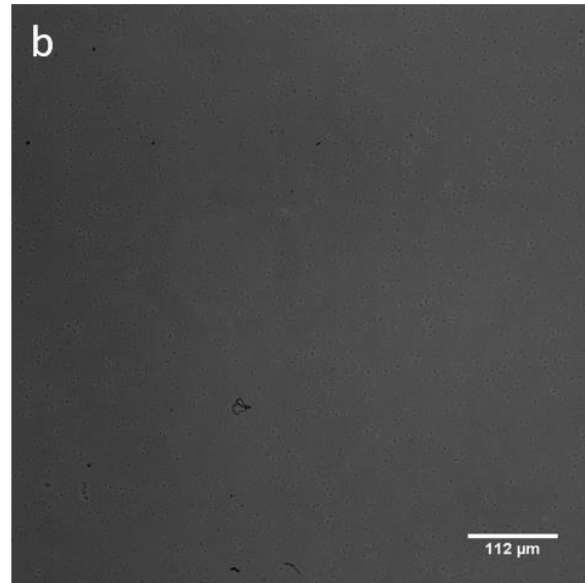
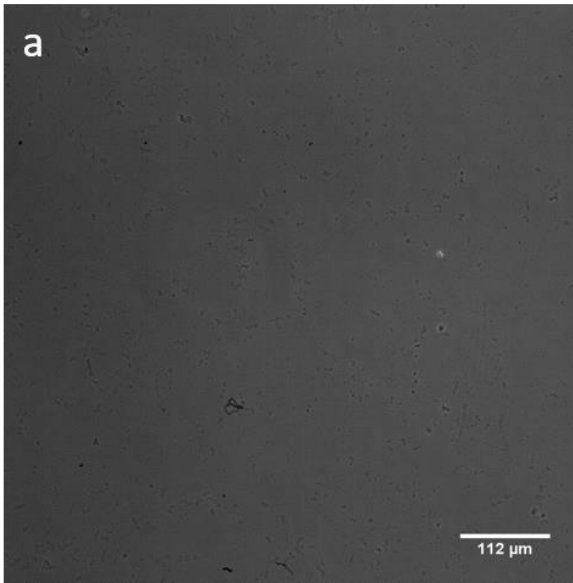


*BW25113, incubated with 100 nM of mannose-based inhibitor linked (Gly-Ser)<sub>3</sub> colicin E9 conjugate, using a starting OD<sub>600</sub> of 0.5. a) active sample, b) vortexed control, both taken at x 20 magnification*

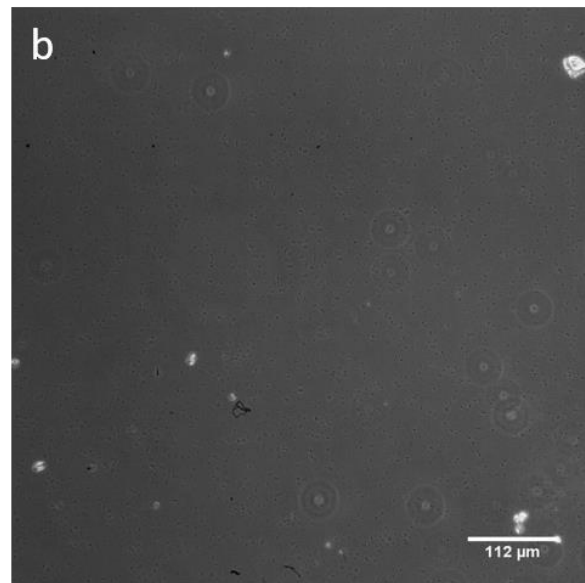
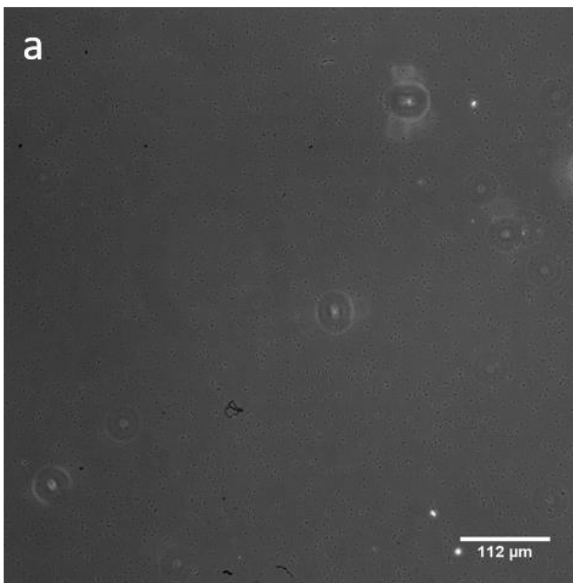


## Appendix

*BW25113, incubated with 1  $\mu\text{M}$  of mannose-based inhibitor linked (Gly-Ser)<sub>6</sub> colicin E9 conjugate, using a starting OD<sub>600</sub> of 0.5. a) active sample, b) vortexed control, both taken at x 20 magnification*

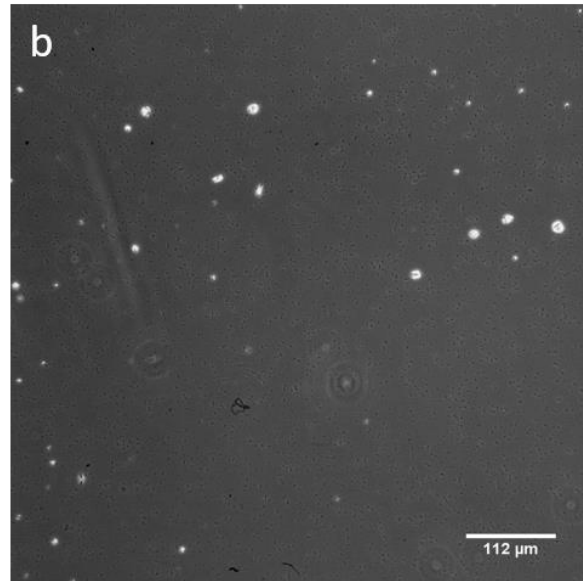
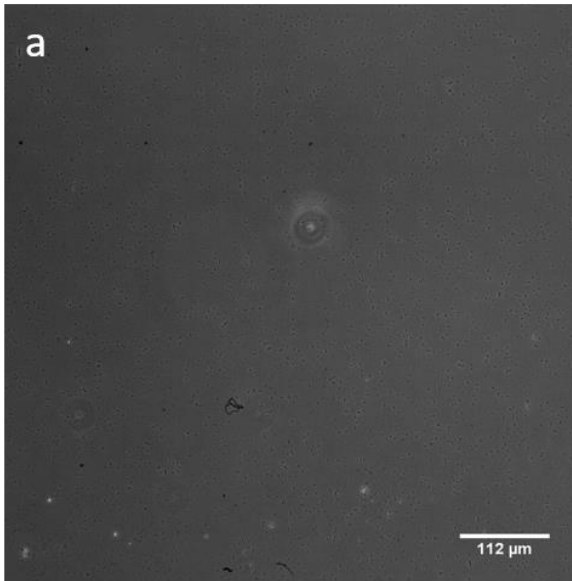


*BW25113, incubated with 100 nM of mannose-based inhibitor linked (Gly-Ser)<sub>6</sub> colicin E9 conjugate, using a starting OD<sub>600</sub> of 0.5. a) active sample, b) vortexed control, both taken at x 20 magnification*

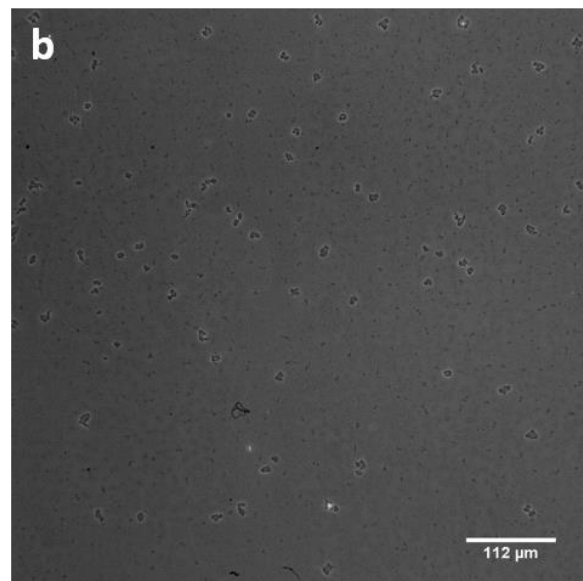
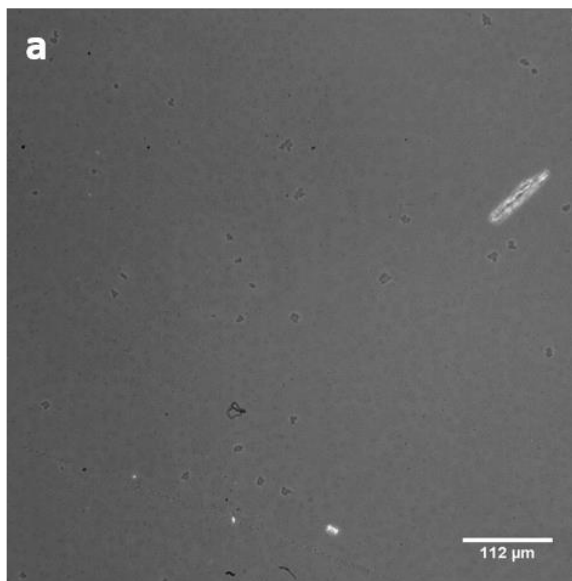


## Appendix

*BW25113, incubated with 10 nM of mannose-based inhibitor linked (Gly-Ser)<sub>6</sub> colicin E9 conjugate 10 nM, using a starting OD<sub>600</sub> of 0.5. a) active sample, b) vortexed control, both taken at x 20 magnification*

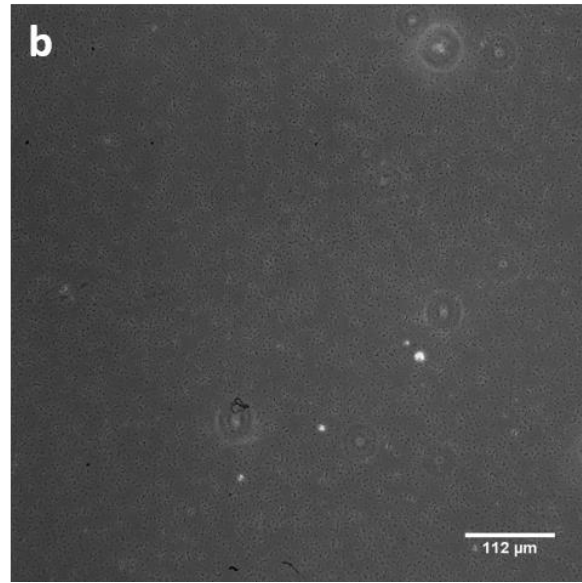
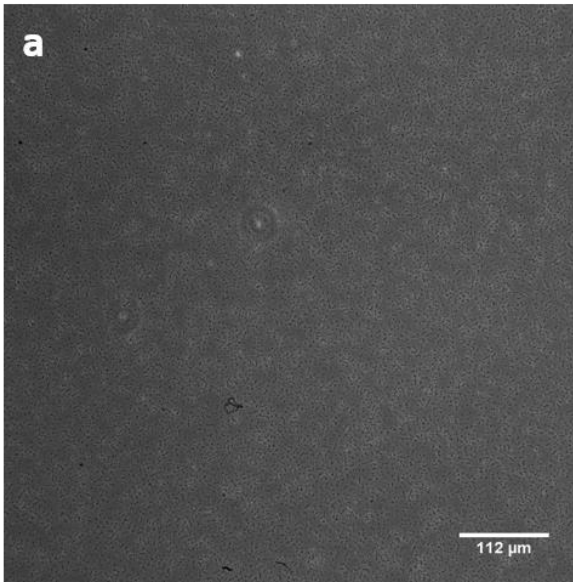


*JW3596, incubated with 1 μM of mannose-based inhibitor linked (Gly-Ser) colicin E9 conjugate, using a starting OD<sub>600</sub> of 2. a) active sample, b) vortexed control, both taken at x 20 magnification*

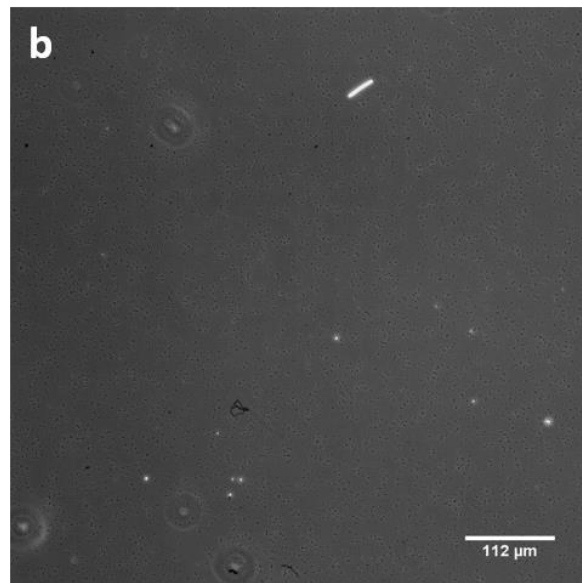
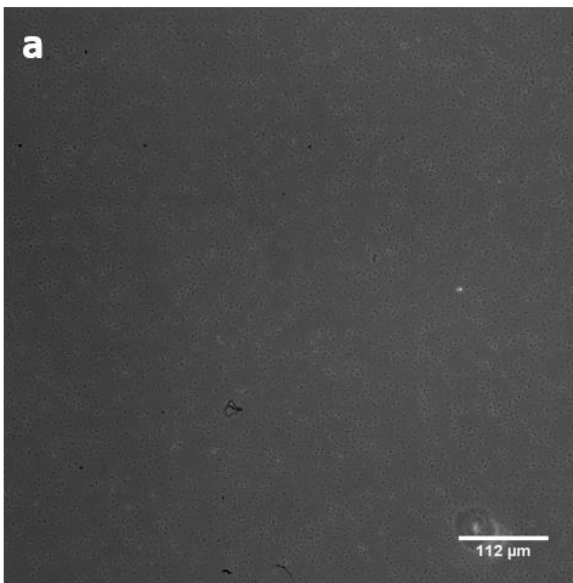


## Appendix

*JW3596, incubated with 100 nM of mannose-based inhibitor linked (Gly-Ser) colicin E9 conjugate, using a starting  $OD_{600}$  of 2. a) active sample, b) vortexed control, both taken at x 20 magnification*



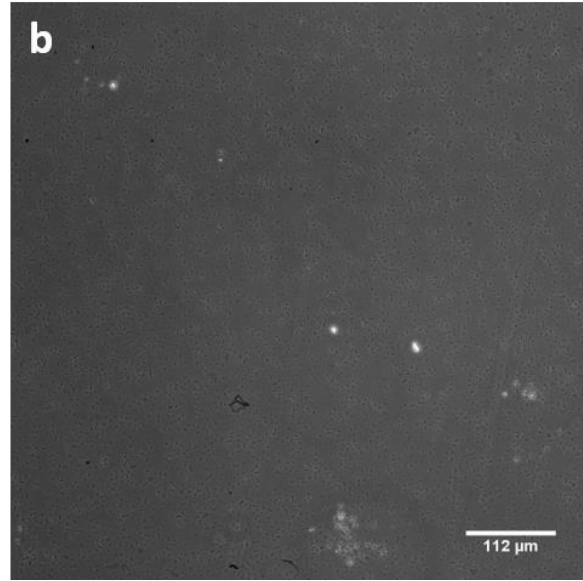
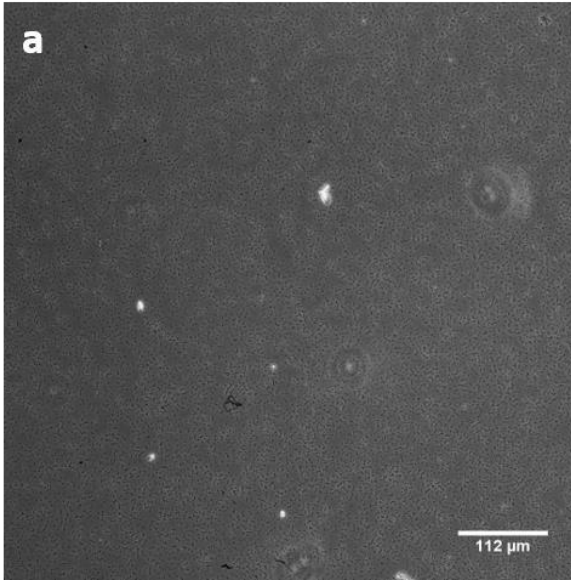
*JW3596, incubated with 10 nM of mannose-based inhibitor linked (Gly-Ser) colicin E9 conjugate 10 nM, using a starting  $OD_{600}$  of 2. a) active sample, b) vortexed control, both taken at x 20 magnification*



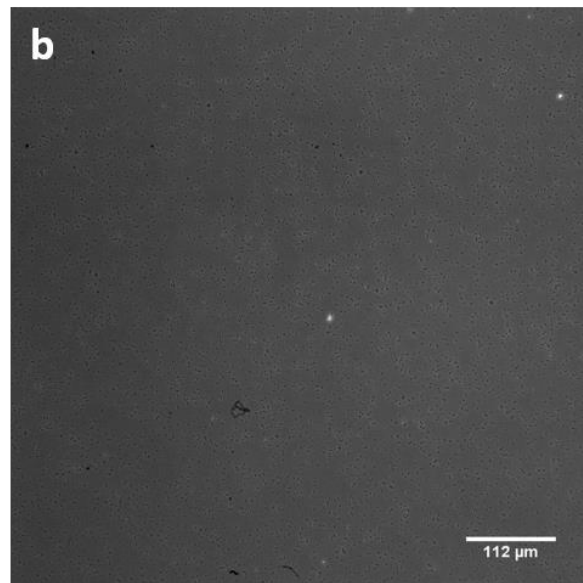
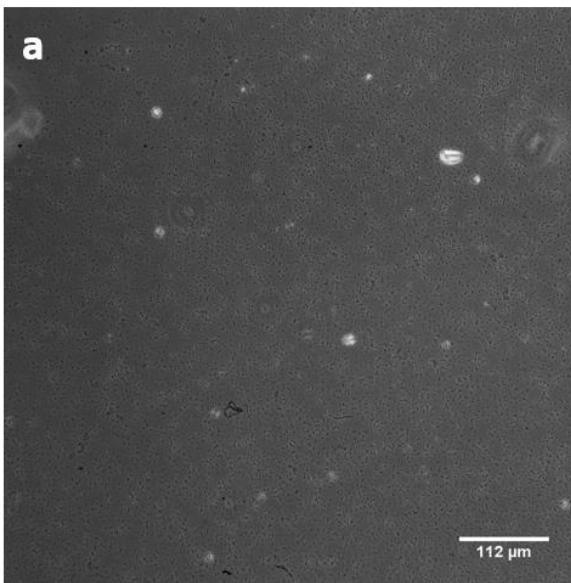


## Appendix

*JW3596, incubated with 1  $\mu\text{M}$  of mannose-based inhibitor linked (Gly-Ser)<sub>3</sub> colicin E9 conjugate, using a starting OD<sub>600</sub> of 2. a) active sample, b) vortexed control, both taken at x 20 magnification*

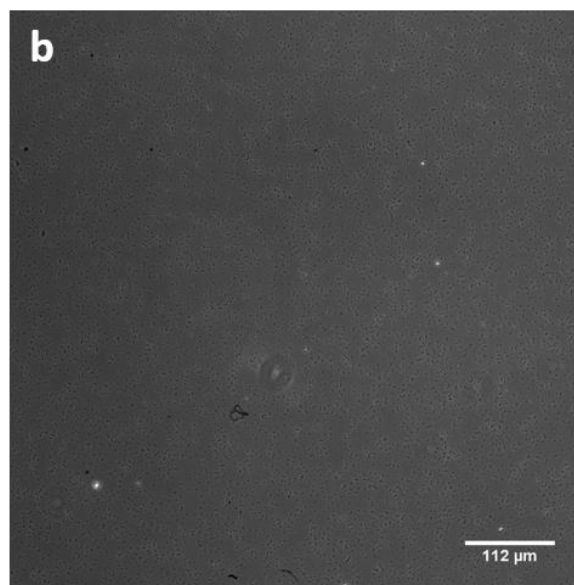
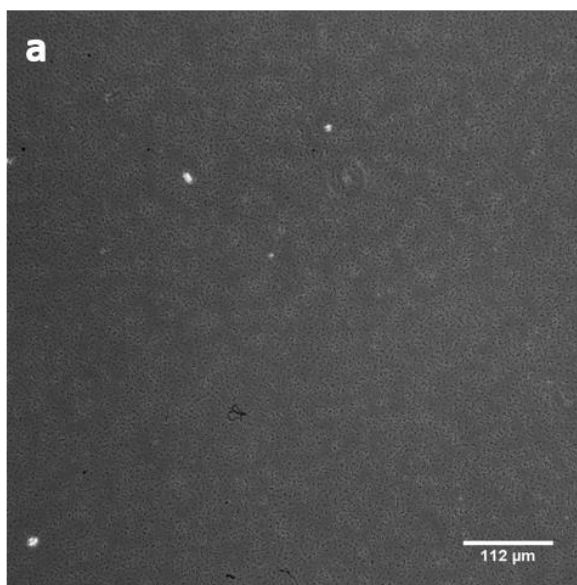


*JW3596, incubated with 100 nM of mannose-based inhibitor linked (Gly-Ser)<sub>3</sub> colicin E9 conjugate, using a starting OD<sub>600</sub> of 2. a) active sample, b) vortexed control, both taken at x 20 magnification*

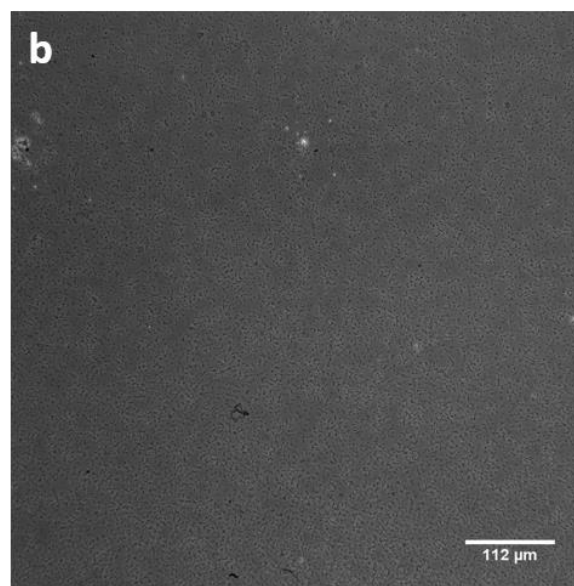
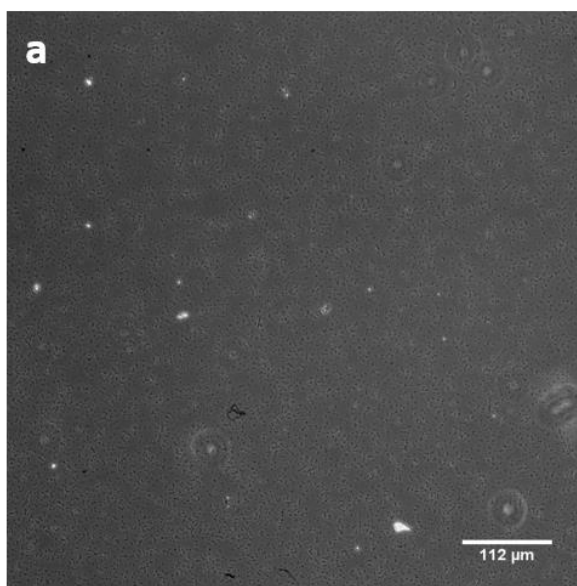


## Appendix

*JW3596, incubated with 10 nM of mannose-based inhibitor linked (Gly-Ser)<sub>3</sub> colicin E9 conjugate, using a starting OD<sub>600</sub> of 2. a) active sample, b) vortexed control, both taken at x 20 magnification*

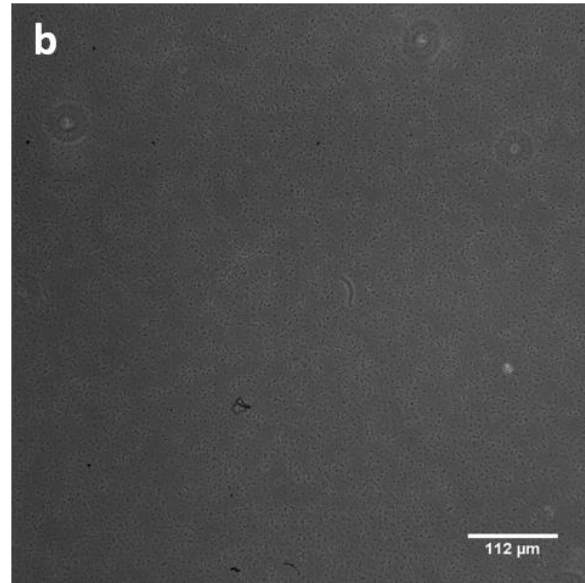
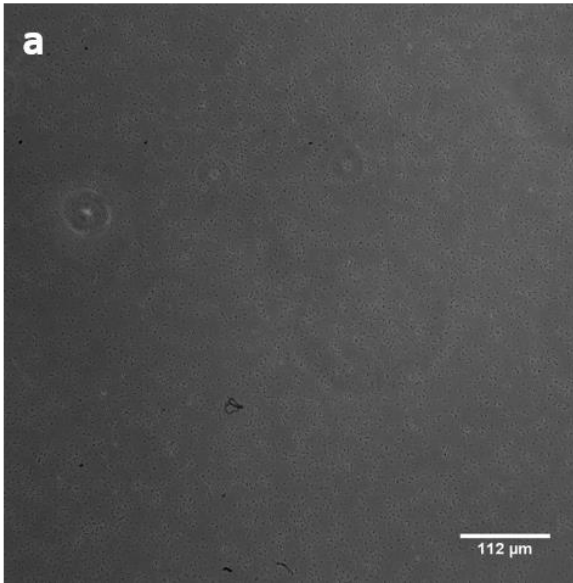


*JW3596, incubated with 1 μM of mannose-based inhibitor linked (Gly-Ser)<sub>6</sub> colicin E9 conjugate, using a starting OD<sub>600</sub> of 2. a) active sample, b) vortexed control, both taken at x 20 magnification*

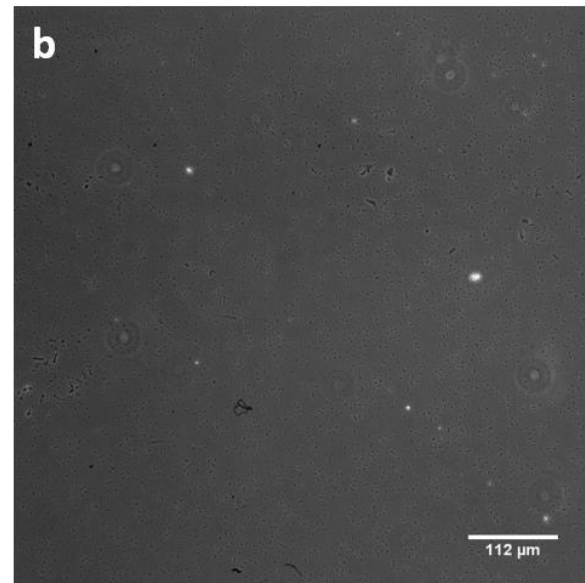
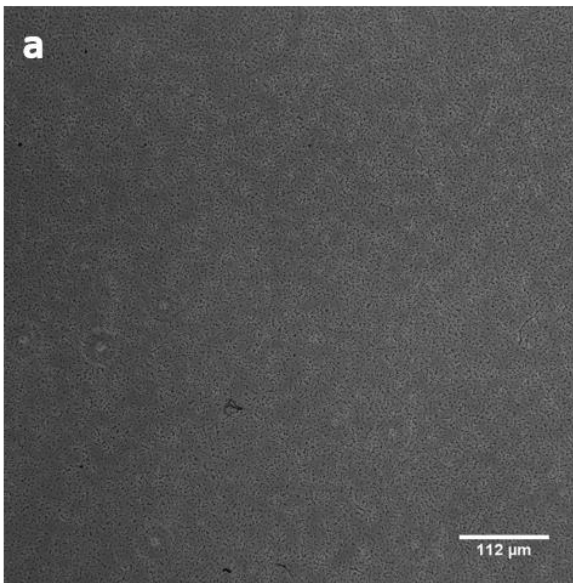


## Appendix

*JW3596, incubated with 100 nM of mannose-based inhibitor linked (Gly-Ser)<sub>6</sub> colicin E9 conjugate, using a starting OD<sub>600</sub> of 2. a) active sample, b) vortexed control, both taken at x 20 magnification*

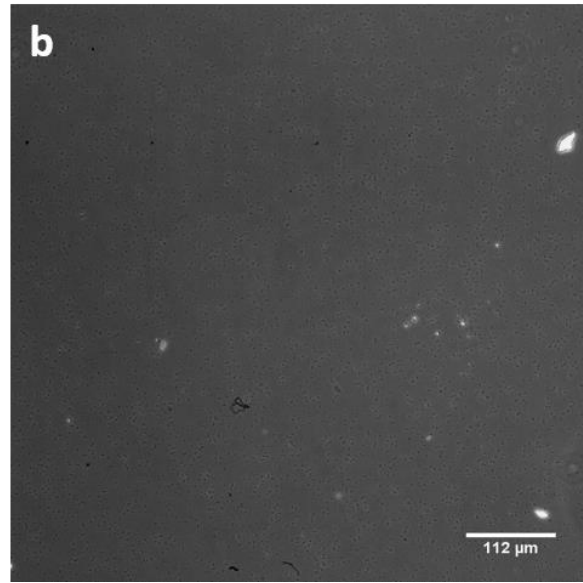
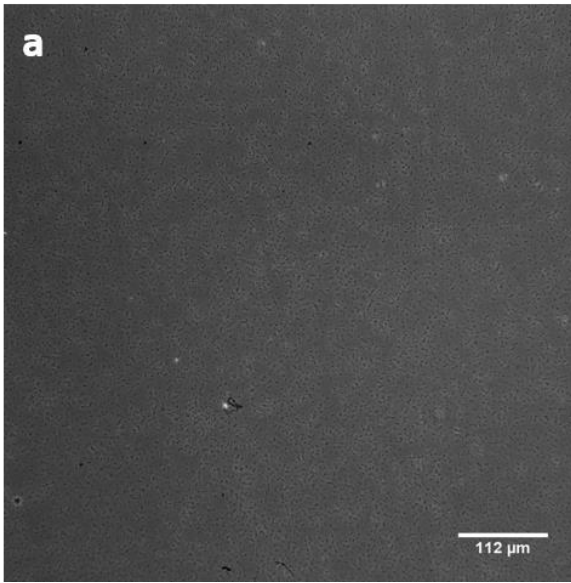


*JW3596, incubated with 10 nM of mannose-based inhibitor linked (Gly-Ser)<sub>6</sub> colicin E9 conjugate, using a starting OD<sub>600</sub> of 2. a) active sample, b) vortexed control, both taken at x 20 magnification*

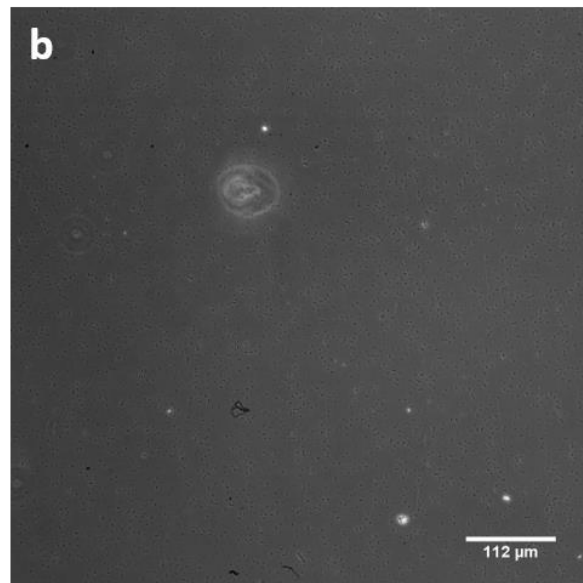
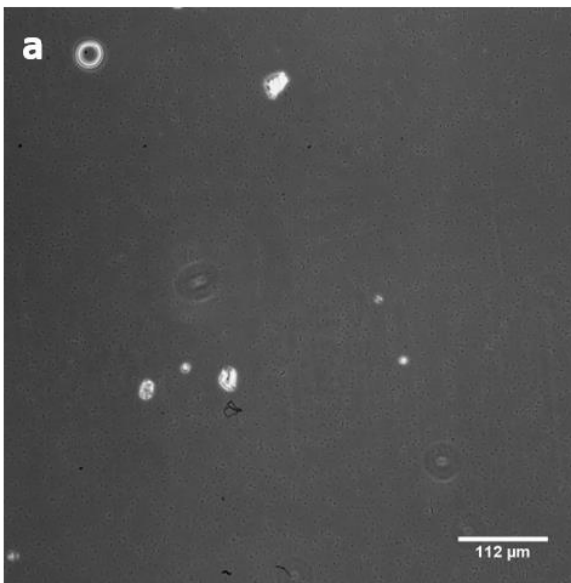


## Appendix

*JW3596, incubated with 1  $\mu$ M of mannose-based inhibitor linked (Gly-Ser) colicin E9 conjugate, using a starting  $OD_{600}$  of 1. a) active sample, b) vortexed control, both taken at x 20 magnification*

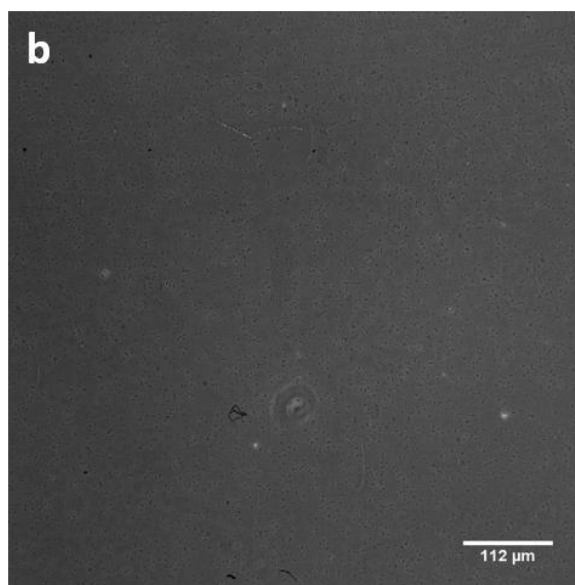
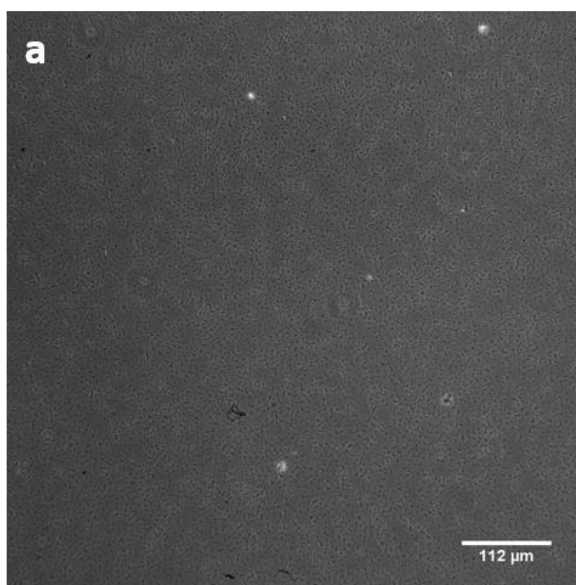


*JW3596, incubated with 100 nM of mannose-based inhibitor linked (Gly-Ser) colicin E9 conjugate, using a starting  $OD_{600}$  of 1. a) active sample, b) vortexed control, both taken at x 20 magnification*

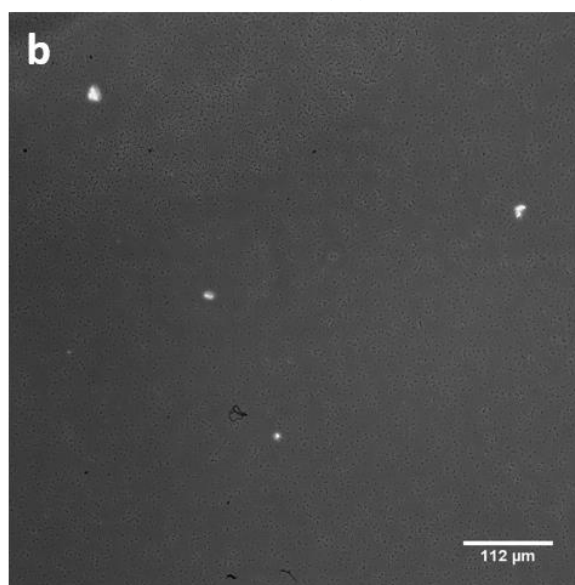
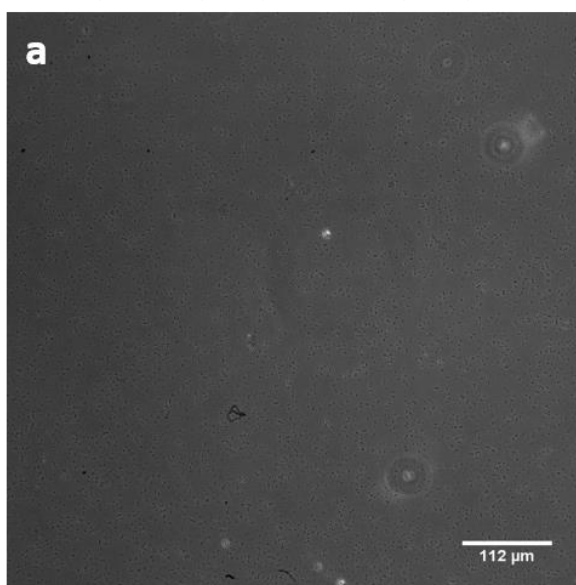


## Appendix

*JW3596, incubated with 10 nM of mannose-based inhibitor linked (Gly-Ser) colicin E9 conjugate 10 nM, using a starting OD<sub>600</sub> of 1. a) active sample, b) vortexed control, both taken at x 20 magnification*

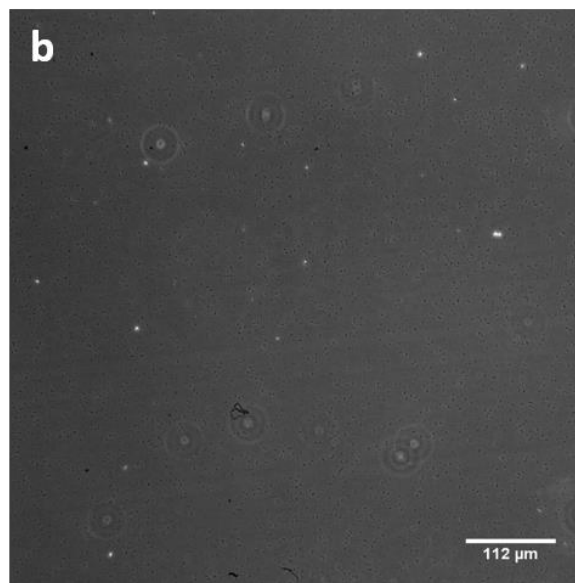
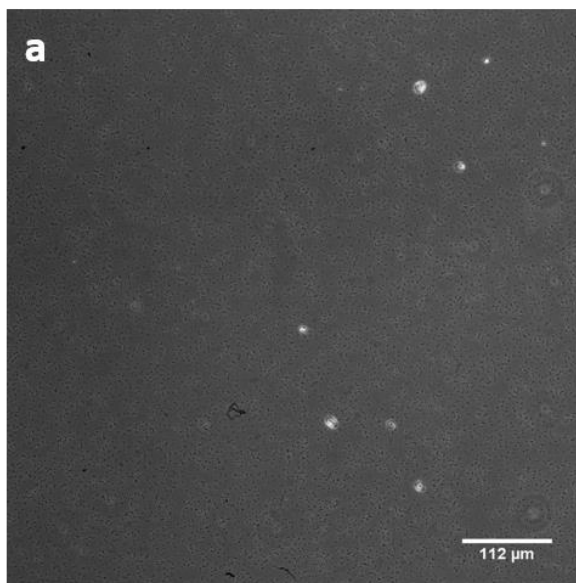


*JW3596, incubated with 1 μM of mannose-based inhibitor linked (Gly-Ser)<sub>3</sub> colicin E9 conjugate, using a starting OD<sub>600</sub> of 1. a) active sample, b) vortexed control, both taken at x 20 magnification*

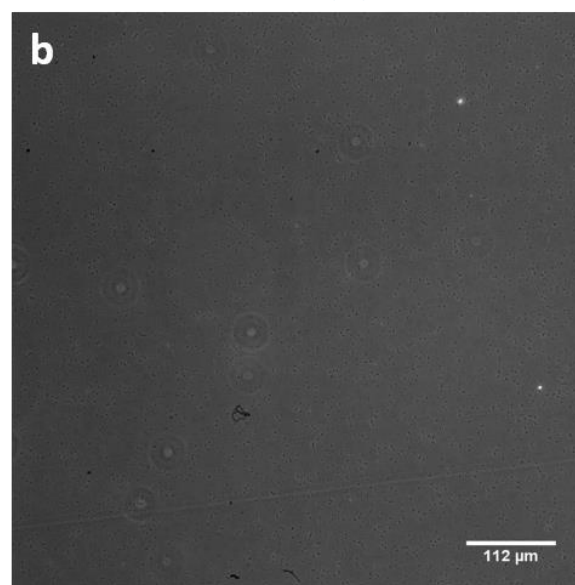
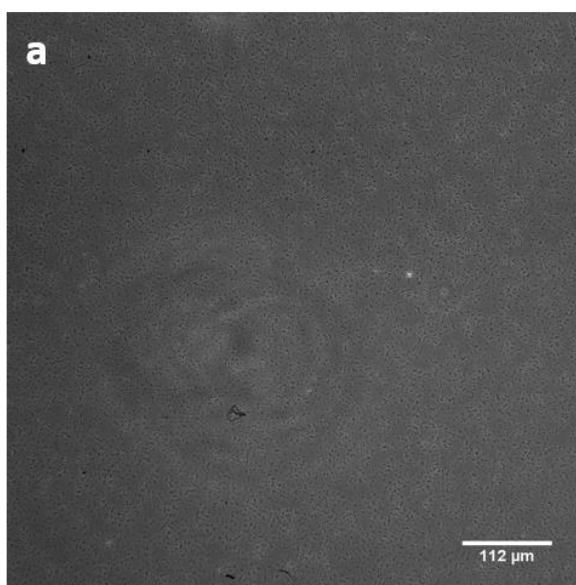


## Appendix

*JW3596, incubated with 100 nM of mannose-based inhibitor linked (Gly-Ser)<sub>3</sub> colicin E9 conjugate, using a starting OD<sub>600</sub> of 1. a) active sample, b) vortexed control, both taken at x 20 magnification*

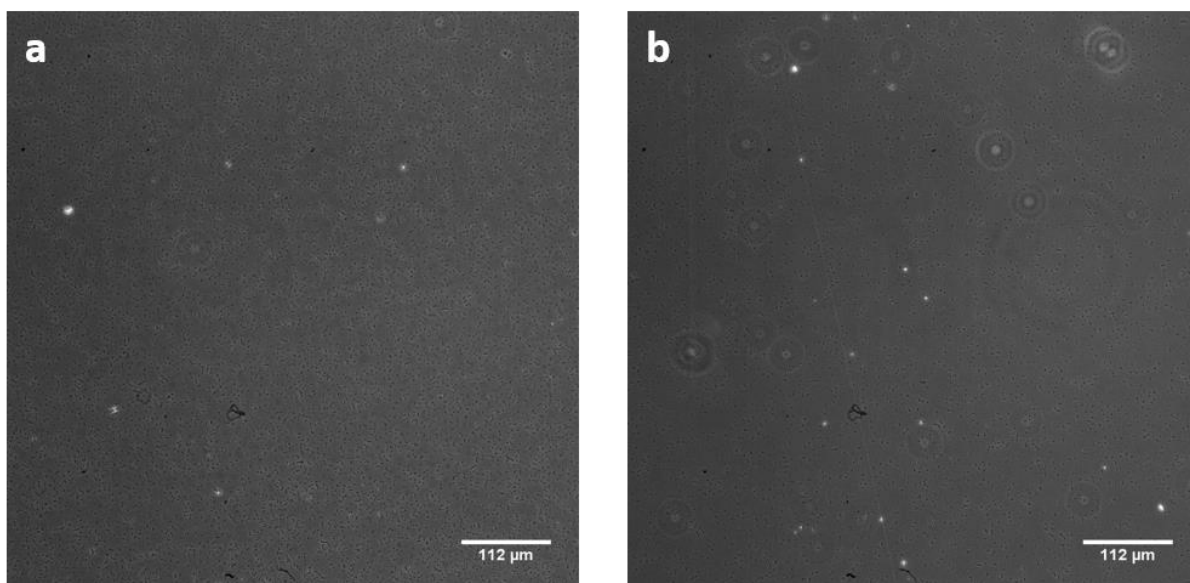


*JW3596, incubated with 10 nM of mannose-based inhibitor linked (Gly-Ser)<sub>3</sub> colicin E9 conjugate, using a starting OD<sub>600</sub> of 1. a) active sample, b) vortexed control, both taken at x 20 magnification*

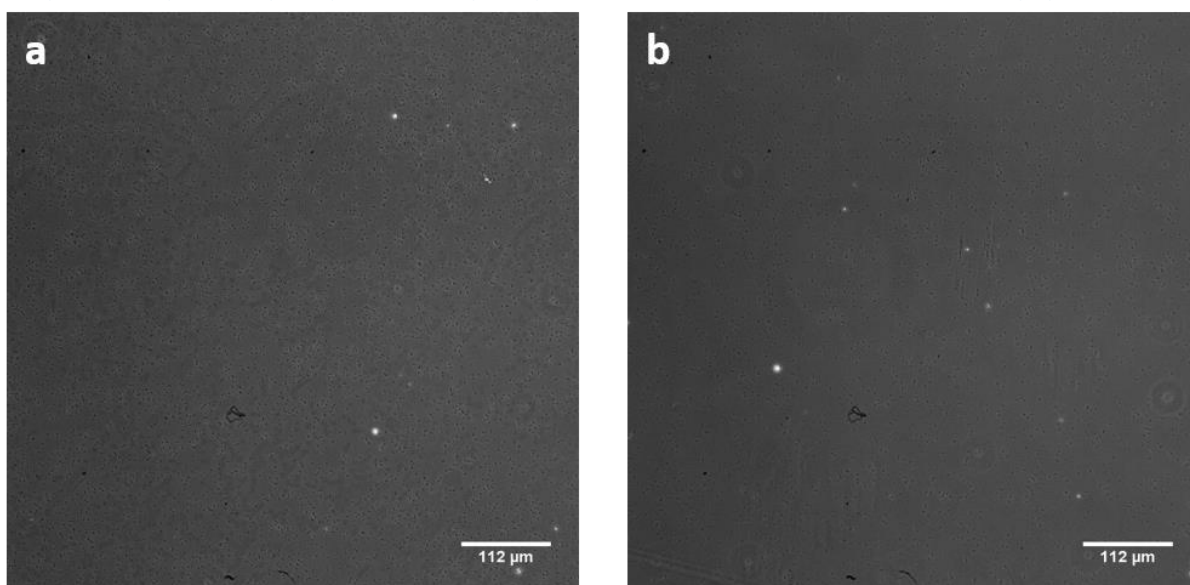


## Appendix

*JW3596, incubated with 1  $\mu$ M of mannose-based inhibitor linked (Gly-Ser)<sub>6</sub> colicin E9 conjugate, using a starting OD<sub>600</sub> of 1. a) active sample, b) vortexed control, both taken at x 20 magnification*

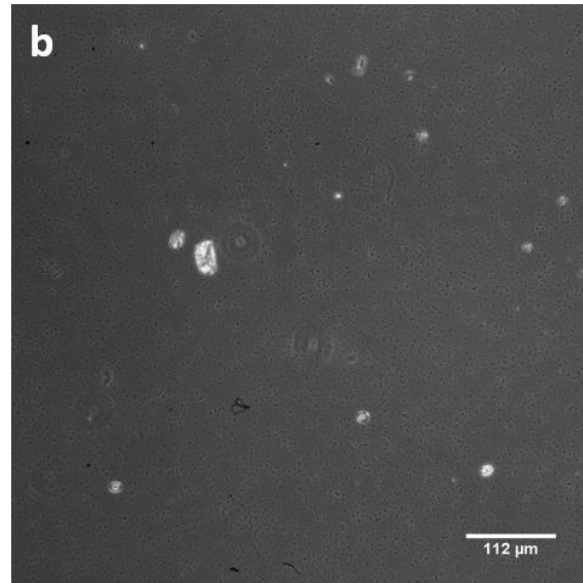
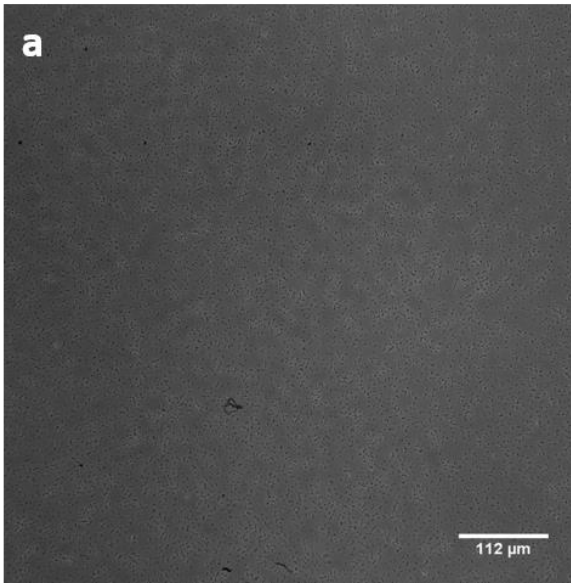


*JW3596, incubated with 100 nM of mannose-based inhibitor linked (Gly-Ser)<sub>6</sub> colicin E9 conjugate, using a starting OD<sub>600</sub> of 1. a) active sample, b) vortexed control, both taken at x 20 magnification*

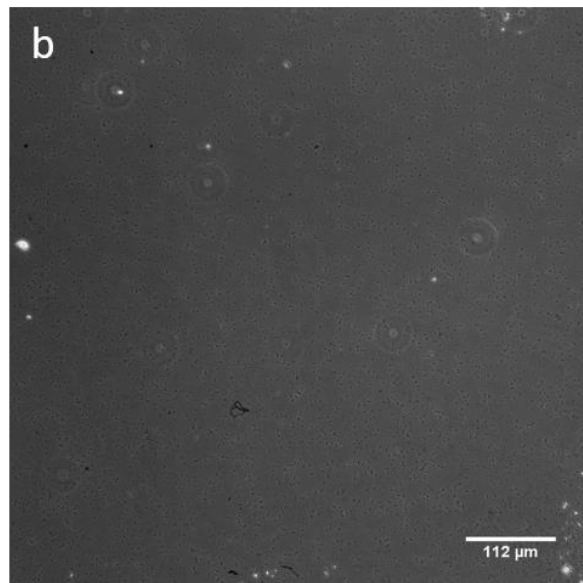
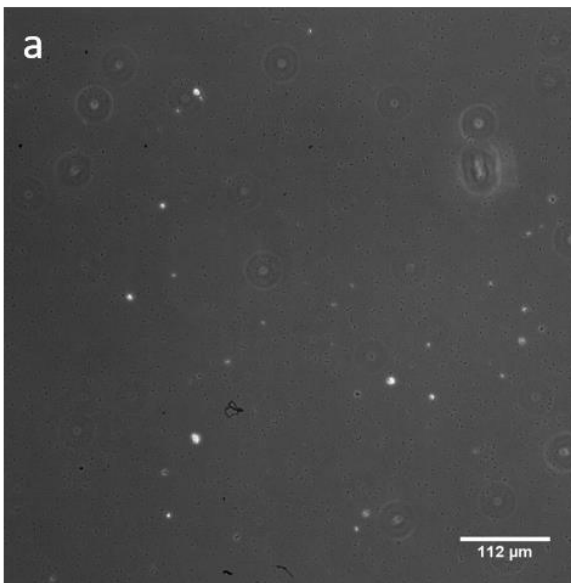


## Appendix

*JW3596, incubated with 10 nM of mannose-based inhibitor linked (Gly-Ser)<sub>6</sub> colicin E9 conjugate, using a starting OD<sub>600</sub> of 1. a) active sample, b) vortexed control, both taken at x 20 magnification*



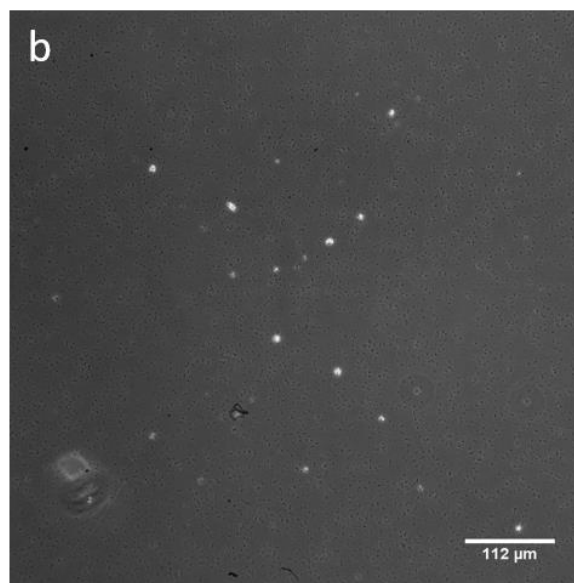
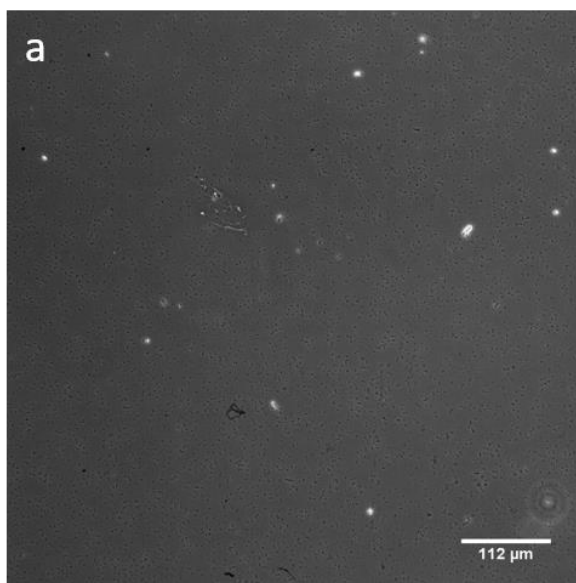
*JW3596, incubated with 1 μM of mannose-based inhibitor linked (Gly-Ser) colicin E9 conjugate, using a starting OD<sub>600</sub> of 0.5. a) active sample, b) vortexed control, both taken at x 20 magnification*



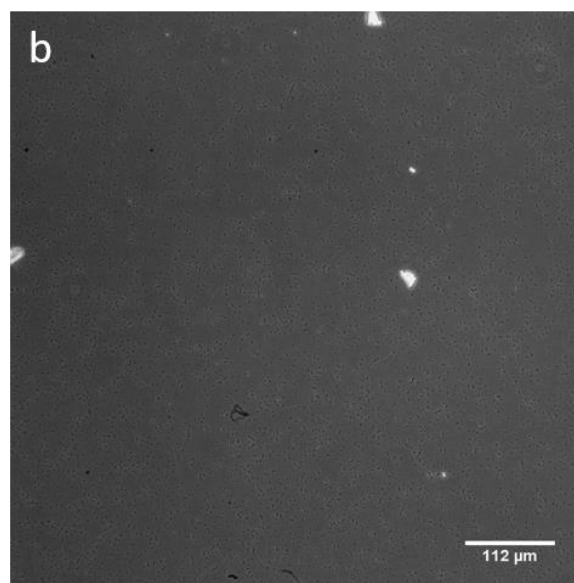
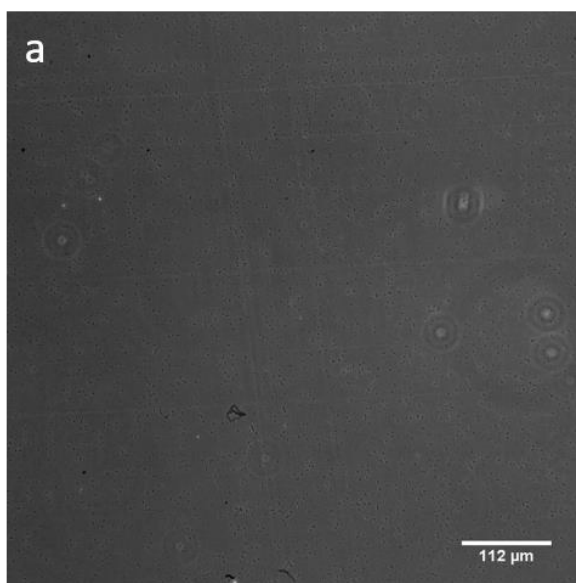


## Appendix

*JW3596, incubated with 100 nM of mannose-based inhibitor linked (Gly-Ser) colicin E9 conjugate, using a starting  $OD_{600}$  of 0.5. a) active sample, b) vortexed control, both taken at x 20 magnification*

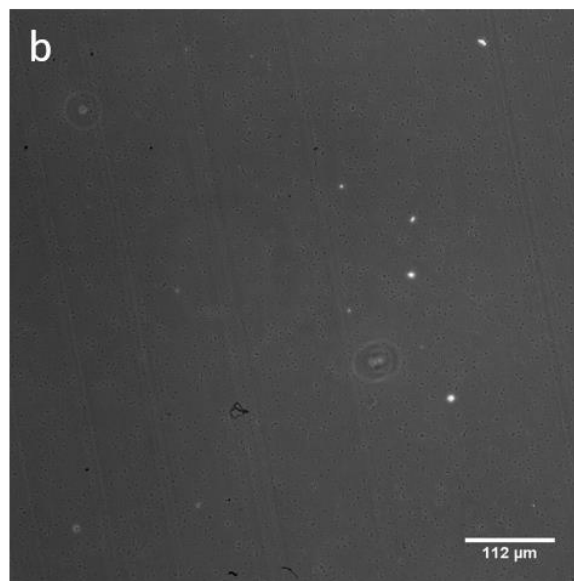
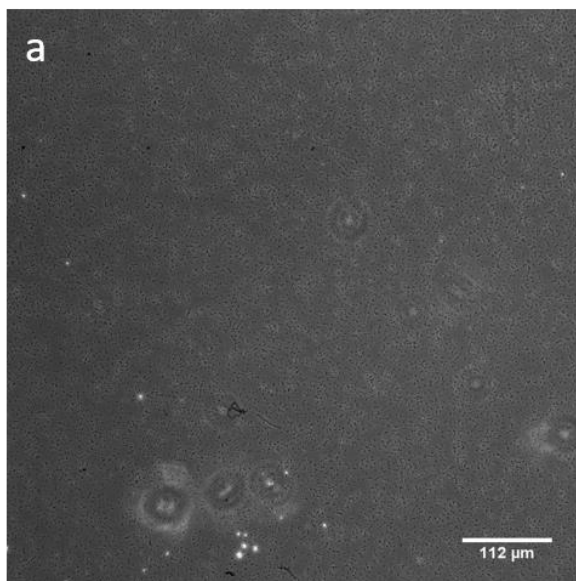


*JW3596, incubated with 10 nM of mannose-based inhibitor linked (Gly-Ser) colicin E9 conjugate, using a starting  $OD_{600}$  of 0.5. a) active sample, b) vortexed control, both taken at x 20 magnification*

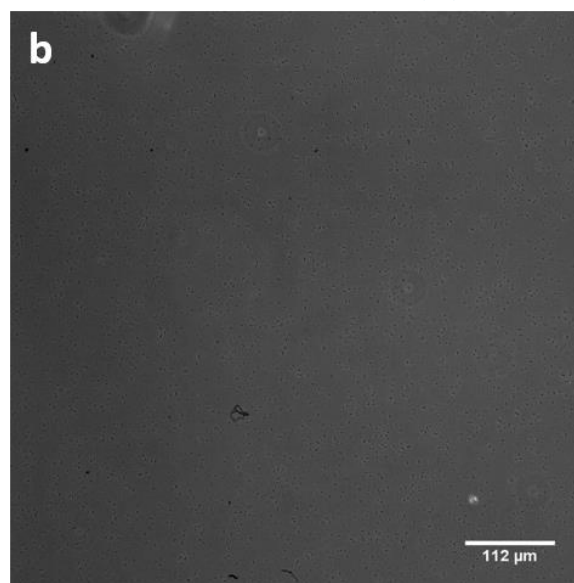
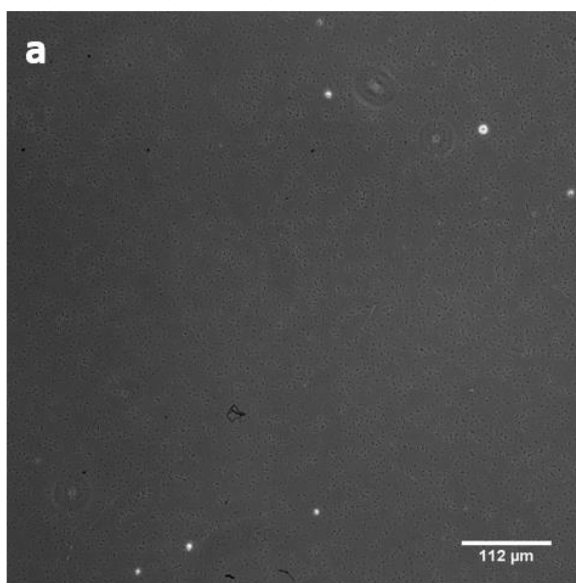


## Appendix

*JW3596, incubated with 1  $\mu\text{M}$  of mannose-based inhibitor linked (Gly-Ser)<sub>3</sub> colicin E9 conjugate, using a starting OD<sub>600</sub> of 0.5. a) active sample, b) vortexed control, both taken at x 20 magnification*

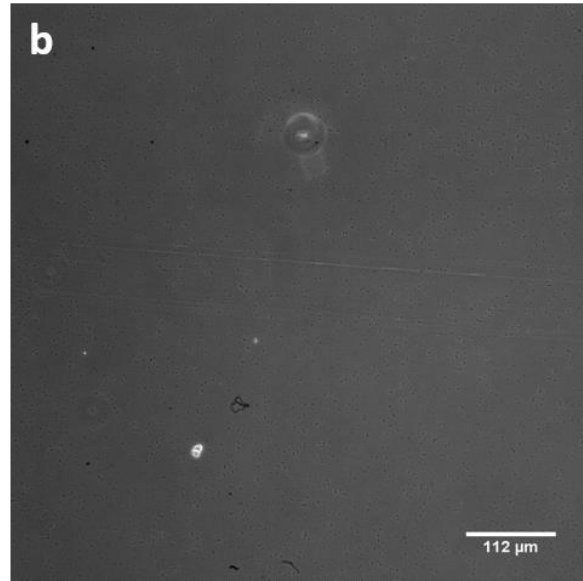
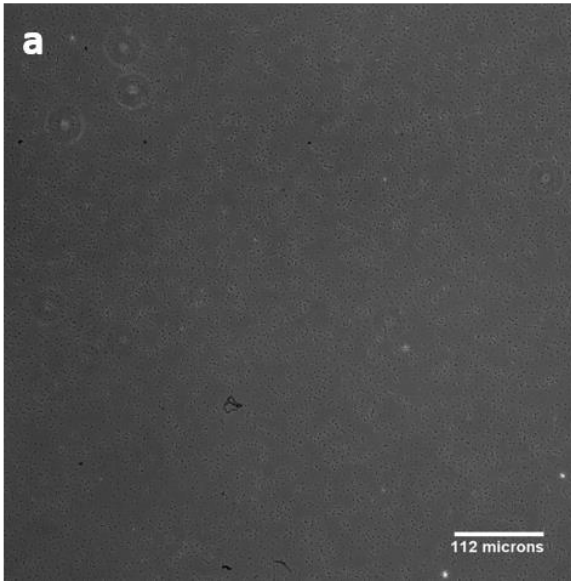


*JW3596, incubated with 100 nM of mannose-based inhibitor linked (Gly-Ser)<sub>3</sub> colicin E9 conjugate, using a starting OD<sub>600</sub> of 0.5. a) active sample, b) vortexed control, both taken at x 20 magnification*

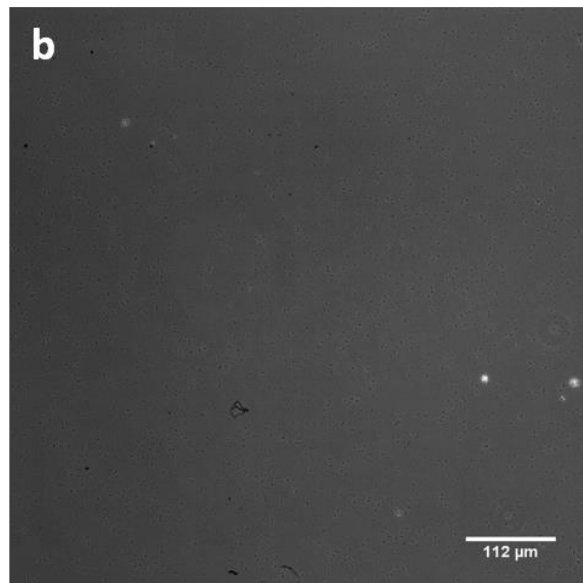
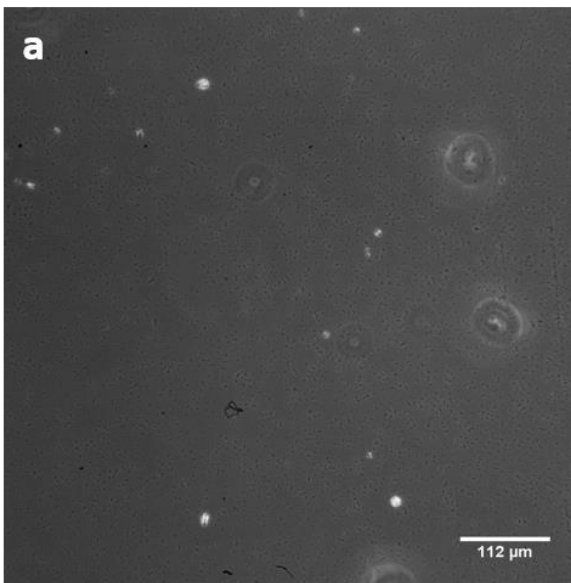


## Appendix

*JW3596, incubated with 10 nM of mannose-based inhibitor linked (Gly-Ser)<sub>3</sub> colicin E9 conjugate, using a starting OD<sub>600</sub> of 0.5. a) active sample, b) vortexed control, both taken at x 20 magnification*

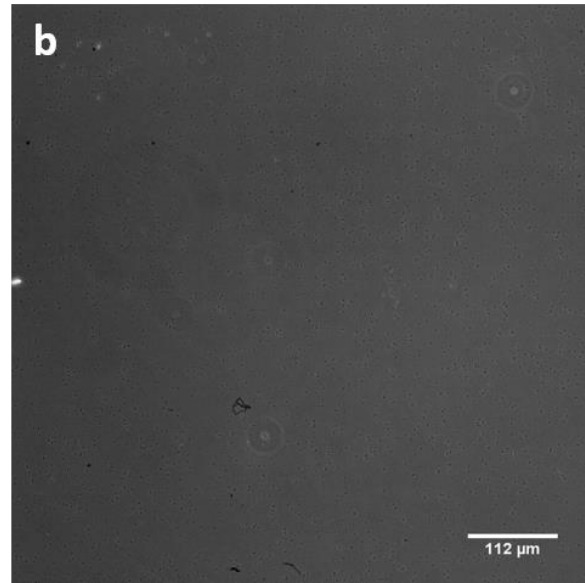
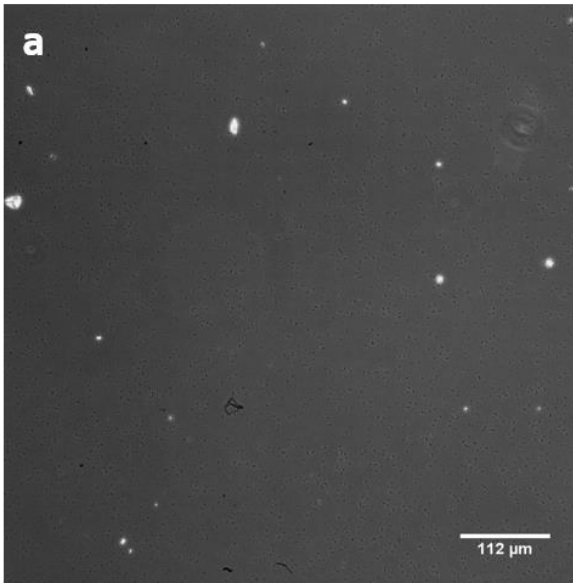


*JW3596, incubated with 1 μM of mannose-based inhibitor linked (Gly-Ser)<sub>6</sub> colicin E9 conjugate, using a starting OD<sub>600</sub> of 0.5. a) active sample, b) vortexed control, both taken at x 20 magnification*

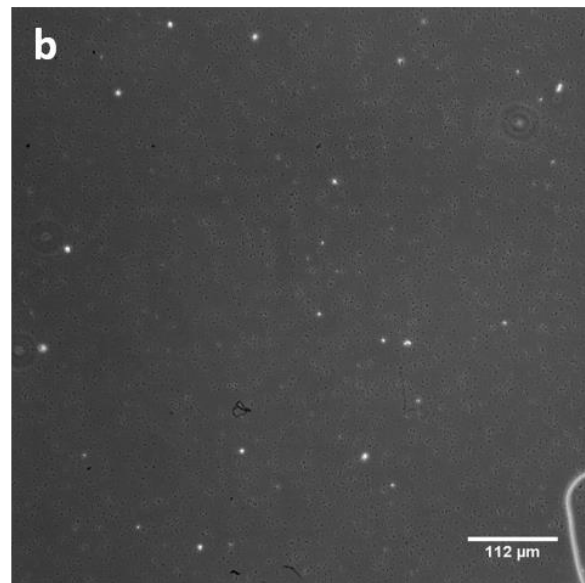
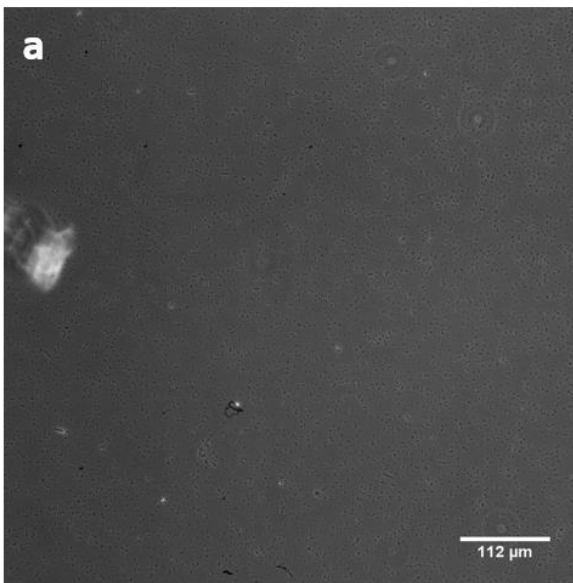


## Appendix

*JW3596, incubated with 100 nM of mannose-based inhibitor linked (Gly-Ser)<sub>6</sub> colicin E9 conjugate, using a starting OD<sub>600</sub> of 0.5. a) active sample, b) vortexed control, both taken at x 20 magnification*



*JW3596, incubated with 10 nM of mannose-based inhibitor linked (Gly-Ser)<sub>6</sub> colicin E9 conjugate, using a starting OD<sub>600</sub> of 0.5. a) active sample, b) vortexed control, both taken at x 20 magnification*

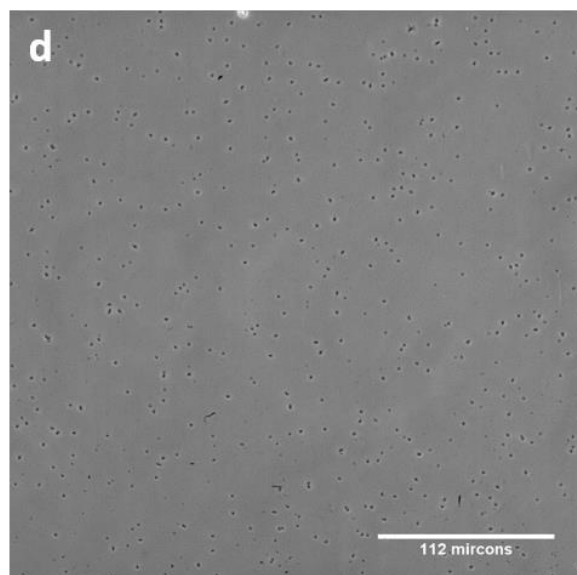
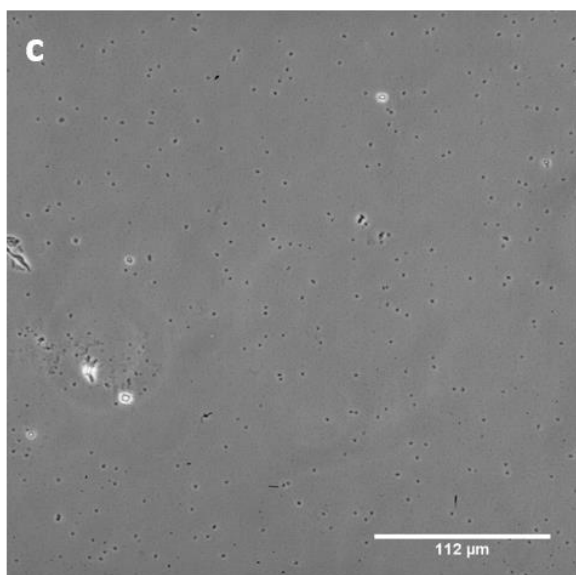
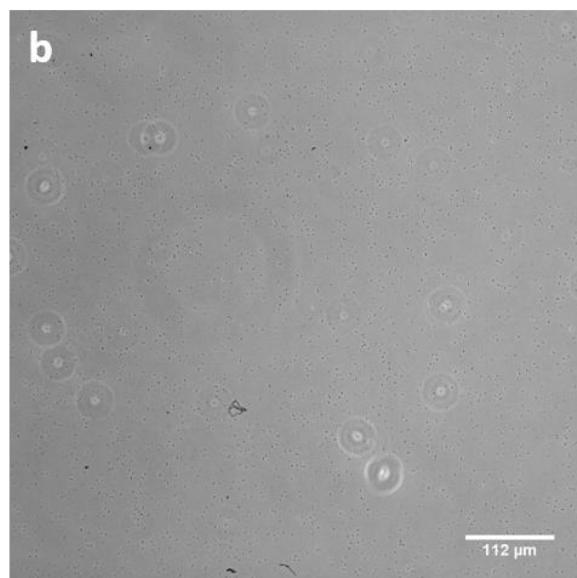
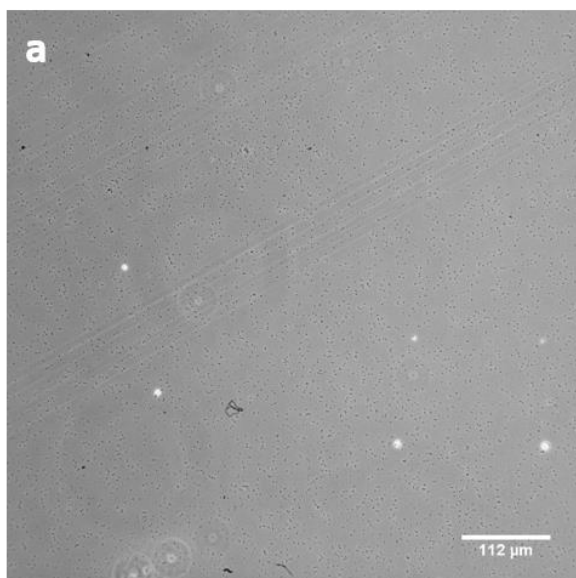


## Appendix

9.3.5 Results of experiment seven, images from the microscopy screen of samples incubated with mannose-based inhibitor linked (Gly-Ser)<sub>6</sub> colicin E9 conjugate

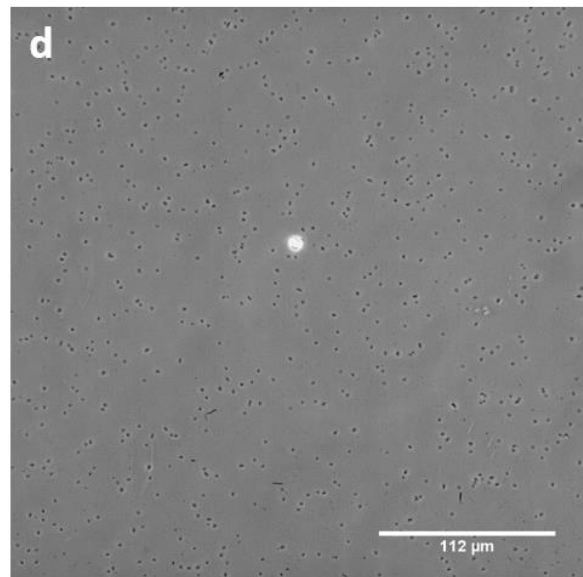
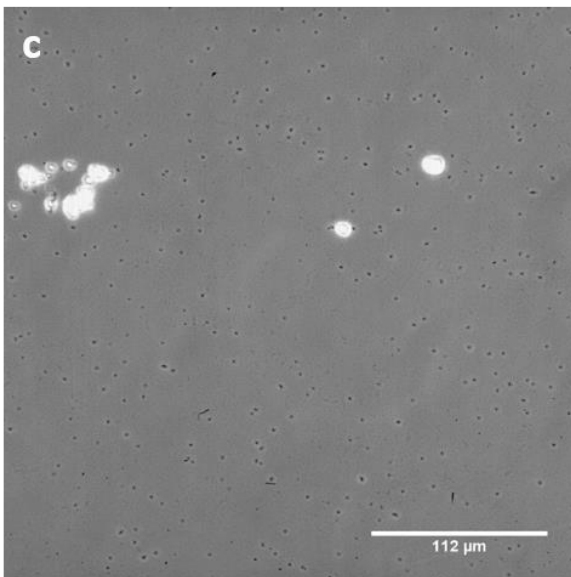
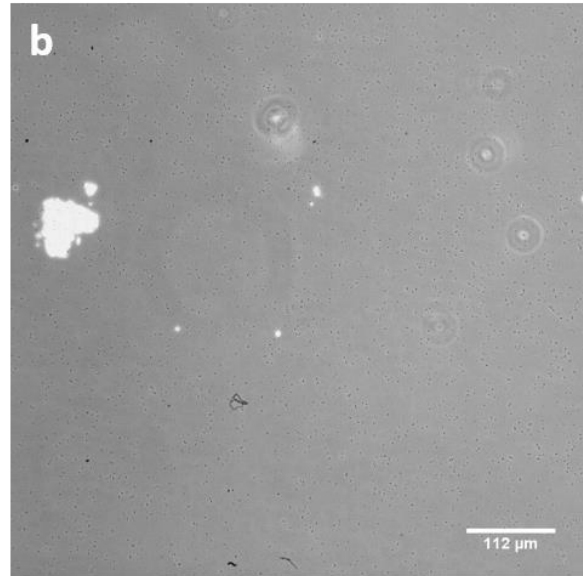
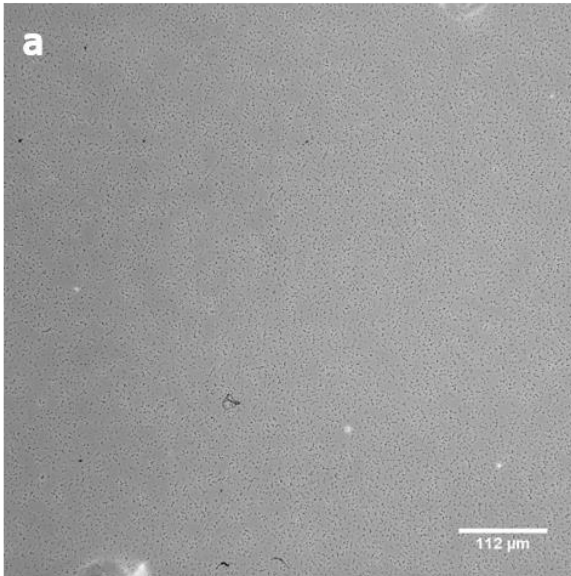
Note, five microscopy images were taken of each active sample and vortex control, at both x 20 and x 40 magnification, all images were analysed to check for sampling bias and one image was selected in included in the below appendix

*BW25113 alone, starting OD<sub>600</sub> = 0.5. a) active sample taken at x 20 magnification, b) vortexed control taken at x 20 magnification, c) active sample taken at x 40 magnification, d) vortexed control taken at x 40 magnification*



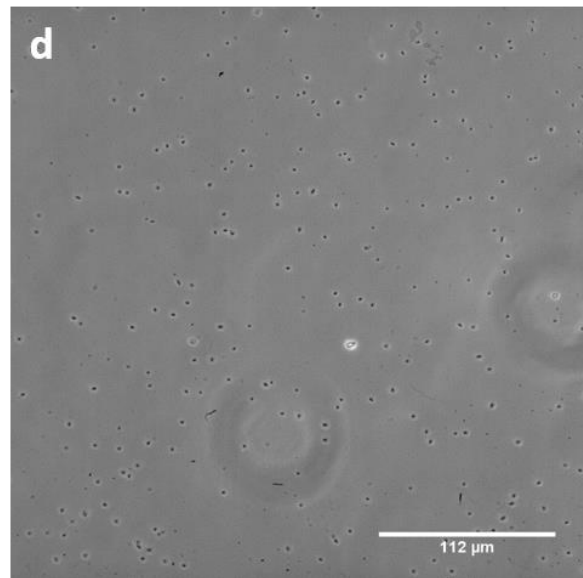
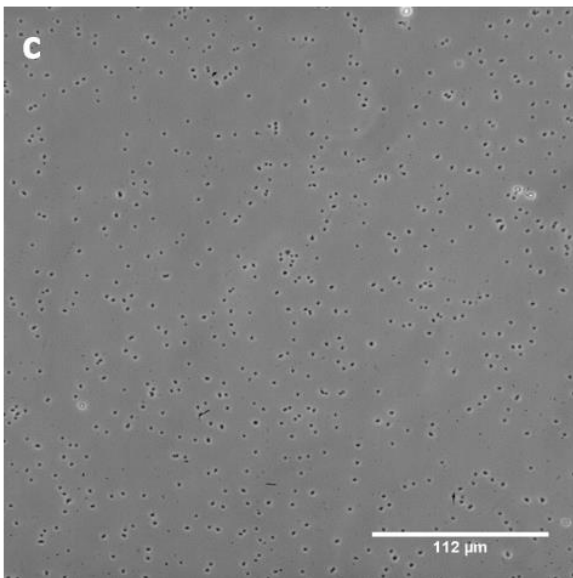
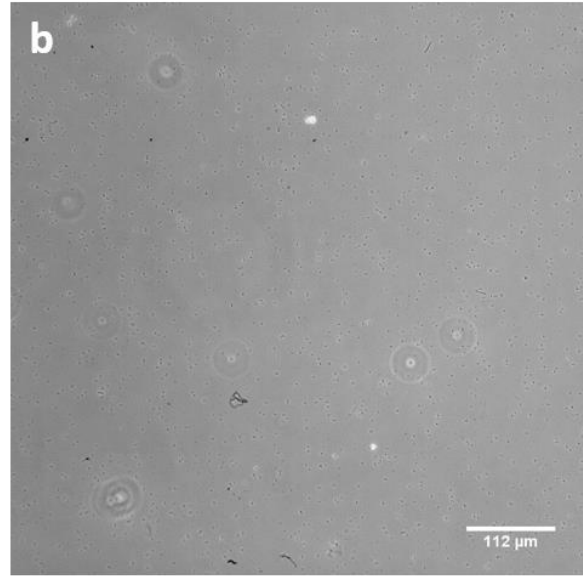
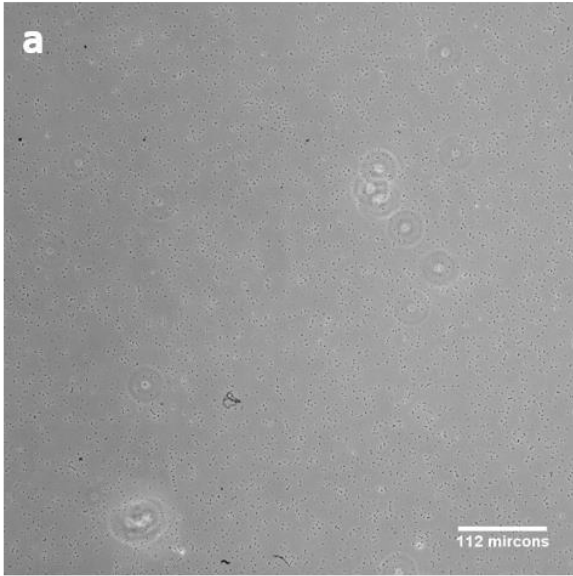
## Appendix

*BW25113* with incubated with  $1 \mu\text{M}$  of mannose-based inhibitor linked  $(\text{Gly-Ser})_6$  colicin E9 conjugate, starting  $\text{OD}_{600} = 0.5$ . a) active sample taken at x 20 magnification, b) vortexed control taken at x 20 magnification, c) active sample taken at x 40 magnification, d) vortexed control taken at x 40 magnification



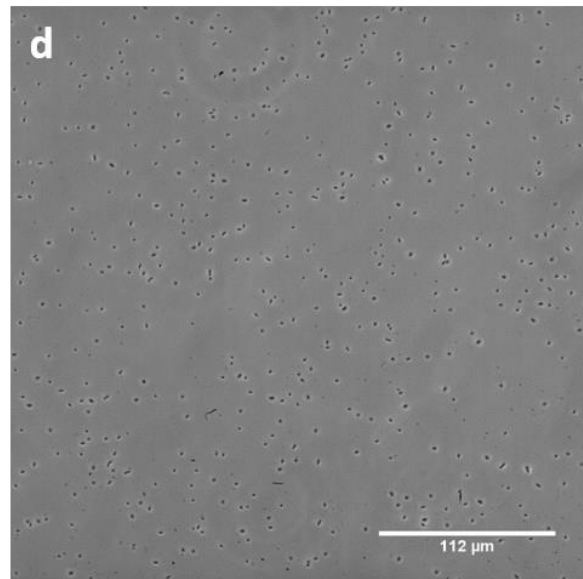
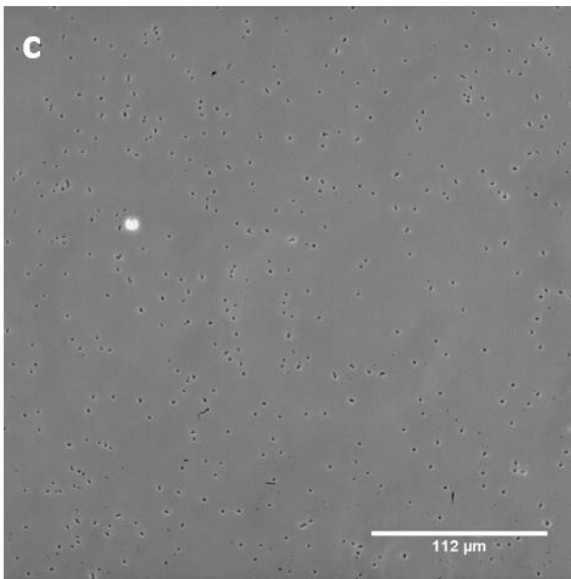
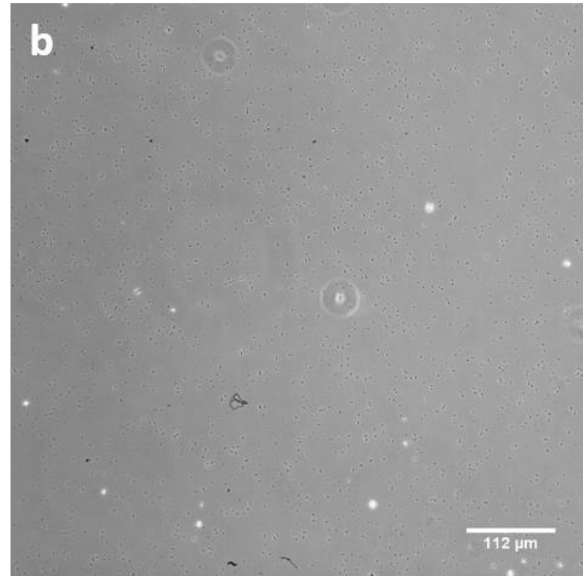
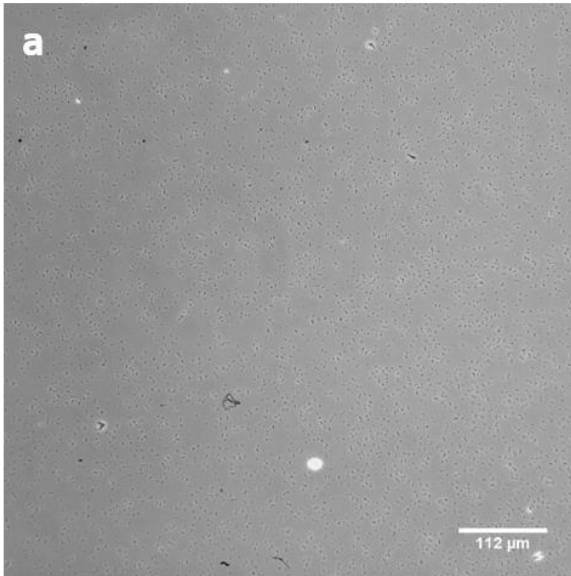
## Appendix

*JW4283* alone, starting  $OD_{600} = 0.5$ . a) active sample taken at x 20 magnification, b) vortexed control taken at x 20 magnification, c) active sample taken at x 40 magnification, d) vortexed control taken at x 40 magnification



## Appendix

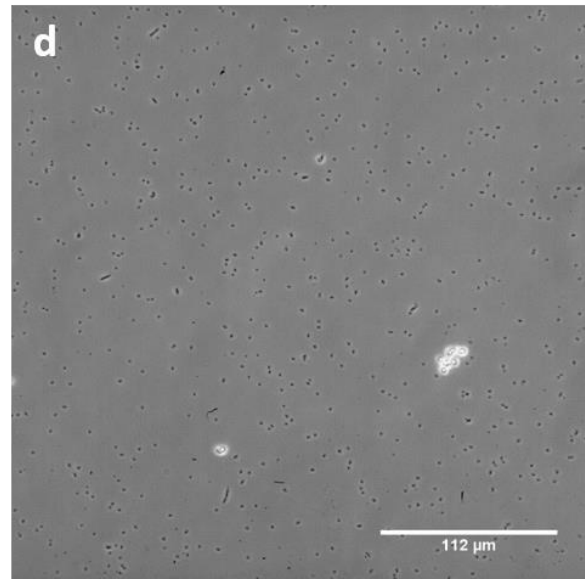
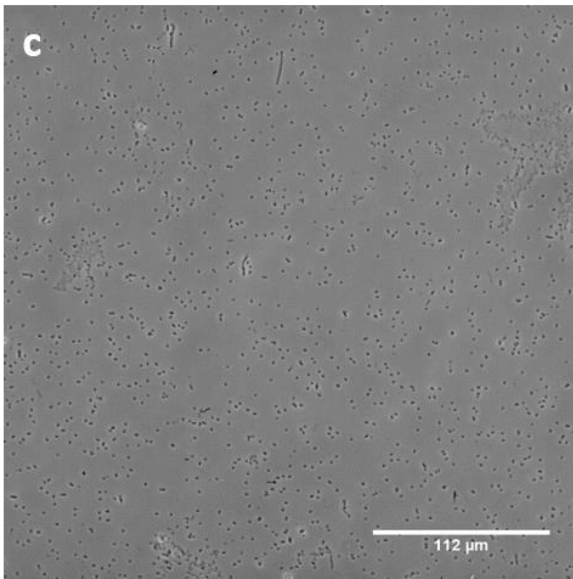
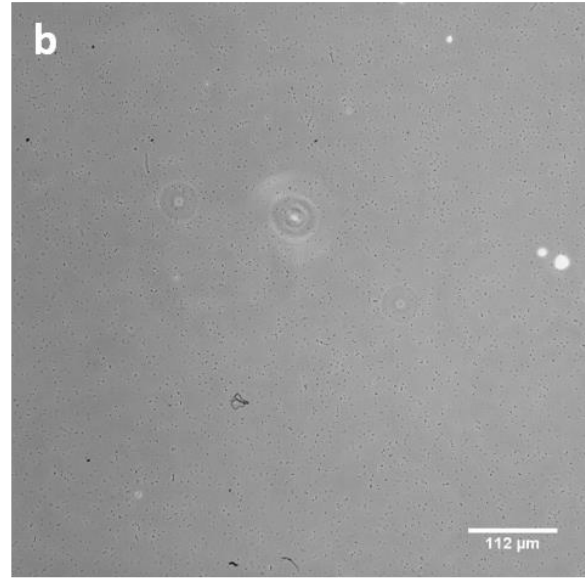
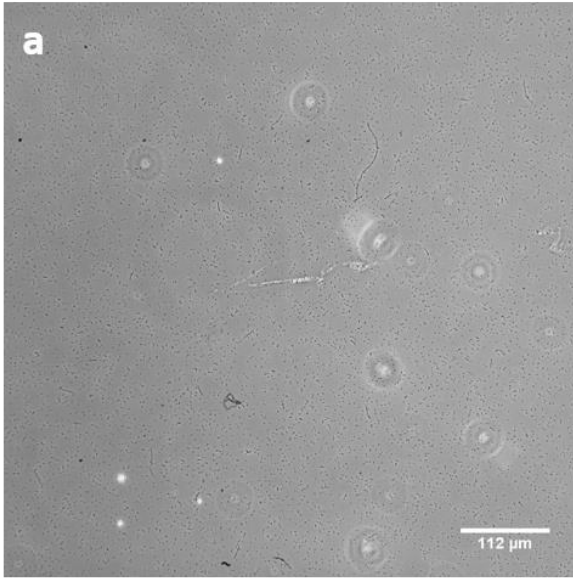
*JW4283* incubated with 1  $\mu\text{M}$  of mannose-based inhibitor linked (Gly-Ser)<sub>6</sub> colicin E9 conjugate, starting  $\text{OD}_{600} = 0.5$ . a) active sample taken at x 20 magnification, b) vortexed control taken at x 20 magnification, c) active sample taken at x 40 magnification, d) vortexed control taken at x 40 magnification





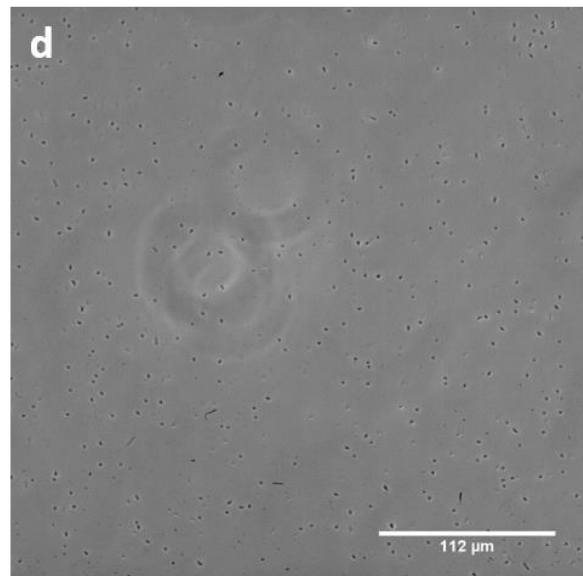
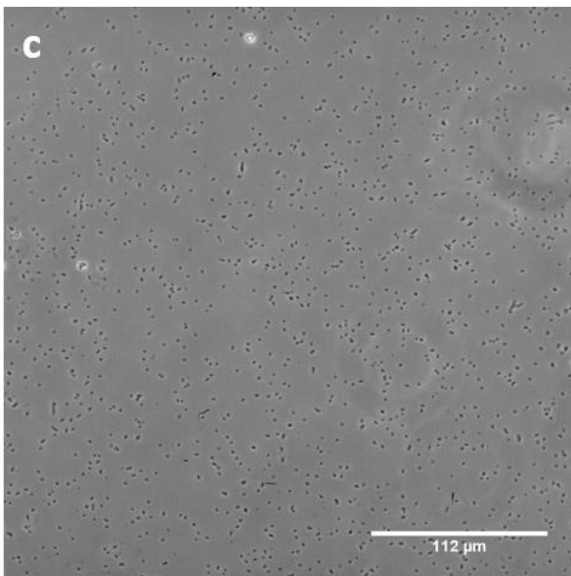
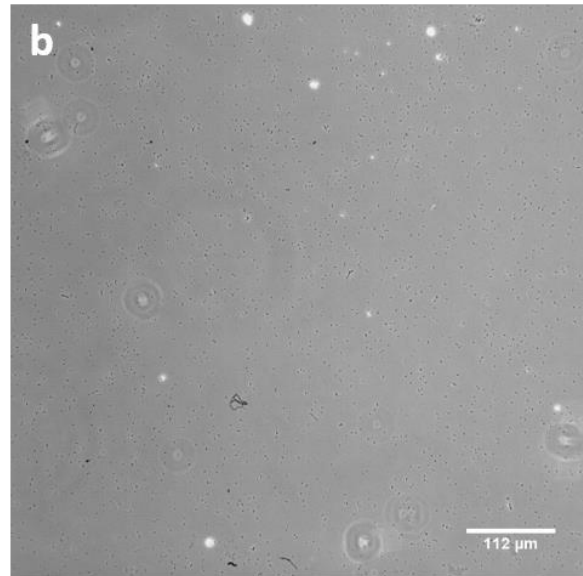
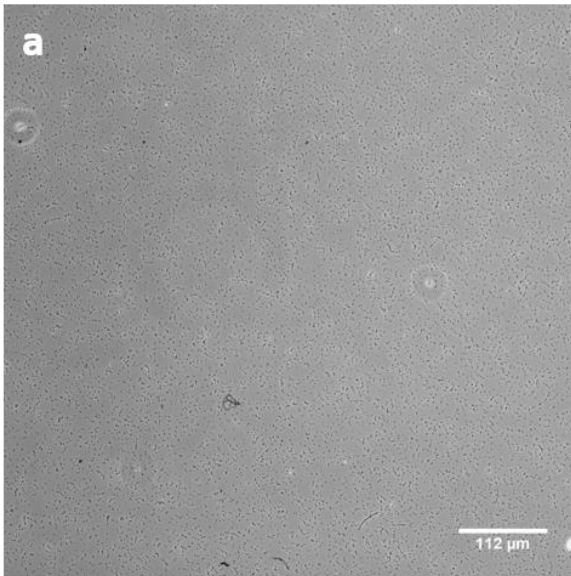
## Appendix

*RK5016 alone, starting  $OD_{600} = 0.5$ . a) active sample taken at x 20 magnification, b) vortexed control taken at x 20 magnification, c) active sample taken at x 40 magnification, d) vortexed control taken at x 40 magnification*



## Appendix

*RK5016* incubated with  $1\ \mu\text{M}$  of mannose-based inhibitor linked  $(\text{Gly-Ser})_6$  colicin E9 conjugate, starting  $\text{OD}_{600} = 0.5$ . a) active sample taken at x 20 magnification, b) vortexed control taken at x 20 magnification, c) active sample taken at x 40 magnification, d) vortexed control taken at x 40 magnification

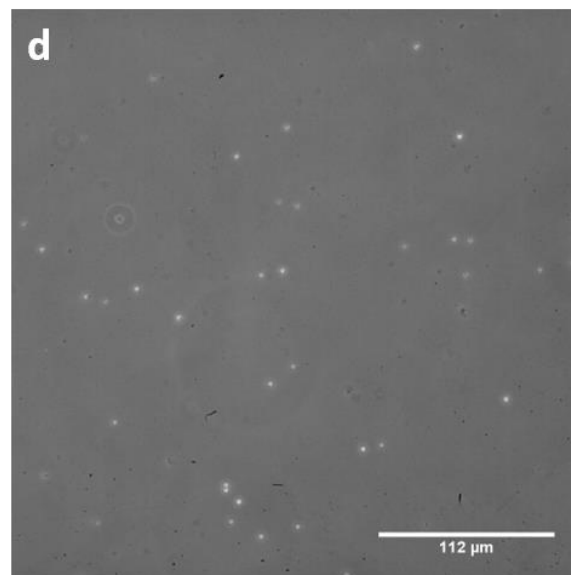
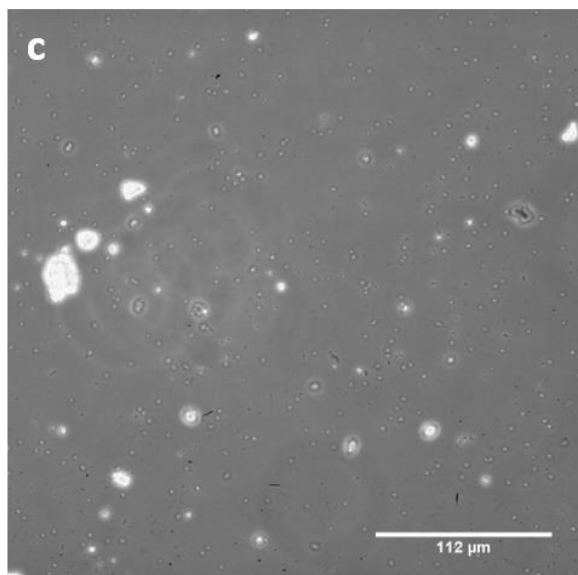
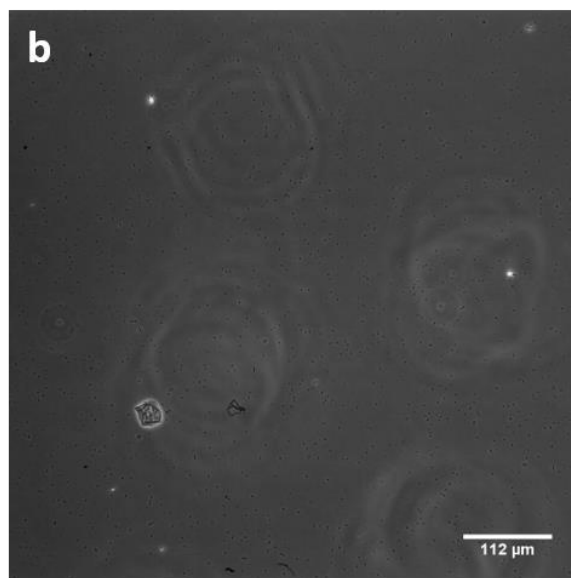
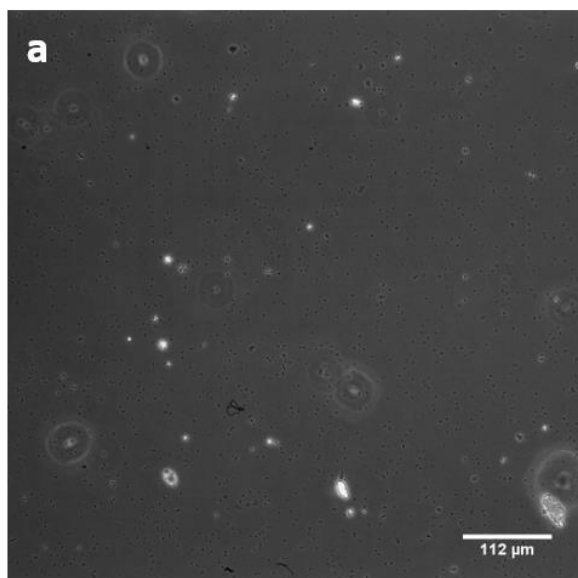


## Appendix

### 9.3.6 Result of experiment eight, microscopy images of samples used in the positive control screen

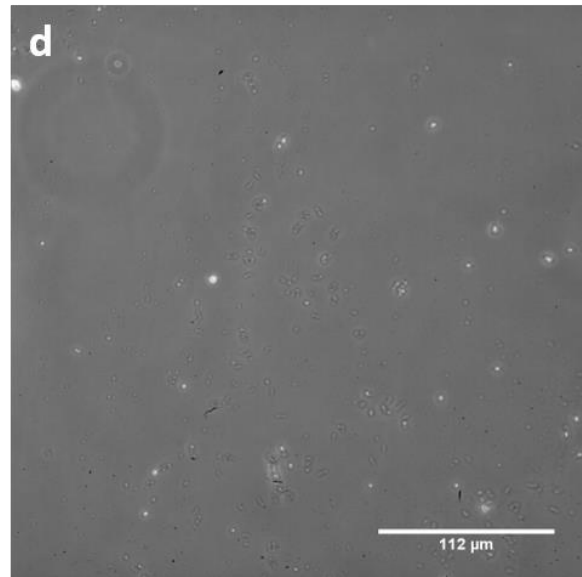
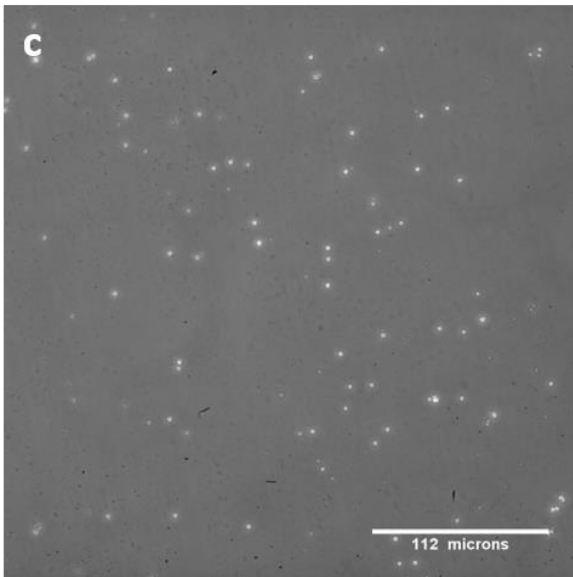
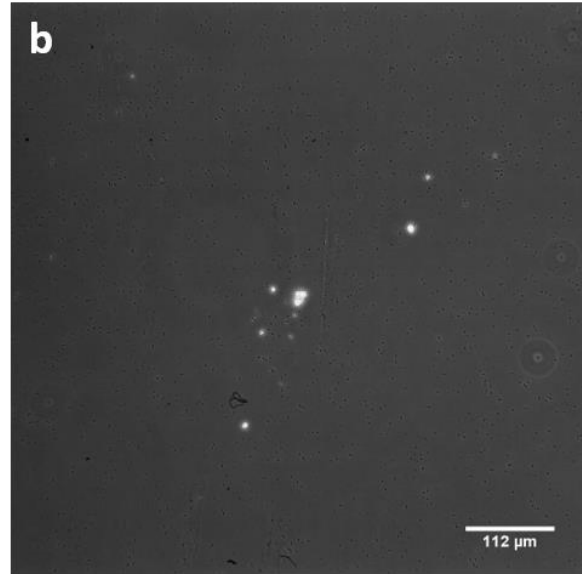
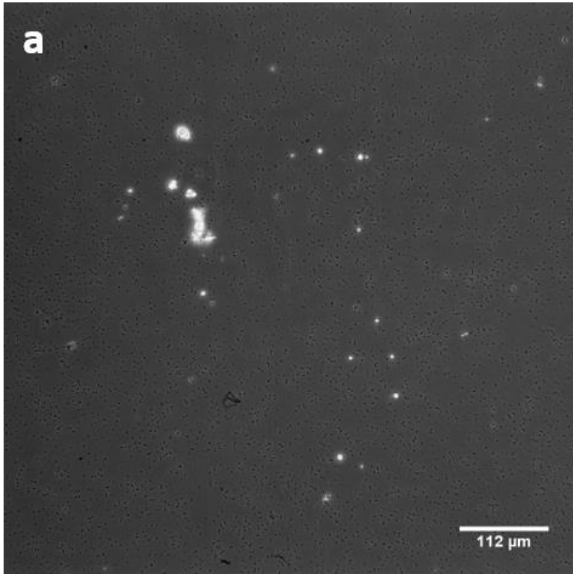
Note, five microscopy images were taken of each active sample and vortex control at both x 20 and x 40 magnification, all images were analysed to check for sampling bias and one image was selected in included in the appendix below

*BW25113 only, starting  $OD_{600}$  0.5. a) active sample taken at x 20 magnification, b) vortexed control taken at x 20 magnification, c) active sample taken at x 40 magnification, d) vortexed control taken at x 40 magnification*



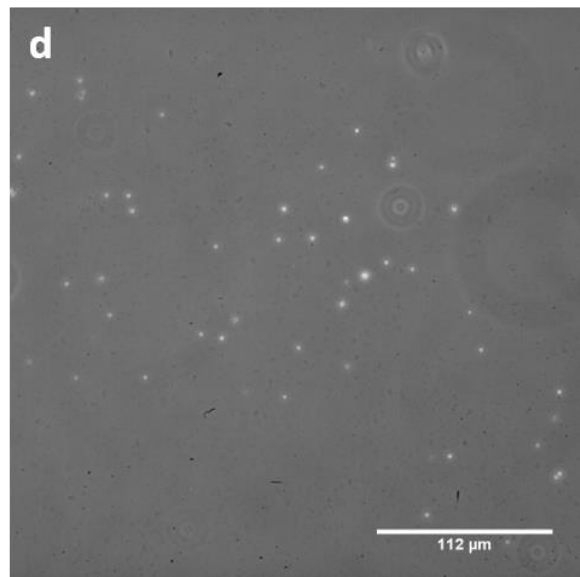
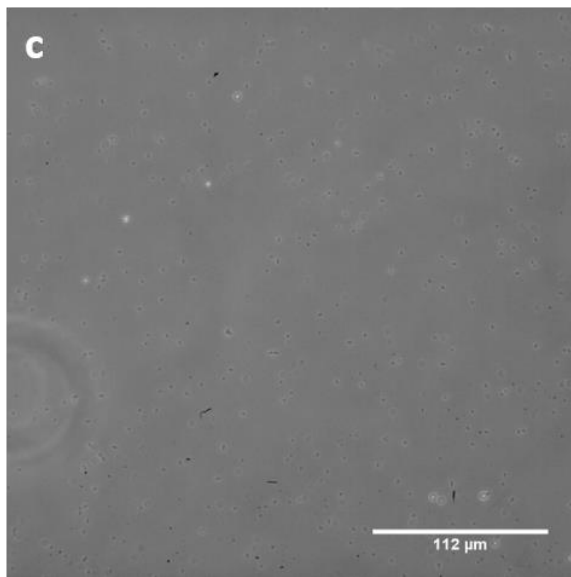
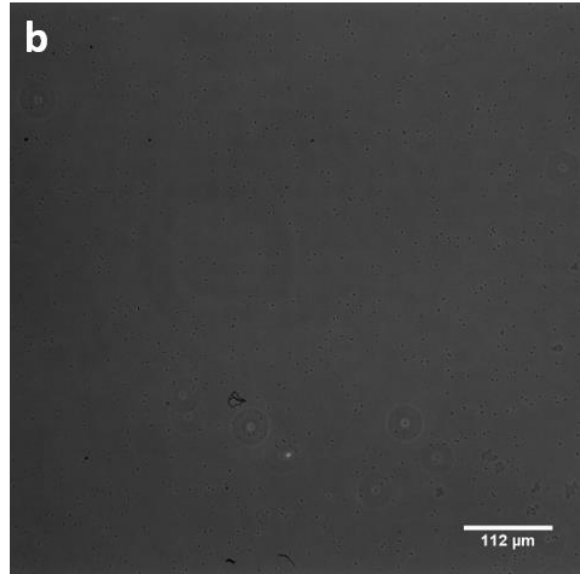
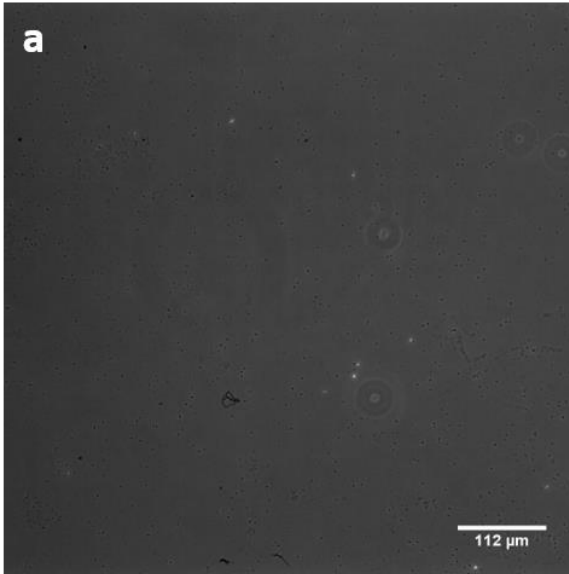
## Appendix

*BW25113* incubated with 10 nM biotin linked colicin E9 conjugate and 2 nM NeutrAvidin, starting  $OD_{600} 0.5$ . a) active sample taken at x 20 magnification, b) vortexed control taken at x 20 magnification, c) active sample taken at x 40 magnification, d) vortexed control taken at x 40 magnification



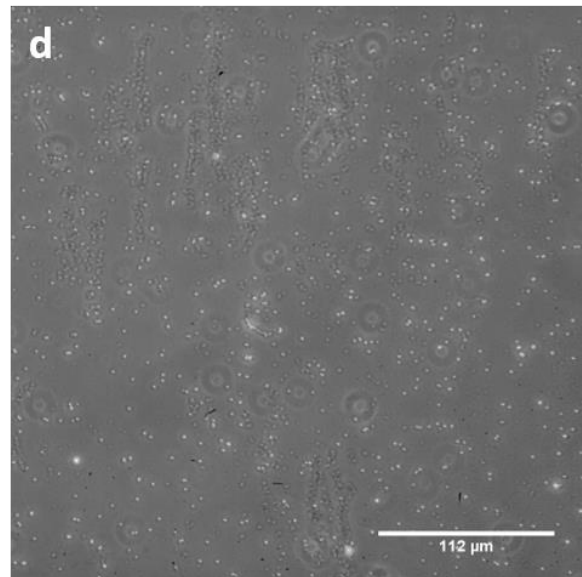
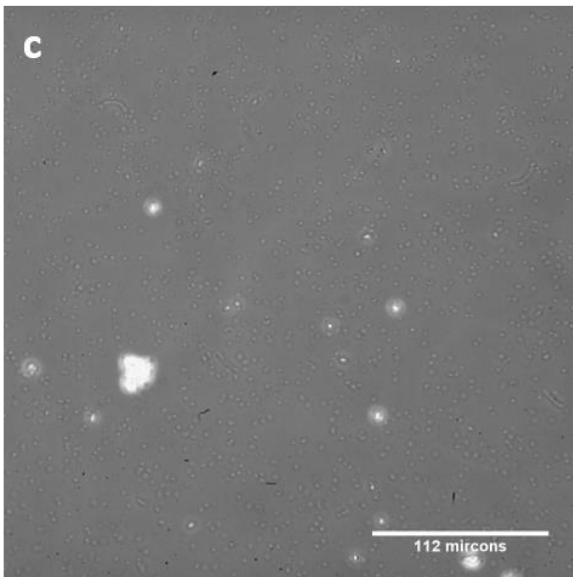
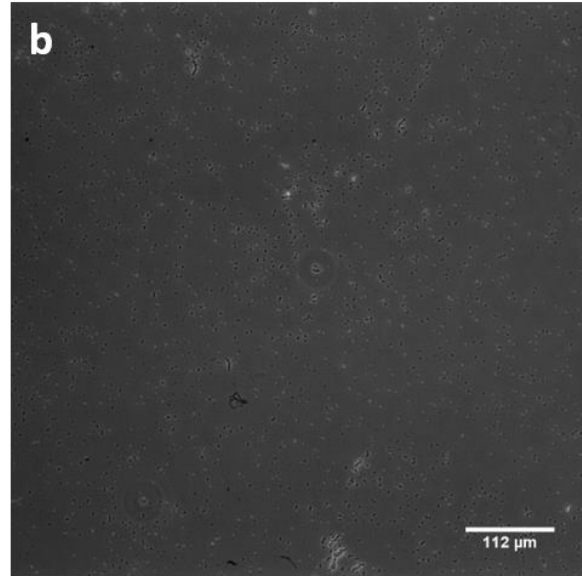
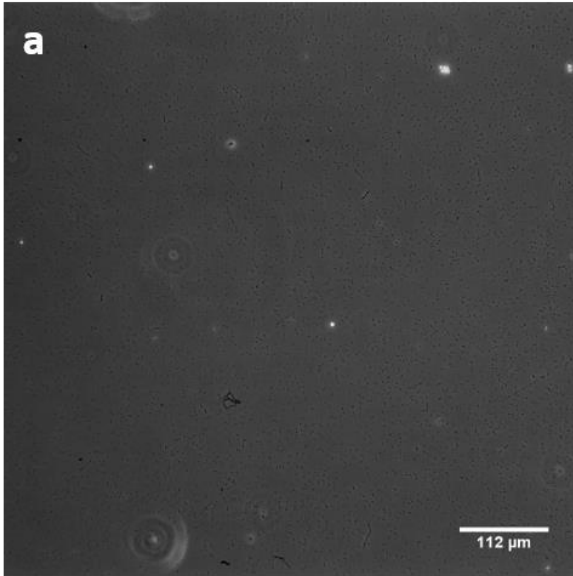
## Appendix

*BW25113* incubated with 2 nM NeutrAvidin, starting  $OD_{600}$  0.5. a) active sample taken at x 20 magnification, b) vortexed control taken at x 20 magnification, c) active sample taken at x 40 magnification, d) vortexed control taken at x 40 magnification



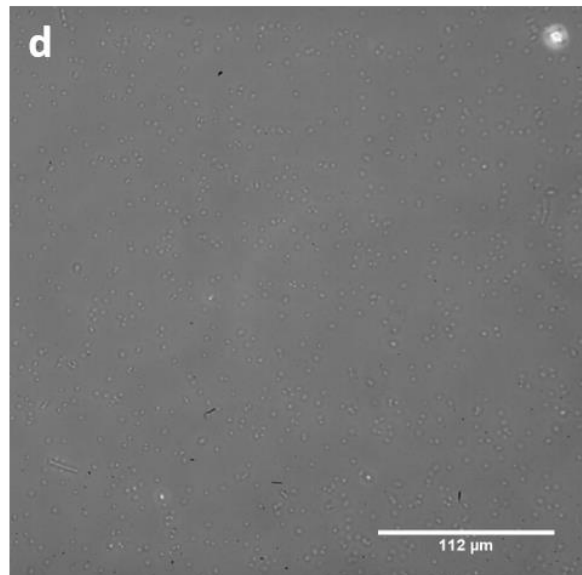
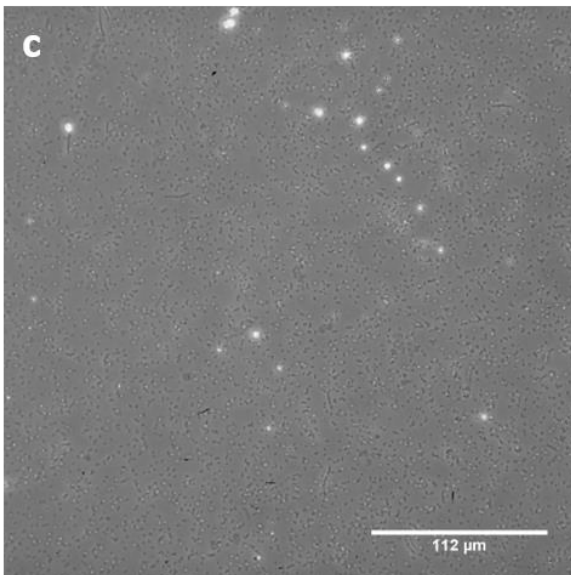
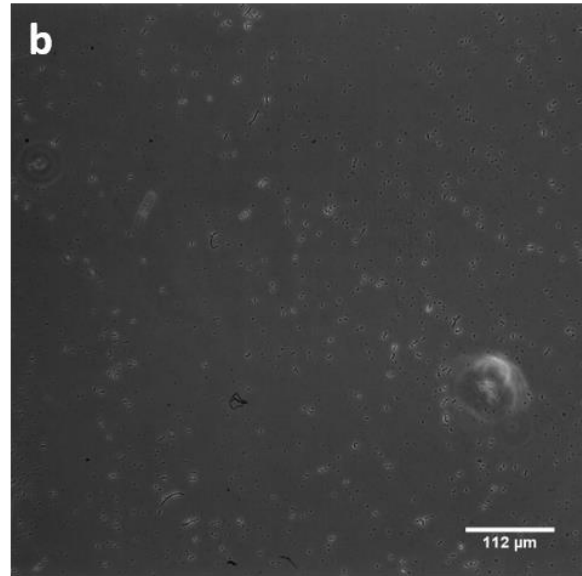
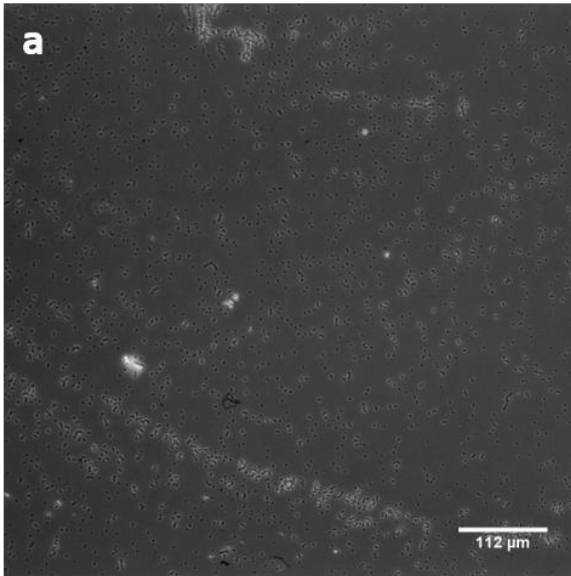
## Appendix

*RK5016 only, Starting  $OD_{600}$  0.5. a) active sample taken at x 20 magnification, b) vortexed control taken at x 20 magnification, c) active sample taken at x 40 magnification, d) vortexed control taken at x 40 magnification*



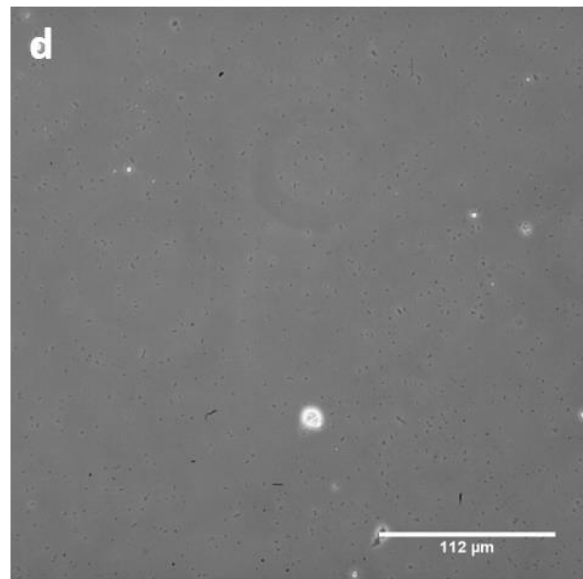
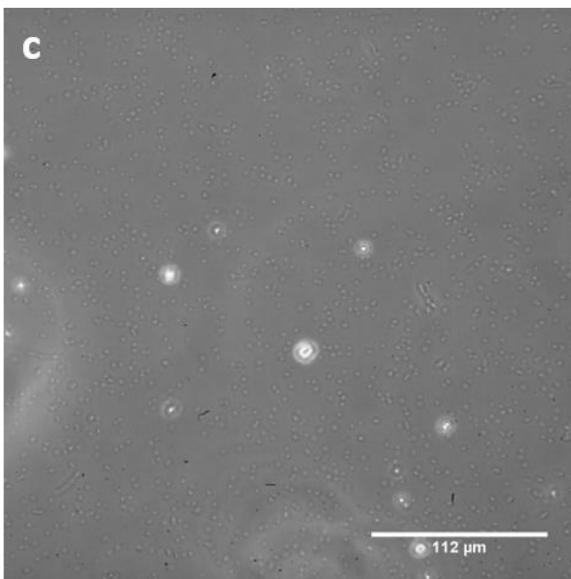
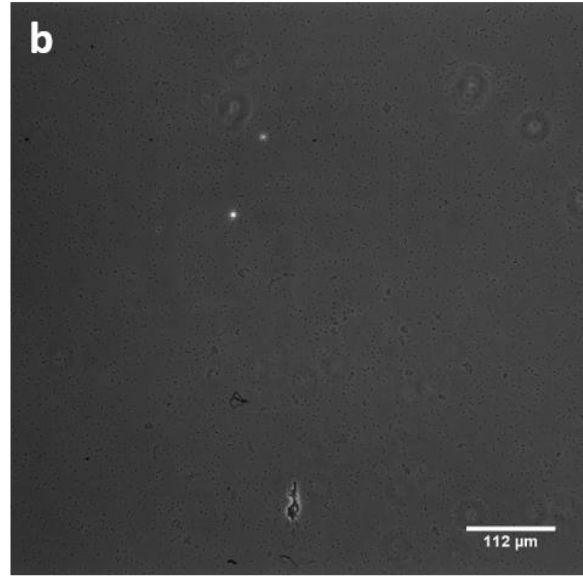
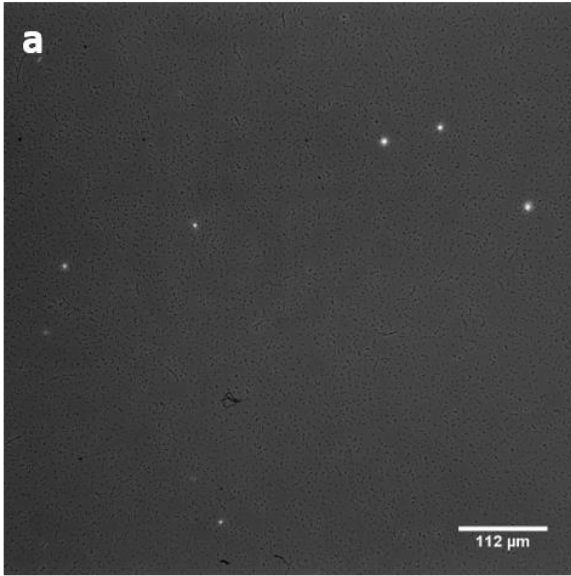
## Appendix

*RK5016 incubated with 10 nM biotin linked colicin E9 conjugate and 2 nM NeutrAvidin, starting  $OD_{600}$  0.5. a) active sample taken at x 20 magnification, b) vortexed control taken at x 20 magnification, c) active sample taken at x 40 magnification, d) vortexed control taken at x 40 magnification*



## Appendix

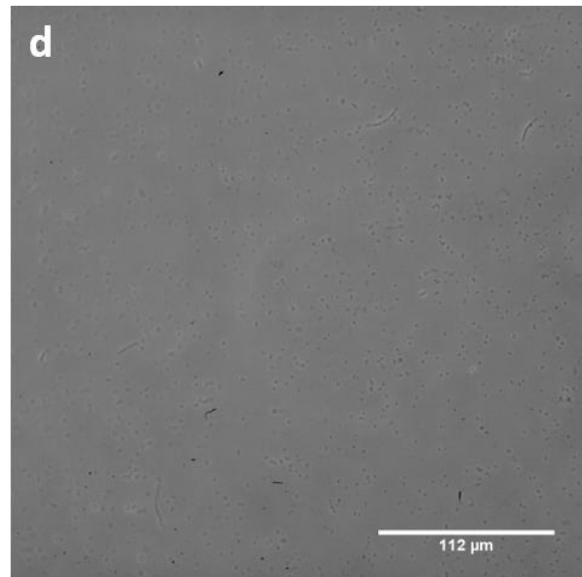
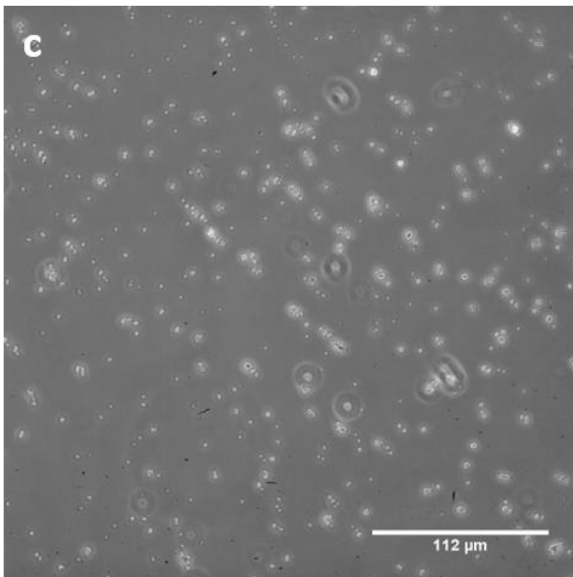
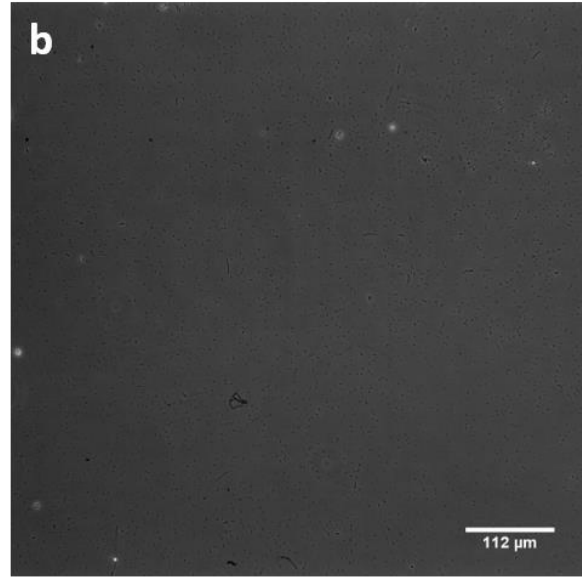
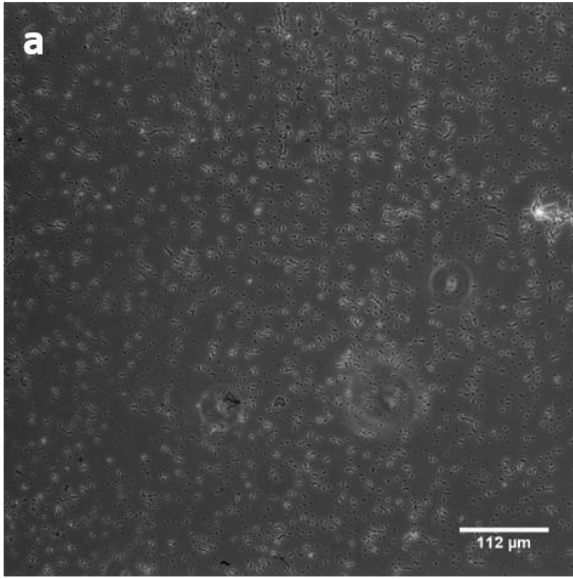
*RK5016 incubated with 10 nM biotin linked colicin E9 conjugate, starting OD<sub>600</sub> 0.5. a) active sample taken at x 20 magnification, b) vortexed control taken at x 20 magnification, c) active sample taken at x 40 magnification, d) vortexed control taken at x 40 magnification*





## Appendix

*RK5016 Incubated with 2 nM NeutrAvidin, starting  $OD_{600}$  0.5. a) active sample taken at x 20 magnification, b) vortexed control taken at x 20 magnification, c) active sample taken at x 40 magnification, d) vortexed control taken at x 40 magnification*

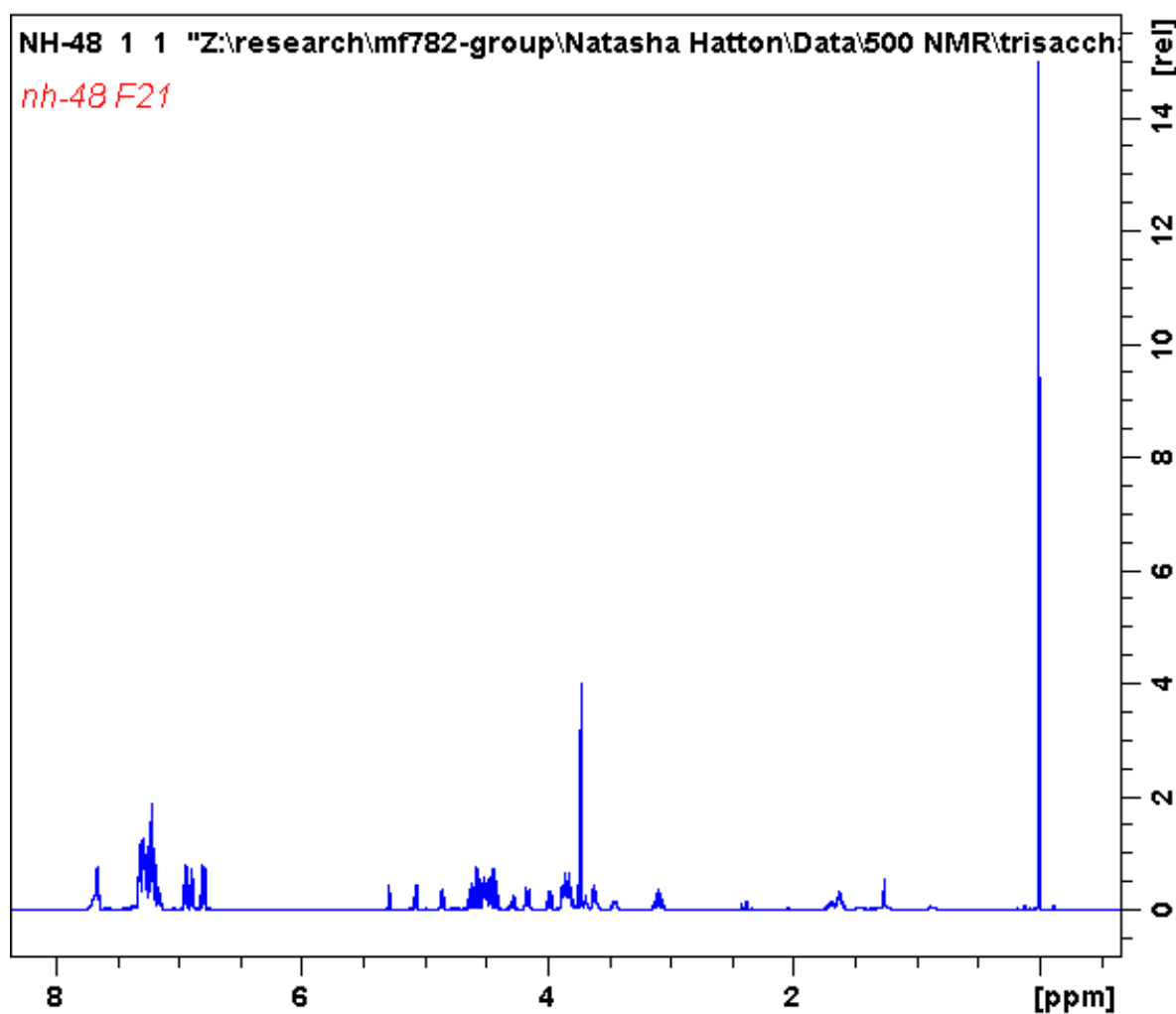
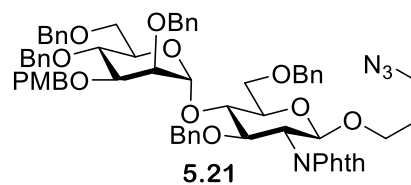


## Appendix

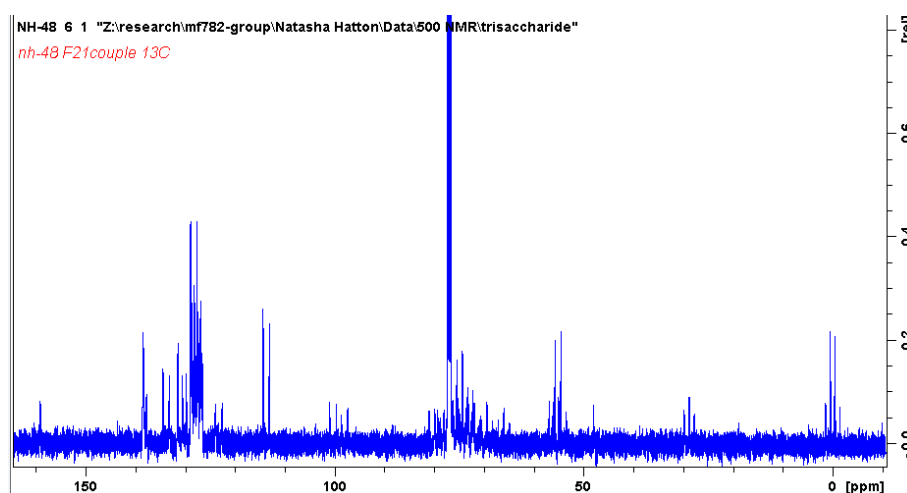
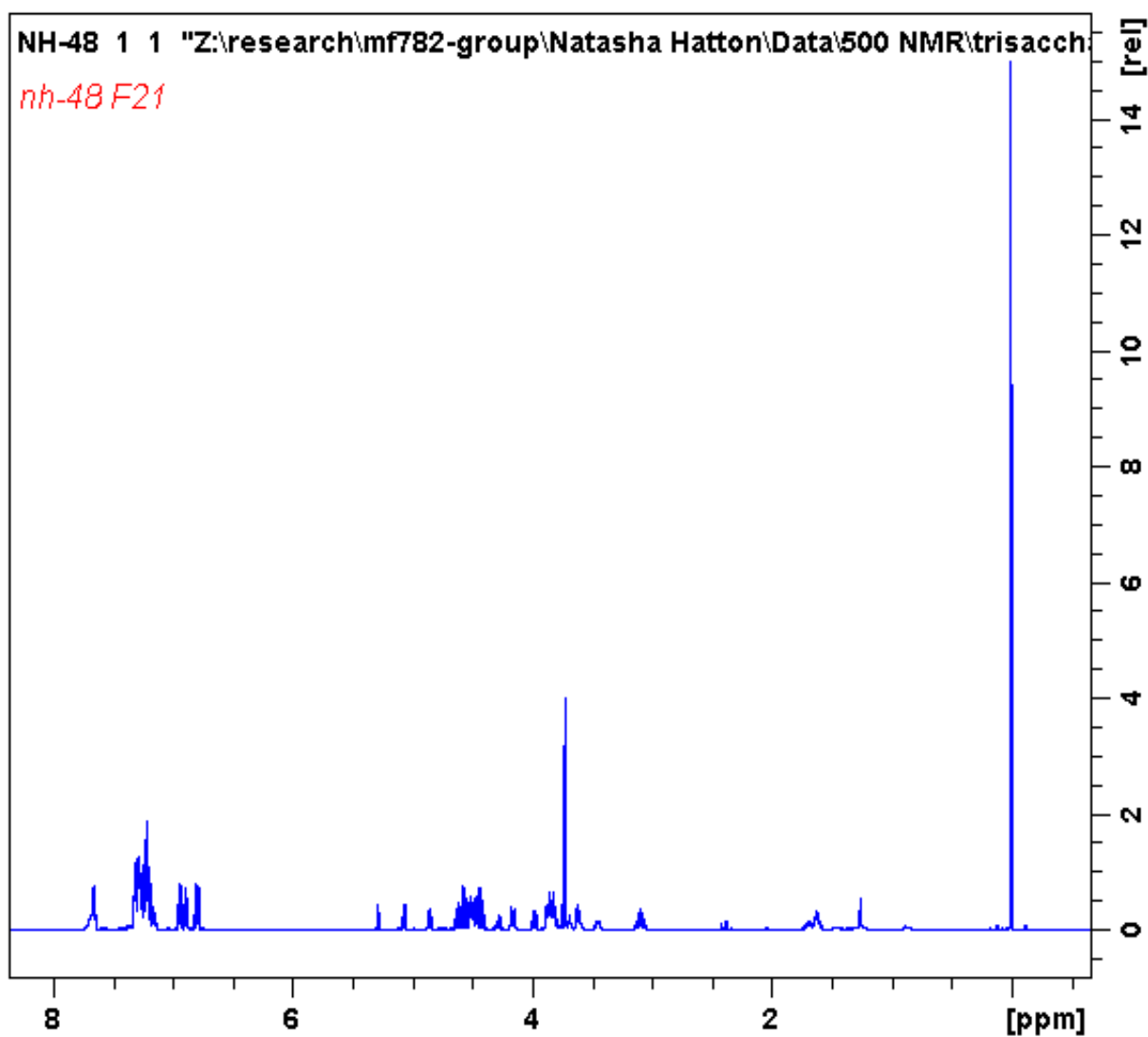
### 9.4 Appendix for Chapter 5

#### 9.4.1 Synthesis of $\beta$ -1,4-D-mannosyl-N-acetyl-D-glucosamine using chemical synthesis

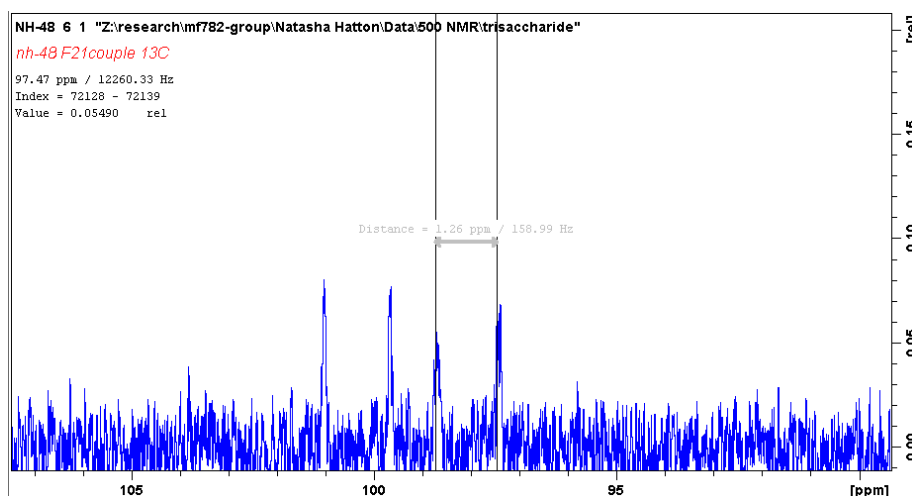
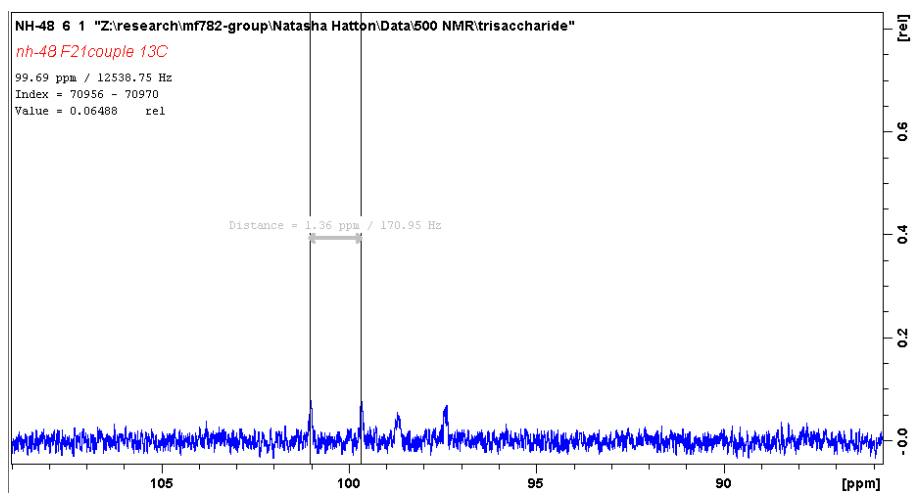
##### 9.4.1.1 2,4,6-O-benzyl-3-O-p-methoxybenzyl- $\alpha$ -D-mannopyranoside-(1 $\rightarrow$ 4) 3-Azidopropyl (3,6-di-O-benzyl-6-D-glucofuranoside) **5.21**



Appendix



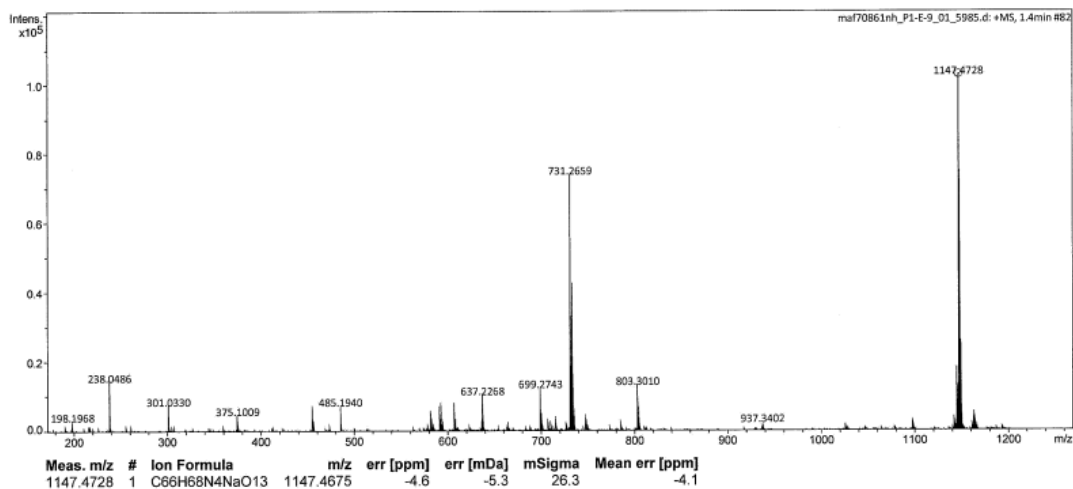
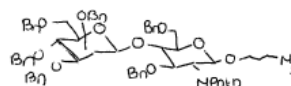
# Appendix



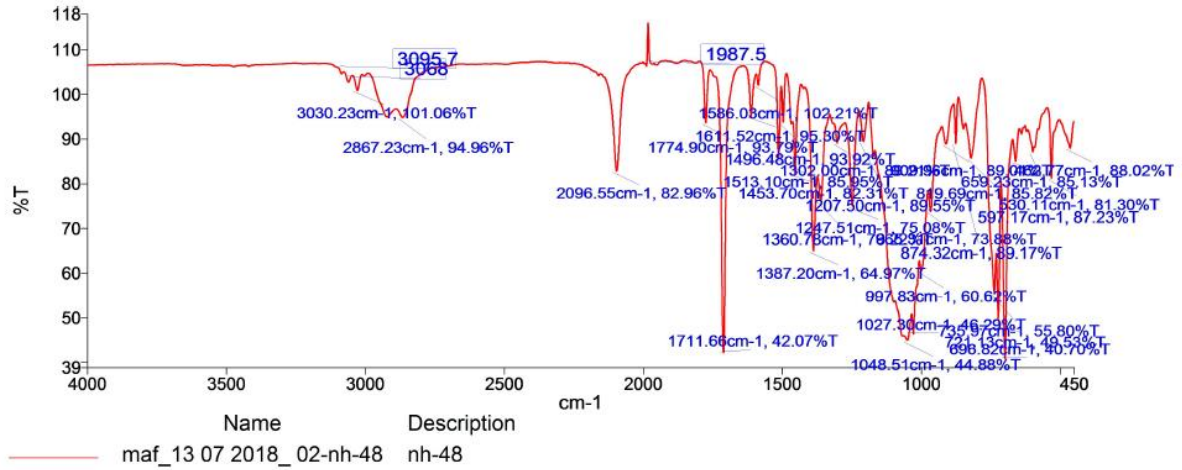
## York - Chemistry - Mass Spectrometry Service Report

*nh-48*

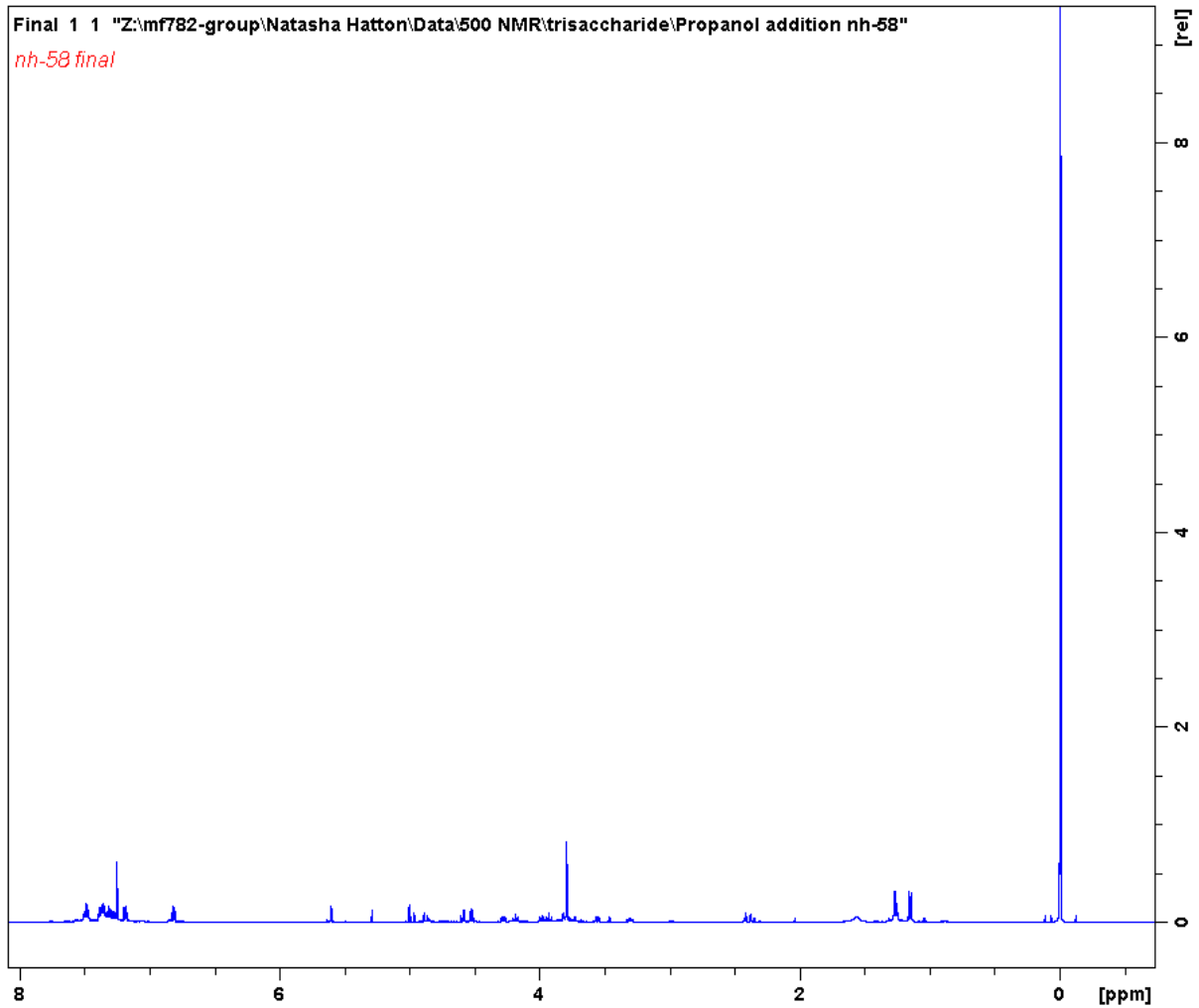
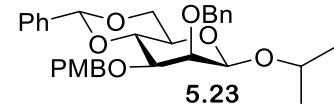
Analysis Information			
Analysis Filename	maf70861nh_P1-E-9_01_5985.d	Acquisition Date	21/06/2018 15:32:43
Method	ESI_low mass_2c1s.m	Instrument	compact
Submission Name	maf70861nh	ESI	Positive



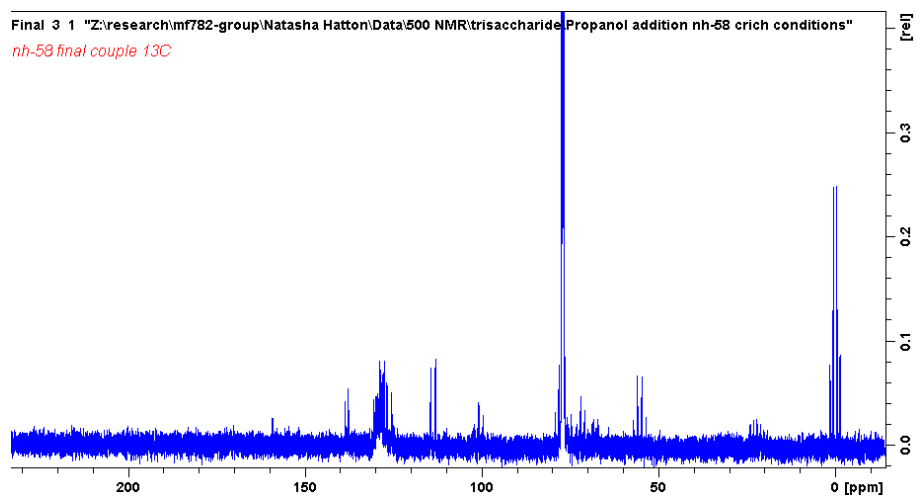
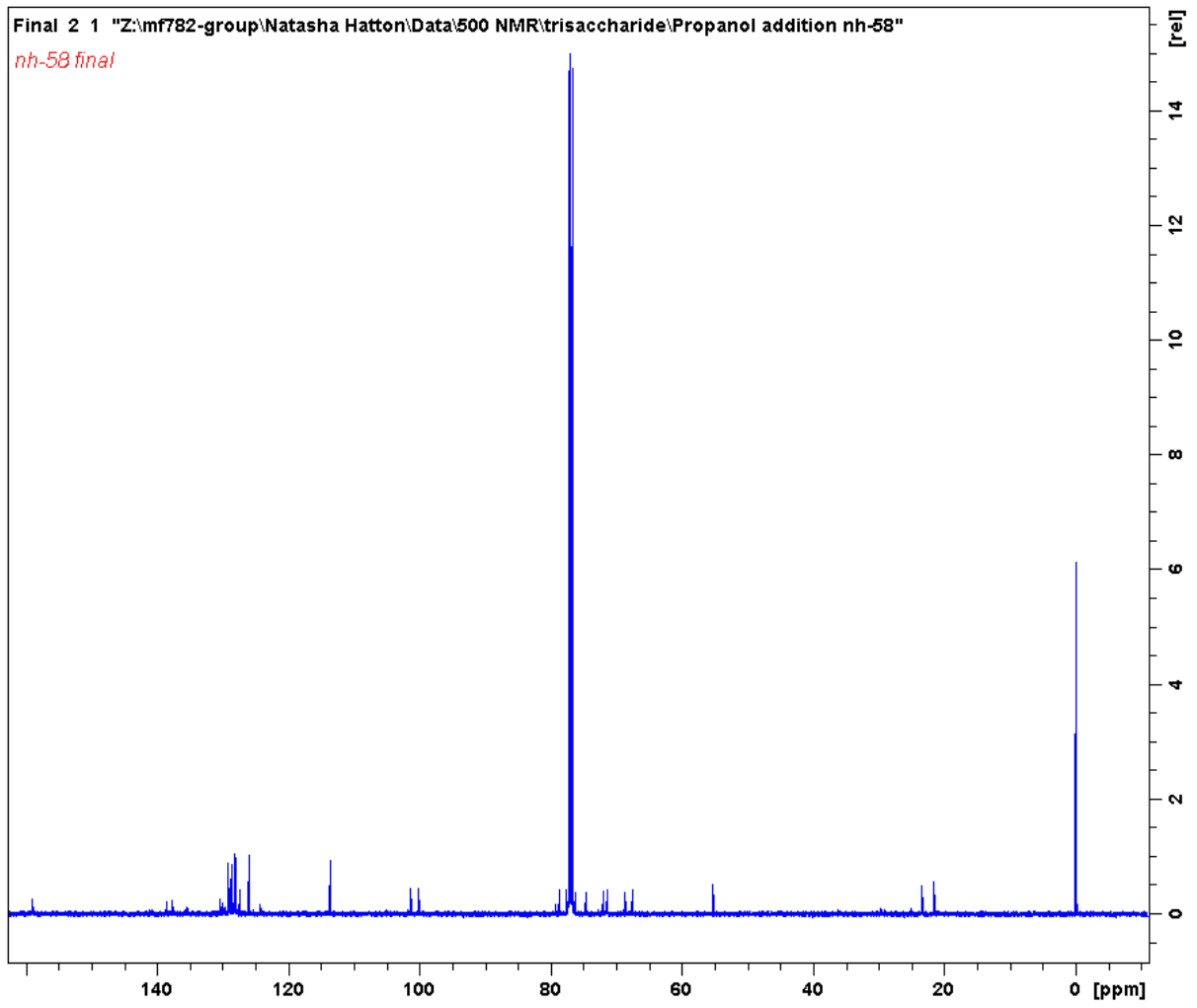
## Appendix



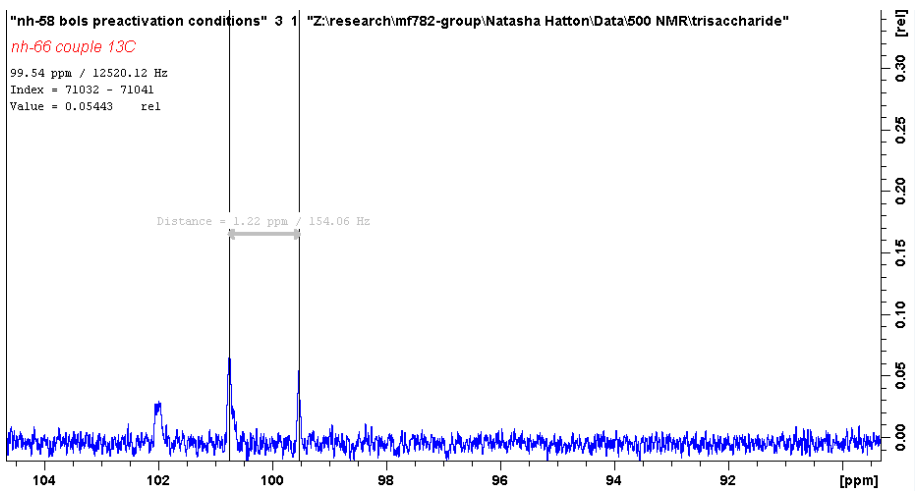
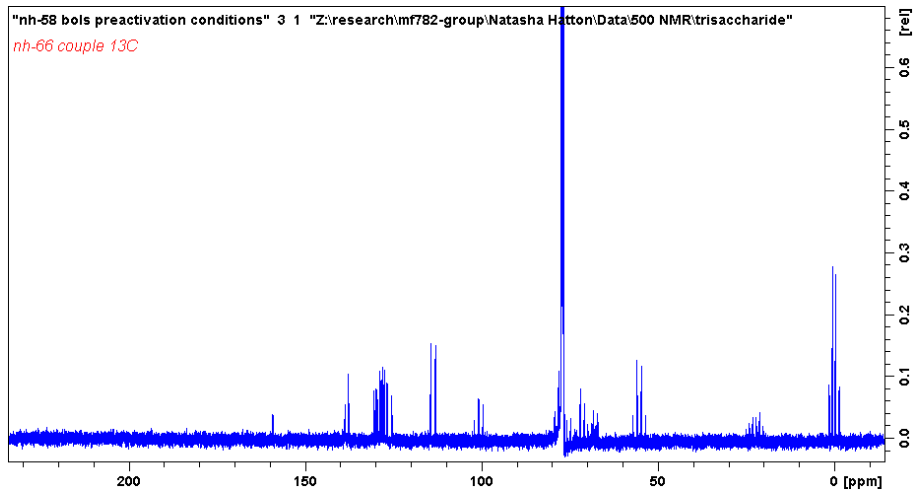
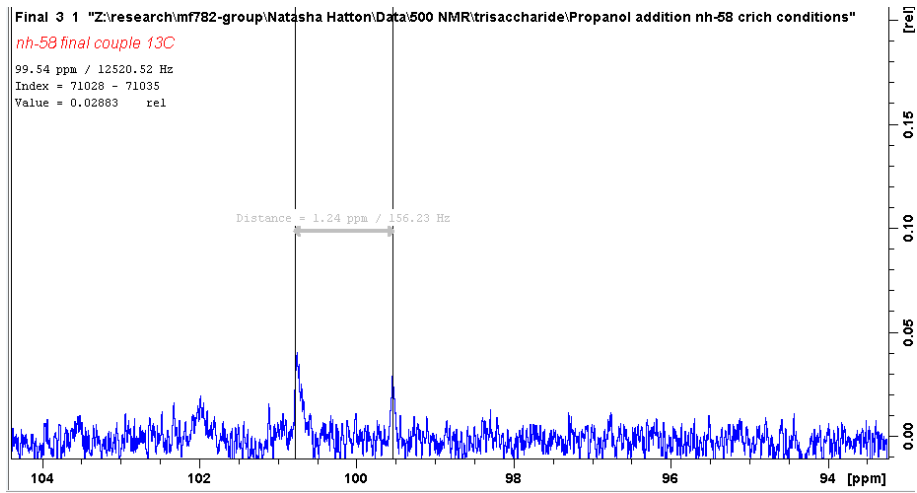
### 9.4.1.2 2-propanol 2-benzyl-4,6-O-benzylidene-3-O-p-methoxybenzyl- $\beta$ -D-mannopyranoside 5.23



Appendix

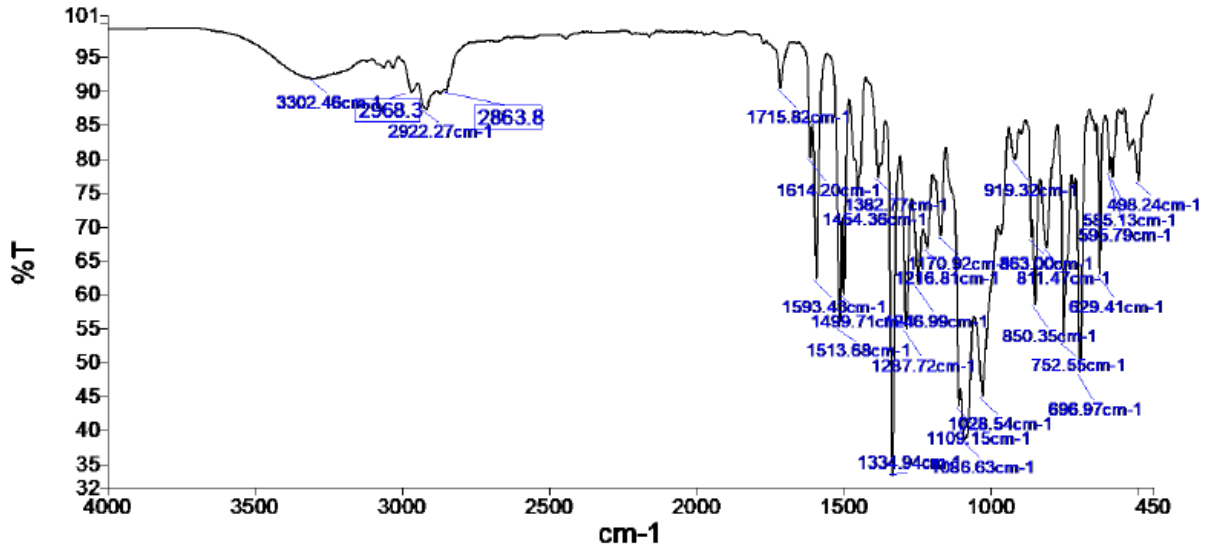
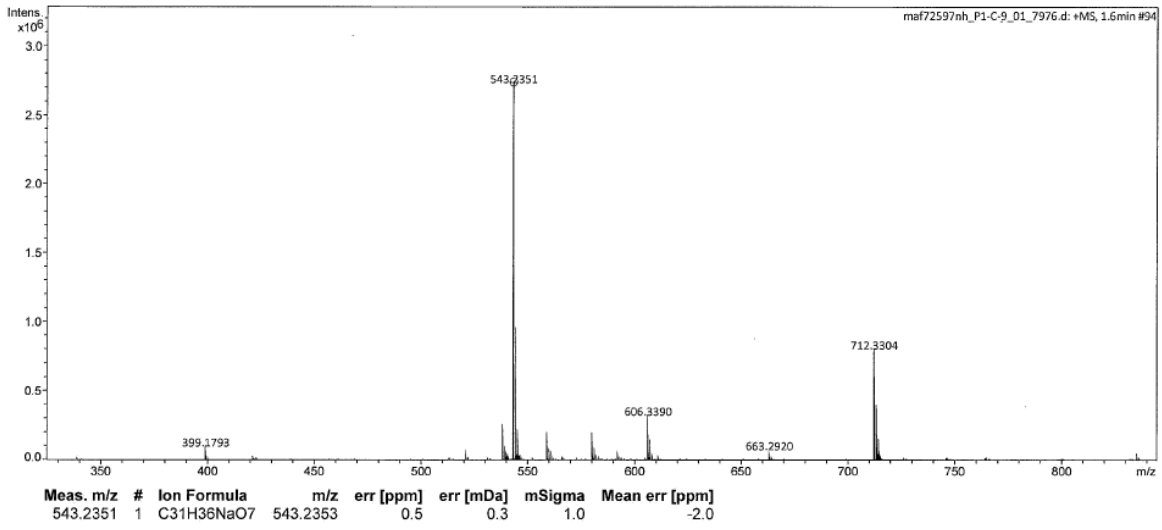


# Appendix



# Appendix

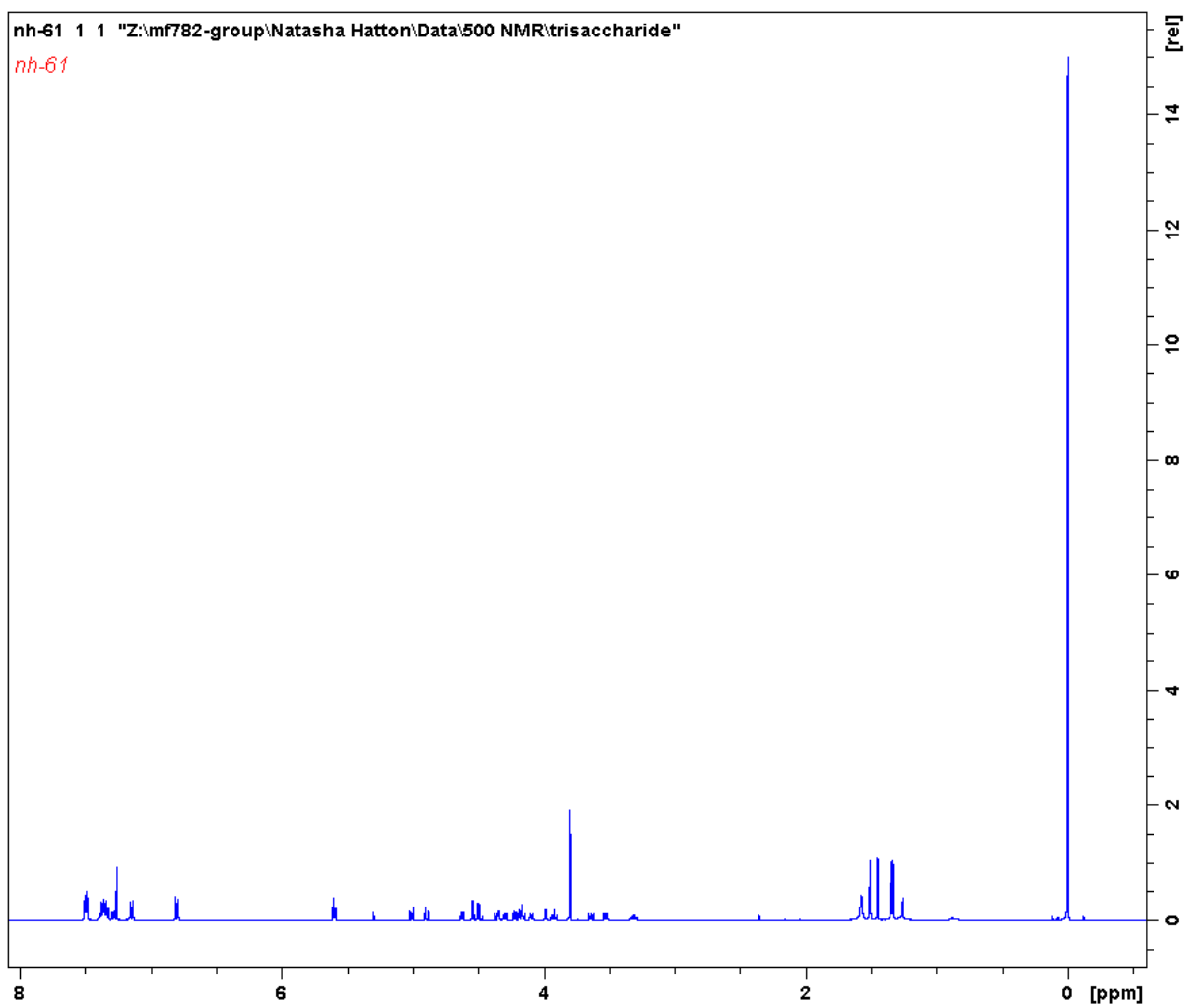
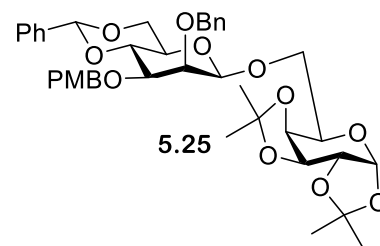
## Mass spectrum



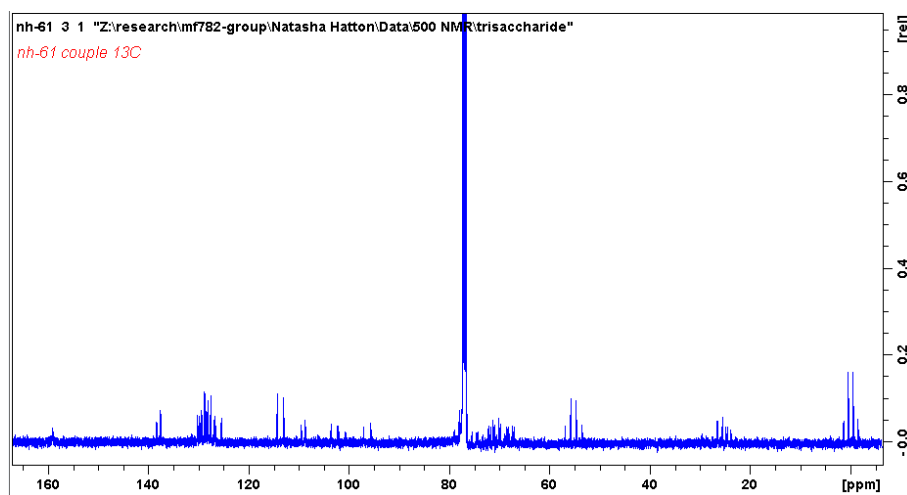
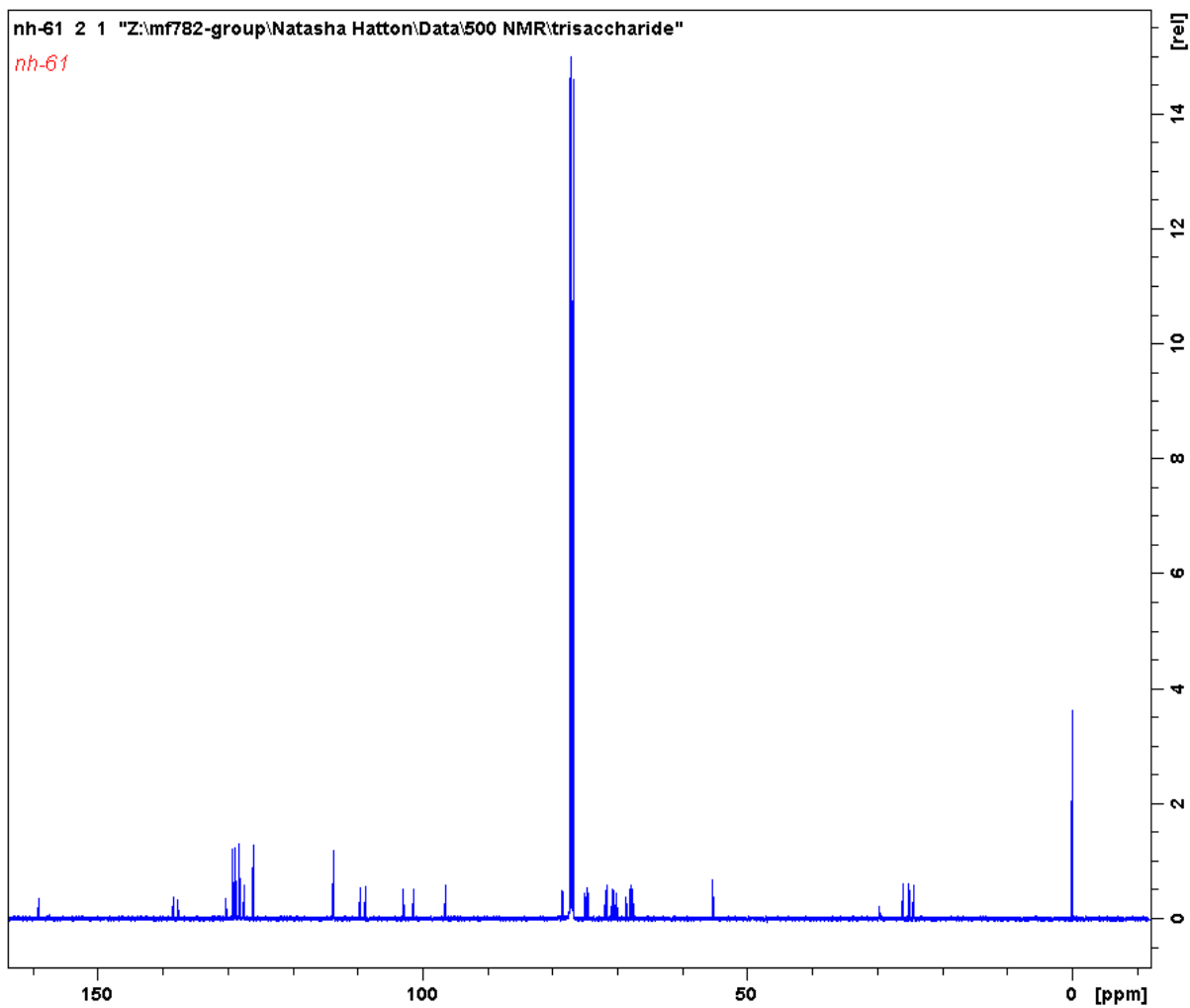


## Appendix

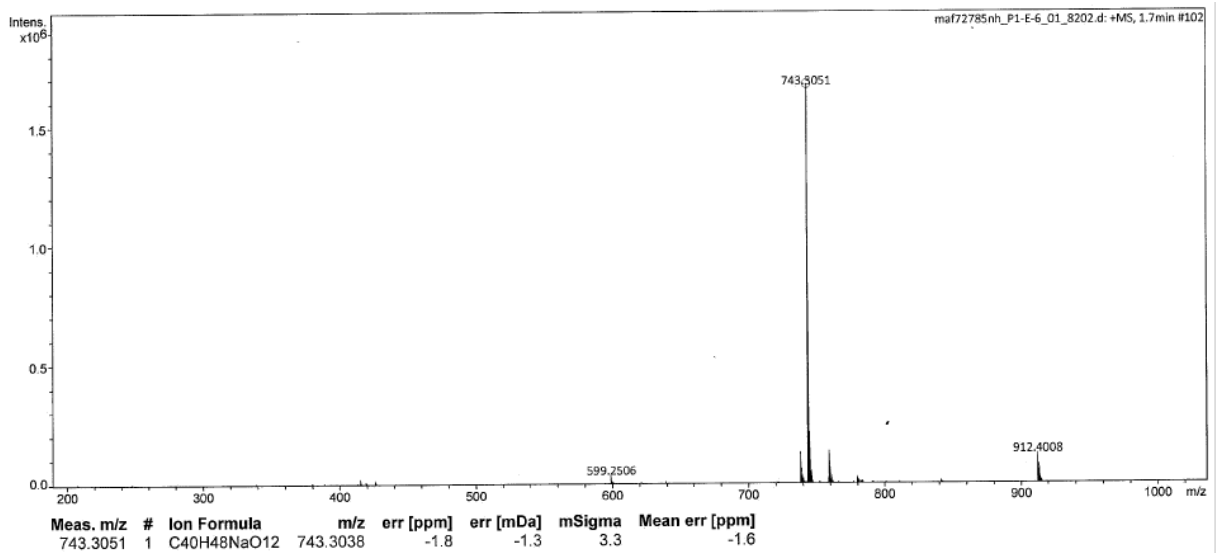
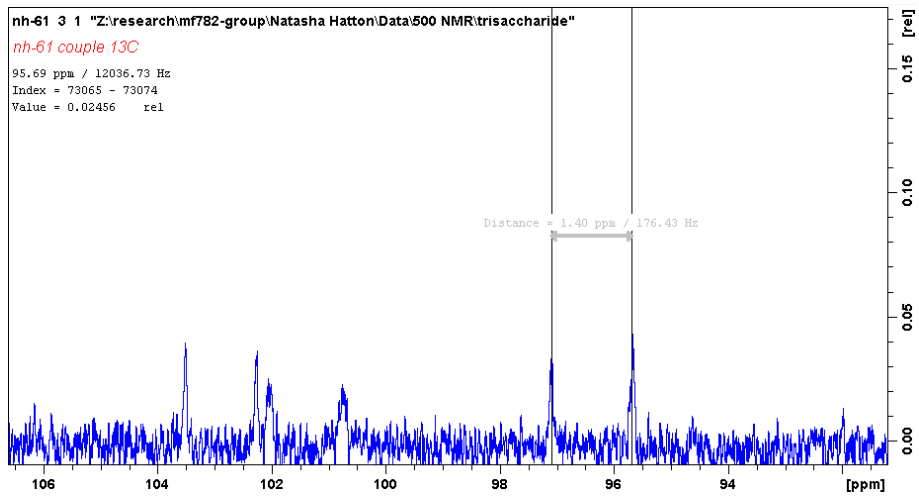
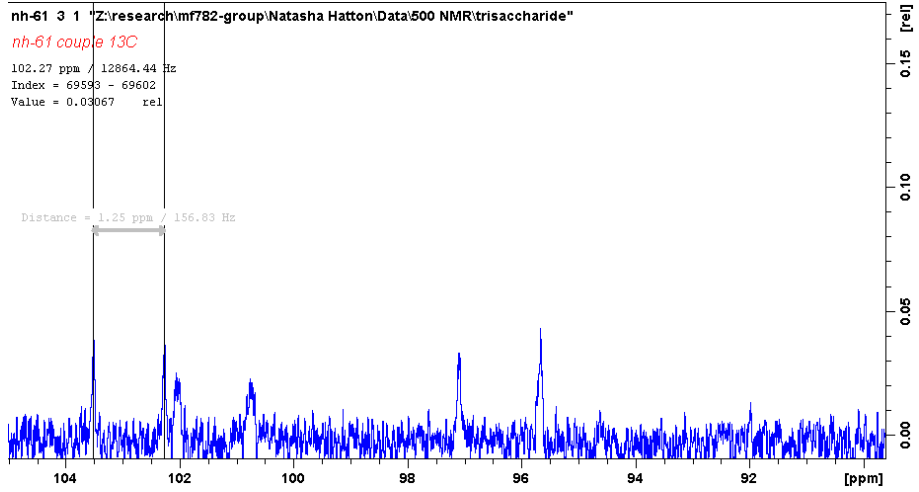
### 9.4.1.3 2-Benzyl-4,6-O-benzylidene-3-O-p-methoxybenzyl- $\beta$ -D-mannopyranoside-(1 $\rightarrow$ 6)-1,2,3,4-di-O-isopropylidene- $\alpha$ -D-galactopyranose 5.25



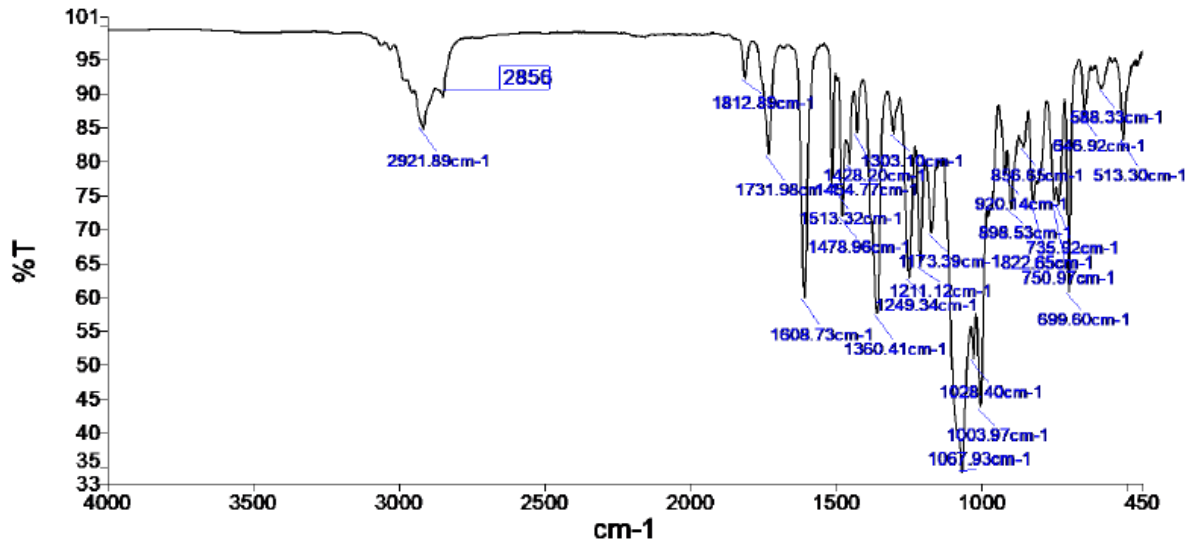
Appendix



# Appendix

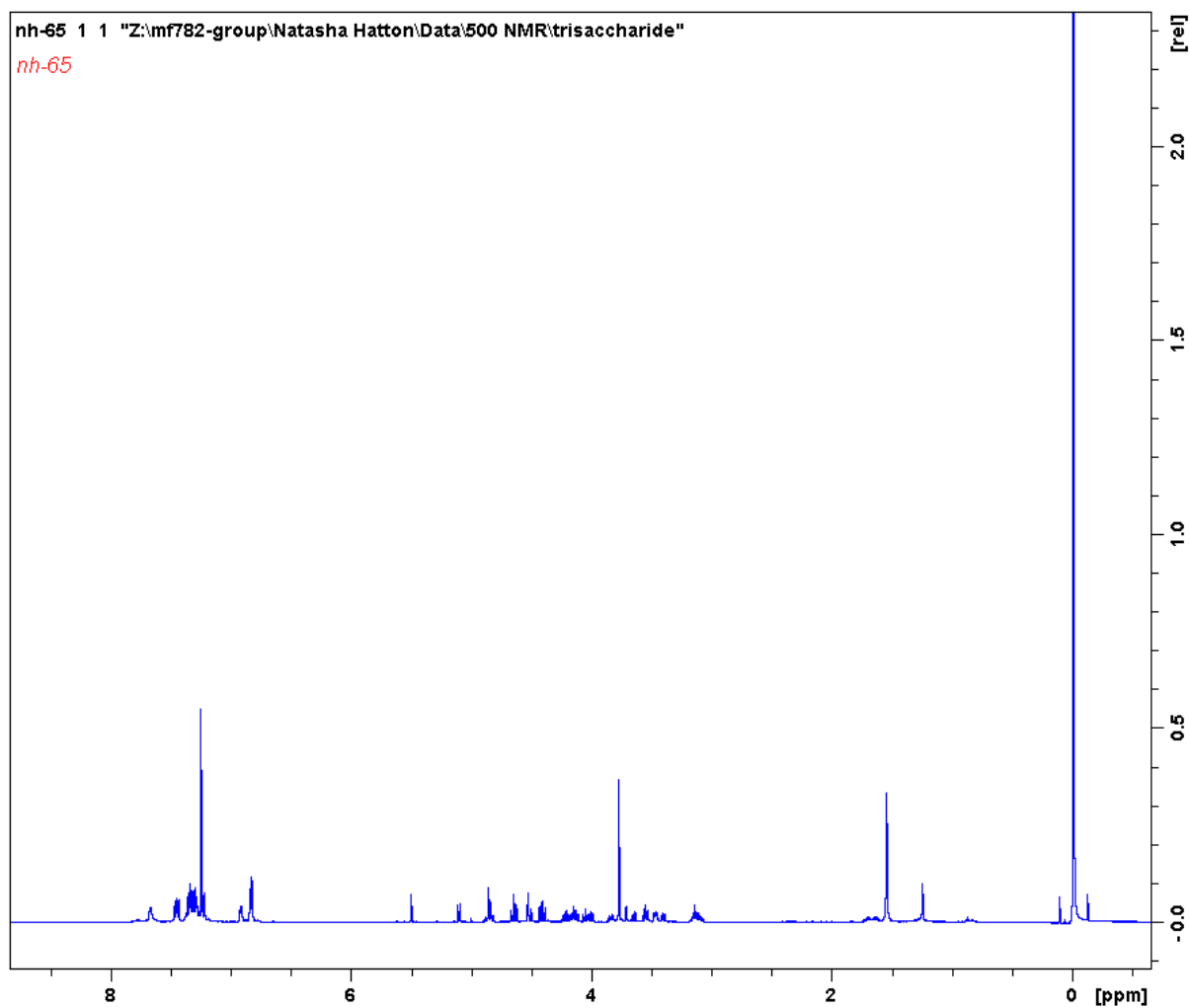
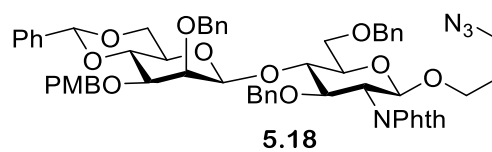


Appendix

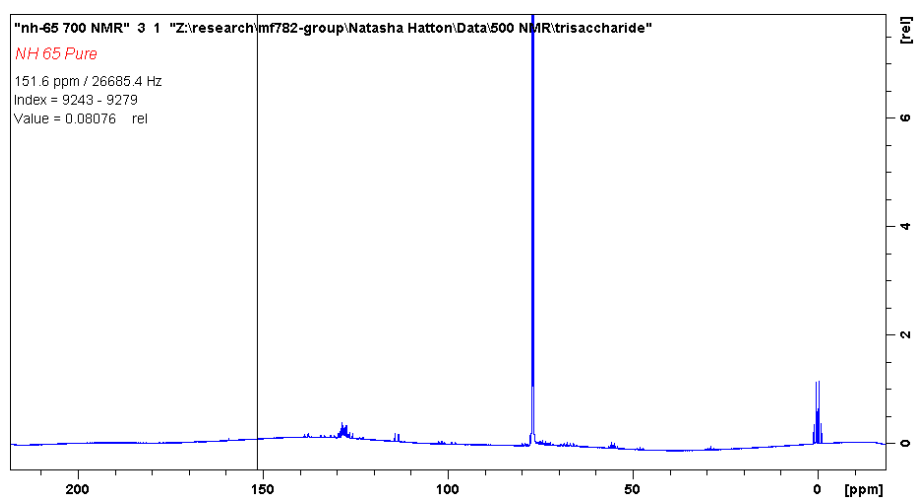
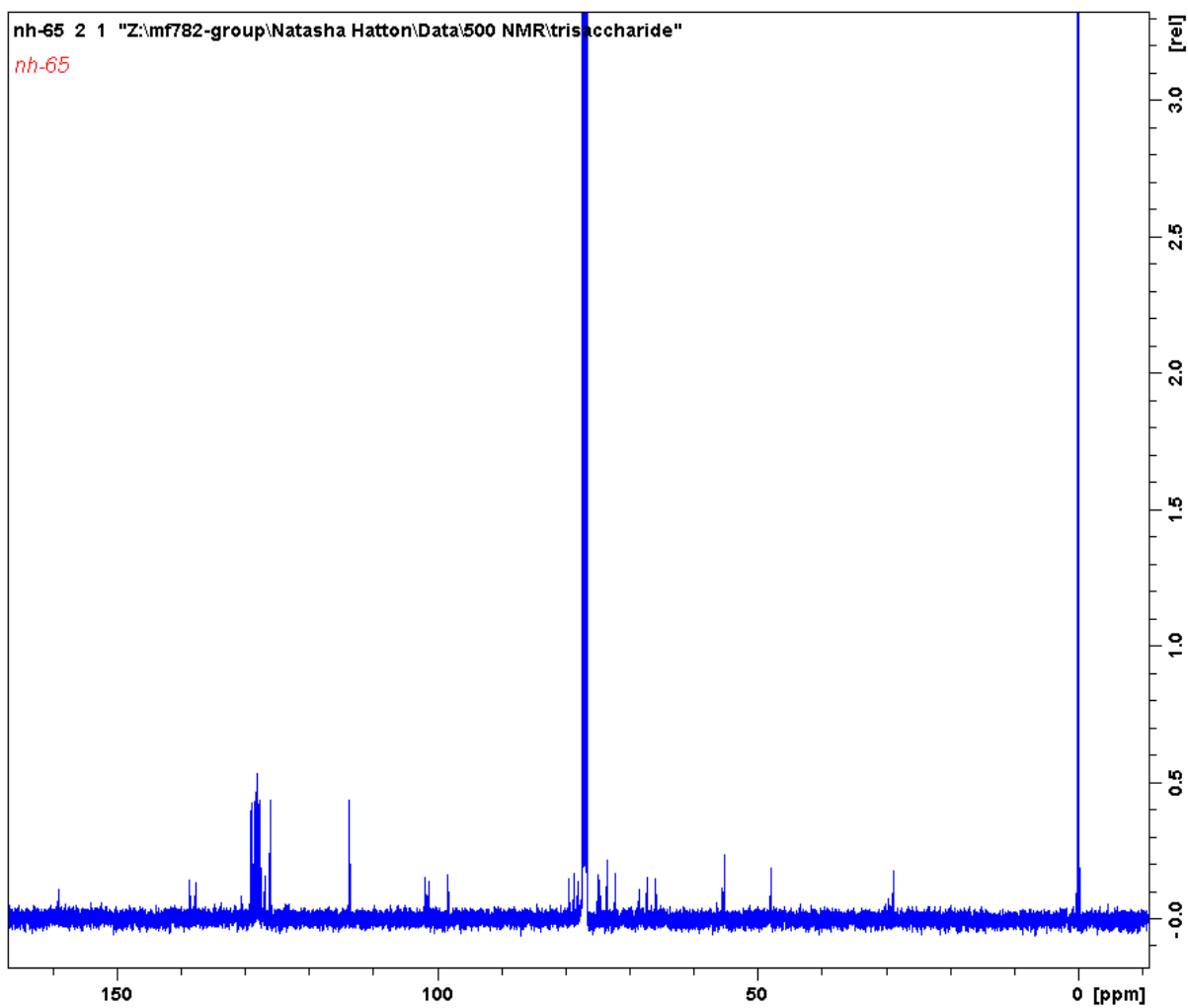


## Appendix

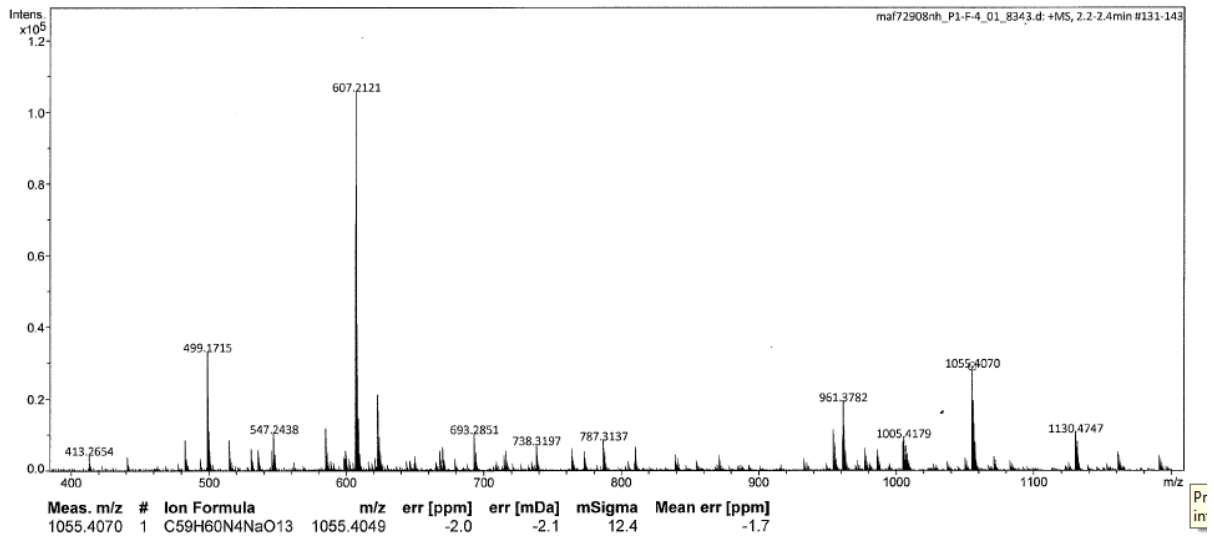
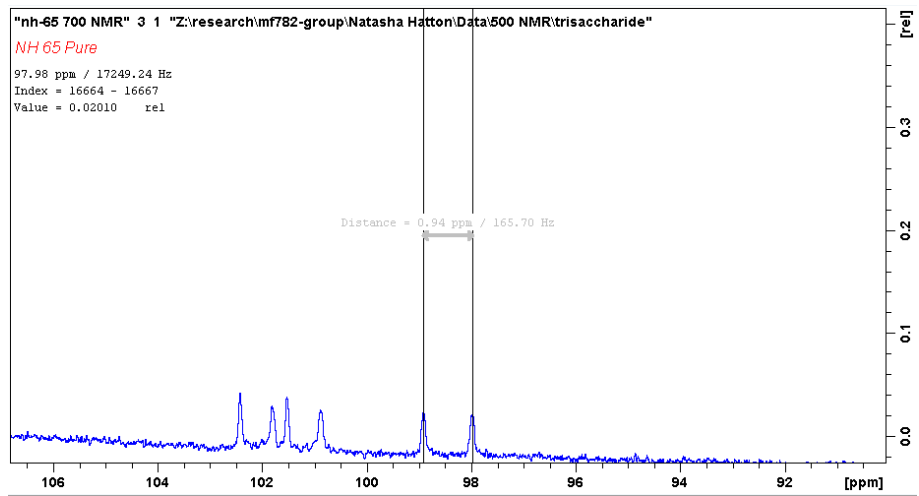
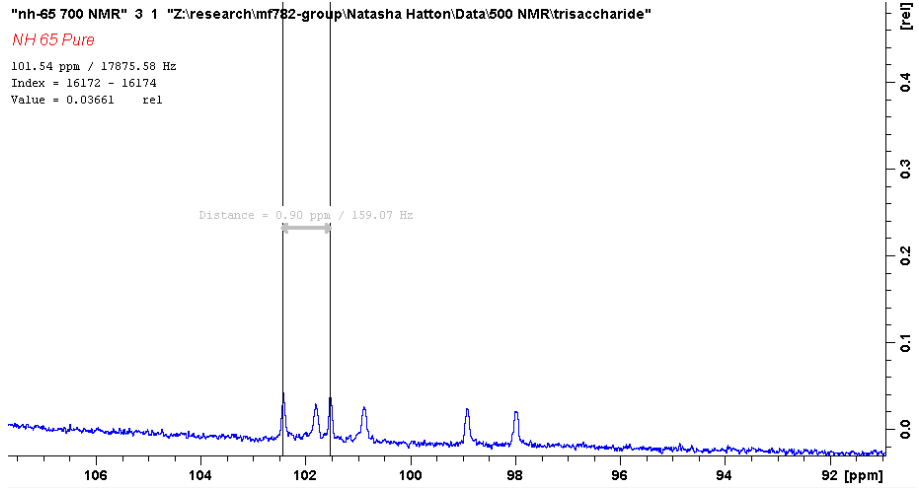
### 9.4.1.4 2-Benzyl-4,6-O-benzylidene-3-O-p-methoxybenzyl- $\beta$ -D-mannopyranoside-(1 $\rightarrow$ 4)-3-Azidopropyl (3,6-di-O-benzyl- $\beta$ -D-glucopyranoside) **5.18**



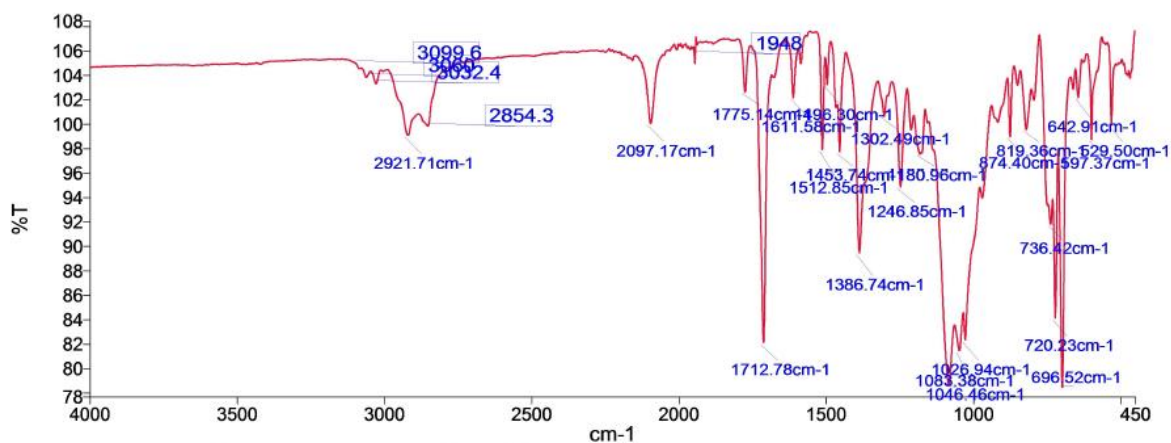
Appendix



# Appendix

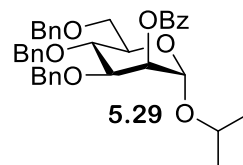


## Appendix



### 9.4.2 Further investigations into the synthesis of trisaccharide 5.19

#### 9.4.2.1 Formation of 2-propyl 2-O-benzoyl-3,4,6-tri-O-benzyl- $\alpha$ -D-mannopyranoside 5.29

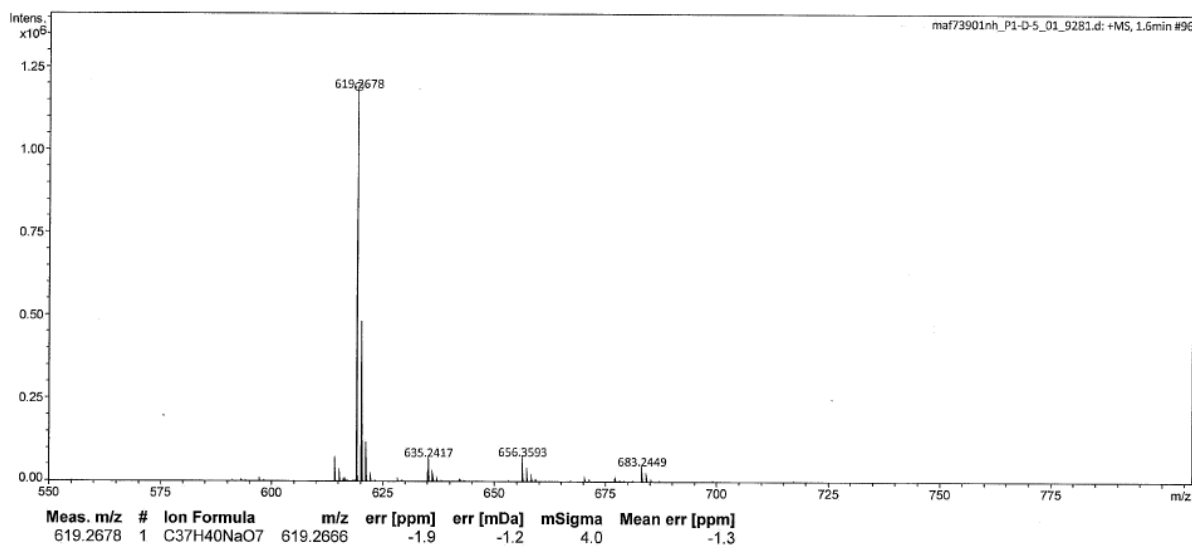


### York - Chemistry - Mass Spectrometry Service Report

NH-66

#### Analysis Information

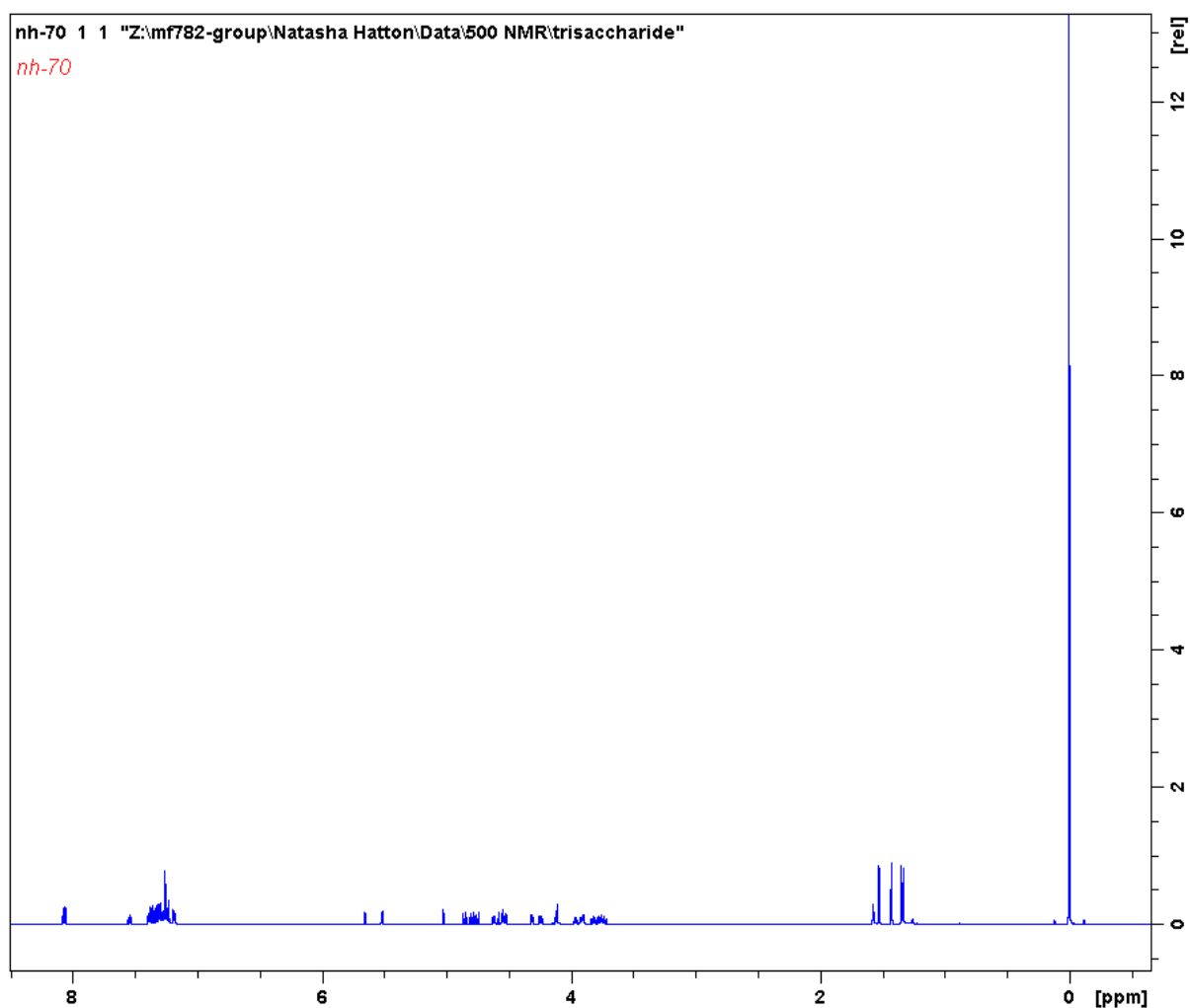
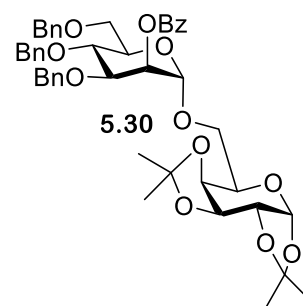
Analysis Filename	maf73901nh_P1-D-5_01_9281.d	Acquisition Date	27/11/2018 12:38:44
Method	ESI_low mass_2c1s.m	Instrument	compact
Submission Name	maf73901nh		Positive



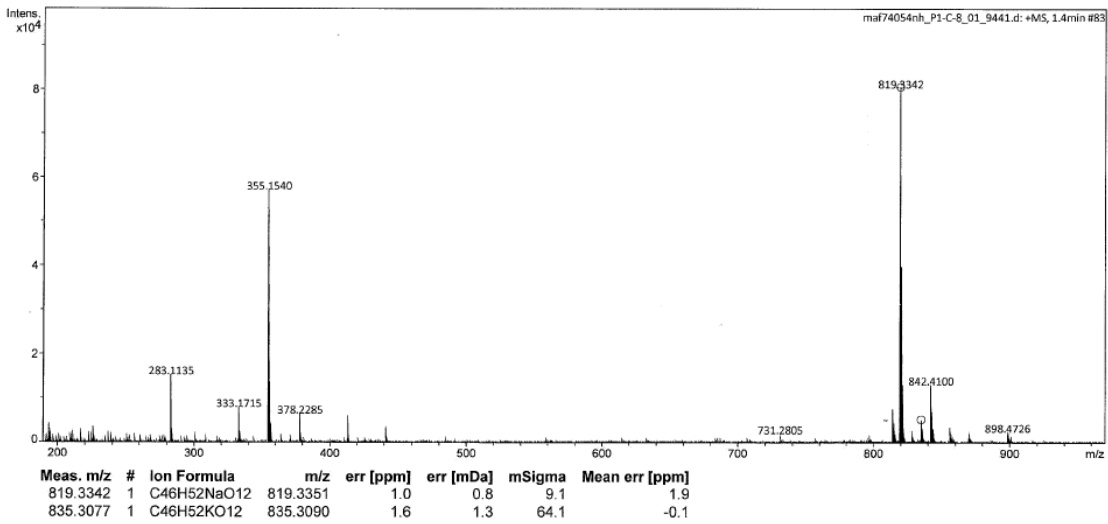
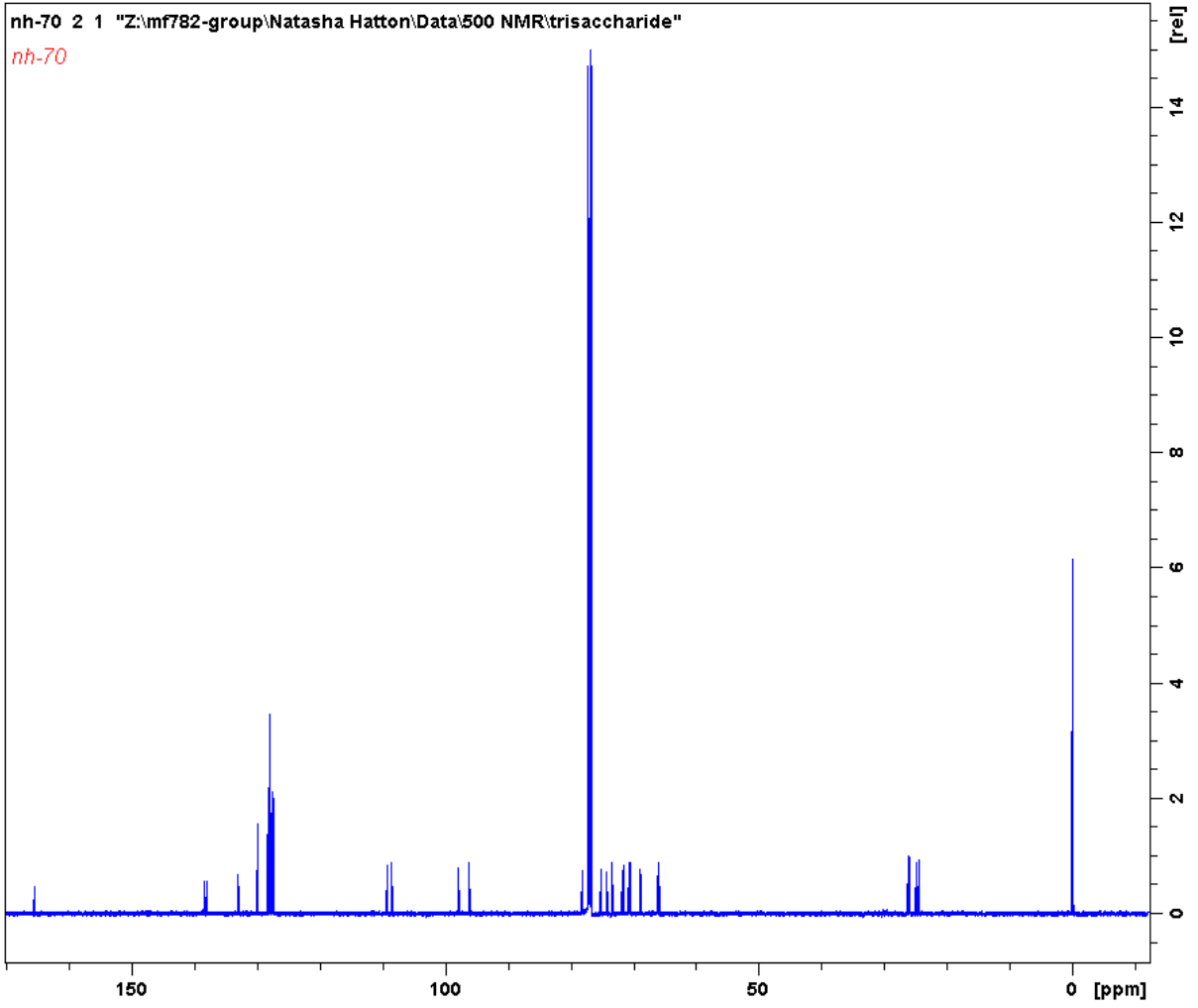


## Appendix

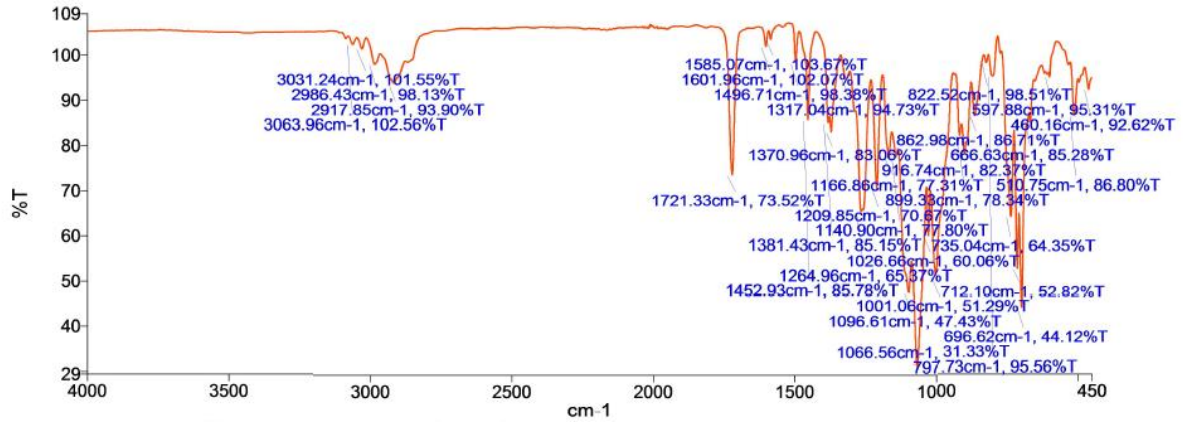
### 9.4.2.2 Formation of 2-O-(benzoyl-3,4,6-tri-O-benzyl- $\alpha$ -D-mannopyranoside)-(1 $\rightarrow$ 6)-1,2,3,4-di-O-isopropylidene- $\alpha$ -D-galactopyranose 5.30



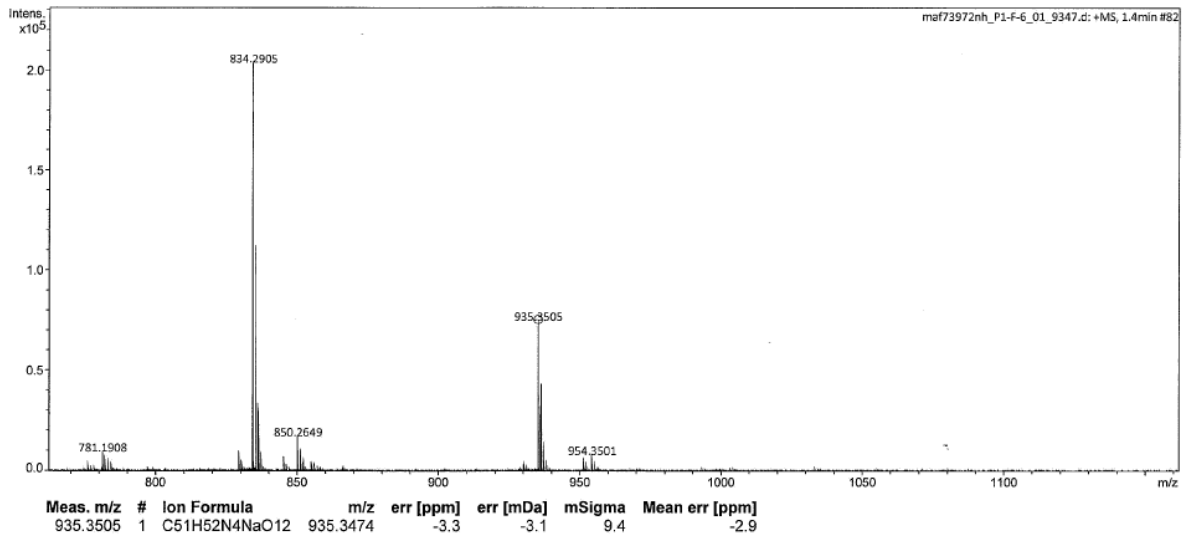
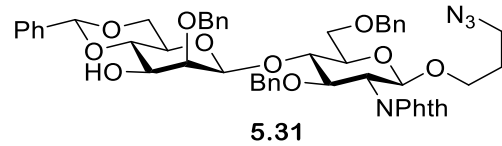
Appendix



## Appendix

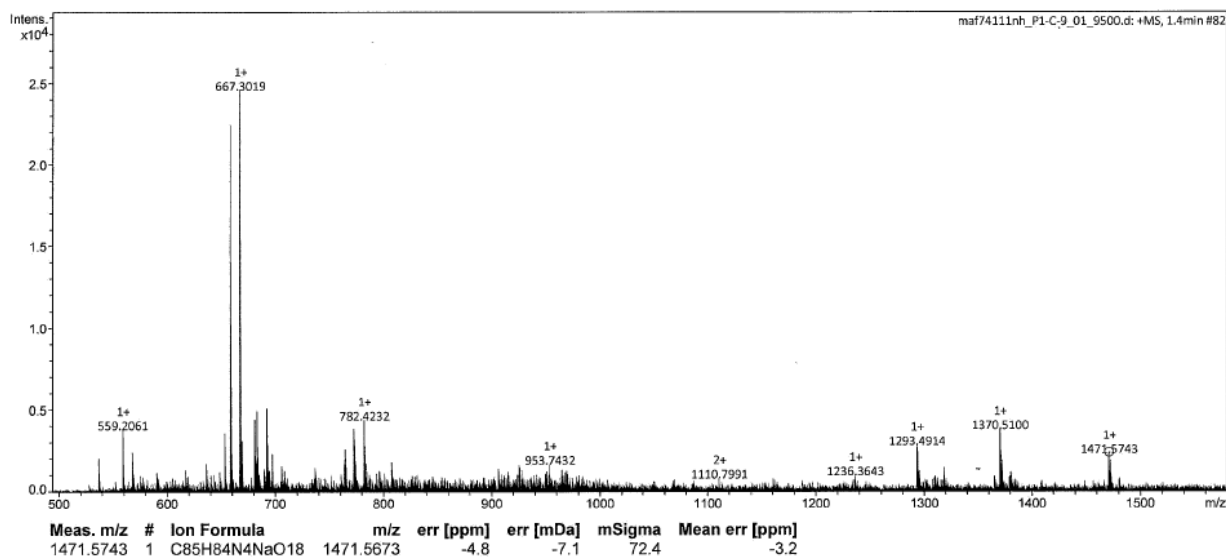
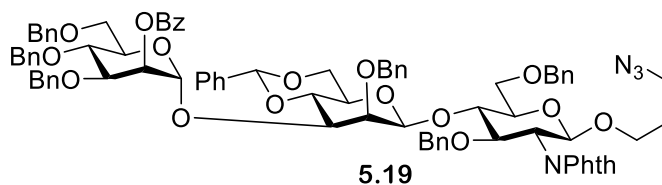


### 9.4.2.3 2-Benzyl-4,6-O-benzylidene- $\alpha$ -D-mannopyranoside-(1 $\rightarrow$ 3)-3-Azidopropyl (3,6-Di-O-benzyl- $\beta$ -D-glucopyranoside) 5.31



## Appendix

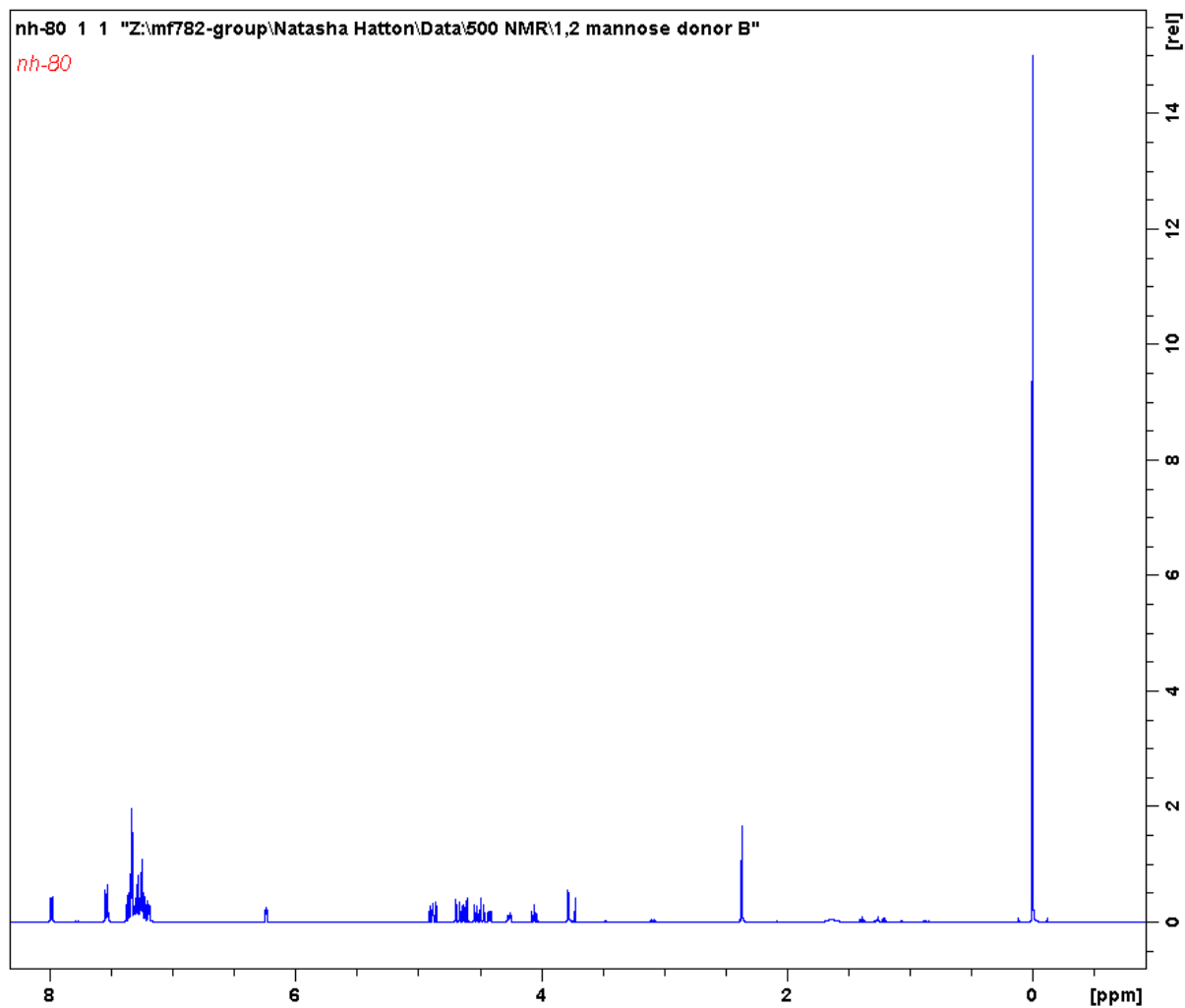
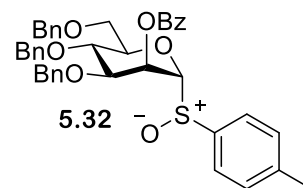
9.4.2.4 2-O-Benzoyl-3,4,6-tri-O-benzyl- $\alpha$ -D-mannopyranoside-(1  $\rightarrow$  3) 2-O-benzyl-4,6-O-benzylidene-3-O-p-methoxybenzyl- $\alpha$ -D-mannopyranoside- (1  $\rightarrow$  4) 3-Azidopropyl (3,6-di-O-benzyl- $\beta$ -D-glucopyranoside) **5.19**



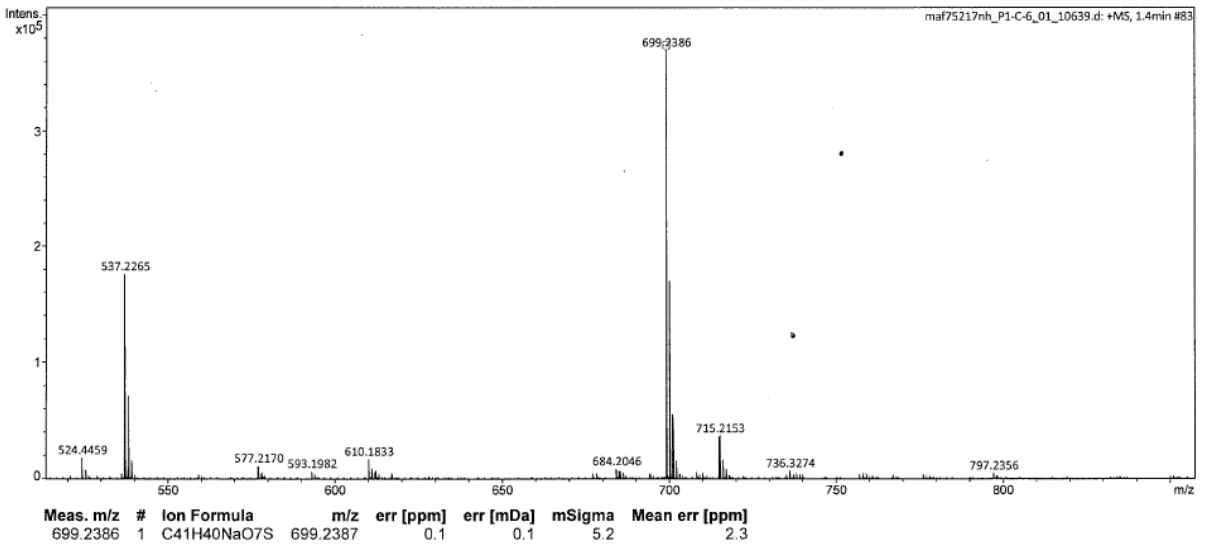
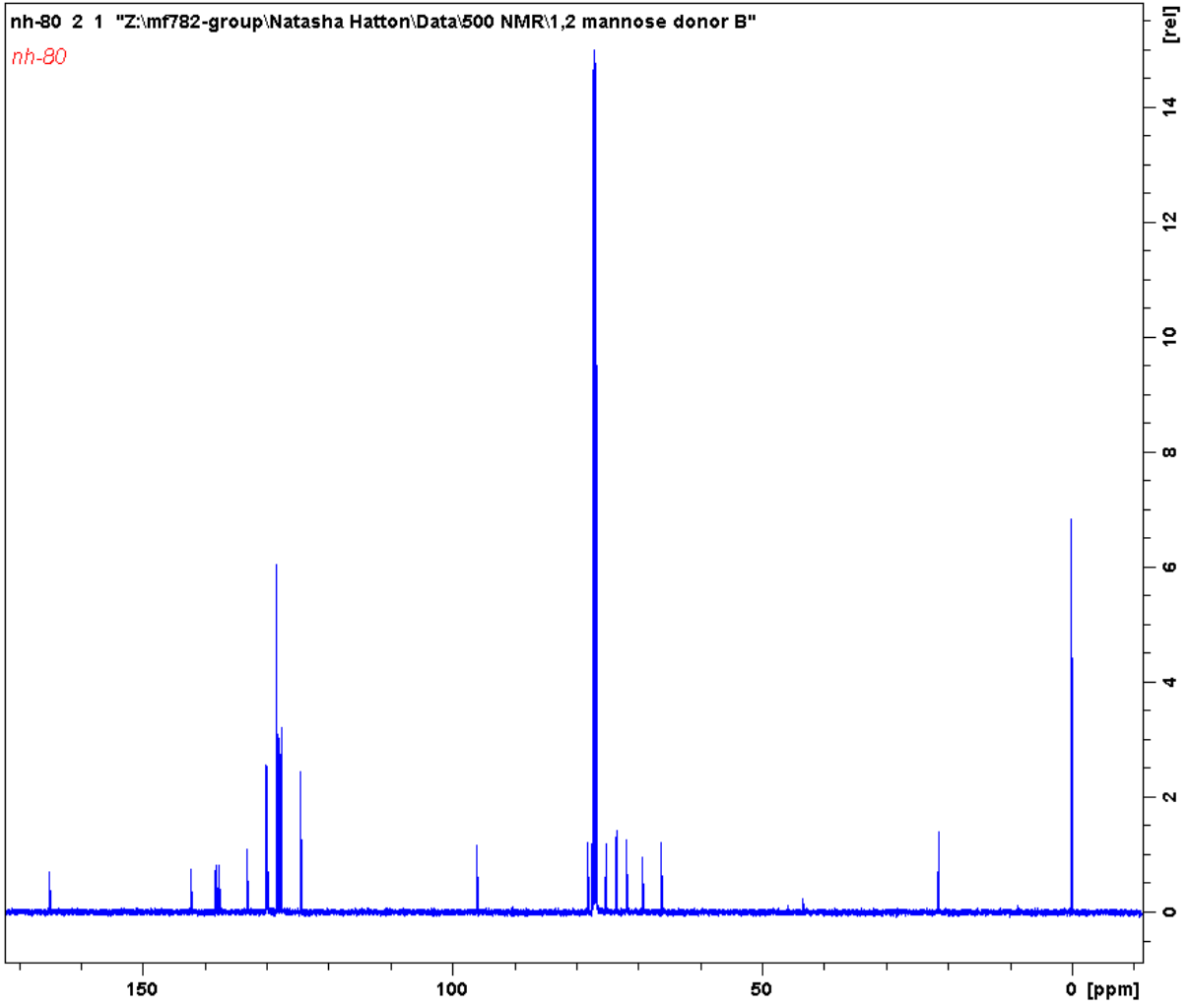
## Appendix

### 9.4.3 Work into the investigation into the optimisation of the $\alpha$ -mannoside glycosylation

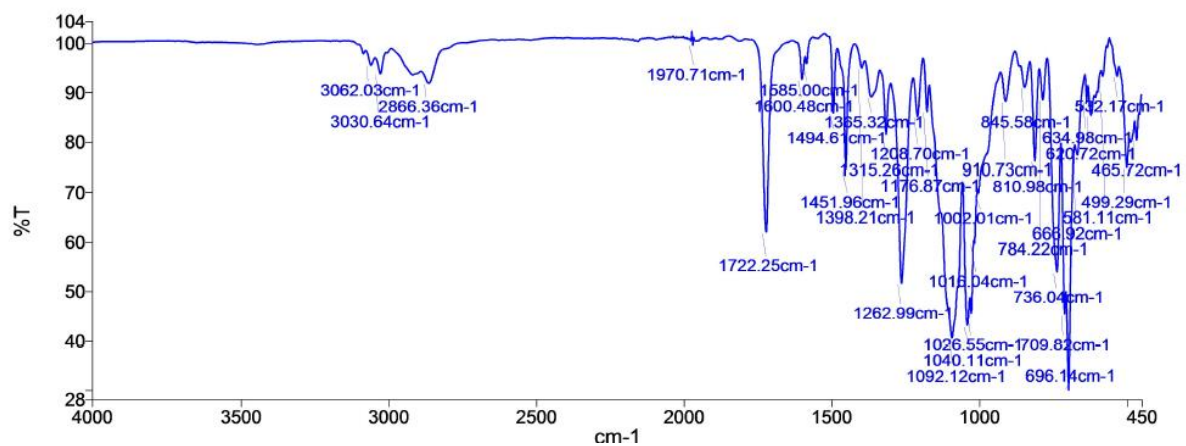
#### 9.4.3.1 4-Methylphenylsulfenyl 2-O-benzoyl-3,4,6-tri-O-benzyl-1-thio- $\alpha$ -D-mannopyranoside **5.32**



Appendix

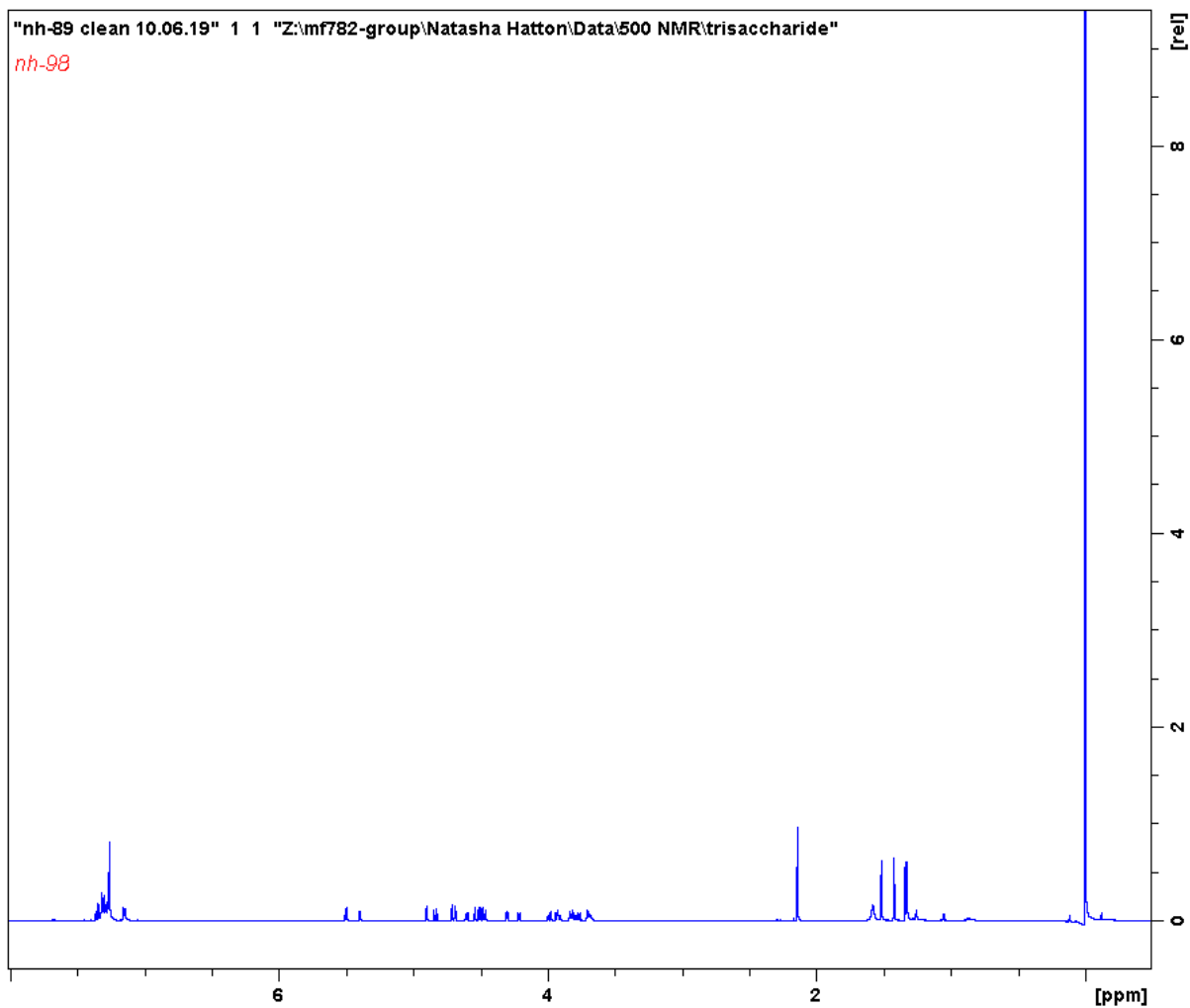
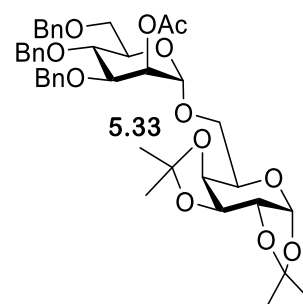


# Appendix



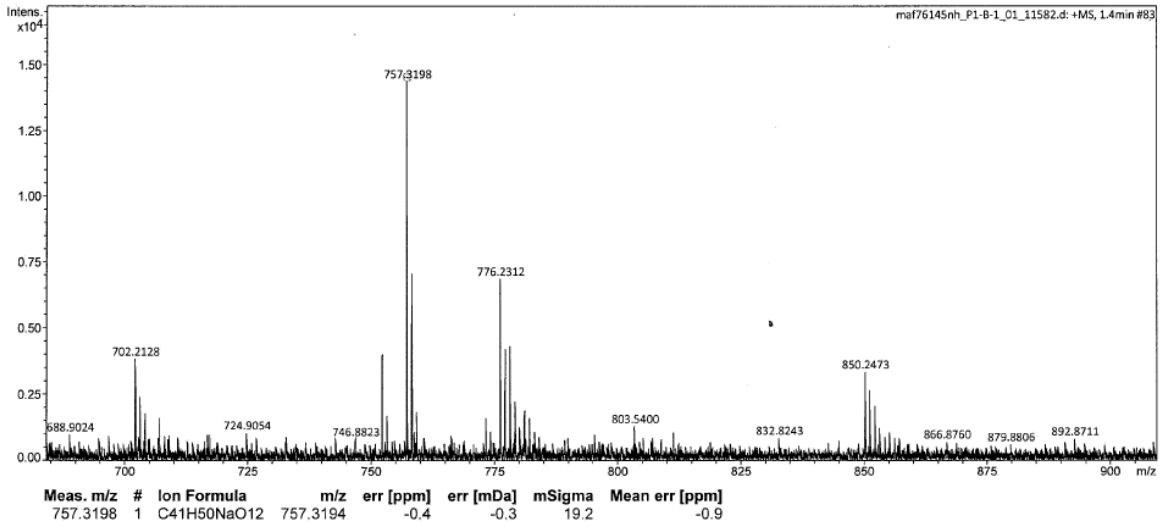
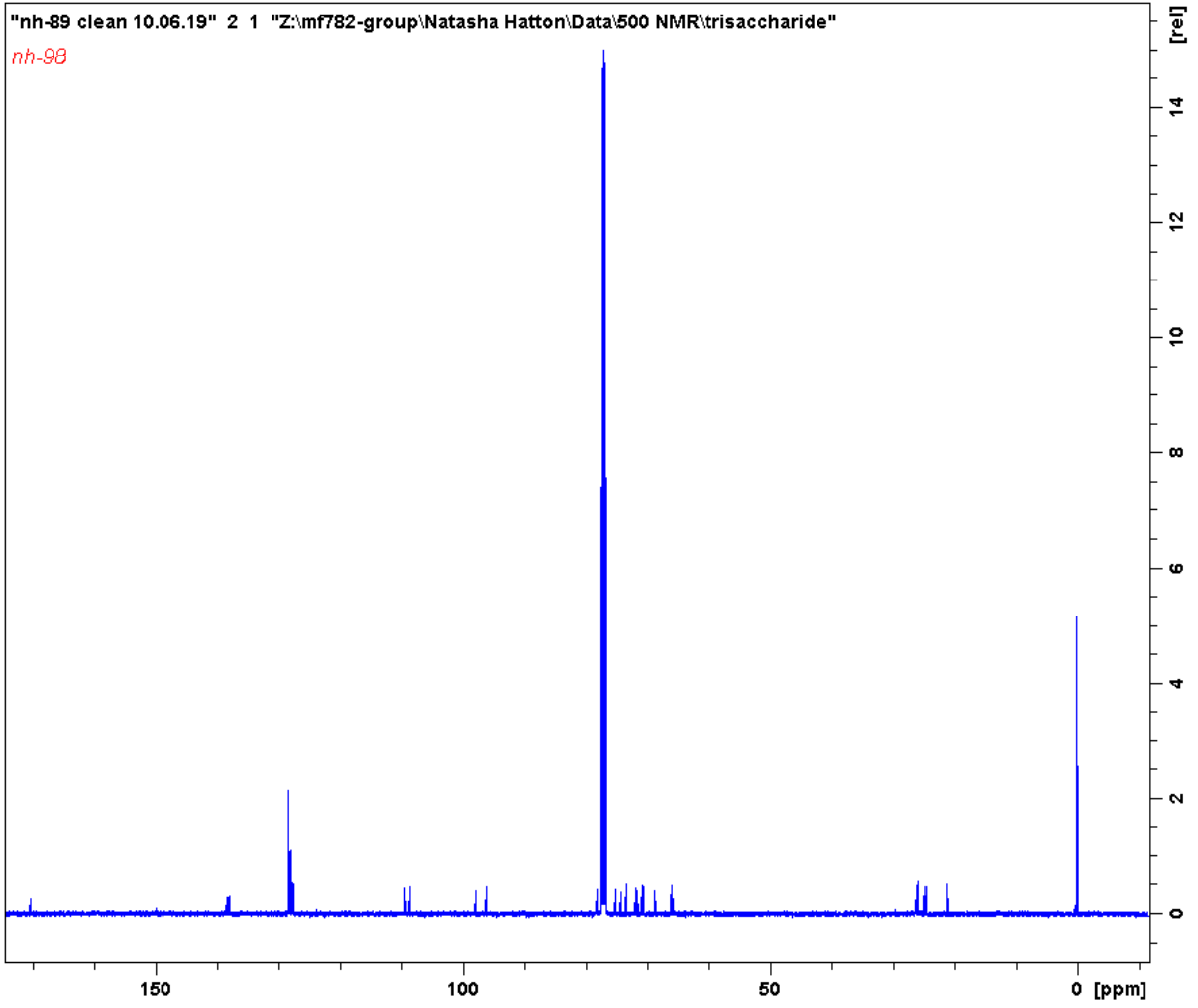
# Appendix

## 9.4.3.2 2-O-(Acetyl-3,4,6-tri-O-benzyl- $\alpha$ -D-mannopyranoside)-(1 $\rightarrow$ 6)-1,2,3,4-di-O-isopropylidene- $\alpha$ -D-galactopyranose 5.33

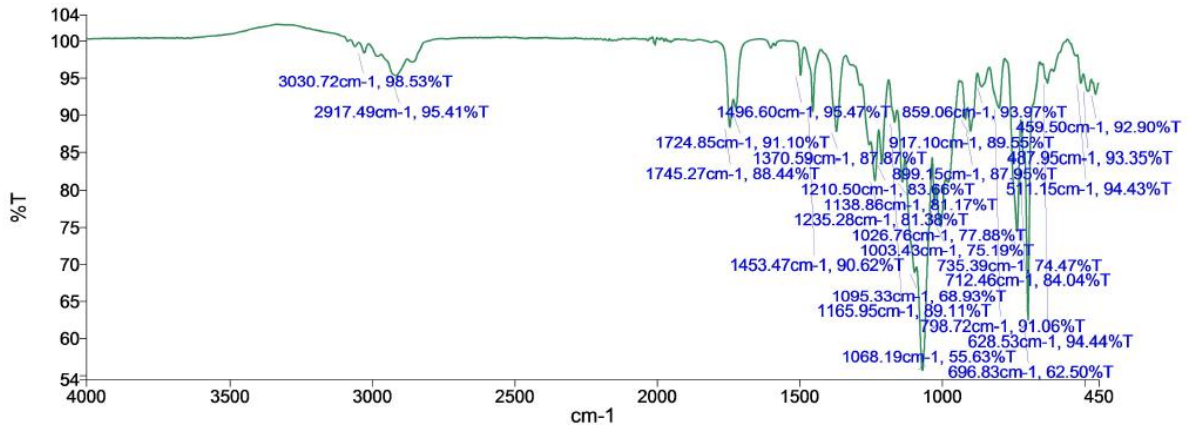




Appendix

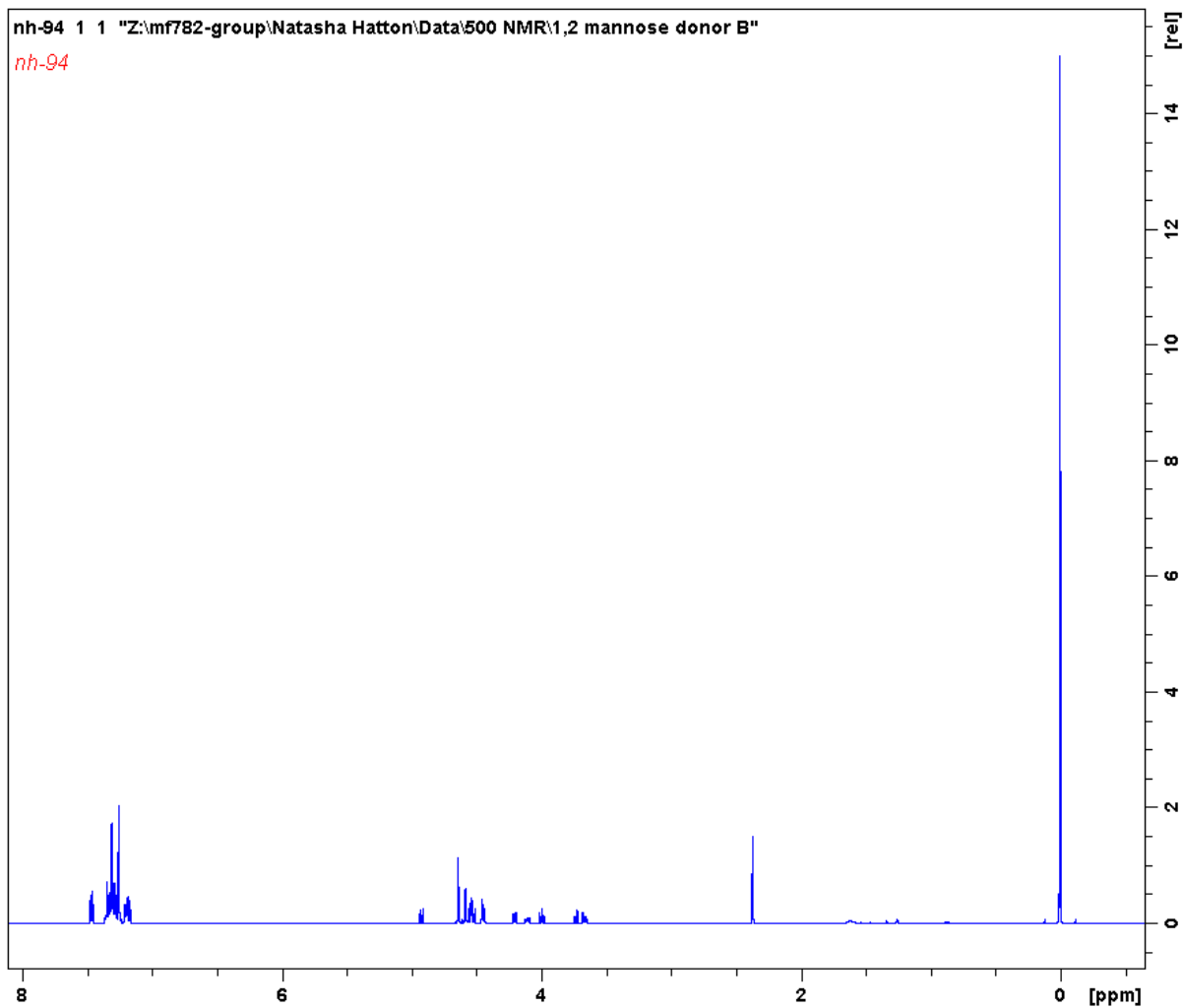
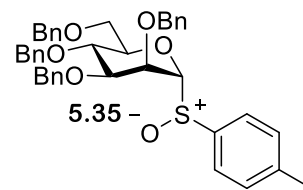


# Appendix

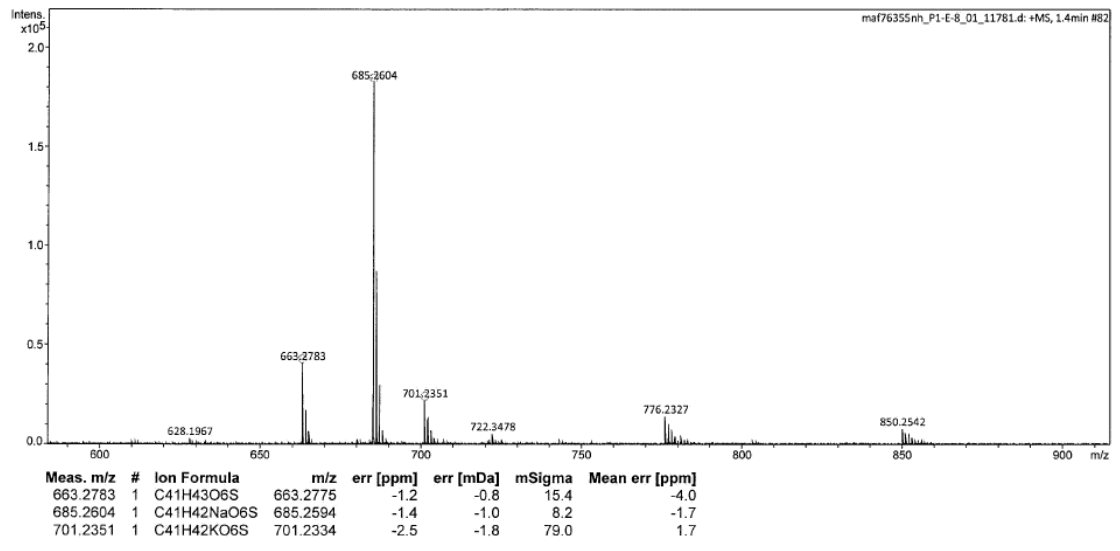
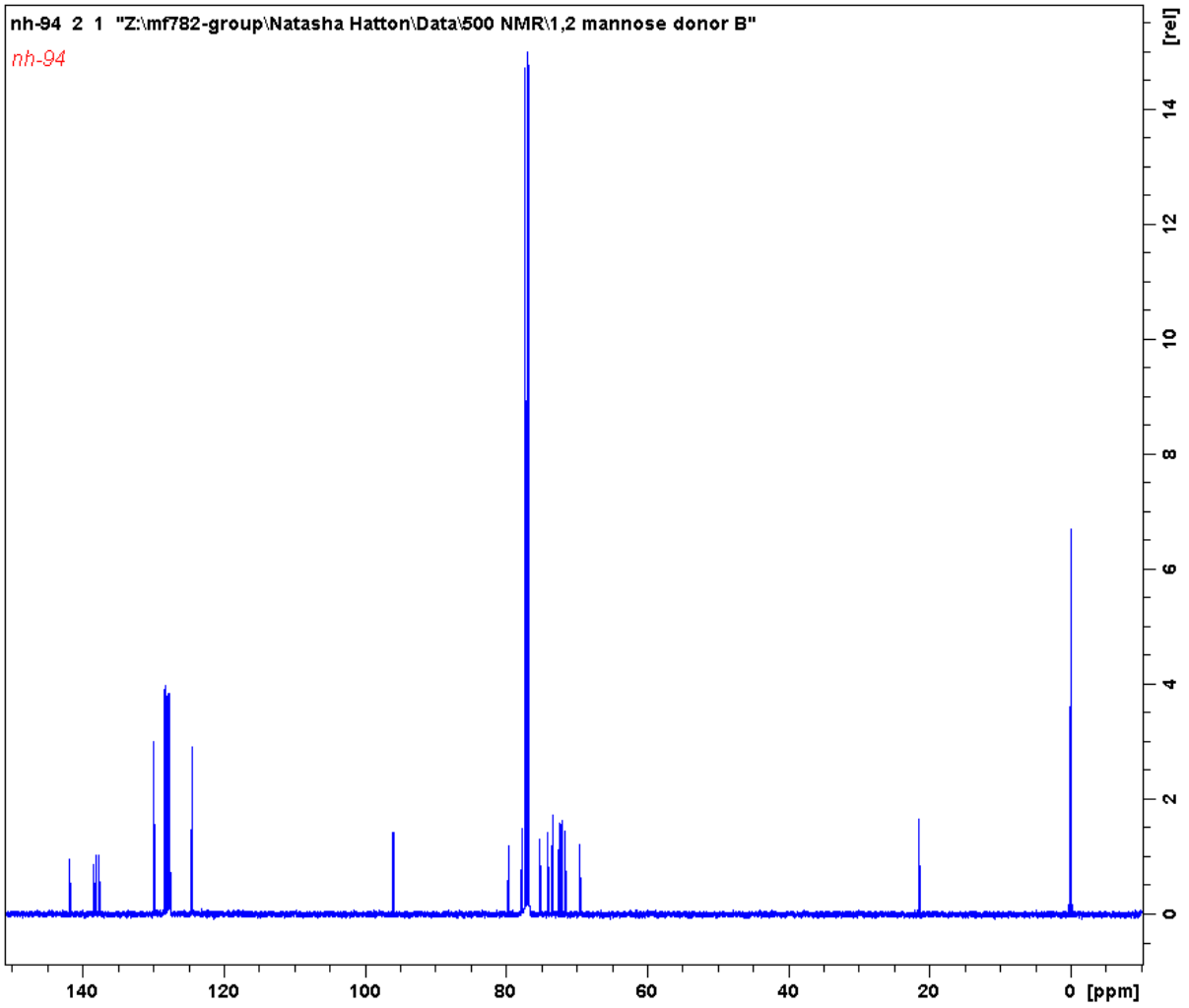


Appendix

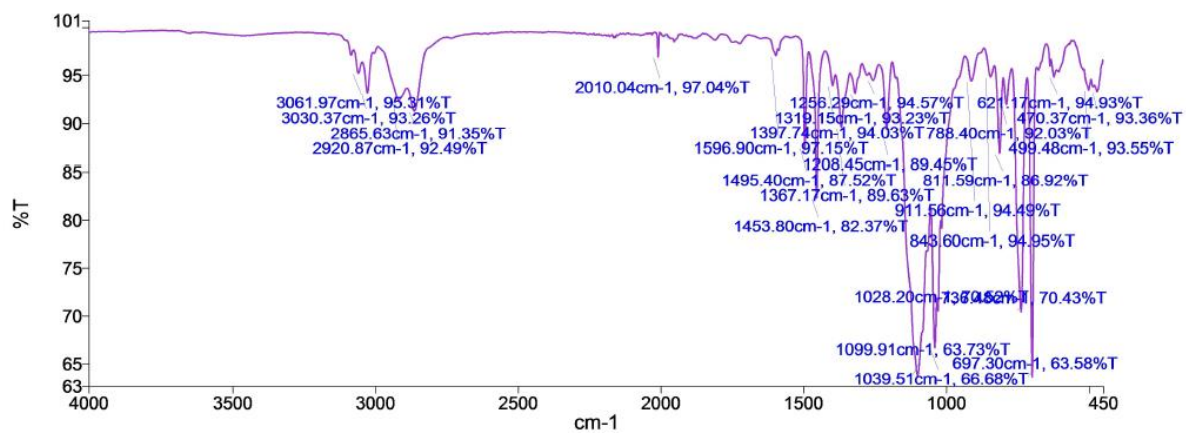
9.4.3.3 4-Methylphenylsulfenyl 2,3,4,6-tetra-O-benzyl-1-thio- $\alpha$ -D-mannopyranoside 5.35



Appendix

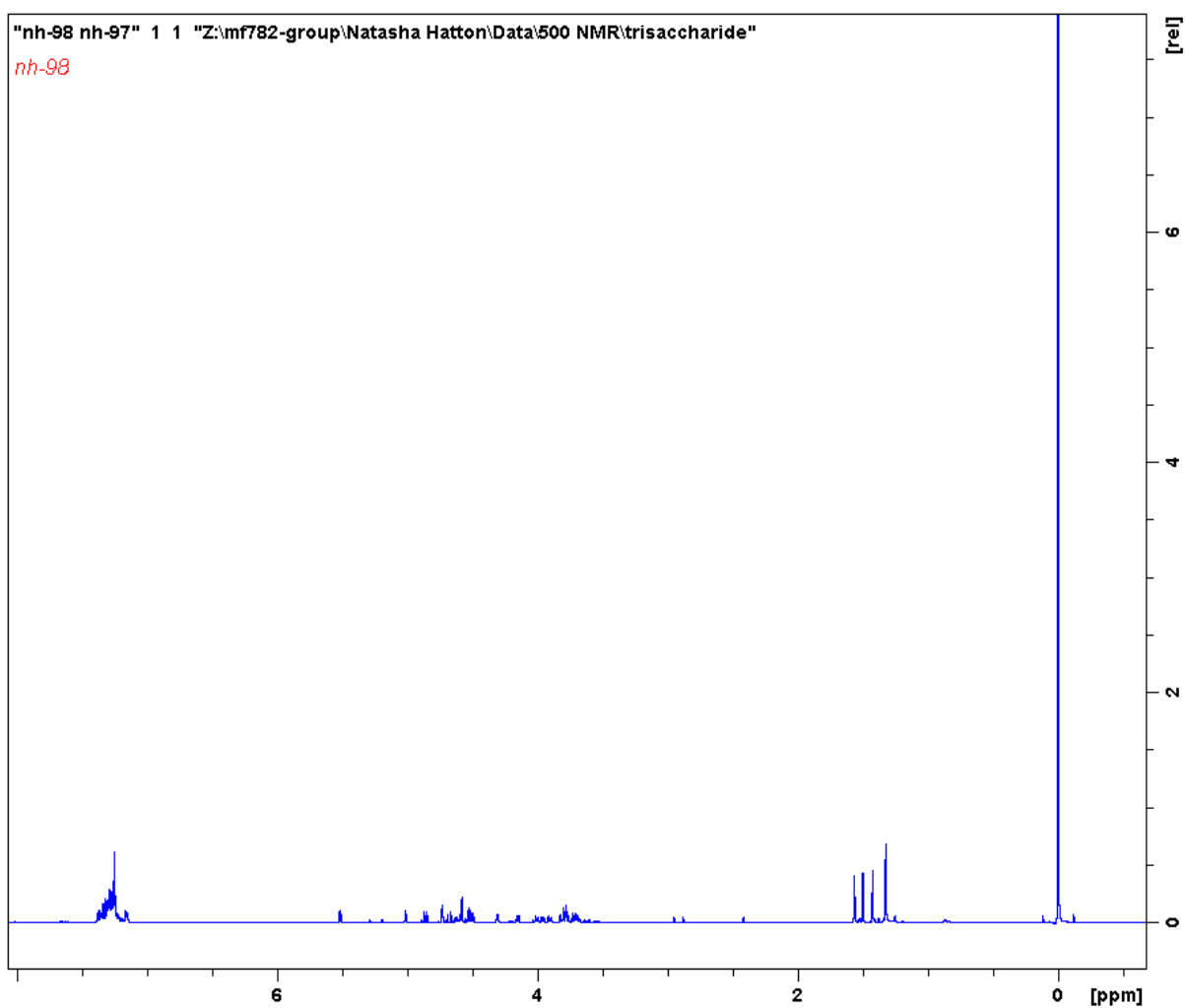
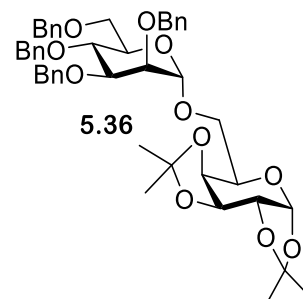


# Appendix

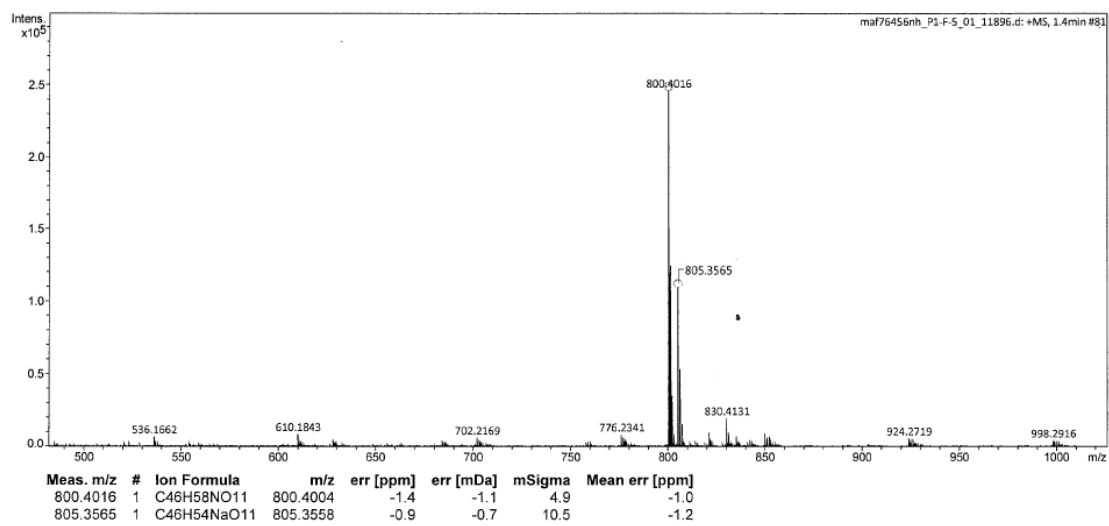
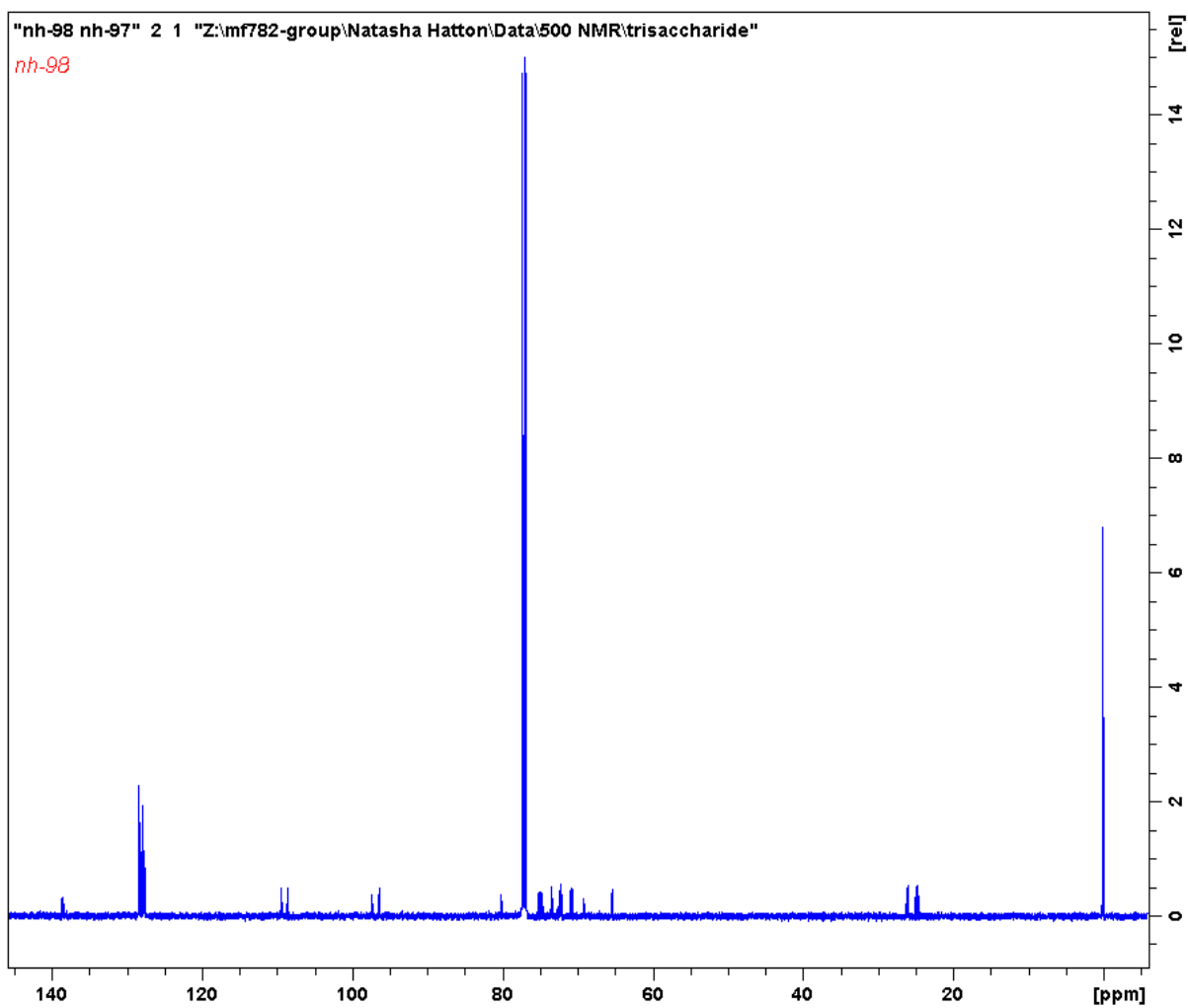


## Appendix

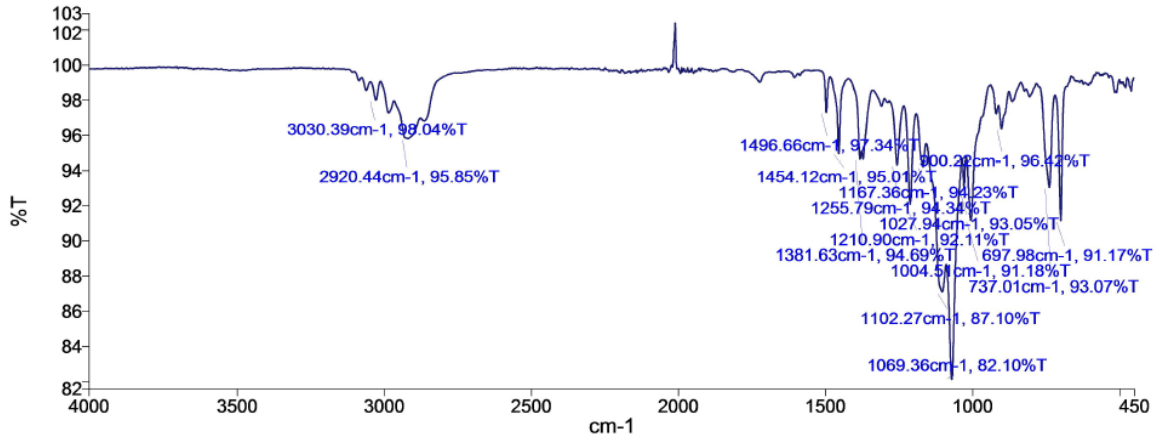
### 9.4.3.4 2,3,4,6-Tetra-O-benzyl- $\alpha$ -D-mannopyranosyl-(1 $\rightarrow$ 6)-1,2:3,4-di-O-isopropylidene- $\alpha$ -D-galactopyranoside 5.36



# Appendix



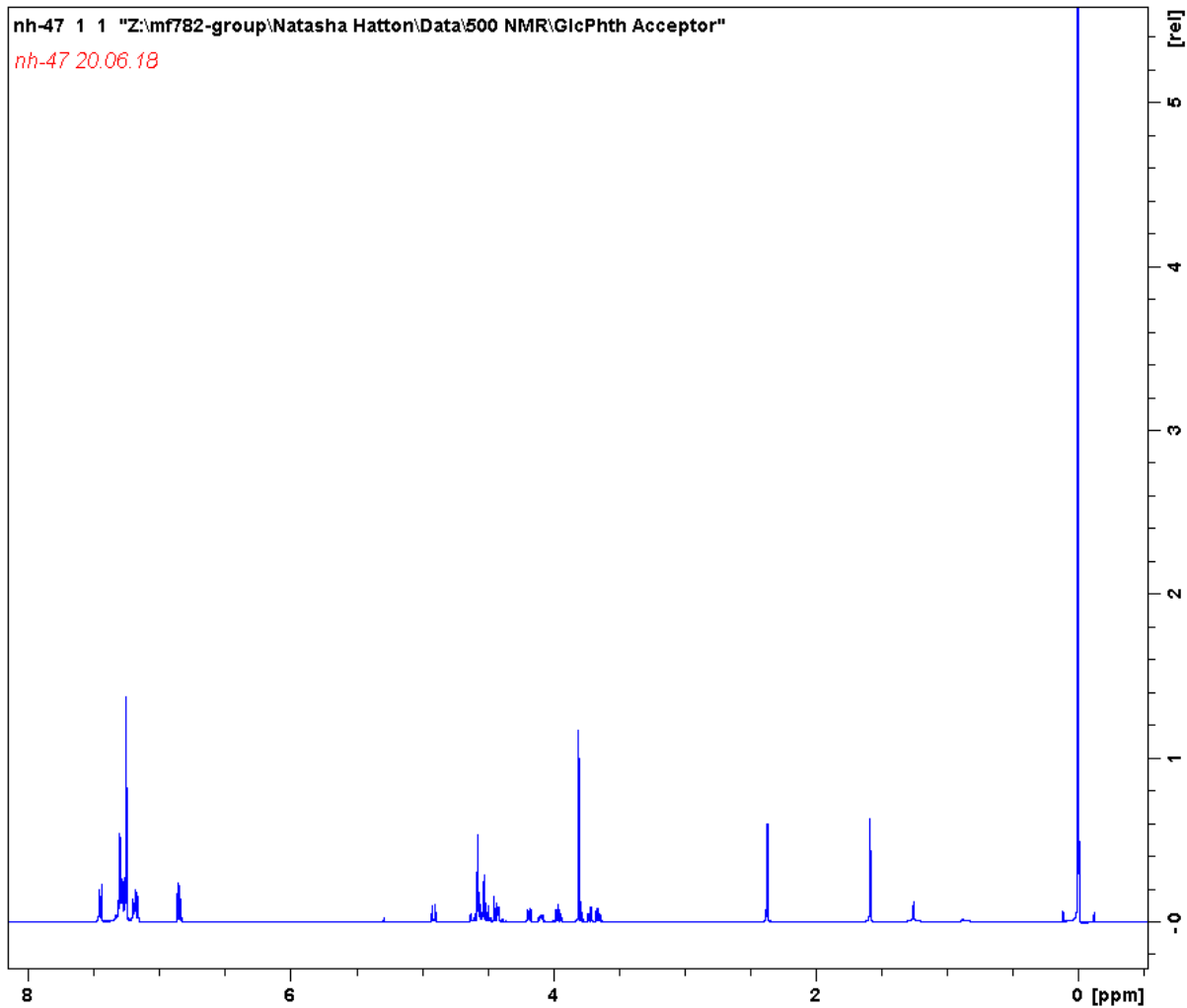
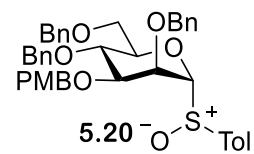
# Appendix



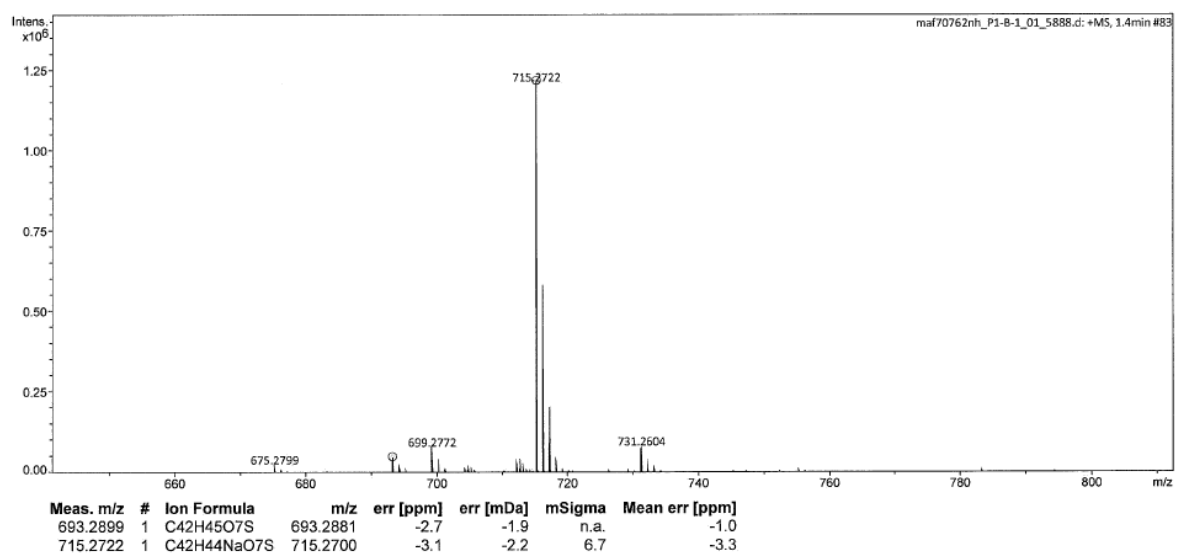
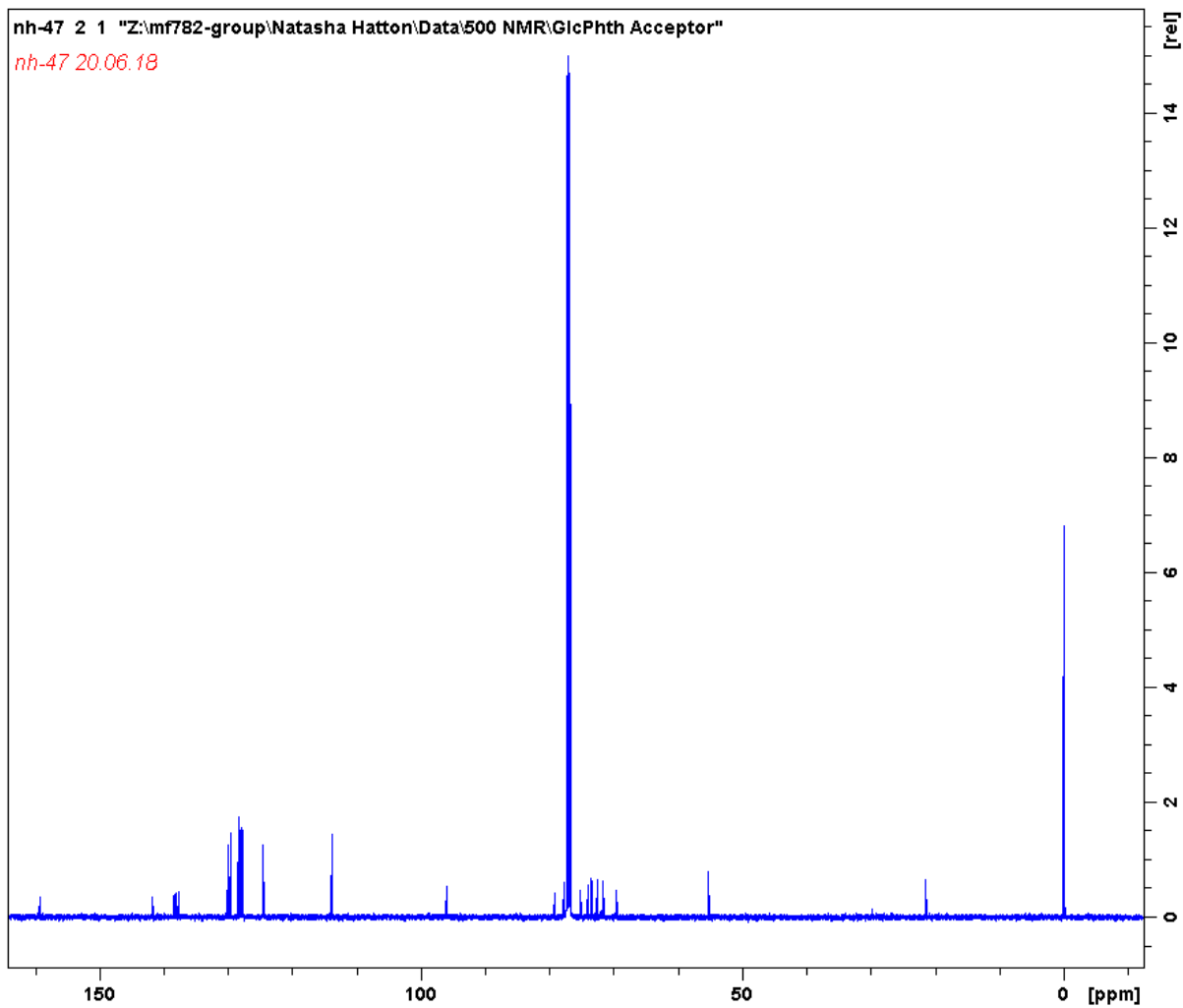


Appendix

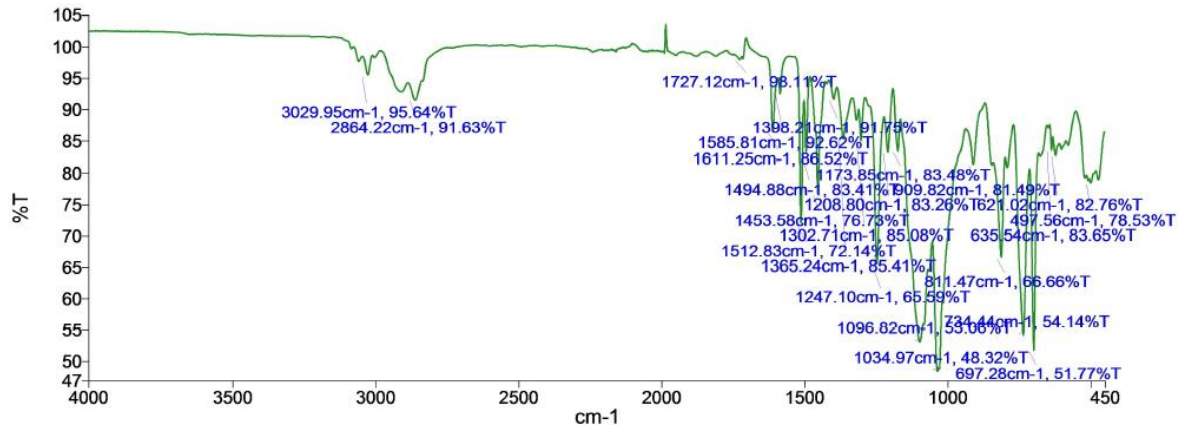
9.4.3.5 4-Methylphenylsulfenyl tri-2, 4, 6-O-benzyl-3-O-p-methoxybenzyl- $\alpha$ -D-mannopyranoside 5.20



# Appendix

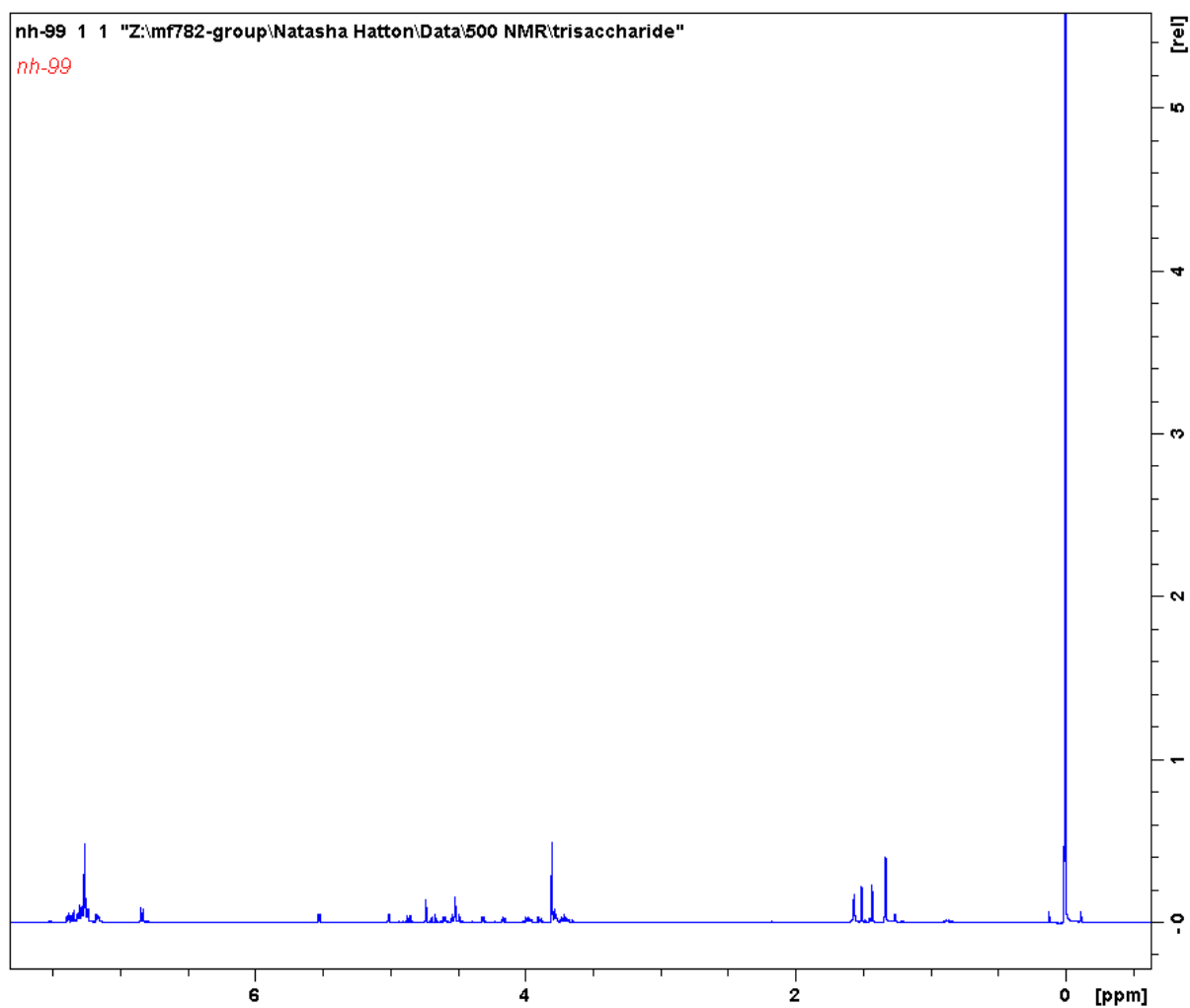
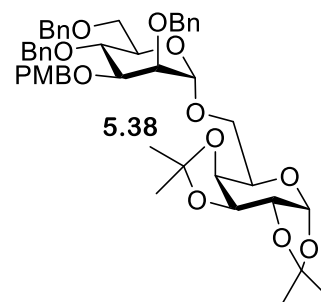


# Appendix

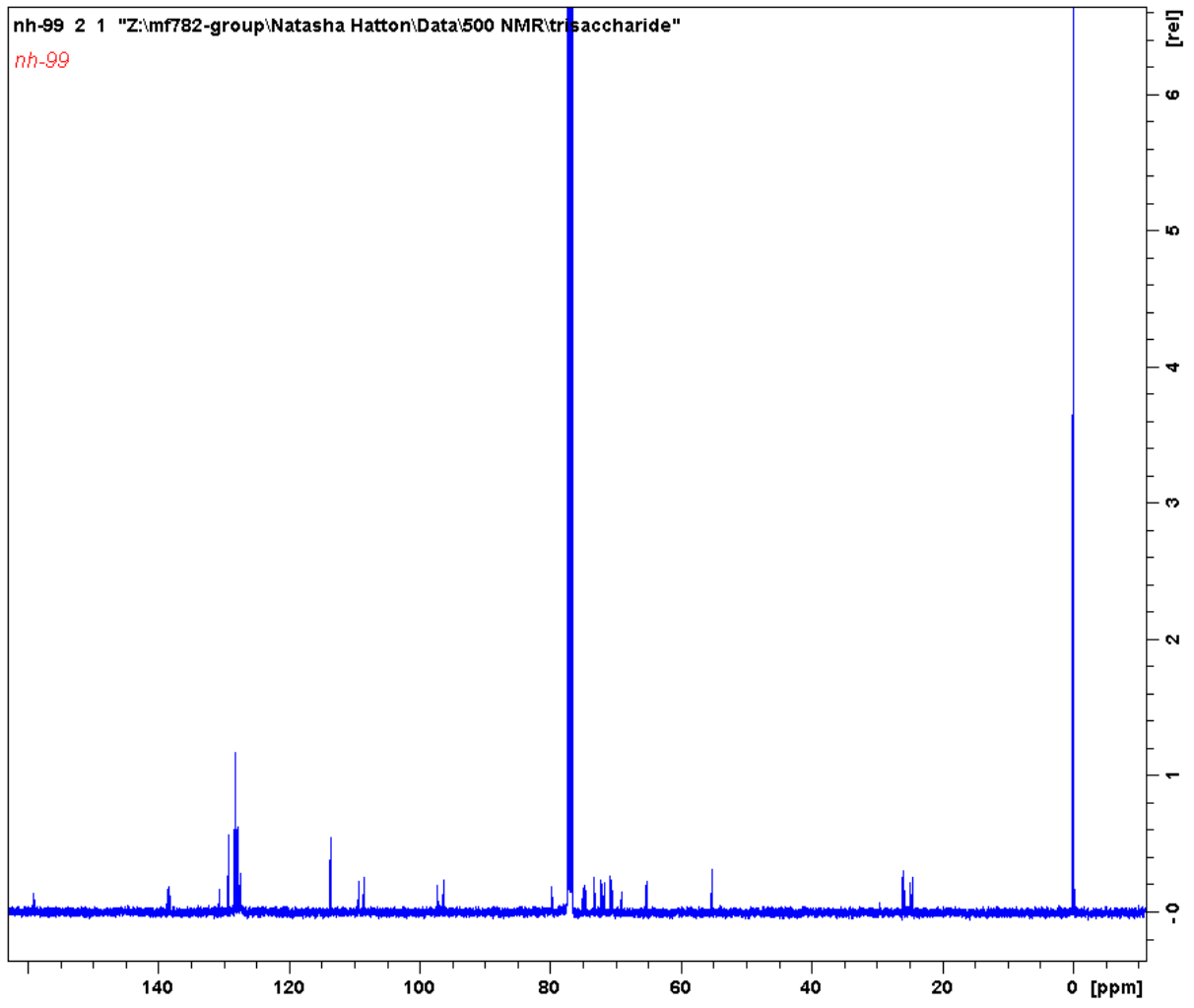


## Appendix

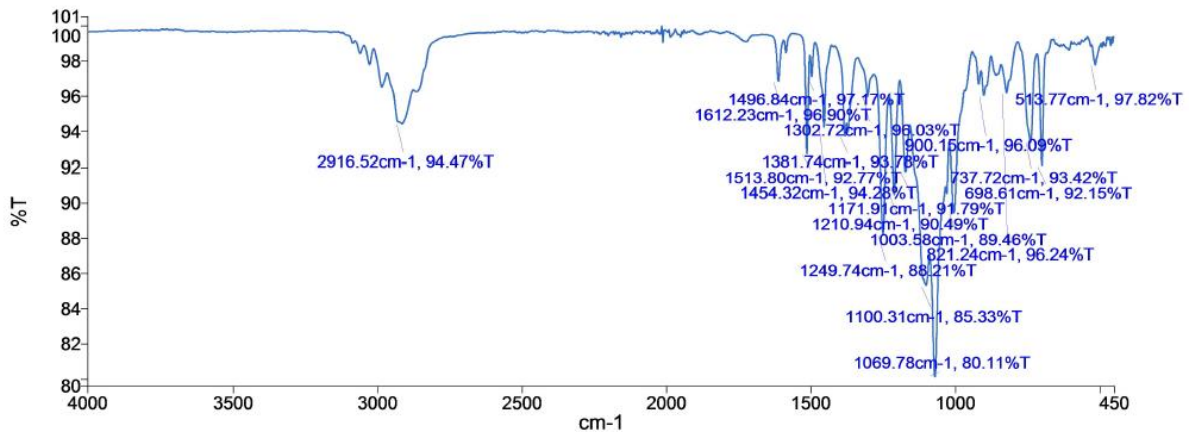
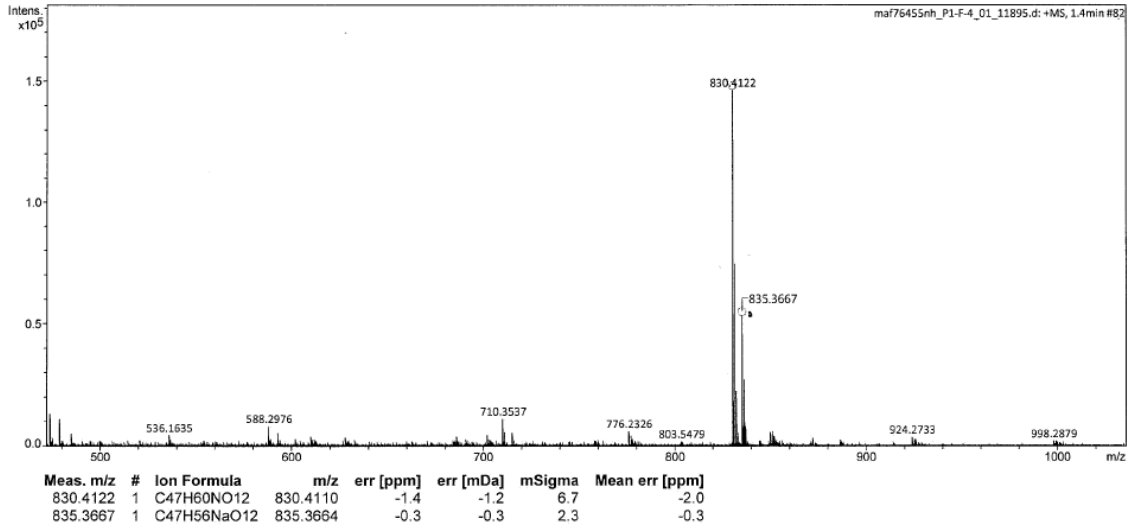
### 9.4.3.6 4-Methylphenyl tri-2, 4, 6-O-benzyl-3-O-p-methoxybenzyl-1-thio- $\alpha$ -D-mannopyranoside -(1->6)-1,2:3,4-di-O-isopropylidene- $\alpha$ -D-galactopyranoside **5.38**



Appendix

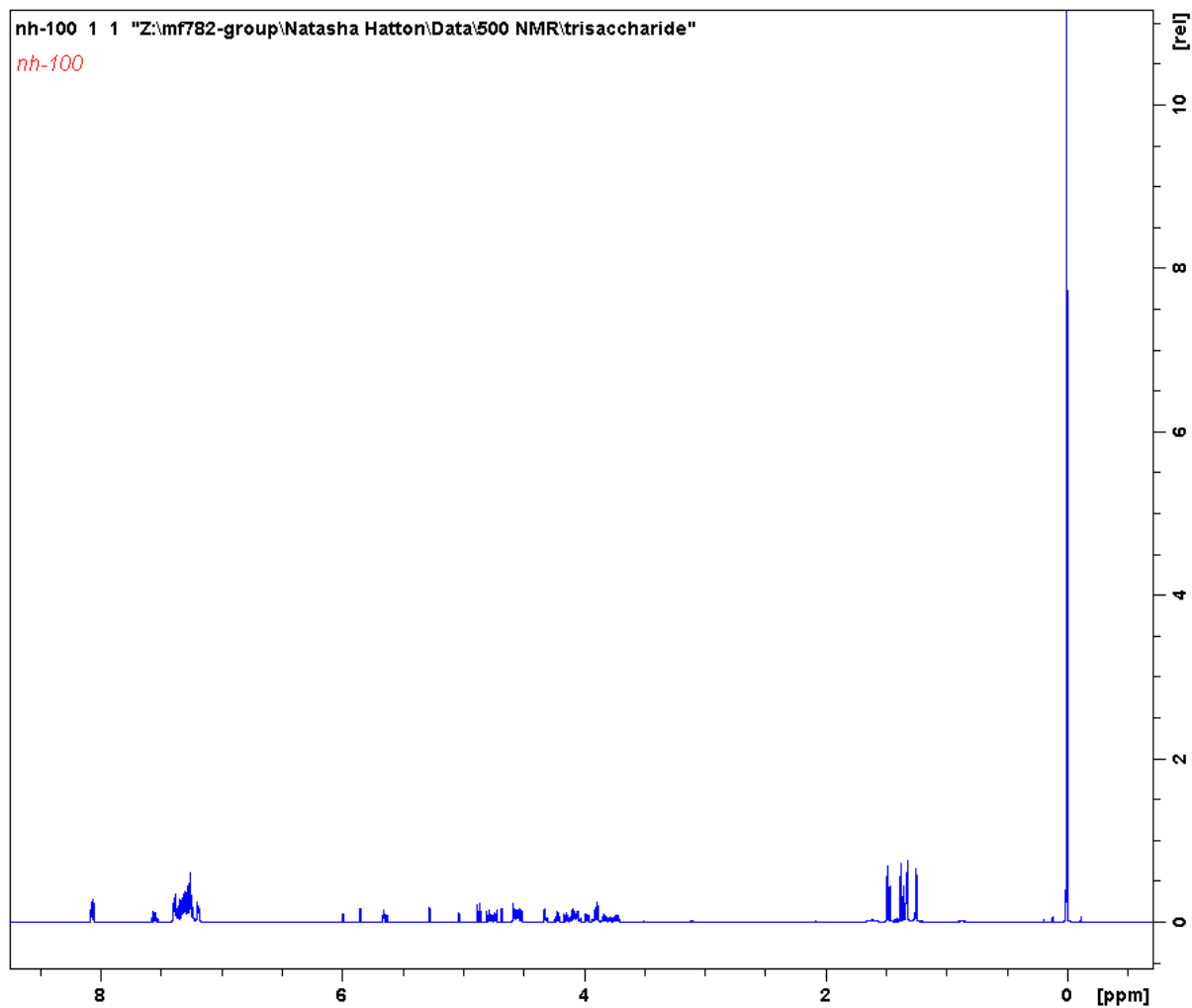
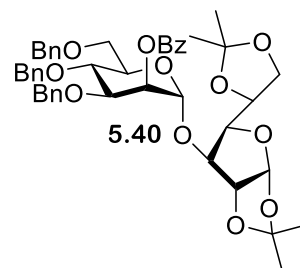


# Appendix

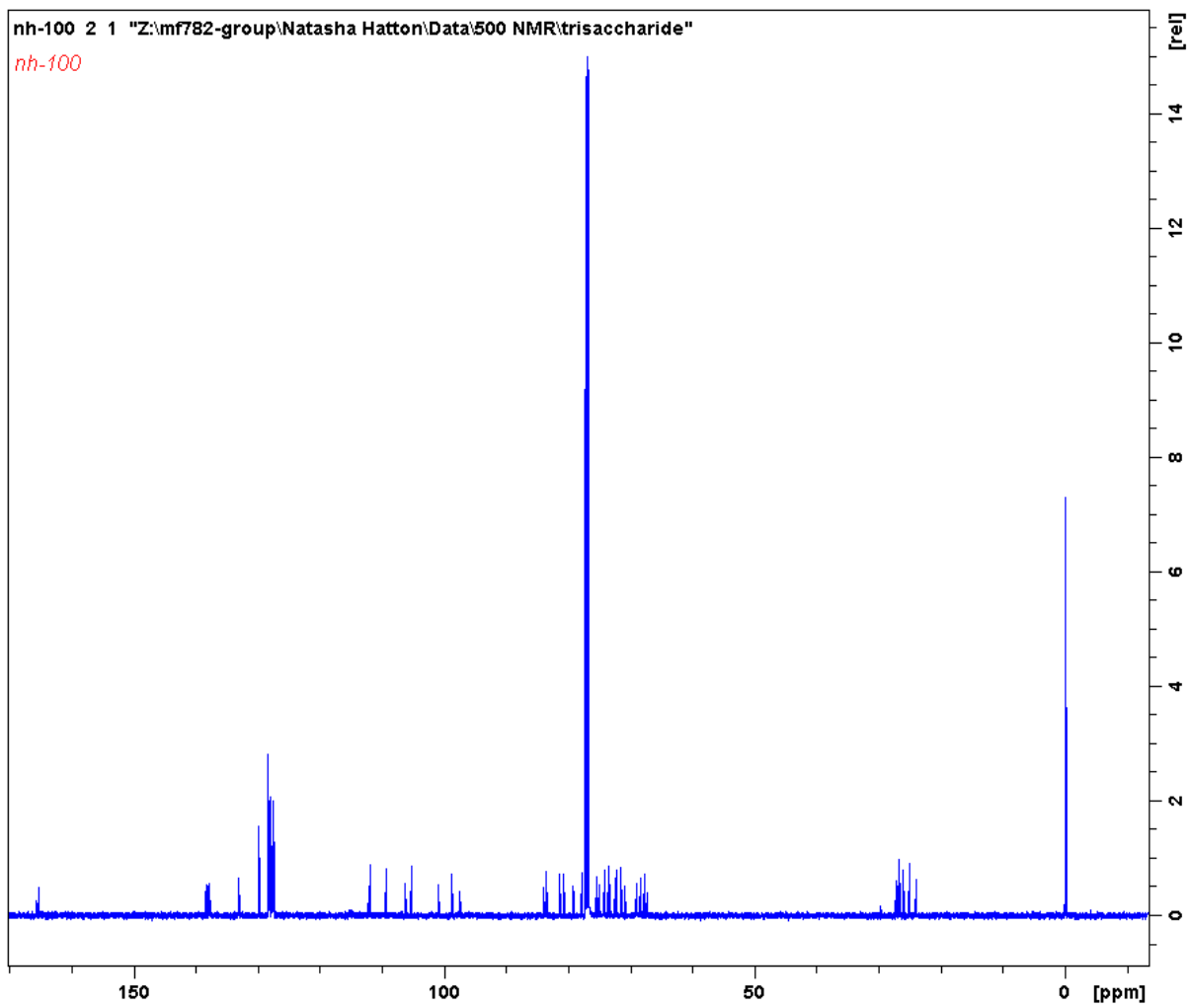


## Appendix

### 9.4.3.7 2-O-(Benzoyl-3,4,6-tri-O-benzyl- $\alpha$ -D-mannopyranoside)-(1 $\rightarrow$ 3)-1,2:5,6-di-O-isopropylidene- $\alpha$ -D-glucofuranose 5.40

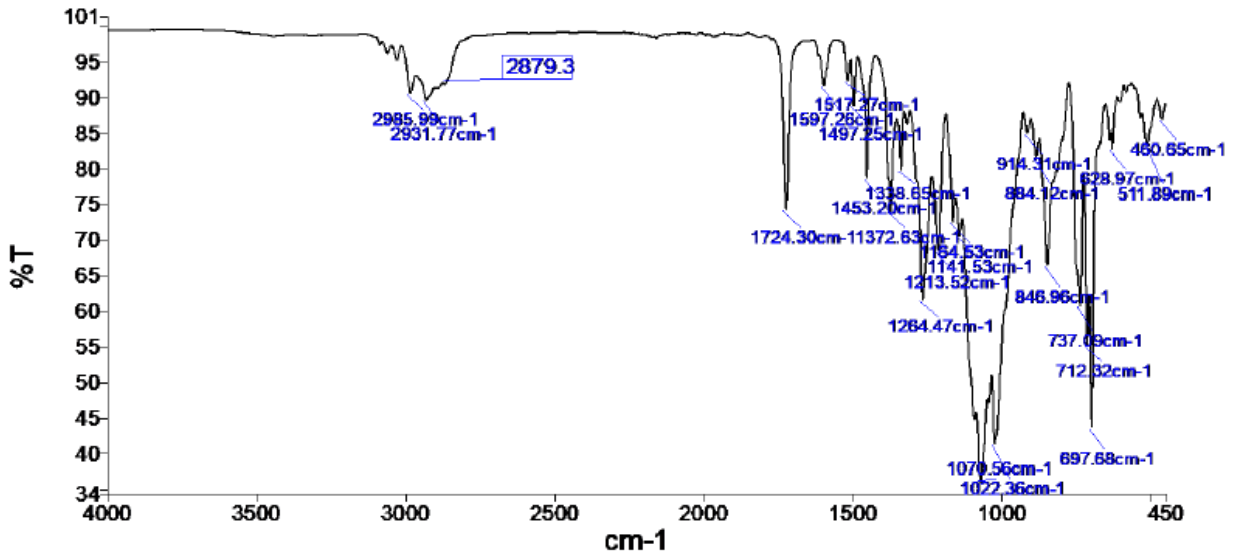
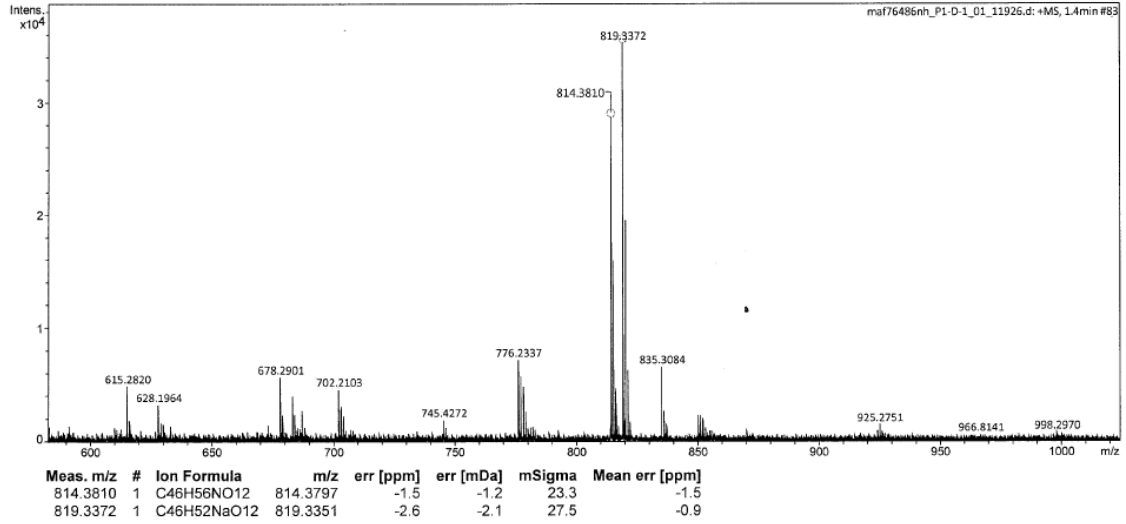


Appendix



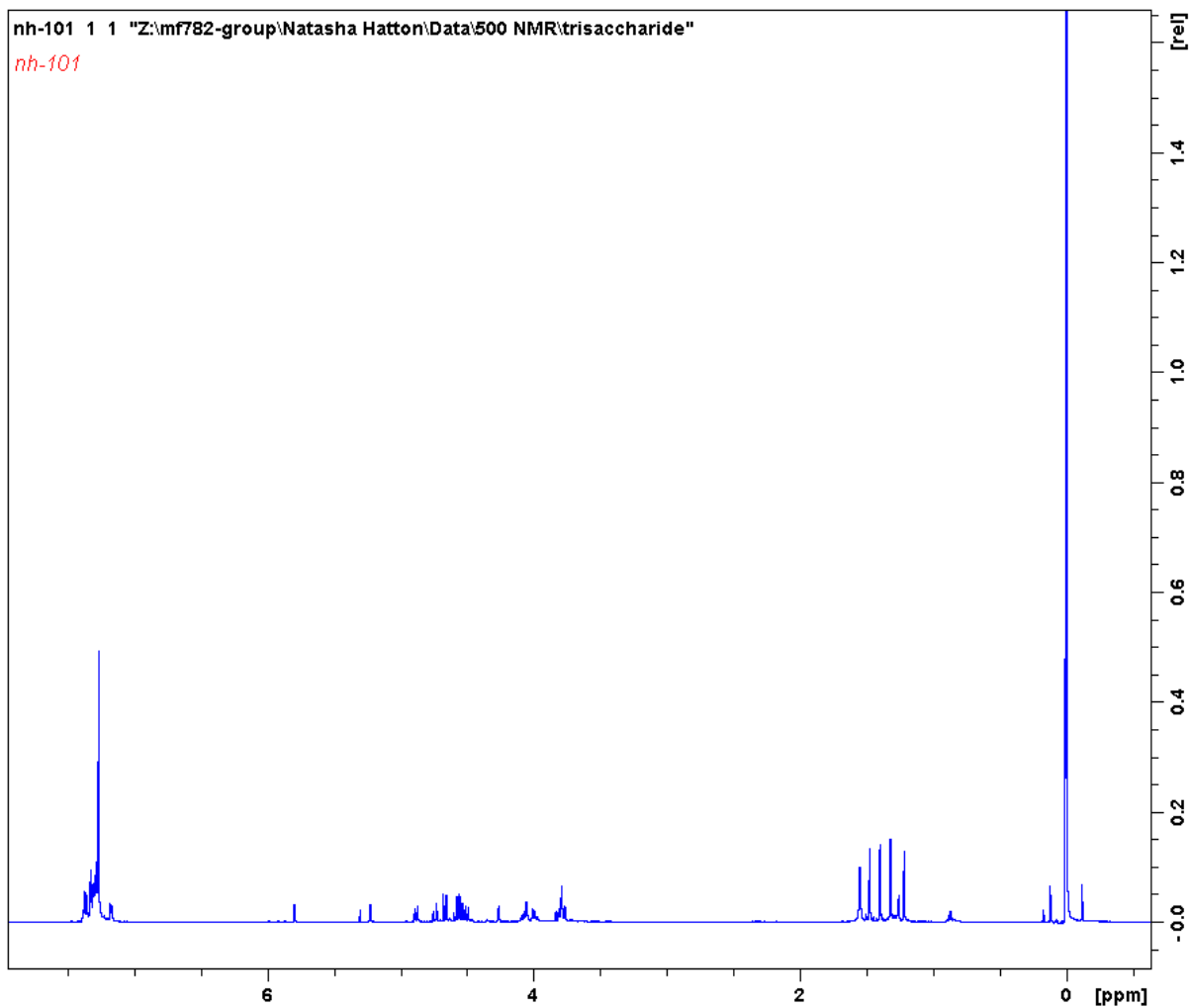
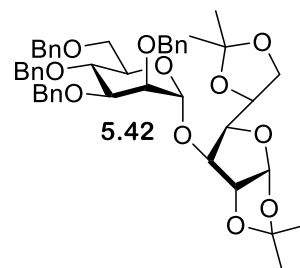


# Appendix

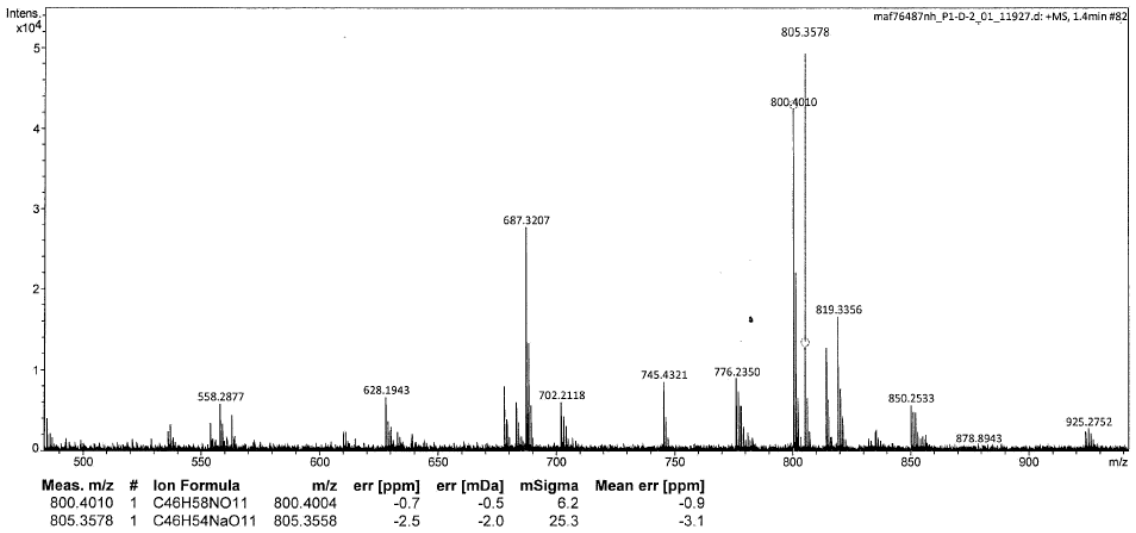
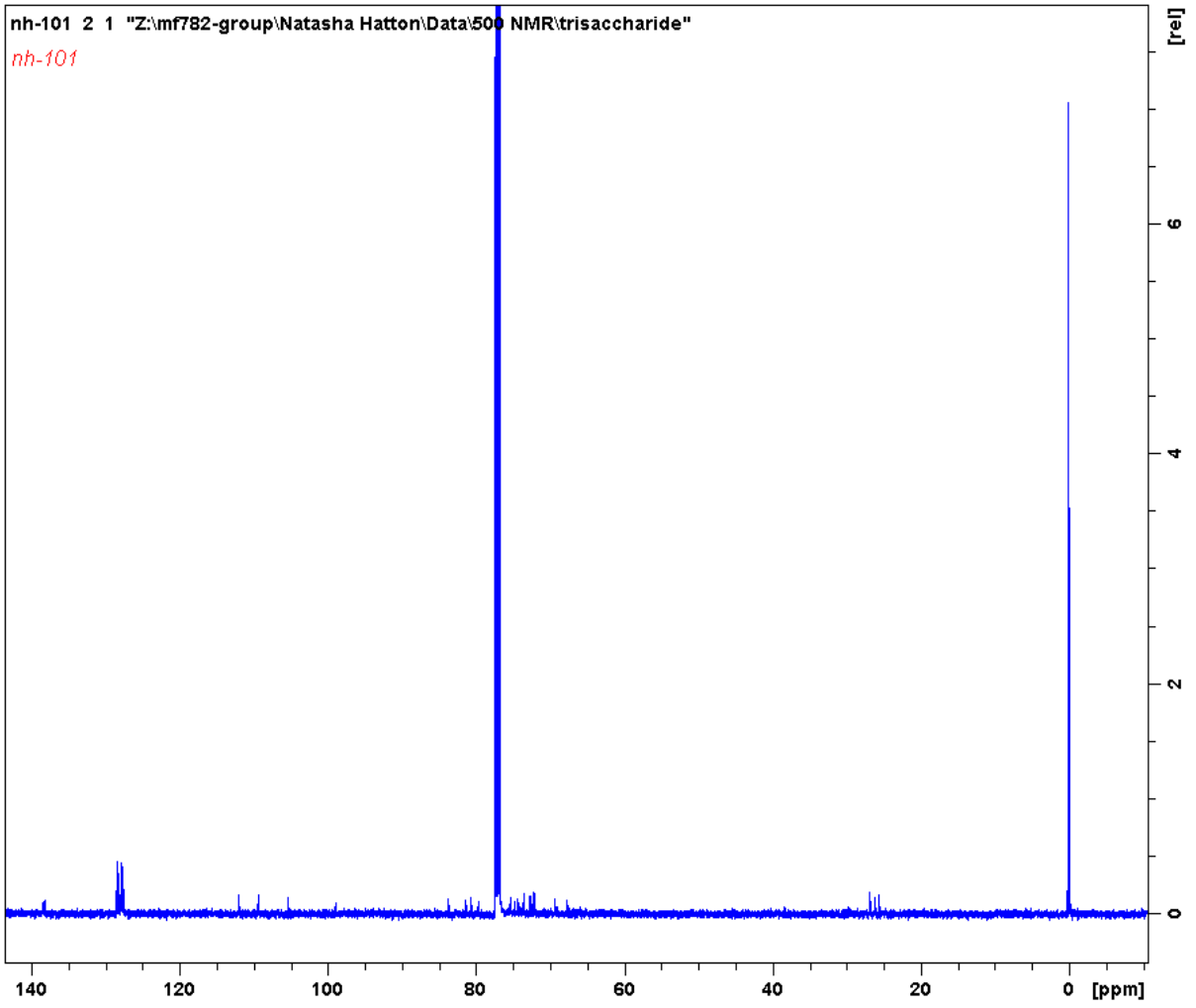


# Appendix

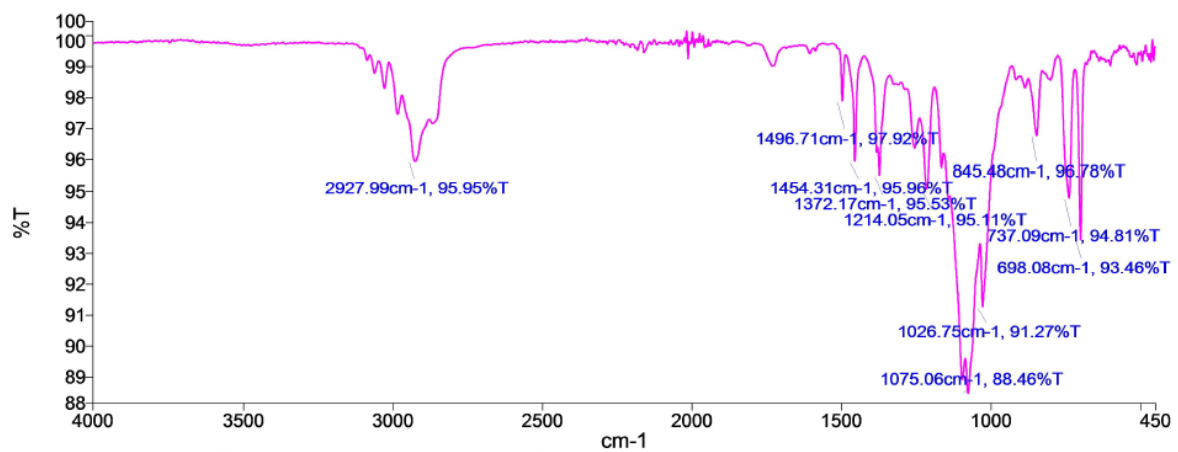
## 9.4.3.8 2,3,4,6-Tetra-O-benzyl- $\alpha$ -D-mannopyranosyl-(1 $\rightarrow$ 3)-1,2:5,6-Di-O-isopropylidene- $\alpha$ -D-glucofuranose 5.42



# Appendix



# Appendix



## Appendix

### 9.5 Appendix for Chapter 6

#### 9.5.1 BT-1033 expression

The BT-1033 gene housed within a pET-24a(+) plasmid was purchased from Genscript.

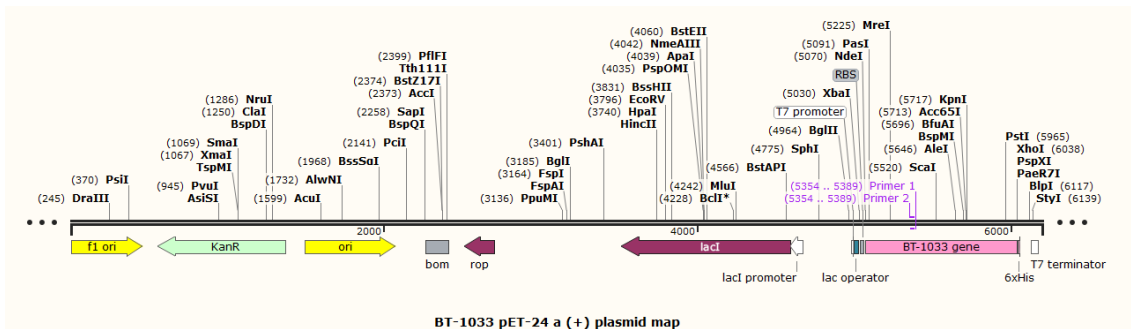


Figure 9-29. Plasmid map of BT-1033 pET-24 a(+), imaged using snap gene

#### Sequence of BT-1033 (no HIS TAG)

catatgaataagattcaaattccttgggaagaacgtcctgtcggatgtacagatgtaatgtggcggttactcgaaaatccggatcatcggacgcta  
tcatattccttcatccaatagtagttttcaacagtgctgtcgtacctttcaaagatggattcgcggcggtattccggttgacaacaaagctgtacag  
atgaacatcttcacaggattcagtaaagatggtattcattgggatattagtcagaccgattcagttcaaagccggtaacacggaaatgattga  
atccgaatataaatgaccgcgtgttacgtggattgaagaccgttattgggtaacttggtgcaacggctatcatggacctactatcggattgct  
ctatacattgattttgtagatttctccaatgcgagaatgcttctcctcttcaatcgtaatggagtactttccgcaaagatagatggcaaat  
atgctatgtaagtcgcccagcgacaatggacatacaccgttcggtgatatttatcagctacagtcggatgatgaatactggggtgaacac  
cgttggtcatgaaagtaactccttccctgaaagtgcctggcagtgtaaccaagattggtgcaggttcggtaccttcttactgatgaaggctggt  
tgctttctatcatggtgttatcactactgcaacggttccggtatgcaatgggttcggcgatactcgataaggatcatcccgaaggtactttat  
cgtaccctgtaatatctgataggtccggctgcacctatgaactcaaggggatgtgccaatggtgattcccattgctggcattgcaggatggt  
gagcgtgtagctgtttattatggagctgcagataccgtttaggaatggcttccgctatatccaggaaataattgattttacaaacgaacgagc  
attatcctcgag

#### HisTrap HP column trace

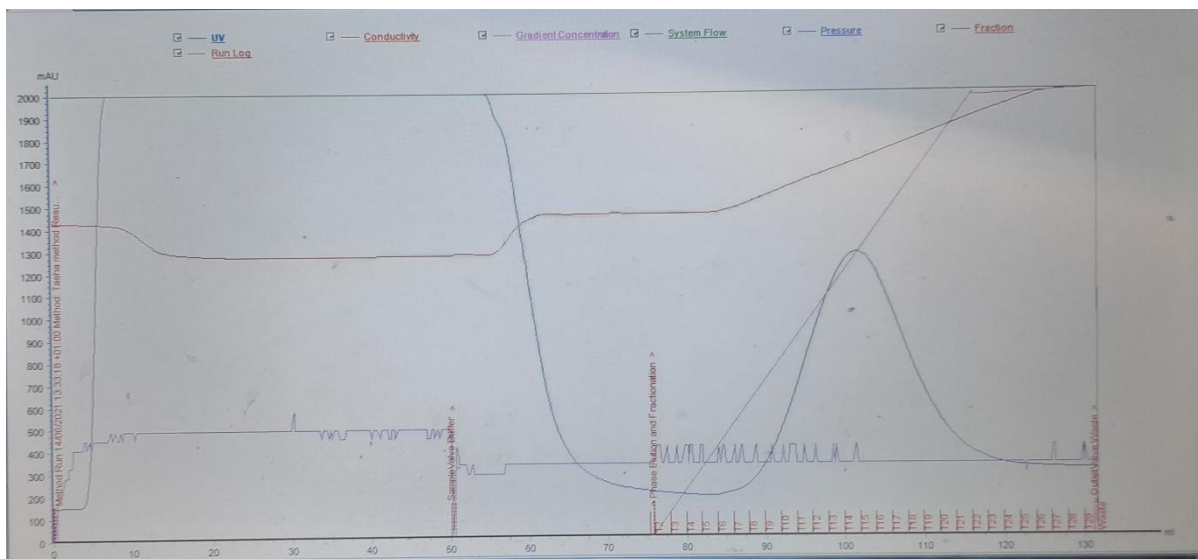


Figure 9-30. HisTrap HP column trace

## Appendix

### Post HisTrap HP column gels

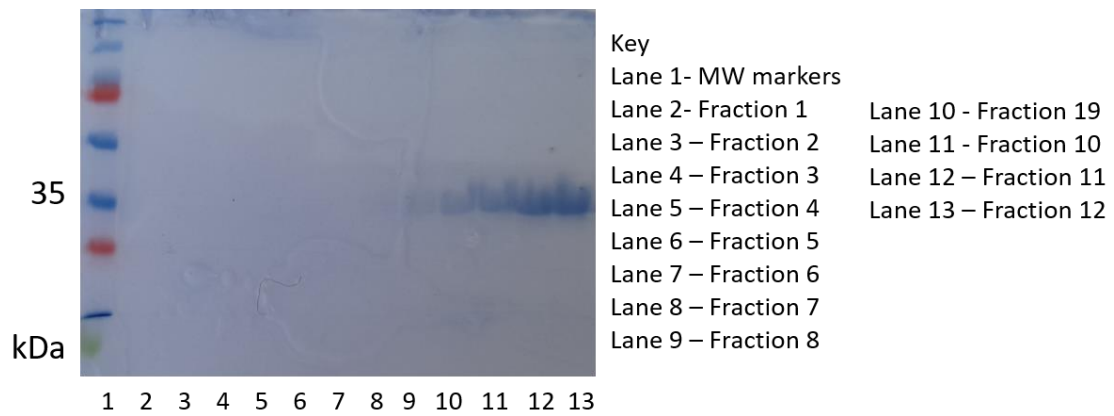


Figure 9-31. Results of SDS-PAGE gel stained with Coomassie of fractions 1-12 extracted from the HisTrap column

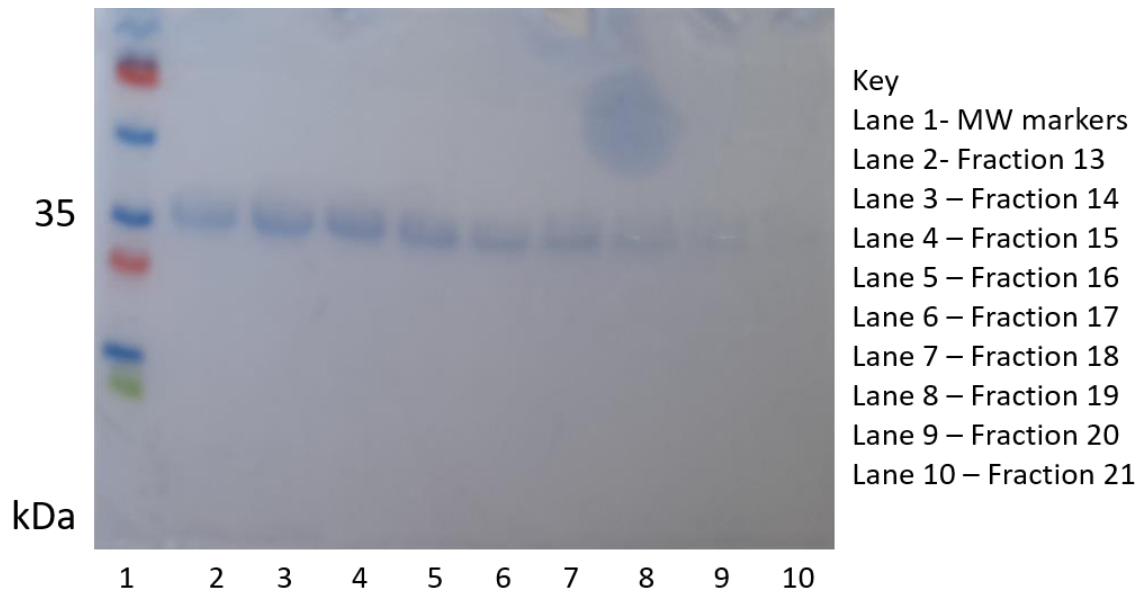


Figure 9-32. Results of SDS-PAGE gel stained with Coomassie of fractions 13-21 extracted from the HisTrap column

## Appendix

### Gel filtration column trace

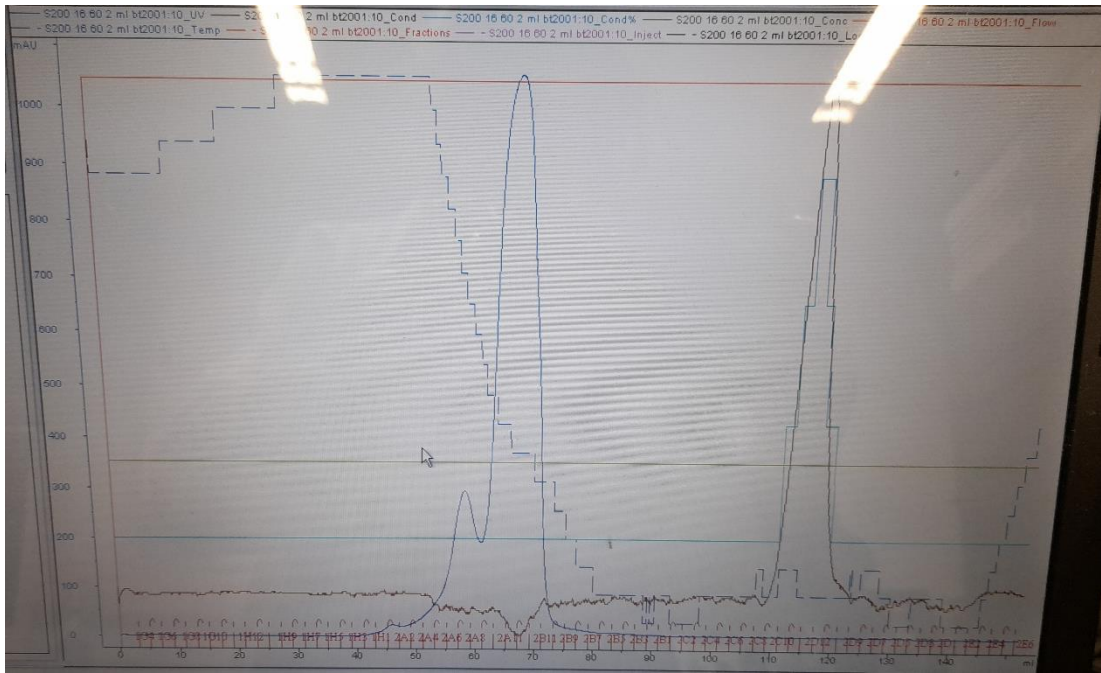


Figure 9-33. Gel filtration column trace

### Post gel filtration gel

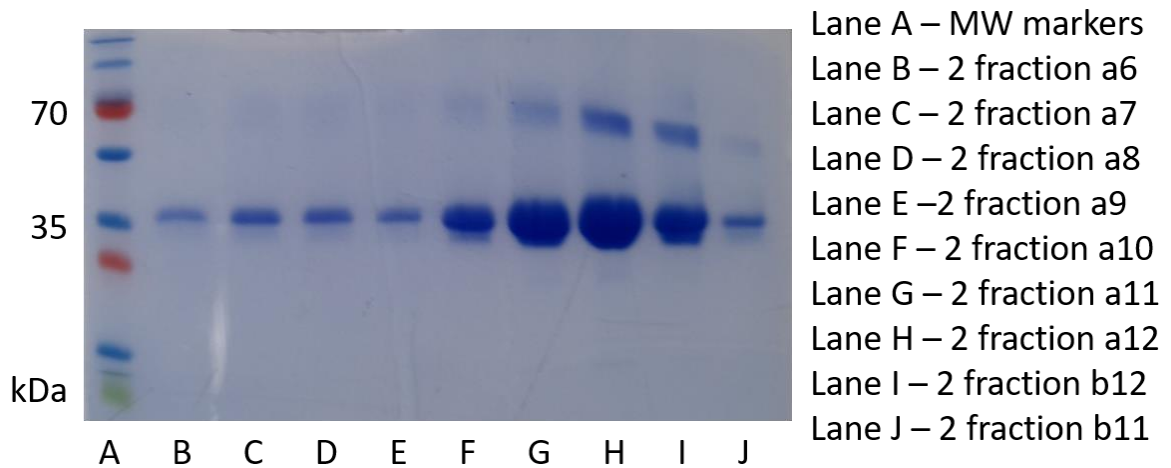


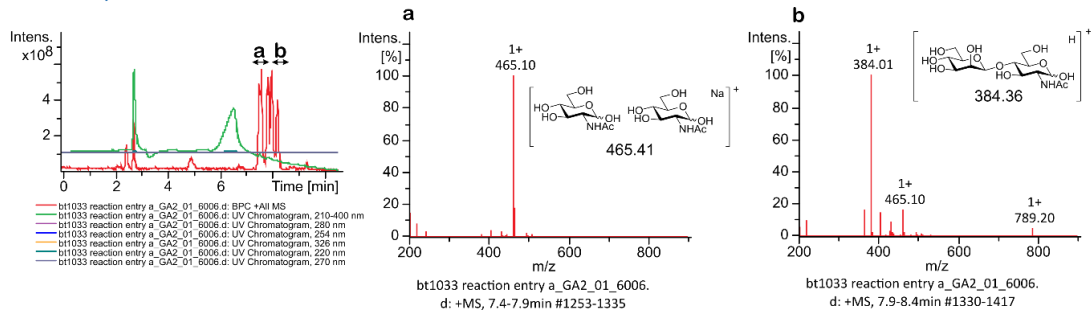
Figure 9-34. Results of SDS-PAGE gel stained with Coomassie of fractions a6 to b11 extracted post gel filtration

## Appendix

### 9.5.2 BT-1033 catalysed reactions 1-42b

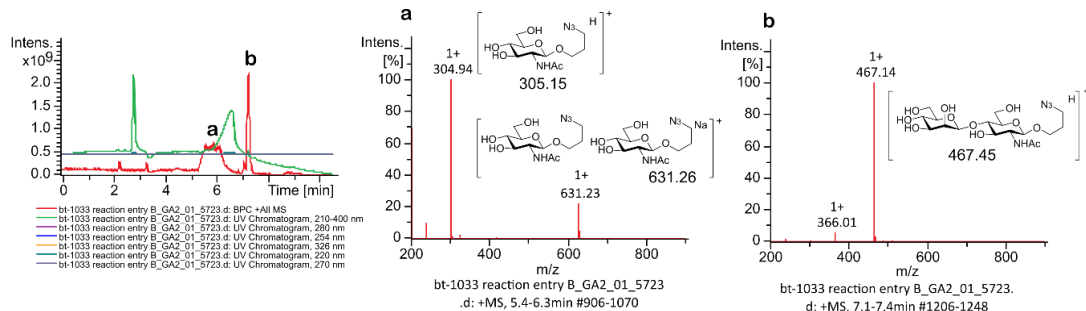
Attached below is the LCMS trace taken post reaction termination, the peaks corresponding to the acceptors and disaccharides masses are highlighted. An LCMS spectrum of each sample post reaction with ITag reagent **6.16** (given to us by the Galan group, University of Bristol) is also attached, the masses for the ITag reagent **6.16** clicked acceptors and disaccharide peaks are shown and their relative intensities are given. These results have been included in Table 38 and used to calculate each reactions conversion rate.

#### Reaction Entry 1

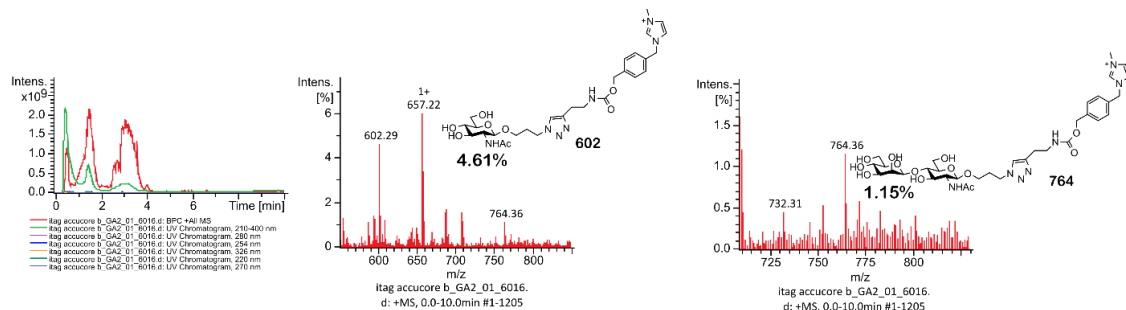


#### Reaction Entry 2

Post reaction LCMS trace



Post reaction with ITag reagent **6.16** LCMS trace

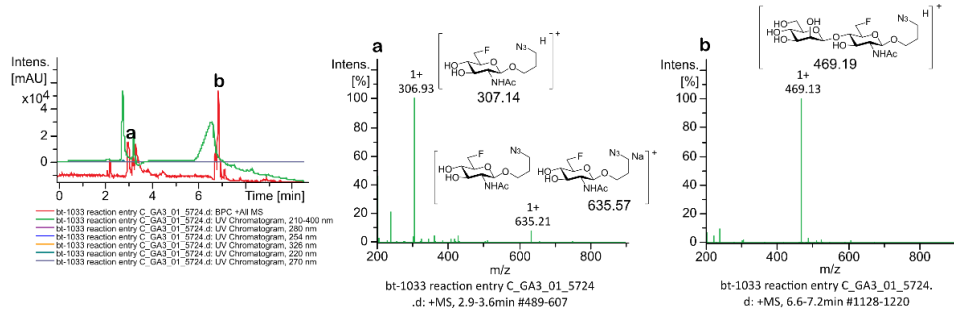




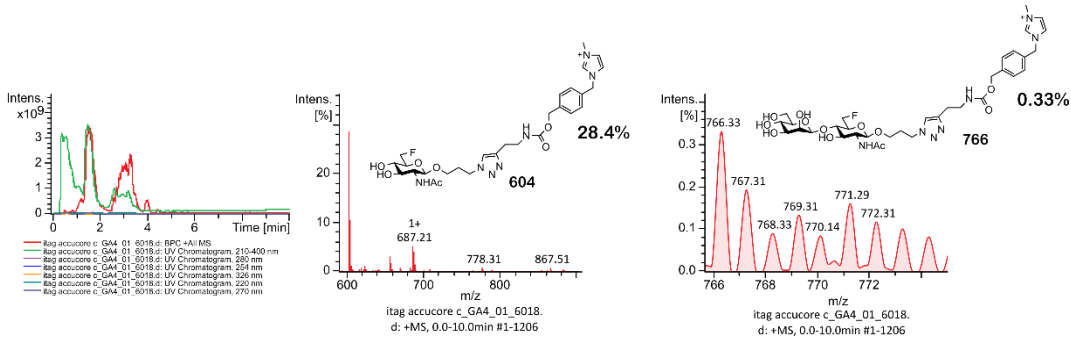
## Appendix

### Reaction Entry 3

#### Post reaction termination LCMS trace

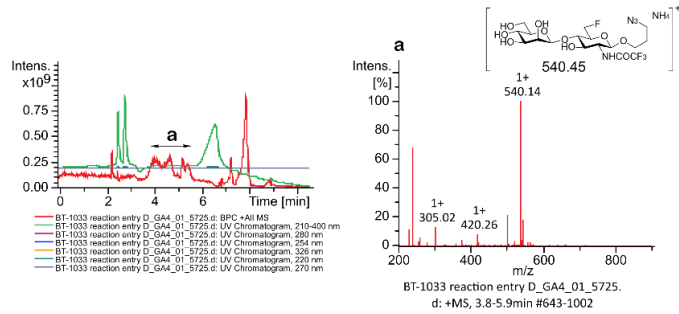


#### Post reaction with ITag reagent 6.16 LCMS trace

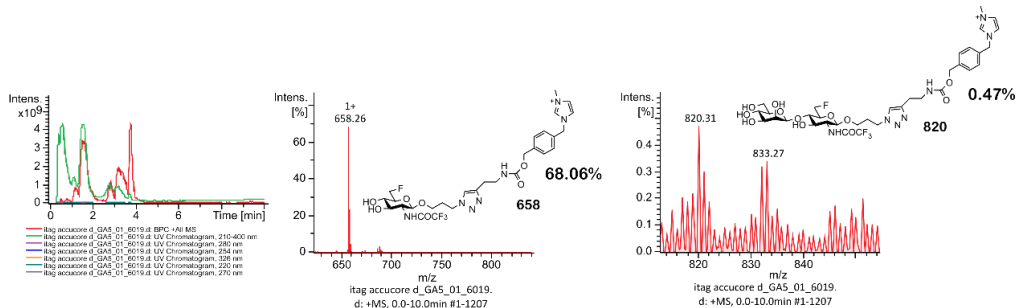


### Reaction Entry 4

#### Post reaction termination LCMS trace



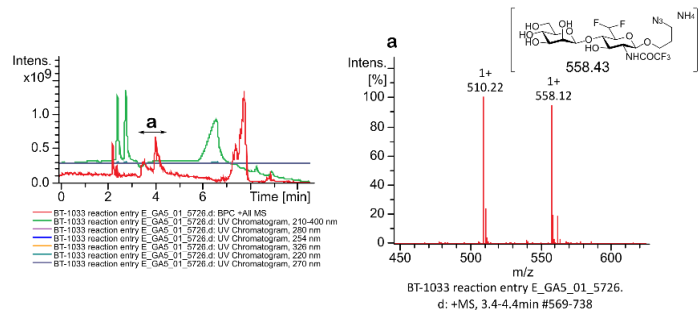
#### Post reaction with ITag reagent 6.16 LCMS trace



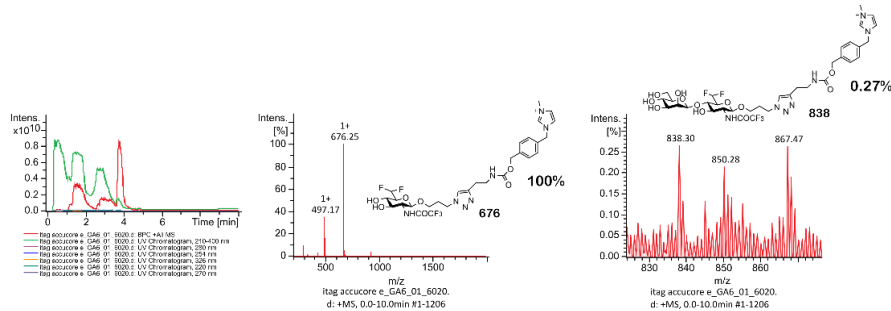
## Appendix

### Reaction Entry 5

#### Post reaction termination LCMS trace

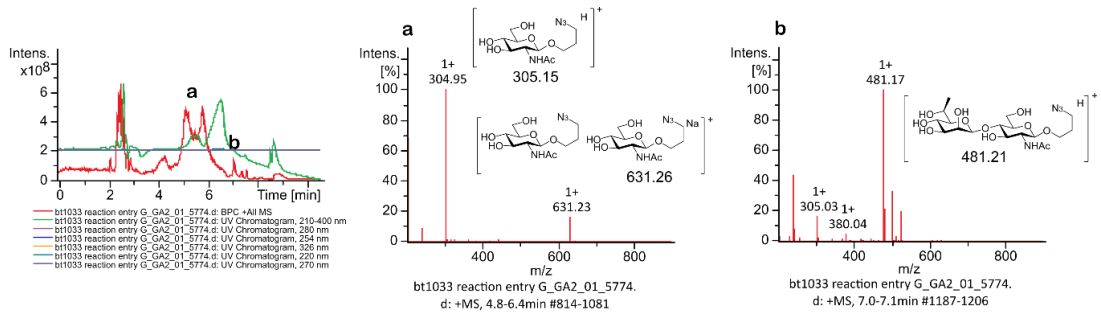


#### Post reaction with ITag reagent 6.16 LCMS trace

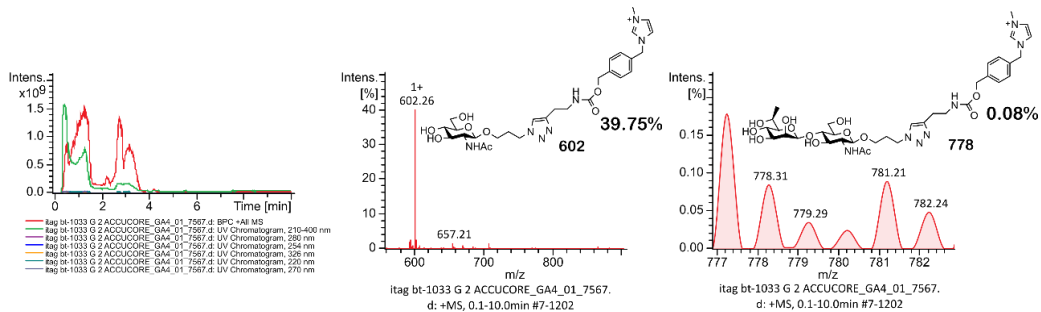


### Reaction Entry 6

#### Post reaction termination LCMS trace



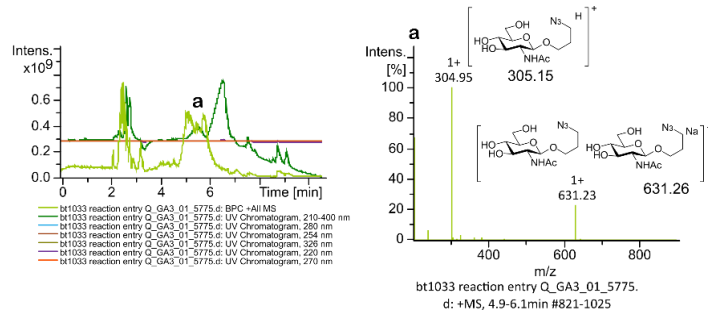
#### Post reaction with ITag reagent 6.16 LCMS trace



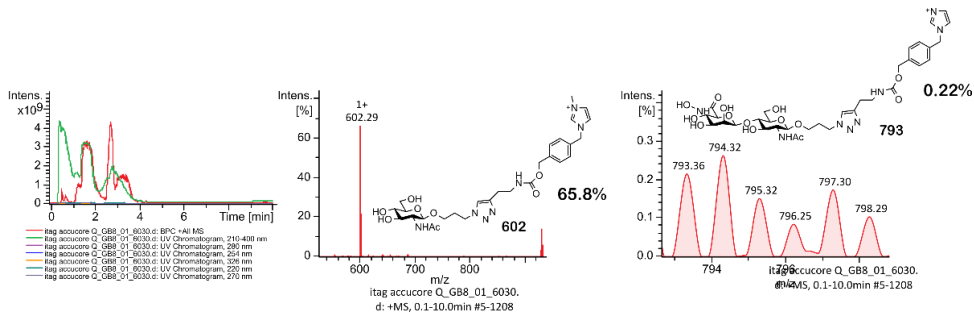
## Appendix

### Reaction Entry 7

#### Post reaction termination LCMS trace

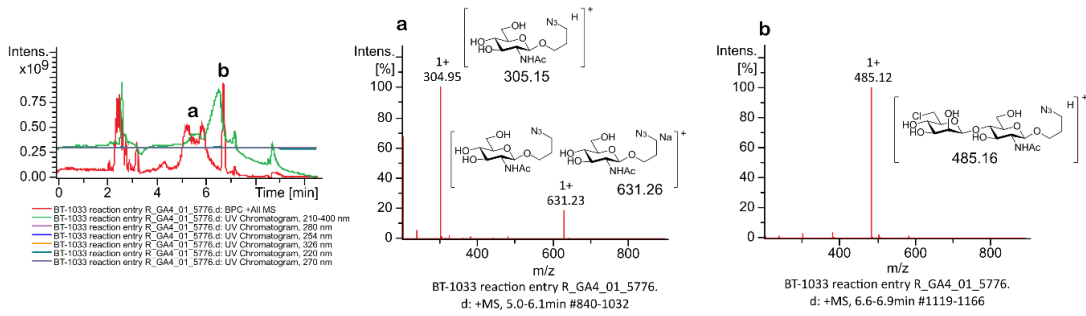


#### Post reaction with ITag reagent 6.16 LCMS trace

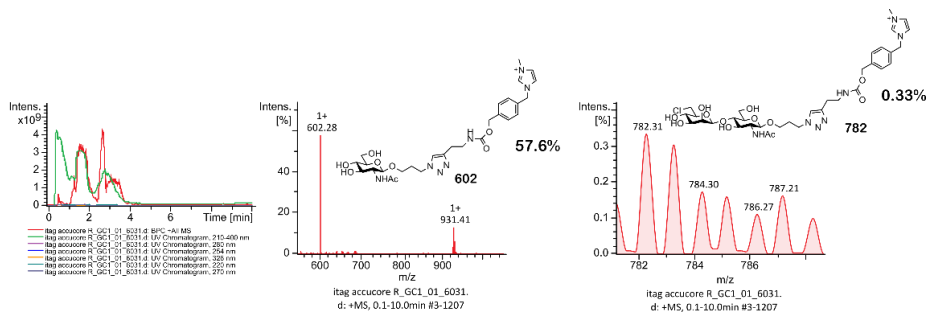


### Reaction Entry 8

#### Post reaction LCMS trace



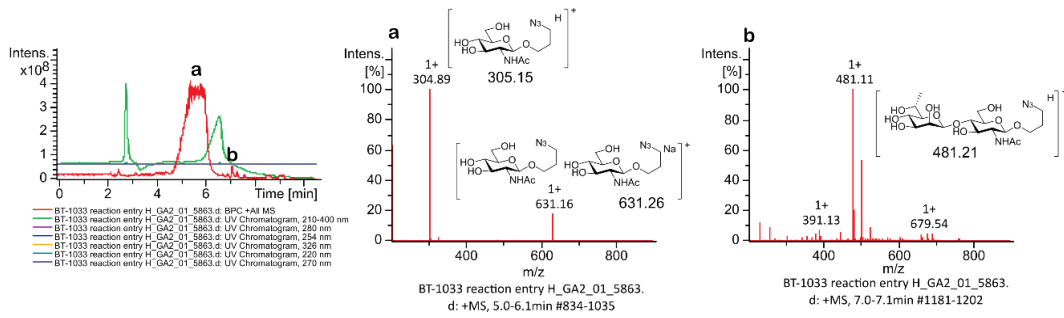
#### Post reaction with ITag reagent 6.16 LCMS trace



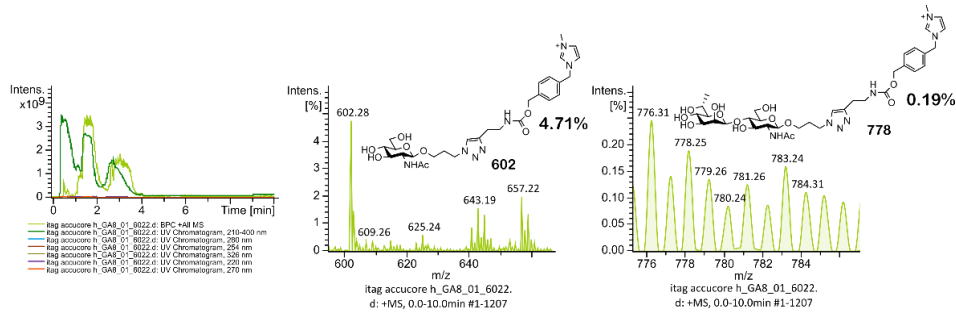
## Appendix

### Reaction Entry 9

#### Post reaction LCMS trace

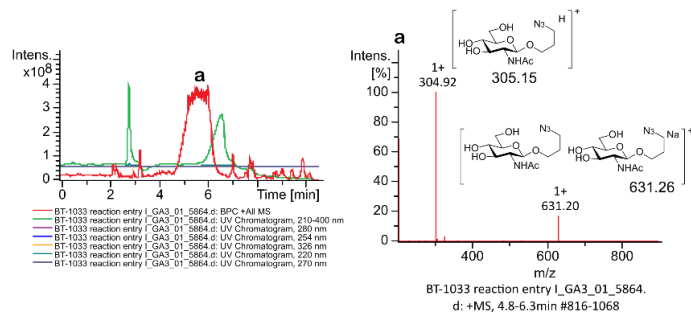


#### Post reaction with ITag reagent 6.16 LCMS trace

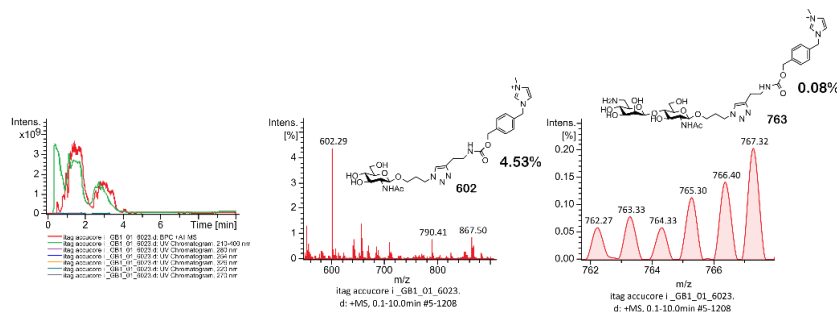


### Reaction Entry 10

#### Post reaction termination LCMS trace



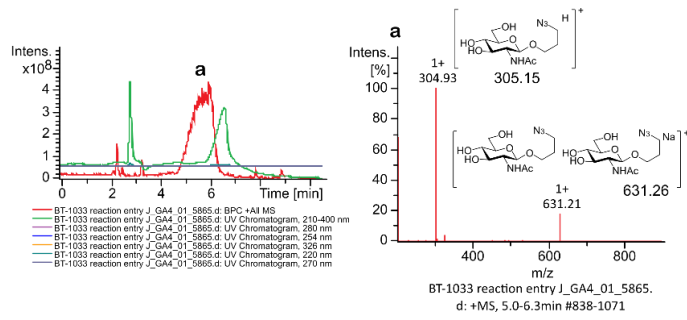
#### Post reaction with ITag reagent 6.16 LCMS trace



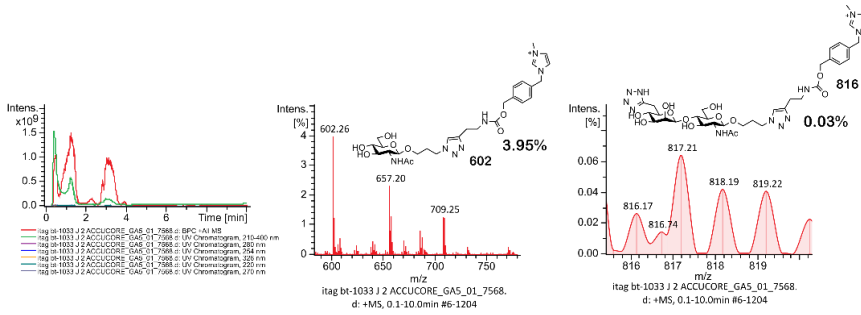
## Appendix

### Reaction Entry 11

#### Post reaction termination LCMS trace

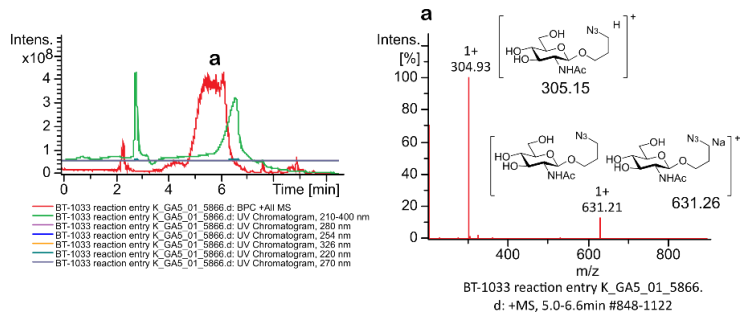


#### Post reaction with ITag reagent 6.16 LCMS trace

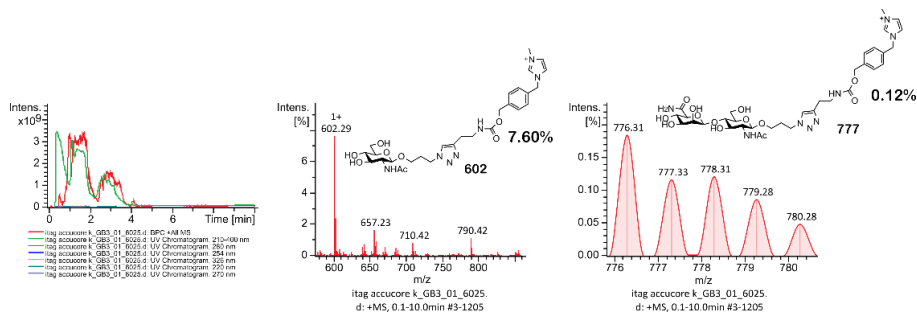


### Reaction Entry 12

#### Post reaction termination LCMS trace



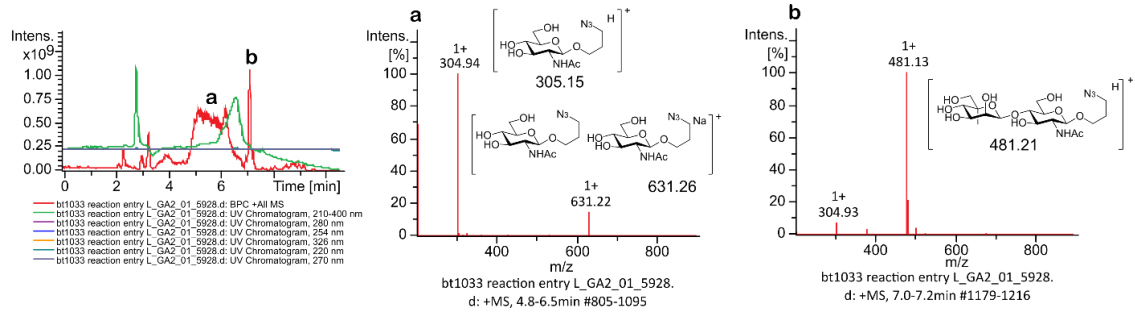
#### Post reaction with ITag reagent 6.16 LCMS trace



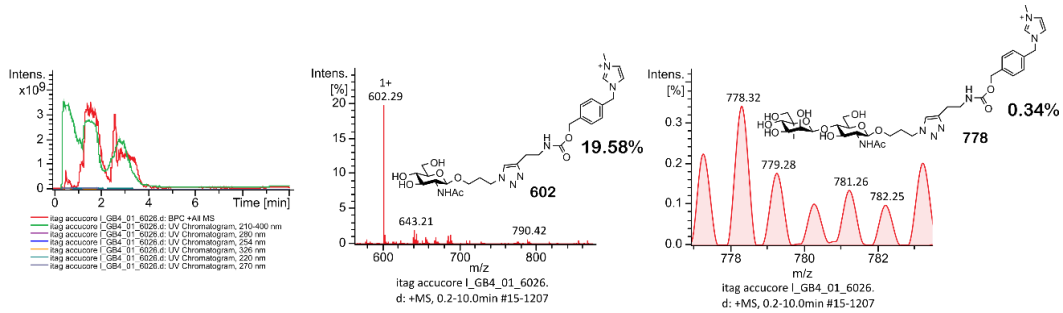
## Appendix

### Reaction Entry 13

#### Post reaction termination LCMS trace

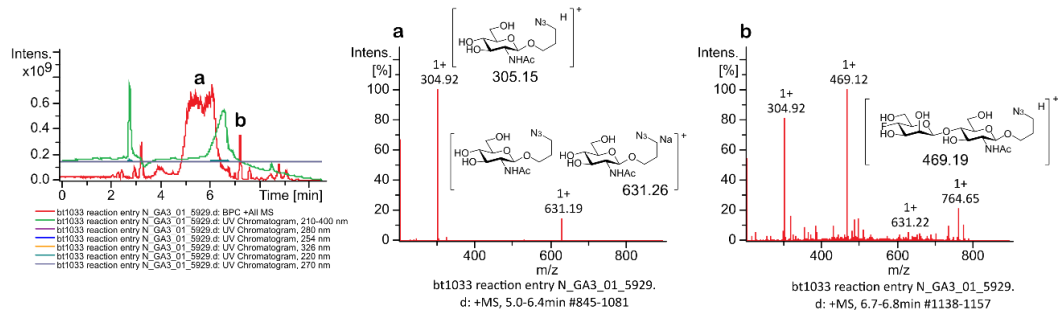


#### Post reaction with ITag reagent 6.16 LCMS trace

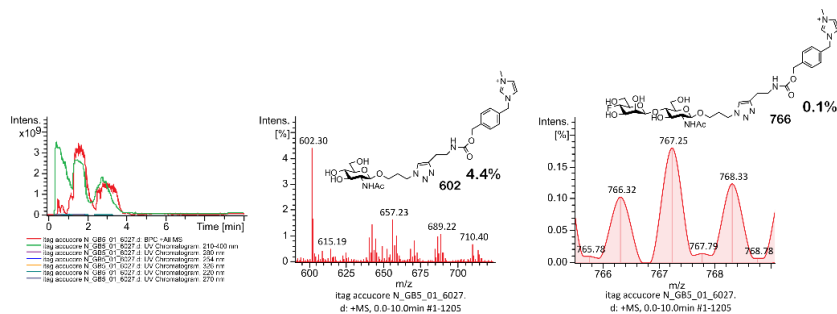


### Reaction Entry 14

#### Post reaction termination LCMS trace



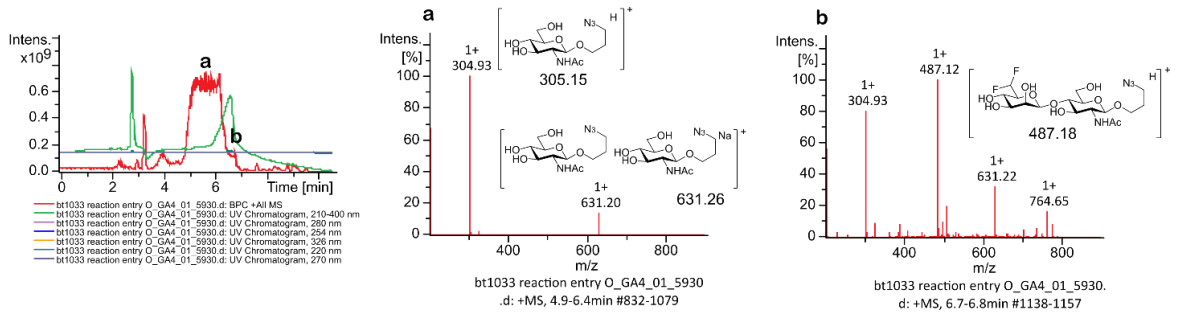
#### Post reaction with ITag reagent 6.16 LCMS trace



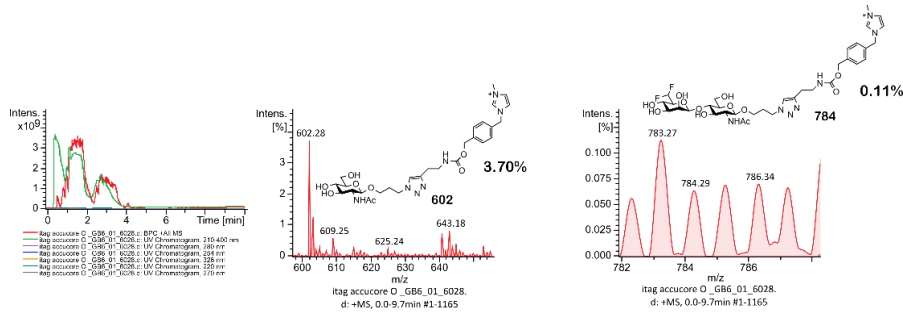
# Appendix

## Reaction Entry 15

### Post reaction termination LCMS trace

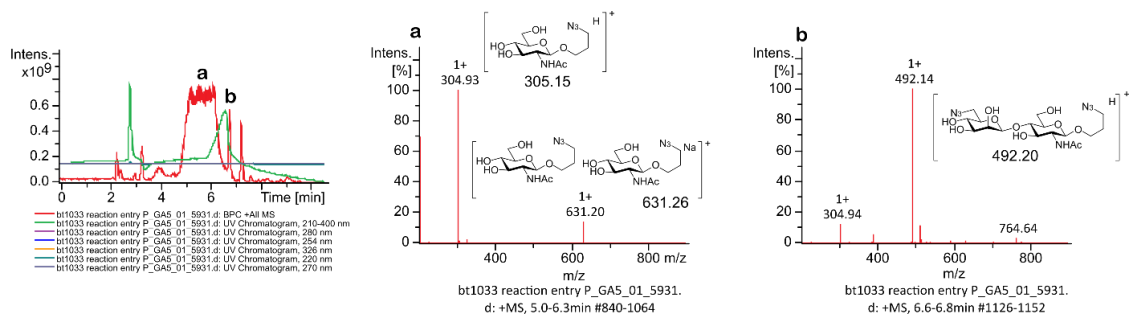


### Post reaction with ITag reagent 6.16 LCMS trace

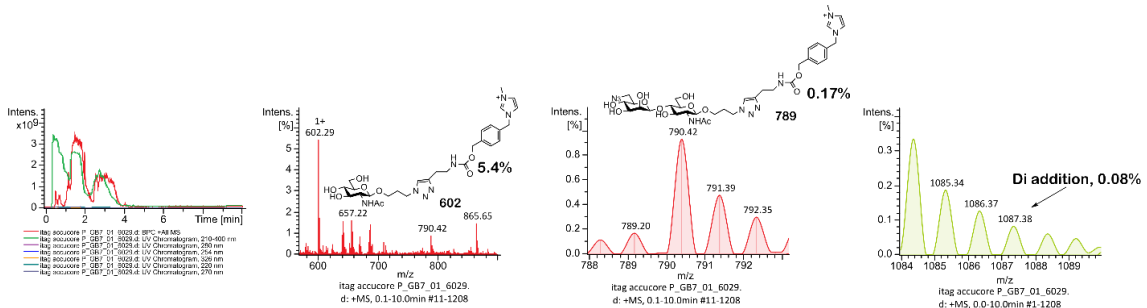


## Reaction Entry 16

### Post reaction termination LCMS trace



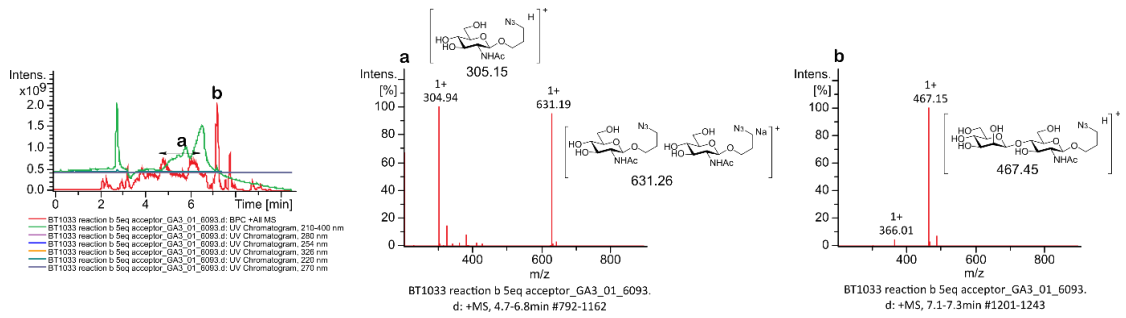
### Post reaction with ITag reagent 6.16 LCMS trace



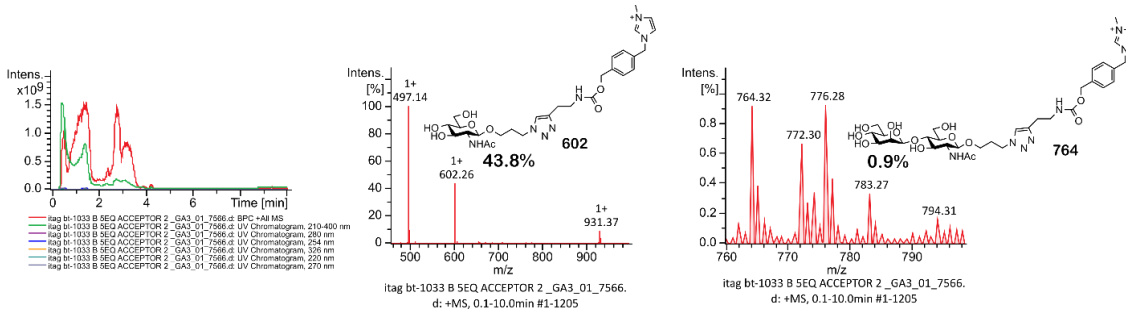
## Appendix

### Reaction Entry 17

#### Post reaction LCMS trace

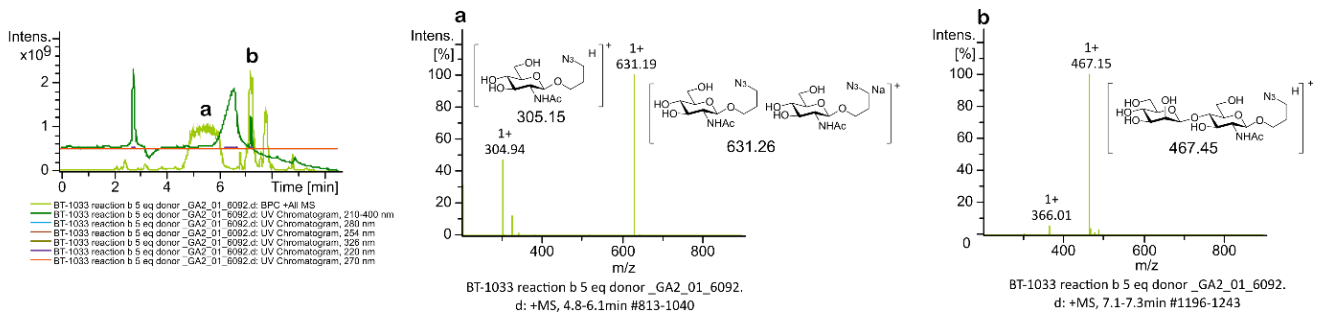


#### Post reaction with ITag reagent 6.16 LCMS trace

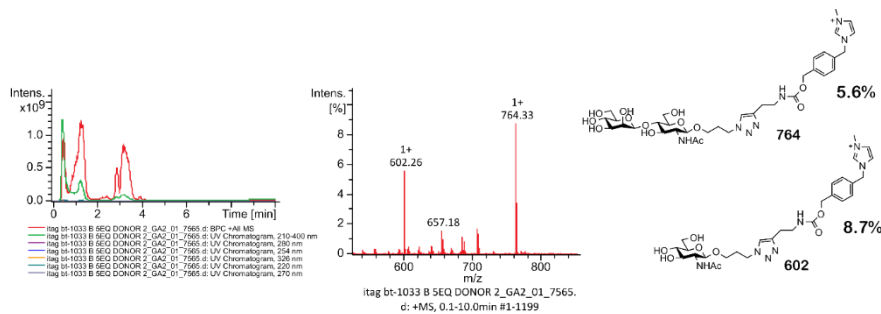


### Reaction Entry 18

#### Post reaction LCMS trace



#### Post reaction with ITag reagent 6.16 LCMS trace

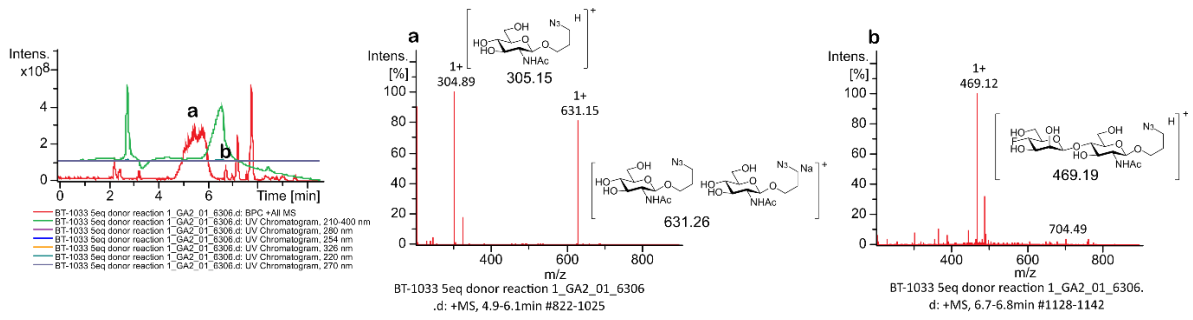




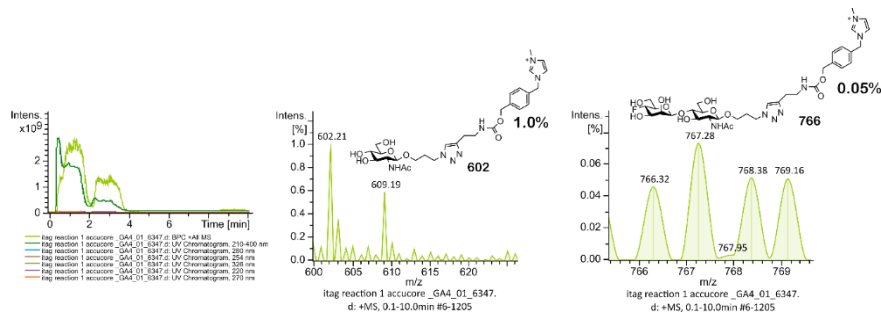
## Appendix

### Reaction Entry 19

#### Post reaction LCMS trace

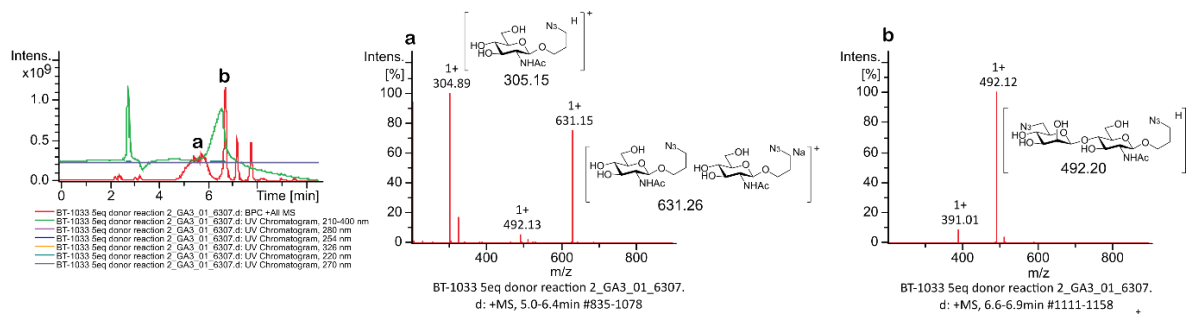


#### Post reaction with ITag reagent 6.16 LCMS trace

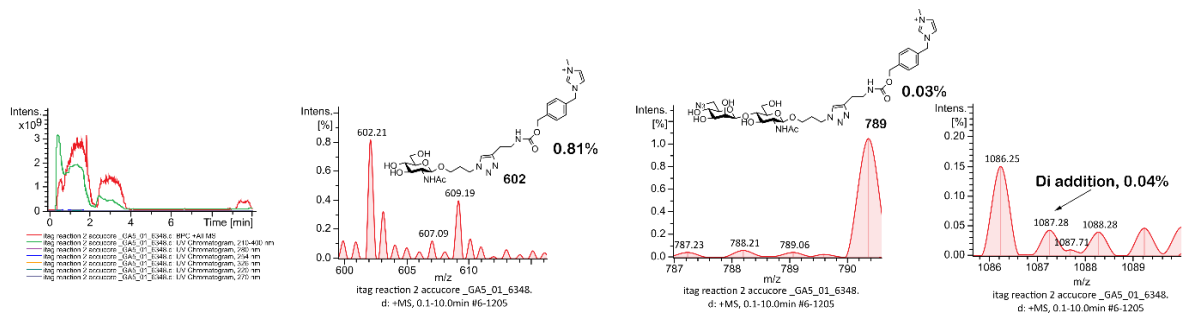


### Reaction Entry 20

#### Post reaction LCMS trace



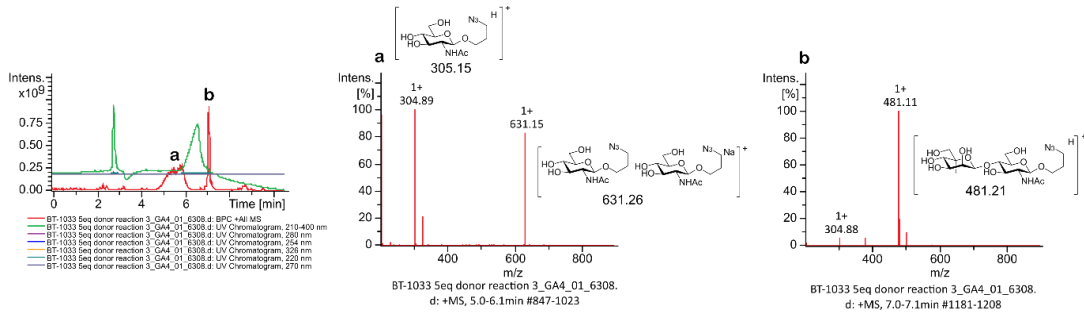
#### Post reaction with ITag reagent 6.16 LCMS trace



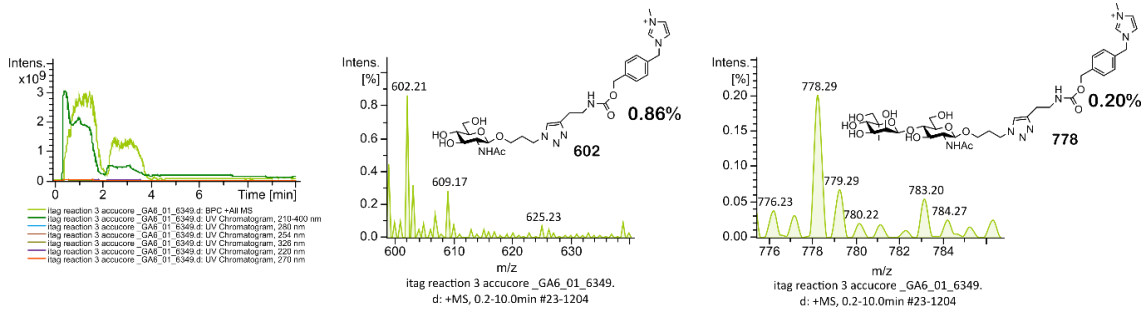
## Appendix

### Reaction Entry 21a

#### Post reaction LCMS trace

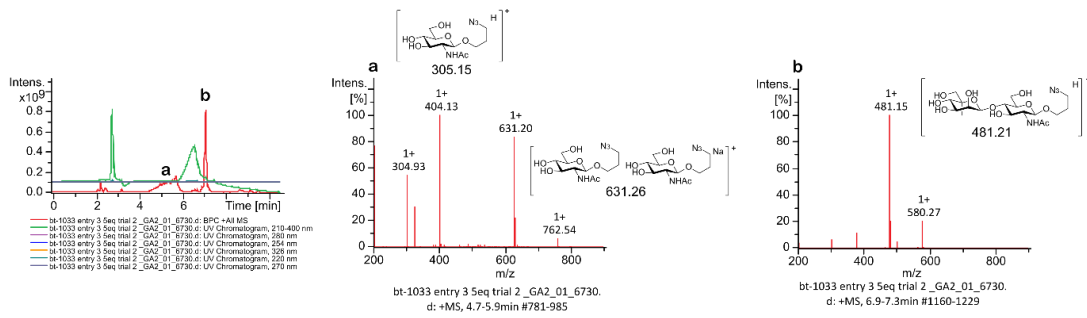


#### Post reaction with ITag reagent 6.16 LCMS trace

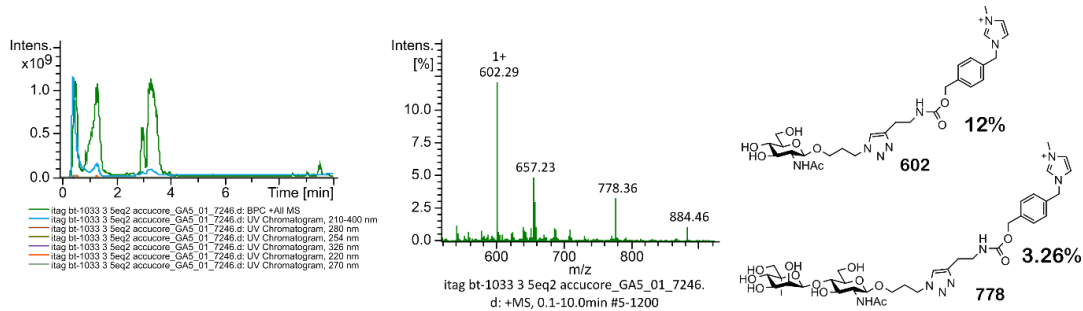


### Reaction Entry 21b

#### Post reaction termination LCMS trace



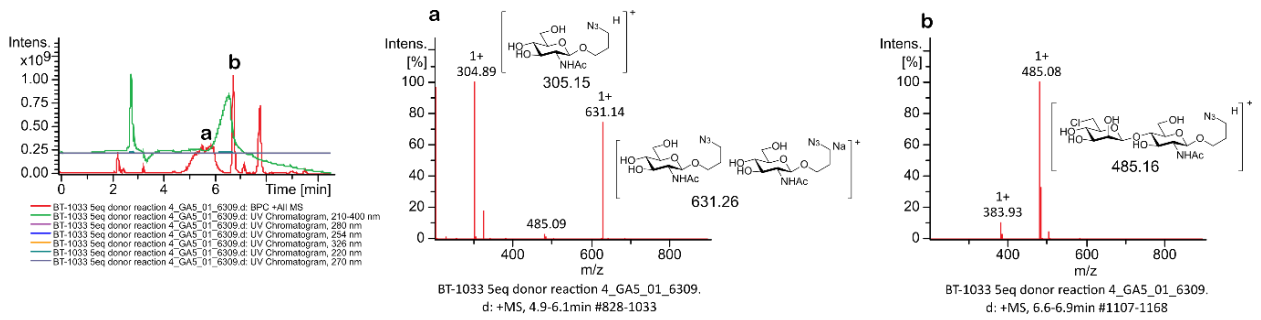
#### Post reaction with ITag reagent 6.16 LCMS trace



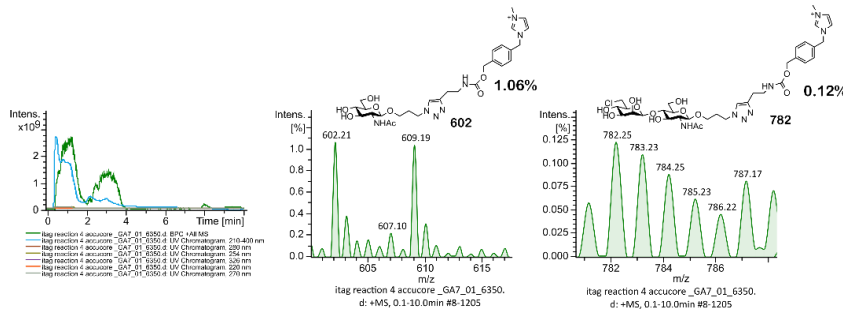
## Appendix

### Reaction Entry 22a

#### Post reaction termination LCMS trace

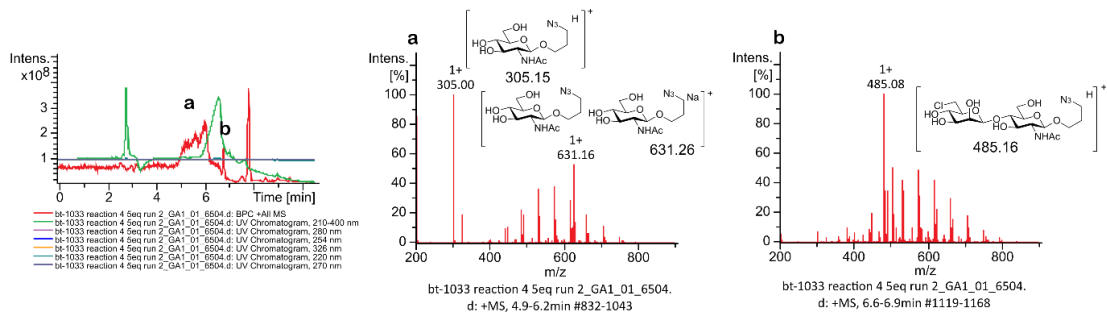


#### Post reaction with ITag reagent 6.16 LCMS trace

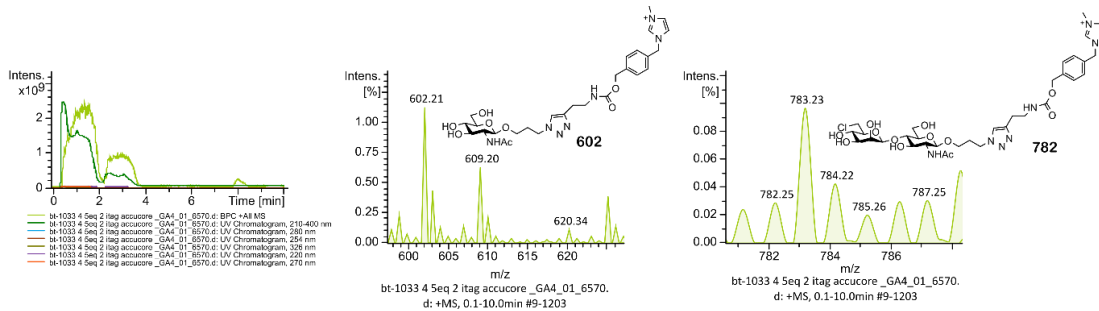


### Reaction Entry 22b

#### Post reaction termination LCMS trace



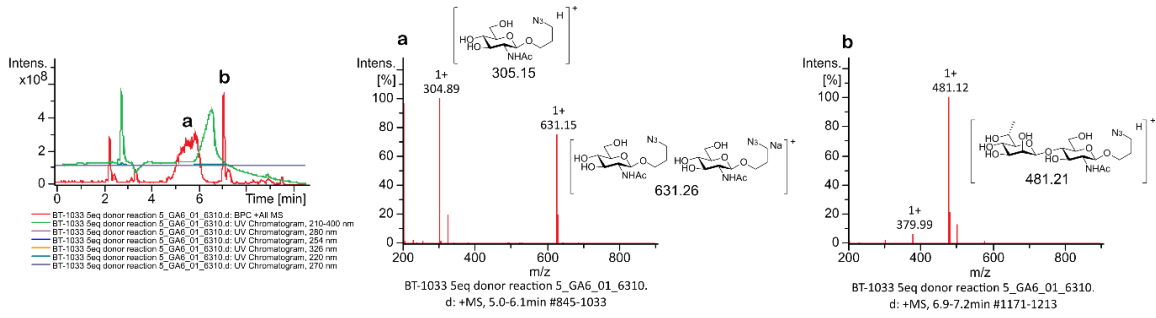
#### Post reaction with ITag reagent 6.16 LCMS trace



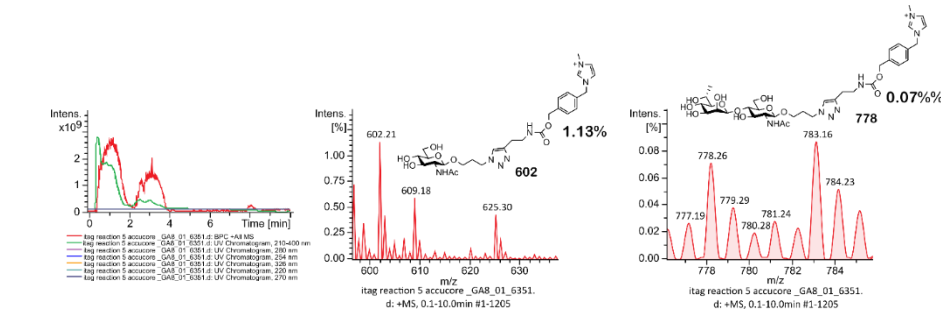
## Appendix

### Reaction trace 23a

#### Post reaction termination LCMS trace

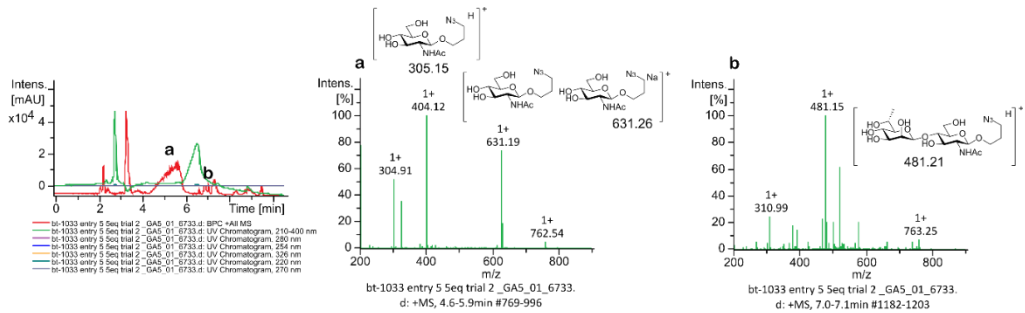


#### Post reaction with ITag reagent 6.16 LCMS trace

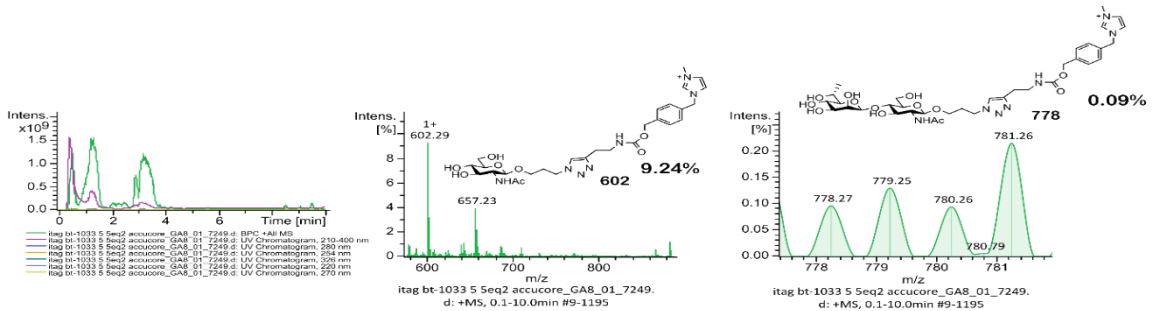


### Reaction Entry 23b

#### Post reaction termination LCMS trace



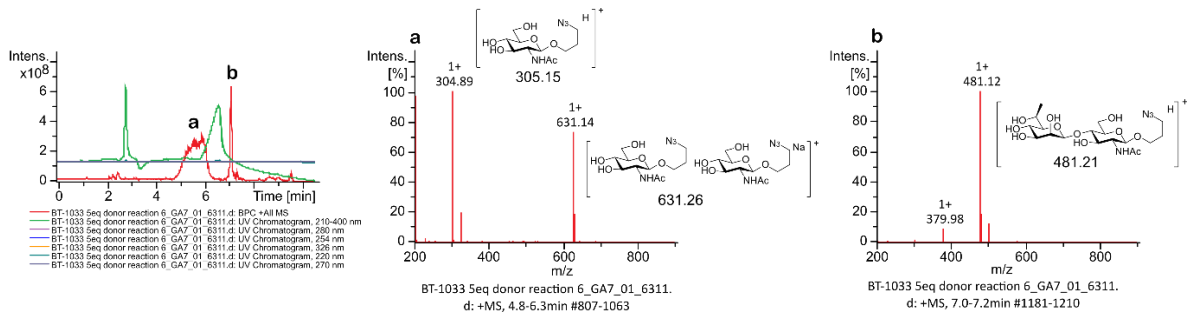
#### Post reaction with ITag reagent 6.16 LCMS trace



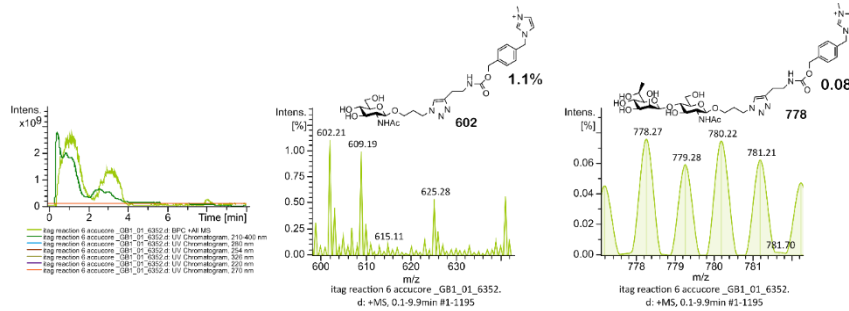
## Appendix

### Reaction trace 24a

#### Post reaction termination LCMS trace

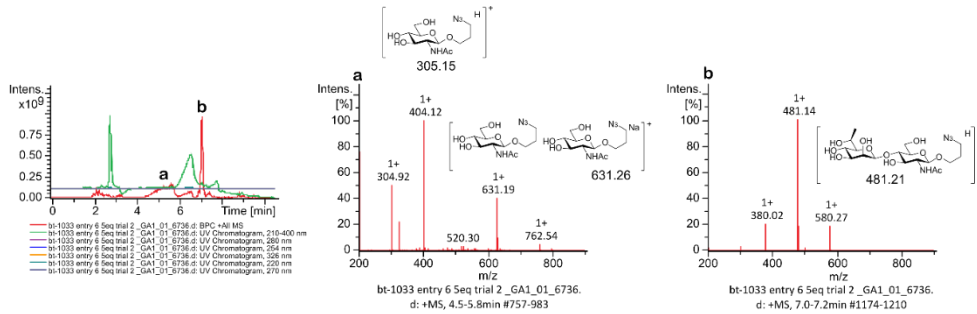


#### Post reaction with ITag reagent 6.16 LCMS trace

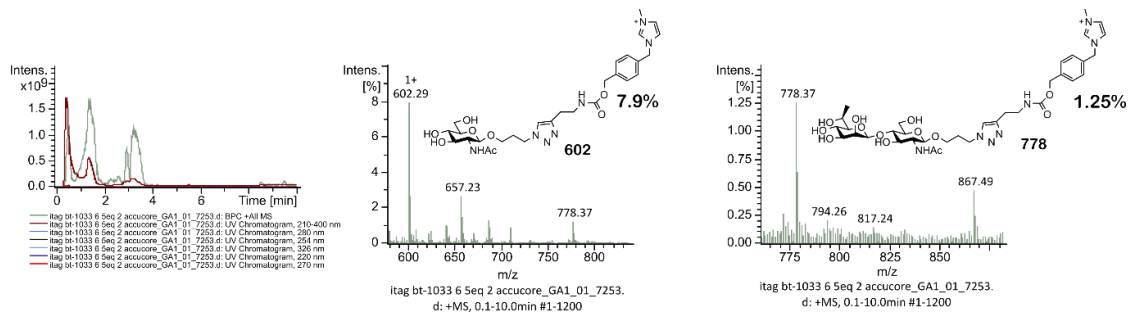


### Reaction Entry 24b

#### Post reaction termination LCMS trace



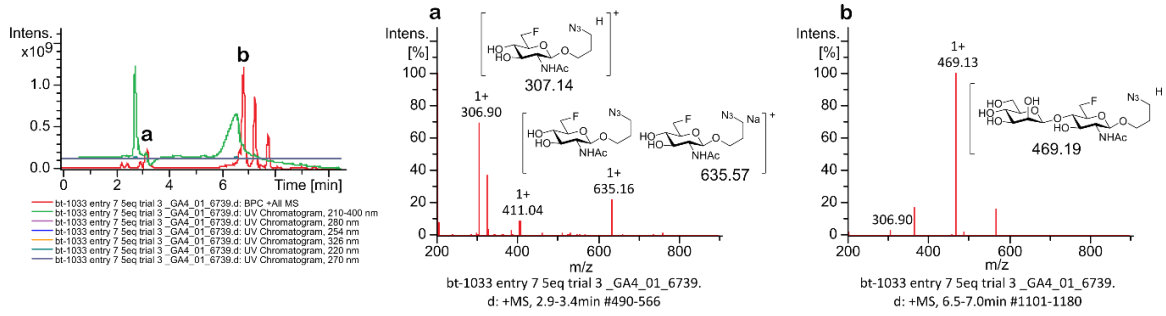
#### Post reaction with ITag reagent 6.16 LCMS trace



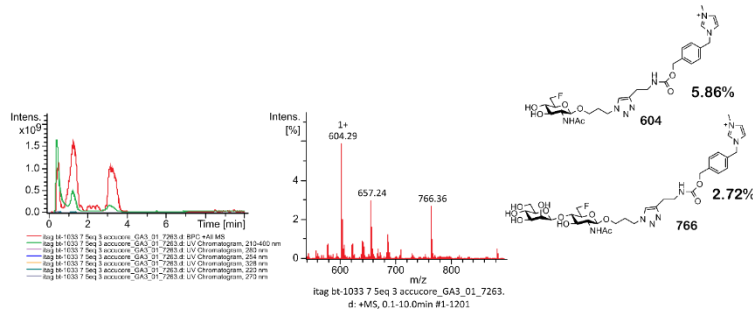
## Appendix

### Reaction trace 25a

#### Post reaction termination LCMS trace

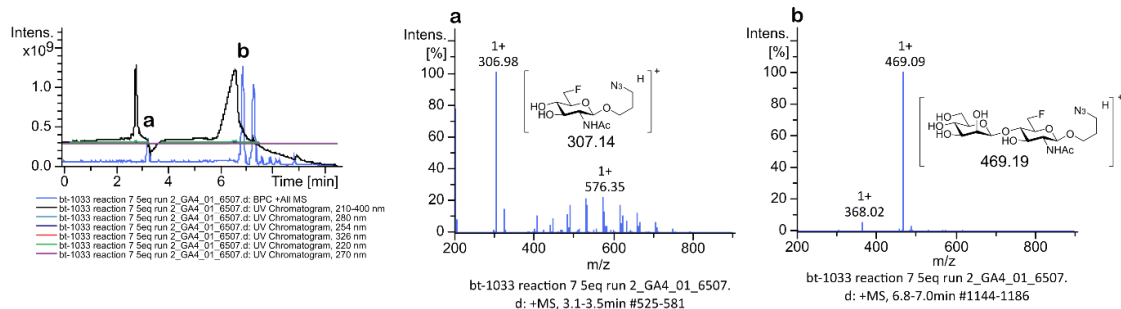


#### Post reaction with ITag reagent 6.16 LCMS trace

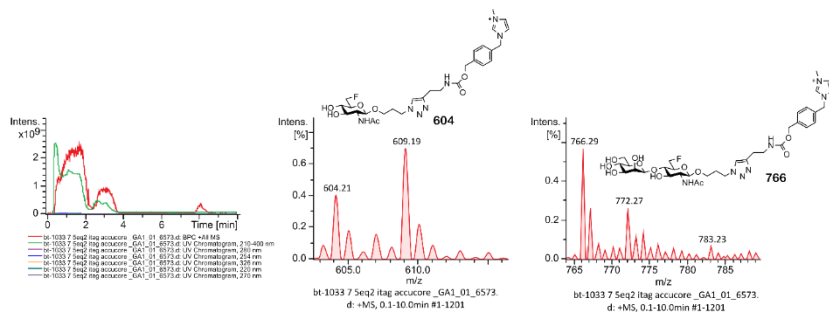


### Reaction Entry 25b

#### Post reaction termination LCMS trace



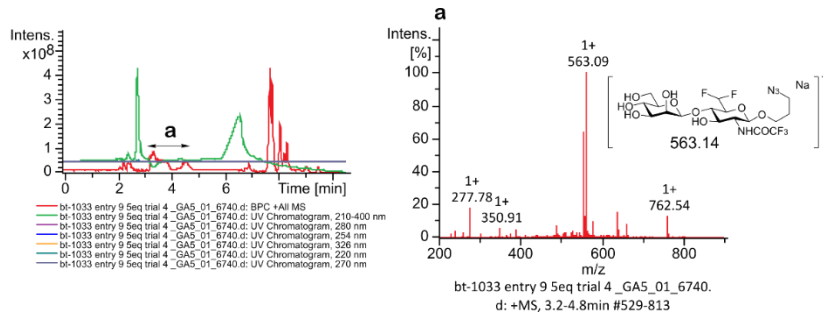
#### Post reaction with ITag reagent 6.16 LCMS trace



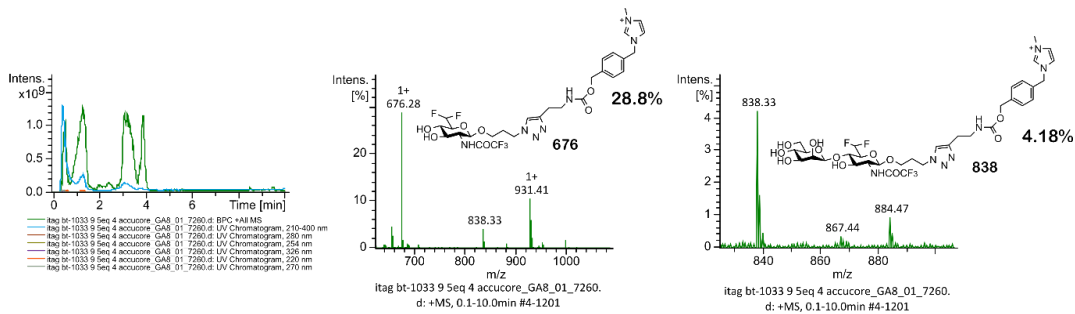
## Appendix

### Reaction Entry 26a

#### Post reaction termination LCMS trace

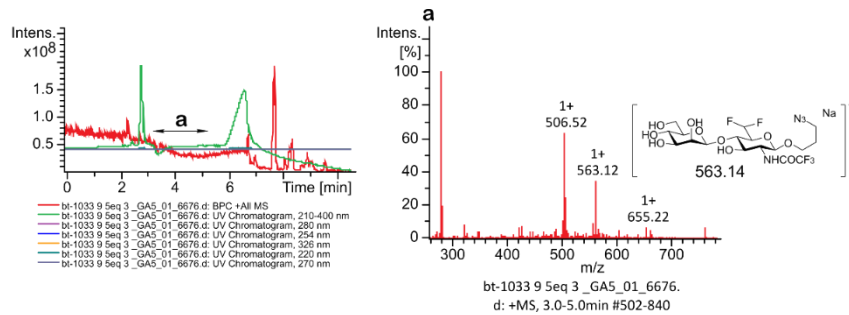


#### Post reaction with ITag reagent 6.16 LCMS trace

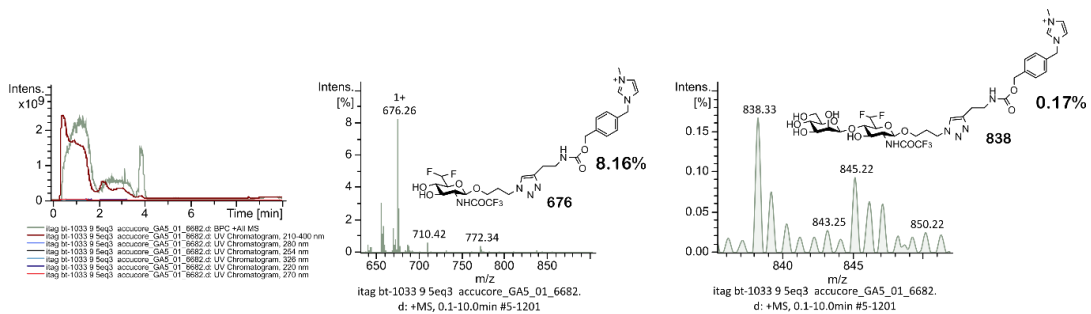


### Reaction Entry 26b

#### Post reaction termination LCMS trace



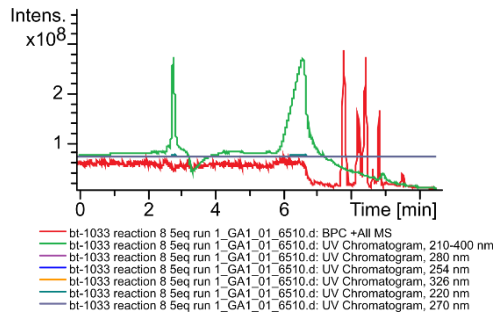
#### Post reaction with ITag reagent 6.16 LCMS trace



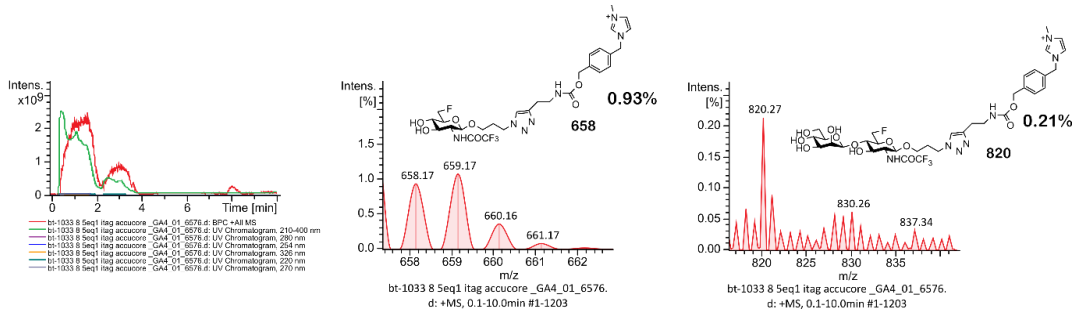
## Appendix

### Reaction Entry 27a

#### Post reaction termination LCMS trace

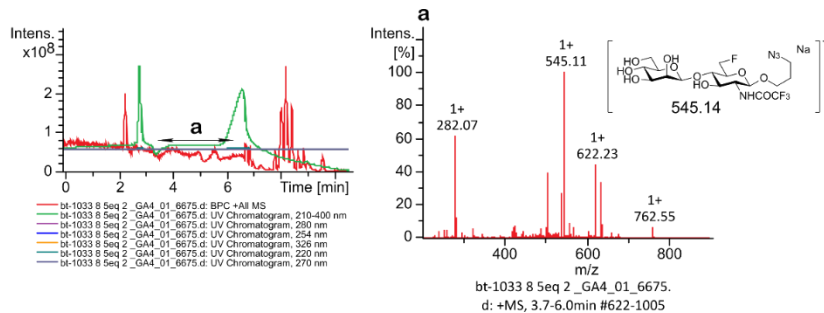


#### Post reaction with ITag reagent 6.16 LCMS trace

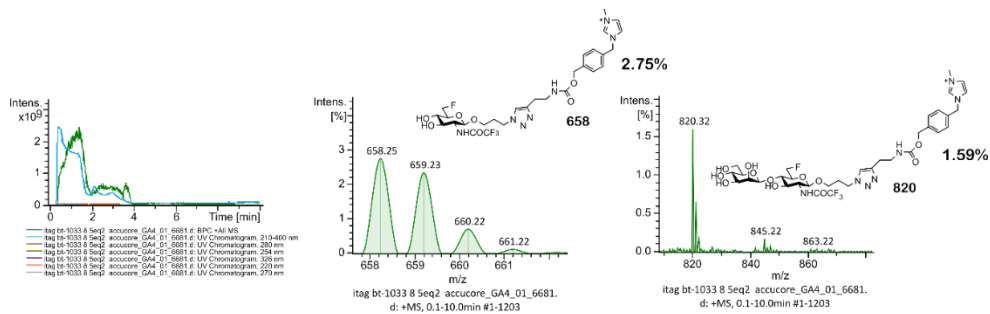


### Reaction Entry 27b

#### Post reaction termination LCMS trace



#### Post reaction with ITag reagent 6.16 LCMS trace

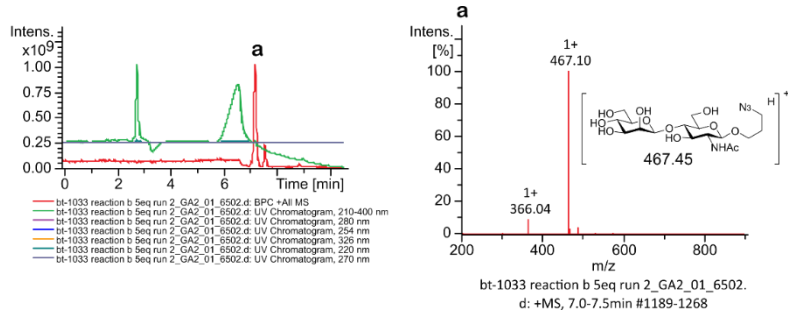




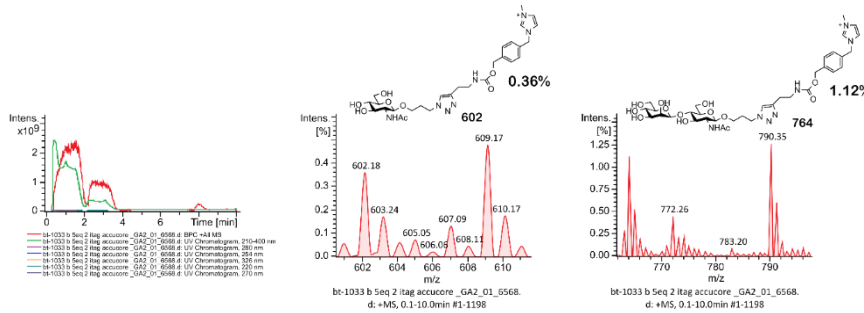
## Appendix

### Reagent Entry 28a

#### Post reaction termination LCMS trace

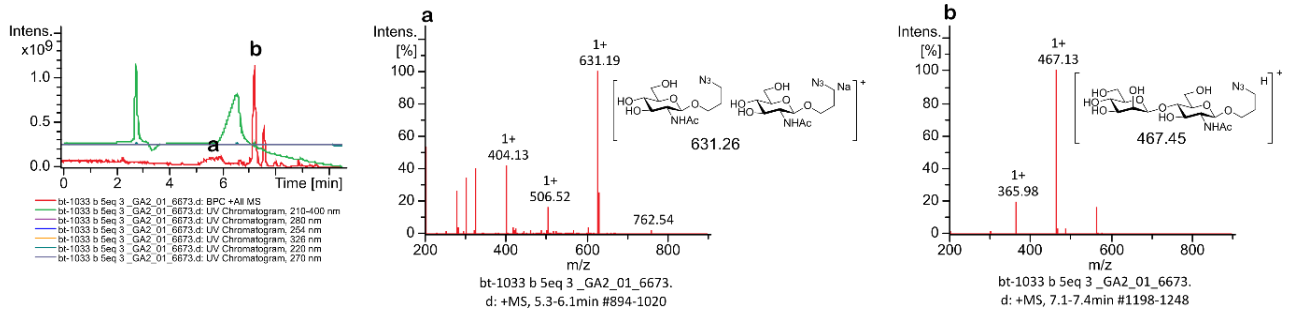


#### Post reaction with ITag reagent 6.16 LCMS trace

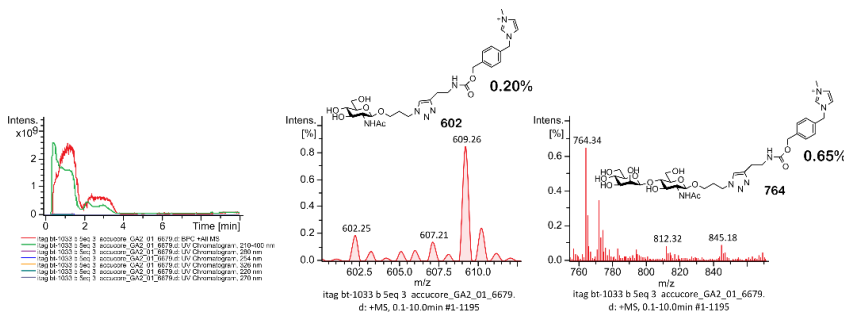


### Reaction Entry 28b

#### Post reaction termination LCMS trace

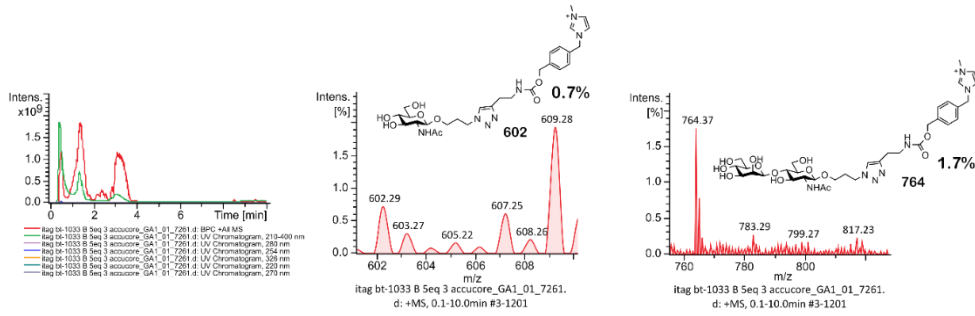


#### Post reaction with ITag reagent 6.16 LCMS trace



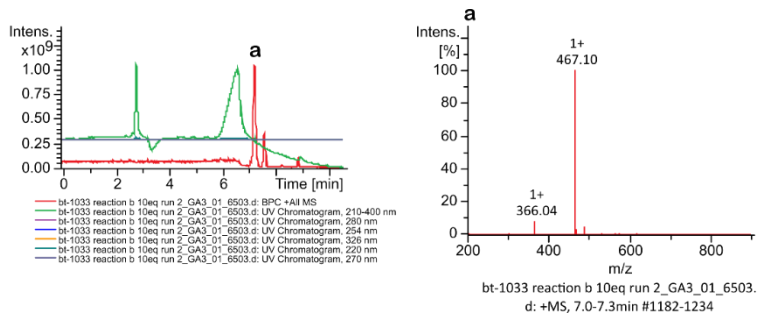
## Appendix

### Post reaction with ITag reagent 6.16 LCMS trace 2<sup>nd</sup> ITag reaction

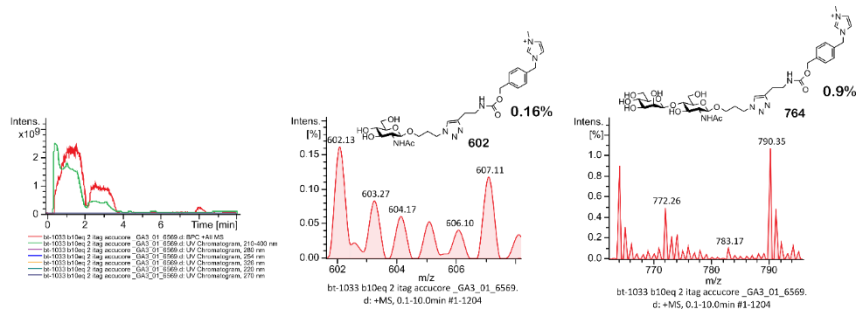


### Reaction Entry 29a

#### Post reaction termination LCMS trace

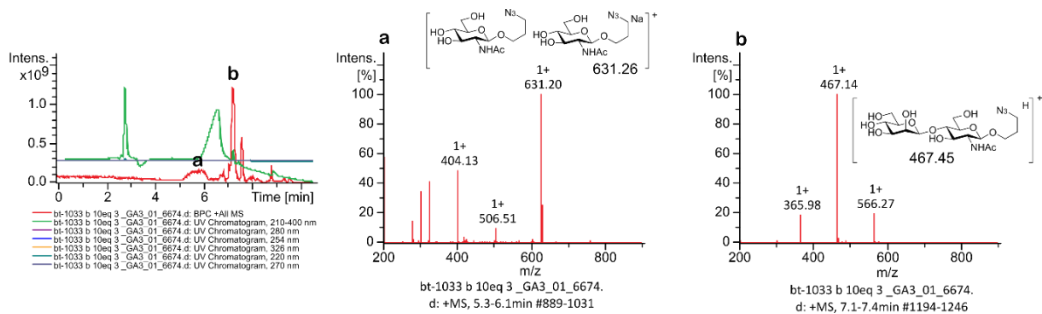


### Post reaction with ITag reagent 6.16 LCMS trace



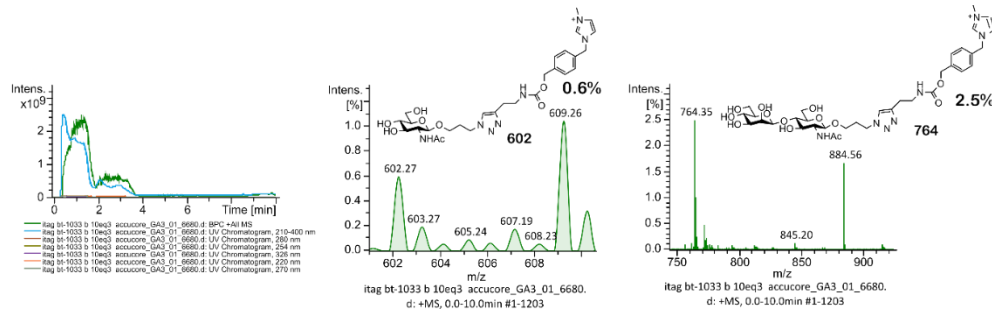
### Reaction Entry 29b

#### Post reaction termination LCMS trace

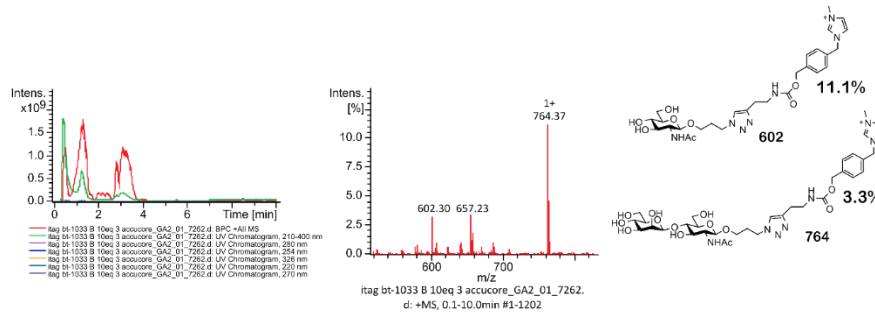


## Appendix

### Post reaction with ITag reagent 6.16 LCMS trace

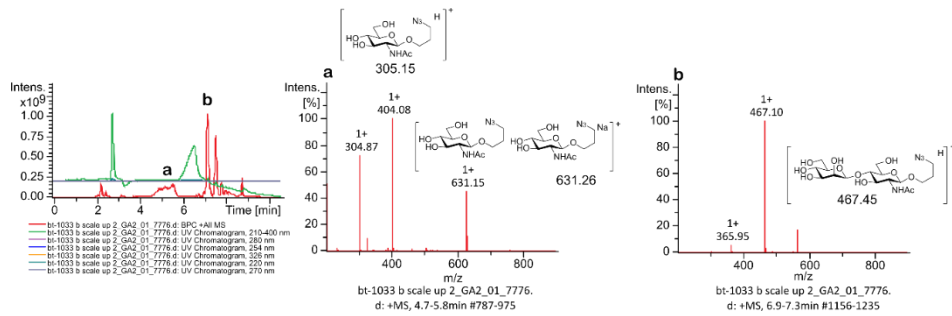


### Post reaction with ITag reagent 6.16 LCMS trace 2<sup>nd</sup> reaction

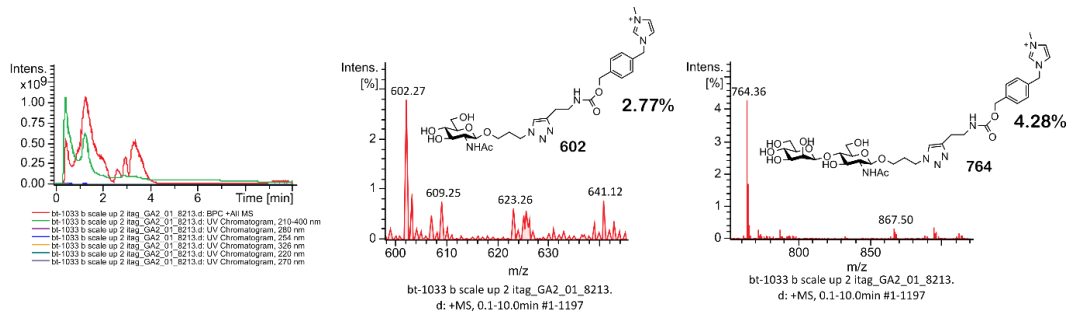


### Reaction Entry 29 scale up

### Post reaction termination LCMS trace



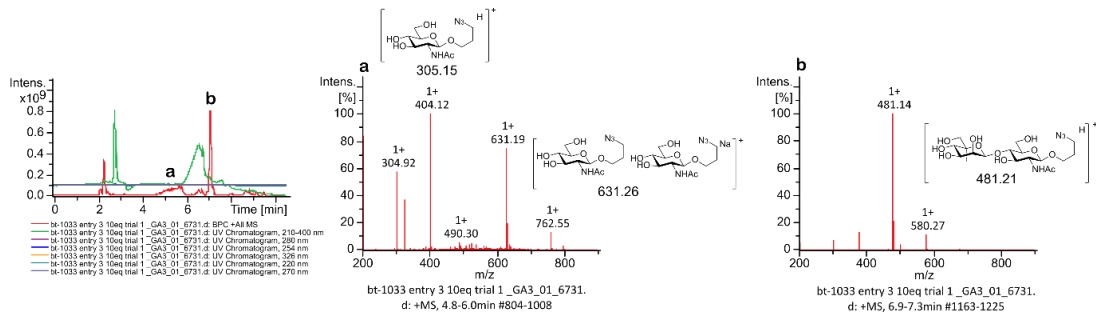
### Post reaction with ITag reagent 6.16 LCMS trace



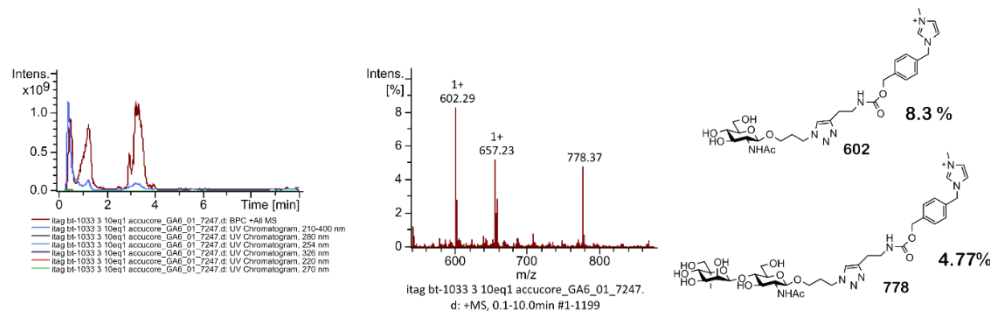
## Appendix

### Reaction Entry 30a

#### Post reaction termination LCMS trace

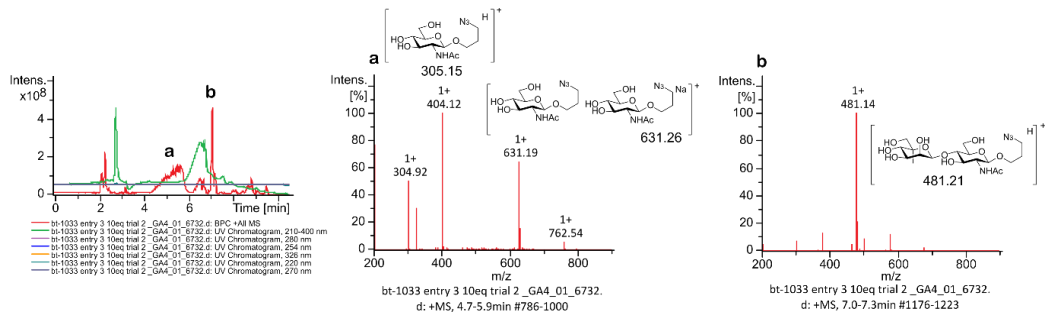


#### Post reaction with ITag reagent 6.16 LCMS trace

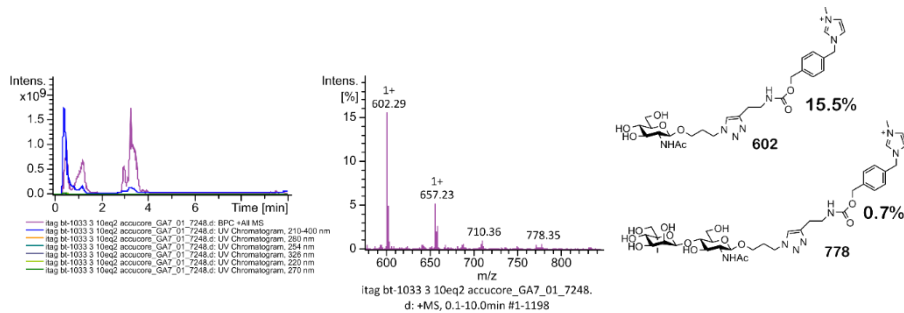


### Reaction Entry 30b

#### Post reaction termination LCMS trace



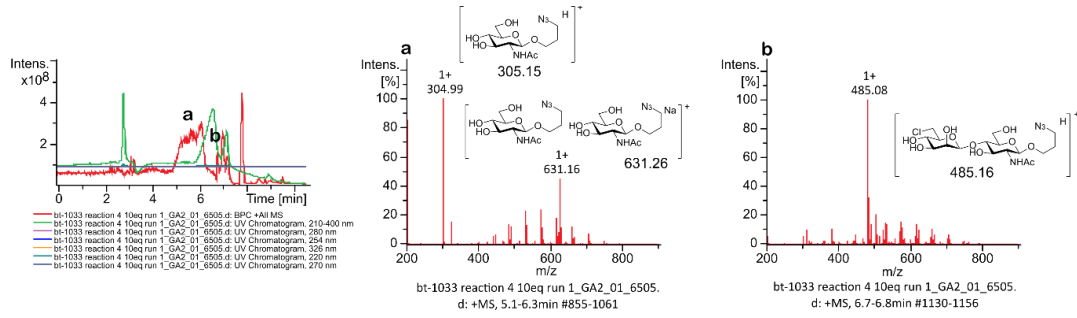
#### Post reaction with ITag reagent 6.16 LCMS trace



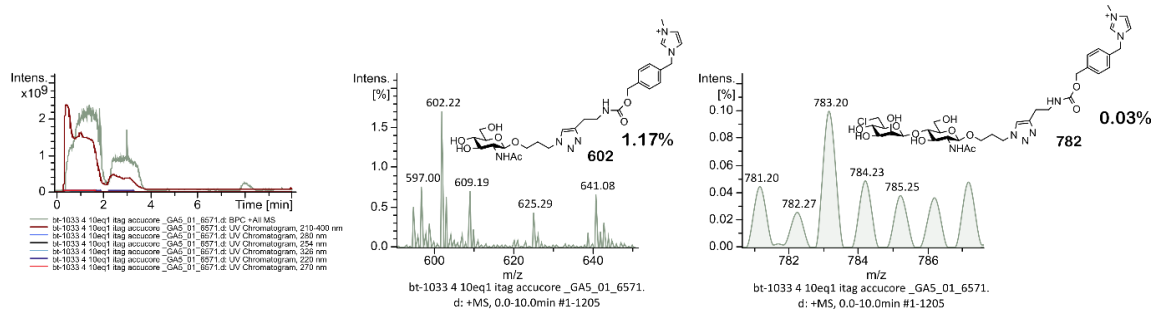
## Appendix

### Reaction Entry 31a

#### Post reaction termination LCMS trace

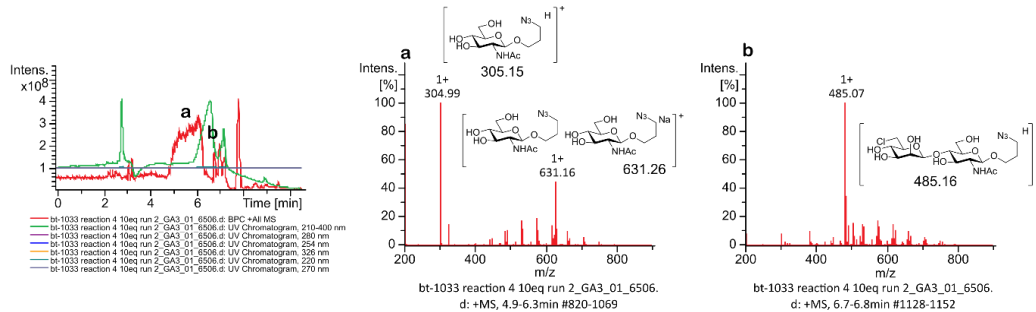


#### Post reaction with ITag reagent 6.16 LCMS trace

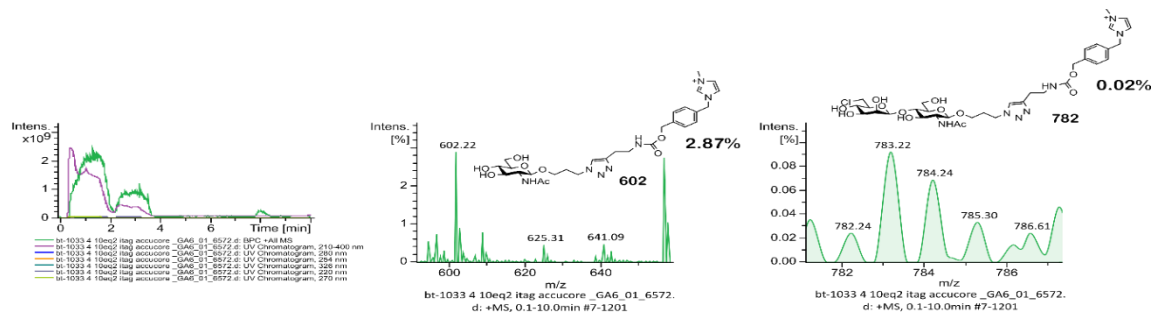


### Reaction Entry 31b

#### Post reaction termination LCMS trace



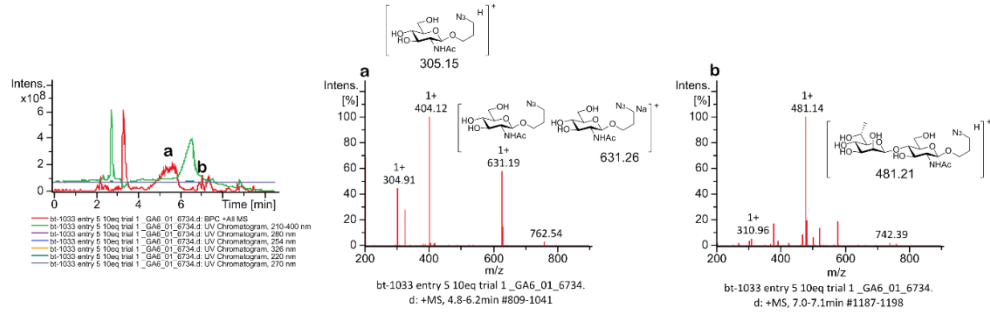
#### Post reaction with ITag reagent 6.16 LCMS trace



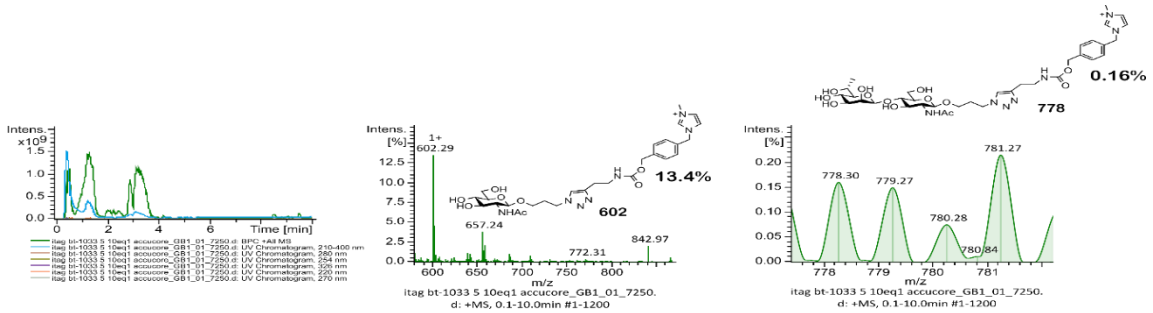
## Appendix

### Reaction Entry 32a

#### Post reaction termination LCMS trace

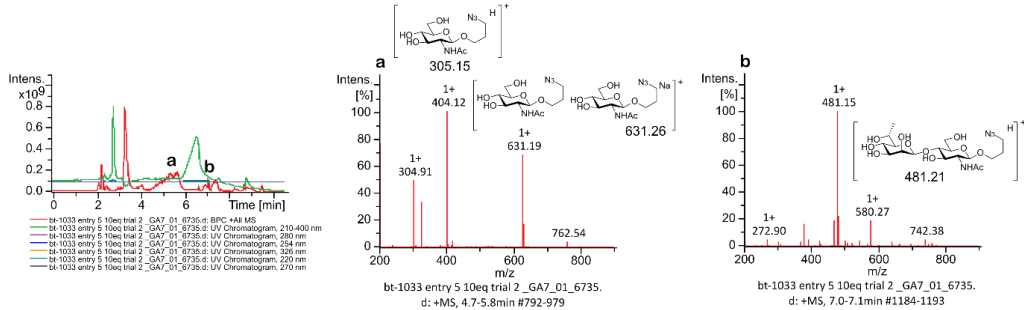


#### Post reaction with ITag reagent 6.16 LCMS trace

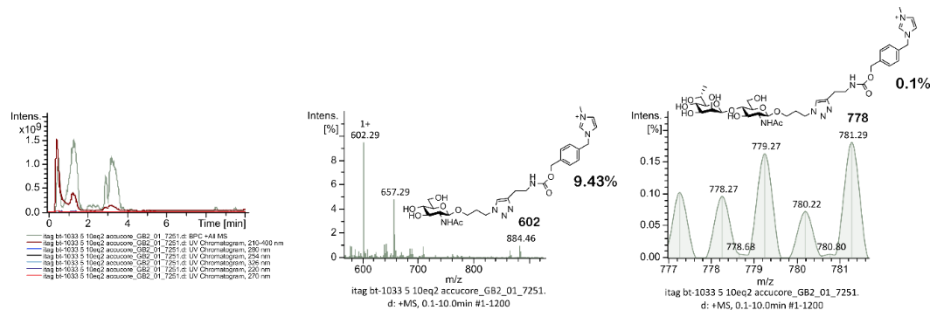


### Reaction Entry 32b

#### Post reaction termination LCMS trace



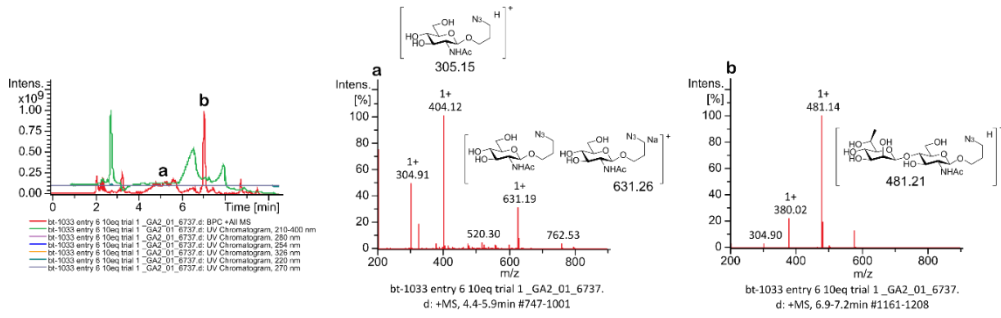
#### Post reaction with ITag reagent 6.16 LCMS trace



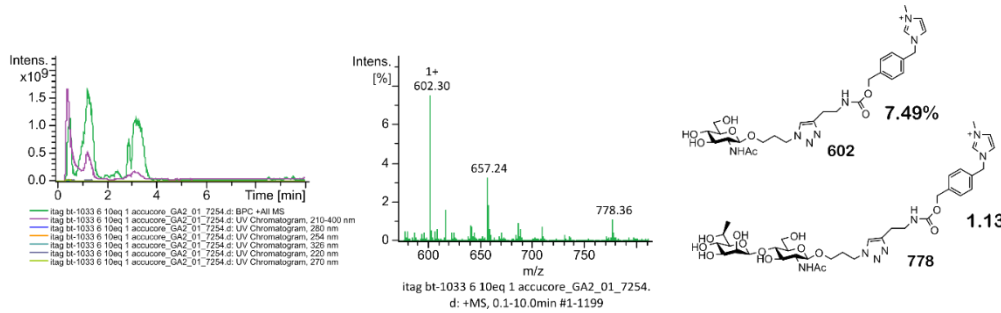
## Appendix

### Reaction Entry 33a

#### Post reaction termination LCMS trace

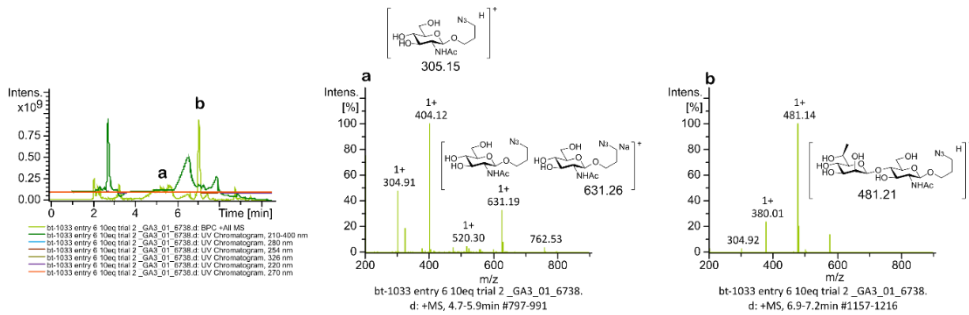


#### Post reaction with ITag reagent 6.16 LCMS trace

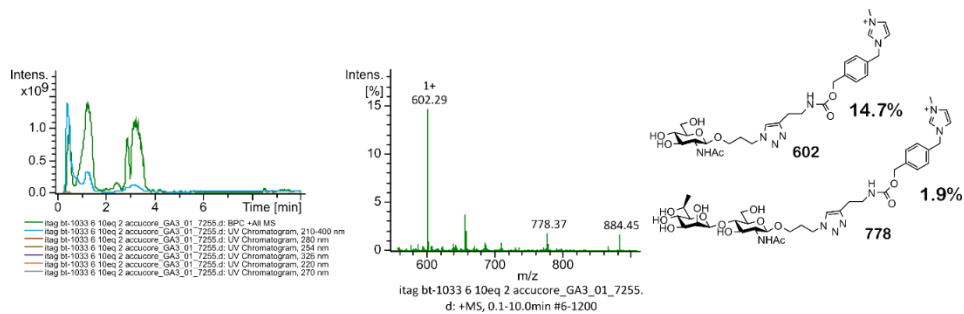


### Reaction Entry 33b

#### Post reaction termination LCMS trace



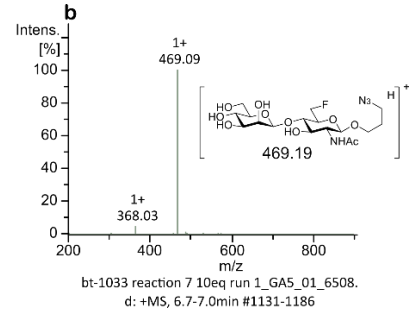
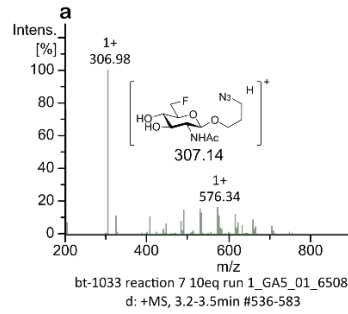
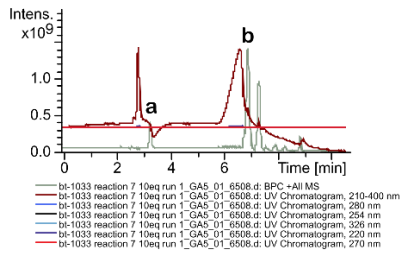
#### Post reaction with ITag reagent 6.16 LCMS trace



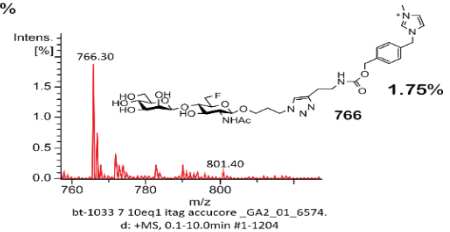
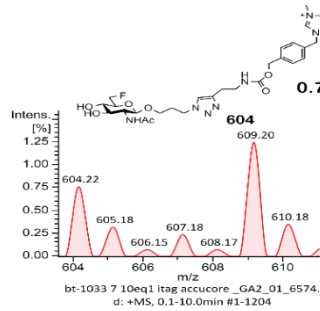
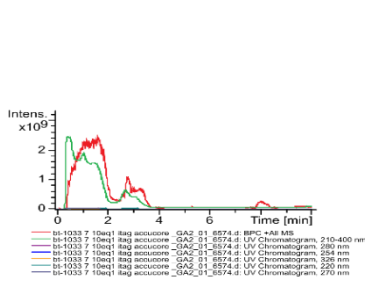
## Appendix

### Reaction Entry 34a

#### Post reaction termination LCMS trace

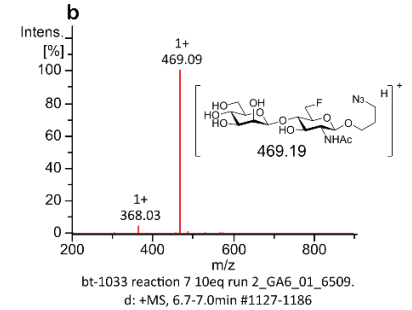
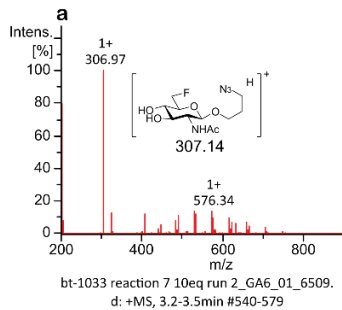
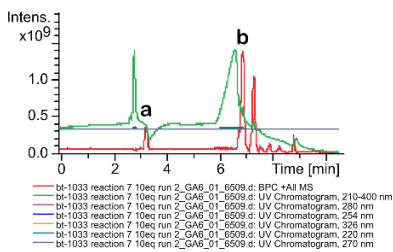


#### Post reaction with ITag reagent 6.16 LCMS trace

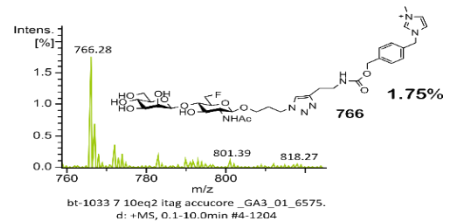
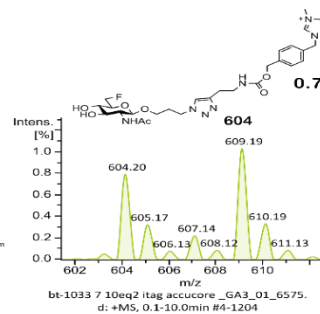
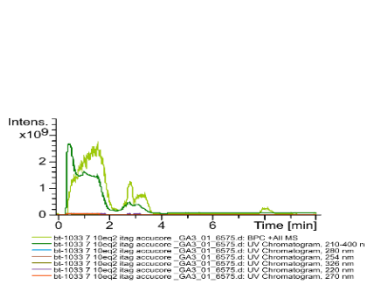


### Reaction Entry 34b

#### Post reaction termination LCMS trace



#### Post reaction with ITag reagent 6.16 LCMS trace

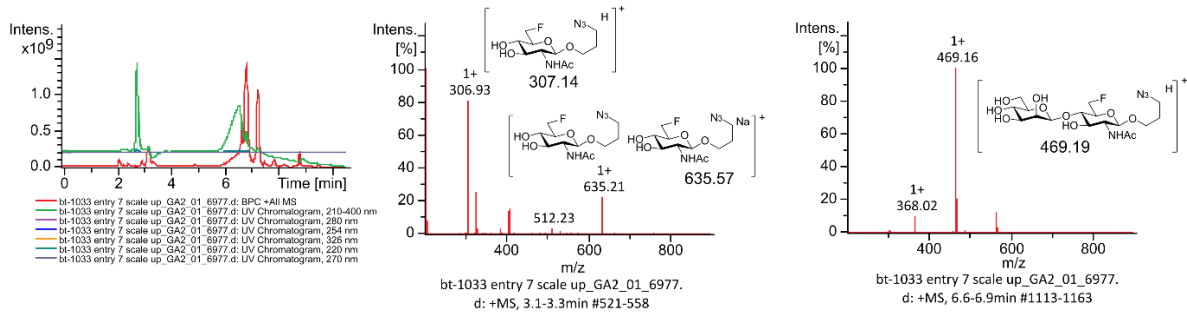




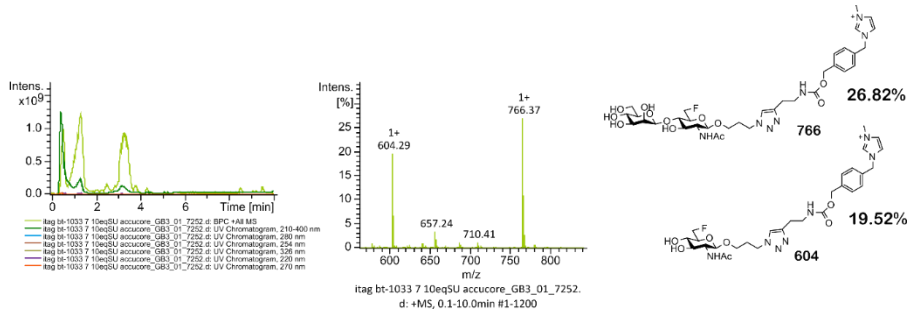
## Appendix

### Reaction Entry 34 scale up

#### Post reaction termination LCMS trace

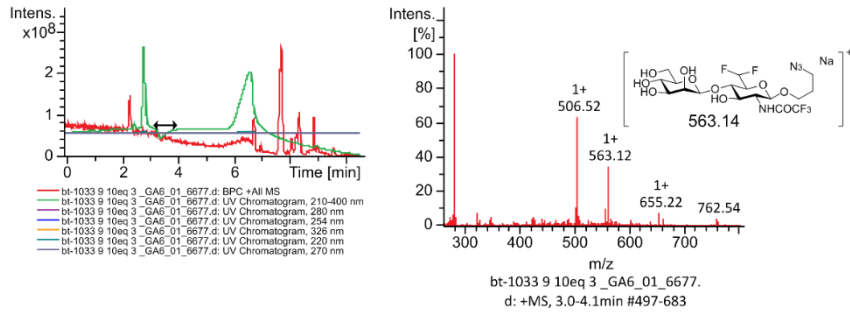


#### Post reaction with ITag reagent 6.16 LCMS trace

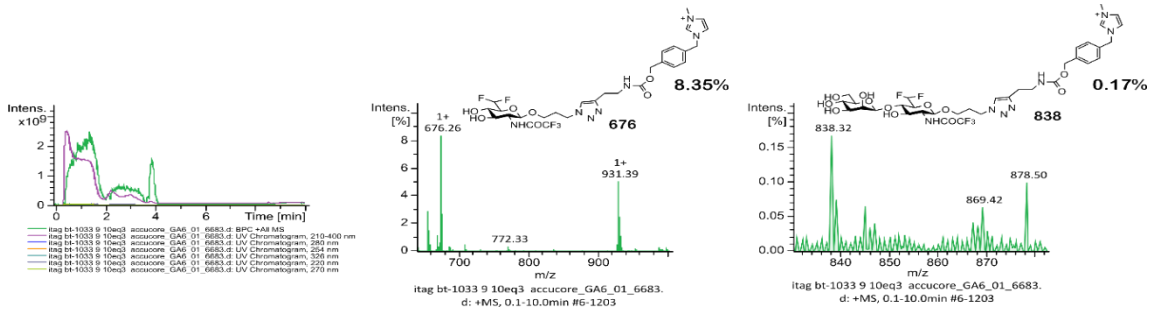


### Reaction Entry 35a

#### Post reaction termination LCMS trace



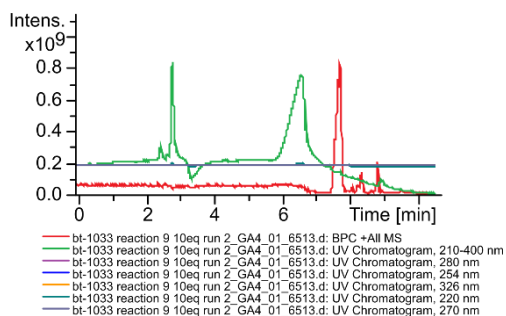
#### Post reaction with ITag reagent 6.16 LCMS trace



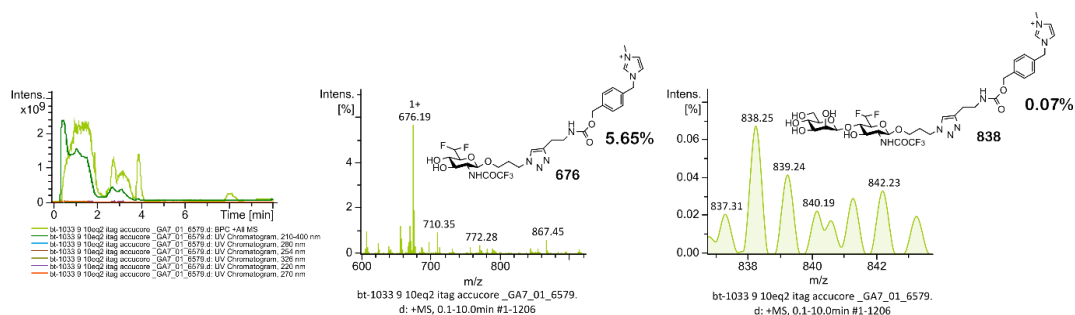
## Appendix

### Reaction Entry 35b

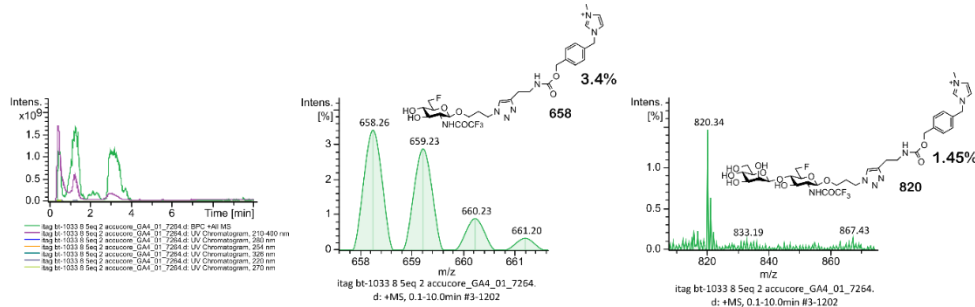
#### Post reaction termination LCMS trace



#### Post reaction with ITag reagent 6.16 LCMS trace

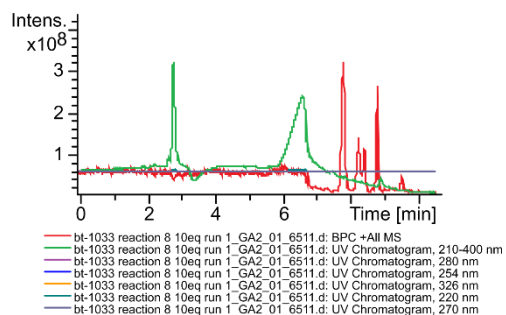


#### Post reaction with ITag reagent LCMS 6.16 trace 2<sup>nd</sup> reaction



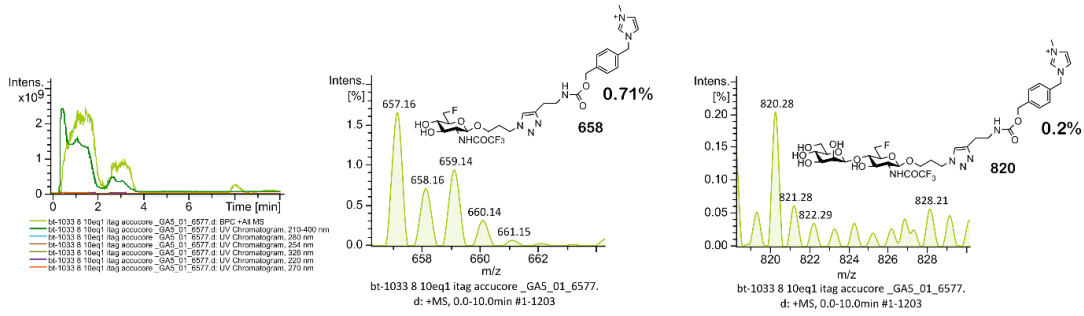
### Reaction Entry 36a

#### Post reaction termination LCMS trace



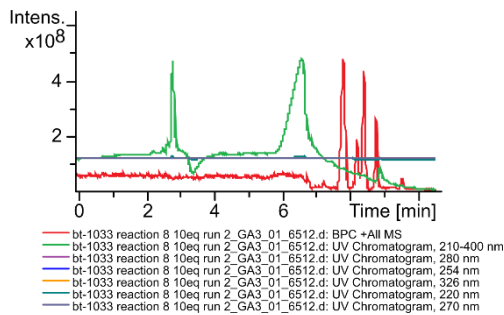
## Appendix

### Post reaction with ITag reagent **6.16** LCMS trace

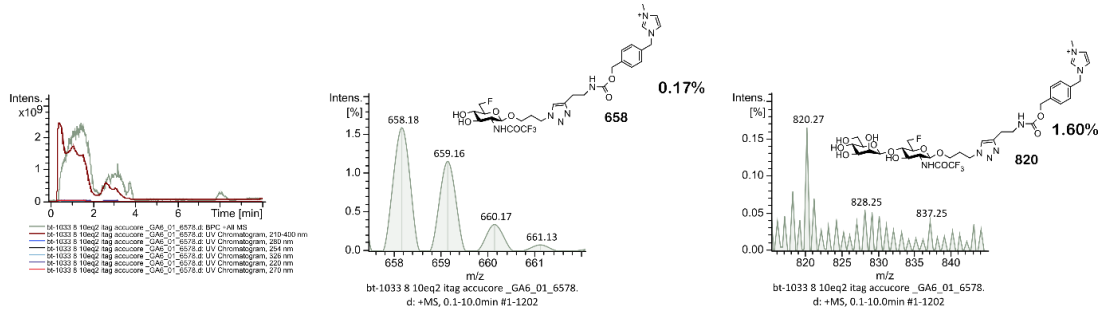


### Reaction Entry 36b

#### Post reaction termination LCMS trace

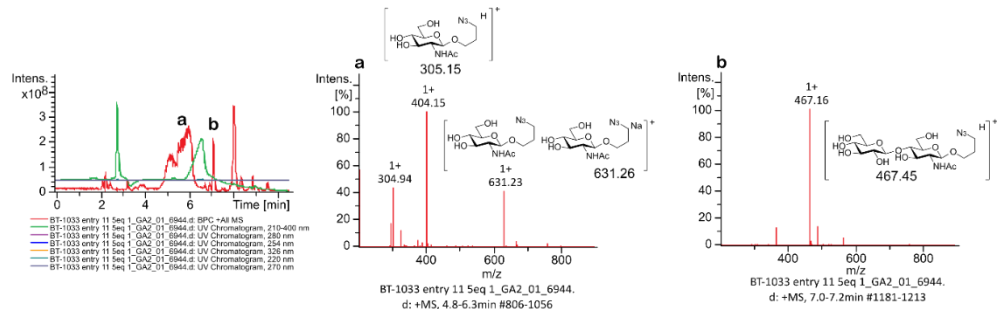


### Post reaction with ITag reagent **6.16** LCMS trace



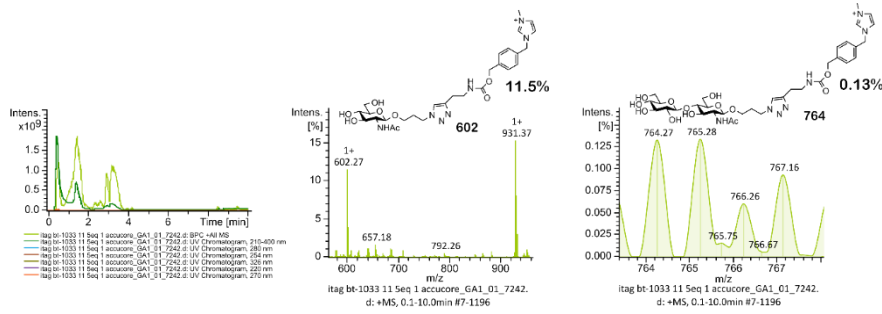
### Reaction Entry 37a

#### Post reaction termination LCMS trace



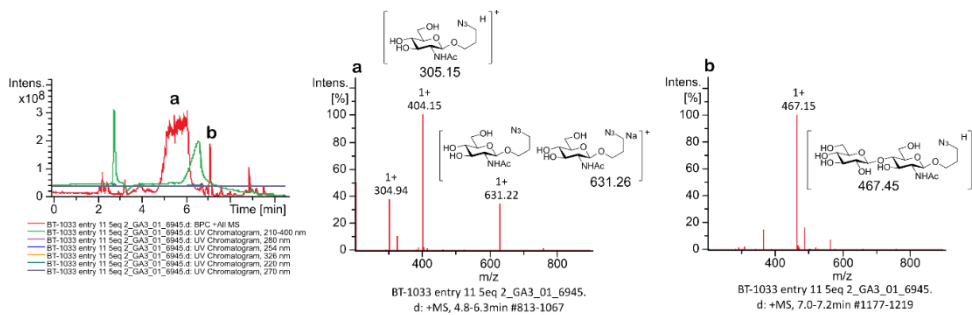
## Appendix

### Post reaction with ITag reagent 6.16 LCMS trace

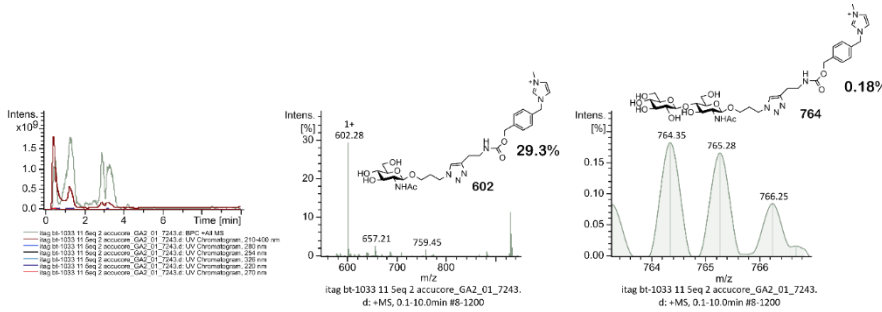


### Reaction Entry 37b

### Post reaction termination LCMS trace

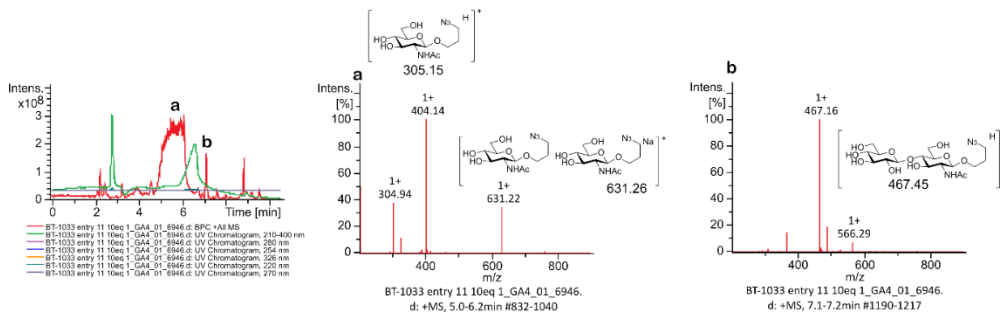


### Post reaction with ITag reagent 6.16 LCMS trace



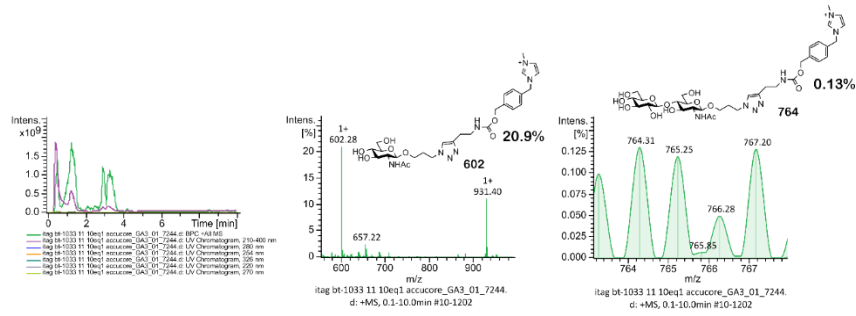
### Reaction Entry 38a

### Post reaction termination LCMS trace



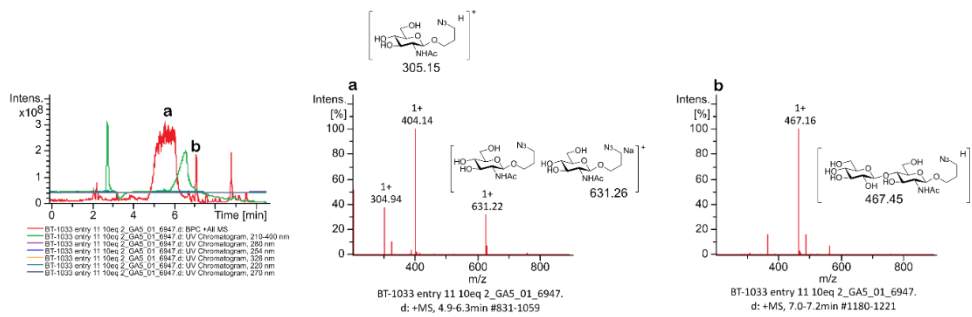
## Appendix

### Post reaction with ITag reagent 6.16 LCMS trace

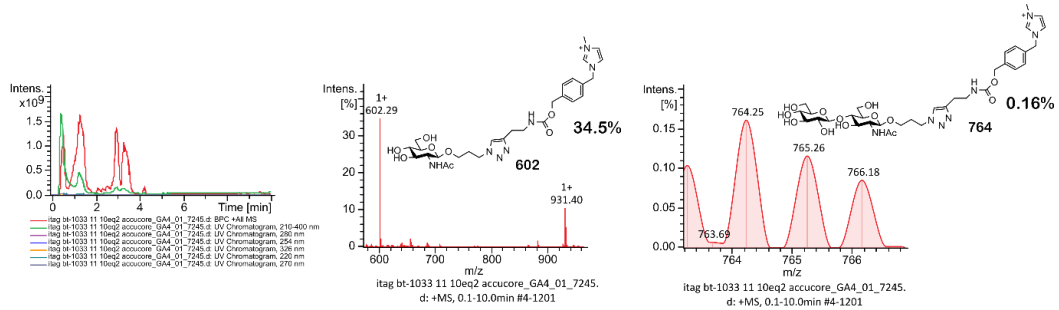


### Reaction Entry 38b

### Post reaction termination LCMS trace

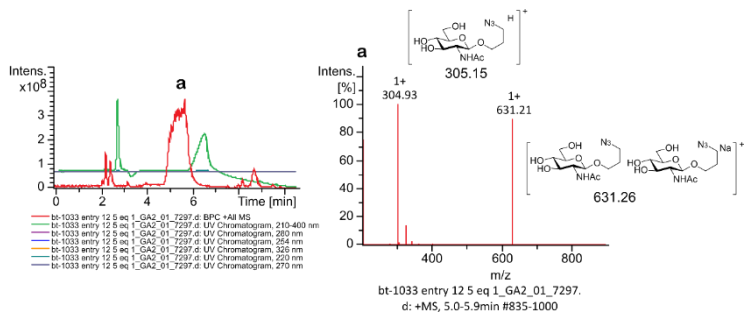


### Post reaction with ITag reagent 6.16 LCMS trace



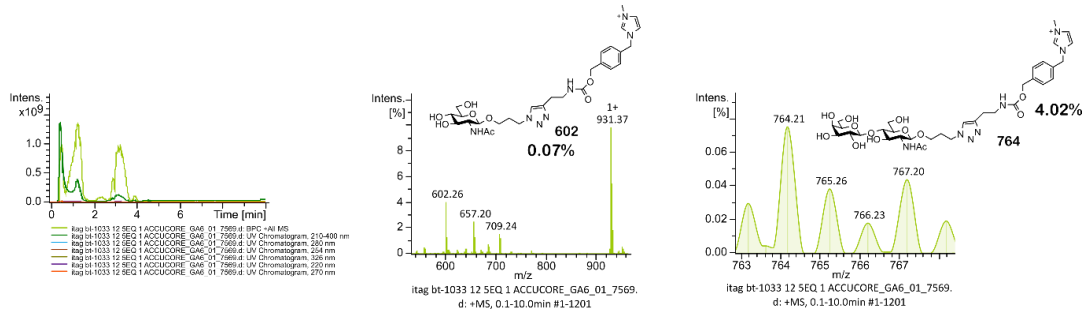
### Reaction Entry 39a

### Post reaction termination LCMS trace



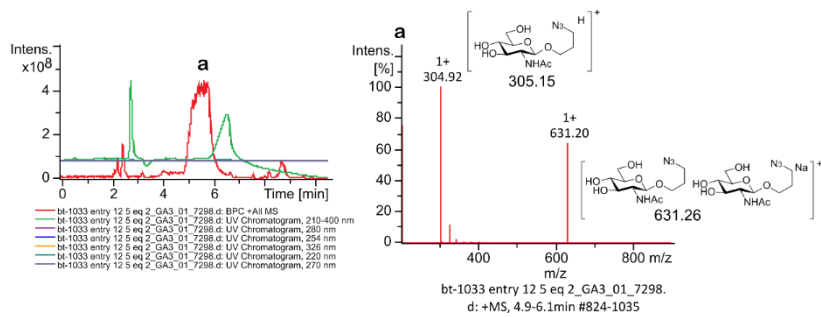
## Appendix

### Post reaction with ITag reagent **6.16** LCMS trace

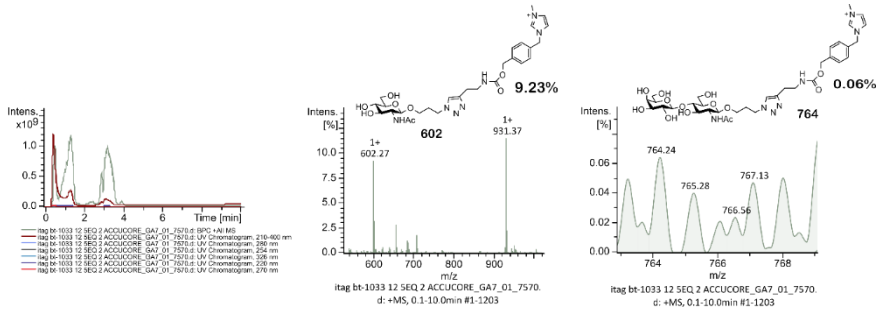


### Reaction Entry 39b

### Post reaction termination LCMS trace

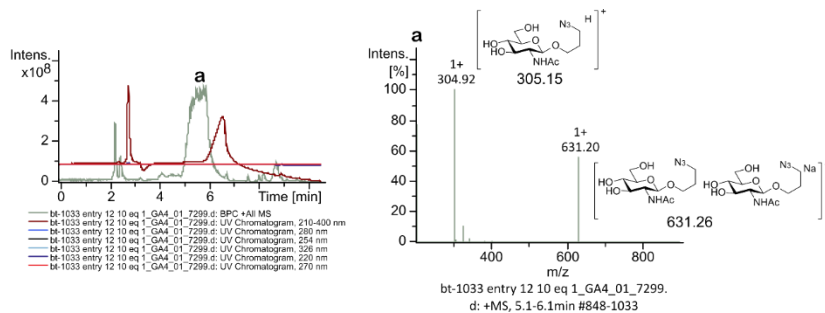


### Post reaction with ITag reagent **6.16** LCMS trace



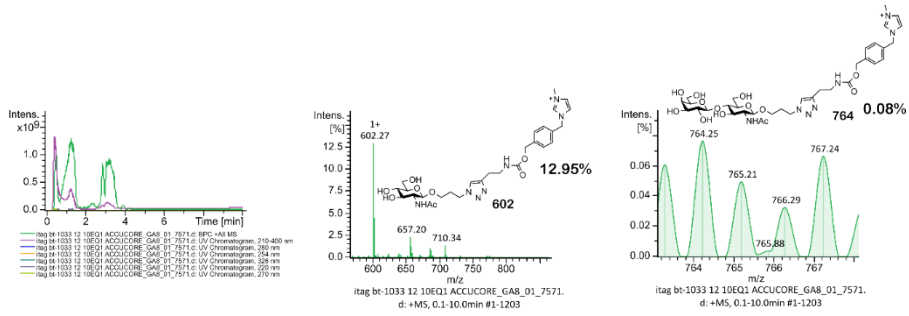
### Reaction Entry 40a

### Post reaction termination LCMS trace



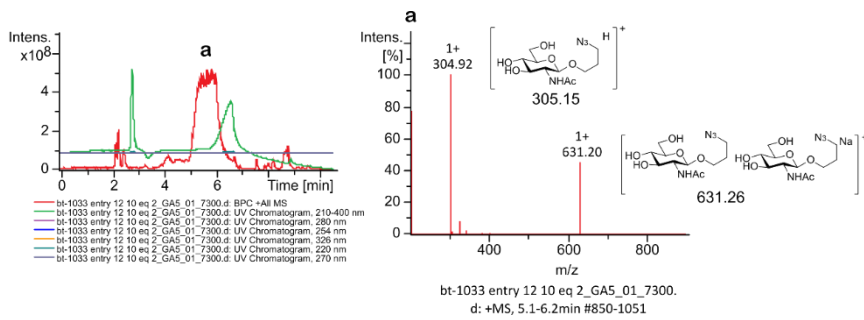
## Appendix

### Post reaction with ITag reagent 6.16 LCMS trace

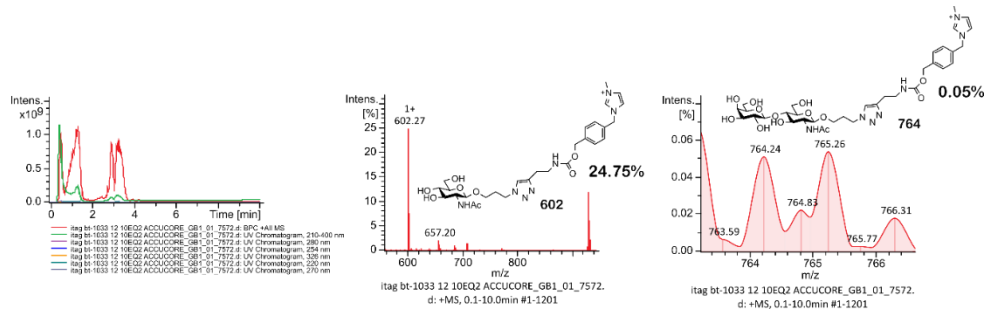


### Reaction Entry 40b

### Post reaction termination LCMS trace

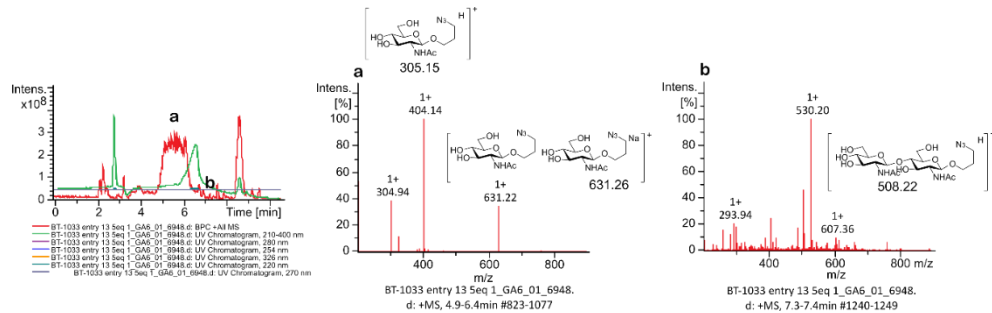


### Post reaction with ITag reagent 6.16 LCMS trace



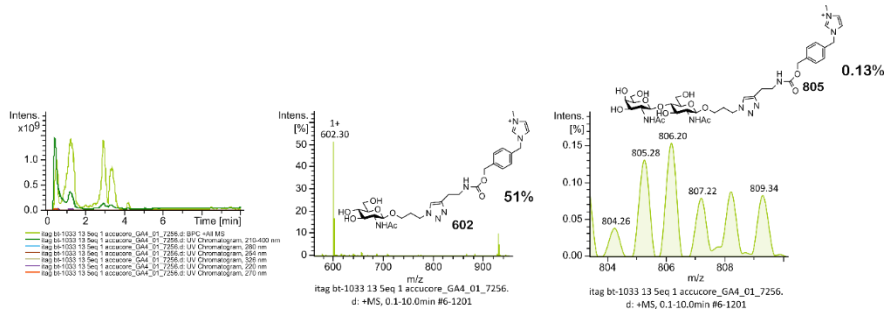
### Reaction Entry 41a

### Post reaction termination LCMS trace



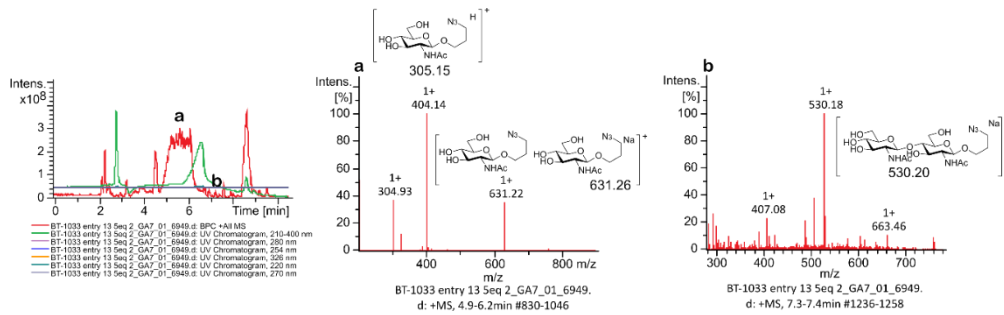
## Appendix

### Post reaction with ITag reagent **6.16** LCMS trace

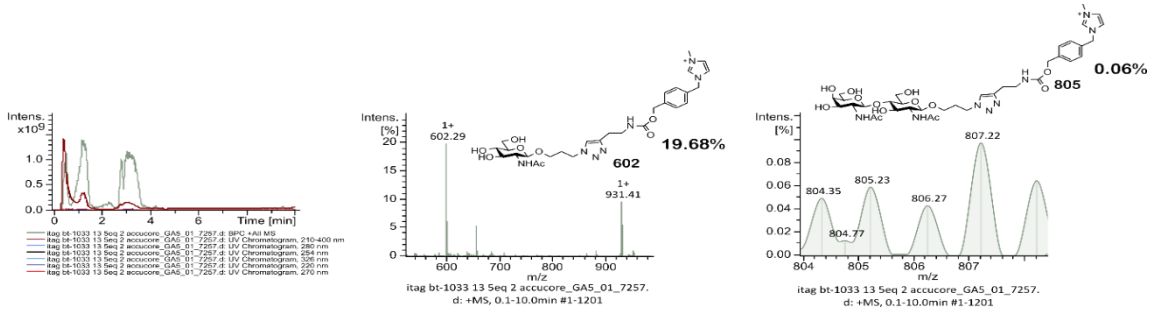


### Reaction Entry 41b

### Post reaction termination LCMS trace

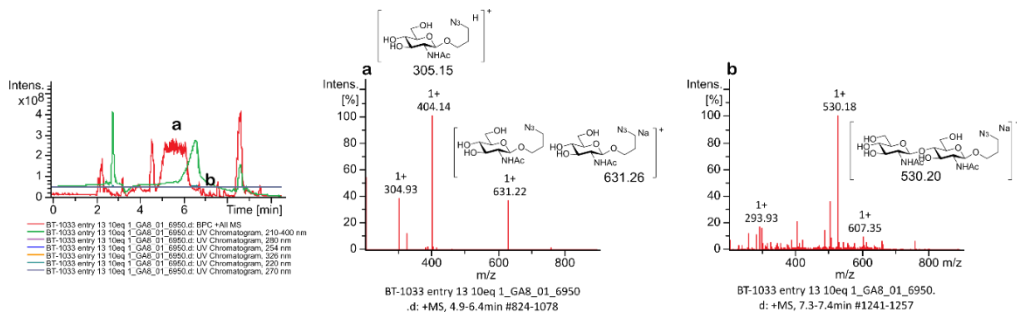


### Post reaction with ITag reagent **6.16** LCMS trace



### Reaction Entry 42a

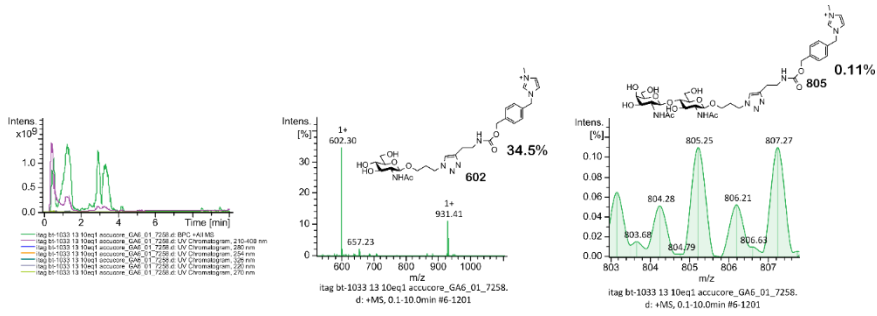
### Post reaction termination LCMS trace





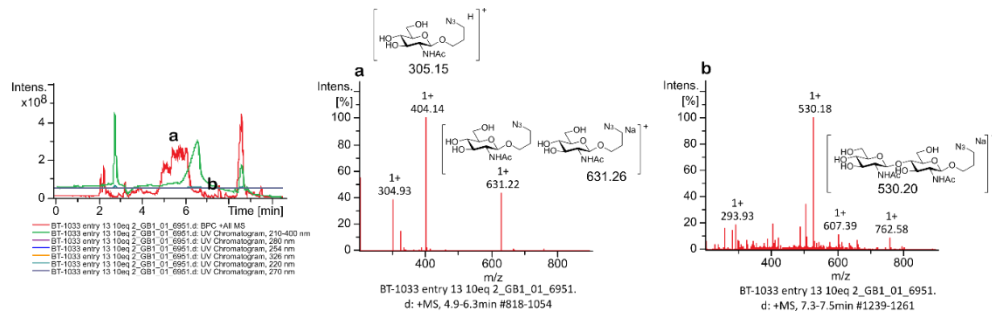
## Appendix

### Post reaction with ITag reagent **6.16** LCMS trace

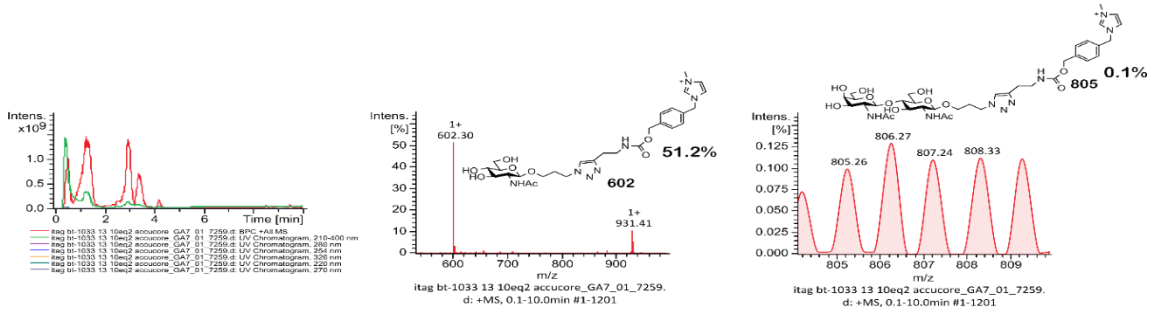


### Reaction Entry 42b

### Post reaction termination LCMS trace



### Post reaction with ITag reagent **6.16** LCMS trace



## Appendix

### 9.5.3 Summary of ITag results

*Table 38. The relative intensities of the ITag reagent 6.16 clicked acceptor and disaccharide peaks in each sample. These results have been used to calculate the total peak contribution of the ITag reagent 6.16 clicked acceptor and disaccharide peaks in each sample. Furthermore, this value can be used to find the percentage contribution of the disaccharide peak and thus the conversion rate of each reaction*

Entry	Percentage of acceptor in LCMS trace	Percentage of disaccharide in LCMS trace	Total peak contributions of acceptor and product	Percentage contribution from disaccharide
				(conversion rate)
2	4.61	1.15	5.76	19.97
3	28.43	0.33	28.76	1.15
4	68.06	0.47	68.53	0.69
5	100	0.06	100.06	0.06
6	39.75	0.08	39.83	0.2
7	65.8	0.22	66.02	0.33
8	57.6	0.33	57.93	0.57
9	4.71	0.19	4.9	3.88
10	4.35	0.08	4.43	1.81
11	3.95	0.03	3.98	0.75
12	7.6	0.12	7.72	1.55
13	19.58	0.34	19.92	1.71
14	4.4	0.1	4.5	2.22
15	3.7	0.06	3.76	1.6
16	5.41	0.17	5.58	3.05
Di addition	5.41	0.08	5.49	1.46
17	43.8	0.91	44.71	2.04
18	5.6	8.71	14.31	60.87
19	1	0.05	1.05	4.76
20	0.81	0.03	0.84	3.57
Di additions	0.81	0.04	0.85	4.71
21a	0.86	0.2	1.06	18.87
21b	12.02	3.26	15.28	21.34
22a	1.06	0.12	1.18	10.17
22b	1.12	0.03	1.15	2.61
23a	1.13	0.07	1.2	5.83
23b	9.24	0.09	9.33	0.96
24a	1.1	0.08	1.18	6.78

## Appendix

24b	7.89	1.25	9.14	13.68
25a	5.86	2.72	8.58	31.7
25b	0.4	0.57	0.97	58.76
26a	28.78	4.18	32.96	12.68
26b	8.16	0.17	8.33	2.04
27a	0.93	0.21	1.14	18.42
27b	2.75	1.59	4.34	36.64
27b 2 <sup>nd</sup> ITag reaction	3.4	1.45	4.85	29.9
28a	0.36	1.12	1.48	75.68
28b	0.19	0.65	0.84	77.38
28b 2 <sup>nd</sup> ITag reaction	0.72	1.74	2.46	70.73
29a	0.16	0.9	1.06	84.91
29b	0.59	2.49	3.08	80.84
29b 2 <sup>nd</sup> ITag reaction	3.28	11.13	14.41	77.24
29 scale up	2.77	4.28	7.05	60.71
30b	15.48	0.7	16.18	4.33
31a	1.7	0.03	1.73	1.73
31b	2.87	0.02	2.89	0.69
32a	13.39	0.16	13.55	1.18
32b	9.43	0.1	9.53	1.05
33a	7.49	1.13	8.62	13.12
33b	14.67	1.88	16.55	11.36
34a	0.76	1.87	2.63	71.1
34b	0.78	1.75	2.53	69.17
34 scale up	19.59	26.82	46.41	57.79
35b	5.65	0.07	5.72	1.22
36a	0.71	0.2	0.91	21.98
36b	1.59	0.17	1.76	9.66
37a	11.54	0.07	11.61	0.6
37b	29.3	0.18	29.48	0.61
38a	20.9	0.13	21.03	0.62
38b	34.46	0.16	34.62	0.46
39a	4.02	0.07	4.09	1.71

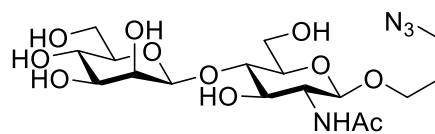
Appendix

39b	9.23	0.06	9.29	0.65
40a	12.23	0.08	12.31	0.65
40b	24.75	0.05	24.8	0.2
41a	51	0.13	51.13	0.25
41b	19.68	0.06	19.74	0.3
42a	34.48	0.11	34.59	0.32
42b	51.2	0.1	51.3	0.19
43a	0.04	0.11	0.15	73.33
43b	2.65	3.87	6.52	59.36
44a	2.05	1.05	3.1	33.87
44b	1.21	0.62	1.83	33.88
45a	12.33	0.17	12.5	1.36
45b	22.61	0.3	22.91	1.31

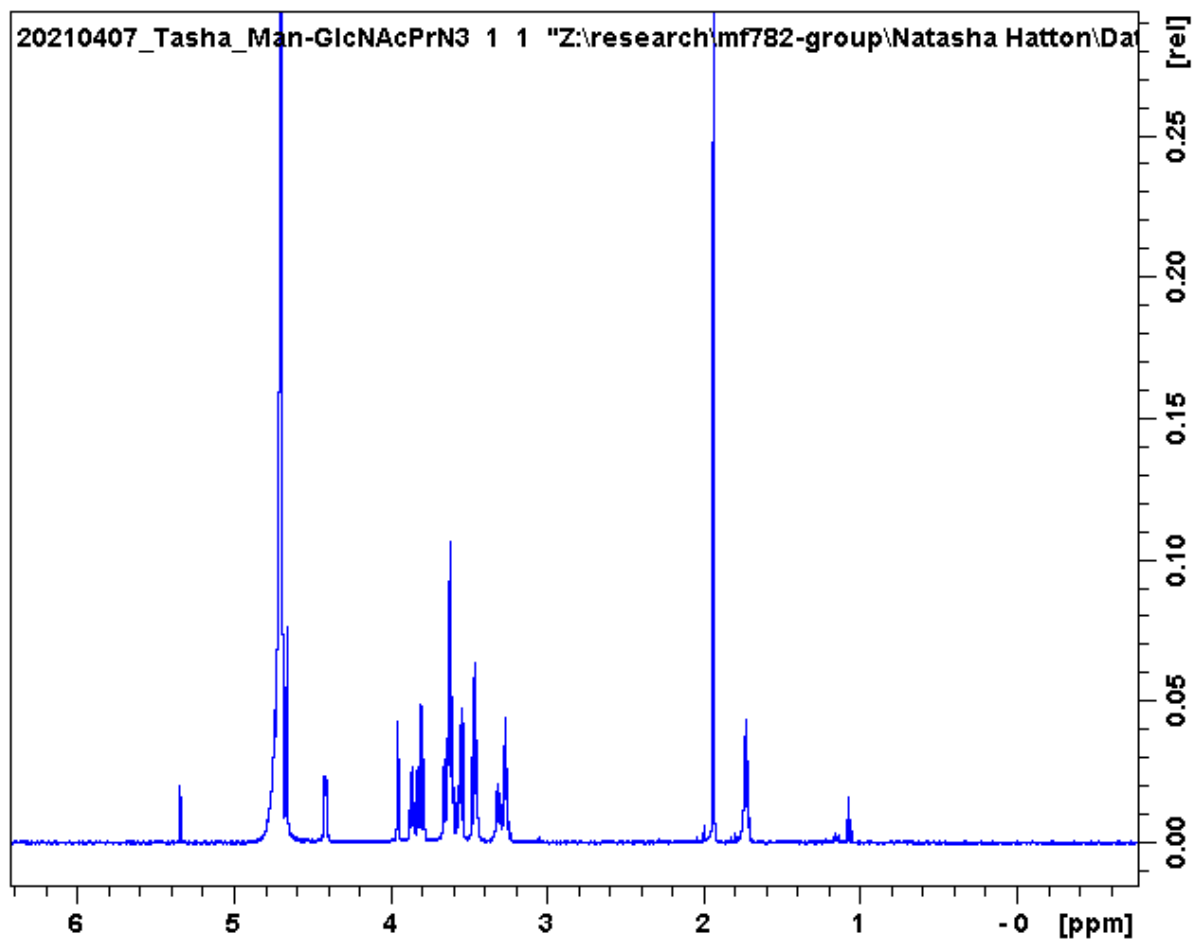
## Appendix

### 9.5.4 NMR data

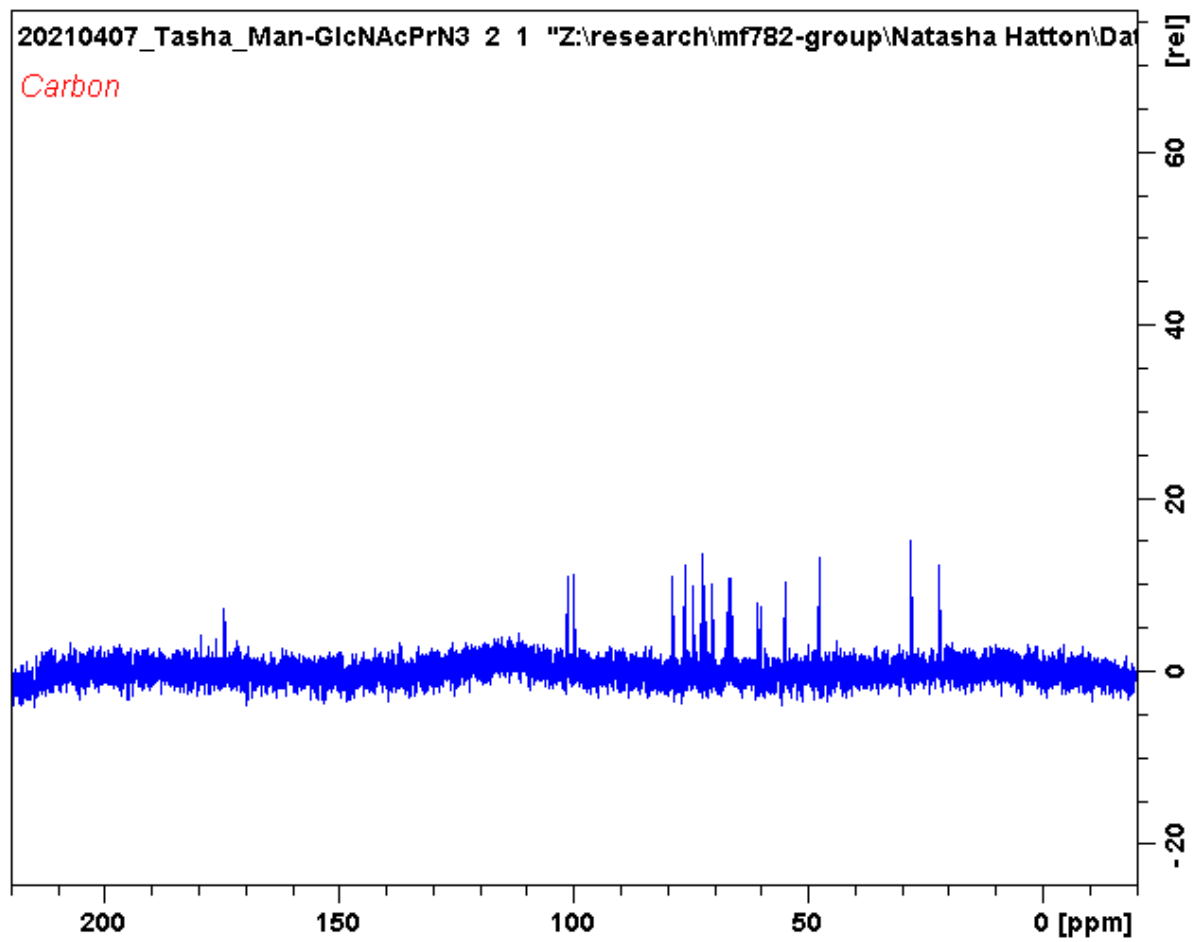
#### 9.5.4.1 NMR spectrum of the disaccharide extracted from entry 29 scale up



### $^1\text{H}$ NMR



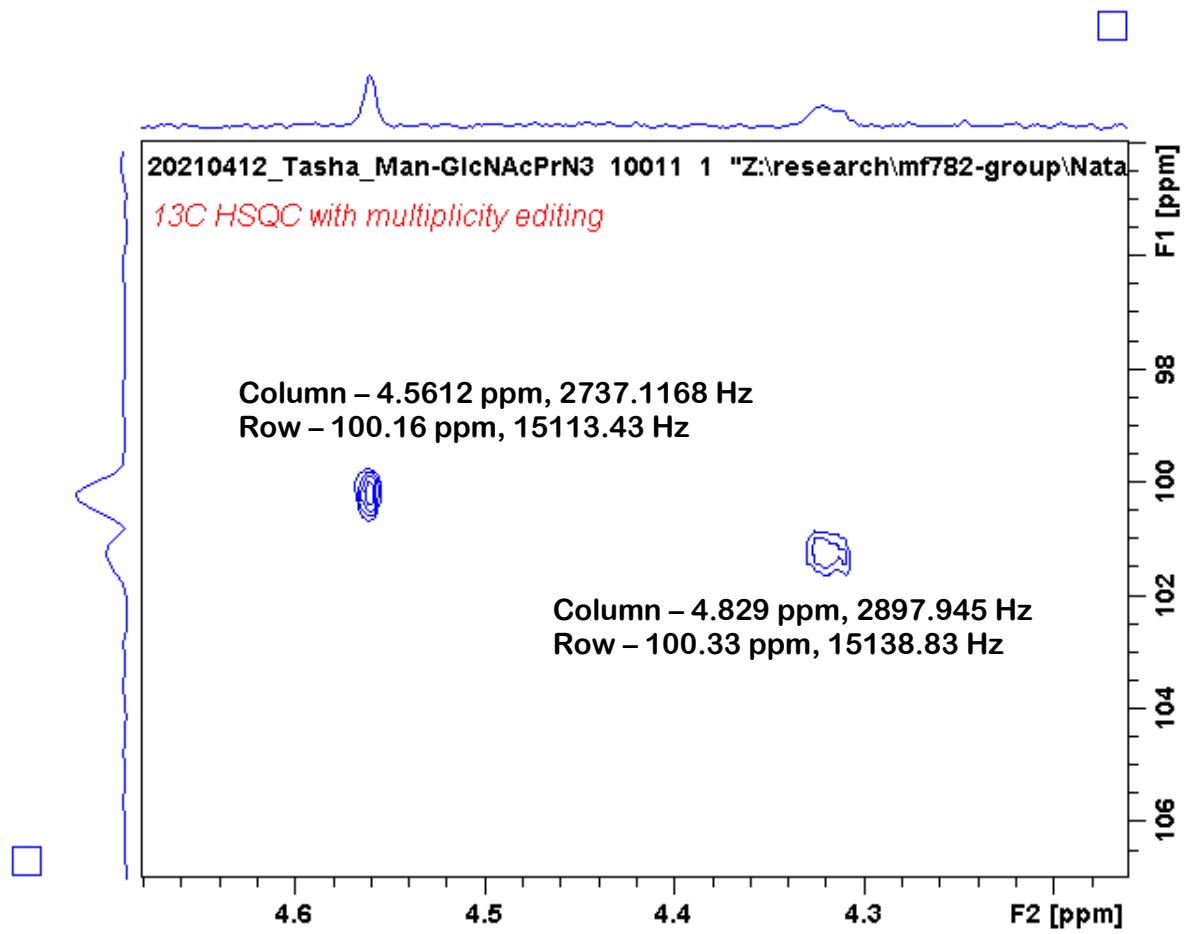
$^{13}\text{C}$  NMR



Appendix

IPAP HSQC (<sup>13</sup>C HSQC with multiplicity editing)

Spectrum 1



Spectrum two

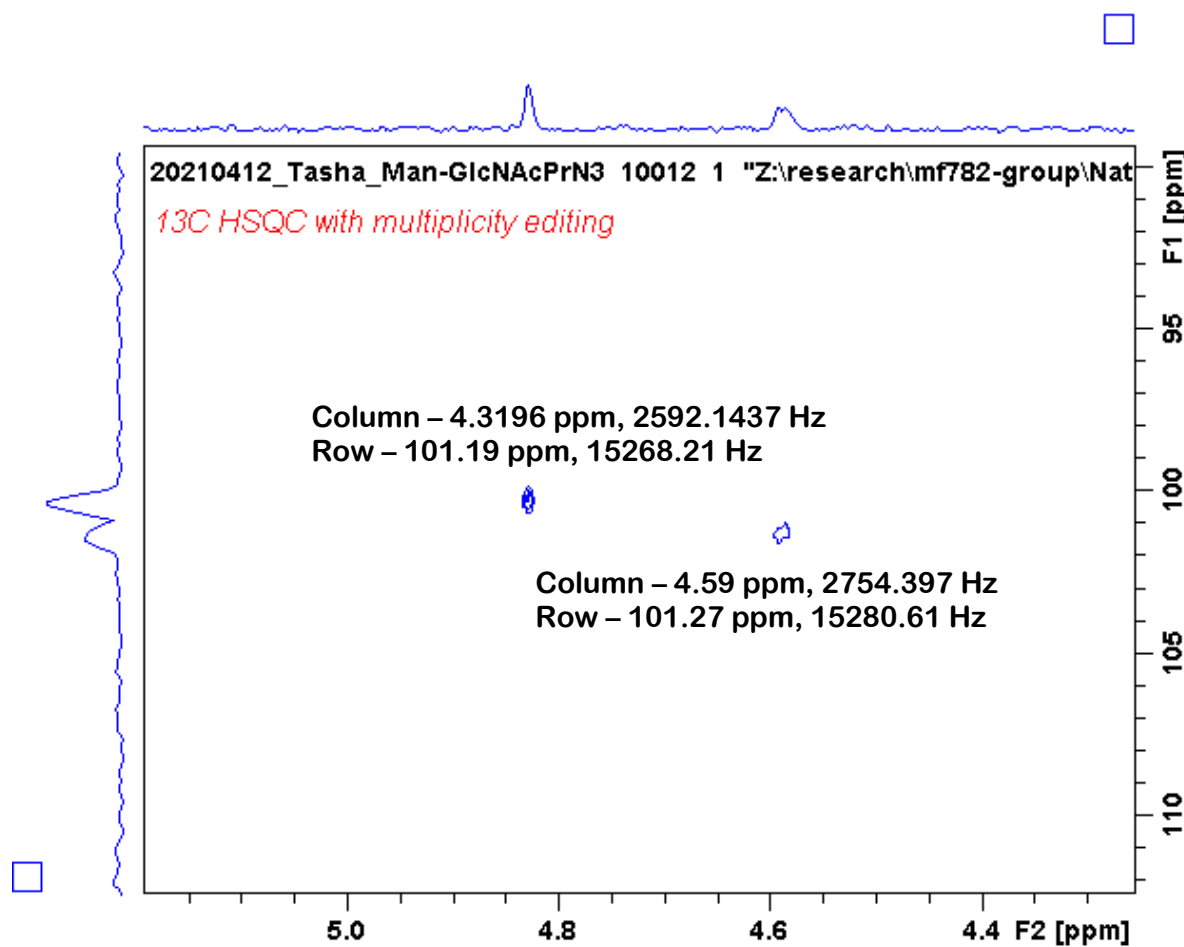


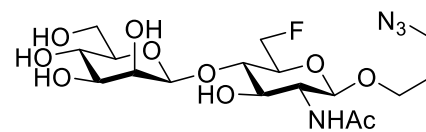
Table 39. Results of the two IPAP HSQC ( $^{13}\text{C}$  HSQC with multiplicity editing) spectra for the two anomeric carbons and analysis of the results to give the  $^1J_{\text{CH}}$  coupling constants.

Carbon	Spectrum one	Spectrum two	$^1J_{\text{CH}}$ coupling constant (Hz)
C-1 mannose	2737.1168	2897.945	160
C-1 Glucosamine	2592.14	2754.40	162

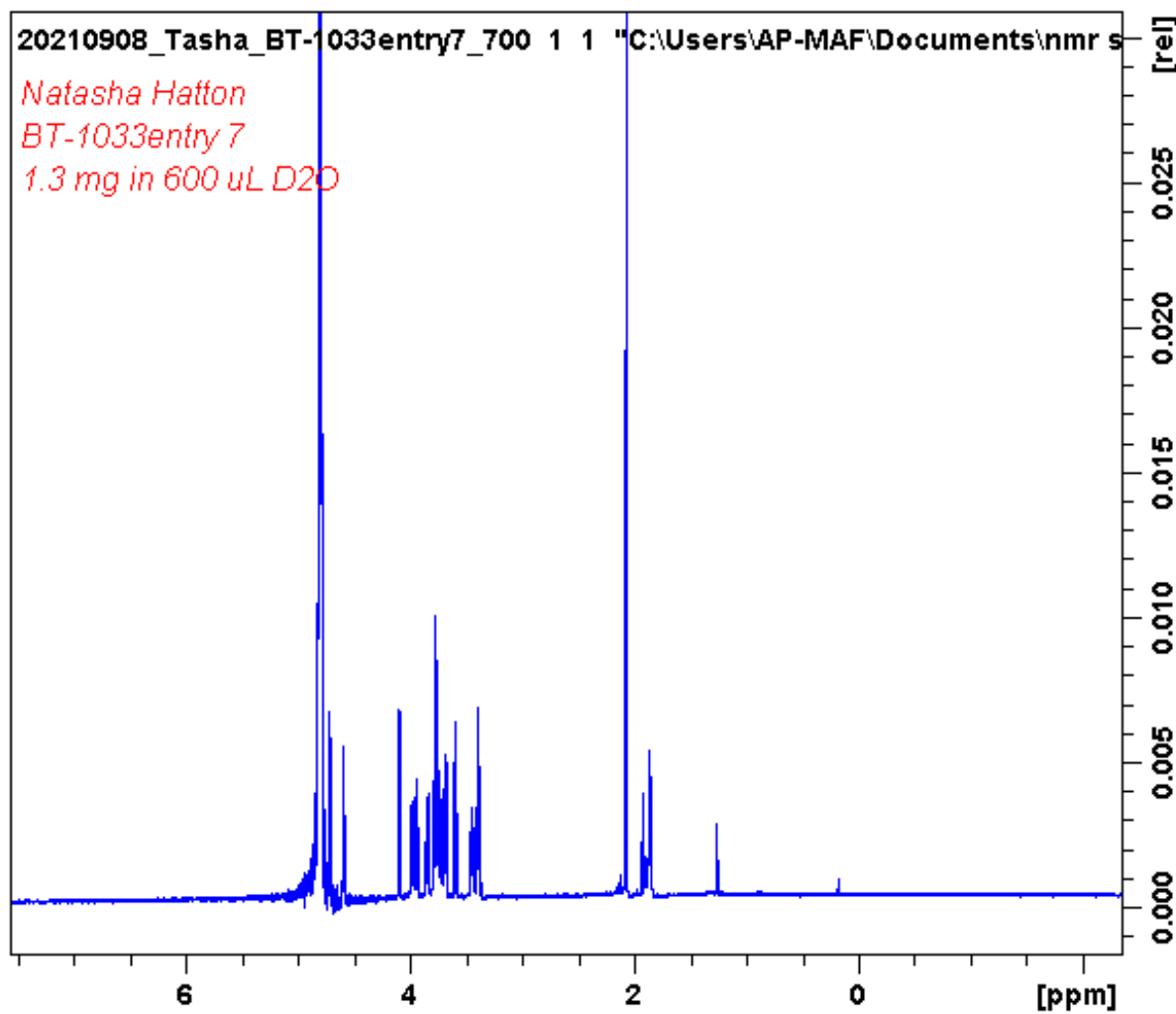


Appendix

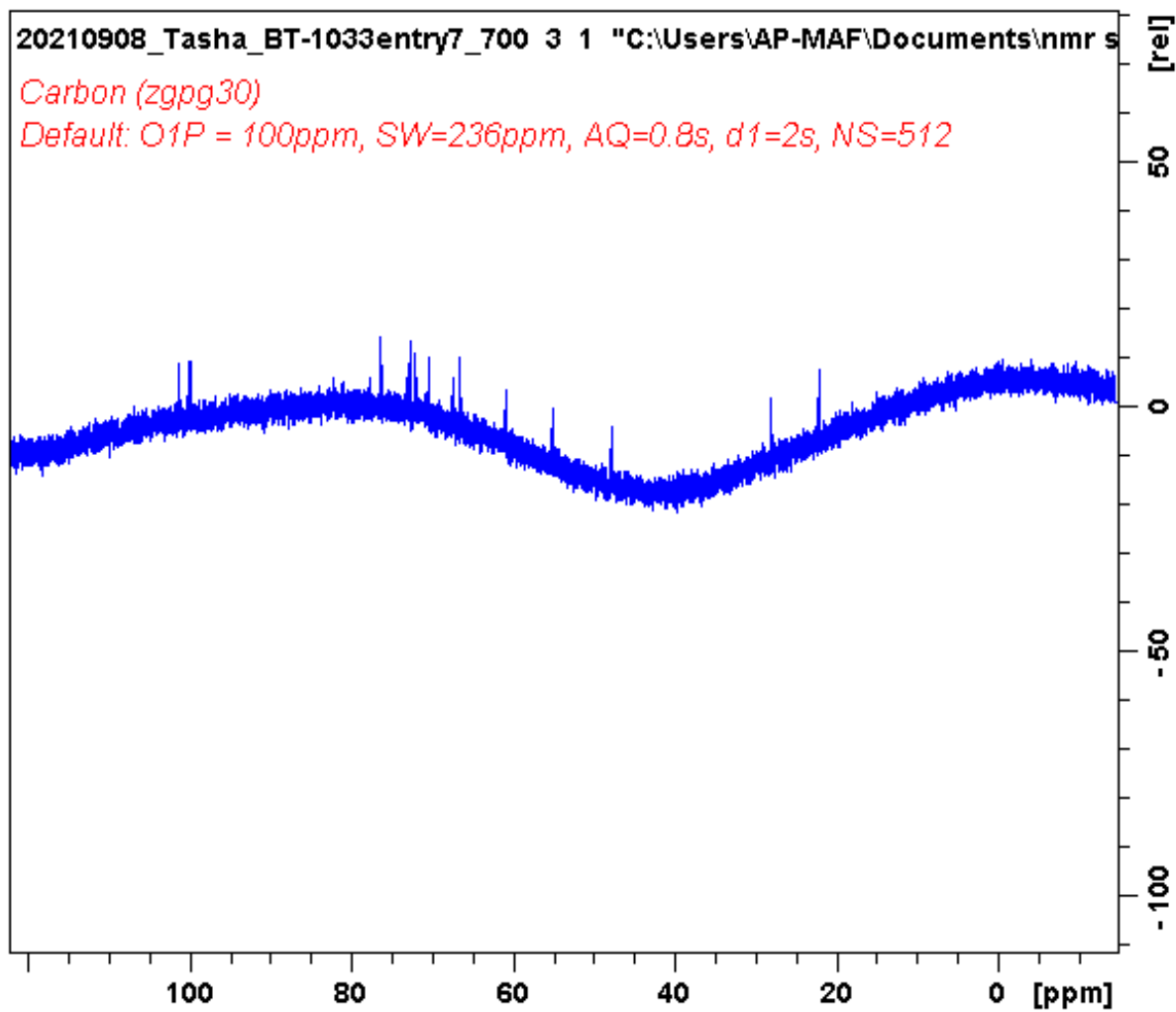
9.5.4.2 NMR spectrums of the disaccharide extracted from entry 34 scale up



<sup>1</sup>H NMR

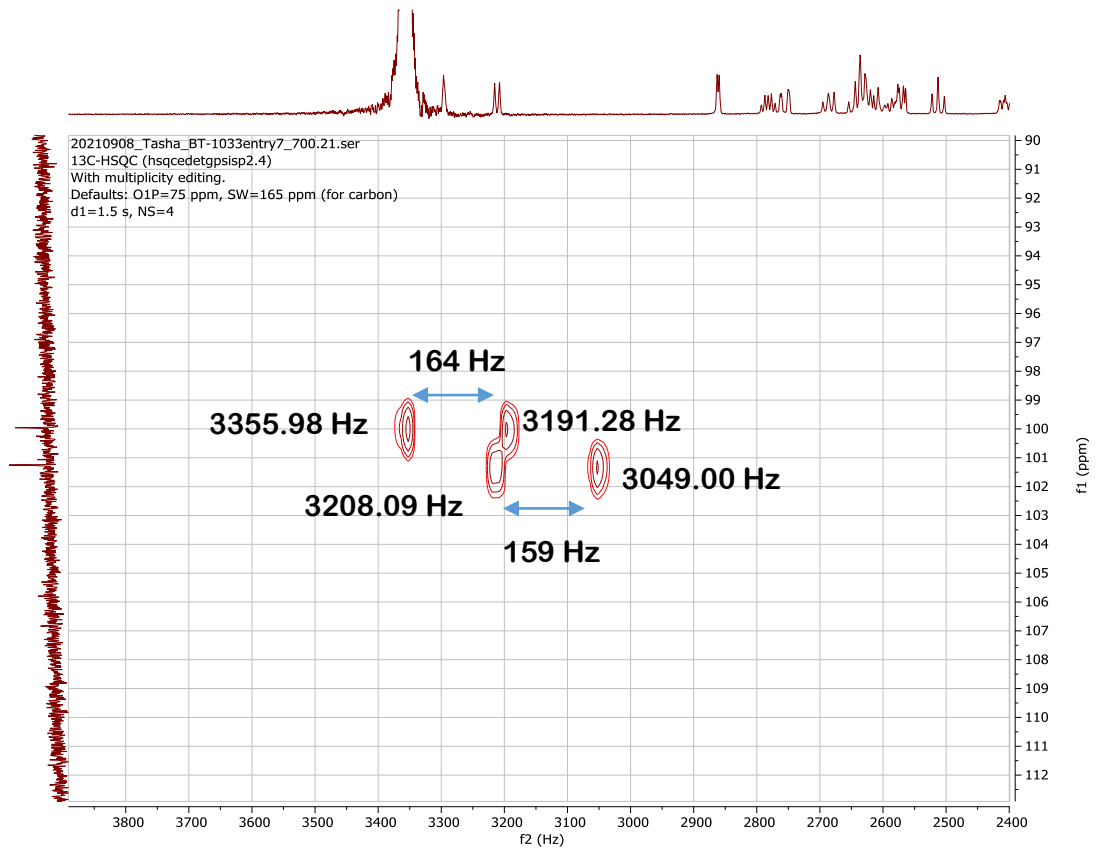


<sup>13</sup>C NMR



Appendix

CLIP-HSQC



## Appendix

### 9.5.5 Crystal trays designs

#### 9.5.5.1 JCSG B8 based plate

	1	2	3	4	5	6
A	0.2 M MgCl <sub>2</sub> , 0.1 M Tris pH 8.0 4% PEG 8000	0.2 M MgCl <sub>2</sub> , 0.1 M Tris pH 7.5 4% PEG 8000	0.2 M MgCl <sub>2</sub> , 0.1 M Tris pH 7.0 4% PEG 8000	0.2 M MgCl <sub>2</sub> , 0.1 M Tris, pH 6.5 4% PEG 8000	0.2 M MgCl <sub>2</sub> , 0.1 M Tris, pH 6.0 4% PEG 8000	0.2 M MgCl <sub>2</sub> , 0.1 M Tris pH 5.5 4% PEG 8000
B	0.2 M MgCl <sub>2</sub> , 0.1 M Tris pH 8.0 6% PEG 8000	0.2 M MgCl <sub>2</sub> , 0.1 M Tris pH 7.5 6% PEG 8000	0.2 M MgCl <sub>2</sub> , 0.1 M Tris, pH 7.0 6% PEG 8000	0.2 M MgCl <sub>2</sub> , 0.1 M Tris, pH 6.5 6% PEG 8000	0.2 M MgCl <sub>2</sub> , 0.1 M Tris pH 6.0 6% PEG 8000	0.2 M MgCl <sub>2</sub> , 0.1 M Tris pH 5.5 6% PEG 8000
C	0.2 M MgCl <sub>2</sub> , 0.1 M Tris pH 8.0 8% PEG 8000	0.2 M MgCl <sub>2</sub> , 0.1 M Tris pH 7.5 8% PEG 8000	0.2 M MgCl <sub>2</sub> , 0.1 M Tris, pH 7.0 8% PEG 8000	0.2 M MgCl <sub>2</sub> , 0.1 M Tris, pH 6.5 8% PEG 8000	0.2 M MgCl <sub>2</sub> , 0.1 M Tris pH 6.0 8% PEG 8000	0.2 M MgCl <sub>2</sub> , 0.1 M Tris pH 5.5 8% PEG 8000
D	0.2 M MgCl <sub>2</sub> , 0.1 M Tris pH 8.0 12% PEG 8000	0.2 M MgCl <sub>2</sub> , 0.1 M Tris pH 7.5 12% PEG 8000	0.2 M MgCl <sub>2</sub> , 0.1 M Tris, pH 7.0 12% PEG 8000	0.2 M MgCl <sub>2</sub> , 0.1 M Tris, pH 6.5 12% PEG 8000	0.2 M MgCl <sub>2</sub> , 0.1 M Tris pH 6.0 12% PEG 8000	0.2 M MgCl <sub>2</sub> , 0.1 M Tris pH 5.5 12% PEG 8000
E	0.2 M MgCl <sub>2</sub> , 0.1 M Tris pH 8.0 10% PEG 8000	0.2 M MgCl <sub>2</sub> , 0.1 M Tris pH 7.5 10% PEG 8000	0.2 M MgCl <sub>2</sub> , 0.1 M Tris, pH 7.0 10% PEG 8000	0.2 M MgCl <sub>2</sub> , 0.1 M Tris, pH 6.5 10% PEG 8000	0.2 M MgCl <sub>2</sub> , 0.1 M Tris pH 6.0 10% PEG 8000	0.2 M MgCl <sub>2</sub> , 0.1 M Tris pH 5.5 10% PEG 8000
F	0.2 M MgCl <sub>2</sub> , 0.1 M Tris pH 8.0 14% PEG 8000	0.2 M MgCl <sub>2</sub> , 0.1 M Tris pH 7.5 14% PEG 8000	0.2 M MgCl <sub>2</sub> , 0.1 M Tris, pH 7.0 14% PEG 8000	0.2 M MgCl <sub>2</sub> , 0.1 M Tris, pH 6.5 14% PEG 8000	0.2 M MgCl <sub>2</sub> , 0.1 M Tris pH 6.0 14% PEG 8000	0.2 M MgCl <sub>2</sub> , 0.1 M Tris pH 5.5 14% PEG 8000
G	0.2 M MgCl <sub>2</sub> , 0.1 M Tris pH 8.0 16% PEG 8000	0.2 M MgCl <sub>2</sub> , 0.1 M Tris pH 7.5 16% PEG 8000	0.2 M MgCl <sub>2</sub> , 0.1 M Tris, pH 7.0 16% PEG 8000	0.2 M MgCl <sub>2</sub> , 0.1 M Tris, pH 6.5 16% PEG 8000	0.2 M MgCl <sub>2</sub> , 0.1 M Tris pH 6.0 16% PEG 8000	0.2 M MgCl <sub>2</sub> , 0.1 M Tris pH 5.5 16% PEG 8000
H	0.2 M MgCl <sub>2</sub> , 0.1 M Tris pH 8.0 18% PEG 8000	0.2 M MgCl <sub>2</sub> , 0.1 M Tris pH 7.5 18% PEG 8000	0.2 M MgCl <sub>2</sub> , 0.1 M Tris, pH 7.0 18% PEG 8000	0.2 M MgCl <sub>2</sub> , 0.1 M Tris, pH 6.5 18% PEG 8000	0.2 M MgCl <sub>2</sub> , 0.1 M Tris pH 6.0 18% PEG 8000	0.2 M MgCl <sub>2</sub> , 0.1 M Tris pH 5.5 18% PEG 8000

## Appendix

## 9.5.5.2 INDEX H8 based plate

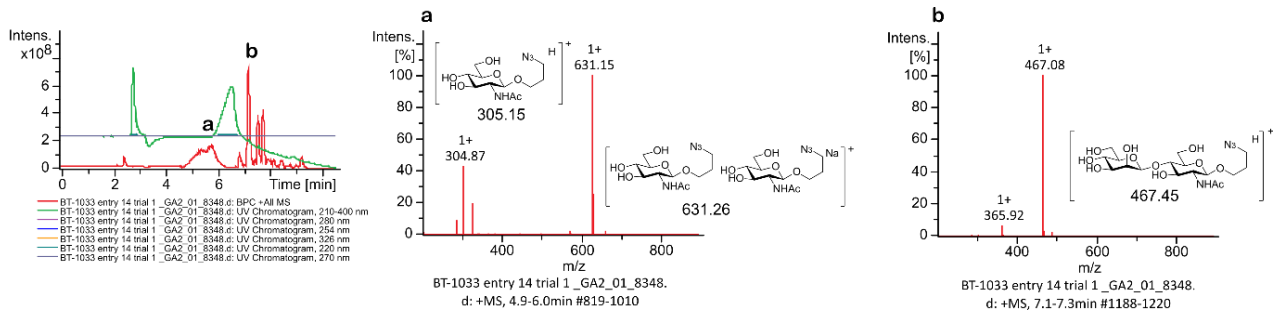
	1	2	3	4	5	6
Protein : reservoir ratio	0.2 : 0.5	0.4 : 0.5	0.5 : 1.0	1.0 : 1.0	1.0 : 0.75	1.0 : 0.5
A	0.1 M magnesium formate dihydrate 9% PEG 3350	0.1 M magnesium formate dihydrate 9% PEG 3350	0.1 M magnesium formate dihydrate 9% PEG 3350	0.1 M magnesium formate dihydrate 9% PEG 3350	0.1 M magnesium formate dihydrate 9% PEG 3350	0.1 M magnesium formate dihydrate 9% PEG 3350
B	0.1 M magnesium formate dihydrate 11% PEG 3350	0.1 M magnesium formate dihydrate 11% PEG 3350	0.1 M magnesium formate dihydrate 11% PEG 3350	0.1 M magnesium formate dihydrate 11% PEG 3350	0.1 M magnesium formate dihydrate 11% PEG 3350	0.1 M magnesium formate dihydrate 11% PEG 3350
C	0.1 M magnesium formate dihydrate 12% PEG 3350	0.1 M magnesium formate dihydrate 12% PEG 3350	0.1 M magnesium formate dihydrate 12% PEG 3350	0.1 M magnesium formate dihydrate 12% PEG 3350	0.1 M magnesium formate dihydrate 12% PEG 3350	0.1 M magnesium formate dihydrate 12% PEG 3350
D	0.1 M magnesium formate dihydrate 15% PEG 3350	0.1 M magnesium formate dihydrate 15% PEG 3350	0.1 M magnesium formate dihydrate 15% PEG 3350	0.1 M magnesium formate dihydrate 15% PEG 3350	0.1 M magnesium formate dihydrate 15% PEG 3350	0.1 M magnesium formate dihydrate 15% PEG 3350
E	0.1 M magnesium formate dihydrate 17% PEG 3350	0.1 M magnesium formate dihydrate 17% PEG 3350	0.1 M magnesium formate dihydrate 17% PEG 3350	0.1 M magnesium formate dihydrate 17% PEG 3350	0.1 M magnesium formate dihydrate 17% PEG 3350	0.1 M magnesium formate dihydrate 17% PEG 3350
F	0.1 M magnesium formate dihydrate 19% PEG 3350	0.1 M magnesium formate dihydrate 19% PEG 3350	0.1 M magnesium formate dihydrate 19% PEG 3350	0.1 M magnesium formate dihydrate 19% PEG 3350	0.1 M magnesium formate dihydrate 19% PEG 3350	0.1 M magnesium formate dihydrate 19% PEG 3350
G	0.1 M magnesium formate dihydrate 20% PEG 3350	0.1 M magnesium formate dihydrate 20% PEG 3350	0.1 M magnesium formate dihydrate 20% PEG 3350	0.1 M magnesium formate dihydrate 20% PEG 3350	0.1 M magnesium formate dihydrate 20% PEG 3350	0.1 M magnesium formate dihydrate 20% PEG 3350
H	0.1 M magnesium formate dihydrate 23% PEG 3350	0.1 M magnesium formate dihydrate 23% PEG 3350	0.1 M magnesium formate dihydrate 23% PEG 3350	0.1 M magnesium formate dihydrate 23% PEG 3350	0.1 M magnesium formate dihydrate 23% PEG 3350	0.1 M magnesium formate dihydrate 23% PEG 3350

## Appendix

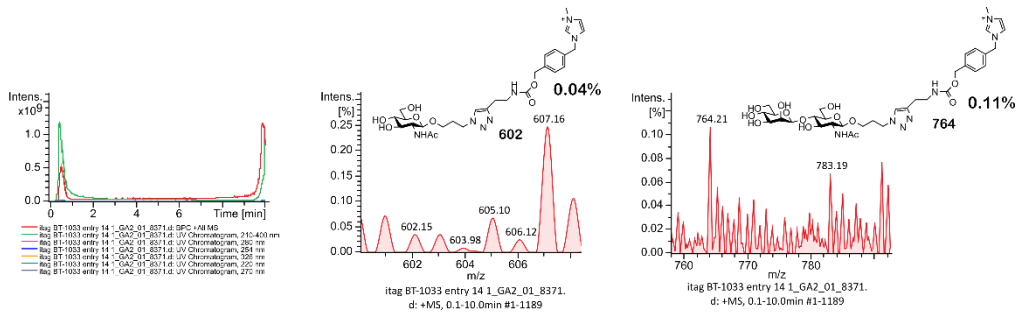
### 9.5.6 BT-1033 catalysed reactions 43a-44b and enzyme free control reactions 45a and 45b

#### Reaction Entry 43a

##### Post reaction termination LCMS trace

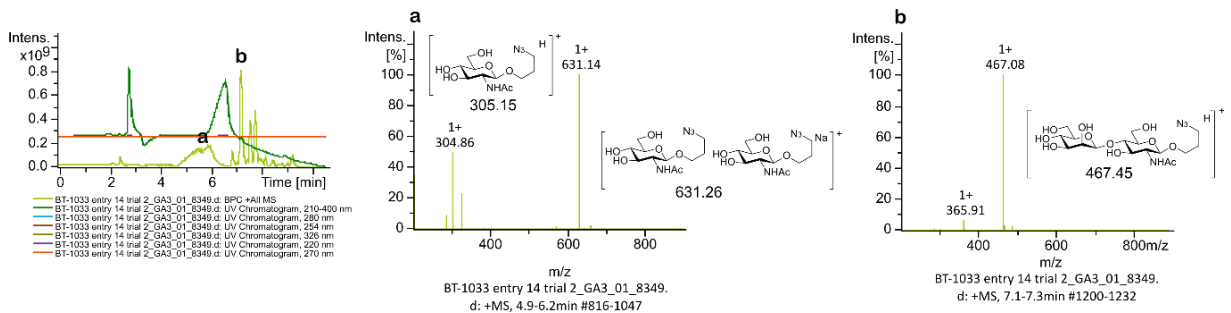


##### Post reaction with ITag reagent 6.16 LCMS trace

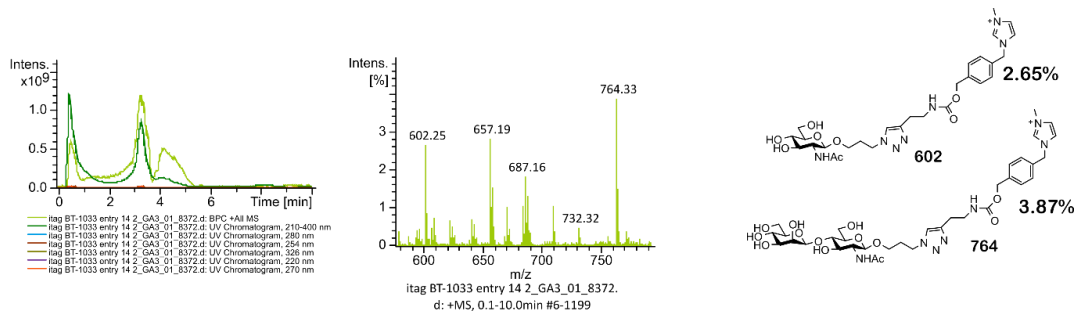


#### Reaction Entry 43b

##### Post reaction termination LCMS trace



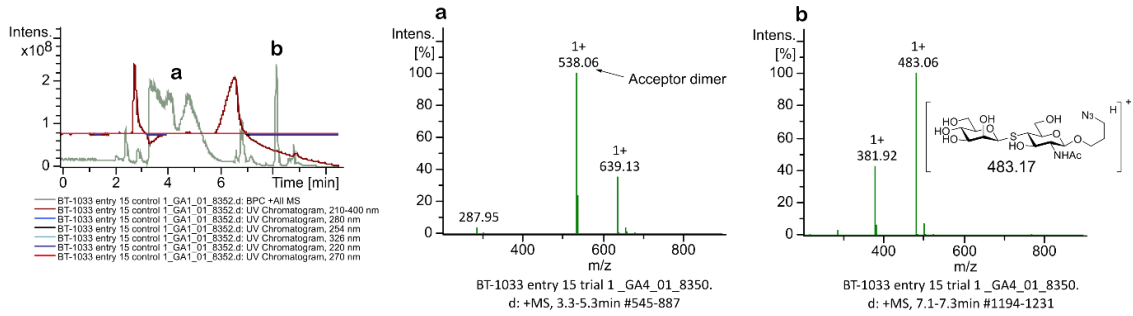
##### Post reaction with ITag reagent 6.16 LCMS trace



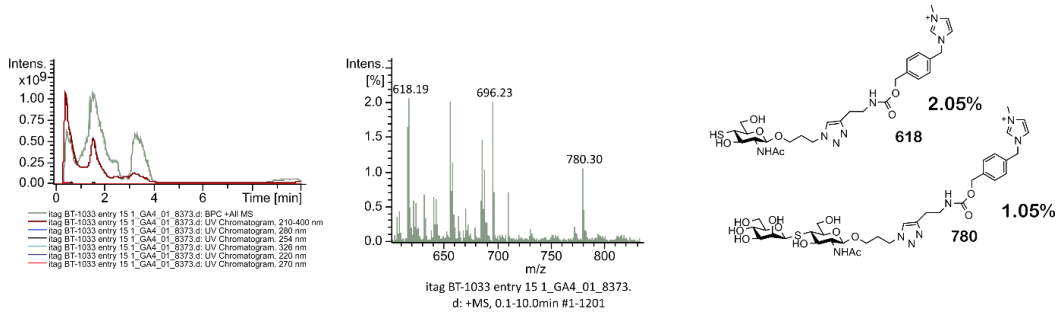
## Appendix

### Reaction Entry 44a

#### Post reaction termination LCMS trace

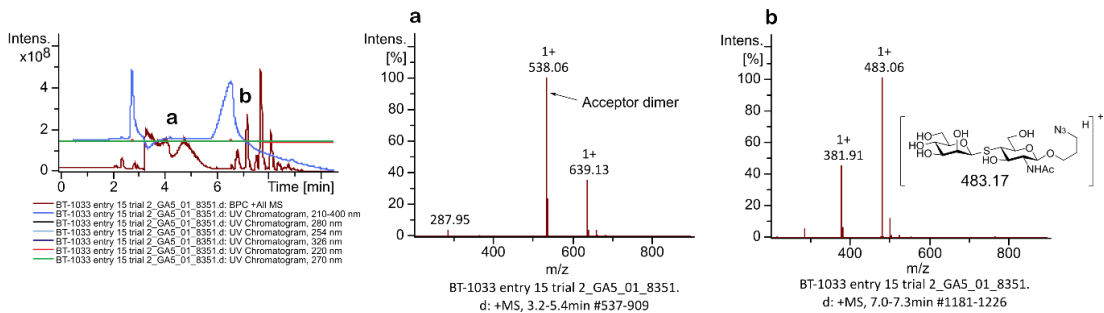


#### Post reaction with ITag reagent 6.16 LCMS trace

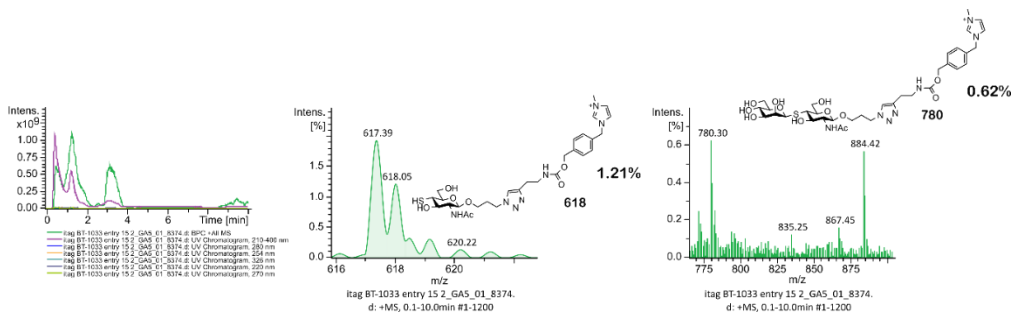


### Reaction Entry 44b

#### Post reaction termination LCMS trace



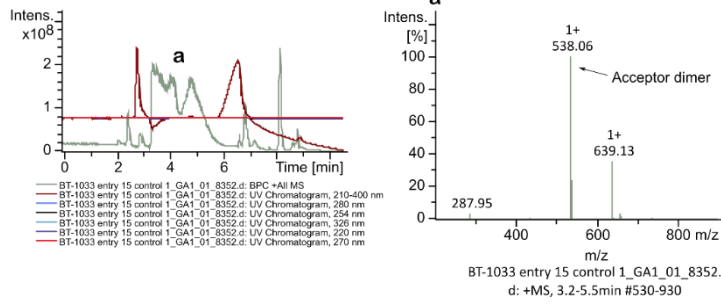
#### Post reaction with ITag reagent 6.16 LCMS trace



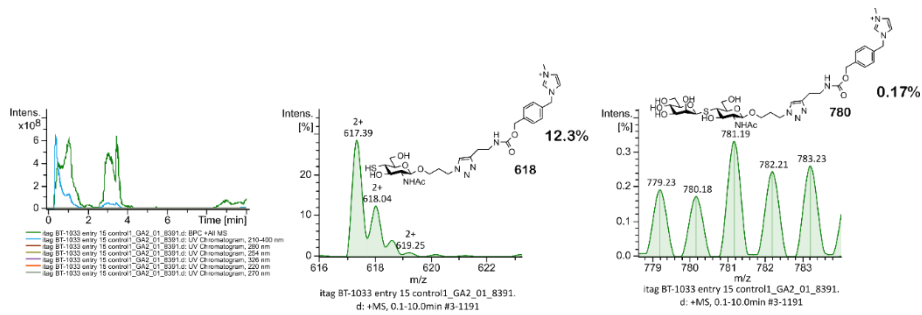
# Appendix

## Reaction Entry 45a

### Post reaction termination LCMS trace

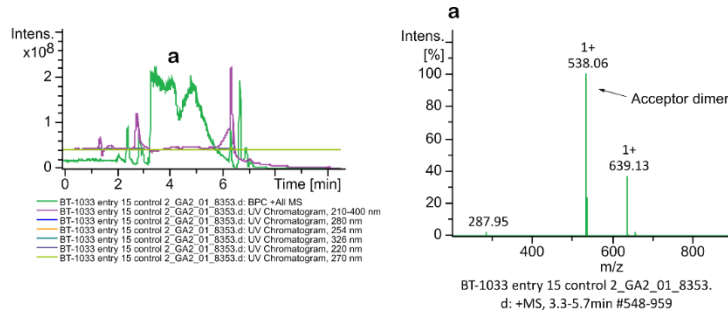


### Post reaction with ITag reagent 6.16 LCMS trace

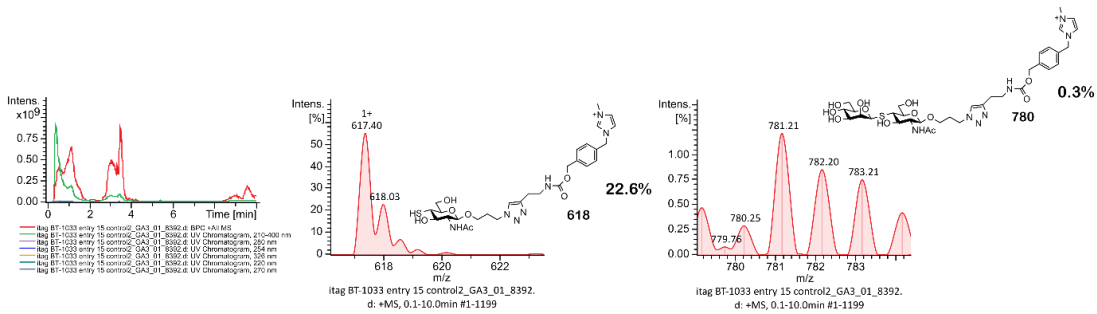


## Reaction Entry 45b

### Post reaction termination LCMS trace



### Post reaction with ITag reagent 6.16 LCMS trace





## Chapter 10 References

1. D. R. Hickling, T. T. Sun and X. R. Wu, *Microbiol. Spectr.*, 2015, **3**, 17.
2. J. Kaufman, M. Temple-Smith and L. Sanci, *BMJ Paediatr. open*, 2019, **3**, e000487-e000487.
3. I. Katnik-Prastowska, J. Lis and A. Matejuk, *Glycoconj. J.*, 2014, **31**, 623-636.
4. C. C. A. Hu, F. X. Liang, G. Zhou, L. Y. Tu, C. H. A. Tang, J. Zhou, G. Kreibich and T. T. Sun, *Mol Biol Cell*, 2005, **16**, 3937-3950.
5. B. Kachar, F. X. Liang, U. Lins, M. X. Ding, X. R. Wu, D. Stoffler, U. Aebi and T. T. Sun, *J. Mol. Biol.*, 1999, **285**, 595-608.
6. G. Lee, *Int Neurorol J*, 2011, **15**, 4-12.
7. M. A. Matuszewski, K. Tupikowski, L. Dolowy, B. Szymanska, J. Dembowski and R. Zdrojowy, *Cent European J Urol*, 2016, **69**, 252-257.
8. UniProt, UniProtKB - O00322 (UPK1A\_HUMAN), <https://www.uniprot.org/uniprot/O00322>, (accessed 01.06.2020, 2020).
9. UniProt, UniProtKB - O75841 (UPK1B\_HUMAN), <https://www.uniprot.org/uniprot/O75841>, (accessed 01.06.2020, 2020).
10. M. S. Najar, C. L. Saldanha and K. A. Banday, *Ind. J. Nephrol*, 2009, **19**, 129-139.
11. C. W. Tan and M. P. Chlebicki, *Singap. Med. J.*, 2016, **57**, 485-489.
12. L. E. Nicolle, *Infect. Dis. Clin. North Am.*, 1997, **11**, 647-&.
13. T. L. Greenhow, Y. Y. Hung, A. M. Herz, E. Losada and R. H. Pantell, *Pediatr. Infect. Dis. J.*, 2014, **33**, 595-599.
14. F. M. E. Wagenlehner, A. Pilatz, K. G. Naber and W. Weidner, *Eur. J. Clin. Invest.*, 2008, **38**, 45-49.
15. B. Foxman, *Dis. Mon.*, 2003, **49**, 53-70.
16. J. A. Ryu and B. Kim, *Radiographics*, 2001, **21**, 1169-1185.
17. T. Klein, D. Abgottsporn, M. Wittwer, S. Rabbani, J. Herold, X. H. Jiang, S. Kleeb, C. Luthi, M. Scharenberg, J. Bezencon, E. Gubler, L. J. Pang, M. Smiesko, B. Cutting, O. Schwarzd and B. Ernst, *J. Med. Chem.*, 2010, **53**, 8627-8641.
18. T. A. Rowe and M. Juthani-Mehta, *Aging Health*, 2013, **9**, 519-528.
19. B. Foxman, *Infect. Dis. Clin. North. Am.*, 2014, **28**, 1-+.
20. A. Ronald, *Am. J. Med.*, 2002, **113**, 14S-19S.
21. M. D. Melekos and K. G. Naber, *Int. J. Antimicrob. Agents*, 2000, **15**, 247-256.
22. M. A. Mulvey, J. D. Schilling, J. J. Martinez and S. J. Hultgren, *Proc. Natl. Acad. Sci. U. S. A.*, 2000, **97**, 8829-8835.
23. B. Wiedemann, A. Heisig and P. Heisig, *Antibiotics*, 2014, **3**, 341-352.
24. N. N. T. Goemaere, K. Grijm, P. T. W. van Hal and M. A. den Bakker, *J. Med. Case Rep*, 2008, **2**, 169.
25. L. Cegelski, G. R. Marshall, G. R. Eldridge and S. J. Hultgren, *Nat. Revi. Microbiol.*, 2008, **6**, 17-27.
26. M. E. Terlizzi, G. Griboaldo and M. E. Maffei, *Front. Microbiol.*, 2017, **8**, 23.
27. M. G. Blango, E. M. Ott, A. Erman, P. Veranic and M. A. Mulvey, *PLoS One*, 2014, **9**, 9.
28. M. A. Mulvey, Y. S. Lopez-Boado, C. L. Wilson, R. Roth, W. C. Parks, J. Heuser and S. J. Hultgren, *Science*, 1998, **282**, 1494-1497.
29. J. J. Martinez, M. A. Mulvey, J. D. Schilling, J. S. Pinkner and S. J. Hultgren, *Embo J.*, 2000, **19**, 2803-2812.
30. D. S. Eto, T. A. Jones, J. L. Sundsbak and M. A. Mulvey, *PLoS Pathog.*, 2007, **3**, 949-961.
31. J. J. Martinez and S. J. Hultgren, *Cell. Microbiol.*, 2002, **4**, 19-28.
32. M. J. Duncan, G. J. Li, J. S. Shin, J. L. Carson and S. N. Abraham, *J. Biol. Chem.*, 2004, **279**, 18944-18951.
33. B. K. Dhakal and M. A. Mulvey, *J. Biol. Chem.*, 2009, **284**, 446-454.
34. J. D. Schilling, M. A. Mulvey and S. J. Hultgren, *J. Infect. Dis.*, 2001, **183**, S36-S40.
35. M. S. Hanson and C. C. Brinton, *Nature*, 1988, **332**, 265-268.

## References

36. C. Spaulding, H. L. Schreiber, W. L. Zheng, K. W. Dodson, J. E. Hazen, M. Conover, F. B. Wang, P. Svenmarker, A. Luna-Rico, O. Francetic, M. Andersson, S. Hultgren and E. H. Egelman, *eLife*, 2018, **7**, 25.
37. M. S. Hanson, J. Hempel and C. C. Brinton, *J. Bacteriol.*, 1988, **170**, 3350-3358.
38. K. A. Krogfelt and P. Klemm, *Microb. Pathog.*, 1988, **4**, 231-238.
39. P. Klemm and G. Christiansen, *Mol. Gen. Gen.*, 1987, **208**, 439-445.
40. K. A. Krogfelt, H. Bergmans and P. Klemm, *Infect. Immun.*, 1990, **58**, 1995-1998.
41. L. K. Mydock-McGrane, T. J. Hannan and J. W. Janetka, *Expert Opin. Drug Discov.*, 2017, **12**, 711-731.
42. M. M. Sauer, R. P. Jakob, T. Lubber, F. Canonica, G. Navarra, B. Ernst, C. Unverzagt, T. Maier and R. Glockshuber, *J. Am. Chem. Soc.*, 2019, **141**, 936-944.
43. I. Le Trong, P. Aprikian, B. A. Kidd, W. E. Thomas, E. V. Sokurenko and R. E. Stenkamp, *J. Struct. Biol.*, 2010, **172**, 380-388.
44. S. Vanwetswinkel, A. N. Volkov, Y. G. J. Sterckx, A. Garcia-Pino, L. Buts, W. F. Vranken, J. Bouckaert, R. Roy, L. Wyns and N. A. J. van Nuland, *J. Med. Chem.*, 2014, **57**, 1416-1427.
45. M. Forero, W. E. Thomas, C. Bland, L. M. Nilsson, E. V. Sokurenko and V. Vogel, *Nano Lett.*, 2004, **4**, 1593-1597.
46. K. Konstantopoulos, W. D. Hanley and D. Wirtz, *Curr. Biol.*, 2003, **13**, R611-R613.
47. R. R. Isberg and P. Barnes, *Cell*, 2002, **110**, 1-4.
48. K. C. Chang and D. A. Hammer, *Biophys. J.*, 1999, **76**, 1280-1292.
49. P. Aprikian, V. Tchesnokova, B. Kidd, O. Yakovenko, V. Yarov-Yarovoy, E. Trinchina, V. Vogel, W. Thomas and E. Sokurenko, *J. Biol. Chem.*, 2007, **282**, 23437-23446.
50. I. Le Trong, P. Aprikian, B. A. Kidd, M. Forero-Shelton, V. Tchesnokova, P. Rajagopal, V. Rodriguez, G. Interlandi, R. Klevit, V. Vogel, R. E. Stenkamp, E. V. Sokurenko and W. E. Thomas, *Cell*, 2010, **141**, 645-655.
51. A. Wellens, C. Garofalo, H. Nguyen, N. Van Gerven, R. Slattegard, J. P. Hernalsteens, L. Wyns, S. Oscarson, H. De Greve, S. Hultgren and J. Bouckaert, *PLoS One*, 2008, **3**, 13.
52. Z. F. Han, J. S. Pinkner, B. Ford, R. Obermann, W. Nolan, S. A. Wildman, D. Hobbs, T. Ellenberger, C. K. Cusumano, S. J. Hultgren and J. W. Janetka, *J. Med. Chem.*, 2010, **53**, 4779-4792.
53. C. Jarvis, Z. F. Han, V. Kalas, R. Klein, J. S. Pinkner, B. Ford, J. Binkley, C. K. Cusumano, Z. Cusumano, L. Mydock-McGrane, S. J. Hultgren and J. W. Janetka, *ChemMedChem*, 2016, **11**, 367-373.
54. D. C. Old, *Journal of Gen. Microbiol.*, 1972, **71**, 149-&.
55. I. E. Salit and E. C. Gotschlich, *J. Exp. Med.*, 1977, **146**, 1169-1181.
56. C. S. Hung, J. Bouckaert, D. Hung, J. Pinkner, C. Widberg, A. DeFusco, C. G. Auguste, R. Strouse, S. Langermann, G. Waksman and S. J. Hultgren, *Mol. Microbiol.*, 2002, **44**, 903-915.
57. A. Wellens, M. Lahmann, M. Touaibia, J. Vaucher, S. Oscarson, R. Roy, H. Remaut and J. Bouckaert, *Biochemistry*, 2012, **51**, 4790-4799.
58. G. Roos, A. Wellens, M. Touaibia, N. Yamakawa, P. Geerlings, R. Roy, L. Wyns and J. Bouckaert, *ACS Med. Chem. Lett.*, 2013, **4**, 1085-1090.
59. L. J. Pang, S. Kleeb, K. Lemme, S. Rabbani, M. Scharenberg, A. Zalewski, F. Schadler, O. Schwardt and B. Ernst, *ChemMedChem*, 2012, **7**, 1404-1422.
60. V. P. O'Brien, T. J. Hannan, H. V. Nielsen and S. J. Hultgren, *Microbiol. Spectr.*, 2016, **4**, 42.
61. A. S. McKee, M. W. Munks and P. Marrack, *Immunity*, 2007, **27**, 687-690.
62. E. M. Grischke and H. Ruttgers, *Urol.Int.*, 1987, **42**, 338-341.
63. P. Das, *Lancet Infect. Dis.*, 2002, **2**, 68-68.
64. A. R. Brumbaugh and H. L. T. Mobley, *Expert Rev. Vaccines*, 2012, **11**, 663-676.
65. H. W. Bauer, V. W. Rahlfs, P. A. Lauener and G. S. S. Blessmann, *Int. J. Antimicrob. Agents*, 2002, **19**, 451-456.

## References

66. H. W. Bauer, S. Alloussi, G. Egger, H. M. Blumlein, G. Cozma, C. C. Schulman and U. T. I. S. G. Multicenter, *Eur. Urol.*, 2005, **47**, 542-548.
67. T. M. Wizemann, J. E. Adamou and S. Langermann, *Emerg. Infect. Dis.*, 1999, **5**, 395-403.
68. S. Langermann, S. Palaszynski, M. Barnhart, G. Auguste, J. S. Pinkner, J. Burlein, P. Barren, S. Koenig, S. Leath, C. H. Jones and S. J. Hultgren, *Science*, 1997, **276**, 607-611.
69. S. Langermann, R. Mollby, J. E. Burlein, S. R. Palaszynski, C. G. Auguste, A. DeFusco, R. Strouse, M. A. Schenerman, S. J. Hultgren, J. S. Pinkner, J. Winberg, L. Guldevall, M. Soderhall, K. Ishikawa, S. Normark and S. Koenig, *J. Infect. Dis.*, 2000, **181**, 774-778.
70. S. Langermann and W. R. Ballou, *J. Infect. Dis.*, 2001, **183**, S84-S86.
71. H. Li and D. H. Walker, *Infect. Immun.*, 1992, **60**, 2030-2035.
72. Gary Eldridge, St. Louis, MO (US); Steven M Martin, St. Louis, MO (US), COMPOSITIONS OF VACCINES AND ADUVANTS AND METHODS FOR THE TREATMENT OF URINARY TRACT INFECTIONS, 9,017,698 B2, 2015.
73. N. Saleh, UTI Vaccine Shows Promise, <https://www.verywellhealth.com/uti-vaccine-shows-promise-4147399>).
74. A. Huttner, C. Hatz, G. van den Dobbelen, D. Abbanat, A. Hornacek, R. Frolich, A. M. Dreyer, P. Martin, T. Davies, K. Fae, I. van den Nieuwenhof, S. Thoelen, S. de Valliere, A. Kuhn, E. Bernasconi, V. Viereck, T. Kavvadias, K. Kling, G. Ryu, T. Hulder, S. Groger, D. Scheiner, C. Alaimo, S. Harbarth, J. Poolman and V. G. Fonck, *Lancet Infect. Dis.*, 2017, **17**, 528-537.
75. B. Xie, G. Zhou, S. Y. Chan, E. Shapiro, X. P. Kong, X. R. Wu, T. T. Sun and C. E. Costello, *J. Biol. Chem.*, 2006, **281**, 14644-14653.
76. N. Sharon, *FEBS Lett.*, 1987, **217**, 145-157.
77. N. Firon, I. Ofek and N. Sharon, *Carbohydr. Res.*, 1983, **120**, 235-249.
78. J. Bouckaert, J. Mackenzie, J. L. de Paz, B. Chipwaza, D. Choudhury, A. Zavialov, K. Mannerstedt, J. Anderson, D. Pierard, L. Wyns, P. H. Seeberger, S. Oscarson, H. De Greve and S. D. Knight, *Mol. Microbiol.*, 2006, **61**, 1556-1568.
79. M. Heuckendorff, J. Bendix, C. M. Pedersen and M. Bols, *Org. Lett.*, 2014, **16**, 1116-1119.
80. D. Crich and S. X. Sun, *J. Org. Chem.*, 1996, **61**, 4506-4507.
81. D. Crich and S. X. Sun, *Tetrahedron*, 1998, **54**, 8321-8348.
82. D. Crich and H. M. Li, *J. Org. Chem.*, 2000, **65**, 801-805.
83. D. Crich and S. X. Sun, *J. Org. Chem.*, 1997, **62**, 1198-1199.
84. M. Heuckendorff, P. S. Bols, C. B. Barry, T. G. Frihed, C. M. Pedersen and M. Bols, *ChemComm.*, 2015, **51**, 13283-13285.
85. D. Crich and O. Vinogradova, *J. Org. Chem.*, 2006, **71**, 8473-8480.
86. D. Crich, M. de la Mora and A. U. Vinod, *J. Org. Chem.*, 2003, **68**, 8142-8148.
87. J. Bouckaert, J. Berglund, M. Schembri, E. De Genst, L. Cools, M. Wuhrer, C. S. Hung, J. Pinkner, R. Slattegard, A. Zavialov, D. Choudhury, S. Langermann, S. J. Hultgren, L. Wyns, P. Klemm, S. Oscarson, S. D. Knight and H. De Greve, *Mol. Microbiol.*, 2005, **55**, 441-455.
88. S. Oscarson and A. K. Tiden, *Carbohydr. Res.*, 1993, **247**, 323-328.
89. N. Firon, S. Ashkenazi, D. Mirelman, I. Ofek and N. Sharon, *Infect. Immun.*, 1987, **55**, 472-476.
90. O. Sperling, A. Fuchs and T. K. Lindhorst, *Org. Biomol. Chem.*, 2006, **4**, 3913-3922.
91. T. K. Lindhorst, S. Kotter, J. Kubisch, U. Krallmann-Wenzel, S. Ehlers and V. Kren, *Eur. J. Org. Chem.*, 1998, **1998**, 1669-1674.
92. Z. F. Han, J. S. Pinkner, B. Ford, E. Chorell, J. M. Crowley, C. K. Cusumano, S. Campbell, J. P. Henderson, S. J. Hultgren and J. W. Janetka, *J. Med. Chem.*, 2012, **55**, 3945-3959.
93. C. K. Cusumano, J. S. Pinkner, Z. Han, S. E. Greene, B. A. Ford, J. R. Crowley, J. P. Henderson, J. W. Janetka and S. J. Hultgren, *Sci. Trans. Med.*, 2011, **3**, 109ra115-109ra115.
94. K. Mayer, D. Eris, O. Schwardt, C. P. Sager, S. Rabbani, S. Kleeb and B. Ernst, *J. Med. Chem.*, 2017, **60**, 5646-5662.

## References

95. M. Vetsch, P. Sebbel and R. Glockshuber, *J. Mol. Biol.*, 2002, **322**, 827-840.
96. W. Schonemann, J. Cramer, T. Muhlethaler, B. Fiege, M. Silbermann, S. Rabbani, P. Datwyler, P. Zihlmann, R. P. Jakob, C. P. Sager, M. Smiesko, O. Schwaradt, T. Maier and B. Ernst, *ChemMedChem*, 2019, **14**, 749-757.
97. C. Grabosch, M. Hartmann, J. Schmidt-Lassen and T. K. Lindhorst, *ChemBioChem*, 2011, **12**, 1066-1074.
98. C. P. Sager, B. Fiege, P. Zihlmann, R. Vannam, S. Rabbani, R. P. Jakob, R. C. Preston, A. Zalewski, T. Maier, M. W. Peczuh and B. Ernst, *Chem. Sci.*, 2018, **9**, 646-654.
99. D. A. Dorta, T. Chalopin, A. Sivignon, J. de Ruyck, T. I. Dumych, R. O. Bilyy, D. Deniaud, N. Barnich, J. Bouckaert and S. G. Gouin, *ChemMedChem*, 2017, **12**, 986-998.
100. S. Brument, A. Sivignon, T. I. Dumych, N. Moreau, G. Roos, Y. Guerardel, T. Chalopin, D. Deniaud, R. O. Bilyy, A. Darfeuille-Michaud, J. Bouckaert and S. G. Gouin, *J. Med. Chem.*, 2013, **56**, 5395-5406.
101. X. H. Jiang, D. Abgottspon, S. Kleeb, S. Rabbani, M. Scharenberg, M. Wittwer, M. Haug, O. Schwaradt and B. Ernst, *J. Med. Chem.*, 2012, **55**, 4700-4713.
102. M. Scharenberg, O. Schwaradt, S. Rabbani and B. Ernst, *J. Med. Chem.*, 2012, **55**, 9810-9816.
103. J. J. Lundquist and E. J. Toone, *Chem. Rev.*, 2002, **102**, 555-578.
104. Y. C. Lee and R. T. Lee, *Acc. Chem. Res.*, 1995, **28**, 321-327.
105. S. Cecioni, A. Imberty and S. Vidal, *Chem. Rev.*, 2015, **115**, 525-561.
106. P. Rassam, N. A. Copeland, O. Birkholz, C. Tóth, M. Chavent, A. L. Duncan, S. J. Cross, N. G. Housden, R. Kaminska, U. Seger, D. M. Quinn, T. J. Garrod, M. S. P. Sansom, J. Piehler, C. G. Baumann and C. Kleanthous, *Nature*, 2015, **523**, 333-336.
107. A. Bernardi, J. Jimenez-Barbero, A. Casnati, C. De Castro, T. Darbre, F. Fieschi, J. Finne, H. Funken, K. E. Jaeger, M. Lahmann, T. K. Lindhorst, M. Marradi, P. Messner, A. Molinaro, P. V. Murphy, C. Nativi, S. Oscarson, S. Penades, F. Peri, R. J. Pieters, O. Renaudet, J. L. Reymond, B. Richichi, J. Rojo, F. Sansone, C. Schaffer, W. B. Turnbull, T. Velasco-Torrijos, S. Vidal, S. Vincent, T. Wennekes, H. Zuilhof and A. Imberty, *Chem. Soc. Rev.*, 2013, **42**, 4709-4727.
108. M. Hartmann, P. Betz, Y. C. Sun, S. N. Gorb, T. K. Lindhorst and A. Krueger, *Chem. Eur. J.*, 2012, **18**, 6485-6492.
109. S. G. Gouin, A. Wellens, J. Bouckaert and J. Kovensky, *ChemMedChem*, 2009, **4**, 749-755.
110. M. Almant, V. Moreau, J. Kovensky, J. Bouckaert and S. G. Gouin, *Chem. Eur. J.*, 2011, **17**, 10029-10038.
111. J. Bouckaert, Z. L. Li, C. Xavier, M. Almant, V. Caveliers, T. Lahoutte, S. D. Weeks, J. Kovensky and S. G. Gouin, *Chem. Eur. J.*, 2013, **19**, 7847-7855.
112. A. Sivignon, X. B. Yan, D. A. Dorta, R. Bonnet, J. Bouckaert, E. Fleury, J. Bernard, S. G. Gouin, A. Darfeuille-Michaud and N. Barnich, *mBio*, 2015, **6**, 9.
113. X. B. Yan, V. La Padula, S. Favre-Bonte and J. Bernard, *Eur. Polym. J.*, 2019, **112**, 170-175.
114. A. Schierholt, M. Hartmann, K. Schwekendiek and T. K. Lindhorst, *Eur. J. Org. Chem.*, 2010, **2010**, 3120-3128.
115. M. Touaibia, T. C. Shiao, A. Papadopoulos, J. Vaucher, Q. G. Wang, K. Benhamioud and R. Roy, *Chem. Commun.*, 2007, DOI: 10.1039/b612471b, 380-382.
116. T. K. Lindhorst, C. Kieburg and U. Krallmann-Wenzel, *Glycoconjug. J.*, 1998, **15**, 605-613.
117. M. Dubber, O. Sperling and T. K. Lindhorst, *Org. Biomol. Chem.*, 2006, **4**, 3901-3912.
118. M. Touaibia, A. Wellens, T. C. Shiao, Q. Wang, S. Sirois, J. Bouckaert and R. Roy, *ChemMedChem*, 2007, **2**, 1190-1201.
119. A. Papadopoulos, T. C. Shiao and R. Roy, *Mol. Pharmaceut.*, 2012, **9**, 394-403.
120. J. D. K. Twibanire, N. K. Paul and T. B. Grindley, *New J. Chem.*, 2015, **39**, 4115-4127.
121. N. Nagahori, R. T. Lee, S. Nishimura, D. Page, R. Roy and Y. C. Lee, *ChemBioChem*, 2002, **3**, 836-844.
122. S. Kötter, U. Krallmann-Wenzel, S. Ehlers and T. K. Lindhorst, *J. Chem. Soc. Perkin Trans. 1*, 1998, DOI: 10.1039/A801985A, 2193-2200.

## References

123. A. Barras, F. A. Martin, O. Bande, J. S. Baumann, J. M. Ghigo, R. Boukherroub, C. Beloin, A. Siriwardena and S. Szunerits, *Nanoscale*, 2013, **5**, 2307-2316.
124. J. F. Nierengarten, J. Iehl, V. Oerthel, M. Holler, B. M. Illescas, A. Munoz, N. Martin, J. Rojo, M. Sanchez-Navarro, S. Cecioni, S. Vidal, K. Buffet, M. Durka and S. P. Vincent, *Chem. Commun.*, 2010, **46**, 3860-3862.
125. M. Durka, K. Buffet, J. Iehl, M. Holler, J. F. Nierengarten, J. Taganna, J. Bouckaert and S. P. Vincent, *Chem. Commun.*, 2011, **47**, 1321-1323.
126. A. Schierholt, M. Hartmann and T. K. Lindhorst, *Carbohydr. Res*, 2011, **346**, 1519-1526.
127. B. Schmidt, S. Sankaran, L. Stegemann, C. A. Strassert, P. Jonkheijm and J. Voskuhl, *J. Mat. Chem. B.*, 2016, **4**, 4732-4738.
128. I. Nierengarten, K. Buffet, M. Holler, S. P. Vincent and J. F. Nierengarten, *Tetrahedron Lett.*, 2013, **54**, 2398-2402.
129. W. Reinisch, X. Hebuterne, A. Buisson, S. Schreiber, P. Desreumaux, J. M. Paillarse and C. Bonny, *J Crohns Colitis*, 2020, **14**, S479-S480.
130. W. Reinisch, X. Hebuterne, A. Buisson, S. Schreiber, P. Desreumaux, C. Primas, J. M. Paillarse and C. Bonny, *Gastroenterology*, 2020, **158**, S1211-S1212.
131. J. Kalia and R. T. Raines, *Curr. Org. Chem.*, 2010, **14**, 138-147.
132. R. V. J. Chari, M. L. Miller and W. C. Widdison, *Angew. Chem.-Int. Edit.*, 2014, **53**, 3796-3827.
133. V. V. Rostovtsev, L. G. Green, V. V. Fokin and K. B. Sharpless, *Angew. Chem.-Int. Edit.*, 2002, **41**, 2596-+.
134. C. W. Tornoe, C. Christensen and M. Meldal, *J. Org. Chem.*, 2002, **67**, 3057-3064.
135. N. J. Agard, J. A. Prescher and C. R. Bertozzi, *J. Am. Chem. Soc.*, 2005, **127**, 11196-11196.
136. M. L. Blackman, M. Royzen and J. M. Fox, *J. Am. Chem. Soc.*, 2008, **130**, 13518-+.
137. M. S. Masri and M. Friedman, *J. Protein Chem.*, 1988, **7**, 49-54.
138. R. J. Spears and M. A. Fascione, *Org. Biomol. Chem.*, 2016, **14**, 7622-7638.
139. R. J. Spears, R. L. Brabham, D. Budhadev, T. Keenan, S. McKenna, J. Walton, J. A. Brannigan, A. M. Brzozowski, A. J. Wilkinson, M. Plevin and M. A. Fascione, *Chem. Sci.*, 2018, **9**, 5585-5593.
140. C. D. Spicer and B. G. Davis, *Nat. Commun.*, 2014, **5**, 14.
141. J. M. Chalker, G. J. L. Bernardes, Y. A. Lin and B. G. Davis, *Chem.-Asian J.*, 2009, **4**, 630-640.
142. C. E. Hopkins, G. Hernandez, J. P. Lee and D. R. Tolan, *Arch. Biochem. Biophys.*, 2005, **443**, 1-10.
143. S. Suttapitugsakul, H. P. Xiao, J. Smeekens and R. H. Wu, *Molecular Biosystems*, 2017, **13**, 2574-2582.
144. J. Morales-Sanfrutos, J. Lopez-Jaramillo, M. Ortega-Munoz, A. Megia-Fernandez, F. Perez-Balderas, F. Hernandez-Mateo and F. Santoyo-Gonzalez, *Org. Biomol. Chem.*, 2010, **8**, 667-675.
145. J. M. Chalker, S. B. Gunnoo, O. Boutureira, S. C. Gerstberger, M. Fernandez-Gonzalez, G. J. L. Bernardes, L. Griffin, H. Hailu, C. J. Schofield and B. G. Davis, *Chem. Sci.*, 2011, **2**, 1666-1676.
146. G. J. L. Bernardes, E. J. Grayson, S. Thompson, J. M. Chalker, J. C. Errey, F. El Oualid, T. D. W. Claridge and B. G. Davis, *Angew. Chem.-Int. Edit.*, 2008, **47**, 2244-2247.
147. J. Ravasco, H. Faustino, A. Trindade and P. M. P. Gois, *Chem.-Eur. J.*, 2019, **25**, 43-59.
148. F. Saito, H. Noda and J. W. Bode, *ACS Chem. Biol.*, 2015, **10**, 1026-1033.
149. A. Beck, L. Goetsch, C. Dumontet and N. Corvaia, *Nat. Rev. Drug Discov.*, 2017, **16**, 315-337.
150. D. J. Betting, K. Kafi, A. Abdollahi-Fard, S. A. Hurvitz and J. M. Timmerman, *J. Immunol.*, 2008, **181**, 4131-4140.
151. C. P. Toseland, *Journal of chemical biology*, 2013, **6**, 85-95.
152. J. H. Ni, S. Singh and L. X. Wang, *Bioconjugate Chem.*, 2003, **14**, 232-238.
153. N. Forte, M. Livanos, E. Miranda, M. Morais, X. P. Yang, V. S. Rajkumar, K. A. Chester, V. Chudasama and J. R. Baker, *Bioconjugate Chem.*, 2018, **29**, 486-492.
154. G. T. Hermanson, *bioconjugation techniques Academic press third addition edn.*, 2013.

## References

155. B. Q. Shen, K. Y. Xu, L. N. Liu, H. Raab, S. Bhakta, M. Kenrick, K. L. Parsons-Reponte, J. Tien, S. F. Yu, E. Mai, D. W. Li, J. Tibbitts, J. Baudys, O. M. Saadi, S. J. Scales, P. J. McDonald, P. E. Hass, C. Eigenbrot, T. Nguyen, W. A. Solis, R. N. Fuji, K. M. Flagella, D. Patel, S. D. Spencer, L. A. Khawllil, A. Ebens, W. L. Wong, R. Vandlen, S. Kaur, M. X. Sliwkowski, R. H. Scheller, P. Polakis and J. R. Junutula, *Nat. Biotechnol.*, 2012, **30**, 184-189.
156. R. I. Nathani, V. Chudasama, C. P. Ryan, P. R. Moody, R. E. Morgan, R. J. Fitzmaurice, M. E. B. Smith, J. R. Baker and S. Caddick, *Org. Biomol. Chem.*, 2013, **11**, 2408-2411.
157. L. M. Tedaldi, M. E. B. Smith, R. I. Nathani and J. R. Baker, *Chem. Commun.*, 2009, DOI: 10.1039/b915136b, 6583-6585.
158. M. E. B. Smith, F. F. Schumacher, C. P. Ryan, L. M. Tedaldi, D. Papaioannou, G. Waksman, S. Caddick and J. R. Baker, *J. Am. Chem. Soc.*, 2010, **132**, 1960-1965.
159. B. Soveges, T. Imre, T. Szende, A. L. Poti, G. B. Cserep, T. Hegedus, P. Kele and K. Nemeth, *Org. Biomol. Chem.*, 2016, **14**, 6071-6078.
160. S. Chatani, D. P. Nair and C. N. Bowman, *Polym. Chem.*, 2013, **4**, 1048-1055.
161. E. M. Sletten and C. R. Bertozzi, *Angew. Chem.-Int. Edit.*, 2009, **48**, 6974-6998.
162. P. Costantino, S. Viti, A. Podda, M. A. Velmonte, L. Nencioni and R. Rappuoli, *Vaccine*, 1992, **10**, 691-698.
163. F. Fiorino, S. Rondini, F. Micoli, L. Lanzilao, R. Alfini, F. Mancini, C. A. MacLennan and D. Medagliani, *Front. Immunol.*, 2017, **8**, 11.
164. S. Rondini, F. Micoli, L. Lanzilao, M. Gavini, R. Alfini, C. Brandt, S. Clare, P. Mastroeni, A. Saul and C. A. MacLennan, *Infect. Immun.*, 2015, **83**, 996-1007.
165. M. J. Matos, B. L. Oliveira, N. Martinez-Saez, A. Guerreiro, P. Cal, J. Bertoldo, M. Maneiro, E. Perkins, J. Howard, M. J. Deery, J. M. Chalker, F. Corzana, G. Jimenez-Oses and G. J. L. Bernardes, *J. Am. Chem. Soc.*, 2018, **140**, 4004-4017.
166. O. Koniev and A. Wagner, *Chem. Soc. Rev.*, 2015, **44**, 5495-5551.
167. R. Brabham and M. A. Fascione, *ChemBioChem*, 2017, **18**, 1973-1983.
168. J. Clayden, N. Greeves and S. Warren, *Organic Chemistry* Oxford University Press, second edition edn., 2012.
169. C. D. Hein, X. M. Liu and D. Wang, *Pharm. Res.*, 2008, **25**, 2216-2230.
170. A. C. Knall and C. Slugovc, *Chem. Soc. Rev.*, 2013, **42**, 5131-5142.
171. S. I. Lim, Y. Mizuta, A. Takasu, Y. H. Kim and I. Kwon, *PLoS One*, 2014, **9**, 10.
172. V. Hong, N. F. Steinmetz, M. Manchester and M. G. Finn, *Bioconjugate Chem.*, 2010, **21**, 1912-1916.
173. J. Li, M. Y. Zheng, W. Tang, P. L. He, W. L. Zhu, T. X. Li, J. P. Zuo, H. Liu and H. L. Jiang, *Bioorg. Med. Chem. Lett.*, 2006, **16**, 5009-5013.
174. V. Hong, S. I. Presolski, C. Ma and M. G. Finn, *Angew. Chem.-Int. Edit.*, 2009, **48**, 9879-9883.
175. P. L. Golas, N. V. Tsarevsky, B. S. Sumerlin and K. Matyjaszewski, *Macromolecules*, 2006, **39**, 6451-6457.
176. C. J. Pickens, S. N. Johnson, M. M. Pressnall, M. A. Leon and C. J. Berkland, *Bioconjugate Chem.*, 2018, **29**, 686-701.
177. S. Jang, K. Sachin, H. J. Lee, D. W. Kim and H. S. Lee, *Bioconjugate Chem.*, 2012, **23**, 2256-2261.
178. S. L. Khatwani, J. S. Kang, D. G. Mullen, M. A. Hast, L. S. Beese, M. D. Distefano and T. A. Taton, *Bioorg. Med. Chem.*, 2012, **20**, 4532-4539.
179. Z. H. Wu, S. L. Liu, M. Hassink, I. Nair, R. Park, L. Li, I. Todorov, J. M. Fox, Z. B. Li, J. E. Shively, P. S. Conti and F. Kandeel, *J. Nucl. Med.*, 2013, **54**, 244-251.
180. N. K. Devaraj, R. Weissleder and S. A. Hilderbrand, *Bioconjugate Chem.*, 2008, **19**, 2297-2299.
181. J. D. Thomas, H. T. Cui, P. J. North, T. Hofer, C. Rader and T. R. Burke, *Bioconjugate Chem.*, 2012, **23**, 2007-2013.
182. A. Darko, S. Wallace, O. Dmitrenko, M. M. Machovina, R. A. Mehl, J. W. Chin and J. M. Fox, *Chem. Sci.*, 2014, **5**, 3770-3776.

## References

183. J. M. Gilmore, R. A. Scheck, A. P. Esser-Kahn, N. S. Joshi and M. B. Francis, *Angew. Chem.-Int. Edit.*, 2006, **45**, 5307-5311.
184. L. S. Witus, C. Netirojjanakul, K. S. Palla, E. M. Muehl, C. H. Weng, A. T. Iavarone and M. B. Francis, *J. Am. Chem. Soc.*, 2013, **135**, 17223-17229.
185. J. D. Cohen, P. Zou and A. Y. Ting, *ChemBioChem*, 2012, **13**, 888-894.
186. D. Schumacher, J. Helma, F. A. Mann, G. Pichler, F. Natale, E. Krause, M. C. Cardoso, C. P. R. Hackenberger and H. Leonhardt, *Angew. Chem.-Int. Edit.*, 2015, **54**, 13787-13791.
187. J. E. Hudak, H. H. Yu and C. R. Bertozzi, *J. Am. Chem. Soc.*, 2011, **133**, 16127-16135.
188. E. L. Smith, J. P. Giddens, A. T. Iavarone, K. Godula, L. X. Wang and C. R. Bertozzi, *Bioconjugate Chem.*, 2014, **25**, 788-795.
189. M. A. Gray, R. N. Tao, S. M. DePorter, D. A. Spiegel and B. R. McNaughton, *ChemBioChem*, 2016, **17**, 155-158.
190. J. Kalia and R. T. Raines, *Angew. Chem.-Int. Edit.*, 2008, **47**, 7523-7526.
191. M. Wendeler, L. Grinberg, X. Y. Wang, P. E. Dawson and M. Baca, *Bioconjugate Chem.*, 2014, **25**, 93-101.
192. A. Tuley, Y. J. Lee, B. Wu, Z. U. Wang and W. R. Liu, *Chem. Commun.*, 2014, **50**, 7424-7426.
193. P. Agarwal, J. van der Weijden, E. M. Sletten, D. Rabuka and C. R. Bertozzi, *Proc. Natl. Acad. Sci. U. S. A.*, 2013, **110**, 46-51.
194. R. L. Brabham, R. J. Spears, J. Walton, S. Tyagi, E. A. Lemke and M. A. Fascione, *Chem. Commun.*, 2018, **54**, 1501-1504.
195. R. L. Brabham, T. Keenan, A. Husken, J. Bilsborrow, R. McBerney, V. Kumar, W. B. Turnbull and M. A. Fascione, *Org. Biomol. Chem.*, 2020, **18**, 4000-4003.
196. J. E. Hudak, R. M. Barfield, G. W. de Hart, P. Grob, E. Nogales, C. R. Bertozzi and D. Rabuka, *Angew. Chem.-Int. Edit.*, 2012, **51**, 4161-4165.
197. R. Rappuoli, E. De Gregorio and P. Costantino, *Proc. Natl. Acad. Sci. U. S. A.*, 2019, **116**, 14-16.
198. W. F. Goebel and O. T. Avery, *J. Exp. Med.*, 1929, **50**, 521-531.
199. O. T. Avery and W. F. Goebel, *J. Exp. Med.*, 1929, **50**, 533-550.
200. R. Rappuoli, *Sci Transl Med*, 2018, **10**, 6.
201. B. Hamasur, M. Haile, A. Pawlowski, U. Schroder, A. Williams, G. Hatch, G. Hall, P. Marsh, G. Kallenius and S. B. Svenson, *Vaccine*, 2003, **21**, 4081-4093.
202. H. Geyer, S. Stirm and K. Himmelspach, *Med. Microbiol. Immunol.*, 1979, **165**, 271-288.
203. X. X. Gu and C. M. Tsai, *Infect. Immun.*, 1993, **61**, 1873-1880.
204. L. Kong, B. Vijaykrishnan, M. Kowarik, J. Park, A. N. Zakharova, L. Neiwert, A. Faridmoayer and B. G. Davis, *Nat. Chem.*, 2016, **8**, 242-249.
205. S. Pecetta, B. Vijaykrishnan, M. R. Romano, D. Proietti, P. Lo Surdo, C. Balocchi, E. Mori, B. G. Davis and F. Berti, *Vaccine*, 2016, **34**, 1405-1411.
206. S. B. Svenson and A. A. Lindberg, *Infect. Immun.*, 1981, **32**, 490-496.
207. S. B. Svenson and A. A. Lindberg, *J. Immunol. Methods*, 1979, **25**, 323-335.
208. G. De Benedetto, L. Salvini, S. Gotta, P. Cescutti and F. Micoli, *Bioconjugate Chem.*, 2018, **29**, 1736-1747.
209. M. Salman, F. St Michael, A. Ali, A. Jabbar, C. Cairns, A. C. Hayes, M. Rahman, M. Iqbal, A. Hague and A. D. Cox, *J. Immunol. Methods*, 2017, **450**, 27-33.
210. S. C. Szu, A. L. Stone, J. D. Robbins, R. Schneerson and J. B. Robbins, *J. Exp. Med.*, 1987, **166**, 1510-1524.
211. S. J. An, Y. K. Yoon, S. Kothari, N. Kothari, J. A. Kim, E. Lee, D. R. Kim, T. H. Park, G. W. Smith and R. Carbis, *Vaccine*, 2011, **29**, 7618-7623.
212. C. Jin, M. M. Gibani, M. Moore, H. B. Juel, E. Jones, J. Meiring, V. Harris, J. Gardner, A. Nebykova, S. A. Kerridge, J. Hill, H. Thomaidis-Brears, C. J. Blohmke, L. M. Yu, B. Angus and A. J. Pollard, *Lancet*, 2017, **390**, 2472-2480.
213. F. Belot, C. Guerreiro, F. Baleux and L. A. Mulard, *Chem.-Eur. J.*, 2005, **11**, 1625-1635.

## References

214. I. L. Acharya, C. U. Lowe, R. Thapa, V. L. Gurubacharya, M. B. Shrestha, M. Cadoz, D. Schulz, J. Armand, D. A. Bryla, B. Trollfors, T. Cramton, R. Schneerson and J. B. Robbins, *New England Journal of Medicine*, 1987, **317**, 1101-1104.
215. K. P. Klugman, H. J. Koornhof, R. Schneerson, M. Cadoz, I. T. Gilbertson, J. B. Robbins, D. Schulz and J. Armand, *Lancet*, 1987, **2**, 1165-1169.
216. E. J. Grayson, G. J. L. Bernardes, J. M. Chalker, O. Boutureira, J. R. Koeppe and B. G. Davis, *Angew. Chem.-Int. Edit.*, 2011, **50**, 4127-4132.
217. A. Pillot, A. Defontaine, A. Fateh, A. Lambert, M. Prasanna, M. Fanuel, M. Pipelier, N. Csaba, T. Violo, E. Camberlein and C. Grandjean, *Front. Chem.*, 2019, **7**, 9.
218. F. Berti and R. Adamo, *Chem. Soc. Rev.*, 2018, **47**, 9015-9025.
219. R. Ribeiro-Viana, M. Sanchez-Navarro, J. Luczkowiak, J. R. Koeppe, R. Delgado, J. Rojo and B. G. Davis, *Nat. Commun.*, 2012, **3**, 8.
220. P. M. Rendle, A. Seger, J. Rodrigues, N. J. Oldham, R. R. Bott, J. B. Jones, M. M. Cowan and B. G. Davis, *J. Am. Chem. Soc.*, 2004, **126**, 4750-4751.
221. T. R. Branson, T. E. McAllister, J. Garcia-Hartjes, M. A. Fascione, J. F. Ross, S. L. Warriner, T. Wennekes, H. Zuilhof and W. B. Turnbull, *Angew. Chem.-Int. Edit.*, 2014, **53**, 8323-8327.
222. M. C. Wiener, D. M. Freymann, P. Williams, P. Ghosh and R. M. Stroud, *Biophys. J.*, 1997, **72**, WAMF1-WAMF1.
223. D. M. Freed, A. K. Khan, P. S. Horanyi and D. S. Cafiso, *Biochemistry*, 2011, **50**, 8792-8803.
224. D. Crich, *Accounts Chem. Res.*, 2010, **43**, 1144-1153.
225. D. Crich, A. Banerjee, W. J. Li and Q. J. Yao, *J. Carbohydr. Chem.*, 2005, **24**, 415-424.
226. D. Crich and H. M. Li, *J. Org. Chem.*, 2002, **67**, 4640-4646.
227. D. Crich and M. Smith, *J. Am. Chem. Soc.*, 2001, **123**, 9015-9020.
228. B. Fraser-Reid and J. C. López, in *Reactivity Tuning in Oligosaccharide Assembly*, eds. B. Fraser-Reid and J. Cristóbal López, Springer Berlin Heidelberg, Berlin, Heidelberg, 2011, DOI: 10.1007/128\_2010\_105, pp. 1-29.
229. H. Paulsen, *Angew. Chem.-Int. Edit. Engl.*, 1982, **21**, 155-173.
230. P. S. Patil, C. C. Lee, Y. W. Huang, M. M. L. Zulueta and S. C. Hung, *Org. Biomol. Chem.*, 2013, **11**, 2605-2612.
231. Z. Y. Zhang and C. H. Wong, *Tetrahedron*, 2002, **58**, 6513-6519.
232. J. Raßloff, Q. Zhang and P. Mischnick, *Cellulose*, 2018, **25**, 4929-4940.
233. H. Helligso and M. Bols, *Accounts Chem. Res.*, 2006, **39**, 259-265.
234. B. Capon, *Quarterly Reviews*, 1964, **18**, 45-111.
235. D. Budhadev, R. Schwoerer and M. A. Fascione, in *Chemical and Biological Synthesis: Enabling Approaches for Understanding Biology*, The Royal Society of Chemistry, 2018, DOI: 10.1039/9781788012805-00243, pp. 243-274.
236. C. S. Callam and T. L. Lowary, *J. Org. Chem.*, 2001, **66**, 8961-8972.
237. R. Litjens, P. Hoogerhout, D. V. Filippov, J. D. C. Codee, L. J. van den Bos, R. van den Berg, H. S. Overkleeft and G. A. van der Marel, *J. Carbohydr. Chem.*, 2005, **24**, 755-769.
238. D. Esposito, M. Hurevich, B. Castagner, C. C. Wang and P. H. Seeberger, *Beilstein J. Org. Chem.*, 2012, **8**, 1601-1609.
239. R. Enugala, L. C. R. Carvalho, M. J. D. Pires and M. M. B. Marques, *Chem.-Asian J.*, 2012, **7**, 2482-2501.
240. G. Blatter, J. M. Beau and J. C. Jacquinet, *Carbohydr. Res.*, 1994, **260**, 189-202.
241. N. Barroca-Aubry, A. Pernet-Poil-Chevrier, A. Domard and S. Trombotto, *Carbohydr. Res.*, 2010, **345**, 1685-1697.
242. J. Bartek, R. Müller and P. Kosma, *Carbohydr. Res.*, 1998, **308**, 259-273.
243. A. Vibert, C. Lopin-Bon and J. C. Jacquinet, *Tetrahedron Lett.*, 2010, **51**, 1867-1869.
244. A. A. Sherman, O. N. Yudina, Y. V. Mironov, E. V. Sukhova, A. S. Shashkov, V. M. Menshov and N. E. Nifantiev, *Carbohydr. Res.*, 2001, **336**, 13-46.
245. D. Urabe, K. Sugino, T. Nishikawa and M. Isobe, *Tetrahedron Lett.*, 2004, **45**, 9405-9407.



## References

246. M. N. Khan and A. A. Khan, *J. Chem. Soc.-Perkin Trans. 2*, 1979, DOI: 10.1039/p29790000796, 796-798.
247. Neelottama Kushwaha and D. Kaushik, *Journal of Applied Pharmaceutical Science*, 2016, **6**, 159-171.
248. D. Crich and V. Dudkin, *J. Am. Chem. Soc.*, 2001, **123**, 6819-6825.
249. P. J. Garegg, H. Hultberg and S. Wallin, *Carbohydr. Res.*, 1982, **108**, 97-101.
250. M. Ohlin, R. Johnsson and U. Ellervik, *Carbohydr. Res.*, 2011, **346**, 1358-1370.
251. J. D. C. Codee, L. J. van den Bos, R. Litjens, H. S. Overkleeft, C. A. A. van Boeckel, J. H. van Boom and G. A. van der Marel, *Tetrahedron*, 2004, **60**, 1057-1064.
252. J. L. Hendel, J. W. Wang, T. A. Jackson, K. Hardmeier, R. De Los Santos and F. I. Auzanneau, *J. Org. Chem.*, 2009, **74**, 8321-8331.
253. Y. Tomabechi, M. A. Squire and A. J. Fairbanks, *Org. Biomol. Chem.*, 2014, **12**, 942-955.
254. R. Das and B. Mukhopadhyay, *ChemistryOpen*, 2016, **5**, 401-433.
255. C. S. Bennett, *Selective Glycosylations*, 2017.
256. N. Tanaka, I. Ogawa, S. Yoshigase and J. Nokami, *Carbohydr. Res.*, 2008, **343**, 2675-2679.
257. E. Cascales, S. K. Buchanan, D. Duche, C. Kleanthous, R. Lloubes, K. Postle, M. Riley, S. Slatin and D. Cavard, *Microbiol. Mol. Biol. Rev.*, 2007, **71**, 158-229.
258. N. G. Housden, S. R. Loftus, G. R. Moore, R. James and C. Kleanthous, *Proc. Natl. Acad. Sci. U. S. A.*, 2005, **102**, 13849-13854.
259. J. Konisky and B. S. Cowell, *J. Biol. Chem.*, 1972, **247**, 6524-&.
260. C. N. Penfold, B. Healy, N. G. Housden, R. Boetzel, M. Vankemmelbeke, G. R. Moore, C. Kleanthous and R. James, *J. Bacteriol.*, 2004, **186**, 4520-4527.
261. S. L. Greig, M. Radjainia and A. K. Mitra, *J. Biol. Chem.*, 2009, **284**, 16126-16134.
262. E. S. Collins, S. B. M. Whittaker, K. Tozawa, C. MacDonald, R. Boetzel, C. N. Penfold, A. Reilly, N. J. Clayden, M. J. Osborne, A. M. Hemmings, C. Kleanthous, R. James and G. R. Moore, *J. Mol. Biol.*, 2002, **318**, 787-804.
263. A. Klein, J. A. Wojdyla, A. Joshi, I. Josts, L. C. McCaughey, N. G. Housden, R. Kaminska, O. Byron, D. Walker and C. Kleanthous, *Biochem. J.*, 2016, **473**, 2799-2812.
264. H. M. Behrens, A. Six, D. Walker and C. Kleanthous, *Emerging Topics in Life Sciences*, 2017, **1**, 65-74.
265. X. Jin, W. Kightlinger, Y.-C. Kwon and S. H. Hong, *Synthetic Biology*, 2018, **3**.
266. S. Hahn-Lobmann, A. Stephan, S. Schulz, T. Schneider, A. Shaverskyi, D. Tuse, A. Giritch and Y. Gleba, *Front. Plant Sci.*, 2019, **10**, 16.
267. J. Chumchalova and J. Smarda, *Folia Microbiol.*, 2003, **48**, 111-115.
268. S. Kaur and S. Kaur, *Front. Pharmacol.*, 2015, **6**, 11.
269. D. R. Dimasi, J. C. White, C. A. Schnaitman and C. Bradbeer, *J. Bacteriol.*, 1973, **115**, 506-513.
270. K. Heller, B. J. Mann and R. J. Kadner, *J. Bacteriol.*, 1985, **161**, 896-903.
271. C. Bradbeer, P. R. Reynolds, G. M. Bauler and M. T. Fernandez, *J. Biol. Chem.*, 1986, **261**, 2520-2523.
272. D. P. Chimento, A. K. Mohanty, R. J. Kadner and M. C. Wiener, *Nat. Struct. Biol.*, 2003, **10**, 394-401.
273. R. J. Kadner, *Mol. Microbiol.*, 1990, **4**, 2027-2033.
274. K. Postle, *J. Bioenerg. Biomembr.*, 1993, **25**, 591-601.
275. V. Braun, *Fems Microbiol. Rev.*, 1995, **16**, 295-307.
276. O. Sharma, E. Yamashita, M. V. Zhalnina, S. D. Zakharov, K. A. Datsenko, B. L. Wanner and W. A. Cramer, *J. Biol. Chem.*, 2007, **282**, 23163-23170.
277. Z. H. Shi, K. F. Chak and H. S. Yuan, *J. Biol. Chem.*, 2005, **280**, 24663-24668.
278. H. Nikaïdo and M. Vaara, *Microbiol. Rev.*, 1985, **49**, 1-32.
279. S. D. Zakharov, M. V. Zhalnina, O. Sharma and W. A. Cramer, *Biochemistry*, 2006, **45**, 10199-10207.

## References

280. K. L. Lou, N. Saint, A. Prilipov, G. Rummel, S. A. Benson, J. P. Rosenbusch and T. Schirmer, *J. Biol. Chem.*, 1996, **271**, 20669-20675.
281. J. Spector, S. Zakharov, Y. Lill, O. Sharma, W. A. Cramer and K. Ritchie, *Biophys. J.*, 2010, **99**, 3880-3886.
282. W. A. Cramer, O. Sharma and S. D. Zakharov, *Biochem. J.*, 2018, **475**, 3903-3915.
283. E. Yamashita, M. V. Zhalnina, S. D. Zakharov, O. Sharma and W. A. Cramer, *Embo J.*, 2008, **27**, 2171-2180.
284. K. S. Jakes and A. Finkelstein, *Mol. Microbiol.*, 2010, **75**, 567-578.
285. S. K. Buchanan, P. Lukacik, S. Grizot, R. Ghirlando, M. M. U. Ali, T. J. Barnard, K. S. Jakes, P. K. Kienker and L. Esser, *Embo J.*, 2007, **26**, 2594-2604.
286. K. Hantke, *FEMS Microbiology Letters*, 1990, **67**, 5-8.
287. N. A. C. Curtis, R. L. Eisenstadt, S. J. East, R. J. Cornford, L. A. Walker and A. J. White, *Antimicrob. Agents Chemother.*, 1988, **32**, 1879-1886.
288. H. Nikaido and E. Y. Rosenberg, *J. Bacteriol.*, 1990, **172**, 1361-1367.
289. I. A. Critchley, M. J. Basker, R. A. Edmondson and S. J. Knott, *J. Antimicrob. Chemother.*, 1991, **28**, 377-388.
290. Y. Tatsumi, T. Maejima and S. Mitsuhashi, *Antimicrob. Agents Chemother.*, 1995, **39**, 613-619.
291. S. K. Buchanan, P. Lukacik, S. Grizot, R. Ghirlando, M. M. Ali, T. J. Barnard, K. S. Jakes, P. K. Kienker and L. Esser, *The EMBO journal*, 2007, **26**, 2594-2604.
292. R. Wallis, K. Y. Leung, A. J. Pommer, H. Videler, G. R. Moore, R. James and C. Kleanthous, *Biochemistry*, 1995, **34**, 13751-13759.
293. W. Li, C. A. Dennis, G. R. Moore, R. James and C. Kleanthous, *J. Biol. Chem.*, 1997, **272**, 22253-22258.
294. J. L. Ramos, A. García-Salamanca, C. Molina-Santiago and Z. Udaondo, in *Brenner's Encyclopedia of Genetics (Second Edition)*, eds. S. Maloy and K. Hughes, Academic Press, San Diego, 2013, DOI: <https://doi.org/10.1016/B978-0-12-374984-0.01096-2>, pp. 176-180.
295. M. Stamatakis and N. V. Mantzaris, *Biophys. J.*, 2009, **96**, 887-906.
296. A. D. Riggs, S. Bourgeois, R. F. Newby and M. Cohn, *J. Mol. Biol.*, 1968, **34**, 365-368.
297. P. Gatti-Lafranconi, W. P. Dijkman, S. R. A. Devenish and F. Hollfelder, *Microb. Cell. Fact.*, 2013, **12**, 10.
298. A. J. E. Gordon, P. A. Burns, D. F. Fix, F. Yatagai, F. L. Allen, M. J. Horsfall, J. A. Halliday, J. Gray, C. Bernelotmoens and B. W. Glickman, *J. Mol. Biol.*, 1988, **200**, 239-251.
299. W. Gilbert and B. Müller-Hill, *Proc. Natl. Acad. Sci. U. S. A.*, 1966, **56**, 1891-1898.
300. C. Martínez-Villaluenga, A. Cardelle-Cobas, N. Corzo, A. Olano and M. Villamiel, *Food Chemistry*, 2008, **107**, 258-264.
301. A. Jobe and S. Bourgeois, *J. Mol. Biol.*, 1972, **69**, 397-408.
302. M. Lewis, *J. Mol. Biol.*, 2013, **425**, 2309-2316.
303. B. H. Wang, B. Ternai and G. Polya, *Phytochemistry*, 1997, **44**, 787-796.
304. B. Decrombrugge, S. Busby and H. Buc, *Science*, 1984, **224**, 831-838.
305. T. P. Malan, A. Kolb, H. Buc and W. R. McClure, *J. Mol. Biol.*, 1984, **180**, 881-909.
306. J. Majors, *Nature*, 1975, **256**, 672-674.
307. M. C. Politz, M. F. Copeland and B. F. Pflieger, *Chem. Commun.*, 2013, **49**, 4325-4327.
308. M. Witvrouw, V. Fikkert, A. Hantson, C. Pannecouque, B. R. O'Keefe, J. McMahon, L. Stamatatos, E. de Clercq and A. Bolmstedt, *J. Virol.*, 2005, **79**, 7777-7784.
309. K. Puget, A. M. Michelson and S. Avrameas, *Anal. Biochem.*, 1977, **79**, 447-456.
310. G. H. G. Thorpe and L. J. Kricka, *Method Enzymol.*, 1986, **133**, 331-353.
311. T. Kobayashi, K. Saga, S. Shimizu and T. Goto, *Agricultural and Biological Chemistry*, 1981, **45**, 1403-1408.

## References

312. J. E. Boyson, R. Erskine, M. C. Whitman, M. Chiu, J. M. Lau, L. A. Koopman, M. M. Valter, P. Angelisova, V. Horejsi and J. L. Strominger, *Proc. Natl. Acad. Sci. U. S. A.*, 2002, **99**, 16180-16185.
313. A. S. Norgren, C. Budke, Z. Majer, C. Heggemann, T. Koop and N. Sewald, *Synthesis*, 2009, DOI: 10.1055/s-0028-1083302, 488-494.
314. N. J. Kruger, in *The Protein Protocols Handbook*, ed. J. M. Walker, Humana Press, Totowa, NJ, 2009, DOI: 10.1007/978-1-59745-198-7\_4, pp. 17-24.
315. R. Nakao, M. Ramstedt, S. N. Wai and B. E. Uhlin, *PLoS One*, 2012, **7**, 13.
316. T. Trunk, H. S. Khalil and J. C. Leo, *Aims Microbiology*, 2018, **4**, 140-164.
317. I. Lerouge and J. Vanderleyden, *Fems Microbiol. Rev.*, 2002, **26**, 17-47.
318. C. Pagnout, B. Sohm, A. Razafitianamaharavo, C. Caillet, M. Offroy, M. Leduc, H. Gendre, S. Jomini, A. Beaussart, P. Bauda and J. F. L. Duval, *Scientific Reports*, 2019, **9**, 9696.
319. J. A. Yethon, E. Vinogradov, M. B. Perry and C. Whitfield, *J. Bacteriol.*, 2000, **182**, 5620-5623.
320. F. G. Sorroche, M. B. Spesia, A. Zorreguieta and W. Giordano, *Appl. Environ. Microbiol.*, 2012, **78**, 4092-4101.
321. S. Bhargava, B. B. Johnson, J. Hwang, T. A. Harris, A. S. George, A. Muir, J. Dorff and I. N. Okeke, *J. Bacteriol.*, 2009, **191**, 4934-4942.
322. D. J. Parker, P. Demetci and G. W. Li, *J. Bacteriol.*, 2019, **201**.
323. L. Nobs, F. Buchegger, R. Gurny and E. Allemann, *European Journal of Pharmaceutics and Biopharmaceutics*, 2004, **58**, 483-490.
324. J. J. Gridley and H. M. I. Osborn, *J. Chem. Soc.-Perkin Trans. 1*, 2000, DOI: 10.1039/a909165c, 1471-1491.
325. T. J. Boltje, T. Buskas and G. J. Boons, *Nat. Chem.*, 2009, **1**, 611-622.
326. M. Bols and C. M. Pedersen, *Beilstein J. Org. Chem.*, 2017, **13**, 93-105.
327. H. Elferink, R. A. Mensink, P. B. White and T. J. Boltje, *Angew. Chem.-Int. Edit.*, 2016, **55**, 11217-11220.
328. G. Hodosi and P. Kovac, *J. Am. Chem. Soc.*, 1997, **119**, 2335-2336.
329. D. Crich, A. Banerjee and Q. J. Yao, *J. Am. Chem. Soc.*, 2004, **126**, 14930-14934.
330. P. Wen and D. Crich, *J. Org. Chem.*, 2015, **80**, 12300-12310.
331. I. Sharma, L. Bohe and D. Crich, *Carbohydr. Res.*, 2012, **357**, 126-131.
332. D. Kahne, S. Walker, Y. Cheng and D. Vanengen, *J. Am. Chem. Soc.*, 1989, **111**, 6881-6882.
333. C. G. Lucero and K. A. Woerpel, *J. Org. Chem.*, 2006, **71**, 2641-2647.
334. S. van der Vorm, T. Hansen, H. S. Overkleeft, G. A. van der Marel and J. D. C. Codee, *Chem. Sci.*, 2017, **8**, 1867-1875.
335. D. Crich and N. S. Chandrasekera, *Angew. Chem.-Int. Edit.*, 2004, **43**, 5386-5389.
336. J. D. C. Codee, L. H. Hossain and P. H. Seeberger, *Org. Lett.*, 2005, **7**, 3251-3254.
337. K. S. Kim, J. H. Kim, Y. J. Lee, Y. J. Lee and J. Park, *J. Am. Chem. Soc.*, 2001, **123**, 8477-8481.
338. H. Nagai, S. Matsumura and K. Toshima, *Carbohydr. Res.*, 2003, **338**, 1531-1534.
339. I. Cumpstey, *Carbohydr. Res.*, 2008, **343**, 1553-1573.
340. F. Barresi and O. Hindsgaul, *J. Am. Chem. Soc.*, 1991, **113**, 9376-9377.
341. F. Barresi and O. Hindsgaul, *Can. J. Chem.-Rev. Can. Chim.*, 1994, **72**, 1447-1465.
342. G. Stork and G. Kim, *J. Am. Chem. Soc.*, 1992, **114**, 1087-1088.
343. G. Stork and J. J. LaClair, *J. Am. Chem. Soc.*, 1996, **118**, 247-248.
344. M. Bols, *J. Chem. Soc.-Chem. Commun.*, 1992, DOI: 10.1039/c39920000913, 913-914.
345. M. Bols, *Tetrahedron*, 1993, **49**, 10049-10060.
346. Y. Ito and T. Ogawa, *Angew. Chem.-Int. Edit. Engl.*, 1994, **33**, 1765-1767.
347. Y. Ito, Y. Ohnishi, T. Ogawa and Y. Nakahara, *Synlett*, 1998, DOI: 10.1055/s-1998-1894, 1102-+.
348. Y. Ito and T. Ogawa, *J. Am. Chem. Soc.*, 1997, **119**, 5562-5566.
349. B. W. Yu, H. van Ingen, S. Vivekanandan, C. Rademacher, S. E. Norris and D. I. Freedberg, *J. Magn. Reson.*, 2012, **215**, 10-22.

## References

350. B. Fraser-Reid, J. C. Lopez, K. V. Radhakrishnan, M. Mach, U. Schlueter, A. M. Gomez and C. Uriel, *J. Am. Chem. Soc.*, 2002, **124**, 3198-3199.
351. W. Wang and F. Kong, *J. Org. Chem.*, 1998, **63**, 5744-5745.
352. T. Desmet and W. Soetaert, *Biocatal. Biotransform.*, 2011, **29**, 1-18.
353. L. L. Lairson and S. G. Withers, *Chem. Commun.*, 2004, DOI: 10.1039/b406490a, 2243-2248.
354. T. Desmet, W. Soetaert, P. Bojarova, V. Kren, L. Dijkhuizen, V. Eastwick-Field and A. Schiller, *Chem.-Eur. J.*, 2012, **18**, 10786-10801.
355. D. L. Zechel and S. G. Withers, *Accounts Chem. Res.*, 2000, **33**, 11-18.
356. A. Ardèvol, J. Iglesias-Fernández, V. Rojas-Cervellera and C. Rovira, *Biochemical Society Transactions*, 2016, **44**, 51-60.
357. N. Soya, Y. Fang, M. M. Palcic and J. S. Klassen, *Glycobiology*, 2011, **21**, 547-552.
358. E. C. O'Neill and R. A. Field, *Carbohydr. Res.*, 2015, **403**, 23-37.
359. T. Nihira, E. Suzuki, M. Kitaoka, M. Nishimoto, K. Ohtsubo and H. Nakai, *J. Biol. Chem.*, 2013, **288**, 27366-27374.
360. Y. X. Ye, W. Saburi, R. Odaka, K. Kato, N. Sakurai, K. Komoda, M. Nishimoto, M. Kitaoka, H. Mori and M. Yao, *FEBS Lett.*, 2016, **590**, 828-837.
361. S. Nakae, S. Ito, M. Higa, T. Senoura, J. Wasaki, A. Hijikata, M. Shionyu, S. Ito and T. Shirai, *J. Mol. Biol.*, 2013, **425**, 4468-4478.
362. C. Mayer, D. L. Jakeman, M. Mah, G. Karjala, L. Gal, R. A. J. Warren and S. G. Withers, *Chem. Biol.*, 2001, **8**, 437-443.
363. M. R. Hayes and J. Pietruszka, *Molecules (Basel, Switzerland)*, 2017, **22**, 1434.
364. M. Jahn and S. G. Withers, *Biocatal. Biotransform.*, 2003, **21**, 159-166.
365. M. Nieto-Domínguez, B. Fernández de Toro, L. I. de Eugenio, A. G. Santana, L. Bejarano-Muñoz, Z. Armstrong, J. A. Méndez-Líter, J. L. Asensio, A. Prieto, S. G. Withers, F. J. Cañada and M. J. Martínez, *Nat. Commun.*, 2020, **11**, 4864.
366. M. Jahn, J. Marles, R. A. J. Warren and S. G. Withers, *Angew. Chem.-Int. Edit.*, 2003, **42**, 352-+.
367. I. Sittel and M. C. Galan, *Org. Biomol. Chem.*, 2017, **15**, 3575-3579.
368. I. Timari, L. Kaltschnee, A. Kolmer, R. W. Adams, M. Nilsson, C. M. Thiele, G. A. Morris and K. E. Kover, *J. Magn. Reson.*, 2014, **239**, 130-138.
369. A. Enthart, J. C. Freudenberger, J. Furrer, H. Kessler and B. Luy, *J. Magn. Reson.*, 2008, **192**, 314-322.
370. L. A. Kelley, S. Mezulis, C. M. Yates, M. N. Wass and M. J. E. Sternberg, *Nat. Protoc.*, 2015, **10**, 845-858.
371. S. Ladeveze, G. Cioci, P. Roblin, L. Mourey, S. Tranier and G. Potocki-Veronese, *Acta Crystallographica Section D-Structural Biology*, 2015, **71**, 1335-1346.
372. K. S. Mehershahi and S. L. Chen, *Genome Announc*, 2017, **5**, e00306-00317.
373. E. T. Saulino, D. G. Thanassi, J. S. Pinkner and S. J. Hultgren, *Embo J.*, 1998, **17**, 2177-2185.
374. D. R. Vianna, L. Ruschel, F. Dietrich, F. Figueiró, F. B. Morrone, R. F. S. Canto, F. Corvello, A. Velho, A. Crestani, H. Teixeira, G. L. von Poser, A. M. O. Battastini and V. L. Eifler-Lima, *MedChemComm*, 2015, **6**, 905-911.
375. Y. H. Su, J. S. Xie, Y. G. Wang, X. Hu and X. F. Lin, *Eur. J. Med. Chem.*, 2010, **45**, 2713-2718.
376. M. Kurosu, K. Li and D. C. Crick, *Org. Lett.*, 2009, **11**, 2393-2396.
377. R. Kowalczyk, P. W. R. Harris, R. P. Dunbar and M. A. Brimble, *Synthesis*, 2009, DOI: 10.1055/s-0029-1216820, 2210-2222.
378. I. Cumpstey, K. Chayajarus, A. J. Fairbanks, A. J. Redgrave and C. M. P. Seward, *Tetrahedron: Asymmetry*, 2004, **15**, 3207-3221.
379. M. K. Patel, B. Vijayakrishnan, J. R. Koeppe, J. M. Chalker, K. J. Doores and B. G. Davis, *Chem. Commun.*, 2010, **46**, 9119-9121.
380. O. Norberg, B. Wu, N. Thota, J. T. Ge, G. Fauquet, A. K. Saur, T. Aastrup, H. Dong, M. D. Yan and O. Ramstrom, *Carbohydr. Res.*, 2017, **452**, 35-42.

## References

381. K. Chayajarus, D. J. Chambers, M. J. Chughtai and A. J. Fairbanks, *Org. Lett.*, 2004, **6**, 3797-3800.
382. Y. H. Lin, B. Ghosh and K. K. T. Mong, *Chem. Commun.*, 2012, **48**, 10910-10912.
383. C. S. Chao, M. C. Chen, S. C. Lin and K. K. T. Mong, *Carbohydr. Res.*, 2008, **343**, 957-964.
384. L. J. Huang and X. F. Huang, *Chem.-Eur. J.*, 2007, **13**, 529-540.
385. C. Coutant and J. C. Jacquinet, *J. Chem. Soc.-Perkin Trans. 1*, 1995, DOI: 10.1039/p19950001573, 1573-1581.
386. A. A. Joseph, V. P. Verma, X. Y. Liu, C. H. Wu, V. M. Dhurandhare and C. C. Wang, *Eur. J. Org. Chem.*, 2012, **2012**, 744-753.
387. A. Cirila, A. R. McHale and J. Mann, *Tetrahedron*, 2004, **60**, 4019-4029.
388. D. Q. Cai, C. C. Xun, F. Tang, X. B. Tian, L. Y. Yang, K. Ding, W. Z. Li, Z. P. Le and W. Huang, *Carbohydr. Res.*, 2017, **449**, 143-152.
389. Y. Y. Lin, S. H. Chan, Y. P. Juang, H. M. Hsiao, J. H. Guh and P. H. Liang, *Eur. J. Med. Chem.*, 2018, **143**, 1942-1958.
390. 2015.
391. J. S. Chen, A. Sankar, Y. J. Lin, P. H. Huang, C. H. Liao, S. S. Wu, H. R. Wu and S. Y. Luo, *RSC Adv.*, 2019, **9**, 33853-33862.
392. S. S. Shiyatare, S. H. Chang, T. I. Tsai, C. T. Ren, H. Y. Chuang, L. Hsu, C. W. Lin, S. T. Li, C. Y. Wu and C. H. Wong, *J. Am. Chem. Soc.*, 2013, **135**, 15382-15391.
393. M. U. Ahmad, S. M. Ali, A. Ahmad, S. Sheikh, P. Chen and I. Ahmad, *Chem. Phys. Lipids*, 2015, **186**, 30-38.
394. J. B. Zhang, B. Zhang, J. F. Zhou, J. Li, C. J. Shi, T. Huang, Z. F. Wang and J. Tang, *J. Carbohydr. Chem.*, 2011, **30**, 165-177.
395. A. Hamed, R. Osman, K. T. Al-Jamal, S. M. Hoayel and A. S. Geneidi, *J. Drug Deliv. Sci. Technol.*, 2019, **51**, 513-523.
396. F. Beiroth, T. Koudelka, T. Overath, S. D. Knight, A. Tholey and T. K. Lindhorst, *Beilstein J. Org. Chem.*, 2018, **14**, 1890-1900.
397. C. Grabosch, K. Kolbe and T. K. Lindhorst, *ChemBioChem*, 2012, **13**, 1874-1879.
398. A. Rostami, A. Colin, X. Y. Li, M. G. Chudzinski, A. J. Lough and M. S. Taylor, *The Journal of Organic Chemistry*, 2010, **75**, 3983-3992.
399. M. J. Lu, Q. B. Lu and J. F. Honek, *Bioorg. Med. Chem. Lett.*, 2017, **27**, 282-287.
400. L. Spitzer, S. Lecommandoux, H. Cramail and F. Jérôme, *Green Chemistry*, 2021, **23**, 1361-1369.
401. X. Elduque, E. Pedroso and A. Grandas, *The Journal of Organic Chemistry*, 2014, **79**, 2843-2853.
402. K. Chauhan, A. Arun, S. Singh, M. Manohar, K. Chuttani, R. Konwar, A. Dwivedi, R. Soni, A. K. Singh, A. K. Mishra and A. Datta, *Bioconjugate Chem.*, 2016, **27**, 961-972.
403. G. Chen, Q. Yin, J. Yin, X. Gu, X. Liu, Q. You, Y.-L. Chen, B. Xiong and J. Shen, *Org. Biomol. Chem.*, 2014, **12**, 9781-9785.
404. Y. J. Zu, C. L. Cai, J. Y. Sheng, L. L. Cheng, Y. L. Feng, S. Zhang, Q. Zhang and Y. H. Chai, *Org. Lett.*, 2019, **21**, 8270-8274.
405. L. Drouin, R. G. Compton, N. Fietkau and A. J. Fairbanks, *Synlett*, 2007, DOI: 10.1055/s-2007-986644, 2711-2717.
406. K. S. Kim, D. B. Fulse, J. Y. Baek, B. Y. Lee and H. B. Jeon, *J. Am. Chem. Soc.*, 2008, **130**, 8537-8547.
407. K. T. Webster, R. Eby and C. Schuerch, *Carbohydr. Res.*, 1983, **123**, 335-340.
408. D. Crich and O. Vinogradova, *J. Am. Chem. Soc.*, 2007, **129**, 11756-11765.